Contributions to siloxane coordination chemistry and silicon based crown-ether analogues *via* s-block metal templated Si-O bond activation

Kumulative Dissertation

Zur Erlangung des Doktorgrades der Naturwissenschaften

(Dr. rer. nat.)

am Fachbereich Chemie der

Philipps-Universität Marburg

vorgelegt von

Fabian Maurice Dankert

aus Varel

Marburg (Lahn) 2020

Erstgutachter: Prof. Dr. Carsten von Hänisch
Zweitgutachter: Prof. Dr. Bernhard Neumüller
Hochschulkennziffer: 1180

Die vorliegende Arbeit wurde von Januar 2017 bis November 2020 unter der Leitung von Herrn Prof. Dr. Carsten von Hänisch am Fachbereich Chemie der Philipps-Universität Marburg angefertigt. Vom Fachbereich Chemie der Philipps-Universität Marburg wurde die Dissertation mit dem Titel

„Contributions to siloxane coordination chemistry and silicon based crown-ether analogues *via* s-block metal templated Si-O bond activation"

angenommen am:

Erstgutachter: Prof. Dr. Carsten von Hänisch
Zweitgutachter: Prof. Dr. Bernhard Neumüller

Tag der Disputation: 15.12.20
Hochschulkennziffer: 1180

Erklärung

Ich erkläre, dass eine Promotion noch an keiner anderen Hochschule als der Philipps-Universität Marburg, Fachbereich Chemie, versucht wurde.

Ich versichere, dass ich meine vorgelegte Dissertation mit dem Titel

„Contributions to siloxane coordination chemistry and silicon based crown-ether analogues *via* s-block metal templated Si-O bond activation“

selbst und ohne fremde Hilfe verfasst, nicht andere als die in ihr angegebenen Quellen oder Hilfsmittel benutzt, alle vollständig oder sinngemäß übernommenen Zitate als solche gekennzeichnet sowie die Dissertation in der vorliegenden oder einer ähnlichen Form noch bei keiner anderen in- oder ausländischen Hochschule anlässlich eines Promotionsgesuchs oder zu anderen Prüfungszwecken eingereicht habe.

11.11.2020	F. Dankert
Datum	Unterschrift

Lebenslauf

Persönliche Daten

Die persönlichen Daten sind nicht Teil der elektronischen Version dieser Dissertation.

Praktika / Nebentätigkeiten

Die Angabe dieser Daten sind nicht Teil der elektronischen Version dieser Dissertation.

Publikationen

(1) F. Dankert, C. Scholl, *PdN-ChiS* **2016**, *6(65)*, 34-40. „Porphyrine: Könige der Aromaten. Aromatenchemie mal anders – Anregungen für den Chemie-LK."

(2) F. Dankert, K. Reuter, C. Donsbach, C. von Hänisch, *Dalton Trans*. **2017**, *46*, 8727. „A structural study of alkaline earth metal complexes with hybrid disila-crown ethers".

(3) K. Reuter, F. Dankert, C. Donsbach, C. von Hänisch, *Inorganics* **2017**, *5(1)*, 11. „Structural Study of Mismatched Disila-Crown Ether Complexes".

(4) F. Dankert, C. Donsbach, C.-N. Mais, K. Reuter, C. von Hänisch, *Inorg. Chem*. **2018**, *57(1)*, 351-359. „Alkali and Alkaline Earth Metal Derivatives of Disila-Bridged Podands: Coordination Chemistry and Structural Diversity".

(5) F. Dankert, K. Reuter, C. Donsbach, C. von Hänisch, *Inorganics* **2018**, *6(1)*, 15. „Hybrid Disila-Crown Ethers as Hosts for Ammonium Cations: The O–Si–Si–O Linkage as an Acceptor for Hydrogen Bonding".

(6) F. Dankert, J. Heine, J. Rienmüller, C. von Hänisch, *CrystEngComm* **2018**, *20*, 5370-5376. „Sila-polyethers as innocent crystallization reagents for heavy alkali metal compounds".

(7) M. R. Buchner, M. Müller, F. Dankert, K. Reuter, C. von Hänisch, *Dalton Trans*. **2018**, *47*, 16393-16397. „The coordination behaviour and reactivity of partially silicon based crown ethers towards beryllium chloride".

(8) F. Dankert, C. von Hänisch, *Inorg. Chem*. **2019**, *58*, 3518-3526. „Insights into the Coordination Ability of Siloxanes Employing Partially Silicon Based Crown Ethers: A Comparative Analysis of s-Block Metal Complexes".

(9) C. Ritter, B. Ringler, F. Dankert, M. Conrad, F. Kraus, C. von Hänisch, *Dalton Trans*. **2019**, *48*, 5253-5262. „Synthesis and crystal structures of novel tertiary butyl substituted (pseudo-)halogen bismuthanes".

(10) F. Dankert, C. Donsbach, J. Rienmüller, R. M. Richter, C. von Hänisch, *Chem. Eur. J*. **2019**, 25, 15934-15943. „Alkaline earth metal template (cross-)coupling reactions with hybrid disila-crown ether analogues".

(11) F. Dankert, F. Weigend, C. von Hänisch, *Inorg. Chem*. **2019**, *58*, 15417-15422. „Not Non-coordinating at all: Coordination Compounds of the Cyclodimethylsiloxanes D_n (D = Me2SiO; n = 6, 7) and Group 2 Metal Cations".

(12) F. Dankert, H. L. Deubner, M. Müller, M. R. Buchner, F. Kraus and C. von Hänisch, *Z. Anorg. Allg. Chem.* **2020**, *646*, 1501-1507. „C-F Bond Cleavage Reactions with Beryllium, Magnesium, Gallium, Hafnium and Thorium Halides".

(13) F. Dankert, L. Erlemeier, C. Ritter, C. von Hänisch, *Inorg. Chem. Front*. **2020**, 7, 2138-2153. „On the molecular architectures of siloxane coordination compounds: (re-)investigating the coordination of the cyclodimethylsiloxanes D_n (n = 5–8) towards alkali metal ions".

(14) M. Jost, R. M. Richter, M. Balmer, B. Peters, F. Dankert, C. von Hänisch, *Dalton Trans*. **2020**, *49*, 5787-5790. „Coordination polymers of alkali metal cyclosiloxazanides with one- and two-dimensional structures".

(15) F. Dankert,* A. Feyh,* C. von Hänisch, *Eur. J. Inorg. Chem*. **2020**, *2020*, 2744-2756. „Chalcogen bonding of SO_2 and s-block metal iodides near room temperature: A remarkable structural diversity". *These authors contributed equally.

(16) T. Dunaj, K. Dollberg, C. Ritter, F. Dankert, C. von Hänisch, *submitted*. **2020**. „2,6-Diisopropylphenyl Substituted Bismuth Compounds: Synthesis, structure and reactivity"

(17) M. R. Buchner, F. Dankert, N. Spang, F. Pielnhofer, C. von Hänisch**,** *accepted***, 2020.** „A Second Modification of Beryllium Bromide: β-BeBr2".

(18) F. Dankert, R. M. Richter, F. Weigend, X. Xie, M. Balmer, C. von Hänisch, *submitted*. **2020**. „ Architecting inorganic crown-ethers by s-block-metal templated Si-O bond activation".

Posterbeiträge

(1) F. Dankert, C. von Hänisch, Materialforschungstag Mittelhessen (Gießen) 2017, 28.06.2017 & GDCh-Wissenschaftsforum Berlin 10.09-14.09.2017.
„Synthesis and Coordination Chemistry of Silicon Based Ligands"

(2) F. Dankert, C. von Hänisch, ^{9}th European Silicon Days Saarbrücken, 09.09-12.09.2018.
„Template assisted synthesis of silicon based crown ether analogues"

(3) F. Dankert, C. von Hänisch, GDCh-Wissenschaftsforum Aachen 15.09.-18.09.2019 & 03.03.-04.03.2020 #RSCPoster Twitter Conference (Online).
„Not non-coordinating at all: Synthesis and coordination chemistry of $[(Me_2Si)_xO]_n$-type crown ether analogues (x = 1, 2; n = 3, 4, 6, 7)"

(4) F. Dankert, C. von Hänisch, Online-Vortragstagung für Anorganische Chemie der Fachgruppen Wöhler-Vereinigung und Festkörperchemie und Materialforschung 29.09.-30.09.2020.
„Architectures based on organics: Synthesis of inorganic crown-ether analogues and their complexes via s-block-metal templated Si-O bond activation"

Danksagung

Danke!
Die Danksagung ist nicht Teil der elektronischen Version dieser Dissertation.

"I have never tried that before, so I think I should definitely be able to do that."
— Astrid Lindgren, Pippi Longstocking

Content

1 Introduction 3

1.1 Macrocyclic Compounds: From Organics to Inorganics 3

1.2 Siloxanes: Synthesis, Structure and Applications 9

1.3 Cyclic Siloxanes and Their Relation to Crown-Ethers 11

1.4 The Si-O bond: A Look at the Building Block of Siloxanes and Silicates 13

1.4.1 Hyperconjugation Interactions in Siloxanes 13

1.4.2 Ionic Bond Model of the Si-O Bond 16

1.4.3 The Si-O-Si Angle as an Important Parameter Regarding Basicity 20

1.4.4 Increased Basicity of Siloxanes Employing Cooperativity Effects 24

1.5 Siloxane coordination compounds 26

1.6 Increasing Cation Binding Ability Employing Disilanes 33

1.6.1 Difference in Hyperconjugation Interactions 33

1.6.2 Difference in Bond Polarity 34

1.6.3 Difference in Ring-Strain 36

1.7 Hybrid Disila Crown-Ethers: Synthesis, Structure, Cation-Binding Ability and Reactivity 37

2 Project Scope 45

3 Cumulative Part 49

4 Unpublished Results 75

4.1 Attempts Synthesizing Disila-Crown Ethers from Disila-Bridged Glycols 75

4.2 The Reactivity of Be-Salts Towards Exclusively Si-Based Systems 77

4.3 Experimental Section 85

4.4 Crystal Structure Data 87

5 Summary 89

5.1 Contributions to the Coordination Chemistry of Disila-Crown Ethers 89

5.2 Contributions to the Coordination Chemistry of D_n Ligands 104

5.3 Siloxane Coordination Chemistry with BeX_2 (X = Cl^-, Br^-, I^-)..... 111

6 Zusammenfassung..... 115

6.1 Beiträge zur Koordinationschemie von Disila-Kronenethern 115

6.2 Beiträge zur Koordinationschemie von D_n Liganden..... 131

6.3 Siloxan-Koordinationschemie mit BeX_2 (X = Cl^-, Br^-, I^-) 138

7 Bibliography..... 143

8 Appendix..... 154

1 Introduction

1.1 Macrocyclic Compounds: From Organics to Inorganics

Macrocyclic compounds, best known as compounds of a natural or synthetic origin bearing at least three donor atoms incorporated in a cyclic backbone,[1] are the centrepiece of host-guest chemistry and thus also supramolecular chemistry. The chemistry of these compounds amazes chemists around the world and is not least driven by their intrinsic beauty and the unexpectedness of their structures.[1] Owing to a cyclic rather than linear structure, macrocyclic compounds bear a cavity in which they can incorporate guest molecules such as metal ions. Hence, linear compounds need to alter their structure during the incorporation process while macrocyclic compounds do not. In many cases, the complexation ability of macrocyclic compounds is thus higher than that of open-chained derivatives having the same amount of donor atoms and/or binding sites.[2] Conclusively, macrocyclic ligand complexes are characterized by high stability and show enhanced resistance to degradation, temperature and are inert toward many acids and bases as the metal centre is firmly bound within the cyclic moiety.[1] Not surprisingly does nature choose macrocyclic ligand frameworks for the use in many important biological processes. To mention just a few, there are chlorophylls, hemeproteins and vitamin B12 which have (except for vitamin B12) the famous porphin-architecture in common which is well-known as the parent structure of the better-known porphyrins (see Figure 1 (top)).[3] As metal centres remain in the porphyrin moiety, they are available for a subsequent metal-assisted biochemistry.

The birth of a synthetic supramolecular chemistry, however, dates back to the year 1967 when Charles PEDERSEN discovered macrocyclic poly-ether ligands which later became known as crown-ethers because of a characteristic crown-like shape (see Figure 1 (middle) for an example).[4–6] Based on the results of PEDERSEN, Jean-Marie LEHN and Donald CRAM expanded the field of macrocyclic ligands shortly after. LEHN for example developed highly ion sensitive molecules which later became known as cryptands (see Figure 1 (bottom)) and CRAM developed supramolecules in the light of substrate recognition.[5–7] Conclusively, nowadays host-guest chemistry is highly characterized by the synthesis of compounds which can serve as model systems for natural products constructed by large rings as ligands.[6]

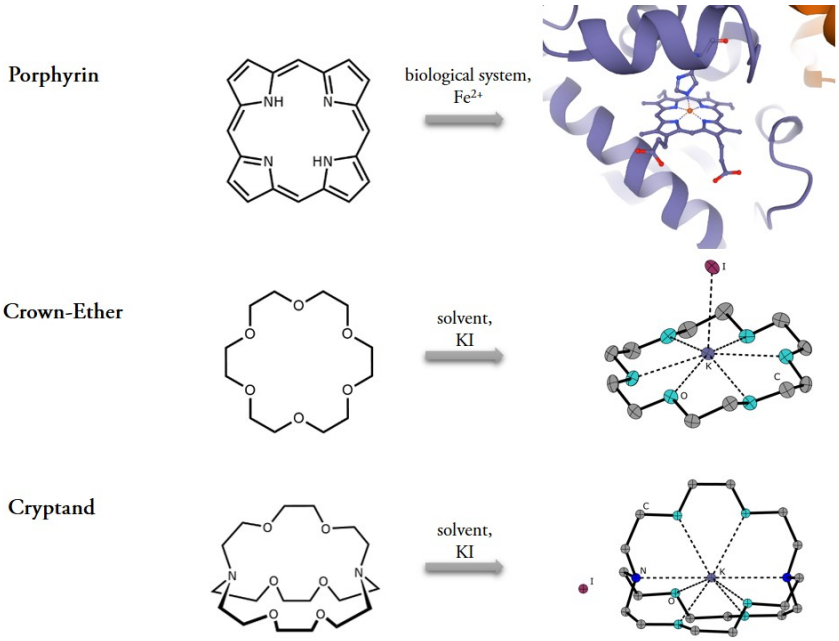

Figure 1: A selection of prominent macrocyclic ligands. Porphin and its implementation into hemoglobin (here: deoxygenated form according to 1GBU.pdb) (top),[8,9] [18]crown-6 and its adduct with KI (middle)[10] and shielding of K^+ by [222]crypt (bottom)[11].

Since the discovery of cyclic polyethers and their complexes, host-guest chemistry has grown rapidly. In particular, crown-type ligands have been reviewed several times and many fields of applications have been established based on the findings.[12–16] The numerous applications range from separation[17,18] and phase-transfer,[19] ion sensing[20,21] to synthetic ion transporters,[22] biomedical applications[23] and many more. Contributions to this chemistry therefore comes from nearly all chemical disciplines but also from biology, physics and nanotechnology making host-guest chemistry highly interdisciplinary. This of course makes the breadth of the topic enormous which, by time, did more and more also arouse the interest of an inorganic chemist.[6]

It should be noted that the research in macrocyclic ligands is mainly based on carbon based systems as carbon is the central element of life, suitable of engaging in the formation of chemical bonds with many other atoms.[24] Similar to conventional host guest chemistry, however, inorganic chemists around the world introduced compounds to host guest chemistry that are (partially) made of an inorganic skeleton and are mostly of a synthetic origin.[25] Studying their chemical structure, binding properties and of course applications gives insights into chemical bonding,

non-covalent interactions and ion recognition. Advances in a chemistry of inorganic macrocycles have been made by time which is evident from a number of review-type articles[26–28] and even books[25] that have been published. Similar to the chemistry of carbon based macrocyclic compounds, a multifarious structural diversity was discovered for inorganic ring-systems.[25] Thus, a detailed view on inorganic ring systems is not provided at this point. To give a few examples referring back to the above-mentioned organic macrocycles, inorganic porphyrinoids have been characterized X-ray crystallographic for instance. In 1980, KREBS and HÜRTER reported on an "inorganic porphine" that has been isolated and characterized investigating boron sulfides.[29] By heating a B_2S_3/S (molar ratio 1:1.5) mixture in a sealed quartz glass tube yielded crystalline B_8S_{16} whose structure has been elucidated be means of single crystal X-Ray diffraction (SC-XRD) analysis. Very recently another inorganic porphyrinoid has been characterized by the DEHNEN-group in the form of the heavy metal porhyrinoid $[Hg_8Te_8(Te_2)_4]^{8-}$ which was accessible by ionothermal treatment of $Na_2[HgTe_2]$ with the ionic liquids (CnC1Im)$[BF_4]$ (n = 10, 12, CnC1Im = 1-(do)decyl-3-methylimidazolium).[30] Both porphyrinoids are displayed in Figure 2. Coordination compounds have not yet been characterized but quantum chemical calculations indicate that such rings are in principle able to act as hosts.[30] Further investigations are still required though. Referring to crown-type structures, no "inorganic crown-ethers" which resemble the organic architecture of cyclic $(C_2H_4O)_n$ have been structurally characterized ever since.

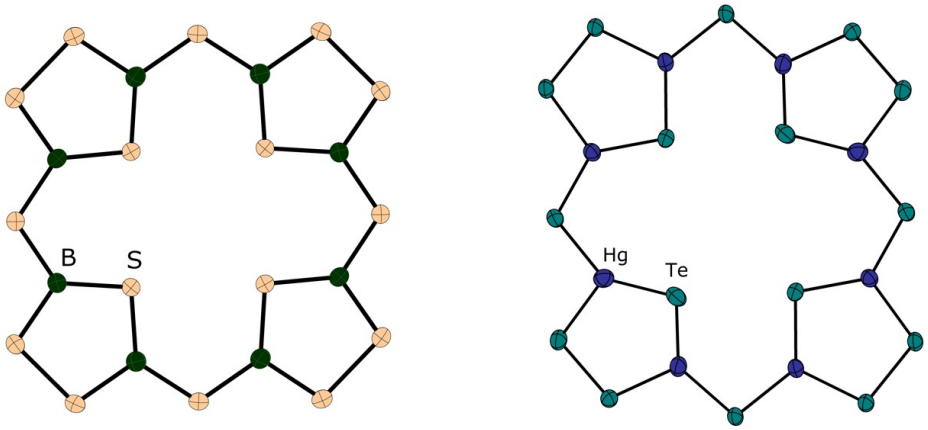

Figure 2: Inorganic porphyrinoids. Molecular B_8S_{16} (left)[29] and ionic $[Hg_8Te_8(Te_2)_4]^{8-}$ (right)[30]. Imidazolium ions of the heavy metal porphyrinoid are omitted for clarity. Thermal ellipsoids set at 50% probability.

Surely there are many crown-type structures published in the literature,[25] but a broader range of coordination behaviour in combination with a sufficient solubility in organic solvents is only observed for cyclophosphazenes[31] and alkylcycloarsoxanes[32]. These systems show the most crown-ether like behaviour so far as these neutral ligands provide a hydrophilic cavity and simultaneously form a hydrophobic shell upon complexation. Hence, host-guest chemistry was successfully employed using these systems as hosts in aliphatic solvents. Selected examples are illustrated in Figure 3. Metal ions considered for incorporation in the above mentioned systems are Na^+,[33] K^+,[33,34] NH_4^+,[35] Cs^+[35] (all embedded into cycloarsoxanes) and Co^{2+},[36] Cu^{2+},[37] Pd^{2+},[38] Pt^{2+}[38] (all embedded into cyclophosphazenes). It should at this point be noted that cycloarsoxanes are ambidentate ligands which are capable of coordinating either by oxygen or arsenic. Above mentioned are only cations which are coordinated by oxygen atoms.

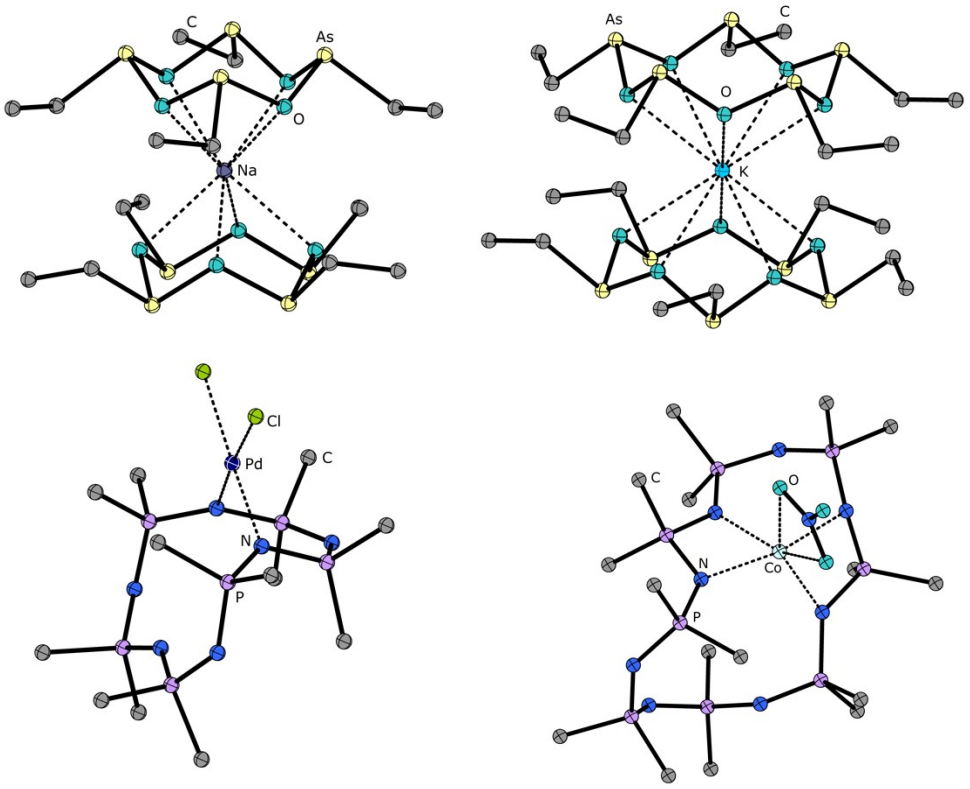

Figure 3: Cyclic arsoxanes in the forms of $[M((As(Et)O)_n)]SCN$ (M = Na^+, K^+, n = 5, 6) (top)[33,34] and phosphazenes in the forms of $[Pd(PMe_2{=}N)_6Cl_2]$ and $[Co(PMe_2{=}N)_nNO_3]NO_3$ (bottom)[36,38]. The SCN^- anions of the arsoxane complexes as well as one of the NO_3^- ions of the respective phosphazene complex are omitted for clarity. Crystal Structures have been published without anisotropic displacement. Atom radii are arbitrarily chosen.

Coordination by arsenic is favoured over oxygen if transition metals are applied for complexation. See ref.[32] for a wide range of these transition metal complexes. However, the selection of coordinated metal ions indicates a considerable binding affinity of these systems towards various cations. The related phosphazane [{P(μ-N*t*Bu)$_2$}$_2$(μ-NH)]$_5$ is a rare example which serves for anion binding. This was demonstrated with H[{P(μ-N*t*Bu)$_2$}$_2$(μ-NH)]$_5$X (X = Cl^-, Br^-), [Li(THF)$_4$][{P(μ-N*t*Bu)$_2$}$_2$(μ-NH)]$_5$I (THF = tetrahydrofuran) or {[{P(μ-N*t*Bu)$_2$}$_2$(μ-NH)]$_5$[PCO]}$^-$.[39–41] Here, the halide ion is trapped inside the cavity through hydrogen bonding (see Figure 4 (top) for an example). By replacing the NH-groups of [{P(μ-N*t*Bu)$_2$}$_2$(μ-NH)]$_n$ with oxygen atoms yields macrocyclic [{P(μ-N*t*Bu)$_2$}$_2$(μ-O)]$_n$ which ultimately joins the crown-family. The ligand [{P(μ-N*t*Bu)$_2$}$_2$(μ-O)]$_4$ has been isolated lately and was presented as the largest crown-like phosph(III)azane of its type.[42]

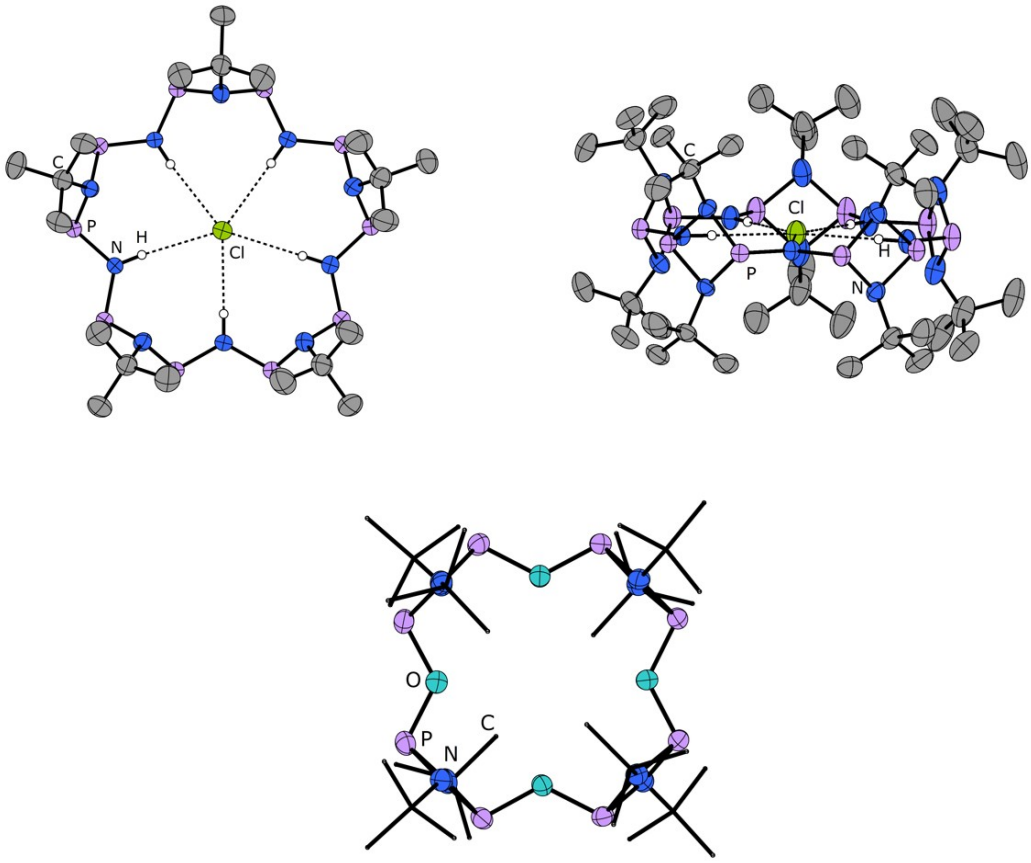

Figure 4: Top-view of the molecular structure of [{P(μ-N*t*Bu)$_2$}$_2$(μ-NH)]$_5$ binding toward Cl^- in the crystal (top left)[39] and side-view (top right)[39] and molecular structure of [{P(μ-N*t*Bu)$_2$}$_2$(μ-O)]$_4$ (bottom)[42]. Carbon atoms of [{P(μ-N*t*Bu)$_2$}$_2$(μ-O)]$_4$ are shown as wires/sticks for clarity. Thermal ellipsoids set at 50% probability.

The structure (Figure 4 (bottom)) is highly related to [12]crown-4 but unfortunately coordination compounds have not yet been isolated due to increased sterics.[42] As outlined by WRIGHT, the most well-developed areas of a p-block element based host–guest chemistry are those with single bonded P–N and formally double bonded P=N frameworks.[27] One of the benefits is, that both of these bonding arrangements are valence isoelectronic with C–C and C=C bonds. In addition, the comparably high bond energies of both of these types of bonding (290 kJ·mol^{-1} for P–N and 420–530 kJ·mol^{-1} for P=N) combined with a relatively low polarity like in carbon-based systems make them promising macrocycles for future host-guest chemistry (for a detailed view on polarity in chemical bonding see Chapter 1.4.2).[27] Practically speaking, suitable inorganic host molecules have to be as similar to organic hosts as possible. As the P–N, P=N and also As–O systems proved to be suitable hosts for a wider range of (metal) ions as they are substantially similar to carbon based systems, it should then also be able to generate stable host-guest compounds based on Si–O building blocks. Looking beyond carbon, silicon has always fascinated chemists as an element with exciting potential.[43]

Indeed have cyclic siloxanes (see chapter 1.3) and their implication in host-guest chemistry been reviewed in mid 2007 by CHIVERS.[28] Host-guest chemistry of this sort of ligands, however, was demonstrated to be highly unsupported. Given the conclusion that well-coordinating inorganic macrocyclic ligands are those which are closely related to carbon based systems, it seems very counter-intuitive that silicon based systems based on Si–O do sparsely serve as host molecules. Silicon and its position just below carbon in the periodic table should be ideal but it is the opposite case. This controversy finally leads to the central part of this thesis. A comprehensive study on the host-guest chemistry including a wide range of metal ions and ligand systems together with NMR (NMR = nuclear magnetic resonance) spectroscopic and quantum chemical calculations is missing so far but is mandatory to evaluate Si-O based macrocycles with regard to metal binding. To introduce the field, the following chapters give an overview on siloxanes, their synthesis and structure as well as the specific Si-O bond character with implications to coordination and/or host-guest chemistry.

1.2 Siloxanes: Synthesis, Structure and Applications

According to the IUPAC compendium of chemical terminology, siloxanes can be understood as hydrides with unbranched or branched chains of alternating silicon and oxygen atoms. This means each silicon atom is separated from its nearest silicon neighbours by single oxygen atoms. The general structure of unbranched siloxanes is $H_3Si(OSiH_2)_nOSiH_3$. Hydrocarbyl derivatives are commonly included.[44] In literature, the term siloxane is often referred to organosilicon compounds. In this respective context, siloxane is an abbreviation for a compound containing silicon, oxygen and alkane.[45] Thus, the general formula $R_3Si(OSiR_2)_nOSiR_3$ is more commonly used with R = H, alkyl, aryl. The synthesis of siloxanes is generally based on the hydrolysis of chlorosilanes.[46] Silanols form as intermediate products which eventually condensate to the respective siloxane (Scheme 1). From industrial importance is also the methanolysis of chlorosilane which avoids HCl waste and makes recycling of chloroalkanes possible which is important for preceded ROCHOW-synthesis.[47]

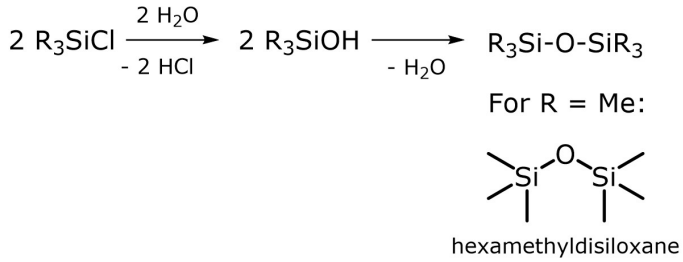

Scheme 1: General synthesis of siloxanes with hexamethyldisiloxane as an example.

Dependent on which respective chlorosilane is hydrolysed, (e.g. Me_3SiCl, Me_2SiCl_2, $MeSiCl_3$ or $SiCl_4$) different functionalities are reached (Figure 5: left).[47] The so obtained structures range from linear (polymeric) over cyclic to cage-like and multidimensional siloxanes (Figure 5: right). Linear polyorganosiloxanes are the most important (industrial and commercial) siloxanes followed by cyclic diorganosiloxanes (known as cyclosiloxanes, see Chapter 1.3). Due to ubiquitous fields of applications, polyorganosiloxanes are nowadays the basis of a multi-million dollar industry.[43] Polydimethylsiloxanes (PDMS), for instance, are characterized by greater stability to high temperature and UV radiation in comparison to organic polymers.

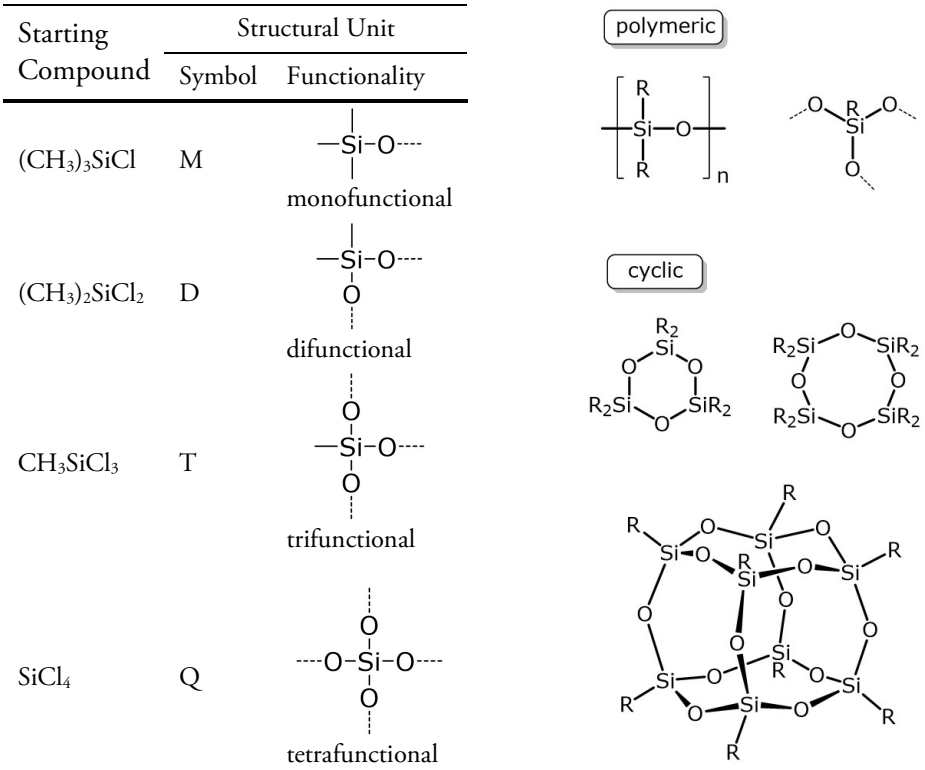

Figure 5: Origin and functionality of siloxane and silicone building-blocks adapted from ref.[47] (left) and different siloxane architectures (right): Diorganopolysiloxane (top left), organopolysiloxane (top right), cyclic siloxanes (middle) and silsesquioxane (bottom).

Further they have good dielectric properties, are strongly hydrophobic, have nearly no surface tension as well as only little temperature dependence of their physical properties. Hence, polydimethylsiloxanes are used in oils, lubricants, rubbers, sealants, resins, insulators and many more.[46–49] The applications of cyclic dimethylsiloxanes overlap with those of PDMS but to mention some more specific ones, they are used in personal care products, cosmetics, cleaning agents as well as coatings for packaging and paints.[50] Silsesquioxanes (common formula $(RSiO_{3/2})_n$) are frequently used on coatings in electronic and optical devices but also in cosmetics, ceramics, resins and in general many fields of material sciences.[51]

As can be seen in Figure 5: right, the simplest siloxanes are build monofunctional having the same repeating unit. Chlorosilanes, however, can also be mixed within the siloxane synthesis. This yields the silicones which can be understood as compounds in which the siloxane polymer often has different Si-O functionalities. Dependent on the respective functionality, the SiR_2O

chain lengths can be adjusted, side groups can be introduced and cross-linking can be established. The material properties of a respective silicone-polymer can thus be substantially fine-tuned.[47] The importance of silicones have impact to all corners of our modern lives which is why silicon chemistry is at the highest level of interest. Current research in polysiloxanes is directed, among other things, towards simple and green synthetic strategies and proceedings in this area were recently highlighted.[52]

1.3 Cyclic Siloxanes and Their Relation to Crown-Ethers

Similar to linear polyorganosiloxanes, cyclic siloxanes are also constituted of the general formula $(SiR_2O)_n$. Systems having rings of alternating silicon and oxygen atoms are generally called cyclosiloxanes.[44] The most widespread used cyclosiloxanes are methyl substituted (R = CH_3) and are also involved in the PDMS synthesis. Due to di-functional building blocks, they are abbreviated as D (with D = Me_2SiO). In comparison to the polymeric species, cyclic siloxanes of D_n type are volatile, which makes a distillation from polymeric species possible. In PDMS synthesis, distilled material is then further processed to a polymer. Strong bases such as KOH or strong acids such as perfluoroalkanesulfonic acids and sulfuric acid are usually used to initiate ring-opening polymerization. This eventually yields clean polymer material.[47,49]

However, cyclodimethylsiloxanes are obtained upon hydrolysis or methanolysis of $(CH_3)_2SiCl_2$. In the process of a modern silicon chemistry also novel synthesis protocols have been published. In this context does CUI report on an NHC catalyzed hydrolytic oxidation of dihydrosilanes.[53] Various Cyclosiloxanes have been obtained in this way. Traditional and novel synthetic pathways are depicted in Scheme 2.

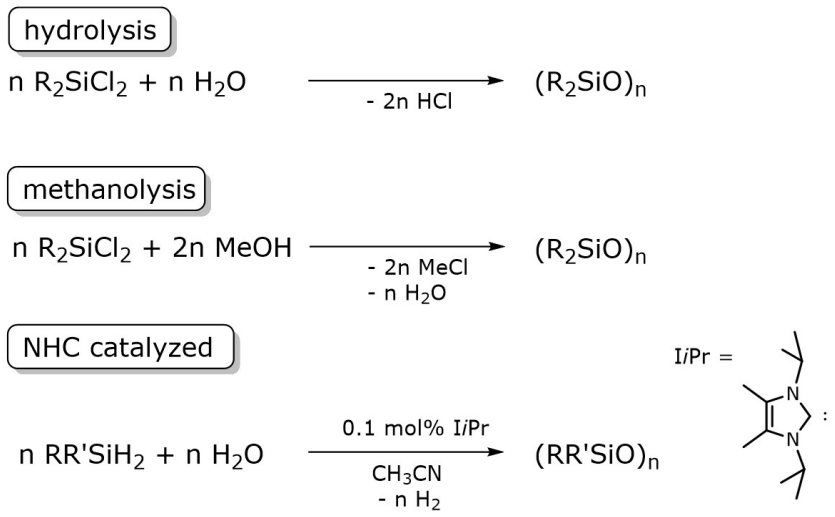

Scheme 2: Traditional synthesis of cyclic and/or polymeric siloxanes vs. NHC catalysed hydrolytic oxidation of hydrosilanes.

The cyclodimethylsiloxanes can structurally be compared to crown-ethers and are formally isoelectronic to ring-silicates. D_n ring sizes up to at least n = 25 have been reported.[54,55] D_6 for example is a crown-like molecule bearing six oxygen donors. C_2H_4 spacers are replaced by $SiMe_2$ here. Hence, D_6 is formally isoelectronic with the ring silicate $[Si_6O_{18}]^{12-}$ (e.g. part of the beryl $Al_2Be_3[Si_6O_{18}]$)[46] and structurally compares well with [18]crown-6 (Figure 6). Even though these crown-type systems have been characterized more than twenty years before the conventional crown-ethers, it seems very counter-intuitive that the host-guest chemistry of these systems has not been extensively studied.[56,57] Instead, they have, not least due to their water repellent properties, evolved into a completely different research area than host-guest chemistry. Conclusively, many works were published since the 1960s which have examined the binding properties of Si-O donors in comparison to C-O donors. Basicity of cyclic and acyclic siloxanes were intensely investigated in terms of hydrogen bonding and proton affinity. Especially IR spectroscopic investigations on hydrogen bonding towards the Si-O-Si linkage had been established as the method of choice. Matching with the material properties of (polymeric) siloxanes, it was found in a number of studies that the electron-donating capacity of the oxygen atom decreases in the sequence C-O-C > C-O-Si > Si-O-Si.[58–67][68–72] Even though given its position in the periodic table, silicon is obviously not exactly a copy of carbon. Especially not in terms of coordination and host-guest chemistry.

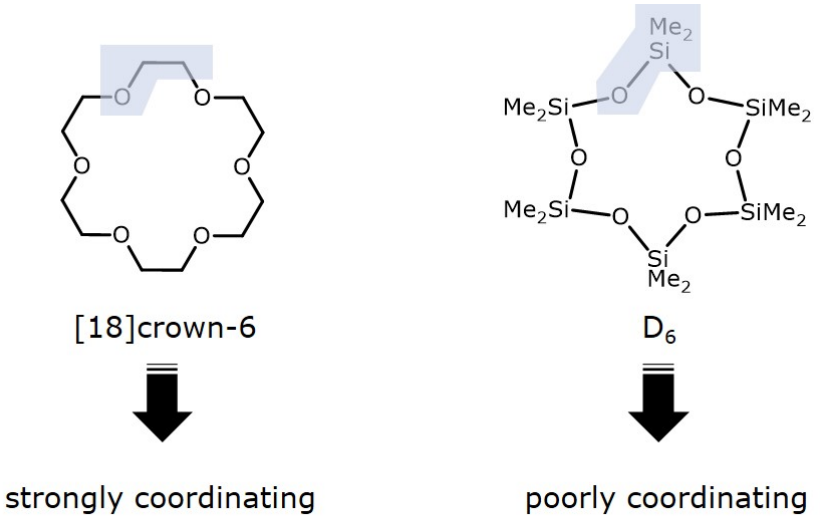

Figure 6: Comparison of organic and silicon based crown-ether moieties with six donor atoms. Marked in light-blue is the repeating unit which is C_2H_4O in conventional crown-ethers and $SiMe_2O$ in silicon based "pseudo" crown-ethers.

To explain a decreased electron-donating capacity, the Si-O bond has been scrutinized over the years and various explanations have been established. A close look at the Si-O bond is part of the next chapter.

1.4 The Si-O bond: A Look at the Building Block of Siloxanes and Silicates

1.4.1 Hyperconjugation Interactions in Siloxanes

For many years now various effects which alter the structural and reactive properties of siloxanes are briskly discussed. Historically, the *3d* orbitals at silicon play a major role. Compared to carbon based systems, *d*-orbitals are available to be occupied with electron density forming π-bonding between d_π and p_π-orbitals.[73–75] Relevant to siloxane coordination, the occupied *2p* orbitals at oxygen donate electron density into the *3d* orbital at silicon.[76,77] Backbonding eventually strengthens the Si-O bond. Hence, electron shifting towards metal ions or hydrogen bonding acceptors requires weakening of the bond first. As a cause, coordination is hindered and the basicity is lowered. This type of backbonding has been the explanation for a lower basicity of siloxanes for decades, especially in the above-mentioned hydrogen bonding studies.[58,60–67,69] By time, the

3*d*-orbitals were identified to be too high in energy. Instead, negative hyperconjugation interactions of the type *p*(O) → σ*(Si-R) (R = H, alkyl, aryl, …) were established to justify the lower basicity of siloxanes compared to ethers.[78–81] These interactions are the most eminent to date. Though also present in organic ethers, these interactions are exceptionally more distinct in siloxanes. This is especially represented by the structural properties of siloxanes compared to ethers. For instance, the calculated R-O-R angles of DME (DME = dimethylether) and HMDME (HMDME = hexamethyldiethylether) have values of 112.7 and 127.9°, respectively. The C-O single bonds have a value of 141 and 145 pm respectively which compares well with the single bond radii of 142 pm.[82] In the respective silicon analogues DSE (DSE = disiloxane) and HMDSE (HMDSE = hexamethyldisiloxane), much larger values of 150.3 and 156.6° are found.[81] Further, the Si-O bond length is calculated to be 165 pm.[81] This value is considerably smaller than the covalent radii sum which predicts a Si-O single bond of 177 pm.[82] Hence, *p*(O) → σ*(Si-R) backbonding dictates the structural behaviour of siloxanes to a larger extent than that of organic ethers. Similar to the backbonding into the *d*-orbitals, backbonding into σ*(Si-R) causes a competing between electron donation towards electrophiles and Si-O bond stabilization. Hence, basicity is lowered and the Si–C bonds are simultaneously weakened.

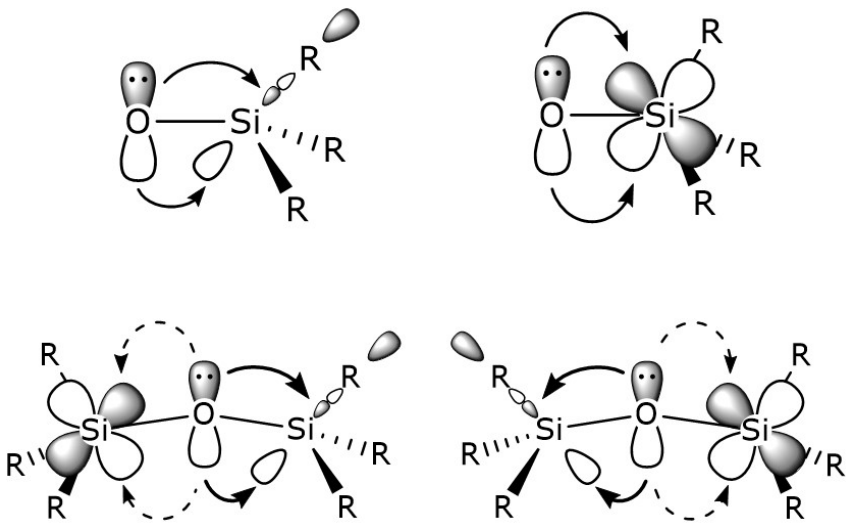

Figure 7: Vicinal hyperconjugation interactions in siloxanes involving d-Orbitals or the the antibonding molecular orbital of the Si-R bonds. *p*(O) → *d*(Si) backbonding (top left), *p*(O) → σ*(Si-R) backbonding (top right) and both interactions (bottom).

Most recent investigations on the Si-O bond does even conclude both, p(O) → d(Si) and p(O) → σ*(Si-R) to be simultaneously present altering the structural properties of siloxanes.[83] Albeit p(O) → d(Si) to much a lesser extent. The respective Si-O bond stabilization effects are depicted in Figure 7. Lately, hyperconjugation interactions have also been investigated for heavier analogues of siloxanes $(ER_3)_2O$ (E = Ge, Sn; R = C, H). p(O) → σ*(E-R) backbonding is also observed here. These interactions were predominantly examined in linear siloxanes involving a single oxygen atom. There are, however, substantial differences, when it comes to siloxanes which contain more than one $SiMe_2O$ repeating unit. In this context does APELOIG discuss the contribution of an anomeric effect which can alter the conformation of siloxanes. Interactions between geminal substituents at the silicon center, especially in terms of oxygen substituents, gives further stabilization of certain conformations. The stabilization is in this case characterized by p(O) → σ*(Si-O) interactions. In case of $H_2Si(OH)_2$, these interactions even surpass p(O) → σ*(Si-H) backbonding.[84] Also CYPRYK pointed out the importance of p(O) → σ*(Si-O) interactions. Contributions from this type of hyperconjugation, among other less significant stabilization effects, reduces the electron density on oxygen significantly.[85,86] Especially the polysiloxanes and thus also cyclosiloxanes, benefit from this effect. This is also the main reason why polysiloxanes are stable while polyoxymultisilylenes (e.g. $(–SiR_2–SiR_2–O)_n$) are not.[85] By implication, disilanyl-bearing cyclosiloxanes are thus more basic than conventional cyclosiloxanes (see chapter 1.6.1 for details). However, a reduced electron density at oxygen eventually means lower basicity. The effects stabilizing a SiH_2O repeating unit in a polymeric siloxane are depicted in Figure 8.

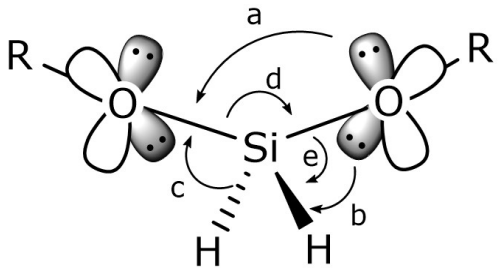

Figure 8: Strongest interactions contributing to the stability of a $–O–SiH_2–O–$ fragment. For clarity, only a single representative of each type of interaction is depicted. p(O) → σ*(Si-O) (a), p(O) → σ*(Si-H) (b), σ(Si-H) → σ*(Si-O) (c), σ(Si-O) → σ*(Si-O) (d), σ(Si-O) → σ*(Si-H) (e).

1.4.2 Ionic Bond Model of the Si-O Bond

A different model to describe the characteristics of the Si–O bond is established with an ionic bond model. Comparing the electronegativity (=EN) differences of a C–O bond with a Si–O bond, it becomes clear that the Si–O bond is substantially more polarized than the C–O bond ($EN_{Allred\text{-}Rochow}$: C 2.50, Si 1.74 and O 3.50).[87] Hence, many studies have been published which presented the Si-O bond as an ionic rather than covalent bond. The ionic consideration of the Si–O bond is contradictory to the above-mentioned explanations but enough evidence is provided in literature to explain the structural and reactive properties of siloxanes.[88–95] An often used LEWIS-formula representation is depicted in Scheme 3. Solely according to the electronegativity differences, silyl-ethers should in general be stronger LEWIS-bases than ethers due to a higher electron density at oxygen.

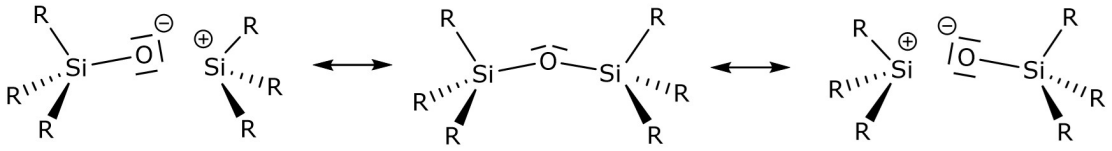

Scheme 3: Lewis-formula representation of the ionic bond model discussed for the siloxane linkage.

Contra-intuitively, this is not the case. So does GILLESPIE point out, that the electron pairs around oxygen are spatially diffuse and are not readily served for electron donation.[91,92] Comprehensive quantum chemical calculations indicate that, the higher the differences in electronegativity between donor atom (=oxygen) and substituents (=X) are, the more spatially diffuse and the more spherical becomes the electron pair around oxygen. Negative charge is increased at oxygen, positive charge increased at X. Consequently does the X-O-X bond angle approach to larger values if EN(X) < EN(O) which is caused by electrostatic repulsions between positively polarized X atoms. *Vice versa*, the bond angle approaches to smaller values if EN(X) approaches EN(O) as the charges at X and O have smaller values. In other words, a sufficient EN(X) consequently supports smaller X-O-X angles and more localized electron density at oxygen.[91] The coherence between electronegativity difference and molecular geometry can be seen in Table 1. The negative charge on oxygen decreases within the first period from Li_2O to $(HO)_2O$. Same observations are made

for the second period as it decreases from Na_2O to $(H_2P)_2O$ indicating an increased covalent character to the bonds. The charge on oxygen is in correlation with the respective electronegativity of the attached atom. Another key factor which determines the ionicity of a respective bond, are the substituents attached to X. An example has been provided for the siloxane linkage (see light grey marked entries). Substitution of hydrogen by fluorine polarizes the already polar Si-O bond even more leading to even larger Si-O-Si angles and shorter Si-O atom distances.[91]

Table 1: Atomic charges (q), X-O-X bond angles [°] and X-O atom distances [pm] obtained from quantum chemical calculations. See ref.[91] for details.

period	molecule	EN(X)[87]	q(O)	q(X)	∠X-O-X	X-O
1	Li_2O	0.97	-1.82	+0.91	180.0	159.6
	$(HBe)_2O$	1.47	-1.79	+1.74	180.0	139.6
	$(H_2B)_2O$	2.01	-1.68	+2.27	126.9	135.4
	$(H_3C)_2O$	2.50	-1.29	+0.78	113.9	139.0
	$(H_2N)_2O$	3.07	-0.51	-0.46	109.8	138.9
	$(HO)_2O$	3.50	-0.04	-0.62	107.8	136.5
2	Na_2O	1.01	-1.77	+0.88	180.0	197.3
	$(HMg)_2O$	1.23	-1.77	+1.69	180.0	178.2
	$(H_2Al)_2O$	1.47	-1.76	+2.45	180.0	167.1
	$(H_3Si)_2O$	1.74	-1.72	+3.05	148.3	162.1
	$(F_3Si)_2O$	1.74	-1.68	+3.13	162.2	158.3
	$(H_2P)_2O$	2.06	-1.59	+0.75	129.8	163.6

By time, the exceptionally high ionicity of Si-O and Si-X bonds gave access to a couple of interesting compounds in the field of general inorganic chemistry and material sciences.[96,97] One example where the ionic Si-O bond character is nicely illustrated, is the occupation of silsesquioxanes with F^- hosts.[97–99] As evident from the molecular electrostatic potential open surface of the hydroxy-substituted parent silsesquioxane POSS (POSS = polyoctahedralsilsesquioxane) it can be seen that the inner core of the cube has an overall positive potential due to the exceptional high polarization of Si (Figure 9: left).[100] The increased electron density on oxygen is directed in the opposite direction and therefore out of the inner-cage. Thus, tetrel bonding (e.g. by F^-) is favourable in the centre of the cube (Figure 9: right).

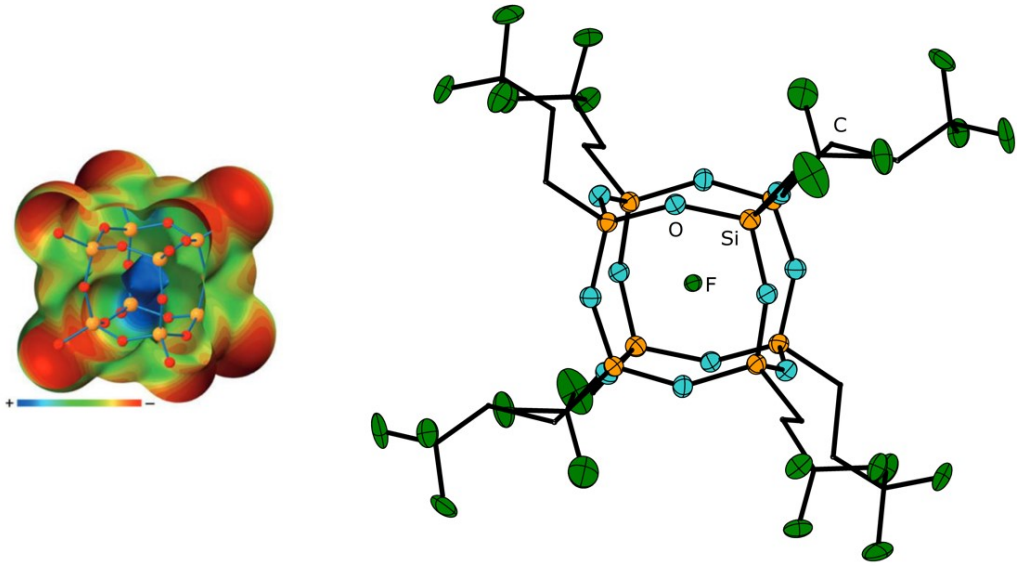

Figure 9: Molecular electrostatic potential open surface of a hydroxyl substituted polyoctahedralsilsesquioxane (left)[100,101] and crystal structure of a caged anion in $[N(n\text{Bu})_4][F@Si_8O_{12}(R_8)]$ (R = 3,3,3-trifluoropropyl; arbitrarily chosen example) (right)[98]. Carbon atoms are depicted as wires/sticks for clarity. Thermal ellipsoids set at 50% probability. Left figure © Wiley-VCH GmbH.

The incorporation of F^- hosts is supported by an EWG (EWG = electron withdrawing group; e.g. CN, CF_3 or in general perfluoroalkanes) substitution at Si.[98,99] A more ionic Si-O linkage is achieved in this way as was also demonstrated for above mentioned $(F_3Si)_2O$.

In terms of investigating cation rather than anion binding *Passmore* and *Rautiainen* performed DFT calculations on 1,3-dimethylsiloxane ($O(SiH_2Me)_2$), diethyl ether (OEt_2) and their respective metal complexes with Li^+ and Ag^+.[94] According to QTAIM (QTAIM = quantum theory of atoms in molecules) analysis the respective complexes have been investigated regarding gas phase stability, charge distribution and energy penalty due to conformational change. Intuitively, the electron density on oxygen of 1,3-dimethylsiloxane turned out to be higher compared to that at oxygen of diethyl ether. Gas phase reactions of the respective ligands with Li^+ and Ag^+, however, revealed that the metal binding of diethyl ether is favoured by approximately 30 $kJ \cdot mol^{-1}$. Under consideration of various anions such as I^-, $[SbF_6]^-$ and $[Al_F]^-$ ($[Al_F]^- = [Al(OC(CF_3)_3)_4]^-$) these values are even higher. QTAIM analysis indicates that the change of charge at the etheric oxygen atom becomes larger than in 1,3-dimethylsiloxane upon complexation.

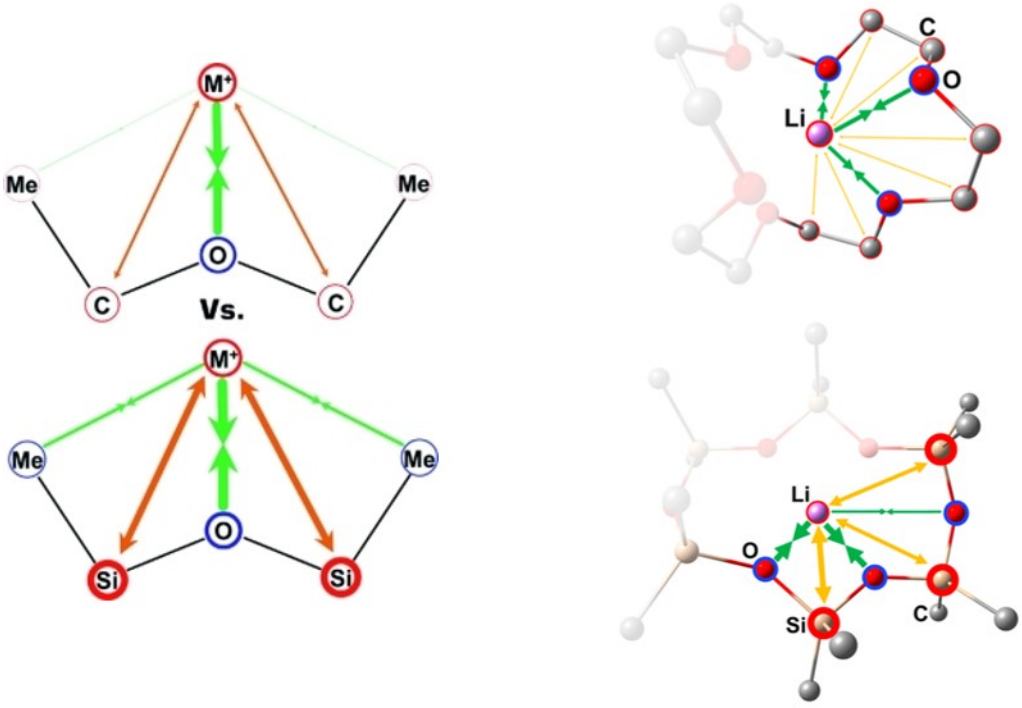

Figure 10: Schematic representation of $M^{+}\cdots X^{\delta+}$ (X = C, Si) repulsive and $M^{+}\cdots O^{\delta-}$ attractive interactions in acyclic (left)[94] and cyclic systems (right)[95]. Repulsive interactions are depicted in yellow/orange whereas attractive interactions are depicted in green. Left figure © Wiley-VCH, Right figure © American Chemical Society.

Hence, the ether is easier to polarize and is activated more easily for metal binding. To polarize the already polar Si-O bond further seams unsupported. A major role in this context plays the deformation energy of the respective ligand upon complexation. Energy decomposition analysis (=EDA) indicates that the "energy penalty" which results through conformational change is exceptionally higher in the siloxane than in the ether. The reason for this is the high polarization of the silicon atoms which results in $M^{+}\cdots Si^{\delta+}$ repulsive interactions. Overall, to achieve the same strength of interaction with electrophiles, the siloxane has to pay higher energy penalty in the form of structural changes.[94] $M^{+}\cdots Si^{\delta+}$ repulsive interactions have later also been reported for metal complexes of cyclic siloxanes by the same research group. Similar to the above mentioned model system, a weaker electrostatic attraction of D_6 toward M^{+} (M = Li, Ag) is found in comparison to [18]crown-6. The reduced ability to incorporate the metal ions is attributed to the repulsion between positively charged silicon atoms and the metal ions.[95] Attractive and repulsive interactions of ethers and siloxanes with metal centers are depicted in Figure 10.

1.4.3 The Si-O-Si Angle as an Important Parameter Regarding Basicity

The previous chapters showed that the relationship between siloxane basicity and Si-O bond character is under debate and tension built between the authors of the respective study as various works have been published which present antipodal concepts. So is the Si–O bond considered to be *covalent* regarding hyperconjugation interactions and exceptionally *ionic* when it comes to spatially diffuse electron pairs and $M^{+}\cdots Si^{\delta+}$ repulsive interactions. Hence, it is necessary to describe the Si–O bond by means of various resonance structures (Scheme 4).

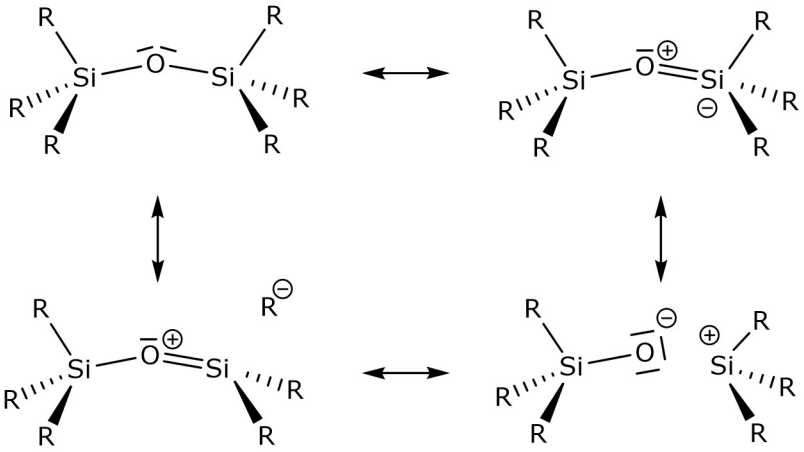

Scheme 4: Resonance structures to represent the intermediate bond character of the Si–O bond. Classic LEWIS formula representation (top left), hypervalent LEWIS formula (e.g. by p(O) → d(Si) backbonding) (top right), no-bond LEWIS structure (e.g. by strong p(O) → σ*(Si-R) backbonding) (bottom left) and ionic LEWIS formula (bottom right).

By time, this controversy on Si-O bond character even prompted authors to establish neologisms. So does GIBBS point out, that the Si-O bond can be understood as the *elusive bond*.[102] Its character is indicated rather to be *intermediate* than either ionic or covalent.[103]

Interestingly, there have been deliberations since the 1960s and also rare experimental evidences since the late 1970s, that the basicity of siloxanes is increased if the Si-O-Si angle is strained.[58,66,68,71,104] Taking this observation into account would mean that hyperconjugation interactions as well as ionicity of a respective siloxane (or silicate) are decreased when approaching

smaller angles. To substantiate a correlation basicity and Si-O-Si angle, further experimental evidence was collected by time and backed up by means of quantum chemical calculations. Persuasive works have been carried out especially in the mineralogy research fields. Silica polymorphs have been analysed regarding location of OH groups. Especially coesite, a high pressure polymorph of SiO_2, opened up for studies of potential electrophilic attack.[105] Coesite, unlike quartz, which has only one non-equivalent Si-O-Si angle, has five non-equivalent Si-O-Si linkages which aroused the researchers attention. According to FTIR (Fourier transform infrared) studies on H-doped coesite crystals, KOCH-MÜLLER et al. reported that hydrogen atoms are bound to four of the five non-equivalent oxide ions.[106] Based on this results, GIBBS et al. performed quantum chemical calculations (e.g. based on the ELF (ELF = electron localization function) approach) and predicted favourably proton docking sites.[107]

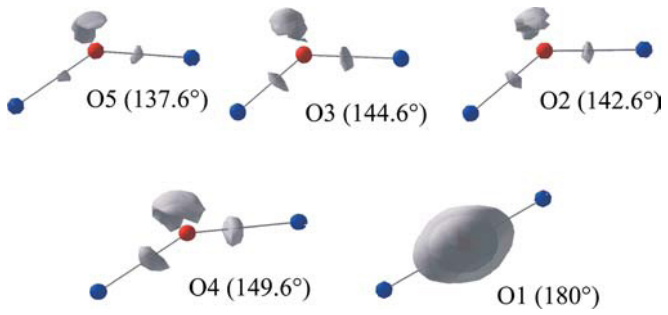

Figure 11: ELF isosurfaces for the five different Si-O-Si linkages in coesite with respect to the non-bonding region.[107] The ELF isosurface value is set at the 98% of the local maximum in the nonbonding region. Red spheres represent oxygen and blue spheres represent silicon. © Springer Nature, Switzerland AG.

The results according to the ELF approach suggest that electron density in coesite is highly localized at O2, O3 and O4 (see Figure 11). Less so in O4 and much less in O1. The local maximum for a nonbonding region is highest at O5 and decreases with larger Si-O-Si angles. Hence, the favourability of a non-bonding region acting as a potential docking site is expected to be larger approaching smaller Si-O-Si angles. The determined docking sites in protonated coesite are for this reason O2-O5 but not O1. Additional studies come from the field of a molecular inorganic

main-group chemistry. GRABOWSKY and co-workers provided a comprehensive study on hydrogen bonding of silanol (H_3SiOH) and water towards DSE which is constrained to Si-O-Si angles ranging from 85 to 165°.[108] As expected from the aforementioned mineralogical studies, the basicity significantly increases when the Si-O-Si angle is decreased. To give some numbers at this point, PES (PES = potential energy surface) scans reveal that approaching a tetrahedral angle (110°) yields silanol···siloxane hydrogen bonding energies of -12 kJ·mol^{-1}. This value is twice as high than at 140° (-6.2 kJ·mol^{-1}). Notable is the broad range of adoptable angles in DSE. The molecule has a high bending potential associated with only a small change of energy in the region of 130 to 180°. The barrier to linearization from the ideal angle (calculated to be 151.4° in this study) is only 0.5 kJ·mol^{-1}. To strain the ideal angle to 130° costs approximately 4.5 kJ·mol^{-1}. By constraining to a tetrahedral angle, however, the amount of energy which is required to adopt this angle, raises almost exponentially. An energy loss of approximately 20 kJ·mol^{-1} is observed here which cannot be overcompensated by the values obtained from hydrogen bonding. Hence, linear siloxanes like DSE are not expected to adopt Si-O-Si angles which enable hydrogen bonding. Instead, the incorporation of an Si-O-Si linkage into a ring system proved to be a successful strategy to verify the correlation between siloxane angle and basicity. BECKMANN and co-workers established the synthesis and characterization of a benzoxadisilole containing a five-membered ring with Si-O-Si moiety as well as a silanol group.[93]

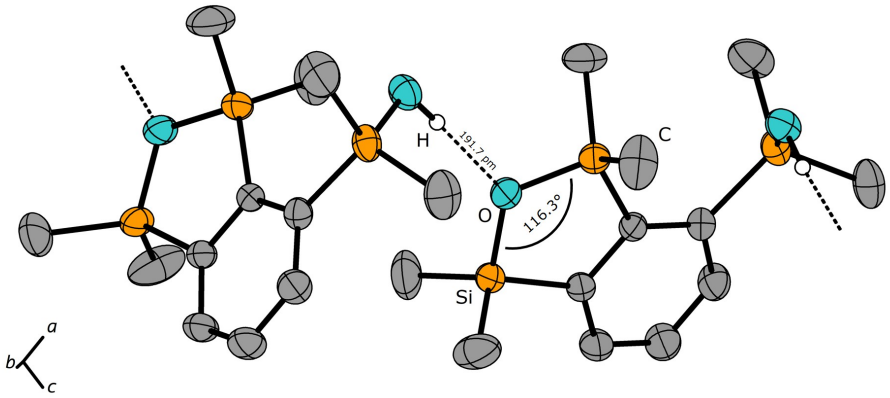

Figure 12: Section of the crystal structure of a benzoxadisilole comprising $(R_3Si)_2O\cdots HO\text{-}SiR_3$ hydrogen bonding.[93] Thermal ellipsoids set at 50% probability.

The respective benzoxadisilole contains a Si-O-Si moiety with an angle of 116.3°. This enables the formation of hydrogen bonds in the solid state with neighbouring silanol groups. Thus, hydrogen bonding determines the crystal packing and dimensionality proving Si-O donors to be a good electron donor at sufficiently small angles (see Figure 12).[93] The depicted structure is a rare example of hydrogen bonding involving siloxanes. Only a handful of such structures were characterized by SC-XRD in the mean time. These involve classic hydrogen bonding as presented above but also protonated oxygen atoms (silyloxonium ions). All structures have (comparably) small Si-O-Si angles in common.[109–112]

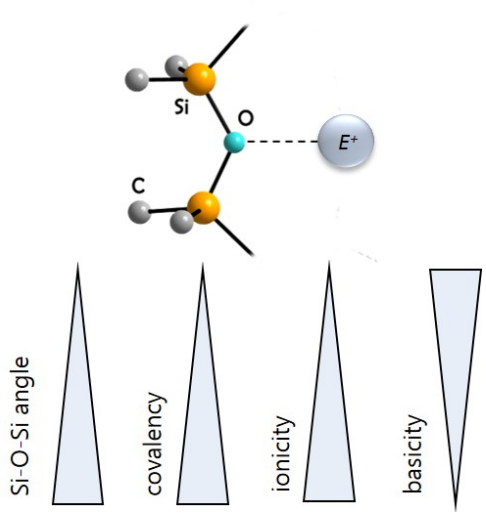

Figure 13: Attractive interaction between an organosiloxane linkage with an electrophile (=E^+) as well as Si-O bond character and basicity in correlation to the Si-O-Si angle.

At this point the correlation between siloxane basicity and Si-O-Si angle is clearly demonstrated by various works of different research areas. Experimental details as well as quantum chemical calculations were provided to substantiate a correlation. The question on how the Si-O bond character is changing in relation to the Si-O-Si angle remains. In a recent work of 2018, GRABOWSKY and co-workers scrutinized the antipodal concepts covalency and ionicity. Meticulously performed quantum chemical calculations have been carried out to resolve an ostensible contradiction. The authors claim the analysis to be a *complementary bonding analysis* that combines methods from different realms and demonstrate that both, covalency and ionicity increase simultaneously towards larger Si-O-Si angles.[113] Taking all herein presented research efforts of

the past years according the Si-O-Si linkage into account, the presented picture of the Si-O-Si bond and basicity can be drawn (see Figure 13). The findings make it important to not overinterpret the results if only one method is used to analyse bonding. The Si-O bond clearly has a unique characteristic.

1.4.4 Increased Basicity of Siloxanes Employing Cooperativity Effects

The previous chapter showed the correlation between Si-O bond character, angle and basicity. Apart from straining the Si-O-Si angle, ALKORTA, MONTERO-CAMPILLO and co-workers very recently demonstrated that non-covalent interactions, in particular tetrel bonding, can alter chemical bonding and thus also LEWIS-basicity.[114–116] Tetrel bonds are known as non-covalent interactions involving tetrel atoms through their σ-hole which is a region of electropositive character.[96] In other words, a tetrel bond is a non-covalent bond between any LEWIS-base and a LEWIS-acid belonging to group 14 elements.[100] An outlook of such interactions regarding siloxanes has been given in chapter 1.4.2. The interaction of F^- with the electropositive center of the silsesquioxane can be understood as such an interaction. ALKORTA, MONTERO-CAMPILLO and co-workers investigated DSE regarding tetrel bonding interactions, LEWIS basicity and cooperativity effects.

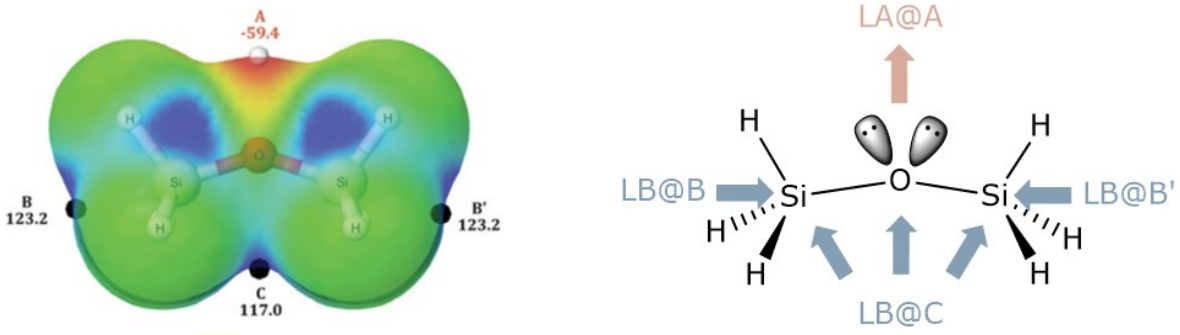

Figure 14: MEP of DSE (left)[115] and possible nucleophilic (blue) and electrophilic (red) docking sites (right). The minimum and maxima ($kJ \cdot mol^{-1}$) are indicated with dots along their corresponding MEP values (left). The MEP is drawn at the 0.001 a.u. electron density isosurface. Left figure © Taylor & Francis Ltd.

A MEP (MEP = molecular electrostatic potential) representation of DSE is depicted in Figure 14 (left). Based on the distributed electron density, it becomes clear that the depicted sites (A, B, B', C) can be occupied by a respective LEWIS acid and/or base (Figure 14, right). Owing to this dual, almost flp (flp = frustrated lewis-pair) character of DSE, the system can form ternary complexes and the different interactions might cooperate between each other.[115] The location of the σ-hole is related to the σ*(Si-R) orbitals whereas maximum electron density is related to *p*(O).[114] To investigate if cooperativity exists, the authors calculated binary complexes with various LEWIS-acids (=LA) at position A first (=DSE:LA), followed by binary complexes with various Lewis-bases at positions B and C (=LB:DSE). Cooperativity between these two types of coordination could then be verified when comparing with ternary complexes of the type LB:DSE:LA. An example is given for the coordination of DSE towards $BeCl_2$ (Figure 15). As can be seen by these gas-phase calculations, coordination of $BeCl_2$ (DSE:LA, as depicted in Figure 15, top left) strains the Si-O-Si angle to a value of 126.6°. The O···Be atom distance has a value of 164.8 pm.[115]

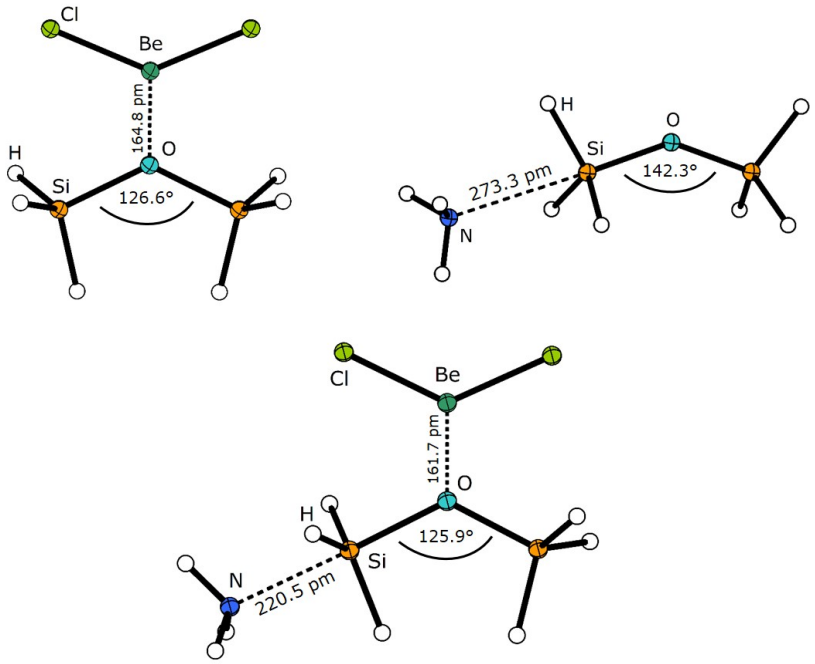

Figure 15: Increased basicity of DSE employing cooperative effects with $BeCl_2$ and NH_3 as an example. Depicted are the $BeCl_2$ adduct at position A (top left), the NH_3 adduct at position B (top) and the ternary complex with both ligands (bottom). The calculated structures have been reproduced from provided .xyz data.[115]

The ternary complex, involving coordination to $BeCl_2$ and simultaneously NH_3, has an Si-O-Si angle of 125.9°, the O···Be atom distance is 161.7 pm and the tetrel bond has a length of 220.5 pm. Thus, combining both, coordination to a LEWIS-acid and tetrel bonding strengthens the beryllium as well as the tetrel bond. To give some more details, it was shown that the total binding energy (=E_b) is raised by ~50 kJ·mol^{-1} (E_b(DSE:LA = -99.2 kJ·mol^{-1}) vs. E_b(LB:DSE:LA = -149.3 kJ·mol^{-1}) even though the energy penalty due to conformational change (=E_r) is ~65kJ/mol higher in the ternary than in the binary complex (E_r(DSE:LA = 79.7 kJ·mol^{-1}) vs. E_r(LB:DSE:LA = 145 kJ·mol^{-1}). This is what the authors call a *cooperative effect* and it was demonstrated for a wide range of (LEWIS) acids and LEWIS bases. These effects can be explained by means of a push-pull system: Coordination of the LEWIS-acid causes increased MEP values at positions B and C. Due to coordination of LB towards DSE, a decreased MEP value is obtained at position A. Hence, cooperativity established by tetrel bonding yields more stable DSE complexes.[115] This synergy was also found to be important in acid catalysed Si-O bond cleavage reactions of DSE involving H^+ and H_2O.[117] Further, tetrel bonding raises the proton affinity of siloxanes. The system NH_3:DSE:NH_3 increases the basicity of DSE to such an extent, that even the proton affinities of carbon related systems can be reached.[114] The conclusion which should be drawn from this chapter is, that weak interactions can have a significant influence on the siloxane linkage. Cooperative effects might become an interesting possibility for stabilizing coordination compounds of weakly coordinating ligands. For the moment, however, these advances are solely based on quantum chemical calculations and thus gas-phase species.

1.5 Siloxane coordination compounds

Reflecting the aforementioned discussion concerning the Si-O bond, it becomes clear that the unique character of this bond requires special activation to obtain stable coordination compounds. Thus, various strategies have been established to bind silicon-based ligands towards electrophiles (especially metal centres). The most common strategy is to deprotonate silanols forming a respective silanolate (R_3SiO^-). This is fairly easy through conversion of silanol and base yielding the respective silanolate salt. In comparison to neutral (crown-)ethers, these ligands have a nega-

tive charge and it is somehow inevitable for the oxygen atom to interact with the metal center. In this way, many silanolate salts have been characterized and also gained some fields of application, mainly catalysis.[118–127] Similar to the above mentioned silanolates have compounds been obtained which bear ligands constituted of *An*-Si(R_2)-O-Si(R_2)-*An* (*An* = any terminal anionic group), $^-$Si(R_2)-O-Si(R_2)$^-$ (silicide-like) or related anionic moieties. These compounds might show $(R_2Si)_2O\cdots M^{n+}$ interactions but these are mostly forced due to an anionic nature of the ligand, similar to the aforementioned silanolates. Obtained complexes involve the cations Li^+,[128–132] Na^+,[133–135] K^+,[131,133,135–137], Rb^+,[135] Cs^+,[133,135,138] Mg^{2+},[139] Sr^{2+},[140] Ba^{2+},[141,142] Sn^{4+},[143,144] $Cr^{2+/3+}$,[145,146] Fe^{3+},[147] Y^{3+},[146,148] Zr^{4+},[149] Sm^{2+},[150] Tm^{3+},[151] Yb^{2+},[150,152–154] Th^{4+},[155–158] U^{4+},[155–159] and UO_2^{2+}[160]. Hence, siloxane$\cdots M^{n+}$ contacts might have been established over the years, but are rather occasionally than purposefully realized. Further, these compounds have barely been published in the context of siloxane coordination chemistry.

In the context of siloxane coordination chemistry, neutral silicon based ligands and their activation for coordination are of special interest. Due to their great resemblance to common (crown-)ethers, the isolation and characterization of neutral siloxane complexes is the only way to learn about the structural aspects, coordination ability and reactivity compared to ethers by all available means. The isolation and characterization of such compounds, however, has been a challenging task over the past years. Attempts isolating stable adducts are made since the late 50s. Given that the basicity of siloxane oxygen atoms are low, these early attempts to coordinate simple silyl ethers like 1,3-dimethyldisiloxane, 1,1,3,3-tetramethyldisiloxane or HMDSE were attempted to bind to highly electrophilic LEWIS-acids such as BF_3 and BCl_3. These attempts, however, failed due to Si-O bond cleavage, even at low-temperature.[161] Over the years, extraction experiments as well as MÖSSBAUER studies then gave, though partially controversial,[162] first insights into metal binding. Alkali metal ions have successfully been extracted from organic phases with various cyclic siloxanes and could also be transferred through lipid bilayers with D_n ligands.[163–166] Observed isomer change in MÖSSBAUER spectroscopy indicated the coordination of HMDSE towards Sn^{4+}.[167] Unfortunately, no solid state structures were obtained back then and thus no structural proof for the silyl-ether coordination could be provided. The first structural proof of a neutral siloxane binding toward a metal centre was finally provided in the 1990s by

CHURCHILL et al.[168] The authors attempted crystallizing the highly reactive potassium species $K[InH(CH_2CMe_3)_3]$ from *n*-pentane. Due to high sensitivity of the compound, the grown single-crystals were, however, to instable and readily shattered. Probably also due to solvent loss. To avoid shattering, the authors then tried to recrystallize the compound from *n*-heptane instead. To protect the material before the solvent was added, it has been covered in small amounts of silicon grease. To the surprise of the authors, D_7 had formed from the silicon polymer upon crystallization. The coordination compound $K_3[K(D_7)][InH(CH_2CMe_3)_3]_4$ has been obtained where one of the potassium ions is coordinated by D_7.[168] $[K(D_7)][K\{C(SiMe_3)_2[SiMe_2(HC{=}CH_2)]\}_2]$ has been reported shortly after. The compound was obtained by recrystallizing $K[C(SiMe_3)_2(SiMe_2(HC{=}CH_2))]$ from methylcyclohexane/Et_2O solution in the presence of silicon grease.[169] Two further examples are published in the mean time where silicon grease has (unintentionally) been used as a precursor for the formation of D_n complexes. An additional potassium compound in the form of the silyl-sodate $[K(D_7)][Na\{SiMe(SitBu_3)\}_2]$[170] was published by the group of LERNER and the zirconium(IV) complex $[Zr(D_6)Br_2][Zr_2Br_9]_2$[171] was published by ERNST. Silicon grease, however, is not inevitably cleaved (e.g. by strong organometallic bases) into cyclic siloxanes. HAIDUC and SAITO reviewed silicon grease as precursor for coordination compounds and demonstrated that various structure motifs (monomers, chains and also cages) can be obtained.[172,173] Thus, a logical consequence was the aspiration to develop synthesis protocols which selectively yield cyclosiloxane complexes.

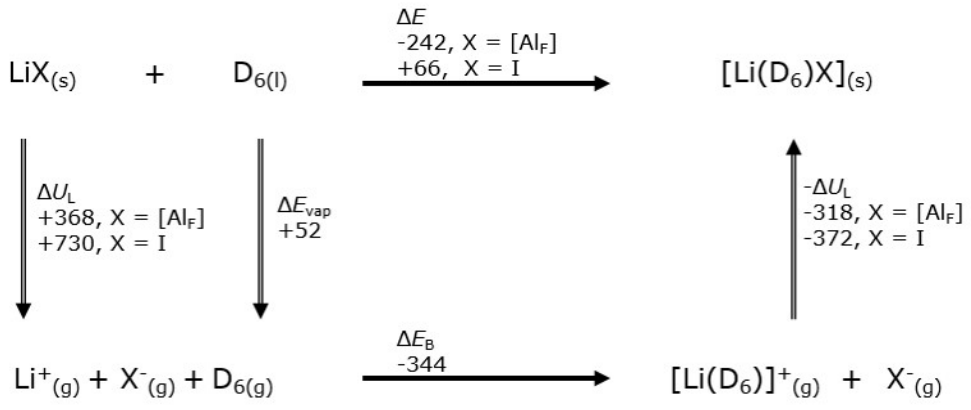

Figure 16: BORN-HABER cycle for the complex formation of LiX (X = I^-, $[AlF]^-$) with D_6.[174] The lattice energies (ΔU_L), energy of vaporization (ΔE_{vap}), binding energies (ΔE_b) and the energies of formation (ΔE) are given in $kJ \cdot mol^{-1}$.

PASSMORE and co-workers studied cyclosiloxane complexes by means of quantum chemical calculations and could, according to suitable BORN-HABER cycles, demonstrate that cation encapsulation becomes favourable when anions are employed, which are weakly coordinating such as the perfluorinated alkoxy-aluminates $[Al_F]^-$ or $[Al_{PhF}]^-$ ($[Al_{PhF}]^-$ = $[Al(OC(CF_3)_2Ph)_4]^-$).[174] WCAs (WCA = weakly coordinating anion) are generally known as anions, where the charge is delocalized over a large area of non-nucleophilic and chemically robust moiety.[175,176] As depicted in Figure 16, the reaction enthalpy calculated from the BORN-HABER cycle shows that the complexation of Li^+ yields 242 kJ·mol^{-1} when $[Al_F]^-$ is employed as an anion. When I^- is employed, the reaction enthalpy becomes positive (ΔE = 66 kJ·mol^{-1}). The main reason accounts for the differences in lattice energy. The aluminate salt has a significant lower lattice energy which is why the vaporization costs only approximately half as much energy than vaporizing the iodide salt. This fact is indeed reflected by the experiment. Direct reaction of D_6 and $Li[Al_F]$ or $Li[Al_{PhF}]$ in DCM (DCM = dichloromethane) yields the respective coordination compound, whereas D_6 is reluctant towards coordination of LiI. Further, direct reaction of the smaller ring D_5 with $Li[Al_F]$ turned out to be successful.[174] Endorsed by the success of these results, the PASSMORE group investigated the coordination chemistry of D_n towards $Ag[SbF_6]$.[177] Conversion of D_5 with $Ag[SbF_6]$ in liquid SO_2 yielded indeed a stable coordination compound but elucidated from SC-XRD, D_7 had formed from the D_5 ligand. Bulk analysis (GC-MS and in-situ $^{29}Si\{^1H\}$ NMR spectroscopy) revealed that besides D_7, significant amounts of D_6 and traces of D_8 have also been part of the reaction mixture. Hence, complexes of these ligands probably also formed even though these complexes had not been elucidated by SC-XRD. The formation of these ligands is attributed to the non-innocent character of the $[SbF_6]^-$ anion. The authors postulate formation of SbF_5 and formation of fluorosilanes as a reactive species. Template directed ring-closure of Ag^+ then yields the respective coordination compounds with $[Ag(D_7)(SbF_6)]$ as the main component.[177] An indirect proof for this assumption was published later on. The chemically robust, non-nucleophilic anions $[Al_F]^-$ and $[FAl(OR_F)_3]$ (R_F = $C(CF_3)_3$) do not promote Ag^+ templated ring-opening polymerization. After conversion of these salts with D_6 in $SO_{2(l)}$, the respective coordination compounds $[Ag(D_6)Al_F]$ and $[Ag(D_6)FAl(OR_F)_3]$ were isolated and characterized.[95] All so far characterized D_n complexes are depicted in Figure 17.

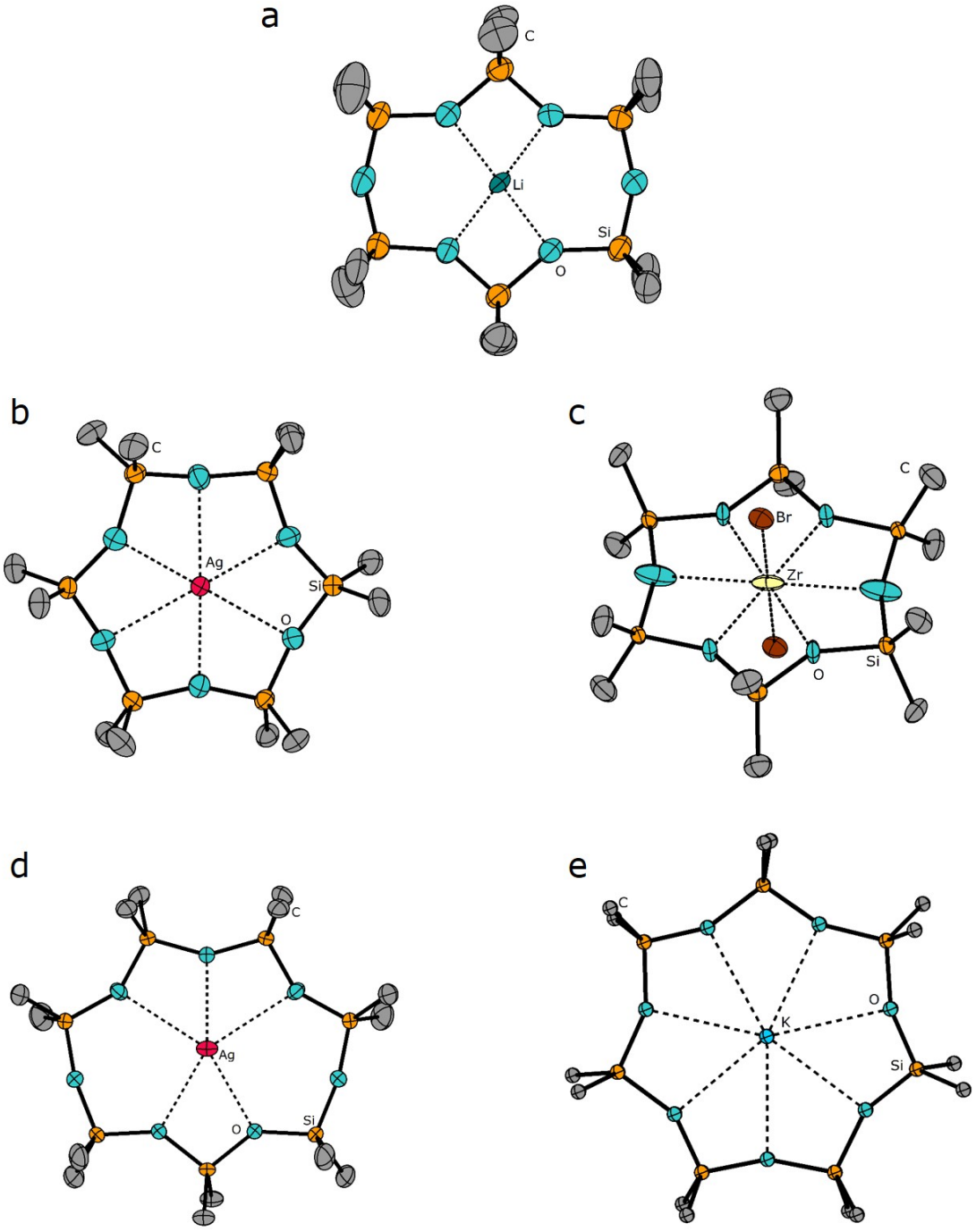

Figure 17: The so far published metal complexes of D_n ligands (n = 6, 7). Weakly coordinating anions are omitted for clarity. Depicted are the cationic parts of $[Li(D_6)Al_F]$ (a),[174] $[Ag(D_6)Al_F]$ (b),[95] $[Zr(D_6)Br_2][Zr_2Br_9]_2$ (c),[171] $[Ag(D_7)(SbF_6)]$ (d),[177] and $K_3[K(D_7)][InH(CH_2CMe_3)_3]_4$ (d)[168]. Thermal ellipsoids set at 50% probability. The crystal structure of $K_3[K(D_7)][InH(CH_2CMe_3)_3]_4$ has been published without anisotropic displacement. Atom radii are arbitrarily chosen here. For the $[K(D_7)]^+$ cation see also refs.[169,170]

The results clearly indicate that the use of weakly coordinating anions can activate siloxane ligands for coordination. However, the examples in Figure 17 are the only examples where cyclosiloxane coordination could be verified by means of SC-XRD to date. Even though there have been additional compounds calculated by means of quantum chemical calculations, no further complexes were isolated so far. WCAs are further known to be able to represent gas phase cations in condensed matter,[178] so it should be possible to obtain more than the species depicted in Figure 17. Examples determined by quantum-chemical calculations are $[Li(D_7)]^+$, $[Li(D_8)]^+$, $[Na(D_5)]^+$, $[K(D_5)]^+$, $[K(D_6)]^+$, $[Rb(D_6)]^+$, $[Ag(D_5)]^+$ and $[Ag(D_8)]^+$.[95,174] Noteworthy in this context are also the determined solid state reaction energies for the formation of simple silyl-ether adducts. The formation of $[Li(O(SiH_2Me)_2][Al_F]$ and $[Ag(O(SiH_2Me)_2][Al_F]$ yields -96 and -102 $kJ \cdot mol^{-1}$, respectively.[94] The values predict stable adducts, but more sophisticated synthesis protocols are required so far to obtain silyl-ether adducts. A successful strategy to obtain a simple silyl ether adduct was not established before 2018. Thus, measured at the first attempts coordinating DSE toward BX_3 (X = F^-, Cl^-),[161] it took 60 years to obtain a simple (and stable) silyl-ether adduct. It has finally been the group of HARDER which succeeded coordinating HDMSE.

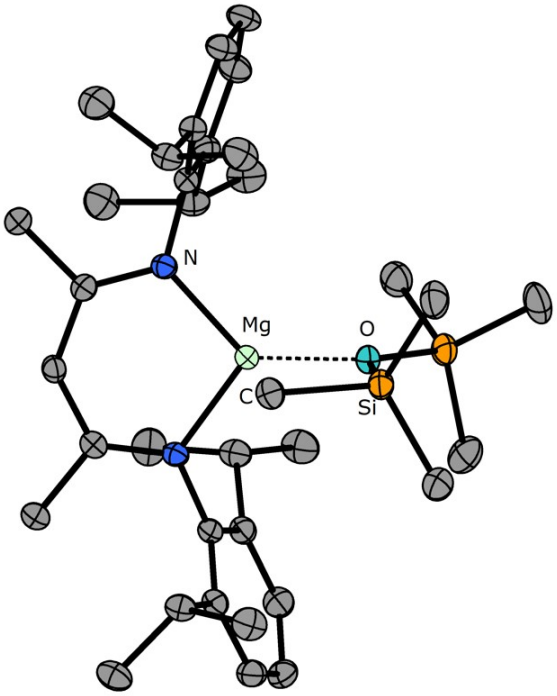

Figure 18: The molecular structure of $[Mg(BDI)HDMSE][B(C_6F_5)_4]$ in the crystal.[179] The $[B(C_6F_5)_4]^-$ anion is omitted for clarity. Thermal ellipsoids set at 50% probability.

The success is based on the synthesis of [Mg(BDI)][$B(C_6F_5)_4$] (BDI = CH[C(CH_3)N-Dipp]$_2$, Dipp = 2,6-diisopropylphenyl) combining both, high LEWIS acidity and a weakly coordinating anion. This dualism activates the silyl-ether for coordination (Figure 18).

Apart from research efforts trying to coordinate silyl-ether adducts consisting exclusively of Si-O donors, the VON HÄNISCH group expanded the field to three-dimensional ligand systems introducing group 15 elements.[180–183] The activation of Si-O donors for coordination was unfortunately unsuccessful in the most cases. A striking result in the field, however, was published in mid 2007. A formal inorganic [2.1.1]cryptand was synthesized, structurally characterized and its coordination toward Li^+ was realized.[180] A stepwise lithiation/silylation process gave access to [P_2{$O(SiiPr_2)_2$}$_2${$SiMe_2(OSiMe_2)_2$}] (=^{inorg}[2.1.1]crypt) which can be activated for coordination after subsequent conversion with Li[Al_F]. The molecular structure in the crystal is depicted in Figure 19. Despite using a three- rather than two-dimensional ligand moiety, the coordination ability of this ligand is comparable with those of D_5 and D_6. Hence, there is a lack of a "cryptate-effect" similar to the lack of a "crown-effect" in D_n ligands as well.

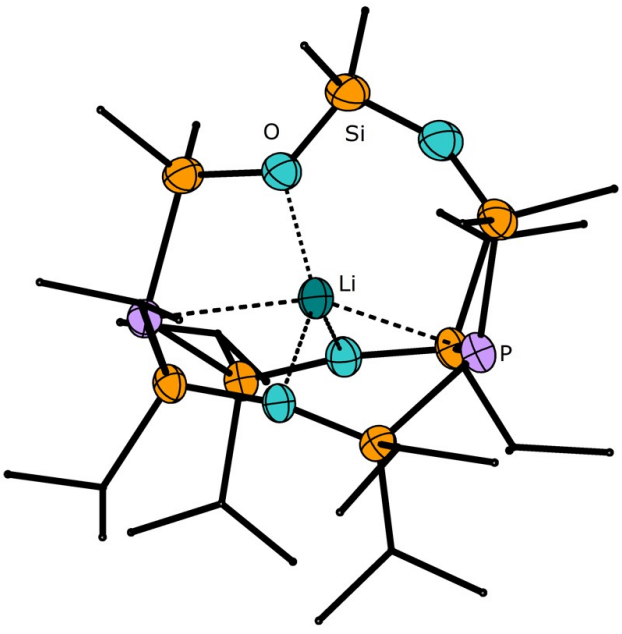

Figure 19: The molecular structure of [Li(^{inorg}[2.1.1]crypt)][Al_F] in the crystal.[180] The [Al_F]$^-$ anion is omitted and carbon atoms are shown as wires/sticks for clarity. Thermal ellipsoids set at 30% probability.

To shortly summarize this chapter, it could be shown that the use of WCAs can highly support siloxane coordination. Rare examples of metal complexes of simple-silyl ethers, cyclosiloxanes and inorganic cryptands have been isolated and structurally characterized employing these anions. The hitherto considered ions for siloxane coordination are Li^+, K^+, Mg^{2+}, Zr^{4+} and Ag^+. Quantum chemical calculations predict further stable siloxane coordination compounds but no more coordination compounds than those above mentioned have been isolated ever since. An interesting possibility to obtain coordination compounds is the ring-opening polymerization. As demonstrated for cationic $[M(D_7)]^+$ (M = K^+, Ag^+) and $[Zr(D_6)Br_2]^{2+}$, (polymeric) siloxane moieties can be cleaved template-driven to ion specific ligand moieties. Cyclic moieties are favoured over open-chained ligands.

1.6 Increasing Cation Binding Ability Employing Disilanes

As shown above, silyl-ether coordination compounds are best obtained employing cyclic ligands. A striking difference between D_n ligands and organic crown ethers, however, is the ligand architecture. Whereas cyclic siloxanes are constituted of $SiMe_2O$ repeating units, crown ethers are constituted of C_2H_4O units. An extension to Si_2Me_4O (=^2D) repeating units regains structural equivalence. The bonding situation in ^2D_n ligands is part of this chapter and the benefits of this linkage in comparison to D_n ligands are discussed.

1.6.1 Difference in Hyperconjugation Interactions

Hyperconjugation interactions have extensively been discussed for (cyclic)siloxanes in chapter 1.4.1. A significant difference compared to common (cyclo-)siloxanes is, that disilanes do not allow for geminal $p(O) \rightarrow \sigma^*(Si\text{-}O)$ backbonding. CYPRYK demonstrated this lack of backbonding on the basis of the $–O–SiH_2–SiH_2–O–$ linkage. As outlined, a different orbital interaction pattern involving the electron pairs of oxygen is present here.[85] The $p(O) \rightarrow \sigma^*(Si\text{-}O)$ backbonding is replaced by $p(O) \rightarrow \sigma^*(Si\text{-}Si)$ backbonding which is substantially weaker. The total energy of the $p(O) \rightarrow \sigma^*(Si\text{-}Si)$ delocalization has a value of approximately 42 $kJ \cdot mol^{-1}$ per unit. The total energy of the $p(O) \rightarrow \sigma^*(Si\text{-}O)$ delocalization, on the contrary, has a value of approximately

88 kJ·mol^{-1} per unit. Thus, the energy penalty upon transformation to a disilane is 46 kJ·mol^{-1} per unit.[85] Hence, electron density at oxygen is significantly more localized at oxygen employing disilanes. This difference in hyperconjugation interaction makes $^2D_2$, for example, a stronger base than all other dimethylcyclosiloxanes including the most reactive cyclosiloxanes D_3 and D_4.[85,86] The orbital interaction pattern relevant for ^2D_n systems is illustrated in Figure 20.

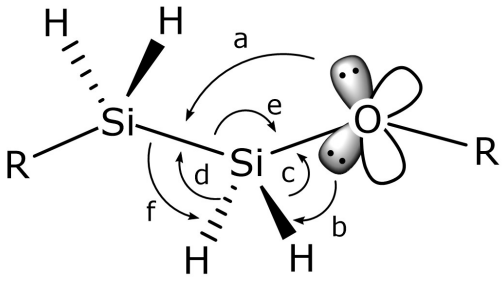

Figure 20: Strongest interactions contributing to the stability of a –SiH_2–SiH_2–O– fragment. For clarity, only a single representative of each type of interaction is depicted. *p*(O) → σ*(Si-Si) (a), *p*(O) → σ*(Si-H) (b), σ(Si-H) → σ*(Si-O) (c), σ(Si-H) → σ*(Si-Si) (d), σ(Si-Si) → σ*(Si-O) (e), σ(Si-Si) → σ*(Si-H) (f).

Noteworthy is, as depicted in Figure 20, that *p*(O) → σ*(Si-H) backbonding interactions are equally present in this linkage as in D_n compounds. As a consequence, one can conclude that the *p*(O) → σ*(Si-O) interactions are the predominant interactions which decrease the availability of the oxygen lone-pair for donation towards electrophiles. At least in (cyclic) systems bearing several repeating units.

1.6.2 Difference in Bond Polarity

The higher differences in electronegativity of the elements Si and O compared to C and O have been discussed in chapter 1.4.3. Transferred to the –O–SiR_2–SiR_2–O– linkage, it is clear that the Si-O bonds of this linkage are also strongly polarized. Even though quantum chemical calculations regarding the ionicity of a –O–SiR_2–SiR_2–O– are not available it is, however, legitimate to assume that this linkage is less ionic than a –O–SiR_2–O– or R_3Si–O–SiR_3 linkage. The first indirect evidence comes from the above-mentioned differences in hyperconjugation interactions. Co-

valency and ionicity are orthogonal rather than antipodal concepts. Thus, an increased basicity must follow a lower ionicity as well. The second evidence comes from the different bonding situation. As can be seen in Figure 21, the –O–SiR_2–SiR_2–O– linkage combines a highly ionic Si-O bond with an unpolar Si-Si bond. As illustrated, this is evident from the ionic resonance energy (i.e. the ionic contribution) of each bond.

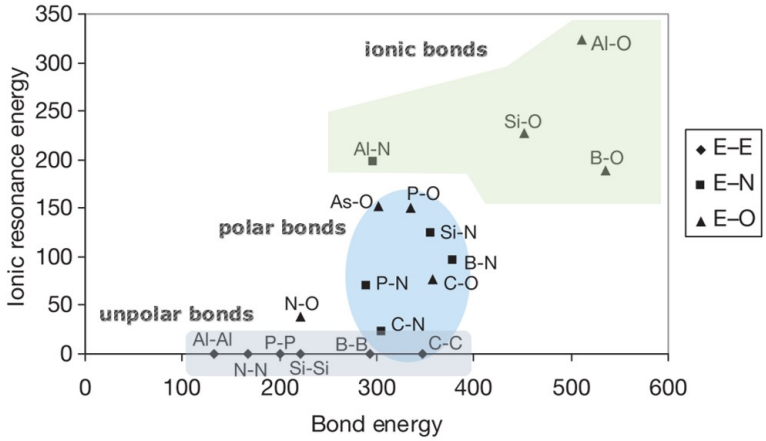

Figure 21: Graph of the ionic resonance energy in correlation to the bond energy (modified, see ref.[27]). Marked in grey: unpolar element-element bonds, blue: polar bonds, green: ionic bonds. Original figure © Elsevier Ltd.

Given the assumption that the ionicity is lowered, the following picture of a –O–SiR_2–SiR_2–O– linkage can be drawn in comparison to –O–SiR_2–O– (Figure 22). Further quantum chemical calculations are still required to strengthen this assumed bonding situation though.

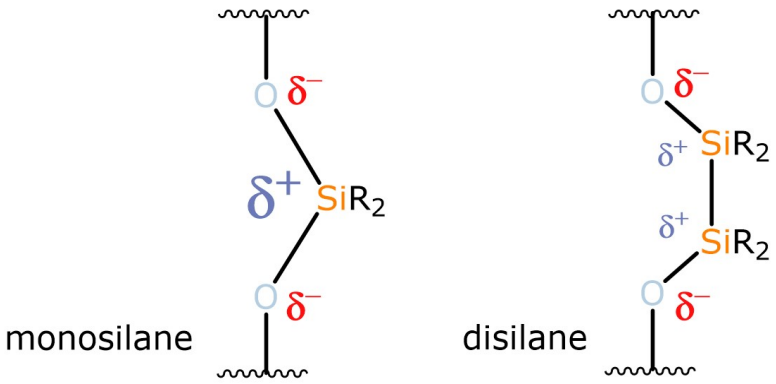

Figure 22: Postulated difference in ionicity of mono- (left) and disilanes (right).

1.6.3 Difference in Ring-Strain

Another crucial difference employing disilanes is the ligand conformation of the silicon-based macrocycle upon complexation. As demonstrated in Figure 23, the central coordination pattern of a (disila-)crown-ether and ion host is a five-membered ring. D_n ligands, however, form four-membered rings upon complexation. Several works show that a difference in ring strain can have a significant impact on the complexation ability and coordination sphere.[184–187]

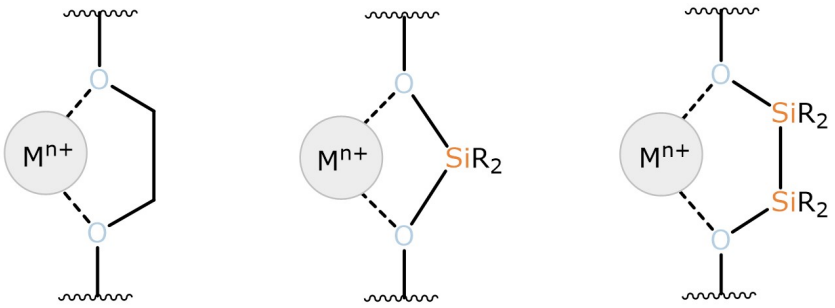

Figure 23: Coordination modes in macrocyclic ligands containing a C_2H_4 unit (left), SiR_2 unit (middle), and Si_2R_4 unit (right).

So has OLLIFF pointed out in the early 80s, that the coordination ability of many D_n ligands might be lowered, solely because of their conformation. By simply using molecular construction kits, possible conformations of D_n rings were found to have either very few oxygen positions available for coordination, or exceptionally long M^{n+}···oxygen atom distances would be required.[165] Experimental evidence was provided in the mid 80s by INOUE and HAKUSHI. Extraction experiments of crown ethers, ring-contracted crown ethers and sila-crown ethers showed that the cation binding ability toward (alkali)metal picrates is exceptionally high for [3n]-crown-n (n = 5, 6) ethers. On the contrary, it is exceptionally low for ring contracted [3n-1]-crown-n ethers as well as mono-sila-crown ethers.[184,186] Hence, disordered conformation of the crown-type macrocycle reduces the cation binding ability significantly. The experimental findings are supported by the fact that a series of ring contracted and sila-crown ethers bearing several –CH_2–CH_2–O– as well as one- or two –SiR_2–O– units have been described in literature,[188–196] but, no coordination compounds have been isolated and crystallographically characterized to date.

1.7 Hybrid Disila Crown-Ethers: Synthesis, Structure, Cation-Binding Ability and Reactivity

Chapter 1.6 gave insights into the bonding situation in cyclic siloxanes bearing disilanes. Evidence is provided that ^2D_n ligands are more basic than D_n ligands. Further, a large enough bite angle can be provided which prevents "disordered" conformations. Hence, more basic ligands in combination with suitable ligand conformations are promising systems for host-guest chemistry. Unfortunately ^2D_n ligands (except for n = 2, 3) are relatively unstable. It has been shown that D_n ligands can easily prepared by hydrolysis of diorganodichlorosilanes (Chapter 1.2). The hydrolysis of 1,1,2,2-tetramethyldisilane, however, yields almost exclusively $^2D_2$.[197] Formation of $^2D_3$ in low yields can also be observed at low temperatures. Higher homologues were not isolated upon hydrolysis of the aforementioned silane. Traces of $^2D_4$ and polymer could so far only be observed in gas-liquid chromatography after ring opening polymerization of $^2D_2$ initiated with triflic acid.[198,199] Hence, synthesis protocols to obtain the macrocycles ^2D_n (n = 3-6) in suitable yield have not yet been established. Host-guest chemistry of these "inorganic" crown-ether analogues could thus not be performed. To obtain meaningful experimental data of disila-bridged macrocycles, the VON HÄNISCH group started embedding Si_2Me_4 bridges into crown-ether moieties. In this way, organic ethers are partially substituted by silicon-based "inorganic" building blocks. Of particular interest are systems with high silicon content but so far, not more than two disila-units could be incorporated into residual C_2H_4O frameworks. Ligands of different ring sizes were characterized and have been successfully used in coordination chemistry. Experimental data regarding their coordination ability could be provided. Furthermore, quantum chemical calculations have been carried out for detailed analysis. A view on the synthesis, coordination ability and also reactivity of these novel ligand systems follows at this point.

Synthesis. The synthesis of (cyclic) hybrid ligand systems consisting of organic and inorganic building blocks is generally achieved through conversion of a respective organic glycol, a chlorosilane and an auxiliary base such as NEt_3.[200–207] Suitable solvents, for instance, are THF (THF = tetrahydrofuran) or Et_2O. Dependent on the chain length of the glycol, crown-ethers of the generally formula 1,2-disila[3n]crown-3 are obtained. Embedding two respective disilane

units into crown-ether moieties was also realized by different paths. The synthesis of such crown ethers dates back to the 70s. HENGGE et al. synthesized 1,2,7,8-tetrasila[12]crown-4 even though the authors did not present this compound as a crown-ether.[208] All compounds presented in Scheme 4 are obtained as colourless, moisture sensitive, viscous oils. The respective crown-ethers are obtained in moderate to good yields and have been thoroughly characterized by means of multinuclear NMR spectroscopy and MS spectrometry.

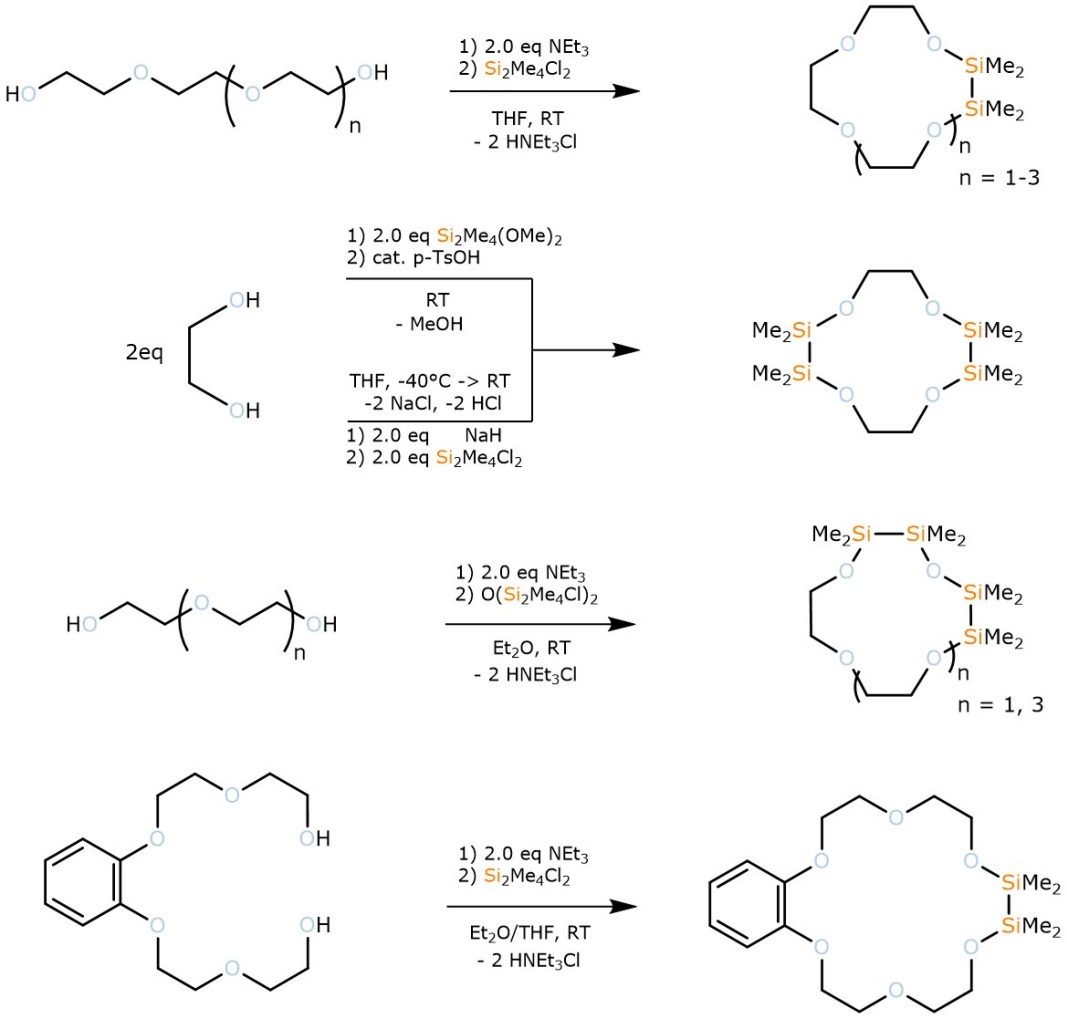

Scheme 5: The synthesis of different hybrid disila-crown ethers.

Structure and cation-binding ability. As the crown-ethers shown in Scheme 5 are colourless viscous oils, no single crystals for structure elucidation were obtained yet. The structure of these hybrid systems has thus been investigated by means of DFT calculations. In general are the methyl groups attached to the silicon atoms in a staggered conformation and these rings are puckered. Figure 24 illustrates three different [12]crown-4 ligands. As can be seen here, this staggered arrangement of the methyl groups is favoured for all respective ligands. Similar observations are also made for larger disila-ligands. All of the ligands presented in Scheme 5 could successfully used in terms of coordination chemistry. So far, it was possible to obtain a wide range of metal complexes which include alkali-metal complexes of Li^{+}-K^{+} as well as alkaline-earth metal complex of Mg^{2+}-Ba^{2+}.[201–204] In the respective complexes, the staggered arrangement of the methyl groups changes to a nearly eclipsed arrangement and all oxygen atoms are directed to the inside of the cavity. This conformational change is connected with an energy penalty (=ΔE_{geom}) upon rearrangement from free crown ether geometries toward the geometry found in the respective complexes.

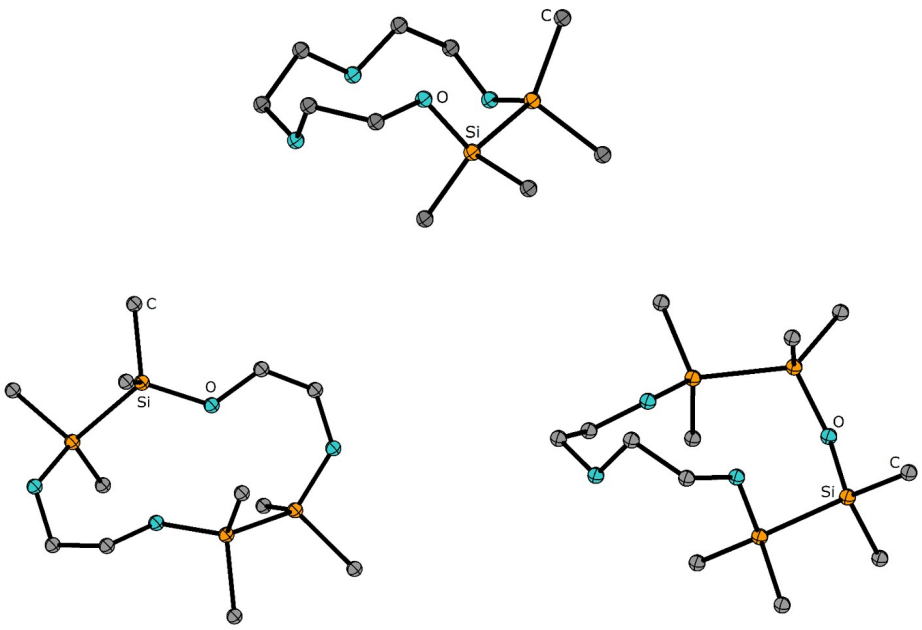

Figure 24: DFT optimized structures of hybrid disila-crown ethers with four donor atoms. 1,2-disila[12]crown-4 (top), 1,2,7,8-tetrasila[12]crown-4 (bottom left) and 1,2,4,5-tetrasila[12]crown-4 (bottom right). The calculated structures have been reproduced from provided .xyz data.[201,202]

Quantum chemical calculations regarding this change of conformation have been carried out for Li^+ complexes as an example. The ligand rearrangement from free 1,2-disila[12]crown-4 to $[Li(1,2\text{-disila}[12]\text{crown-4})]^+$ requires approximately 34 kJ·mol^{-1}. 60 kJ·mol^{-1} are required for rearranging free 1,2,7,8-tetrasila[12]crown-4 to $[Li(1,2,7,8\text{-tetrasila}[12]\text{crown-4})]^+$. Rearrangement of free 1,2,4,5-tetrasila[12]crown-4 to $[Li(1,2,4,5\text{-tetrasila}[12]\text{crown-4})]^+$ requires even 70 kJ·mol^{-1}. It can be seen that the higher the silicon content is, the higher is ΔE_{geom}. Compared to the complexation of Li^+ by organic [12]crown-4, these values are exceptionally higher. The conformational change of organic [12]crown-4 requires only 18 kJ·mol^{-1}. Despite these higher energy penalties, a higher electrostatic interaction between the O atoms of the respective sila-ligands and the metal ions compensates this amount of energy: Relative energies of the Li^+ exchange from [12]crown-4 to 1,2-disila[12]crown-4 yields -10 kJ·mol^{-1}. Li^+ exchange from [12]crown-4 to 1,2,7,8-tetrasila[12]crown-4 or 1,2,4,5-tetrasila[12]crown-4 yields 3 kJ·mol^{-1} and -29.5 kJ·mol^{-1}, respectively (Scheme 6). Hence, the coordination ability of these systems in comparison to the organic counterpart is on even terms. In case of 1,2,4,5-tetrasila[12]crown-4 the complexation ability is even slightly enhanced.[201,202]

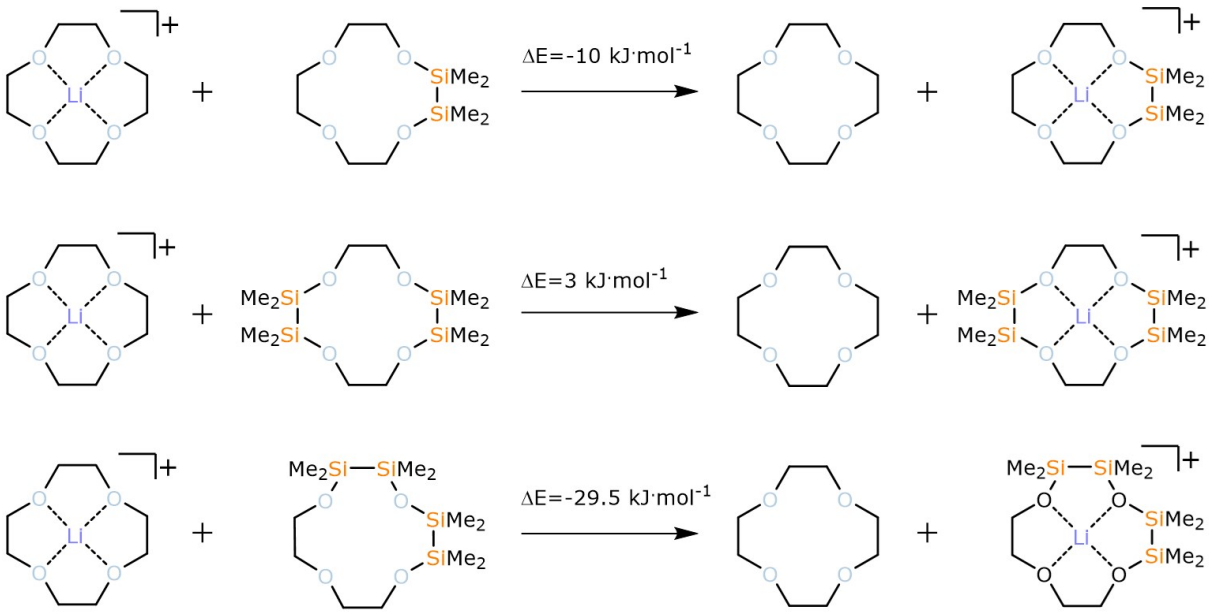

Scheme 6: Relative energies of the lithium exchange from [12]crown-4 to hybrid disila-crown-ethers obtained from DFT calculations.[201,202]

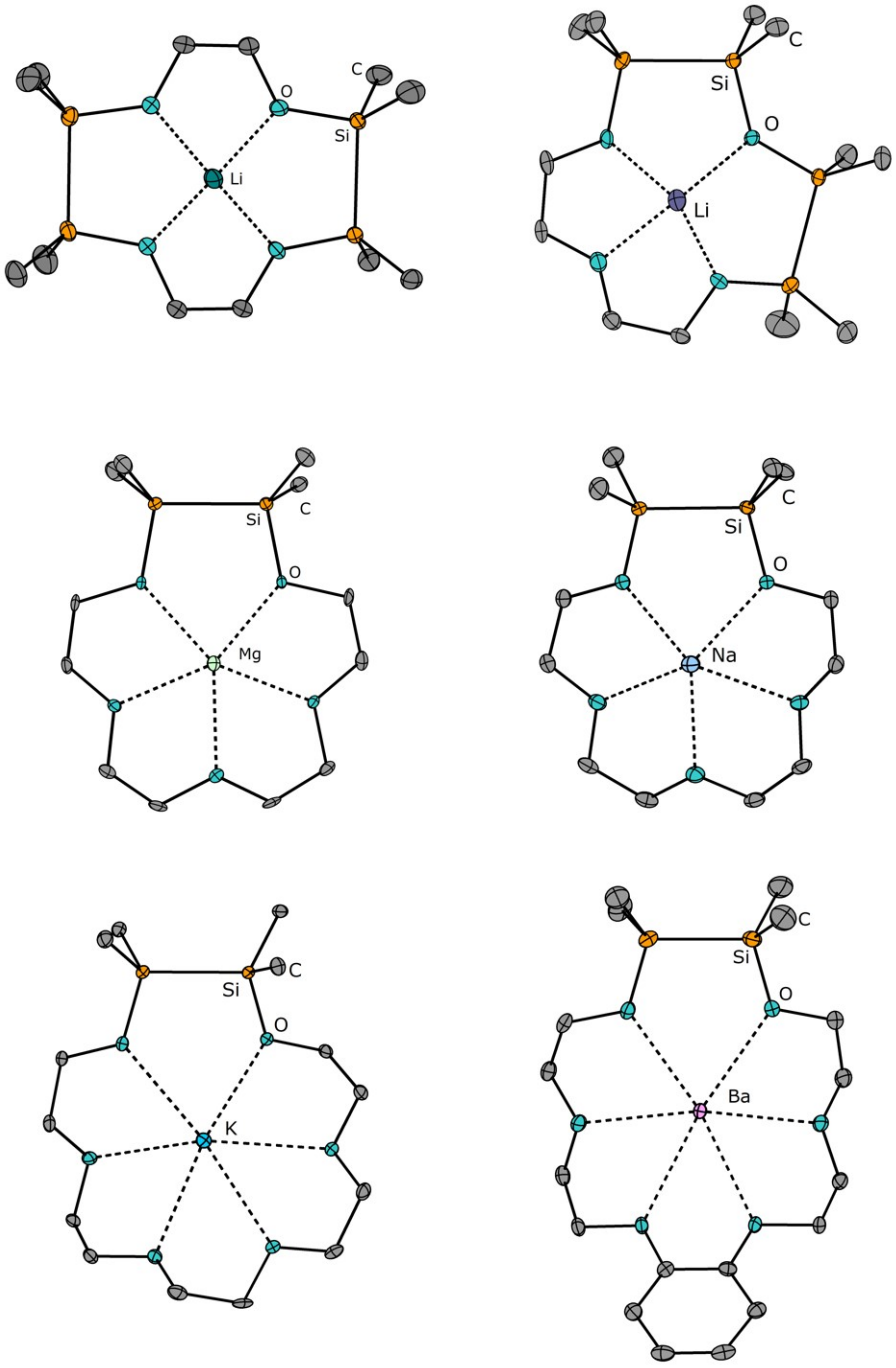

Figure 25: Cationic parts of the molecular structures of different metal complexes of hybrid disila-crown ethers. [Li(1,2,7,8-tetrasila[12]crown-4)PF_6] (top left)[201], [Li(1,2,4,5-tetrasila[12]crown-4)OTf] (top right, OTf = $CF_3SO_3^-$))[202], [Mg(1,2-disila[15]crown-5)Br_2] (mid left)[204], [Na(1,2-disila[15]crown-5)ClO_4] (mid right)[201], [K(1,2-disila[18]crown-6)PF_6] (bottom left)[201] and [Ba(1,2-disila-benzo[18]crown-6)OTf_2] (bottom right)[204]. Thermal ellipsoids set at 50% probability.

Notably, the coordination ability of 1,2,4,5-tetrasila[12]crown-4 is determined to be the highest, even though coordination of Li^+ is realized by an oxygen atom which is bound by two silicon atoms. Thus, the incorporation of disilane-units into ring-systems proved indeed to be a powerful strategy to activate siloxanes for coordination. Besides theoretical investigations, also experimental evidence could be provided. Dynamic ^1H NMR spectroscopic studies revealed that 1,2,7,8-tetrasila[12]crown-4 coordinates reasonably well when compared with [12]crown-4.[201] To shortly sum up at this point, combined experimental and theoretical investigations on hybrid-disila crown ethers revealed, that partially silicon based crown-ethers coordinate on even terms when compared with organic crown ethers. Conclusively, partially silicon based crown-ethers allowed obtaining diverse coordination compounds (Figure 25). Even with comparatively strong coordinating anions such as Br^- and I^-. The respective coordination compounds are obtained by conversion of equimolar ratios of the respective salt and ether. Suitable solvents turned out to be DCM or α,α,α-trifluorotoluene.[201–204]

Drastic decrease in cation binding ability, however, was observed in "mismatched" complexes of hybrid disila-crown ethers. Cations which are too small for the cavity of a respective crown-ether are not coordinated in a coplanar manner by the ligands O atoms. Some oxygen atoms are even reluctant toward coordination in certain cation-ligand combinations (Figure 26). Such drastic reduced coordination ability is for example observed for [Ca(1,2-disila[18]crown-6)OTf_2]. Whereas [18]crown-6 enables all six oxygen donors for coordination, the disila-crown ether enables only five oxygen atoms for coordination due to its larger cavity size. Hence, the cation binding ability of [18]crown-6 was determined to be considerably higher by means of NMR spectroscopy. Interestingly, the non-coordinating oxygen atoms are not inevitably silicon affected. Nevertheless, a suitable match between ionic radius of the cation and crown-ether cavity significantly improves the complex stability and supports coordination of the three types of oxygen donors O_{Si}, $O_{Si/C}$ and O_C. A larger cavity of disilane-substituted crown-ethers than that of organic crown-ethers needs to be taken into account. The inverse case, a relatively large cation in comparison to a smaller cavity size of the ligand had also been under investigation. So does conversion of 1,2-disila[15]crown-5 with $BaOTf_2$ in DCM yield the dinuclear species [Ba_2(1,2-disila[15]crown-5)$_2OTf_4$].

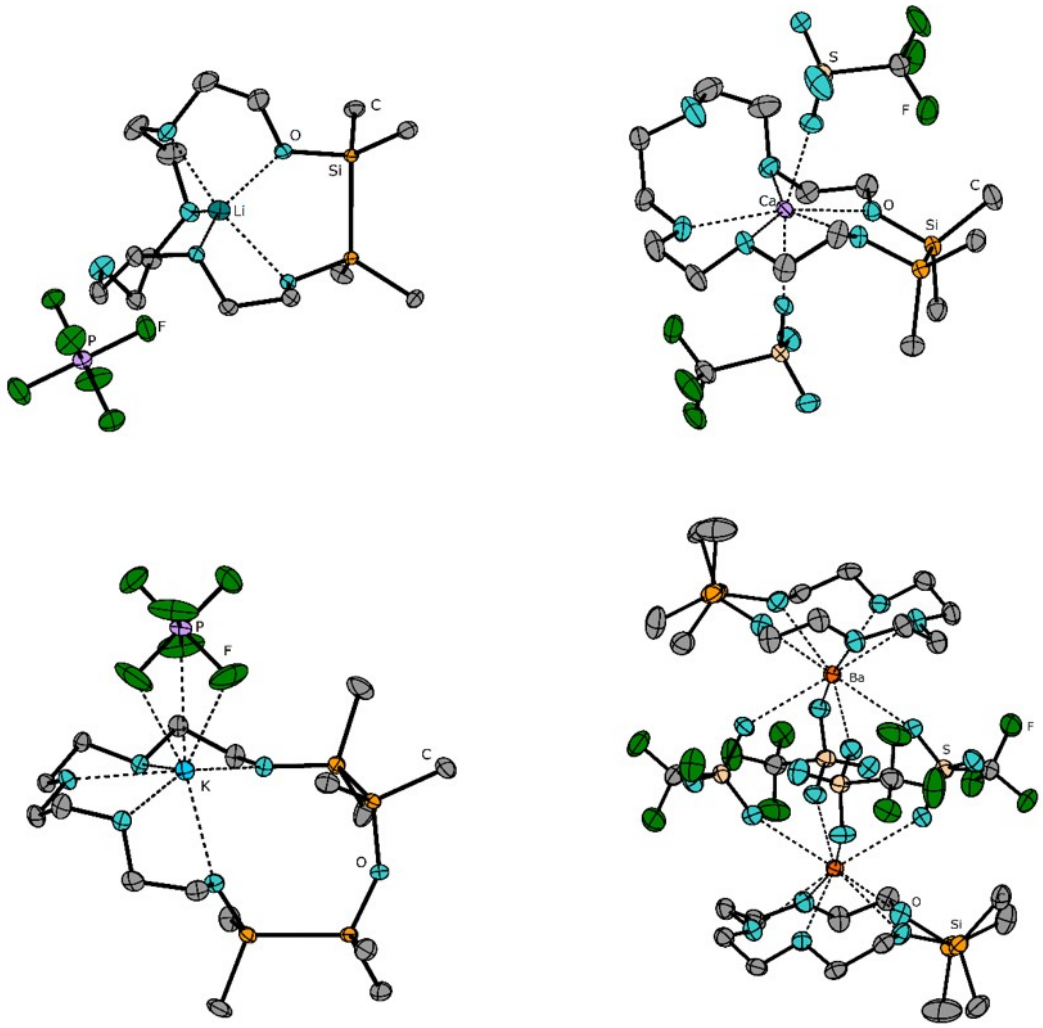

Figure 26: Different mismatched complexes of partially silicon-based crown ethers. [Li(1,2-disila[18]crown-6)]PF_6 (top left)[203], [Ca(1,2-disila[18]crown-6)OTf_2] (top right)[204], [K(1,2,4,5-tetrasila[18]crown-6)PF_6] (bottom left)[203] and [Ba_2(1,2-disila[15]crown-5)$_2OTf_4$] (bottom right)[203]. Thermal ellipsoids set at 50% probability.

Reactivity. Disila-crown ethers proved to be suitable ligands for a range of s-block metal complexes. Hence, the use of these crown-ethers can increase anion reactivity and supports stabilization of different electrophiles. Anion activation has successfully performed upon conversion of LiCl with 1,2-disila[12]crown-4. The incorporation of Li^+ into the macrocycle enhanced the LEWIS-basicity of Cl^- to such an extent, that the chlorosulfite ion $[SO_2Cl]^-$ was formed in a respective LEWIS-acid base reaction with SO_2.[209] The stabilization of elusive electrophiles could

recently be demonstrated stabilizing (low-)valent p-block cations with these hybrid crown-ethers. Preliminary results show that Ga^{3+}, $In^{+/3+}$, Tl^{+}, Ge^{2+}, Sn^{2+}, Pb^{2+}, Sb^{3+} and Bi^{3+} can be incorporated into these crown-ethers. The compound [In(1,2-disila[15]crown-5)][$GaCl_4$] for instance, was even observed to activate C–Cl bonds. The indium ion inserts into the C–Cl bond of DCM and the compound [In(1,2-disila[15]crown-5)(CH_2Cl)Cl] is obtained. The indium ion changes its oxidation state from +1 to +3 in this respective compound.[210] Further bond activations have not yet been established. The molecular structures of the complexes [Li(1,2-disila[12]crown-4)(SO_2Cl)] and [In(1,2-disila[15]crown-5)(CH_2Cl)Cl] are finally illustrated in Figure 27.

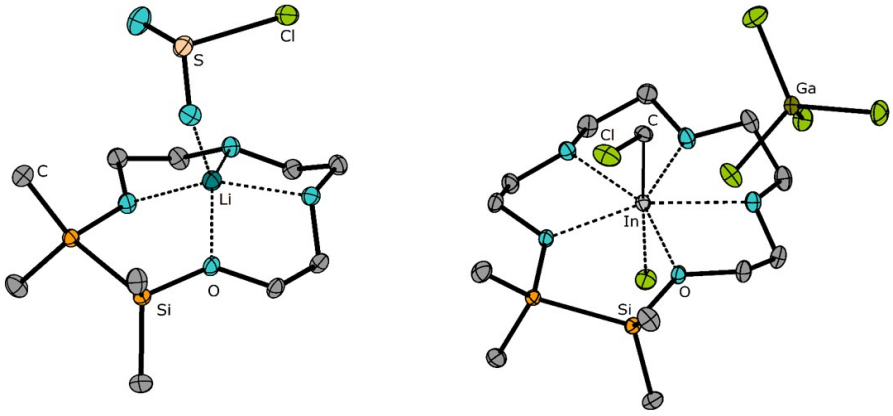

Figure 27: The molecular structures of the complexes [Li(1,2-disila[12]crown-4)(SO_2Cl)] (left)[209] and [In(1,2-disila[15]crown-5)(CH_2Cl)Cl][$GaCl_4$] (right)[210] in the crystal. Thermal ellipsoids set at 50% probability.

2 Project Scope

The previous chapters demonstrated that disila-substituted crown-ethers can effectively bind metal cations and promising results regarding coordination ability of Si-based ligands could be observed by means of SC-XRD and NMR techniques. However, of particular interest are systems with a possibly high silicon-content. So far, stable complexes of ligands with not more than two disilane-units were characterized. Further, it has so far only been obtained one example where siloxane coordination of a $(Si_2Me_4)_2O$ fragment was realized. Central part of this work is therefore to establish and investigate strategies to obtain ligands with more than two disilane-units. Associated with this research design is finding suitable coordination partners for these ligands.

A first strategy to obtain more silicon-rich crown-ethers is establishing novel building blocks for the synthesis of hybrid crown-ethers. Instead of reacting 1,1,2,2-tetramethyldichlorodisilane with one-equivalent of glycol, the reaction with two equivalents glycol at low-temperatures might be useful to obtain such a building block. In this way, disila-bridged polyethylene glycols are obtained which then could be used as educts for further reactions with $(Si_2Me_4Cl)_2O$ in the presence of a base such as NEt_3 or also Cs_2CO_3 (Scheme 7). Additionally, the obtained glycols can be converted with metal salts first. The ring-closure upon $(ClSi_2Me_4)_2O$ addition follows as the next step. By lowering the chain length of the glycol, the silicon content might be adjustable.

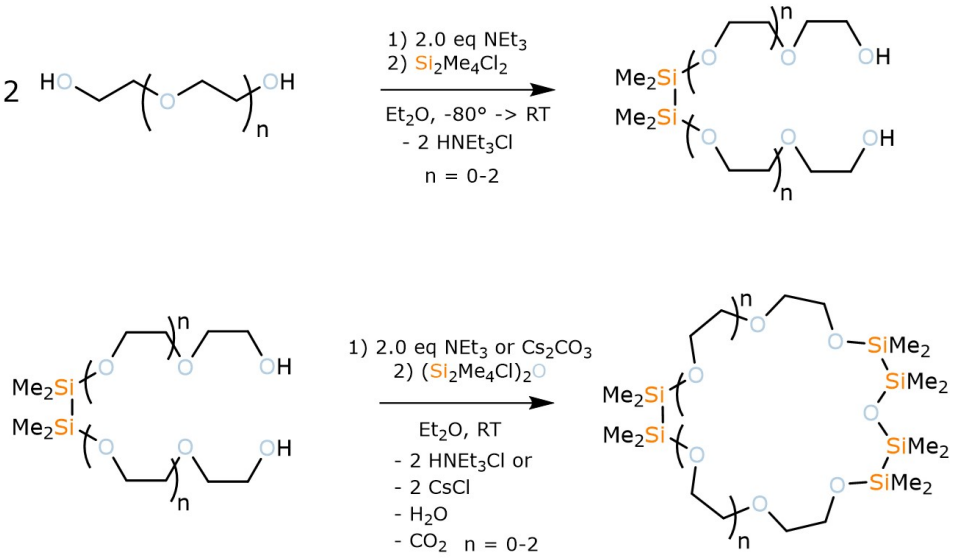

Scheme 7: Possible synthesis of silicon-based crown-ethers bearing three disilane units.

A second strategy is to obtain novel ligand moieties by metal templated ring-opening oligomerization. It was shown by the potassium and silver complexes of D_n ligands that siloxanes are vulnerable towards ring-opening if suitable cation-anion combinations are provided.[28] Thus, a key target in this thesis are template reactions with disila-bridged ligand moieties. To evaluate suitable coordination partners for siloxane-ligands and thus templates, a systematic study regarding the influence of different metal centers toward the Si-O-Si linkage is necessary. Taken the ionic radii of s-block metal ions into account, 1,2,4,5-tetrasila-benzo[15]crown-5 is an ideal ligand for such a study (Scheme 8). The cavity of this ligand is larger than that of [15]crown-5 but smaller than that of [18]crown-6. Hence, a series of cations might be incorporated into this ligand. Combined NMR and X-ray crystallographic investigations can then give valuable insights which coordination partners are most suitable. These, in turn, might then be suitable for template reactions which require effective Si-O bond activation. Upon conversion of suitable building-blocks in the presence of a metal template which can activate the Si-O bond, silicon-rich crown-ether analogues might be obtained which are not available by other means. Of special interest are ligands, whose cavity is too small for the given template ion. (Cross-)coupling of different sila-ethers are an interesting possibility (Scheme 9).

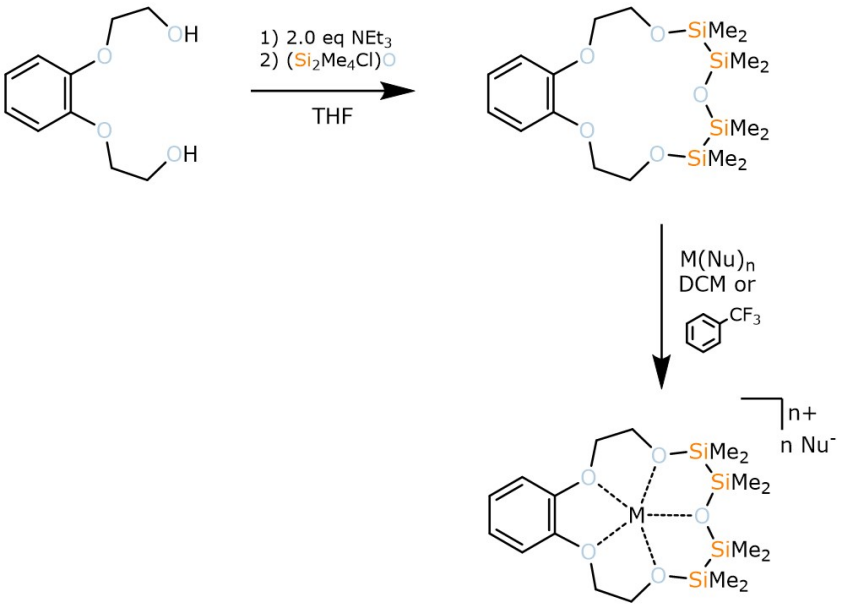

Scheme 8: Possible synthesis of a silicon based crown ether which can be used for a comparative analysis of different metal complexes.

To establish the synthesis and investigating the coordination ability of an exclusively disila-bridged crown-ether analogue is of particular interest in this context. Isolating stable complexes of $^{2}D_{n}$ type (n = 3-6) ligands could finally give meaningful results in how far inorganic crown-ethers can challenge organic crown-ethers and D_{n} ligands. This, however, requires ring-opening of an exclusively silicon-based precursor. $^{2}D_{2}$ might serve as a promising building block here.

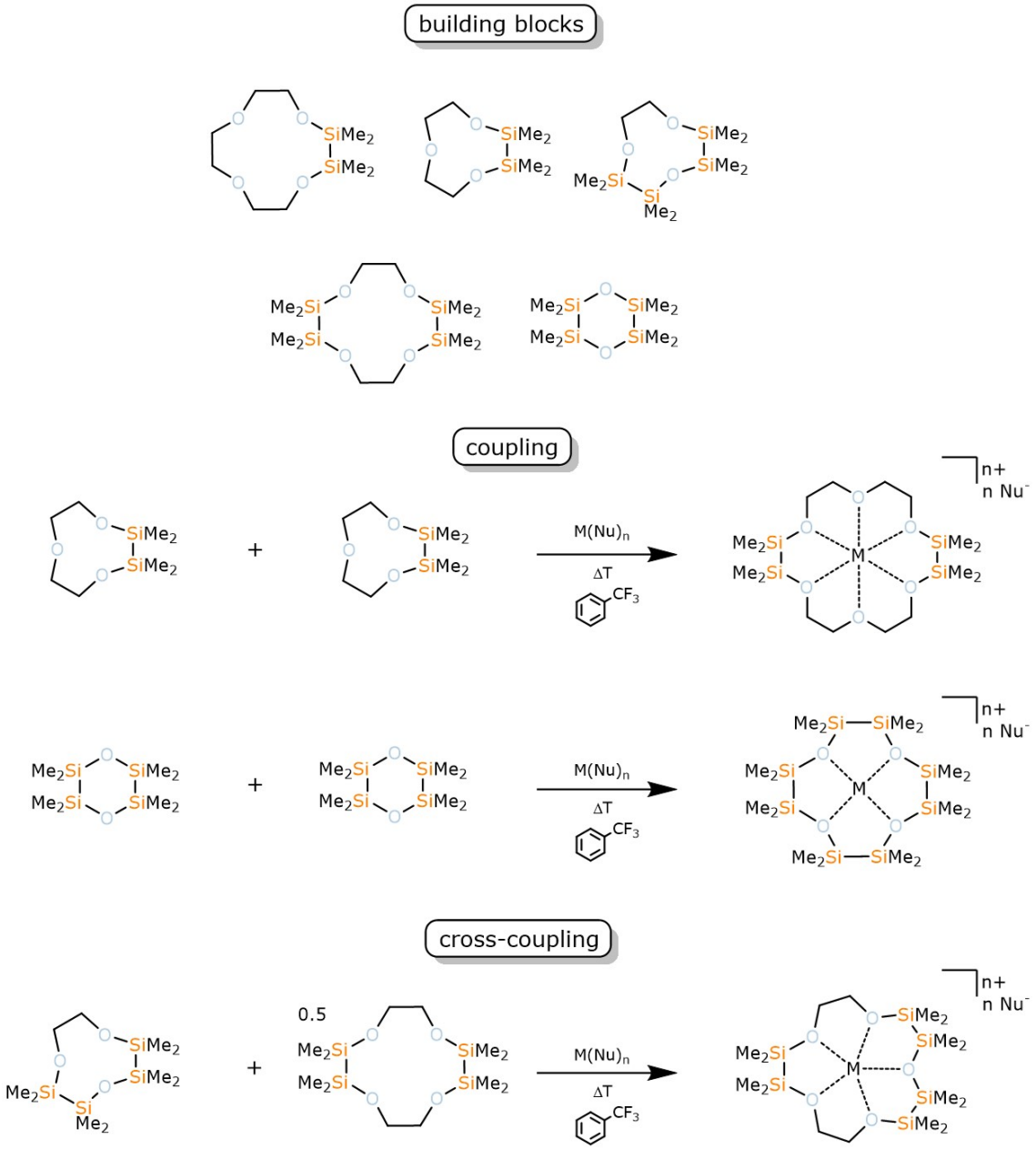

Scheme 9: A selection of possible building blocks for templated synthesis and three different examples of (cross-)coupling reactions to obtain silicon-rich crown ether analogues.

Another major part of this thesis is to examine the limits of siloxane coordination stepwise. Therefore, not only disila-bridged ligands but also D_n ligands are taken into account. It should be noted that, so far, only complexes of four different cations (Li^+, K^+, Ag^+, Zr^{4+}) were obtained with D_n ligands. It has been shown that weakly coordinating anions can support coordination, but less is known about the influence of the nature of the cation. Thus, the research effort regarding disila-ligands, e.g. finding suitable coordination partners for siloxane donors, shall also be transferred to D_n ligands. The possibilities but also limits of siloxane coordination chemistry with D_n ligands are of special interest. In general, the aim is to find new ways to activate the Si-O bond for coordination and to expand the field of siloxane coordination chemistry. Overall, the assumed picture of siloxane-based ligands as poorly coordinating ligands is about to be scrutinized in this way.

3 Cumulative Part

General information:

The cumulative part shortly summarizes each paper in chronological order. This order differs from that in the summary part as the results have been published independently from each other. Each paper had been undergoing the peer review process with at least two independent referees reviewing the respective paper regarding scientific correctness before publication. Each paper can be found in the appendix section in the same chronological order with the supplementary information included. Manuscripts which are denoted as *"submitted manuscript"* have not yet been peer reviewed or are being peer reviewed in the mean time. Publishing the respective manuscript in a peer reviewed journal as soon as possible is highly intended. All articles or prepared manuscripts have been or are about to be finished through contribution of all listed authors. Authors marked with asterisk (*) are the respective corresponding authors. Authors marked with hashtag (#) contributed equally. A description of the respective personal contribution is provided for each paper or manuscript.

Inorganic Chemistry **2018**, *57*, 351-359 **#1**

Alkali and Alkaline Earth Metal Derivatives of Disila-Bridged Podands: Coordination Chemistry and Structural Diversity

Fabian Dankert, Carsten Donsbach, Christopher-Nils Mais, Kirsten Reuter and Carsten von Hänisch*

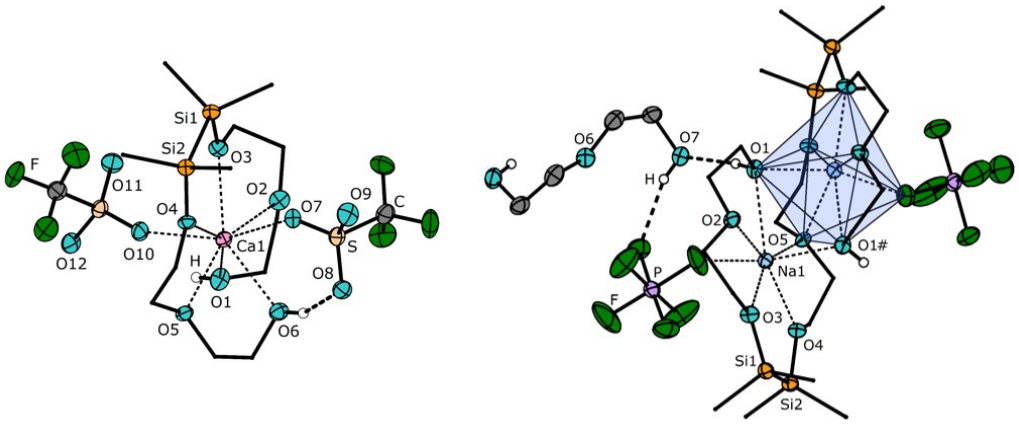

Within this study, the synthesis and coordination chemistry of disila-bridged polyethylene glycols towards various s-block metal salts is explored. Structural diversity is observed in the variety of ligand and salt. Two disila-bridged polyethylene glycols were successfully synthesized through conversion of two equivalents of a respective glycol and 1,1,2,2-tetramethyldichlorodisilane in the presence of NEt_3 as base in diethylether. Low temperatures are crucial. The ligands 8,9-disila-EO5 and 11,12-disila-EO7 (EO5 = pentaethylene glycol, EO7 = heptaethylene glycol) were obtained in this way. Through conversion of these ligands with different s-block metal salts in DCM or α,α,α-trifluorotoluene yielded the respective coordination compounds. The alkaline earth metal complexes [Ca(8,9-disila-EO5)OTf_2], [Sr(8,9-disila-EO5)I_2], [Sr(11,12-disila-EO7)I]I, and [Ba(11,12-disila-EO7)OTf_2] were successfully characterized, also by means of SC-XRD. As evident from the solid state structures, the respective ligands helically encapsulate the cation. Within the reaction of the alkali metal salt $NaPF_6$ with 8,9-disila-EO5, the sodium ion acts as a template during the complexation process. Under elimination of

one molecule of diethylene glycol, the dinuclear species [Na_2(8,9,17,18-tetrasila-EO8)(PF_6)$_2$]·EO2 (EO8 = octaethylene glycol, EO2 = diethylene glycol) was obtained. Thus, a first template-driven reaction was observed for disila-ligands. The sodium ions create a [15]crown-5-like coordination environment and EO2 is eliminated forming this novel ligand moiety. Quantum chemical investigations showed that the coordination ability of these ligand systems is on even terms when compared to organic glycols. This finding, however, is only applicable for sufficiently hard cations. The attempt to coordinate Cs^+ upon conversion of 11,12,disila-EO7 with CsOTf failed, leading to recrystallization of anhydrous CsOTf. Additional quantum chemical calculations show that the soft Cs^+ cation does only barely share interactions with the silicon-bound oxygen atoms whereas cations like Ca^{2+} and Sr^{2+} share strong interactions.

Descriptions of the personal contributions:

Fabian Dankert (F.D.) conducted the synthesis, characterization and crystallization of the compounds, performed the DFT calculations and partially conducted the single-crystal diffraction experiments. Further, F.D. wrote the manuscript and contributed to the refinement of the respective crystallographic data. Carsten Donsbach (C.D.) contributed to the crystallographic refinement of all compounds and accomplished the X-ray crystallographic data collection of compound **7**. As part of a practical course, Christopher-Nils Mais (C.-N. M.) contributed to the synthesis, characterization and crystallization of all compounds. Kirsten Reuter (K.R.) instructed F.D. how to perform the DFT calculations. Carsten von Hänisch (C.v.H.) contributed to the manuscript preparation and led the research project.

Inorganics **2018**, *6(1)*, 15 **#2**

Hybrid Disila-Crown Ethers as Hosts for Ammonium Cations: The O–Si–Si–O Linkage as an Acceptor for Hydrogen Bonding

Fabian Dankert, Kirsten Reuter, Carsten Donsbach and Carsten von Hänisch*

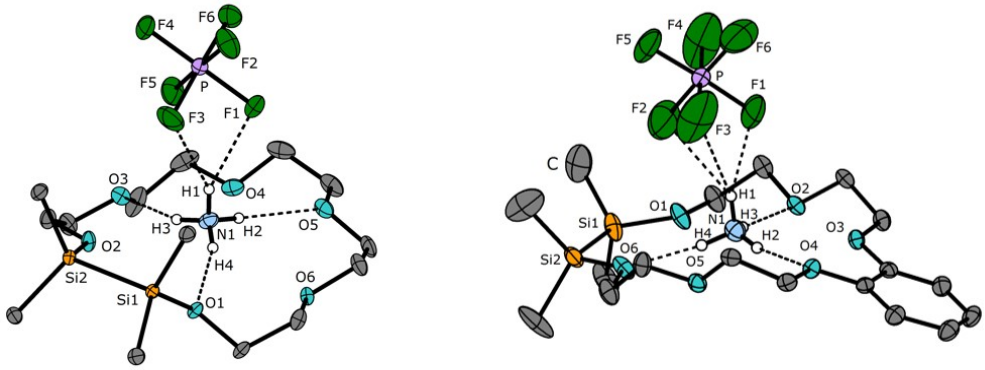

Based on the success to incorporate a wide range of metal ions into disila-bridged crown-ether analogues, it was demonstrated in this contribution that these ligands can also serve as hydrogen bond acceptors. The reaction of 1,2-disila[18]crown-6 and 1,2-disila-benzo[18]crown-6 with NH_4PF_6 in DCM turned out to be successful. It was shown by means of NMR and IR spectroscopy, that the ammonium ion had successfully been incorporated in the middle of the crown-ether cavity. In addition, the single crystal structures of the complexes [NH_4(1,2-disila[18]crown-6)]PF_6 and [NH_4(1,2-disila-benzo[18]crown-6)]PF_6·DCM were determined. The hydrogen atom positions of NH_4^+ were located and refined as isotropic atoms. No hint is found of a preference of the purely organic ethers to form hydrogen bonds on a structural level.

Descriptions of the personal contributions:

Fabian Dankert (F.D.) performed the synthesis and analytics of compound **4**, interpretations of all the analytical data, contributed to the X-ray crystallographic refinement, and wrote the manu-

script. Kirsten Reuter (K.R.) performed the synthesis of compound **3** and the collection of the respective analytical data. Carsten Donsbach (C.D.) accomplished the crystal structure solution and refinement of compound **4**. Carsten von Hänisch (C.v.H.) contributed to the interpretation and manuscript preparation and led the overarching research project.

CrystEngComm **2018**, *20*, 5370-5376 **#3**

Sila-polyethers as *innocent* crystallization reagents for heavy alkali metal compounds

Fabian Dankert, Johanna Heine, Julia Rienmüller and
Carsten von Hänisch*

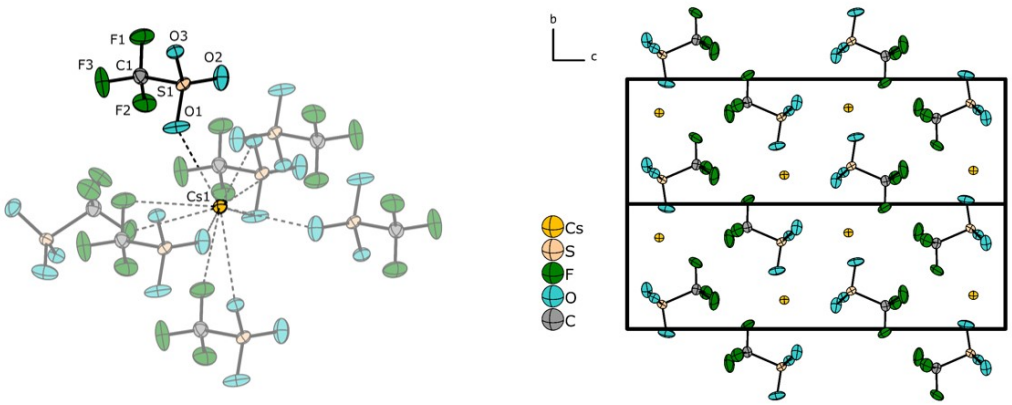

Open-chained disila-polyethers were found to be reluctant towards coordination of heavier and thus soft alkali-metal ion. In this contribution this unique coordination behaviour could be utilized and a novel approach to recrystallize elusive alkali metal salts is presented. It was shown that 8,9-disila-EO5, 11,12-disila-EO7 and 1,2,10,11-tetrasila[18]crown-6 can act as a solubilizer and promote recrystallization of heavy alkali metal compounds such as RbOTf, CsOTf and Cs_2Ox ($Ox = C_2O_4^{2-}$). The crystal structures of the mentioned salts have previously been solved from powder diffraction data. Sila-polyethers, however, allow obtaining single-crystals for structural analysis when an inert atmosphere and a weakly-coordinating solvent such as DCM is employed. In this way, the crystal structures of these salts could be confirmed by SC-XRD. In case of CsOTf, the general findings of the previous study were not only confirmed but also expanded. Single crystal structure analysis allowed us to determine that α-CsOTf crystallizes in the monoclinic space group $P2_1/n$ (no. 14) with a = 5.4549(6) Å, b = 6.0582(4) Å, c = 18.339(2) Å

and β = 91.022(9)°, V = 605.71(10) Å^3 and Z = 4. This resembles a superstructure of the previously reported structure doubled in the crystallographic *c* axis. The organic counterparts of the sila-polyethers were found to form stable coordination compounds with the respective salts. This was, for instance, demonstrated upon conversion of EO5 with MOTf (M = Rb^+, Cs^+). The complexes [Rb_3(EO5)OTf_3] and [Cs(EO5)OTf] have successfully been characterized. In conclusion, it is the sila-group in the polyethers, that allows these ligands to act as an efficient crystallization aid without being included in the final compound.

Descriptions of the personal contributions:

Fabian Dankert (F.D.) performed the synthesis, characterization as well as recrystallization of the triflate salts, performed the SC-XRD experiments regarding CsOTf and wrote the manuscript. Johanna Heine (J.H.) contributed to the manuscript preparation and performed the SC-XRD experiments of Cs_2Ox and RbOTf. Julia Rienmüller (J.R.) accomplished the synthesis and characterization of **3**-**6** as well as recrystallized Cs_2Ox as part of a practical course. Carsten von Hänisch (C.v.H) contributed to the manuscript preparation and led the overarching research project.

Dalton Transactions **2018**, *47*, 16393-16397 **#4**

The coordination behaviour and reactivity of partially silicon based crown ethers towards beryllium chloride

Magnus R. Buchner,* Matthias Müller, Fabian Dankert, Kirsten Reuter and Carsten von Hänisch

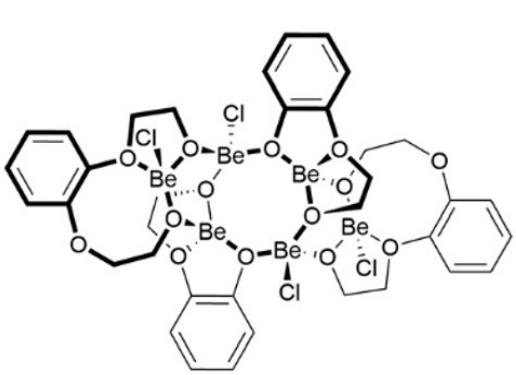

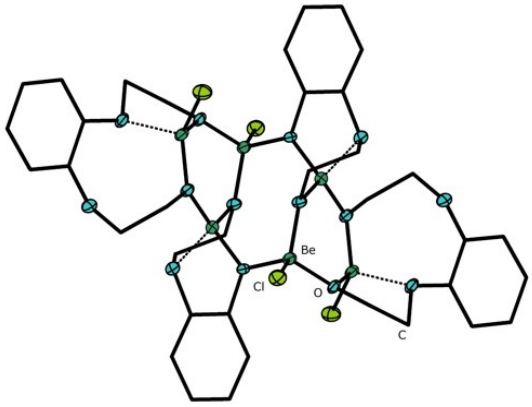

This contribution describes the coordination behaviour of different disila-crown ethers towards beryllium chloride and has been elaborated with the BUCHNER group. In this collaborative research, two compounds have been isolated and characterized which demonstrate that the beryllium salt cleaves the sila-crown ethers 1,2-disila[12]crown-4 and 1,2-disila-benzo[12]crown-4 to hexanuclear coordination compounds with different glycolate ligands. The central coordination motifs in the obtained compounds elucidated by SC-XRD are eight-membered Be–O-heterocycles which are annulated by two six-membered Be–O-cycles. A mechanism for the ligand cleavage has been proposed based on multinuclear NMR spectroscopy. Central parts in this mechanism are an exocyclic coordination of $BeCl_2$ followed by subsequent Si–O bond cleavage reactions under formation of chlorosilanes. In case of 1,2-disila-benzo[12]crown-4 also C–O bond cleavage occurs. The favoured tetrahedral coordination mode around beryllium is most likely a major factor directing the ligands into the observed coordination environments.

Descriptions of the personal contributions:

Magnus R. Buchner (M.R.B.) accomplished the synthesis and characterization of all compounds containing Be, wrote the manuscript including the supporting information and led the overarching research project. Matthias Müller (M.M.) provided $BeCl_2$ and accomplished the single crystal structure determination of compound **4**. Fabian Dankert (F.D.) accomplished the synthesis and characterization of compound **3**, accomplished the single crystal structure determination of compound **5**, contributed to the manuscript preparation and designed the inside back cover. Kirsten Reuter (K.R.) provided different sila-crown ethers. Together with M. R. B., Carsten von Hänisch (C.v.H.) led the overarching research project, gave valuable support and contributed to the manuscript preparation.

Inorganic Chemistry **2019**, *58*, 3518-3526 **#5**

Insights into the Coordination Ability of Siloxanes Employing Partially Silicon Based Crown Ethers: A Comparative Analysis of s-Block Metal Complexes

Fabian Dankert and Carsten von Hänisch*

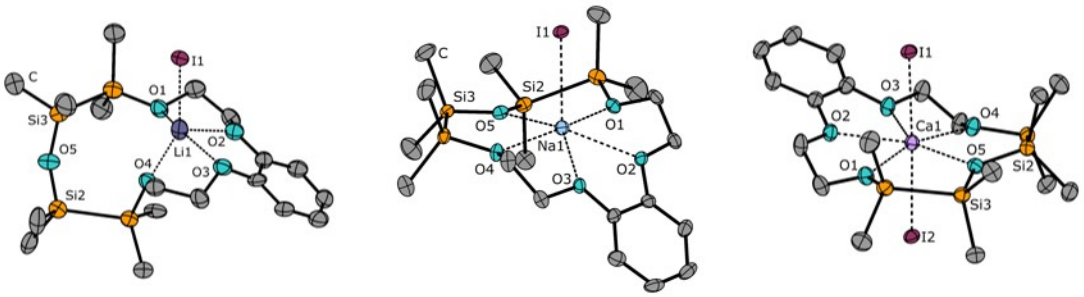

In this contribution the synthesis and coordination chemistry of the partially silicon substituted crown-ether 1,2,4,5-tetrasila-benzo[15]crown-5 is presented. The synthesis of this crown-ether turned out to be successful upon conversion of the corresponding glycol and $(Si_2Me_4Cl)_2O$ in THF in presence of NEt_3. As this ligand is larger than organic [15]crown-5 but smaller than [18]crown-6, a wide range of metal ions can be embedded into the cavity. Conversion of this sila-crown ether with s-block metal iodides allowed obtaining five different complexes showing a good complexation ability of this ligand. [M_A(1,2,4,5-tetrasila-benzo[15]crown-5)I] (M_A = Li^+, Na^+) and [M_{EA}(1,2,4,5-tetrasila-benzo[15]crown-5)I_2] (M_{EA} = Mg^{2+}, Ca^{2+}, Sr^{2+}) could be isolated and characterized, also by means of SC-XRD. The solid state structures show different coordination modes dependent on which cation is used for incorporation. Depending on the ionic radii of the respective cations, the coordination modes of the siloxane backbones are substantially different and it could be shown that these coordination modes can be distinguished with ^{29}Si NMR spectroscopy. Whereas the small Li^+ ion shows no interaction with the siloxane backbone in the solid state and in solution, the Mg^{2+} ion shows weak interactions. Moderate interactions are ob-

served for the larger Na^+ ion and strong interactions are found for Ca^{2+} and Sr^{2+}. In conclusion, those cations which exhibit a hard character and fit perfectly with the cavity of the ligand can activate Si embedded oxygen atoms for effective coordination. As demonstrated in this paper, especially alkaline earth metal ions activate siloxanes for coordination. This argumentation was further strengthened when comparing the complexes [K(1,2,4,5-tetrasila[18]crown-6)PF_6] and [Ba_2(1,2,4,5-tetrasila[18]crown-6)$_2I_4$]. The latter compound has been prepared upon conversion of 1,2,4,5-tetrasila[18]crown-6 with BaI_2. Even though K^+ and Ba^{2+} have almost identical ionic radii at given coordination numbers, it is evident from SC-XRD and ^{29}Si NMR chemical shift, that the attraction between siloxane donors is stronger when an alkaline earth metal is employed for coordination. Moderate interactions are found in [Ba_2(1,2,4,5-tetrasila[18]crown-6)$_2I_4$] whereas no interactions are found in literature known [K(1,2,4,5-tetrasila[18]crown-6)PF_6].

Descriptions of the personal contributions:

Fabian Dankert (F.D.) conducted the synthesis, characterization and crystallization of all compounds, performed the single-crystal X-ray diffraction experiments of the compounds **2**-**6** as well as the refinement of the crystal data and wrote the manuscript. Carsten von Hänisch (C.v.H.) contributed to the manuscript preparation and led the overarching research project.

Chemistry – A European Journal **2019**, *25*, 15934-15943 **#6**

Alkaline Earth Metal Template (Cross-)Coupling Reactions with Hybrid Disila-Crown Ether Analogues

Fabian Dankert, Carsten Donsbach, Julia Rienmüller, Roman M. Richter and Carsten von Hänisch*

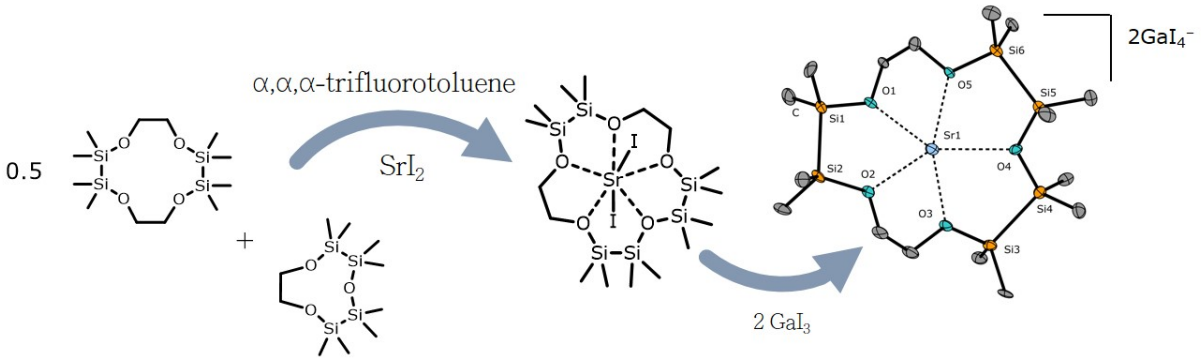

Siloxanes were found to share strong interactions with alkaline earth metal ions. Based on these general findings, various ligand building blocks were reacted with alkaline earth metal iodides at reflux conditions in α,α,α-trifluorotoluene. In this way, template controlled reactions were established and novel silicon-based crown-ethers could be obtained. The reaction of 1,2,7,8-tetrasila[12]crown-4 with 1,2-disila[9]crown-3 in the presence of MgI_2 yielded exclusively [Mg(1,2,7,8-tetrasila[12]crown-4)I_2]. Hence, the Mg^{2+} ion fits well into the cavity of this ligand so there is no driving force for a ring-opening and subsequent reorganization of these ligands. The same reaction with CaI_2 employed yielded [Ca(1,2,7,8-tetrasila[15]crown-5)I_2]. As can be seen by the novel ligand formed, half an equivalent of 1,2,7,8-tetrasila[12]crown-4 is merged with one equivalent of 1,2-disila[9]crown-3. The larger Sr^{2+} cation was used for a similar reaction. By cross-coupling 1,2,7,8-tetrasila[12]crown-4 and 1,2,4,5-tetrasila[9]crown-3 with SrI_2, the first ever hexasila-crown ether could be successfully synthesized and characterized in the form of [Sr(1,2,4,5,10,11-hexasila[15]crown-5)I_2]. This is the first compound bearing more disilane than ethylene units. Three further examples for Sr^{2+} templated synthesis could also be established by

coupling two equivalents of 1,2-disila[9]crown-3, 1,2-disila[12]crown-4 or 1,2-disila-benzo[12]crown-4. After coupling, the compounds [Sr(1,2,10,11-tetrasila[18]crown-6)I_2], [Sr(1,2,13,14-tetrasila[24]crown-8)I_2], and [Sr(1,2,13,14-tetrasila-dibenzo[24]crown-8)I_2] were obtained and successfully characterized. Using various anions, the (cross-)coupled ligands were also observed in suitable X-ray structures within the mentioned complexes. All these ligands could so far not been synthesized by other means. The mechanism behind these reactions was postulated and suggests an exocyclic coordination of the metal center first, before the ligand is ring-opened under formation of a glycolate ligand with terminal iodosilane functionality. The glycolate does then attack a further equivalent of sila-crown building block to eventually form the novel ligand moiety in a template assisted substitution reaction. These template reactions have only been successful employing iodide salts.

Descriptions of the personal contributions:

Fabian Dankert (F.D.) conducted the synthesis, characterization and crystallization of the compounds, performed the single-crystal X-ray diffraction experiments for the compounds **1-3a**, contributed to the X-ray crystallographic data refinement and wrote the manuscript. Carsten Donsbach (C.D.) assisted with the single-crystal structure determination, especially for the compounds **4a-6** and significantly contributed to the refinement of the respective compounds. Julia Rienmüller (J.R.) and Roman M. Richter (R.M.R.) contributed to the synthesis, characterization and crystallization of the compounds **1**, **2**, **2a**, **3** and **3a** as part of a practical course. Carsten von Hänisch (C.v.H.) contributed to the manuscript preparation and led the overarching research project.

Inorganic Chemistry **2019**, *58*, 15417-15422 **#7**

Not Non-Coordinating at All: Coordination Compounds of the Cyclodimethylsiloxanes D_n (D = Me_2SiO; n = 6, 7) and Group 2 Metal Cations

Fabian Dankert, Florian Weigend and
Carsten von Hänisch*

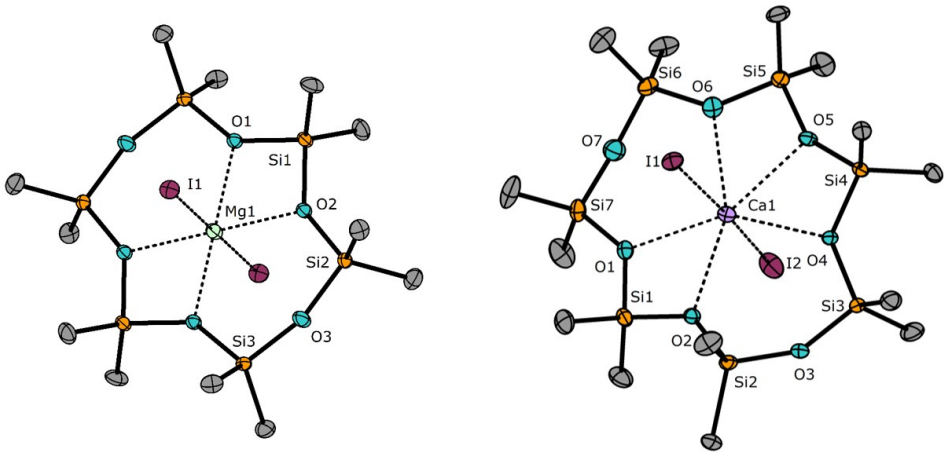

This paper presents the coordination chemistry of D_n ligands towards alkaline earth metal cations. Based on the general findings that alkaline earth metal cations can strongly activate siloxane donors for coordination, alkaline earth metal iodides were reacted with D_6 and D_7. Counterintuitively, the conversion of D_6 with MgI_2 and D_7 with CaI_2 yields indeed stable complexes. $[Mg(D_6)I_2]$ and $[Ca(D_7)I_2]$ have successfully been characterized, also by means of SC-XRD. This shows that the nature of the cation is important and has to be taken into account when it comes to siloxane coordination chemistry. Even though relatively strong iodide salts are employed here, which do also have high lattice energies, stable coordination compounds are obtained. Hence, in terms of early alkaline earth metal cations, there is no necessity of a (bulky) WCA. Upon conversion of D_7 with SrI_2, coordination could only been observed in ^{29}Si NMR spectroscopy in solution when examining a freshly prepared sample of SrI_2 and D_7 in CD_2Cl_2. No X-ray structure

could be obtained and no reaction is observed when BaI_2 is employed for reaction. This revealed a cross-over point where siloxane-coordination of D_n ligands is possible with the relatively strong coordinating iodide anion. To obtain coordination compounds of Sr^{2+} and Ba^{2+}, $M_{EA}I_2$ (M_{EA} = Sr^{2+}, Ba^{2+}) was treated *in-situ* with GaI_3 which serves as an anion acceptor. Conversion of the GaI_4^- salt with D_7 then yielded the compounds $[M_{EA}(D_7)(GaI_4)_2]$. Due to a disorder-problematic, suitable X-ray structures have in both cases only been obtained as aqua complexes $[Sr(D_7)\{GaI_4\}(H_2O)]GaI_4$ and $[Ba(D_7)\{GaI_4\}(H_2O)_{0.94}\{GaI_4\}_{0.06}][GaI_4]_{0.94}$. This resistance against traces of moisture, however, further proofs that the siloxane ligand coordinates reasonably well towards the alkaline earth metal cations. In addition to this experimental work, quantum chemical treatments were carried out based on suited BORN-HABER cycles to clarify why stable complexes were obtained for MgI_2 and CaI_2 but not for SrI_2 and BaI_2 and how matters change when GaI_3 is employed. In agreement with the experiment, negative reaction enthalpies are determined for MgI_2 and CaI_2 when reacted with D_6 and D_7. Reaction enthalpies close to zero are found for SrI_2 and positive reaction enthalpies are found for BaI_2. When GaI_4^- is employed, the formation of complexes is much more favourable as higher energy gains were determined. Hence, also stable complexes with Sr^{2+} and Ba^{2+} were obtained. A small WCA such as GaI_4^- is therefore sufficient for siloxane coordination chemistry with the heavier alkaline earth metals and D_n ligands.

Descriptions of the personal contributions:

Fabian Dankert (F.D.) conducted the synthesis, characterization and crystallization of all compounds, performed the single-crystal X-ray diffraction experiments and wrote the manuscript. Florian Weigend (F.W.) conducted the quantum chemical calculations and contributed to the manuscript preparation. Carsten von Hänisch (C.v.H.) gave valuable support, established the cooperation with F.W. and contributed to the manuscript preparation. Further, C.v.H. led the overarching research project.

Zeitschrift für anorgische und allgemeine Chemie **2020**, *646*, 1501-1507.

C–F Bond Cleavage Reactions with Beryllium, Magnesium, Gallium, Hafnium, and Thorium Halides

#8

Fabian Dankert, H. Lars Deubner, Matthias Müller, Magnus R. Buchner, Florian Kraus and Carsten von Hänisch*

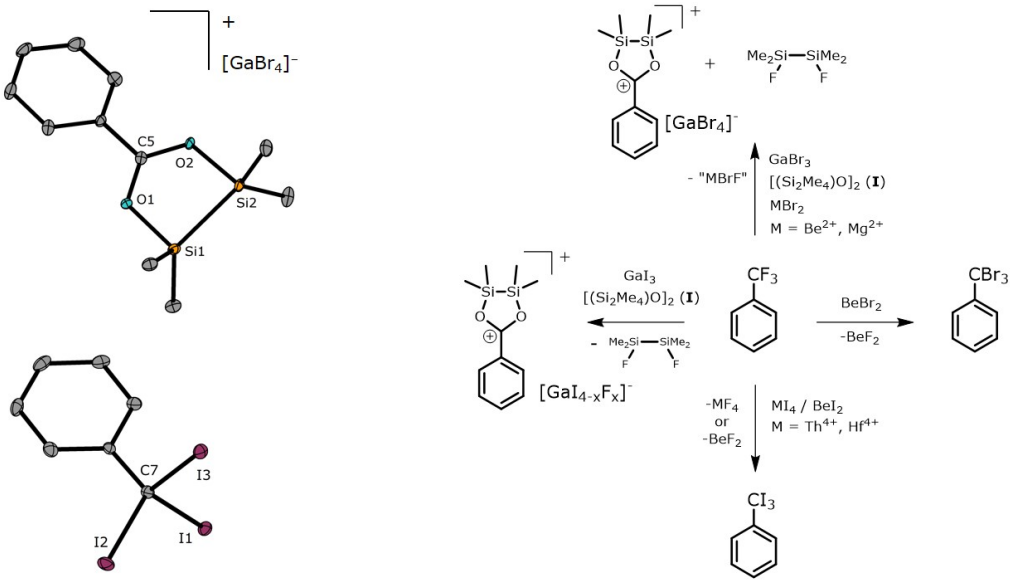

This work presents unexpected stoichiometric C–F bond cleavage reactions. In many reaction protocols, α,α,α-trifluorotoluene has been established as a suitable solvent for siloxane coordination chemistry. Some attempts to obtain siloxane coordination compounds, however, failed due to C–F bond activation. When employing LEWIS acidic systems such as $MBr_2/GaBr_3$ (M = Be^{2+}, Mg^{2+}) or salts with hard cations such as $BeBr_2$, GaI_3, ThI_4 or HfI_4, this solvent is cleaved to form various interesting reaction products. In the presence of $^2D_2$ and $MBr_2/GaBr_3$ (M = Be^{2+}, Mg^{2+}) or neat GaI_3, α,α,α-trifluorotoluene is cleaved to the siloxy-stabilized carbenium compounds [Ph-C($O_2Si_2Me_4$)]GaX_4 (X = Br or X = I/F). Driving force for this reaction is the formation of $(SiMe_2F)_2$ which has been detected by investigating reaction mixtures with ^{29}Si NMR

spectroscopy. If no siloxane is present in the reaction mixture, the CF_3 moiety is deconstructed to a CX_3 moiety (X = Br, I). After α,α,α-trifluorotoluene was reacted with MI_4 (M = Hf^{4+}, Th^{4+}) or BeX_2 (X = Br^-, I^-) a halodefluorination reaction yielded α,α,α-tribromotoluene or α,α,α-triiodotoluene. The mechanism behind the formation of these rare carbenium species has been postulated based on these results. Central parts are C–F bond activation by the respective LEWIS-acids followed by F^--abstraction. The initial formed cation is then stabilized by $^2D_2$ which is itself eventually cleaved to form the respective carbenium ion $[Ph\text{-}C(O_2Si_2Me_4)]^+$ and $(SiMe_2F)_2$. Facile C–F bond cleavage reactions are reported for the Hf^{4+} and Th^{4+} cation for the first time in this contribution.

Descriptions of the personal contributions:

Fabian Dankert (F.D.) conducted the synthesis, characterization and crystallization of compounds **I**, **II**, **1**-**3**, performed the single-crystal X-ray diffraction experiments and wrote the manuscript. H. Lars Deubner (H.L.D.) conducted the synthesis of HfI_4 and ThI_4 and contributed to the manuscript preparation. Matthias Müller (M.M.) synthesized and provided $BeBr_2$. Magnus R. Buchner (M.R.B.) significantly contributed to the NMR spectroscopic part and contributed to the manuscript preparation. Florian Kraus (F.K.) and Carsten von Hänisch (C.v.H.) led the overarching research project and also contributed to the manuscript preparation.

Inorganic Chemistry Frontiers **2020**, *7*, 2138-2153 **#9**

On the molecular architectures of siloxane coordination compounds: (re-)investigating the coordination of the cyclodimethylsiloxanes D_n (n = 5–8) towards alkali metal ions

Fabian Dankert, Lukas Erlemeier, Christian Ritter and Carsten von Hänisch*

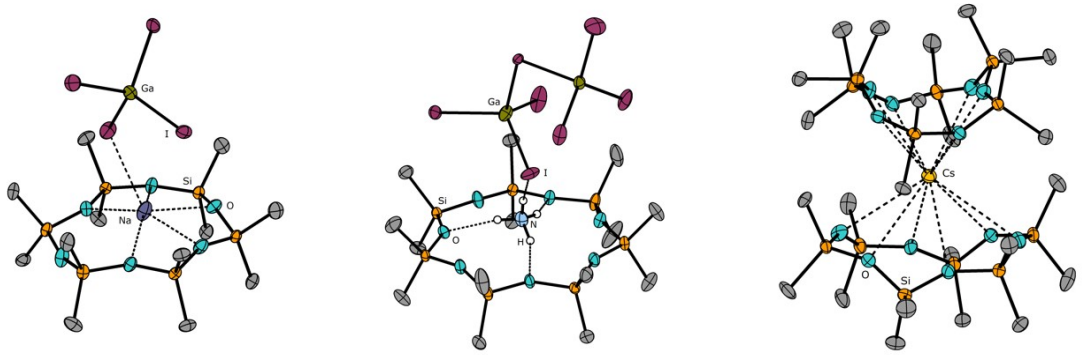

Based on the success obtaining stable D_n alkaline earth metal compounds and employing GaI_4^- as anion, this paper presents a comprehensive study on the molecular architectures of D_n coordination compounds of the alkali metal ions. All alkali metal ions, except for Cs^+, have been incorporated into D_n (n = 5-8) ligands employing the $MI/D_n/GaI_3$ system. The limits of silyl-ether coordination have been explored stepwise. Li^+ has been successfully incorporated into D_5 and D_6 ligands. D_5, however, is highly sensitive towards ring-opening forming D_6. Two respective compounds are isolated and characterized: $[Li_2(D_5)(D_6)(GaI_4)_2]$ and $[Li(D_6)GaI_4]$. The larger Na^+ ion was incorporated into D_6 and D_7. The compounds $[Na(D_6)GaI_4]$ and $[Na(D_7)(DCM)GaI_4]$ were determined by SC-XRD. A coordination of D_7, however, is favoured over that of D_6 which was elucidated by means of ^{29}Si NMR spectroscopy and mass spectrometry. The affinity of D_7 to bind K^+ has been known for a while and thus expectedly $[K(D_7)(DCM)GaI_4]$ was obtained after D_7 was reacted with KI and GaI_3 and subsequently recrystallized from DCM. The limits of this

system to form stable silyl-ether adducts is reached when RbI and GaI_3 were converted with the large cyclic siloxane D_8. Cumbersomely, $[Rb(D_8)(DCM)GaI_4]$ was characterized via an X-ray structure, as well as by means of mass spectrometry, but the compound starts decomposing readily in solution. A caesium compound has not been obtained for GaI_4^- employed as an anion. As this promising $MI/D_n/GaI_3$ system allowed obtaining a series of novel coordination compounds, NH_4^+ was also employed for complex formation. Counterintuitively, the first ever non-metal-cyclosiloxane coordination compound was synthesized in this way. After the conversion of D_6 with NH_4I and GaI_3, the compound $[NH_4(D_7)]Ga_2I_7$ was obtained. At low temperatures, the compound is stable in solution and meaningful spectroscopic data could be provided proving hydrogen bonding interactions of an exclusively silicon based macrocycle and NH_4^+. Hence, no cooperative effects between ethers and silyl-ethers are needed for stabilization. To further investigate the D_n coordination, especially to obtain meaningful spectroscopic data for heavy alkali metal complexes and evaluating the ability of D_n ligands to form sandwich complexes, salts of the weakly coordinating Al_F^- anion have been employed for reaction. The salts MAl_F ($M = K^+$, Rb^+, Cs^+) have been successfully synthesized for this purpose and were converted with various D_n ligands at a given stoichiometry. With this weakly coordinating anion, stable complexes of the type $[M(D_8)Al_F]$ ($M = Rb^+$, Cs^+) were obtained, structurally characterized and silyl-ether coordination was realized also for these heavy alkali metal ions. Finally, when converting an excess of D_5 with KAl_F and D_6 with $CsAl_F$ the complexes $[K(D_5)_2]Al_F$ and $[Cs(D_6)_2]Al_F$ are obtained. These are the first ever characterized sandwich-type complexes bearing a cyclosiloxane ligand.

Descriptions of the personal contributions:

This publication partially represents the bachelor thesis of Lukas Erlemeier (L.E.) which was accomplished under the supervision of Fabian Dankert (F.D.). F.D. conducted the synthesis, characterization and crystallization of compounds **4**, **6-8**, **11** and **12**, performed the single-crystal X-ray diffraction experiments of all compounds, the X-ray crystallographic refinement, designed the outside front-cover of the article and wrote the manuscript. L.E. contributed to the synthesis, characterization and crystallization of the compounds **1-3**, **5**, **8** and **9** as well as the MAl_F ($M = K^+$, Rb^+, Cs^+) salts. Christian Ritter (C.R.) contributed to the X-ray crystallographic refinement.

Carsten von Hänisch (C.v.H.) also supervised the bachelor thesis of L.E., contributed to the manuscript preparation and led the overarching research project.

Important note:

During the refereeing process for this paper, a closely related and in part overlapping publication describing the syntheses and structures of $M[Al(OR^F)_4]$ ($M = K^+, Rb^+$) did appear in the journal *Dalton Transactions*. The reference is: P. J. Malinowski, T. Jaroń, M. Domańska, J. M. Slattery, M. Schmitt and I. Krossing, *Dalton Trans.*, 2020,**49**, 7766-7773. DOI: 10.1039/D0DT00592D.

European Journal of Inorganic Chemistry **2020**, *2020*, 2744-2756 **#10**

Chalcogen Bonding of SO_2 and s-Block Metal Iodides Near Room Temperature: A Remarkable Structural Diversity

Fabian Dankert,[#] Anne Feyh,[#] and
Carsten von Hänisch*

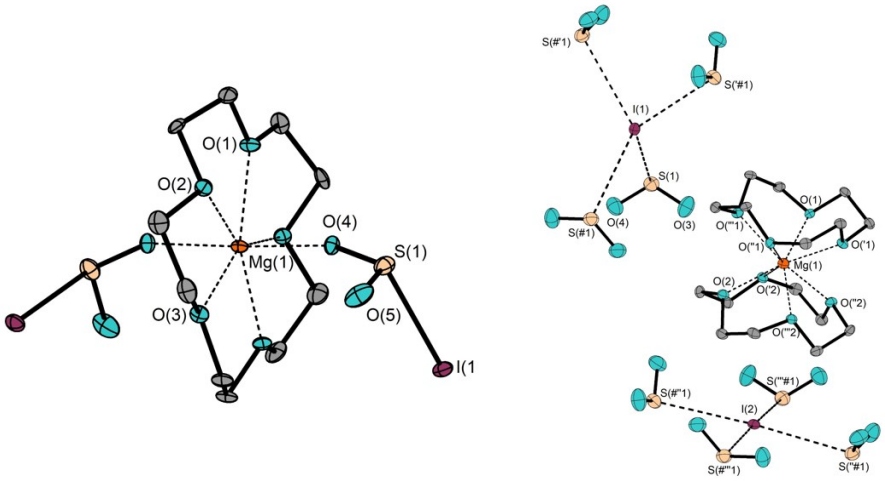

Based on the promising results regarding s-block metal chloride solvation with SO_2, this paper presents the solvation of SO_2 towards s-block metal iodides. This contribution therefore contributes to the recent discussion around chalcogen bonds rather than siloxane-coordination chemistry. These bonds have been purposefully realized by reacting s-block metal iodides with SO_2 in the presence of a crown-ether. Chalcogen bonding between I^- and SO_2 was established to form one-dimensional networks in the compounds [Li([12]crown-4)H_2O]I·SO_2, [Na([15]crown-5)(SO_2)I], [K([18]crown-6)(SO_2)I], [NH_4([18]crown-6)]I·SO_2, [Rb([18]crown-6)I(SO_2)]·2SO_2 and [Cs([18]crown-6)(SO_2)$_2$I] all of which were obtained by 1:1 complexation of the respective iodide salt and crown-ether in liquid SO_2. Two-dimensional networks were obtained in the alkaline earth compounds [Mg([12]crown-4)$_2$]I_2·4SO_2 and [Ba_2([18]crown-6)$_2$(SO_2I)(SO_2)$_2$$I_3$]·$SO_2$.

Beside these network compounds, also structures have been determined by SC-XRD which show the formation of the rare iodosulfite ion. The S···I atom distances found in this study (<300pm) are substantially shorter than those reported in literature. Thus, structural more precise details for this anion are provided and its structure is revisited. This anion was observed in the compounds $[Na([12]crown\text{-}4)_2]ISO_2$, $[Mg([15]crown\text{-}5)(ISO_2)_2]$ and $[Ca_2([18]crown\text{-}6)(SO_2I)_3]I_3$ as well as the aforementioned barium compound. One more compound is obtained which shows an SO_2 adduct of the composition $[I_2(SO_2)_5]^{2-}$. This is found to be present in $[Na([12]crown\text{-}4)_2]I{\cdot}2.75SO_2$. As can be seen by the number of obtained and characterized compounds, large organocations, such as formed by crown-ether complexes allows obtaining stable compounds for structural analysis at room temperature. One-and two-dimensional coordination polymers are observed in these compounds which, in conclusion, are determined by the respective chalcogen bonds. Thus, non-covalent $O_2S{\cdots}I^-$ interactions are strong enough to determine the crystal packing and dimensionality. In general, this chemistry reminds of that of poly-(pseudo)halides.

Descriptions of the personal contributions:

This publication partially represents the thesis (so called "Examensarbeit für das Lehramt an Gymnasien") of Anne Feyh (A.F.) which was accomplished under the supervision of Fabian Dankert (F.D.). A.F. conducted the synthesis and characterization of all compounds and contributed to interpretations. F.D. performed the single-crystal X-ray diffraction experiments of all compounds, the X-ray crystallographic refinement and wrote the manuscript. Carsten von Hänisch (C.v.H.) contributed to the manuscript preparation and led the overarching research project.

Inorganic Chemistry **2020** (*accepted article*) **#11**

A Second Modification of Beryllium Bromide: β-BeBr2

Magnus R. Buchner,* Fabian Dankert, Nils Spang, Florian Pielnhofer, and Carsten von Hänisch*

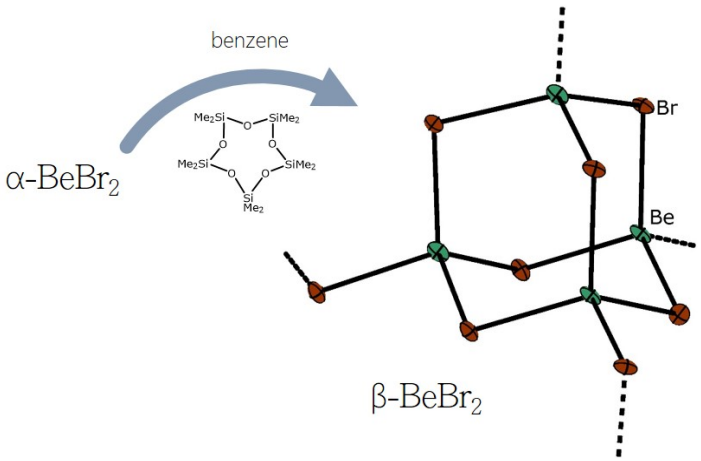

This contribution describes the serendipitous crystallization of β-$BeBr_2$ from benzene solution in the presence of D_5. When α-$BeBr_2$ is reacted with D_5 in benzene, the salt partially dissolves in the solvent. By time, block-shaped single crystals of β-$BeBr_2$ are then obtained which were suitable for SC-XRD. β-$BeBr_2$ crystallizes in the tetragonal space group $I4_1/acd$ (No. 142) with a = 11.2117(7), c = 19.2922(13) and Z = 32 and is thus isostructural to β-$BeCl_2$ and β-BeI_2. Further characterized has β-$BeBr_2$ by means of IR and Raman spectroscopy. Measured spectra compare reasonably well with calculated ones. This phase of $BeBr_2$ was unknown to date and various attempts to obtain and/or observe this phase, e.g. *via* variable temperature powder X-ray diffraction, failed. Thus the possibility of D_n ligands to act as a solubilizer and crystallization aid is extraordinarily demonstrated here.

Descriptions of the personal contributions:

This is a collaborative work of the groups BUCHNER and VON HÄNISCH. Magnus R. Buchner (M.R.B.) wrote the manuscript including the supporting information, led the overarching research project and gave Fabian Dankert (F.D.) valuable insights into beryllium chemistry. F. D. conducted the synthesis and crystallization of β-$BeBr_2$, performed the single-crystal X-ray diffraction experiment, refined the respective reflection data and contributed to the manuscript preparation. Nils Spang (N.S.) gave F.D. valuable insights into beryllium chemistry (especially laboratory procedures), conducted the characterization by means of IR- and Raman spectroscopy and contributed to the manuscript preparation. Florian Pielnhofer (F.P.) performed the quantum chemical calculations and contributed to the manuscript preparation. Carsten von Hänisch (C.v.H.) did also lead the overarching research project.

submitted manuscript **2020** **#12**

Architecting inorganic crown-ethers by s-block-metal templated Si-O bond activation

Fabian Dankert, Roman M. Richter, Florian Weigend,* Xiulan Xie, Markus Balmer, and Carsten von Hänisch*

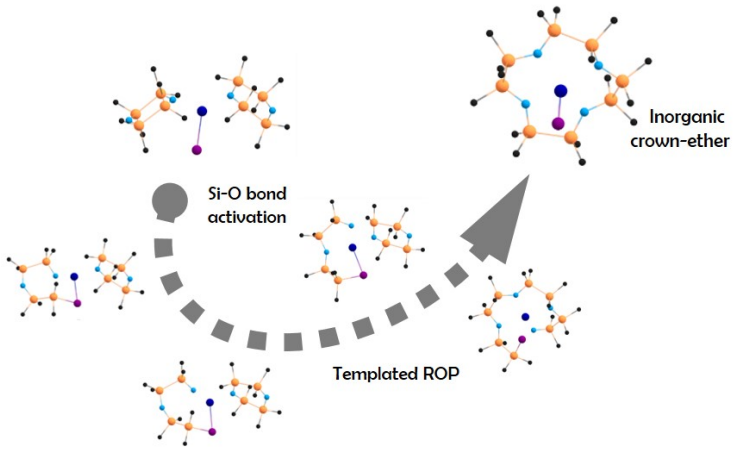

In this work, the template approach was successfully transferred to exclusively silicon-based ligands. Employing a *Lewis*-acidic s-block metal iodide/GaI_3 system allowed obtaining various complexes of unprecedented ligand systems when $^2D_2$ is used as a precursor for ring-opening oligomerization. By conversion of $^2D_2$ with *in situ* generated $M(GaI_4)_n$ we could observe the formation of $^2D_3$ for M = Li^+ (n = 1) whereas M = Na^+, Mg^{2+}, Ca^{2+} and Sr^{2+} (n = 1 or 2) form $^2D_4$. The coordination compounds $[Li(^2D_3)GaI_4]$ and $[M(^2D_4)(GaI_4)_2]$ were successfully characterized by means of multinuclear NMR spectroscopy and, except for the Mg^{2+} species also by means of SC-XRD. The Mg^{2+} species was found to be extraordinarily sensitive towards traces of moisture. Hence, also the proton complex $[H(^2D_3)]Ga_2I_7$ could successfully be characterized. A crucial step in the formation of these compounds is an exocyclic coordination of M^{n+} which is evident from an obtained X-ray structure $[Li_2(^2D_2)(GaI_4)_2]$. Exocyclic coordination indicates Si-O bond elongation and a smaller Si-O bond angle. Hence, Si-O bond activation occurs before ring-opening and

the above mentioned compounds are obtained. As long as the template is bound within the ligand moiety, these compounds are stable in solution which was elucidated by means of DOSY NMR studies. When it is removed, however, also higher oligomers can be observed by means of LIFDI$^+$ MS spectrometry. All free ligand species, however are unstable and react back to the monomer $^2D_2$ proving that this ring-opening is reversible. To shed light on the binding ability of such ligands and to understand the mechanism behind these template reactions, meticulous quantum chemical calculations were performed. As calculated for Li^+ and Na^+ as examples, energies of exchange reactions calculated by means of density functional theory show that M^+ is bound stronger to $^2D_4$ or D_6 than to $^2D_3$ or D_5, the former being nearly competitive to the organic crown ethers [3n]-crown-n (n = 4-6). The binding of M^+ to $^2D_2$ is clearly de-preferred. The mechanism behind these template reactions suggests an exocyclic Si-O bond activation which is also found in the experiment. Then, iodosilane-formation occurs under Si-O bond cleavage and simultaneous formation of a silanolate end-group. Template-driven, the silanolate attacks a second equivalent of $^2D_2$ which is then brought into a suitable conformation for ring-closure. Backbiting forms an Si-O bond and an iodide anion is released from the silane. The sila-crown ether is eventually formed.

Descriptions of the personal contributions:

This is a collaborative work of the VON HÄNISCH group and Florian WEIGEND (F.W.). Fabian Dankert (F.D.) conducted the synthesis, characterization and SC-XRD experiments of all compounds. Further, F.D. wrote the manuscript and accomplished the solution and refinement of the reflection data of all compounds except that of compound **1**. Roman-Malte Richter (R.M.R.) contributed to the synthesis, characterization and crystallization of the compounds **I**, **II**, **1**, **4** and **4a** as part of a practical course. F.W. performed the quantum chemical calculations and contributed to the manuscript preparation. Xiulan Xie (X.X.) performed the DOSY NMR experiments and contributed to the NMR spectroscopic part of the manuscript. M. Balmer (M.B.) significantly assisted with the solution and refinement of the reflection data of compound **1**. Carsten von Hänisch (C.v.H.) established the cooperation with F.W., contributed to the manuscript preparation and led the overarching research project.

4 Unpublished Results

4.1 Attempts Synthesizing Disila-Crown Ethers from Disila-Bridged Glycols

As was demonstrated in publication **#1**, the synthesis and characterization of two disila-bridged polyethylene glycols was successfully performed. This is true for di- (=EO2) and triethylene glycol (EO3) employed in the reaction. When similar reaction conditions were employed and two equivalents of ethylene glycol were reacted with $Si_2Me_4Cl_2$, however, no disila-bridged polyethylene glycol could be obtained. This is due to rapid formation of 1,2,7,8-tetrasila[12]crown-4 and further, slight impurities which is evident from ^{29}Si NMR chemical shift. The respective resonance of 1,2,7,8-tetrasila[12]crown-4 is found at 10.8 ppm in deuterated dichloromethane and was also observed for the main product of the above-mentioned reaction reaction.[201] Hence, 8,9-disila-EO5 and 11,12-disila-EO7 could successfully be characterized but not 5,6-disila-EO3 (Scheme 10). To further functionalize these glycols and to obtain silicon-rich crown-ether analogues, the ligands 8,9-disila-EO5 and 11,12-disila-EO7 were planned to be converted with two equivalents of NEt_3 and $(Si_2Me_4Cl)_2O$. Unfortunately, the synthesis of crown-ethers failed. It turned out that the open-chained species are instable toward base addition as elimination of glycol and intramolecular ring-closure occurs.

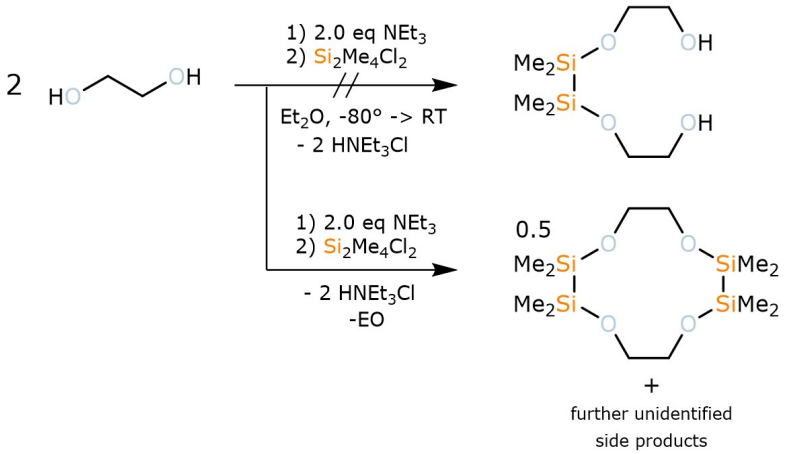

Scheme 10: Attempted synthesis of 5,6-disila-EO3 and observed pathway.

This could be shown for 8,9-disila-EO5 as an example. ^{1}H, ^{13}C and ^{29}Si NMR spectroscopy compare well with those published in publication **#3**. The decomposition of 8,9-disila-EO5 in the presence of NEt_3 is drawn in Scheme 11 (left). An initial step here might be the formation of $HNEt_3^+$(8,9-disila-EO5$^-$) which is in equilibrium with NEt_3 and 8,9-disila-EO5.

With Cs_2CO_3, another base was evaluated. This approach, however, resulted in a complete destruction of the ligand system which is most likely due to H_2O formation. In ref.[202], ligands bearing a tetrasila-moiety were determined to be stable towards H_2O. In this attempted synthesis, however, H_2O leads to a complete deconstruction. As demonstrated in Scheme 11 (right), 8,9-disila-EO5 and $(Si_2Me_4Cl)_2O$ are most likely deconstructed to [Cs(EO2)Cl] and $^{2}D_2$. After workup, exclusively $^{2}D_2$ was found to be present. This compound was elucidated by means of SC-XRD and multinuclear NMR spectroscopy. Both were in accordance with those reported in the publications **#8** and **#12**.

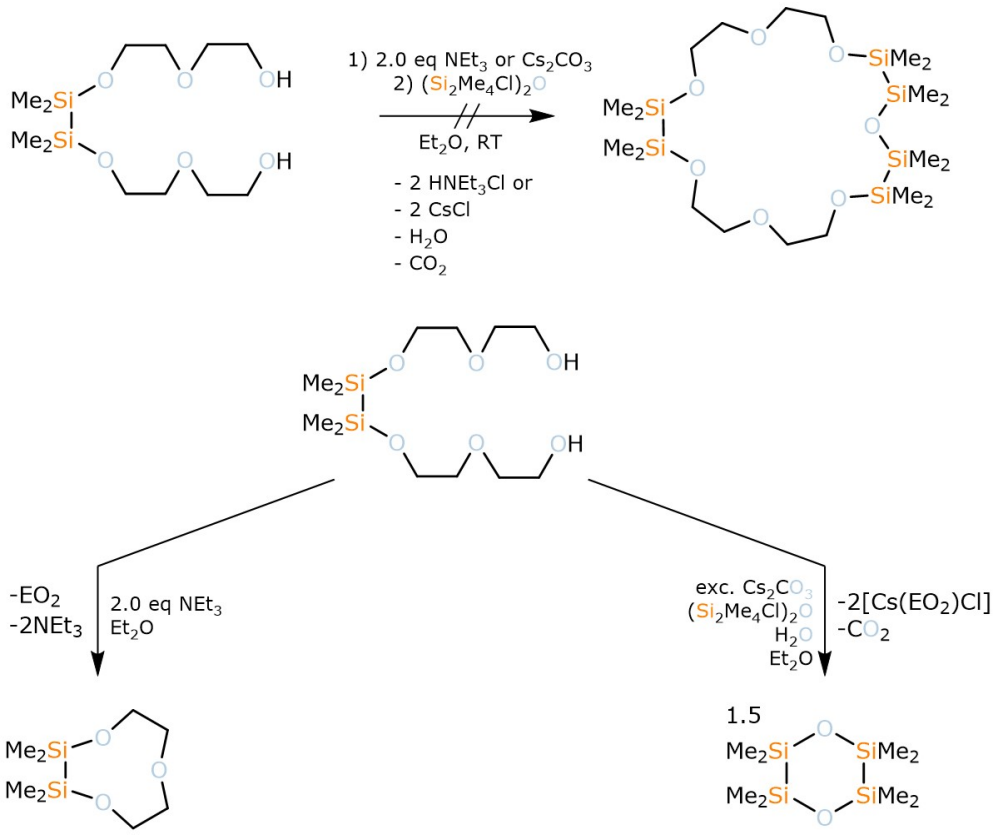

Scheme 11: Attempted synthesis of a hexasila-crown ether and observed problematic upon base addition and H_2O sensitivity.

Hence, also this synthesis route is not expedient. As a last option to obtain sila-crown ethers from disila-polyethylene glycols, it was also tried to directly convert the obtained complexes of publication **#1** with $(Si_2Me_4Cl)_2O$ in DCM. So far, however, no reaction was observed.

Even though the synthesis of sila-crown ethers failed following the presented routes, these results clearly show the problems with "conventional" synthetic approaches. The template approach has thus been established as an elegant way to bypass the given problematics.

4.2 The Reactivity of Be-Salts Towards Exclusively Si-Based Systems

As was demonstrated in a number of publications, early s-block metal ions share strong interactions with siloxane donors. In case of the early alkaline earth meal ions, even salts with a relatively strong iodide ion were successfully embedded into D_n ligands. Further, the publications of this thesis show that the Si-O bond can be effectively activated for coordination and ring-opening reactions. Thus, it was clear that the beryllium ion should also be investigated concerning siloxane coordination chemistry. As shown in publication **#4**, hybrid disila-crown ethers are deconstructed to glycolates. Hence, the reactivity of BeX_2 (X = Cl^-, Br^-, I^-) was also investigated towards D_n ligands as well as $^2D_2$ to obtain exclusively silicon-based system. Preliminary results are presented in this chapter.

The first attempts coordinating a siloxane ligand toward BeX_2 (X = Br^-, I^-) failed. By investigating the reaction of $D_{5/6}$ with BeX_2 in C_6D_6, no significant conversion of the metal salt is observed. As demonstrated in publication **#11**, solely recrystallization of β-BeX_2 is observed and a new phase of $BeBr_2$ is about to be published. Things are different when BeX_2 is converted with the more basic siloxane D_3.

Table 2: NMR chemical shifts [ppm] after conversion of D_3 with BeX_2 (1:1 ratio, *J. Young* NMR tube after 9 days) in C_6D_6. The chemical shift after 9 days was chosen here, as a freshly prepared sample of D_3+$BeCl_2$ shows no conversion.

nucleus	$BeCl_2$	$BeBr_2$	BeI_2
^1H	0.29 (s)	0.41 (s)	0.99 (s)
^9Be	0.91 (br, s)	1.10 (br, s)	1.49+6.45 (s+br, s)
$^{13}C\{^1H\}$	3.7 (s)	5.7 (s)	9.9 (s)
^{29}Si	7.3 (s)	4.3 (s)	2.0 (s)

The siloxane has a small cavity which is why an exocyclic coordination mode of Be^{2+} is feasible. When examining an equimolar reaction of BeX_2 with D_3 in C_6D_6 solution in an NMR tube, indeed conversion can be observed. The observed chemical shifts for selected NMR active nuclei are summarized in table 2. When comparing these resonances with other siloxane coordination compounds such as the alkaline earth metal complexes published in publication **#7**, it becomes clear that the beryllium salts react differently. They prefer the formation of species with tetrahedral coordinated beryllium which is evident from ^{9}Be chemical shift. ^{29}Si NMR chemical shift shows a low-field chemical shift which indicates strong interactions of the siloxane linkage with the hard beryllium ions but taking the ^{13}C chemical shift into account, it is, however, evident that the structures formed, cannot be cyclic siloxanes coordinating a LEWIS acid. The range of ^{13}C chemical shift for cyclic siloxanes coordinating to M^{2+} (M = Mg–Ba) is the following: 1.4 to 2.2 ppm (see publication **#7**). Despite the fact, that NMR spectra were recorded in CD_2Cl_2 rather than C_6D_6, the ^{13}C chemical shift in C_6D_6 is not expected to shift up to 7 ppm, which is observed upon conversion of D_3 with BeI_2. Hence, one can carefully conclude, that the species formed in solution are no siloxane coordination compounds bearing a cyclic siloxane. To substantiate the whole argumentation, it would be nice to have an X-ray structure of the respective species. An X-ray structure, however, was only been obtained for the product upon converting D_3 with BeI_2. Colourless blocks suitable for SC-XRD are obtained after about one week in the NMR tube. As elucidated by means of SC-XRD, the trinuclear species $[Be_3(\mu\text{-}OSiMe_2I)_4I_2]$ (**1**$^{\text{unp}}$) is obtained. The D_3 moiety is deconstructed to iodosiloxanato ligands which compares well with the observations made in solution (see also Scheme 12).

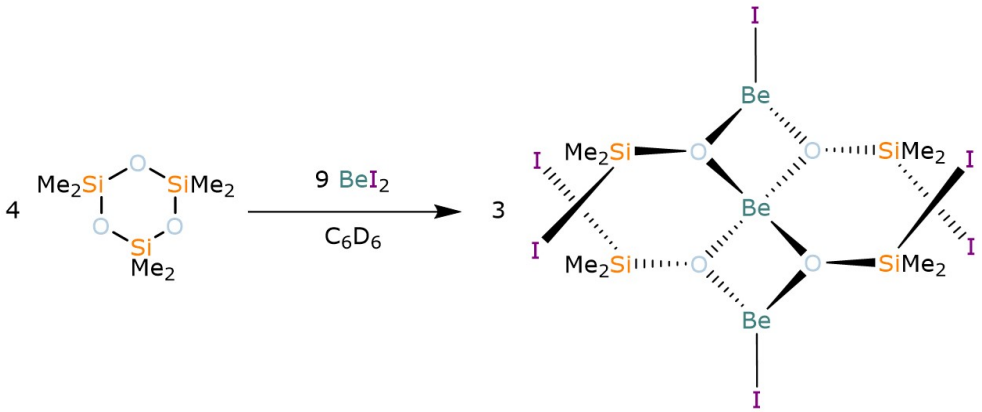

Scheme 12: Observed reaction of BeI_2 with D_3.

Interestingly, the solid state structure (see Figure 28) shows three-coordinated beryllium atoms. Given that two resonances in the ^{9}Be NMR are are found, it is most likely that solid state structure and structure in solution are indeed consistent. This X-ray structure is a first example which shows the proposed Si–I bond in ring-opening polymerizations initiated with early s-block metal iodides.

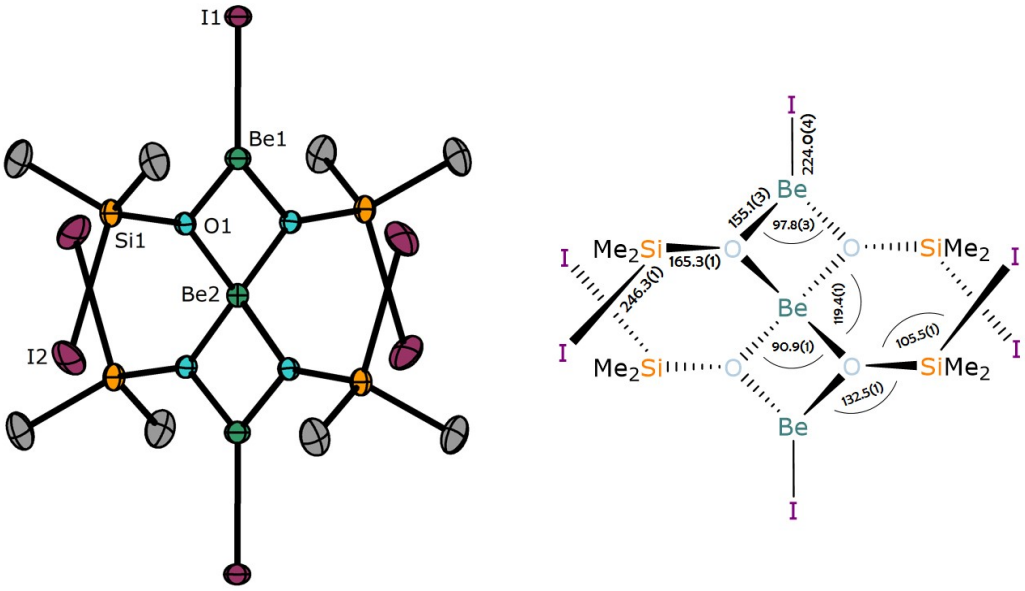

Figure 28: The molecular structures of $[Be_3(\mu\text{-}OSiMe_2I)_4I_2]$ in the crystal (left) and selected geometric features of this trinuclear complex. Bond lengths/angles are depicted in [pm]/[°]. Non-labelled atoms are symmetry generated using 1-x, 1-y, z; 1-y, x, 1-z and y, 1-x, 1-z. Thermal ellipsoids set at 50% probability.

Taking the observed X-ray structure and observed chemical shifts, especially a single resonance in ^{9}Be-NMR, into account it is most likely that BeX_2 (X = Cl^-, Br^-) might form the following species in solution: $[Be(\mu\text{-}OSiMe_2X)_2]_n$ (For X = Cl: **2**^{unp}, X = Br: **3**^{unp}). As broad resonances are observed and the signal to noise ratio is quite poor, however, isostructural compounds to compound **1**^{unp} might also be present in solution. Further investigations, especially long-term NMR spectroscopy could give further insides. As these results are dependent from the cooperation partners of the Be-laboratory, the partners might then also carefully manipulate the reaction mixtures, e.g. by carefully removing the solvent. In this way, single crystals for the bromo and chloro species

might also be obtained in the near future. The examination of the coordination behaviour of D_n systems towards beryllium salts is at an early stage, so further studies are underway.

First compounds were also obtained when $^2D_2$ was reacted with BeX_2 (X = Cl^-, Br^-, I^-), so advances have also been achieved with disila-ligands. The NMR spectroscopic investigation does unfortunately not give a clear view on the species formed in solution. Unfortunately, all chemical shifts are outside an expected range for siloxane coordination chemistry (table 3). Hence, also when $^2D_2$ is employed for chemical reaction, no sila-crown ether formation or $RSiMe_2O\cdots Be^{2+}$ coordination can be observed in solution. The observed range could hint for either Si-O bond cleavage or the formation of the respective halidosilanes $(SiMe_2X)_2$ (X = Cl^-, Br^-, I^-). The latter might have been published in literature[211,212] but ^{29}Si NMR chemical shift is missing in case of (X = Br^-, I^-). Further, ^{1}H and ^{13}C NMR chemical shift have been published but do not compare with the values found within this study.

Table 3: NMR chemical shifts [ppm] after conversion of $^2D_2$ with BeX_2 (1:1 ratio, *J. Young* NMR tube after different reaction periods) in C_6D_6.

time period	nucleus	$BeCl_2$	$BeBr_2$	BeI_2
2 days	^{1}H	0.27 (s)*, 0.33 (s)	0.27 (s)*, 0.47 (s)	0.27 (s)*, 0.56 (s), 0.66 (s), 0.99 (s)
	^{9}Be	2.11 (br, s)**	1.33 (s), 2.05 (s), 2.89 (s)	0.84 (s), 1.60 (s), 7.58 (br, s)**
	^{13}C{^{1}H}	2.6 (s)*, 1.0 (s)	2.5 (s)*, 0.8 (s)	0.6 (s), 2.5 (s)*, 2.6 (s), 3.7 (s)
	^{29}Si	3.3 (s)*, 17.5 (s)	3,3 (s)*, 10.6 (s)	-12.3 (s), -7.84 (s), 3.33 (s)*, 12.9 (s)
9 days	^{1}H	0.26 (s)*, 0.33 (s)	0.26 (s), 0.27 (s)*, 0.48 (s), 0.52 (s)	0.27 (s)*, 0.66 (s)
	^{9}Be	2.16 (br, s)**	1.33 (s), 1.97 (s), 2.89 (s)	0.85 (s), 1.17 (s), 1.66 (br)
	^{13}C{^{1}H}	2.6 (s)*, 1.0 (s)	0.8 (s), 1.28 (s), 1.7 (s), 2.5 (s)*	0.6 (s), 2.5 (s)*
	^{29}Si	3.2 (s)*, 17.3 (s)	2.2 (s), 3.2 (s) 10.4 (s), 11.7 (s)	-12.5 (s), 3.2 (s)*

* resonance referring to $^2D_2$

** very poor signal to noise ratio

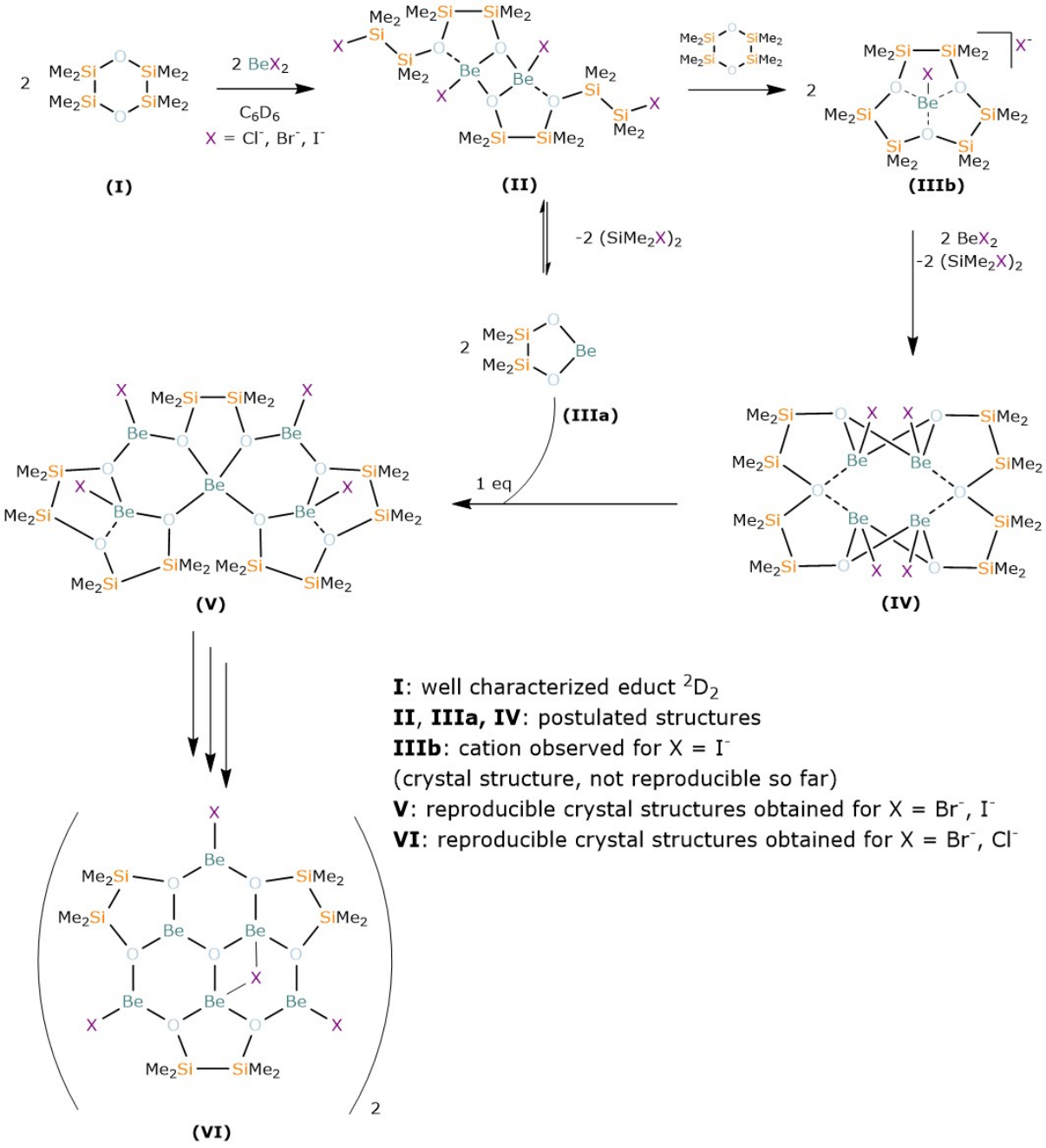

Scheme 13: Proposed and partially simplified mechanism for the deconstruction of $^2D_2$ with BeX_2.

Suspiciously, though, is the ^{29}Si NMR chemical shift of 17.5 ppm after conversion of $BeCl_2$ with $^2D_2$. This resonance compares reasonably well with values found for $(SiMe_2Cl)_2$ (see publication **#4**). Hence, a more sophisticated study on the chemical shift of halidosilanes should be performed to verify halidosilane or silanolate formation. At this point, however one can solely con-

clude that in all three cases, as evident from ^{1}H, $^{13}C\{^{1}H\}$, ^{9}Be and ^{29}Si NMR chemical shift, conversion clearly takes place. What species are present in solution remains unclear. Please note that these are preliminary results and a more sophisticated analysis has not yet been performed. Luckily, single crystals were obtained for all performed reactions. Indeed, Si-O bond cleavage occurs in all cases. Mainly two different structure motifs are observed which lets one conclude that the deconstruction of $^{2}D_2$ is independent from the metal salt as it follows the same reaction path. Based on the obtained X-ray structures, a strongly simplified mechanism for the deconstruction of $^{2}D_2$ with BeX_2 salts is drawn in Scheme 13. As drawn here, $^{2}D_2$ (**I**) is ring-opened by the beryllium salt (see **II**) to form a silanolate (**III**a) or a $^{2}D_3$ ligand moiety (**III**b) next. The cation of **III**b was once observed in an X-ray structure. Due to the fact that the formation of this ligand with BeX_2 could not be reproduced, a representation is studiously avoided though. **II**, **III**a and **IV** represent postulated structures which are plausible intermediates which eventually lead to the formation of compound **V**.

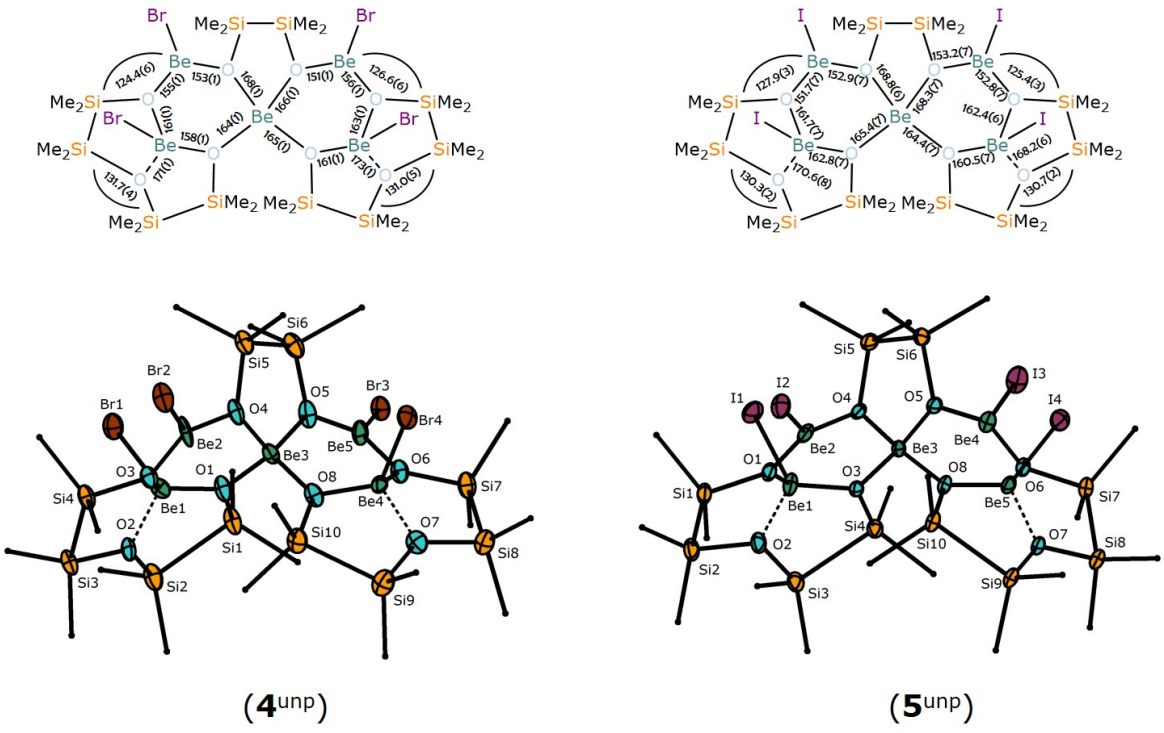

Figure 29: Geometric features and the molecular structures of pentanuclear beryllium complexes with silanolato ligands in crystal form. Bond lengths/angles are depicted in [pm]/[°]. Co-crystalline C_6D_6 molecules are omitted and carbon atoms depicted as wires/sticks for clarity. Thermal ellipsoids set at 50% probability.

V is a pentanuclear beryllium compound which consists of two beryllo-sila-crown ether moieties as well as a bridging disilanolate ligand. Central structural motif here are two six-membered Be-O cycles which form a spiro compound. This molecular structure in the crystal has been obtained for BeX_2 (X = Br^-: $\mathbf{4}^{unp}$, X = I^-: $\mathbf{5}^{unp}$). The compounds have an intact siloxane-moiety which is why siloxane coordination towards the beryllium ion could be observed for the first time here. Hence, with these obtained compounds, all s-block metal ions except for the radioactive ones could successfully coordinated to neutral siloxane donors. The geometric features of the compounds are displayed in figure 29. In case of BeX_2 (X = Cl^-, Br^-) further single crystal structures could be determined.

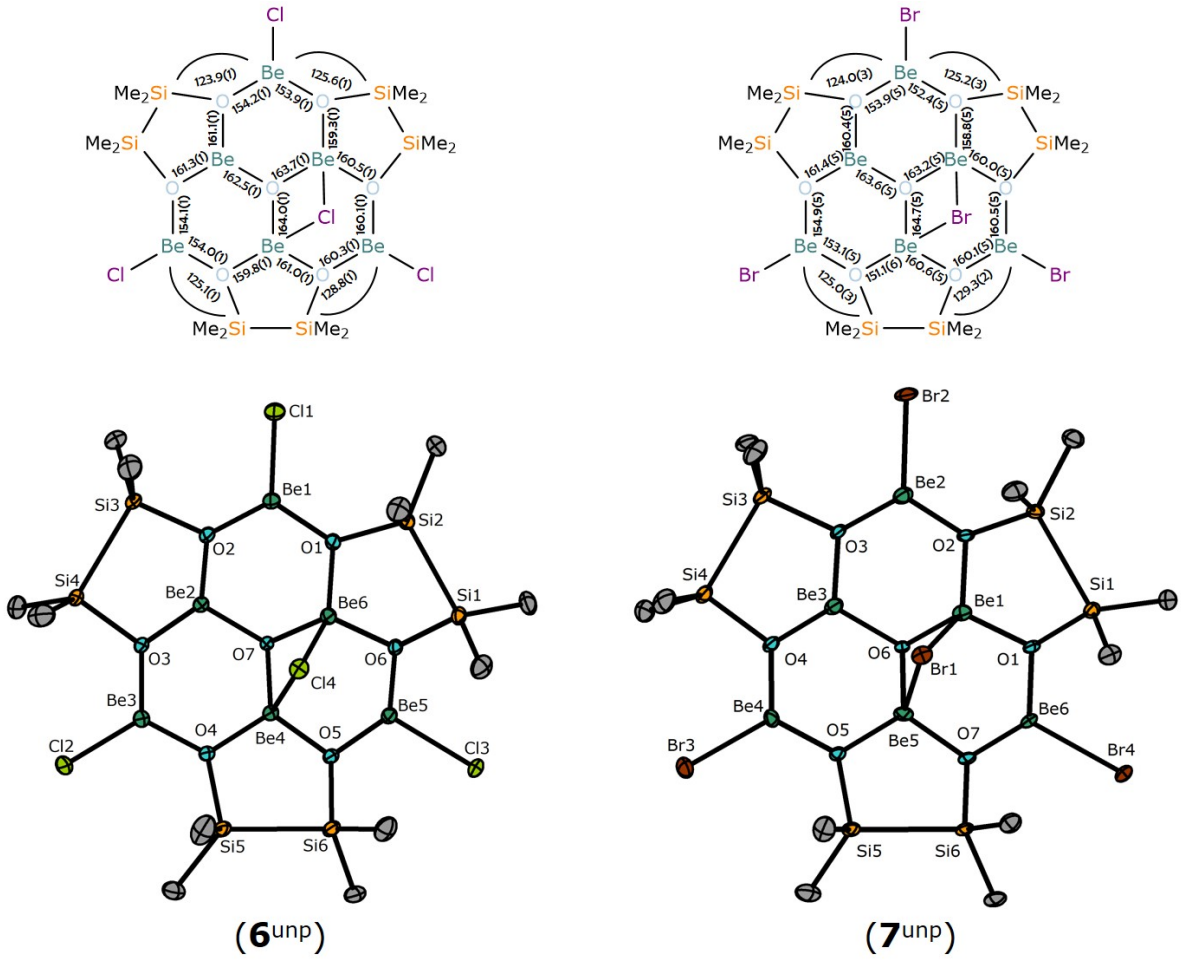

Figure 30: Geometric features and the molecular structures of the monomers of a dodecanuclear beryllium complex in crystal form. Bond lengths/angles are depicted in [pm]/[°]. Co-crystalline C_6D_6 molecules are omitted for clarity. Thermal ellipsoids set at 50% probability.

The oxophilic Be^{2+} ion deconstructs the siloxane to an extent: disiloxanato ligands are formed which find themselves in dodecanuclear cluster compounds **6**^{unp} (X = Cl^-) and **7**^{unp} (X = Br^-) which anon follow the structure motif **VI** (Scheme **13**). Half a molecule of these cluster compounds consist of three $Me_4Si_2O_2^{2-}$ ligands which are attached to three Be-O six-membered cycles (Figure 30). The symmetry generated parts of the respective structure, find themselves inverted on top of this cluster unit (Figure 31). The connection between the cluster units is build by terminal halide ligands as well as a central O^{2-} ion. The O^{2-} ion shows that even $Me_4Si_2O_2^{2-}$ units are partially deconstructed. These dodecanuclear cluster compounds are two very rare examples of large Be-O cluster compounds.

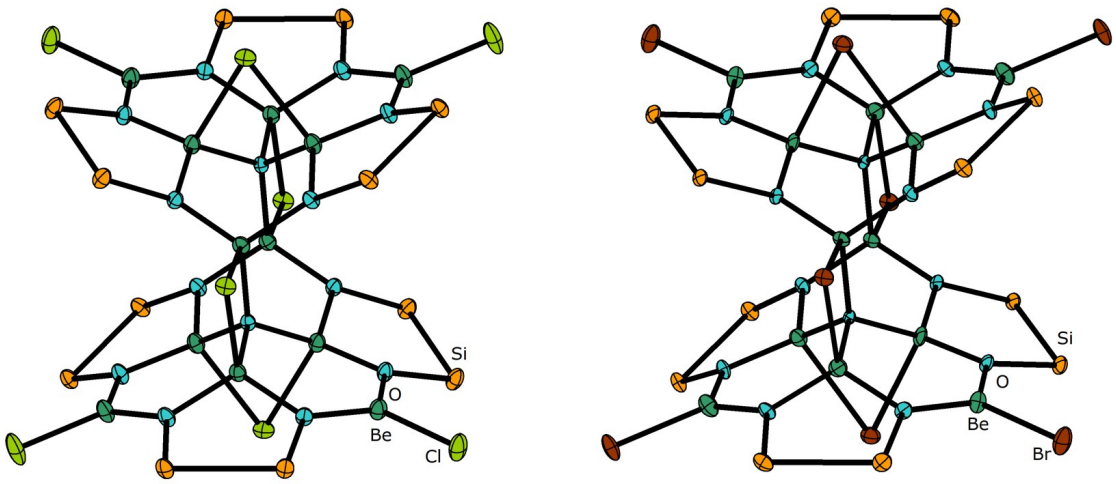

Figure 31: Molecular structures of dodecanuclear beryllium complexes in crystal form. The structures are reduced to the inorganic skeleton and co-crystalline C_6D_6 molecules are omitted for clarity. Thermal ellipsoids set at 50% probability.

To sum up the beryllium chemistry at this point, interesting new compounds have been elucidated by means of X-ray crystallography. The first neutral siloxane···Be^{2+} contact has been established and first insights of the reaction behaviour of beryllium salts towards different siloxane systems could be provided. The results presented herein, especially berylliums tendency to form large Be-O cluster systems, might not inevitably give insights into siloxane coordination chemistry but might give valuable insights for metal induced immune responses.[213] The behaviour in

solution, however, is not yet fully understood which is why further investigations are necessary. Clear is, that a cascade of substitution reactions must take place to form these unprecedented coordination compounds. Further studies are underway with the endeavour to publish these results in chemistry-related peer-reviewed journals in the near future.

4.3 Experimental Section

Note: The experimental section is reduced to the beryllium chemistry. A reaction protocol for both compounds, 1,2-disila[9]crown-3 and $^2D_2$ had already been published and the compounds have been examined by means of multinuclear NMR spectroscopy as well as SC-XRD in case of $^2D_2$. Please see publications **#3**, **#8** and **#12**. The depicted pathways were just mentioned to demonstrate for what sake disila-bridged polyethylene glycols were synthesized at first.

General information regarding Be-chemistry: All work was carried out excluding moisture and air in an atmosphere of dried and purified argon (5.0, Praxair) using vacuum glass lines and a glovebox (MBraun). Solvents were dried and freshly distilled before use. Berylliumhalides were synthesized and provided by the BUCHNER group. All further work was performed by the thesis author F. DANKERT except for recording the NMR spectra which was done by M. R. BUCHNER. The laboratory work was supervised by N. SPANG and M. R. BUCHNER due to safety reasons. Please further note:

Caution! Beryllium and its compounds are regarded as toxic and carcinogenic. As the biochemical mechanisms that cause beryllium associated diseases are still unknown, special (safety) precautions are strongly advised.[214] Due to the expected extreme toxicity of the beryllium compounds no elemental analysis or mass spectrometry could be performed of these compounds. The NMR spectroscopic data of all compounds are already summarized in tables **2** and **3**.

Synthesis of compounds ***1^{unp}–3^{unp}***: A 10 mg portion of BeX_2 (0.13 mmol for X = Cl^-, 0.06 mmol for X = Br^-, 0.04 mmol for X = I^-) together with D_3 (29 mg, 0.13 mmol for X = Cl^-; 14 mg, 0.06 mmol for X = Br^-; 9 mg, 0.04 mmol for X = I^-) are placed in a *J. Young* NMR tube. Subsequently 0.6 mL of C_6D_6 are added. The resulting suspension is sonicated for at least 30

min. and is then kept at ambient temperature for several days. In this time period, colourless blocks were obtained for compound **1**^{unp} at the bottom of the tube. In case of **2**^{unp} and **3**^{unp}, almost clear solutions are obtained. So far no single crystals were obtained for these species.

Synthesis of compounds ***4***^{unp}*–****7***^{unp}: A 10 mg portion of BeX_2 (0.13 mmol for X = Cl^-, 0.06 mmol for X = Br^-, 0.04 mmol for X = I^-) together with $^2D_2$ (33 mg, 0.13 mmol for X = Cl^-; 16 mg, 0.06 mmol for X = Br^-; 10 mg, 0.04 mmol for X = I^-) are placed in a *J. Young* NMR tube. Subsequently 0.6 mL of C_6D_6 are added. The resulting suspension is sonicated for at least 30 min. and is then kept at ambient temperature for several days. In different time periods, single crystals of **4**^{unp}–**7**^{unp} are obtained at the bottom of the tube. **4**^{unp} and **5**^{unp} are obtained as colourless platelets whereas **6**^{unp} and **7**^{unp} are obtained as colourless needles.

4.4 Crystal Structure Data

Single crystal X-ray diffraction experiments were carried out on a *Bruker* D8 Quest diffractometer at 100(2) K with MoKα radiation and respective X-ray optics (λ = 0.71073). All structures were solved by direct methods and refinement with full-matrix-least-squares against F^2 using SHELXT- and SHELXL-2015 on OLEX2 platform.[215–217] The respective crystal data and selected experimental parameters of the structure determinations are summarized in Tables 4 and 5.

Table 4: Selected crystal structure data of the structure determinations of the compounds **1^{unp}**, **4^{unp}**·C_6D_6, and **5^{unp}**·C_6D_6.

Compound	**1^{unp}**	**4^{unp}**·C_6D_6	**5^{unp}**·$3C_6D_6$
Empirical formula	$C_8H_{24}Be_3I_6O_4Si_4$	$C_{26}H_{66}Be_5Br_4O_8Si_{10}$*	$C_{38}H_{78}Be_5I_4O_8Si_{10}$
Formula weight	1085.06	1152.37	1496.55
Crystal colour, habit	colourless, block	colourless, platelet	colourless, platelet
Temperature/K	100(2)	100(2)	100(2)
Crystal system	tetragonal	monoclinic	monoclinic
Space group	*I*-42*m*	$P2_1/c$	$P2_1/c$
a/Å	10.1534(5)	12.894(3)	13.0397(8)
b/Å	10.1534(5)	39.350(8)	39.761(2)
c/Å	14.8717(9)	12.880(3)	13.1403(7)
α/°	90	90	90
β/°	90	117.978(5)	105.019(2)
γ/°	90	90	90
Volume/Å^3	1533.15(18)	5771(2)	6580.1(6)
Z	2	4	4
ϱ_{calc}g/cm^3	2.350	1.326	1.511
μ/mm^{-1}	6.244	3.030	2.115
F(000)	980.0	2344.0	2968.0
Crystal size/mm^3	0.348 × 0.182 × 0.179	0.321 × 0.109 × 0.08	0.252 × 0.202 × 0.118
Radiation	MoKα (λ = 0.71073)	MoKα (λ = 0.71073)	MoKα (λ = 0.71073)
2Θ range for data collection/°	4.858 to 61.134	4.738 to 50.962	3.828 to 52.864
Reflections collected	12302	47385	130188
Independent reflections	1248 [R_{int} = 0.0291, R_{sigma} = 0.0150]	10342 [R_{int} = 0.0839, R_{sigma} = 0.0825]	13528 [R_{int} = 0.0394, R_{sigma} = 0.0230]
Data/restraints/parameters	1248/0/40	10342/0/495	13528/0/606
Goodness-of-fit on F^2	1.116	1.107	1.294
Final R indexes [I>=2σ (I)]	R_1 = 0.0098, wR_2 = 0.0208	R_1 = 0.0992, wR_2 = 0.2317	R_1 = 0.0466, wR_2 = 0.0939
Final R indexes [all data]	R_1 = 0.0102, wR_2 = 0.0208	R_1 = 0.1169, wR_2 = 0.2389	R_1 = 0.0522, wR_2 = 0.0954
Largest diff. peak/hole / e Å^{-3}	0.37/-0.32	2.12/-0.83	1.99/-1.19
Absolute structure parameter	0.005(8)	-	-

*The SQUEEZE implementation was applied.

Table 5: Selected crystal structure data of the structure determinations of the compounds **1**^{unp}, **4**^{unp}·C_6D_6, and **5**^{unp}·C_6D_6.

Compound	**6**^{unp}·C_6D_6	**7**^{unp}·C_6D_6
Empirical formula	$C_{36}H_{84}Be_{12}Cl_8O_{14}Si_{12}$	$C_{36}H_{84}Be_{12}Br_8O_{14}Si_{12}$
Formula weight	1481.90	1837.58
Crystal colour, habit	colourless, needle	colourless, needle
Temperature/K	100(2)	100(2)
Crystal system	monoclinic	monoclinic
Space group	$P2_1/c$	$P2_1/c$
a/Å	12.8020(11)	12.640(3)
b/Å	24.359(2)	12.098(3)
c/Å	12.1211(8)	24.857(7)
α/°	90	90
β/°	98.080(2)	99.122(7)
γ/°	90	90
Volume/Å^3	3742.4(5)	3753.1(17)
Z	2	2
ϱ_{calc}g/cm^3	1.315	1.626
μ/mm^{-1}	0.540	4.513
F(000)	1528.0	1816.0
Crystal size/mm^3	0.617 × 0.257 × 0.138	0.17 × 0.09 × 0.04
Radiation	MoKα (λ = 0.71073)	MoKα (λ = 0.71073)
2Θ range for data collection/°	4.638 to 56.784	4.27 to 50.744
Reflections collected	168816	59631
Independent reflections	9374 [R_{int} = 0.0481, R_{sig-ma} = 0.0173]	6854 [R_{int} = 0.0603, R_{sig-ma} = 0.0297]
Data/restraints/parameters	9374/0/383	6854/0/382
Goodness-of-fit on F^2	1.075	1.146
Final R indexes [I>=2σ (I)]	R_1 = 0.0256, wR_2 = 0.0609	R_1 = 0.0377, wR_2 = 0.0781
Final R indexes [all data]	R_1 = 0.0316, wR_2 = 0.0630	R_1 = 0.0480, wR_2 = 0.0810
Largest diff. peak/hole / e Å^{-3}	0.41/-0.28	1.04/-0.66
Absolute structure parameter	-	-

5 Summary

In starting to summarize the results of this thesis, the following sections are reasonable. Results according to the synthesis and coordination chemistry of silicon-rich crown-ether analogues based on disilanes are presented first. The second part summarizes the results regarding the coordination chemistry of D_n ligands. A third part is represented by siloxane coordination chemistry regarding beryllium halides. Beryllium chemistry had been established as a logical extension due to presented results in the first two parts. Important note: The order of the presented results deviates from that presented in the cumulative part (chapter 5) and unpublished results are included.

5.1 Contributions to the Coordination Chemistry of Disila-Crown Ethers

The synthesis of disila-bridged polyethylene glycols has been successfully performed following the reaction protocol displayed in Scheme 14. The reaction was successful for di- and triethylene glycol at but not for ethylene glycol (=EO). 8,9-disila-EO5 and 10,11-disila-EO7 have been characterized by means of multinuclear NMR spectroscopy as well as MS spectrometry.

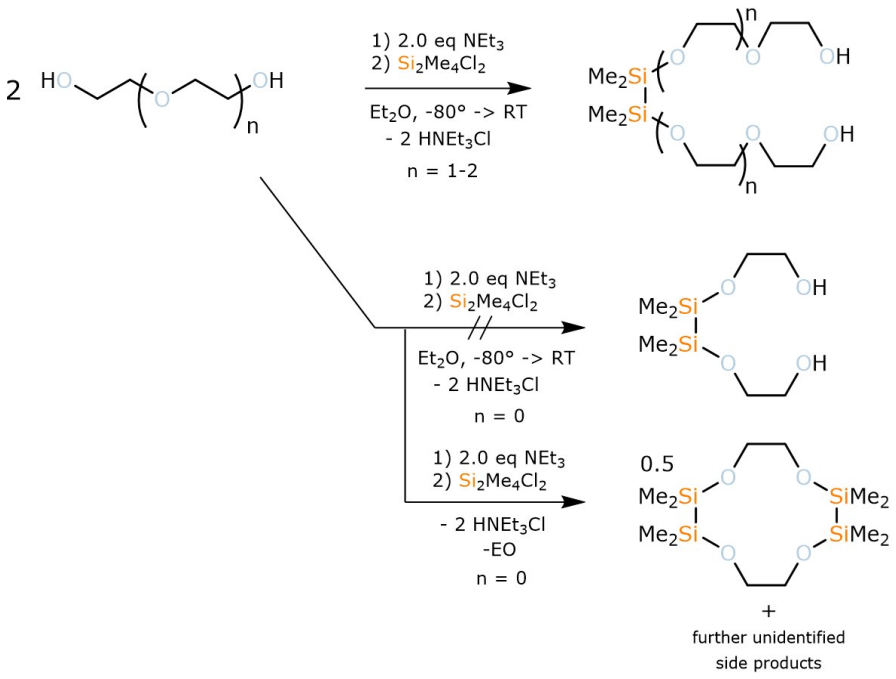

Scheme 14: Successful and unsuccessful syntheses of a respective disila-bridged glycol.

The attempt to use these glycols for the synthesis of hexasila-crown ethers failed. The problematic lays in the deconstruction of the ligand moiety in the presence of a base such as NEt_3 or Cs_2CO_3 (Scheme 15, top). Hence, a subsequent reaction of a disila-glycol with $(Si_2Me_4Cl)_2O$ could not be performed. This strategy to obtain more silicon-rich crown-ethers might have failed, but these ligands opened up for a structural study on various coordination compounds and showed an interesting reactivity towards various metal ions (Scheme 15, bottom).

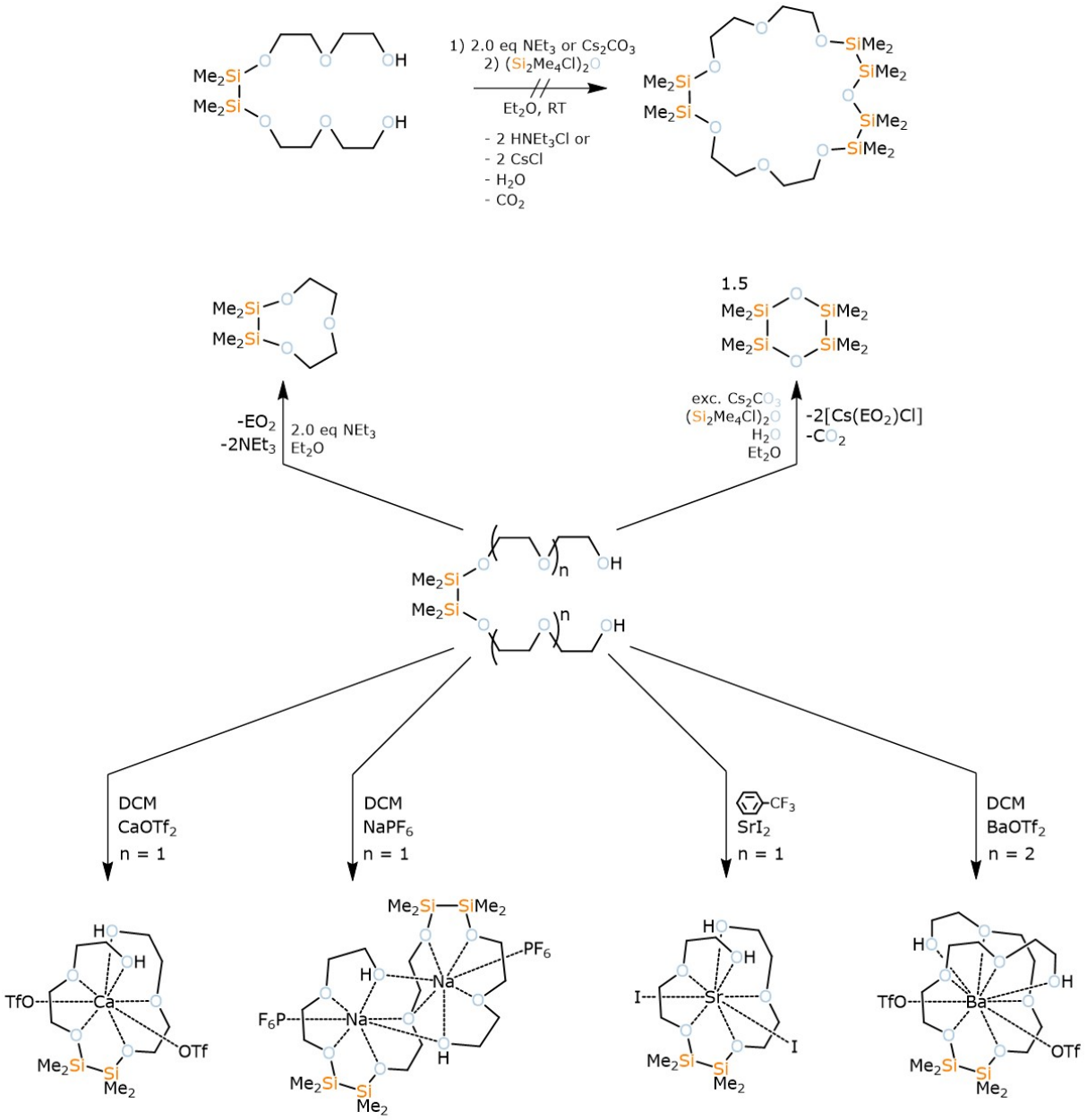

Scheme 15: Attempted synthesis of a hexasila-crown ether and the coordination chemistry of disila-bridged glycols (selected examples).

The depicted coordination compounds could all been observed in suitable X-ray structures showing the successful synthesis of the ligands on the one hand and on the other hand, that also open-chained ligands can form stable adducts with various s-block metal cations (see also Figure 32). Special attention aroused the reaction of $NaPF_6$ with 8,9-disila-EO5. Under elimination of one equivalent of EO2 a tetrasila-octaethylene glycol unit was obtained which coordinates two Na^+ ions. The coordination geometry around the Na^+ ions is coplanar, showing that the symmetric arrangement of the oxygen donors has most likely been the driving force for the formation of this ligand. The coordination pattern is similar to that of 1,2-disila[15]crown-5. This has been the first example of a template-driven reaction proving that also disila-ligands can in principle be activated for (ring-)opening oligomerization.

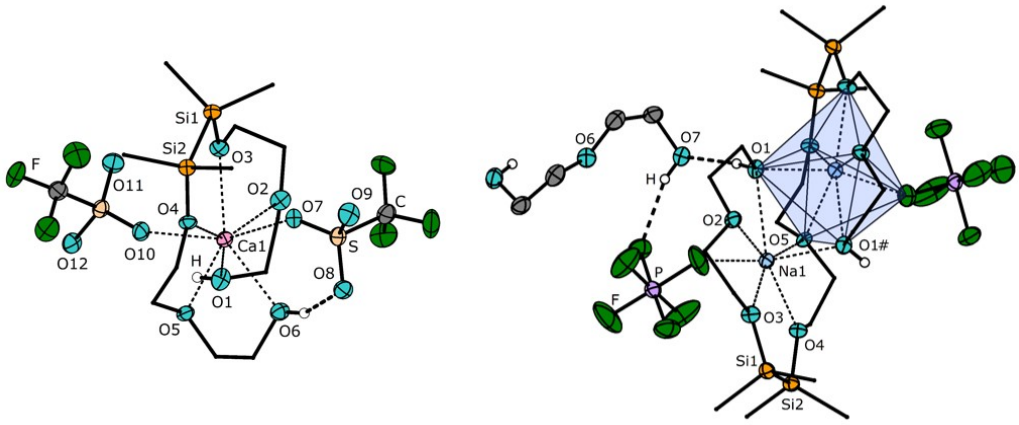

Figure 32: The molecular structures of [Ca(8,9-disila-EO5)$(OTf)_2$] and [Na_2(8,9,17,18-tetrasila-EO8)$(PF_6)_2$]·EO2 in the crystal: Two examples of disila-glycols coordinating s-block metal ions. Carbon atoms are partially depicted as wires/sticks for clarity. Thermal ellipsoids set at 50% probability.

Whereas stable complexes were obtained for the cations Na^+, Ca^{2+}–Ba^{2+}, no stable complexes were obtained for Cs^+. Conversion of 10,11-disila-EO7 with CsOTf in DCM yields a colourless solution proving that the ligand dissolves the salt in an organic solvent. However, removal of the solvent did not yield a respective coordination compound but crystalline α-CsOTf. First evidence is given here, that disila-ligands show an ion selectivity for hard s-block metal ions. Indeed quantum chemical calculations could confirm this assumption. Strong interactions of the silicon-backbone are observed for M_{EA}^{2+} (M_{EA} = Ca^{2+}, Sr^{2+}) but not for Cs^+. To substantiate this ion selectivity and

to evaluate if it is possible to somehow incorporate heavy alkali-metal compounds into hybrid disila-ligands, MOTf (M = Rb^+, Cs^+) had been converted with different ligands such as 8,9-disila-EO5, 11,12-disila-EO7 or 1,2,10,11-tetrasila[18]crown-6. In all cases, however, the reaction failed as expected. Interestingly, the reaction allowed the recrystallization of the respective triflate salt from the solvent DCM. Hence, it was possible to determine the single-crystal structures of these salts. The crystal structures of these salts had previously been elucidated by means of powder X-ray diffraction. Single-crystal structure determination could not yet been successfully performed due to disorder problems, hygroscopic nature of the salts and poor crystal quality in general. The combination of a sila-polyether, an inert-atmosphere and weakly coordinating solvent such as DCM allowed obtaining suitable crystals for SC-XRD. In this way, the crystal structures of these triflate salts could be confirmed by SC-XRD. In case of CsOTf, the general findings of a previous study were not only confirmed but also expanded. Single crystal structure analysis allowed us to determine that α-CsOTf crystallizes in the monoclinic space group $P2_1/n$ (no. 14) with a = 5.4549(6) Å, b = 6.0582(4) Å, c = 18.339(2) Å and β = 91.022(9)°, V = 605.71(10) $Å^3$ and Z = 4. This resembles a superstructure of the previously reported structure doubled in the crystallographic *c* axis (Figure 33).

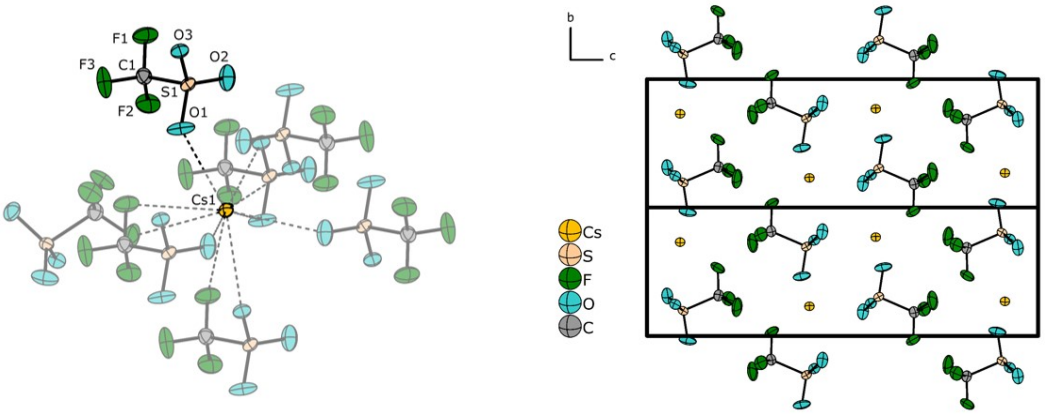

Figure 33: The structure of CsOTf in crystal form at 100K. Left: Coordination sphere around Cs^+ and right: Cell package depicted as a supercell along [100]. Thermal ellipsoids set at 50% probability.

The recrystallization method is not restricted to triflate salts. Also the crystal structure of Cs_2Ox ($Ox = C_2O_4^{2-}$) could be determined after recrystallizing in this way. To demonstrate the necessity of a sila-polyether, heavy alkali-metal triflates were converted with all-carbon polyethers. For instance, the reaction of EO5 with MOTf ($M = Rb^+$, Cs^+) yields the complexes $[Rb_3(EO5)OTf_3]$ and [Cs(EO5)OTf]. Hence, it is the sila-group in the polyethers, that allows these ligands to act as an efficient crystallization aid without being included in the final compound. 8,9-disila-EO5, 11,12-disila-EO7 and 1,2,10,11-tetrasila[18]crown-6 can act as a solubilizer and promote recrystallization of heavy alkali metal compounds. Taking these observations into account, hybrid disila-ligands coordinate strongly toward early and thus hard s-block metal salts but not heavy and thus soft alkali metal compounds. A remaining question was at this point of course how hybrid disila-ligands behave regarding hydrogen-bonding situations. Establishing hydrogen bonding and incorporation of a guest turned out to be successful in the use of ammonium hexafluorophosphate as the salt and 1,2-disila[18]crown-6 as well as 1,2-disila-benzo[18]crown-6 as the ligands of choice. The reaction of 1,2-disila[18]crown-6 and 1,2-disila-benzo[18]crown-6 with NH_4PF_6 in DCM turned out to be successful (Scheme 16). It was shown by means of NMR and IR spectroscopy, that the ammonium ion had successfully been incorporated in the centre of the crown-ether. Low-field shift in ^{29}Si NMR is observed and according to IR spectroscopy, three instead of only one N–H stretching vibrations are observed in both compounds. These show significant redfield shifts in comparison to free NH_4PF_6. In addition, the single crystal structures of the complexes $[NH_4(1,2\text{-disila}[18]\text{crown-}6)]PF_6$ and $[NH_4(1,2\text{-disila-benzo}[18]\text{crown-}6)]PF_6$ were successfully determined (Figure 34).

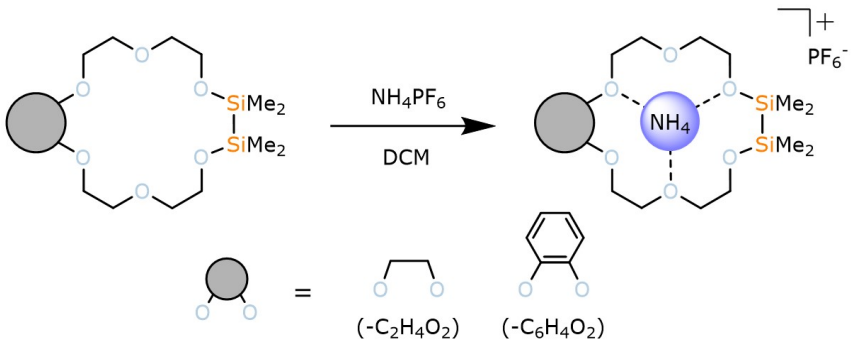

Scheme 16: Synthesis of NH_4^+ complexes of hybrid disila-crown ethers.

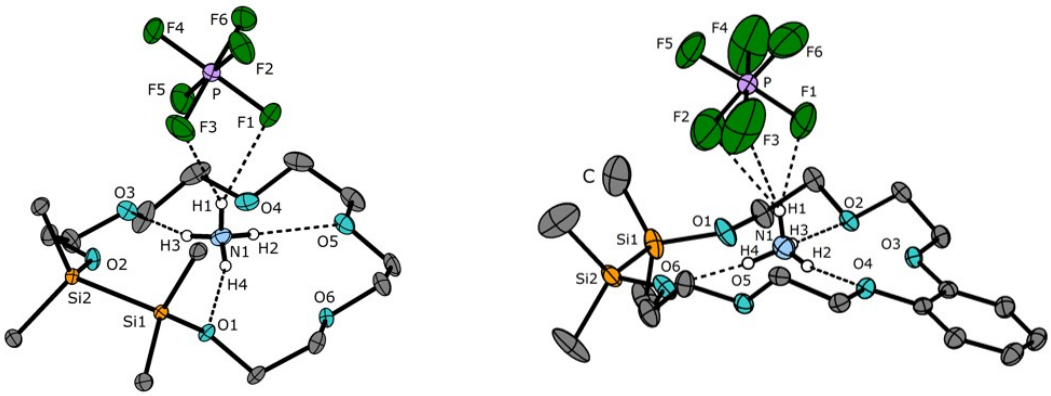

Figure 34: Two disila-crown ether complexes showing hydrogen bonding interactions: $[NH_4$(1,2-disila-[18]crown-6)$]PF_6$ and $[NH_4$(1,2-disila-[18]crown-6)$]PF_6$ in crystal form. Thermal ellipsoids set at 50% probability. Co-crystalline DCM molecules are omitted for clarity.

Taking the results of this thesis as well as those of past works into account, hybrid disila-ligands show a tendency to bind the alkali metal ions Na^+-K^+, the pseudo alkali metal ion NH_4^+ and the alkaline-earth metal ions Mg^{2+}-Ba^{2+}. An ion selectivity towards early, hard s-block metal ions is indicated. The next step in understanding siloxane-donors was of course to evaluate how different s-block cations can activate a $(Si_2Me_4)_2O$ linkage for coordination and if a similar tendency towards coordination of the early s-block metal ions is also found here. The synthesis of 1,2,4,5-tetrasila-benzo[15]crown-5 was successfully performed by conversion of the respective glycol with $(Si_2Me_4Cl)_2O$ in the presence of NEt_3 in THF (Scheme 17, top). Due to the great availability and based on earlier success to incorporate these salts into various ligands, s-block metal iodides have been chosen for incorporation into this ligand. Indeed the conversion of various s-block metal iodides turned out to be successful and the respective 1:1 complexes were obtained after equimolar reaction of ligand and salt in α,α,α-trifluorotoluene (Scheme 17, bottom). All coordination compounds could be observed in suitable X-ray structures. Depending on the ionic radii, different coordination modes are observed which could be well-represented by means of ^{29}Si NMR in solution. The NMR experiment turned out to be a very good indicator for the strength of interaction between a metal ion and the siloxane backbone as the chemical shift reacts very sensitive toward coordination. So does Li^+ share no interaction with the siloxane oxygen at-

om, Mg^{2+} shares weak interactions, Na^{+} shares moderate interactions and Ca^{2+}/Sr^{2+} share strong interactions (Figure 35). Taking these observations depicted in Figure 35 into account, such cations which exhibit a hard character and fit perfectly with the cavity of the ligand can activate Si embedded oxygen atoms for effective coordination.

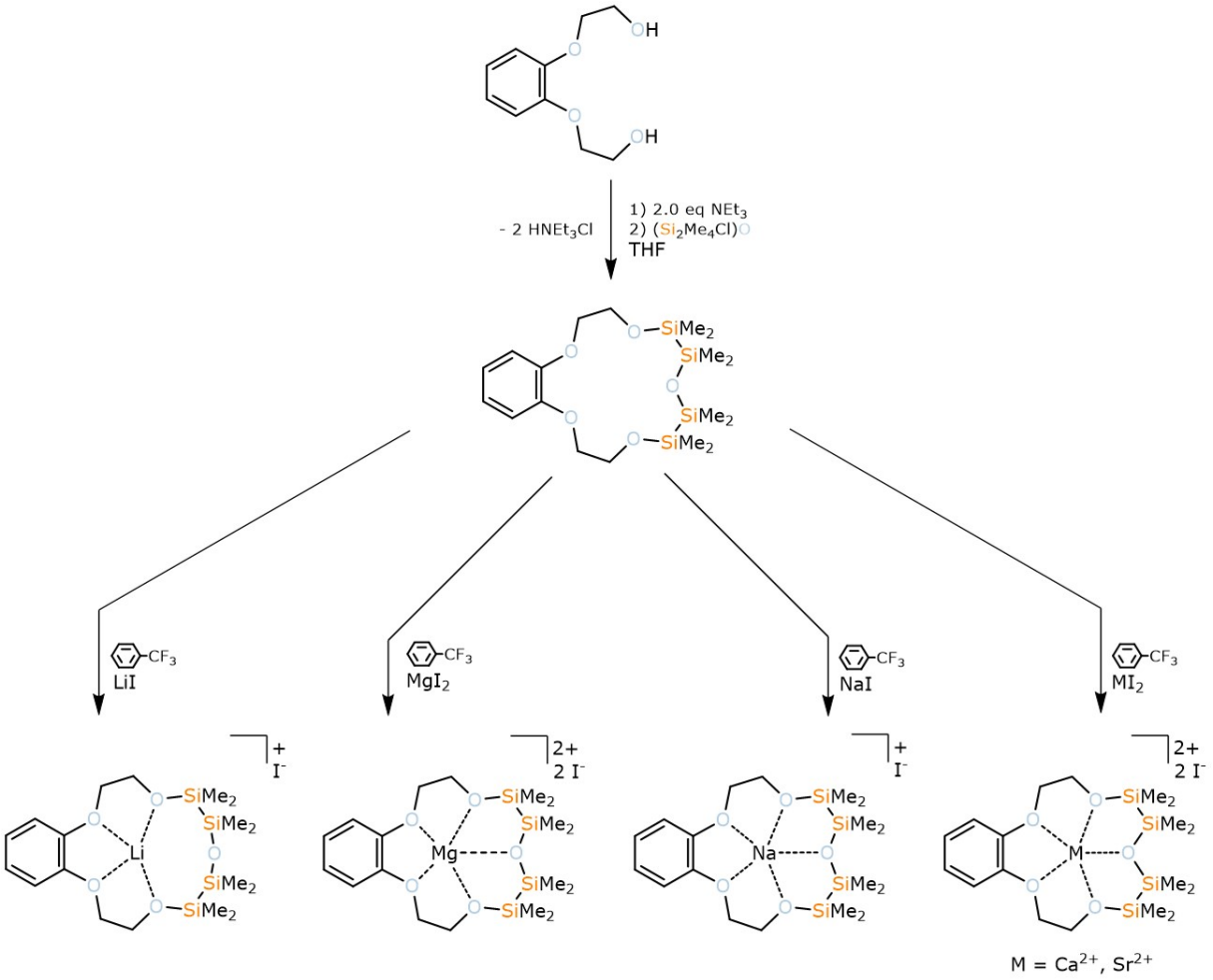

Scheme 17: Synthesis of s-block metal complexes of 1,2,4,5-tetrasila-benzo[15]crown-5.

The hardest used cation Mg^{2+} might only show weak interactions with the siloxane backbone but, similar to Li^{+}, is also too small for the cavity of the ligand. Hence, the interaction of the siloxane backbone with Na^{+} can be stronger than that of Mg^{2+}. Nevertheless, especially the hard alkaline earth metal ions seem to activate the siloxane backbone for coordination. This argumentation was further strengthened when comparing the complexes [K(1,2,4,5-tetrasila[18]crown-6)PF_6] and

[Ba_2(1,2,4,5-tetrasila[18]crown-6)$_2I_4$]. The latter compound was successfully synthesized upon conversion of 1,2,4,5-tetrasila[18]crown-6 with BaI_2. Even though K^+ and Ba^{2+} have almost identical ionic radii at given coordination numbers, it is evident from SC-XRD and ^{29}Si NMR chemical shift, that the attraction between siloxane donors is stronger when the alkaline earth metal ion Ba^{2+} is employed for coordination. Moderate interactions are found in [Ba_2(1,2,4,5-tetrasila[18]crown-6)$_2I_4$] ($\Delta\delta$(^{29}Si, inner Si-atoms) = 8.3 ppm) whereas no interactions are found in the literature-known compound [K(1,2,4,5-tetrasila[18]crown-6)PF_6]. Overall, strong evidence is provided at this point that it is an early s-block metal ion which shares the strongest interaction with siloxane donors given that a suitable match of ligand and ion size is present.

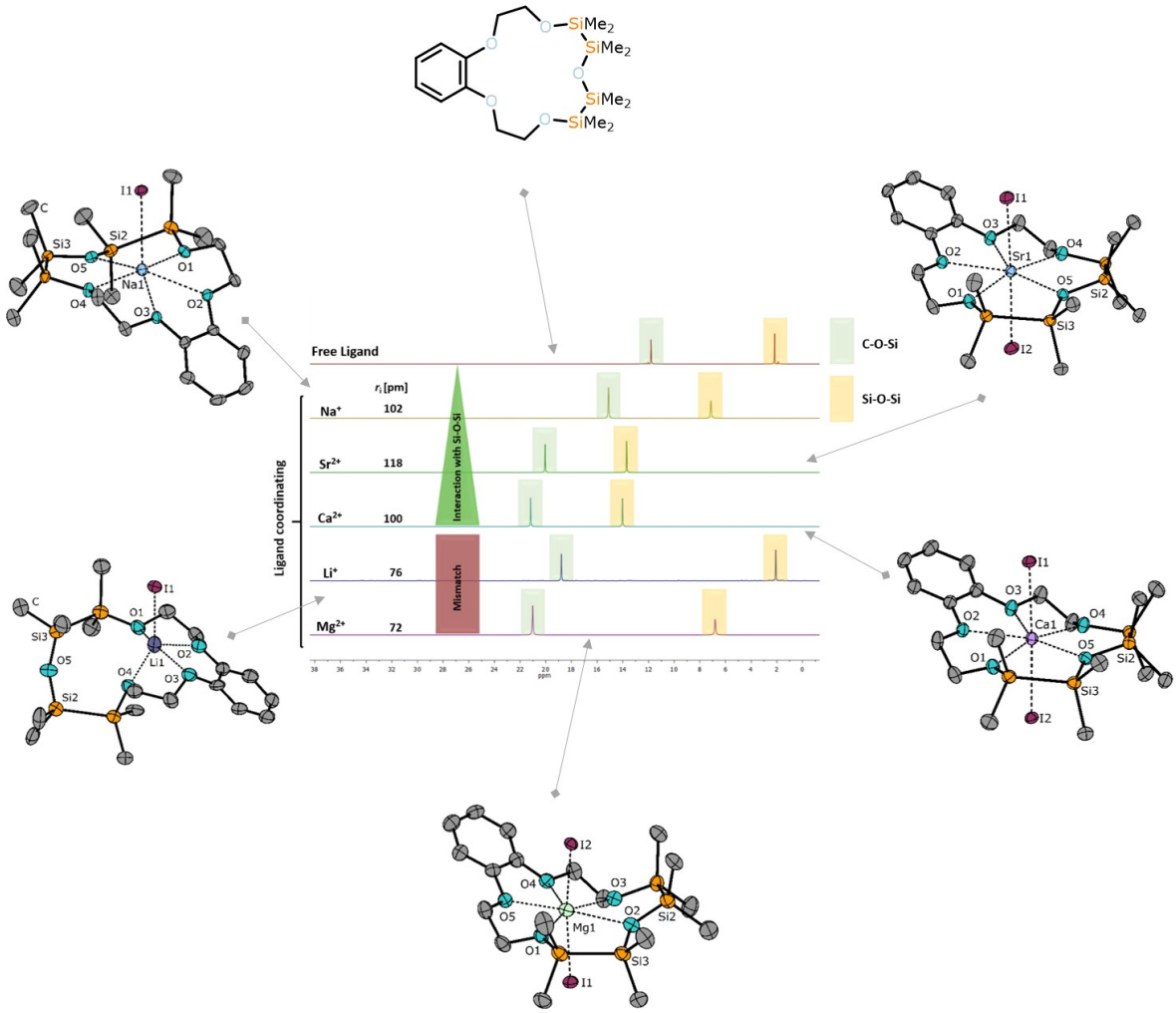

Figure 35: Tetrasila-crown ether complexes of 1,2,4,5-tetrasila-benzo[15]crown-5 in crystal form and ^{29}Si NMR spectra representing the respective coordination mode in solution. Thermal ellipsoids set at 50% probability. Co-crystalline solvent molecules are omitted for clarity.

The findings were, as the next step, transferred to template reactions. To obtain novel ligand systems, a number of reactions were performed with alkaline earth metal iodides and small siloxane building blocks. Different reactions turned out to be successful and indeed, novel ligands were obtained which can, so far, not be synthesized by other means (Scheme 18).

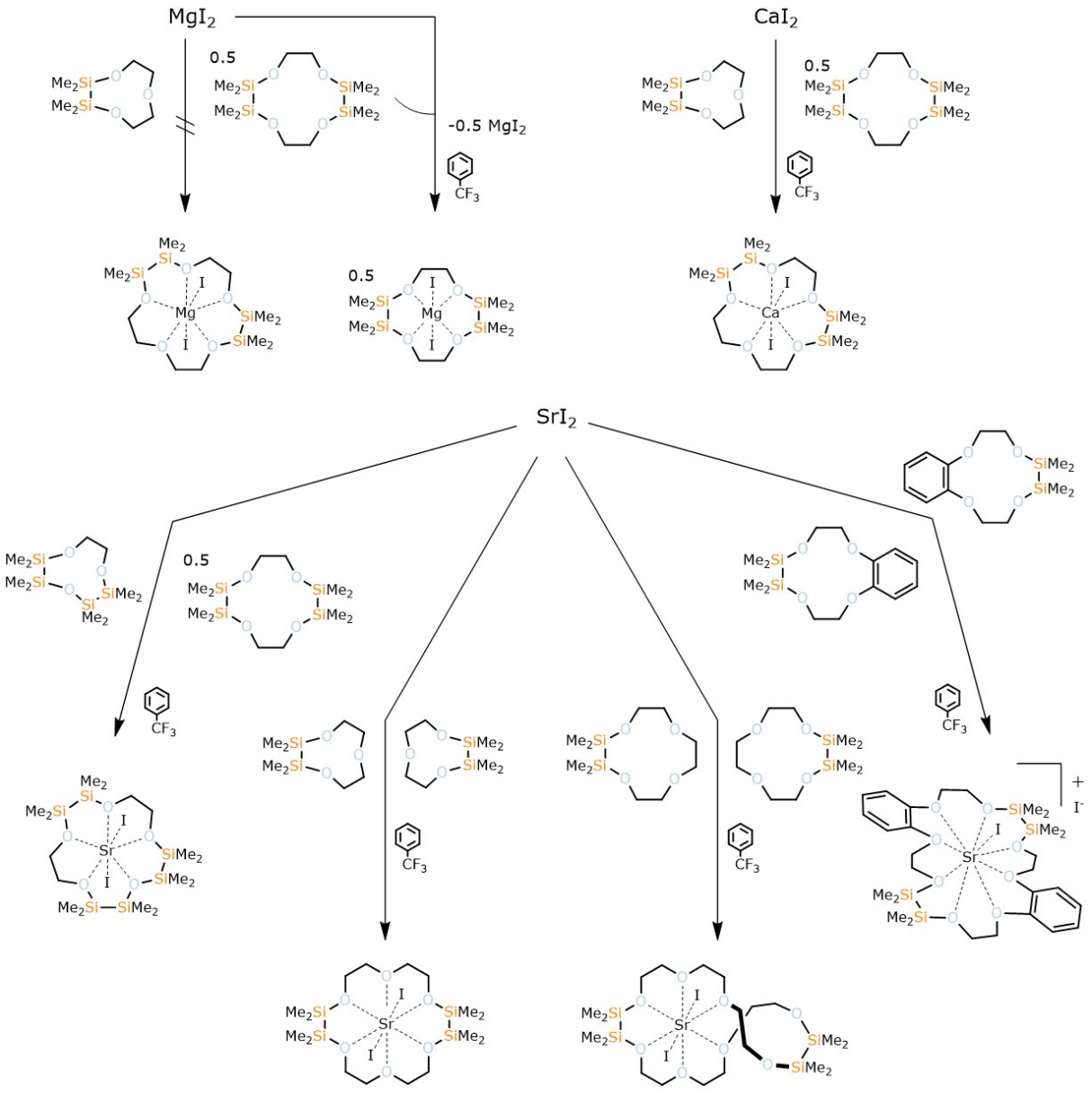

Scheme 18: Alkaline-earth metal templated synthesis of novel hybrid disila-crown ether analogues.

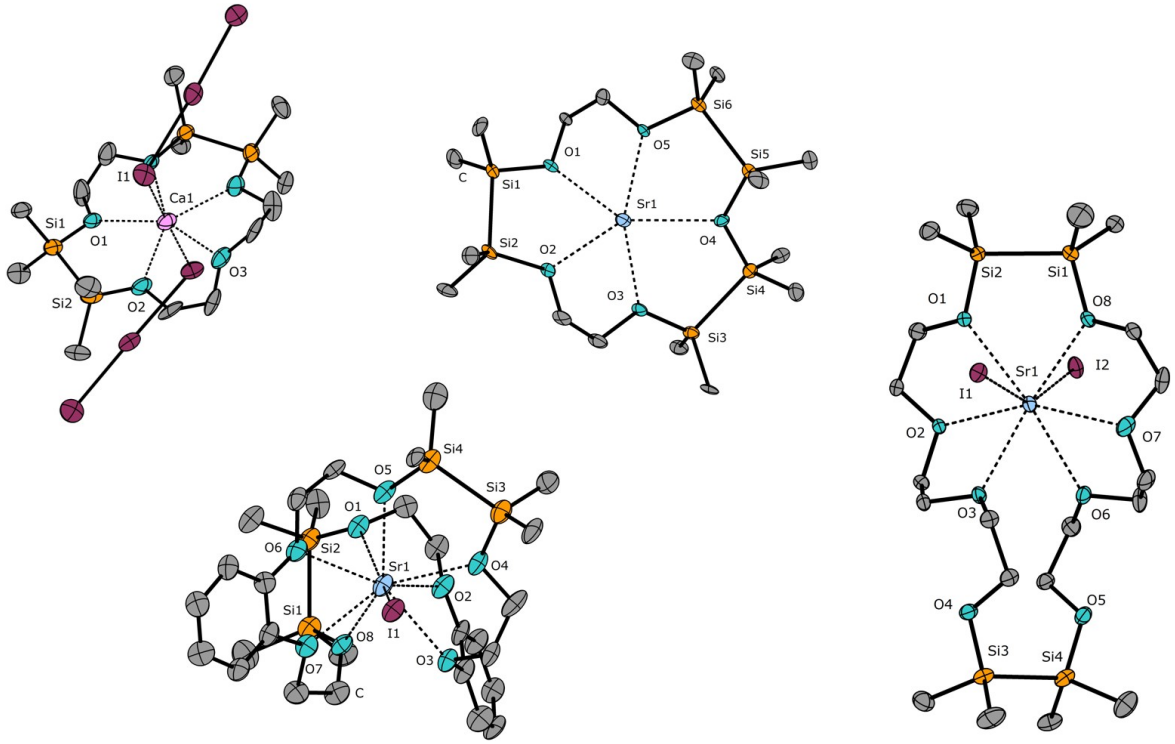

Figure 36: Selected X-ray structures of alkaline earth metal complexes with novel disila-crown ethers obtained *via* templated synthesis. Thermal ellipsoids set at 40% (both left structures) and 50% probability (both right structures). The GaI_4^- ions of [Sr(1,2,4,5,10,11-hexasila[15]crown-5)$(GaI_4)_2$], the non-coordinating iodide ion of [Sr(1,2,13,14-tetrasila-dibenzo[24]crown-8)I]I and co-crystalline solvent molecules are omitted for clarity.

A 1:2 reaction of 1,2,7,8-tetrasila[12]crown-4 with 1,2-disila[9]crown-3 in the presence of MgI_2 was carried out to obtain the silicon based crown-ether analogue 1,2,7,8-tetrasila[15]crown-5. Due to the small ionic radius of Mg^{2+}, however, the reaction failed yielding exclusively [Mg(1,2,7,8-tetrasila[12]crown-4)I_2]. The Mg^{2+} ion fits well into the cavity of this ligand so there is no driving force for a ring-opening and subsequent reorganization of these ligands even though Mg^{2+} shares strong interactions with the silicon affected oxygen atoms of ligand 1,2,7,8-tetrasila[12]crown-4. When employing CaI_2, however, the targeted ligand was obtained showing that smaller ligand moieties can indeed be coupled to ion-specific crown-ether analogues if a hard s-block metal ion is employed. This is a unique reaction behaviour of such sila-polyethers. Organic crown-ethers have not yet been reported to undergo ring-expansions when mismatched combinations of ligand size and ion radius are employed. Further reactions were

performed with SrI_2. The larger Sr^{2+} ion allowed obtaining four further silicon-based ligands upon (cross-)coupling. Probably the most remarkable crown-ether was obtained by cross-coupling 1,2,7,8-tetrasila[12]crown-4 and 1,2,4,5-tetrasila[9]crown-3. The first ever hexasila-crown ether could be successfully synthesized and characterized in the form of [Sr(1,2,4,5,10,11-hexasila[15]crown-5)I_2]. With this ligand, a hexasila-crown ether moiety was finally obtained which was not accessible by the disila-glycol route. Further ligands which have been obtained are 1,2,10,11-tetrasila[18]crown-6, 1,2,13,14-tetrasila[24]crown-8 and 1,2,13,14-tetrasila-dibenzo[24]crown-8 all of which are obtained as their SrI_2 complexes after coupling two equivalents of 1,2-disila[9]crown-3, 1,2-disila[12]crown-4 or 1,2-disila-benzo[12]crown-4. All ligands were also observed in suitable X-ray structures when different anions were employed. As the iodide complexes partially showed no tendency to crystallize, iodide ion acceptors such as elemental iodine or GaI_3 found application. Selected X-ray structures are depicted in Figure 36. In the context of templated synthesis, also barium iodide and alkaline earth metal bromides have been tried. So far, however, these coupling reactions have not been successful using these salts for chemical reaction. The mechanism behind these reactions is postulated to be an exocyclic coordination of the metal center and thus Si-O bond activation first, before the ligand is ring-opened under formation of a glycolate ligand with terminal iodosilane functionality. The glycolate does then attack a further equivalent of a sila-crown building block to eventually form the novel ligand moiety in a template assisted substitution reaction. An initial, effective Si-O bond activation together with suitable nucleophiles seem to be crucial factors which decide whether such a template reaction takes place or not.

As the template reactions depicted in Scheme 18 showed a promising reaction behaviour of alkaline earth metal toward siloxane ligands, it was now tried to obtain ^2D_n ligands with an exclusively silicon-based backbone. Therefor now various magnesium and also beryllium salts found application which were thought to effectively activate Si-O bond moieties for ROP. $^2D_2$ was the precursor of choice and was subsequently brought to reaction in α,α,α-trifluorotoluene. Serendipitously, LEWIS acidic systems were not found to yield silicon-based crown-ethers but to support C-F bond cleavage (Figure 37).

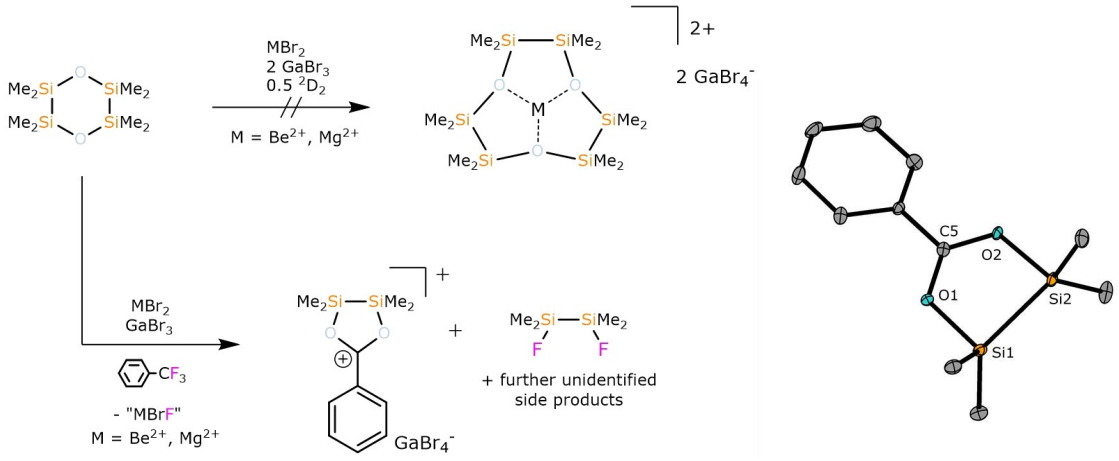

Figure 37: Attempted synthesis of an exclusively silicon-based crown-ether and observed pathway (left) and X-ray structure of the cation of $[Ph\text{-}C(O_2Si_2Me_4)]GaBr_4$. Thermal ellipsoids set at 50% probability. The $GaBr_4^-$ counter ion is omitted for clarity.

In case of a $M_{EA}Br_2/GaBr_3/^2D_2$ (M_{EA} = Be^{2+}, Mg^{2+}) mixture in α,α,α-trifluorotoluene, the chemically rather inert CF_3 group of the solvent is fully deconstructed to form rare siloxy-stabilized carbenium ions. It is most likely that the C-F bond is activated and a transient $Ph\text{-}CF_2^+$ cation then reacts with $^2D_2$. Under formation of $(SiMe_2F)_2$ and further unidentified side products, $[Ph\text{-}C(O_2Si_2Me_4)]GaBr_4$ is obtained and a herein characterized example for such a rare species. As the deconstruction of α,α,α-trifluorotoluene could also observed when reacted with miscellaneous salts with a hard metal ion such as BeI_2, GaI_3, HfI_4 and ThI_4, it was clear that in some cases another solvent should be used to successfully obtain an exclusively silicon-based crown-ether.

Alternatively, Ph-F was used to prevent side-reactions. $^2D_2$ was successfully converted with various s-block metal iodides in the presence of GaI_3 (Scheme 19). The latter serves, similar as demonstrated for $[Sr(1,2,4,5,10,11\text{-hexasila[15]crown-5})(GaI_4)_2]$, as an iodide ion acceptor and increases the respective LEWIS acidity of the s-block ion. By conversion of $^2D_2$ with *in situ* generated $M(GaI_4)_n$ we could now observe the formation of $^2D_3$ for M = Li^+ (n = 1) whereas M = Na^+, Mg^{2+}, Ca^{2+} and Sr^{2+} (n = 1 or 2) form $^2D_4$. The coordination compounds $[Li(^2D_3)GaI_4]$ and $[M(^2D_4)(GaI_4)_2]$ were successfully characterized by means of multinuclear NMR spectroscopy and, except for the Mg^{2+} species also by means of SC-XRD (see Figure 38 for selected examples).

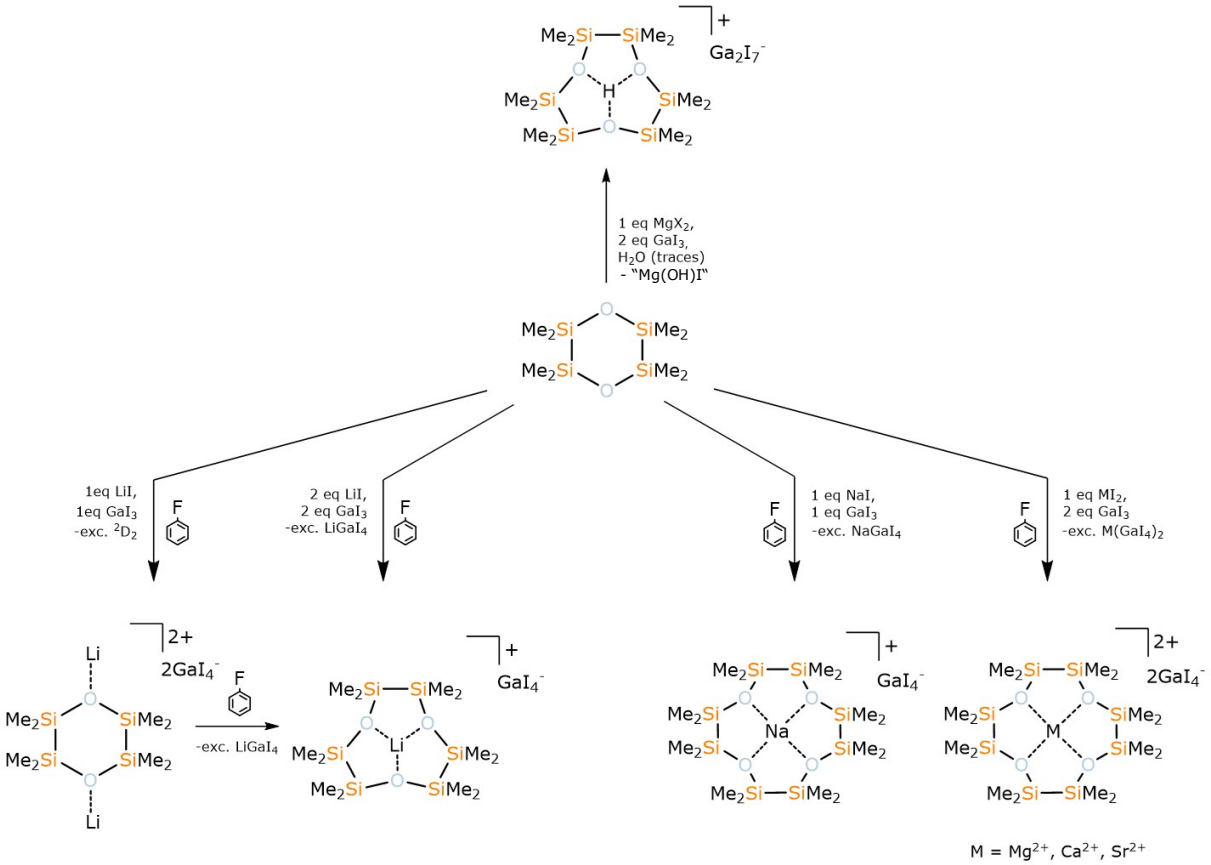

Scheme 19: Templated synthesis of inorganic crown-ether analogues.

Serendipitously, another example of a $^2D_3$ complex was obtained for M = H^+ when a Mg^{2+} salt was employed for reaction. $[H(^2D_3)]Ga_2I_7$ could be obtained and structurally characterized after the reaction was performed with presence of traces of water. At this point it should be mentioned that the time period between the first published results regarding disila-crown ethers and these fully-disila crown ethers measures more than four years. Taking the starting point of this project into account, this time period does even measure more than six years. The template approach, suitable coordination partners as well as an inert solvent are the key determinants which made the success in obtaining these sila-crown ethers finally possible.

A crucial step in in the formation of these compounds is an exocyclic coordination of M^{n+} as was also postulated for hybrid disila-systems. This could now also experimentally verified from the obtained X-ray structure $[Li_2(^2D_2)(GaI_4)_2]$. The compound was obtained after reacting $^2D_2$ and $LiGaI_4$ with regard to short reaction times. Crystal structure determination shows Si-O bond

elongation and a smaller Si-O bond angle. Hence, Si-O bond activation occurs before ring-opening occurs and the above-drawn compounds are obtained. The inorganic crown-ether analogues are stable in solution which was elucidated by means of DOSY NMR even though these systems have a high tendency towards ring-opening. This is true as long as the template bound within the ligand moiety. MeCN addition releases the templates from the crown-ethers which eventually leads to oligo- but also monomerization.

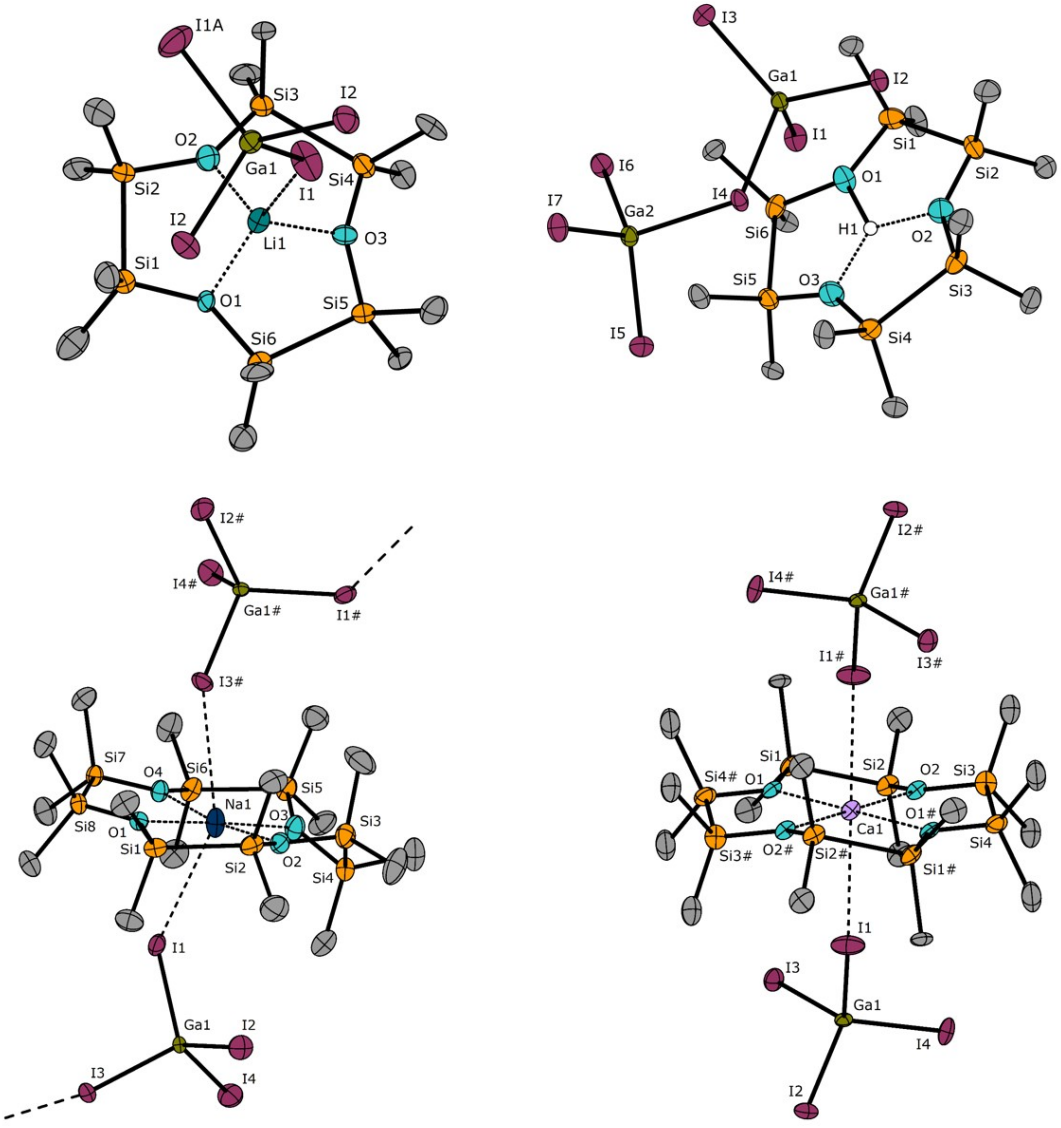

Figure 38: s-block element complexes of $^{2}D_{3}$ (top) and $^{2}D_{4}$ (bottom) in crystal form. Atoms depicted with # are symmetry generated using x, 3/2-y, 1/2+z or 1-x,1-y, 1-z. Co-crystalline solvent molecules as well as disordered parts of the structures are omitted for clarity. Thermal ellipsoids set at 50% probability.

$^2D_2$, $^2D_4$, $^2D_5$ and $^2D_6$ were identified and characterized by means of multinuclear NMR spectroscopy and/or MS spectrometry. All free ligand species, however, are unstable over a longer time period and react back to the monomer $^2D_2$. Ring-opening oligomerization is thus found to be reversible. This makes inorganic crown-ethers attractive for separation techniques as the precursor might be recycled. To shed light on the tendency of such ligands to bind M^{n+} and to understand the mechanism behind these template reactions, meticulous quantum chemical calculations were performed in cooperation with Dr. F. WEIGEND. As calculated for Li^+ and Na^+ as examples, energies of exchange reactions calculated by means of density functional theory show that M^+ is bound stronger to $^2D_4$ or D_6 than to $^2D_3$ or D_5, the former being nearly competitive to the organic crown ethers [3n]-crown-n (n = 4-6). The binding of M^+ to $^2D_2$ is clearly de-preferred whereas the binding towards [15]crown-5 and [18]crown-6 is mostly preferred. The mechanism behind these template reactions compares well with the one postulated for the templated synthesis of hybrid disila-ligands (Figure 39). An exocyclic Si-O bond activation is suggested which is also found in the experiment. Then, silanolate formation occurs under Si-O bond cleavage and simultaneous formation of a iodosilane end-group. Template-driven, the silanolate attacks a second equivalent of $^2D_2$ which is then brought into a suitable conformation for ring-closure. Backbiting forms an Si-O bond and an iodide anion is released from the silane. The sila-crown ether is eventually formed.

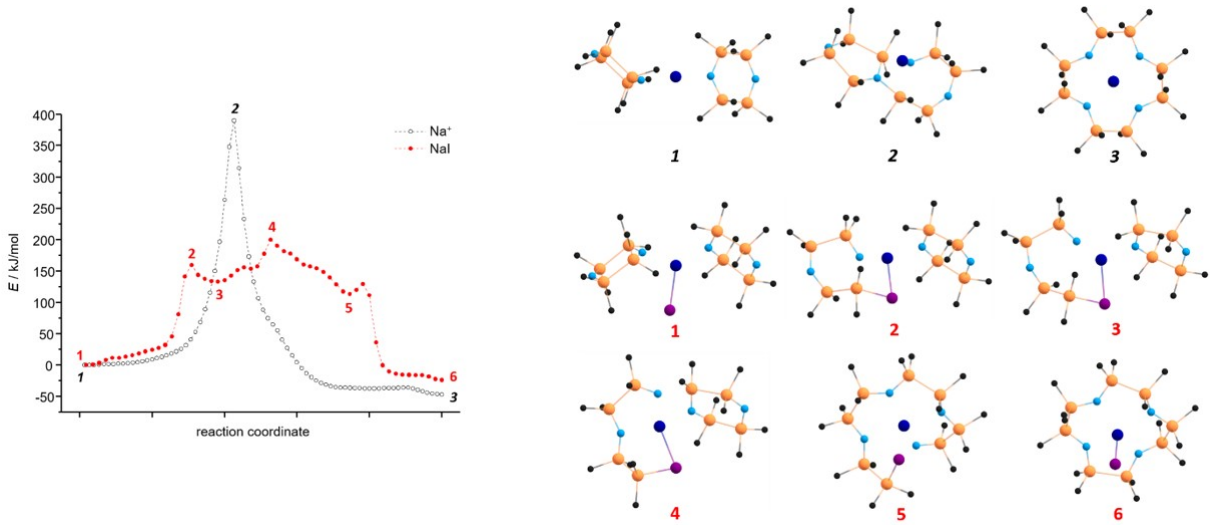

Figure 39: Energy profiles for the pathways from $[Na(^2D_2)_2]^+$ to $[Na(^2D_4)]^+$ (left) and extremum structures of the respective path (right) obtained from DFT calculations.

The significance of the presence of I^- was also substantiated. The quantum chemical calculations show that the transformation from $[Na(^2D_2)_2]^+$ to $[Na(^2D_4)]^+$ exhibits a single barrier which amounts to almost 400 kJ/mol but becomes much lower in presence of I^- (160 kJ/mol).

Taking all compounds and reactivity of silicon based ligands toward various s-block metal salts into account it could in conclusion be shown that it is very well possible to obtain silicon-rich crown-ether analogues. They are accessible by template-assisted reactions with preceding Si-O bond activation. Both types of ligands, hybrid-disila crown ether analogues as well as exclusively disilanyl bearing systems can be ring-opened and show a considerable coordination ability toward hard s-block metal cations. A series of side-reactions such as C-F bond cleavage can perturb the silyl-ether coordination which is why inert solvents are recommended for this chemistry. How far the larger ring ^2D_n (n = 5, 6) can be used for coordination chemistry will be part of upcoming work.

5.2 Contributions to the Coordination Chemistry of D_n Ligands

The contributions to a coordination chemistry of disila-crown ethers gave valuable insights into the coordination ability of siloxanes. As was comprehensibly shown with 1,2,4,5-tetrasila-benzo-[15]crown-5 as ligand, siloxanes prefer early s-block metal ions embedded into a matching coordination geometry. The idea was now to investigate various D_n ligands towards different hard s-block metal ions such as the alkaline-earth metal ions. As s-block metal iodides were found to be suitable salts in the aforementioned study with 1,2,4,5-tetrasila-benzo-[15]crown-5 as a ligand, these salts were straight forwardly converted with D_n (n = 6, 7) ligands which were presented as weakly coordinating ligands in past works (see introduction part).

Counter-intuitively, the conversion of these iodides turned out to be successful for Mg^{2+} and Ca^{2+} as cation. Sr^{2+} and Ba^{2+} were embedded into such rings as their GaI_4^- salts which was also shown for various disila-ligands (Scheme 20). This ultimately proves that no bulky, perfluorinated anion such as Al_F^- is necessary to obtain stable adducts of cyclic dimethylsiloxanes with metal cations. The X-ray structures of $[Mg(D_6)I_2]$ and $[Ca(D_7)I_2]$ were successfully determined (see Figure 40, top) and even show metal···anion bonds which were further described to perturb

silyl-ether bonding. Thus, this success of binding salts with relatively strong coordinating I^- ion further demonstrates that the nature of the cation has to be taken into account when siloxane coordination chemistry is discussed. This was further confirmed with suitable BORN-HABER cycles obtained from quantum chemical approaches. Despite the relatively strong coordinating iodide ion, the overall energy gains for complexation of MgI_2 has a value of -328 kJ/mol for D_6 employed and -313 kJ/mol when D_7 employed. Slightly lower values are obtained for CaI_2. These are -125 kJ/mol for D_6 and -109 kJ/mol for D_7. Things are different when the slightly softer ions Sr^{2+} and Ba^{2+} are employed for chemical reaction. -10 kJ/mol (D_6) and -3 kJ/mol (D_7) are obtained for SrI_2. +87 kJ/mol (D_6) and +79 kJ/mol (D_7) are obtained for BaI_2. These values are finely represented by the experiment. As demonstrated, stable complexes of MgI_2 and CaI_2 are obtained. In case of SrI_2, a respective coordination compound was only observed by means of ^{29}Si NMR in solution ($\delta(SrI_2@D_7)$ = -9.2 ppm) and no evidence for coordination is found in case of BaI_2. A crossover point was thus detected which demonstrates how far the silyl-ether coordination is possible with the iodide anion on an experimental level.

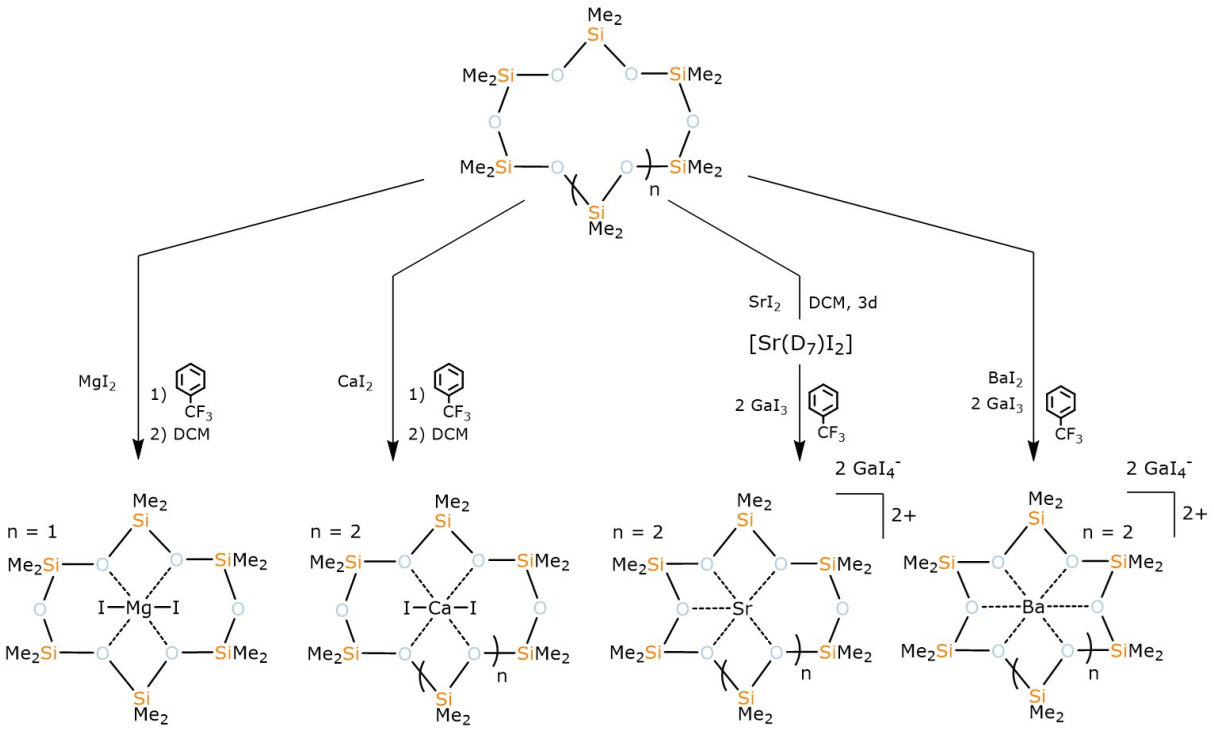

Scheme 20: Synthesis of alkaline earth metal complexes with D_n ligands.

Again it is the presence of GaI_3 which allows for obtaining stable complexes of Sr^{2+} and Ba^{2+}. Adding two equivalents of GaI_3 to a suspension of D_7 and MI_2 (M = Sr^{2+}, Ba^{2+}) yielded the respective D_7 complexes which then could also be investigated by means of SC-XRD as the coordination compounds $[Sr(D_7)\{GaI_4\}(H_2O)]GaI_4$ and $[Ba(D_7)\{GaI_4\}(H_2O)_{0.94}\{GaI_4\}_{0.06}][GaI_4]_{0.94}$ (Figure 40, bottom). The energy gain employing the GaI_4^- anion is about 240 kJ/mol. Hence, initially unsupported silyl-ether coordination of Sr^{2+} and Ba^{2+} could be shown to be clearly exothermal with this small WCA.

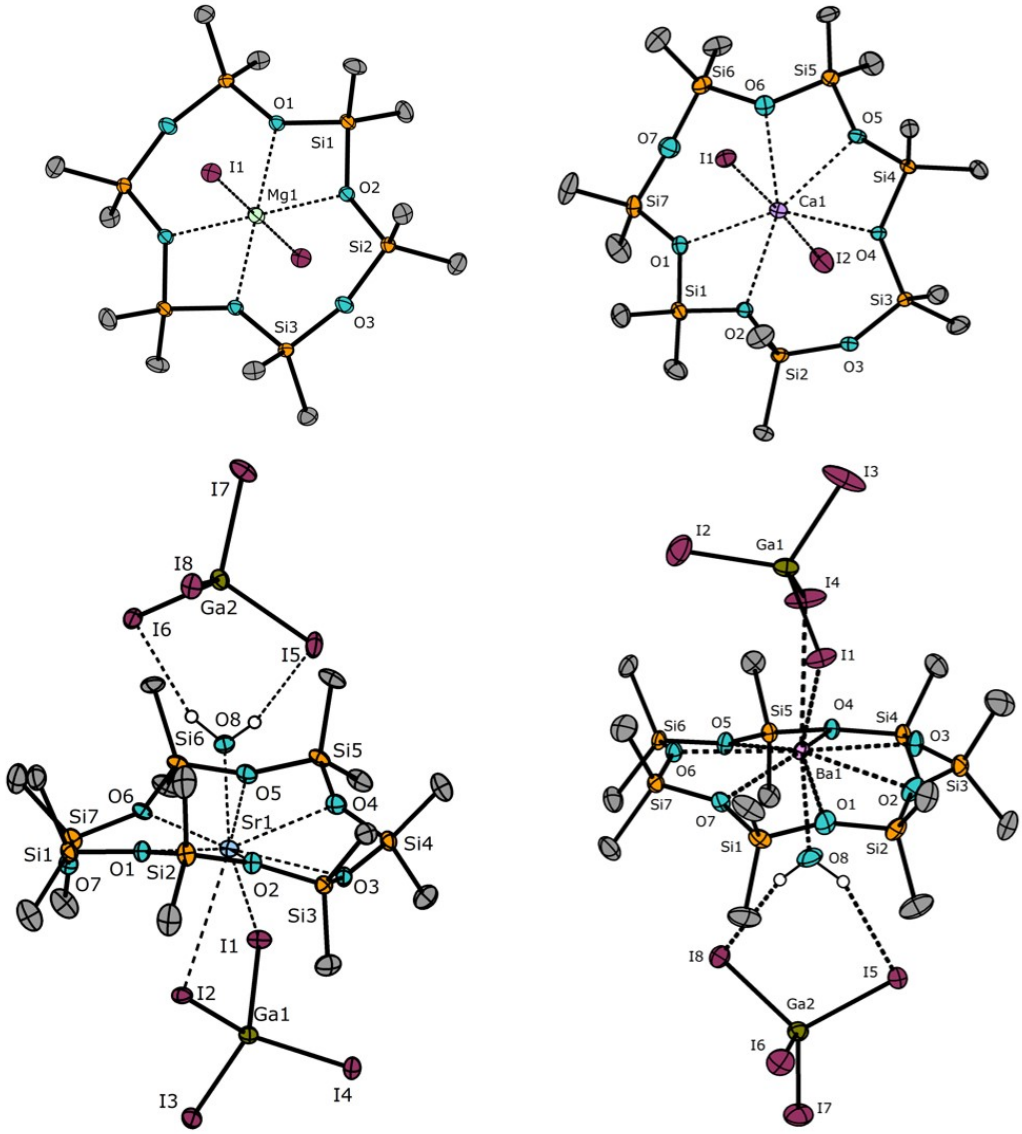

Figure 40: Alkaline-earth metal complexes of D_6 and D_7. Co-crystalline solvent molecules as well as disordered parts of the structures are omitted for clarity. Thermal ellipsoids set at 50% probability.

The energy gain employing GaI_4^-, gave rise to the question if also alkali-metal complexes are accessible with this small WCA and indeed a great selection of alkali metal complexes could be obtained when this anion is employed (Scheme 21). It was shown that Li^+ can be bound in D_5 and D_6 ligands, Na^+ can be bound in D_6 and D_7 ligands and K^+ was, as expected from previous works, bound in D_7 (see Figure 41). Similar as observed for several disila-ligands, also these cyclic siloxanes were observed to be vulnerable towards ring-opening polymerization reaction. For example was D_5 ring-opened to D_6 when converted with $LiGaI_4$ in α,α,α-trifluorotoluene.

As was already successfully shown for hybrid disila-ligands, also NH_4^+ was employed for complexation reacting one equivalent of NH_4I and two equivalents of GaI_3.

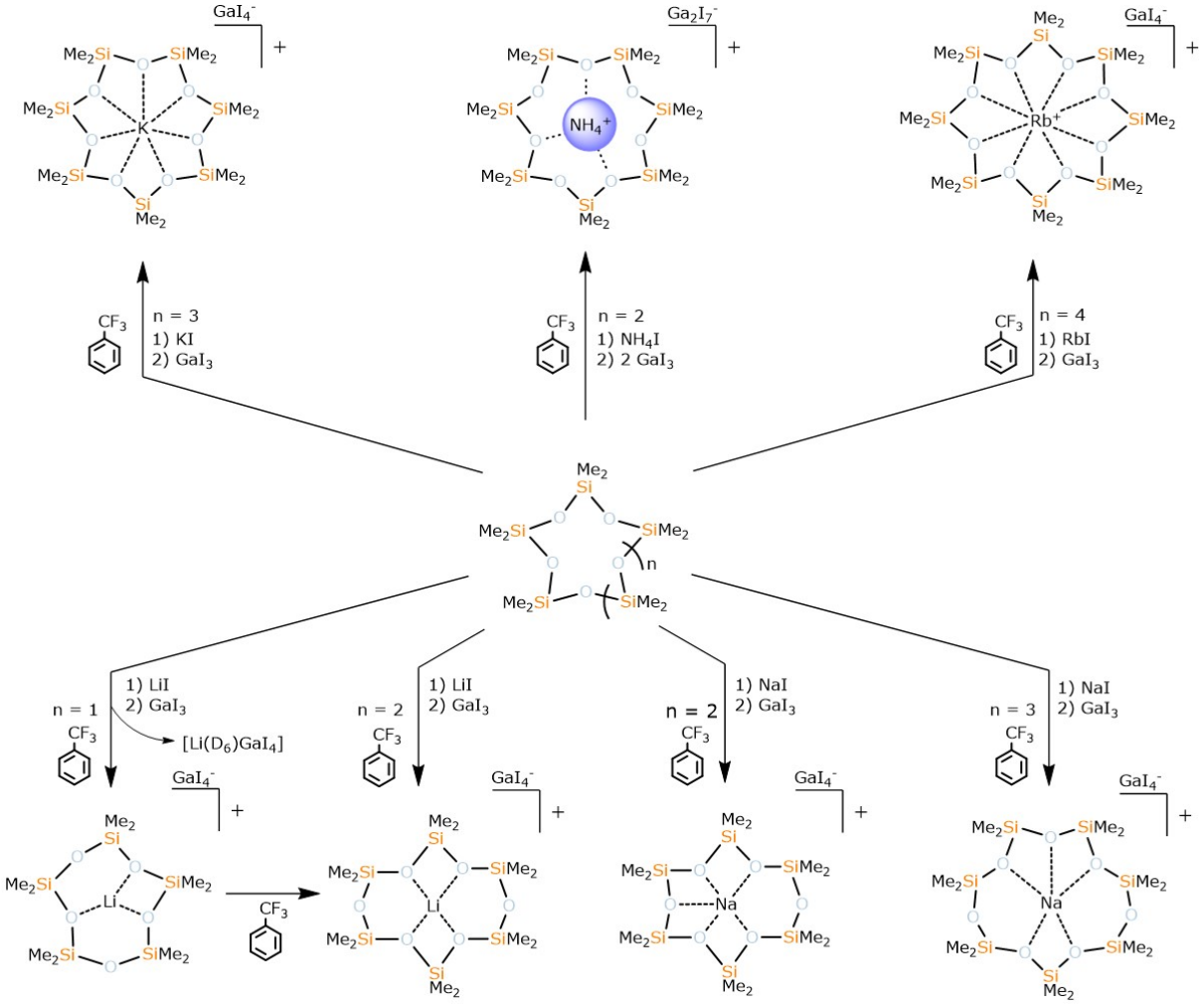

Scheme 21: Synthesis of alkali metal and NH_4^+ complexes with D_n ligands employing the small WCAs GaI_4^- and $Ga_2I_7^-$.

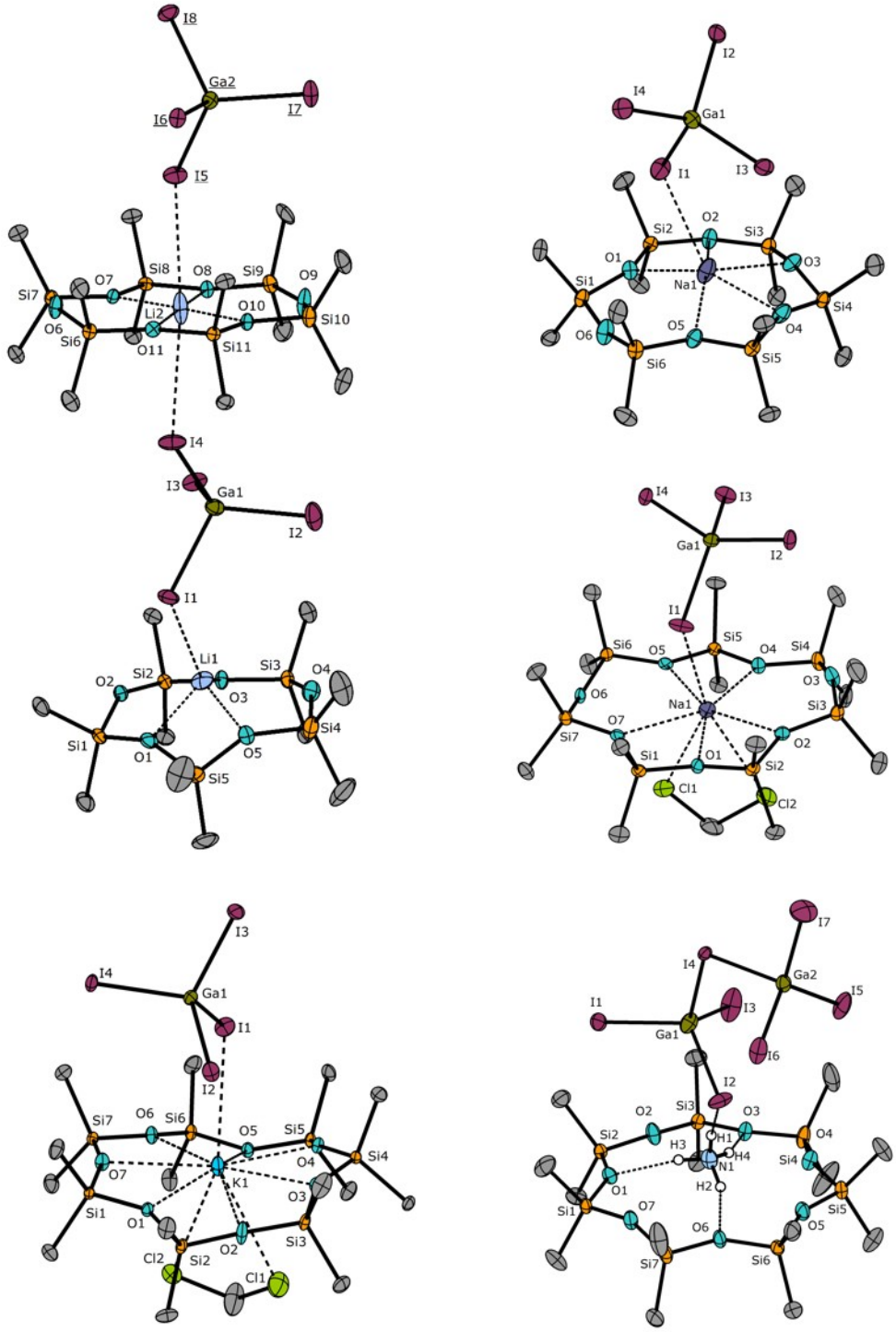

Figure 41: Alkali metal (and NH_4^+) complexes of D_5, D_6 and D_7 employing the small WCAs GaI_4^- and $Ga_2I_7^-$. Co-crystalline solvent molecules as well as disordered parts of the structures are omitted for clarity. Underlined atom labels indicate symmetry generation using 1+x, y, -1+z. Thermal ellipsoids set at 50% probability.

In this way, the first ever characterized non-metal complex of a cyclic siloxane was obtained but which, in contrast to the metal complexes, shows high sensitivity and decomposes readily in solution. The complex was obtained as $[NH_4(D_7)]Ga_2I_7$ after conversion of D_6 with NH_4I and GaI_3. Hydrogen atoms of a determined X-ray structure were located crystallographically and showed a similar coordination pattern as observed in the above-mentioned compounds $[NH_4$(1,2-disila[18]crown-6)$]PF_6$ and $[NH_4$(1,2-disila-benzo[18]crown-6)$]PF_6$. Further, IR and NMR spectroscopic investigations verified the hydrogen-bonding interactions with the $SiMe_2O$-moieties. That this compound is stabilized by three hydrogen bonds involving Si-O-Si groups is remarkable. This bonding situation is clearly counter-intuitive which is why the limits of siloxane coordination chemistry was then be explored further. As silyl-ether coordination towards heavy alkali metal compounds has been strictly avoided so far it was clear at this point, that also Rb^+ and Cs^+ should be tried to be embedded into cyclic siloxanes.

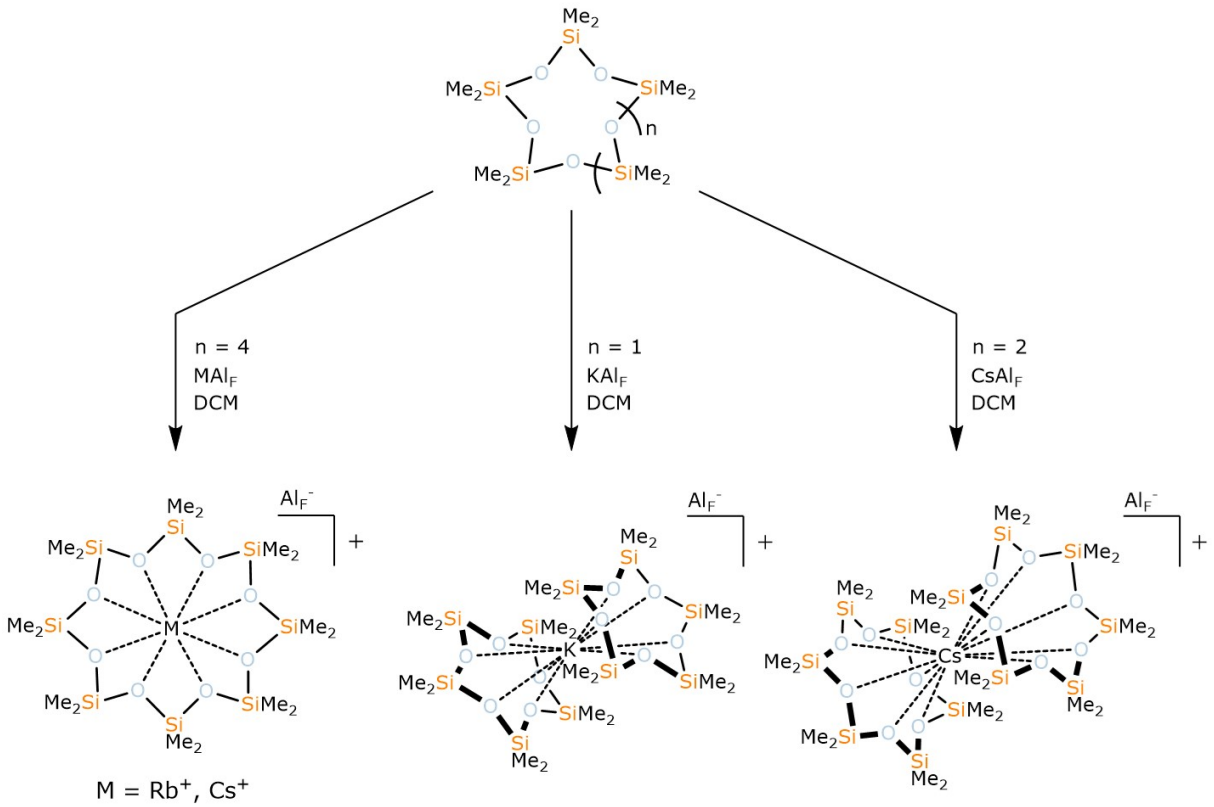

Scheme 22: Synthesis of (heavy) alkali metal complexes with D_n ligands employing the bulky Al_F^- ion.

This so far failed for Cs^+ when *in situ* generated $CsGaI_4$ and D_8 were converted in α,α,α-trifluorotoluene. In case of $RbGaI_4$, silyl-ether coordination was finally observed which was demonstrated by means of MS spectrometry and an X-ray structure of the compound $[Rb(D_8)(DCM)GaI_4]$. As this compound showed major instability, was obtained in very poor yields and as no meaningful spectroscopic data was obtained for this heavy alkali metal compound, the Al_F^- anion now found application (see Scheme 22). As demonstrated in this thesis though, no bulky WCA is in general necessary for the alkali metal ions Li^+-K^+. Rb^+ therefore reveals a crossover point for the small WCA GaI_4^-.

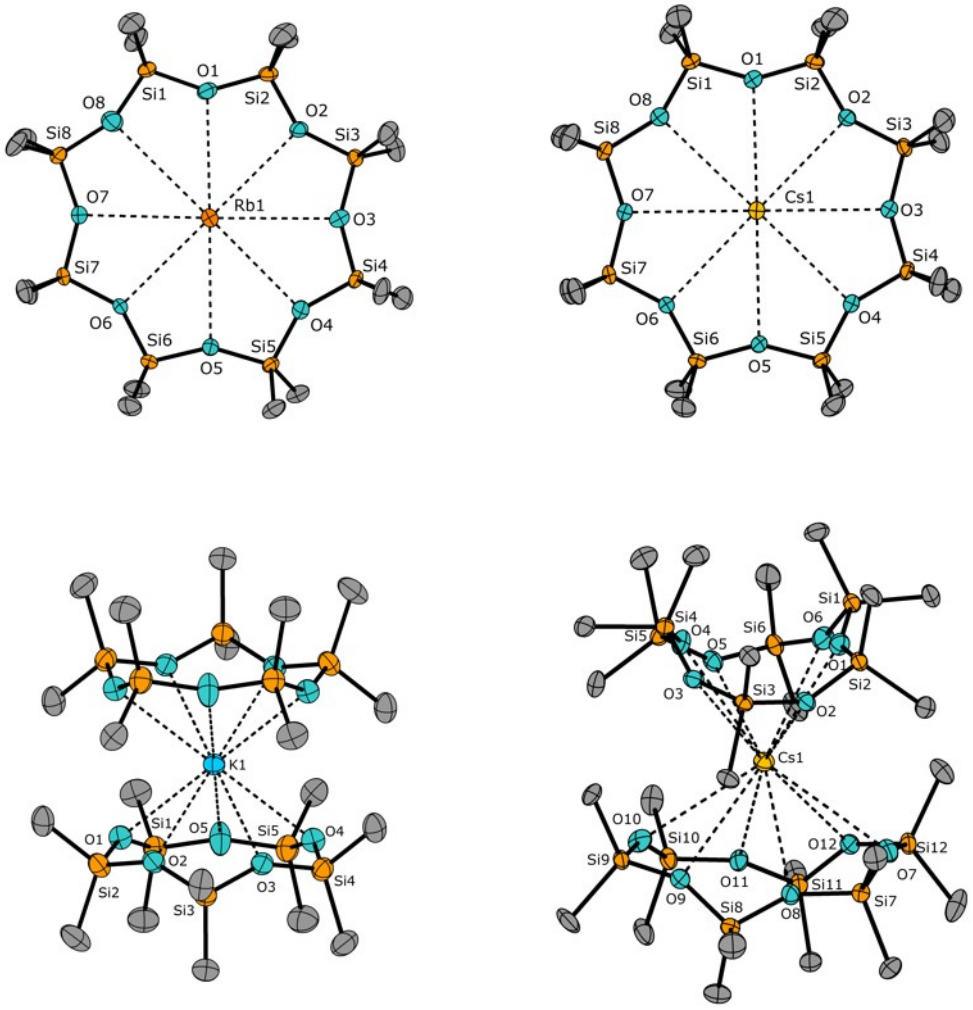

Figure 42: Alkali metal complexes of D_5, D_6 and D_8 employing the bulky WCA Al_F^-. Co-crystalline solvent molecules as well as the anions of the structures are omitted for clarity. Non-labelled atoms are symmetry generated using 1-x, -y, 1-z. Thermal ellipsoids set at 30% (for the potassium compound) or 50% probability, respectively.

Employing the bulky WCA, coordination compounds were finally obtained for both cations, Rb^+ and Cs^+ in suitable yields and meaningful spectroscopic data could be obtained. With these two compounds, all s-block metal ions except for Be^{2+} and the radioactive ones were successfully embedded into D_n ligands (Figure 42). While investigating the coordination chemistry of siloxane ligands it is conspicuous that these ligands are vulnerable toward ring-opening polymerization reactions and tend to form ligand moieties which show coplanar coordination modes toward a respective cation rather than exocyclic coordination. A remaining question was at this point whether it is possible to observe different coordination modes e.g. through combining relatively large cations with relatively small ligands. Also for this purpose the bulky, non-nucleophilic Al_F^- was successfully used. The reactions of excess D_5 with KAl_F and D_6 with $CsAl_F$ in dichloromethane turned out to be expedient. First ever sandwich type complexes in the forms of $[K(D_5)_2]Al_F$ and $[Cs(D_6)_2]Al_F$, could successfully be characterized.

5.3 Siloxane Coordination Chemistry with BeX_2 ($X = Cl^-, Br^-, I^-$)

In the last chapters siloxanes were described to share strong interactions especially with early s-block metal ions. Especially alkaline earth metal ions were found to share strong interactions with siloxane donors. As a logical extension of the project scope, different beryllium halides were thus investigated regarding their reactivity towards various silicon-based ligands.

For this purpose, hybrid disila-ligands have been converted with $BeCl_2$ at first. Two compounds have been isolated and characterized which demonstrate that the beryllium salt cleaves the sila-crown ethers 1,2-disila[12]crown-4 and 1,2-disila-benzo[12]crown-4 to hexanuclear coordination compounds with different glycolate ligands (Scheme 23). The central coordination motifs in the obtained compounds elucidated by SC-XRD are eight-membered Be–O-heterocycles which are annulated by two six-membered Be–O-cycles. Congruent with NMR spectroscopic and X-ray crystallographic investigations, the mechanism behind the formation of these compounds follows an exocyclic coordination of $BeCl_2$ followed by subsequent Si–O bond cleavage reactions under formation of chlorosilanes. In case of 1,2-disila-benzo[12]crown-4 even C–O bond cleavage occurs.

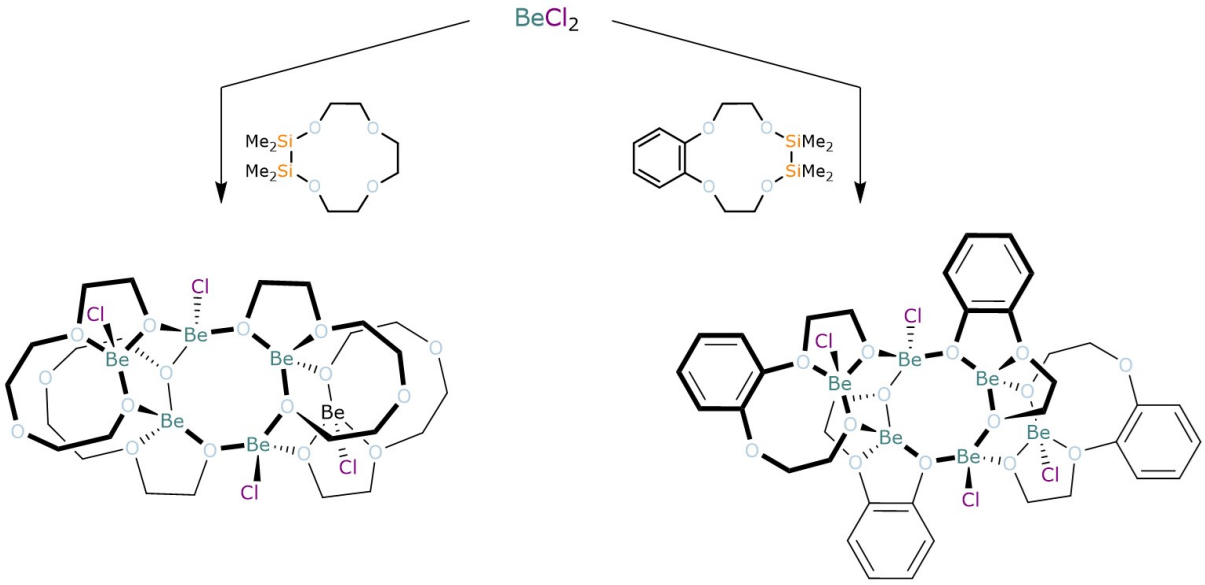

Scheme 23: Deconstruction of hybrid disila[12]crown-4 ethers with $BeCl_2$.

As the hybrid disila-crown ethers are deconstructed to various glycolates, the reactivity of BeX_2 (X = Cl^-, Br^-, I^-) was then investigated towards D_n ligands as well as $^2D_2$ with the intention to obtain silicon-based rather than organic ligand systems.

First investigations on the coordination chemistry of $BeBr_2$ and BeI_2 toward D_5 and D_6 did not yield siloxane coordination compounds which would have been expected after obtaining the promising results regarding alkaline earth metal complexes with D_n ligands. Serendipitously, though, not only had β-BeI_2 been identified by means of SC-XRD but also the so far unknown phase β-$BeBr_2$. This phase has never been observed and could not yet been obtained by other means. Hence, this is another example of a siloxane ligand acting as a solubilizer. To observe reaction of a D_n ligand towards BeX_2 (X = Cl^-, Br^-, I^-) anyway, the smaller more reactive cyclic siloxane D_3 was converted. Chemical reaction was observed for all salts and in the form of $[Be_3(\mu\text{-}OSiMe_2I)_4I_2]$ also an X-ray structure was obtained. The compound resembles a trinuclear complex with iodosiloxanato ligands showing that Si-O bond breakage occurs when employing this more reactive cyclic siloxane (Scheme 24). Similar observations were made when $^2D_2$ is converted with BeX_2. Two major structure motifs are observed: a pentanuclear coordination environment

with two intact siloxane donors and a dodecanuclear cluster compound primarily consisting of disiloxanato ligands. In case of BeX_2 (X = Br^-, I^-) the pentanuclear species could be obtained and the dodecanuclear species in case of BeX_2 (X = Cl^-, Br^-). As the pentanuclear compounds have an intact siloxane moiety which is coordinating Be^{2+}, all s-block metal ions, except for the radioactive ones, could thus by successfully coordinated to neutral siloxane donors.

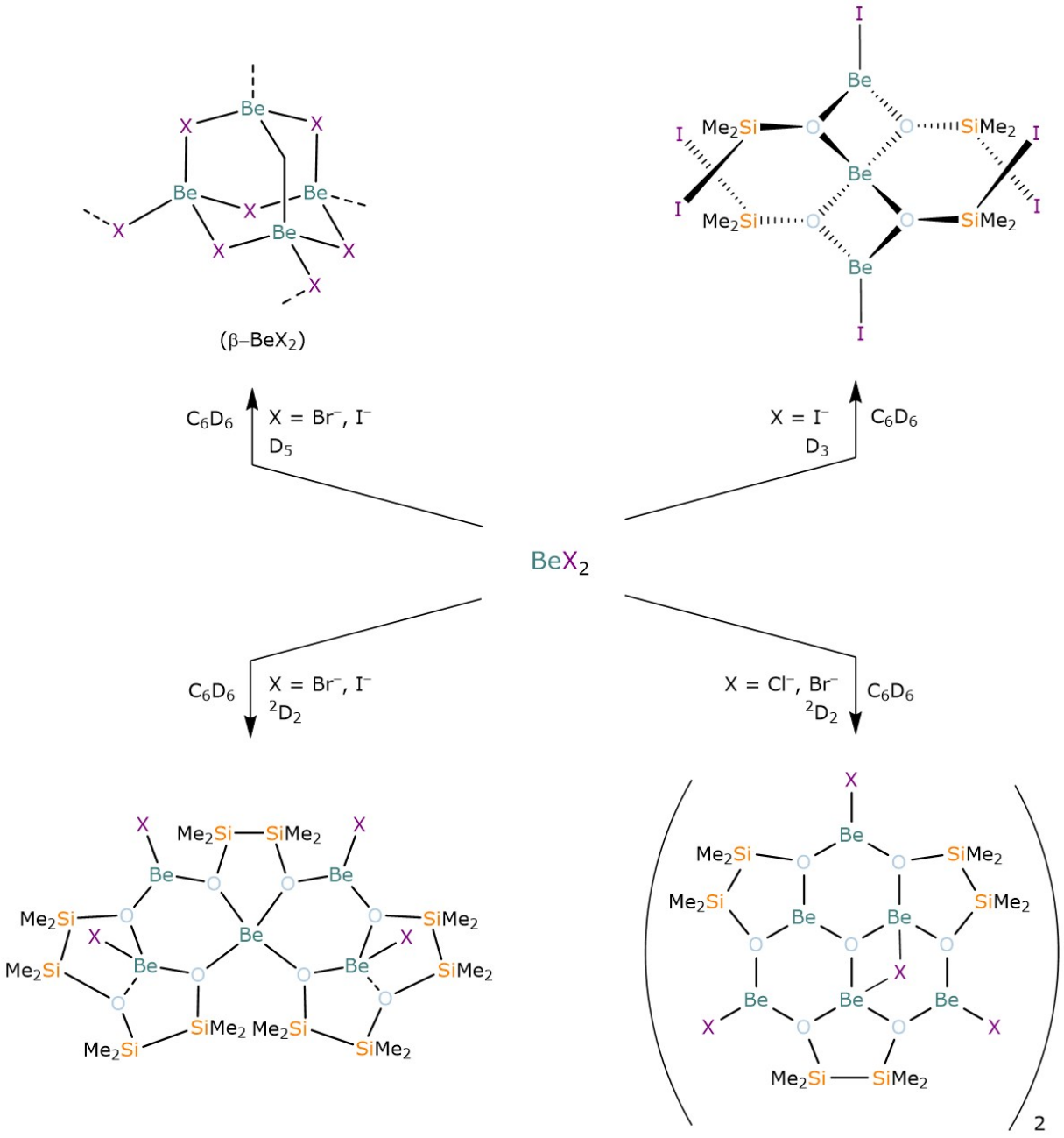

Scheme 24: Preliminary results of a siloxane coordination chemistry with BeX_2.

A problem so far are unclear results by means of NMR spectroscopy. Further investigations are therefore necessary but it should be noted that the beryllium chemistry with siloxane based ligands is also at an early stage. For the amount of time working on this project, promising results were obtained (Figure 43). This chemistry surely has a lot more to offer.

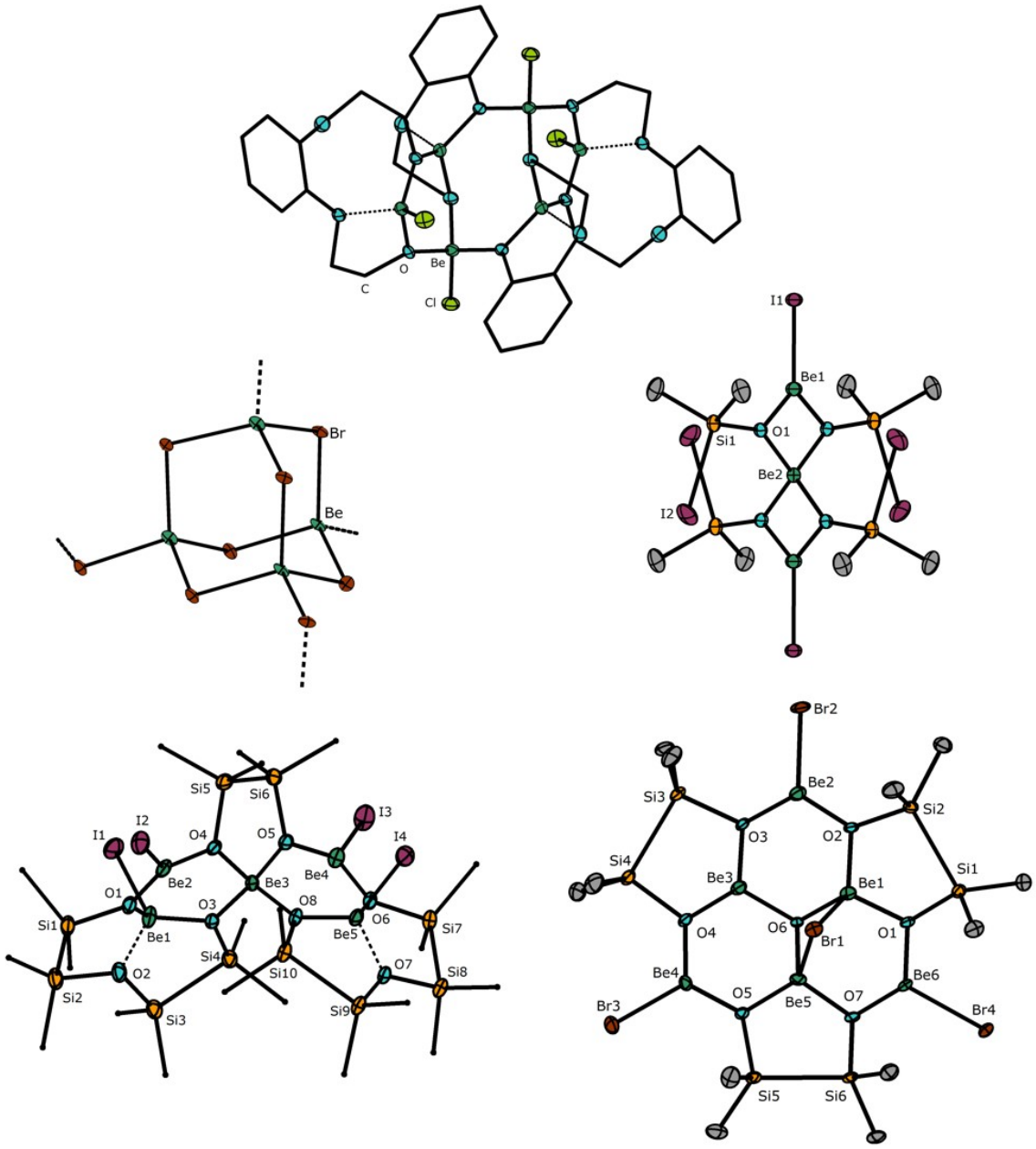

Figure 43: Selected X-ray structures of beryllium containing compounds. Co-crystalline C_6D_6 molecules are omitted and carbon atoms are partially depicted as wires/sticks for clarity. The non-labelled atoms are symmetry generated using different symmetry codes. Thermal ellipsoids set at 50% probability.

6 Zusammenfassung

Für die Zusammenfassung der im Rahmen dieser Dissertation erarbeiteten Ergebnisse, ist es sinnvoll die verschiedenen Themengebiete einzeln darzustellen. Die Ergebnisse bezüglich der Synthese und Koordinationschemie siliziumreicher Kronenether folgen zu Anfang. Als nächstes folgen die Ergebnisse hinsichtlich der Koordinationschemie mit D_n Ligandsystemen. Mit der Berylliumchemie wurde zudem ein dritter Teil als logische Erweiterung des Themengebietes etabliert, der abschließend dargestellt werden soll. Wichtige Notiz: Die Reihenfolge der hier zusammengefassten Ergebnisse unterscheidet sich von jener im kumulativen Teil. Des Weiteren sind unveröffentlichte Ergebnisse ebenfalls miteinbezogen.

6.1 Beiträge zur Koordinationschemie von Disila-Kronenethern

Die Synthese von disila-verbrückten Polyethylenglykolen stellte sich gemäß der Reaktionsbedingungen skizziert in Schema 14 als erfolgreich dar. Die dargestellte Reaktion war erfolgreich für Di- und Triethylenglykol, scheiterte jedoch beim Einsatz von Ethylenglykol. Entsprechend wurden 8,9-Disila-EO5 und 10,11-Disila-EO7 erfolgreich per NMR Spektroskopie und MS Spektrometrie charakterisiert.

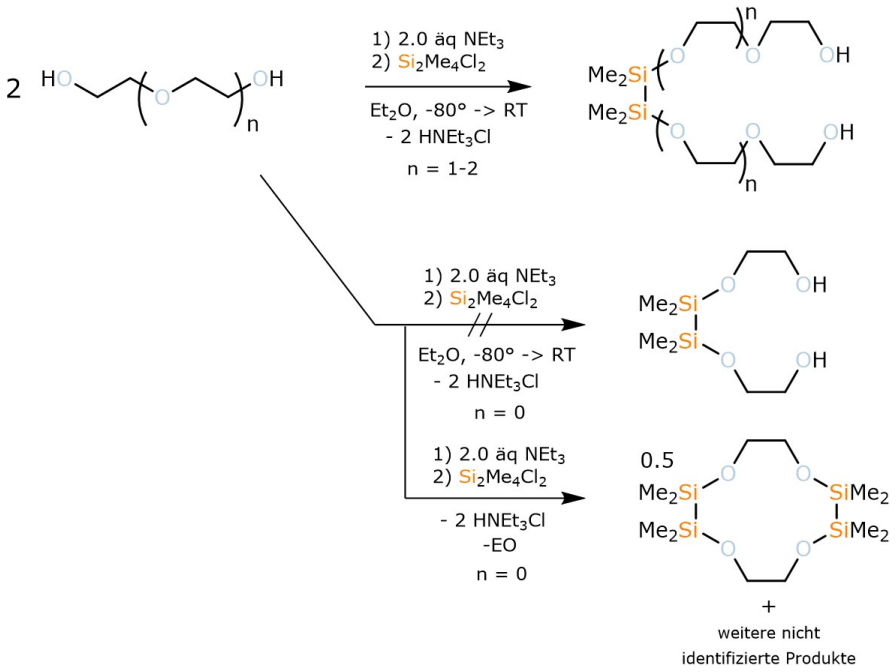

Schema 14: Gelungene und gescheiterte Synthesen verschiedener disila-verbrückter Glykole.

Der Versuch diese Glykole weiter zu funktionalisieren und diese als Baustein für Hexasilakronenether zu nutzen scheiterte. Die Problematik lag darin, dass sich die Liganden unter Zugabe der etablierten Basen NEt_3 und Cs_2CO_3 zersetzen (Schema 15, oben). Daher konnte bisher keine Umsetzung mit $O(Si_2Me_4Cl)_2$ erfolgen. Entsprechend scheiterte zwar diese Strategie zur Darstellung siliziumreicher Kronenether, dennoch konnten einige Koordinationsverbindungen disila-verbrückter Glykole erfolgreich synthetisiert und dabei eine interessante Reaktivität gegenüber verschiedener Metallionen beobachtet werden (Schema 15, unten).

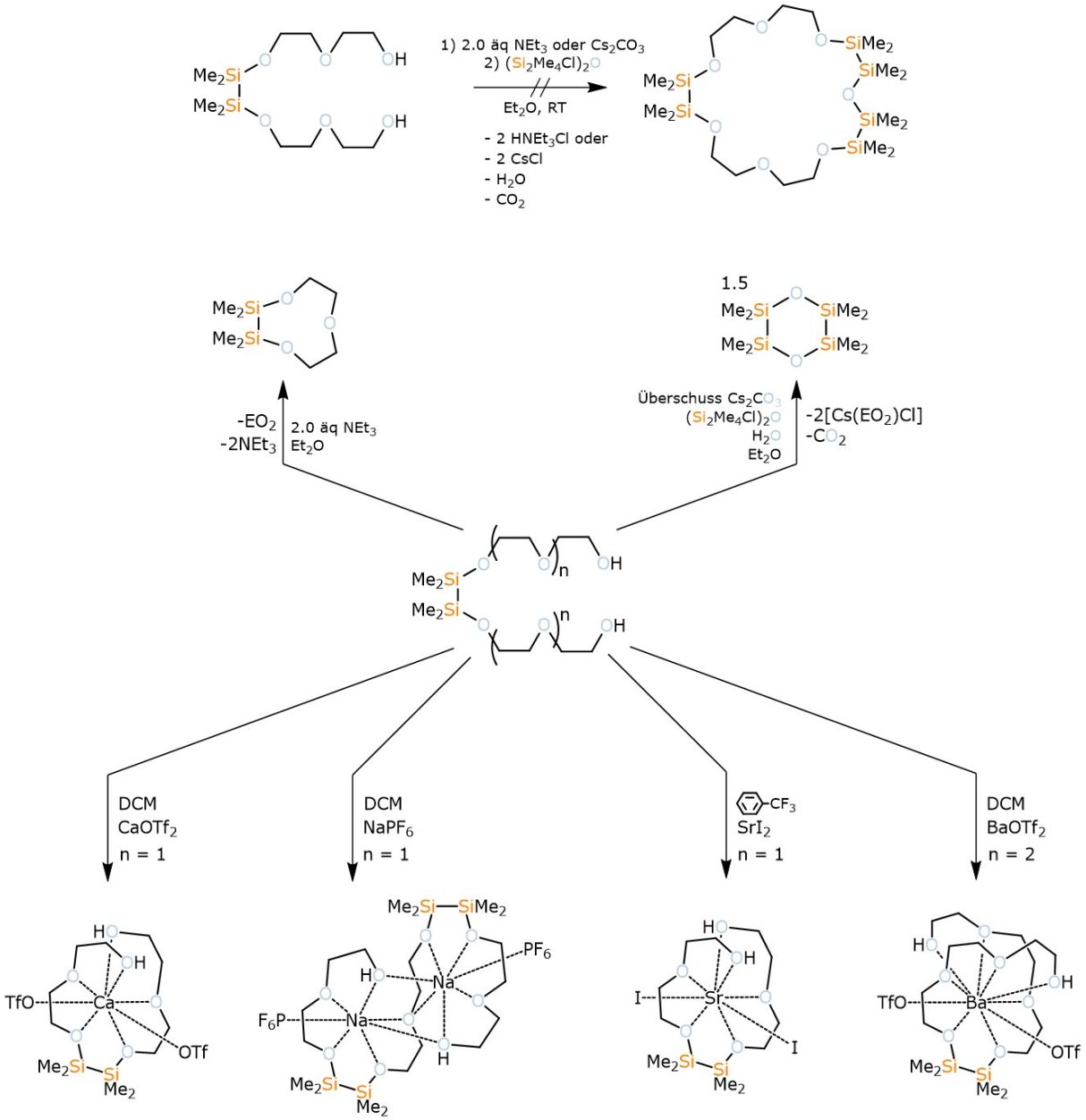

Schema 15: Geplante Synthese eines Hexasilakronenethers und Koordinationschemie disila-verbrückter Glykole (ausgewählte Beispiele).

Die dargestellten Koordinationsverbindungen konnten allesamt in geeigneten Einkristallstrukturen beobachtet werden, was einerseits die gelungene Synthese der Liganden bestärkt und andererseits zeigt, dass auch offenkettige Ligandsysteme stabile Koordinationsverbindungen mit verschiedenen s-block Metallionen bilden können (siehe u.a. Abbildung 32). Besondere Aufmerksamkeit hat vor allem die Reaktion von $NaPF_6$ mit 8,9-Disila-EO5 erregt. Unter Eliminierung von einem Äquivalent EO2 wurde die Bildung eines tetrasila-Oktaethylenglykolliganden beobachtet, der zwei Natriumionen bindet. Die Anordnung der Sauerstoffatome um die Na^+ Zentren herum ist coplanar, sodass diese symmetrische Anordnung vermutlich die Triebkraft dieser Reaktion ist. Das Koordinationsmuster gleicht jenem von [Na(1,2-Disila[15]Krone-5)ClO_4]. Insgesamt ist die Reaktion ein erstes Beispiel einer templatgesteuerten Reaktion. Dies zeigte, dass disilan-basierte Liganden ganz offensichtlich für Ringöffnungspolymerisationen aktiviert werden können.

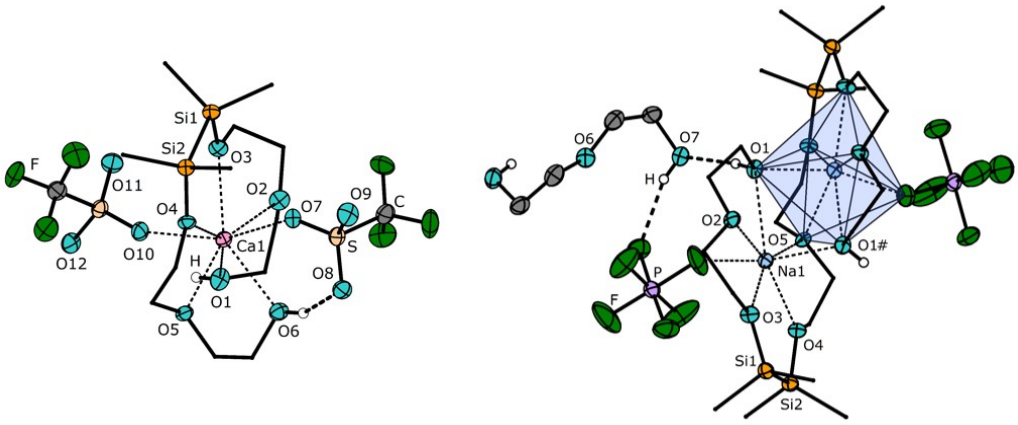

Abbildung 32: Die Molekülstrukturen von [Ca(8,9-Disila-EO5)$(OTf)_2$] und [Na_2(8,9,17,18-Tetrasila-EO8)$(PF_6)_2$]·EO2 im Kristall: Zwei Beispiele für s-block Metallionen koordiniert von Disilaglykolen. Kohlenstoffatome sind als wires/sticks dargestellt aus Gründen der Übersichtlichkeit. Schwingungsellipsoide zeigen eine Aufenthaltswahrscheinlichkeit von 50%.

Während Komplexbildung für die Kationen Na^+, Ca^{2+}–Ba^{2+} beobachtet wurde, konnten bspw. keine Koordinationsverbindungen für Cs^+ hergestellt werden. Die Umsetzung von 10,11-Disila-EO7 mit CsOTf in DCM liefert eine farblose Lösung, was demonstriert, dass ein solcher Ligand das Salz in einem organischen Lösungsmittel löst. Beim Entfernen des Lösungsmittels und entsprechender Aufarbeitung wird die Bildung von wasserfreiem α-CsOTf beobachtet, welches aus dem öligen Liganden kristallisiert. Anhand der Beobachtung war festzustellen, dass es Anzeichen

für eine Kationenselektivität gibt. Harte s-block Metallionen scheinen bevorzugt gebunden zu werden. Mittels quantenchemischer Rechnungen wird diese Annahme bekräftigt: Starke Wechselwirkung des siliziumbasierten Rückgrats sind für M_{EA}^{2+} (M_{EA} = Ca^{2+}, Sr^{2+}) beobachtet worden. Das Gegenteil hingegen für Cs^{+}. Um diese Ionenselektivität weiter zu untersuchen und zu evaluieren, ob es unter Umständen doch möglich ist, Koordinationsverbindungen der schweren Alkalimetalle zu synthetisieren, wurden die Triflatsalze MOTf (M = Rb^{+}, Cs^{+}) mit verschiedenen Liganden wie 8,9-Disila-EO5, 11,12-Disila-EO7 oder 1,2,10,11-Tetrasila[18]Krone-6 in DCM umgesetzt. Alle Reaktionen waren jedoch erfolglos. Interessanterweise führte die Umsetzung der entsprechenden Salze in allen Fällen zur teilweisen Umkristallisation der Salze. Demnach erfolgte die Einkristallstrukturbestimmung dieser Salze. Wie frühere Arbeiten zeigen, konnten die Kristallstrukturen dieser Salze nur über Röntgenpulverdiffraktometrie ermittelt werden. Einkristallstukturen hingegen konnten nicht bestimmt werden, was auf hohe Hygroskopie, schlechte Kristallqualität und Fehlordnungsproblematiken zurückgeführt wurde. Die Kombination eines Silapolyethers, einer Inertgasatmosphäre sowie ein schwach koordinierendes Lösungsmittel wie DCM, führte zum Erhalt von Einkristallen, die nun geeignet für eine Strukturanalyse waren. Die Ergebnisse früherer Studien wurden per Einkristalldiffraktometrie bestätigt.

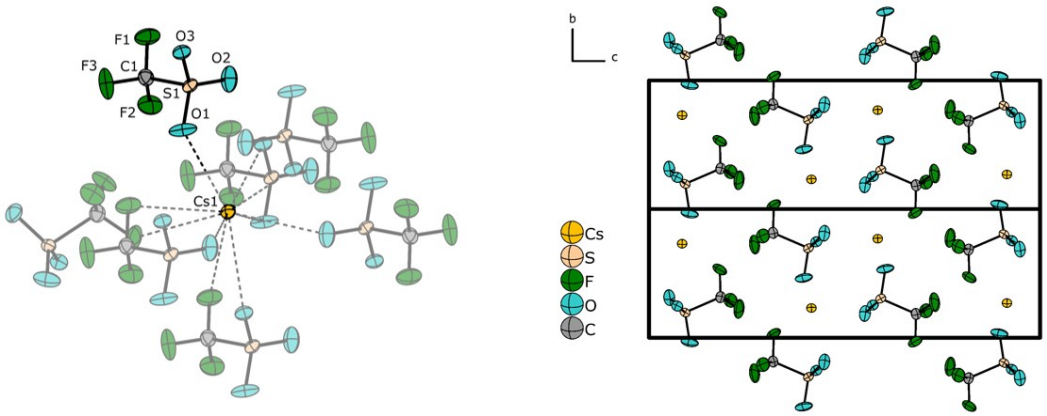

Abbildung 33: Die Struktur von CsOTf im Kristall bei 100 K. Links: Koordinationssphäre des Cs^{+} Ions und rechts: Zellpackungsdiagramm als Superzelle entlang [100]. Schwingungsellipsoide zeigen eine Aufenthaltswahrscheinlichkeit von 50%.

Dies stellt eine Überstruktur der bisher publizierten Kristallstruktur dar, was u.a. in einer verdoppelten kristallographischen *c* Achse deutlich wird (Abbildung 33). Diese Methode zur Kristallisation ist nicht beschränkt auf Triflatsalze. So konnte ebenfalls die Einkristallstruktur von Cs_2Ox ($Ox = C_2O_4^{2-}$) ermittelt werden. Um die Notwendigkeit eines Sila-polyethers zu verdeutlichen, wurden die Triflatsalze MOTf (M = Rb, Cs) ebenfalls mit einem organischen Polyether zur Reaktion gebracht. Die Reaktion mit EO5 lieferte die Komplexe $[Rb_3(EO5)OTf_3]$ und [Cs(EO5)OTf]. Demnach ist es also in der Tat das Siliziumrückgrat, was den oben genannten Liganden erlaubt als effektive Kristallisationshilfe zu dienen und eben keine Koordinationsverbindungen einzugehen. 8,9-Disila-EO5, 11,12-Disila-EO7 und 1,2,10,11-Tetrasila[18]Krone-6 sind demnach brauchbare Lösungsvermittler und fördern die Kristallisation schwer zu fassender Alkalimetallsalze. Basierend auf den bis hierhin dargelegten Ergebnissen, sind hybride Disila-Liganden gute Liganden gegenüber leichten und demnach harten s-block Metallsalzen. Weniger gute Liganden sind sie gegenüber den schweren und demnach weichen Alkalimetallsalzen. Fraglich war an dieser Stelle inwiefern sich derartige Liganden gegenüber Ionen verhalten, die Wasserstoffbrückenbindungen ausbilden. Für eine derartige Untersuchung boten sich 1,2-Disila[18]Krone-6 und 1,2-Disila-Benzo[18]Krone-6 als Liganden und NH_4PF_6 als Salz an. Die Reaktion in DCM verlief glatt wie in Schema 16 dargestellt. Der erfolgreiche Einbau des NH_4^+ Ions zeigte sich dann anhand von NMR und IR Spektroskopie. Tieffeldshift im ^{29}Si NMR Spektrum und drei rotfeldverschobene N–H Streckschwingungen sowie letztlich die Kristallstrukturen der Verbindungen $[NH_4(1,2\text{-Disila}[18]\text{Krone-6})]PF_6$ und $[NH_4(1,2\text{-Disila-Benzo}[18]\text{Krone-6})]PF_6$ zeigen den erfolgreichen Einbau des Ammoniumions (Abbildung 34).

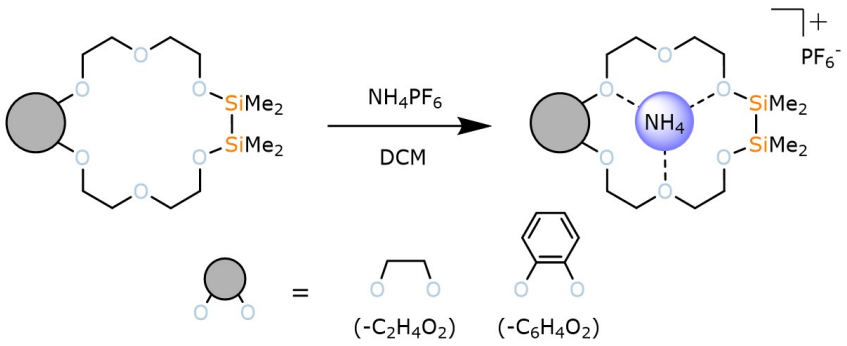

Schema 16: Synthese von NH_4^+ Komplexen mit hybriden Disila-Kronenethern.

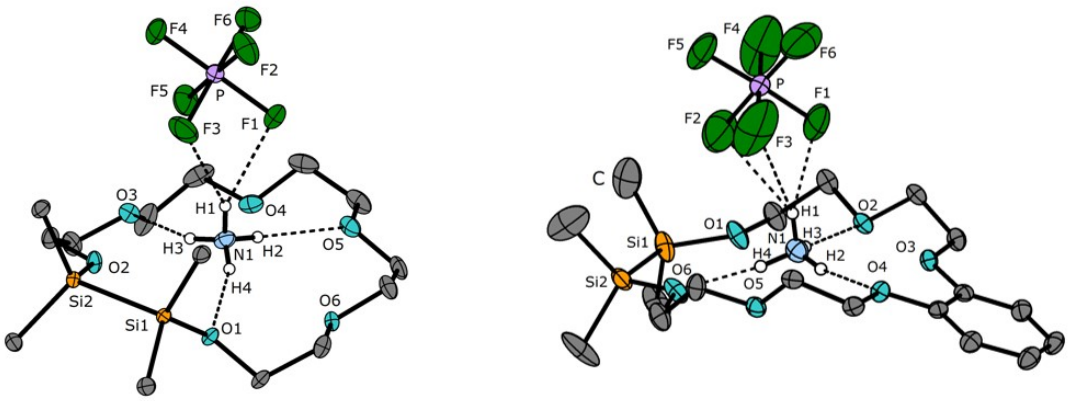

Abbildung 34: Zwei Disila-Kronenether Komplexe die sich durch Wasserstoffbrückenbindungen auszeichnen: $[NH_4(1,2\text{-Disila-}[18]\text{Krone-}6)]PF_6$ und $[NH_4(1,2\text{-Disila-}[18]\text{Krone-}6)]PF_6$ im Kristall. Schwingungsellipsoide zeigen eine Aufenthaltswahrscheinlichkeit von 50%. Co-kristalline DCM Moleküle sind aus Gründen der Übersicht ausgeblendet.

Anhand der bisher erhaltenen Ergebnisse sowie den bereits publizierten Ergebnissen hinsichtlich Disila-Kronenether und ihren Metallkomplexen, ist ersichtlich, dass diese Liganden eine Tendenz dazu ausbilden die Ionen Na^+-K^+, das pseudo Alkalimetallion NH_4^+ sowie die Erdalkalimetallionen Mg^{2+}-Ba^{2+} zu binden. Eine Ionenselektivität hin zu harten s-block Metallionen ist angedeutet. Als nächster Schritt, um die Donoreigenschaften von Siloxanverbindungen näher zu untersuchen, wurde ermittelt, wie verschiedene s-Block Metallionen ein $(Si_2Me_4)_2O$ Rückgrat zur Koordination aktivieren können und ob eine ähnliche Tendenz gegenüber den leichten s-Block Metallionen gefunden wird. Die Synthese des dafür geeigneten Kronenethers 1,2,4,5-Tetrasila-Benzo[15]Krone-5 verlief erfolgreich, nachdem $(Si_2Me_4Cl)_2O$ mit dem entsprechenden Glykol in THF unter Anwesenheit der Base NEt_3 umgesetzt wurde (Schema 17, oben). Weitere Umsetzungen erfolgten dann mit s-Block Metalliodiden, um zu den entsprechenden Komplexen zu gelangen. Die Wahl fiel auf diese Salze aufgrund der großen Verfügbarkeit sowie früherer Erfolge diese Salze mit verschiedenen Disila-Liganden zu komplexieren. In der Tat sind auch hier die entsprechenden 1:1 Komplexe nach äquimolarer Reaktion von Ligand und Salz in α,α,α-Trifluortoluol zugänglich (Schema 17, unten). Für alle dargestellten Koordinationsverbindungen wurden Kristallstrukturen angefertigt. Abhängig vom entsprechenden Ionenradius konnten verschiedene Koordinationsmodi des Liganden beobachtet und zudem mit Hilfe von ^{29}Si NMR Spektroskopie in

Lösung bestätigt werden. Das NMR Experiment zeigte sich als hervorragende Sonde für die Stärke der Interaktion des Siloxanrückgrats mit dem Metallion, da die ^{29}Si NMR Verschiebung sehr empfindlich gegenüber Koordination reagiert: Li^+ zeigt keine Wechselwirkung mit dem Siloxanrückgrat, Mg^{2+} zeigt schwache Wechselwirkungen, Na^+ moderate Wechselwirkungen und Ca^{2+} sowie Sr^{2+} zeigen schließlich starke Wechselwirkungen (Abbildung 35).

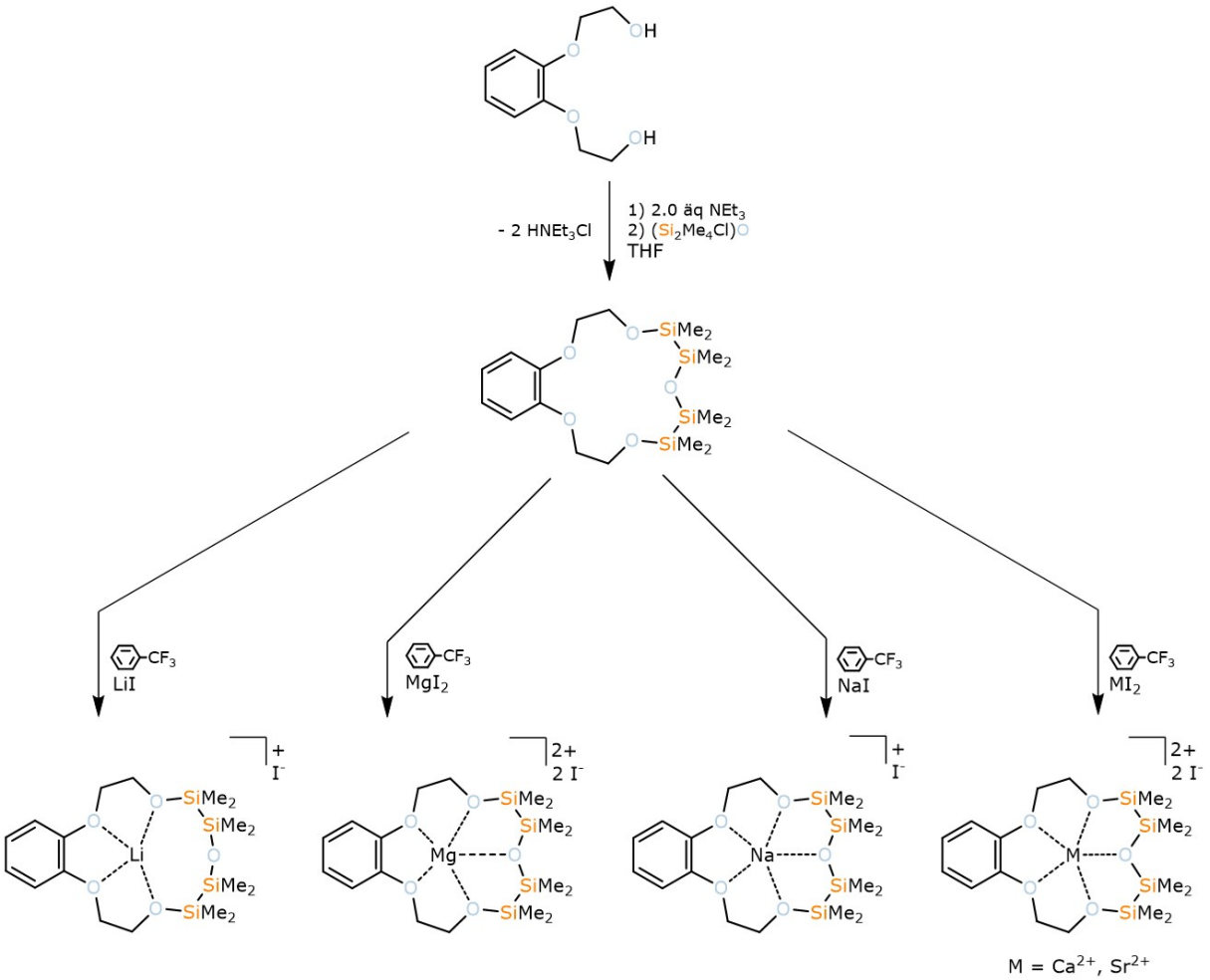

Schema 17: Synthese von s-block Metallkomplexen des Liganden 1,2,4,5-Tetrasila-Benzo[15]Krone-5.

Bei Betrachtung der in Abbildung 35 skizzierten Ergebnisse kann geschlussfolgert werden, dass es eben jene Kationen sind, die die Si-O Bindung für Koordination aktivieren, die einen harten Charakter besitzen und zusätzlich gut in den Hohlraum des Liganden passen. Das härteste hier eingesetzte Kation, Mg^{2+}, zeigt zwar nur schwache Wechselwirkungen mit dem Siloxanliganden, ist aber ebenso wie Li^+ zu klein für die Kavität des Liganden. Demnach kann die Wechselwirkung

mit einem weniger harten Kation wie Na^+ stärker sein, als jene mit dem harten Mg^{2+}-Ion. Dennoch sind es vor allem die harten Erdalkalimetallionen, welche die Si-O Bindung zur Koordination aktivieren können, was im Rahmen dieser Arbeit zusätzlich im Vergleich von [K(1,2,4,5-Tetrasila[18]Krone-6)PF_6] und [Ba_2(1,2,4,5-Tetrasila[18]Krone-6)$_2I_4$] deutlich wird. Der Bariumkomplex wurde synthetisiert, indem 1,2,4,5-Tetrasila[18]Krone-6 mit BaI_2 umgesetzt wurde.

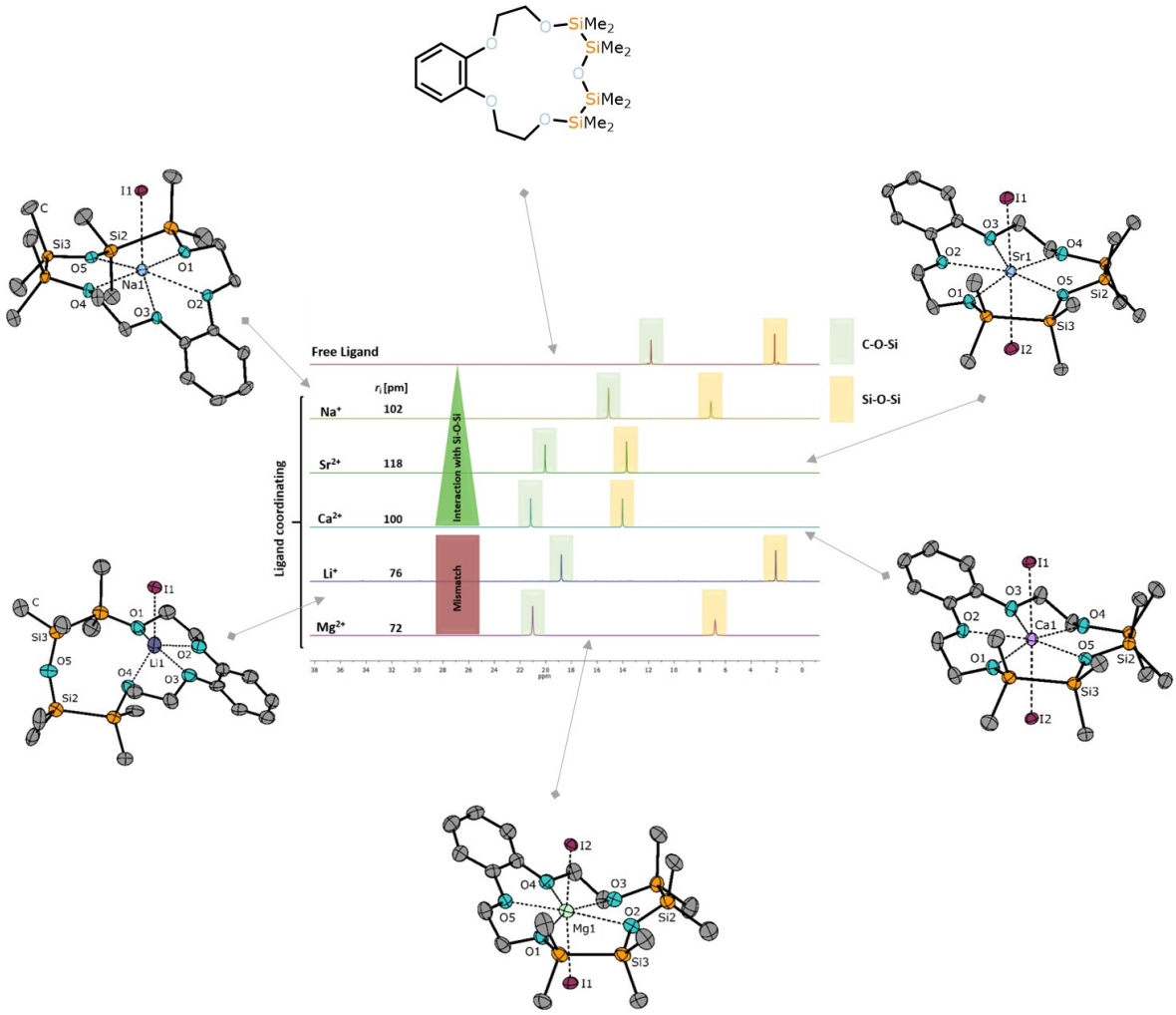

Abbildung 35: Tetrasila-Kronenether-Komplexe in Kristallform und dazugehörige ^{29}Si NMR Spektren. Schwingungsellipsoide zeigen eine Aufenthaltswahrscheinlichkeit von 50%. Co-kristalline Lösungsmittelmoleküle sind aus Gründen der Übersicht ausgeblendet.

Trotz der Tatsache, dass K^+ und Ba^{2+} bei gegebener Koordinationszahl nahezu denselben Ionenradius aufweisen, zeigten die Röntgenstrukturanalyse sowie das ^{29}Si NMR Experiment, dass die Wechselwirkung des Siloxanliganden deutlich stärker gegenüber dem Ba^{2+} Ion ausfällt: Moderate

Wechselwirkungen des Siloxanrückgrats zeigen sich gegenüber Ba^{2+} ($\Delta\delta(^{29}Si$, innere Si-Atome) = 8.3 ppm) während keine Wechselwirkung beobachtet wird gegenüber K^+ in der literaturbekannten Verbindung [K(1,2,4,5-Tetrasila[18]Krone-6)PF_6]. Das Gesamtbild zeigt damit klar, dass es v.a. harte s-Block Metallionen sind, die besonders starke Wechselwirkungen mit Siloxanen eingehen können solange dies ein geeigneter Hohlraum zulässt.

Die bis hierhin gewonnenen Erkenntnisse sind in einem nächsten Schritt auf templatgesteuerte Reaktionen angewandt worden. Um nun auch neuartige Ligandsysteme zu erhalten, sind eine Reihe an Reaktionen durchgeführt worden, bei denen Erdalkalimetalliodide mit kleinen Ligandbausteinen umgesetzt wurden. Hierbei zeigten sich einige Reaktionen als erfolgreich und in der Tat waren so neue Ligandsysteme zugänglich, welche bisher nicht über andere Wege synthetisiert werden konnten (Schema 18). Eine 1:2 Reaktion von 1,2,7,8-Tetrasila[12]Krone-4 mit 1,2-Disila[9]Krone-3 unter Anwesenheit von MgI_2 wurde versucht, um den siliziumbasierten Kronenether 1,2,7,8-Tetrasila[15]Krone-5 zu erhalten. Aufgrund des kleinen Ionenradius‘ von Mg^{2+} scheiterte die Reaktion anfänglich, da die Bildung von [Mg(1,2,7,8-Tetrasila[12]Krone-4)I_2] beobachtet wurde. Das Mg^{2+} Ion findet in der Kavität von 1,2,7,8-Tetrasila[12]Krone-4 Platz, sodass es keine Triebkraft für eine Ringöffnungsoligomerisierung gibt. Wiederholung der Reaktion mit CaI_2 zeigte hingegen die Bildung des angestrebten Liganden. Dies demonstriert klar, dass kleine Silakronenether durch Umsetzung mit einem harten s-Block Metallion zu ionenspezifischen Kronenethern gekuppelt werden können. Dies ist ein einzigartiges Reaktionsverhalten von Sila-Kronenethern, denn derartige Ring-Expansionen wurden für organische Kronenether bisher nicht beschrieben. Weitere Reaktionen wurden mit SrI_2 durchgeführt. Das größere Sr^{2+} Kation erlaubte den Erhalt von vier weiteren, neuartigen Disila-Kronenethern durch (Kreuz-)Kupplung. Das wohl bemerkenswerteste Beispiel wurde durch Kreuzkupplung von 1,2,7,8-Tetrasila[12]Krone-4 und 1,2,4,5-Tetrasila[9]Krone-3 beobachtet: Mit dem Strontiumkomplex [Sr(1,2,4,5,10,11-Hexasila[15]Krone-5)I_2] konnte der erste Hexasila-Kronenether synthetisiert und charakterisiert werden.

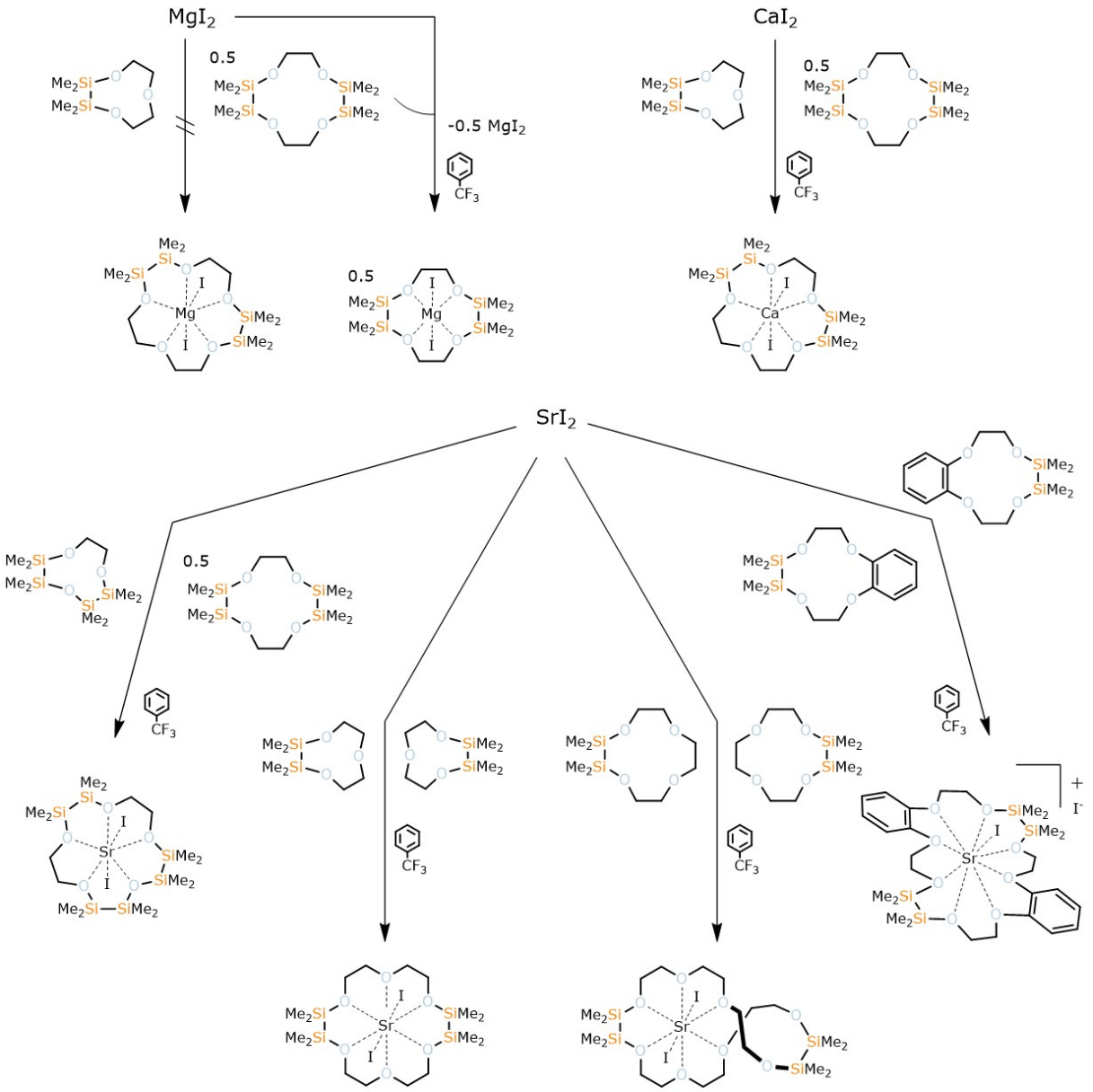

Schema 18: Synthese von neuartigen Disila-Kronenethern unter Templatwirkung verschiedener Erdalkalimetallsalze.

Mit diesem Liganden wurde also schließlich jener Hexasilakronenether synthetisiert, der über die zuvor dargestellte Disilaglykol-Route nicht zugänglich war. Die drei weiteren Liganden, die nach Kupplung des jeweiligen Bausteins synthetisiert wurden, sind 1,2,10,11-Tetrasila[18]Krone-6, 1,2,13,14-Tetrasila[24]Krone-8 und 1,2,13,14-Tetrasila[24]Krone-8.

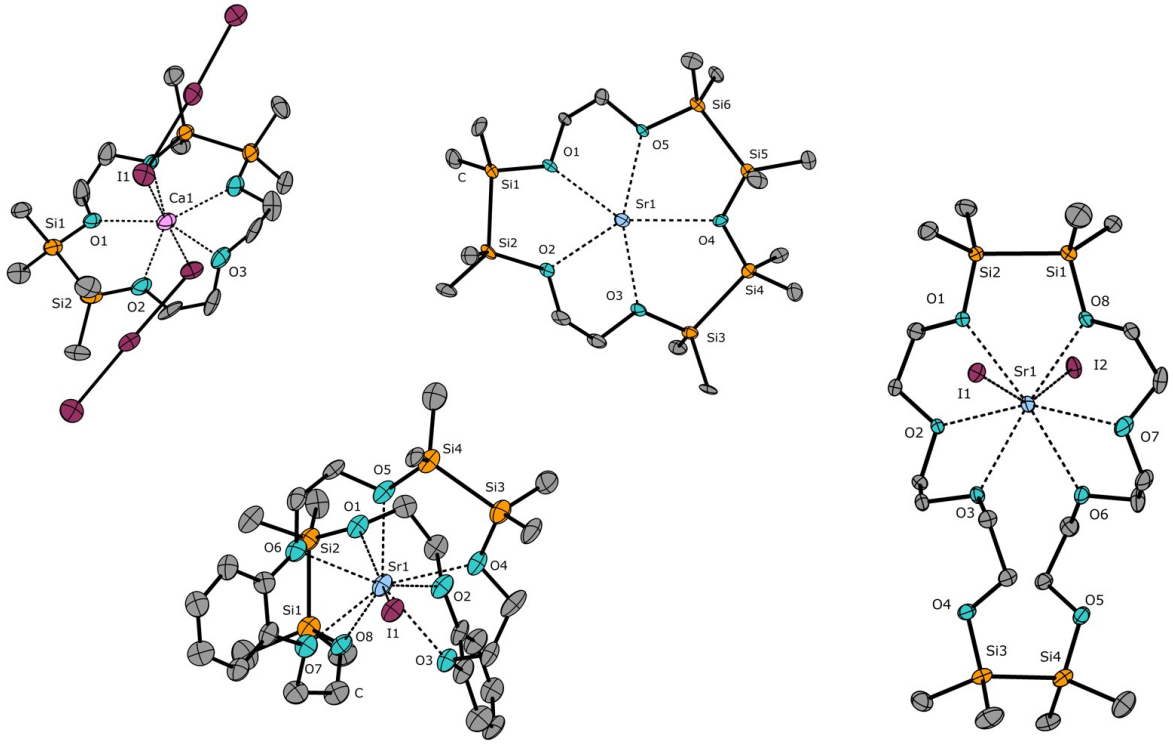

Abbildung 36: Ausgewählte Kristallstrukturen von verschiedenen Erdalkalimetallkomplexen die mittels templatgesteuerter Reaktion synthetisiert wurden. Schwingungsellipsoide zeigen eine Aufenthaltswahrscheinlichkeit von 40% (links dargestellte Strukturen) und 50% (rechts dargestellte Strukturen). Das GaI_4^- Ion von [Sr(1,2,4,5,10,11-Hexasila[15]Krone-5)$(GaI_4)_2$], das nicht-koordinierende Iodidion von [Sr(1,2,13,14-Tetrasiladibenzo[24]Krone-8)I]I sowie co-kristalline Lösungsmittelmoleküle sind aus Gründen der Übersicht nicht dargestellt.

Die genannten Liganden sind ebenfalls in geeigneten Einkristallstrukturen beobachtet worden. Mehrere Iodidokomplexe konnten allerdings nicht brauchbar kristallisiert werden, sodass verschiedene Gegenionen genutzt wurden, um eine Kristallisation zu fördern. Elementares Iod sowie GaI_3 stellten sich dabei als sinnvolle Reagenzien heraus, um das Iodidion in ein anders Ion, wie I_3^- oder GaI_4^- zu überführen. Ausgewählte Kristallstrukturen sind in Abbildung 36 dargestellt. Im Rahmen dieser templatgesteuerten Reaktionen wurden auch BaI_2 sowie eine verschiedene Erdalkalimetallbromide getestet. Bisher jedoch ohne Erfolg. Ein Mechanismus hinter diesen Reaktionen wurde postuliert: Als erster Schritt erfolgt eine exocyclische Koordination des Metallions an den Silakronenether wobei die Si-O Bindung aktiviert wird. Anschließend wird der Ring geöffnet unter Ausbildung eines Glykolats mit terminaler Iodosilanfunktionalität. Dieses Glykolat greift

dann nucleophil einen weiteren Silakronenether an, um anschließend in einer templatgesteuerten Reaktion Substitutionsreaktion den entsprechenden Kronenether zu bilden. Eine vorausgeschaltete, effektive Si-O Bindungsaktivierung, zusammen mit geeigneten Nucleophilen (hier offensichtlich Iodidionen) scheinen wichtige Faktoren zu sein, die entscheiden, ob eine templatgesteuerte Reaktion erfolgreich verläuft oder nicht.

Die in Schema 18 dargelegten Ergebnisse zeigen ein vielversprechendes Reaktionsverhalten von Silakronenethern gegenüber Erdalkalimetallionen. Im nächsten Schritt wurde nun versucht einen Kronenether herzustellen, bei dem das Rückgrat vollständig disilansubstituiert ist. Für dieses Vorhaben kamen nun verschiedenste Magnesium- und auch Berylliumsalze zum Einsatz. Angedacht war, den kleinen dafür notwendigen Precursor $^2D_2$ entsprechend zu aktivieren und eine Ringöffnungspolymerisation, analog wie oben dargestellt, zu initiieren. Als Lösungsmittel wurde erneut α,α,α-Trifluortoluol gewählt. Es zeigte sich jedoch, dass unter diesen Bedingungen nun keine Bildung des Sila-Kronenethers beobachtet wird, sondern dass diese LEWIS-aciden Systeme C-F Bindungen aktivieren. Im Falle einer $M_{EA}Br_2/GaBr_3/^2D_2$-Mischung in α,α,α-Trifluortoluol wird die für chemisch inert gehaltene CF_3 Gruppe des Lösungsmittels vollständig dekonstruiert und es kommt zur Bildung eines seltenen siloxy-stabilisierten Carbeniumions (Abbildung 37).

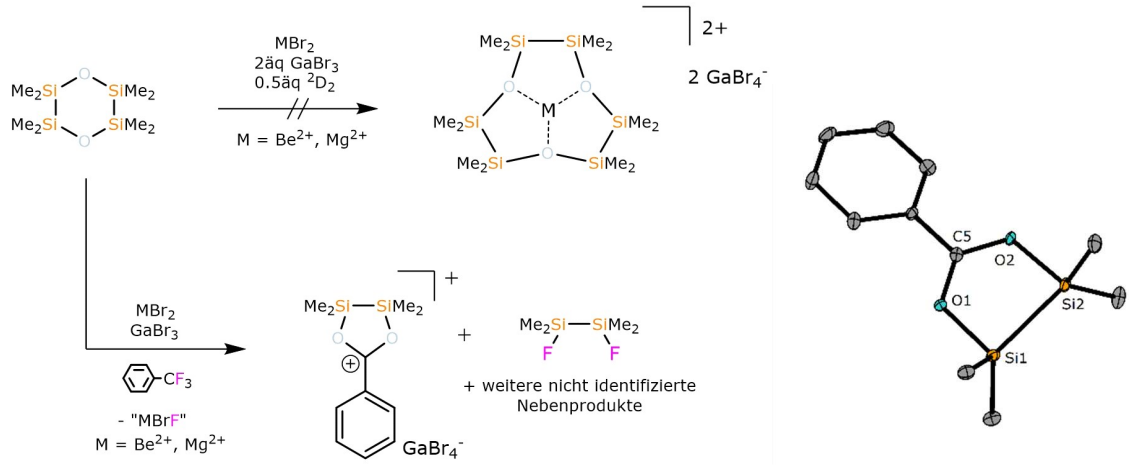

Abbildung 37: Angedachte Synthese eines siliziumbasierten Kronenethers und beobachteter Reaktionspfad (links) und Kristallstruktur des Kations in $[Ph\text{-}C(O_2Si_2Me_4)]GaBr_4$ (rechts). Schwingungsellipsoide zeigen eine Aufenthaltswahrscheinlichkeit von 50%. Das Gegenion $GaBr_4^-$ ist aus Gründen der Übersicht nicht dargestellt.

Beim Reaktionsverlauf ist es wahrscheinlich, dass sich übergangsweise ein Ph-CF_2^+ Kation bildet, welches dann mit dem Precursor $^2D_2$ reagiert. Unter Bildung von $(SiMe_2F)_2$ und weiteren bisher nicht identifizierten Nebenprodukten bildet sich [Ph-C($O_2Si_2Me_4$)]$GaBr_4$. Nachdem im weiteren Forschungsverlauf beobachtet wurde, dass sich α,α,α-Trifluortoluol in der Gegenwart von weiteren Salzen mit hartem Metallkation wie BeI_2, GaI_3, HfI_4, ThI_4 zersetzt, sind also bei gewissen Reaktionen andere Lösungsmittel als α,α,α-Trifluortoluol von Nöten.

Die Wahl fiel folglich auf Ph-F, um derartige Nebenreaktionen zu vermeiden. $^2D_2$ konnte nun erfolgreich mit verschiedenen s-Block Metalliodiden in der Gegenwart von GaI_3 umgesetzt werden (siehe u.a. Schema 19). Letzteres dient als Iodidionenakzeptor wie bspw. auch für [Sr(1,2,4,5,10,11-Tetrasila[15]Krone-5)$(GaI_4)_2$] gezeigt wurde. Unter Umsatz mit *in-situ* generiertem $M(GaI_4)_n$ zeigte sich die Bildung von $^2D_3$ für M = Li^+ (n = 1), während bei M = Na^+, Mg^{2+}, Ca^{2+}, Sr^{2+} (n = 1 oder 2) die Bildung von $^2D_4$ beobachtet wird.

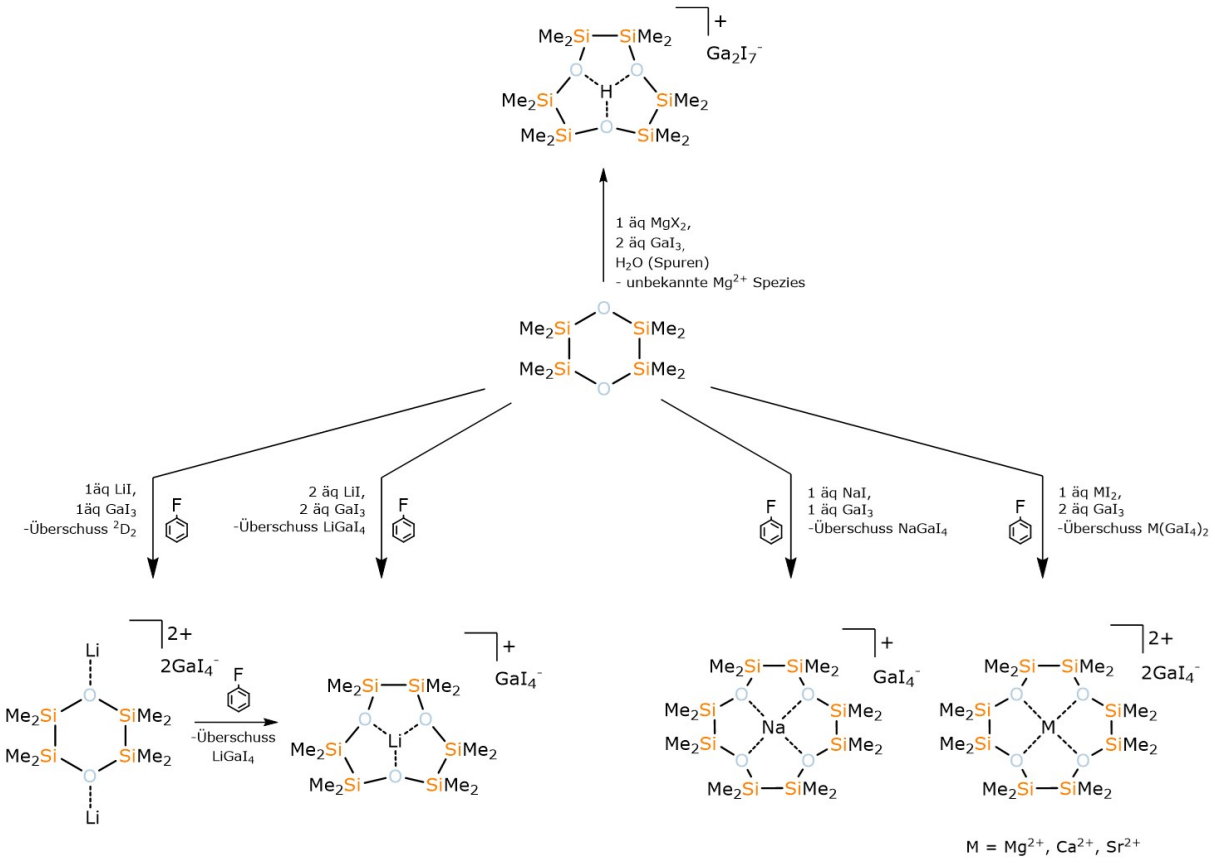

Schema 19: Templatgesteuerte Synthese von anorganischen Kronenethern.

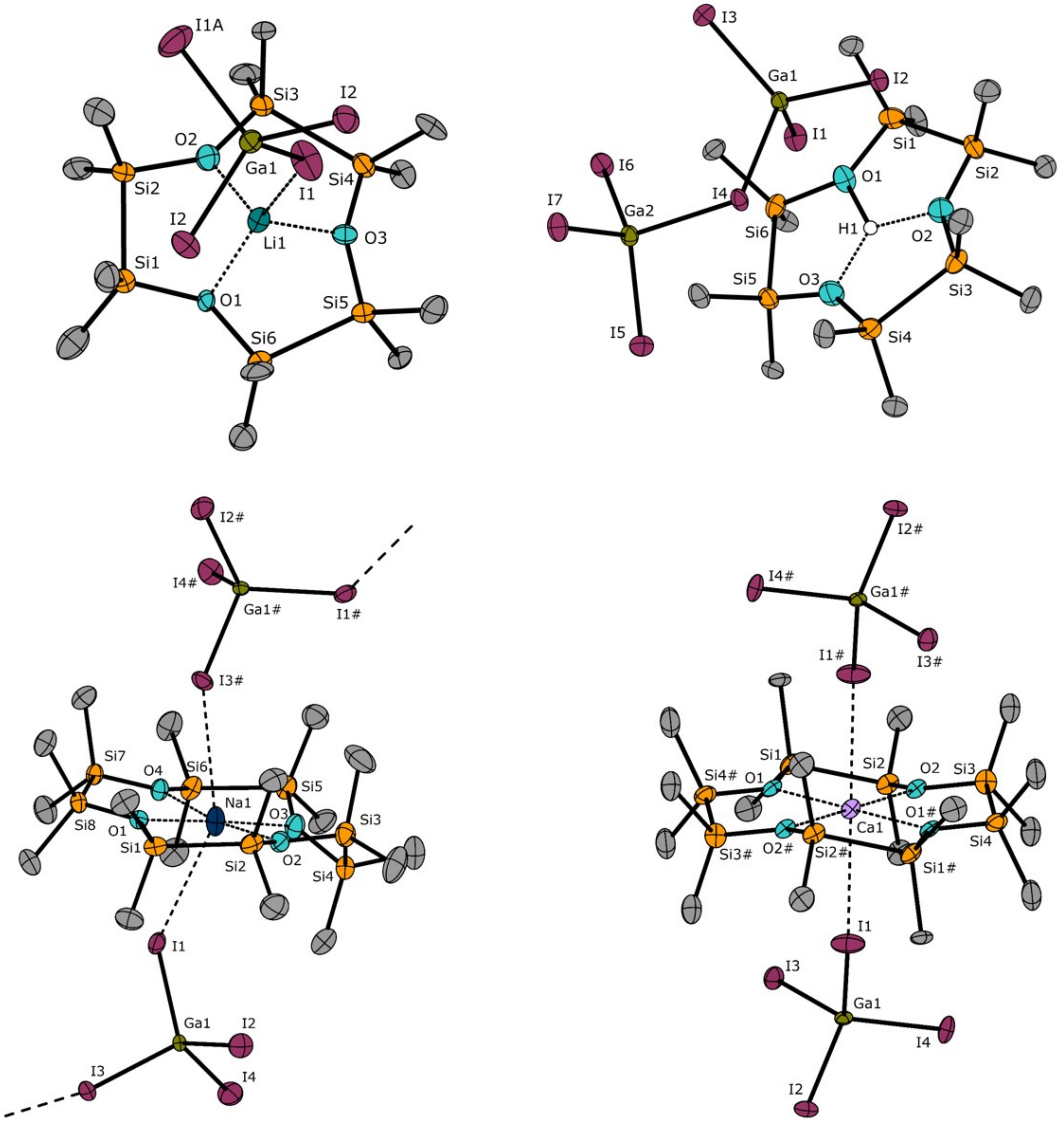

Abbildung 38: s-Block Komplexverbindungen der Liganden $^2D_3$ (oben) und $^2D_4$ (unten) in Kristallform. Atome markiert mit # sind symmetriegeneriert über x, 3/2-y, 1/2+z oder 1-x,1-y, 1-z. Co-kristalline Lösungsmittelmoleküle sind aus Gründen der Übersicht nicht dargestellt. Schwingungsellipsoide zeigen eine Aufenthaltswahrscheinlichkeit von 50%.

Die Verbindungen $[Li(^2D_3)GaI_4]$ und $[M(^2D_4)(GaI_4)_2]$ konnten alle per NMR Spektroskopie aller gängigen NMR aktiven Kerne sowie per Röntgenstrukturanalyse (gilt nicht für M = Mg^{2+}) charakterisiert werden. Darüber hinaus konnte die Bildung eines weiteren Komplexes mit $^2D_3$ Ligand beobachtet werden. $[H(^2D_3)]Ga_2I_7$ ist charakterisiert worden, nachdem die Reaktion mit einem Magnesiumsalz durchgeführt und das Produkt mit Spuren von Feuchtigkeit kontaminiert wurde.

An dieser Stelle sei erwähnt, dass die Zeitspanne zwischen den ersten publizierten Ergebnissen hinsichtlich Disilakronenether und den hier beschriebenen Ergebnissen mehr als vier Jahre beträgt. Wird der Startpunkt dieses Forschungsprojektes zugrunde gelegt, so misst die Zeitspanne sogar mehr als sechs Jahre. Templatgesteuerte Synthesen, geeignete Koordinationspartner sowie ein inertes Lösungsmittel stellten sich als Schlüsselfaktoren heraus, die diesen Erfolg schließlich möglich machten. Ein wichtiger Schritt in der Bildung dieser Kronenether stellt die exozyklische Koordination von M^{n+} an den Precursor $^2D_2$ dar, ähnlich wie es auch für die Ringöffnungsoligomerisation hybrider Liganden postuliert wurde. Dies konnte nun auch experimentell gestützt werden nach Erhalt der Kristallstruktur der Verbindung $[Li_2(^2D_2)(GaI_4)_2]$. Die Verbindung bleibt erhalten, wenn $LiGaI_4$ mit $^2D_2$ unter Berücksichtigung von vergleichsweise kurzen Reaktionszeiten zur Reaktion gebracht wird. Die Kristallstrukturbestimmung zeigt eine Verlängerung der Si-O Bindung und eine Verkleinerung des Si-O-Si Winkels. Folglich wird die Si-O Bindung aktiviert bevor die Ringöffnungsoligomerisation stattfindet und sich die oben dargestellten Verbindungen bilden. Die dargestellten Kronenether sind weitestgehend stabil in Lösung, was sich per DOSY NMR bestätigen ließ. Solange das Templat innerhalb des Rings gebunden bleibt, bleibt auch die Ligandstruktur erhalten. Nach Zugabe von MeCN konnte das Metallion vom Kronenether entfernt werden. Dies führte zur Oligo- aber auch zur Monomerisierung dieser neuartigen Liganden. Die freien Liganden $^2D_2$, $^2D_4$, $^2D_5$ und $^2D_6$ konnten per NMR spektroskopischen und/oder massenspektrometrischen Untersuchungen nachgewiesen werden. Die oligomerisierten Liganden zeigten sich in Lösung jedoch über einen längeren Zeitraum hinweg als instabil und reagieren zurück zum Monomer $^2D_2$. Die Ringöffnungspolymerisation scheint demnach reversibel zu sein und eröffnet daher, auch durch Recycling des Precursors, eine potentielle Anwendung im Bereich von Extraktionstechniken. Um das Koordinationsvermögen dieser neuartigen Liganden sowie den Mechanismus hinter diesen templatgesteuerten Reaktionen besser zu verstehen, wurden abschließend aufwändige quantenchemische Rechnungen durch den Kooperationspartner Herrn PD Dr. Florian WEIGEND durchgeführt. Beispielhaft für Li^+ und Na^+ konnte per DFT Rechnungen ermittelt werden, dass $^2D_4$ eine ähnliche Koordinationsfähigkeit besitzt wie D_6 und klar besser koordiniert als $^2D_2$, $^2D_3$ oder D_5. $^2D_4$ und D_6 sind in der Gasphase sogar teilweise mit der Koordinationsfähigkeit der organischen Kronenether [3n]-Krone-n (n = 4-6) vergleich-

bar. [15]Krone-5 und [18]Krone-6 zeigen jedoch klar die höchsten Affinitäten gegenüber M^+. Der ermittelte Mechanismus der templatgesteuerten Reaktionen vergleicht sich gut mit dem für die hybriden Ligandsysteme postulierten Mechanismus (Abbildung 39). Eine exocyclische Si-O Bindungsaktivierung ist, wie auch im Experiment gefunden, vorliegend. Im nächsten Schritt entsteht ein Silanolat mit terminaler Iodosilanfunktionalität. Templatgesteuert greift das Silanolat ein weiteres Molekül $^2D_2$ nukleophil an, welches dann in eine geeignete Konformation überführt wird, um den offenkettigen Liganden zu einem Ring zu schließen. Unter Rückbildung einer Si-O Bindung tritt schließlich das Iodidion als Nucleofug aus und der Kronenether ist erfolgreich geformt. Die Signifikanz des I^--Ions in der Reaktion wurde ebenfalls näher untersucht. Die quantenchemischen Rechnungen zeigen, dass die Umwandlung von $[Na(^2D_2)_2]^+$ zu $[Na(^2D_4)]^+$ eine einzelne Ernergiebarriere von 400 kJ/mol besitzt. In dem Beisein von I^- wird diese Barriere deutlich verringert (160 kJ/mol).

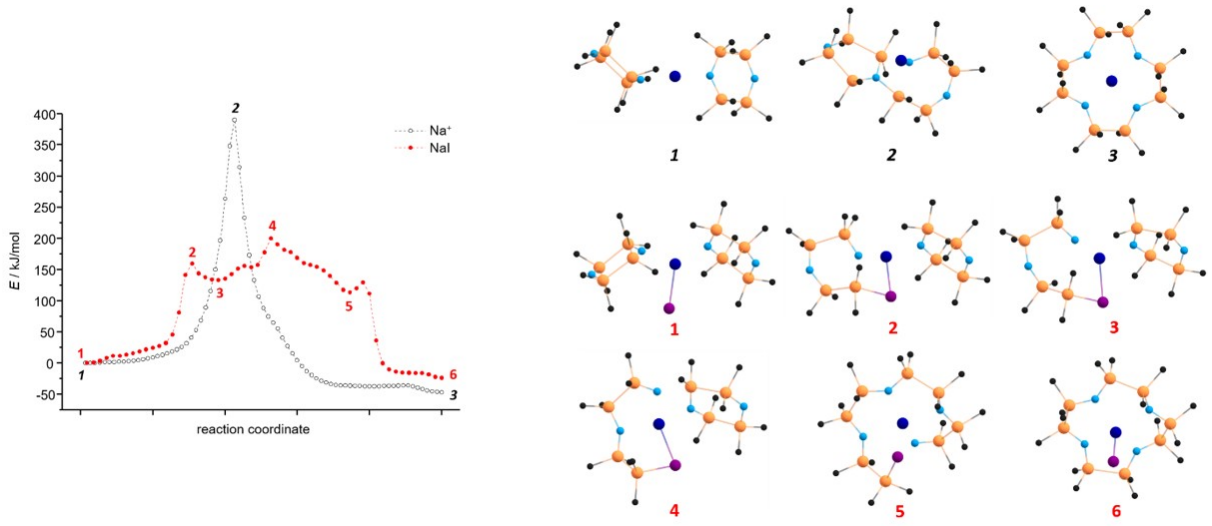

Abbildung 39: Energieprofile der Reaktionspfade von $[Na(^2D_2)_2]^+$ zu $[Na(^2D_4)]^+$ (links) und Strukturen lokaler Extrema des jeweiligen Pfades (rechts) ermittelt anhand von DFT Rechnungen.

Anhand der im Rahmen dieser Dissertation erarbeiteten Ergebnisse ist es ersichtlich, dass es sehr gut möglich ist siliziumreiche Kronenether darzustellen und zu charakterisieren. Sie sind zugänglich über templatgesteuerte Reaktionen mit vorgeschalteter Si-O Bindungsaktivierung. Beide Ligandtypen, hybride Disilakronenether sowie vollständig disilanbasierte Liganden können

in Ringöffnungsoligomerisation genutzt werden und zeigen eine hinreichende Koordinationsfähigkeit gegenüber harten s-Block Metallionen. Eine Reihe von Nebenreaktionen kann Siloxankoordination stören, weshalb inerte Lösungsmittel für eine solche Chemie stark empfohlen sind. Inwieweit die größeren Liganden des Typs $^{2}D_n$ (n = 5, 6) in der Koordinationschemie genutzt werden können, wird sich hoffentlich in zukünftigen Forschungsprojekten zeigen.

6.2 Beiträge zur Koordinationschemie von D_n Liganden

Die oben dargelegten Beiträge zur Koordinationschemie von Disila-Kronenethern gaben wertvolle Erkenntnisse hinsichtlich des Koordinationsverhaltens von Siloxanverbindungen. Wie überzeugend, u.a. anhand von 1,2,4,5-Tetrasila-Benzo-[15]Krone-5 gezeigt werden konnte, sind es die frühen s-Block Metallionen, die starke Wechselwirkungen mit Siloxanliganden eingehen, solange ein passender Rahmen für eine solche Koordination zur Verfügung gestellt wird.

Die Idee war es daher zunächst zu untersuchen, wie sich die als schwach koordinierend beschriebenen D_n Liganden gegenüber den Erdalkalimetallionen verhalten. Entsprechend wurden Erdalkalimetalliodide mit den Siloxanen D_6 und D_7 zur Reaktion gebracht. Kontraintuitiv war die Reaktion für die Kationen Mg^{2+} und Ca^{2+} erfolgreich. Sr^{2+} und Ba^{2+} konnten mit diesen Liganden komplexiert werden, nachdem erneut das GaI_4^--Salz *in-situ* hergestellt wurde (Schema 20). Dies zeigt deutlich, dass kein sterisch anspruchsvolles, perfluoriertes, schwach koordinierendes Anion notwendig ist, um stabile Koordinationsverbindungen cyclischer Dimethylsiloxane zu synthetisieren. Die Kristallstrukturen von $[Mg(D_6)I_2]$ und $[Ca(D_7)I_2]$ konnten erfolgreich ermittelt werden und dass trotz der Tatsache, dass Metall···Anion Wechselwirkungen mit diesen Anionen beobachtet werden. Folglich demonstriert der erfolgreiche Einbau eines Kations mit relativ stark koordinierendem Anion, dass die Natur des Kations berücksichtigt werden muss, wenn die Koordinationschemie von Siloxanen diskutiert wird. Mit Hilfe von geeigneten BORN-HABER Zyklen, konnte diese Annahme weiter unterstützt werden. Trotz eines relativ stark koordinierendem I^--Ions sind nennenswerte Reaktionsenthalpien von -328 kJ/mol (D_6) und -313 kJ/mol (D_7) bei der Komplexierung von MgI_2 ermittelt worden.

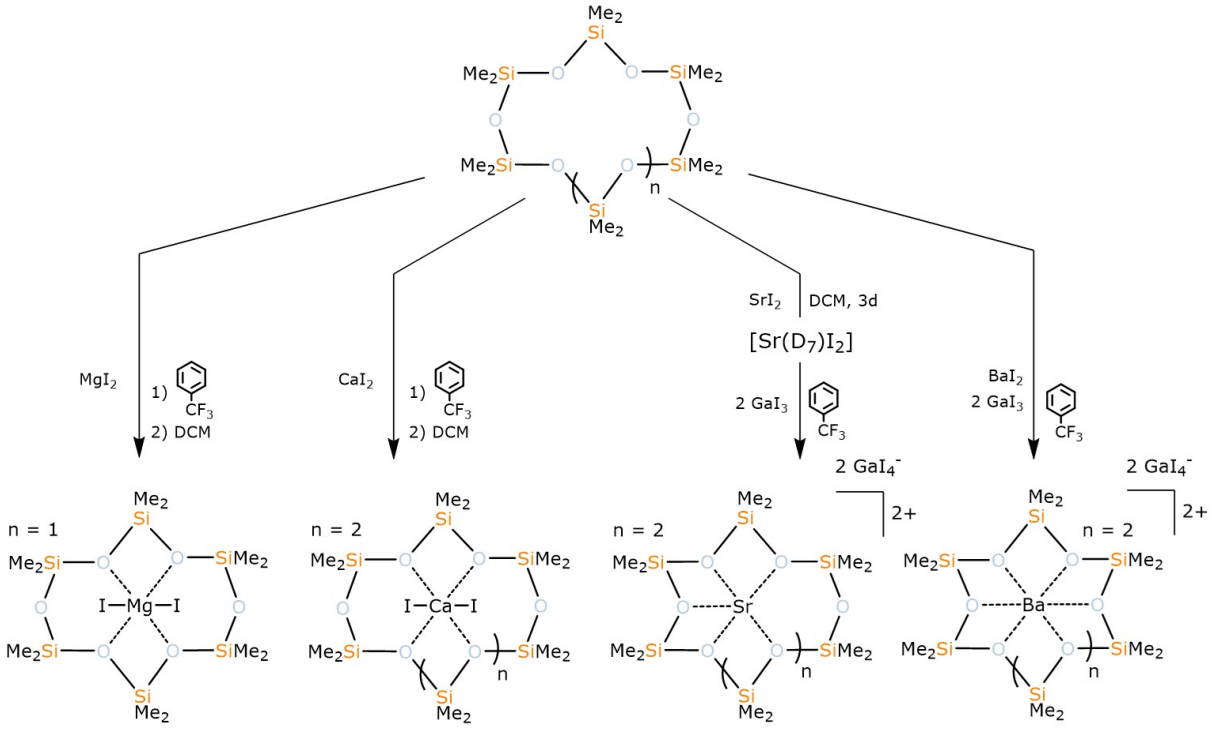

Schema 20: Synthese von Erdalkalimetallkomplexen mit D_n Liganden.

Etwas niedrigere Werte ergeben sich für CaI_2. Diese messen -125 kJ/mol für D_6 und -109 kJ/mol für D_7. Bei den etwas weicheren Ionen Sr^{2+} und Ba^{2+} ändern sich diese Werte hinzu positiven Reaktionsenthalpien. -10 kJ/mol (D_6) und -3 kJ/mol (D_7) werden errechnet für die Reaktion mit SrI_2. +87 kJ/mol (D_6) und +79 kJ/mol (D_7) werden errechnet für die Reaktion mit BaI_2. Das Experiment gab die theoretischen Befunde sehr gut wieder: Wie gezeigt, sind stabile Komplexe mit MgI_2 und CaI_2 synthetisiert worden. Im Falle von SrI_2 und D_7 konnte eine Koordinationsverbindung nur in Lösung per ^{29}Si NMR Spektroskopie beobachtet werden ($\delta(SrI_2@D_7)$ = -9.2 ppm) und im Falle von BaI_2 und D_7 gab es keinen Nachweis für eine Koordination des Liganden. Entsprechend wurde hier die Grenze ermittelt, bis zu der eine Siloxankoordination mit dem relativ stark koordinierendem I^--Ion möglich ist. Erneut ist es das kleine WCA GaI_4^- welches den Erhalt einer Siloxankoordinationsverbindung, in diesem Fall von Sr^{2+} und Ba^{2+}, ermöglichte. Nach Zugabe von zwei Äquivalenten GaI_3 zu einer Suspension aus MI_2 und D_7 werden die entsprechenden 1:1 Komplexe hergestellt. Röntgenografisch konnten dann die Komplexe in Form von $[Sr(D_7)\{GaI_4\}(H_2O)]GaI_4$ und $[Ba(D_7)\{GaI_4\}(H_2O)_{0.94}\{GaI_4\}_{0.06}][GaI_4]_{0.94}$ ermittelt werden (Ab-

bildung 40). Der Energiegewinn durch den Austausch von I^- gegen GaI_4^- ist zusätzlich ermittelt worden und mit 240 kJ/mol groß genug, sodass auch die Synthese von Strontium- respektive Bariumkomplexen gelang. Dieser enorme Energiegewinn und die Vielzahl an erfolgreich synthetisierten Verbindungen mit einem GaI_4^- Ion warf dann die Frage auf, ob nicht auch die weniger bevorzugten Alkalimetallionen in D_n Liganden gebunden werden können und in der Tat wurden so eine ganze Reihe verschiedener Komplexe hergestellt (Schema 21).

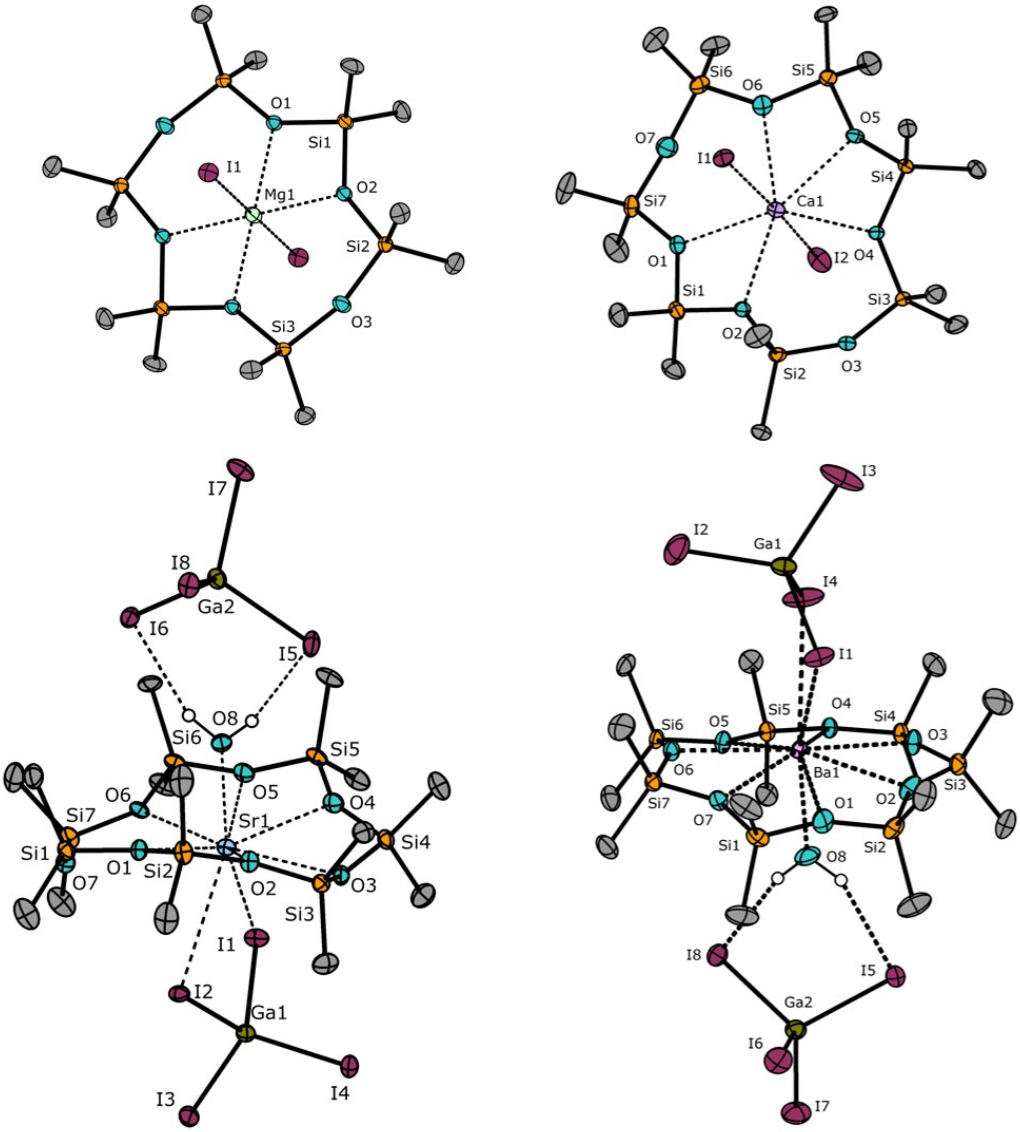

Abbildung 40: Erdalkalimetallkomplexe mit D_6 und D_7. Co-kristalline Lösungsmittelmoleküle sowie fehlgeordnete Teile der Strukturen sind aus Gründen der Übersichtlichkeit nicht dargestellt. Schwingungsellipsoide zeigen eine Aufenthaltswahrscheinlichkeit von 50%.

Es konnte gezeigt werden, dass Li^+ in D_5 und D_6 gebunden werden kann, Na^+ in D_6 sowie D_7 und letztlich K^+ erwartungsgemäß in D_7 (Abbildung 41). Wie bereits für Disilaliganden gezeigt, so sind auch die D_n Liganden empfindlich gegenüber Ringöffnungsoligomerisation. So ist bspw. bei der Reaktion von $LiGaI_4$ mit D_5 ein D_6 Ring entstanden. Des Weiteren konnte mit hybriden Disilakronenethern der erfolgreiche Einbau des NH_4^+-Ions demonstriert werden. Deshalb wurde nun neben den Metallionen auch das NH_4^+-Ion versucht mit einem solchen D_n Ring zu binden. Umgesetzt wurden hierfür D_6, NH_4I und GaI_3 im Verhältnis 1:1:2. Auf diesem Wege wurde so auch der erste Nichtmetall-Komplex eines D_n Liganden dargestellt. Im Gegensatz zu den bisher genannten Cyclosiloxankomplexes zeigte der Komplex $[NH_4(D_7)]Ga_2I_7$ allerdings eine große Temperaturempfindlichkeit in Lösung.

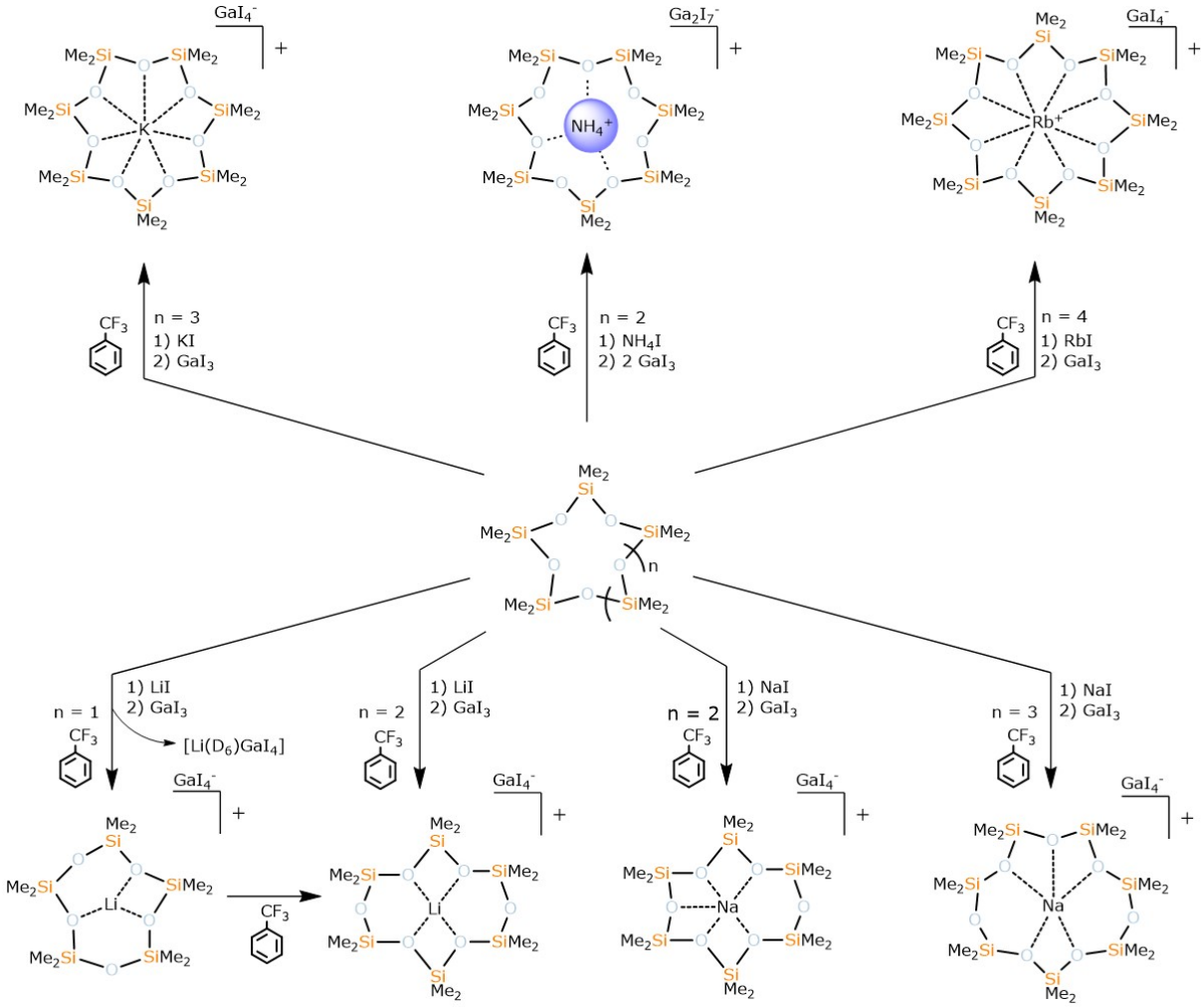

Schema 21: Synthese von Alkalimetall- sowie NH_4^+-Komplexen mit D_n Liganden unter Anwendung der kleinen WCAs GaI_4^- und $Ga_2I_7^-$.

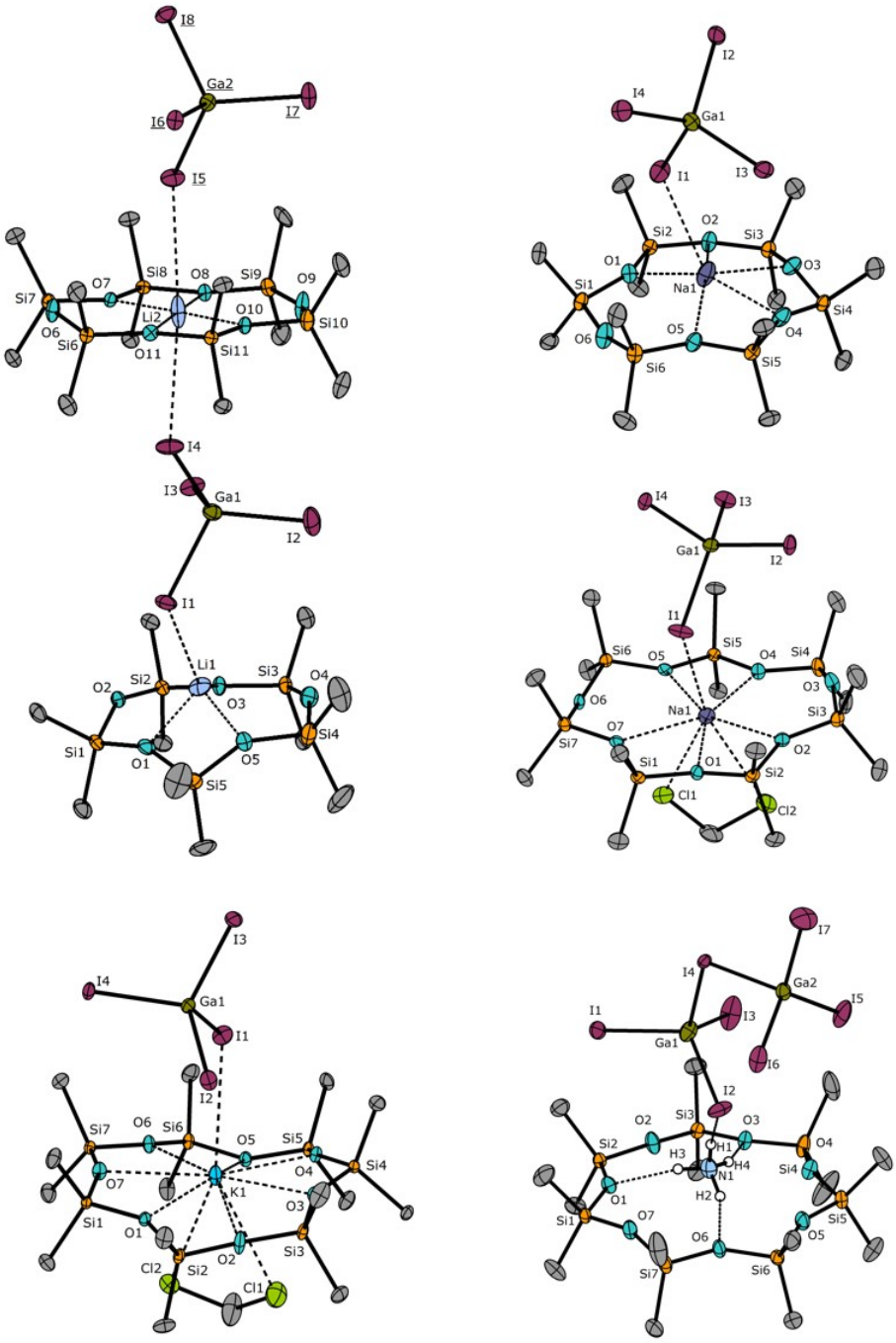

Abbildung 41: Alkalimetall- und NH_4^+-Komplexe mit D_n Liganden und den kleinen WCAs GaI_4^- und $Ga_2I_7^-$. Co-kristalline Lösungsmittelmoleküle und fehlgeordnete Teile der Strukturen sind aus Gründen der Übersicht nicht dargestellt. Unterstrichene Atomkennzeichnung zeigt eine Symmetriegenerierung über 1+x, y, -1+z. Schwingungsellipsoide zeigen eine Aufenthaltswahrscheinlichkeit von 50%.

Die Wasserstoffatome einer ermittelten Kristallstruktur der Verbindung konnten kristallographisch lokalisiert und als unabhängiges isotropes Atom verfeinert werden. Das dadurch erzeugte Koordinationsmuster entspricht jenem von den oben genannten Verbindungen $[NH_4(1,2\text{-Disila}[18]\text{Krone-6})]PF_6$ und $[NH_4(1,2\text{-Disila-Benzo}[18]\text{Krone-6})]PF_6$. IR und NMR Spektroskopische Untersuchungen bestätigten die Interaktion des NH_4^+ Ions mit den $SiMe_2O$ Einheiten. Die Tatsache, dass die Si-gebundenen Sauerstoffatome mit dem NH_4^+ Kation hinreichend wechselwirken und die Verbindung entsprechend stabilisiert wird, ist beeindruckend. Die Bindungssituation ist klar kontra-intuitiv sodass die Grenzen der Koordinationschemie dieser Liganden noch weiter erforscht wurden.

Die Koordination von Siloxanliganden gegenüber schweren Alkalimetallionen wurde bisher klar vermieden, sodass an dieser Stelle noch ausstand Rb^+ und Cs^+ in einem Cyclosiloxan zu binden. Der gleichen Strategie folgend, konnte im Falle der Reaktion von D_8 mit *in-situ* generiertem $CsGaI_4$ bisher keine Reaktion festgestellt werden.

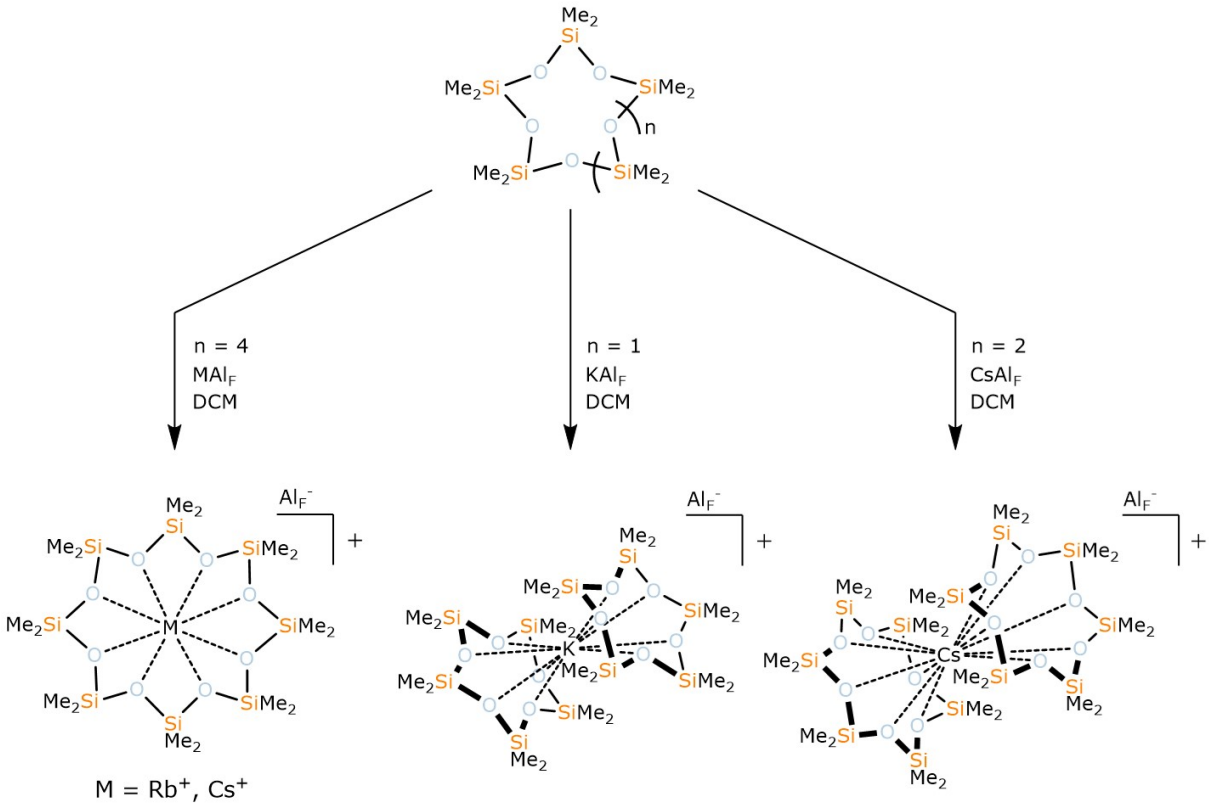

Schema 22: Synthese verschiedener Alkalimetallkomplexe mit D_n (n = 5, 6, 8) Liganden und dem sterisch anspruchsvollem Al_F^- ion.

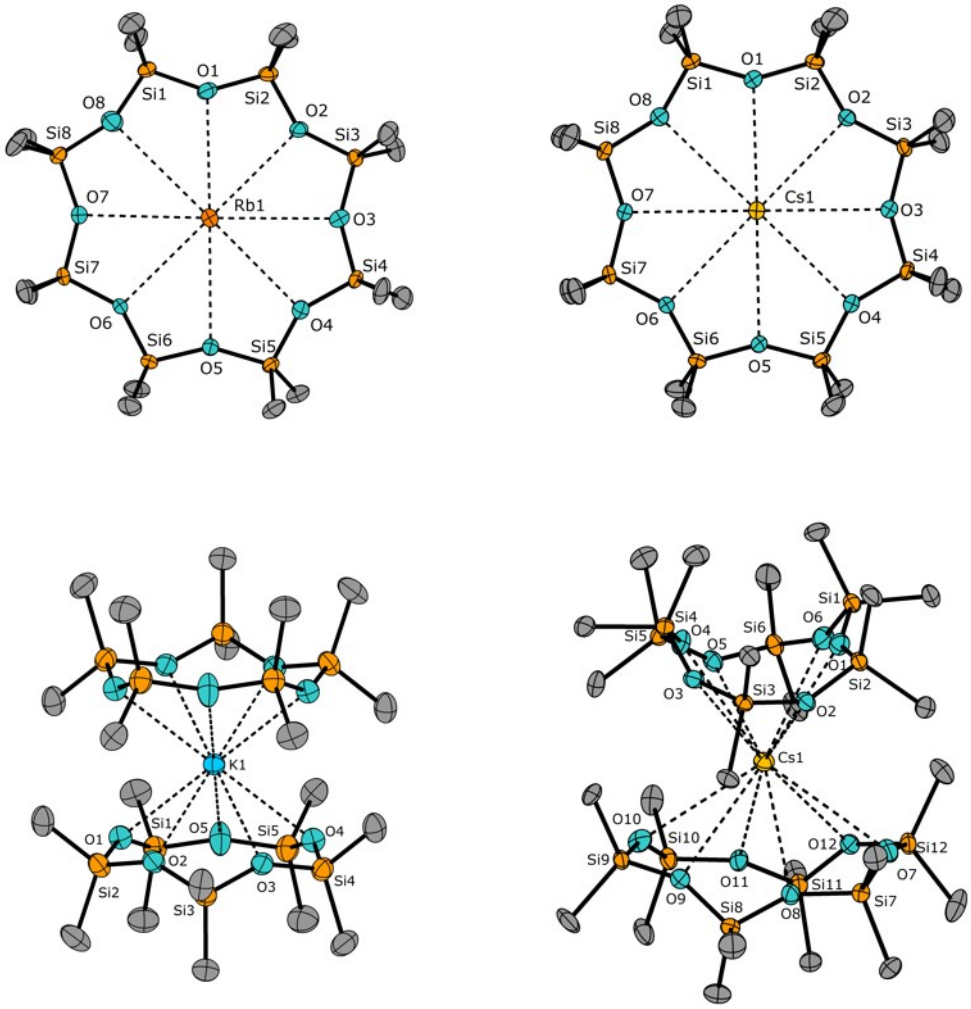

Abbildung 42: Alkalimetallkomplexe von verschiedenen Alkalimetallkomplexe mit D_n (n = 5, 6, 8) Liganden und dem sterisch anspruchsvollem Al_F^- ion im Kristall. Co-kristalline Lösungsmittelmoleküle sowie die Anionen sind aus Gründen der Übersicht nicht dargestellt. Atome ohne Kennzeichnung sind symmetriegeneriert über 1-x, -y, 1-z. Schwingungsellipsoide zeigen eine Aufenthaltswahrscheinlichkeit von 30% (für die Kaliumverbindung) bzw. 50%.

Im Falle von $RbGaI_4$ hingegen konnte eine Reaktion beobachtet werden. Ein hochaufgelöstes Massenspektrum von $[Rb(D_8)]^+$ sowie eine Kristallstruktur wiesen die Verbindung $[Rb(D_8)(DCM)GaI_4]$ nach. Leider zeigte diese Verbindung eine hohe Instabilität, wurde nur in sehr niedrigen Ausbeuten isoliert und bisher konnten keine sinnvollen spektroskopischen Daten der Verbindung hervorgebracht werden. Daher fand nun das große, sterisch anspruchsvolle Al_F^--Ion Anwendung (Schema 22). Da bis hierher kein derartiges Anion notwendig war, stellt das Rb^+

Ion offensichtlich die Grenze dar, inwieweit Siloxankoordination mit dem kleinen WCA GaI_4^- möglich ist. Mit Hilfe des Al_F^--Ions konnten schließlich auch stabile Rb^+ und Cs^+ Verbindungen in brauchbaren Ausbeuten isoliert werden. Spektroskopische Daten sowie geeignete Kristallstrukturen wurden erarbeitet. Mit der Synthese der Verbindungen $[Rb(D_8)(DCM)GaI_4]$ und $[M(D_8)Al_F]$ ($M = Rb^+, Cs^+$) sind nun an dieser Stelle alle nicht-radioaktiven s-Block Metallionen bis auf Be^{2+} in D_n Liganden gebunden worden (Abbildung 42). Die Untersuchungen hinsichtlich der D_n Koordinationschemie zeigen, dass sich D_n Liganden teilweise flexibel gegenüber den Kationen anpassen und die Sauerstoffatome des Liganden das Kation bevorzugt co-planar koordinieren. Eine abschließende Frage die sich stellte war, ob auch andere Koordinationsmodi beobachtet werden können. So z.B. wenn vergleichsweise große Kationen mit vergleichsweise kleinen Liganden umgesetzt werden. Auch für dieses Vorhaben wurde das sterisch anspruchsvolle, nicht-nukleophile Al_F^--Ion gewählt. Die Reaktionen von einem Überschuss D_5 und KAl_F in DCM sowie einem Überschuss D_6 und $CsAl_F$ in DCM verliefen erfolgreich. Die ersten jemals beobachteten Sandwich-Komplexe dieser Substanzklasse konnten in Form von $[K(D_5)_2]Al_F$ und $[Cs(D_6)_2]Al_F$ erfolgreich charakterisiert werden.

6.3 Siloxan-Koordinationschemie mit BeX_2 ($X = Cl^-, Br^-, I^-$)

In den letzten Kapiteln ist deutlich geworden, dass Siloxanverbindungen vor allem mit frühen s-Block Metallionen, so vor allem den Erdalkalimetallionen wechselwirken. Als logische Erweiterung des Projekthorizonts wurden in Kooperation mit dem AK BUCHNER verschiedene Berylliumhalogenide hinsichtlich ihrer Reaktivität gegenüber siliziumbasierten Liganden geprüft.

Anfänglich wurden mit 1,2-Disila[12]Krone-4 und 1,2-Disila-Benzo[12]Krone-4 zunächst hybride Systeme mit $BeCl_2$ zur Reaktion gebracht. Hierbei wurden zwei Verbindungen isoliert und charakterisiert, die eindrucksvoll demonstrieren, dass das Berylliumsalz hybride Kronenether spaltet. Die Kristallstrukturen zeigten hexanukleare Koordinationsverbindungen mit verschiedenen Glykolatliganden (Schema 23). Das zentrale Koordinationsmuster dieser Verbindungen stellt einen achtgliedrigen Be-O Heterozyklus dar, welcher anliegend zwei Be-O Sechsringe trägt. Übereinstimmend mit erhaltenen NMR Daten sowie den Kristallstrukturen konnte

zudem ein Mechanismus zur Bildung dieser Glykolatliganden formuliert werden. Der Mechanismus hinter der Bildung dieser Verbindungen startet mit der exozyklischen Koordination des Be^{2+}-Ions an den Silakronenether. Es folgt der Si-O Bindungsbruch unter Formation von Chlorosilanen. Zurück bleiben die genannten Glykolatliganden, welche schließlich fest an die Berylliumionen gebunden sind. Im Falle von 1,2-Disila-Benzo[12]Krone-4 erfolgen zudem C-O Bindungsbrüche.

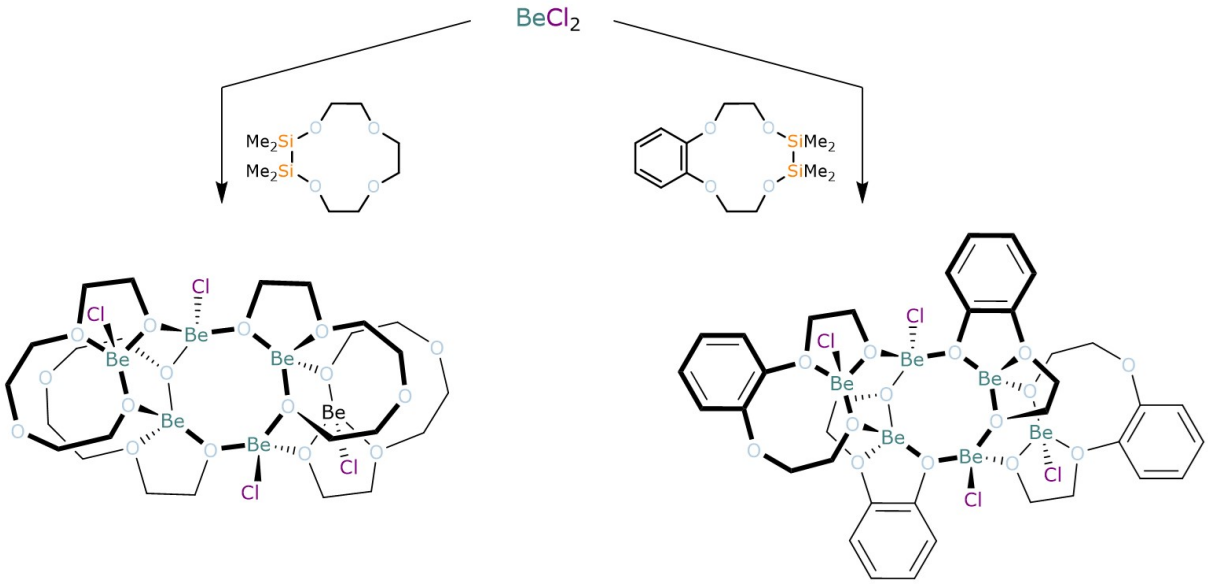

Schema 23: Spaltung von hybriden Disila[12]Krone-4 Ethern durch $BeCl_2$.

Nachdem die hybriden Disilakronenether zu Glykolaten zersetzt wurden, wurde die Reaktivität von BeX_2 (X = Cl^-, Br^-, I^-) nun gegenüber D_n Liganden sowie $^2D_2$ untersucht, mit der Intention siliziumbasierte Systeme zu erhalten, die eine Siloxankoordination zeigen.

Die ersten Untersuchungen hinsichtlich einer Koordinationschemie von $BeBr_2$ und BeI_2 gegenüber D_5 and D_6 zeigten keinerlei Nachweis dafür, dass Koordinationsverbindungen erzeugt wurden. Zufälligerweise jedoch, konnten nicht nur Einkristalle von β-BeI_2 identifiziert werden, sondern auch Einkristalle der bis dato unbekannten Phase β-$BeBr_2$. Diese Phase konnte bis heute trotz verschiedener Bemühungen nicht beobachtet und/oder hergestellt werden. Entsprechend kam es hier zwar nicht zur Ausbildung eines Siloxankomplexes, aber ein weiteres eindrucksvolles Beispiel zeigt an dieser Stelle, wie siliziumbasierte Liganden als Lösungsvermittler dienen können.

Um eine Reaktion eines zyklischen Siloxans mit Berylliumsalzen zu erzwingen, wurde als nächstes das deutlich reaktivere cyclische Dimethylsiloxan D_3 mit den Berylliumhalogeniden BeX_2 (X = Cl^-, Br^-, I^-) umgesetzt. Ein Umsatz zeigt sich für alle Berylliumsalze und in Form von $[Be_3(\mu\text{-}OSiMe_2I)_4I_2]$ ist sogar die Kristallisation einer Siloxanatospezies gelungen. Der Komplex ist trinuklear und weist μ-verbrückende Iodosiloxanato Liganden auf. Diese zeigen klar, dass reaktivere Siloxane wie D_3 ebenfalls unter Si-O Bindungsbruch reagieren (Schema 24). Die Umsetzung von $^2D_2$ mit BeX_2 (X = Cl^-, Br^-, I^-) demonstriert dies erneut.

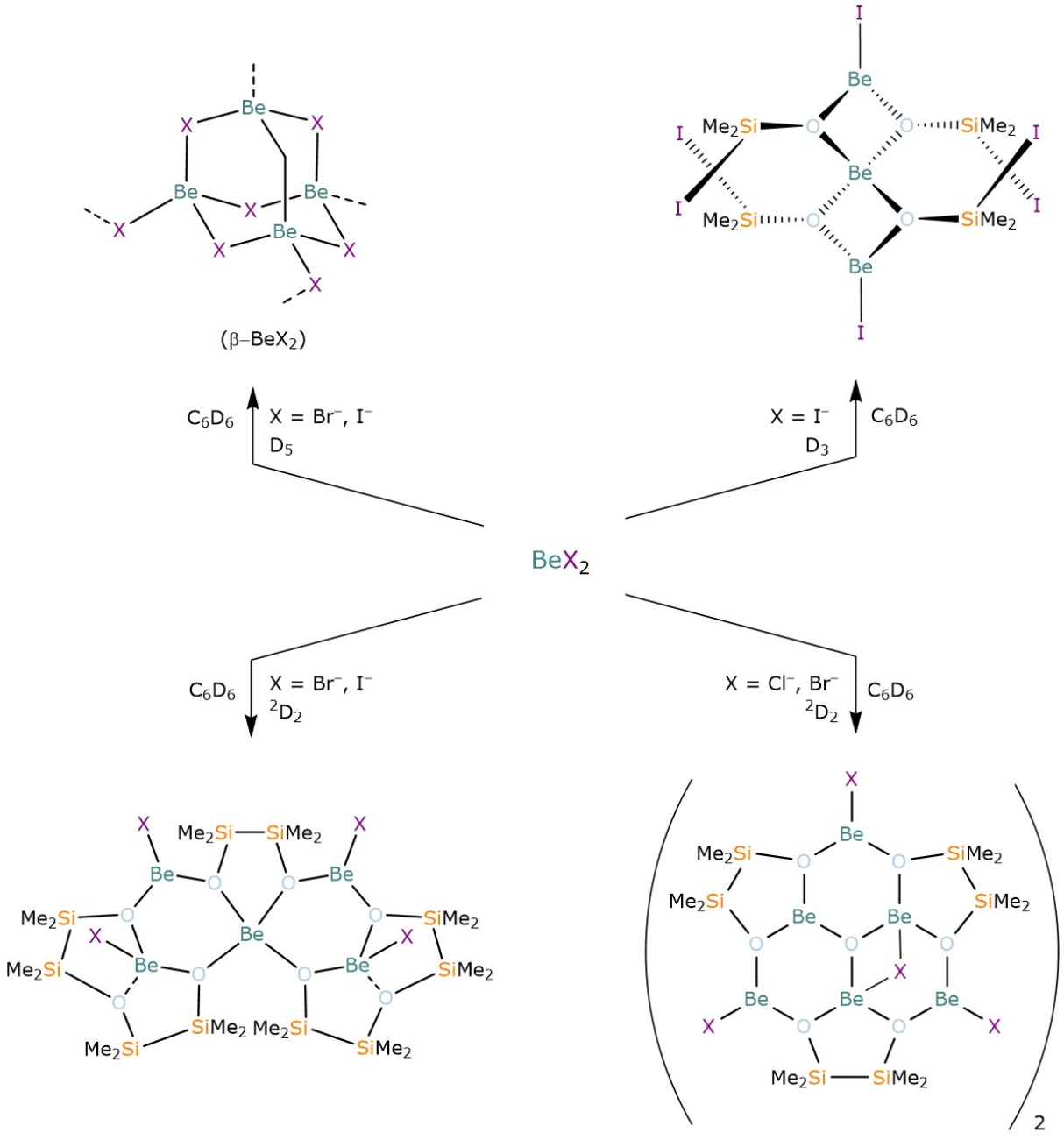

Schema 24: Vorläufige Ergebnisse einer Siloxankoordinationschemie mit BeX_2.

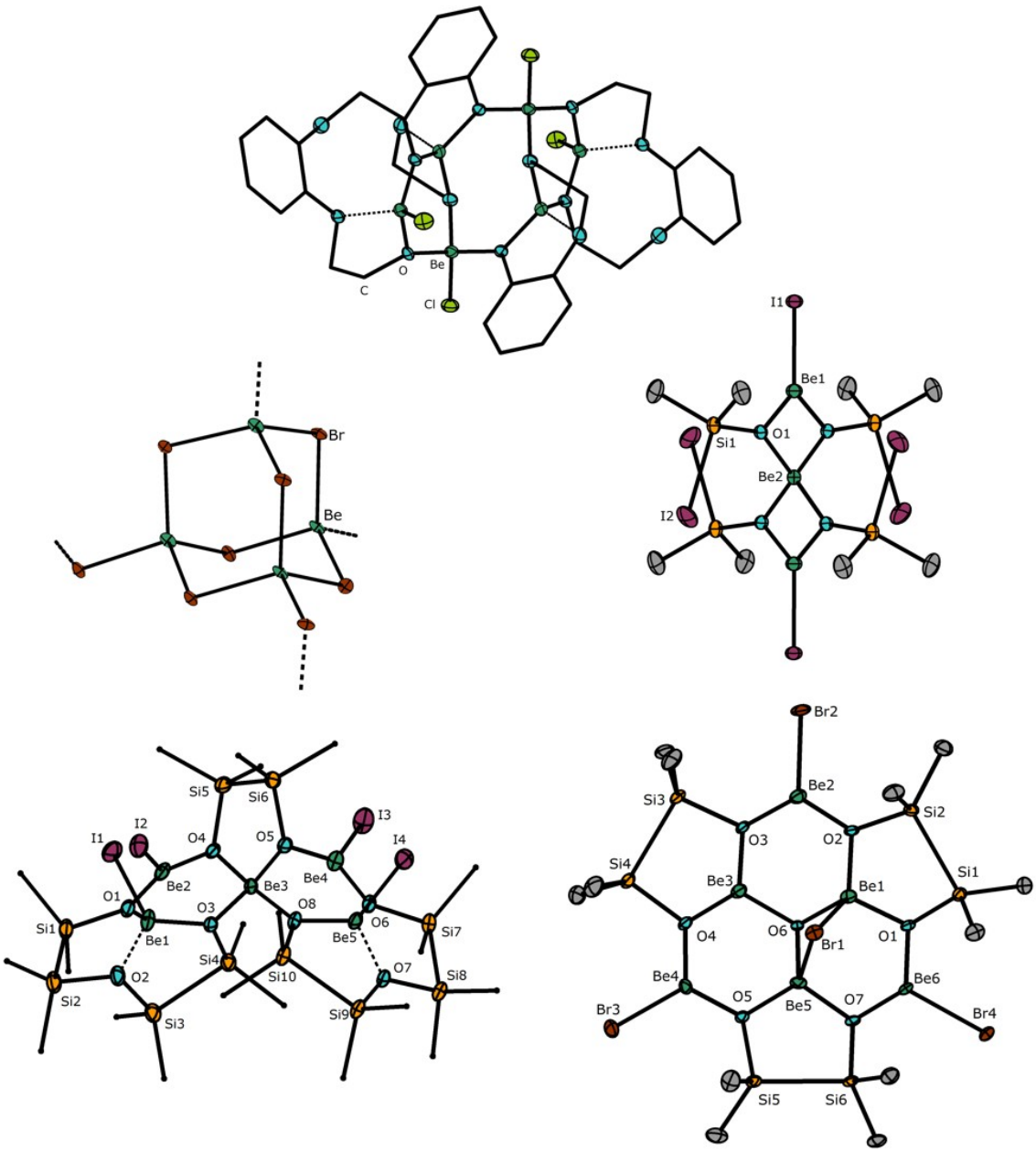

Abbildung 43: Ausgewählte Kristallstrukturen berylliumhaltiger Verbindungen. Co-kristalline C_6D_6 Moleküle sind aus Gründen der Übersicht nicht dargestellt und Kohlenstoffatome sind teilweise aus selbigem Grund als wires/sticks Modell dargestellt. Atome ohne Kennzeichnung sind symmetriegeneriert über verschiedene Symmetriecodes. Schwingungsellipsoide zeigen eine Aufenthaltswahrscheinlichkeit von 50%

Zwei Strukturmotive wurden hauptsächlich beobachtet. Einerseits wird ein pentanuklearer Komplex mit zwei intakten Siloxaneinheiten sowie einem Disiloxanatoliganden und andererseits ein zwölfkerniger Cluster beobachtet, welcher primär aus Disiloxanatoliganden besteht. Im Falle von

BeX_2 (X = Br^-, I^-) gelingt der Erhalt der pentanuklearen Spezies, während im Falle von BeX_2 (X = Cl^-, Br^-) die dodekanukleare Spezies hervorgebracht wird. Die jeweilige Strukturaufklärung anhand von Einkristalldiffraktometrie bestätigte dies.

Da die pentanuklearen Komplexe eine intakte Siloxaneinheit besitzen, welche ein Berylliumkation koordinativ absättigt, kann hier zudem geschlussfolgert werden, dass im Rahmen dieser Dissertation das Binden aller s-Block (Metall-)Ionen an Siloxanliganden gelang. Leider sind die NMR spektroskopischen Untersuchungen im Rahmen der Berylliumchemie problematisch. Unklare Resultate erfordern weitere Untersuchungen. Letztlich ist die Berylliumchemie allerdings noch nicht erschöpfend behandelt worden und weitere Experimente sind geplant. Anhand der bisher erzielten Ergebnisse ist klar, dass diese Chemie noch vielversprechendes Potential hat.

7 Bibliography

[1] R. Delgado, *Rev. Port. Quim.* **1995**, *2*, 18–29.

[2] T. Ogoshi, T.-A. Yamagishi, *Chapter 1. Historical Background of Macrocyclic Compounds*, in *Pillararenes*. **2016**, 1–22. DOI: 10.1039/9781782622321.

[3] L. F. Lindoy, K. M. Park, S. S. Lee, *Chem. Soc. Rev.* **2013**, *42*, 1713–1727.

[4] C. J. Pedersen, *J. Am. Chem. Soc.* **1967**, *89*, 2495–2496.

[5] C. J. Pedersen, *Angew. Chem., Int. Ed.* **1988**, *27*, 1021–1027.

[6] S. Kubik, *Chem. Unserer Zeit* **2017**, *51*, 372–383.

[7] D. J. Cram, *Angew. Chem.* **1988**, *100*, 1041–1052.

[8] G. B. Vásquez, M. Karavitis, X. Ji, I. Pechik, W. S. Brinigar, G. L. Gilliland, C. Fronticelli, *Biophys. J.* **1999**, *76*, 88–97.

[9] D. Sehnal, A. Rose, J. Koča, S. Burley, S. Velankar, *Proc. Work. Mol. Graph. Vis. Anal. Mol. Data* **2018**, 29–33.

[10] C. Arnal-Herault, M. Barboiu, E. Petit, M. Michau, A. Der Van Lee, *New J. Chem.* **2005**, *29*, 1535–1539.

[11] D. Moras, B. Metz, R. Weiss, *Acta Crystallogr. Sect. B Struct. Crystallogr. Cryst. Chem.* **1973**, *29*, 383–388.

[12] H. An, J. S. Bradshaw, R. M. Izatt, *Chem. Rev.* **1992**, *92*, 543–572.

[13] H. Tsukube, *Coord. Chem. Rev.* **1996**, *148*, 1–17.

[14] J. W. Steed, *Coord. Chem. Rev.* **2001**, *215*, 171–221.

[15] G. W. Gokel, W. M. Leevy, M. E. Weber, *Chem. Rev.* **2004**, *104*, 2723–2750.

[16] A. Swidan, C. L. B. Macdonald, *Chem. Soc. Rev.* **2016**, *45*, 3883–3915.

[17] R. Mohammadzadeh Kakhki, *J. Inclusion Phenom. Macrocyclic Chem.* **2013**, *75*, 11–22.

[18] A. A. Elbashir, H. Y. Aboul-Enein, *Curr. Pharm. Anal.* **2010**, *6*, 101–113.

[19] D. Landini, F. Montanari, F. M. Pirisi, *J. Chem. Soc. Chem. Commun.* **1974**, 879–880.

[20] G. Aragay, J. Pons, A. Merkoçi, *Chem. Rev.* **2011**, *111*, 3433–3458.

[21] F. A. Christy, P. S. Shrivastav, *Crit. Rev. Anal. Chem.* **2011**, *41*, 236–269.

[22] G. W. Gokel, I. A. Carasel, *Chem. Soc. Rev.* **2007**, *36*, 378–389.

[23] M. Kralj, L. Tušek-Božić, L. Frkanec, *ChemMedChem* **2008**, *3*, 1478–1492.

[24] N. R. Pace, *Proc. Natl. Acad. Sci. U.S.A* **2001**, *98*, 805–808.

[25] T. Chivers, I. Manners, *Inorganic Rings and Polymers of the P-Block Elements. From Fundamentals to Applications*, **2009**. RSC Publishing.

[26] S. G. Calera, D. S. Wright, *Dalton Trans.* **2010**, *39*, 5055–5065.

[27] D. S. Wright, *Host-Guest Chemistry - p-Block Systems*, in *Comprehensive Inorganic Chemistry II (Second Edition): From Elements to Applications.* Elsevier Ltd., **2013**, 953–966.

[28] J. S. Ritch, T. Chivers, *Angew. Chem., Int. Ed.* **2007**, *46*, 4610–4613.

[29] B. Krebs, H.-U. Hürter, *Angew. Chem., Int. Ed.* **1980**, *19*, 481–482.

[30] C. Donsbach, K. Reiter, D. Sundholm, F. Weigend, S. Dehnen, *Angew. Chem., Int. Ed.* **2018**, *57*, 8770–8774.

[31] R. T. Oakley, S. J. Rettig, N. L. Paddock, J. Trotter, *J. Am. Chem. Soc.* **1985**, *107*, 6923–6936.

[32] W. S. Sheldrick, I. M. Müller, *Coord. Chem. Rev.* **1999**, *182*, 125–173.

[33] W. S. Sheldrick, T. Häusler, *Z. Anorg. Allg. Chem.* **1993**, *619*, 1984–1990.

[34] M. Heller, O. Teichert, W. S. Sheldrick, *Z. Anorg. Allg. Chem.* **2005**, *631*, 709–714.

[35] T. Häusler, W. S. Sheldrick, *Chem. Ber.* **1997**, *130*, 371–376.

[36] K. D. Gallicano, N. L. Paddock, S. J. Rettig, J. Trotter, *Can. J. Chem.* **1981**, *59*, 2435–2440.

[37] W. C. Marsh, N. L. Paddock, C. J. Stewart, J. Trotter, *J. Chem. Soc., Chem. Commun.* **1970**, 1190–1191.

[38] N. L. Paddock, T. N. Ranganathan, S. J. Rettig, R. D. Sharma, J. Trotter, *Can. J. Chem.* **1981**, *59*, 2429–2434.

[39] A. Bashall, A. D. Bond, E. L. Doyle, F. García, S. Kidd, G. T. Lawson, M. C. Parry, M. McPartlin, A. D. Woods, D. S. Wright, *Chem. Eur. J.* **2002**, *8*, 3377–3385.

[40] F. García, J. M. Goodman, R. A. Kowenicki, I. Kuzu, M. McPartlin, M. A. Silva, L. Riera, A. D. Woods, D. S. Wright, *Chem. Eur. J.* **2004**, *10*, 6066–6072.

[41] A. J. Plajer, F. J. Rizzuto, H. Niu, S. Lee, J. M. Goodman, D. S. Wright, *Angew. Chem., Int. Ed.* **2019**, *58*, 10655–10659.

[42] S. Gonzalez Calera, D. J. Eisler, J. M. Goodman, M. McPartlin, S. Singh, D. S. Wright, *Dalton Trans.* **2009**, *2*, 1293.

[43] C. Marschner, T. Don Tilley, *Dalton Trans.* **2017**, *46*, 8699–8700.

[44] A. D. McNaught, A. Wilkinson, S. J. Chalk, *IUPAC Compendium of Chemical Terminology*, IUPAC, Research Triagle Park, NC, **2019**.

[45] M. Alaee, D. G. Wang, T. Gouin, *Chemosphere* **2013**, *93*, 709–710.

[46] A. F. Hollemann, N. Wiberg, *Lehrbuch der Anorganischen Chemie*. Walter de Gruyter, Berlin **2007**.

[47] H.-H. Moretto, M. Schulze, G. Wagner, *Silicones* in *Ullmann's Encyclopedia of Indutrial Chemistry Vol. 32*, Wiley-VCH Verlag GmbH & Co. KGaA, Weinheim, Germany, **2000**, 675–712. DOI: 10.1002/14356007.a24_057.

[48] M. P. Wolf, G. B. Salieb-Beugelaar, P. Hunziker, *Prog. Polym. Sci.* **2018**, *83*, 97–134.

[49] C. Rücker, K. Kümmerer, *Chem. Rev.* **2015**, *115*, 466–524.

[50] H. Fromme, *Cyclic Volatile Methylsiloxanes: Occurrence and Exposure* in *Encyclopedia of Environmental Health Elsevier Inc.*, **2019**, 805-812. DOI: 10.1016/B978-0-12-409548-9.11241-2.

[51] R. H. Baney, M. Itoh, A. Sakakibara, T. Suzuki, *Chem. Rev.* **1995**, *95*, 1409–1430.

[52] F. Vidal, F. Jäkle, *Angew. Chem.* **2019**, *131*, 5904–5929.

[53] G. Qing, C. Cui, *Dalton Trans.* **2017**, *46*, 8746–8750.

[54] J. F. Brown, G. M. J. Slusarczuk, *J. Am. Chem. Soc.* **1965**, *87*, 931–932.

[55] D. Seyferth, C. Prud'homme, G. H. Wiseman, *Inorg. Chem.* **1983**, *22*, 2163–2167.

[56] W. Patnode, D. F. Wilcock, *J. Am. Chem. Soc.* **1946**, *68*, 358–363.

[57] M. J. Hunter, J. F. Hyde, E. L. Warrick, H. J. Fletcher, *J. Am. Chem. Soc.* **1946**, *68*, 667–672.

[58] R. West, L. S. Whatley, K. J. Lake, *J. Am. Chem. Soc.* **1961**, *83*, 761–764.

[59] C. M. Huggins, *J. Phys. Chem.* **1961**, *65*, 1881–1884.

[60] M. D. Joesten, R. S. Drago, *J. Am. Chem. Soc.* **1962**, *84*, 3817–3821.

[61] E. W. Abel, D. A. Armitage, D. B. Brady, *Trans. Faraday Soc.* **1966**, *62*, 3459–3462.

[62] J. T. Wang, C. H. Van Dyke, *Inorg. Chem.* **1967**, *6*, 1741–1743.

[63] N. Viswanathan, C. H. Van Dyke, *J. Chem. Soc. A* **1968**, *5*, 487.

[64] A. Marchand, J. Mendelsohn, M. Lebedeff, J. Valade, *J. Organomet. Chem.* **1969**, *17*, 379–388.

[65] A. N. Egorochkin, N. S. Vyazankin, S. Y. Khorshev, *Russ. Chem. Rev.* **1972**, *41*, 425–438.

[66] M. G. Voronkov, V. P. Mileshkevich, Y. A. Yuzhelevskii, *Russ. Chem. Rev.* **1976**, *45*, 1167–1178.

[67] A. N. Egorochkin, S. E. Skobeleva, *Russ. Chem. Rev.* **1979**, *48*, 1198–1211.

[68] R. West, L. S. Wilson, D. L. Powell, *J. Organomet. Chem.* **1979**, *178*, 5–9.

[69] E. Popowski, J. Schulz, K. Feist, H. Kelling, H. Jancke, *Z. Anorg. Allg. Chem.* **1988**, *558*, 206–216.

[70] B. D. Shepherd, *J. Am. Chem. Soc.* **1991**, *113*, 5581–5583.

[71] Y. L. Frolov, M. G. Voronkov, N. V. Strashnikova, N. I. Shergina, *J. Mol. Struct.* **1992**, *270*, 205–215.

[72] E. Yilgör, E. Burgaz, E. Yurtsever, I. Yilgör, *Polymer.* **2000**, *41*, 849–857.

[73] L. O. Brockway, F. T. Wall, *J. Am. Chem. Soc.* **1934**, *56*, 2373–2379.

[74] D. P. Craig, A. Maccoll, R. S. Nyholm, L. E. Orgel, L. E. Sutton, *J. Chem. Soc.* **1954**, 332.

[75] F. G. A. Stone, D. Seyferth, *J. Inorg. Nucl. Chem.* **1955**, *1*, 112–118.

[76] G. Engelhardt, H. Kriegsmann, *Z. Anorg. Allg. Chem.* **1965**, *336*, 286–294.

[77] G. Engelhardt, *J. Organomet. Chem.* **1968**, *11*, 243–252.

[78] M. Cypryk, Y. Apeloig, *Organometallics* **1997**, *16*, 5938–5949.

[79] S. Shambayati, S. L. Schreiber, J. F. Blake, S. G. Wierschke, W. L. Jorgensen, *J. Am. Chem. Soc.* **1990**, *112*, 697–703.

[80] F. Weinhold, R. West, *Organometallics* **2011**, *30*, 5815–5824.

[81] F. Weinhold, R. West, *J. Am. Chem. Soc.* **2013**, *135*, 5762–5767.

[82] B. Cordero, V. Gómez, A. E. Platero-Prats, M. Revés, J. Echeverría, E. Cremades, F. Barragán, S. Alvarez, *Dalton Trans.* **2008**, 2832.

[83] I. T. Moraru, P. M. Petrar, G. Nemeş, *J. Phys. Chem. A* **2017**, *121*, 2515–2522.

[84] Y. Apeloig, A. Stanger, *J. Organomet. Chem.* **1988**, *346*, 305–313.

[85] M. Cypryk, *Macromol. Theory Simul.* **2001**, *10*, 158–164.

[86] M. Cypryk, J. Kurjata, J. Chojnowski, *J. Organomet. Chem.* **2003**, *686*, 373–378.

[87] E. J. Little, M. M. Jones, *J. Chem. Educ.* **1960**, *37*, 231.

[88] H. Oberhammer, E. James, *J. Am. Chem. Soc.* **1980**, *102*, 7241–7244.

[89] T. Kudo, S. nagase, *J. Am. Chem. Soc.* **1985**, *107*, 2589–2595.

[90] M. S. Gordon, T. J. Packwood, M. T. Carroll, J. A. Boatz, *J. Phys. Chem.* **1991**, *95*, 4332–4337.

[91] R. J. Gillespie, S. A. Johnson, *Inorg. Chem.* **1997**, *36*, 3031–3039.

[92] R. J. Gillespie, E. A. Robinson, *Chem. Soc. Rev.* **2005**, *34*, 396–407.

[93] S. Grabowsky, M. F. Hesse, C. Paulmann, P. Luger, J. Beckmann, *Inorg. Chem.* **2009**, *48*, 4384–4393.

[94] J. Passmore, J. M. Rautiainen, *Eur. J. Inorg. Chem.* **2012**, 6002–6010.

[95] T. S. Cameron, A. Decken, I. Krossing, J. Passmore, J. M. Rautiainen, X. Wang, X. Zeng, *Inorg. Chem.* **2013**, *52*, 3113–3126.

[96] A. Bauzá, T. J. Mooibroek, A. Frontera, *Chem. Rec.* **2016**, *16*, 473–487.

[97] S. E. Anderson, D. J. Bodzin, T. S. Haddad, J. A. Boatz, J. M. Mabry, C. Mitchell, M. T. Bowers, *Chem. Mater.* **2008**, *20*, 4299–4309.

[98] P. G. Taylor, A. R. Bassindale, Y. El Aziz, M. Pourny, R. Stevenson, M. B. Hursthouse, S. J. Coles, *Dalton Trans.* **2012**, *41*, 2048–2059.

[99] Y. El Aziz, P. G. Taylor, A. R. Bassindale, S. J. Coles, M. B. Pitak, *Organometallics* **2016**, *35*, 4004–4013.

[100] I. Alkorta, J. Elguero, A. Frontera, *Crystals* **2020**, *10*, DOI: 10.3390/cryst10030180.

[101] A. Bauzá, T. J. Mooibroek, A. Frontera, *Angew. Chem., Int. Ed.* **2013**, *52*, 12317–12321.

[102] G. V. Gibbs, J. W. Downs, M. B. Boisen, *Rev. Mineral. Geochem.* **1994**, *29*, 331–368.

[103] G. V. Gibbs, K. M. Rosso, D. M. Teter, M. B. Boisen, M. S. T. Bukowinski, *J. Mol. Struct.* **1999**, *485–486*, 13–25.

[104] M. G. Voronkov, Y. A. Yuzhelevskii, V. P. Mileshkevich, *Russ. Chem. Rev.* **1975**, *44*, 355–372.

[105] G. V. Gibbs, D. F. Cox, T. D. Crawford, M. B. Boisen, M. Lim, *Phys. Chem. Miner.*

2002, *29*, 307–318.

[106] M. Koch-Müller, Y. Fei, E. Hauri, Z. Liu, *Phys. Chem. Miner.* **2001**, *28*, 693–705.

[107] G. V. Gibbs, D. F. Cox, M. B. Boisen, R. T. Downs, N. L. Ross, *Phys. Chem. Miner.* **2003**, *30*, 305–316.

[108] S. Grabowsky, J. Beckmann, P. Luger, *Aust. J. Chem.* **2012**, *65*, 785–795.

[109] M. Ichinohe, N. Takahashi, A. Sekiguchi, *Chem. Lett.* **1999**, *28*, 553–554.

[110] M. Morisue, T. Kusukawa, S. Watase, *Eur. J. Inorg. Chem.* **2020**, *2020*, 1885–1893.

[111] A. Schäfer, M. Reißmann, A. Schäfer, M. Schmidtmann, T. Müller, *Chem. Eur. J.* **2014**, *20*, 9381–9386.

[112] C. Eaborn, P. B. Hitchcock, P. D. Lickiss, *J. Organomet. Chem.* **1984**, *264*, 119–126.

[113] M. Fugel, M. F. Hesse, R. Pal, J. Beckmann, D. Jayatilaka, M. J. Turner, A. Karton, P. Bultinck, G. S. Chandler, S. Grabowsky, *Chem. Eur. J.* **2018**, *24*, 15275–15286.

[114] C. Martín-Fernández, M. M. Montero-Campillo, I. Alkorta, J. Elguero, *J. Phys. Chem. A* **2017**, *121*, 7424–7431.

[115] C. Martín-Fernández, M. M. Montero-Campillo, I. Alkorta, J. Elguero, *Mol. Phys.* **2018**, *116*, 1539–1550.

[116] I. Alkorta, M. M. Montero-Campillo, O. Mó, J. Elguero, M. Yáñez, *J. Phys. Chem. A* **2019**, *123*, 7124–7132.

[117] M. Cypryk, Y. Apeloig, *Organometallics* **2002**, *21*, 2165–2175.

[118] L. King, A. C. Sullivan, *Coord. Chem. Rev.* **1999**, *189*, 19–57.

[119] B. Marciniec, H. Maciejewski, *Coord. Chem. Rev.* **2001**, *223*, 301–335.

[120] M. M. Levitsky, B. G. Zavin, A. N. Bilyachenko, *Russ. Chem. Rev.* **2007**, *76*, 847–866.

[121] T. J. Boyle, L. A. M. Ottley, *Chem. Rev.* **2008**, *108*, 1896–1917.

[122] M. M. Levitskii, V. V. Smirnov, B. G. Zavin, A. N. Bilyachenko, A. Y. Rabkina, *Kinet. Catal.* **2009**, *50*, 490–507.

[123] V. Lorenz, A. Edelmann, S. Gießmann, C. G. Hrib, S. Blaurock, F. T. Edelmann, *Z. Anorg. Allg. Chem.* **2010**, *636*, 2172–2191.

[124] C. Krempner, *Eur. J. Inorg. Chem.* **2011**, 1689–1698.

[125] M. M. Levitsky, A. N. Bilyachenko, *Coord. Chem. Rev.* **2016**, *306*, 235–269.

[126] M. M. Levitsky, Y. V. Zubavichus, A. A. Korlyukov, V. N. Khrustalev, E. S. Shubina, A. N. Bilyachenko, *J. Cluster Sci.*, **2019**, *30*, 1283–1316.

[127] B. Freitag, P. Stegner, K. Thum, C. A. Fischer, S. Harder, *Eur. J. Inorg. Chem.* **2018**, *2018*, 1938–1944.

[128] M. Veith, A. Koban, K. Fries, P. Spaniol, R. Elsässer, A. Rammo, V. Huch, U. Kleinsteuber, *Organometallics* **1998**, *17*, 2612–2618.

[129] C. Eaborn, S. M. El-Hamruni, P. B. Hitchcock, J. D. Smith, *Chem. Commun.* **1998**, *5*, 1277–1278.

[130] E. Iravani, A. Dashti-Mommertz, B. Neumüller, *Z. Anorg. Allg. Chem.* **2003**, *629*, 1136–1146.

[131] L. J. Bowman, K. Izod, W. Clegg, R. W. Harrington, J. D. Smith, C. Eaborn, *J. Chem. Soc. Dalton Trans.* **2005**, *6*, 502–508.

[132] M. Veith, A. Rammo, R. Heim, V. Huch, *Z. Anorg. Allg. Chem.* **2010**, *636*, 320–324.

[133] A. N. Bilyachenko, A. Yalymov, M. Dronova, A. A. Korlyukov, A. V. Vologzhanina, M. A. Es'Kova, J. Long, J. Larionova, Y. Guari, P. V. Dorovatovskii, E. S. Shubina, M. M. Levitsky, *Inorg. Chem.* **2017**, *56*, 12751–12763.

[134] S. Beaini, G. B. Deacon, A. P. Erven, P. C. Junk, D. R. Turner, *Chem. Asian J.* **2007**, *2*, 539–550.

[135] M. Jost, R. M. Richter, M. Balmer, B. Peters, F. Dankert, C. von Hänisch, *Dalton Trans.* **2020**, *49*, 5787–5790.

[136] S. Chitsaz, B. Neumüller, K. Dehnicke, *Z. Anorg. Allg. Chem.* **2003**, *629*, 592–594.

[137] R. Zitz, J. Baumgartner, C. Marschner, *Eur. J. Inorg. Chem.* **2018**, *2018*, 2380–2386.

[138] A. A. Korlyukov, A. V. Vologzhanina, M. I. Buzin, N. V. Sergienko, B. G. Zavin, A. M. Muzafarov, *Cryst. Growth Des.* **2016**, *16*, 1968–1977.

[139] R. J. Schwamm, J. R. Harmer, M. Lein, C. M. Fitchett, S. Granville, M. P. Coles, *Angew. Chem., Int. Ed.* **2015**, *54*, 10630–10633.

[140] S. Harder, B. Freitag, P. Stegner, J. Pahl, D. Naglav, *Z. Anorg. Allg. Chem.* **2015**, *641*, 2129–2134.

[141] J. A. Darr, S. R. Drake, D. J. Williams, A. M. Z. Slawin, *J. Chem. Soc., Chem. Commun.*

1993, *352*, 866–868.

[142] A. Steiner, G. T. Lawson, B. Walfort, D. Leusser, D. Stalke, *J. Chem. Soc., Dalton Trans.* **2001**, *6*, 219–221.

[143] M. Schulte, M. Schürmann, K. Jurkschat, *Chem. Eur. J.* **2001**, *7*, 347–355.

[144] M. Schulte, G. Gabriele, M. Schürmann, K. Jurkschat, A. Duthie, D. Dakternieks, *Organometallics* **2003**, *22*, 328–336.

[145] F. Haftbaradaran, G. Mund, R. J. Batchelor, J. F. Britten, D. B. Leznoff, *Dalton Trans.* **2005**, 2343–2345.

[146] E. W. Y. Wong, A. K. Das, M. J. Katz, Y. Nishimura, R. J. Batchelor, M. Onishi, D. B. Leznoff, *Inorg. Chim. Acta* **2006**, *359*, 2826–2834.

[147] G. Mund, R. J. Batchelor, R. D. Sharma, C. H. W. Jones, D. B. Leznoff, *J. Chem. Soc. Dalton Trans.* **2002**, 136–137.

[148] W. A. Herrmann, R. Anwander, V. Dufaud, W. Scherer, *Angew. Chem., Int. Ed.* **1994**, *33*, 1285–1286.

[149] N. A. H. Male, M. Thornton-Pett, M. Bochmann, *J. Chem. Soc., Dalton Trans.* **1997**, *35*, 2487–2494.

[150] R. Zitz, J. Hlina, M. Aghazadeh Meshgi, H. Krenn, C. Marschner, T. Szilvási, J. Baumgartner, *Inorg. Chem.* **2017**, *56*, 5328–5341.

[151] L. J. Bowman, K. Izod, W. Clegg, R. W. Harrington, *J. Organomet. Chem.* **2007**, *692*, 806–812.

[152] L. J. Bowman, K. Izod, W. Clegg, R. W. Harrington, *Organometallics* **2007**, *26*, 2646–2651.

[153] R. Zitz, J. Baumgartner, C. Marschner, *Organometallics* **2019**, *38*, 1159–1167.

[154] A. Willauer, A. Dabrowska, R. Scopelliti, M. Mazzanti, *Chem. Commun.* **2020**, DOI 10.1039/D0CC04197A.

[155] K. C. Jantunen, R. J. Batchelor, D. B. Leznoff, *Organometallics* **2004**, *23*, 2186–2193.

[156] K. C. Jantunen, F. Haftbaradaran, M. J. Katz, R. J. Batchelor, G. Schatte, D. B. Leznoff, *Dalton Trans.* **2005**, *50*, 3083.

[157] C. E. Hayes, R. H. Platel, L. L. Schafer, D. B. Leznoff, *Organometallics* **2012**, *31*, 6732–

6740.

[158] C. E. Hayes, Y. Sarazin, M. J. Katz, J. F. Carpentier, D. B. Leznoff, *Organometallics* **2013**, *32*, 1183–1192.

[159] C. E. Hayes, D. B. Leznoff, *Organometallics* **2010**, *29*, 767–774.

[160] M. K. Assefa, G. Wu, T. W. Hayton, *J. Am. Chem. Soc.* **2020**, *142*, 8738–8747.

[161] H. J. Emeléus, M. Onyszchuk, *J. Chem. Soc.* **1958**, 604–609.

[162] Y. A. Yuzhelevskii, V. V. Pchelintsev, N. N. Fedoseeva, *Vysok. Soedin., Ser. B* **1976**, *18*, 873.

[163] C. J. Olliff, P. Ladbrook, *Bioelectrochem Bioenerg.* **1979**, *6*, 105–109.

[164] C. J. Olliff, G. R. Pickering, K. J. Rutt, *J. Inorg. Nucl. Chem.* **1980**, *42*, 1201–1202.

[165] C. J. Olliff, G. R. Pickering, K. J. Rutt, *J. Inorg. Nucl. Chem.* **1980**, *42*, 288–289.

[166] H. C. Marsmann, M. Seifert, *Z. Naturforsch. B* **1991**, *46*, 693–694.

[167] B. Csákvári, E. Csákvári, P. Gömöry, A. Vértes, *J. Radioanal. Chem.* **1975**, *25*, 275–282.

[168] M. R. Churchill, C. H. Lake, S.-H. L. Chao, O. T. Beachley, *J. Chem. Soc., Chem. Commun.* **1993**, *53*, 1577–1578.

[169] C. Eaborn, P. B. Hitchcock, K. Izod, J. D. Smith, *Angew. Chemie, Int. Ed.* **1996**, *34*, 2679–2680.

[170] I. Sänger, M. Gärtner, M. Bolte, M. Wagner, H. W. Lerner, *Z. Anorg. Allg. Chem.* **2018**, *644*, 925–929.

[171] R. D. Ernst, A. Glöckner, A. M. Arif, *Z. Kristallogr. - New Cryst. Struct.* **2007**, *222*, 333–334.

[172] I. Haiduc, *Organometallics* **2004**, *23*, 3–8.

[173] L. C. Pop, M. Saito, *Coord. Chem. Rev.* **2016**, *314*, 64–70.

[174] A. Decken, J. Passmore, X. Wang, *Angew. Chem.* **2006**, *118*, 2839–2843.

[175] I. Krossing, I. Raabe, *Angew. Chem., Int. Ed.* **2004**, *43*, 2066–2090.

[176] I. M. Riddlestone, A. Kraft, J. Schaefer, I. Krossing, *Angew. Chem.* **2018**, *130*, 14178–14221.

[177] A. Decken, F. A. LeBlanc, J. Passmore, X. Wang, *Eur. J. Inorg. Chem.* **2006**, *7*, 4033–4036.

[178] I. Krossing, A. Reisinger, *Coord. Chem. Rev.* **2006**, *250*, 2721–2744.

[179] J. Pahl, H. Elsen, A. Friedrich, S. Harder, *Chem. Commun.* **2018**, *54*, 7846–7849.

[180] C. von Hänisch, O. Hampe, F. Weigend, S. Stahl, *Angew. Chem.* **2007**, *119*, 4859–4863.

[181] C. von Hänisch, F. Weigend, O. Hampe, S. Stahl, *Chem. Eur. J.* **2009**, *15*, 9642–9646.

[182] A. Kracke, C. von Hänisch, N. Kramer, *Eur. J. Inorg. Chem.* **2012**, 2975–2979.

[183] C. Bimbös, M. Jost, C. von Hänisch, K. Harms, *Eur. J. Inorg. Chem.* **2013**, *3*, 4645–4653.

[184] M. Ouchi, Y. Inoue, T. Kanzaki, T. Hakushi, *Bull. Chem. Soc. Jpn.* **1984**, *57*, 887–888.

[185] K. H. Pannell, C. K. La Neave, E. Rico, B. Arkles, *Pharmacol., Biochem. Behav.* **1984**, *21*, 77–80.

[186] Y. Inoue, M. Ouchi, T. Hakushi, *Bull. Chem. Soc. Jpn.* **1985**, *58*, 525–530.

[187] U. Das, G. Zhang, B. Hu, A. S. Hock, P. C. Redfern, J. T. Miller, L. A. Curtiss, *ACS Catal.* **2015**, *5*, 7177–7185.

[188] R. H. Krieble, C. A. Burkhard, *J. Am. Chem. Soc.* **1947**, *69*, 2689–2692.

[189] H. T. Phung, P. B. Chi, F. Kober, *Z. Anorg. Allg. Chem.* **1981**, *472*, 75–82.

[190] B. Arkles, K. King, R. Anderson, W. Peterson, *Organometallics* **1983**, *2*, 454–457.

[191] G. Oddon, M. W. Hosseini, *Tetrahedron Lett.* **1993**, *34*, 7413–7416.

[192] B. Rezzonico, M. Grignon-Dubois, M. Laguerre, J. M. Léger, *Organometallics* **1998**, *17*, 2656–2664.

[193] T. J. Liu, D. Wang, Y. Z. Wang, G. Z. Xu, *Phosphorus, Sulfur Silicon Relat. Elem.* **1998**, *140*, 237–244.

[194] R. Buschbeck, H. Lang, S. Agarwal, V. K. Saini, V. K. Gupta, *Synthesis.* **2004**, *2*, 1243–1248.

[195] S. Bruña, I. Martínez-Montero, A. M. González-Vadillo, C. Martín-Fernández, M. M. Montero-Campillo, O. Mó, I. Cuadrado, *Macromolecules* **2015**, *48*, 6955–6969.

[196] N. Yamasaki, J. Masamoto, *J. Polym. Sci., Part A: Polym. Chem.* **2004**, *42*, 520–533.

[197] A. I. Chernyavskii, A. P. Pleshkova, *Russ. Chem. Bull.* **2006**, *55*, 748–750.

[198] J. Kurjata, J. Chojnowski, *Macromol. Chem. Phys.* **1993**, *194*, 3271–3286.

[199] J. Chojnowski, J. Kurjata, *Macromolecules* **1994**, *27*, 2302–2309.

[200] D. J. Harrison, D. R. Edwards, R. McDonald, L. Rosenberg, *Dalton Trans.* **2008**, *9226*, 3401.

[201] K. Reuter, M. R. Buchner, G. Thiele, C. von Hänisch, *Inorg. Chem.* **2016**, *55*, 4441–4447.

[202] K. Reuter, G. Thiele, T. Hafner, F. Uhlig, C. von Hänisch, *Chem. Commun.* **2016**, *52*, 13265–13268.

[203] K. Reuter, F. Dankert, C. Donsbach, C. von Hänisch, *Inorganics* **2017**, *5*, 1–12.

[204] F. Dankert, K. Reuter, C. Donsbach, C. von Hänisch, *Dalton Trans.* **2017**, *46*, 8727–8735.

[205] H. Li, L. J. Hope-Weeks, C. Krempner, *Chem. Commun.* **2011**, *47*, 4117–4119.

[206] H. Li, A. J. A. Aquino, D. B. Cordes, W. L. Hase, C. Krempner, *Chem. Sci.* **2017**, *8*, 1316–1328.

[207] V. D. Thalangamaarachchige, H. Li, D. B. Cordes, D. K. Unruh, C. Krempner, *Inorg. Chem.* **2017**, *56*, 9869–9879.

[208] E. Hengge, E. Brandstätter, W. Veigl, *Monatsh. Chem.* **1977**, *108*, 1425–1430.

[209] K. Reuter, S. S. Rudel, M. R. Buchner, F. Kraus, C. von Hänisch, *Chem. Eur. J.* **2017**, *23*, 9607–9617.

[210] M. Köster, *Untersuchungen zu disilanbasierten Makrocyclen als Liganden für p- und d-Block Metallionen sowie zu siloxanbasierten Käfigverbindungen*. Dissertation **2019**, Marburg. DOI: 10.17192/z2020.0076.

[211] W. Einholz, W. Gollinger, W. Haubold, *Z. Naturforsch. B* **1990**, *45*, 25–30.

[212] G. Fritz, B. Grunert, *Z. Anorg. Allg. Chem.* **1981**, *473*, 59–79.

[213] M. R. Buchner, *Chem. Commun.* **2020**, *56*, 8895–8907.

[214] D. Naglav, M. R. Buchner, G. Bendt, F. Kraus, S. Schulz, *Angew. Chem., Int. Ed.* **2016**, *55*, 10562–10576.

[215] G. M. Sheldrick, *Acta Crystallogr. Sect. A Found. Adv.* **2015**, *71*, 3–8.

[216] G. M. Sheldrick, *Acta Crystallogr. Sect. C Struct. Chem.* **2015**, *71*, 3–8.

[217] O. V. Dolomanov, L. J. Bourhis, R. J. Gildea, J. A. K. Howard, H. Puschmann, *J. Appl. Crystallogr.* **2009**, *42*, 339–341.

8 Appendix

In this final section, the respective paper of this cumulative dissertation are attached in chronological order. Supplementary Information is provided if existing. Copyright belongs to the respective publisher.

1) F. Dankert, C. Donsbach, C.-N. Mais, K. Reuter, C. von Hänisch, *Inorg. Chem.* **2018**, *57(1)*, 351-359. „Alkali and Alkaline Earth Metal Derivatives of Disila-Bridged Podands: Coordination Chemistry and Structural Diversity". Copyright © 2018, American Chemical Society.
2) F. Dankert, K. Reuter, C. Donsbach, C. von Hänisch, *Inorganics* **2018**, *6(1)*, 15. „Hybrid Disila-Crown Ethers as Hosts for Ammonium Cations: The O–Si–Si–O Linkage as an Acceptor for Hydrogen Bonding". Published by MDPI (open access).
3) F. Dankert, J. Heine, J. Rienmüller, C. von Hänisch, *CrystEngComm* **2018**, *20*, 5370-5376. „Sila-polyethers as innocent crystallization reagents for heavy alkali metal compounds". Copyright © 2018, Published by The Royal Society of Chemistry (RSC).
4) M. R. Buchner, M. Müller, F. Dankert, K. Reuter, C. von Hänisch, *Dalton Trans.* **2018**, *47*, 16393-16397. „The coordination behaviour and reactivity of partially silicon based crown ethers towards beryllium chloride". Copyright © 2018, The Royal Society of Chemistry.
5) F. Dankert, C. von Hänisch, *Inorg. Chem.* **2019**, *58*, 3518-3526. „Insights into the Coordination Ability of Siloxanes Employing Partially Silicon Based Crown Ethers: A Comparative Analysis of s-Block Metal Complexes". Copyright © 2019, American Chemical Society.
6) F. Dankert, C. Donsbach, J. Rienmüller, R. M. Richter, C. von Hänisch, *Chem. Eur. J.* **2019**, *25*, 15934-15943. „Alkaline earth metal template (cross-)coupling reactions with hybrid disila-crown ether analogues". Copyright © Wiley-VCH GmbH, Weinheim.

7) F. Dankert, F. Weigend, C. von Hänisch, *Inorg. Chem.* **2019**, *58*, 15417-15422. „Not Non-coordinating at all: Coordination Compounds of the Cyclodimethylsiloxanes D_n (D = Me_2SiO; n = 6, 7) and Group 2 Metal Cations". Copyright © 2019, American Chemical Society.

8) F. Dankert, H. L. Deubner, M. Müller, M. R. Buchner, F. Kraus and C. von Hänisch, *Z. Anorg. Allg. Chem.* **2020**, *646*, 1501-1507. „C-F Bond Cleavage Reactions with Beryllium, Magnesium, Gallium, Hafnium and Thorium Halides". Copyright © Wiley-VCH GmbH, Weinheim.

9) F. Dankert, L. Erlemeier, C. Ritter, C. von Hänisch, *Inorg. Chem. Front.* **2020**, 7, 2138-2153. „On the molecular architectures of siloxane coordination compounds: (re-)investigating the coordination of the cyclodimethylsiloxanes Dn (n = 5–8) towards alkali metal ions". Copyright © 2018, The Royal Society of Chemistry.

10) F. Dankert,* A. Feyh,* C. von Hänisch, *Eur. J. Inorg. Chem.* **2020**, *2020*, 2744-2756. „Chalcogen bonding of SO_2 and s-block metal iodides near room temperature: A remarkable structural diversity". *These authors contributed equally. Copyright © Wiley-VCH GmbH, Weinheim.

11) M. R. Buchner, F. Dankert, N. Spang, F. Pielnhofer, C. von Hänisch, *accepted manuscript*, *Inorg. Chem.* **2020**. „A Second Modification of Beryllium Bromide: β-$BeBr_2$". Copyright © 2020, American Chemical Society.

12) F. Dankert, R. M. Richter, F. Weigend, X. Xie, M. Balmer, C. von Hänisch, *unpublished manuscript*. **2020**. „Architecting inorganic crown-ethers by s-block-metal templated Si-O bond activation".

Inorganic Chemistry

Article

Cite This: Inorg. Chem. 2018, 57, 351−359

pubs.acs.org/IC

Alkali and Alkaline Earth Metal Derivatives of Disila-Bridged Podands: Coordination Chemistry and Structural Diversity

Fabian Dankert, Carsten Donsbach, Christopher-Nils Mais, Kirsten Reuter, and Carsten von Hänisch*

Fachbereich Chemie and Wissenschaftliches Zentrum für Materialwissenschaften (WZMW), Philipps-Universität Marburg, Hans-Meerwein-Straße 4, 35043 Marburg, Germany

Supporting Information

ABSTRACT: Within this study, the synthesis and coordination chemistry of open-chain ligands bearing disila-units is presented. Instead of basic 1:1 complexes, structural diversity was discovered in the variety of ligand and salt. Stable complexes of alkali and alkaline earth metal complexes were obtained by equimolar reactions of different salts with the disila-bridged podands 8,9-disila-EO5 (**1**) and 11,12-disila-EO7 (**2**) (EO5 = pentaethylene glycol; EO7 = heptaethylene glycol). The respective alkaline earth metal complexes of the type $[Ca(8,9\text{-disila-EO5})(OTf)_2]$ (**3**), $[Sr(8,9\text{-disila-EO5})I_2]$ (**5**), $[Sr(11,12\text{-disila-EO7})I]I$ (**6**), and $[Ba(11,12\text{-disila-EO7})OTf_2]$ (**7**) (OTf = $CF_3SO_3^-$) were characterized via single-crystal X-ray diffraction analyses. Within the reaction of the alkali metal salt $NaPF_6$ with **1**, the sodium ion acts as a template during the complexation process. Under elimination of one molecule of diethylene glycol, the dinuclear species $[Na_2(8,9,17,18\text{-tetrasila-EO8})(PF_6)_2]\cdot EO2$ (**4**) (EO8 = octaethylen glycol, EO2 = diethylene glycol) is obtained, in which the sodium cations are 7-fold coordinated within a disilane-bearing framework. The reaction of **2** with CsOTf failed, leading to recrystallization of anhydrous CsOTf. By means of DFT calculations it was shown that the disila-bearing ligands are burdened with negative hyperconjugation interactions between the silicon and the oxygen atoms, but the coordination by sufficiently hard cations can easily overcompensate the competing polarization. In contrast, soft Lewis acids barely share interactions with silicon-bonded oxygen atoms. All findings are consistent with observations made in solution according to ^{29}Si NMR spectroscopical studies.

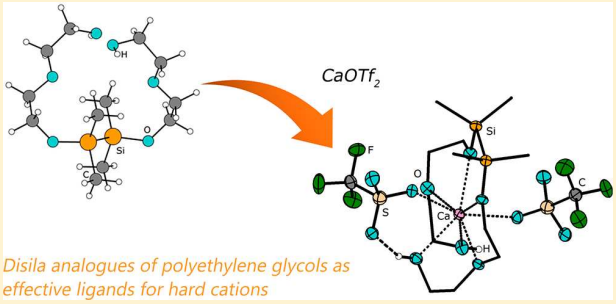

Disila analogues of polyethylene glycols as effective ligands for hard cations

Downloaded via UNIV OF MARBURG on April 3, 2020 at 13:14:44 (UTC).
See https://pubs.acs.org/sharingguidelines for options on how to legitimately share published articles.

INTRODUCTION

Cyclosiloxanes are well-known as part of silicon grease; they are able to act like crown ether type ligands and are thus described as pseudocrown ethers or inorganic crown ethers.[1] With the discovery of cyclosiloxane complexes, an increased interest in the development of macrocyclic compounds and their metal complexes was the direct consequence and a structural diversity was discovered rapidly (Scheme 1a−d). These ligands can basically be divided into cyclosiloxanes, hybrid (di)sila-crown ethers, and cryptands. Some exotic ligands such as silicon-containing oxathio-crown ethers were also described in the literature.[2] In comparison to the corresponding organic crown type ligands, a significantly lower coordination ability of ligands bearing $SiMe_2$ units was found.[1] Hitherto known cyclosiloxane complexes are mostly constituted of a weakly coordinating anion such as Al_F (Al_F = $[Al\{OC(CF_3)_3\}_4]^-$), $[SbF_6]^-$, or $[InH\{CH_2C(CH_3)\}_3]^-$ as counterion, in which the charge is widely spread over a non-nucleophilic, chemically robust moiety.[3−6] Only $[Zr(D_6)Br_2][Zr_2Br_9]_2$ (D = Me_2SiO) is a unique example of a cyclosiloxane complex bearing a more strongly coordinating halide anion.[7] Historically, the low basicity was attributed to backbonding of an occupied p-orbital into unoccupied d-orbitals (p(O) → d(Si)).[8,9] Replaced by the theory of negative hyperconjugation between p(O) → σ*(Si−C), this approach was disestablished later.[10−12] To date, negative hyperconjugation is one of the most eminent models to describe the lower basicity, and it is remarkably present in permethylated siloxanes.[13,14] In contrast, however, an ionic consideration of the Si−O bond is also discussed.[15−17] A strong attraction between negatively polarized oxygen atoms and Lewis acids is intercepted because of repulsive interactions between the positively polarized silicon atoms and the Lewis acid.[12,18] Since cyclosiloxanes bear $-SiMe_2-$ rather than $-CH_2CH_2-$ units, there is also a significant structural repugnance.

Furthermore, small changes in the macrocyclic framework affect the coordination ability immensely. Contracted crown ethers of the type [3*n*−1]crown-*n* (*n* = 5, 6) exhibit an eminently lower complexation ability.[28,29] To subject the lower ability of silicon bonded oxygen atoms to scrutiny, there have been approaches to regain structural analogy to organic crown ether compounds inserting $-Si_2Me_4-$ units. Lately, the ligands 1,2-disila-[3*n*]crown-*n* (*n* = 4−6), 1,2,7,8-tetrasila[12]crown-4, 1,2,4,5-tetrasila[12]crown-4, and 1,2-disila-benzo[18]crown-6 were characterized (see Scheme 1e−h).[24,25,27] It was found that

Received: October 11, 2017
Published: December 12, 2017

© 2017 American Chemical Society

DOI: 10.1021/acs.inorgchem.7b02590
Inorg. Chem. 2018, 57, 351−359

Scheme 1. Selection of Characterized Mono- and Bicyclic Macrocycles Bearing Sila- or Disila-Units[a]

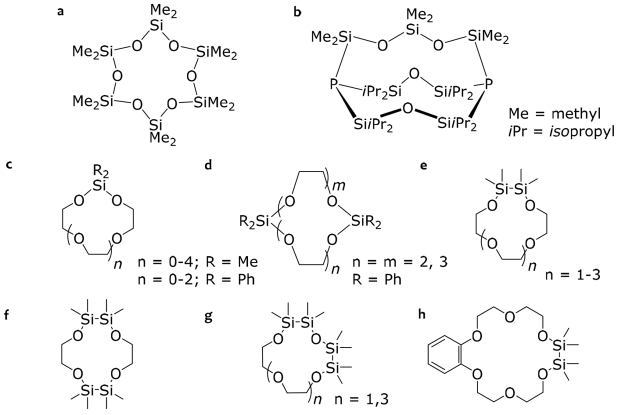

[a](a) Cyclosiloxanes,[1] (b) cryptands,[19] (c and d) sila-crown ethers,[20−23] (e) disila-crown ethers,[24] (f and g) tetrasila-crown ethers,[24−26] and (h) benzo disila-crown ethers.[27] This list is not intended to be exhaustive.

these ligands willingly form stable complexes with alkali and alkaline earth metal salts, even with strongly coordinating counterions. Complexation abilities seem to be on even terms compared to those of organic crown compounds as confirmed by NMR as well as DFT studies.[24] Most recent works even hint at a considerably higher complexation ability of the partially silicon substituted crown ether 1,2,4,5-tetrasila[12]crown-4 toward Li^+ compared to that of [12]crown-4.[25] Furthermore, a study on mismatched crown ether complexes revealed that there is no superiority in the coordination ability of fully carbon bonded oxygen atoms on a structural level.[26] Finally, the potential of disila-units could be shown with the cyclic aluminum disiloxide $\{[R_4Si_2O_2]_2[Al(Me)_2]_2\}^{2-}$ stabilizing the formal $[AlMe]^{2+}$ cation (R = $SiMe_3$).[30] However, less attention has been paid to open-chain ligands, also known as podands, such as common glymes and polyethylene glycols bearing sila-units. Podands are known to have a lower complexation ability than crown-type ligands[31] but are able to build stable metal complexes, which was shown by a number of publications.[32−34] For this reason, they also have widespread applications, e.g., as catalysts in anion-promoted reactions or in chemical analytics in which podands are described as useful tools for compound separation and concentration determination.[35] This motivated us to extend the coordination chemistry to open-chain ligands which incorporate Si_2Me_4 units as well as C_2H_4 bridges in between the oxygen atoms.

EXPERIMENTAL SECTION

General. All working procedures were carried out with rigorous exclusion of oxygen and moisture using Schlenk techniques under argon gas. Solvents were dried and freshly distilled before use. Alkali and alkaline earth metal salts were stored and handled under argon atmosphere using a glovebox. NMR spectra were recorded on a Bruker AV III HD 300 MHz or AV III 500 MHz. MestReNova package was used for analyzation.[36] Infrared (IR) spectra of the respective samples were measured using attenuated total reflectance (ATR) mode on a Bruker Model Alpha FT-IR. OPUS-Software package was applied throughout.[37] MS spectrometry was measured on JEOL AccuTOF-GC (FD and LIFDI) or LTQ-FT (ESI). Elemental analysis was carried out on a Vario MicroCube.

Synthesis and Crystallization. *Compounds 1 and 2.* First, 31.6 mmol of the appropriate glycol (3.1 mL of diethylene glycol or 4.25 mL of triethylene glycol, respectively), 4.4 mL of triethylamine (31.6 mmol) and 10 mL of diethyl ether were placed in a 100 mL Schlenk-flask. The solution was vigorously stirred and cooled to −80 °C. After cooling, 3.0 mL of 1,2-dichloro-1,1,2,2-tetramethyldisilane (15.8 mmol) in 15 mL of diethyl ether was dropped into the cold solution over a period of 45 min. While dropping the silane into the reaction vessel, cooling was stopped in order to slowly warm the solution to room temperature. The resulting pale white suspension was further stirred for 1 h and then freed from the solvent. The residue was extracted with 20 mL of toluene followed by filtration. Removing the solvent under reduced pressure gives a dull oil that was extracted with 5 mL of acetonitrile. The solvent was once again removed under reduced pressure to obtain ligands **1** and **2** as colorless oils (**1**: 2.16 g, 42%; **2**: 2.80 g, 43%).

Analytical Data for 1. ^{1}H NMR (300 MHz, CD_3CN): 0.17 (s, 12H, $SiCH_3$), 3.11 (br, s, 2H, OH), 3.49−3.52 (m, 4H, CH_2), 3.57−3.62 (m, 8H, CH_2), 3.72−3.75 (m, 4H, CH_2) ppm. $^{13}C\{^1H\}$ NMR (75 MHz, CD_3CN): 0.51 (s, $SiCH_3$), 62.1 (s, CH_2), 63.5 (s, CH_2), 73.2 (s, CH_2), 73.3 (s, CH_2) ppm. $^{29}Si\{^1H\}$ NMR (99 MHz, CD_3CN): 10.6 (s, $SiCH_3$) ppm. MS (ESI^+): 349.1474 $[M+Na]^+$ (10) 365.1424 $[M+K]^+$ (15). IR (cm^{-1}): 3440 (m, br, $\tilde{\nu}_s$ O−H), 2948 (m), 2867 (m), 1728 (vw), 1457 (w), 1398 (w), 1354 (w), 1326 (w), 1294 (s), 1245 (s), 1082 (s), 929 (s), 824 (s), 788 (s), 762 (vs), 718 (m), 628 (s), 542 (w), 503 (w).

Analytical Data for 2. ^{1}H NMR (300 MHz, CD_3CN): 0.22 (s, 12H, $SiCH_3$), 3.01 (br, s, 2H, OH), 3.47−3.52 (m, 8H, CH_2), 3.56 + 3.58 (s, 12H, CH_2), 3.67−3.72 (m, 4H, CH_2) ppm. $^{13}C\{^1H\}$ NMR (75 MHz, CD_3CN): −0.07 (s, $SiCH_3$), 62.0 (s, CH_2), 63.8 (s, CH_2), 71.1 (s, CH_2), 71.3 (s, CH_2), 73.3 (s, CH_2), 73.4 (s, CH_2) ppm. $^{29}Si\{^1H\}$ NMR (99 MHz, CD_3CN): 12.0 (s, $SiCH_3$) ppm. MS (ESI^+): 437.1991 $[M+H]^+$ (60). IR (cm^{-1}): 3444 (m, br, $\tilde{\nu}_s$ O−H), 2867 (m), 1456 (w), 1399 (w), 1351 (w), 1294 (w), 1245 (s), 1079 (vs), 940 (s), 886 (w), 826 (s), 790 (w), 764 (s), 629 (m), 514 (w).

Compound 3. First, 260 mg of **1** (0.80 mmol) was dissolved in 10 mL of DCM. Then, 257 mg of $CaOTf_2$ (0.80 mmol) was added. The solution was stirred overnight, and the slightly cloudy solution was freed from the solvent. The residue was washed well with 8 mL of *n*-pentane followed by drying *in vacuo* to receive **3** as a pale white powder (479 mg, 90%). For single crystal growth, the powder was dissolved in 5 mL of DCM, filtered and layered with 20 mL of *n*-pentane. Single crystals in the shape of colorless blocks among colorless needles were obtained within 2 days (see Supporting Information for further information). ^{1}H NMR (300 MHz, CD_2Cl_2): 0.38 (s, 12H, $SiCH_3$), 3.74−3.81 (m, 8H, CH_2), 3.88−3.97 (m, 8H, CH_2), 5.14 (t, 2H, OH, $^3J_{HH}$ = 6.1 Hz) ppm. $^{13}C\{^1H\}$ NMR (75 MHz, CD_2Cl_2): −1.38 (s, $SiCH_3$), 60.5 (s, CH_2), 62.1 (s, CH_2), 72.2 (s, CH_2), 72.9 (s, CH_2), 120.5 (q, CF_3, $^1J_{CF}$ = 318 Hz) ppm. $^{29}Si\{^1H\}$ NMR (99 MHz, CD_2Cl_2): 19.4 (s, $SiCH_3$) ppm. ^{19}F NMR (283 MHz, CD_2Cl_2): 79.6 (s, CF_3) ppm. MS (LIFDI$^+$): 515.07289 $[M-OTf]^+$ (100), 349.1545 [8,9-disila-EO5+Na]$^+$ (5). IR (cm^{-1}): 3491 + 3337 (br, m, $\tilde{\nu}_s$ O−H), 2963 (w), 2894 (w), 1461 (w), 1406 (w), 1353 (s), 1299 (s), 1243 (s), 1225 (s), 1168 (s), 1106 (m), 1057 (s), 1029 (vs), 943 (s), 916 (s), 865 (m), 818 (s), 795 (s), 774 (s), 733 (m), 636 (s), 574 (s), 516 (s). CHN calcd for $C_{14}H_{30}CaF_6O_{12}S_2Si_2$: C, 25.30; H, 4.55; S, 9.65. Found: C, 24.86; H, 4.162; S, 9.16.

Compound 4. First, 85 mg of **1** (0.26 mmol) and 44 mg of $NaPF_6$ (0.26 mmol) were dissolved in 10 mL of DCM. The solution was stirred for 2 h followed by filtration. The clear solution is then freed from the solvent. The residue is well washed with 5 mL of *n*-pentane followed by drying *in vacuuo* to receive **4** as a colorless, sticky oil (60 mg, 47%). For single crystal growth the oil was stored at ambient temperature for 3 days. Single crystals grew in shape of colorless platelets out of the solvent free oil. MS (LIFDI$^+$): 349.1469 [8,9-disila-EO5+Na]$^+$ (20), 569.2428 $[M-2PF_6-Na]^+$ (100). IR (cm^{-1}): 3594 + 3364 (br, m, $\tilde{\nu}_s$ O−H), 2955 (w), 2892 (w), 1460 (w), 1398 (w), 1354 (w), 1302 (w), 1250 (s), 1119 (s), 1050 (s), 955 (m), 933 (m), 832 (vs), 794 (vs), 769 (vs), 741 (s), 635 (w), 556 (s). CHN calcd for $C_{20}H_{50}F_{12}Na_2O_9P_2Si_4{\cdot}0.5EO2$: C, 28.23; H, 5.92. Found: C, 28.69; H, 5.45.

DOI: 10.1021/acs.inorgchem.7b02590
Inorg. Chem. 2018, 57, 351−359

Scheme 2. Synthesis and Coordination Chemistry of Disila-Bridged Polyethyleneglycols

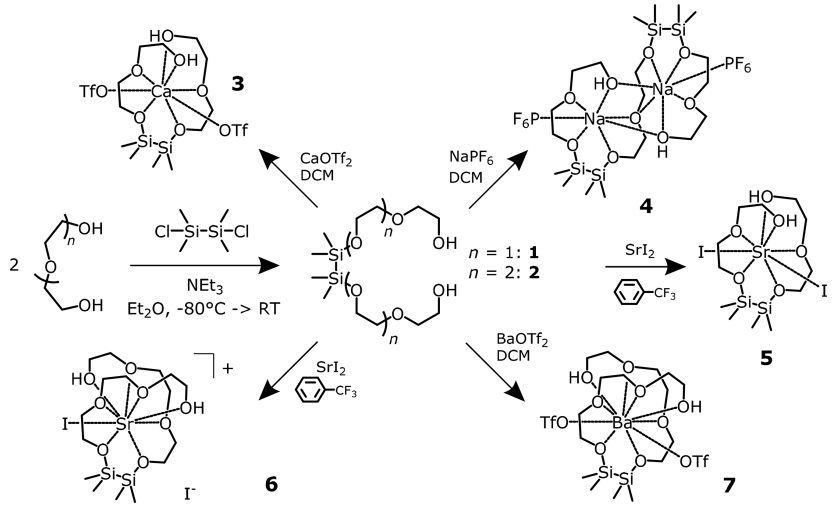

Compound **5**. First, 210 mg of **1** (0.643 mmol) was dissolved in 10 mL of *α*,*α*,*α*-trifluorotoluene. Afterward, 220 mg of SrI_2 (0.643 mmol) was added. The solution was stirred overnight and filtered afterward. The resulting solid was extracted with 2 mL of DCM and combined with the filtrate. The solvent mixture was removed under reduced pressure and the residue was washed with two portions of 5 mL of *n*-pentane. The resulting solid was then dried *in vacuo* to receive **5** as a colorless powder (266 mg, 62%). For single crystal growth, the solid was dissolved in 4 mL of DCM and filtered. Layering the filtrate with 20 mL of *n*-pentane yielded single crystals in form of colorless blocks among colorless planks within 2 days (see the Supporting Information for further information). ^{1}H NMR (300 MHz, CD_2Cl_2): 0.49 (s, 12H, SiCH_3), 3.75 (t, 2H, O*H*, $^3J_{HH}$ = 6.5 Hz), 3.85−3.90 (m, 8H, CH_2), 3.94−4.00 (m, 4H, CH_2), 4.04−4.07 (m, 4H, CH_2) ppm. ^{13}C{^{1}H} NMR (75 MHz, CD_2Cl_2): −0.2 (s, $SiCH_3$), 61.9 (s, CH_2), 62.8 (s, CH_2), 72.7 (s, CH_2), 73.0 (s, CH_2) ppm. ^{29}Si{^{1}H} NMR (99 MHz, CD_2Cl_2): 18.7 (s, *Si*CH_3) ppm. MS (ESI$^+$): 349.1474 [8,9-disila-EO5 + Na]$^+$ (100), 413.0555 [M − I]$^+$ (6). IR (cm^{-1}) $\tilde{\nu}$ = 3297 (m, br, $\tilde{\nu}_s$ O−H), 2936 (m), 2878 (w), 1451 (w), 1392 (w), 1351 (w), 1302 (m), 1248 (w), 1106 (s), 1060 (vs), 1032 (s), 943 (s), 923 (vs), 882 (m), 863 (m), 837 (s), 813 (s), 792 (s), 767 (vs), 728 (s), 634 (m), 546 (m), 503 (m), 452 (m). CHN calcd for $C_{12}H_{30}I_2O_6Si_2Sr$·0.5DCM C, 21.13; H, 4.40. Found: C, 20.94; H, 4.41.

Compound **6**. First, 124 mg of **2** (0.299 mmol) were dissolved in 10 mL of *α*,*α*,*α*-trifluorotoluene. Then, 102 mg of SrI_2 (0.299 mmol) were added. The solution was stirred overnight and filtered afterward. The resulting solid was extracted with 2 mL of DCM and combined with the filtrate. The solvent mixture was removed under reduced pressure and the residue was washed with two portions of 8 mL of *n*-pentane. The resulting solid was then dried *in vacuo* to obtain **6** as a colorless powder (145 mg, 64%). For single crystal growth, the solid was dissolved in 5 mL of DCM and 2 mL of *α*,*α*,*α*-trifluorotoluene. After filtration, reducing to a volume of approximately 3 mL and cooling the clear solution to −24 °C allowed us to obtain crystals in the shape of colorless planks after 4 days for single crystal XRD studies. ^{1}H NMR (300 MHz, CD_2Cl_2): 0.52 (s, 12H, SiCH_3), 3.86−3.88 (m, 4H, CH_2), 3.93−3.96 (m, 12H, CH_2), 3.98 (s, 8H, CH_2), 5.33 (s, 2H, O*H*) ppm. ^{13}C{^{1}H} NMR (75 MHz, CD_2Cl_2): 0.2 (s, $SiCH_3$), 60.4 (s, CH_2), 62.9 (s, CH_2), 69.3 (s, CH_2), 69.6 (s, CH_2), 71.5 (s, CH_2), 72.7 (s, CH_2) ppm. ^{29}Si{^{1}H} NMR (99 MHz, CD_2Cl_2): 19.1 (s, *Si*CH_3) ppm. MS (ESI$^+$): 437.1990 [11,12-disila-EO8 + Na]$^+$ (100), 629.0211 [M − I]$^+$ (7). IR (cm^{-1}): 3282.48 + 3174.42 (br, m, $\tilde{\nu}_s$ O−H), 2944 (w), 2930 (w), 2877 (w), 1451 (w), 1347 (w), 1283 (w), 1247 (w), 1223 (m), 1126 (m), 1100 (s), 1059 (vs), 957 (s), 937 (s), 896 (m), 868 (m), 845 (s), 823 (s), 802 (s), 772 (s), 720 (s), 631 (m), 585 (m), 529 (m), 456 (w), 435 (w), 409 (vw). CHN calcd for $C_{16}H_{38}I_2O_8Si_2Sr$ C, 25.42; H, 5.07. Found: C, 25.68; H, 4.89.

Compound **7**. First, 164 mg of **2** (0.396 mmol) was dissolved in 15 mL of DCM, and 172 mg of $BaOTf_2$ (0.396 mmol) was added. The solution was then stirred overnight and filtered afterward. The solvent was removed under reduced pressure, and the residue was washed with two portions of 15 mL of *n*-pentane. The resulting solid was dried *in vacuo* to receive **7** as a pale white powder (248 mg, 75%). For crystal growth, the powder was dissolved in 4 mL of DCM followed by filtration. After layering with 10 mL of *n*-pentane, crystals suitable for single crystal XRD studies were obtained in the shape of colorless blocks after 1 day. ^{1}H NMR (300 MHz, CD_2Cl_2): 0.35 (s, 12H, SiCH_3), 3.62−3.65 (m, 4H, CH_2), 3.71−3.73 (m, 4H, CH_2), 3.77 (s, 8H, CH_2), 3.79−3.86 (m, 8H, CH_2), 4.91 (t, 2H, O*H*, $^3J_{HH}$ = 6.6 Hz) ppm. ^{13}C{^{1}H} NMR (75 MHz, CD_2Cl_2): −1.1 (s, $SiCH_3$), 61.4 (s, CH_2), 63.1 (s, CH_2), 70.3 (s, CH_2), 70.6 (s, CH_2), 72.3 (s, CH_2), 73.0 (s, CH_2), 122.1 (q, CF_3, $^1J_{CF}$ = 309 Hz) ppm. ^{29}Si NMR (99 MHz, CD_2Cl_2): 16.8 (s, *Si*CH_3) ppm. ^{19}F NMR (283 MHz, CD_2Cl_2): −79.47 (s, CF_3) ppm. IR (cm^{-1}): 3445 (br, m, OH), 2945 (m), 2916 (w), 2882 (w), 1466 (w), 1405 (vw), 1350 (w), 1259 (vs), 1223 (m), 1152 (s), 1104 (s), 1068 (s), 1054 (s), 1034 (s), 951 (s), 933 (m), 897 (m), 863 (m), 842 (m), 817 (m), 794 (s), 768 (s), 754 (m), 722 (s), 685 (w), 635 (vs), 573 (m), 516 (s), 453 (vw); MS: (LIFDI+) 701.0685 [M−OTf]$^+$ (40); CHN calcd for $C_{18}H_{38}BaF_6O_{14}S_2Si_2$ C, 25.43; H, 4.51; S 7.54. Found: C, 25.07; H, 4.395; S 7.24.

RESULTS AND DISCUSSION

In the first step, the disila-bearing ligands were prepared through reaction of two equivalents of an appropriate diol, two equivalents of triethylamine as an auxiliary base and one equivalent of 1,1,2,2-tetramethyl-1,2-dichlorodisilane. With EO2 (EO2 = diethylene glycol) and EO3 (EO3 = triethylene glycol), the ligands 8,9-disila-EO5 (**1**) and 11,12-disila-EO7 (**2**) (EO5 = pentaethylene glycol; EO7 = heptaethylene glycol) could be obtained as colorless oils. With the use of alkali or alkaline earth metal salts and a suitable solvent, coordination chemistry can easily be performed (Scheme 2).

Treatment of **1** with anhydrous $CaOTf_2$ (OTf = $CF_3SO_3^-$) in dichloromethane yielded the respective coordination compound [Ca(8,9-disila-EO5)(OTf)$_2$] (**3**). Within the crystallization procedure two types of crystal habits were obtained: **3** crystallizing in form of colorless blocks and colorless needles. Both resemble two different polymorphs of the same compound, as the same molecular structure was determined upon refinement of the X-ray diffraction data, but with different hydrogen bonding patterns (see the Supporting

DOI: 10.1021/acs.inorgchem.7b02590
Inorg. Chem. 2018, 57, 351−359

Information). Herein, the discussion is restricted to the diffraction data obtained from the colorless needles in which **3** crystallizes in the centrosymmetric, monoclinic space group $P2_1/n$. The molecular structure reveals an 8-fold coordinated calcium cation with podand oxygen atoms as well as two triflate anions coordinating (Figure 1). Within the molecular structure

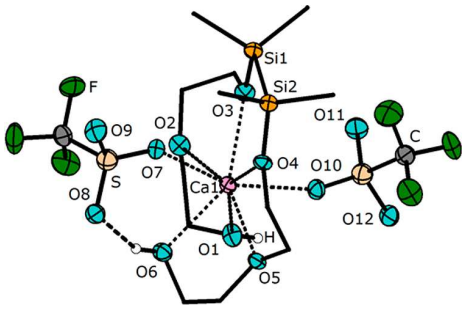

Figure 1. Molecular structure of **3** in the crystal. Thermal ellipsoids are represented at the 50% probability level. Carbon-bonded hydrogen atoms are omitted, and carbon atoms of the podand are represented as wireframes for clarity. Selected bond lengths [pm]: Ca1−O1 246.3(2), Ca1−O2 249.5(3), Ca1−O3 245.5(2), Ca1−O4 250.3(2), Ca1−O5 244.7(2), Ca1−O6 245.2(2), Ca1−O7 243.3(2), Ca1−O10 238.2(2), Si1−Si2 233.6(1). Selected bond angles [deg]: O1−Ca1−O2 66.54(8), O2−Ca1−O3 67.82(8), O3−Ca1−O4 77.78(7), O4−Ca1−O5 68.16(7), O5−Ca1−O6 67.50(8), O7−Ca1−O10 152.54(8).

of **3** in the crystal, intramolecular hydrogen bonding between H6 and the triflate bonded O8 is found. Intermolecular hydrogen bonding is present between two molecules each of which forming isolated dimers along the crystallographic *a* axis. (see Figure 2).

Using the alkali metal salt $NaPF_6$, we aimed at synthesizing the corresponding alkali metal complex of the ligand **1**. The ion diameter of Na^+ is 204 pm and thus very similar to that of Ca^{2+} with 200 pm.[38] However, in the reaction of **1** with $NaPF_6$ the

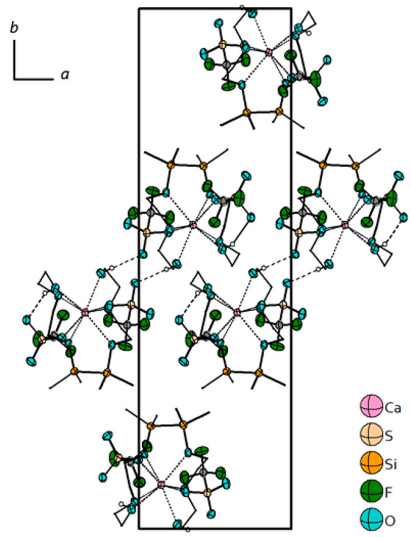

Figure 2. Cell package of **3** and hydrogen bonding along [001]. Thermal ellipsoids are represented at the 50% probability level. Carbon-bonded hydrogen atoms are omitted, and carbon atoms of the podand are represented as wireframes for clarity.

sodium cation acts as a template: Under elimination of 1 equiv of EO2 (EO2 = diethylene glycol) the dinuclear species $[Na_2(8,9,17,18\text{-tetrasila-EO8})(PF_6)_2]$ (**4**) (EO8 = octaethylene glycol) was formed. The formation of **4** was confirmed via single-crystal X-ray diffraction analysis as well as by mass-spectrometry and elemental analysis. In FD^+ mass spectrometry, $[Na(8,9,17,18\text{-tetrasila-EO8})]^+$ was detected at 569.2428 *m/z*. The ^1H, ^{13}C, and ^{29}Si NMR spectra of the dissolved crystals show a mixture of at least two species, and monitoring of ligand **1** with $NaPF_6$ via ^{13}C NMR spectroscopy shows the formation of various unidentified products. This indicates that sila ether **1** is not stable in solution if $NaPF_6$ is present. Due to these Si−O bond cleavage reactions not all of the signals in the NMR spectra could be assigned. Compound **4** crystallizes in the noncentrosymmetric orthorhombic space group *Aea*2. The molecular structure determined via X-ray diffraction analysis reveals the dinuclear complex **4** with one cocrystalline molecule of EO2 (see Figure 3).

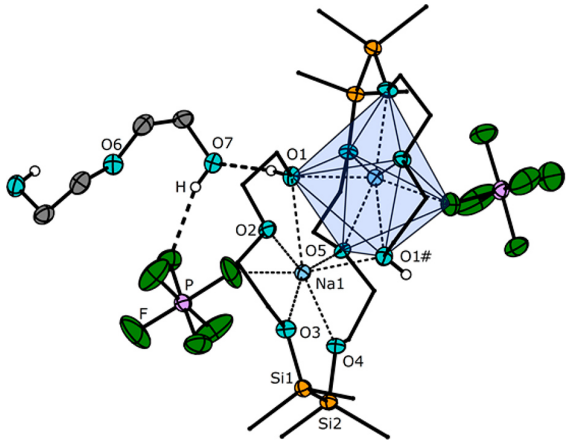

Figure 3. Molecular structure of **4·EO2** in the crystal. Thermal ellipsoids are represented at the 50% probability level. Carbon-bonded hydrogen atoms are omitted, and carbon atoms of the podand represented as wireframes for clarity. Sodium cations are coordinated in the shape of a pentagonal bipyramid (see light blue). All nonlabeled atoms are symmetry generated by $1-x,1-y,+z$ or $1-x,-y,z$. Selected bond lengths [pm]: Na1−O1 265.9(3), Na1−O1$^{\#}$ 234.5(3), Na1−O2 244.7(3), Na1−O3 242.0(3), Na1−O4 243.3(3), Na1−O5 253.3(3), Na1···Na1$^{\#}$ 337.7(3), Na1···O7 440.6(3), Na1−F1 226.9(3), Si1−Si2 233.8(2). Selected bond angles [deg]:O1−Na1−O2 65.8(1), O1$^{\#}$−Na1−O1 87.8(1), O1$^{\#}$−Na1−O2 93.9(1), O1$^{\#}$−Na1-O3 95.3(1), O1$^{\#}$−Na1−O4 85.4(1), O1$^{\#}$−Na1−O5 77.86(9), O2−Na1−O3 68.9(1), O3−Na1−O4 82.9(1), O4−Na1−O5 69.73(8), O1$^{\#}$−Na1−F1 161.6(1), Na1−O1−Na1$^{\#}$ 84.6(1), Na1−O5−Na1$^{\#}$ 83.6(1).

The sodium cation Na1 is in an almost coplanar arrangement with the oxygen atoms O1−O5; this is apparent from the deviation of the spanned plane by the oxygen atoms, which is only 18 pm. The sodium cations are coordinated both in a nearly pentagonal-bipyramidal geometry by six O atoms from the podand framework and one F atom from the $[PF_6]^-$ anion which is located next to the Na position. The coordination bipyramids are distorted to each other by about 48°, resulting in a face-to-face connection. The alignment of the oxygen atoms around the metal ions in the product seems to be the driving force for the elimination of diethylene glycol and formation of this novel dinuclear species. As known from basic

DOI: 10.1021/acs.inorgchem.7b02590
Inorg. Chem. 2018, 57, 351−359

crown ether chemistry, the sodium ion matches very finely with a ring diameter somewhere between [15]crown-5 and [18]-crown-6.[39]

A look at the molecular structure reminds of two aligned crown ethers aligned in this way. The O–Na bond lengths within this dinuclear coordination compound are similar to those of the dinuclear species $[Na_2(dibenzo\text{-}[36]crown\text{-}12)(PF_6)_2]$ or the familiar disila-crown ether complex $[Na(1,2\text{-}disila[15]crown\text{-}5)ClO_4]$. In these respective complexes, the sodium cations are coordinated by five oxygen atoms of the crown ether and two donor atoms of the PF_6 or the ClO_4 anion each.[24,40] The cocrystalline EO2 molecules act as linkers forming hydrogen bonding between the podand and the PF_6 anion leading to a one-dimensional hydrogen bonding network along the crystallographic *b* axis (see Figure 4).

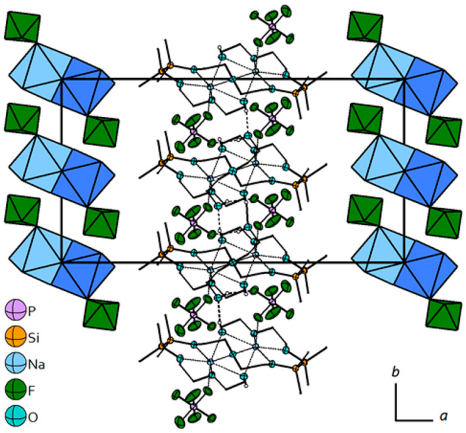

Figure 4. Cell package of **4** and hydrogen bonding along [001]. Thermal ellipsoids are represented at the 50% probability level. Carbon-bonded hydrogen atoms are omitted, and carbon atoms of the podand are represented as wireframes for clarity. Pentagonal bipyramidal coordinated sodium ions are in light and dark blue, respectively. PF_6-octahedra are tagged in green.

Treatment of **1** with anhydrous SrI_2 in *α,α,α*-trifluorotoluene at ambient temperature led to the coordination compound $[Sr(8,9\text{-}disila\text{-}EO5))I_2]$ (**5**). Crystallization yielded colorless blocks among colorless needles. Both crystal habits were suitable for single-crystal XRD analysis and revealed the same molecular structure. Within the determined crystal structure of the colorless needles, co-crystalline DCM was found to be present (see the Supporting Information).

No such solvent molecule was found upon refinement of the diffraction data of the colorless blocks. Within this study, the structural discussion is restricted to the solvent free crystal structure in which **5** crystallizes in the centrosymmetric, monoclinic space group $P2_1/c$. The molecular structure reveals that all oxygen atoms as well as the two iodide anions participate in the coordination of the metal ion, resulting in a total coordination number of 8 (Figure 5). Similar to the findings in the solid state structures of disila-crown ether complexes, the distances between the metal ion and the silicon affected oxygen atoms O3 and O4 are on equal levels to those of the fully carbon substituted oxygen atoms.

Treatment of the larger ligand **2** with anhydrous SrI_2 in *α,α,α*-trifluorotoluene also turned out to be successful and yielded $[Sr(11,12\text{-}disila\text{-}EO7)I]I$ (**6**) (see the Supporting Information for information and representation). Both crystal

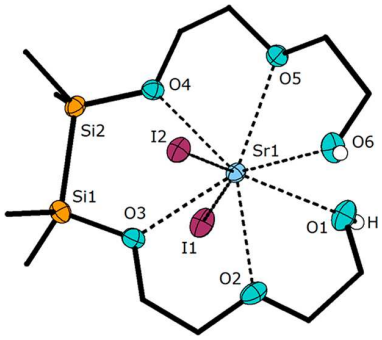

Figure 5. Molecular structure of **5** in the crystal. Thermal ellipsoids are represented at the 50% probability level. Carbon-bonded hydrogen atoms as well as solvent molecules are omitted, and carbon atoms of the podand are represented as wireframes for clarity. Selected bond lengths [pm]: Sr1–O1 261.18(8), Sr1–O2 257.0(2), Sr1–O3 255.8(2), Sr1–O4 257.0(2), Sr1–O5 259.5(3), Sr1–O6 254.9(2), Sr1–I1 338.1(1), Sr1–I2 334.6(1), Si1–Si2 234.4(1). Selected bond angles [deg]: O1–Sr1–O2 65.92(9), O2–Sr1–O3 65.53(8), O3–Sr1–O4 78.98(7), O4–Sr1–O5 64.83(7), O5–Sr1–O6 64.63(8), I1–Sr1–I2 145.66(1).

structures (**5** and **6**) represent a one-dimensional hydrogen bonding network (see Figure 6 and the Supporting Information).

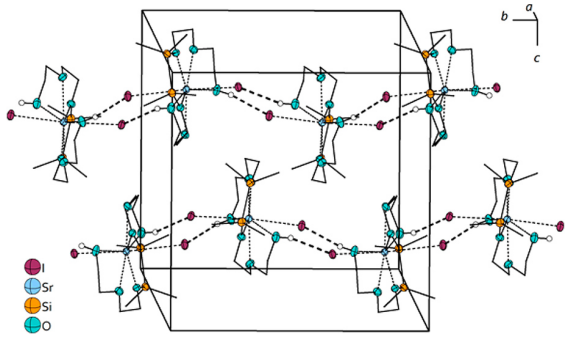

Figure 6. Cell package of **5** and hydrogen bonding along [100]. Thermal ellipsoids are represented at the 50% probability level. Carbon-bonded hydrogen atoms are omitted, and carbon atoms represented as wireframes for clarity.

By treatment of **2** with anhydrous $BaOTf_2$ in DCM, the next heavier alkaline earth metal cation was complexated and the compound $[Ba(11,12\text{-}disila\text{-}EO7)(OTf)_2]$ (**7**) could be obtained. **7** crystallizes in the non-centrosymmetric, tetragonal space group $P4_32_12$. The molecular structure reveals that all oxygen atoms as well as the two triflate groups are placed in the coordination sphere of the metal ion giving a total coordination number of 10 (Figure 7). The oxygen atoms O(1–4) are in well-nigh coplanar arrangement with the barium cation. However, with a value of 93 pm the metal ion deviates from the calculated mean plane spanned by the oxygen atoms more than the Sr^{2+} cation does in **5** and also in **6**.

The $O2^{\#}$–$4^{\#}$–Ba1–O5 angles are getting larger as the glycolic chain helically encapsulates the metal ion. These are 114.61(5), 162.79(5), and 126.07(5)°, respectively. The distances between barium and the silicon affected oxygen atom O1 have almost the same value as observed for the fully carbon substituted oxygen atoms O2–O4. This is also observed

DOI: 10.1021/acs.inorgchem.7b02590
Inorg. Chem. 2018, 57, 351–359

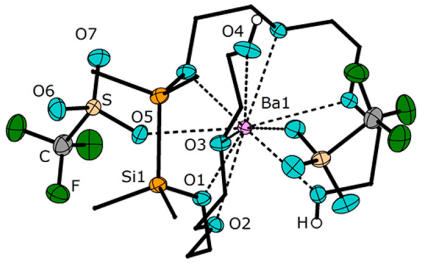

Figure 7. Molecular structure of 7 in the crystal. Thermal ellipsoids are represented at the 50% probability level. Hydrogen atoms are omitted, and carbon atoms of the podand are represented as wireframes for clarity. All nonlabeled atoms are symmetry generated by $1 - y$, $1 - x$, $3/2 - z$. Selected bond lengths [pm]: Ba1–O1 282.2(1), Ba1–O2 283.0(2), Ba1–O3 284.0(2), Ba1–O4 274.8(2), Ba1–O5 281.6(2), Si1–Si1$^{\#}$ 235.4(1), Selected bond angles [deg]: O1–Ba1–O1$^{\#}$ 72.94(6), O1–Ba1–O2 60.72(5), O2–Ba1–O3 58.77(4), O3–Ba1–O4 57.98(5), O4–Ba1–O5 87.04(6), O4$^{\#}$–Ba1–O5 126.07(5).

for disila-crown ether complexes and for strontium species **5** and **6**. The crystal structure itself features a three-dimensional hydrogen bonding network (Figure 8). This is made up by H4 and O7^{f} contacts (see Table 1).

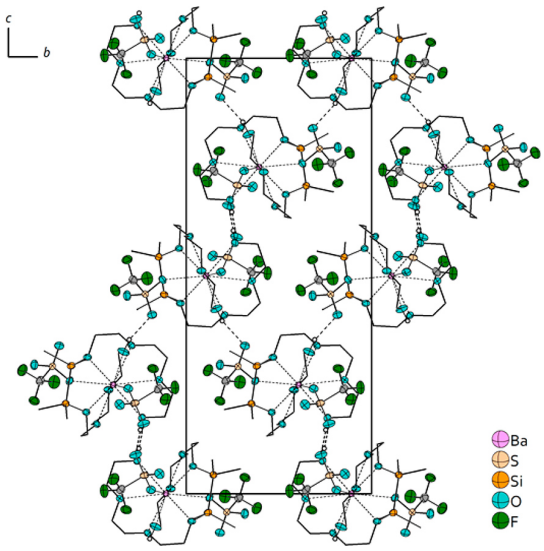

Figure 8. Cell package of 7 and hydrogen bonding along [100]. Thermal ellipsoids are represented at the 50% probability level. Carbon-bonded hydrogen atoms are omitted, and carbon atoms of the podands represented as wireframes for clarity.

The complexation of the alkaline earth metal triflates $M(OTf)_2$ (M = Ca and Ba) was successful, so we also tried to analogously complexate CsOTf with larger ligand **2** in DCM. Even though the salt dissolves, single crystals of solvent- and ligand-free α-CsOTf grew out from the reaction mixture after 3 weeks, which were analyzed by single crystal X-ray diffraction.[41] Beside crystallographic studies, we decided to perform DFT calculations for a better understanding of the coordination chemistry of silicon based polyethers. The optimized structure of **1** shows a staggered conformation of the silicon-bonded methyl groups. The two glycolic side arms attached to the disilane fragment find themselves in a twisted arrangement to each other within C_1-symmetry. The optimized structure of

Table 1. Hydrogen Bonding Data Observed in the Crystal Structures of 3–5 and 7 (pm, deg)[a]

compound	D–H···A	H···A	D···A	D–H···A
3	O1–H1···O12[b]	199(1)	276(2)	156(1)
	O6–H6···O8	198(1)	273(1)	151(1)
4	O5–H5···O7[c]	198(1)	279(1)	169(2)
	O7–H7···F3[c]	214(1)	294(1)	163(2)
5	O1–H1···I2[d]	280(1)	348(1)	138(1)
	O6–H6···I1[e]	261(1)	339(1)	155(1)
7	O4–H4···O7[f]	207(3)	288(3)	163(2)

[a]Hydrogen bond geometries according to HFIX83. D = donor; A = acceptor. [b]Symmetry code: $2 - x$, $1 - y$, $1 - z$. [c]Symmetry code $1 - x$, $-y$, z. [d]Symmetry code $1 - x$, $1/2 + y$, $1/2 - z$. [e]Symmetry code $1 - x$, $-1/2 + y$, $1/2 - z$; [f]Symmetry code $3/2 - x$, $-1/2 + y$, $7/4 - z$.

EO5 can best be described as an [18]crown-6-like molecule out of which one ethylene bridge is replaced by a hydrogen bonding contact of 188.2 pm (see Figure 9).

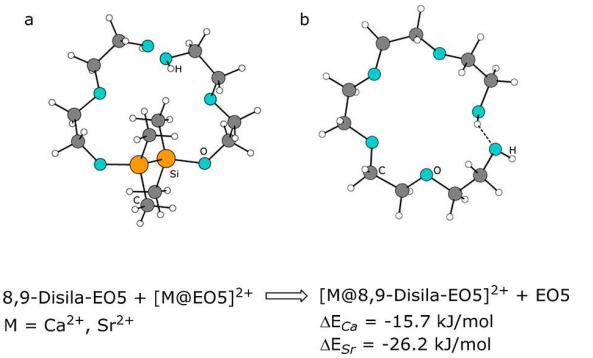

Figure 9. Optimized structures of **1** (a) and its organic analogue EO5 (b) in their local minima. Relative energies of the alkaline earth metal exchange from EO5 to 8,9-disila-EO5 as obtained at the BP86/def2-TZVP level of theory. For related structures and XYZ data, see the Supporting Information.

The average Si–O and Si–C atom distances of **1** are 168.92 and 187.70 pm, respectively. Caused by the complexation process, Si–O average distances of 172.58 pm for [Ca^{2+}@**1**] and 171.98 pm for [Sr^{2+}@**1**] are observed. Si–C distances change to 186.94 ppm in [Ca^{2+}@**1**] and 187.09 ppm [Sr^{2+}@**1**]. With these respective changes, it can be summarized that the average Si–O bond lengths of the ligand are enlarged whereas the Si–C bonds are shortened due to the complexation of **1** with the alkaline earth metal cations Ca^{2+} and Sr^{2+}. This is consistent with the concept of negative hyperconjugation, but the loss of complexation ability caused by this effect is obviously overcompensated. With the use of different salts, stable complexes were obtained, so within respective complexes **3**–**7** negative hyperconjugation seems to be only of minor importance. While comparing the relative change of bond lengths (ΔL_r), it is notable that the harder Ca^{2+} cation causes higher changes (ΔL_r^{Ca}(Si–O) = 3.66 pm and ΔL_r^{Ca}(Si–C) = −0.76 pm) in comparison to Sr^{2+} (ΔL_r^{Sr}(Si–O) = 3.05 pm and ΔL_r^{Sr}(Si–C) = −0.61 pm), which depicts a higher attraction between the silicon-bonded oxygen atoms and a hard metal ion. For this reason, the optimized structures of [Sr^{2+}@**2**] and [Ba^{2+}@**2**] were also compared in order to strengthen the argument that a harder cation shares higher interactions with silicon-bonded oxygen atoms and promotes the diminishing of

DOI: 10.1021/acs.inorgchem.7b02590
Inorg. Chem. 2018, 57, 351–359

negative hyperconjugation interactions. The average Si−O and Si−C atom distances of **2** are 168.87 and 188.15 pm, respectively, and thus close to those of the optimized structure of **1**. As the complexation process of **1** with Ca^{2+} and Sr^{2+} does, the alkaline earth metal ions Sr^{2+} and Ba^{2+} strengthen the Si−C bond and weaken the Si−O bond within the ligand **2**. The relative change of bond lengths are in line with the trend: The harder Sr^{2+} cation causes higher changes ($\Delta L_r'^{Sr}$(Si−O) = 2.4 pm and $\Delta L_r'^{Sr}$(Si−C) = −0.91 pm) in comparison to those with Ba^{2+} ($\Delta L_r'^{Ba}$(Si−O) = 1.87 pm and $\Delta L_r'^{Ba}$(Si−C) = −0.61 pm). A harder cation shares stronger interactions with silicon-bonded oxygen atoms and promotes the diminishing of negative hyperconjugation interactions. Conversely, one can say that soft Lewis acids barely share interactions with silicon bonded oxygen atoms. These findings are consistent with observations made in solution according to ^{29}Si NMR studies. The harder the cation, the more low-field-shifted the signals in deuterated dichloromethane, which is caused by withdrawal of electron density. The ^{29}Si NMR shift of the Ca^{2+} containing complex **3** appears at 19.4 ppm, the one of the Sr^{2+} containing complex **5** at 18.7 ppm. Compound **6** shows a singlet at 19.1 ppm and **7** at 16.8 ppm. Furthermore, related structures described in the literature prove the findings made with quantum chemical calculations in this work: The harder the cation, the higher the low field shifts in relation to the free ligands the appearance of the singlet in [Li(1,2-disila[12]crown-4)OTf] at 15.4 ppm, the one in [Na(1,2-disila[15]crown-5)ClO_4] at 14.1 ppm, and the one in [K(1,2-disila[18]crown-6)PF_6] at 13.0 ppm.[24] Overall, this leads to an understanding of why the reaction of **2** with CsOTf only leads to recrystallization of CsOTf or why MCl·3SO_2 (M = Rb, Cs) is obtained in the reaction of MCl with 1,2-disila[12]crown-4 in liquid SO_2.[42]

According to ^{29}Si NMR experiments, it seems that there is an interaction between these ligands and a salt, which is high enough to dissolve the salts. Yet, the soft cations are not able to significantly weaken negative hyperconjugation interactions and yield a solid state structure of the complex since the lattice energy of the uncomplexated salt cannot be overcompensated. The calculated model of $[Cs@\mathbf{2}]^+$ (see Figure 10) proves the findings comparing the relative change of bond lengths with the changes caused by complexation of an alkaline earth metal. $\Delta L_r'^{Cs}$(Si−O) as well $\Delta L_r'^{Cs}$(Si−C) are close to zero, indicating only a poor electrostatic interaction (see Table 2).

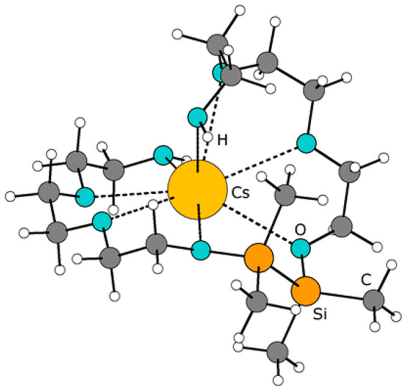

Figure 10. Optimized structure at the BP86/def2-TZVP level of theory of $[Cs@\mathbf{2}]^+$ in its local minimum (C_1 symmetric). For XYZ data, see the Supporting Information.

It would be interesting to see in how far these silicon-based ligands and the inverse case with the Be^{2+} cation interact. With high regard to safety procedures, we strive for beryllium chemistry with silicon-based ligands, so further studies are underway.[43] At this point it is still unclear to what extend these disila-analogues of polyethylene glycols can challenge organic glycols according to their coordination ability. For this reason, the exchange of the M^{2+} ion (M = Ca, Sr) from EO5 to 8,9-disila-EO5 was calculated by means of DFT employing the BP86 functional and def2-TZVP basis sets under inclusion of dispersion interactions and charge compensation. These are energetically favored by 16 kJ/mol (M = Ca) or 26 kJ/mol (M = Sr), respectively (see Figure 9). Taking the typical error of DFT calculations into account, the coordination ability is on even terms or even slightly higher. Hence it can be assumed that at least Si/C-bonded oxygen atoms do not exhibit a lower basicity than etheric oxygen atoms; at least for sufficiently hard cations.

SUMMARY AND CONCLUSIONS

Within this study, the synthesis of disila-analogues of polyetheleneglycols and group 1 and 2 coordination chemistry with these ligands turned out to be successful. With the variation of ligand and salt a structural diversity was observed. Ligands **1** and **2** willingly form stable complexes with alkali and alkaline earth metal complexes showing a respectable complexation ability higher than those of common siloxanes. Whereas the complexation of alkaline earth metal salts yielded 1:1 complexes **3** and **5**−**7**, the use of the alkali metal salt $NaPF_6$ yielded dinuclear complex **4**, in which the sodium ions are coordinated in a tetrasila-analogue of EO8. Template chemistry was performed under elimination of diethylene glycol. Within the respective crystal structures of **3**−**7** hydrogen bonding is present with **3** forming isolated dimers, **4**−**6** forming a one-dimensional network, and **7** forming a three-dimensional network. The complexation of **2** with CsOTf failed, leading to recrystallization of α-CsOTf. Quantum chemical calculations according to the BP86/def2-TZVP basis set revealed the general trend that a harder cation interacts with silicon-based ligands stronger than soft cations do and led to further understanding in how silicon-based ligands interact with Lewis acids and why the complexation of **2** with CsOTf was doomed to fail. Sufficiently hard cations diminish negative hyperconjugation interactions immensely and share high electrostatic interactions with Lewis acids that can easily overcompensate a competing polarization. This was shown by a comparison of the calculated complexes with free ligand structures, ^{29}Si NMR spectroscopical studies and the alkaline earth metal exchange from EO5 to 8,9-disila-EO5. The relative change of bond lengths (ΔL_r) increases with the hardness of the cation. So the ^{29}Si NMR shift undergoes a higher downfield shift the harder the coordinated cation is. The exchange of alkaline earth metal ions is favored by 15.7 kJ/mol for Ca^{2+} or 26.2 kJ/mol for Sr^{2+}, respectively. Soft cations, however, do only interact barely with the herein presented ligands with $\Delta L_r'$ values close to zero combined with only a slight shift in the ^{29}Si NMR spectrum. Considering all observations, it can be concluded that silicon-based ligands bearing disilane-units are effective ligands for the complexation of especially hard cations, and a better understanding of the Si−O bond is achieved. The reaction behavior of silicon based ligands toward Be^{2+} cations is subject of future research.

DOI: 10.1021/acs.inorgchem.7b02590
Inorg. Chem. 2018, 57, 351−359

Table 2. Experimental and Calculated Average Distances [pm] and Angles [deg] of Disila-Analogues of Polyethylene Glycols and Their Group 1 and 2 Metal Complexes

		bond length (Å)					bond angle (deg)	
compound	method	M–O_C[a]	M–O_{Si}[b]	Si–Si	Si–O	Si–C	C–O–Si	C–Si–Si–C
1	DFT[c]			235.03	168.93	188.05	126.73	58.04
2	DFT[c]			235.72	168.87	188.09	124.10	83.77
3	XRD[d]	246.4(2)	247.9(2)	233.6(1)	167.9(2)	184.8(3)	119.8(1)	2.7(1)
$[Ca@\mathbf{1}]^{2+}$	DFT[c]	236.92	236.36	235.84	172.58	186.95	118.8(3)	32.6
4	XRD[d]	249.6(3)	242.7(3)	233.8(2)	167.2(3)	185.6(5)	121.3(2)	15.3(3)
5	XRD[d]	258.3(5)	256.3(8)	234.4(1)	167.6(1)	185.8(4)	121.2(2)	3.9(1)
$[Sr@\mathbf{1}]^{2+}$	DFT[c]	255.51	255.80	235.49	171.98	187.09	122.21	41.27
6	XRD[d]	263.4(1)	261.5(1)	235.1(2)	167.4(1)	186.1(2)	120.7(2)	2.2(3)
$[Sr@\mathbf{2}]^{2+}$	DFT[c]	261.71	257.30	235.50	171.27	187.24	121.13	37.97
7	XRD[d]	280.6(1)	282.2(1)	235.4(1)	167.1(1)	186.4(2)	121.9(1)	19.6(1)
$[Ba@\mathbf{2}]^{2+}$	DFT[c]	280.68	279.53	235.57	170.74	187.54	119.47	20.58
$[Cs@\mathbf{2}]^{+}$	DFT[c]	316.68	317.92	234.93	168.81	188.11	124.6	60.08

[a]Completely carbon bonded oxygen atoms. [b]Silicon affected oxygen atoms. [c]BP86 functional at the def2-TZVP level of theory. [d]Structures determined by single crystal X-ray diffraction analysis.

■ ASSOCIATED CONTENT

Supporting Information

The Supporting Information is available free of charge on the ACS Publications website at DOI: 10.1021/acs.inorgchem.7b02590.

Summary of additional crystal structures and XYZ data obtained from DFT calculations (PDF)

Accession Codes

CCDC 1576407–1576413 contain the supplementary crystallographic data for this paper. These data can be obtained free of charge via www.ccdc.cam.ac.uk/data_request/cif, or by emailing data_request@ccdc.cam.ac.uk, or by contacting The Cambridge Crystallographic Data Centre, 12 Union Road, Cambridge CB2 1EZ, UK; fax: +44 1223 336033.

■ AUTHOR INFORMATION

Corresponding Author

*E-mail: haenisch@chemie.uni-marburg.de.

ORCID

Carsten von Hänisch: 0000-0002-6298-8937

Notes

The authors declare no competing financial interest.

■ ACKNOWLEDGMENTS

This work was financially supported by the Deutsche Forschungsgemeinschaft (DFG). F.D. thanks the NMR (Dr. X. Xie, G. Häde, Dr. R. Wagner, and C. Mischke), MS (Dr. U. Linne and co-workers) and X-ray Departments (M. Marsch, R. Riedel, and Dr. K. Harms), Philipps-Universität Marburg, for measurement time and their kind advice. F.D. thanks Dr. M. Kapitein for his valuable help with DFT calculations and Dr. M. R. Buchner for his kind advice regarding NMR issues.

■ REFERENCES

(1) Ritch, J. S.; Chivers, T. Siliciumanaloga von Kronenethern und Cryptanden: ein neues Kapitel in der Wirt-Gast-Chemie? *Angew. Chem.* **2007**, *119*, 4694–4697; *Angew. Chem., Int. Ed.* **2007**, *46*, 4610–4613.

(2) Bruña, S.; Martínez-Montero, I.; González-Vadillo, A. M.; Martín-Fernández, C.; Montero-Campillo, M. M.; Mó, O.; Cuadrado, I. Ferrocene and Silicon-Containing Oxathiocrown Macrocycles and Linear Oligo-Oxathioethers Obtained via Thiol-Ene Chemistry of a Redox-Active Bifunctional Vinyldisiloxane. *Macromolecules* **2015**, *48*, 6955–6969.

(3) Decken, A.; Passmore, J.; Wang, X. Cyclic Dimethylsiloxanes as Pseudo Crown Ethers: Syntheses and Characterization o Li-$(Me_2SiO)_5[Al\{OC(CF_3)_3\}_4]$, $Li(Me_2SiO)_6[Al\{OC(CF_3)_3\}_4]$, and Li-$(Me_2SiO)_6[Al\{OC(CF_3)_2PH\}_4]$. *Angew. Chem.* **2006**, *118*, 2839–2843; *Angew. Chem., Int. Ed.* **2006**, *45*, 2773–2777.

(4) Churchill, M. R.; Lake, C. H.; Chao, S.-H. L.; Beachley, O. T. Silicon Grease as a Precursor to a Pseudo Crown Ether Ligand: Crystal Structure of $[K^+]_3[K(Me_2SiO)_7^+][InH(CH_2CMe_3)_3^-]_4$. *J. Chem. Soc., Chem. Commun.* **1993**, *1*, 1577–1578.

(5) Eaborn, C.; Hitchcock, P. B.; Izod, K.; Smith, J. D. Zwei Diorganopotassate und die Struktur von $[K(C_6H_6)][K\{C(SiMe_3)_2(SiMe_2Ph)\}_2]$. *Angew. Chem.* **1995**, *107*, 2936–2937; *Angew. Chem., Int. Ed. Engl.* **1996**, *34*, 2679–2680.

(6) Krossing, I.; Raabe, I. Nichtkoordinierende Anionen - Traum oder Wirklichkeit? Eine Übersicht zu möglichen Kandidaten. *Angew. Chem.* **2004**, *116*, 2116–2142; *Angew. Chem., Int. Ed.* **2004**, *43*, 2066–2090.

(7) Ernst, R. D.; Glöckner, A.; Arif, A. M. Crystal structure of hexakis(dimethyl-μ-oxosilane)dibromozirconium(IV) bis(nonabromodizirconate(IV)), $[Zr\{(CH_3)_2SiO\}_6Br_2][Zr_2Br_9]_2$. *Z. Kristallogr. - New Cryst. Struct.* **2007**, *222*, 333–334.

(8) Emeléus, H. J.; Onyszchuk, M. The Reaction of Methyldisiloxanes and 1:1-Dimethyldisilthiane with Boron and Hydrogen Halides. *J. Chem. Soc.* **1958**, *0*, 604–609.

(9) Stone, F. G. A.; Seyferth, D. The chemistry of silicon involving propable use of d-type orbitals. *J. Inorg. Nucl. Chem.* **1955**, *1*, 112–118.

(10) Shambayati, S.; Schreiber, S. L.; Blake, J. F.; Wierschke, S. G.; Jorgensen, W. L. Structure and Basicity of Silyl Ethers: a Crystallographic and ab Initio Inquiry into the Nature of Silicon-Oxygen Interactions. *J. Am. Chem. Soc.* **1990**, *112*, 697–703.

(11) Cypryk, M.; Apeloig, Y. Ab Initio Study of Silyloxonium Ions. *Organometallics* **1997**, *16*, 5938–5949.

(12) Passmore, J.; Rautiainen, J. M. On The Lower Lewis Basicity of Siloxanes Compared to Ethers. *Eur. J. Inorg. Chem.* **2012**, *2012*, 6002–6010.

(13) Weinhold, F.; West, R. The nature of the silicon-oxygen bond. *Organometallics* **2011**, *30*, 5815–5824.

(14) Weinhold, F.; West, R. Hyperconjugative Interactions in Permethylated Siloxanes and Ethers: The Nature of the SiO Bond. *J. Am. Chem. Soc.* **2013**, *135*, 5762–5767.

(15) Oberhammer, H.; Boggs, J. E. Importance of (p-d)π Bonding in the Siloxane Bond. *J. Am. Chem. Soc.* **1980**, *102*, 7241–7244.

(16) Gillespie, R. J.; Johnson, S. A. Study of Bond Angles and Bond Lengths in Disiloxane and Related Molecules in Terms of the

DOI: 10.1021/acs.inorgchem.7b02590
Inorg. Chem. 2018, 57, 351–359

Topology of the Electron Density and Its Laplacian. *Inorg. Chem.* **1997**, *36*, 3031−3039.
(17) Grabowsky, S.; Hesse, M. F.; Paulmann, C.; Luger, P.; Beckmann, J. How to Make the Ionic Si-O Bond More Covalent and the Si-O-Si Linkage a Better Acceptor for Hydrogen Bonding. *Inorg. Chem.* **2009**, *48*, 4384−4393.
(18) Cameron, T. S.; Decken, A.; Krossing, I.; Passmore, J.; Rautiainen, J. M.; Wang, X.; Zeng, X. Reactions of a Cyclodimethylsiloxane $(Me_2SiO)_6$ with Silver Salts of Weakly Coordinating Anions; Crystal Structures of $[Ag(Me_2SiO)_6][Al]$ ($[Al]$ = $[FAl\{OC(CF_3)_3\}_3]$, $[Al\{OC(CF_3)_3\}_4]$) and Their Comparison with $[Ag(18\text{-Crown-}6)]_2[SbF_6]_2$. *Inorg. Chem.* **2013**, *52*, 3113−3126.
(19) von Hänisch, C.; Hampe, O.; Weigend, F.; Stahl, S. Ein anorganischer Cryptand: schrittweise Synthese und Koordination von Li^+-Ionen. Angew. *Angew. Chem.* **2007**, *119*, 4859−4863; *Angew. Chem., Int. Ed.* **2007**, *46*, 4775−4779.
(20) Phung, P.; Chi, B.; Kober, F. Synthese anorganischer Tintenfisch-Moleküle. *Z. Anorg. Allg. Chem.* **1981**, *472*, 75−82.
(21) Arkles, B.; King, K.; Anderson, R.; Peterson, W. Silacrowns: phase-transfer catalysts. *Organometallics* **1983**, *2*, 454−457.
(22) Oddon, G.; Hosseini, M. W. Silacrown Ethers: Synthesis of Macrocyclic Diphenylpolyetheleneglycol Mono- and Disilanes. *Tetrahedron Lett.* **1993**, *34*, 7413−7416.
(23) Buschbeck, R.; Lang, H.; Agarwal, S.; Saini, V. K.; Gupta, V. K. Carbosilane Dendrimers with End-Grafted Silacrown- and Crown-Ether Units. *Synthesis* **2004**, *2004*, 1243−1248.
(24) Reuter, K.; Buchner, M. R.; Thiele, G.; von Hänisch, C. Stable Alkali-Metal Complexes of hybrid Disila-Crown Ethers. *Inorg. Chem.* **2016**, *55*, 4441−4447.
(25) Reuter, K.; Thiele, G.; Hafner, T.; Uhlig, F.; von Hänisch, C. Synthesis and coordination ability of a partially silicon based crown ether. *Chem. Commun.* **2016**, *52*, 13265−13268.
(26) Reuter, K.; Dankert, F.; Donsbach, C.; von Hänisch, C. Structural Study of Mismatched Disila-Crown Ether Complexes. *Inorganics* **2017**, *5*, 11.
(27) Dankert, F.; Reuter, K.; Donsbach, C.; von Hänisch, C. A structural study of alkaline earth metal complexes with hybrid disila-crown ethers. *Dalt. Trans.* **2017**, *46*, 8727−8735.
(28) Ouchi, M.; Inoue, Y.; Kanzaki, T.; Hakushi, T. Ring-contracted Crown Ethers: 14-Crown-5, 17-Crown-6, and their Sila-analogues. Drastic Decrease in Cation-binding Ability. *Bull. Chem. Soc. Jpn.* **1984**, *57*, 887−888.
(29) Inoue, Y.; Ouchi, M.; Hakushi, T. Molecular Design of Crown Ethers. 3. Extraction of Alkaline Earth and heavy Metal Picrates with 14- to 17-Crown-5 and 17- to 22-Crown-6. *Bull. Chem. Soc. Jpn.* **1985**, *58*, 525−530.
(30) Krempner, C.; Reinke, H.; Weichert, K. Synthesis and Structure of Cyclic Aluminium Disiloxides. *Organometallics* **2007**, *26*, 1386−1392.
(31) Swinburne, A. N.; Steed, J. W. Podands. *Supramolecular Chemistry: From Molecules to Nanomaterials*, **2012**, 10.1002/9780470661345.smc058.
(32) Rogers, R. D.; Jezl, M. L.; Bauer, C. B. Effects of Polyethylene Glycol on the Coordination Sphere of Strontium in $SrCl_2$ and $Sr(NO3)_2$ Complexes. *Inorg. Chem.* **1994**, *33*, 5682−5692.
(33) Gschwind, F.; Fromm, K. M. Tetraethylene glycol Adducts of Alkaline Earth Halides. *Z. Anorg. Allg. Chem.* **2011**, *637*, 1871−1879.
(34) Tang, S.; Zhao, H. Glymes as Versatile Solvents for Chemical reactions and Processes: from the Laboratory to Industry. *RSC Adv.* **2014**, *4*, 11251−11287.
(35) Steed, J. W.; Atwood, J. L. *Supramolecular Chemistry*, 2nd ed.; Royal Society of Chemistry: Cambridge, U.K., 2009.
(36) Willcott, M. R. MesRe Nova. *J. Am. Chem. Soc.* **2009**, *131*, 13180−13180.
(37) *OPUS*; Bruker Opt. GmbH: Billerica, MA, 2012.
(38) Trömel, M. Metallradien, Ionenradien und Wertigkeiten fester metallischer Elemente. *Z. Naturforsch., B: J. Chem. Sci.* **2000**, *55*, 243−247.
(39) Lamb, J. D.; Izatt, R. M.; Swain, C. S.; Christensen, J. J. A Systematic Study of the Effect of macrocycle Ring Size and Donor Atom Type on the Log *K*, ΔH, and $T\Delta S$ of Reactions at 25 °C in Methanol of Mono- and Divalent Cations with Crown Ethers. *J. Am. Chem. Soc.* **1980**, *102*, 475−479.
(40) Maud, J. M.; Stoddart, J. F.; Colquhoun, H. M.; Williams, D. J. The isolation and x-ray crystal structure of a complex between sodium hexafluorophosphate and dibenzo-36-crown-12. *Polyhedron* **1984**, *3*, 675−679.
(41) Hildebrandt, L.; Dinnebier, R.; Jansen, M. Crystal Structure and Ionic Conductivity of Cesium Trifluoromethyl Sulfonate, $CsSO_3CF_3$. *Z. Anorg. Allg. Chem.* **2005**, *631*, 1660−1666.
(42) Reuter, K.; Rudel, S. S.; Buchner, M. R.; Kraus, F.; von Hänisch, C. Crown ether complexes of alkali metal chlorides from SO_2. *Chem. - Eur. J.* **2017**, *23*, 9607−9617.
(43) Naglav, D.; Buchner, M. R.; Bendt, G.; Kraus, F.; Schulz, S. Auf neuen Pfaden - per Anhalter durch die Berylliumchemie. *Angew. Chem.* **2016**, *128*, 10718−10733; *Angew. Chem., Int. Ed.* **2016**, *55*, 10562−10576.

DOI: 10.1021/acs.inorgchem.7b02590
Inorg. Chem. 2018, 57, 351−359

"ALKALI AND ALKALINE EARTH METAL DERIVATIVES OF DISILA-BRIDGED PODANDS: COORDINATION CHEMISTRY AND STRUCTURAL DIVERSITY"

Electronic Supporting Information (ESI)

Fabian Dankert,[†] Carsten Donsbach[†], Christopher-Nils Mais[†], Kirsten Reuter[†], C. v. Hänisch*[†]

This electronic supporting information is part of the article "Alkali and Alkaline Earth Metal Derivatives of Disila-bridged Podands: Coordination Chemistry and Structural Diversity" and summarizes additional X-ray structures as well as XYZ-Data obtained from DFT calculations, which were not included but mentioned in the full text article.

[†] Fachbereich Chemie and Wissenschaftliches Zentrum für Materialwissenschaften (WZMW) Philipps-Universität Marburg, Hans-Meerwein-Straße, 35043 Marburg, Germany, E-Mail: haenisch@chemie.uni-marburg.de

Table of contents

1. Crystal Structures 2
   1.1 Compound **3a** 3
   1.2 Compound **5a** 4
   1.3 Compound **6** 6
2. XYZ-Data of Optimized Structures 8
   2.1 Compound **1** 8
   2.2 Compound **2** 10
   2.3 EO5 12
   2.4 [Ca@**1**]$^{2+}$ 14
   2.5 [Ca@EO5]$^{2+}$ 16
   2.6 [Sr@**1**]$^{2+}$ 18
   2.7 [Sr@EO5]$^{2+}$ 20
   2.8 [Sr@**2**]$^{2+}$ 22
   2.9 [Ba@**2**]$^{2+}$ 24
   2.10 [Cs@**2**]$^{+}$ 26
3. References 28

1. Crystal Structures

General: Single crystal X-ray diffraction studies were carried out using a Bruker D8 Quest (**6**), Stoe IPDS2T (**4**) or Stoe IPDS2 (**3**, **3a**, **5**, **5a**, **7**) diffractometer at 100(2) K with MoK_α radiation and X-ray optics or graphite monochromatization, respectively ($\lambda = 0.71073$). All structures were solved by direct methods and refinement with full-matrix-least-squares against F^2 using SHELXT- and SHELXL-2015 on OLEX2 platform.[1-3] Crystallographic data for compounds **3-7** are denoted as follows: CCDC Nos. 1576410 (**3**), 1576407 (**3a**), 1576412 (**4**), 1576408 (**5**), 1576411 (**5a**), 1576409 (**6**·2DCM) and 1576413 (**7**). Crystallographic information files (CIF) can be obtained free of charge from the Cambridge Crystallographic Data Centre (CCDC) (link: www.ccdc.cam.ac.uk/data_request/cif). All CIFs are also provided as associated content. Visualization of all structures was performed with Diamond software package Version 4.4.0.[4] Thermal ellipsoids are represented at the 50% probability level.

Compound ***3*** $C_{14}H_{30}CaF_6O_{12}S_2Si_2$, monoclinic, $P2_1/n$, Z = 4, 100 K, a = 8.849(5) Å, b = 30.056(9) Å, c = 10.424(4) Å, $\beta = 95.94(4)°$, $V = 2757(2)$ Å^3, $\rho = 1.601$ g cm^{-3}, numerical absorption correction using STOE X-AREA and X-RED32.[5] $\mu = 0.559$ mm^{-1}, T_{min}, T_{max} = 0.9087, 0.9847, 2Θ range 4.156-50°, reflections measured 15265, independent reflections 4863 [R(int) = 0.0720], 338 parameters, R-index [$I \geq 2\sigma(I)$] 0.0341, wR_2 (all data) 0.0834, GOOF 0.718, $\Delta\rho_{max}$, $\Delta\rho_{min}$ 0.37/–0.23 e Å^3.

Compound ***4*** $C_{24}H_{60}F_{12}Na_2O_{12}P_2Si_4$, orthorhombic, *Aea*2, Z = 4, 100 K, a = 24.032(5) Å, b = 12.882(3) Å, c = 14.870(3) Å, $V = 4603.3(16)$ Å^3, $\rho = 1.427$ g cm^{-3}, numerical absorption correction using STOE X-AREA and X-RED32.[5] $\mu = 0.314$ mm^{-1}, T_{min}, T_{max} = 0.9578, 0.9819, 2Θ range 3.39-54.204°, reflections measured 13877, independent reflections 5061 [R(int) = 0.0647], 260 parameters, R-index [$I \geq 2\sigma(I)$] 0.0390, wR2 (all data) 0.0658, GOOF 0.867, $\Delta\rho_{max}$, $\Delta\rho_{min}$ 0.30/-0.25 e Å^3, flack parameter 0.14(15).

Compound ***5*** $C_{12}H_{30}I_2O_6Si_2Sr$, monoclinic, $P2_1/c$, Z = 4, 100 K, a = 11.177(2) Å, b = 14.960(3) Å, c = 14.723(3) Å, $\beta = 106.62(3)°$, $V = 2359.0(9)$ Å^3, $\rho = 1.881$ g cm^{-3}, numerical absorption correction using STOE X-AREA and X-RED32.[5] $\mu = 5.024$ mm^{-1}, T_{min}, T_{max} = 0.3006, 0.3863, 2Θ range 3.802-52°, reflections measured 13104, independent reflections 4634 [R(int) = 0.0558], 212 parameters, R-index [$I \geq 2\sigma(I)$] 0.0310, wR_2 (all data) 0.0755, GOOF 1.049, $\Delta\rho_{max}$, $\Delta\rho_{min}$ 1.97/-0.84 e Å^3.

Compound ***6****·2DCM* $C_{18}H_{42}Cl_4I_2O_8Si_2Sr$, monoclinic, *Cc*, Z = 4, 100 K, a = 11.1204(5) Å, b = 20.5826(9) Å, c = 15.1592(7) Å, $\beta = 91.658(2)°$, $V = 3468.3(3)$ Å^3, $\rho = 1.773$ g cm^{-3}, multi-scan absorption correction using SADABS-2014/5.[6] $\mu = 3.747$ mm^{-1}, T_{min}, T_{max} = 0.6170, 0.7457, 2Θ range 4.784-52.036°, reflections measured 36376, independent reflections 6686 [R(int) = 0.667], 322 parameters, R-index [$I \geq 2\sigma(I)$] 0.0238, wR_2 (all data) 0.0470, GOOF 1.042, $\Delta\rho_{max}$, $\Delta\rho_{min}$ 1.61/-1.01e Å^3, flack parameter 0.015(7).

Compound 7 $C_{18}H_{38}BaF_6O_{14}S_2Si_2$, tetragonal, $P4_32_12$, Z = 4, 100 K, a = b = 11.3169(16) Å, c = 26.605(5) Å, $V = 3407.4(12)$ Å^3, $\rho = 1.657$ g cm^{-3}, numerical absorption correction using STOE X-AREA and X-RED32.[5] $\mu = 1.447$ mm^{-1}, T_{min}, T_{max} = 0.6712, 0.7517, 2Θ range 3.912-54.18°, reflections measured 31108, independent reflections 3754 [R(int) = 0.0362], 198 parameters, R-index [$I \geq 2\sigma(I)$] 0.0146, wR_2 (all data) 0.0363, GOOF 1.012, $\Delta\rho_{max}$, $\Delta\rho_{min}$ 0.61/-0.17e Å^3, flack parameter 0.038(9).

Computational Details:

All calculations were performed with the program system TURBOMOLE V7.1.1.[7] The resolution of identity (RI) approximation, dispersion corrections, and the conductor-like screening model (COSMO) were applied throughout, the latter set to default. For all calculations, the BP86 functional was chosen, utilizing a def2-TZVP basis set.[8]

1.1 Compound 3a

After recrystallization of [Ca(8,9-Disila-EO5)$(OTf)_2$] from a mixture of dichloromethane and *n*-pentane, two sorts of crystal habits were obtained. The complex crystallizes in form of colorless blocks as well as colorless needles. This section represents the diffraction data of the colorless blocks. Within these respective crystals, the complex crystallizes in the centrosymmetric space group *C2*/*c*. The molecular structure within the crystal only features intramolecular hydrogen bonding by way of the terminal hydroxyl groups and two triflate anions. No dimer or network formation occurs as was discussed in the full-text. Intramolecular hydrogen bonding is present between H1 and O5^a. For further information according symmetry and geometry, see table 1 below.

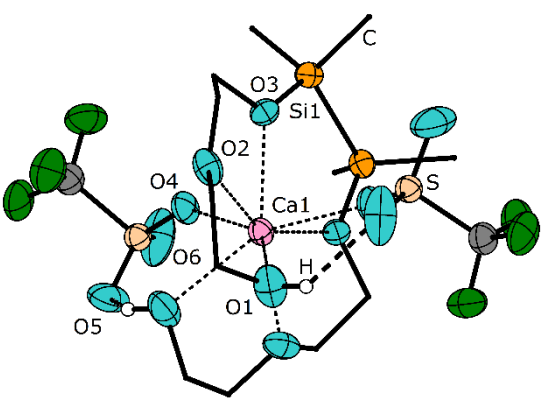

Figure 1. Molecular structure and intramolecular hydrogen bonding of **3a** in the crystal. Carbon bonded hydrogen atoms are omitted and carbon atoms of the podand are represented as wireframes for clarity. Non-labled atoms are symmetry generated: *a* = 1-x, y, 3/2-z.

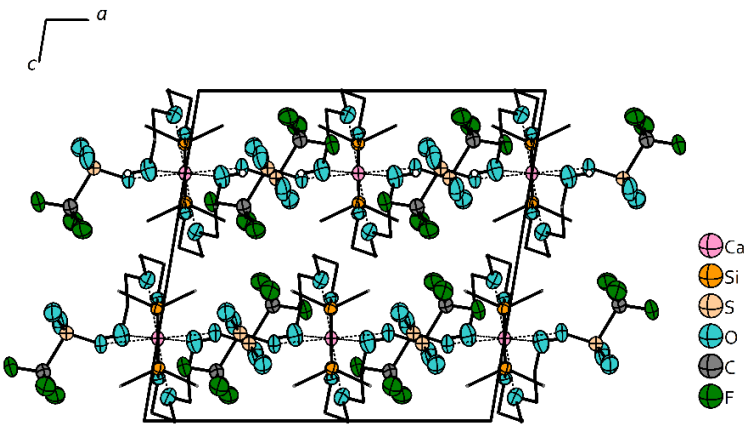

Figure 2. Cell package of **3a** along [010]. Carbon bonded hydrogen atoms are omitted and carbon atoms of the podand are represented as wireframes for clarity.

Table 1. Hydrogen bond geometries in the crystal structure of **3a** (pm, °)

compound	*D*–H···*A*	H···*A*	*D*···*A*	*D*–H···*A*
3a	O1-H1···O5[a]	212(2)	277(3)	134(1)

Hydrogen bond geometries according to HFIX83. Symmetry code is [a] 1-x, y, 3/2-z.

1.2 Compound 5a

Similar to compound **3**, recrystallization from a mixture of DCM and *n*-pentane yields two sorts of crystals. In this case colorless blocks among colorless planks. Diffraction data of the colorless blocks are discussed in the full-text. This section represents the diffraction data of the colorless needles. Within these respective crystals, [Sr(8,9-Disila-EO5)I_2] crystallizes in the triclinic space group *P*-1 with presence of cocrystalline solvent molecules (see CIF-file compound 5a.cif). The hydrogen-bonding pattern is similar to that discussed in the full-text. However, the crystal structure reveals that intermolecular hydrogen bonds are present between H1 and I1[b] as well as between H6 and I2[c] (see table 1 for symmetry codes). Hydrogen-bonding chains along the crystallographic *b* axis reveal a one-dimensional hydrogen-bonding network.

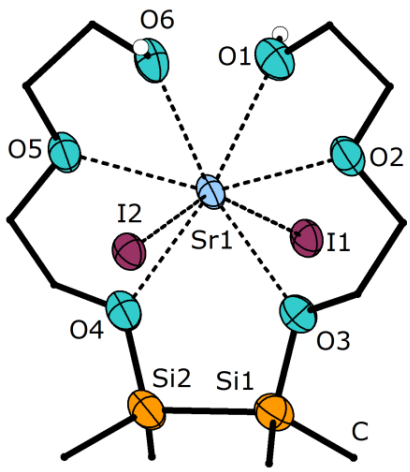

Figure 3. Molecular structure of **5a** in the crystal. Carbon bonded hydrogen atoms are omitted and carbon atoms of the podand are represented as wireframes for clarity.

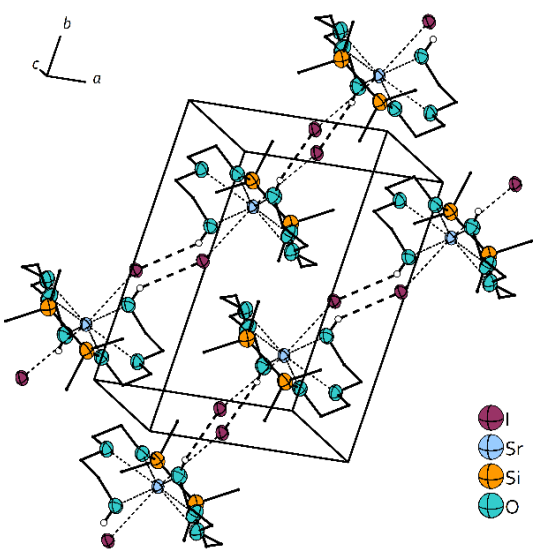

Figure 4. Cell package of **5a** and hydrogen bonding approximately along [001]. Carbon bonded hydrogen atoms are omitted and carbon atoms of the podand are represented as wireframes for clarity.

Table 2. Hydrogen bond geometries in the crystal structure of **5a** (pm, °)

compound	*D*–H···*A*	H···*A*	*D*···*A*	*D*–H···*A*
5a	O1-H1···I1[b]	281(1)	364(6)	167(3)
	O6-H6···I2[c]	278(1)	352(5)	148(3)

Hydrogen-bond geometries according to HFIX83. Symmetry codes are [b] 1-x, y, 3/2-z and [c] -x, 1-y, 1-z

1.3 Compound 6

6 crystallizes in the non-centrosymmetric, monoclinic space group *Cc*. In comparison to **5,** the enlarged chain size of **2** leads to the replacement of one of the iodide anions in the coordination sphere of the Sr^{2+} cation. A close look at the crystal structure reveals that intermolecular hydrogen bonds are present in between H1 and I2[c] as well as between H6 and I1[d] (see table 3 for symmetry codes). Hydrogen-bonding chains along the crystallographic *b* axis reveal a one-dimensional hydrogen-bonding network.

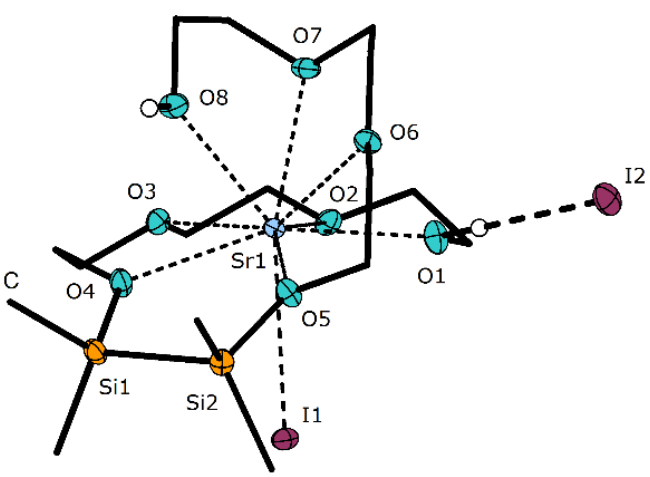

Figure 5. Molecular structure of **6** in the crystal. Carbon bonded hydrogen atoms as well as solvent molecules are omitted and carbon atoms of the podand are represented as wireframes for clarity. Selected bond lengths [pm]: Sr1-O1: 257.7(4), Sr1-O2: 265.8(4), Sr1-O3: 263.9(4), Sr1-O4: 262.8(4), Sr1-O5: 260.3(4), Sr1-O6: 263.1(4), Sr1-O7: 262.2(4), Sr1-O8: 267.5(4), Sr1-I1: 341.6(1), Si1-Si2 235.1(2). Selected bond angles [°]: O1-Sr1-O2 61.0(1), O2-Sr1-O3 62.1(1), O3-Sr1-O4 64.1(1), O4-Sr1-O5 74.0(1), O5-Sr1-O6 63.3(1), O6-Sr1-O7 63.9(1), O7-Sr1-O8 61.1(2), I1-Sr1-O3 83.2(1), I1-Sr1-O6 129.7(1), I1-Sr1-O7 147.9(1).

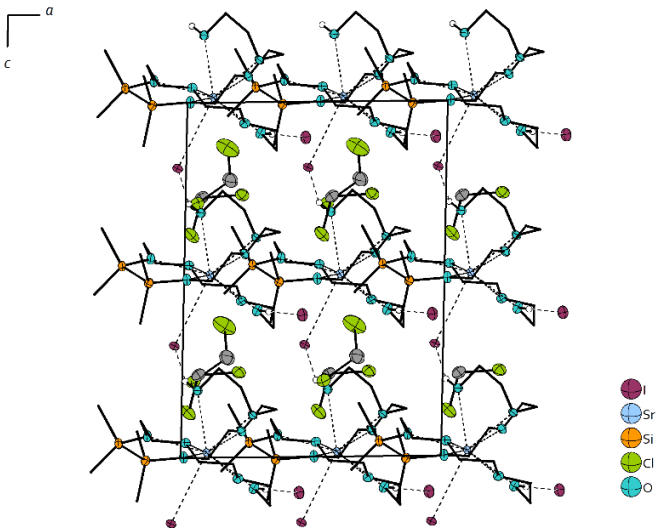

Figure 6. Cell package of **6**·2DCM and hydrogen bonding along [010]. Thermal ellipsoids are represented at the 50% probability level. Carbon bonded hydrogen atoms are omitted and carbon atoms of the podands are represented as wireframes for clarity.

The molecular structure reveals that all oxygen atoms as well as a single iodine atom participate in the coordination of the metal ion, giving a total coordination number of nine (Fig. 5). The ligand behaviour is similar to that of the smaller ligand **1**. As was found in the crystal structure, intermolecular hydrogen bonds between hydrogen atoms bound to the terminal hydroxyl groups and the iodide anions are present. This is the case between H1 and free I2 as well as between H8 and a neighboring iodine atom I1^{d} (see table 3 for further details). Hence, neighboring molecules are linked, resulting in a one-dimensional network along the crystallographic *c* axis (see Figure **6**).

Table 3. Hydrogen bond geometries in the crystal structure of **6** (pm, °)

compound	*D*–H···*A*	H···*A*	*D*···*A*	*D*–H···*A*
6	O1-H1···I2	258(4)	345(1)	178(4)
	O8-H8···I1^{d}	272(4)	351(1)	153(4)

Hydrogen bond geometries according to HFIX83. Symmetry code is ^{d} x, 1-y, -1/2+z

2. XYZ-Data of Optimized Structures

General: All calculations were performed with the program system TURBOMOLE V7.1.1.[5] The resolution of identity (RI) approximation, dispersion corrections, and the conductor-like screening model (COSMO) were applied throughout, the latter set to default. For all calculations, the BP86 functional was chosen, utilizing a def2-TZVP basis set.[6] Molecular Structure design: Diamond Version 4.4.0.[4]

2.1 **Compound 1**

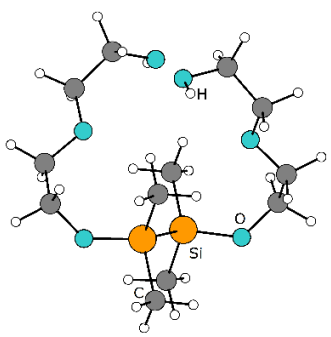

O	4.81863	12.93966	7.50062
O	5.66825	12.93377	12.08012
O	3.54057	8.11130	10.22880
O	6.94787	8.10758	9.34443
O	3.95803	10.00817	7.79212
O	6.52973	10.00174	11.78198
Si	5.88780	12.83596	8.80449
C	4.59722	11.94903	6.49995
Si	4.60318	12.83593	10.77264
C	5.88792	11.93979	13.07766
H	2.62576	8.35934	10.45399
C	3.57779	7.83751	8.82121
H	7.85547	8.38377	9.12275
C	6.91340	7.83192	10.75166
C	3.02262	8.94211	7.94183
C	3.49444	10.96781	6.84351
C	7.46653	8.93688	11.63144
C	6.99161	10.95994	12.73311
C	7.04465	11.37144	8.63996
C	6.88957	14.43499	8.76134
H	5.52252	11.38723	6.28517
H	4.30336	12.47705	5.57820
C	3.44120	11.37466	10.92870
C	3.60686	14.43830	10.81798
H	4.96226	11.37715	13.28875
H	6.17992	12.46472	14.00174

H	3.01386	6.91353	8.59551
H	4.63617	7.67282	8.57777
H	7.48138	6.90982	10.97534
H	5.85613	7.66230	10.99677
H	2.79330	8.51350	6.94540
H	2.06702	9.31987	8.36074
H	2.61308	11.51096	7.23777
H	3.18548	10.45198	5.91215
H	7.69674	8.50811	12.62753
H	8.42148	9.31646	11.21266
H	7.87301	11.50431	12.34084
H	7.29969	10.44211	13.66362
H	6.49096	10.42410	8.64105
H	7.71522	11.35830	9.51255
H	7.66299	11.44102	7.73145
H	7.50446	14.48898	7.84946
H	7.56086	14.48566	9.63265
H	6.23537	15.31869	8.78918
H	3.99372	10.42711	10.96033
H	2.79982	11.34433	10.03503
H	2.79418	11.46039	11.81552
H	2.99703	14.49503	11.73306
H	2.93111	14.48972	9.95019
H	4.26343	15.32005	10.78551

2.2 Compound 2

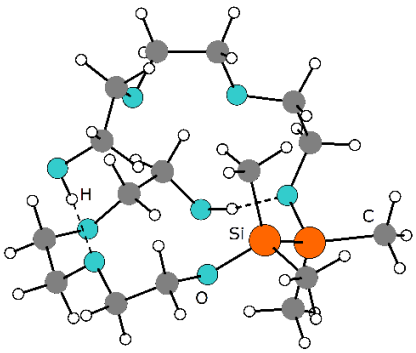

O	6.75613	6.03512	4.80672
O	7.87837	7.03340	9.07701
O	6.06230	11.69679	8.48712
O	7.81514	11.30892	6.20481
O	7.72255	9.98708	9.88261
O	5.53975	6.27851	7.32009
O	3.84617	8.59249	7.31804
O	8.01931	8.66199	4.96339
H	6.37887	6.18316	5.70904
C	6.40857	7.16116	3.99468
C	7.75313	8.17122	8.19990
C	7.62210	5.78405	8.44026
Si	4.37635	11.53881	8.39371
C	6.83477	12.73087	7.86273
C	8.25000	11.10042	4.86216
C	7.07530	12.50978	6.38319
H	7.04727	10.56160	9.44251
C	8.45664	9.36266	8.81487
C	4.10880	6.20812	7.34195
C	6.15094	5.44080	8.31044
Si	3.65406	10.12434	6.65193
C	3.53300	7.39623	6.60838
C	7.56770	8.10277	3.73068
C	8.93533	9.74817	4.79600
H	5.59110	7.72905	4.46300
H	6.04606	6.79330	3.01996
H	6.69190	8.40318	8.01034
H	8.21155	7.93499	7.22351
H	8.09170	5.01211	9.06893
H	8.10619	5.75766	7.44579
C	3.91079	10.73831	10.02534
C	3.60184	13.24446	8.21761
H	7.80019	12.76063	8.38948
H	6.34511	13.70948	7.99458
H	8.96208	11.89360	4.56211
H	7.39085	11.13597	4.16587
H	6.11744	12.45695	5.83254

H	7.63790	13.38028	5.99245
H	9.42268	9.03878	9.23374
H	8.64576	10.09104	8.01160
H	3.76388	6.22406	8.39028
H	3.75898	5.27016	6.87241
H	6.04194	4.37437	8.03402
H	5.64639	5.59923	9.27981
C	1.82949	10.44608	6.29168
C	4.62475	10.26680	5.04990
H	3.93135	7.43020	5.57923
H	2.43966	7.25726	6.53484
H	8.39924	7.56606	3.23384
H	7.21467	8.89389	3.04129
H	9.48184	9.65652	3.84215
H	9.66827	9.67900	5.61517
H	2.82739	10.55030	10.06246
H	4.18332	11.38193	10.87496
H	4.42386	9.77194	10.13120
H	3.83699	13.71542	7.25215
H	3.92939	13.91975	9.02255
H	2.50744	13.14671	8.27966
H	1.21610	10.35378	7.19949
H	1.44398	9.73868	5.54107
H	1.69650	11.46327	5.89260
H	4.56534	11.29330	4.65797
H	4.22137	9.59856	4.27445
H	5.68001	10.01632	5.22431

2.3 EO5

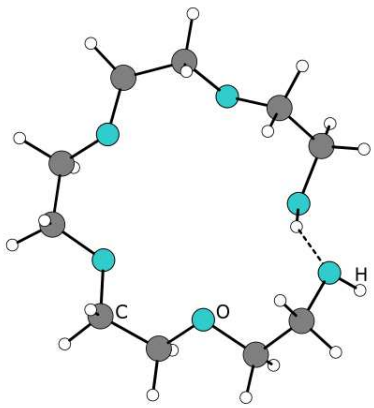

O	13.34907	6.60025	10.26224
O	14.29285	6.79227	7.37972
O	14.28120	9.19595	5.71900
O	11.99793	10.82315	6.22834
O	11.83214	11.15657	9.12385
O	13.79618	9.36369	10.33142
C	13.63065	5.54432	9.31856
H	14.00915	6.53372	10.97561
C	14.75890	5.87008	8.36096
C	15.32236	7.16280	6.46390
C	14.72479	7.91160	5.29601
C	13.56063	9.87952	4.69768
C	12.98947	11.15786	5.26450
C	11.45124	11.95255	6.90487
C	10.80442	11.46303	8.18084
C	11.46780	10.14247	10.05451
C	12.63597	9.87805	10.98713
H	13.86984	4.61561	9.85944
H	12.70377	5.38488	8.74993
H	15.09967	4.93530	7.87176
H	15.62084	6.28991	8.91606
H	16.08233	7.78607	6.97259
H	15.82909	6.25863	6.07498
H	13.87706	7.33261	4.88124
H	15.48997	8.00521	4.50002
H	14.22225	10.12198	3.84308
H	12.74024	9.23940	4.31877
H	12.55814	11.75704	4.43873
H	13.79230	11.75605	5.73656
H	12.24864	12.67844	7.14971
H	10.70384	12.46751	6.27078
H	10.20452	10.56197	7.95942
H	10.12321	12.23553	8.58540
H	10.59148	10.45351	10.65849

H	11.19318	9.21632	9.51220
H	12.28796	9.19526	11.78452
H	12.94027	10.82212	11.46486
H	13.58593	8.45104	10.02017

2.4 $[Ca@1]^{2+}$

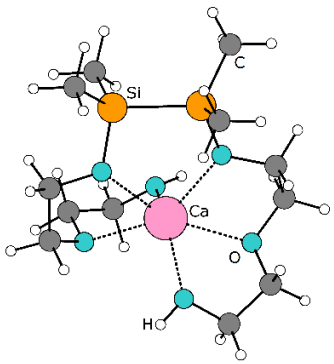

Ca	2.62701	17.60118	7.66301
O	3.45657	19.05387	6.00809
O	1.49338	19.51885	8.48373
O	4.26965	16.42574	6.36553
O	4.32058	16.78269	9.05498
O	0.91582	16.59835	6.40409
O	0.84714	16.91841	9.09933
Si	3.06943	20.73483	5.97522
C	4.56736	18.55566	5.20914
Si	1.17135	20.80090	7.37342
C	0.55749	19.30981	9.57631
C	4.41573	17.05655	5.07013
C	5.52011	16.22036	7.06993
H	4.32763	16.68380	10.02351
C	5.17797	15.76323	8.46314
H	0.97538	16.20759	5.51441
C	-0.06425	15.84911	7.18097
C	0.76569	17.91715	10.14386
C	-0.39572	16.67731	8.39325
C	2.65344	21.22620	4.22095
C	4.52393	21.68914	6.65830
H	4.55305	19.01238	4.20927
H	5.51037	18.82832	5.70457
C	1.01231	22.40820	8.30988
C	-0.38894	20.36150	6.43510
H	0.73858	20.04922	10.36892
H	-0.46989	19.44304	9.20686
H	5.27443	16.62842	4.53338
H	3.49828	16.81110	4.51876
H	6.11222	15.45246	6.55071
H	6.09219	17.16036	7.10179
H	6.09761	15.66084	9.05266
H	4.64180	14.80296	8.44828
H	-0.97148	15.69071	6.58406

H	0.36321	14.87640	7.46510
H	-0.03991	17.66963	10.85029
H	1.72565	17.85008	10.67314
H	-1.09503	16.13897	9.04931
H	-0.84841	17.63268	8.08791
H	2.25649	22.25238	4.21676
H	3.54047	21.20848	3.57163
H	1.88815	20.56275	3.79421
H	4.78355	21.34711	7.66987
H	5.40846	21.58525	6.01287
H	4.27018	22.75811	6.71306
H	0.90377	23.23736	7.59509
H	0.12516	22.40674	8.95977
H	1.90236	22.59929	8.92520
H	-0.29283	19.38503	5.93865
H	-1.27137	20.33634	7.09123
H	-0.57424	21.11883	5.65897

2.5 $[Ca@EO5]^{2+}$

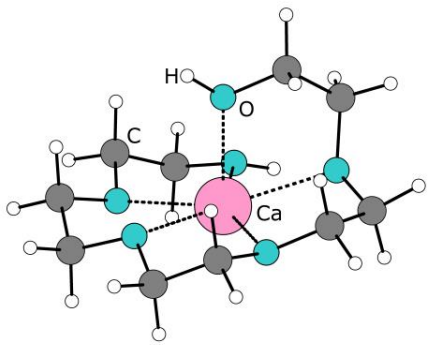

Ca	12.71043	8.45184	7.65935
O	12.34604	6.62763	9.13188
O	14.34466	6.74821	7.32210
O	14.37044	9.13103	6.08350
O	12.06311	10.48395	6.55193
O	11.10593	9.62129	8.99626
O	13.84080	9.66242	9.32631
C	13.14183	5.43423	8.89244
H	11.47066	6.35875	9.46352
C	14.51626	5.88289	8.46771
C	15.58353	7.19293	6.72502
C	15.21422	8.07843	5.56246
C	13.88469	10.04086	5.07045
C	13.10359	11.12053	5.77400
C	11.29260	11.42616	7.33243
C	10.38363	10.62767	8.24388
C	11.67224	10.02370	10.26902
C	13.06689	10.59793	10.12604
H	13.21729	4.84171	9.81433
H	12.66696	4.83186	8.10422
H	15.12422	5.00924	8.18902
H	15.02727	6.43843	9.27121
H	16.17633	7.74197	7.47488
H	16.16231	6.32655	6.37151
H	14.66001	7.51492	4.79483
H	16.11972	8.51252	5.11319
H	14.73264	10.49080	4.53304
H	13.25542	9.48715	4.35497
H	12.65576	11.80075	5.03385
H	13.75275	11.69836	6.45152
H	11.98031	12.07534	7.89600
H	10.68503	12.05671	6.66445
H	9.64924	10.06705	7.65136
H	9.84909	11.29962	8.92999
H	11.01122	10.75049	10.76125
H	11.70262	9.10425	10.86796

H	13.51715	10.69773	11.12381
H	13.06473	11.58144	9.63676
H	14.76955	9.95365	9.31146

2.6 $[Sr@1]^{2+}$

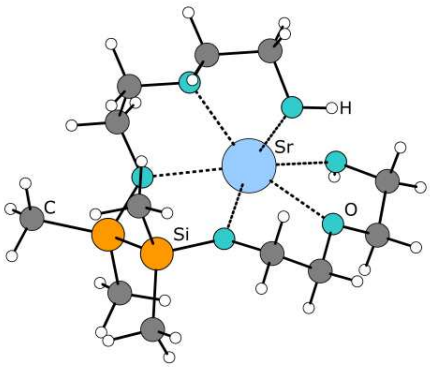

Sr	3.39456	6.38770	4.36394
O	1.56639	5.66257	2.75498
O	3.07103	4.62871	6.21260
O	1.28251	6.73072	5.79650
O	4.49975	4.15751	3.97234
O	4.08234	6.41304	1.88647
O	5.49953	7.74918	3.85863
Si	-0.05225	5.31186	3.21893
C	2.10206	5.15656	1.50225
C	1.89178	4.72877	7.03565
C	3.44572	3.26719	5.91825
Si	-0.26213	6.78616	5.04316
C	1.51585	6.18886	7.11789
H	5.19765	3.99737	3.31298
C	4.72605	3.30338	5.12553
C	5.03988	7.41459	1.48372
C	3.03786	6.18517	0.92028
H	5.51227	8.71025	4.01717
C	6.09620	7.47330	2.56303
C	-1.20470	5.73465	1.80535
C	-0.16471	3.49528	3.66148
H	1.29276	4.96168	0.78505
H	2.63332	4.21393	1.70226
H	2.10106	4.33198	8.04179
H	1.07912	4.13453	6.58347
H	2.63745	2.78492	5.34365
H	3.60220	2.70888	6.85408
C	-1.59940	6.28917	6.24987
C	-0.45643	8.54098	4.42779
H	0.62744	6.30700	7.75209
H	2.33389	6.77239	7.56390
H	5.55048	3.71344	5.72829
H	4.98314	2.28685	4.80012
H	4.52908	8.38489	1.36330

H	5.49929	7.12828	0.52373
H	3.47182	5.80898	-0.01962
H	2.50761	7.13165	0.72045
H	6.59759	6.50076	2.65820
H	6.84761	8.23435	2.31874
H	-2.24400	5.66806	2.16111
H	-1.09828	5.03981	0.95970
H	-1.03461	6.75885	1.44523
H	0.51506	3.22937	4.48315
H	0.08405	2.86425	2.79513
H	-1.18865	3.24816	3.97835
H	-1.46177	5.26853	6.63298
H	-2.56439	6.31941	5.72181
H	-1.65833	6.98334	7.10058
H	-0.47271	9.24786	5.27034
H	-1.39896	8.64074	3.86948
H	0.36473	8.82314	3.75299

2.7 $[Sr@EO5]^{2+}$

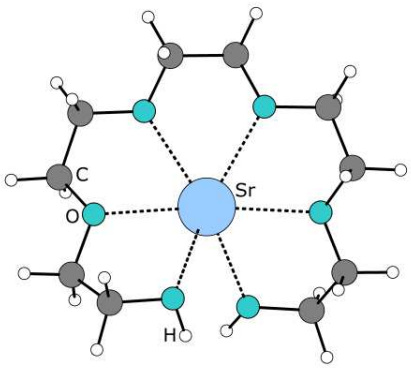

Sr	13.19678	8.86964	8.03509
O	12.72610	6.64696	9.26220
O	14.53322	6.82558	7.22320
O	14.42122	9.12780	5.76545
O	12.07990	10.51134	6.37475
O	11.76168	10.72801	9.08231
O	13.35895	9.13717	10.60722
C	13.40996	5.45692	8.78716
H	12.88229	6.75288	10.21873
C	14.76884	5.81706	8.22711
C	15.68868	7.20990	6.45241
C	15.17951	7.99848	5.27240
C	13.63693	9.74233	4.71971
C	12.92549	10.94216	5.28449
C	11.31523	11.60600	6.92883
C	10.68519	11.14312	8.21752
C	11.37291	10.46018	10.44528
C	12.63999	10.23578	11.22915
H	13.51031	4.72316	9.59671
H	12.77622	5.03532	7.99615
H	15.23788	4.93231	7.76790
H	15.43974	6.21416	9.00788
H	16.37675	7.80339	7.07737
H	16.21949	6.31596	6.09057
H	14.52025	7.36870	4.65391
H	16.02099	8.35468	4.65824
H	14.29681	10.06821	3.90033
H	12.91841	9.00360	4.32707
H	12.31085	11.40112	4.49418
H	13.64298	11.69061	5.65938
H	11.99086	12.45529	7.11939
H	10.53676	11.91543	6.21440
H	9.98911	10.30330	8.05407
H	10.13371	11.97863	8.67562
H	10.83028	11.32417	10.85882
H	10.71503	9.57532	10.47860

H	12.38931	9.98100	12.26864
H	13.26709	11.13909	11.21218
H	14.18544	8.99626	11.10349

2.8 $[Sr@2]^{2+}$

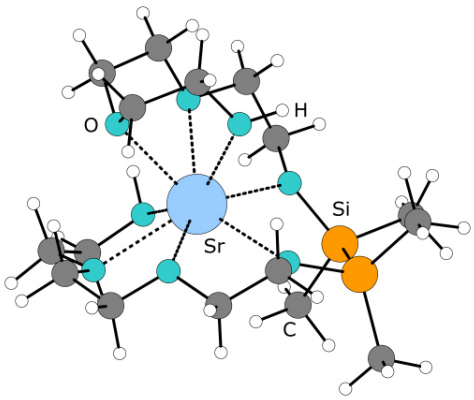

Sr	6.41271	9.04361	6.95671
O	6.12754	8.97800	4.38307
O	7.47531	7.35973	8.67478
O	5.46929	11.45137	7.04761
O	8.12097	10.94280	6.21954
O	7.84341	10.07927	8.88402
O	5.58089	6.55317	6.88406
O	3.88821	8.73851	6.66800
O	8.46100	8.21440	5.62052
H	5.51028	9.47825	3.82213
C	7.13844	8.37918	3.53973
C	8.69941	7.83280	9.26805
C	7.58331	6.04510	8.09506
Si	3.98071	11.66228	7.87122
C	6.48844	12.48012	7.06891
C	9.04151	10.57404	5.17522
C	7.48692	12.21492	5.97135
H	8.56590	10.53904	8.41463
C	8.39504	9.18279	9.87711
C	4.16178	6.34318	6.74211
C	6.18560	5.58704	7.76691
Si	2.70501	9.95919	6.86222
C	3.58386	7.50258	5.97185
C	8.02016	7.52399	4.42867
C	9.53426	9.16828	5.45457
H	7.70953	9.16494	3.02526
H	6.67213	7.73297	2.78074
H	9.48488	7.90463	8.49473
H	9.03633	7.12971	10.04716
H	8.03232	5.34659	8.81838
H	8.22542	6.08891	7.19924
C	4.27505	11.37936	9.70080
C	3.29678	13.37023	7.53472
H	6.98083	12.48685	8.05338

H	6.03563	13.46706	6.89476
H	9.90230	11.26314	5.17181
H	8.53231	10.65161	4.20227
H	6.98465	12.18215	4.98980
H	8.24524	13.01462	5.96003
H	7.62527	9.08094	10.65304
H	9.29984	9.61199	10.32657
H	3.70771	6.27970	7.74522
H	3.97053	5.40221	6.20057
H	6.21572	4.59796	7.28282
H	5.58330	5.51890	8.68753
C	1.32752	9.30940	7.94992
C	2.07315	10.46794	5.17409
H	4.01933	7.55903	4.96390
H	2.49731	7.35888	5.87870
H	7.45029	6.66232	4.80235
H	8.88905	7.15768	3.86220
H	10.20848	8.84182	4.64940
H	10.09049	9.14807	6.40184
H	3.32846	11.47379	10.25294
H	4.98237	12.11841	10.10489
H	4.67742	10.37513	9.89830
H	3.25152	13.57875	6.45668
H	3.89348	14.15391	8.02347
H	2.27362	13.43088	7.93522
H	1.71994	8.96001	8.91503
H	0.79147	8.47819	7.46810
H	0.59837	10.11008	8.14447
H	1.33612	11.27731	5.28336
H	1.57959	9.62952	4.66082
H	2.88915	10.83584	4.53611

2.9 $[Ba@2]^{2+}$

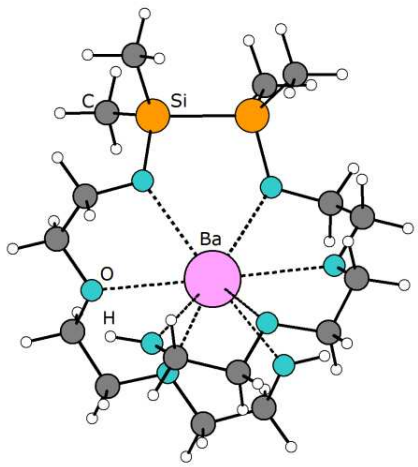

Ba	6.93005	4.38601	19.95330
O	7.99789	5.49142	17.55909
O	5.82499	3.31820	22.34789
O	9.72062	4.85489	19.68904
O	6.46257	1.59525	20.21822
O	5.32045	5.99184	18.32759
O	5.32487	5.99592	21.57990
O	8.66901	3.58659	21.90452
O	7.73153	2.64688	18.00291
C	9.36174	5.94734	17.58516
C	7.15032	6.33551	16.76368
C	5.36941	1.95424	22.32178
C	4.98065	4.16561	23.14318
C	10.19505	4.94078	18.33244
C	10.53178	3.96230	20.47738
C	6.37639	1.12108	21.57490
C	7.35597	0.78439	19.43047
Si	4.32874	7.30007	18.79678
C	5.72692	5.86687	16.94435
Si	4.01725	6.98850	21.11092
C	5.44951	5.58901	22.96304
H	8.33880	3.52542	22.81848
C	10.04968	4.00902	21.90288
H	7.79227	2.97699	17.08888
C	7.30962	1.26606	18.00482
H	9.74704	6.03949	16.55619
H	7.43800	6.26247	15.70125
H	4.37967	1.90634	21.83572

H	5.27703	1.56905	23.35077
H	5.05327	3.87764	24.20555
H	10.13021	3.94722	17.85711
H	11.24745	5.26916	18.32651
H	10.45394	2.93868	20.06959
H	7.36978	1.18625	22.05053
H	6.04830	0.06858	21.58092
H	7.03933	-0.27031	19.47423
H	8.37936	0.86296	19.83870
C	5.19838	8.92094	18.42729
C	2.69936	7.20434	17.87473
H	5.06629	6.44559	16.28128
H	5.63154	4.80670	16.66473
C	2.39587	6.11989	21.48062
C	4.11410	8.61775	22.03310
H	4.87074	6.24953	23.62618
H	6.50963	5.68416	23.24290
H	10.66149	3.32836	22.51287
H	10.13146	5.03031	22.30653
H	7.99073	0.65431	17.39526
H	6.28851	1.18377	17.60081
H	4.58218	9.75736	18.79059
H	5.35075	9.06488	17.34710
H	6.17373	8.97531	18.93105
H	2.20855	6.23466	18.03743
H	2.83326	7.35399	16.79326
H	2.02593	7.99456	18.23976
H	1.55973	6.73695	21.11811
H	2.25231	5.96694	22.56077
H	2.34052	5.14489	20.97629
H	5.08369	9.10848	21.86965
H	3.96543	8.48369	23.11468
H	3.32363	9.29134	21.66892
H	3.93227	4.05395	22.81852
H	7.26220	7.38400	17.08792
H	9.40937	6.93723	18.07093
H	11.58631	4.27953	20.43378

2.10 [Cs@2]$^+$

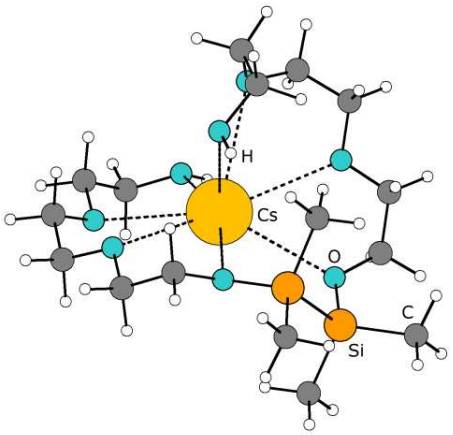

Cs	6.89073	8.95690	7.52147
O	6.10076	8.03609	4.58876
O	7.85991	6.40947	9.17603
O	5.44906	11.78262	7.74237
O	7.79043	11.61812	6.03314
O	9.75002	8.59158	8.74968
O	5.21226	6.30172	7.89942
O	3.74580	8.70580	7.13559
O	8.79546	9.05343	4.99909
H	5.15225	8.21066	4.45371
C	6.81800	8.73024	3.55175
C	9.28432	6.26292	9.13115
C	7.19378	5.22117	8.73787
Si	3.76344	11.82540	7.83461
C	6.29575	12.88881	7.41529
C	8.53364	11.52078	4.81802
C	6.90817	12.74150	6.03997
H	10.19364	9.37496	9.11994
C	9.94593	7.50572	9.67302
C	3.79072	6.43841	7.96735
C	5.70076	5.38424	8.88098
Si	3.00464	10.06870	6.47179
C	3.31173	7.36560	6.87546
C	8.30298	8.51237	3.76493
C	9.45648	10.31941	4.89489
H	6.57412	9.80507	3.56950
H	6.54753	8.33381	2.55752
H	9.61310	6.07880	8.09088
H	9.59210	5.39695	9.74584
H	7.51701	4.36154	9.35354

H	7.45407	5.00416	7.68507
C	3.27677	11.53492	9.62498
C	3.09371	13.47275	7.22280
H	7.09765	12.93759	8.16946
H	5.74292	13.84083	7.44906
H	9.15251	12.42767	4.67607
H	7.84833	11.44952	3.95335
H	6.11817	12.60915	5.27594
H	7.46738	13.66510	5.79828
H	9.51945	7.75283	10.66051
H	11.02120	7.29448	9.80127
H	3.49306	6.83667	8.95507
H	3.31071	5.45040	7.83377
H	5.22247	4.39653	8.74337
H	5.45335	5.74438	9.89701
C	1.13331	9.88316	6.51282
C	3.57386	10.32028	4.69241
H	3.70143	7.01901	5.90256
H	2.21116	7.31009	6.83970
H	8.50152	7.42985	3.80119
H	8.85574	8.93628	2.90970
H	10.12311	10.32920	4.01462
H	10.07736	10.40141	5.79907
H	2.18148	11.49237	9.72307
H	3.65091	12.34453	10.26991
H	3.68748	10.58168	9.98703
H	3.39653	13.68249	6.18720
H	3.41761	14.31026	7.85833
H	1.99397	13.43894	7.25103
H	0.77759	9.65722	7.52835
H	0.78362	9.08990	5.83566
H	0.66542	10.82599	6.19146
H	3.06336	11.19231	4.25633
H	3.33635	9.45416	4.05390
H	4.65478	10.51612	4.64477

3. References

[1] Sheldrick, G. M. SHELXT - Integrated space-group and crystal-structure determination. Acta Crystallogr., Sect. A: Fundam. Crystallogr., **2015**, *A71*, 3–8.

[2] Sheldrick, G. M. Crystal structure refinement with SHELXL. *Acta Crystallogr., Sect. C: Cryst. Struct. Commun.*, **2015**, *71*, 3–8.

[3] O. V. Dolomanov, L. J. Bourhis, R. J. Gildea, J. A. K. Howard and H. Puschmann, *OLEX2*: a complete structure solution, refinement and analysis program. *J. Appl. Crystallogr.*, **2009**, *42*, 339–341.

[4] H. Putz, K. Brandenburg, *Diamond-Crystal and Molecular Structure Visualization.* Crystal Impact: Bonn, Germany, **2012**.

[5] Stoe & Cie, *X-AREA* and *X-RED32*, Stoe & Cie, Darmstadt, Germany, **2009**.

[6] Bruker *SADABS* Bruker AXS Inc., Madison, Wisconsin, USA, **2014**.

[7] (a) Turbomole Version 7.0.1, Turbomole GmbH 2016. Turbomole is a development of University of Karlsruhe and Forschungszentrum Karlsruhe 1989–2007, Turbomole GmbH since 2007; (b) Furche, F.; Ahlrichs, R.; Hättig, C.; Klopper, W.; Sierka, M.; Weigend, F. Turbomole. *Wiley Interdiscip. Rev.: Comput. Mol. Sci.*, **2014**, *4*, 91–100.

[8] (a) Weigend, F.; Ahlrichs, R. Balanced basis sets of split valence, triple zeta valence and quadruple zeta valence quality for H to Rn: Design and assessment of accuracy. *Phys. Chem. Chem. Phys.*, **2005**, *7*, 3297–3305; (b) Weigend, F. Accurate Coulomb-fitting basis sets for H to Rn. *Phys. Chem. Chem. Phys.*, **2006**, *8*, 1057–1065; (c) Dolg, M.; Stoll, H.; Savin, A.; Preuss, H. Energy-adjusted pseudopotentials for the rare earth elements. *Theor. Chim. Acta*, 1989, **75**, 173–194; (d) Stoll, H.; Metz, B.; Dolg, M., Relativistic energy-consistent pseudopotentials–recent developments. *J. Comput. Chem.*, 2002, **23**, 767–778; (e) Grimme, S.; Antony, J.; Ehrlich, S.; Krieg, H. A consistent and accurate ab initio parametrization of density functional dispersion correction (DFT-D) for the 94 elements H-Pu. *J. Chem. Phys.*, **2010**, *132*, 154104; (f) Grimme, S.; Ehrlich, S.; Goerigk, I. Effect of the damping function in dispersion corrected density functional theory. *J. Comput. Chem.*, **2011**, *32*, 1456–1465.

inorganics

MDPI

Article

Hybrid Disila-Crown Ethers as Hosts for Ammonium Cations: The O–Si–Si–O Linkage as an Acceptor for Hydrogen Bonding

Fabian Dankert, Kirsten Reuter, Carsten Donsbach and Carsten von Hänisch *

Fachbereich Chemie and Wissenschaftliches Zentrum für Materialwissenschaften (WZMW), Philipps-Universität Marburg, Hans-Meerwein Straße 4, D-35032 Marburg, Germany; fabian.dankert@staff.uni-marburg.de (F.D.); kirsten.reuter@staff.uni-marburg.de (K.R.); donsbach@students.uni-marburg.de (C.D.)

* Correspondence: haenisch@chemie.uni-marburg.de; Tel.: +49-06421-2825612

Received: 11 December 2017; Accepted: 11 January 2018; Published: 16 January 2018

Abstract: Host-guest chemistry was performed with disilane-bearing crown ethers and the ammonium cation. Equimolar reactions of 1,2-disila[18]crown-6 (**1**) or 1,2-disila-benzo[18]crown-6 (**2**) and NH_4PF_6 in dichloromethane yielded the respective compounds $[NH_4$(1,2-disila[18]crown-6)$]PF_6$ (**3**) and $[NH_4$(1,2-disila-benzo[18]crown-6)$]PF_6$ (**4**). According to X-ray crystallographic, NMR, and IR experiments, the uncommon hydrogen bonding motif $O_{(Si)}\cdots H$ could be observed and the use of cooperative effects of ethylene and disilane bridges as an effective way to incorporate guest molecules was illustrated.

Keywords: siloxanes; host-guest chemistry; supramolecular chemistry; main group coordination chemistry; hydrogen bonding

1. Introduction

Siloxane bonding has been intensely discussed for the past seventy years. However, siloxane bonding is not yet fully understood. Its discussion regarding the basicity is, to the best of our knowledge, nowadays based on two different explanatory models. Both are important in order to give insights into the Si–O bond, the associated Lewis basicity, and binding properties. As one model, negative hyperconjugation interactions are discussed especially for permethylated siloxanes [1,2]. These interactions are understood as a donation of electron density in the case $p(O) \rightarrow \sigma^*(Si–C)$, which is competing with the coordination towards a Lewis acid and vice versa. Hence, the basicity of silicon bonded oxygen atoms turns out to be lower [3–5]. The other explanatory model considers the Si–O bond as highly ionic. The electronegativity gradient in the Si–O bond is considerably larger than in the C–O bond, which causes significantly different binding properties of siloxanes in comparison to ethers. Gillespie and Robinson emphasize that the electron pairs located directly at the oxygen atoms are spatially diffused, resulting in a lower basicity [6]. Furthermore, one could argue that the partially negatively charged oxygen atoms should show strong interactions with Lewis acids. However, this argument is disproved by repulsive interactions between a positively charged silicon atom and a Lewis acid, which was recently shown via quantum chemical calculations [7,8]. Overall, this leads to an understanding of why the coordination of siloxanes turns out to be cumbersome. The whole discussion is stripped down to monosilanes, which results in a structural discrepancy regarding (cyclic) poly-silaethers. The conformation of the ligand significantly affects the coordination properties, which was shown for ring-contracted crown ethers [9,10]. Considering all those arguments, we tried to regain structural analogy towards organic (crown type) ligands with the insertion of disilane-units. Simple substitution of $–SiMe_2–$ units with $–Si_2Me_4–$ units in a residuary $–C_2H_4O–$ framework yields

disilane-bearing ligands with a respectable coordination ability very close to their organic analogs. Alkali and alkaline earth metal salts could easily be coordinated by ligands of this class, so the coordination ability of siloxane compounds should be reconsidered [11–15]. However, the discussion around siloxane bonding is not restricted to the coordination of Lewis acids and includes the ability to form hydrogen bonds. Hydrogen-bonding patterns vary with the use of different substituents within a silicon-based system (see Scheme 1).

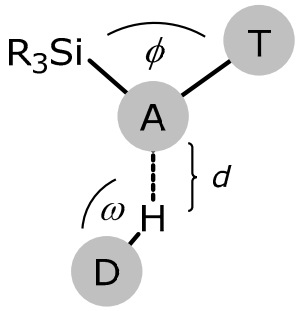

Scheme 1. Model of hydrogen-bonding involving silicon-based systems in which A = acceptor (especially O), D = donor-bearing atom (O/N), T = tetrel (C/Si), *d* = length of the respective hydrogen bonding contact, and ϕ as well as ω are relevant bond angles setting up the hydrogen bonding pattern.

The ability of these systems to form a hydrogen bond has been discussed since the early sixties, especially by the group of West. Early examinations order the affinity to form hydrogen bonds in the sequence R_3COCR_3 > R_3COSiR_3 >> $R_3SiOSiR_3$ according to IR-spectroscopic and thermodynamic studies, as well as NMR experiments [16–18]. Also, recent research confirms a low hydrogen bonding affinity of the oxygen atoms within ligands of the type $R_3SiOSiR_3$ [19]. This is also reflected by the fact that a lot more solid state structures with hydrogen bonding between D–H and R_3CDSiR_3 (D = O, N) than between D–H and $R_3SiOSiR_3$ are known to date. These results reflect the fact that a screening of the Cambridge Crystallographic Database (CCDC) reveals no more than twenty structures that exhibit hydrogen bonding between D–H and R_3CDSiR_3 (D = O, N) and just a handful of structures showing contacts in between D–H and $R_3SiOSiR_3$ in the solid state [20]. Taking all observations into account, the hydrogen bonding of siloxanes continues to be an uncommon motif and is declared as an unusual phenomenon [21]. However, it is possible to increase the ability of siloxanes to form hydrogen bonds by decreasing the ϕ-angle, which could be shown in several publications and was also supported by experimental data provided by the group of Beckmann [5,17,21–23]. The relatively small pool of experimental data motivated us to extend the coordination chemistry of hybrid disila-crown ethers to ammonium cations.

2. Results

The ability of organic crown ethers to act as host molecules is discussed regarding different systems with hydronium- and ammonium ions as the simplest hosts. Recrystallization of equimolar ratios of salt and an appropriate crown ether from organic and/or aqueous solution yields crown ether complexes with the general formula [M(CE)]A, where M = H_3O^+ or NH_4^+, CE = crown ether, and A = anion. Mainly crown ethers of the [18]crown-6 type are used, but the anion structure varies with A = Cl^-, Br_3^-, I_3^-, ClO_4^-, $[BF_4]^-$, $[PF_6]^-$ $[SbCl_6]^-$, and many more [24–33]. In the case of hybrid crown-ethers, aqueous solutions and traces of moisture lead to the entire decomposition of the ligand. Siloxane cleavage with aqueous solutions is common for this kind of ligand and has already been discussed in other publications [11,34,35]. For this reason, hydrogen bonding towards hydronium cations could not be performed. However, the incorporation of a guest turned out to be successful in the use of ammonium hexafluorophosphate as the salt and 1,2-disila[18]crown-6 (**1**), as well as 1,2-disila-benzo[18]crown-6 (**2**) as the ligands of choice. The ligands were prepared using methods

described in the literature (see Scheme 2) [11,15]. Subsequent reaction of these ligands with NH_4PF_6 in anhydrous dichloromethane yielded the respective complexes [NH_4(1,2-disila[18]crown-6)]PF_6 (**3**) and [NH_4(1,2-disila-benzo[18]crown-6]PF_6 (**4**). Neat **3** is a colorless powder which can be recrystallized from dichloromethane. The resulting colorless blocks were analyzed via XRD. **3** crystallizes in the non-centrosymmetric monoclinic space group $P2_1$ as an enantiopure product very similar to the corresponding potassium complex [K(1,2-disila[18]crown-6)PF_6] according to the lattice constants [11]. As also observed for organic crown ether complexes, the ammonium cation is trapped in the cavity of the sila-crown ether beneath the anion bound to every second oxygen atom of the ligand **1**. The hydrogen bonding system of the ammonium cation now features three different binding modes due to the insertion of the O–Si–Si–O linkage and the presence of the $[PF_6]^-$ anion. Hence, etheric oxygen atoms, one silicon substituted oxygen atom, and two of the fluorine atoms of the $[PF_6]^-$ anion are participating (see Figure 1). The F···H contacts show distances that are well within the range of hydrogen bonding for this system. Freely chosen systems for comparison are [NH4([18]crown-6)]PF_6, [NH_4(dibenzo[18]crown-6)]PF_6, and [NH_4(benzo[15]crown-5)]PF_6 [32,36,37].

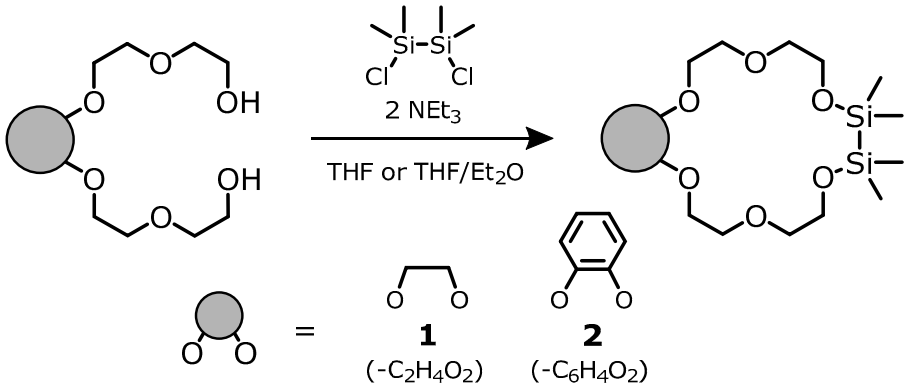

Scheme 2. Synthesis of 1,2-disila[18]crown-6 and 1,2-disila-benzo[18}crown-6 [11,15].

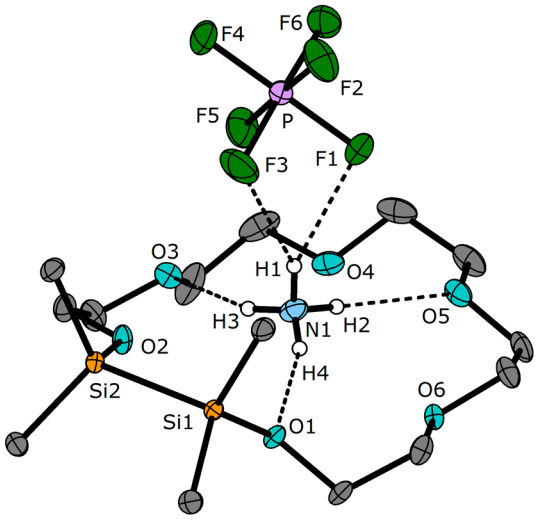

Figure 1. The molecular structure of compound **3** in the solid state. Thermal ellipsoids represent a probability level of 50%. The disordered part of the ligand with a lower occupancy and all carbon bonded hydrogen atoms are omitted for clarity, whereas hydrogen atoms of the ammonium cation are represented with arbitrary atomic radii. The latter were refined with DFIX [0.91] commands. Selected contacts and bond lengths [pm]: H1···F1 222(3), H1···F2 236(3), H2···O5 206(3), H3···O3 203(6), H4···O1 205(3), Si1–Si2 234.8(1).

Compound **3** is a rare example combining hydrogen bonding situations towards etheric oxygen atoms, as well as partially silicon substituted oxygen atoms in the same molecule. This enables a comparative analysis of the respective hydrogen bond donating properties of the different oxygen atoms. The hydrogen bonding data for **3** and related compounds-based on the representation in Scheme 1 are presented in Table 1. The respective hydrogen bonding patterns of **3** show no significant divergence between the $O_{(organic)}\cdots H$ and $O_{(Si)}\cdots H$ contacts. Hence, there is no hint of a preference of the etheric oxygen atoms to form hydrogen bonding. The N–H4···O1 contact has a rather short value of 205 pm, but is still in agreement with those in the related compounds. So, it can be assumed that the use of cooperative effects of ether and disilane bridges seems to be an effective way to incorporate guest molecules.

Table 1. Hydrogen bonding geometry in **3**, **4**, and related silicon based systems.

Compound or CSD Refcode [1]	D–H [2]	A	*d* [pm]	T [3]	ω [°]	ϕ [°]	Ref. [4]
3	N–H2	O5	206	C_E	160	113	*
	N–H3	O3	203	C_E	156	108	*
	N–H4	O1	205	C	159	122	*
4	N–H2	O4	214	C_E	165	117	*
	N–H3	O2	209	C_E	151	110	*
	N–H4	O6	200	C	172	118	*
VONMOB	N–H	O	226	C	174	128	[38]
MEQFOD	N–H	O	247	C	141	131	[39]
ITUBUI	N–H	O	198–210	C	157–160	130–132	[40]
MOLYUO	O–H	O	192	Si	167	116	[23]
TAKFOB	O–H	O	257–260	Si	148–152	139–148	[41]
ZEMXAQ	O–H	O	199	Si	156	116	[42]
EGEKAC	O–H	O	199–200	C	155–161	114–115	[43]
PERWIS	O–H	O	199	C	166	123	[44]
REXXAT	O–H	O	199	C	173	111	[45]

[1] Choice of CSD Codes is based on ref. [20]. Geometric criteria for the search were similar to those in ref [21]. CCDC ConQuest Version 1.19 was used for the search; [2] See Scheme 1 for abbreviations; [3] Subscript E denotes that the hydrogen bonding refers to an etheric oxygen atom: two carbon atoms are located next to one oxygen atom; [4] * = published within this work.

The successful incorporation of the ammonium cation in the silicon containing [18]crown-6 ether and its interesting bonding relations prompted us to synthesize another ammonium complex using the similar ligand **2**. Thereby, we obtained compound **4** as a white powder, which was further recrystallized from a mixture of dichloromethane and cyclopentane, yielding colorless rods suitable for single crystal X-ray diffraction analysis (see Figure 2 and Table 2). **4** crystallizes in the monoclinic space group *Cc* and reveals a trapped ammonium cation in the middle of the crown ether cavity bound to every second oxygen atom of the ligand **2**. The $[PF_6]^-$ anion and one molecule of co-crystalline DCM are located above and beneath the ammonium cation. In comparison to compound **3**, the ammonium cation is located closer to the calculated mean plane spanned by the donor atoms of the crown ether with 45 pm in the case of **4** and 59 pm in the case of **3**. The hydrogen bonding geometry of **4** is slightly different to that of **3** because of the rather rigid, *ortho*-bridging phenyl unit (see Table 1). Similar to the $O_{(organic)}\cdots H$ and $O_{(Si)}\cdots H$ in **3**, the respective hydrogen bonding contacts show no significant divergence. However, due to the incorporation of co-crystalline DCM, an intrinsic disorder causes problems with the crystal structure refinement. For this reason, several restraints on distances and anisotropic displacement parameters were used during the refinement. Hence, the hydrogen-bonding situation between the ligand and ammonium cation should be considered carefully and is not discussed in detail as done for **3**. Recrystallization attempts from other solvents failed. Nonetheless, the crystal structure clearly indicates the participation of the silicon bonded oxygen atom regarding hydrogen bonding.

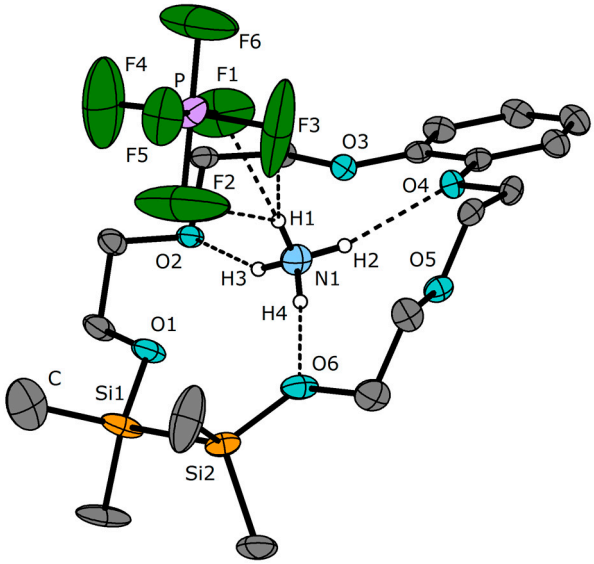

Figure 2. The molecular structure of compound **4** in the solid state. Thermal ellipsoids represent a probability level of 50%. The disordered part of the ligand with a lower occupancy and all carbon bonded hydrogen atoms, as well as the DCM molecule, are omitted for clarity. The hydrogen atoms of the ammonium cation are represented with arbitrary atomic radii. The latter were refined with DFIX [0.91] commands. Selected contacts and bond lengths [pm]: H1···F1 212(4) pm, H1···F2 247(5), H1···F3 279(5), H2···O4 213(6), H3···O2 209(5), H4···O6 200(3), Si1–Si2 233.9(3).

Table 2. X-ray crystallographic data for compounds **3** and **4**·DCM.

	3	**4·DCM**
Empirical formula	$C_{14}H_{36}F_6NO_6PSi_2$	$C_{19}H_{38}Cl_2F_6NO_6PSi_2$
Formula weight [g·mol^{-1}]	515.59	648.55
Crystal colour, shape	colourless block	colourless rod
Crystal size [mm]	0.487 × 0.432 × 0.346	0.076 × 0.106 × 0.522
Crystal system	monoclinic	monoclinic
Space group	$P2_1$	Cc
Formula units	2	4
Temperature [K]	100(2)	100(2)
Unit cell dimensions [Å, °]	a = 10.4542(5) b = 12.3869(6) c = 10.6140(5) β = 117.912(1)	a = 14.9582(7) b = 12.6454(6) c = 16.3325(8) β = 104.950(2)
Cell volume [Å^3]	1214.57(10)	2984.8(2)
ρ calc [g/cm^3]	1.410	1.443
μ [mm^{-1}]	0.286	0.422
2θ range [°]	4.342 to 50.568	4.280 to 53.570
Reflections measured	34532	68974
Independent reflections	4419	6355
R_1 (I > 2σ(I))	0.0203	0.0535
wR_2 (all data)	0.0529	0.1329
GooF	1.076	1.035
Largest diff. peak/hole [e·Å^{-3}]	0.24/−0.27	0.51/−0.44
Flack parameter	0.004(14)	0.048(16)

The interactions between the silicon affected oxygen atoms and the hydrogen atoms of the ammonium cation are further verified by NMR and IR experiments. As observed for the metal complexes of disila-crown ethers, a characteristic downfield shift of the singlet in the $^{29}Si\{^1H\}$ and the

singlet of the $SiMe_2$-groups in the ^1H NMR spectra is observed for both compounds **3** and **4**. The ^{29}Si NMR shift is 13.7 ppm in the case of **3** and 16.2 ppm in the case of **4**. For this reason, both compounds show a dynamic process regarding the H-bonding situation. Rapid exchange results in the described equivalency of the silicon atoms. Even in VT NMR experiments, subsequently cooling the solution to 190 K did not result in an inequivalence of the $SiMe_2$ groups. The respective NMR shifts are in the range of sodium and potassium metal ion complexes of disila-crown ethers [11,14].

The ^1H NMR spectra represent the singlets for the $SiMe_2$ groups at 0.29 (**3**) and 0.30 (**4**) ppm, respectively. For the ammonium cations, triplets were observed at 6.44 ppm for **3** and at 6.64 ppm for **4** in the ^1H NMR spectra. As mentioned above, IR spectroscopic data also indicate an interaction of the ammonium cation with the silicon bonded oxygen atom. In comparison to pure NH_4PF_6, three instead of only one NH stretching vibrations are observed in both compounds. The respective signals are found at 3333 cm^{-1} in NH_4PF_6; 3317, 3188, and 3086 cm^{-1} in **3**; and 3298, 3225, and 3066 cm^{-1} in **4**, comprising a significant red-shift in the coordinated cases [46]. This is in accordance with the solid-state structures found upon single crystal X-ray diffraction analysis, as three different binding modes of the NH_4-related hydrogen atoms are revealed.

3. Materials and Methods

3.1. Laboratory Procedures and Techniques

All working procedures were performed by the use of Schlenk techniques under Ar gas. Solvents were dried and freshly distilled before use. Ammonium hexafluorophosphate was stored and handled under Ar atmosphere using a glovebox of MBRAUN-type. NMR spectra were recorded on a Bruker AV III HD 300 MHz or AV III 500 MHz spectrometer (Bruker, Ettlingen, Germany), respectively. The MestReNova package was used for analyzation [47]. Infrared (IR) spectra of the respective samples were measured using attenuated total reflectance (ATR) mode on a Bruker Model Alpha FT-IR (Bruker, Billerica, MA, USA) stored in the glove box. OPUS-software package was applied throughout [48]. ESI-MS spectrometry was performed with an LTQ-FT (Waltham, MA, USA) and LIFDI-MS with an AccuTOF-GC device (Akishima, Tokyo, Japan). Elemental analysis data cannot be provided due to the presence of fluorine in the samples, which harms the elemental analysis devices.

3.2. Crystal Structures

Single crystal X-ray experiments were carried out using a Bruker D8 Quest diffractometer (Bruker, Billerica, MA, USA) at 100(2) K with Mo Kα radiation and X-ray optics (λ = 0.71073). All structures were solved by direct methods and refinement with full-matrix-least-squares against F^2 using *SHELXT*- and *SHELXL*-2015 on the OLEX2 platform. Crystallographic data for compounds **3** and **4** are denoted as follows: CCDC Nos. 1589283 (**3**), 1589284 (**4**·DCM) [49–51]. Crystallographic information files (CIF, see Supplementary Materials) can be obtained free of charge from the Cambridge Crystallographic Data Centre (CCDC) (link: www.ccdc.cam.ac.uk/data_request/cif). Visualization of all structures was performed with Diamond software package Version 4.4.0 [52]. Thermal Ellipsoids are drawn at the 50% probability level.

3.3. Experimental Section

The sila-crown ethers 1,2-disila[18]crown-6 (**1**) and 1,2-disila-benzo[18]crown-6 (**2**) were synthesized according to methods reported in literature [11,15]. Compounds **3** and **4** were synthesized as follows.

[NH_4(1,2-disila[18]crown-6)]PF_6 (**3**): 106 mg of **1** (0.30 mmol, 1.0 eq) was dissolved in 15 mL of dichloromethane. A total of 59 mg of NH_4PF_6 (1.2 eq, 0.36 mmol) was then added. Stirring the suspension for 72 h gave a cloudy solution, which was filtered followed by the removal of the solvent under reduced pressure. The raw product was washed with 5 mL of *n*-pentane and dried in vacuo. A total of 147 mg of **3** was obtained as a pale white powder in 94% yield. For single crystal growth,

3 was dissolved in dichloromethane and the solvent was removed until saturation of the solution. Cooling to −32 °C yielded colorless blocks after a few days. ^{1}H NMR: (300 MHz, CD_2Cl_2) δ = 0.29 (s, 12H, Si(CH_3)$_2$), 3.55–3.88 (m, 4H, CH_2), 3.64 (s, 12H, CH_2), 3.74–3.76 (m, 4H, CH_2), 6.44 (t, $^{1}J_{NH}$ = 54 Hz, 4H, NH_4) ppm; ^{13}C{^{1}H} NMR: (75 MHz, CD_2Cl_2) δ = −1.2 (s, Si(CH_3)$_2$), 62.9 (s, CH_2), 70.7 (s, CH_2), 70.8 (s, CH_2), 70.9 (s, CH_2), 72.9 (s, CH_2) ppm; ^{19}F NMR: (283 MHz) δ = −72.5 (d, $^{1}J_{PF}$ = 713 Hz, PF_6) ppm; ^{29}Si{^{1}H} NMR: (99 MHz, CD_2Cl_2) δ = 13.7 (s, *Si*(CH_3)$_2$) ppm; ^{31}P NMR: (203 MHz, CD_2Cl_2) δ = −140.3 (hept, $^{1}J_{PF}$ = 713 Hz, PF_6) ppm. MS: LIFDI(+) *m*/*z* (%): 370.20784 [M–PF_6]$^{+}$ (100), IR (cm^{-1}): 3317 + 3188 + 3086 (m, br, $\tilde{\nu}_s$ N–H), 2891 (m), 1453 (m), 1425.98 (m), 1352 (w), 1249 (m), 1097 (s), 1075 (s), 1060 (s), 953 (s) 920 (s), 830 (vs), 791 (vs), 769 (s), 739 (s), 713 (s), 626 (m), 556 (s), 518 (w).

[NH_4(1,2-disila-benzo[18]crown-6)]PF_6 (**4**): 140 mg of **2** (0.35 mmol, 1.0 eq) was dissolved in 10 mL of Dichloromethane. Subsequent addition of 69 mg of NH_4PF_6 (0.35 mmol, 1.0 eq) and stirring of the suspension for three hours yielded a clear solution that was subsequently freed of the solvent. The raw product was well washed with 8 mL of *n*-pentane, followed by drying in vacuo. A total of 200 mg of **4** was obtained as a pale white powder in 95% yield. For single crystal growth, **4** was dissolved in 2 mL of dichloromethane, layered with 15 mL cyclopentane, and finally stored at −32 °C to obtain colorless rods after a few days. ^{1}H NMR: (300 MHz, CD_2Cl_2) δ = 0.30 (s, 12H, Si(CH_3)$_2$), 3.63–3.71 (m, 4H, CH_2), 3.74–3.83 (m, 4H, CH_2), 3.85–3.95 (m, 4H, CH_2), 4.15–4.23 (m, 4H, CH_2), 6.64 (t, $^{1}J_{NH}$ = 54 Hz, 4H, NH_4) ppm; 6.86–7.04 (m, 4H, C_6H_4). ^{13}C{^{1}H} NMR: (75 MHz, CD_2Cl_2) δ = 2.5 (s, Si(CH_3)$_2$), 62.02 (s, CH_2), 68.6 (s, CH_2), 69.6 (s, CH_2), 72.8 (s, CH_2), 113.6 (s, C_{Ar}H), 122.4 (s, C_{Ar}H), 148.3 (s, $C_{Ar,\,q}$) ppm; ^{19}F NMR: (283 MHz) δ = −72.9 (d, $^{1}J_{PF}$ = 712 Hz, PF_6) ppm; ^{29}Si{^{1}H} NMR: (99 MHz, CD_2Cl_2) δ = 16.2 (s, Si(CH_3)$_2$) ppm; ^{31}P NMR (203 MHz, CD_2Cl_2): −143.8 (hept, $^{1}J_{PF}$ = 713 Hz, PF_6) ppm. MS: ESI(+) *m*/*z* (%): 418.2080 [M–PF_6]$^{+}$ (100), IR (cm^{-1}): 3298, 3225, 3066 (m, br, $\tilde{\nu}_s$ N–H), 2946 (m), 2878 (m), 1594 (w), 1505 (m), 1454 (m), 1425 (m), 1249 (s), 1209 (s), 1121 (m) 1069 (s), 957 (m), 830 (vs), 791 (vs), 765 (vs), 738 (vs), 632 (w), 555 (vs).

4. Conclusions

In this work, the incorporation of guest molecules into disilane-bearing crown ethers was discussed. The complexation of ammonium cations by the ligands **1** and **2** turned out to be successful. Within the respective complexes **3** and **4**, H-bonding between a silicon affected oxygen atom and the ammonium cation was purposefully realized. So far, related H-bonding was only observed as an occasional occurrence in solid-state structures. In addition, $O_{(organic)}\cdots H$ and $O_{(Si)}\cdots H$ contacts show no significant divergence on a structural level. Hence, there is no hint for a preference of the etheric oxygen atoms to form hydrogen bonding. The interaction of the protons related to the ammonium cation with the silicon affected oxygen atoms was verified by NMR- and IR-spectroscopic experiments. It can be concluded that the use of cooperative effects of ethylene and disilane bridges is an effective way to incorporate guest molecules. We are currently aiming for the synthesis of all-disilane substituted crown ether analogs. Systems of the type SiSi–O–SiSi will help advance our understanding of the siloxane linkage in combination with hydrogen bonding.

Supplementary Materials: The following are available online at www.mdpi.com/2304-6740/6/1/15/s1, Cif and cif-checked files.

Acknowledgments: This work was financially supported by the Deutsche Forschungsgemeinschaft (DFG). Fabian Dankert gratefully acknowledges the kind advice and meticulous data collection of Michael Marsch (X-ray department, Philipps-University Marburg). Fabian Dankert further thanks N. Mais for his help with synthetic work.

Author Contributions: Fabian Dankert performed the synthesis and analytics of compound **4**, interpretations of all the analytical data, contributed to the X-ray crystallographic refinement, and wrote the manuscript. Kirsten Reuter performed the synthesis of compound **3** and the collection of the respective analytical data. Carsten Donsbach accomplished the crystal structure solution and refinement of compound **4**. Carsten von Hänisch contributed to the interpretation and manuscript preparation and led the overarching research project.

Conflicts of Interest: The authors declare no conflict of interest.

References

1. Weinhold, F.; West, R. The nature of the silicon–oxygen bond. *Organometallics* **2011**, *30*, 5815–5824. [CrossRef]
2. Weinhold, F.; West, R. Hyperconjugative Interactions in Permethylated Siloxanes and Ethers: The Nature of the SiO Bond. *J. Am. Chem. Soc.* **2013**, *135*, 5762–5767. [CrossRef] [PubMed]
3. Ritch, J.S.; Chivers, T. Siliciumanaloga von Kronenethern und Cryptanden: Ein neues Kapitel in der Wirt-Gast-Chemie? *Angew. Chem.* **2007**, *119*, 4694–4697. [CrossRef]
4. Shambayati, S.; Blake, J.F.; Wierschke, S.G.; Jorgensen, W.L.; Schreiber, S.L. Structure and Basicity of Silyl Ethers: A Crystallographic and ab Initio Inquiry into the Nature of Silicon–Oxygen Interactions. *J. Am. Chem. Soc.* **1990**, *112*, 697–703. [CrossRef]
5. Cypryk, M.; Apeloig, Y. Ab Initio Study of Silyloxonium Ions. *Organometallics* **1997**, *16*, 5938–5949. [CrossRef]
6. Gillespie, R.J.; Robinson, E. Models of molecular geometry. *Chem. Soc. Rev.* **2005**, *34*, 396–407. [CrossRef] [PubMed]
7. Passmore, J.; Rautiainen, J.M. On The Lower Lewis Basicity of Siloxanes Compared to Ethers. *Eur. J. Inorg. Chem.* **2012**, *2012*, 6002–6010. [CrossRef]
8. Cameron, T.S.; Decken, A.; Krossing, I.; Passmore, J.; Rautiainen, J.M.; Wang, X.; Zeng, X. Reactions of a Cyclodimethylsiloxane $(Me_2SiO)_6$ with Silver Salts of Weakly Coordinating Anions; Crystal Structures of $[Ag(Me_2SiO)_6][Al]$ ([Al] = $[FAl\{OC(CF_3)_3\}_3]$, $[Al\{OC(CF_3)_3\}_4]$) and Their Comparison with $[Ag(18\text{-Crown-}6)]_2[SbF_6]_2$. *Inorg. Chem.* **2013**, *52*, 3113–3126. [CrossRef] [PubMed]
9. Ouchi, M.; Inoue, Y.; Kanzaki, T.; Hakushi, T. Ring-contracted Crown Ethers: 14-Crown-5, 17-Crown-6, and Their Sila-analogues. Drastic Decrease in Cation-binding Ability. *Bull. Chem. Soc. Jpn.* **1984**, *57*, 887–888. [CrossRef]
10. Inoue, Y.; Ouchi, M.; Hakushi, T. Molecular Design of Crown Ethers. 3. Extraction of Alkaline Earth and Heavy Metal Picrates with 14- to 17-Crown-5 and 17- to 22-Crown-6. *Bull. Chem. Soc. Jpn.* **1985**, *58*, 525–530. [CrossRef]
11. Reuter, K.; Buchner, M.R.; Thiele, G.; von Hänisch, C. Stable Alkali-Metal Complexes of Hybrid Disila-Crown Ethers. *Inorg. Chem.* **2016**, *55*, 4441–4447. [CrossRef] [PubMed]
12. Reuter, K.; Thiele, G.; Hafner, T.; Uhlig, F.; von Hänisch, C. Synthesis and coordination ability of a partially silicon based crown ether. *Chem. Commun.* **2016**, *52*, 13265–13268. [CrossRef] [PubMed]
13. Reuter, K.; Rudel, S.S.; Buchner, M.R.; Kraus, F.; von Hänisch, C. Crown ether complexes of alkali metal chlorides from SO_2. *Chem. Eur. J.* **2017**, *23*, 9607–9617. [CrossRef] [PubMed]
14. Reuter, K.; Dankert, F.; Donsbach, C.; von Hänisch, C. Structural Study of Mismatched Disila-Crown Ether Complexes. *Inorganics* **2017**, *5*, 11. [CrossRef]
15. Dankert, F.; Reuter, K.; Donsbach, C.; von Hänisch, C. A structural study of alkaline earth metal complexes with hybrid disila-crown ethers. *Dalton Trans.* **2017**, *46*, 8727–8735. [CrossRef] [PubMed]
16. West, R.; Whatley, L.S.; Lake, K.J. Hydrogen Bonding Studies. V. The Relative Basicities of Ethers, Alkoxysilanes and Siloxanes and the Nature of the Silicon–Oxygen Bond. *J. Am. Chem. Soc.* **1961**, *83*, 761–764. [CrossRef]
17. West, R.; Wilson, L.S.; Powell, D.L. Basicity of siloxanes, alkoxysilanes and ethers toward hydrogen bonding. *J. Organomet. Chem.* **1979**, *178*, 5–9. [CrossRef]
18. Popowski, E.; Schulz, J.; Feist, K.; Kelling, H.; Jancke, H. Basizität und 29Si-NMR-spektroskopische Untersuchungen von Ethoxysiloxanen. *Z. Anorg. Allg. Chem.* **1988**, *558*, 206–216. [CrossRef]
19. Yilgör, E.; Burgaz, E.; Yurtsever, E.; Yilgör, I. Comparison of hydrogen bonding in polydimethylsiloxane and polyether based urethane and urea copolymers. *Polymer* **2000**, *41*, 849–857. [CrossRef]
20. Jeffrey, G.A. *An Introduction to Hydrogen Bonding*; Oxford University Press: Oxford, UK, 1997.
21. Grabowsky, S.; Beckmann, J.; Luger, P. The Nature of Hydrogen Bonding Involving the Siloxane Group. *Aust. J. Chem.* **2012**, *65*, 785–795. [CrossRef]
22. Frolov, Y.L.; Voronkov, M.G.; Strashnikova, N.V.; Shergina, N.I. Hydrogen bonding involving the siloxane group. *J. Mol. Struct.* **1992**, *270*, 205–215. [CrossRef]
23. Grabowsky, S.; Hesse, M.F.; Paulmann, C.; Luger, P.; Beckmann, J. How to Make the Ionic Si–O Bond More Covalent and the Si–O–Si Linkage a Better Acceptor for Hydrogen Bonding. *Inorg. Chem.* **2009**, *48*, 4384–4393. [CrossRef] [PubMed]

24. Behr, J.P.; Dumas, P.; Moras, D. The H_3O^+ Cation: Molecular Structure of an Oxonium-Macrocyclic Polyether Complex. *J. Am. Chem. Soc.* **1982**, *104*, 4540–4543. [CrossRef]
25. Atwood, J.L.; Bott, S.G.; Means, C.M.; Coleman, A.W.; Zhang, H.; May, M.T. Synthesis of salts of the hydrogen dichloride anion in aromatic solvents. 2. Syntheses and crystal structures of [K·18-crown-6][Cl–H–Cl], [Mg·18-crown-6][Cl–H–Cl]$_2$, [H_3O·18-crown-6][Cl–H–Cl], and the Related [H_3O·18-crown-6][Br–H–Br]. *Inorg. Chem.* **1990**, *29*, 467–470. [CrossRef]
26. Atwood, J.L.; Bott, S.G.; Robinson, K.D.; Bishop, E.J.; May, M.T. Preparation and X-ray structure of [H_3O^+ ·18-crown-6]-[($H_5O_2^+$)(Cl^-)$_2$], a compound containing both H_3O^+ and $H_5O_2^+$ crystallized from aromatic solution. *J. Crystallogr. Spectrosc. Res.* **1991**, *21*, 459–462. [CrossRef]
27. Atwood, J.L.; Junk, P.C.; May, M.T.; Robinson, K.D. Synthesis and X-ray structure of [H_3O^+ · 18-crown-6] [Br–Br–Br^-]; a compound containing both H_3O^+ and a linear and symmetrical Br_3^- ion crystallized from aromatic solution. *J. Chem. Crystallogr.* **1994**, *24*, 243–245. [CrossRef]
28. Saleh, M.I.; Kusrini, E.; Fun, H.-K.; Teh, J.B.-J. Dicyclohexano-18-crown-6 hydroxonium tribromide. *Acta Cryst.* **2007**, *E63*, o3790–o3791. [CrossRef]
29. Kloo, L.; Svensson, P.H.; Taylor, M.J. Investigations of the polyiodides $H_3O{\cdot}I_x$ (x = 3, 5 or 7) as dibenzo-18-crown-6 complexes. *J. Chem. Soc. Dalton Trans.* **2000**, 1061–1065. [CrossRef]
30. Cheng, M.; Liu, X.; Luo, Q.; Duan, X.; Pei, C. Cocrystals of ammonium perchlorate with a series of crown ethers: Preparation, structures, and properties. *CrystEngComm* **2016**, *18*, 8487–8496. [CrossRef]
31. Feinberg, H.; Columbus, I.; Cohen, S.; Rabinovitz, M.; Shoham, G.; Selig, H. Crystallographic evidence for different modes of interaction of BF_3/BF_4^- species with water molecules and 18-crown-6. *Polyhedron* **1993**, *12*, 2913–2919. [CrossRef]
32. Dapporto, P.; Paoli, P.; Matijašić, I.; Tušek-Božić, L. Crystal structures of complexes of ammonium and potassium hexafluorophosphate with dibenzo-18-crown-6. Molecular mechanics studies on the uncomplexed macrocycle. *Inorg. Chim. Acta* **1996**, *252*, 383–389. [CrossRef]
33. Ponomarova, V.V.; Rusanova, J.A.; Rusanov, E.B.; Domasevitch, K.V. Unusual centrosymmetric structure of [M(18-crown-6)]$^+$ (M = Rb, Cs and NH_4) complexes stabilized in an environment of hexachloridoantimonate(V) anions. *Acta Crystallogr. Sect. C Struct. Chem.* **2015**, *71*, 867–872. [CrossRef] [PubMed]
34. Hurd, D.T. On the Mechanism of the Acid-catalyzed Rearrangement of Siloxane Linkages in Organopolysiloxanes. *J. Am. Chem. Soc.* **1955**, *77*, 2998–3001. [CrossRef]
35. Cypryk, M.; Apeloig, Y. Mechanism of the Acid-Catalyzed Si–O Bond Cleavage in Siloxanes and Siloxanols. A Theoretical Study. *Organometallics* **2002**, *21*, 2165–2175. [CrossRef]
36. Wu, D.H.; Wu, Q.Q. Ammonium hexafluoridophosphate-18-crown-6 (1/1). *Acta Crystallogr. Sect. E Struct. Rep. Online* **2010**, *66*, 2–9. [CrossRef] [PubMed]
37. Shephard, D.S.; Zhou, W.; Maschmeyer, T.; Matters, J.M.; Roper, C.L.; Parsons, S.; Johnson, B.F.G.; Duer, M.J. Ortsspezifische Derivatisierung von MCM-41: Molekulare Erkennung und Lokalisierung funktioneller Gruppen in mesoporösen Materialien durch hochauflösende Transmissionselektronenmikroskopie. *Angew. Chem.* **1998**, *110*, 2847–2851. [CrossRef]
38. Kociok-Köhn, G.; Molloy, K.C.; Price, G.J.; Smith, D.R.G. Structural characterisation of trimethylsilyl-protected DNA bases. *Supramol. Chem.* **2008**, *20*, 697–707. [CrossRef]
39. Ha, H.-J.; Choi, C.-J.; Ahn, Y.-G.; Yun, H.; Dong, Y.; Lee, W.K. Cycloaddition of Lewis Acid-Induced *N*-Methyleneanilines as Azadienes to 1,2-Bistrimethylsilyloxycyclobutene and Oxidative Ring Expansion to 1,2,4,5-Tetrahydro-1-benzazocine-3,6-diones. *J. Org. Chem.* **2000**, *65*, 8384–8386. [CrossRef] [PubMed]
40. Becker, B.; Baranowska, K.; Chojnacki, J.; Wojnowski, W. Cubane-like structure of a silanethiol—Primary amine assembly—A novel, unusual hydrogen bond pattern. *Chem. Commun.* **2004**, 620–621. [CrossRef] [PubMed]
41. Polishchuk, A.P.; Makarova, N.N.; Astapova, T.V. X-ray diffraction investigation of *trans*-2,8-dihydroxy-2,8-diphenyl-4,4′,6,6′,10,10′, 12,12′-octamethylcyclohexasiloxane and *trans*-2,8-dihydroxy-2,4,4′,6,6′,8,10,10′, 12,12′-decamethyl-5-carbahexacyclosiloxane. *Crystallogr. Rep.* **2002**, *47*, 798–804. [CrossRef]
42. Spielberger, A.; Gspaltl, P.; Siegl, H.; Hengge, E.; Gruber, K. Syntheses, structures and properties of dihydroxypermethylcyclosilanes and permethyloxahexasilanorbornanes. *J. Organomet. Chem.* **1995**, *499*, 241–246. [CrossRef]

43. Driver, T.G.; Franz, A.K.; Woerpel, K.A. Diastereoselective Silacyclopropanations of Functionalized Chiral Alkenes. *J. Am. Chem. Soc.* **2002**, *124*, 6524–6525. [CrossRef] [PubMed]
44. Myers, A.G.; Dragovich, P.S. A Reaction Cascade Leading to 1,6-didehydro[10]annulene → 1,5-dehydronaphthalene Cyclization Initiated by Thiol Addition. *J. Am. Chem. Soc.* **1993**, *115*, 7021–7022. [CrossRef]
45. Veith, M.; Rammo, A. Synthese und Struktur eines neuartigen molekularen λ^5-Organospirosilikats und dessen dynamisches Verhalten in Lösung. *J. Organomet. Chem.* **1996**, *521*, 429–433. [CrossRef]
46. Heyns, A.M.; van Schalkwyk, G.J. A study of the infrared and Raman spectra of ammonium hexafluorophosphate NH_4PF_6 over a wide range of temperatures. *Spectrochim. Acta Part A Mol. Spectrosc.* **1973**, *29*, 1163–1175. [CrossRef]
47. Willcott, M.R. MestRe Nova. *J. Am. Chem. Soc.* **2009**, *131*, 13180. [CrossRef]
48. *OPUS*; Version 7.2; Bruker Opt. GmbH: Ettlingen, Germany, 2012.
49. Sheldrick, G.M. *SHELXT*—Integrated space-group and crystal-structure determination. *Acta Crystallogr. Sect. A Found. Adv.* **2015**, *71*, 3–8. [CrossRef] [PubMed]
50. Sheldrick, G.M. Crystal structure refinement with *SHELXL*. *Acta Crystallogr. Sect. C Struct. Chem.* **2015**, *71*, 3–8. [CrossRef] [PubMed]
51. Dolomanov, O.V.; Bourhis, L.J.; Gildea, R.J.; Howard, J.A.K.; Puschmann, H. *OLEX2*: A complete structure solution, refinement and analysis program. *J. Appl. Crystallogr.* **2009**, *42*, 339–341. [CrossRef]
52. *Diamond*; Version 4.4.1; Crystal and Molecular Structure Visualization; Putz, H. & Brandenburg, K. GbR: Bonn, Germany, 2017.

© 2018 by the authors. Licensee MDPI, Basel, Switzerland. This article is an open access article distributed under the terms and conditions of the Creative Commons Attribution (CC BY) license (http://creativecommons.org/licenses/by/4.0/).

CrystEngComm

PAPER

View Article Online
View Journal | View Issue

Check for updates

Cite this: *CrystEngComm*, 2018, **20**, 5370

Sila-polyethers as *innocent* crystallization reagents for heavy alkali metal compounds†

Fabian Dankert, Johanna Heine, Julia Rienmüller and Carsten von Hänisch *

In this study, we report on a novel approach for the crystallization of previously elusive rubidium and caesium salts. Stirring alkali metal salts in dichloromethane together with sila-polyethers such as 8,9-disila-EO5 (**1**) (EO5 = pentaethylene glycol), 11,12-disila-EO7 (**2**) (EO7 = heptaethylene glycol) and 1,2,10,11-tetrasila[18]crown-6 (**3**) under an inert-gas atmosphere yields crystalline materials of the respective salts suitable for single crystal diffraction analysis. This allowed the single crystal structure determination of the salts MOTf (M = Rb^+, Cs^+ and OTf = $CF_3SO_3^-$) and Cs_2Ox (Ox = $C_2O_4^{2-}$) whose structures had previously been solved from powder diffraction data. In contrast, the use of all-carbon polyethers like [18]crown-6 and EO5 under similar reaction conditions yields coordination compounds of the respective salts such as [M([18]crown-6)OTf], [Rb_3(EO5)OTf_3] (**5**) and [Cs(EO5)OTf] (**6**). This lets us conclude that it is the sila group in the polyethers that allows these ligands to act as a very efficient crystallization aid without being included in the final compound.

Received 4th July 2018,
Accepted 12th August 2018

DOI: 10.1039/c8ce01097h

rsc.li/crystengcomm

Published on 23 August 2018. Downloaded by University of Marburg on 4/3/2020 2:12:38 PM.

Introduction

The coordination chemistry of silicon-based ligands has been intensely discussed in the past years and is still a subject of ongoing research.[1] With respect to recent publications, the coordination ability of this kind of ligand is better than previously thought. Disilane-bearing systems are able to form stable complexes with alkali and alkaline earth metal salts. Compounds consisting of $[M_A(L)]^+$ and $[M_{EA}(L)]^{2+}$ cations and different anions were characterized (M_A = Li^+–K^+ and M_{EA} = Mg^{2+}–Ba^{2+}, L = 1,2-disila[3*n*]crown-*n* {*n* = 4–6}, 1,2,4,5-tetrasila[12]crown-4, 1,2,7,8-tetrasila[12]crown-4 or 1,2-disilabenzo[18]crown-6).[2–4]

The coordination ability of these systems in comparison with their all-carbon counterparts turned out to be on even terms. However, at this point no stable complexes of rubidium and caesium salts and sila-polyethers could be obtained. In our recent findings on the coordination chemistry of disila-bridged polyethylene glycols, we concluded that this type of ligand is effective for the coordination of hard cations.[5] According to DFT (DFT = density functional theory) calculations, it was shown that hard cations have a significant influence on the bonding situation in the siloxane linkage. Soft cations, however, show only weak interactions with the siloxane linkage and consequently, the attempt to complex CsOTf (OTf = $CF_3SO_3^-$) with 11,12-disila-EO7 (EO7 = heptaethylene glycol) failed. Unexpectedly, single crystals of CsOTf grew out of the solvent-free ligand after workup procedures. This is surprising, as the single crystal growth of anhydrous alkali metal triflates and similar anions such as oxalate is described to be very difficult due to disorder problems, the hygroscopic nature of the anions and poor crystal quality in general.[6–8] For example, no single crystal structure determination for RbOTf, CsOTf and Cs_2Ox could be performed, but instead Jansen and coworkers solved the crystal structures from powder diffraction data.[6–8] In this work, we show that the sila-polyethers 8,9-disila-EO5 (**1**) (EO5 = pentaethylene glycol), 11,12-disila-EO7 (**2**) (EO7 = heptaethylene glycol) and 1,2,10,11-tetrasila[18]crown-6 (**3**), shown in Scheme 1a and c, can be used as effective crystallization reagents for these

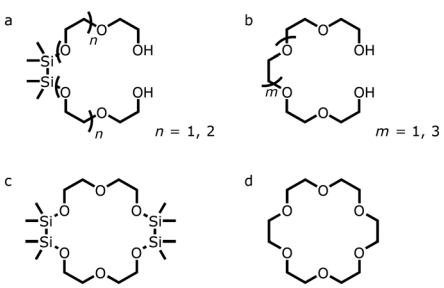

Scheme 1 Sila-ligands used in this work and their organic counterparts. a: 8,9-disila-EO5 for *n* = 1 (**1**), 11,12-disila-EO7 for *n* = 2 (**2**), b: EO5 for *m* = 1 and EO7 for *m* = 3, c: 1,2,10,11-tetrasila[18]crown-6 and d: [18]crown-6.

Fachbereich Chemie and Wissenschaftliches Zentrum für Materialwissenschaften (WZMW), Philipps-Universität Marburg, Hans-Meerwein-Straße 4, D-35032, Marburg, Germany. E-mail: haenisch@chemie.uni-marburg.de

† Electronic supplementary information (ESI) available. CCDC 1852230 (5). CSD 434771–434774. For ESI and crystallographic data in CIF or other electronic format see DOI: 10.1039/c8ce01097h

This journal is © The Royal Society of Chemistry 2018

Published on 23 August 2018. Downloaded by University of Marburg on 4/3/2020 2:12:38 PM.

elusive salts. Similar to a chemical transport agent used in a solid state reaction, sila-polyethers allow for the partial dissolution and recrystallization of the salts without being included in the product (see Scheme 2).

In contrast to this, the use of analogous all-carbon polyethers (Scheme 1b and d) leads to the compounds [M([18]crown-6)OTf], $[Rb_3(EO5)OTf_3]$ (**5**) and [Cs(EO5)OTf] (**6**), where the alkali metal cations are complexed with the polyether.

Results and discussion

Synthesis of sila-polyethers

Silicon-based ligands bearing disilane units are generally synthesized by combining 1,1,2,2-tetramethyl-1,2-dichlorodisilane, the appropriate amount of glycol and triethylamine as a base.

The synthesis of 8,9-disila-EO5 (EO5 = pentaethylene glycol) (**1**) and 11,12-disila-EO7 (EO7 = heptaethylene glycol) (**2**) has been published in an earlier work.[5] 1,2,10,11-Tetrasila-[18]crown-6 (**3**) along with 1,2-disila[9]crown-3 (**4**) is synthesized from EO2 (EO2 = diethylene glycol) and 1,1,2,2-tetramethyl-1,2-dichlorodisilane (see Scheme 3). Both ligands are obtained as viscous oils. After condensing the volatile substance **4**, both compounds can be isolated separately.

General procedure for the re-crystallization of rubidium and caesium salts using sila-polyethers

The re-crystallization process is performed by adding a silicon-based ligand (**1**, **2** or **3**) to a suspension of the salt in dichloromethane and subsequent stirring of the suspension under an inert gas atmosphere. Depending on the chosen salt and ligand, the interaction differs slightly. However, all workup procedures allowed us to obtain single crystals of the selected salts (see the Experimental section). For example, RbOTf is stirred for 70 min in dichloromethane together with 1,2,10,11-disila[18]crown-6. Only a fraction of the salt dissolves within this period, but nevertheless single crystals of α-RbOTf are formed among the powder and can be isolated for single crystal X-ray diffraction. RbOTf, CsOTf and Cs_2Ox are also slightly soluble in pure DCM (DCM = dichloromethane), but only microcrystalline powders can be obtained from recrystallization attempts without any sila-polyether. A similar behaviour was also observed in previous

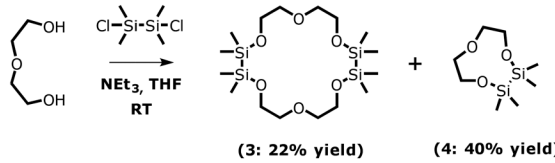

Scheme 3 Synthesis of the disilane-substituted crown ether analogues 1,2,10,11-tetrasila[18]crown-6 (**3**) and 1,2-disila[9]crown-3 (**4**).

works as the compounds $MCl{\cdot}3SO_2$ ($M = Rb^+$, Cs^+) can be obtained as single crystals from liquid sulphur dioxide using a sila-crown ether as a crystallization auxiliary.[9]

The crystal structures of α-MOTf (M = Rb, Cs)

Using crystals grown from a melt, Jansen and coworkers also determined the crystal structure of RbOTf *via* single crystal diffraction analysis. But due poor crystal quality, a subsequent refinement did not converge to an acceptable *R* value and high-resolution X-ray powder diffraction data were used to validate the single crystal structure.[6] In this work, single crystals of α-RbOTf were obtained using sila-polyethers as crystallization reagents. Colourless platelets (see Fig. 1: left) were investigated *via* single crystal diffraction analyses and the powder data of the group of Jansen could be affirmed (see the ESI† for details). α-RbOTf crystallizes in the monoclinic space group *Cm* (no. 8) with $a = 19.2895(8)$ Å, $b = 23.4587(9)$ Å, $c = 5.0673(2)$ Å, $\beta = 100.992(2)°$, $V = 2250.92(16)$ Å^3 and $Z = 4$. Investigating the crystal structure of different CsOTf phases, Jansen and coworkers had experienced similar difficulties in growing single crystals as for the rubidium salt and subsequently solved and refined the structures from high resolution X-ray powder diffraction data collected from a synchrotron light source.[7]

Using sila-polyethers, we were able to grow good quality, trapezoid-like single crystals (see Fig. 1: right) of α-CsOTf (see the ESI† for details). In this case, we were not only able to affirm the general findings of the previous study, but could also expand upon them. Single crystal structure analysis allowed us to determine that α-CsOTf crystallizes in the monoclinic space group $P2_1/n$ (no. 14) with $a = 5.4549(6)$ Å, $b = 6.0582(4)$ Å, $c = 18.339(2)$ Å and $\beta = 91.022(9)°$, $V = 605.71(10)$ Å^3 and $Z = 4$, a superstructure, doubled in *c*, of the

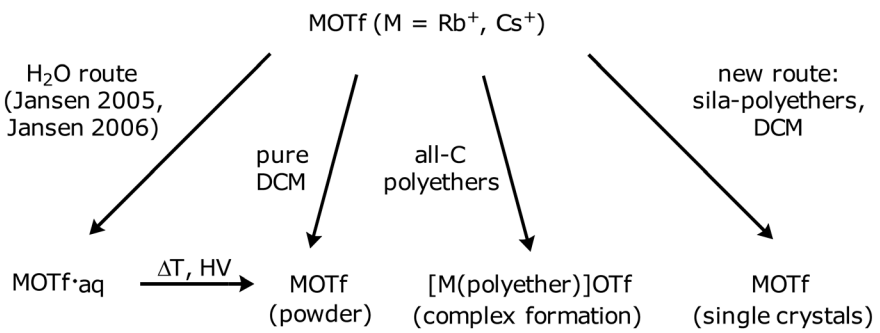

Scheme 2 Preparation and crystallization attempts for heavy alkali metal triflates.

Published on 23 August 2018. Downloaded by University of Marburg on 4/3/2020 2:12:38 PM.

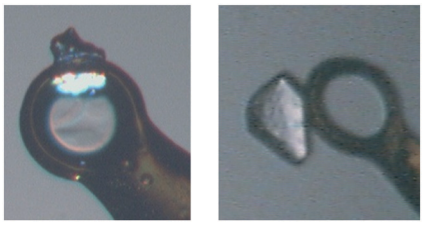

Fig. 1 Single crystals of heavy alkali metal triflates. Left: Colourless platelet of RbOTf and right: trapezoid-like crystal of CsOTf. Snaps recorded on an IPDS2T or IPDS2 diffractometer, respectively using X-AREA and applications therein.

crystal structure originally reported by Jansen. Fig. 2 shows the asymmetric unit of our determination of α-CsOTf as well as the coordination sphere of the cesium cation.

A side-by-side comparison of excerpts of the original structure and our structure is displayed in Fig. 3. As can be seen, the superstructure allows for two different orientations of the OTf^- anions. This results in slight differences in the Cs coordination environment and other structural details (see the ESI†). But, originating from the light atom part of the crystal structure, the superstructure reflections are very weak, as a simulation of the powder patterns from both the original and the new structure determination shows (Fig. 4). To exclude the observation that the superstructure is a result of the measurement at 100 K, we determined the single crystal structure at room temperature (see the ESI† for details). No significant differences between both structures can be observed, showing that no phase transition occurs in CsOTf between 100 K and room temperature. In the end, we cannot exclude the fact that the crystallization method in our case has produced a different polymorph of CsOTf than that found by Jansen, but it is likely that the additional level of detail we found was simply unavailable even from high quality powder data.

The crystal structure of Cs_2Ox

Besides the triflate anions, the oxalate anion was chosen to illustrate that salts of various anions can be recrystallized.

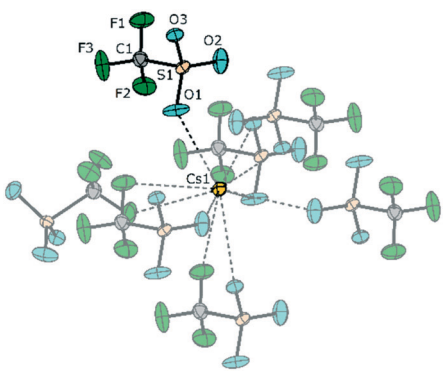

Fig. 2 Asymmetric unit of α-CsOTf and the Cs^+ coordination sphere as determined by single crystal X-ray diffraction analysis at 100 K (this work). Transparent triflate groups are symmetry-generated. Thermal ellipsoids shown at the 50% probability level.

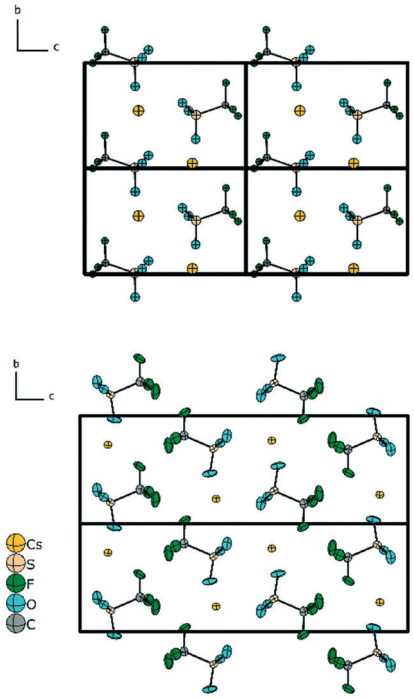

Fig. 3 Excerpts of the crystal structure of α-CsOTf (top) solved in $P2_1$ (Jansen's work)[7] and (bottom) solved in $P2_1/n$ in a supercell doubled along the *c* axis (this work).

Colourless blocks were investigated *via* single crystal diffraction analyses and the powder data of the group of Jansen could be validated with suitable *R* values (selected crystals as can be seen in Fig. 5). The crystals showed cell parameters similar to those reported previously.[8] The compound crystallizes in the monoclinic space group $P2_1/c$ (no. 14) with a = 6.5506(4) Å, b = 10.8879(6) Å, c = 8.5685(6) Å, β = 97.405(2)°, V = 606.03(7) Å^3 and Z = 4 (Fig. 6). At this point, it should be noted that the triflates and oxalates described here are highly sensitive to moisture. After the crystal preparation and single

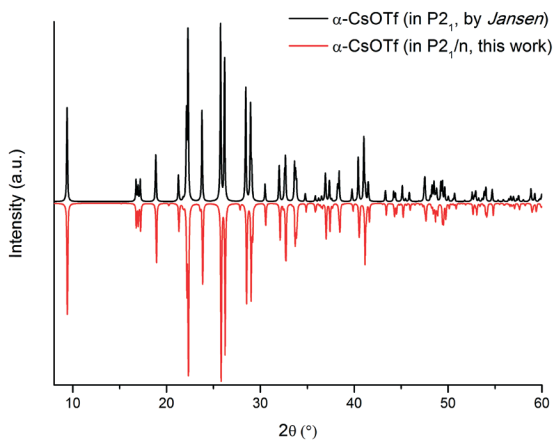

Fig. 4 Simulation of the powder patterns of α-CsOTf from Jansen's original structure determination[7] and from the single crystal structure determination in this work. Very weak superstructure reflections can be discerned in the second dataset, for example, at 20° and 28°.

This journal is © The Royal Society of Chemistry 2018

Published on 23 August 2018. Downloaded by University of Marburg on 4/3/2020 2:12:38 PM.

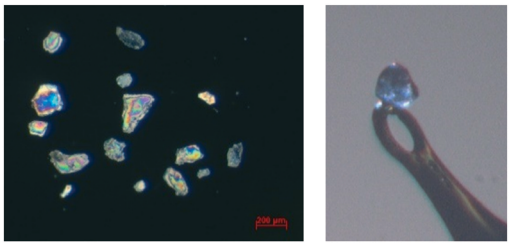

Fig. 5 A selection of block-shaped single crystals of Cs_2Ox (left; recorded with a Zeiss Discovery V8 microscope using a Zeiss AxioCam and the AxioVs40×64 V4.9.1 software package) and a single crystal suitable for XRD (right; recorded on a STOE IPDS2T diffractometer using X-AREA and applications therein).

crystal diffraction experiment for Cs_2Ox, we looked at the single crystals we stored in oil for preservation. Even though the crystals were stored in inert oil, a few colourless rods had formed which were not observed before. The rods turned out to be the literature-known compound $Cs_2Ox{\cdot}H_2O$.[10]

This finding may help to explain some of the difficulties experienced in previous attempts to obtain single crystals of these compounds, as they typically involved a dehydration step after an aqueous synthesis procedure. It also underlines the advantage of using our non-aqueous re-crystallization route to obtain single crystals of these highly sensitive compounds.

Interaction of rubidium and caesium salts with all-carbon polyethers

One remaining question is of course whether it is strictly necessary to use sila-polyethers for our re-crystallization method when all-carbon polyethers like [18]crown-6 and EO5 are readily available from commercial sources. For crown-ethers, complex formation with rubidium and caesium cations is well known, for example, in the complexes [M([18]crown-6)OTf] (M = Rb^+, Cs^+) both of which are monomeric contact ion pairs.[11] Numerous other crown ether complexes of rubidium and caesium salts are known, but complexes of open chain polyether ligands are highly limited, including rare examples of complexes of a ferulic acid derivative and glymes.[12–14]

However, with respect to the triflate anion we decided to investigate the ligand behaviour of EO5 towards RbOTf and CsOTf in order to demonstrate that sila-polyethers have to be used rather than all-carbon polyether ligands. The reaction of one equivalent of EO5 and RbOTf in DCM leads to rapid dissolution of the salt among thinly dispersed powder. After workup procedures, single crystals were obtained in the shape of colourless platelets. In this case, no crystals of α-RbOTf were obtained but the trinuclear complex $[Rb_3(EO5)OTf_3]$ (5) (see Fig. 7). This compound reveals three crystallographically different rubidium atoms within the asymmetric unit. The coordination numbers vary, with nine for Rb1 and eight for Rb2 and Rb3, respectively. The respective coordination patterns are displayed in Fig. 8.

As shown in the molecular structure, the compound can be divided into three parts. The three crystallographically different rubidium atoms share interaction with the EO5 molecule as the triflate groups saturate the metal ions. All three rubidium atoms display almost the same Rb–O distances with 289.9(2)–3.296(3) pm for Rb1, 282.4(2)–314.4(2) pm for Rb2 and 283.9(2)–314.7(2) pm for Rb3. This does overall compare very well with those distances reported previously (see Table 1). The Rb2–O11 distance of 3.601 pm should be considered as a weak contact. Such a long Rb–O contact was also observed in [Rb(FAD)pic] (FAD = ferulic acid derivative; pic = picrate $\{C_6H_2N_3O_7^-\}$) which has a length of 356.2 pm.[12]

The Rb–O distances depend on several factors such as the coordination number of the central ion, the donor strength and the steric demand of co-ligands. Common for this kind of compound, the triflate anions find themselves in a staggered arrangement with C_{3v} symmetry. As this coordination compound of RbOTf and EO5 clearly indicates the preference to form a stable complex, we also repeated the experiment

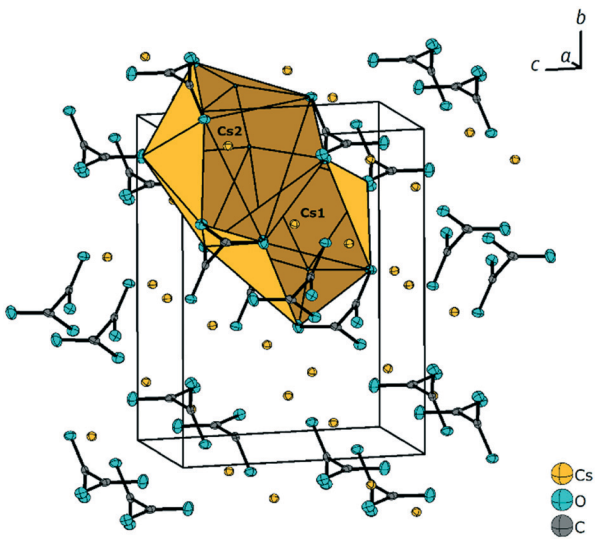

Fig. 6 Excerpt of the crystal structure of Cs_2Ox and illustration of the caesium coordination spheres. Thermal ellipsoids shown at the 50% probability level.

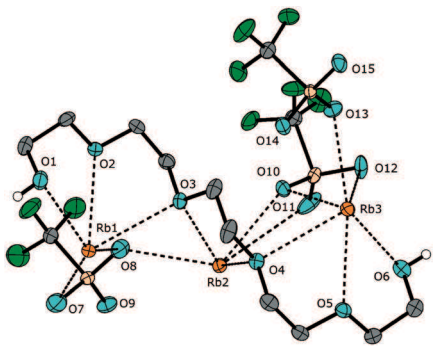

Fig. 7 The molecular structure of $[Rb_3(EO_5)OTf_3]$ in the crystal as determined by single crystal X-ray diffraction analysis. Thermal ellipsoids shown at the 50% probability level. Hydrogen atoms were treated with DFIX [0.83] commands.

Published on 23 August 2018. Downloaded by University of Marburg on 4/3/2020 2:12:38 PM.

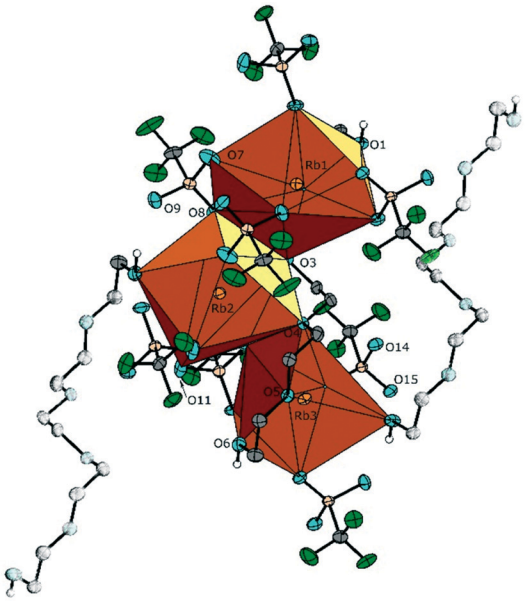

Fig. 8 Illustration of the coordination spheres of the three crystallographically different rubidium atoms in $[Rb_3(EO5)OTf_3]$. Thermal ellipsoids shown at the 50% probability level.

Table 1 Selected bond lengths [pm] for compound **5** and average Rb–O distances in related compounds

				CN of Rb[a]	Ref.
$[Rb_3(EO5)OTf_3]$					
Rb1–O1	308.6(2)	Rb1–O9[c]	294.3(2)	9	*b*
Rb1–O2	293.6(1)	Rb1–O12[d]	289.9(2)		
Rb1–O3	307.7(2)	Rb1–O14[e]	308.1(2)		
Rb1–O7	329.6(3)	Rb1–O15[e]	306.9(2)		
Rb1–O8	308.7(3)				
Rb2–O3	298.3(2)	Rb2–O8	293.1(2)	8	*b*
Rb2–O4	314.2(2)	Rb2–O10	291.5(2)		
Rb2–O6[f]	307.7(2)	Rb2–O11	360.1(3)		
Rb2–O7[e]	285.3(2)	Rb2–O11[f]	282.4(2)		
Rb3–O1[e]	314.7(2)	Rb3–O10	293.2(2)	8	*b*
Rb3–O4	304.3(2)	Rb3–O12	308.5(2)		
Rb3–O5	289.7(2)	Rb3–O13	289.5(2)		
Rb3–O6	306.7(2)	Rb3–O15[g]	283.9(2)		
[Rb([18]crown-6)OTf]					
Rb–O	290.6(6)–305.8(6)			8	11
[Rb(FAD)pic][h]					
Rb–O	291.7(6)–314.5(6)			9	12

[a] CN = coordination number. [b] This work. [c] $1-x, 1-y, -z$. [d] $1+x, +y, +z$. [e] $1-x, 2-y, 1-z$. [f] $-x, 1-y, -z$. [g] $-x, 2-y, 1-z$. [h] FAD = ferulic acid derivative – see ref. 12 for further information; pic = picrate ($C_6H_2N_3O_7^-$).

with CsOTf. Similar to the rubidium salt, the caesium salt readily dissolves under these conditions. After removal of the solvent, however, no crystals could be obtained as the compound remains a colourless, sticky oil. Attempts at crystallizing at low temperatures with weak-coordinating solvents such as dichloromethane and liquid sulphur dioxide failed. Nevertheless this proves the necessity for a silicon-based ligand as no single crystals of CsOTf could be obtained. For the sake of completeness, the oil was analysed by means of mass spectrometry. An ESI(+) spectrum reveals the interaction of the caesium cation with EO5. Fig. 9 shows the ESI(+) mass spectra of a mixture of EO5 and CsOTf in acetonitrile. Single charged signals were observed at m/z = 133.1 $[Cs]^+$, 261.2 $[Na@EO5]^+$, 371.1 $[Cs@EO5]^+$. With these respective signals, no higher binding stoichiometry was found. Therefore EO5 forms a stable complex in a 1:1 stoichiometry with CsOTf so the obtained oil is best described as [Cs(EO5)OTf] (**6**). The signal found at 261.2 m/z is caused by sodium ions which are a common impurity in the mass spectrometer.

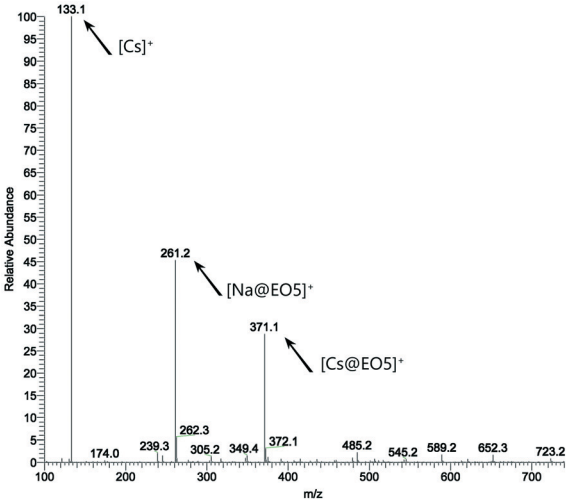

Fig. 9 ESI(+)-MS spectrum of a mixture of EO5 and CsOTf in acetonitrile.

Conclusions

In this work, we presented a novel crystallization technique using sila-polyethers as auxiliaries. Selected crystallization agents were 1,2-disila-EO5 (**1**), 1,2-disila-EO7 (**2**), and 1,2,10,11-tetrasila[18]crown-6 (**3**). **3** was synthesized from EO2 and 1,1,2,2-tetramethyldichlorodisilane. Stirring RbOTf, CsOTf or Cs_2Ox together with one of these crystallization agents in dichloromethane yielded the crystalline material of the respective salt, which could be analysed *via* single-crystal X-ray diffraction analysis. The single-crystal X-ray diffraction data compared well with the powder data published by the group of Jansen adding a new level of detail for α-CsOTf.[6–8] We show that to recrystallize the rubidium and caesium salts without the formation of a coordination complex with the polyether, it is strictly necessary to use sila-polyethers instead of the all-carbon analogues: even when using the open chain polyether EO5, a trinuclear complex $[Rb_3(EO5)OTf_3]$ or a mononuclear complex [Cs(EO5)OTf] is observed in the reaction with the respective salt. Both compounds have been analysed by single-crystal X-ray diffraction and/or mass spectrometry, respectively.

As we were successful in obtaining previously elusive single crystals of three heavy alkali metal salts, we hope that there will be a broader application of our method as a means

 This journal is © The Royal Society of Chemistry 2018

Published on 23 August 2018. Downloaded by University of Marburg on 4/3/2020 2:12:38 PM.

to grow crystals of various anhydrous rubidium and caesium salts for single crystal structure determination and high precision measurements of physical properties such as conductivity across different crystallographic directions.

Experimental section

General

All manipulations were carried out under rigorous exclusion of oxygen and moisture using a Schlenk-line under an inert gas atmosphere. Solvents were dried over a suitable drying reagent and freshly distilled before use. Alkali metal salts were stored and handled under an argon atmosphere using a glovebox. NMR spectra were recorded on a Bruker AV III HD 300 MHz or AV III 500 MHz. The infrared (IR) spectra of the respective samples were measured using attenuated total reflectance (ATR) mode on a Bruker Model Alpha FT-IR operated with the OPUS software package.[15] MS-spectrometry was conducted on a LTQ-FT device. Compounds **1** and **2** are synthesized using methods reported in the literature.[5]

Synthesis of 1,2,10,11-tetrasila[18]crown-6 (3) and 1,2-disila[9]crown-3 (4)

1 mL of EO2 (0.106 mmol, 1.0 eq.) is dissolved in 20 mL of THF (THF = tetrahydrofuran) together with 2.14 mL of triethylamine (0.21 mmol, 2.0 eq.). Subsequently, 2 mL of 1,1,2,2-tetramethyldichlorodisilane (0.106 mmol, 1.0 eq.) dissolved in 20 mL of THF are added dropwise over a period of 15 min. The suspension is stirred overnight followed by removal of the solvent under reduced pressure. The residue is then extracted with 50 mL of *n*-pentane followed by filtration. The clear solution is freed of the solvent and the remaining dull oil is extracted with 5 mL of acetonitrile. After decanting and removal of the solvent under reduced pressure, a colourless viscous oil is obtained which is a mixture of compounds **3** and **4**. The compounds are purified by condensing the volatile substance **4**. For this purpose, the oil was heated to 320 °C under dynamic high vacuum conditions (1×10^{-3} mbar) using a heat gun. **4** is trapped in another flask under cooling with liquid nitrogen. Both compounds are obtained as colourless oils in 22% yield for **3** and 40% yield for **4**.

Analytical data for 3

^{1}H NMR: (300 MHz, CD_3CN) 0.22 (s, 24H, SiCH_3), 3.48 (t, 8H, CH_2, $^{3}J_{HH}$ = 5.1 Hz), 3.69 (t, 8H, CH_2, $^{3}J_{HH}$ = 5.1 Hz) ppm; ^{13}C{^{1}H} NMR: (75 MHz, CD_3CN) 0.08 (s, SiCH_3), 63.9 (s, CH_2), 73.4 (s, CH_2) ppm; ^{29}Si NMR: (59 MHz, CD_3CN) 10.1 (s, $SiCH_3$) ppm; IR (cm^{-1}): 2950 (m), 2867 (m), 1457 (w), 1398 (w), 1354 (w), 1293 (w), 1245 (s), 1139 (s), 1086 (vs), 942 (m), 825 (s), 788 (vs), 761 (vs), 629 (m), 541 (w), 493 (w); MS: (ESI +) *m*/*z* (%) 441.1978 $[M + H]^+$ (10).

Analytical data for 4

^{1}H NMR: (300 MHz, CD_3CN) 0.17 (s, 12H, SiCH_3), 3.58–3.61 (m, 4H, CH_2), 3.72–3.75 (m, 4H, CH_2) ppm; ^{13}C{^{1}H} NMR: (75 MHz, CD_3CN) 0.4 (s, SiCH_3), 63.4 (s, CH_2), 73.2 (s, CH_2) ppm; ^{29}Si NMR: (59 MHz, CD_3CN) 11.6 (s, $SiCH_3$) ppm; IR (cm^{-1}): 2949 (m), 2867 (m), 1729 (vw), 1457 (w), 1389 (w), 1354 (w), 1294 (w), 1244 (s), 1131 (s), 1086 (vs), 929 (m), 824 (s), 788 (vs), 761 (vs), 621 (m), 542 (w), 502 (w); MS: ESI(+) *m*/*z* (%) 221.1025 $[M + H]^+$ (10).

Crystallization of RbOTf

40 mg of finely ground RbOTf are placed in a Schlenk tube equipped with a small stirring bar (1 × 0.5 cm, 0.39 × 0.19″) under argon gas. Subsequently, 5 mL of DCM and 0.2 mL of **1** or **3** are added. The solution is stirred vigorously for 70 min. Single crystals of RbOTf are obtained in the form of colourless platelets.

Crystallization of CsOTf

200 mg of finely ground CsOTf are placed in a Schlenk tube equipped with a stirring bar (2 × 1 cm, 0.8 × 0.4″) under argon gas. After addition of 10 mL of DCM and 0.2 mL of **2**, the mixture was stirred vigorously for 2 hours. After dissolution, the solution was freed of the solvent to obtain a colourless oil. This was washed with 5 mL of *n*-pentane. After a few weeks, trapezoid-like single crystals in the form of colourless platelets grew out of the solvent-free oil.

Crystallization of Cs_2Ox

50 mg of finely ground Cs_2Ox are placed in a Schlenk tube equipped with a stirring bar (2 × 1 cm, 0.8 × 0.4″) under argon gas. Subsequently, 10 mL of DCM and 0.2 mL of **1** or **3** are added. The solution is stirred vigorously for 90 min. Single crystals of Cs_2Ox are obtained in the form of colourless blocks.

Synthesis of $[Rb_3(EO5)OTf_3]$ (5)

0.103 g of EO5 (0.432 mmol, 1.0 eq.) together with 0.101 g finely ground RbOTf (0.432 mmol, 1.0 eq.) are dissolved in 10 mL of DCM. The resulting suspension is stirred overnight. The almost clear solution is then centrifuged followed by decantation. Removal of the solvent under reduced pressure yields a colourless sticky oil out of which colourless platelets grew after one day. The determination of the yield is crucial as the single crystals cannot be picked one by one out of the oil as they melt in the glovebox-atmosphere.

^{1}H NMR: (300 MHz, CD_2Cl_2) 3.53–3.56 (m, 4H, CH_2), 3.60 (s, 12H, CH_2), 3.69–3.72 (m, 4H, CH_2), 3.91 (s, 2H, OH) ppm; ^{13}C{^{1}H} NMR: (75 MHz, CD_2Cl_2) 61.5 (s, CH_2), 70.3 (s, CH_2), 70.5 (s, CH_2), 70.7 (s, CH_2), 72.9 (s, CH_2), 121.2 (q, $^{1}J_{CF}$ = 319.7 Hz, CF_3) ppm; ^{19}F NMR (283 MHz, CD_2Cl_2): −78.98 (s, CF_3) ppm; MS: ESI(+) *m*/*z* (%): 323.0529 $[EO5 + Rb]^+$ (100); IR (cm^{-1}): 3457 (m, br, $\tilde{\nu}_s$ O–H), 2876 (m), 1661 (w), 1455 (w), 1351 (m), 1253 (s), 1224 (s), 1157 (s), 1091 (vs), 1028 (vs), 947 (s), 888 (m), 830 (m), 756 (w), 637 (vs), 573 (m), 516 (s).

Published on 23 August 2018. Downloaded by University of Marburg on 4/3/2020 2:12:38 PM.

Synthesis of [Cs(EO5)OTf] (6)

0.102 g of EO5 (0.432 mmol, 1.0 eq.) together with 0.120 g finely ground CsOTf (0.432 mmol, 1.0 eq.) are dissolved in 10 mL of DCM. The salt readily dissolves and the clear solution is stirred for further 2.5 h. Removal of the solvent under reduced pressure yields a colourless sticky oil. No single crystals grew out of the oil even after several weeks. The yield is quantitative.

^{1}H NMR: (300 MHz, CD_2Cl_2) 3.52–3.55 (m, 4H, CH_2), 3.60 (s, 12H, CH_2), 3.52–3.55 (m, 4H, CH_2), 4.42 (s, 2H, O*H*) ppm; ^{13}C{^{1}H} NMR: (75 MHz, CD_2Cl_2) 61.7 (s, *C*H_2), 70.4 (s, *C*H_2), 70.6 (s, *C*H_2), 70.7 (s, *C*H_2), 72.9 (s, *C*H_2), 119.8 (q, $^1J_{CF}$ = 318.3 Hz, *C*F_3) ppm; ^{19}F NMR (283 MHz, CD_2Cl_2): −79.79 (s, CF_3) ppm; MS: ESI(+) *m*/*z* (%): 132.9049 $[Cs]^+$ (100), 371.0466 $[EO5 + Cs]^+$ (30); IR (cm^{-1}): 3464 (m, br, $\tilde{\nu}_s$ O–H), 2961 (w), 2876 (m), 1455 (w), 1350 (w), 1259 (s), 1224 (s), 1158 (s), 1091 (vs), 1027 (vs), 946 (m), 886 (m), 800 (m), 757 (w), 637 (s), 574 (m), 516 (m), 437 (vw).

Crystal structures

Single crystal X-ray diffraction experiments were performed on a Bruker D8 Quest (RbOTf, Cs_2Ox), an IPDS2 (CsOTf) or an IPDS2T (5) diffractometer, respectively. Measurements were performed at 100 K and 293 K with MoKα radiation, graphite monochromatization and/or respective X-ray optics. The structures were solved by direct methods and refined with full-matrix-least-squares against F^2 using *SHELXT* and *SHELXL* on the *OLEX2* platform.[16–18] The crystallographic data for compound 5 is deposited in the Cambridge Crystallographic Data Centre (CCDC); No. 1852230. For crystallographic details, see below. The respective single-crystal X-ray structures of the alkali metal salts were deposited at the Fachinformationszentrum Karlsruhe (FIZ) and can be obtained on quoting the CSD-numbers 434772 (RbOTf), 434773 (CsOTf 100 K), 434774 (CsOTf 293 K) and 434771 (Cs_2Ox). Please see the ESI† for the crystallographic details of these compounds.

Crystal data of 5

$C_{13}H_{22}F_9O_{15}Rb_3S_3$, triclinic, $P\bar{1}$, Z = 2, 100 K, a = 11.520(4) Å, b = 12.109(4) Å, c = 12.548(3) Å, α = 112.79(2)°, β = 100.47(3)°, γ = 102.10(2)°, V = 1509.3(8) Å^3, ρ = 2.072 g cm^{-3}, numerical absorption correction using STOE X-AREA and X-RED32,[19] μ = 3.980 mm^{-1}, T_{min}, T_{max} = 0.2706, 0.6809, 2Θ range 3.84–60.00°, reflections measured 23 023, independent reflections 8793 [R(int) = 0.0635], 396 parameters, R-index [$I >= 2\sigma(I)$] 0.0328, wR_2 (all data) 0.08118, GoF 1.001, $\Delta\rho_{max}$, $\Delta\rho_{min}$ 1.26/−0.76 e Å^3.

Conflicts of interest

There are no conflicts to declare.

Acknowledgements

This work was financially supported by the Deutsche Forschungsgemeinschaft (DFG). Dr. B. Weinert and Dr. C. Donsbach are gratefully acknowledged for their valuable help with powder or X-ray crystallographic data, respectively. Further, F. D. thanks the MS (Dr. U. Linne and co-workers) and X-ray Departments (M. Marsch, R. Riedel, and Dr. K. Harms), Philipps-Universität, Marburg, for measurement time. In particular, Dr. K. Harms is gratefully acknowledged for his valuable help with X-ray experiments and his kind advice.

Notes and references

1 J. S. Ritch and T. Chivers, *Angew. Chem., Int. Ed.*, 2007, **46**, 4610–4613.
2 K. Reuter, M. R. Buchner, G. Thiele and C. von Hänisch, *Inorg. Chem.*, 2016, **55**, 4441–4447.
3 F. Dankert, K. Reuter, C. Donsbach and C. von Hänisch, *Dalton Trans.*, 2017, **46**, 8727–8735.
4 K. Reuter, G. Thiele, T. Hafner, F. Uhlig and C. von Hänisch, *Chem. Commun.*, 2016, **52**, 13265–13268.
5 F. Dankert, C. Donsbach, C.-N. Mais, K. Reuter and C. von Hänisch, *Inorg. Chem.*, 2018, **57**, 351–359.
6 L. Hildebrandt, R. Dinnebier and M. Jansen, *Inorg. Chem.*, 2006, **45**, 3217–3223.
7 L. Hildebrandt, R. Dinnebier and M. Jansen, *Z. Anorg. Allg. Chem.*, 2005, **631**, 1660–1666.
8 R. E. Dinnebier, S. Vensky, M. Panthöfer and M. Jansen, *Inorg. Chem.*, 2003, **42**, 1499–1507.
9 K. Reuter, S. S. Rudel, M. R. Buchner, F. Kraus and C. von Hänisch, *Chem. – Eur. J.*, 2017, **23**, 9607–9617.
10 M. T. Weller, P. F. Henry and M. E. Light, *Acta Crystallogr., Sect. B: Struct. Sci.*, 2007, **63**, 426–432.
11 M. Gjikaj and A. Adam, *Z. Anorg. Allg. Chem.*, 2006, **632**, 2475–2480.
12 Y. Miyake, A. Hosoda, M. Takagaki, E. Nomura and H. Taniguchi, *Chem. Commun.*, 2002, 132–133.
13 A. V. Zabula, B. S. Dolinar and R. West, *J. Organomet. Chem.*, 2014, **751**, 458–461.
14 C. Näther, H. Bock, Z. Havlas and T. Hauck, *Organometallics*, 1998, **17**, 4707–4715.
15 OPUS, *Version 7.2; Bruker Opt. GmbH*, Ettlingen, Germany, 2012.
16 G. M. Sheldrick, *Acta Crystallogr., Sect. A: Found. Adv.*, 2015, **71**, 3–8.
17 G. M. Sheldrick, *Acta Crystallogr., Sect. C: Struct. Chem.*, 2015, **71**, 3–8.
18 O. V. Dolomanov, L. J. Bourhis, R. J. Gildea, J. A. K. Howard and H. Puschmann, *J. Appl. Crystallogr.*, 2009, **42**, 339–341.
19 Stoe & Cie, *X-AREA and X-RED32*, Stoe & Cie, Darmstadt, Germany, 2009.

 This journal is © The Royal Society of Chemistry 2018

Electronic Supplementary Material (ESI) for CrystEngComm.
This journal is © The Royal Society of Chemistry 2018

Electronic Supplementary Information on

Sila-polyethers as *innocent* crystallization reagents for heavy alkali metal compounds

Fabian Dankert, Johanna Heine, Julia Rienmüller and Carsten von Hänisch*

Department of Chemistry and Material Sciences Center, Philipps-Universität Marburg, Hans-Meerwein-Straße, 35043 Marburg, Germany.

Experimental details

Crystallographic details

RbOTf

Empirical formula	$C_4F_{12}O_{12}Rb_4S_4$
Formula weight	938.16
Temperature/K	100.0
Crystal system	monoclinic
Space group	*Cm*
a/Å	19.2895(8)
b/Å	23.4587(9)
c/Å	5.0673(2)
α/°	90
β/°	100.992(2)
γ/°	90
Volume/Å^3	2250.92(16)
Z	4
ϱ_{calc}g/cm^3	2.768
μ/mm^{-1}	9.166
F(000)	1760.0

Crystal size/mm^3	0.151 × 0.083 × 0.063
Radiation	MoKα (λ = 0.71073)
2Θ range for data collection/°	4.302 to 50.668
Index ranges	-23 ≤ h ≤ 23, -28 ≤ k ≤ 25, -6 ≤ l ≤ 6
Reflections collected	33902
Independent reflections	4201 [R_{int} = 0.0680, R_{sigma} = 0.0352]
Data/restraints/parameters	4201/458/317
Goodness-of-fit on F^2	1.092
Final R indexes [I>=2σ (I)]	R_1 = 0.0558, wR_2 = 0.1081
Final R indexes [all data]	R_1 = 0.0644, wR_2 = 0.1122
Largest diff. peak/hole / e Å^{-3}	1.18/-2.24
Flack parameter	0.51(3)

Details of crystal structure refinement: The structure was refined as an inversion twin (BASF 0.50618). All CF_3 groups and most SO_3 groups showed significant disorder, either by rotation about the C-S bond of the triflate anion or tilting of the C-S bond. Disordered atoms were refined isotropically and a number of strict SADI, DFIX and ISOR restraints had to be used to stabilize the refinement. Occupancies of disordered groups were constrained to values yielding a chemically reasonably disorder model. One triflate anion is disordered about the mirror plane in such a way that the PART instruction cannot be used to generate a correct bonding pattern here, although the overall disorder model is reasonable here.

α-CsOTf (100 K)

Empirical formula	$CCsF_3O_3S$
Formula weight	281.98
Temperature/K	100(2)
Crystal system	monoclinic
Space group	$P2_1/n$
a/Å	5.4549(6)
b/Å	6.0582(4)
c/Å	18.339(2)
α/°	90
β/°	91.922(9)
γ/°	90
Volume/Å^3	605.71(10)
Z	4
ϱ_{calc}g/cm^3	3.092
μ/mm^{-1}	6.456
F(000)	512.0
Crystal size/mm^3	0.09 × 0.066 × 0.036
Radiation	MoKα (λ = 0.71073)
2Θ range for data collection/°	4.444 to 57.996
Index ranges	$-7 \le h \le 7$, $-8 \le k \le 8$, $-24 \le l \le 24$
Reflections collected	22166
Independent reflections	1609 [R_{int} = 0.0676, R_{sigma} = 0.0224]
Data/restraints/parameters	1609/0/82
Goodness-of-fit on F^2	1.088
Final R indexes [I>=2σ (I)]	R_1 = 0.0207, wR_2 = 0.0502
Final R indexes [all data]	R_1 = 0.0239, wR_2 = 0.0511
Largest diff. peak/hole / e Å^{-3}	1.28/-0.86

α-CsOTf (293 K)

Empirical formula	$CCsF_3O_3S$
Formula weight	281.98
Temperature/K	293(2)
Crystal system	monoclinic
Space group	$P2_1/n$
a/Å	5.4705(11)
b/Å	6.1497(8)
c/Å	18.759(4)
α/°	90
β/°	91.357(16)
γ/°	90
Volume/Å^3	630.9(2)
Z	4
ϱ_{calc}g/cm^3	2.969
μ/mm^{-1}	6.198
F(000)	512.0
Crystal size/mm^3	0.09 × 0.066 × 0.036
Radiation	MoKα (λ = 0.71073)
2Θ range for data collection/°	4.344 to 57.992
Index ranges	$-7 \le h \le 7$, $-8 \le k \le 8$, $-25 \le l \le 25$
Reflections collected	14785
Independent reflections	1680 [R_{int} = 0.0729, R_{sigma} = 0.0310]
Data/restraints/parameters	1680/0/82
Goodness-of-fit on F^2	0.979
Final R indexes [I>=2σ (I)]	R_1 = 0.0388, wR_2 = 0.0989
Final R indexes [all data]	R_1 = 0.0579, wR_2 = 0.1048
Largest diff. peak/hole / e Å^{-3}	1.53/-0.73

$Cs_2C_2O_4$ (100 K)

Empirical formula	$C_2Cs_2O_4$
Formula weight	353.84
Temperature/K	100.0
Crystal system	monoclinic
Space group	$P2_1/c$
a/Å	6.5506(4)
b/Å	10.8879(6)
c/Å	8.5685(6)
α/°	90
β/°	97.405(2)
γ/°	90
Volume/Å3	606.03(7)
Z	4
ϱcalcg/cm3	3.878
μ/mm-1	11.955
F(000)	616.0
Crystal size/mm3	0.117 × 0.081 × 0.066
Radiation	MoKα (λ = 0.71073)
2Θ range for data collection/°	6.082 to 50.54
Index ranges	-7 ≤ h ≤ 7, -13 ≤ k ≤ 13, -10 ≤ l ≤ 10
Reflections collected	6053
Independent reflections	1095 [Rint = 0.0329, Rsigma = 0.0217]
Data/restraints/parameters	1095/0/73
Goodness-of-fit on F2	1.099
Final R indexes [I>=2σ (I)]	R_1 = 0.0149, wR_2 = 0.0282
Final R indexes [all data]	R_1 = 0.0199, wR_2 = 0.0293
Largest diff. peak/hole / e Å-3	0.55/-0.58

Comparison of α-CsOTf (100 K), α-CsOTf (293 K) and α-CsOTf (Jansen)

Table S1: Comparison of unit cell parameters of single crystal measurements of α-CsOTf at 100 K and 293 K with data from previous work by *Jansen*.[1]

	α-CsOTf	**α-CsOTf**	**α-CsOTf (from powder data)[1]**
Temperature/K	100	293	294
Crystal system	monoclinic	monoclinic	monoclinic
Space group	$P2_1/n$	$P2_1/n$	$P2_1$
a/Å	5.4549(6)	5.4705(11)	9.7406(2)
b/Å	6.0582(4)	6.1497(8)	6.1640(1)
c/Å	18.339(2)	18.759(4)	5.4798(1)
β/°	91.922(9)	91.357(16)	104.998(1)
Volume/Å^3	605.71(10)	630.9(2)	317.81(10)
Z	4	4	2

Table S2: Comparison of interatomic distances obtained from single crystal measurements of α-CsOTf at 100 K and 293 K with data from previous work by *Jansen*[1].

Interatomic distances in Å	**α-CsOTf (100 K, this work)**	**α-CsOTf (293 K, this work)**	**α-CsOTf (from powder data)**
S-C	1.819(3)	1.776(8)	1.805(7)
S-O	1.436(2)-1.438(2)	1.383(6) - 1.468(5)	1.432(10) - 1.444(13)
C-F	1.322(3)-1.328(3)	1.253(11) - 1.377(9)	1.311(11) - 1.320(15)
Cs-O	3.010(1)-3.361(1)	3.057(5) - 3.409(4)	2.969(12) - 3.330(16)
Cs-F	3.287(1)-3.653(2)	3.381(6) - 3.657(7)	3.492(12)- 3.847(11)

References

[1] L. Hildebrandt, R. Dinnebier and M. Jansen, *Z. Anorg. Allg. Chem.*, 2005, **631**, 1660–1666.

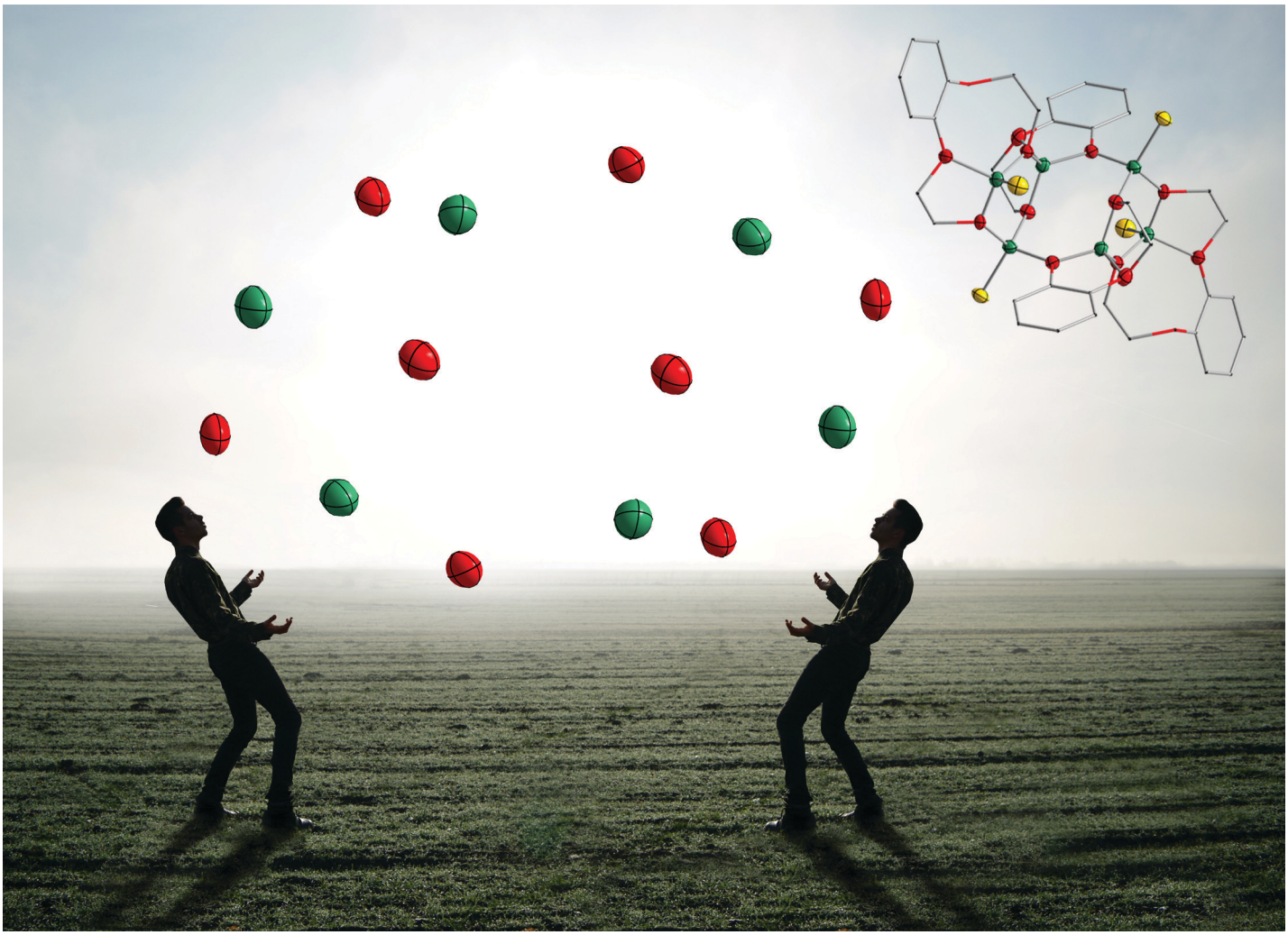

Showcasing collaborative research from the Magnus R. Buchner and Carsten von Hänisch labs at the Philipps-Universität Marburg, Germany.

The coordination behaviour and reactivity of partially silicon based crown ethers towards beryllium chloride

Reaction of sila-crown ethers with $BeCl_2$ results in the formation of eight-membered Be—O-heterocycles, which are annulled by two six-membered Be—O-cycles. The process leading to these unprecedented ring systems was studied with NMR and IR spectroscopy.

As featured in:

See Magnus R. Buchner *et al.*, *Dalton Trans.*, 2018, **47**, 16393.

ROYAL SOCIETY OF CHEMISTRY

rsc.li/dalton

Registered charity number: 207890

Dalton Transactions

COMMUNICATION

View Article Online
View Journal | View Issue

Published on 12 October 2018. Downloaded by University of Marburg on 4/3/2020 2:09:10 PM.

Check for updates

Cite this: *Dalton Trans.*, 2018, **47**, 16393

Received 2nd October 2018,
Accepted 11th October 2018

DOI: 10.1039/c8dt03963a

rsc.li/dalton

The coordination behaviour and reactivity of partially silicon based crown ethers towards beryllium chloride†

Magnus R. Buchner, *[a] Matthias Müller,[a] Fabian Dankert, [b] Kirsten Reuter[b] and Carsten von Hänisch [b]

Through reactions of 1,2-disila[12]crown-4 or 1,2-disila-benzo[12]crown-4 ethers with $BeCl_2$ eight-membered Be–O-heterocycles, which are annulated by two six-membered Be–O-cycles were obtained and characterised. The reactions leading to these unusual ring systems have been investigated by NMR and IR spectroscopy as well as reactions with further ligand derivatives.

While carbon based ethers and crown ethers are of high importance in solution chemistry their silicon based analogues show extremely poor coordination behaviour,[1,2] which is showcased by the inaccessibility of silyl ether complexes of strong Lewis acids.[3–5] This reluctance to form dative bonds towards metal cations has been ascribed to delocalisation of the oxygen centred lone pairs into empty d-orbitals of the silicon atom,[1,6] negative hyperconjugation[2,7–11] and more recently also to electrostatic repulsion between the partially positive charged silicon atom and the metal cation.[12,13] However it could be demonstrated lately that the complex stability of lithium complexes with [12]crown-4 and its silicon derivatives, in which one or two ethylene bridges had been substituted by $–SiMe_2SiMe_2–$ groups, increases with silicon content.[14] This has been explained through minimization of the electrostatic repulsion by a large enough bite angle[15] as well as only minute influence of negative hyperconjugation.[16] Therefore the higher electron density at the oxygen atom compared to organic crown ethers leads to a higher basicity and better coordination properties. Reactions of alkali and alkaline earth metal ions with larger sila-crown ethers and disila-bridged podands revealed that the ring strain of the formed complexes is the dominant factor determining which oxygen atoms coordinate to the metal.[14,17,18] However, Be^{2+}, the hardest s-block *Lewis* acid had not been investigated so far, presumably due to its alleged extreme toxicity.[19] Though in consideration of the fact that highly Lewis acidic magnesium complexes are able to form stable adducts to unsupported silyl ethers[5] and that binding of disila-ligands is most effective for hard cations,[18] it was evident that a study with beryllium compounds was long overdue. Here we therefore present the first study on the coordination behaviour of sila-crown ethers towards a beryllium salt.

Only one decade ago the coordination of beryllium salts towards organic crown ethers was investigated. It could be shown, that $BeCl_2$ coordinates exocyclic to only two oxygen atoms of [15]crown-5 or [18]crown-6, with both chlorine atoms still bound to the beryllium atom.[20,21] In contrast to this, [12]crown-4 displaces one chloride ion from the $BeCl_2$ moiety in the presence of a chloride ion acceptor, resulting in the formation of five-coordinated, cationic beryllium complex **1** (Fig. 1).[22] Lately, it could also be shown that the coordination modes observed in the solid state are also present in solution, that no chloride ion abstractor is necessary to generate cation **1** and that in solution mostly non-coordinated crown ether is present.[23] The reactivity of beryllium compounds towards silyl ethers is even less explored and it is only known, that $[Ph_4P]_2[Be_2Cl_6]$ can ring-open $(OSiMe_2)_3$ under the cleavage of Me_2SiCl_2 and the generation of disiloxanato-bridged tetranuclear chloroberyllates[24] and that Me_3SiO^- can act as a brid-

[a]*Anorganische Chemie, Nachwuchsgruppe Berylliumchemie, Fachbereich Chemie, Philipps-Universität Marburg, Hans-Meerwein-Straße 4, 35032 Marburg, Germany. E-mail: magnus.buchner@chemie.uni-marburg.de*

[b]*Fachbereich Chemie and Wissenschaftliches Zentrum für Materialwissenschaften (WZMW), Philipps-Universität Marburg, Hans-Meerwein-Straße 4, 35032 Marburg, Germany. E-mail: haenisch@chemie.uni-marburg.de*

†Electronic supplementary information (ESI) available: Details on the experimental procedures and analytical data. CCDC 1866609 and 1866610. For ESI and crystallographic data in CIF or other electronic format see DOI: 10.1039/c8dt03963a

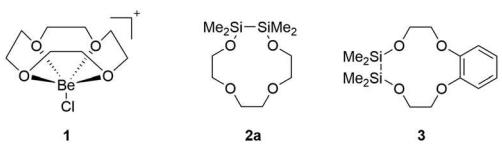

1 2a 3

Fig. 1 Cationic [12]crown-4 berylliumchloride complex **1** and disila-derivatives of [12]crown-4 (**2a** & **3**).

Published on 12 October 2018. Downloaded by University of Marburg on 4/3/2020 2:09:10 PM.

ging ligand for di-nuclear acido beryllates.[25] According to these compounds we decided to start the investigation with the reactivity of 1,2-disila[12]crown-4 (**2a**) and 1,2-disila-benzo [12]crown-4 (**3**) towards $BeCl_2$ in dichloromethane.

When $BeCl_2$ is reacted with a dichloromethane solution of ligand **2a** it takes several days to dissolve the $BeCl_2$ and in the case of ligand **3** several weeks. In contrast to this, the same reaction with organic [12]crown-4 takes only minutes for complete conversion.[23] Reaction monitoring *via* ^{1}H, ^{13}C and ^{29}Si NMR spectroscopy confirms that the present solid is $BeCl_2$ since non-coordinated ligands **2a** and **3** are observed after several days or weeks respectively. Additionally, the formation of a $Cl(Me_2)Si–Si(Me_2)O$-group bound to a carbon nucleus[26] and also of $Cl(Me_2)Si–Si(Me_2)Cl$[27] – as the reaction proceeds – is observed for both ligands (Fig. S1–S6†). In ^{9}Be NMR spectroscopy the formation of one permanent signal at 2.7 ppm ($\omega_{1/2}$ = 45 Hz) and two transient signals at 3.4 ($\omega_{1/2}$ = 61 Hz) and 2.0 ppm ($\omega_{1/2}$ = 49 Hz) is observed in the presence of ligand **2a** (Fig. S7†), while for crown ether **3** only one signal at 3.1 ppm ($\omega_{1/2}$ = 59 Hz) is present (Fig. S8†). These signals are all in the typical range of tetrahedral coordinated beryllium nuclei,[28] but are significantly different to the signal of $[BeCl([12]crown-4)]^{+}$ at 4.2 ppm.[23]

After two months (**2a**) or two weeks (**3**) crystals suitable for X-ray diffraction analysis of compounds **4** and **5** formed on the wall of the reaction vessels respectively (Scheme 1, see also Table S1† for the crystallographic details). Hexa-nuclear complex **4** comprises of one eight-membered Be–O-heterocycle which is annulated by two six-membered Be–O-cycles (Fig. 2). Neither the annulation of Be-heterocycles nor the formation of eight-membered ring systems have previously been observed in beryllium chemistry. Compound **4** can be described as a dimer comprising of two equivalent tri-nuclear complexes, in which one beryllium atom is coordinated by one chlorine atom and the oxygen atoms in the 1, 4 and 10 position of a triethylene glycolate. The second beryllium atom is also coordinated in the same fashion to a second triethylene glycolate, however also tethered to the oxygen atom in position 10 of the first glycolate. The third beryllium atom is coordinated to one chlorine atom and to one oxygen atom of each of the glycolates respectively and dimerization completes its coordination sphere. This also leads to every alcoholate oxygen atom being coordinated to two beryllium atoms. Complex **5** exhibits the same structural motive, with the exception, that the all

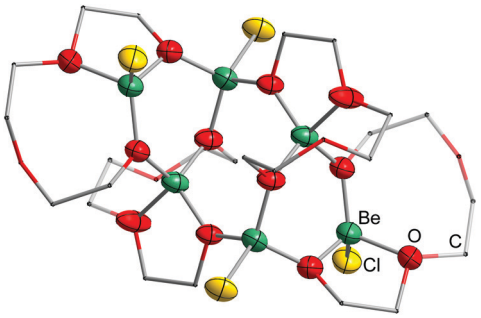

Fig. 2 Molecular structure of compound **4** in the solid state. Displacement ellipsoids are shown at the 70% probability level at 100 K, hydrogen atoms are omitted and non-beryllium-bound atoms are depicted as a wireframe image for clarity.

oxygen-coordinated beryllium atom is coordinated at the 1, 4 and 7 position of a di-glycolate (Fig. 3). The $Be–O_{alcoholate}$ (**4**: 1.596(4)–1.623(4) Å, **5**: 1.574(3)–1.650(3) Å) and Be–Cl-bond lengths (**4**: 2.020(4)–2.049(3) Å, **5**: 1.988(3)–2.001(3) Å) are comparable to $[BeCl(\mu_2\text{-}OEt)(piperidine)]_2$ (Be–O: 2.032(2) Å; Be–Cl: 2.032(2) Å)[29] but the latter are longer than in ether (1.978(3) Å)[30] or crown ether (1.958(2)–1.978(2) Å)[20,21] adducts to $BeCl_2$. Also the $Be–O_{ether}$-bond lengths (**4**: 1.715(4)–1.730(4) Å, **5**: 1.763(3)–1.803(3) Å) are significantly longer than in known crown ether (1.665(2)–1.699(2) Å)[20,21] and ether beryllium complexes (1.683(3) & 1.655(3) Å).[30] The O–Be–O angles in the five-

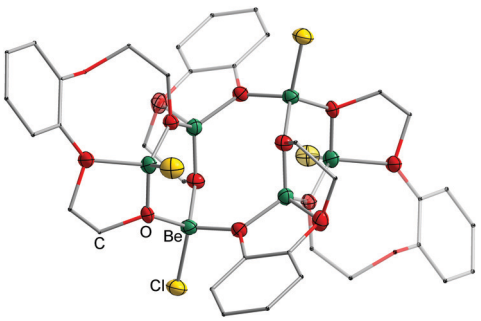

Fig. 3 Molecular structure of compound **5** in the solid state. Displacement ellipsoids are shown at the 70% probability level at 100 K, hydrogen atoms are omitted and non-beryllium-bound atoms are depicted as a wireframe image for clarity.

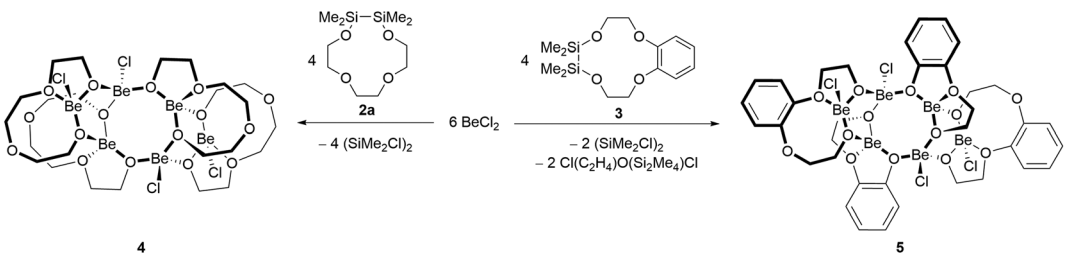

Scheme 1 Reaction of $BeCl_2$ with disila[12]crown-4-ethers **2a** and **3** in dichloromethane, yielding hexa-nuclear complexes **4** and **5**.

This journal is © The Royal Society of Chemistry 2018

Published on 12 October 2018. Downloaded by University of Marburg on 4/3/2020 2:09:10 PM.

membered rings are between 93.5(2)° and 96.9(2)°, which is similar to the beryllium atoms coordinated exocyclicly to [15] crown-5 (92.98(9)°)[20] and [18]crown-6 (92.4(1)°).[21] All other O–Be–O and the O–Be–Cl angles are with 104.0(2)°–117.2(2)° very close to ideal tetrahedral coordination around the beryllium atoms.

To investigate the formation of complexes **4** and **5** we reacted $BeCl_2$ with triethylene glycol (**6**) and triethylene glycol monomethylether (**7**) in dichloromethane. In the case of ligand **6** the $BeCl_2$ dissolved instantaneously under gas evolution and a clear solution was obtained. In the ^1H and ^{13}C NMR spectra of this solution three very broad signals could be observed, while the ^9Be NMR spectrum revealed again one signal at 2.7 ppm ($\omega_{1/2}$ = 18 Hz). We therefore deduct, that the beryllium nucleus is κ^4O-coordinated by doubly deprotonated triethylene glycol to give compound **8a** (Scheme 2, see also Fig. S11†) and that this species is also formed from disila[12] crown-4 (**2a**) and $BeCl_2$ under the formation of $Cl(Me_2)Si–Si(Me_2)Cl$. The reaction with ether **7** led to the formation of huge amounts of a colourless, voluminous precipitate, which dissolved at temperatures above 80 °C. The ^{13}C NMR spectrum of this suspension revealed five very broad signals, while two very broad singlets and one broad multiplet were observed *via* ^1H NMR spectroscopy. The ^9Be NMR spectrum showed one signal at 3.6 ppm ($\omega_{1/2}$ = 30 Hz). We assign these signals to κ^3O-coordinated BeCl-complex **9** in solution. However the solubility behaviour suggests an equilibrium between compound **9** and cationic κ^4O-coordinated species **9′** (Scheme 2).

Based on these results and on the presence of the $Cl(Me_2)Si–Si(Me_2)O$-group we assumed that the signal at 3.4 ppm in the ^9Be NMR spectrum of the reaction of $BeCl_2$ with ligand **2a** is caused by a similar κ^3O-coordinated BeCl-complex (**10a** in Scheme 3). To verify this we performed the analogous reaction with 1,2,7,8-tetrasila[12]crown-4 (**2b**). *In situ* reaction monitoring by ^{29}Si NMR spectroscopy revealed – besides the formation of $Cl(Me_2)Si–Si(Me_2)Cl$ – a signal set for a $Cl(Me_2)Si–Si(Me_2)O$-group and an additional signal for a $O(Me_2)Si–Si(Me_2)O$-group, as expected (Fig. S12†). This together with two signals in the ^9Be NMR spectrum at 3.4 ($\omega_{1/2}$ = 69 Hz) and 2.5 ppm ($\omega_{1/2}$ = 53 Hz) (Fig. S13†) confirms the presence of κ^3O-coordinated BeCl-compound **10**. In the case of ligand **3**, the solubility of the resulting product is too low, so that the ^9Be NMR spectrum shows only one broad signal, which can be assigned to corresponding phenyl derivatives of complexes **8** and **10**. Surprisingly, the formation of only minor amounts of $Cl(Me_2)Si–Si(Me_2)Cl$ and $Cl(Me_2)Si–Si(Me_2)O$-groups was observed by

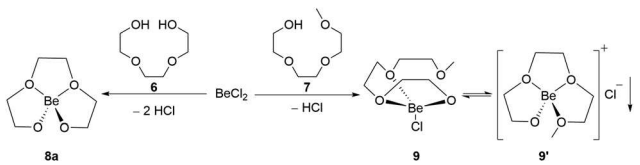

Scheme 2 Reaction of $BeCl_2$ with triethylene glycol (**6**) and triethylene glycole monomethylether (**7**) in dichloromethane.

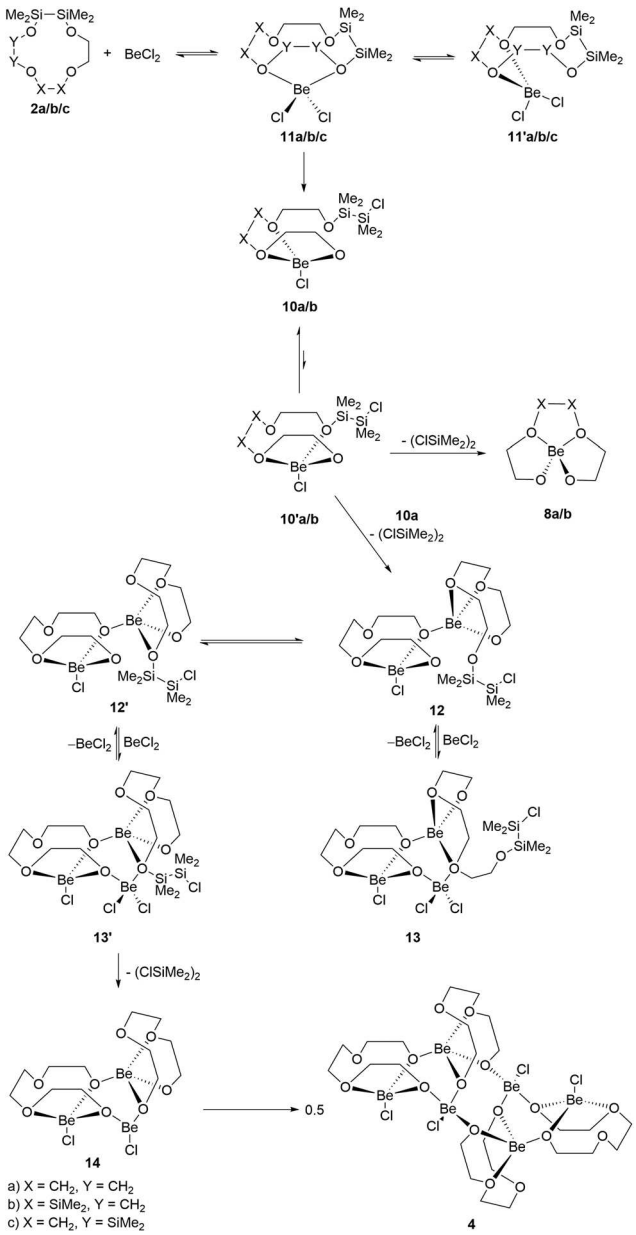

Scheme 3 Proposed reaction cascade leading to the formation of hexa-nuclear compound **4**.

^{29}Si NMR spectroscopy when 1,2,4,5-tetrasila[12]crown-4 (**2c**) was reacted with $BeCl_2$ even though no free ligand could be detected (Fig. S14 & S15†). The downfield shift of the ligand signals suggests coordination to the metal, however this shift is less pronounced than for a corresponding lithium complex.[16] Therefore we assume that not all oxygen atoms of ligand **2c** coordinate and that the $BeCl_2$ moiety is still intact. Close examination of the ^1H, ^{13}C and ^{29}Si NMR spectra of the reaction of crown ether **2a** with $BeCl_2$ also revealed corresponding signals in the first days of the reaction. This is evidence, that the first step in the reaction is the κ^2O-coordination of sila-crown ether to $BeCl_2$ resulting in complexes **11** or **11′**, which exhibit fast interchange on the NMR timescale. This is

Published on 12 October 2018. Downloaded by University of Marburg on 4/3/2020 2:09:10 PM.

supported by IR-spectroscopy of reactions of $BeCl_2$ with ligands **2a**, **2c** and **3** after 2 h reaction time, which shows a bathochromic shift of the C–O-/Si–O-bands of 51, 53 and 43 cm^{-1} together with the presence of Be–Cl-bands at 484, 481 and 528 cm^{-1}, respectively (Fig. S17–S22†). In compounds with the complex cation **1** the bathochromic shift of the C–O-band compared to free [12]crown-4 is more pronounced ($\Delta\nu$ = 63 cm^{-1}) and the Be–Cl-bands are found at significantly higher wavenumbers (737–665 cm^{-1}),[22,23] which suggests that no cationic, five-coordinated complexes are present in the case of the sila-crown ethers. This is also supported by the position of the Be–Cl-bands of [$BeCl_2$([15]crown-5)] and [$(BeCl_2)_2$([18] crown-6)] at 651 and 570 cm^{-1} respectively.[20,21] Furthermore, the IR spectroscopic data suggests a significant weakening of the Be–Cl-bond and an increasing donor ability in the order **3** < **2a** < **2c**. In line with this, a reduction of the ring size to disila[9]crown-3 (**15**; Fig. 4) leads to practically no conversion of $BeCl_2$ (Fig. S16†) due to worse coordination to $BeCl_2$, while larger ring sizes in disila[15]crown-5 (**16**) and disila-benzo[18] crown-6 (**17**) result in comparable reaction rates to di- and tetrasila[12]crown-4 ethers concerning the formation of $Cl(Me_2)Si–Si(Me_2)Cl$ and $Cl(Me_2)Si–Si(Me_2)O$-groups.

In conclusion, we propose the following pathway for the reaction of $BeCl_2$ with sila[12]crown-4 crown ethers (Scheme 3). $BeCl_2$ is κ^2*O*-coordinated by ligands **2a–c** and **3** leading to complexes **11** and **11′**. In the case of 1,2,4,5-tetrasila [12]crown-4 (**2c**) no further reaction occurs, which is currently under further investigation, while for the other ligands the Be-coordination leads to strong polarization of the Si–O- and Be–Cl-bonds facilitating nucleophilic attack of the chlorine at the silicon. This leads to the formation of complex **10**. Intramolecular coordination shift to compound **10′** results in polarisation of the second Si–O-bond, enabling either intra- or intermolecular attack at the silicon atom, leading to compounds **8** or **12**, respectively. The latter reaction seems only feasible for disila[12]-crown-4-ethers **2a** and **3**. Compound **12** or its isomer **12′** can than act as a chelate ligand for a further equivalent of $BeCl_2$ resulting in compounds **13** and **13′** respectively. The signal at 2.0 ppm in the ^{9}Be NMR spectrum of the reaction of ligand **2a** with $BeCl_2$ is presumably caused by compounds **12**/**12′** and/or **13**/**13′**. Direct coordination of two beryllium atoms seems necessary to polarize the last remaining Si–O-bond to an extent that $Cl(Me_2)Si–Si(Me_2)Cl$ can be eliminated, resulting in the formation of tri-nuclear complex **14**. The coordination environment of the tri-coordinate beryllium atom is then saturated through dimerization to compound **4**. In the case of disila-benzo[12]crown-4 (**3**) the polarisation of the C–O-bond adjacent to the aryl ring in the compound corresponding to complex **13** is apparently high enough, that this bond can be broken under the formation of a C–Cl-bond. This results eventually in the generation of hexa-nuclear species **5**.

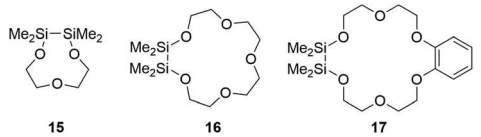

Fig. 4 Further sila-crown ethers that were tested for their coordination properties towards $BeCl_2$.

Conflicts of interest

There are no conflicts to declare.

Acknowledgements

M. R. B. thanks Prof. F. Kraus for moral and financial support as well as for the provision of lab space. The authors thank the NMR- and X-ray departments of the Philipps-Universität Marburg for their assistance and the DFG for financial support.

Notes and references

1 R. West, L. S. Whatley and K. J. Lake, *J. Am. Chem. Soc.*, 1961, **83**, 761.
2 J. S. Ritch and T. Chivers, *Angew. Chem., Int. Ed.*, 2007, **46**, 4610.
3 H. J. Emeléus and M. Onyszchuk, *J. Chem. Soc.*, 1958, 604.
4 B. D. Shepherd, *J. Am. Chem. Soc.*, 1991, **113**, 5581.
5 J. Pahl, H. Elsen, A. Friedrich and S. Harder, *Chem. Commun.*, 2018, **54**, 7846.
6 S. Grabowsky, M. F. Hesse, C. Paulmann, P. Luger and J. Beckmann, *Inorg. Chem.*, 2009, **48**, 4384.
7 C. G. Pitt, *J. Organomet. Chem.*, 1973, **61**, 49.
8 H. Oberhammer and J. E. Boggs, *J. Am. Chem. Soc.*, 1980, **102**, 7241.
9 A. Decken, J. Passmore and X. Wang, *Angew. Chem., Int. Ed.*, 2006, **118**, 2839.
10 F. Weinhold and R. West, *Organometallics*, 2011, **30**, 5815.
11 F. Weinhold and R. West, *J. Am. Chem. Soc.*, 2013, **135**, 5762.
12 A. Decken, F. A. LeBlanc, J. Passmore and X. Wang, *Eur. J. Inorg. Chem.*, 2006, 4033.
13 T. S. Cameron, A. Decken, I. Krossing, J. Passmore, J. M. Rautiainen, X. Wang and X. Zeng, *Inorg. Chem.*, 2013, **52**, 3113.
14 K. Reuter, F. Dankert, C. Donsbach and C. von Hänisch, *Inorganics*, 2017, **5**, 11.
15 K. Reuter, M. R. Buchner, G. Thiele and C. von Hänisch, *Inorg. Chem.*, 2016, **55**, 4441.
16 K. Reuter, G. Thiele, T. Hafner, F. Uhlig and C. von Hänisch, *Chem. Commun.*, 2016, **52**, 13265.
17 F. Dankert, K. Reuter, C. Donsbach and C. von Hänisch, *Dalton Trans.*, 2017, **46**, 8727.
18 F. Dankert, C. Donsbach, C.-N. Mais, K. Reuter and C. von Hänisch, *Inorg. Chem.*, 2018, **57**, 351.

 This journal is © The Royal Society of Chemistry 2018

Published on 12 October 2018. Downloaded by University of Marburg on 4/3/2020 2:09:10 PM.

19 D. Naglav, M. R. Buchner, G. Bendt, F. Kraus and S. Schulz, *Angew. Chem., Int. Ed.*, 2016, **55**, 10562.
20 B. Neumüller, K. Dehnicke and R. Puchta, *Z. Anorg. Allg. Chem.*, 2008, **634**, 1473.
21 R. Putcha, R. Kolbig, F. Weller, B. Neumüller, W. Massa and K. Dehnicke, *Z. Anorg. Allg. Chem.*, 2010, **636**, 2364.
22 B. Neumüller and K. Dehnicke, *Z. Anorg. Allg. Chem.*, 2006, **632**, 1681.
23 M. R. Buchner and M. Müller, *Z. Anorg. Allg. Chem.*, 2018, DOI: 10.1002/zaac.201800334.
24 B. Neumüller and K. Dehnicke, *Z. Anorg. Allg. Chem.*, 2004, **630**, 1846.
25 B. Neumüller and K. Dehnicke, *Z. Anorg. Allg. Chem.*, 2006, **632**, 931.
26 U. Herzog, N. Schulze, K. Trommer and G. Roewer, *J. Organomet. Chem.*, 1997, **547**, 133.
27 A. Chernyavskii, D. Larkin and N. Chernyavskaya, *J. Organomet. Chem.*, 2003, **679**, 17.
28 P. G. Plieger, K. D. John, T. S. Keizer, T. M. McCleskey, A. K. Burrell and R. L. Martin, *J. Am. Chem. Soc.*, 2004, **126**, 14651.
29 M. P. Dressel, S. Nogai, R. J. F. Berger and H. Schmidbaur, *Z. Naturforsch., B: J. Chem. Sci.*, 2003, **58**, 173.
30 K. Ruhlandt-Senge, R. A. Bartlett, M. M. Olmstead and P. P. Power, *Inorg. Chem.*, 1993, **32**, 1724.

Electronic Supplementary Material (ESI) for Dalton Transactions.
This journal is © The Royal Society of Chemistry 2018

Table of contents:

General experimental techniques	2
Synthesis and characterization	3
Crystallographic details	5
NMR spectra	6
IR spectra	14
References	17

General experimental techniques

All manipulations were performed either under solvent vapour pressure or dry argon using glovebox and *Schlenk* techniques. Dichloromethane was dried by refluxing over CaH_2 and CD_2Cl_2 was dried over CaH_2 and vacuum transferred directly into the *J. Young* NMR tubes. $BeCl_2$,[1] 1,2-disila[12]crown-4,[2] 1,2,4,5-tetrasila[12]crown-4,[3] 1,2,7,8-tetrasila[12]crown-4,[2] 1,2-disila[9]crown-3,[4] 1,2-disila[15]crown-5,[2] 1,2-disila-benzo[18]crown-6[5] and 2,2'-[1,2-phenylenebis(oxy)]diethanol[6] were prepared according to literature procedures. Due to the expected extreme toxicity of the beryllium compounds no elemental analysis or mass spectrometry could be performed of these.

NMR spectroscopy

^{1}H, ^{9}Be, ^{13}C and ^{29}Si NMR spectra were recorded on *Bruker* Avance III HD 300 and Avance III 500 NMR spectrometers. ^{1}H NMR (300 / 500 MHz) and ^{13}C NMR (76 / 126 MHz) chemical shifts are given relative to the solvent signal CD_2Cl_2 (5.32 and 53.8 ppm) while ^{9}Be (42 / 70 MHz) used 0.43 [M] $BeSO_4$ in D_2O and ^{29}Si (60 / 99 MHz) used neat $SiMe_4$ as an external standard. NMR spectra were processed with the MestReNova software.[7]

IR spectroscopy

IR spectra were recorded on a *Bruker* alpha FT-IR spectrometer equipped with a diamond ATR unit in an argon filled glovebox. Processing of the spectra was performed with the OPUS software package[8] and OriginPro 2017.[9]

Single crystal X-ray diffraction

Single crystals were selected under exclusion of air in perfluorinated polyether (Fomblin YR 1800, *Solvay Solexis*) and mounted using the *MiTeGen* MicroLoop system. X-ray diffraction data were collected using the monochromated Mo-K_α radiation of a *Stoe* IPDS2 diffractometer equipped with an Image Plate detector or the monochromated Mo-K_α radiation of a *Bruker* D8 Quest diffractometer equipped with a microfocus source and a *CMOS* Photon 100 detector. The diffraction data were reduced with the X-Area software.[10] The structures were solved using Direct Methods (SHELXS-2013/1 & SHELXT-2015) and refined against F^2 (SHELXL-2016/4) using the ShelXle (**4**) and OLEX2 (**5**) software packages.[11] All atoms were located by Difference Fourier synthesis and non-hydrogen atoms were refined anisotropically. Hydrogen atoms were refined isotropically.

Mass spectrometry

Mass spectrometry was performed on a *Thermo Fischer Scientific* LTQ-FT Ultra using a electrospray ionization (ESI) source.

Synthesis and characterization

1,2-disila-benzo[12]crown-4 (3):
1.00 g of 2,2'-[1,2-Phenylenebis(oxy)]diethanol (6.02 mmol, 1.00 eq) and 1.67 mL of NEt_3 (12.04 mmol, 2.0 eq) were dissolved in 50 ml of THF. Subsequently, 1.14 ml of $Si_2Me_4Cl_2$ (6.02 mmol, 1.0 eq) dissolved in 50 ml of THF was added over a period of 60 min. The resulting white suspension was then stirred overnight and freed of the solvent in vacuo. The residue was extracted with 50 ml of *n*-pentane followed by filtration. Removing the solvent under reduced pressure yielded the crown ether as a colourless oil (1.32 g, 70%). For purification, the crown ether was sublimated by slowly raising the temperature to 90 °C under fine vacuum ($1 \cdot 10^{-3}$ mbar) and was then obtained as a colourless wax.
^{1}H NMR: (300 MHz, CD_2Cl_2) δ = 0.24 (s, 12H, SiCH_3), 3.96-3.99 (m, 4H, CH_2), 4.04-4.08 (m, 4H, CH_2), 6.92 (s, 4H, CH_{AR}) ppm. ^{13}C{^{1}H} NMR: (126 MHz, CD_2Cl_2) δ = 0.8 (s, SiCH_3), 63.6 (s, CH_2), 72.5 (s, CH_2), 116.8 (s, C_{AR}), 122.5 (s, C_{AR}), 150.5 (s, C_{ARq}). ^{29}Si{^{1}H} NMR (60 MHz, CD_2Cl_2) δ = 11.5 ppm (s, $SiCH_3$). HR-MS(ESI$^+$): m/z calcd. for $[C_{14}H_{24}O_4Si_2+H]^+$: 313.1291; found: 313.1285 (100). Anal. calcd. for $C_{14}H_{24}O_4Si_2$: C, 53.81; H 7.74. Found: C, 53.67; H, 7.76.

***In situ* NMR monitoring:**
5.0 mg (0.06 mmol) $BeCl_2$ and 0.06 mmol of the ligand were placed in a *J. Young* NMR tube and 0.5 ml CD_2Cl_2 were vacuum transferred into the tube. NMR spectra were recorded in regular time intervals (see NMR spectra below).

Crystallisation of compounds 4 and 5:
$BeCl_2$ (5.0 mg, 0.06 mmol) and 0.06 mmol of ligand **2a** or **3** were placed in a *J. Young* NMR tube and 0.5 ml CD_2Cl_2 were vacuum transferred into the tube. After standing at ambient temperature for two months crystals of compounds **4** suitable for single crystal X-ray diffraction analysis grew on the wall of the vessel, while layering of the reaction solution with benzene led to the formation of crystals of compound **5**.

Synthesis of samples for IR spectroscopy:
8.0 mg (0.10 mmol) $BeCl_2$ and 0.10 mmol of ligand **2a**, **2c** or **3** respectively were weighed into a *Schlenk* tube and 5.0 ml dichloromethane was added *via* cannula and the reaction mixture was stirred for two hours at ambient temperature. Afterwards the solvent was removed *in vacuo* and the received colourless oils were analysed via ATR FT-IR spectroscopy.

Spectroscopic data:

[Be(O(C_2H_4O)$_3$)] (8a): ^{1}H NMR (300 MHz, CD_2Cl_2) δ = 3.75 (bs, $\omega_{1/2}$ = 6.3 Hz, 4H, CH_2), 3.83 (bs, $\omega_{1/2}$ = 15.0 Hz, 4H, CH_2), 4.16 (bs, $\omega_{1/2}$ = 18.7 Hz, 4H, CH_2). ^{9}Be NMR (42 MHz, CD_2Cl_2) δ = 2.7 ($\omega_{1/2}$ = 18.3 Hz). ^{13}C NMR (126 MHz, CD_2Cl_2) δ = 64.2 (bs, $\omega_{1/2}$ = 43.8 Hz, CH_2), 70.0 (bs, $\omega_{1/2}$ = 62.0 Hz, CH_2), 70.9 (bs, $\omega_{1/2}$ = 108.5 Hz, CH_2).

[Be(O(C_2H_4O)($SiMe_2SiMe_2O$)(C_2H_4O)] (8b): ^{9}Be NMR (70 MHz, CD_2Cl_2) δ = 3.4 ($\omega_{1/2}$ = 69.0 Hz). Due to extremely broad signals and the presence of compounds **10b** and **2b** no signal assignment could be performed in the ^{1}H, ^{29}Si and ^{13}C NMR spectra.

[Be(O(C_2H_4O)(C_6H_4O)(C_2H_4O))] (8Ph): ^{9}Be NMR (42 MHz, CD_2Cl_2) δ = 3.1 ($\omega_{1/2}$ = 59.1 Hz). Due to extremely broad signals and the presence of compounds **10Ph** and **3** no signal assignment could be performed in the ^{1}H and ^{13}C NMR spectra.

[BeCl(O(C$_2$H$_4$O)$_3$Me)] (9): ^{1}H NMR (300 MHz, CD_2Cl_2) δ = 3.27 – 3.70 (m, 4H, CH_2), 3.87 (bs, $\omega_{1/2}$ = 25.6 Hz, 7H, CH_2, CH_3), 4.14 (bs, $\omega_{1/2}$ = 15.7 Hz, 4H, CH_2). ^{9}Be NMR (42 MHz, CD_2Cl_2) δ = 3.6 ($\omega_{1/2}$ = 30.1 Hz). ^{13}C NMR (126 MHz, CD_2Cl_2) δ = 59.4 (bs, $\omega_{1/2}$ = 61.1 Hz, CH$_3$), 63.8 (bs, $\omega_{1/2}$ = 37.9 Hz, CH$_2$), 70.4 (bs, $\omega_{1/2}$ = 21.7 Hz, CH$_2$), 71.1 (bs, $\omega_{1/2}$ = 53.6 Hz, CH$_2$), 72.1 (bs, $\omega_{1/2}$ = 81.8 Hz, CH$_2$).

[BeCl(O(C$_2$H$_4$O)$_3$SiMe$_2$SiMe$_2$Cl)] (10a): ^{1}H NMR (500 MHz, CD_2Cl_2) δ = 0.31 (s, 6H, OSiMe_2SiMe$_2$Cl), 0.51 (s, 6H, OSiMe$_2$SiMe_2Cl), 3.49 – 3.53 (m, 4H, CH_2), 3.58 (s, 4H, CH_2), 3.71 – 3.76 (m, 4H, CH_2). ^{9}Be NMR (70 MHz, CD_2Cl_2) δ = 3.4 ($\omega_{1/2}$ = 60.5 Hz). ^{13}C NMR (126 MHz, CD_2Cl_2) δ −1.0 (OSiMe_2SiMe$_2$Cl), 2.7 (OSiMe$_2$SiMe_2Cl), 63.9 (CH$_2$), 71.1 (CH$_2$), 73.0 (CH$_2$). ^{29}Si NMR (99 MHz, CD_2Cl_2) δ = 11.5 (s, OSiMe$_2$SiMe$_2$Cl), 18.4 (s, OSiMe$_2$$SiMe_2$Cl).

[BeCl(O(C$_2$H$_4$O)(SiMe$_2$SiMe$_2$O)(C$_2$H$_4$O)SiMe$_2$SiMe$_2$Cl)] (10b): ^{1}H NMR (500 MHz, CD_2Cl_2) δ = 0.26 (s, 12H, OSiMe$_2$$SiMe_2$O), 0.31 (s, 6H, OSi$Me_2$SiMe$_2$Cl), 0.51 (s, 6H, OSiMe$_2SiMe_2$Cl), 3.67 (s, 2H, C$H_2$), 3.82 (s, 6H, C$H_2$). ^{9}Be NMR (70 MHz, CD_2Cl_2) δ = 2.5 ($\omega_{1/2}$ = 53.2 Hz). ^{13}C NMR (126 MHz, CD_2Cl_2) δ = −1.0 (OSiMe_2SiMe$_2$Cl), −0.1 (OSiMe$_2$$SiMe_2$O), 2.8 (OSiMe$_2SiMe_2$Cl), 65.7 ($CH_2$), 67.0 ($CH_2$). ^{29}Si NMR (99 MHz, CD_2Cl_2) δ = 11.6 (s, OSiMe$_2$$SiMe_2$O), 11.8 (s, O$SiMe_2$SiMe$_2$Cl), 18.6 (s, OSiMe$_2$$SiMe_2$Cl).

[BeCl(O(C$_2$H$_4$O)(C$_6$H$_4$O)(C$_2$H$_4$O)SiMe$_2$SiMe$_2$Cl)] (10Ph): ^{1}H NMR (500 MHz, CD_2Cl_2) δ = 0.36 (s, 6H, OSiMe_2SiMe$_2$Cl), 0.52 (s, 6H, OSiMe$_2$SiMe_2Cl), 3.96 – 4.00 (m, 4H, CH_2), 4.05 – 4.08 (m, 4H, CH_2), 6.86 – 6.98 (m, 2H, H_{Ar}), 7.18 – 7.26 (m, 2H, H_{Ar}). ^{9}Be NMR (42 MHz, CD_2Cl_2) δ = 3.1 ($\omega_{1/2}$ = 59.1 Hz). ^{13}C NMR (126 MHz, CD_2Cl_2) δ = −1.0 (OSiMe_2SiMe$_2$Cl), 2.7 (OSiMe$_2$SiMe_2Cl), 63.2 (CH$_2$), 70.7 (CH$_2$), 114.6 (C_{Ar}H), 121.8 (C_{Ar}H), 149.3 (C_{Ar}). ^{29}Si NMR (99 MHz, CD_2Cl_2) δ = 12.2 (s, OSiMe$_2$SiMe$_2$Cl), 18.3 (s, OSiMe$_2$$SiMe_2$Cl).

[BeCl$_2$(1,2-disila[12]crown-4)] (11a): ^{1}H NMR (500 MHz, CD_2Cl_2) δ = 0.24 (s, 12H, SiMe_2), 3.60 (s, 4H, CH_2), 3.69 – 3.72 (m, 4H, CH_2). ^{13}C NMR (126 MHz, CD_2Cl_2) δ −0.1 (SiMe_2), 0.0 (SiMe_2), 63.6 (CH$_2$), 71.2 (CH$_2$), 73.1 (CH$_2$). ^{29}Si NMR (99 MHz, CD_2Cl_2) δ = 11.4 (SiMe$_2$). FT-IR (cm^{-1}): 2951 (m), 2884 (m), 1458 (w), 1395 (w), 1350 (w), 1293 (w), 1248 (m, Si-Me), 1136 (m, Si-O/C-O), 1083 (s, Si-O/C-O), 1046 (s, Si-O/C-O), 930 (s), 822 (m), 789 (s, Si-Me), 767 (s, Si-Me), 728 (s), 687 (w), 671 (w), 628 (s), 522 (m), 484 (s, Be-Cl), 404 (m).

[BeCl$_2$(1,2,4,5-tetrasila[12]crown-4)] (11c): ^{1}H NMR (500 MHz, CD_2Cl_2) δ = 0.19 (s, 6H, SiMe_2), 0.20 (s, 6H, SiMe_2), 3.58 – 3.64 (m, 4H, CH_2), 3.74 – 3.77 (m, 4H, CH_2). ^{13}C NMR (126 MHz, CD_2Cl_2) δ = 0.41 (SiMe_2OSiMe_2), 2.5 (SiMe_2OCH$_2$), 63.2 (CH$_2$OSiMe$_2$), 73.1 (CH$_2$OCH$_2$). ^{29}Si NMR (99 MHz, CD_2Cl_2) δ = 3.8 (s, SiOSi), 10.7 (SiOC). FT-IR (cm^{-1}): 2949 (m), 2882 (w), 1593 (w), 1501 (m), 1454 (m), 1399 (w), 1248 (s, Si-Me), 1218 (m), 1126 (m, Si-O/C-O), 1091 (s, Si-O/C-O), 1042 (s, Si-O/C-O), 926 (s), 822 (m), 791 (m), 763 (s, Si-Me), 742 (s, Si-Me), 683 (m), 634 (s), 598 (m), 481 (s, Be-Cl), 406 (m).

[BeCl$_2$(1,2-disila-benzo[12]crown-4)] (11Ph): FT-IR (cm^{-1}): 2945 (m), 2880 (m), 1593 (w), 1501 (m), 1452 (m), 1399 (w), 1356 (w), 1328 (w), 1289 (w), 1250 (s, Si-Me), 1216 (m), 1126 (m, Si-O/C-O), 1089 (s, Si-O/C-O), 1046 (s, Si-O/C-O), 938 (s), 830 (s), 787 (s), 767 (s, Si-Me), 738 (s, Si-Me), 632 (m), 528 (m, Be-Cl), 483 (m).

Crystallographic details

Table S1: Crystallographic details of compounds **4** & **5**

	4 · CH_2Cl_2	**5** · 2 C_6H_6
empirical formula	$C_{25}H_{50}Be_6Cl_6O_{16}$	$C_{48}H_{52}Be_6Cl_4O_{14}$
color and appearance	colourless block	colourless block
molecular mass / g mol^{-1}	873.41	1048.75
cryst. syst.	monoclinic	triclinic
space group type (No.)	*C*2/*c* (15)	$P\bar{1}$ (2)
a / Å	19.481(4)	9.8872(5)
b / Å	9.549(2)	12.0013(6)
c / Å	21.762(4)	12.2122(6)
α / °	90	108.235(2)
β / °	106.72(3)	103.883(2)
γ / °	90	106.623(2)
volume / Å^3	3877.2(15)	1229.35(11)
Z	4	1
λ / Å	0.71073 (Mo-K_α)	0.71073 (Mo-K_α)
T / K	100(2)	100(1)
μ / mm^{-1}	0.509	0.307
Θ_{max}	26.371	24.91
hkl_{max}	$-24 \le h \le 24$	$-11 \le h \le 11$
	$-11 \le k \le 11$	$-14 \le k \le 14$
	$-19 \le l \le 27$	$-14 \le l \le 14$
crystal size / mm^3	0.11 · 0.10 · 0.09	0.26 · 0.16 · 0.09
R_{int}, R_σ	0.081, 0.057	0.022, 0.039
$R(F)$ ($I \ge 2\sigma(I)$, all data)	0.053, 0.064	0.040, 0.049
$wR(F^2)$ ($I \ge 2\sigma(I)$, all data)	0.140, 0.148	0.096, 0.100
S (all data)	1.069	1.046
data, parameter, restraints	3895, 226, 0	4297, 325, 0
$\Delta\rho_{max}$, $\Delta\rho_{min}$ / e Å^{-3}	0.693 / −0.488	0.552 / −0.310

NMR spectra

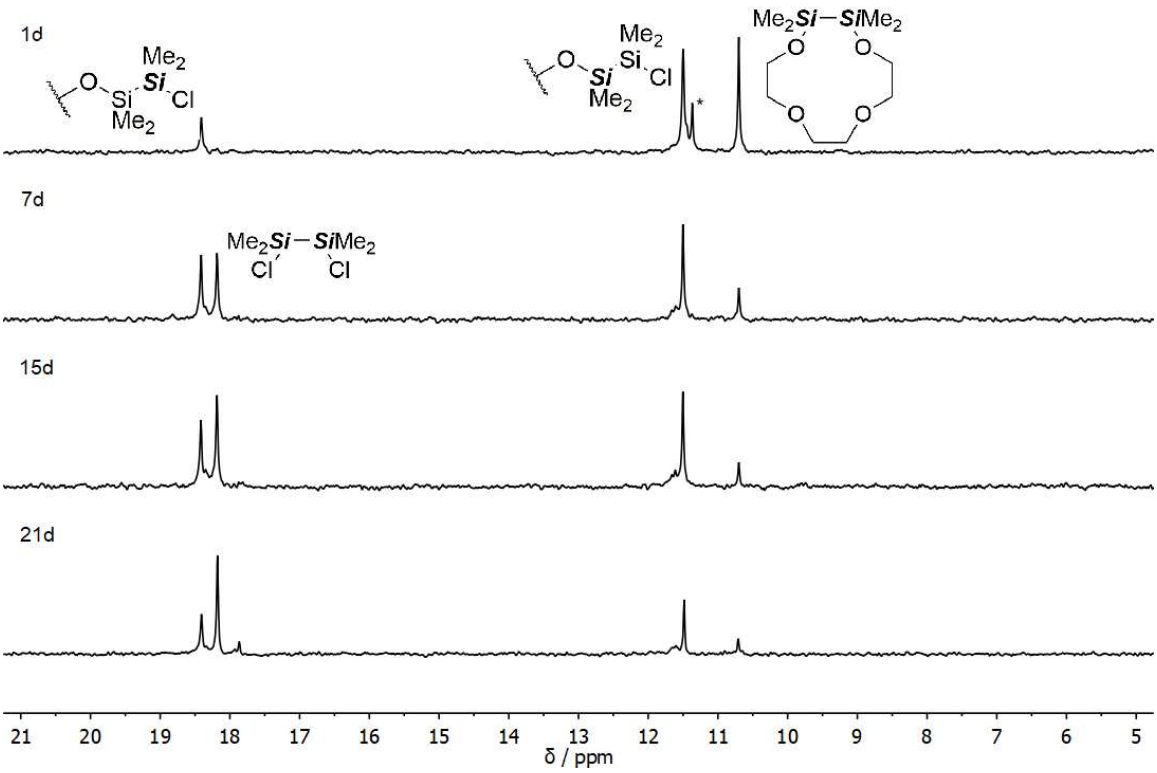

Figure S1: ^{29}Si NMR spectra of the reaction of $BeCl_2$ with ligand **2a** after different reaction times in CD_2Cl_2. The signal marked with an asterisk presumably originates from compound **11a**.

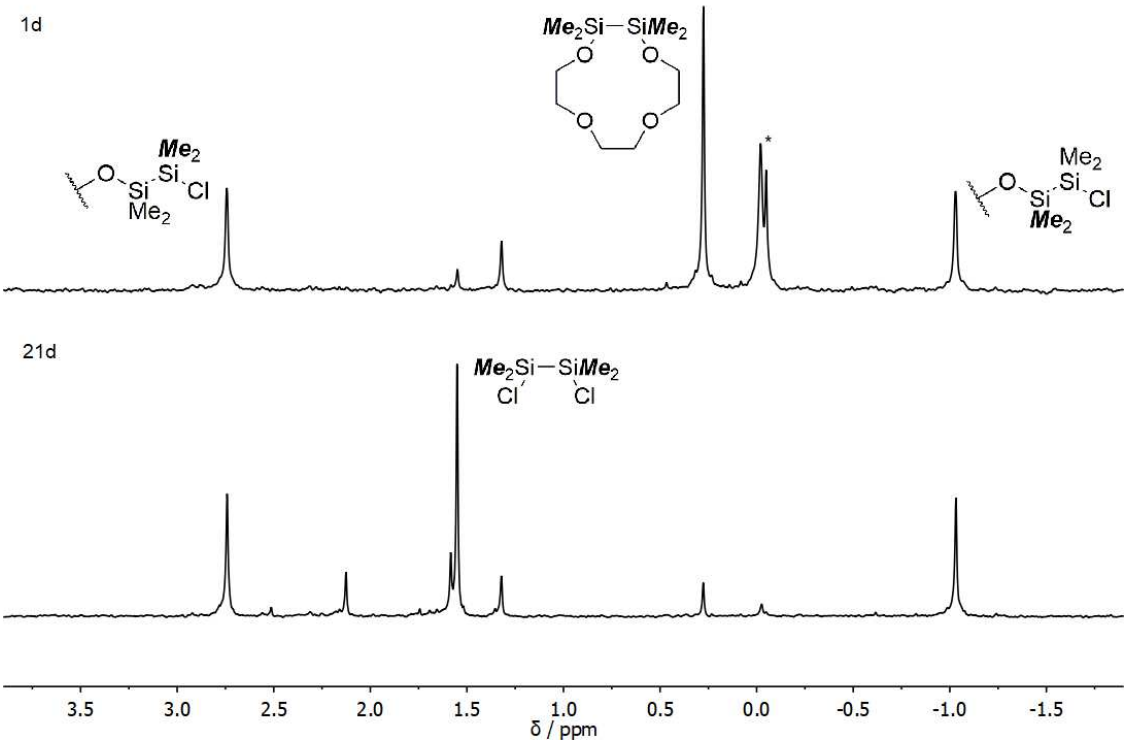

Figure S2: ^{13}C NMR spectra of the reaction of $BeCl_2$ with ligand **2a** after different reaction times in CD_2Cl_2. The signal marked with an asterisk presumably originates from compound **11a**.

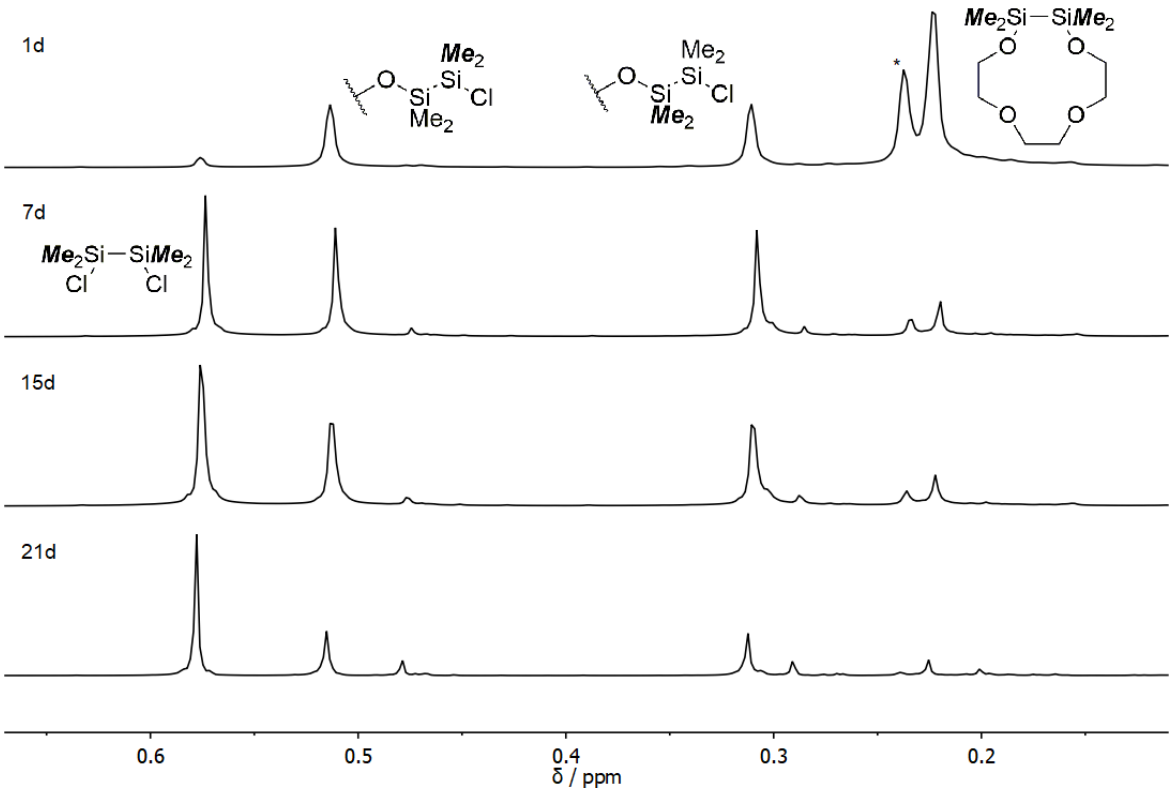

Figure S3: ^{1}H NMR spectra of the reaction of $BeCl_2$ with ligand **2a** after different reaction times in CD_2Cl_2. The signal marked with an asterisk presumably originates from compound **11a**.

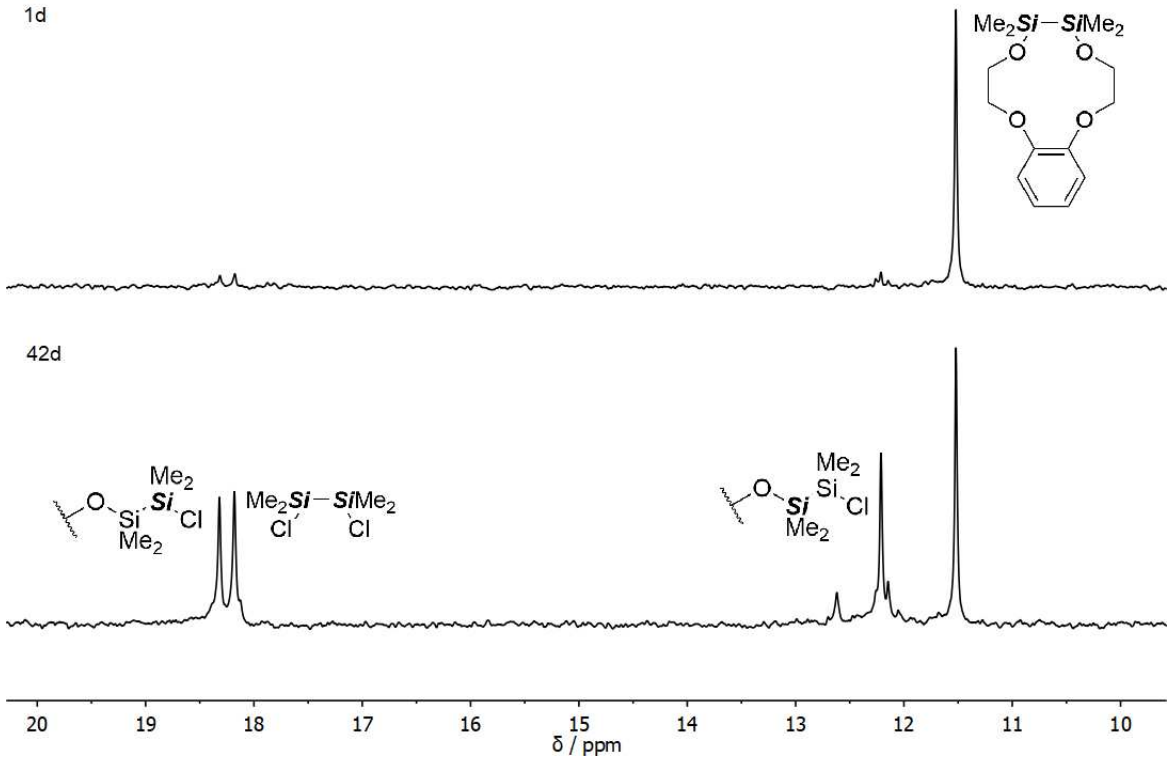

Figure S4: ^{29}Si NMR spectra of the reaction of $BeCl_2$ with ligand **3** after different reaction times in CD_2Cl_2.

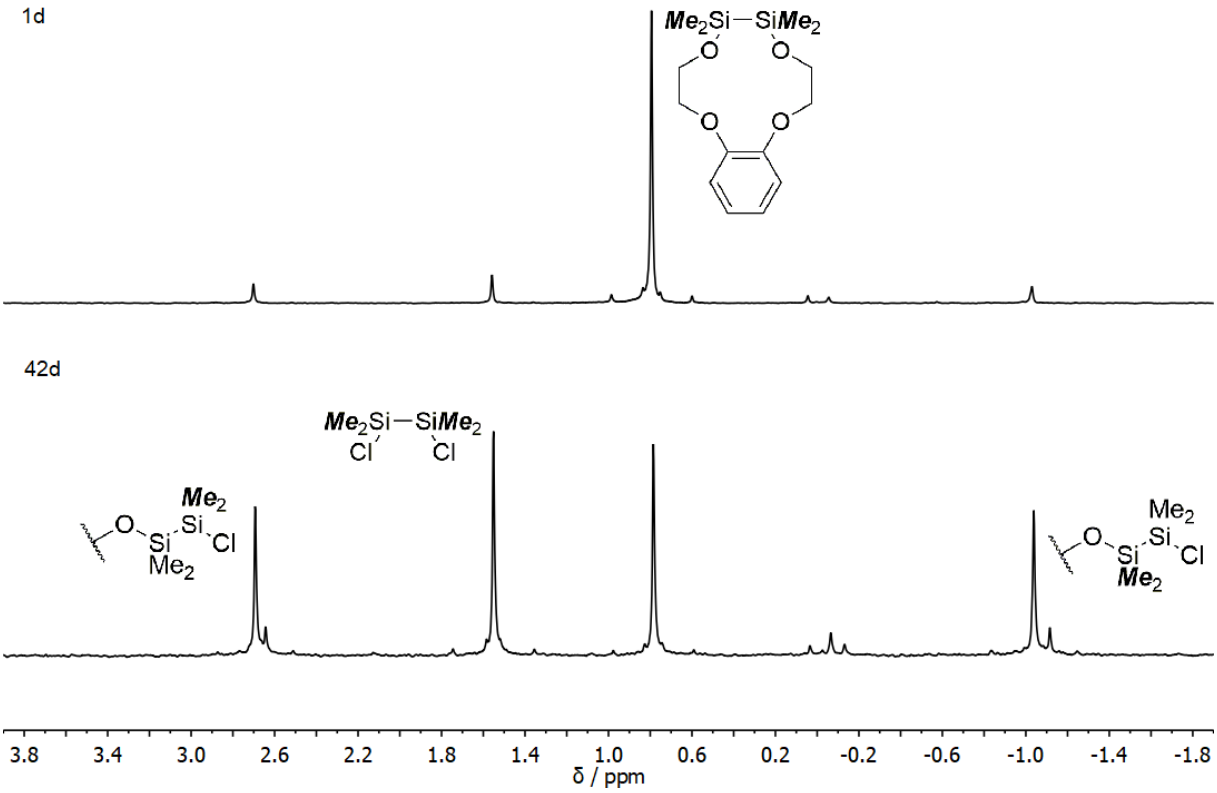

Figure S5: ^{13}C NMR spectra of the reaction of $BeCl_2$ with ligand **3** after different reaction times in CD_2Cl_2.

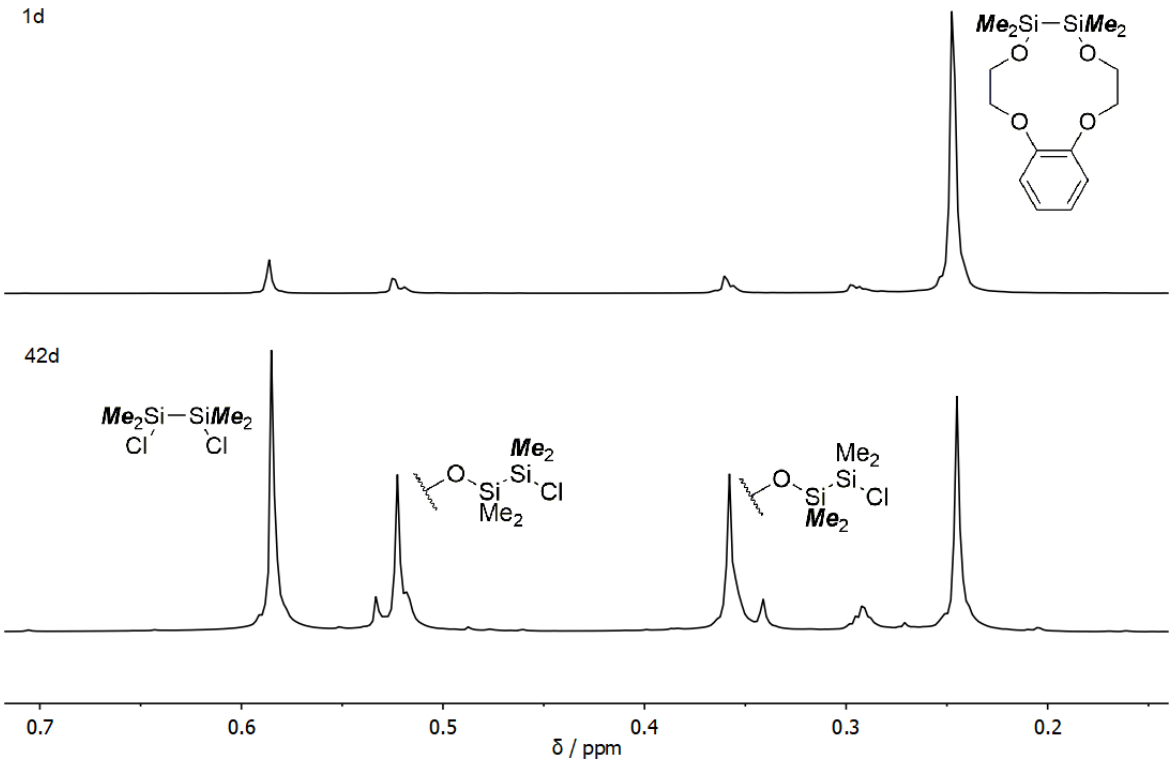

Figure S6: ^{1}H NMR spectra of the reaction of $BeCl_2$ with ligand **3** after different reaction times in CD_2Cl_2.

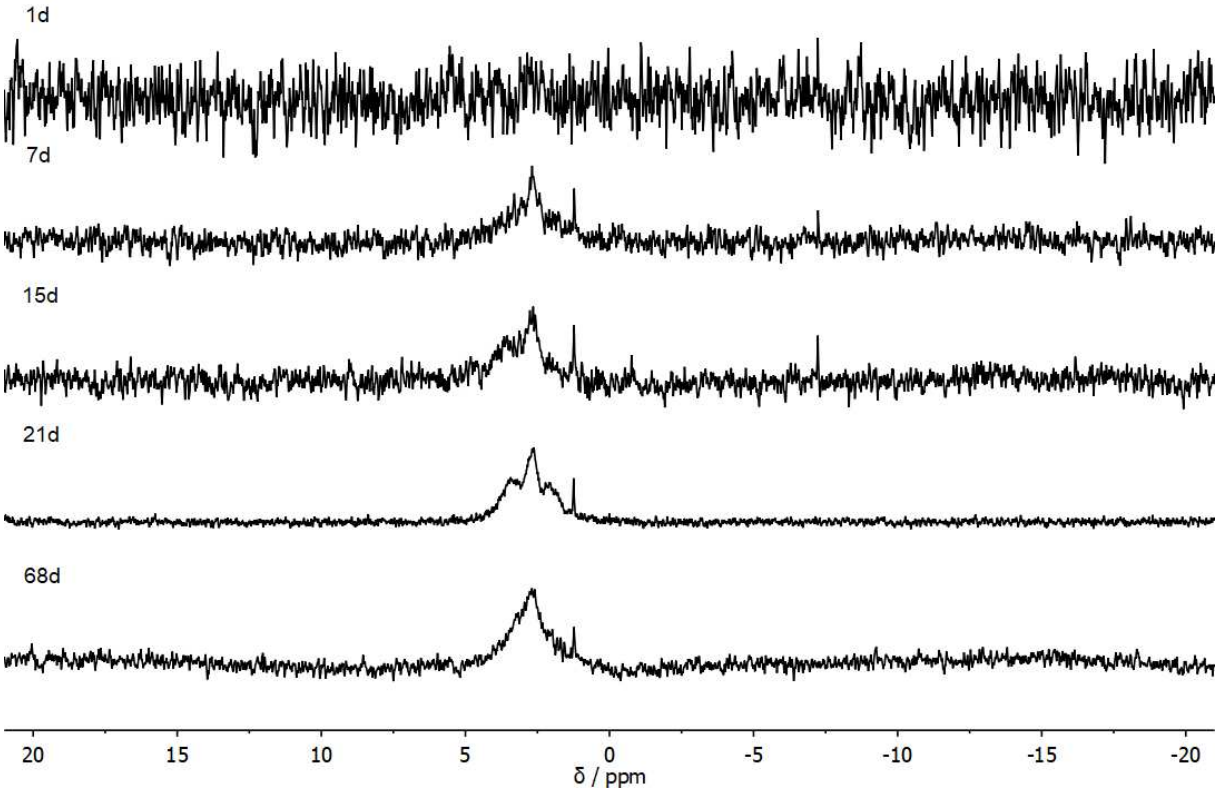

Figure S7: ^{9}Be NMR spectra of the reaction of $BeCl_2$ with ligand **2a** after different reaction times in CD_2Cl_2.

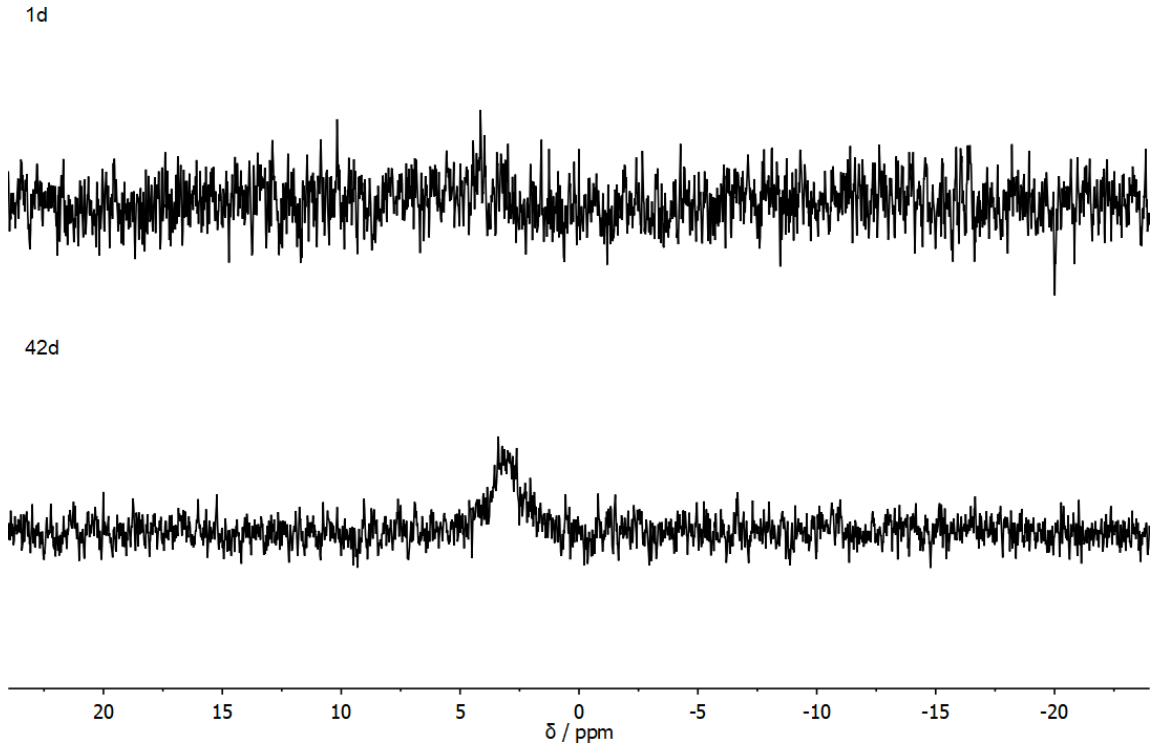

Figure S8: ^{9}Be NMR spectra of the reaction of $BeCl_2$ with ligand **3** after different reaction times in CD_2Cl_2.

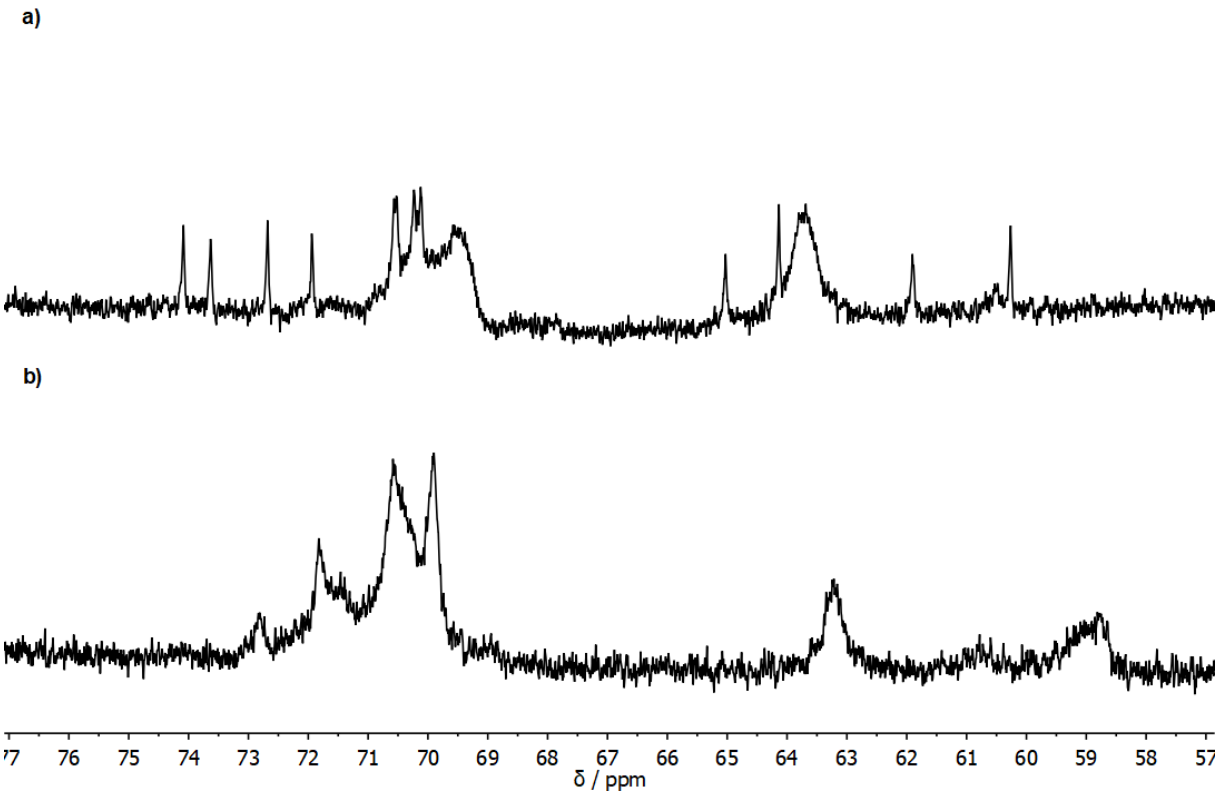

Figure S9: ^{13}C NMR spectra of the reaction of $BeCl_2$ with a) ligand **6** and b) ligand **7** in CD_2Cl_2.

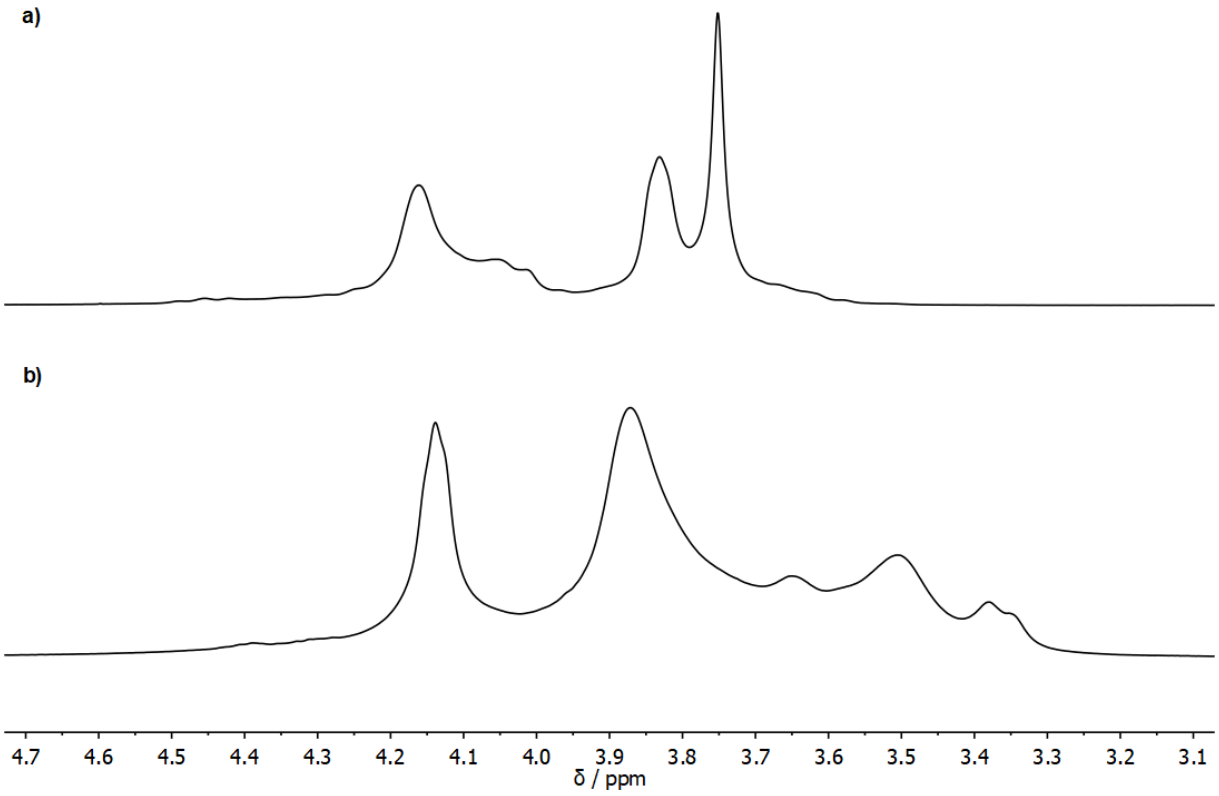

Figure S10: ^{1}H NMR spectra of the reaction of $BeCl_2$ with a) ligand **6** and b) ligand **7** in CD_2Cl_2.

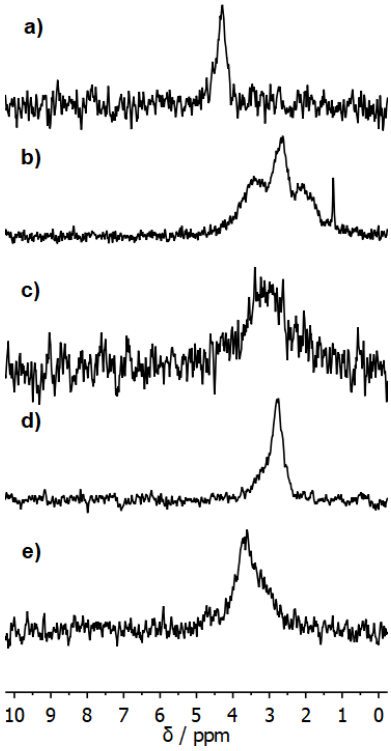

Figure S11: ^{9}Be NMR spectra of $BeCl_2$ with [12]crown-4 (a), ligands **2a** (b), **3** (c), **6** (d) or **7** (e) in CD_2Cl_2 respectively.

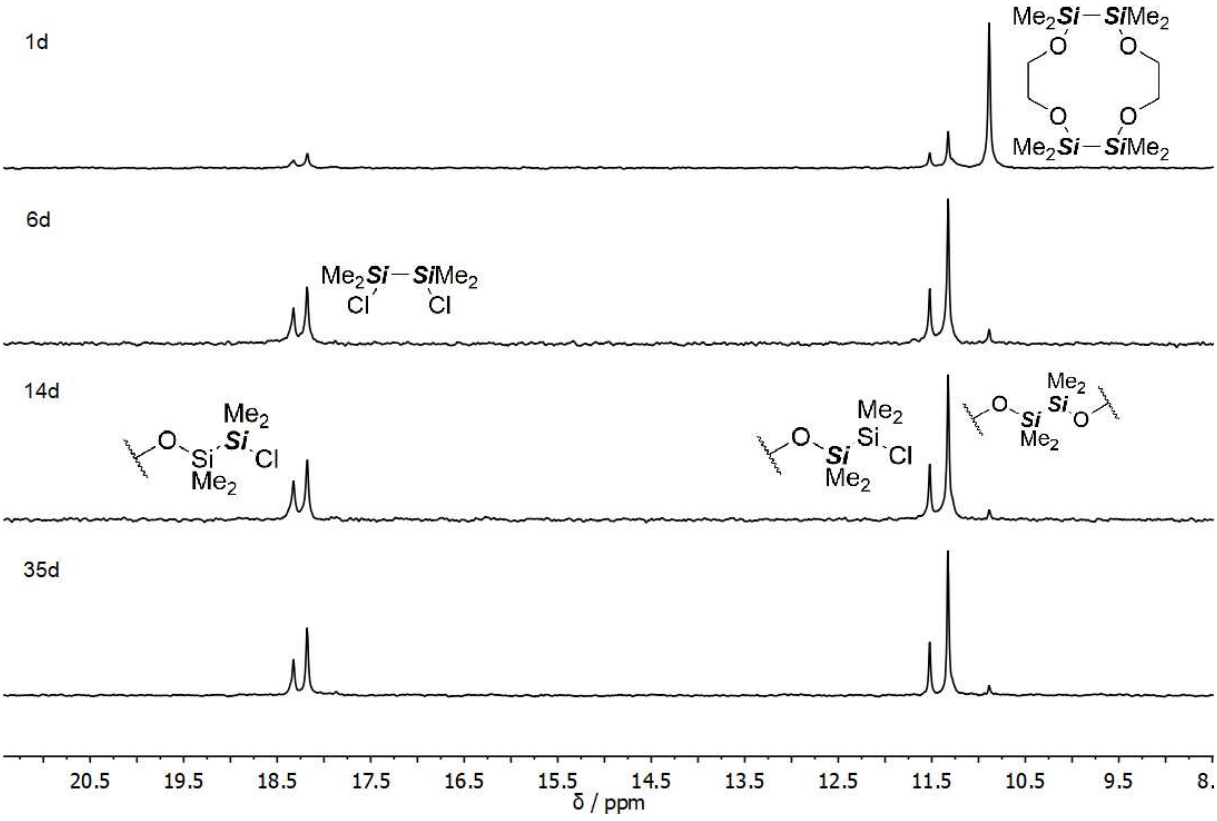

Figure S12: ^{29}Si NMR spectra of the reaction of $BeCl_2$ with ligand **2b** after different reaction times in CD_2Cl_2.

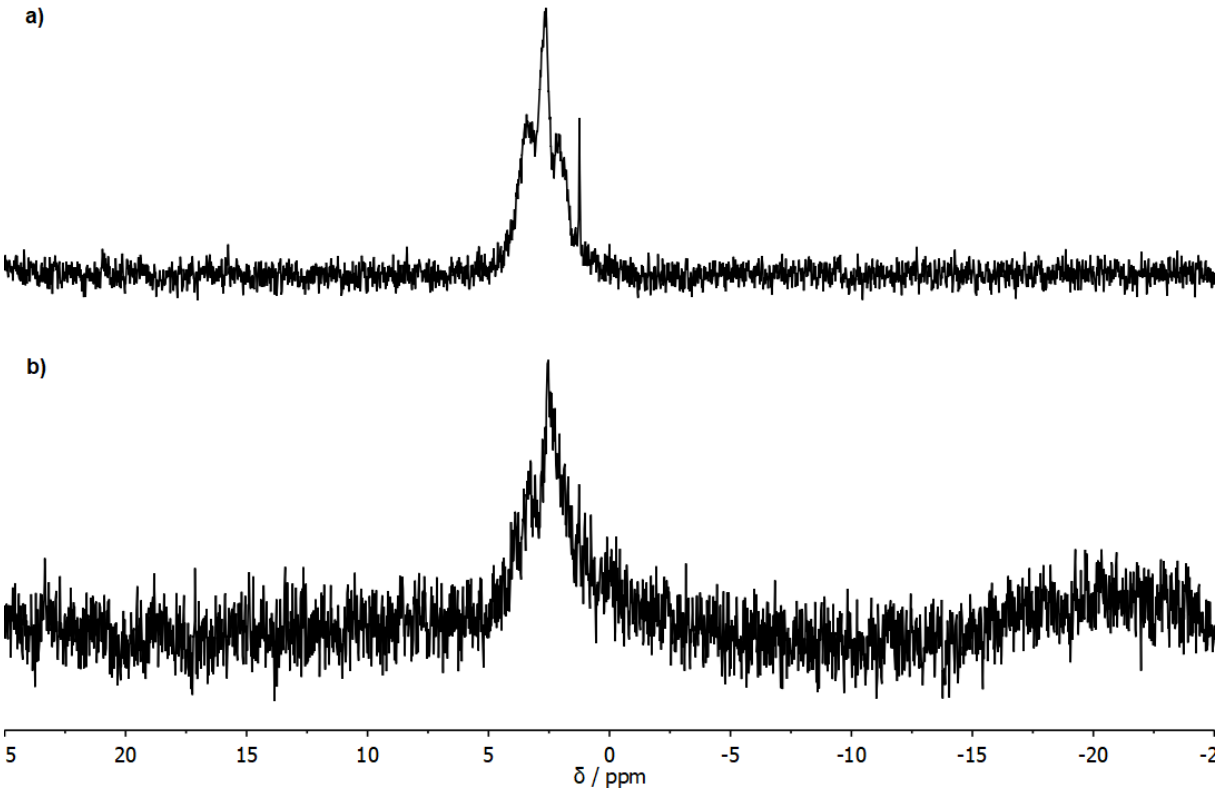

Figure S13: ^{9}Be NMR spectra of the reaction of $BeCl_2$ with a) ligand **2a** and b) ligand **2b** in CD_2Cl_2.

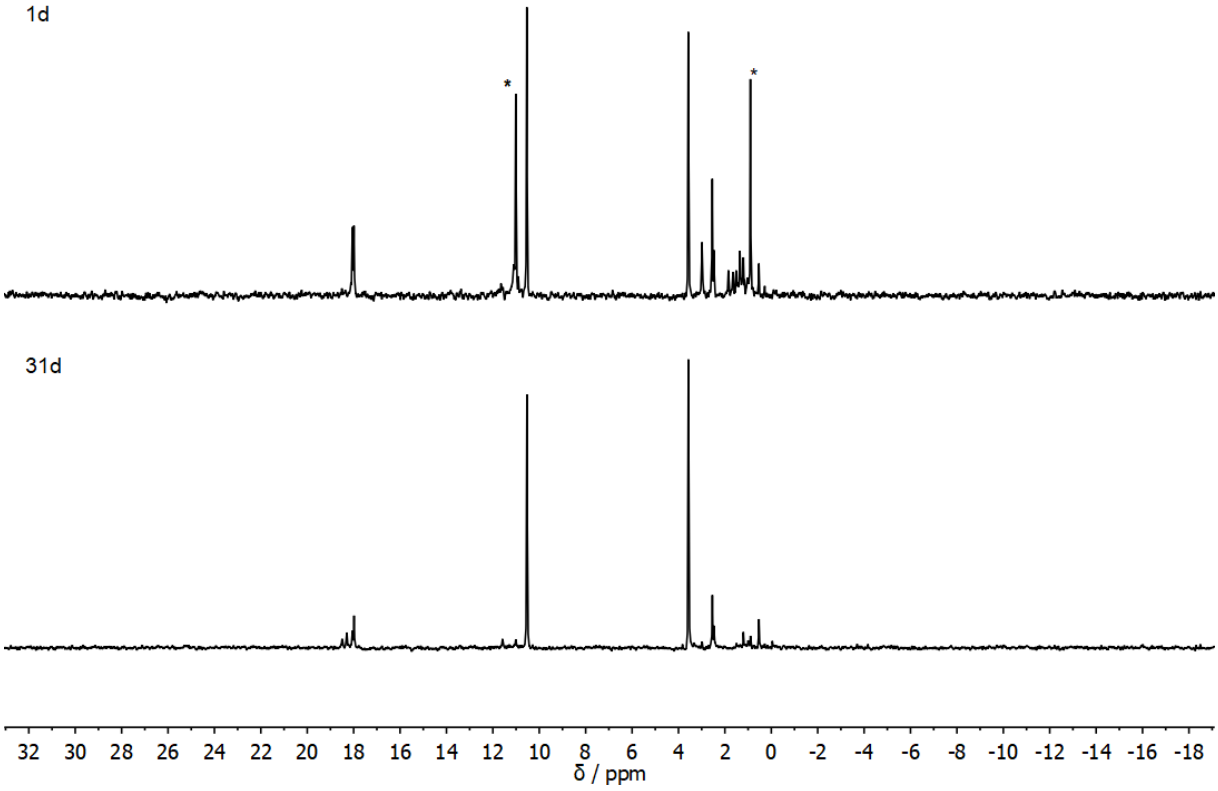

Figure S14: ^{29}Si NMR spectra of the reaction of $BeCl_2$ with ligand **2c** after different reaction times in CD_2Cl_2. Free ligand is marked with an asterisk.

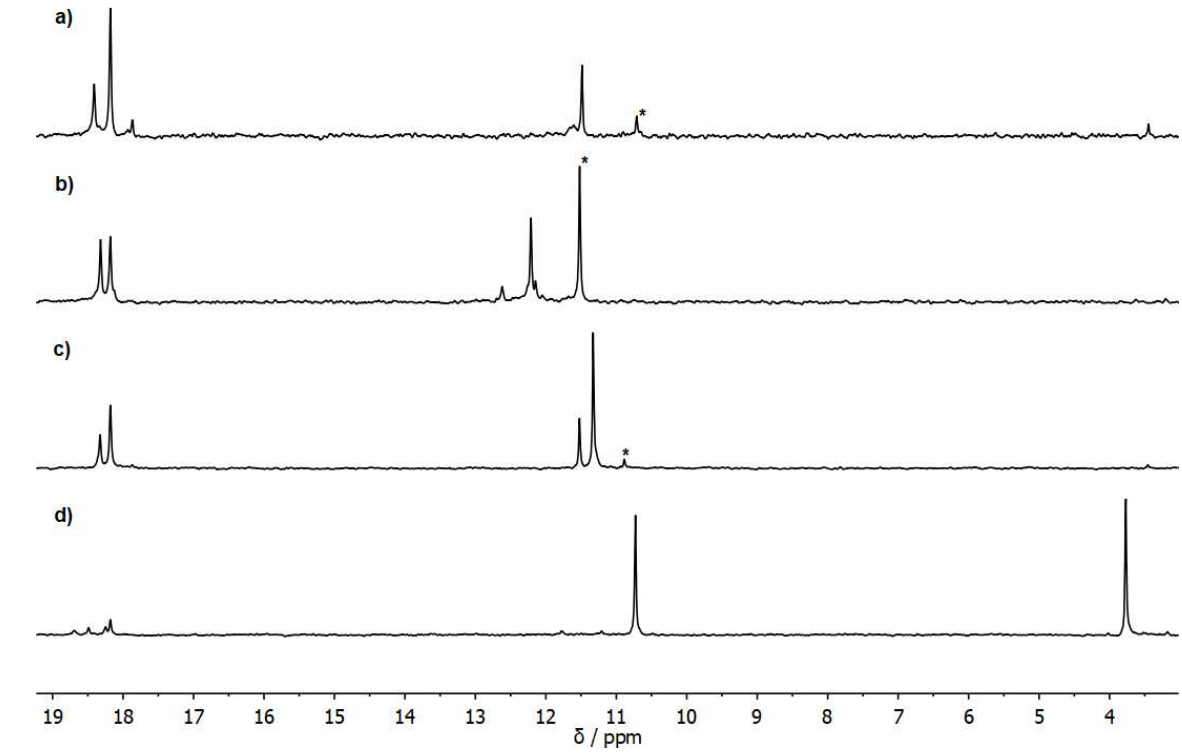

Figure S15: ^{29}Si NMR spectra of the reaction of $BeCl_2$ with ligands a) **2a**, b) **3**, c) **2b** and d) **2c** in CD_2Cl_2. Free ligand is marked with an asterisk.

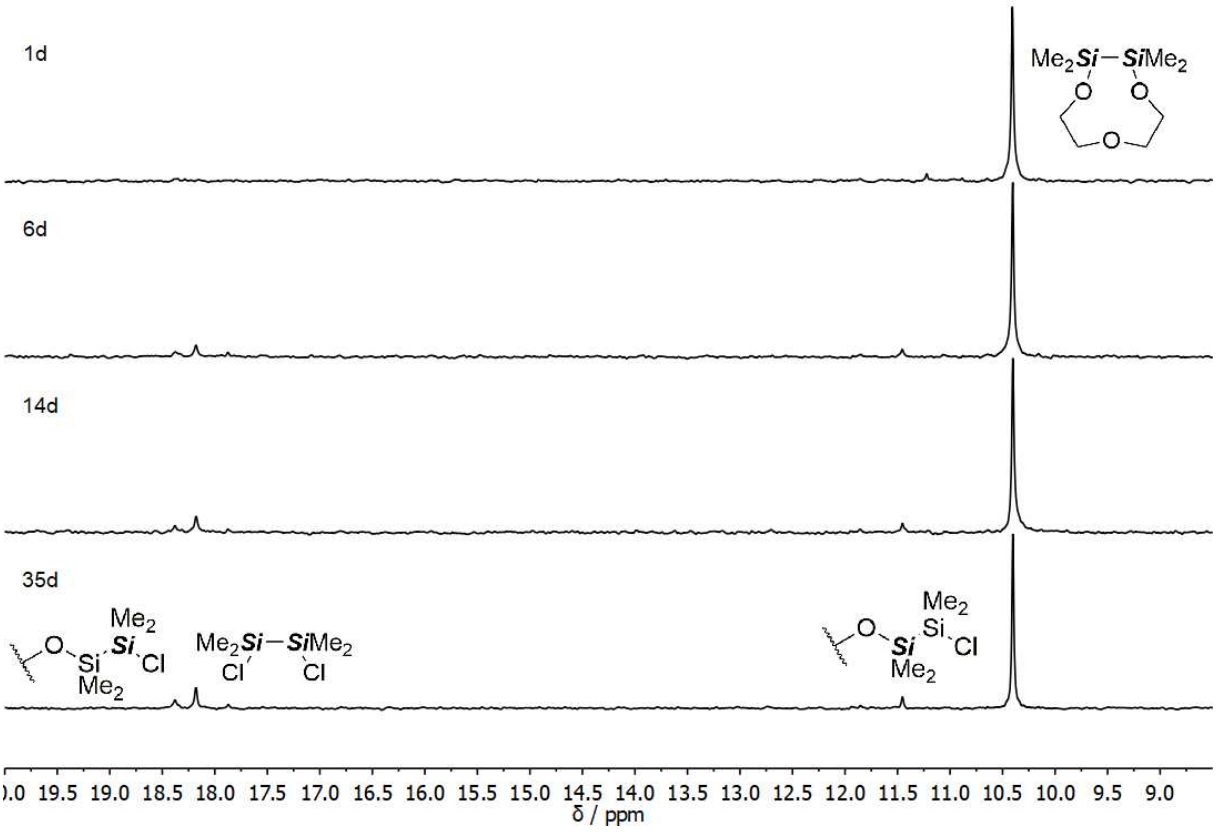

Figure S16: ^{29}Si NMR spectra of the reaction of $BeCl_2$ with ligand **15** after different reaction times in CD_2Cl_2.

IR spectra

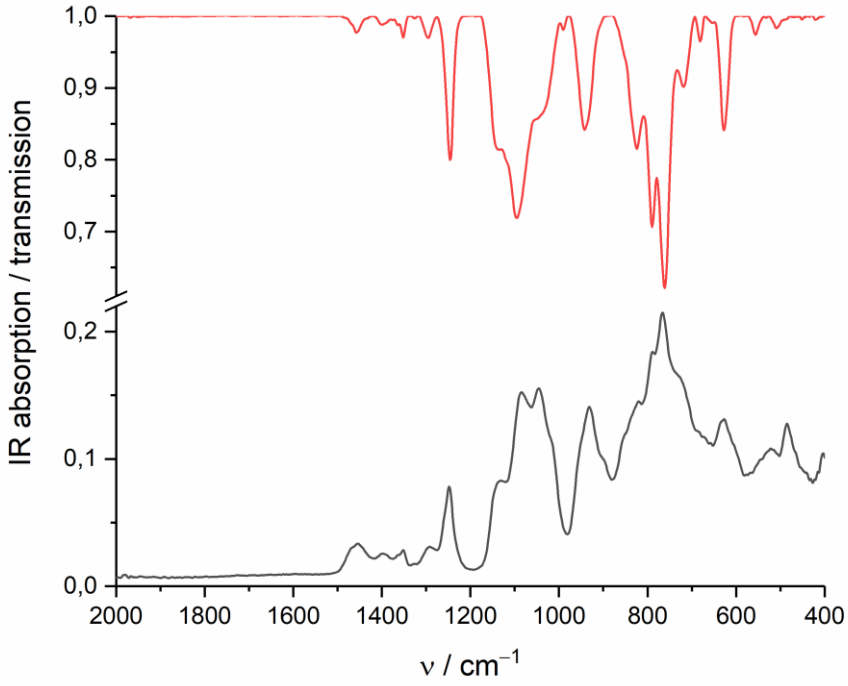

Figure S17: Detail of the FT-IR spectra of 1,2-disila[12]crown-4 (**2a**) before (red) and after reaction with $BeCl_2$ (black).

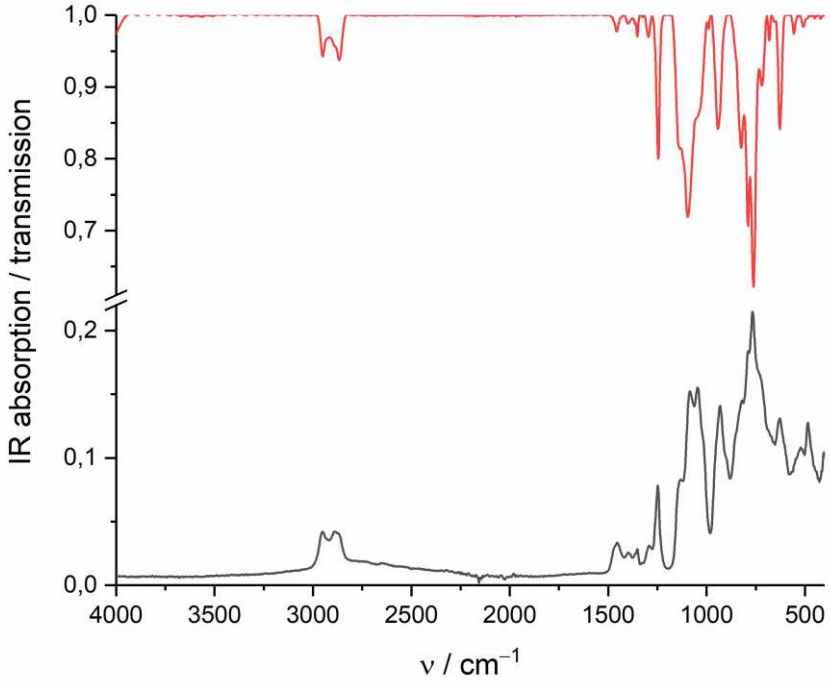

Figure S18: FT-IR spectra of 1,2-disila[12]crown-4 (**2a**) before (red) and after reaction with $BeCl_2$ (black).

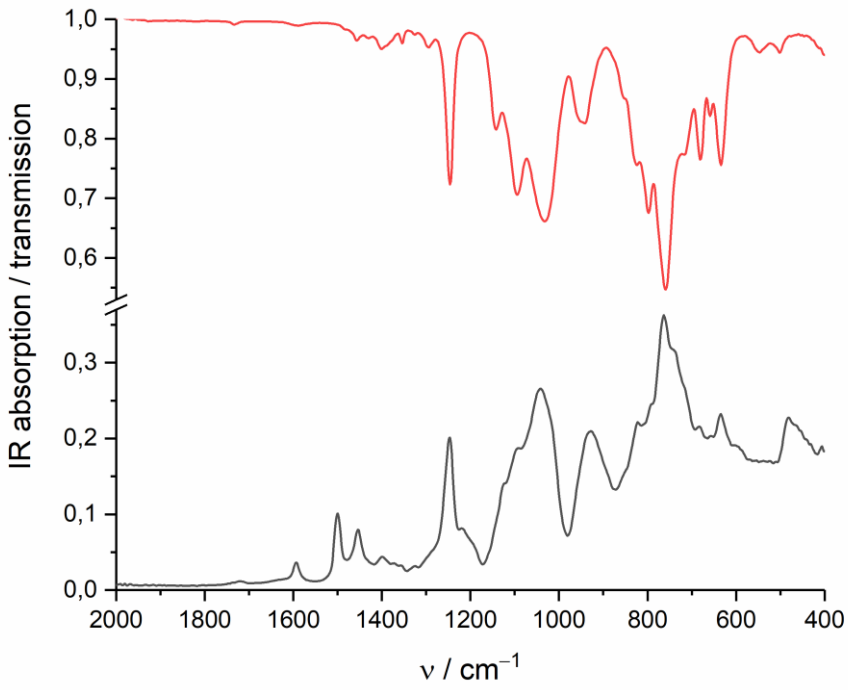

Figure S19: Detail of the FT-IR spectra of 1,2,4,5-tetrasila[12]crown-4 (**2c**) before (red) and after reaction with $BeCl_2$ (black).

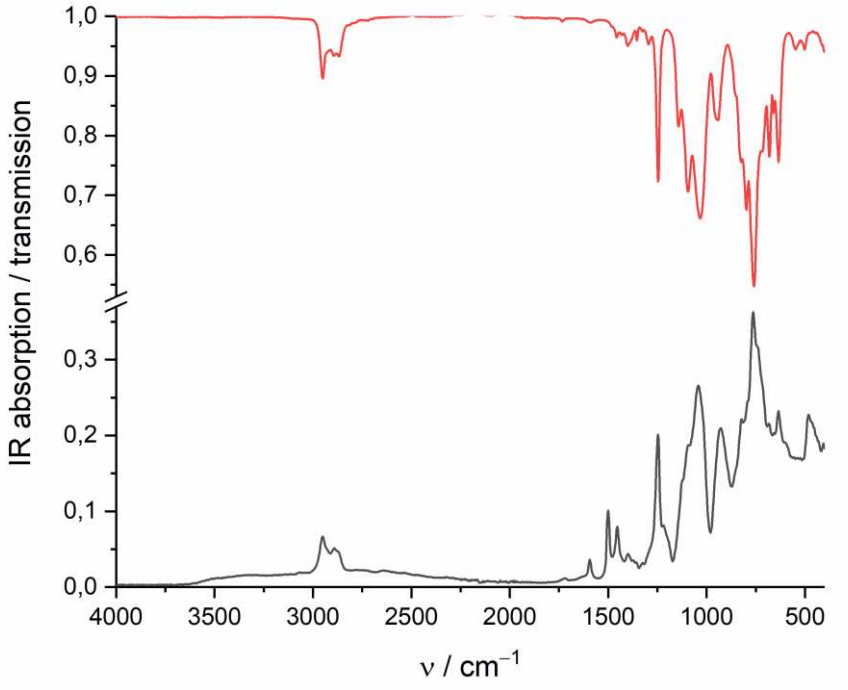

Figure S20: FT-IR spectra of 1,2,4,5-tetrasila[12]crown-4 (**2c**) before (red) and after reaction with $BeCl_2$ (black).

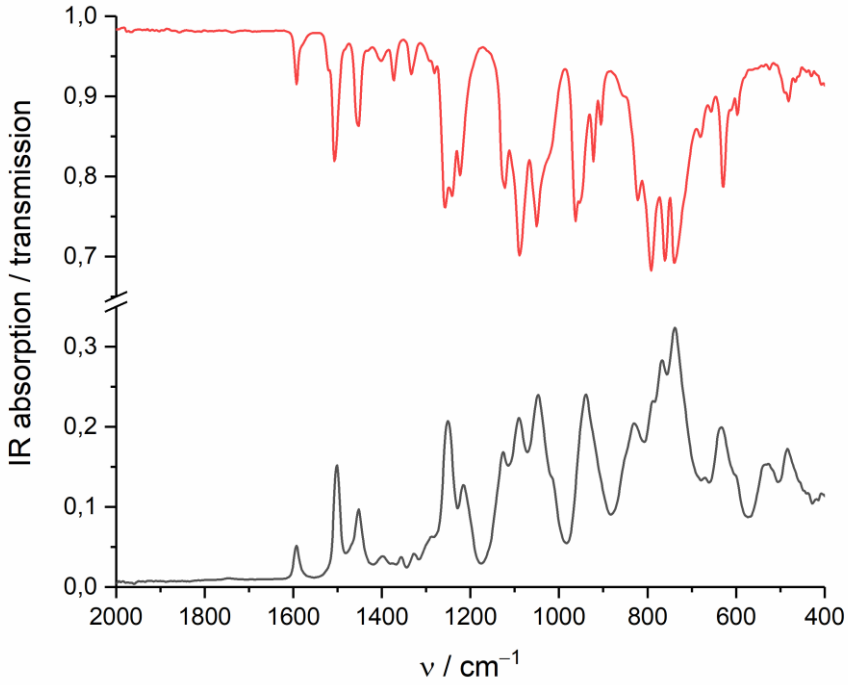

Figure S21: Detail of the FT-IR spectra of 1,2-disila-benzo[12]crown-4 (**3**) before (red) and after reaction with $BeCl_2$ (black).

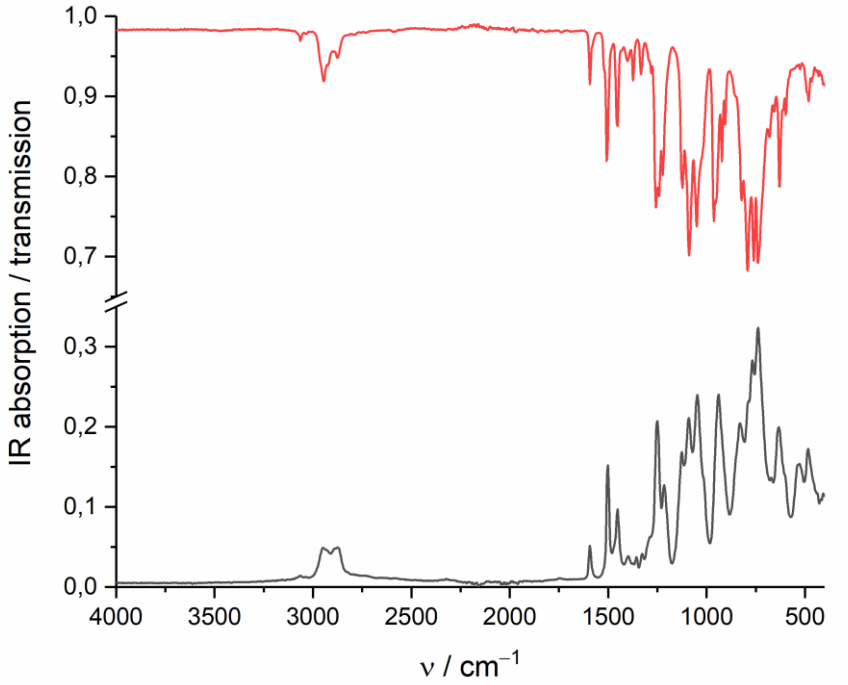

Figure S22: FT-IR spectra of 1,2-disila-benzo[12]crown-4 (**3**) before (red) and after reaction with $BeCl_2$ (black).

References

[1] M. Müller, F. Pielnhofer, M. R. Buchner, *Dalton Trans.* **2018**, doi: 10.1039/C8DT01756E.

[2] K. Reuter, M. R. Buchner, G. Thiele, C. von Hänisch, *Inorg. Chem.* **2016**, *55*, 4441.

[3] K. Reuter, G. Thiele, T. Hafner, F. Uhlig, C. von Hänisch, *Chem. Commun.* **2016**, *52*, 13265.

[4] F. Dankert, J. Heine, J. R. C. von Hänisch, *CrystEngComm* **2018**, doi: 10.1039/C8CE01097H.

[5] F. Dankert, K. Reuter, C. Donsbach, C. von Hänisch, *Dalton Trans.* **2017**, *46*, 8727.

[6] M. A. Peshkova, N. V. Timofeeva, A. L. Grekovich, S. M. Korneev, K. N. Mikhelson, *Electroanalysis* **2010**, *22*, 2147–2156.

[7] MestReNova, Mestrelab Research S.L., Santiago de Compostela, Spain **2011**.

[8] OPUS, Bruker Optik GmbH, Ettlingen, Germany **2009**.

[9] OriginPro 2017, OriginLab Corporation, Northampton, MA, USA **2017**.

[10] a) *X-Area*, Stoe & Cie GmbH, Darmstadt, Germany, **2011**; b) *X-Shape*, Stoe & Cie GmbH, Darmstadt, Germany, **2009**; c) *X-Red32*, Stoe & Cie GmbH, Darmstadt, Germany, **2009** .

[11] a) G. M. Sheldrick, *SHELXS-2013/1*, Göttingen, Germany, **2013**; b) G. M. Sheldrick, *Acta Crystallogr., Sect. A: Fundam. Crystallogr.* 2015, **71**, 3; c) G. M. Sheldrick, *SHELXL-2016/4*, Göttingen, Germany, **2016**; d) C. B. Hübschle, G. M. Sheldrick, B. Dittrich, *J. Appl. Crystallogr.* **2011**, *44*, 1281; e) O. V. Dolomanov, L. J. Bourhis, R. J. Gildea, J. A. K. Howard and H. Puschmann, *J. Appl. Crystallogr.* 2009, **42**, 339 .

Inorganic Chemistry
Article
Cite This: Inorg. Chem. 2019, 58, 3518−3526
pubs.acs.org/IC

Insights into the Coordination Ability of Siloxanes Employing Partially Silicon Based Crown Ethers: A Comparative Analysis of s-Block Metal Complexes

Fabian Dankert and Carsten von Hänisch*

Fachbereich Chemie and Wissenschaftliches Zentrum für Materialwissenschaften (WZMW), Philipps-Universität Marburg, Hans-Meerwein-Straße 4, 35043 Marburg, Germany

ABSTRACT: Herein we present the synthesis and coordination chemistry of the partially silicon based crown ether analogues 1,2,4,5-tetrasila-benzo[15]crown-5 (**1**) and 1,2,4,5-tetrasila[18]crown-6 (**7**). Stable complexes of alkali and alkaline earth metal iodides could be obtained showing the good coordination ability of these ligands. The complexes $[M_A(1,2,4,5\text{-tetrasila-benzo}[15]\text{crown-}5)I]$ (M_A = Li^+ (**2**), Na^+ (**4**)) and $[M_{EA}(1,2,4,5\text{-tetrasila-benzo}[15]\text{crown-}5)I_2]$ (M_{EA} = Mg^{2+} (**3**), Ca^{2+} (**5**), Sr^{2+} (**6**)) were obtained by equimolar reaction of **1** with the respective alkali or alkaline earth metal iodide. Depending on the ionic radii of the respective cations, the coordination modes of the siloxane backbone are significantly different and could be well-represented by means of ^{29}Si NMR spectroscopy. In addition, we were able to generate the unusual dinuclear complex $[Ba_2(1,2,4,5\text{-tetrasila}[18]\text{crown-}6)_2I_4]$ (**8**) by reaction of **7** with BaI_2. All compounds were characterized via single crystal X-ray diffraction (XRD) analysis.

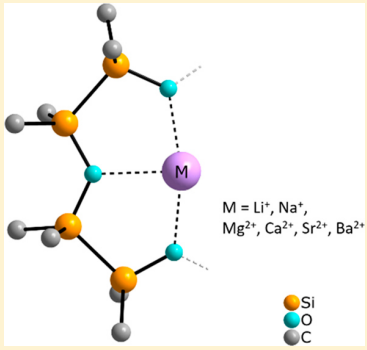

INTRODUCTION

The silicon analogues of crown ethers and cryptands opened a new chapter in host−guest chemistry, and the imitation of organic analogues can help to understand the Si−O bond, especially regarding the Lewis basicity of silicon affected oxygen atoms.[1] The Lewis basicity of siloxane compounds has been intensely discussed over the past years, but all considerations of the Si−O bond conclude a lower basicity of the oxygen atoms in comparison to those bonds in carbon related systems. On one hand, negative hyperconjugation interactions are discussed. These occur in especially permethylated systems and are, in this context, understood as a donation of electron density in this case $p(O) \rightarrow \sigma^*(Si-C)$. A subsequent coordination to a metal center is hindered due to a competing polarization.[2,3] On the other hand, the Si−O bond is considered highly ionic. This causes spatially diffuse electron pairs.[4] Furthermore, repulsive interactions between the positively polarized silicon atoms and a Lewis acid occur.

Both effects are disadvantageous in terms of complex formation.[5,6] With the insertion of Si_2Me_4 units rather than $SiMe_2$ units into a residual C_2H_4O framework (see Scheme 1b,c), we could demonstrate that these effects have to be taken into account but low basicity also originates from different architecture of cyclosiloxanes in comparison to crown ethers (Scheme 1a). Crown ethers bearing a single disilane unit readily form stable complexes with alkali and alkaline earth metal salts, and the coordination ability is comparable to that of the purely organic crown ethers which is confirmed by means of NMR experiments and DFT calculations.[7−10] Furthermore, even hydrogen bonding could be established as the incorporation of ammonium cations was realized.[12] Very recently new insights into the Si−O bond were given as ligands bearing a single O−Si−Si−O linkage were found to be effective for the incorporation of exclusively hard cations. Negative hyperconjugation interactions in these disilane-bearing systems are easily overcompensated when a hard group 1 or 2 metal ion is coordinated. The harder the cation is, the higher the impact is on the siloxane linkage, and a higher bonding energy is the outcome.[13,14] Especially group 2 metal ions seem to readily form stable complexes with ligands bearing a Si−O moiety.[13,15,16] The group of Harder very recently introduced the synthesis and structure of the

Scheme 1. Binding Modes of Crown Ethers (a) and Disilanyl-Bearing Crown Ethers (b−d): (b) Hybrid Crown Ethers Bearing a Single Disilane Unit,[7−10] (c) Hybrid Crown Ethers Bearing Disilane Units Opposite Each Other,[7] and (d) Hybrid Crown Ethers Bearing Two Adjacent Disilane Units[9,11,a]

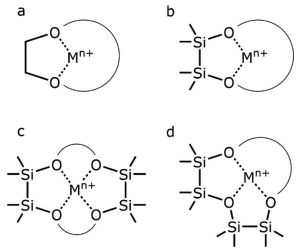

[a]Curves represent different organic spacers. See cited works for further information.

Received: January 11, 2019
Published: February 21, 2019

Downloaded via UNIV OF MARBURG on April 3, 2020 at 12:59:18 (UTC).
See https://pubs.acs.org/sharingguidelines for options on how to legitimately share published articles.

© 2019 American Chemical Society

DOI: 10.1021/acs.inorgchem.9b00086
Inorg. Chem. 2019, 58, 3518−3526

fascinating magnesium complex $[Mg(BDI)\{O(SiMe_3)_2\}]^+$ (BDI = $CH[C(CH_3)N\text{-}Dipp]_2$ where Dipp = 2,6-diisopropylphenyl) and demonstrated unsupported silyl ether coordination by means of XRD and ^{29}Si NMR experiments.[17] While the coordination chemistry of ligands bearing a single O−Si−Si−O linkage has advanced quite well, the coordination chemistry of ligands bearing two or more adjacent disilane units (see Scheme 1d) is at an early stage. With [Li(1,2,4,5-tetrasila[12]-crown-4)OTf] (OTf = $CF_3SO_3^-$) only one example is known so far in which the uncommon binding motif $(Si_2Me_4)_2O\cdots LA$ (LA = Lewis acid) could be observed.[11] The ligand shows a fair complexation ability, but additional experimental data is necessary in order to understand the coordination chemistry of a ligand with the $O-Si_2Me_4-O-Si_2Me_4-O$ moiety. We herein report on novel s-block coordination compounds representing the uncommon binding motif $(Si_2Me_4)_2O\cdots LA$. The influence of different Lewis acids toward the siloxane linkage is discussed by means of single crystal X-ray diffraction analysis and ^{29}Si NMR chemical shift.

RESULTS AND DISCUSSION

In past works we were able to generate 1,2,4,5-tetrasila[12]-crown-4 and 1,2,4,5-tetrasila[18]crown-6.[9,11] In this work we aimed to synthesize a tetrasila-crown ether with a size between these two ligands. 1,2,4,5-Tetrasila-benzo[15]crown-5 (**1**) is accessible by reaction of the corresponding glycol and the 1,5-dichloro-tetrasilaether $(ClSi_2Me_4)_2O$ presented in Scheme 2.

Scheme 2. Preparation of Ligand 1

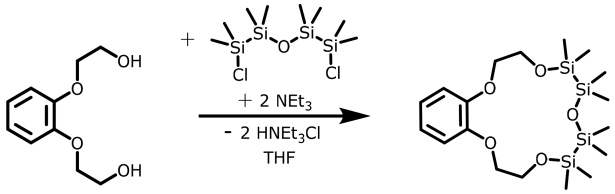

1

The crown ether **1** can be obtained after workup procedures in 98% yield. The cavity size of this ligand is larger than that of [15]crown-5 but slightly smaller than that of [18]crown-6. For this reason the ligand is capable of complexing a wide range of s-block ions, e.g., Na^+, Ca^{2+}, Sr^{2+}, but also Li^+ and Mg^{2+} in a mismatched fashion. These (mismatched) complexes can be an indicator of whether siloxane embedded oxygen atoms interact with a Lewis acid in the solid state and whether coordination modes are maintained in solution. Treatment of **1** with LiI in α,α,α-trifluorotoluene yields the coordination compound [Li(1,2,4,5-tetrasila-benzo[15]crown-5)I] (**2**). Neat **2** is a slightly yellow powder which can be recrystallized after dissolution in benzene, overlayering with *n*-pentane and cooling the solution at −24 °C for several weeks. Colorless needles were obtained that are suitable for a single crystal X-ray diffraction (XRD) experiment. The molecular structure within the crystal reveals a 5-fold-coordinated lithium ion (see Figure 1). The central ion is coordinated by two of the Si and C substituted oxygen atoms of the siloxane backbone, two oxygen atoms of the organic framework, and the iodide anion.

The Li^+ ion is far too small for the cavity of ligand **1** so the fully Si substituted O atom is not coordinated. The flexible siloxane backbone remains in a staggered conformation with

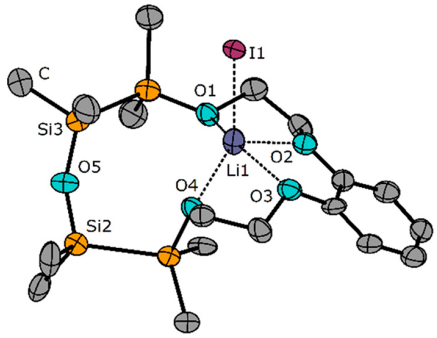

Figure 1. Molecular structure of **2** in the crystal. Thermal ellipsoids represent the 50% probability level. Hydrogen atoms and solvent molecules of benzene are omitted for clarity. Only one out of four independent molecules per asymmetric unit is shown. Selected bond lengths [pm]: O1−Li1 227.6(15), O2−Li1 201.6(14), O3−Li1 227.6(15), O4−Li1 203.1(16), O5···Li1 451.8(1), I1−Li1 273.1(15). Selected bond angles [deg]: O1−Li1−O2 105.0(6), O2−Li1−O3 72.5(5), O3−Li1−O4 75.4(5), Si2−O5−Si3 147.9(5).

the oxygen atom turned outward which is apparent from the large O5···Li distance of 451.8(1) pm. The Si−O−Si angle, an important parameter regarding siloxane basicity,[18−23] is comparatively large. The Si2−O5−Si3 angle has a value of about 148°. Taking all observations into account, no interaction of O5 with Li^+ can be observed in the solid state. The $^{29}Si\{^1H\}$ NMR experiment shows two respective singlets for the siloxane backbone with one significantly low-field shifted and one slightly high-field shifted (δ = 18.8 and 2.1 ppm) in comparison to free ligand **1**. This small shift of the $^{29}Si\{^1H\}$ signal for Si2 and Si3 ($\Delta\delta_{Si2/Si3}$ = −0.1 ppm) indicates that the conformation of the ligand is also maintained in solution with O5 showing no interactions with the Li^+ ion.

However, fully Si substituted oxygen atoms are still capable of coordinating Li^+ ions which was shown by the partially silicon based crown ether 1,2,4,5-tetrasila[12]crown-4. In the presence of LiOTf (OTf = $CF_3SO_3^-$), a remarkable downfield shift is observed from 0.9 to 9.4 ppm in deuterated dichloromethane.[11] At this point, it can be summarized that the ^{29}Si NMR experiment is a very good indicator of the strength of the interaction of a Lewis acid with the siloxane backbone as the shift is very sensitive toward coordination. A quite similar ligand behavior to that observed in **2** is also expected for the magnesium cation ($r_i[Mg^{2+}]_{CN6}$ = 72 pm; CN = coordination number)[24] which is in a diagonal relationship with lithium ($r_i[Li^+]_{CN6}$ = 72 pm).[24] The magnesium complex [Mg(1,2,4,5-tetrasila-benzo[15]crown-5)I_2] (**3**) is obtained after addition of MgI_2 to a solution of **1** in α,α,α-trifluorotoluene.

After workup and recrystallization from dichloromethane (DCM)/*n*-pentane solution, colorless platelets could be obtained which were suitable for XRD. The coordination sphere of the Mg^{2+} cation can be interpreted as a highly distorted pentagonal bipyramid with all of the oxygen atoms as well as the two iodide anions coordinating to the metal center (see Figure 2). Whereas the fully organic and the Si/C substituted oxygen atoms share strong interactions with the Mg^{2+} cation, the fully Si substituted oxygen atom has much weaker interactions with the metal center. The ionic radius of Mg^{2+} is, at 72 pm (CN6), very close to that of Li^+ at 76 pm (CN6).[24] Surprisingly the siloxane backbone is still pointed to the inside of the crown ether cavity, but the O2−Mg1 distance

DOI: 10.1021/acs.inorgchem.9b00086
Inorg. Chem. 2019, 58, 3518−3526

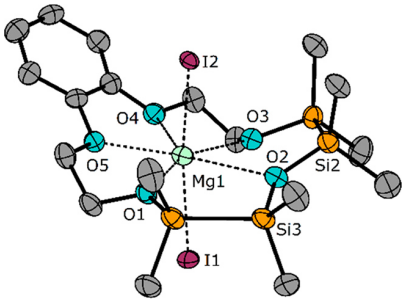

Figure 2. Molecular structure of **3** in the crystal. Thermal ellipsoids represent the 50% probability level. Hydrogen atoms omitted for clarity. Only one out of four independent molecules per asymmetric unit is shown. Selected bond lengths [pm]: O1−Mg1 227.0(3), O2−Mg1 299.8(8), O3−Mg1 220.3(3), O4−Mg1 227.2(3), O5−Mg1 227.7(3), I1−Mg1 279.0(1), I2−Mg1 279.5(1). Selected bond angles [deg]: O1−Mg1−O2 77.3(1), O1−Mg1−O5 71.6(1), O2−Mg1−O3 74.2(1), O3−Mg1−O4 72.1(1), O4−Mg1−O5 65.8(1), I1−Mg1−I2 167.2(1), Si2−O2−Si3 133.9(2).

at 299.8(8) pm is significantly longer than the other O−Mg atom distances (220.3(2)−227.7(3) pm). Even though the O2−Mg1 atomic distance is very long, it is less than the sum of the van der Waals radii.[25] Thus, a weak contact can be inferred. A contact is obviously enforced due to the more Lewis acidic magnesium cation. In addition, the Si2−O2−Si3 angle is, at 133.9(2)°, comparatively small. A weak interaction is further underpinned by observations made in solution since a slight NMR shift for Si2 and Si3 of $\Delta\delta_{Si2/Si3}$ = 4.6 ppm is observed between **3** and free ligand **1**. A stronger interaction with the siloxane backbone is observed for the larger Na^+ ion. After reaction of **1** with NaI in *α,α,α*-trifluorotoluene, the complex [Na(1,2,4,5-tetrasila-benzo[15]crown-5)I] (**4**) can be obtained as a colorless powder, Figure 3. As the compound showed no tendency to crystallize from various solvent mixtures, we were finally able to obtain just a few single crystals from melting the bulk compound and slowly cooling to ambient temperature. Colorless platelets were analyzed via XRD. The molecular structure within the crystal reveals a 6-fold-coordinated sodium ion placed in the middle of the crown

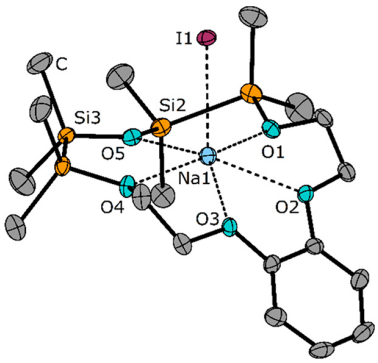

Figure 3. Molecular structure of **4** in the crystal. Thermal ellipsoids represent the 50% probability level. Hydrogen atoms are omitted for clarity. Only one out of two independent molecules per asymmetric unit is shown. Selected bond lengths [pm]: O1−Na1 243.2(2), O2−Na1 252.4(3), O3−Na1 255.3(2), O4−Na1 237.2(2), O5−Na1 274.1(3), I1−Na1 304.4(1). Selected bond angles [deg]: O1−Na1−O2 66.2(1), O1−Na1−O5 80.3(1), O2−Na1−O3 56.6(1), O3−Na1−O4 66.6(1), O4−Na1−O5 82.7(1), Si2−O2−Si3 133.8(1).

ether cavity. The sodium ion matches well with the spanned mean plane of the five oxygen atoms as it is placed only about 43 pm above this plane.

For comparison, in [Na([15]crown-5)I] the sodium ion is located 80 pm above this plane.[26] Thus, the sodium ion matches better with the cavity of **1** than with that of [15]crown-5. The coordination of the three different types of O atoms is very similar to those in the complex [Li(1,2,4,5-tetrasila[12]crown-4)OTf]. Whereas the Si/C substituted O atoms show the shortest distances to the metal center (237.2(2) and 243.2(2) pm), the completely silicon bonded oxygen is the longest (274.1(3) pm).[11] Just like in [Li(1,2,4,5-tetrasila[12]crown-4)OTf], the completely Si substituted oxygen atom in **4** has about a 30 pm greater distance to the metal center than the Si/C substituted atom and about a 20 pm greater distance than the C substituted atom. The Si2−O5−Si3 angle is decreasing to a value of 133.8(1)° with O5 pointing to Na^+.

This Si−O−Si angle is also very close to the Si−O−Si angle in the related lithium compound [Li(1,2,4,5-tetrasila[12]-crown-4)OTf] where an angle of 134.3(1)° is found.[11] The O5−Na1 distance, however, is now much closer to the residual O−Na distances indicating a stronger interaction of the siloxane backbone with the metal center than in **3**. Observations made in solution confirm this argument as the NMR chemical shift of $\Delta\delta_{Si2/Si3}$ = 4.9 ppm for silicon atoms Si2 and Si3 is observed in comparison to that of free ligand **1**. This shift is larger than in **3**. Thus, a good match with the cavity size of the silicon based crown ether is very important along with the hardness of the cation and has to be taken into account when siloxane basicity is discussed. Overall the siloxane backbone in **4** shares moderate interactions with the Na^+ metal center. As the Na^+ cation matches very well with the cavity of **1**, the Ca^{2+} cation should also be a very suitable cation for complexation.

As calcium is in a diagonal relationship with sodium, the ionic radius is almost the same at 106 pm (CN7).[24] Adding CaI_2 to a solution of **1** in *α,α,α*-trifluorotoluene yields [Ca(1,2,4,5-tetrasila-benzo[15]crown-5)I_2] (**5**). After workup procedures, single crystals for X-ray diffraction were obtained from DCM/*n*-pentane solution in the shape of colorless platelets. The molecular structure within the crystal reveals a pentagonal bipyramidal coordinated calcium ion in ligand **1** (see Figure 4). As can be seen here, the harder Ca^{2+} cation has a more significant influence toward the bonding situation of the siloxane linkage. As the O_C−M as well as the $O_{C/Si}$−M distances are close to those in compound **4**, the O_{Si}−M atomic distance is significantly shorter. It is now 256.0(1) pm and for this reason much closer now to the residual O−M distances. Thus, the Si−O−Si angle is also further decreased to a value of 125.9(1)° which one of the smallest angles observed so far for siloxane ligands binding to a metal center. In solution, this leads to a remarkable NMR chemical low-field shift of the silicon atoms Si2 and Si3. The respective signal is found at 14.0 ppm. This is the most low-field shifted value for all herein characterized coordination compounds ($\Delta\delta_{Si2/Si3}$ = 11.8 ppm). The slightly larger Sr^{2+} cation ($r_i[Sr^{2+}]_{CN7}$ = 121 pm)[24] can be incorporated into **1** using analogous procedures and can also be recrystallized from DCM/*n*-pentane solution. The coordination compound [Sr(1,2,4,5-tetrasila-benzo[15]crown-5)I_2] (**6**) crystallizes isostructurally to **5** (see Figure 5) and for this reason also indicates a very good matching of Sr^{2+} with ligand **1**. In comparison to **5**, the crown ether is now stretched as the

DOI: 10.1021/acs.inorgchem.9b00086
Inorg. Chem. 2019, 58, 3518−3526

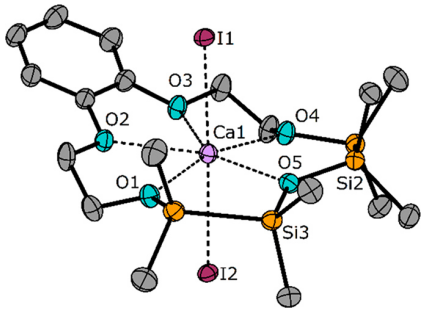

Figure 4. Molecular structure of **5** in the crystal. Thermal ellipsoids represent the 50% probability level. Hydrogen atoms are omitted for clarity. Selected bond lengths [pm]: O1−Ca1 242.9(1), O2−Ca1 249.8(1), O3−Ca1 247.8(1), O4−Ca1 241.8(1), O5−Ca1 256.0(1), I1−Ca1 305.4(1), I2−Ca1 307.4(1). Selected bond angles [deg]: O1−Ca1−O2 66.5(1), O1−Ca1−O5 83.0(1), O2−Ca1−O3 61.9(1), O3−Ca1−O4 66.7(1), O4−Ca1−O5 82.4(1), I1−Ca1−I2 176.8(1), Si2−O2−Si3 125.9(1).

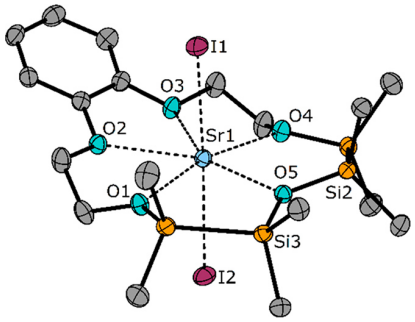

Figure 5. Molecular structure of **6** in the crystal. Thermal ellipsoids represent the 50% probability level. Hydrogen atoms are omitted for clarity. Selected bond lengths [pm]: O1−Sr1 252.4(2), O2−Sr1 258.9(2), O3−Sr1 257.1(2), O4−Sr1 252.3(2), O5−Sr1 260.8(2), I1−Sr1 317.9(1), I2−Sr1 320.5(1). Selected bond angles [deg]: O1−Sr1−O2 65.2(1), O1−Sr1−O5 84.7(1), O2−Sr1−O3 60.7(1), O3−Sr1−O4 65.5(1), O4−Sr1−O5 84.0(1), I1−Sr1−I2 175.6(1), Si2−O2−Si3 129.9(1).

Si−O−Si angle is increased to a value of 129.9(1)°. Despite the larger Si−O−Si angle, a strong Sr−O5 interaction is observed. This is due to the larger ionic radius for Sr^{2+}. Hence, the O_{Si}−M atomic distance is, with 260.8(2) pm, again very close to those of the $O_{C/Si}$−M (252.3(2) and 252.4(2) pm) but especially the O_C−M (258.9(2) and 257.1(2) pm) distances. Similar to that of **5**, the NMR chemical shift of **6** is distinct.

The respective signal of Si2 and Si3 is found at 13.7 ppm ($\Delta\delta_{Si2/Si3}$ = 11.5 ppm). On a structural level, Sr^{2+} rather than Ca^{2+} seems to be the most suitable cation for ligand **1** as the O_{Si}−M distance is in better harmony with the O_C−M distances. As observed in solution, however, the Ca^{2+} cation shares stronger interactions which follow the general trend that hard cations share stronger interactions with the siloxane backbone than soft ions do.[13] In this work, experimental details hint that harder cations share stronger interactions not only with oxygen atoms bonded to silicon as well as carbon but also with oxygen atoms bonded exclusively to silicon, as long as the cation is not far too small for the cyclic ligand as for example in complex **2**. Taking all these observations into account one can conclude that a perfect match of a hard cation with the crown ether cavity can make siloxane oxygen atoms available for effective coordination. As the coordination chemistry of hard group 1 and 2 metal ions turned out to be successful, the ^{29}Si NMR chemical shifts are summarized in Figure 6. As can be seen here, the shifts are highly sensitive toward coordination, and the choice of the Lewis acid and ligand can reveal very different coordination modes which are very well-represented in solution. No interactions of the Si−O−Si moiety of ligand **1** with M could be observed with M = Li^+; weak interactions with M = Mg^{2+}, moderate interactions with M = Na^+, and strong interactions with M = Ca^{2+} and Sr^{2+} could be observed. This class of ligand opens up for further investigations hard group 2 cations such as Be^{2+}, which are currently underway.[27,28]

For barium, the heaviest nonradioactive alkaline earth metal, we decided to choose 1,2,4,5-tetrasila[18]crown-6 (**7**) as a ligand for complexation. As the ionic radius of Ba^{2+} ($r_i[Ba^{2+}]_{CN9}$ = 147 pm)[24] is even larger, the cavity of **1** is too small for 1:1 complex formation. As is evident from the disila-crown ether analogue of [15]crown-5, it could be shown that this crown ether yields a dinuclear species [Ba_2(1,2-disila[15]crown-5)OTf_4].[9] Thus, **7**, which is accessible by

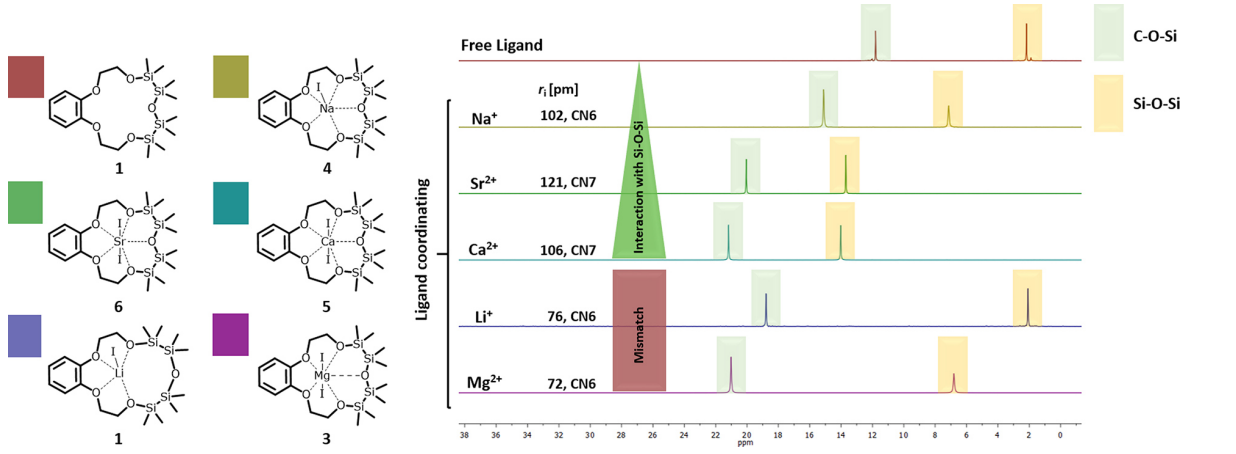

Figure 6. ^{29}Si NMR chemical shifts of alkali and alkaline earth metal complexes of the partially silicon based crown ether 1,2,4,5-tetrasila-benzo[15]crown-5 (**1**) in deuterated dichloromethane at 300 K.

DOI: 10.1021/acs.inorgchem.9b00086
Inorg. Chem. 2019, 58, 3518−3526

reaction of tetraethylene glycol with $O(Si_2Me_4Cl)_2$,[9] was the ligand of choice. Reaction of **7** with BaI_2 yields a slight yellow powder which can be recrystallized from DCM/*n*-pentane solution. Crystals suitable for XRD were obtained in the shape of colorless needles. Unusually, the molecular structure in the crystal reveals the dinuclear species $[Ba_2(1,2,4,5\text{-tetrasila}[18]\text{-crown-}6)_2I_4]$ (**8**) (Figure 7). In contrast to this molecular structure, [Ba(1,2-disila[18]crown-6)OTf_2] and [Ba(1,2-disila-benzo[18]crown-6)OTf_2] are monomeric contact ion pairs.[10]

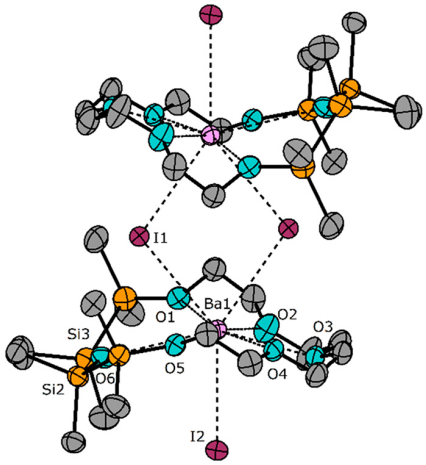

Figure 7. Molecular structure of **7** in the crystal. Thermal ellipsoids represent the 40% probability level. Hydrogen atoms are omitted for clarity. All nonlabeled atoms are symmetry generated over $1 - x$, $1 - x$, $2 - z$. Selected bond lengths [pm]: O1−Ba1 286.7(5), O2−Ba1 278.8(6), O3−Ba1 291.3(1), O4−Ba1 284.6(5), O5−Ba1 283.4(5), O6−Ba1 338.8(1), I1−Ba1 352.0(1), I2−Ba1 342.3(1), Ba1···Ba1# 560.1(1). Selected bond angles [deg]: O1−Ba1−O2 55.9(1), O1−Ba1−O6 65.6(1), O2−Ba1−O3 56.6(1), O3−Ba1−O4 57.4(1), O4−Ba1−O5 59.7(1), O5−Ba1−O6 71.1(1), I1−Ba1−I2 139.4(1), Ba1−I1−Ba1# 105.1(1), Si2−O2−Si3 133.5(4).

The central barium cations are coordinated by all of the crown ether oxygen atoms, but similar to compound **3** the O_{Si}−M distance is at 338.8(1) pm by far the longest. Beside the crown ethers, three iodide anions coordinate to each metal ion. Two iodide anions act as bridges between the Ba^{2+} ions and saturate the coordination sphere. Barium is overall 9-fold-coordinated in a highly distorted crown ether environment. We discussed the enlarged cavity size of **7** in a previous work as we targeted synthesis of the corresponding alkali metal complex [K(1,2,4,5-tetrasila[18]crown-6)PF_6].[9] The potassium ion is with 151 pm (CN8)[24] slightly larger than the Ba^{2+} cation, but the coordination mode is significantly different. As shown via XRD and ^{29}Si NMR chemical shift, the siloxane backbone shares no interaction with the potassium cation. Barium, however, does share moderate interactions with it. Even though the O_{Si}−M distance is very long, the NMR experiment proves the interaction of O6 with Ba^{2+} as can be seen by a shift of $\Delta\delta_{Si2/Si3}$ = 8.3 ppm in comparison to free ligand **7**.

CONCLUSION

In a recent work, we described the synthesis of the hybrid tetrasila-crown ether 1,2,4,5-tetrasila[12]crown-4. This crown ether and its respective lithium complex have been the only examples where a O−Si_2Me_4−O−Si_2Me_4−O unit coordinate a metal cation.[11] This promising result motivated us to extend the coordination chemistry to other partially silicon based crown ethers bearing a O−Si_2Me_4−O−Si_2Me_4−O moiety. In this work we synthesized the partially silicon based crown ether 1,2,4,5-tetrasila-benzo[15]crown-5 (**1**). The ligand turned out to be suitable for complexation of a wide range of s-block ions. Furthermore, salts of the strongly coordinating anion I^- were suitable, showing a fair complexation ability of this ligand. By equimolar reaction of **1** with alkali or alkaline earth metal iodides, we obtained the alkali metal complexes **2** and **4** and the alkaline earth metal complexes **3**, **5**, and **6**.

Depending on the ionic radii, different coordination modes were established which could be well-represented by observations made in solution. The ^{29}Si NMR experiment turned out to be a very good indicator for the strength of interaction between a Lewis acid and the siloxane backbone as the chemical shift is very sensitive toward coordination. Whereas the Li^+ cation shows no interaction with the siloxane oxygen atom, the harder magnesium cation enforces coordination. Both experiments, XRD and NMR, are consistent. However, both cations were too small for the cavity of **1**. The larger Na^+ ion fits well, and thus, the NMR chemical shift is more distinct although the Na^+ ion is less hard than the Mg^{2+} cation. Ca^{2+} and Sr^{2+}, both cations which match well with the cavity of **1**, exhibit a hard character and for this reason share very strong interactions with the siloxane backbone. The molecular structures of compounds **5** and **6** show comparatively small Si−O−Si angles, and the NMR chemical shift is significantly more low-field shifted in comparison to all other characterized compounds. It might be concluded that there is a special ion selectivity of partially silicon based crown ethers. This will be the subject of future research. Those cations which exhibit a hard character and fit perfectly with the cavity of the ligand can activate Si embedded oxygen atoms for effective coordination. In this study, the O_{Si}−M distance is in best harmony with the O_C−M distances in compound **6** on a structural level and compound **5** regarding NMR chemical shift as the attraction of O_{Si} with M being the strongest observed here. However, if given a choice where to place the ion in the cavity, the O_{Si}−M distance is the largest in all compounds. The results are summarized in Scheme 3. A siloxane coordination with barium as the central ion could be established by reaction of **7** with BaI_2. The dinuclear complex $[Ba_2(1,2,4,5\text{-tetrasila}[18]\text{crown-}6)_2I_4]$ (**8**) could be characterized, and the argument that a harder cation interacts with silicon based ligands stronger than soft cations do could be further strengthened. Overall, the successful incorporation of a wide range of s-block metal ions is promising for future coordination chemistry of siloxane compounds. Further, the coordination chemistry of siloxane embedded oxygen atoms toward Lewis acids has been advanced and challenges the widespread opinion of (cyclo)siloxanes as weakly coordinating ligands.

EXPERIMENTAL SECTION

General. All manipulations were carried out with rigorous exclusion of oxygen and moisture using basic Schlenk techniques establishing an inert-gas atmosphere. Solvents were dried and freshly distilled before use. Compound **7** and the organic fragment of **1** were synthesized using methods described in the literature.[9,29] Alkali and alkaline earth metal salts were dried *in vacuo* and handled under an argon atmosphere using a glovebox of MBraun-type. NMR spectra were recorded on different Bruker spectrometers including an AV III HD 300 MHz or an AV III 500 MHz. Infrared (IR) spectra of the respective samples were measured using the attenuated total

DOI: 10.1021/acs.inorgchem.9b00086
Inorg. Chem. 2019, 58, 3518−3526

Scheme 3. Coordination Chemistry of the Partially Silicon Based Crown Ethers 1,2,4,5-tetrasila[15]crown-5 (1) and 1,2,4,5-tetrasila[18]crown-6 (7)

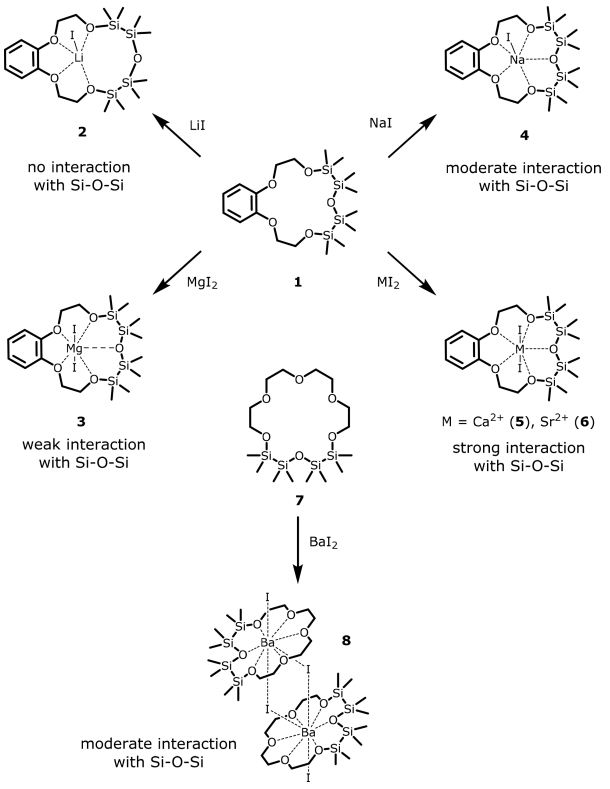

reflectance (ATR) mode on the Bruker-type spectrometer Alpha FT-IR. ESI mass spectra were acquired with an LTQ-FT Ultra mass spectrometer (Thermo Fischer Scientific). The resolution was set to 100.000. Elemental analysis was carried out on a Vario MicroCube. In the case of the alkali metal compounds **2** and **4**, we have not been able to obtain an accurate CH-analysis. This is probably due to the wax-like, greasy characteristics of the compounds and/or formation of SiC.

Synthesis and Crystallization. *1,2,4,5-Tetrasila-benzo[15]-crown-5 (**1**).* A 0.676 g portion of 2,2′-[1,2-phenylenebis(oxy)]-diethanol (3.41 mmol, 1.0 equiv) and 0.89 mL of NEt_3 (6.42 mmol, 2.0 equiv) are dissolved in 25 mL of THF (THF = tetrahydrofuran). Subsequently, 1 mL of $O(Si_2Me_4Cl)_2$ (3.41 mmol, 1.0 equiv) dissolved in 25 mL of THF is added over a period of 60 min. The resulting white suspension is then stirred overnight and is freed of the solvent. The residue is extracted with 50 mL of *n*-pentane followed by filtration. Removing the solvent under reduced pressure yields crown ether **1** as a colorless oil (1.500 g, 98%).

^{1}H NMR (300 MHz, C_6D_6): δ = 0.31 (s, 12H, Si(CH_3)$_2$), 0.32 (s, 12H, Si(CH_3)$_2$), 3.81−3.90 (m, 8H, CH_2), 6.69−6.83 (m, 4H, CH_{Ar}) ppm. ^{13}C{^{1}H} NMR (125 MHz, C_6D_6): δ = −0.3 (s, Si(CH_3)$_2$), 2.8 (s, Si(CH_3)$_2$), 63.0 (s, CH_2), 71.1 (s, CH_2), 115.0 (s, CH_{Ar}), 121.6 (s, CH_{Ar}), 150.1 (s, $CH_{Ar,q}$) ppm. ^{29}Si{^{1}H} NMR (60 MHz, C_6D_6): δ = 12.7 (s, *Si*CH_3), 3.8 (s, *Si*CH_3) ppm. ^{29}Si{^{1}H} NMR (60 MHz, CD_2Cl_2): 11.8 (s, *Si*CH_3), 2.2 (s, *Si*CH_3). ESI(+) *m*/*z* (%): 445.1730 [M + H]$^+$ (5), 467.1553 [M + Na]$^+$ (100). IR (cm^{-1}): 2949 (m), 2871 (w), 1593 (w), 1501 (m), 1452 (w), 1399 (w), 1372 (w), 1328 (w), 1246 (s), 1221 (m), 1124.58 (s), 1098 (s), 1033 (vs), 953 (m), 924 (m), 824 (m), 797 (s), 761 (vs), 738 (vs), 681 (m), 660 (m), 635 (m), 552 (w), 485 (w), 461 (w).

*[Li(1,2,4,5-tetrasila-benzo[15]crown-5)I] (**2**).* A 0.120 g portion of 1,2,4,5-tetrasila-benzo[15]crown-5 (0.27 mmol) is dissolved in 10 mL of *α*,*α*,*α*-trifluorotoluene. Subsequently, 0.036 g (0.27 mmol) of LiI is added. The resulting suspension is stirred vigorously and is heated to reflux several times. The suspension is allowed to cool to ambient temperature and is then stirred overnight. The solvent is removed under reduced pressure and the remaining solid dissolved in 5 mL DCM. After centrifugation and decantation, the solvent is yet again removed under reduced pressure to obtain a slight yellow, greasy solid. After washing with 3 mL of *n*-pentane, **2** is obtained as a slight yellow wax-like powder (0.151 g, 97%). For single crystal growth, the powder is dissolved in 3 mL of benzene and layered with 20 mL of *n*-pentane. Storage at −24 °C yields a few single crystals in the shape of colorless needles within a few weeks.

^{1}H NMR (300 MHz, CD_2Cl_2): δ = 0.27 (s, 12H, Si(CH_3)$_2$), 0.34 (s, 12H, Si(CH_3)$_2$), 4.25 (s, 8H, CH_2), 6.98−7.07 (m, 4H, CH_{Ar}) ppm. ^{7}Li NMR (117 MHz, CD_2Cl_2): δ = 0.33 (s, *Li*I). ^{13}C{^{1}H} NMR (125 MHz, CD_2Cl_2): δ = −0.5 (s, Si(CH_3)$_2$), 2.7 (s, Si(CH_3)$_2$), 62.1 (s, CH_2), 71.1 (s, CH_2), 114.4 (s, CH_{Ar}), 123.5 (s, CH_{Ar}), 147.5 (s, $CH_{Ar,\ q}$) ppm. ^{29}Si{^{1}H} NMR (60 MHz, CD_2Cl_2): δ = 18.8 (s, *Si*CH_3), 2.1 (s, *Si*CH_3) ppm. ESI(+) *m*/*z* (%): 451.1807 [M − I]$^+$ (100). IR (cm^{-1}): 2961 (m), 2886 (w), 1597 (w), 1502 (m), 1457 (w), 1400 (w), 1372 (w), 1324 (w), 1257 (s), 1207 (w), 1018 (vs), 933 (s), 858 (m), 796 (vs), 765 (vs), 685 (s), 661 (m), 641 (m), 606 (w), 554 (w), 453 (w).

*[Mg(1,2,4,5-tetrasila-benzo[15]crown-5)I$_2$] (**3**).* A 0.140 g portion of 1,2,4,5-tetrasila-benzo[15]crown-5 (0.32 mmol) is dissolved in 10 mL of *α*,*α*,*α*-trifluorotoluene. Subsequently, 0.088 g (0.32 mmol) of MgI_2 is added. The resulting suspension is stirred vigorously overnight. The solvent is removed under reduced pressure, and the remaining solid is dissolved in 10 mL DCM. After centrifugation and decantation, the solvent is yet again removed under reduced pressure to obtain a slight yellow powder. Washing the powder with 4 mL of *n*-pentane yields **3** as a colorless powder (0.200 g, 88%). For single crystal growth, the powder is dissolved in 4 mL of DCM and layered with 25 mL of *n*-pentane. Single crystals in the shape of colorless platelets are obtained after 3 days.

^{1}H NMR (300 MHz, CD_2Cl_2): δ = 0.46 (s, 12H, Si(CH_3)$_2$), 0.48 (s, 12H, Si(CH_3)$_2$), 4.29−4.31 (m, 4H, CH_2), 4.39−4.41 (m, 4H, CH_2), 6.93−6.96 (m, 2H, CH_{Ar}), 7.07−7.11 (m, 2H, CH_{Ar}) ppm. ^{13}C{^{1}H} NMR (125 MHz, CD_2Cl_2): δ = 0.0 (s, Si(CH_3)$_2$), 3.86 (s, Si(CH_3)$_2$), 60.9 (s, CH_2), 67.7 (s, CH_2), 111.6 (s, CH_{Ar}), 123.3 (s, CH_{Ar}), 144.7 (s, $CH_{Ar,q}$) ppm. ^{29}Si{^{1}H} NMR (60 MHz, CD_2Cl_2): δ = 21.0 (s, *Si*CH_3), 6.8 (s, *Si*CH_3) ppm. MS ESI(+) *m*/*z* (%): 595.0546 [M − I]$^+$ (100), 911.3201 [2M − MgI_2 + Na]$^+$ (5), 1039.2207 [2M − I]$^+$ (20). IR (cm^{-1}): 2960 (w), 2891 (vw), 1598 (vw), 1504 (m), 1457 (w), 1401 (vw), 1333 (vw), 1252 (s), 1200 (m), 1125 (m), 1032 (s), 936 (s), 857 (m), 800 (vs), 767 (vs), 746 (vs), 714 (s), 649 (m), 607 (m), 540 (w), 455 (vw). CHN Calcd for $C_{18}H_{36}I_2MgO_5Si_4$·0.5DCM: C, 29.03; H, 4.87. Found: C, 28.93; H, 4.84.

*[Na(1,2,4,5-tetrasila-benzo[15]crown-5)I] (**4**).* A 0.350 g portion of 1,2,4,5-tetrasila-benzo[15]crown-5 (0.79 mmol) is dissolved in 10 mL of *α*,*α*,*α*-trifluorotoluene. Subsequently, 0.118 g (0.79 mmol) of NaI is added. The resulting suspension is stirred vigorously and is heated to reflux several times. The suspension is allowed to cool to ambient temperature and is then stirred overnight. The solvent is removed under reduced pressure and the remaining solid dissolved in 10 mL of DCM. After centrifugation and decantation, the solvent is yet again removed under reduced pressure to obtain a greasy solid. After washing several times with 3 mL portions of *n*-pentane, **4** is obtained as a slight yellow wax-like powder (0.250 g, 53%). For single crystal growth the compound is gently melted several times using a heat gun. A few very small single crystals in the shape of colorless platelets are then obtained by allowing the melt to slowly cool to ambient temperature.

^{1}H NMR (300 MHz, CD_2Cl_2): δ = 0.35 (s, 12H, Si(CH_3)$_2$), 0.35 (s, 12H, Si(CH_3)$_2$), 4.08−4.12 (m, 4H, CH_2), 4.16−4.20 (m, 4H, CH_2), 6.86−6.98 (m, 4H, CH_{Ar}) ppm. ^{13}C{^{1}H} NMR (125 MHz, CD_2Cl_2): δ = −0.6 (s, Si(CH_3)$_2$), 3.1 (s, Si(CH_3)$_2$), 61.5 (s, CH_2), 69.3 (s, CH_2), 112.0 (s, CH_{Ar}), 122.0 (s, CH_{Ar}), 147.5 (s, $CH_{Ar,\ q}$) ppm. ^{29}Si{^{1}H} NMR (60 MHz, CD_2Cl_2): δ = 15.1 (s, *Si*CH_3), 7.1 (s, *Si*CH_3) ppm. MS ESI(+) *m*/*z* (%): 467.1545 [M − I]$^+$ (100). IR (cm^{-1}): 2949 (m), 2876 (w), 1596 (w), 1504 (s), 1456 (m), 1402 (w), 1372 (w), 1333 (w), 1248 (s), 1216 (s), 1125 (s), 1081 (s),

DOI: 10.1021/acs.inorgchem.9b00086
Inorg. Chem. 2019, 58, 3518−3526

1044 (s), 952 (vs), 931 (s), 854 (m), 827 (m), 805 (s), 765 (vs), 727 (s), 694 (s), 638 (m), 602 (w), 533 (w), 457 (w).

*[Ca(1,2,4,5-tetrasila-benzo[15]crown-5)I$_2$] (**5**).* A 0.222 g portion of 1,2,4,5-tetrasila-benzo[15]crown-5 (0.50 mmol) is dissolved in 10 mL of α,α,α-trifluorotoluene. Subsequently, 0.147 g (0.50 mmol) of CaI_2 is added. The resulting suspension is stirred vigorously overnight. The solvent is removed under reduced pressure and the remaining solid dissolved in 10 mL of DCM. After centrifugation and decantation, the solvent is yet again removed under reduced pressure. The residue is washed with 4 mL of *n*-pentane, and **5** is then obtained as a pale white powder (0.330 g, 89%). For single crystal growth, the powder is dissolved in 4 mL of DCM and layered with 20 mL of *n*-pentane. Single crystals in the shape of colorless platelets are obtained overnight.

^{1}H NMR (300 MHz, CD_2Cl_2): δ = 0.51 (s, 12H, Si(CH_3)$_2$), 0.60 (s, 12H, Si(CH_3)$_2$), 4.34−4.41 (m, 8H, CH_2), 6.94−6.98 (m, 2H, CH_{Ar}), 7.04−7.09 (m, 2H, CH_{Ar}) ppm. ^{13}C{^{1}H} NMR (125 MHz, CD_2Cl_2): δ = −0.45 (s, Si(CH_3)$_2$), 4.13 (s, Si(CH_3)$_2$), 62.4 (s, CH_2), 69.0 (s, CH_2), (s, CH_2), 111.6 (s, CH_{Ar}), 123.2 (s, CH_{Ar}), 146.0 (s, $CH_{Ar,\,q}$) ppm. ^{29}Si{^{1}H} NMR (60 MHz, CD_2Cl_2): δ = 21.2 (s, *Si*CH_3), 14.0 (s, *Si*CH_3) ppm. MS ESI(+) *m*/*z* (%): 467.1544 [M − CaI_2 + Na]$^+$ (50), 611.0321 [M − I]$^+$ (40), [2M − CaI_2 − I]$^+$ (10). IR (cm^{-1}): 2943 (w), 2882 (w), 1505 (w), 1459 (w), 1394 (w), 1350 (w), 1255 (s), 1126 (w), 1076 (s), 1042 (s), 974 (m), 948 (s), 931 (s), 855 (m), 798 (vs), 772 (vs), 735 (s), 721 (s), 634 (w), 515 (w), 458 (w), 426 (w). CHN Calcd for $C_{18}H_{36}I_2CaO_5Si_4$: C, 29.27; H, 4.91. Found: C, 29.19; H, 4.82.

*Synthesis of [Sr(1,2,4,5-tetrasila-benzo[15]crown-5)I$_2$] (**6**).* A 0.222 g portion of 1,2,4,5-tetrasila-benzo[15]crown-5 (0.50 mmol) is dissolved in 10 mL of α,α,α-trifluorotoluene. Subsequently, 0.170 g (0.50 mmol) of SrI_2 is added. The resulting suspension is stirred vigorously overnight. The solvent is removed under reduced pressure and the remaining solid dissolved in 10 mL of DCM. After centrifugation and decantation the solvent is yet again removed under reduced pressure to obtain a white powder. The residue is washed with 4 mL of *n*-pentane, and **6** is then obtained as a pale white powder (0.351 g, 89%). For single crystal growth, the powder is dissolved in 4 mL of DCM and layered with 20 mL of *n*-pentane. Single crystals in the shape of colorless platelets are obtained overnight.

^{1}H NMR (300 MHz, CD_2Cl_2): δ = 0.56 (s, 12H, Si(CH_3)$_2$), 0.63 (s, 12H, Si(CH_3)$_2$), 4.38−4.49 (m, 4H, CH_2), 4.45−4.47 (m, 4H, CH_2), 7.03−7.06 (m, 2H, CH_{Ar}), 7.11−7.13 (m, 2H, CH_{Ar}) ppm. ^{13}C{^{1}H} NMR (125 MHz, CD_2Cl_2): δ = −0.80 (s, Si(CH_3)$_2$), 3.42 (s, Si(CH_3)$_2$), 62.2 (s, CH_2), 69.3 (s, CH_2), (s, CH_2), 111.8 (s, CH_{Ar}), 122.9 (s, CH_{Ar}), 145.6 (s, $CH_{Ar,\,q}$) ppm. ^{29}Si{^{1}H} NMR (60 MHz, CD_2Cl_2): δ = 20.1 (s, *Si*CH_3), 13.7 (s, *Si*CH_3) ppm. MS ESI(+) *m*/*z* (%): 467.1544 [M − SrI_2 + Na]$^+$ (10), 658.9751 [M − I]$^+$ (100), 1444.8566 [2M − I]$^+$ (15). IR (cm^{-1}): 2942 (w), 2879 (w), 1596 (vw), 1502 (m), 1453 (w), 1249 (w), 1190 (w), 1122 (m), 1074 (s), 1035 (s), 947 (s), 922 (m), 898 (m), 846 (m), 798 (vs), 772 (vs), 718 (s), 691 (m), 638 (w), 603 (vw), 573 (vw), 530 (vw), 451 (w). CHN Calcd for $C_{18}H_{36}I_2SrO_5Si_4$: C, 27.50; H, 4.62. Found: C, 28.13; H, 4.54.

*Synthesis of [Ba$_2$(1,2,4,5-tetrasila[18]crown-6)$_2$I$_4$] (**8**).* A 0.100 g portion 1,2,4,5-tetrasila[18]crown-6 (0.23 mmol) is dissolved in 10 mL of α,α,α-trifluorotoluene. Subsequently, 0.090 g (0.23 mmol) of BaI_2 is added. The resulting suspension is heated to reflux several times and stirred vigorously for 1 week. The solvent is removed under reduced pressure and the remaining solid dissolved in 8 mL of DCM. After centrifugation and decantation, the solvent is yet again removed under reduced pressure. Washing the residue with two 4 mL portions of *n*-pentane yields **8** as a yellow powder (0.180 g, 95%). For single crystal growth, the powder is dissolved in 4 mL of DCM and layered with 20 mL of *n*-pentane. Single crystals in the shape of colorless needles are obtained within 2 days.

^{1}H NMR (300 MHz, CD_2Cl_2): δ = 0.42 (s, 12H, Si(CH_3)$_2$), 0.49 (s, 12H, Si(CH_3)$_2$), 3.82−3.84 (m, 4H, CH_2), 3.94 (s, 8H, CH_2), 4.08−4.09 (m, 4H, CH_2), ppm. ^{13}C{^{1}H} NMR (125 MHz, CD_2Cl_2): δ = −0.30 (s, Si(CH_3)$_2$), 4.03 (s, Si(CH_3)$_2$), 63.6 (s, CH_2), 70.7 (s, CH_2), 70.9 (s, CH_2), 73.3 (s, CH_2) ppm. ^{29}Si{^{1}H} NMR (60 MHz, CD_2Cl_2): δ = 18.3 (s, *Si*CH_3), 10.2 (s, *Si*CH_3) ppm. MS ESI(+) *m*/*z* (%): 509.1440 [M − BaI_2 − 2I]$^{2+}$ (30), 705.0019 [0.5M − I]$^+$ (30). IR (cm^{-1}): 2962 (m), 2908 (w), 2879 (w), 1466 (w), 1401 (w), 1347 (w), 1258 (s), 1085 (s), 1064 (s), 1019 (s), 950 (m), 928 (m), 855 (m), 797 (vs), 763 (vs), 720 (m), 696 (m), 634 (m), 519 (w), 448 (w). CHN Calcd for $C_{32}H_{80}I_4Ba_2O_{12}Si_8$·0.5DCM: C, 22.66; H, 4.73. Found: C, 22.49; H, 4.70.

Crystal Structures. Single crystal X-ray diffraction experiments were performed on a Bruker D8 Quest (**4**), STOE IPDS2 (**3**, **5**, **6**), STOE IPDS2T (**2**), or a STOE STADIVARI (**8**) diffractometer, respectively. Measurements were performed at 100 K with Mo Kα (λ = 0.71073 Å) or Cu Kα (λ = 1.54184 Å) radiation, graphite monochromatization, and/or respective X-ray optics. The structures were solved by direct methods and refinement with full-matrix-least-squares against F^2 using *SHELXT* and *SHELXL* on the *OLEX2* platform.[30−32] The crystallographic data for all compounds are deposited in the Cambridge Crystallographic Data Centre (CCDC). The deposition numbers are 1871016 (**2**), 1871015 (**3**), 1871018 (**4**), 1871019 (**5**), 1871014 (**6**), and 1871017 (**8**).

*Crystal Data for **2**·0.5C$_6$H$_6$.* $C_{21}H_{39}ILiO_5Si_4$, triclinic, $P\bar{1}$, Z = 8, 100(2) K, a = 10.2359(9) Å, b = 23.042(2) Å, c = 26.871(3) Å, α = 93.509(8)°, β = 90.275(7)°, γ = 92.139(7)°, V = 6321.1(10) Å^3, ρ = 1.298 g cm^{-3}, spherical absorption correction using STOE X-AREA and LANA,[32] μ = 1.190 mm^{-1}, T_{min}, T_{max} = 0.2116, 0.9235, 2Θ range 3.422−50.00°, reflections measured 49 969, independent reflections 22 236 [R(int) = 0.1054], 1185 parameters, R-index [$I \geq 2\sigma(I)$] 0.0677, wR_2 (all data) 0.1776, GOF 0.921, $\Delta\rho_{max}$, $\Delta\rho_{min}$ 1.15/−1.31 e Å^3.

*Crystal Data for **3**.* $C_{18}H_{36}I_2MgO_5Si_4$, triclinic, $P\bar{1}$, Z = 8, 100(2) K, a = 17.9132(11) Å, b = 18.8637(12) Å, c = 19.2796(11) Å, α = 94.842(5)°, β = 100.546(5)°, γ = 93.294(5)°, V = 6364.2(7) Å^3, ρ = 1.509 g cm^{-3}, spherical absorption correction using STOE X-AREA and LANA,[33] μ = 2.169 mm^{-1}, T_{min}, T_{max} = 0.2908, 0.6373, 2Θ range 2.854−56.998°, reflections measured 81 360, independent reflections 32 228 [R(int) = 0.0361], 1113 parameters, R-index [$I \geq 2\sigma(I)$] 0.0455, wR_2 (all data) 0.1244, GOF 1.019, $\Delta\rho_{max}$, $\Delta\rho_{min}$ 3.76/−1.43 e Å^3.

*Crystal Data for **4**.* $C_{18}H_{36}INaO_5Si_4$, monoclinic, $P2_1/n$, Z = 8, 100(2) K, a = 13.1247(6) Å, b = 21.0454(10) Å, c = 20.7966(9) Å, β = 97.757(2)°, V = 5691.8(4) Å^3, ρ = 1.388 g cm^{-3}, multiscan absorption correction using SADABS2016,[34] μ = 1.332 mm^{-1}, T_{min}, T_{max} = 0.6940, 0.7452, 2Θ range 4.346−50.816°, reflections measured 121 055, independent reflections 10 476 [R(int) = 0.1016], 539 parameters, R-index [$I \geq 2\sigma(I)$] 0.0425, wR_2 (all data) 0.0750, GOF 1.070, $\Delta\rho_{max}$, $\Delta\rho_{min}$ 0.83/−0.63 e Å^3.

*Crystal Data for **5**.* $C_{18}H_{36}CaI_2O_5Si_4$, monoclinic, $P2_1/c$, Z = 4, 100(2) K, a = 18.5850(16) Å, b = 9.7165(6) Å, c = 18.0271(14) Å, β = 110.406(6)°, V = 3051.1(4) Å^3, ρ = 1.608 g cm^{-3}, spherical absorption correction using X-AREA and LANA,[33] μ = 2.410 mm^{-1}, T_{min}, T_{max} = 0.1713, 0.4121, 2Θ range 4.566−58.00°, reflections measured 26 254, independent reflections 8101 [R(int) = 0.0281], 279 parameters, R-index [$I \geq 2\sigma(I)$] 0.0298, wR_2 (all data) 0.0763, GOF 0.989, $\Delta\rho_{max}$, $\Delta\rho_{min}$ 1.39/−0.49 e Å^3.

*Crystal Data for **6**.* $C_{18}H_{36}SrI_2O_5Si_4$, monoclinic, $P2_1/c$, Z = 4, 100(2) K, a = 18.737(10) Å, b = 9.797(6) Å, c = 18.118(10) Å, β = 110.85(4), V = 3108(3) Å^3, ρ = 1.680 g cm^{-3}, spherical absorption correction using X-AREA and LANA,[33] μ = 3.898 mm^{-1}, T_{min}, T_{max} = 0.1185, 0.1765, 2Θ range 4.538−57.00°, reflections measured 20 092, independent reflections 7840 [R(int) = 0.0281], 279 parameters, R-index [$I \geq 2\sigma(I)$] 0.0261, wR_2 (all data) 0.0567, GOF 0.925, $\Delta\rho_{max}$, $\Delta\rho_{min}$ 0.94/−0.33 e Å^3.

*Crystal Data for **8**.* $C_{32}H_{80}Ba_2I_4O_{12}Si_8$, monoclinic, $P2_1/n$, Z = 2, 100(2) K, a = 10.7039(7) Å, b = 18.8316(13) Å, c = 16.4914(12) Å, β = 103.155(5), V = 3237.0(4) Å^3, ρ = 1.707 g cm^{-3}, spherical absorption correction using X-AREA and LANA,[33] μ = 26.144 mm^{-1}, T_{min}, T_{max} = 0.0201, 0.0009, 2Θ range 7.234−136.00°, reflections measured 28 610, independent reflections 5885 [R(int) = 0.0518], 270 parameters, R-index [$I \geq 2\sigma(I)$] 0.0573, wR_2 (all data) 0.1685, GOF 1.058, $\Delta\rho_{max}$, $\Delta\rho_{min}$ 2.60/−1.56 e Å^3.

DOI: 10.1021/acs.inorgchem.9b00086
Inorg. Chem. 2019, 58, 3518−3526

■ ASSOCIATED CONTENT

Accession Codes

CCDC 1871014−1871019 contain the supplementary crystallographic data for this paper. These data can be obtained free of charge via www.ccdc.cam.ac.uk/data_request/cif, or by emailing data_request@ccdc.cam.ac.uk, or by contacting The Cambridge Crystallographic Data Centre, 12 Union Road, Cambridge CB2 1EZ, UK; fax: +44 1223 336033.

■ AUTHOR INFORMATION

Corresponding Author

*E-mail: haenisch@chemie.uni-marburg.de.

Author Contributions

The manuscript was written through contributions of all authors. All authors have given approval to the final version of the manuscript.

Notes

The authors declare no competing financial interest.

■ ACKNOWLEDGMENTS

This work was financially supported by the Deutsche Forschungsgemeinschaft (DFG). Dr. C. Donsbach and C. Ritter are gratefully acknowledged for their valuable help with X-ray crystallographic data. Further, F.D. thanks the MS (Dr. U. Linne and co-workers−especially J. Bamberger) and X-ray Departments (M. Marsch, R. Riedel, and Dr. K. Harms), Philipps-Universität, Marburg, for measurement time. In particular, R. Riedel is gratefully acknowledged for data collection of compounds **4** and **8**.

■ REFERENCES

(1) Ritch, J. S.; Chivers, T. Silicon analogues of crown ethers and cryptands: A new chapter in host-guest chemistry? *Angew. Chem., Int. Ed.* **2007**, *46*, 4610−4613. Ritch, J. S.; Chivers, T. *Angew. Chem.* **2007**, *119*, 4694−4697.

(2) Weinhold, F.; West, R. The nature of the silicon-oxygen bond. *Organometallics* **2011**, *30*, 5815−5824.

(3) Weinhold, F.; West, R. Hyperconjugative Interactions in Permethylated Siloxanes and Ethers: The Nature of the SiO Bond. *J. Am. Chem. Soc.* **2013**, *135*, 5762−5767.

(4) Gillespie, R. J.; Robinson, E. A. Models of molecular geometry. *Chem. Soc. Rev.* **2005**, *34*, 396.

(5) Passmore, J.; Rautiainen, J. M. On The Lower Lewis Basicity of Siloxanes Compared to Ethers. *Eur. J. Inorg. Chem.* **2012**, *2012*, 6002−6010.

(6) Cameron, T. S.; Decken, A.; Krossing, I.; Passmore, J.; Rautiainen, J. M.; Wang, X.; Zeng, X. Reactions of a Cyclodimethylsiloxane $(Me_2SiO)_6$ with Silver Salts of Weakly Coordinating Anions; Crystal Structures of $[Ag(Me_2SiO)_6][Al]$ ([Al] = $[FAl\{OC(CF_3)_3\}_3]$, $[Al\{OC(CF_3)_3\}_4]$) and Their Comparison with $[Ag(18\text{-Crown-6})]_2[SbF_6]_2$. *Inorg. Chem.* **2013**, *52*, 3113−3126.

(7) Reuter, K.; Buchner, M. R.; Thiele, G.; von Hänisch, C. Stable Alkali-Metal Complexes of hybrid Disila-Crown Ethers. *Inorg. Chem.* **2016**, *55*, 4441−4447.

(8) Reuter, K.; Rudel, S. S.; Buchner, M. R.; Kraus, F.; von Hänisch, C. Crown Ether Complexes of Alkali-Metal Chlorides from SO_2. *Chem. - Eur. J.* **2017**, *23*, 9607−9617.

(9) Reuter, K.; Dankert, F.; Donsbach, C.; von Hänisch, C. Structural Study of Mismatched Disila-Crown Ether Complexes. *Inorganics* **2017**, *5*, 11.

(10) Dankert, F.; Reuter, K.; Donsbach, C.; von Hänisch, C. A structural study of alkaline earth metal complexes with hybrid disila-crown ethers. *Dalton Trans.* **2017**, *46*, 8727−8735.

(11) Reuter, K.; Thiele, G.; Hafner, T.; Uhlig, F.; von Hänisch, C. Synthesis and coordination ability of a partially silicon based crown ether. *Chem. Commun.* **2016**, *52*, 13265−13268.

(12) Dankert, F.; Reuter, K.; Donsbach, C.; von Hänisch, C. Hybrid Disila-Crown Ethers as Hosts for Ammonium Cations: The O−Si−Si−O Linkage as an Acceptor for Hydrogen Bonding. *Inorganics* **2018**, *6*, 15.

(13) Dankert, F.; Donsbach, C.; Mais, C.-N.; Reuter, K.; von Hänisch, C. Alkali and Alkaline Earth Metal Derivatives of Disila-Bridged Podands: Coordination Chemistry and Structural Diversity. *Inorg. Chem.* **2018**, *57*, 351−359.

(14) Martín-Fernández, C.; Montero-Campillo, M. M.; Alkorta, I.; Elguero, J. Weak interactions and cooperativity effects on disiloxane: a look at the building block of silicones. *Mol. Phys.* **2018**, *116*, 1539−1550.

(15) Harder, S.; Freitag, B.; Stegner, P.; Pahl, J.; Naglav, D. Strontium Chemistry with Silicone Grease. *Z. Anorg. Allg. Chem.* **2015**, *641*, 2129−2134.

(16) Freitag, B.; Stegner, P.; Thum, K.; Fischer, C. A.; Harder, S. Tetranuclear Strontium and Barium Siloxide/Amide Clusters in Metal-Ligand Cooperative Catalysis. *Eur. J. Inorg. Chem.* **2018**, *2018*, 1938−1944.

(17) Pahl, J.; Elsen, H.; Friedrich, A.; Harder, S. Unsupported metal silyl ether coordination. *Chem. Commun.* **2018**, *54*, 7846−7849.

(18) Cypryk, M.; Apeloig, Y. Ab Initio Study of Silyloxonium Ions. *Organometallics* **1997**, *16*, 5938−49.

(19) West, R.; Wilson, L. S.; Powell, D. L. Basicity of siloxanes, alkoxysilanes and ethers toward hydrogen bonding. *J. Organomet. Chem.* **1979**, *178*, 5−9.

(20) Grabowsky, S.; Hesse, M. F.; Paulmann, C.; Luger, P.; Beckmann, J. How to Make the Ionic Si-O Bond More Covalent and the Si-O-Si Linkage a Better Acceptor for Hydrogen Bonding. *Inorg. Chem.* **2009**, *48*, 4384−4393.

(21) Grabowsky, S.; Beckmann, J.; Luger, P. The Nature of Hydrogen Bonding Involving the Siloxane Group. *Aust. J. Chem.* **2012**, *65*, 785.

(22) Frolov, Y. L.; Voronkov, M. G.; Strashnikova, N. V.; Shergina, N. I. Hydrogen bonding involving the siloxane group. *J. Mol. Struct.* **1992**, *270*, 205−215.

(23) Fugel, M.; Hesse, M. F.; Pal, R.; Beckmann, J.; Jayatilaka, D.; Turner, M. J.; Karton, A.; Bultinck, P.; Chandler, G. S.; Grabowsky, S. Covalency and Ionicity Do Not Oppose Each Other-Relationship Between Si−O Bond Character and Basicity of Siloxanes. *Chem. - Eur. J.* **2018**, *24*, 15275−15286.

(24) Shannon, R. Revised Effective Ionic Radii and Systematic Studies of Interatomic distances in Halides and Chalcogenides. *Acta Crystallogr., Sect. A: Cryst. Phys., Diffr., Theor. Gen. Crystallogr.* **1976**, *A32*, 751−767.

(25) Mantina, M.; Chamberlin, A. C.; Valero, R.; Cramer, C. J.; Truhlar, D. G. Consistent van der Waals Radii for the Whole Main Group. *J. Phys. Chem. A* **2009**, *113*, 5806−5812.

(26) Buchanan, G. W.; Gerzain, M.; Bensimon, C. 1,4,7,10,13-Pentaoxacyclopentadecane (15-crown-5) sodium iodide complex, $C_{10}H_{20}O_5NaI$. *Acta Crystallogr., Sect. C: Cryst. Struct. Commun.* **1994**, *50*, 1016−1019.

(27) Buchner, M. R.; Müller, M.; Dankert, F.; Reuter, K.; von Hänisch, C. The coordination behaviour and reactivity of partially silicon based crown ethers towards beryllium chloride. *Dalton Trans.* **2018**, *47*, 16393−16397.

(28) Naglav, D.; Buchner, M. R.; Bendt, G.; Kraus, F.; Schulz, S. Off the Beaten Track-A Hitchhiker's Guide to Beryllium Chemistry. *Angew. Chem., Int. Ed.* **2016**, *55*, 10562−10576. Naglav, D.; Buchner, M. R.; Bendt, G.; Kraus, F.; Schulz, S. *Angew. Chem.* **2016**, *128*, 10718−10733.

(29) Peshkova, M. A.; Timofeeva, N. V.; Grekovich, A. L.; Korneev, S. M.; Mikhelson, K. N. Novel Ionophores for Barium-Selective Electrodes: Synthesis and Analytical Characterization. *Electroanalysis* **2010**, *22*, 2147−2156.

DOI: 10.1021/acs.inorgchem.9b00086
Inorg. Chem. 2019, 58, 3518−3526

(30) Sheldrick, G. M. Crystal structure refinement with SHELXL. *Acta Crystallogr., Sect. C: Struct. Chem.* **2015**, *71*, 3−8.
(31) Sheldrick, G. M. SHELXT - Integrated space-group and crystal-structure determination. *Acta Crystallogr., Sect. A: Found. Adv.* **2015**, *A71*, 3−8.
(32) Dolomanov, O. V.; Bourhis, L. J.; Gildea, R. J.; Howard, J. A. K.; Puschmann, H. *OLEX2* a complete structure solution, refinement and analysis program. *J. Appl. Crystallogr.* **2009**, *42*, 339−341.
(33) *X-AREA and LANA*; Stoe & Cie: Darmstadt, Germany, 2009.
(34) *SADABS*; Bruker AXS Inc.: Madison, WI, 2016.

DOI: 10.1021/acs.inorgchem.9b00086
Inorg. Chem. 2019, 58, 3518−3526

ChemPubSoc Europe

DOI: 10.1002/chem.201904209

CHEMISTRY A European Journal Full Paper

Alkaline Earth Metals

Alkaline Earth Metal Template (Cross-)Coupling Reactions with Hybrid Disila-Crown Ether Analogues

Fabian Dankert, Carsten Donsbach, Julia Rienmüller, Roman M. Richter, and Carsten von Hänisch*[a]

Dedicated to Professor Jean-Marie Lehn on the occasion of his 80th birthday

Abstract: Alkaline earth metal iodides were used as templates for the synthesis of novel silicon-based ligands. Siloxane moieties were (cross-)coupled and ion-specific, silicon-rich crown ether analogues were obtained. The reaction of 1,2,7,8-tetrasila[12]crown-4 (**I**) and 1,2-disila[9]crown-3 (**II**) with MgI_2 yielded exclusively [Mg(1,2,7,8-tetrasila[12]crown-4)I_2] (**1**). The larger Ca^{2+} ion was then employed for cross-coupling of **I** and **II** and yielded the complex [Ca(1,2,7,8-tetrasila[15]crown-5)I_2] (**2**). Cross-coupling of **I** and 1,2,4,5-tetrasila[9]crown-3 (**III**) with SrI_2 enables the synthesis of the silicon-dominant 1,2,4,5,10,11-hexasila[15]crown-5 ether complex of SrI_2 (**3**). Further, the compounds [Sr(1,2,10,11-tetrasila[18]crown-6)I_2] (**4**), [Sr(1,2,13,14-tetrasila[24]crown-8)I_2] (**5**), and [Sr(1,2,13,14-tetrasila-dibenzo[24]crown-8)I_2] (**6**) were obtained by coupling **I**, 1,2-disila[12]crown-4 (**IV**) or 1,2-disila-benzo[12]crown-4 (**V**), respectively. Using various anions, the (cross-)coupled ligands were also observed in an X-ray structure within the mentioned complexes. These template-assisted (cross-)couplings of various ligands are the first of their kind and a novel method to obtain macrocycles and/or their metal complexes to be established. Further, the Si–O bond activations presented herein might be of importance for silane or even organic functionalization.

Introduction

It is well known for crown ethers to form coordination compounds with metal centers across a wide range of the periodic table. These complexes are generally very stable and these polyethers as well as related systems such as cryptands, or in general, multidentate ligands, gained many fields of applications since their discovery in the mid-sixties. The synthesis of such polyethers, however, is often not trivial because the molecules of the starting materials need to be brought into a suitable conformation for the formation of a specific (most often cyclic) product. The synthesis of these cyclic ethers is therefore mostly metal-template assisted.[1]

Templates are known to provide a suitable coordination sphere for the starting materials, which favors the linkage to ring closure and allows obtaining cyclic ligand systems in much higher yields.[1] Some prominent examples are summarized in Scheme 1. Over the years, also silicon-based polyethers, their syntheses as well as their coordination behavior towards different Lewis acids were studied.[5] For a long time, template-assisted syntheses of cyclosiloxanes were only observed (accidently) by using highly reactive starting materials in the presence of silicon grease (Scheme 2).[6–10] Ring transformations in the presence of metal cations were described later and the generation of sila-polyethers by metal-templated ring-opening polymerization was presented as an interesting possibility to obtain novel silicon-based ring systems.[5,11,12] The coordination behavior of silicon-based macrocycles, however, is significantly different to that of organic ethers, which is accompanied by the characteristics of the Si–O bond. Different explanations for the reduced capability of binding Lewis acids shown by siloxanes were provided in the literature.

Most recently, both concepts—covalency and ionicity—were considered as harmonious models to understand the basicity of siloxanes. Regarding a covalent model, negative hyperconjugation interactions are described in the case $p(O)\rightarrow\sigma^*(Si–C)$.[14,15] This strengthening of the Si–O bond then competes with the shift of electron density towards Lewis acids. Concerning the ionic model, the highly polarized Si–O bond features spatially diffuse electron pairs around the O-atom and repulsive interaction in between $Si^{\delta+}$ and $metal^{n+}$ disturbs silyl ether bonding.[16–18] Both, covalency and ionicity gain simultaneously in importance when the Si-O-Si angle increases and basicity lowers.[19–21] Given that the understanding of the Si–O bond

[a] F. Dankert, Dr. C. Donsbach, J. Rienmüller, R. M. Richter, Prof. Dr. C. von Hänisch
Fachbereich Chemie and Wissenschaftliches Zentrum für Materialwissenschaften (WZMW), Philipps-Universität Marburg
35032, Marburg (Germany)
E-mail: haenisch@staff.uni-marburg.de

The ORCID identification number(s) for the author(s) of this article can be found under:
https://doi.org/10.1002/chem.201904209.

© 2019 The Authors. Published by Wiley-VCH Verlag GmbH & Co. KGaA. This is an open access article under the terms of the Creative Commons Attribution License, which permits use, distribution and reproduction in any medium, provided the original work is properly cited.

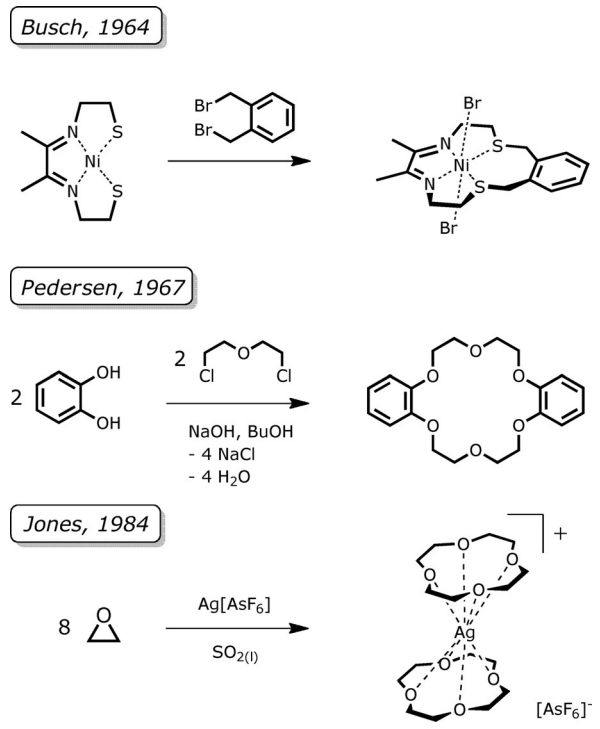

Scheme 1. A selection of metal-template syntheses of cyclic organic crown-type ligands. In all examples, the metal center acts as a convex template to promote ring closure and/or expansion.[2–4]

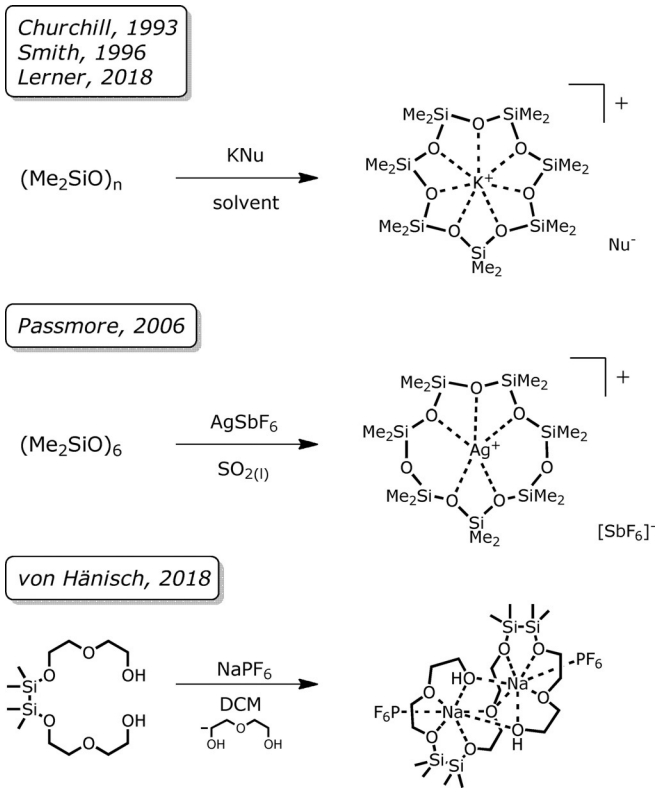

Scheme 2. A selection of metal-template syntheses of cyclic sila-crown-type ligands. In all examples, the metal center acts as a convex template to promote ring expansion. For details, please see the cited literature.[6,7,11–13]

was established in this case, research in the field of coordination chemistry with cyclosiloxanes and related ligand systems showed clearly that these effects have to be taken into account. Nonetheless, the coordination chemistry turned out to be very suitable for early Group 1 and 2 metal ions, especially within disila-ligands, which provide more suitable bite angles than cyclosiloxanes of D_n type ($D = Me_2SiO$, $n = 6$, 7).[22–26] The nature of a cation, which shall be complexed within siloxane moieties, is preferably hard.[13,27–31] In the case of the early alkaline earth-metal ions, even the commercially available cyclosiloxanes are able to dissolve salts characterized by a high lattice energy and stable complexes were obtained.[32] Soft cations like Rb^+ and Cs^+ so far relucted silyl ether coordination.[33,34] Overall, sila-ligands are suitable ligands for early s-block-metal coordination chemistry and opened a new chapter in host–guest chemistry over the years. In this contribution, we report the synthesis of novel hybrid disila-crown ether moieties, which are accessible by alkaline earth metal-template synthesis. First outlooks of a targeted template synthesis of hybrid disila-ligands were given in past works. Scheme 2 represents sila-ligands formed by metal templates.

Apart from siloxane coordination chemistry, the metal···O–Si interaction should also be put in context to Si–O bond activation. From the perspective of Si–O bond activation, weakening of Si–O bonds is of considerable significance regarding the conversion of silicates to silanes. Especially dicatecholato-silicate(IV) complexes are frequently used as precursors for either silane synthesis or functionalization of various organic molecules.[35–43] Most recently, a collaborative research of Ollivier and co-workers together with Fensterbank and co-workers demonstrated a new synthesis for ketones, in this context employing acyl chlorides.[44]

Results and Discussion

Starting with the Mg^{2+} ion, we aimed at synthesizing a [15]crown-5 ether by cross-coupling the ligands 1,2,7,8-tetrasila[12]crown-4 (**I**) and 1,2-disila[9]crown-3 (**II**). However, the reaction in α,α,α-trifluorotoluene heated at reflux failed (Scheme 3). Instead, [Mg(1,2,7,8-tetrasila[12]crown-4)I_2] (**1**) was obtained and, as can be seen from the molecular structure determined by single-crystal X-ray diffraction analysis (SC-XRD), the moiety of crown ether **I** is large enough to bind Mg^{2+} (Figure 1). This is probably due to the insertion of two disilane units with Si–Si bonds of 236.0(1) and 236.3(1) pm. The coordination mode of Mg^{2+} in the siloxane framework of **1** is very similar to that of [Mg(D_6)I_2] and the octahedral coordination towards Mg^{2+} is preferred.[32] Also in solution, a strong interaction of ligand **I** with Mg^{2+} is present because the $^{29}Si\{^1H\}$ NMR chemical shift is observed at 22.8 ppm and thus, a strong low-field shift in comparison with **I** ($\delta = 10.8$ ppm)[20] is observed.

The fivefold, coplanar coordination by sila-crown ligands towards the larger Ca^{2+} ion was described earlier and, as can be seen from various examples, seems to match perfectly.[26,32] Hence, we repeated the reaction of **I** and **II** with CaI_2. After workup procedures two new signals in the $^{29}Si\{^1H\}$ NMR are observed at 19.6 and 19.9 ppm. Crystallization of the reaction

 © 2019 The Authors. Published by Wiley-VCH Verlag GmbH & Co. KGaA, Weinheim

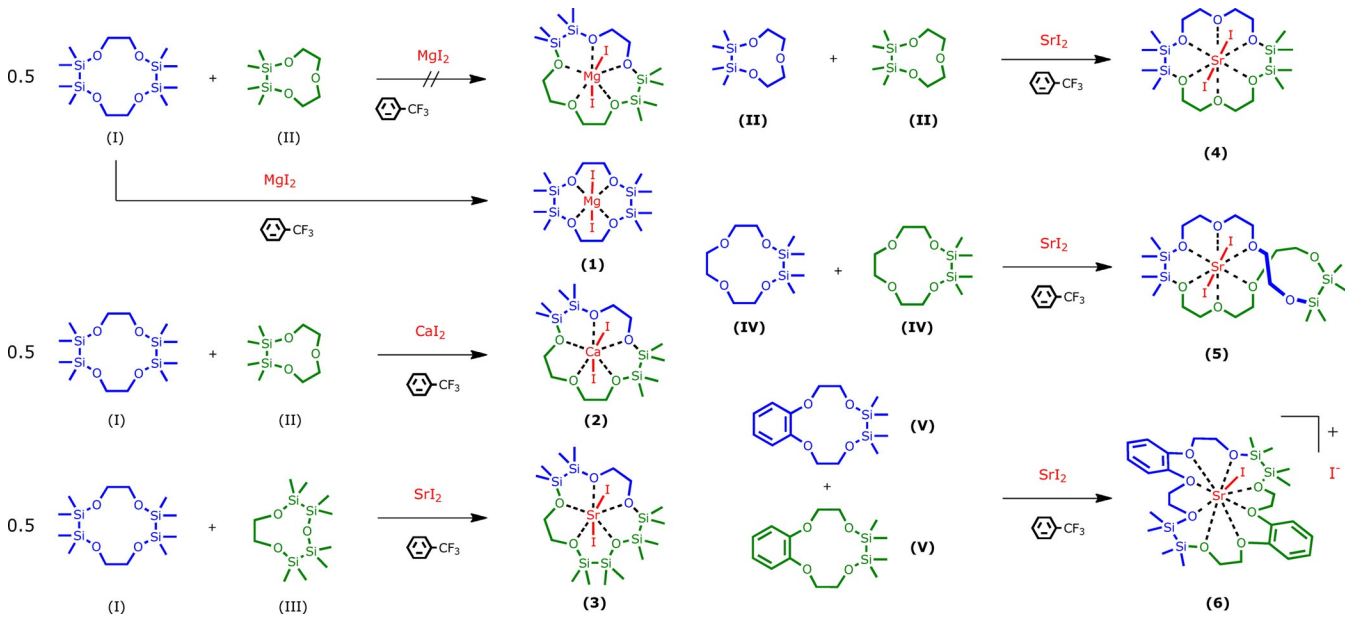

Scheme 3. Alkaline earth metal-template cross-coupling reactions (left) and coupling reactions (right) of the silicon-based crown ethers **1**–**6**.

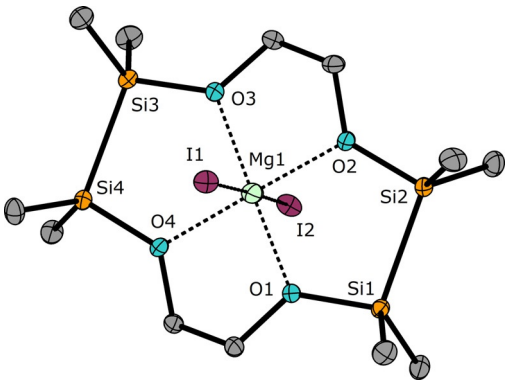

Figure 1. Molecular structure of **1** in the crystal. Thermal ellipsoids represent the 50% probability level. Hydrogen atoms are omitted for clarity. Selected bond lengths [pm]: O1–Mg1 198.8(3), O2–Mg1 199.9(3), O3–Mg1 199.4(3), O4–Mg1 200.3(3), Si1–Si2 236.3(1), Si3–Si4 236.0(1). I1–Mg1 305.4(2), I2–Mg1 302.8(2). Selected bond angles [°]: O1-Mg1-O2 96.1(1), O3-Mg1-O4 98.2(1), I1-Mg1-I2 176.6(1).

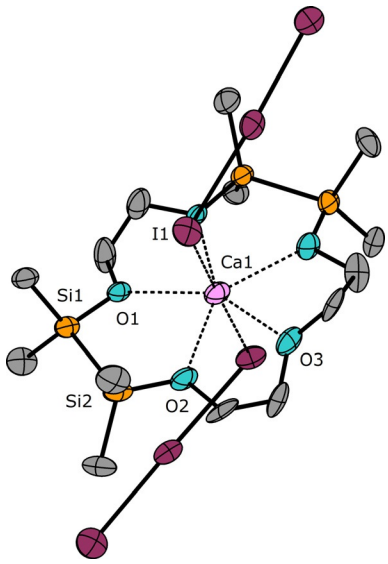

Figure 2. Molecular structure of **2a** in the crystal. Thermal ellipsoids represent the 40% probability level. Hydrogen atoms are omitted for clarity. Non-labeled atoms are symmetry generated over $1-x, y, {}^{1}/_{2}-z$. Selected bond lengths [pm]: O1–Ca1 239.3(7), O2–Ca1 245.2(9), O3–Ca1 236.4(9), Si1–Si2 234.4(3), I1–Ca1 312.6(1). Selected bond angles [°]: O1-Ca1-O2 77.6(2), I1-Ca1-I1# 177.6(1).

product **2** however, was unsuccessful from different solvents and temperatures also due to poor solubility. We therefore expanded the anion I^- to I_3^- upon iodine addition. The compound [Ca(1,2,7,8-tetrasila[15]crown-5)$(I_3)_2$] (**2a**) then was crystallized and the molecular structure was determined by means of SC-XRD (Figure 2). Compound **2a** contains the new ligand 1,2,7,8-tetrasila[15]crown-5, which was formed by a cross-coupling reaction of the ligands **I** and **II** mediated by the Ca^{2+} ions. The cross-coupling of sila-ligands is an elegant way to obtain novel macrocycles. The synthesis of these macrocycles cannot yet be realized by conventional silane chemistry and thus, the alkaline earth metal template opens up new synthetic pathways of such new ligands. The O_{Si}–Ca^{2+} distances measure 239.3(7) and 245.2(9) pm and compare well to the complex [Ca(1,2-disila[18]crown-6)OTf_2] (OTf = $CF_3SO_3^-$).[26]

The synthesis of [Sr(1,2,4,5,10,11-hexasila[15]crown-5)I_2] (**3**) is another example of a cross-coupling reaction in which an alkaline earth metal cation is used. **3** represents the first hybrid disila-crown ether bearing more disilane than ethylene units. The even larger Sr^{2+} cation can be used as a convex template to cross-couple **I** and 1,2,4,5-tetrasila[9]crown-3 (**III**), which is accessible applying reaction conditions reported before.[27] The reaction yields a silicon-based [15]crown-5 ether merging half an equivalent of **I** and one equivalent of **III**. Due to three disilane units within the ligand framework, the Sr^{2+} cation fits well

 © 2019 The Authors. Published by Wiley-VCH Verlag GmbH & Co. KGaA, Weinheim

in the cavity of the obtained ligand. With 19.44, 19.27, and 13.32 ppm, three resonances are observed in the $^{29}Si\{^1H\}$ NMR spectrum, all of which compare well to those of $O_{Si}\cdots Sr^{2+}$ coordination compounds characterized before.[26,27] A crystal structure of **3** could not be obtained, even after iodine addition. Hence, the Lewis acidic salt GaI_3 was added as an acceptor for the iodide anion. It is notable, that also in **3a**, the SiSi—O—SiSi fragment of the siloxane framework provides a small Si-O-Si angle, which measures 121.1(6)°. The $O_{Si-O-Si}\cdots Sr^{2+}$ distance might be the longest $O\cdots Sr^{2+}$ distance observed in **3a**, but the high basicity of siloxanes towards Group 2 ions is clearly emphasized.

After several months, a few single crystals of [Sr(1,2,4,5,10,11-hexasila[15]crown-5)$(GaI_4)_2$] (**3a**) were obtained, which were analyzed through SC-XRD (Figure 3). The $O_{Si}\cdots Sr^{2+}$ distances (concerning Si—O—C as well as Si—O—Si donor groups) compare well to various complexes of Sr^{2+} and sila ligands, which were reported before.[26,27] Using the Sr^{2+} cation as a template, we were able to observe reactions of other disila-crown ethers as well. The small cavity of **II** does not allow for 1:1 complexation of Sr^{2+} and thus, a total of two equivalents of **II** react to form the 1,2,10,11-tetrasila[18]crown-6 ether. [Sr(1,2,10,11-tetrasila[18]crown-6)I_2] (**4**) is obtained as a colorless powder and in solution, a resonance at 17.5 ppm in the $^{29}Si\{^1H\}$ NMR spectrum was observed. Given that we were also experiencing problems with the crystallization of this compound, the X-Ray structure could only be determined upon iodine addition. According to a reduced niggli formula, compound $^1_\infty$[Sr(1,2,10,11-tetrasila[18]crown-6$I_{2/2}$]I_3 (**4a**) was obtained as brown platelets which were investigated through SC-XRD. As shown by the molecular structure in the crystal, the ligand does not perfectly match with the Sr^{2+} cation because a coplanar arrangement of the donor atoms is not observed (see Figure 4). However, all oxygen atoms of the crown ether still manage to participate in the coordination. Upon iodine addition, one I_3^- anion is formed, which does not coordinate the central ion in the solid state. This enables the formation of [Sr(1,2,10,11-tetrasila[18]crown-6)I]$^+$ fragments to build infinite chains along [001] which is most likely the driving force for crystallization. The $O_{Si}\cdots Sr^{2+}$ distances in **4a** compare well to those in compound **3a** and [Sr(1,2-disila[18]crown6)I_2].[24]

At this point, it is clear that (cross-)coupling reactions are possible with different alkaline earth metal iodides. We tried to understand how the reaction works and the mechanism behind the formation of these unprecedented macrocycles, but unfortunately, we were unable to characterize any intermediate products by means of NMR spectroscopy or SC-XRD. We can assure that heating at reflux is needed to cleave the smaller rings. Further, we can assure that the reaction does only occur if an iodide salt is employed. Other alkaline earth metal halides do not form these ligands. This lets us conclude that one key step in the formation of the (cross-)coupling product has to be a nucleophilic substitution reaction. Furthermore, as evident from different works, we could convincingly show that the Si—O bond is significantly weakened due to coordinating an alkaline earth metal ion. Thus, the Si—O bond instead of the C—O bond is cleaved, which is also represented by the herein obtained macrocycles. A proposed mechanism for the formation of the cross coupling products is depicted in Scheme 4 for **4** as an example. As drawn here, the sila-ligand

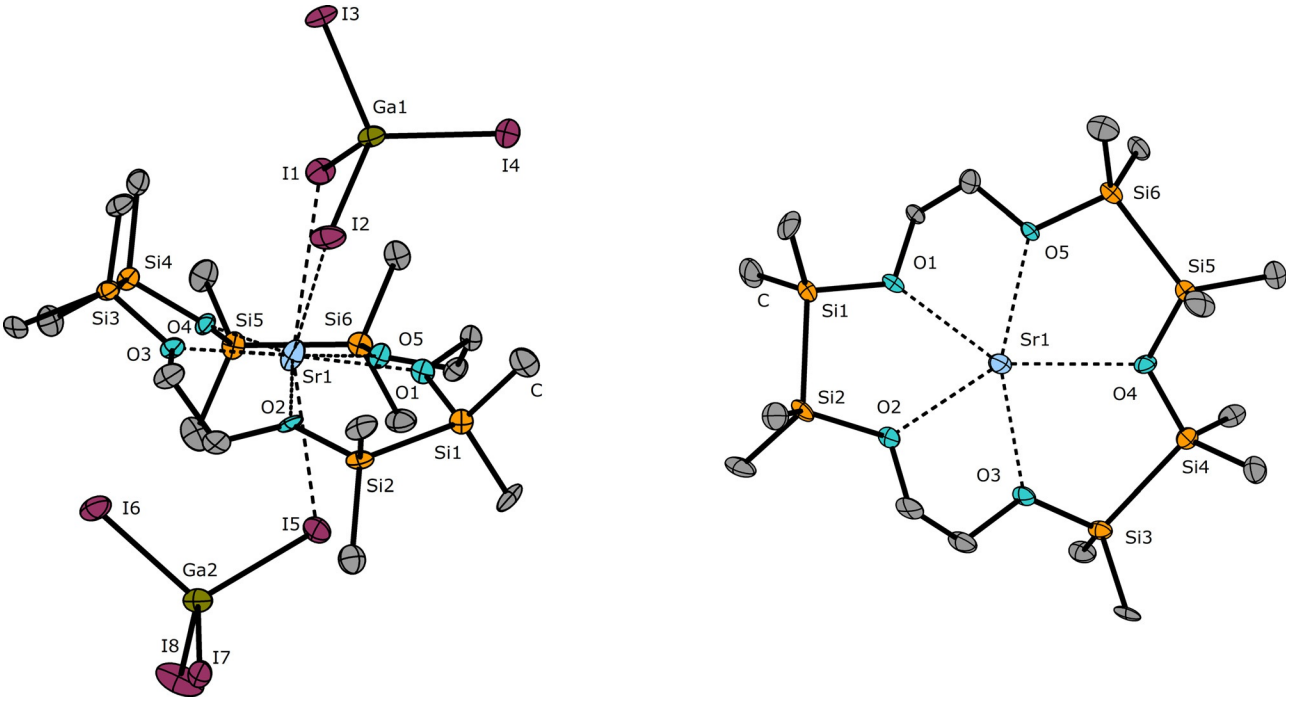

Figure 3. Molecular structure of **3a** in the crystal. Contact-ion pair (left) and top view (right). Thermal ellipsoids represent the 50% probability level. Hydrogen atoms are omitted for clarity. Selected bond lengths [pm]: O1—Sr1 251.6(9), O2—Sr1 257.4(7), O3—Sr1 250.5(7), O4—Sr1 272.4(9), O5—Sr1 253.5(7), Si1—Si2 235.5(5), Si3—Si4 236.8(4), Si5—Si6 234.46. I1—Sr1 347.1(1), I2—Sr1 399.8(1), I5—Sr1 343.2(1). Selected bond angles [°]: O1-Sr1-O2 73.8(3), O3-Sr1-O4 79.4(3), O4-Sr1-O5 77.0(3).

 © 2019 The Authors. Published by Wiley-VCH Verlag GmbH & Co. KGaA, Weinheim

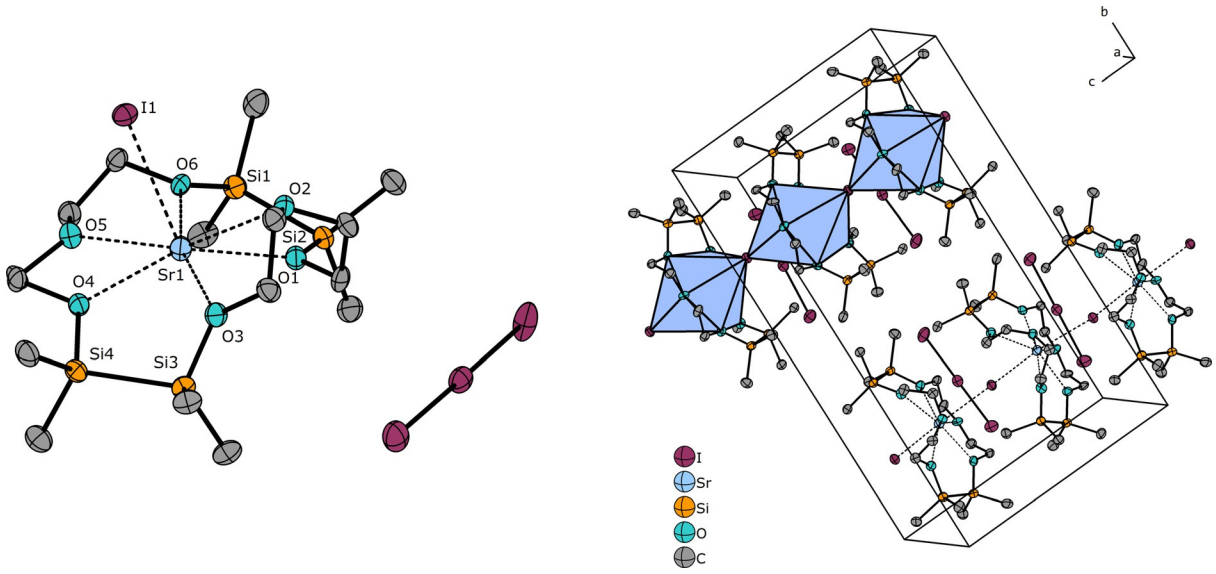

Figure 4. Molecular structure of **4a** in the crystal (left) and cell package approximately along [100] (right). Thermal ellipsoids represent the 50% probability level. Hydrogen atoms are omitted for clarity. Selected bond lengths [pm]: O1–Sr1 262.8(4), O2–Sr1 270.7(5), O3–Sr1 277.6(5), O4–Sr1 265.9(4), O5–Sr1 261.1(4), O6–Sr1 265.4(4), Si1–Si2 231.8(3), Si3–Si4 233.8(3), I1–Sr1 327.5(1). Selected bond angles [°]: O1-Sr1-O2 71.6(1), O3-Sr1-O4 69.5(1), I1-Sr1-O2 78.8(3).

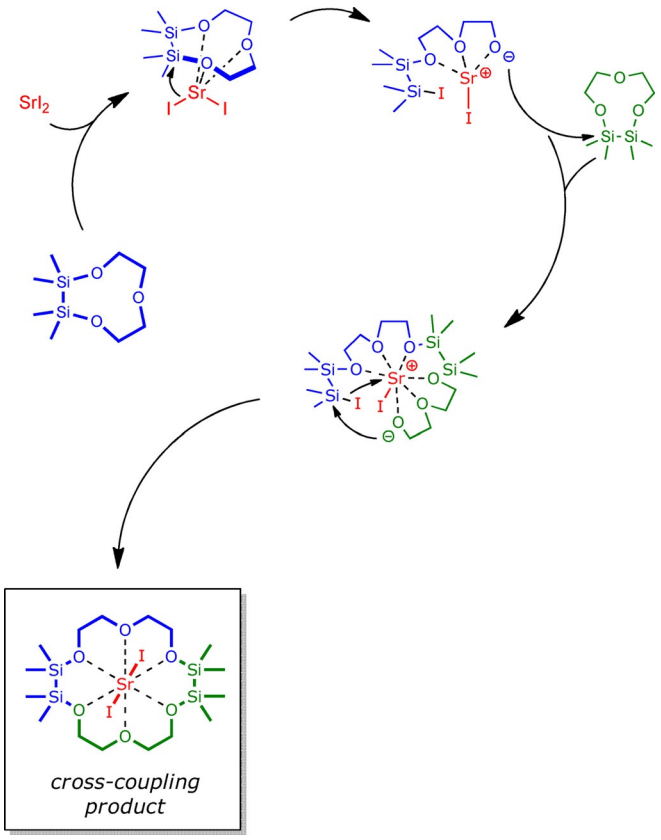

Scheme 4. Proposed mechanism for the formation of compound **4**.

is polarized by the Lewis acid first, which makes it electrophilic and thus accessible for nucleophilic attack of I^-. Afterwards, the Si–O bond is cleaved. Subsequently, the intermediate then has to cleave the second sila-crown. At this point of the reaction, the alkaline earth metal ion acts as a convex template, in which the open-chained ligand species is brought into a suitable conformation for ring closure, which is the final step of the presented reactions. We want to emphasize, that such a mechanism was also postulated by Harder in a past work.[31]

Further reactions of SrI_2 with the ligands 1,2-disila[12]crown-4 (**IV**) and 1,2-disila-benzo[12]crown-4 (**V**) were performed. Both ligands are too small for Sr^{2+} and thus, template-assisted ring opening yielded novel species by intermolecular coupling of the respective crown ether. The reaction of **IV** with SrI_2 results in the formation of the first disilanyl-bearing [24]crown-8 ether. [Sr(1,2,13,14-tetrasila[24]crown-8)I_2] (**5**) was obtained by coupling two equivalents of **IV** (Figure 5). The molecular structure in the crystal reveals that six out of eight oxygen atoms, as well as the two iodide anions, are coordinating. The overall eightfold coordinated Sr^{2+} cation is therefore embedded in a *pseudo*-1,2-disila[18]crown-6 moiety. Given that the two oxygen atoms of the second disilane fragment do not coordinate, a twisting of the crown ether is observed. The driving force of this reaction is the arrangement of six of the coordinating crown ether oxygen atoms forming an [18]crown-6-like coordination sphere similar to that observed in **4**. The $O_{Si}\cdots Sr^{2+}$ distances in **5** are, however, slightly shorter than those in [Sr(1,2-disila[18]crown6)I_2].[26] A single $^{29}Si\{^1H\}$ NMR resonance signal for **5** is observed at 15.2 ppm. A split of this resonance at low temperature of 190 K was not observed.

Thus, the exchange between the coordinating disilane units is too fast on the NMR time scale and results in the described equivalency. At this point, it should be noted that the spectroscopic investigation of the compound is challenging. Compound **5** decomposes readily with only traces of moisture forming [Sr(11,12-disila-EO7)I]I (EO7 = heptaethylene glycol).[13]

The twisting of the crown ether is most likely a suitable preorganization for the formation of the open-chained EO7 ligand

 © 2019 The Authors. Published by Wiley-VCH Verlag GmbH & Co. KGaA, Weinheim

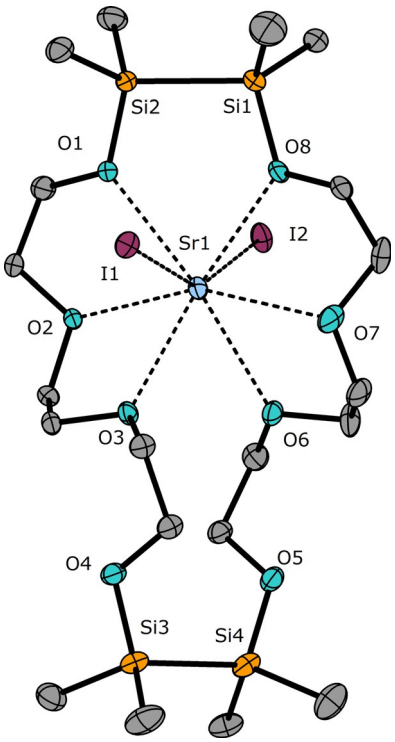

Figure 5. Molecular structure of **5** in the crystal. Thermal ellipsoids represent the 50% probability level. Hydrogen atoms are omitted for clarity. Selected bond lengths [pm]: O1–Sr1 265.8(1), O2–Sr1 261.9(1), O3–Sr1 262.8(1), O4···Sr1 543.1(1), O5···Sr1 539.2(2), O6–Sr1 270.3(2), O7–Sr1 266.3(2), O8–Sr1 261.9(2), Si1–Si2 234.4(1), Si3–Si4 238.2(1), I1–Sr1 335.2(4), I2–Sr1 326.4(4). Selected bond angles [°]: O1-Sr1-O8 76.6(5), O3-Sr1-O6 67.6(1), I1-Sr1-I2 150.9(1).

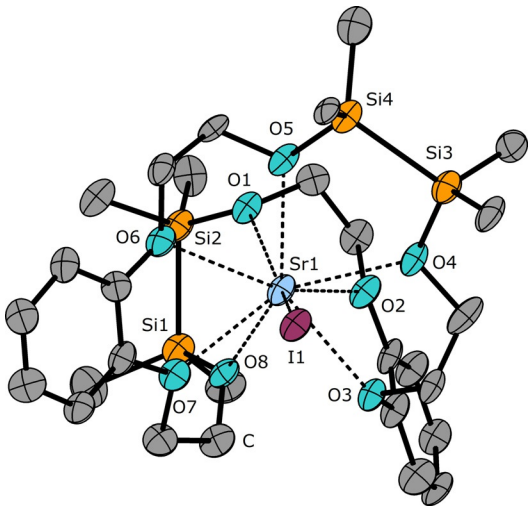

Figure 6. Molecular structure of the cationic part of **6** in the crystal. Thermal ellipsoids represent the 40% probability level. Hydrogen atoms as well as a single iodide anion are omitted for clarity. Selected bond lengths [pm]: O1–Sr1 265.0(10), O2–Sr1 274.1(8), O3–Sr1 266.0(9), O4–Sr1 263.9(9), O5–Sr1 260.8(10), O6–Sr1 270.1(8), O7–Sr1 263.8(10), O8–Sr1 271.9(9), Si1–Si2 234.6(7), Si3–Si4 234.8(5), I1–Sr1 329.9(1). Selected bond angles [°]: O4-Sr1-O5 72.8(3), O6-Sr1-O7 58.4(3).

and explains its high sensitivity. [Sr(1,2,13,14-tetrasila-dibenzo[24]crown-8)I]I (**6**) is more stable and was characterized by state-of-the-art methods including SC-XRD (Figure 6). After a 2:1 reaction of **V** with SrI_2, **V** performs intermolecular coupling as well. Here, the dibenzo crown ether helically encapsulates the central ion under replacement of one iodide anion. All eight oxygen atoms do now participate in the coordination of Sr^{2+}. Even though the ligand in **6** is more rigid than that of **5**, shielding of the central ion is observed. This might be a result of slightly reduced basicity of benzo crown ethers in general. The replacement of iodide by oxygen donor groups is favored over metal–anion interactions and is most likely also present in solution because the $^{29}Si\{^1H\}$ NMR chemical shift is with 19.8 ppm very distinct for Sr^{2+} coordination.

One of the remaining questions is of course whether it is possible to remove the metal center for possible use of such new ligand in coordination chemistry. We are currently investigating this subject, but are still at an early stage. To give an outlook, we performed exchange reactions. As an example, an excess of **6** was reacted with [222]cryptand and indeed we were able to obtain free ligand 1,2,13,14-tetrasila-dibenzo[24]crown-8 (**7**) after workup. The metal-free ligand species was characterized by means of HR-ESI MS as well as NMR spectroscopy. In HR-ESI$^+$ MS, *m/z* relations of 625.2502 $[\mathbf{7}+H]^+$ (100) as well as 647.2320 $[\mathbf{7}+Na]^+$ (100) were found. In addition, $^{29}Si\{^1H\}$ NMR spectroscopy revealed highfield chemical shift and a single resonance at 11.5 ppm is found. This value compares well to the free ligand **V** and also to related metal-free disila-ligand systems.[22,24,26,28,33] The problem so far is that a significant amount of the cryptand remains in the oily residue after conversion, so no further coordination chemistry could be performed yet. To which extent this will be possible, not only for the ligands presented herein, is of current interest and will be subject of further research.

So far, we also tried (cross)-coupling reactions with BaI_2, or other alkaline earth metal halides such as chlorides and bromides but various attempts failed. The method obtaining the novel macrocycles herein is for this reason restricted to iodide salts.

Conclusions

In this study alkaline earth metal iodides were successfully used for the coupling reaction of different silicon-based crown ether analogues to form novel ligand environments. The work presents Si–O bond-cleavage reactions driven by a macrocyclic effect due to metal-template reaction of the respective silicon-based ligands. Given that the Mg^{2+} ion is too small to cross-couple small silicon-based ligands, a cross-coupling reaction was established with the larger Ca^{2+} and Sr^{2+} ions. Furthermore, the Sr^{2+} ion was used for coupling reactions of three different disila-crown ethers. Barium as a template for coupling reaction, however, turned out to be unsuccessful. Although the organic [12]crown-4 is too small for the Mg^{2+} ion, the cavity of the disilane-bearing analogue 1,2,7,8-tetrasila[12]-crown-4 (**I**) ether matches fine with the Mg^{2+} ion and the complex [Mg(1,2,7,8-tetrasila12crown-4)I_2] (**1**) was obtained. [Ca(1,2,7,8-tetrasila[15]crown-5)I_2] (**2**) and [Sr(1,2,4,5,10,11-hexasila[15]crown-5)I_2] (**3**) were synthesized by cross-coupling reac-

© 2019 The Authors. Published by Wiley-VCH Verlag GmbH & Co. KGaA, Weinheim

tion of the small rings **I** and **II** for **2**, and **I** and **III** for **3**. The ligand in **3** represents the first crown ether with more disilane than ethylene units between the donor atoms. Finally, [Sr(1,2,10,11-tetrasila[18]crown-6)I_2] (**4**), [Sr(1,2,13,14-tetrasila[24]crown-8)I_2] (**5**) and [Sr(1,2,13,14-tetrasila-dibenzo[24]crown-8)I]I (**6**) were characterized and obtained by template-driven dimerization of **II**, **IV**, or **V** with SrI_2. The ligand moieties observed in **2**–**6** cannot yet be synthesized by conventional silane chemistry and for this reason, the template-assisted (cross-)coupling of various ligands is an elegant way to obtain novel macrocycles and/or their metal complexes. Overall, this work gives an outlook on Group 2 ion-catalyzed silane syntheses, especially due to the fact that first attempts showed that the metal ion can, in principle, be removed from a novel silaether. We also hope that there will be a broader application of the presented Si–O bond activations as a mean of molecule functionalization.

Experimental Section

General

All manipulations were carried out with rigorous exclusion of oxygen and moisture using basic Schlenk techniques establishing an inert-gas atmosphere with a vacuum line. All solvents were dried and freshly distilled before use. The alkaline earth metal salts MgI_2 (Alfa Aesar, 99,996%), CaI_2 and SrI_2 (Alfa Aesar, 99%), BaI_2 (abcr, 99.995%) and GaI_3 (abcr, 99%) were finely ground and stored in a Mbraun glovebox under Ar. NMR spectra were recorded on a Bruker AV III HD 300 MHz or AV III 500 MHz spectrometer, respectively. Infrared (IR) spectra of the respective samples were measured using attenuated total reflectance (ATR) mode on the Bruker-type spectrometer Alpha FT-IR. ESI mass spectra were acquired with a LTQ-FT Ultra mass spectrometer (Thermo Fischer Scientific) and LIFDI mass spectra were acquired on a JEOL AccuTOF-GCv device. The resolution was set to 100.000. Elemental analysis was carried out on a Vario MicroCube. In case of complex **2** and **3**, we were not able to obtain an accurate elemental analysis. This is probably due to the wax-like, greasy characteristics of the compounds and/or formation of SiC during the measurement. The crown-ethers **I**, **II**, **IV**, and **V** were synthesized according to literature-known procedures.[22,28,33] Compound **7** can only be obtained with major impurities of [222]crypt.

Synthesis of 1,2,4,5-tetrasila[9]crown-3 (III)

Ethylene glycol (0.19 mL, 3.41 mmol, 1.00 equiv) and NEt_3 (0.94 mL, 6.84 mmol, 2.0 equiv) were dissolved in THF (50 mL). Subsequently, $O(Si_2Me_4Cl)_2$[23] (1 mL, 3.41 mmol, 1.00 equiv) dissolved in THF (50 mL) was added over a period of 60 min. The resulting white suspension was then stirred overnight and the solvent was removed in vacuo. The residue was extracted with *n*-pentane (50 mL) followed by filtration. Removing the solvent under reduced pressure yielded the crown ether as a colorless oil (0.74 g, 70%).

^{1}H NMR (300 MHz, CD_3CN): $\delta = 0.18$ (s, 12H, $Si(CH_3)_2$), 0.20 (s, 12H, $Si(CH_3)_2$), 3.69 ppm (s, 4H, CH_2); $^{13}C\{^1H\}$ NMR (125 MHz, CD_3CN): $\delta =$ 0.1 (s, $Si(CH_3)_2$), 2.8 (s, $Si(CH_3)_2$), 66.0 ppm (s, CH_2); $^{29}Si\{^1H\}$ NMR (60 MHz, CD_3CN): $\delta = 1.5$ (s, $Si(CH_3)_2$), 11.4 ppm (s, $Si(CH_3)_2$). HR-MS: ESI(+) *m/z* (%): 309.1196 $[M+H]^+$ (100), 639.2143 $[2M+Na]^+$ (100); IR: 2951 (m), 2896 (w), 2867 (w), 1457 (vw), 1388 (vw), 1247 (s), 1140 (m), 1089 (s), 1027 (s), 927 (m), 854 (m), 795 (s), 761 (vs.), 721 (m), 681 (m), 660 (m), 633 (m), 553 (m), 506 (vw), 487 cm^{-1} (m).

Synthesis of [Mg(1,2,7,8-tetrasila[12]crown-4)I_2] (1)

Compound **I** (0.100 g, 0.29 mmol) was dissolved in α,α,α-trifluorotoluene (10 mL). Subsequently, MgI_2 (0.079 g, 0.29 mmol) was added. Stirring the mixture at 60 °C for 90 min gave a white suspension. Removing the solvent under reduced pressure yielded a white precipitate which was extracted with DCM (10 mL) followed by filtration. After washing with *n*-pentane (4 mL), and drying in vacuo, **1** was obtained as a colorless powder (0.139 g, 77%). For single-crystal growth, the powder was dissolved in DCM (4 mL) and layered with *n*-pentane (20 mL). Single crystals were obtained overnight as colorless needles.

^{1}H NMR (300 MHz, CD_2Cl_2): $\delta = 0.59$ (s, 24H, $Si(CH_3)_2$), 4.23 ppm (s, 8H, CH_2); $^{13}C\{^1H\}$ NMR (125 MHz, CD_2Cl_2): $\delta = -0.46$ (s, $Si(CH_3)_2$), 62.8 ppm (s, CH_2); $^{29}Si\{^1H\}$ NMR (60 MHz, CD_2Cl_2): $\delta = 22.8$ ppm (s, $Si(CH_3)_2$). MS: ESI(+) *m/z* (%): 503.0270 $[M-I]^+$ (15); IR: 2949 (vw), 2888 (vw), 1450 (w), 1398 (vw), 1369 (vw), 1247 (m), 1103 (m), 1056 (s), 1022 (s), 934 (vs.), 915 (s), 868 (m), 840 (m), 818 (s), 802 (s), 780 (vs.), 715 (s), 645 (m), 464 cm^{-1} (m). CHN calcd for $C_{12}H_{32}I_2MgO_4Si_4 \cdot CH_2Cl_2$ C, 21.81; H, 4.79. Found C, 21.66; H, 4.90.

Synthesis of [Ca(1,2,7,8-tetrasila[15]crown-5)I_2] (2)

Compound **I** (0.156 g, 0.44 mmol) together with **II** (0.195 g, 0.88 mmol) were dissolved in α,α,α-trifluorotoluene (10 mL). Subsequently, CaI_2 (0.259 g, 0.88 mmol) was added. Heating the mixture at reflux for 90 min resulted in a white suspension. Removing the solvent under reduced pressure yielded a white precipitate which was extracted with of DCM (10 mL) followed by filtration. After washing with two portions of *n*-pentane (4 mL each), and drying in vacuo, **1** was obtained as a colorless powder (0.316 g, 52%). For single-crystal growth, **2** (30 mg, 0.04 mmol) and I_2 (22 mg, 0.09 mmol) were dissolved in DCM (4 mL) and filtered. The filtrate was then layered with *n*-pentane (20 mL). A few brown platelets of **2a** were obtained after more than two weeks at ambient temperature.

^{1}H NMR (300 MHz, CD_2Cl_2): $\delta = 0.47$ (s, 12H, $SiCH_3$), 0.48 (s, 12H, $SiCH_3$), 3.95–4.03 ppm (m, 12H, CH_2); $^{13}C\{^1H\}$ NMR (75 MHz, CD_2Cl_2): $\delta = -0.7$ (s, $SiCH_3$), −0.7 (s, $SiCH_3$), 63.2 (s, CH_2), 64.8 (s, CH_2), 71.2 ppm (s, CH); $^{29}Si\{^1H\}$ NMR (60 MHz, CD_2Cl_2): $\delta = 19.6$ (s, $SiCH_3$), 19.9 ppm (s, $SiCH_3$). MS: ESI(+) *m/z* (%): 419.1521 $[M-CaI_2+Na]^+$ (100), 397.1705 $[M-CaI_2+H]^+$ (5). IR: 2947 (m), 2881 (w), 1455 (vw), 1400 (vw), 1248 (s), 1057 (s), 1029 (s), 943 (s), 795 (s), 768 (vs.), 723 (s), 635 (m), 505 cm^{-1} (vw).

Synthesis of [Sr(1,2,7,8,10,11-hexasila[15]crown-5)I_2] (3)

Compounds **I** (0.100 g, 0.29 mmol) and **III** (0.170 g, 0.55 mmol) were dissolved in α,α,α-trifluorotoluene (10 mL). Subsequently, SrI_2 (0.188 g, 0.56 mmol) was added. Heating the mixture at reflux for 90 min resulted in a white suspension. Removing the solvent under reduced pressure yielded a white precipitate which was extracted with DCM (10 mL), followed by filtration. After washing with two portions of *n*-pentane (4 mL each) and drying in vacuo, **3** was obtained as a colorless, greasy solid (0.185 g, 40%). For single-crystal growth, product **3** (0.030 g, 0.04 mmol) and GaI_3 (0.018 g, 0.04 mmol) were dissolved in α,α,α-trifluorotoluene (5 mL). The suspension was stirred 30 min and gently warmed to 60 °C for 5 min. The mixture was then freed of the solvent, extracted with DCM (3 mL) and filtered. The filtrate was then concentrated until

 © 2019 The Authors. Published by Wiley-VCH Verlag GmbH & Co. KGaA, Weinheim

the saturation point was reached and stored at −32 °C. A few colorless platelets of **3a** were obtained after more than four weeks. ^{1}H NMR (300 MHz, CD_2Cl_2): δ = 0.44 (s, 12H, Si(CH_3)$_2$), 0.47 (s, 12H, Si(CH_3)$_2$), 0.56 (s, 12H, Si(CH_3)$_2$), 3.96 ppm (s, 8H, CH_2); ^{13}C{^{1}H} NMR δ = −0.5 (s, Si(CH_3)$_2$), −0.5 (s, Si(CH_3)$_2$), 4.1 (s, Si(CH_3)$_2$), 65.3 (s, CH_2), 65.4 ppm (s, CH_2); ^{29}Si{^{1}H} NMR (60 MHz, CD_2Cl_2): δ = 13.3 (s, *Si*(CH_3)$_2$), 19.3 (s, *Si*(CH_3)$_2$), 19.4 ppm (s, *Si*(CH_3)$_2$). MS: ESI(+) *m/z* (%): 698.9902 [M−I]$^+$ (100), 507.1697 [M−SrI_2+Na]$^+$ (30). IR: 2960 (w), 2879 (vw), 1456 (vw), 1400 (vw), 1369 (vw), 1258 (s), 1074 (s), 1024 (s), 951 (s), 894 (m), 851 (m), 794 (vs.), 769 (vs.), 712 (s), 634 (m), 557 (m), 497 (w), 448 cm^{-1} (w).

Synthesis of [Sr(1,2,10,11-tetrasila[18]crown-6)I_2] (4)

Compound **II** (0.258 g, 1.17 mmol) was dissolved in α,α,α-trifluorotoluene (10 mL). Subsequently SrI_2 (0.200 g, 0.59 mmol) was added. Heating the mixture at reflux for 60 min. resulted in a white suspension. Removing the solvent under reduced pressure gave a white precipitate which was extracted with DCM (20 mL) followed by filtration. Upon washing with *n*-pentane (5 mL) and removal of the solvent, **4** was obtained as a pale white powder (0.259 g, 56%). For single crystal growth, product **4** (30 mg 0.04 mmol) and I_2 (10 mg, 0.04 mmol) were dissolved in DCM (4 mL). Layering the solution with *n*-pentane (20 mL) yielded single crystals of **4a** as brown blocks after three days.

^{1}H NMR (300 MHz, CD_2Cl_2): δ = 0.45 (s, 12H, SiCH_3), 3.88 (t, $^3J_{HH}$ = 4.6 Hz, 8H, CH_2), 4.08 ppm (t, $^3J_{HH}$ = 4.6 Hz, 8H, CH_2); ^{13}C{^{1}H} NMR (125 MHz, CD_2Cl_2): δ = 0.1 (s, SiCH_3), 63.0 (s, CH_2), 72.8 ppm (s, CH_2); ^{29}Si{^{1}H} NMR (60 MHz, CD_2Cl_2): δ = 17.5 ppm (s, *Si*CH_3). MS: ESI(+) *m/z* (%): 264.0475 [M−2I]$^{2+}$ (93), 447.2058 [M−SrI_2+Li]$^+$ (3), 463.1797 [M−SrI_2+Na]$^+$ (55), 479.1537 [M−SrI_2+K]$^+$ (15), 655.0003 [M−I]$^+$ (16). IR: 2943 (w), 2880 (w), 1459 (w), 1398 (vw), 1353 (w), 1247 (m), 1069 (s), 1039 (s), 944 (s), 927 (s), 861 (s), 840 (s), 819 (s), 795 (s), 768 (vs.), 718 (s), 629 (m), 546 (w), 523 cm^{-1} (w). CHN calcd for $C_{16}H_{40}I_2O_6Si_4Sr$: C, 24.57; H, 5.15. Found: C, 25.42; H, 5.35.

Synthesis of [Sr(1,2,13,14-tetrasila[24]crown-8)I_2] (5)

Compound **IV** (0.209 g, 0.79 mmol) was dissolved in α,α,α-trifluorotoluene (15 mL). Subsequently SrI_2 (0.135 g, 0.40 mmol) was added. Heating the mixture at reflux for three hours resulted in a white suspension. Removing the solvent under reduced pressure yielded a white precipitate which was extracted with DCM (20 mL), followed by filtration. The product **5** was then obtained as a colorless powder after removal of the solvent (0.252 g, 74%). For single-crystal growth, the powder was dissolved in DCM (4 mL) and layered with *n*-pentane (20 mL). Single crystals were obtained overnight as colorless needles.

^{1}H NMR (300 MHz, CD_2Cl_2): δ = 0.37 (s, 24H, Si(CH_3)$_2$), 3.94 (s, 8H, CH_2), 3.95 ppm (s, 16H, CH_2); ^{13}C{^{1}H} NMR (125 MHz, CD_2Cl_2): δ = −0.09 (s, SiCH_3), 62.8 (s, CH_2), 70.5 (s, CH_2), 73.5 ppm (s, CH_2); ^{29}Si{^{1}H} NMR (60 MHz, CD_2Cl_2): δ = 15.2 ppm (s, *Si*CH_3). MS: ESI(+) *m/z* (%): 551.2311 [M−SrI_2+Na]$^+$ (82); IR: 2961 (m), 2943 (m), 2882 (w), 1454 (w), 1396 (w), 1366 (w), 1349 (w), 1302 (w), 1259 (s), 1091 (s), 1073 (s), 1039 (s), 1017 (s), 951 (s), 931 (s), 861 (m), 840 (m), 791 (vs.), 764 (s), 732 (s), 661 (s), 636 (m), 563 (w), 492 (w), 424 cm^{-1} (w). CHN calcd for $C_{20}H_{48}I_2O_8Si_4Sr$: C, 27.86; H, 5.67. Found: C, 27.60; H, 5.67.

Synthesis of [Sr(1,2,13,14-tetrasila-dibenzo[24]crown-8)I]I (6)

Compound **V** (0.200 g, 0.64 mmol) was dissolved in α,α,α-trifluorotoluene (15 mL). Subsequently, SrI_2 (0.109 g, 0.32 mmol) was added. Heating the mixture at reflux for three hours resulted in a white suspension. Removing the solvent under reduced pressure yielded a white precipitate which was extracted with DCM (20 mL) followed by filtration. The product **6** was then obtained as a colorless powder after removal of the solvent (0.200 g, 65%). For single-crystal growth, the powder was dissolved in DCM (3 mL) and layered with *n*-pentane (20 mL). Single crystals were obtained overnight as colorless platelets.

^{1}H NMR (300 MHz, CD_2Cl_2): δ = 0.45 (s, 24H, SiCH_3), 4.15 (t, 8H, CH_2, $^3J_{HH}$ = 4.6 Hz), 4.42 (t, 8H, CH_2, $^3J_{HH}$ = 4.6 Hz), 7.02–7.16 ppm (m, 8H, CH_{Ar}); ^{13}C{^{1}H} NMR (125 MHz, CD_2Cl_2): δ = 0.0 (s, SiCH_3), 62.4 (s, CH_2), 72.6 (s, CH_2), 116.1 (s, CH_{Ar}), 124.9 (s, CH_{Ar}), 147.4 ppm (s, C_qH_{Ar}); ^{29}Si{^{1}H} NMR (60 MHz, CD_2Cl_2): δ = 19.8 ppm (s, *Si*CH_3). MS: ESI(+) *m/z* (%): 647.2311 [M−SrI_2+Na]$^+$ (78), 839.0525 [M−I]$^+$ (35); IR: 2946 (w), 2885 (w), 1595 (w), 1500 (s), 1456 (m), 1400 (w), 1366 (w), 1250 (vs.), 1191 (m), 1161 (m), 1115 (m), 1063 (s), 934 (vs.), 916 (vs.), 862 (m), 837 (m), 817 (s), 774 (s), 750 (vs.), 734 (s), 711 (s), 630 (w), 605 (w), 533 (w), 516 (w), 484 (w), 456 (w), 422 cm^{-1} (w). CHN calcd for $C_{28}H_{48}I_2O_8Si_4Sr{\cdot}0.5\,CH_2Cl_2$: C, 33.93; H, 4.90. Found: C, 33.92; H, 4.68.

Synthesis of 1,2,13,14-tetrasila-dibenzo[24]crown-8 (7)

Compound **6** (0.190 g, 0.19 mmol, excess) was dissolved in DCM (10 mL) and [222]cryptand (0.050 mg, 0.13 mmol, 0.7 equiv) was added. The resulting suspension was stirred overnight to give a clear solution. The solvent was removed under reduced pressure to give an oily, greasy residue. Extracting with *n*-pentane (10 mL) and subsequent filtering of the suspension yielded a clear solution. Removing the solvent under reduced pressure gave a greasy crown ether-[222]cryptand mixture (0.13 g). [222]crypt contamination was more than 30%.

^{1}H NMR (300 MHz, CD_2Cl_2): δ = 0.24 (s, 24H, SiCH_3), 3.96–4.01 (m, 8H, CH_2), 4.02–4.08 (m, 8H, CH_2), 6.91 ppm (m, 8H, CH_{AR}); ^{13}C{^{1}H} NMR (125 MHz, CD_2Cl_2): δ = 0.8 (s, SiCH_3), 63.5 (s, CH_2), 72.5 (s, CH_2), 116.7 (s, C_{AR}), 122.5 (s, C_{AR}), 150.5 ppm (s, C_{ARq}); ^{29}Si{^{1}H} NMR (60 MHz, CD_2Cl_2): δ = 11.5 ppm (s, *Si*CH_3). MS: HR-ESI(+) *m/z* (%): 625.2502 [M+H]$^+$ (100), 647.2320 [M+Na]$^+$ (100). IR: 2945 (w), 2869 (w), 1593 (w), 1501 (s), 1452 (m), 1396 (w), 1370 (w), 1328 (w), 1247 (s), 1221 (m), 1124 (s), 1098 (s), 1053 (s), 948 (m), 923 (m), 823 (m), 790 (s), 763 (vs.), 740 (s), 631 (m), 450 cm^{-1} (w).

Crystallography

Single-crystal X-ray diffraction experiments were carried out on a Bruker D8 Quest (**3a**, **5**), STOE IPDS2 (**1**·DCM, **6**), STOE IPDS2T (**2a**) or a STOE STADIVARI (**4a**) diffractometer, respectively. Measurements were performed at 100 K with MoKα (λ = 0.71073 Å) or CuKα (λ = 1.54184 Å) radiation, graphite monochromatization or respective X-ray optics. The structures were solved by direct methods and refinement with full-matrix-least-squares against F^2 using *SHELXT* and *SHELXL* on *OLEX2* platform.[45–47] The crystallographic data for all compounds is deposited in the Cambridge Crystallographic Data Centre (CCDC).[51] Due to severe disorder of solvent molecules in the crystal structure of **3a** and **6**, we applied the SQUEEZE operation. A selection of respective crystal data is given below.

Crystal data of 1·DCM: $C_{13}H_{34}Cl_2I_2MgO_4Si_4$, monoclinic, $P2_1$, Z = 2, 100(2) K, a = 8.173(3), b = 12.204(4), c = 14.204(8) Å; β = 93.02(4)°, V = 1414.8(11) Å^3, ρ = 1.680 g cm^{-3}, numerical absorption correction using STOE X-AREA and X-RED32.[48] μ = 2.618 mm^{-1}, T_{min}, T_{max} = 0.5303, 0.8053, 2Θ range 4.402–58.996°, reflections measured 21 645, independent reflections 7891 [R(int) = 0.0451, 244 parame-

 © 2019 The Authors. Published by Wiley-VCH Verlag GmbH & Co. KGaA, Weinheim

ters, R-index [$I \geq 2\sigma(I)$] 0.0244, wR_2 (all data) 0.0590, GoF 1.047, $\Delta\rho_{max}$, $\Delta\rho_{min}$ 1.27/−0.52 e Å^3.

Crystal data of 2a: $C_{14}H_{36}CaI_6O_5Si_4$, monoclinic, *C*2/*c*, $Z=4$, 100(2) K, $a=11.408(3)$, $b=12.970(2)$, $c=25.570$ Å; $\beta=92.38(2)^\circ$, $V=3484.7(16)$ Å^3, $\rho=2.284$ g cm^{-3}, spherical absorption correction using STOE X-AREA and LANA.[49] $\mu=5.654$ mm^{-1}, T_{min}, $T_{max}=0.1989$, 0.4381, 2Θ range 3.458–50.994°, reflections measured 13 999, independent reflections 3250 [R(int) = 0.0924], 154 parameters, R-index [$I \geq 2\sigma(I)$] 0.0548, wR_2 (all data) 0.1400, GoF 1.072, $\Delta\rho_{max}$, $\Delta\rho_{min}$ 1.56/−0.91 e Å^3.

Crystal data of 3a: $C_{16}H_{44}Ga_2I_8O_5Si_6Sr$, monoclinic, $P2_1/c$, $Z=4$, 100(2) K, $a=23.3580(16)$, $b=11.3585(7)$, $c=20.6920(14)$ Å; $\beta=111.998(4)^\circ$, $V=5090.2(6)$ Å^3, $\rho=2.254$ g cm^{-3}, spherical absorption correction using STOE X-AREA and LANA,[49] $\mu=7.110$ mm^{-1}, T_{min}, $T_{max}=0.4793$, 0.7452, 2Θ range 4.232–50.738°, reflections measured 171 072, independent reflections 9287 [R(int) = 0.1514], 355 parameters, R-index [$I \geq 2\sigma(I)$] 0.0675, wR_2 (all data) 0.1863, GoF 1.076, $\Delta\rho_{max}$, $\Delta\rho_{min}$ 4.17/−1.57 e Å^3.

Crystal data of 4a: $C_{16}H_{40}I_4O_6Si_4Sr$, monoclinic, $P2_1/c$, $Z=4$, 100(2) K, $a=12.0422(5)$, $b=22.2125(6)$, $c=12.8413(4)$ Å; $\beta=95.734(3)^\circ$, $V=3417.7(2)$ Å^3, $\rho=2.014$ g cm^{-3}, spherical absorption correction using STOE X-AREA and LANA,[49] $\mu=32.123$ mm^{-1}, T_{min}, $T_{max}=0.212$, 0.360, 2Θ range 7.378–50.994°, reflections measured 26 969, independent reflections 6337 [R(int) = 0.0854], 288 parameters, R-index [$I \geq 2\sigma(I)$] 0.0391, wR_2 (all data) 0.0894, GoF 0.804, $\Delta\rho_{max}$, $\Delta\rho_{min}$ 1.23/−1.51 e Å^3.

Crystal data of 5: $C_{20}H_{48}I_2O_8Si_4Sr$, triclinic, *P*-1, $Z=2$, 110(2) K, $a=8.4870(4)$, $b=14.9819(7)$, $c=15.4929(7)$ Å, $\alpha=105.457(2)^\circ$, $\beta=102.187(2)^\circ$, $\gamma=99.376(2)^\circ$, $V=1804.98(15)$ Å^3, $\rho=1.601$ g cm^{-3}, multiscan absorption correction using SADABS2016[50], $\mu=3.371$ mm^{-1}, T_{min}, $T_{max}=0.5094$, 0.8894, 2Θ range 4.642–57.786°, reflections measured 54 208, independent reflections 9456 [R(int) = 0.0442], 365 parameters, R-index [$I \geq 2\sigma(I)$] 0.0323, wR_2 (all data) 0.0540, GoF 1.034, $\Delta\rho_{max}$, $\Delta\rho_{min}$ 1.21/−0.80 e Å^3.

Crystal data of 6·1.5DCM: $C_{29.5}H_{51}Cl_3I_2O_8Si_4Sr$, triclinic, *P*-1, $Z=4$, 100(2) K, $a=11.9953(8)$ Å, $b=16.0514(12)$ Å, $c=24.936(2)$ Å, $\alpha=76.567(6)^\circ$, $\beta=85.494(6)^\circ$, $\gamma=86.477(6)^\circ$, $V=4650.7(6)$ Å^3, $\rho=1.562$ g cm^{-3}, numerical absorption correction using STOE X-AREA and X-RED32,[48] $\mu=2.801$ mm^{-1}, T_{min}, $T_{max}=0.5094$, 0.8894, 2Θ range 4.642–57.786°, reflections measured 52 818, refined as a two component twin, 901 parameters, R-index [$I \geq 2\sigma(I)$] 0.0780, wR_2 (all data) 0.2325, GoF 0.871, $\Delta\rho_{max}$, $\Delta\rho_{min}$ 2.32/−1.74 e Å^3.

Acknowledgements

This work was financially supported by the Deutsche Forschungsgemeinschaft (DFG). F.D. thanks MS (Dr. U. Linne and co-workers) and X-ray Departments (M. Marsch, R. Riedel, and Dr. K. Harms), Philipps-Universität, Marburg, for measurement time. In particular, R. Riedel is gratefully acknowledged for data collection of compound **5**. Also Dr. M. R. Buchner is gratefully acknowledged for his valuable help with NMR experiments.

Conflict of interest

The authors declare no conflict of interest.

Keywords: alkaline earth metals · cross-coupling · crown ethers · ligand design · Si–O bond activation

[1] R. Hoss, F. Vögtle, *Angew. Chem. Int. Ed. Engl.* **1994**, *33*, 375 – 384; *Angew. Chem.* **1994**, *106*, 389 – 398.
[2] M. C. Thompson, D. H. Busch, *J. Am. Chem. Soc.* **1964**, *86*, 213 – 217.
[3] C. J. Pedersen, *J. Am. Chem. Soc.* **1967**, *89*, 7017 – 7036.
[4] P. G. Jones, T. Gries, H. Grützmacher, H. W. Roesky, J. Schimkowiak, G. M. Sheldrick, *Angew. Chem. Int. Ed. Engl.* **1984**, *23*, 376; *Angew. Chem.* **1984**, *96*, 357.
[5] J. S. Ritch, T. Chivers, *Angew. Chem. Int. Ed.* **2007**, *46*, 4610 – 4613; *Angew. Chem.* **2007**, *119*, 4694 – 4697.
[6] M. R. Churchill, C. H. Lake, S.-H. L. Chao, O. T. Beachley, *J. Chem. Soc. Chem. Commun.* **1993**, *1*, 1577 – 1578.
[7] C. Eaborn, P. B. Hitchcock, K. Izod, J. D. Smith, *Angew. Chem. Int. Ed. Engl.* **1996**, *34*, 2679 – 2680; *Angew. Chem.* **1995**, *107*, 2936 – 2937.
[8] A. Decken, J. Passmore, X. Wang, *Angew. Chem. Int. Ed.* **2006**, *45*, 2773 – 2777; *Angew. Chem.* **2006**, *118*, 2839 – 2843.
[9] L.-C. Pop, M. Saito, *Coord. Chem. Rev.* **2016**, *314*, 64 – 70.
[10] I. Haiduc, *Organometallics* **2004**, *23*, 3 – 8.
[11] A. Decken, F. A. LeBlanc, J. Passmore, X. Wang, *Eur. J. Inorg. Chem.* **2006**, 4033 – 4036.
[12] I. Sänger, M. Gärtner, M. Bolte, M. Wagner, H.-W. Lerner, *Z. Anorg. Allg. Chem.* **2018**, *644*, 925 – 929.
[13] F. Dankert, C. Donsbach, C.-N. Mais, K. Reuter, C. von Hänisch, *Inorg. Chem.* **2018**, *57*, 351 – 359.
[14] F. Weinhold, R. West, *Organometallics* **2011**, *30*, 5815 – 5824.
[15] F. Weinhold, R. West, *J. Am. Chem. Soc.* **2013**, *135*, 5762 – 5767.
[16] R. J. Gillespie, E. A. Robinson, *Chem. Soc. Rev.* **2005**, *34*, 396.
[17] J. Passmore, J. M. Rautiainen, *Eur. J. Inorg. Chem.* **2012**, 6002 – 6010.
[18] T. S. Cameron, A. Decken, I. Krossing, J. Passmore, J. M. Rautiainen, X. Wang, X. Zeng, *Inorg. Chem.* **2013**, *52*, 3113 – 3126.
[19] S. Grabowsky, J. Beckmann, P. Luger, *Aust. J. Chem.* **2012**, *65*, 785.
[20] S. Grabowsky, M. F. Hesse, C. Paulmann, P. Luger, J. Beckmann, *Inorg. Chem.* **2009**, *48*, 4384 – 4393.
[21] M. Fugel, M. F. Hesse, R. Pal, J. Beckmann, D. Jayatilaka, M. J. Turner, A. Karton, P. Bultinck, G. S. Chandler, S. Grabowsky, *Chem. Eur. J.* **2018**, *24*, 15275 – 15286.
[22] K. Reuter, M. R. Buchner, G. Thiele, C. von Hänisch, *Inorg. Chem.* **2016**, *55*, 4441 – 4447.
[23] K. Reuter, G. Thiele, T. Hafner, F. Uhlig, C. von Hänisch, *Chem. Commun.* **2016**, *52*, 13265 – 13268.
[24] K. Reuter, F. Dankert, C. Donsbach, C. von Hänisch, *Inorganics* **2017**, *5*, 11.
[25] F. Dankert, K. Reuter, C. Donsbach, C. von Hänisch, *Inorganics* **2018**, *6*, 15.
[26] F. Dankert, K. Reuter, C. Donsbach, C. von Hänisch, *Dalton Trans.* **2017**, *46*, 8727 – 8735.
[27] F. Dankert, C. von Hänisch, *Inorg. Chem.* **2019**, *58*, 3518 – 3526.
[28] M. R. Buchner, M. Müller, F. Dankert, K. Reuter, C. von Hänisch, *Dalton Trans.* **2018**, *47*, 16393 – 16397.
[29] J. Pahl, H. Elsen, A. Friedrich, S. Harder, *Chem. Commun.* **2018**, *54*, 7846 – 7849.
[30] B. Freitag, P. Stegner, K. Thum, C. A. Fischer, S. Harder, *Eur. J. Inorg. Chem.* **2018**, 1938 – 1944.
[31] S. Harder, B. Freitag, P. Stegner, J. Pahl, D. Naglav, *Z. Anorg. Allg. Chem.* **2015**, *641*, 2129 – 2134.
[32] F. Dankert, F. Weigend, C. von Hänisch, *Inorg. Chem.* **2019**, DOI: 10.1021/acs.inorgchem.9b02519.
[33] F. Dankert, J. Heine, J. Rienmüller, C. von Hänisch, *CrystEngComm* **2018**, *20*, 5370 – 5376.
[34] K. Reuter, S. S. Rudel, M. R. Buchner, F. Kraus, C. von Hänisch, *Chem. Eur. J.* **2017**, *23*, 9607 – 9617.
[35] A. Boudin, G. Cerveau, C. Chutt, R. J. P. Corriu, C. Reye, *Tetrahedron* **1989**, *45*, 171 – 180.
[36] A. Boudin, G. Cerveau, C. Chuit, R. J. P. Corriu, C. Reye, *Angew. Chem. Int. Ed. Engl.* **1986**, *25*, 473 – 474; *Angew. Chem.* **1986**, *98*, 472 – 473.
[37] A. Boudin, G. Cerveau, C. Chuit, R. J. P. Corriu, C. Reye, *Bull. Chem. Soc. Jpn.* **1988**, *61*, 101 – 106.
[38] A. Boudin, G. Cerveau, C. Chuit, R. J. P. Corriu, C. Reye, *J. Organomet. Chem.* **1989**, *362*, 265 – 272.
[39] A. Boudin, G. Cerveau, C. Chuit, R. J. P. Corriu, C. Reye, *Organometallics* **1988**, *7*, 1165 – 1171.

 © 2019 The Authors. Published by Wiley-VCH Verlag GmbH & Co. KGaA, Weinheim

[40] N. R. Patel, C. B. Kelly, M. Jouffroy, G. A. Molander, *Org. Lett.* **2016**, *18*, 764 – 767.
[41] C. Lévêque, L. Chenneberg, V. Corcé, C. Ollivier, L. Fensterbank, *Chem. Commun.* **2016**, *52*, 9877 – 9880.
[42] C. Lévêque, L. Chenneberg, V. Corcé, J. P. Goddard, C. Ollivier, L. Fensterbank, *Org. Chem. Front.* **2016**, *3*, 462 – 465.
[43] J. P. Phelan, R. J. Wiles, S. B. Lang, C. B. Kelly, G. A. Molander, *Chem. Sci.* **2018**, *9*, 3215 – 3220.
[44] E. Levernier, V. Corcé, L. M. Rakotoarison, A. Smith, M. Zhang, S. Ognier, M. Tatoulian, C. Ollivier, L. Fensterbank, *Org. Chem. Front.* **2019**, *6*, 1378 – 1382.
[45] G. M. Sheldrick, *Acta Crystallogr. Sect. C* **2015**, *71*, 3 – 8.
[46] G. M. Sheldrick, *Acta Crystallogr. Sect. A* **2015**, *71*, 3 – 8.
[47] O. V. Dolomanov, L. J. Bourhis, R. J. Gildea, J. A. K. Howard, H. Puschmann, *J. Appl. Crystallogr.* **2009**, *42*, 339 – 341.
[48] X-AREA and X-RED32; Stoe & Cie: Darmstadt, Germany, **2009**.
[49] X-AREA and LANA; Stoe & Cie: Darmstadt, Germany, **2009**.
[50] SADABS; Bruker AXS Inc.: Madison, WI, **2016**.
[51] CCDC 1952843 (**1**·DCM), 1952841 (**2a**), 1952846 (**3a**), 1952844 (**4a**), 1952842 (**5**), and 1952845 (**6**·1.5 CH_2Cl_2) contain the supplementary crystallographic data for this paper. These data are provided free of charge by The Cambridge Crystallographic Data Centre.

Manuscript received: September 12, 2019
Accepted manuscript online: October 9, 2019
Version of record online: November 4, 2019

 © 2019 The Authors. Published by Wiley-VCH Verlag GmbH & Co. KGaA, Weinheim

Inorganic Chemistry
Article
Cite This: Inorg. Chem. 2019, 58, 15417−15422
pubs.acs.org/IC

Not Non-Coordinating at All: Coordination Compounds of the Cyclodimethylsiloxanes D_n (D = Me_2SiO; n = 6, 7) and Group 2 Metal Cations

Fabian Dankert,[†] Florian Weigend,[‡] and Carsten von Hänisch*,[†]

[†]Fachbereich Chemie and Wissenschaftliches Zentrum für Materialwissenschaften (WZMW), Philipps-Universität Marburg, 35032 Marburg, Germany

[‡]Institut für Nanotechnologie, Karlsruher Institut für Technologie, Hermann-von-Helmholtz-Platz 1, 76344 Leopoldshafen-Eggenstein, Germany

Supporting Information

ABSTRACT: We present the coordination chemistry of the cyclodimethylsiloxanes D_6 and D_7 toward alkaline earth metal salts. The coordination chemistry of these macrocycles toward alkaline earth metals has been unprecedented to date, and we could show that these ligands coordinate better than previously thought. Direct reaction of alkaline earth metal salts with these ligands yields stable complexes even with a relatively strongly coordinating iodide anion. A handful of counterintuitive coordination compounds could be characterized by single-crystal X-ray diffraction analysis. Quantum chemical calculations of suited Born−Haber cycles showed that these complexes are indeed stable, for Mg^{2+} and Ca^{2+} even with iodide employed as the anion and for Sr^{2+} and Ba^{2+} in the presence of GaI_3.

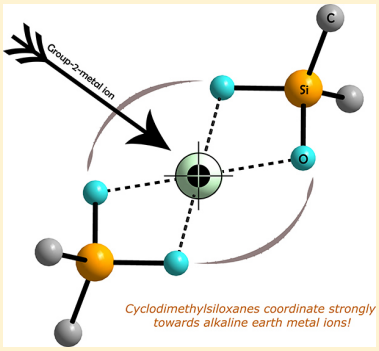

INTRODUCTION

More than ten years after the silicon analogues of crown ethers and cryptands were reviewed and presented as the prospect of a new chapter in host−guest chemistry,[1] the coordination chemistry of these systems is still at an early stage. There are still just a few examples where siloxane coordination chemistry could be established, and there are open questions in how far these types of ligands are capable to form stable complexes with metal centers. Since the discovery of the first metal complexes in the 1990s, complexes of common cyclosiloxanes were only obtained using highly reactive reagents or weakly coordinating anions. Quantum chemical calculations by Passmore and co-workers referring to a Born−Haber cycle (BHC) demonstrated that the complexation of alkali metal halides by cyclic silyl ethers is an overall positively enthalpic process.[2] The hitherto considered ions are Li^+, K^+, Zr^{4+}, and Ag^+ (Scheme 1).[2−9]

So far, fully silicon- and oxygen-based macrocycles have not been used as ligands for remaining s-block, d-block, or p-block elements. This is probably due to their unusual weak Lewis basicity, which is explained by negative hyperconjugation interactions of the type $p(O) \rightarrow \sigma^*(Si{-}C)$[2,10−12] and more recently also by metal$^+\cdots Si^{\delta+}$ electrostatic repulsion.[7,12] Lately, we demonstrated that the reduced complexation ability is also the result of a different architecture of crown ethers.[13−15] Whereas cyclosiloxanes are constituted of monosilanes ($-SiMe_2-$), organic crown ethers exhibit ethylene bridges ($-CH_2CH_2-$) between the oxygen atoms. Thus, the insertion of disilanes ($-SiMe_2SiMe_2-$) leads to minimization of the electrostatic repulsion between the cation and the positively polarized Si atom by a large enough bite angle.

Hybrid disila-crown ethers are able to form stable complexes with alkali and alkaline earth metal salts even with halides.[13,14,16−18] The coordination ability of this type of crown ether is on even terms, which was confirmed by means of NMR spectroscopy and quantum chemical calculations.[13,14,18] The nature of the cation, however, is also an important parameter to our understanding of the Si−O bond in relation to the metal silyl ether attraction. Yet, though few research activities have been performed, the latest results indicate that silyl ether bonding toward metal centers is most effective for group 2 ions.[18,20−24] Overall negative hyperconjugation interactions are easily overcompensated using a hard group 2 cation for complexation.[18] Most recently, this was demonstrated by Harder and co-workers. Silyl ether coordination of hexamethyldisiloxane toward Mg^{2+} was established, and the synthesis and structure of the magnesium complex $[Mg(BDI)\{O(SiMe_3)_2\}]^+$ (BDI = $CH[C(CH_3)N\text{-}Dipp]_2$ with Dipp = 2,6-diisopropylphenyl) was introduced.[21] Unfortunately, fully Si-substituted crown ethers with a disilane backbone are synthetically not yet available. We therefore started investigating the commercially available cyclosiloxanes for the coordination ability toward hard group 2 ions.

Received: August 20, 2019
Published: October 29, 2019

Downloaded via UNIV OF MARBURG on April 3, 2020 at 13:17:18 (UTC).
See https://pubs.acs.org/sharingguidelines for options on how to legitimately share published articles.

© 2019 American Chemical Society

DOI: 10.1021/acs.inorgchem.9b02519
Inorg. Chem. 2019, 58, 15417−15422

Scheme 1. Characterized Metal Complexes of Cyclosiloxanes and Hybrid Disila-Crown-Ether Analogues[a]

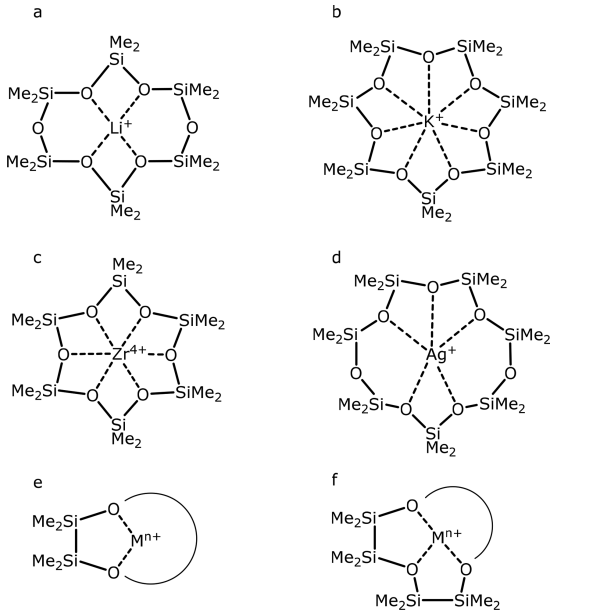

[a](a)[2] Binding of D_6 towards Li^+; observed with $[Al(OR_F)_4]^-$ anions (R_F = $C(CF_3)_3$, $C(CF_3)_2Ph$). (b)[3−5] Binding of D_7 towards K^+; observed in $[K]_3[InHCH_2CMe_3)_3]_4[K(D_7)]$, $K[C(SiMe_3)_2(SiMe_2(CH{=}CH_2))][K(D_7)]$, or more recently also in $[K(D_7)][(^tBu_3Si)_2MeSi\text{-}Na\text{-}SiMe(Si^tBu_3)_2]$. (c)[6] Silyl ether bonding towards Zr^{4+} was observed in $[Zr(D_6)Br_2][Zr_2Br_9]_2$. (d)[7,8] The $[Ag(D_7)]^+$ cation was characterized as the salt of $[SbF_6]^-$, and with $[Ag(D_6)][Al(OR_F)_4]$ and $[Ag(D_6)][AlF(OR_F)_3]$ (R_F = $C(CF_3)_3$) there are also complexes of D_6 characterized. (e, f)[13−19] Binding modes of hybrid disila-crown ethers. Stable complexes of the alkali metal ions Li^+, Na^+, and K^+, the alkaline earth metal cations Mg^{2+}, Ca^{2+}, Sr^{2+}, and Ba^{2+}, and the NH_4^+ cation, as well as different anions including halides, could be isolated. Curves represent different organic spacers.

RESULTS AND DISCUSSION

In starting to investigate the coordination behavior of D_6 and D_7 toward alkaline earth metal salts, we straight forwardly converted the cyclic siloxanes with a respective alkaline earth metal iodide in *α,α,α*-trifluorotoluene. Counterintuitively, the reaction of the cyclosiloxane D_6 with MgI_2 directly yields the corresponding coordination compound $[Mg(D_6)I_2]$ (**1**) without the necessity of a WCA (WCA = weakly coordinating anion) (Scheme 2). A few single crystals of $[Mg_2(D_6)_2\{Mg_2I_6\}I_2]$ (**2**) could also be obtained by varying the crystallization procedures (see the Supporting Information). As a result of the diagonal relationship to lithium, the coordination mode of Mg^{2+} in **1** is similar to that of the $[Li(D_6)]^+$ cation.[2] The Mg^{2+} cation is octahedrally coordinated with O_{Si}−Mg bond lengths of 212.7(1) and 212.8(1) pm. The oxygen atoms O3 and O3# do not show interactions with the central ion in the solid state (O···Mg distances of 315.1(1) pm). By means of NMR spectroscopy in solution, only one signal is observed for all $SiMe_2$ groups. Even cooling of the solution to 190 K did not cause a split of signals. Thus, rapid exchange results in the described equivalency of the Si atoms. The ^{29}Si NMR chemical shift in deuterated dichloromethane, an important parameter regarding siloxane coordination chemistry,[25] is with a δ = −4.8 ppm very distinct (δ_{D6} = −22.2 ppm). Significant downfield shift indicates a strong interaction of the siloxane with Mg^{2+} in solution. The Si−O−Si angles, another important parameter regarding siloxane basicity,[26−28] are comparatively small for those angles bearing a coordinating oxygen atom ($\angle_{coord.}$ = 142.4(1)° and 142.1(1)°). Si−O−Si angles with a non-coordinating oxygen atom exhibit significantly larger values ($\angle_{non\text{-}coord.}$ = 161.2(1)°). As a cause of the coordination, the ring is fully planar with transannular angles of 180.00°. It is notable that the two iodide anions are also coordinating the central ion with an I−Mg distance of 287.4(1) pm. Anion−metal interactions were described to be very unfavorable in terms of complex formation with cyclosiloxanes. This was meticulously described via calculation of BHCs in previous works.[2] Thus, the coordination of simple cyclosiloxanes toward alkaline earth metal ions is significantly different than to that of alkali metals. Siloxane coordination is better than previously thought as salts characterized by a high lattice energy can be complexed. Attempts at coordinating these ligands with metal halides is obviously not doomed to fail, which was concluded in previous works.[1,2] As a salt including a relatively strong coordinating anion was successfully complexed, the impact of negative hyperconjugation interactions is of minor importance for the early group 2 metal ions in combination with cyclosiloxane bonding.

Thus, the larger calcium ion could also be incorporated into the fully silicon-based macrocycle D_7 by direct reaction with CaI_2. In this compound the Ca^{2+} ion (r_i $[Ca^{2+}]_{CN7}$ = 106 pm[29]) represents the same coordination mode which was also observed for the silver complex $[Ag(D_7)][SbF_6]$.[8] In the solid state only five of the overall seven O atoms participate in the coordination of Ca^{2+}, and the Si−$O_{coord.}$ angles vary from 132.8(1)° to 152.0(1)°. Thus, the ligand cannot provide a matching geometry where preferably small Si−O−Si angles can be established. In the CaI_2 complex of the hybrid disila-crown ether 1,2,4,5-tetrasila[15]crown-5, an Si−$O_{coord.}$−Si angle of 125.9(1)° is established, indicating that oxygen atoms bind more effectively toward Ca^{2+}.[25] However, D_7 still manages to incorporate CaI_2 in the macrocycle with a ligand behavior that is similar to that of D_6 in **1**. The $p(O) \rightarrow \sigma^*(Si\text{−}C)$ negative hyperconjugation interactions are present in both compounds. For example, in **3** the Si−O average distances are found to be larger in the Si−$O_{coord.}$ bonds in comparison to the Si−$O_{non\text{-}coord.}$ bonds (164.3(3)−166.7(3) pm vs 161.2(3)−162.5(2) pm). The $^{29}Si\{^1H\}$ NMR chemical shift in deuterated dichloromethane is less distinct but still shows, with δ = −7.8 ppm, a remarkable downfield shift. Moving on to the next heavier alkaline earth metal, the attempt to incorporate SrI_2 into the macrocycle D_7 is difficult. Therefore, long reaction times are necessary and the compound $[Sr(D_7)I_2]$ (**4**) can only be obtained as a greasy residue which is contaminated with free ligand D_7. **4** cannot be isolated in a significant yield, which is the reason why the characterization of the compound is restricted to NMR spectroscopy. For this purpose, the reaction was once carried out in deuterated dichloromethane, and the reaction mixture was filtered directly into a J. Young NMR tube. The filtrate gives two resonance signals in the ^{29}Si NMR spectrum. The one referring to the free ligand D_7 is observed at δ = −22.2 ppm. One smaller signal is observed at δ = −9.2 ppm, which can be assigned to **4** due to downfield shift. Conversion of in situ generated compound **4** with two equivalents of GaI_3, however, significantly increases the solubility, and the compound could be fully characterized.

DOI: 10.1021/acs.inorgchem.9b02519
Inorg. Chem. 2019, 58, 15417−15422

Scheme 2. Synthesis of Compounds 1 and 3, including the Respective Molecular Structures in the Crystal[a]

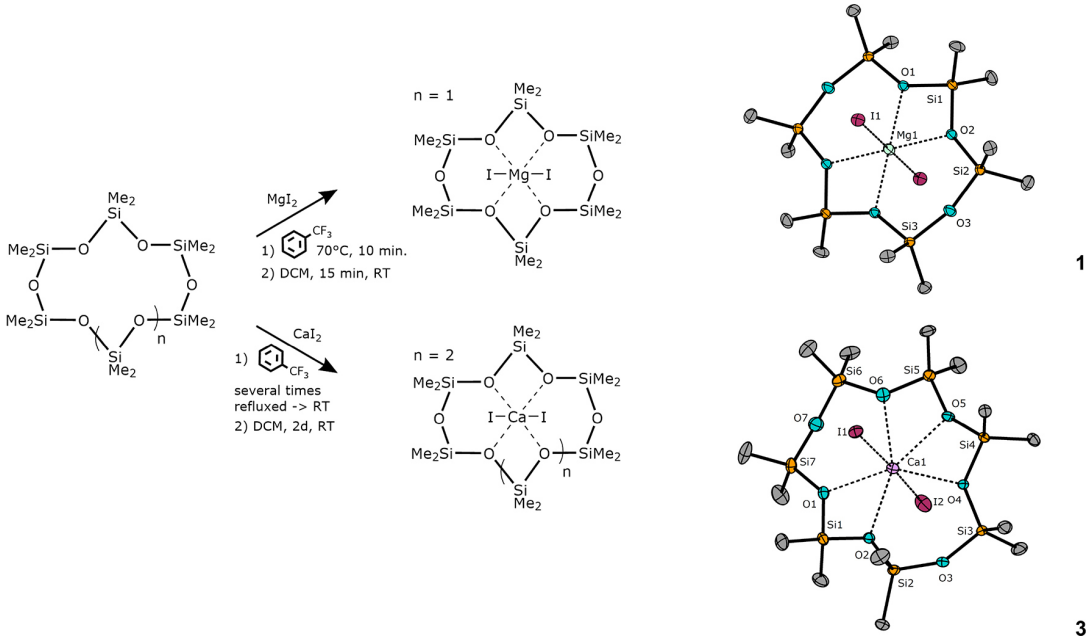

[a]Thermal displacement ellipsoids are drawn at the 50% probability level. For selected interatomic distances and angles, see the Supporting Information.

After workup, $[Sr(D_7)][GaI_4]_2$ (**4a**) can be obtained as a colorless powder. There might now be a weakly coordinating anion involved, but it is still remarkable that there is no need of a bulky, perfluorinated alkoxymetallate such as those reviewed earlier.[1] The compound can be crystallized from DCM solution and subsequent cooling to −24 °C for several days. Severe disorder of the $[GaI_4]^-$ anions, as well as the siloxane, causes problems with the crystal structure refinement. No suitable disorder model could be established and the refinement did not converge to an acceptable *R*-value, so no reliable refinement is obtained. To prevent disorder we recrystallized the compound several times to then obtain colorless needles.

After the XRD experiment, it could be shown that $[Sr(D_7)\{GaI_4\}(H_2O)][GaI_4]$ (**4b**) was formed, including an additional water molecule in the coordination sphere of the cation (Scheme 3). The refinement did now converge to acceptable *R*-values. Obviously, traces of moisture do not immediately replace the siloxane ligand, which further illustrates the effectiveness of siloxane bonding toward group 2 metal ions. The D_7 ligand is still too large for the Sr^{2+} cation (r_i $[Sr^{2+}]_{CN9}$ = 131 pm[29]) as it is placed to one side of the siloxane moiety ($Sr-O_{coord.}$ = 264.6(4)−283.6(4) pm vs $Sr\cdots O_{non\text{-}coord.}$ = 356.3(4) pm). All oxygen atoms of D_7 could be activated for coordination as the even larger barium cation was incorporated. This was possible by direct reaction of D_7 with one equivalent of BaI_2 and two equivalents of GaI_3. Conversion of exclusively BaI_2 did not result in any kind of complex formation as we did not observe an NMR chemical shift or a suitable *m*/*z* relation in ESI^+ and $LIFDI^+$ MS spectrometry. Conversion of BaI_2 into the $[GaI_4]^-$ salt in the presence of D_7 yields a colorless powder which could then be characterized by X-ray diffraction and turned out to be $[Ba(D_7)][GaI_4]_2$ (**5**). Similar to the potassium cation, barium fits very well with the cavity of D_7, which is closely related to almost identical ionic radii (r_i $[K^+]_{CN9}$ = 155 pm and r_i $[Ba^{2+}]_{CN10}$ = 152 pm[29]). The disorder problematic in the crystal structure of $[Ba(D_7)][GaI_4]_2$ is the same as in **4**. Thus, we crystallized the compound open to air to afford block-shaped single crystals of the composition $[Ba(D_7)\{GaI_4\}(H_2O)_{0.94}\{GaI_4\}_{0.06}][GaI_4]_{0.94}$ (**5a**). The central ion is also saturated by a water molecule, and $[GaI_4]^-$ rather than siloxane replacement occurs.

At this point we could demonstrate that the commercially available cyclosiloxanes can be effectively used as ligands for group 2 metal cations and prepared compounds that are clearly counterintuitive. It is not impossible to obtain stable complexes with relatively strong coordinating anions according to what was concluded in past works. Quantum chemical treatments were carried out in order to find out why the reactions yield crystalline MD_nI_2 for M = Mg, Ca, but not for M = Sr, Ba, and to clarify how matters change when GaI_3 and additional water molecules are present. For this, the energies, *E*, for the reactions from liquid D_n and solid MI_2 to solid MD_nI_2 were estimated by calculation of BHCs as suggested by Passmore,[2] see Figure 1, bottom. The structures of all involved compounds were calculated for the gas phase at the level B3LYP[30]/dhf-TZVP.[31] Energies E_1 and E_4 were estimated from the molecular volume as proposed by Jenkins[32] and Preiss.[33] E_2 is from an empirical formula,[34] and the energy E_3 of the gas phase reaction was calculated from the energy differences of products and reactants, which finally yields the energy E_{BHC} from energy conservation. For details see the Supporting Information. E_{BHC}, as well as E_1-E_4, are shown in Figure 1, and respective numbers are listed in the Supporting Information together with the Cartesian coordinates for all compounds.

For M^{2+} = Mg^{2+}, Ca^{2+}, E_{BHC} is negative, see Figure 1, and thus reactions from liquid D_n and solid MI_2 to solid MD_nI_2 are exothermal; for M^{2+} = Ba^{2+}, E_{BHC} is positive and for Sr^{2+} is close to zero, which is in line with the above mentioned

DOI: 10.1021/acs.inorgchem.9b02519
Inorg. Chem. 2019, 58, 15417−15422

Scheme 3. Synthesis Path of Heavy Alkaline Earth Metal Complexes with D_7 and Molecular Structures of the Aqua Complexes 4b and 5a in the Crystal[a]

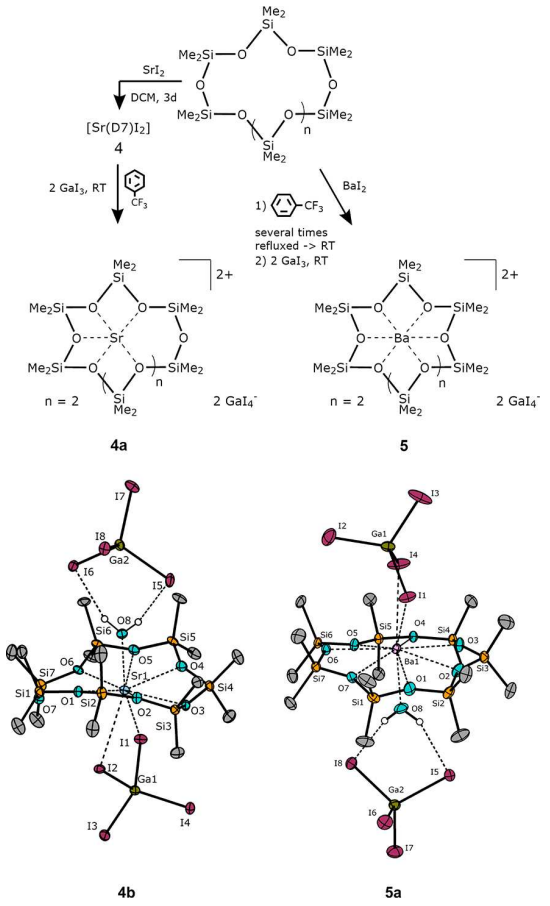

[a]Thermal displacement ellipsoids are drawn at the 50% probability level. For selected interatomic distances and angles, see the Supporting Information.

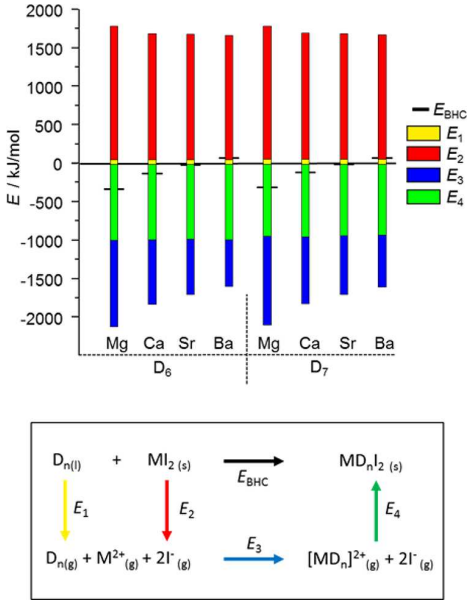

Figure 1. BHC (bottom) for the calculation of the reaction energy, E_{BHC} (bars, top), as well as individual contributions (columns, top) for M = Mg, Ca, Sr, Ba and n = 6, 7. E_{BHC} for M = Mg/Ca/Sr/Ba amounts to −328/−125/−10/+87 kJ/mol for n = 6 and to −313/−109/−3/+79 kJ/mol for n = 7, respectively.

experimental findings. The reason for this trend is mainly the strongly decreasing energy gain E_3 of the gas phase reaction yielding $[MD_n]^{2+}$ from Mg^{2+} to Ba^{2+}, whereas the other energy contributions depend much less on the choice of M. Next, we estimate the role of GaI_3 within the BHC. The simplest way for this is the consequent replacement of I^- by GaI_4^- in the BHC. This reduces E_2 by 516−548 kJ/mol (depending on the choice of the parameters for obtaining the energy from the volume, see Table S6) and E_4 by ca. 93−114 kJ/mol (see Table S6), which leads to an overall energy gain of ca. 400 kJ/mol in E_{BHC}. According to these considerations, the formation of even $BaD_n(GaI_4)_2$ is exothermal by more than 300 kJ/mol. Alternatively, and maybe somewhat closer to the experimental conditions, the process could be considered as follows. One keeps the original reactants, D_n and MI_2, but adds GaI_3. Then, in addition to D_n and MI_2, GaI_3 also needs to be vaporized, which requires ca. 60 kJ/mol.[35] The gas phase reaction $I^- + GaI_3 \rightarrow GaI_4^-$ is exothermal by 197 kJ/mol, and the change in the absolute value of E_4 when replacing I^- with GaI_4^- is the same as above, ca. 100 kJ/mol. E_{BHC} thus is lowered by $2 \times 197 - 60 - 100 \approx 240$ kJ/mol. For Ba^{2+}, this yields ca. 160 kJ/mol for E_{BHC}. This is less than the value obtained above, but again the formation of $MD_n(GaI_4)_2$ is shown to be clearly exothermal also for Ba^{2+} and Sr^{2+}. The presence of water is considered analogously. Vaporization requires ca. 40 kJ/mol.[36] The gas phase reaction $(MD_n)^{2+} + H_2O \rightarrow (MD_n{\cdot}H_2O)^{2+}$ is exothermal by 84 kJ/mol. The changes in E_4 are negligible (ca. 5 kJ/mol, see Table S4), so E_{BHC} is lowered by a further ca. 40 kJ/mol. Finally, we estimate the temperature dependence of E by calculating thermal corrections for E_3 from energies at 0 K to free enthalpies at 300 K obtained from partition sums within the standard harmonic oscillator approximation[37] with unscaled frequencies. These corrections are small compared to the effects of the presence of GaI_3 and H_2O; they only slightly lower the energy gain in E_3 and, thus, E_{BHC} by 6 kJ/mol ($M^{2+} = Ba^{2+}$, n = 6, 7) to 9 kJ/mol ($M^{2+} = Mg^{2+}$, n = 6, 7). To summarize, the calculation of E_{BHC} indicates that for X = I^- the formation of complexes is favorable for Mg^{2+} and Ca^{2+}, but not for Sr^{2+} ($E_{BHC} \approx 0$) and Ba^{2+} ($E_{BHC} \approx 80$ kJ/mol). Exchange of I^- with GaI_4^- makes the formation of complexes much more favorable, which means stability also for the complexes of Sr^{2+} and Ba^{2+}. A further (less pronounced) increase of stability is due to the presence of water. Temperature effects on the enthalpy are negligible.

CONCLUSIONS

The coordination chemistry of the cyclodimethylsiloxanes D_6 and D_7 has been reported. Counterintuitively, we have shown that it is very possible to obtain stable complexes even with a relatively strong coordinating iodide anion. $[Mg(D_6)I_2]$ (**1**) and $[Ca(D_7)I_2]$ (**3**) could be fully characterized, and it was shown by means of SC-XRD as well as $^{29}Si\{^1H\}$ NMR spectroscopy that silyl ether coordination is present in the solid state and in solution. Cumbersomely, $[Sr(D_7)I_2]$ (**4**) was characterized by NMR spectroscopy and reveals a crossover point which demonstrates how far silyl ether coordination is possible on an experimental level when employing the iodide anion. A respective barium iodide complex could not be

DOI: 10.1021/acs.inorgchem.9b02519
Inorg. Chem. 2019, 58, 15417−15422

observed by any characterization method. Using GaI_3 as an abstractor for I^-, we were also able to obtain single-crystal structures of D_7 and Sr^{2+} and Ba^{2+}. The respective complexes $[M(D_7)][GaI_4]_2$ (M = Sr (**4a**) and M = Ba (**5**)) were characterized, i.e., $[Sr(D_7)\{GaI_4\}(H_2O)][GaI_4]$ (**4b**) and $[Ba(D_7)\{GaI_4\}(H_2O)_{0.94}\{GaI_4\}_{0.06}][GaI_4]_{0.94}$ (**5a**), crystallographically. This lets us conclude that early alkaline earth metal ions share strong interactions with cyclosiloxanes even without a WCA. Heavier alkaline earth metals might need the formation of GaI_4^- as the WCA, but still, no perfluorinated, bulky WCA is necessary, which was often assumed in past works. These experimentally based conclusions were supported by means of quantum chemical calculations referring suitable BHCs, where the gas phase reactions of MI_2 (M = Mg, Ca) with D_6 and D_7 turned out to be exothermal, the conversion of SrI_2 close to zero, and BaI_2 clearly endothermal. The exchange of I^- with GaI_4^- makes the formation of the complexes much more favorable, which means that also the complexes of Sr^{2+} and Ba^{2+} are stable.

Overall, this work highly challenges the general assumption of sila-crowns as weakly coordinating ligands. The question of how far sila-crowns with a disilane backbone can challenge the ligands presented herein is still matter of ongoing research, so further studies are underway. Fundamental research in the field of silyl−ether coordination, however, is crucially improved upon, and in our eyes, neutral silicon-based ligands have a high potential in main-group coordination chemistry. Earlier considerations of these systems as weakly coordination ligands should be dropped.

■ ASSOCIATED CONTENT

Supporting Information

The Supporting Information is available free of charge on the ACS Publications website at DOI: 10.1021/acs.inorgchem.9b02519.

Synthesis and crystallization, single-crystal X-ray diffraction analysis, and quantum chemical calculations sections containing experimental, crystallographic, and theoretical details (PDF)

Accession Codes

CCDC 1921174−1921178 contain the supplementary crystallographic data for this paper. These data can be obtained free of charge via www.ccdc.cam.ac.uk/data_request/cif, or by emailing data_request@ccdc.cam.ac.uk, or by contacting The Cambridge Crystallographic Data Centre, 12 Union Road, Cambridge CB2 1EZ, UK; fax: +44 1223 336033.

■ AUTHOR INFORMATION

Corresponding Author

*E-mail: haenisch@chemie.uni-marburg.de.

ORCID

Fabian Dankert: 0000-0002-6806-4794

Florian Weigend: 0000-0001-5060-1689

Carsten von Hänisch: 0000-0002-6298-8937

Author Contributions

The manuscript was written through contributions of all authors. All authors have given approval to the final version of the manuscript.

Funding

This work was financially supported by the Deutsche Forschungsgemeinschaft (DFG).

Notes

The authors declare no competing financial interest.

■ ACKNOWLEDGMENTS

M. Köster is acknowledged for fruitful discussion in the laboratory. F.D. thanks the Mass Spectrometry (especially J. Bamberger) and X-ray Departments (M. Marsch, R. Riedel, and Dr. K. Harms), Philipps-Universität, Marburg, for measurement time and their kind advice.

■ REFERENCES

(1) Ritch, J. S.; Chivers, T. Silicon analogues of crown ethers and cryptands: A new chapter in host-guest chemistry? *Angew. Chem., Int. Ed.* **2007**, *46*, 4610−4613. Ritch, J. S.; Chivers, T. *Angew. Chem.* **2007**, *119*, 4694−4697.

(2) Decken, A.; Passmore, J.; Wang, X. Cyclic Dimethylsiloxanes as Pseudo Crown Ethers: Syntheses and Characterization of $Li(Me_2SiO)_5[Al\{OC(CF_3)_3\}_4]$, $Li(Me_2SiO)_6[Al\{OC(CF_3)_3\}_4]$, and $Li(Me_2SiO)_6[Al\{OC(CF_3)_2Ph\}_4]$. *Angew. Chem.* **2006**, *118*, 2839−2843; *Angew. Chem., Int. Ed.* **2006**, *45*, 2773−2777.

(3) Churchill, M. R.; Lake, C. H.; Chao, S.-H. L.; Beachley, O. T. Silicon Grease as a Precursor to a Pseudo Crown Ether Ligand: Crystal Structure of $[K^+]_3[K(Me_2SiO)_7^+][InH(CH_2CMe_3)_3^-]_4$. *J. Chem. Soc., Chem. Commun.* **1993**, *1*, 1577−1578.

(4) Eaborn, C.; Hitchcock, P. B.; Izod, K.; Smith, J. D. Two Diorganopotassates: Crystal Structure of $[K(C_6H_6)][K\{C(SiMe_3)_2(SiMe_2Ph)\}_2]$. *Angew. Chem., Int. Ed. Engl.* **1996**, *34*, 2679−2680; *Angew. Chem.* **1995**, *107*, 2936−2937.

(5) Sänger, I.; Gärtner, M.; Bolte, M.; Wagner, M.; Lerner, H.-W New Aspects with Regard to Silanide Chemistry in Particular Formation and Structure of the First Disilyl Sodate $[K(Me_2SiO)_7][(^tBu_3Si)_2MeSi\text{-}Na\text{-}SiMe(^tBu_3Si)_2]$. *Z. Anorg. Allg. Chem.* **2018**, *644*, 925−929.

(6) Ernst, R. D.; Glöckner, A.; Arif, A. M. Crystal structure of hexakis(dimethyl-μ-oxosilane)dibromozirconium(IV) bis(nonabromodizirconate(IV)), $[Zr\{(CH_3)_2SiO\}_6Br_2][Zr_2Br_9]_2$. *Z. Kristallogr. - New Cryst. Struct.* **2007**, *222*, 333−334.

(7) Cameron, T. S.; Decken, A.; Krossing, I.; Passmore, J.; Rautiainen, J. M.; Wang, X.; Zeng, X. Reactions of a Cyclodimethylsiloxane $(Me_2SiO)_6$ with Silver Salts of Weakly Coordinating Anions; Crystal Structures of $[Ag(Me_2SiO)_6][Al]$ ([Al] = $[Fal\{OC(CF_3)_3\}_3]$, $[Al\{OC(CF_3)_3\}_4]$) and Their Comparison with $[Ag(18\text{-Crown-}6)]_2[SbF_6]_2$. *Inorg. Chem.* **2013**, *52*, 3113−3126.

(8) Decken, A.; LeBlanc, F. A.; Passmore, J.; Wang, X. Cyclodimethylsiloxane $(Me_2SiO)_m$ (m = 3−6) Ring Transformations on Reactions with $AgSbF_6$; Crystal Structure of $Ag(Me_2SiO)_7SbF_6$. *Eur. J. Inorg. Chem.* **2006**, *2006*, 4033−4036.

(9) von Hänisch, C.; Hampe, O.; Weigend, F.; Stahl, S. Stepwise Synthesis and Coordination Compound of an Inorganic Cryptand. *Angew. Chem., Int. Ed.* **2007**, *46*, 4775−4779. Stahl, S. Ein anorganischer Cryptand: schrittweise Synthese und Koordination von Li+-Ionen. *Angew. Chem.* **2007**, *119*, 4859−4863.

(10) Weinhold, F.; West, R. Hyperconjugative Interactions in Permethylated Siloxanes and Ethers: The Nature of the SiO Bond. *J. Am. Chem. Soc.* **2013**, *135*, 5762−5767.

(11) Weinhold, F.; West, R. The nature of the silicon-oxygen bond. *Organometallics* **2011**, *30*, 5815−5824.

(12) Passmore, J.; Rautiainen, J. M. On The Lower Lewis Basicity of Siloxanes Compared to Ethers. *Eur. J. Inorg. Chem.* **2012**, *2012*, 6002−6010.

(13) Reuter, K.; Buchner, M. R.; Thiele, G.; von Hänisch, C. Stable Alkali-Metal Complexes of hybrid Disila-Crown Ethers. *Inorg. Chem.* **2016**, *55*, 4441−4447.

(14) Reuter, K.; Thiele, G.; Hafner, T.; Uhlig, F.; von Hänisch, C. Synthesis and coordination ability of a partially silicon based crown ether. *Chem. Commun.* **2016**, *52*, 13265−13268.

DOI: 10.1021/acs.inorgchem.9b02519
Inorg. Chem. 2019, 58, 15417−15422

(15) Dankert, F.; Reuter, K.; Donsbach, C.; von Hänisch, C. A structural study of alkaline earth metal complexes with hybrid disila-crown ethers. *Dalton Trans.* **2017**, *46*, 8727−8735.
(16) Reuter, K.; Dankert, F.; Donsbach, C.; von Hänisch, C. Structural Study of Mismatched Disila-Crown Ether Complexes. *Inorganics* **2017**, *5*, 11.
(17) Reuter, K.; Rudel, S. S.; Buchner, M. R.; Kraus, F.; von Hänisch, C. Crown ether complexes of alkali metal chlorides from SO_2. *Chem. - Eur. J.* **2017**, *23*, 9607−9617.
(18) Dankert, F.; Donsbach, C.; Mais, C.-N.; Reuter, K.; von Hänisch, C. Alkali and Alkaline Earth Metal Derivatives of Disila-Bridged Podands: Coordination Chemistry and Structural Diversity. *Inorg. Chem.* **2018**, *57*, 351−359.
(19) Dankert, F.; Reuter, K.; Donsbach, C.; von Hänisch, C. Hybrid Disila-Crown Ethers as Hosts for Ammonium Cations: The O−Si−Si−O Linkage as an Acceptor for Hydrogen Bonding. *Inorganics* **2018**, *6*, 15.
(20) Buchner, M. R.; Müller, M.; Dankert, F.; Reuter, K.; von Hänisch, C. The coordination behaviour and reactivity of partially silicon based crown ethers towards beryllium chloride. *Dalton Trans.* **2018**, *47*, 16393−16397.
(21) Pahl, J.; Elsen, H.; Friedrich, A.; Harder, S. Unsupported metal silyl ether coordination. *Chem. Commun.* **2018**, *54*, 7846−7849.
(22) Freitag, B.; Stegner, P.; Thum, K.; Fischer, C. A.; Harder, S. Tetranuclear Strontium and Barium Siloxide/Amide Clusters in Metal-Ligand Cooperative Catalysis. *Eur. J. Inorg. Chem.* **2018**, *2018*, 1938−1944.
(23) Harder, S.; Freitag, B.; Stegner, P.; Pahl, J.; Naglav, D. Strontium Chemistry with Silicone Grease. *Z. Anorg. Allg. Chem.* **2015**, *641*, 2129−2134.
(24) Martín-Fernández, C.; Montero-Campillo, M. M.; Alkorta, I.; Elguero, J. Weak interactions and cooperativity effects on disiloxane: a look at the building block of silicones. *Mol. Phys.* **2018**, *116*, 1539−1550.
(25) Dankert, F.; von Hänisch, C. Insights into the Coordination Ability of Siloxanes Employing Partially Silicon Based Crown Ethers: A Comparative Analysis of s-Block Metal Complexes. *Inorg. Chem.* **2019**, *58*, 3518−3526.
(26) Grabowsky, S.; Hesse, M. F.; Paulmann, C.; Luger, P.; Beckmann, J. How to Make the Ionic Si-O Bond More Covalent and the Si-O-Si Linkage a Better Acceptor for Hydrogen Bonding. *Inorg. Chem.* **2009**, *48*, 4384−4393.
(27) Grabowsky, S.; Beckmann, J.; Luger, P. The Nature of Hydrogen Bonding Involving the Siloxane Group. *Aust. J. Chem.* **2012**, *65*, 785.
(28) Fugel, M.; Hesse, M. F.; Pal, R.; Beckmann, J.; Jayatilaka, D.; Turner, M. J.; Karton, A.; Bultinck, P.; Chandler, G. S.; Grabowsky, S. Covalency and Ionicity Do Not Oppose Each Other-Relationship Between Si−O Bond Character and Basicity of Siloxanes. *Chem. - Eur. J.* **2018**, *24*, 15275−15286.
(29) Shannon, R. Revised Effective Ionic Radii and Systematic Studies of Interatomic distances in Halides and Chalcogenides. *Acta Crystallogr., Sect. A: Cryst. Phys., Diffr., Theor. Gen. Crystallogr.* **1976**, *A32*, 751−767.
(30) Lee, C.; Yang, W.; Parr, R. G. Development of the Colle-Salvetti correlation-energy formula into a functional of the electron density. *Phys. Rev. B: Condens. Matter Mater. Phys.* **1988**, *37*, 785−789.
(31) Weigend, F.; Baldes, A. Segmented contracted basis sets for one- and two-component Dirac−Fock effective core potentials. *J. Chem. Phys.* **2010**, *133*, 174102.
(32) Jenkins, H. D. B.; Roobottom, H. K.; Passmore, J.; Glasser, L. Relationships among Ionic Lattice Energies, Molecular (Formula Unit) Volumes, and Thermochemical Radii. *Inorg. Chem.* **1999**, *38*, 3609−3620.
(33) Preiss, U.; Slattery, J. M.; Krossing, I. In Silico Prediction of Molecular Volumes, Heat Capacities, and Temperature-Dependent Densities of Ionic Liquids. *Ind. Eng. Chem. Res.* **2009**, *48*, 2290−2296.
(34) Wilcock, D. F. Vapor Pressure-Viscosity Relations in Methylpolysiloxanes. *J. Am. Chem. Soc.* **1946**, *68*, 691−696.
(35) Stølevik, R.; Eriksson, L.; Werner, P.-E.; Westdahl, M.; Lucanska, B.; Krätsmar-Smogrovic, J.; Valent, A.; Alminger, T.; Erickson, M.; Grundevik, I.; Hagin, I.; Hoffman, K.-J.; Johansson, S.; Larsson, S.; Löfberg, I.; Ohlson, K.; Persson, B.; Skånberg, I.; Tekenbergs-Hjelte, L. Prediction of Entropy of Vaporization Based on Correlation with the Normal Boiling Point. *Acta Chem. Scand.* **1989**, *43*, 860−867.
(36) McCullough, J. P.; Pennington, R. E.; Waddington, G. A Calorimetric Determination of the Vapor Heat Capacity and Gas Imperfection of Water. *J. Am. Chem. Soc.* **1952**, *74*, 4439−4442.
(37) McQuarrie, D. A.; Simon, J. D. *Molecular Thermodynamics*; University Science Books: 1999.

DOI: 10.1021/acs.inorgchem.9b02519
Inorg. Chem. 2019, 58, 15417−15422

Not Non-coordinating at all: Coordination Compounds of the Cyclodimethylsiloxanes D_n (D = Me_2SiO; n = 6, 7) and Group-2-Metal Cations

Fabian Dankert,[†] Florian Weigend,[‡] and Carsten von Hänisch[†]*

*Email: haenisch@staff.uni-marburg.de

[†] Department of Chemistry and Material Sciences Center, Philipps-Universität Marburg, Hans-Meerwein-Straße, 35032 Marburg, Germany.

[‡] Institut für Nanotechnologie, Karlsruher Institut für Technologie, Hermann-von-Helmholtz-Platz 1, 76344 Leopoldshafen-Eggenstein, Germany.

Content

1. Synthesis and Crystallization 3

1.1 General Information 3

1.2 Synthesis of $[Mg(D_6)I_2]$ (1) and $[Mg_2(D_6)_2I_2\{Mg_2I_6\}]$ (2) 4

1.3 Synthesis of $[Ca(D_7)I_2]$ (3) 6

1.4 Synthesis of $[Sr(D_7)I_2]$ (4) 7

1.5 Synthesis of $[Sr(D_7)\{GaI_4\}_2]$ (4a) and $[Sr(D_7)\{GaI_4\}(H_2O)]$ (4b) 8

1.6 Synthesis of $[Ba(D_7)\{GaI_4\}_2]$ (5) and $[Ba(D_7)\{GaI_4\}(H_2O)_{0.94}\{GaI_4\}_{0.06}][GaI_4]_{0.94}$ (5a) 9

2. Single crystal X-Ray diffraction analysis 10

2.1 General Information 10

2.2 Crystallographic Data 11

2.3 Ellipsoid and cell plots 13

3. Quantum chemical calculations 22

3.1 General Information 22

3.2 Calculated energy values and cartesian coordinates of optimized structures 24

4. References 36

1. Synthesis and Crystallization

1.1 General Information

All manipulations were carried out with rigorous exclusion of oxygen and moisture using basic Schlenk techniques under argon gas if not stated otherwise. Solvents were dried and freshly distilled before use and subsequently stored over molecular sieve (3Å). The cyclosiloxanes D_6 and D_7 (≥95%) were purchased from TCI and used as received. The alkaline earth metal salts MgI_2 (Alfa Aesar, 99,996%), CaI_2 and SrI_2 (Alfa Aesar, 99%), BaI_2 (abcr, 99.995%) and GaI_3 (abcr, 99%) were used as received and handled under argon atmosphere using a glovebox of MBraun-type. In all respective reactions we strictly avoided the use of silicon-grease. For all glass valves and joints PTFE paste (Carl Roth) was used. NMR spectra were recorded on different Bruker Spectrometer types e.g. AV III HD 300 MHz or AV III 500 MHz. Infrared (IR) spectra of the respective samples were measured using attenuated total reflectance (ATR) mode on the Bruker-type spectrometer Alpha FT-IR. The OPUS-Software package was applied throughout. ESI mass spectra were acquired with a LTQ-FT Ultra mass spectrometer (Thermo Fischer Scientific). The resolution was set to 100.000. Elemental analysis was carried out on a Vario MicroCube.

1.2 Synthesis of $[Mg(D_6)I_2]$ (1) and $[Mg_2(D_6)_2I_2\{Mg_2I_6\}]$ (2)

0.250 g of D_6 (0.56 mmol) are dissolved in 5 mL of α,α,α-trifluorotoluene. Subsequently, 0.156 g (0.32 mmol) of MgI_2 are added. The suspension is heated and kept at 70 °C for 10 min. under vigorous stirring. The solvent is removed under reduced pressure and the remaining solid is dissolved in 10 mL DCM. The solution is then stirred for another 15 min at ambient temperature followed by filtration. After filtration the solvent is again removed under reduced pressure to obtain a slight yellow powder. Washing the powder with 4 mL of *n*-pentane yields **1** as a slight yellow powder (0.364 g, 90%). For single crystal growth, the powder is dissolved in 5 mL of DCM and layered with 15 mL of *n*-pentane. The solution is then placed at -24°C to obtain single crystal in the shape of colourless platelets after a few days. Attempts crystallizing the compound from DCM/benzene/n-pentane solution (1:1:8) at ambient temperature also yielded colourless platelets of **1** after a few days. Storing the solution for more than two weeks, however, also yields a few much smaller colourless platelets of whose X-ray structure represent compound **2**·0.5C_6H_6.

Analytical Data: ^{1}H NMR: (300 MHz, CD_2Cl_2) δ = 0.47 (s, 36H, Si(C*H*$_3$)$_2$) ppm. ^{13}C{^{1}H} NMR*:* (75 MHz, CD_2Cl_2) 2.1 (s, SiCH_3) ppm. ^{29}Si{^{1}H} NMR: (99 MHz, CD_2Cl_2) δ = -4.8 (s, *Si*(CH$_3$)$_2$) ppm. HR-MS: ESI(+) m/z (%): 595.0016 $[M\text{-}I]^+$ (100). IR (cm^{-1}): 2962 (w), 2900 (vw), 1412 (vw), 1257 (s), 1097 (s), 998 (s), 947 (s), 852 (m), 820 (s), 794 (vs), 722 (s), 709 (s), 593 (m), 555 (s), 510 (w), 429 (vw); CHN calcd. for $C_{12}H_{36}I_2MgO_6Si_6$ C, 19.93; H, 5.02. Found C, 19.92; H, 4.88.

Comment on compound 2: A targeted, straight-forward synthesis of **2** failed, even using the required 2:1 stoichiometry or even higher amounts of MgI_2. The reaction conditions were varied, and longer reaction times stirring the mixtures for about one week did not result in the selective formation of **2**, but mainly **1**. Applying these manipulations we were able to obtain a rather greyish powder. The elemental analysis indicates a lowering of C- and H-values but still comparing well with compound **1**. Also, the crop did not show chemical shift in comparison to compound **1**. The same set of signals is found.

Thus, the crop may only contain very small amounts of compound **2** and however, due to the described reaction behaviour and observed problems in the targeted synthesis of **2**, we were not able to characterize the compound in another way than single crystal X-ray diffraction analysis.

1.3 Synthesis of [Ca(D_7)I_2] (3)

0.160 g of D_7 (0.31 mmol) are dissolved in 5 mL of α,α,α-trifluorotoluene. Subsequently, 0.090 g (0.31 mmol) of CaI_2 are added. The suspension is several times heated to reflux under vigorous stirring over a period of 30 min. The solvent is removed under reduced pressure and the remaining solid is dissolved in 15 mL DCM. The solution is then stirred for another two days at ambient temperature followed by filtration. After filtration the solvent is again removed under reduced pressure to obtain a white wax-like powder (0.180 g, 71%). Single crystals were obtained after the powder was handled under glovebox-atmosphere. The compound partially melts under glove-box conditions and crystallizes as soon as the Schlenk tube is kept at ambient temperature outside the glovebox. A few single crystals in the shape of colourless platelets are obtained after a few days.

Analytical Data: ^{1}H NMR: (300 MHz, CD_2Cl_2) δ = 0.39 (s, 42H, Si(CH_3)$_2$) ppm. ^{13}C{^{1}H} NMR: (75 MHz, CD_2Cl_2) δ = 1.9 (s, $SiCH_3$) ppm. ^{29}Si NMR: (99 MHz, CD_2Cl_2) δ = -7.8 (s, *Si*(CH_3)$_2$) ppm. IR (cm^{-1}): 2961 (w), 1411 (vw), 1260 (s), 1094 (s), 1057 (s), 1015 (m), 964 (s), 857 (s), 818 (s), 792 (vs), 716 (s), 616 (w), 575 (w), 553 (m), 525 (w), 408 (w). MS: ESI(+) m/z (%): 684.9985 [M-I]$^+$ (100). CHN calcd. for $C_{14}H_{42}CaI_2O_7Si_7$ C, 20.68; H, 5.21; found C, 21.28; H, 5.52.

1.4 Synthesis of $[Sr(D_7)I_2]$ (4)

0.180 g of D_7 (0.35 mmol) are dissolved in 10 mL of α,α,α-trifluorotoluene. Subsequently, 0.118 g (0.35 mmol) of SrI_2 are added. The suspension is several times heated to reflux under vigorous stirring. The solvent is removed under reduced pressure and the remaining solid is dissolved in 15 mL DCM. The solution is then stirred for at least three days at ambient temperature followed by filtration. After filtration the solvent is again removed under reduced pressure to obtain the crude compound **4** among D_7 as a colourless grease. A yield determination is obsolet, also by means of NMR spectroscopy, as an equilibrium causes precipitation of uncomplexated SrI_2. To obtain any analytical data of the compound we recommend to directly extract the crude compound **4** with deuterated dichloromethane and filtering the solution into a *J-Young* NMR tube.

Analytical Data: ^{1}H NMR: (300 MHz, CD_2Cl_2) δ = 0.36 (s, 42H, Si(CH_3)$_2$) ppm. ^{13}C{^{1}H} NMR: (75 MHz, CD_2Cl_2) δ = 1.42 (s, SiCH_3) ppm. ^{29}Si NMR: (99 MHz, CD_2Cl_2) δ = -9.2 (s, *Si*(CH_3)$_2$) ppm.

1.5 Synthesis of $[Sr(D_7)\{GaI_4\}_2]$ (4a) and $[Sr(D_7)\{GaI_4\}(H_2O)]$ (4b)

0.125 g of D_7 (0.24 mmol) are dissolved in 10 mL of α,α,α-trifluorotoluene. Subsequently, 0.082 g (0.24 mmol) of SrI_2 are added. The suspension is several times heated to reflux under vigorous stirring. At ambient temperature 0.216 g GaI_3 (0.48 mmol) are added to the pale white suspension. The mixture is stirred overnight and the solvent is removed under reduced pressure. The remaining solid is dissolved in 10 mL of DCM. After subsequent filtration the solvent is again removed under reduced pressure to obtain **4a** (0.363 g, 86%) as a colourless powder. For crystallization, a DCM solution of **4a** is exposed to moisture for at least two hours opening the reaction vessel. Placing the solution at -32°C for a few days yields colourless needles of **4b**·DCM.

Analytical Data of 4a: ^{1}H NMR: (300 MHz, CD_2Cl_2) δ = 0.47 (s, 42H, $Si(CH_3)_2$) ppm. $^{13}C\{^{1}H\}$ NMR: (75 MHz, CD_2Cl_2) δ = 2.2 (s, $SiCH_3$) ppm. ^{29}Si NMR: (99 MHz, CD_2Cl_2) δ = -5.3 (s, $Si(CH_3)_2$) ppm. IR (cm^{-1}): 2958 (w), 1622 (w), 1608 (w), 1410 (vw), 1266 (s), 1088 (w), 978 (s), 856 (s), 815 (vs), 792 (vs), 717 (s), 531 (m). CHN calcd. for $C_{14}H_{42}SrGa_2I_8O_7Si_7$ C, 9.55; H, 2.40; found C, 8.88; H, 2.29.

Analytical Data of 4b: ^{1}H NMR: (300 MHz, CD_2Cl_2) δ = 0.45 (s, 42H, $Si(CH_3)_2$), 4.03 (s, 2H, OH_2) ppm. $^{13}C\{^{1}H\}$ NMR: (75 MHz, CD_2Cl_2) δ = 2.1 (s, $SiCH_3$) ppm. ^{29}Si NMR: (99 MHz, CD_2Cl_2) δ = -5.9 (s, $Si(CH_3)_2$) ppm. IR (cm^{-1}): 3411 (w), 2956 (w), 1623 (m), 1408 (vw), 1392 (vw), 1267 (s), 1078 (w), 1054 (w), 974 (s), 855 (m), 815 (s), 792 (vs), 737 (m), 717 (s), 531 (m), 481 (w), 466 (w), 445 (w), 428 (w). CHN calcd. for $C_{14}H_{44}SrGa_2I_8O_8Si_7$·DCM C, 9.66; H, 2.49; found C, 9.91; H, 2.61.

1.6 Synthesis of $[Ba(D_7)\{GaI_4\}_2]$ (5) and $[Ba(D_7)\{GaI_4\}(H_2O)_{0.94}\{GaI_4\}_{0.06}][GaI_4]_{0.94}$ (5a)

0.098 g of D_7 (0.19 mmol) are dissolved in 10 mL of α,α,α-trifluorotoluene. Subsequently, 0.074 g (0.19 mmol) of BaI_2 are added. The suspension is several times heated to reflux under vigorous stirring. At ambient temperature 0.170 g GaI_3 (0.38 mmol) are added to the pale white suspension. The mixture is stirred overnight and the solvent is removed under reduced pressure. The remaining solid is dissolved in 10 mL of DCM. After subsequent filtration the solvent is again removed under reduced pressure to obtain **4a** (0.300 g, 87%) as a colourless powder. For crystallization, a DCM/benzene solution (1:1) of **5** is exposed to moisture for two hours opening the reaction vessel. Placing the solution at -32°C for a few days yields colourless blocks of **5a**·$0.5C_6H_6$.

Analytical Data of 5: ^{1}H NMR: (300 MHz, CD_2Cl_2) δ = 0.46 (s, 42H, Si(CH_3)$_2$) ppm. ^{13}C{^{1}H} NMR: (75 MHz, CD_2Cl_2) δ = 2.1 (s, SiCH_3) ppm. ^{29}Si NMR: (99 MHz, CD_2Cl_2) δ = -5.8 (s, *Si*(CH_3)$_2$) ppm. IR (cm^{-1}): 2956 (w), 1407 (vw), 1266 (s), 1043 (w), 983 (vs), 856 (s), 814 (s), 792 (vs), 715 (s), 526 (s). CHN calcd. for $C_{14}H_{42}BaGa_2I_8O_7Si_7$ C, 9.28; H, 2.34; found C, 9.40; H, 2.25.

Analytical Data of 5a: ^{1}H NMR: (300 MHz, CD_2Cl_2) δ = 0.45 (s, 42H, Si(CH_3)$_2$), 2.99 (s, 2H, OH_2) ppm. ^{13}C{^{1}H} NMR: (75 MHz, CD_2Cl_2) δ = 2.1 (s, SiCH_3) ppm. ^{29}Si NMR: (99 MHz, CD_2Cl_2) δ = -6.4 (s, *Si*(CH_3)$_2$) ppm. IR (cm^{-1}): 3489 (w), 3437 (w), 2955 (vw), 1595 (m), 1306 (m), 1265 (m), 1234 (m), 1203 (m), 1149 (m), 1126 (m), 982 (vs), 857 (m), 817 (s), 793 (s), 715 (m), 553 (m), 527 (s), 424 (vw). After drying the compound *in vacuo*, loss of water and formation of **5** is observed. Thus no elemental analysis was performed in this case.

2. Single crystal X-Ray diffraction analysis

2.1 General Information

Single crystal X-ray diffraction experiments were carried out on a Bruker D8 Quest (**3**, **4b**, **5**) or a IPDS2T (**1**, **2**) diffractometer at 100(2) K with MoKα radiation and X-ray optics or graphite monochromatization, respectively (λ = 0.71073). All structures were solved by direct methods and refinement with full-matrix-least-squares against F^2 using SHELXT- and SHELXL-2015 on OLEX2 platform.[1-3] Crystallographic data for the compounds **1-3**, **4b**, **5a** are denoted as follows: CCDC Nos. 1921174 (**1**), 1921176 (**2**·0.5C_6H_6), 1921178 (**3**), 1921175 (**4b**·DCM), 1921177 (**5a**·0.5C_6H_6). Crystallographic information files (CIF) can be obtained free of charge from the Cambridge Crystallographic Data Centre (CCDC) (link: www.ccdc.cam.ac.uk/data_request/cif). The respective crystal data and selected experimental parameters of the structure determinations are summarized in Table S1 and Table S2. Visualization of all structures was performed with the Diamond software package Version 4.4.0. All Ellipsoid plots represent the 50% probability level.

2.2 Crystallographic Data

Table S1. Selected crystal structure data of the structure determinations of compounds **1**, **2**·0.5C_6H_6 and **3**

Compound	**1**	**2**·0.5C_6H_6	**3**
Empirical formula	$C_{12}H_{36}I_2MgO_6Si_6$	$C_{36}H_{84}I_8Mg_4O_{12}Si_{12}$	$C_{14}H_{42}CaI_2O_7Si_7$
Formula weight	723.06	2158.55	812.98
Crystal colour, habit	colourless, platelet	colourless, platelet	colourless, platelet
Temperature/K	100(2)	100(2)	100(2)
Crystal system	monoclinic	triclinic	orthorhombic
Space group	$P2_1/n$	$P\bar{1}$	$P2_12_12_1$
a/Å	10.6451(6)	9.7032(8)	14.5174(7)
b/Å	13.2541(9)	12.6357(12)	14.9034(8)
c/Å	10.8015(6)	16.9673(15)	32.6588(17)
α/°	90	84.329(7)	90
β/°	96.697(5)	81.614(7)	90
γ/°	90	80.167(7)	90
Volume/Å^3	1513.60(16)	2022.0(3)	7066.0(6)
Z	2	1	8
ϱ_{calc}g/cm^3	1.587	1.773	1.528
μ/mm^{-1}	2.357	3.317	2.189
F(000)	716.0	1036.0	3248.0
Crystal size/mm^3	0.314 × 0.215 × 0.125	0.42 × 0.075 × 0.021	0.259 × 0.19 × 0.187
Radiation	MoKα (λ = 0.71073)	MoKα (λ = 0.71073)	MoKα (λ = 0.71073)
2Θ range for data collection/°	4.884 to 60	3.28 to 57.998	4.634 to 50.654
Reflections collected	16071	26721	321842
Independent reflections	4405 [R_{int} = 0.0300, R_{sigma} = 0.0205]	10748 [R_{int} = 0.0476, R_{sigma} = 0.0608]	12879 [R_{int} = 0.0403, R_{sigma} = 0.0119]
Data/restraints/parameters	4405/0/130	10748/0/337	12879/0/588
Goodness-of-fit on F^2	1.032	0.988	1.057
Final R indexes [I>=2σ (I)]	R_1 = 0.0230, wR_2 = 0.0614	R_1 = 0.0394, wR2 = 0.0815	R_1 = 0.0152, wR_2 = 0.0350
Final R indexes [all data]	R_1 = 0.0268, wR_2 = 0.0628	R_1 = 0.0744, wR2 = 0.0881	R_1 = 0.0162, wR_2 = 0.0353
Largest diff. peak/hole / e Å^{-3}	0.79/-1.00	0.84/-1.15	0.53/-0.53
Absolute structure parameter	-	-	0.491(7)

Table S2. Selected crystal structure data of the structure determinations of compounds **4b**·DCM and **5a**·0.5C_6H_6

Compound	**4b·DCM**	**5a**·0.5C_6H_6
Empirical formula	$C_{15}H_{46}Cl_2Ga_2I_8O_8Si_7Sr$	$C_{17}H_{46.88}BaGa_2I_8O_{7.94}Si_7$
Formula weight	1864.31	1867.07
Crystal colour, habit	colourless, needle	colourless, block
Temperature/K	100(2)	100(2)
Crystal system	monoclinic	monoclinic
Space group	$P2_1/c$	$P2_1/c$
a/Å	22.8633(12)	22.5082(11)
b/Å	11.2286(6)	12.1806(5)
c/Å	22.4046(12)	21.5584(10)
α/°	90	90
β/°	99.884(2)	109.613(2)
γ/°	90	90
Volume/Å^3	5666.4(5)	5567.6(4)
Z	4	4
ϱ_{calc}g/cm^3	2.185	2.227
μ/mm^{-1}	6.510	6.275
F(000)	3424.0	3410.0
Crystal size/mm^3	0.532 × 0.189 × 0.097	0.277 × 0.143 × 0.114
Radiation	MoKα (λ = 0.71073)	MoKα (λ = 0.71073)
2Θ range for data collection/°	4.324 to 50.586	4.528 to 50.672
Reflections collected	59856	222243
Independent reflections	10286 [R_{int} = 0.0322, R_{sigma} = 0.0232]	10110 [R_{int} = 0.0322, R_{sigma} = 0.0100]
Data/restraints/parameters	10286/0/403	10110/1/472
Goodness-of-fit on F^2	1.208	1.047
Final R indexes [I>=2σ (I)]	R_1 = 0.0436, wR_2 = 0.0909	R_1 = 0.0339, wR_2 = 0.0786
Final R indexes [all data]	R_1 = 0.0478, wR_2 = 0.0923	R_1 = 0.0360, wR_2 = 0.0799
Largest diff. peak/hole / e Å^{-3}	2.30/-0.86	3.07/-1.96
Absolute structure parameter	-	-

2.3 Ellipsoid and cell plots

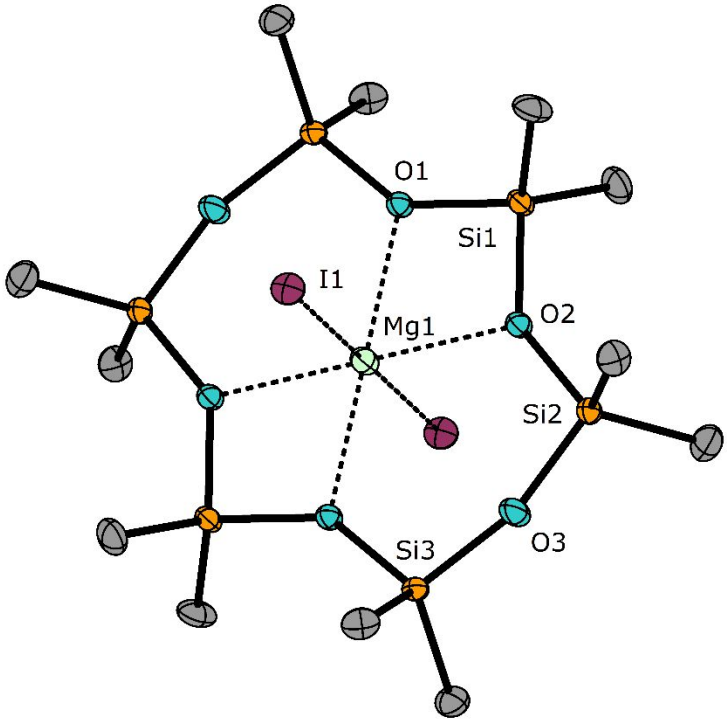

Figure S1. Molecular structure of **1** in the crystal. Thermal displacement ellipsoids are drawn at 50% probability. All nonlabeled atoms are symmetry generated over # = 1-x, 1-y, 1-z. Selected bond lengths [pm]: O1-Mg1 212.8(1), O2-Mg1 212.3(1), O3···Mg1 315.1(1), I1-Mg1 287.4(1). Selected bond angles [°]: O1-Mg1-O2 70.5(1), O2-Mg1-O1# 109.4(1), Si1-O1-Si3# 142.4(1), Si1-O2-Si2 142.1(1), Si2-O3-Si3 161.2(1).

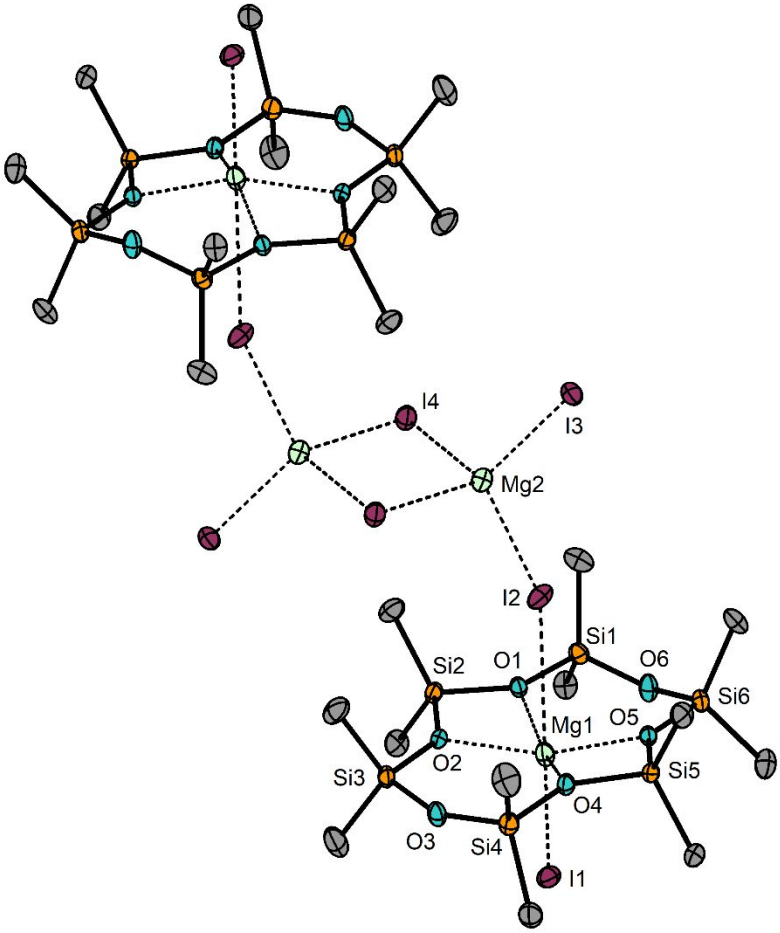

Figure S2. Molecular structure of **2** in the crystal. Thermal displacement ellipsoids are drawn at 50% probability. All nonlabeled atoms are symmetry generated over # = 1-x, 1-y, 1-z. Selected bond lengths [pm]: O1-Mg1 208.7(3), O2-Mg1 209.1(2), O3···Mg1 325.5(3), O4-Mg1 210.8(3), O5-Mg1 209.1(2), O6···Mg1 309.9(3), I1-Mg1 270.8(1), I2-Mg1 353.2(1), I2-Mg2 268.4(1), I3-Mg2 265.1(1), I4-Mg2 278.2(1), Mg2···Mg2# 363.9(3). Selected bond angles [°]: O1-Mg1-O2 71.5(1), O2-Mg1-O4 102.1(1), O4-Mg1-O5 70.8(1), O1-Mg1-O5 106.1(1), I2-Mg2-I3 112.7(1), I3-Mg2-I4 111.0(1), Mg2-I4-Mg2# 81.7(1).

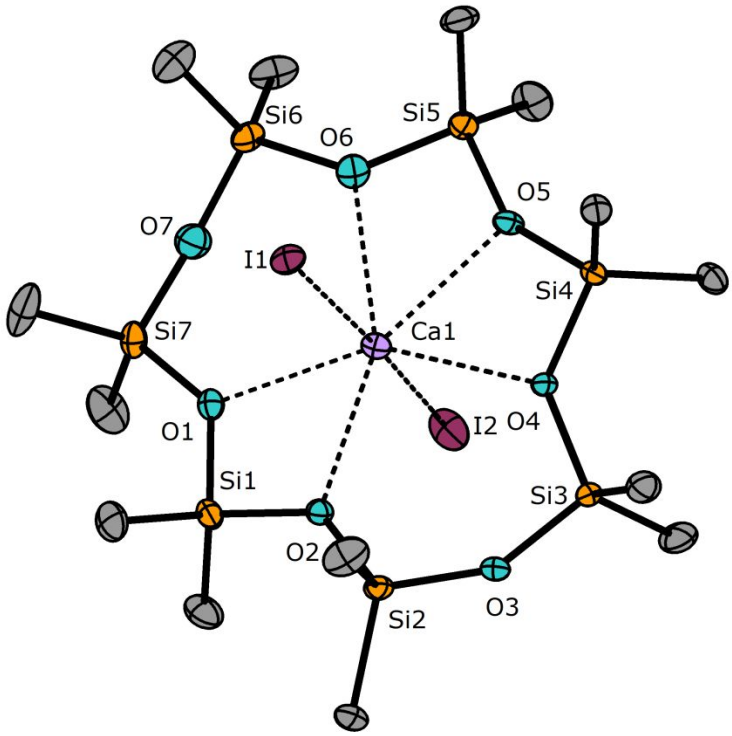

Figure S3. Molecular structure of **3** in the crystal. Thermal displacement ellipsoids are drawn at 50% probability. Only one of two independent molecules per asymmetric unit is shown. Selected bond lengths [pm]: O1-Ca1 246.6(2), O2-Ca1 250.2(2), O3···Ca1 375.9(1), O4-Ca1 260.0(1), O5-Ca1 244.8(2), O6-Ca1 259.5(3), O7···Ca1 351.8(3), I1-Ca1 305.6(1), I2-Ca1 302.0(1). Selected bond angles [°]: O1-Ca1-O2 61.0(1), O1-Ca1-O6 94.4(1), O2-Ca1-O4 87.0(1), O4-Ca1-O5 59.1(1), O5-Ca1-O6 58.5(1), Si1-O1-Si7 135.9(1), Si1-O2-Si2 133.9(1), Si2-O3-Si3 149.4(2), Si3-O4-Si4 133.7(1), Si4-O5-Si5 149.6(1), Si5-O6-Si6 139.1(2), Si6-O7-Si7 152.8(2).

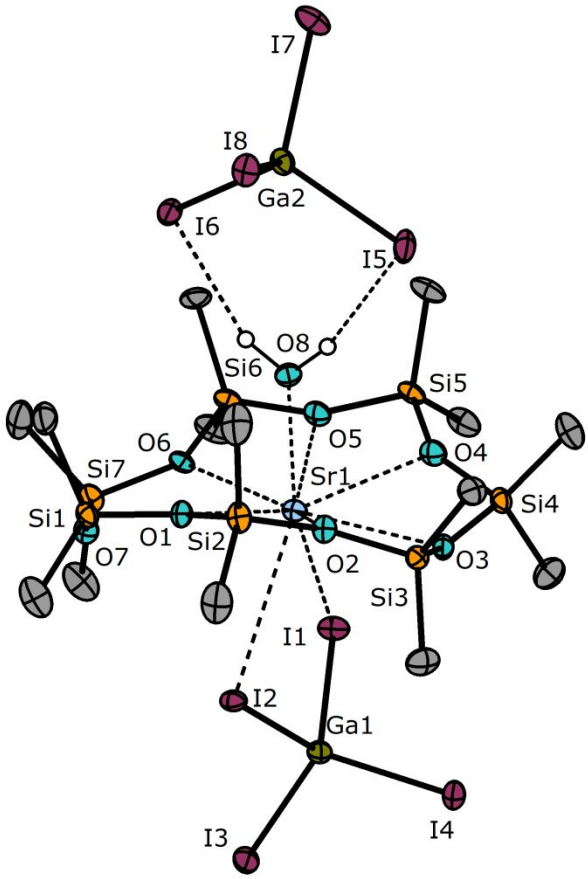

Figure S4. Molecular structure of **4b** in the crystal. Thermal displacement ellipsoids are drawn at 50% probability. Hydrogen atoms are drawn with arbitrary radii. Selected bond lengths [pm]: O1-Sr1 2.765(5), O2-Sr1 2.649(5), O3-Sr1 2.837(5), O4-Sr1 2.674(5), O5-Sr1 2.753(5), O6-Sr1 2.646(5), O7···Sr1 356.3(4), O8-Sr1 2.469(5), I1-Sr1 3.5706(8), I2-Sr1 3.4397(8). Selected bond angles [°]: O1-Sr1-O2 55.4(1), O1-Sr1-O6 86.6(1), O2-Sr1-O3 54.4(1), O3-Sr1-O4 53.7(1) O4-Sr1-O5 54.8(1), O5-Sr1-O6 55.4(1), Si1-O7-Si7 150.2(4), Si1-O1-Si2 139.7(3), Si2-O2-Si3 147.9(3), Si3-O3-Si4 145.9(4), Si4-O4-Si5 147.9(4), Si5-O5-Si6 155.7(4), Si6-O6-Si7 134.6(3).

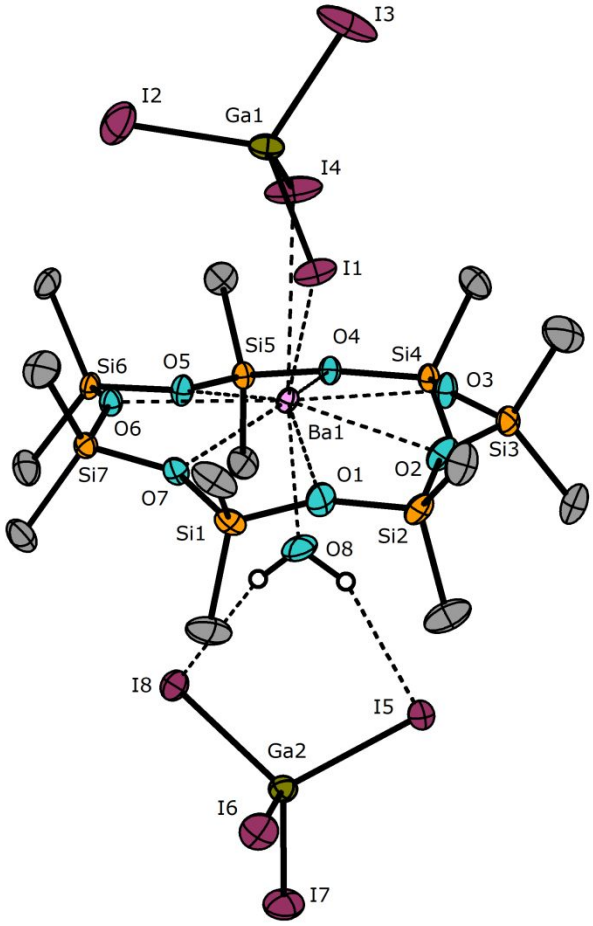

Figure S5. Molecular structure of 5a in the crystal. Thermal displacement ellipsoids are drawn at 50% probability. Only one of two independent molecules per asymmetric unit is shown Hydrogen atoms are drawn with arbitrary radii. Selected bond lengths [pm]: O1-Ba1 295.0(3), O2-Ba1 291.4(3), O3-Ba1 288.5(3), O4-Ba1 292.0(3), O5-Ba1 291.0(3), O6-Ba1 292.0(3), O7-Ba1 285.9(3), O8-Ba1 263.3(5), I1-Ba1 362.5(2), I4-Ba1 356.2(2). Selected bond angles [°]: O1-Ba1-O2 55.5(1), O2-Ba1-O3 51.4(1), O3-Ba1-O4 51.3(9), O4-Ba1-O5 50.98(9), O5-Ba1-O6 51.07(9), O6-Ba1-O7 51.43(9), Si1-O7-Si7 147.8(2), Si1-O1-Si2 152.5(3), Si2-O2-Si3 150.9(3), Si3-O3-Si4 148.5(3), Si4-O4-Si5 149.4(2), Si5-O5-Si6 148.8(2), Si6-O6-Si7 148.1(2).

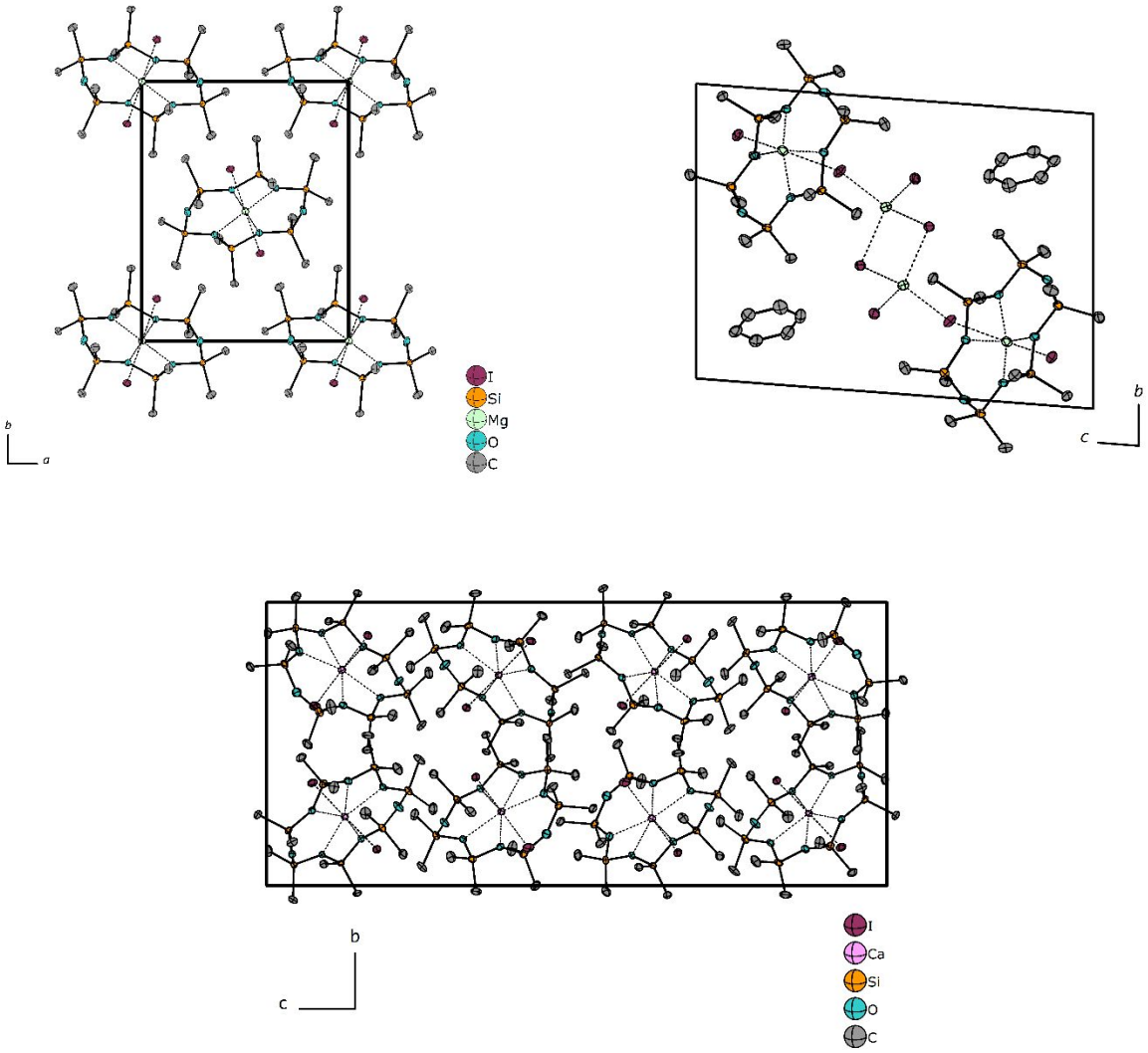

Figure S6. Cell plot of compound **1** (top left, along [001]), compound **2**·C_6H_6 (top right, along [100]) and compound **3** (bottom, along [100]).

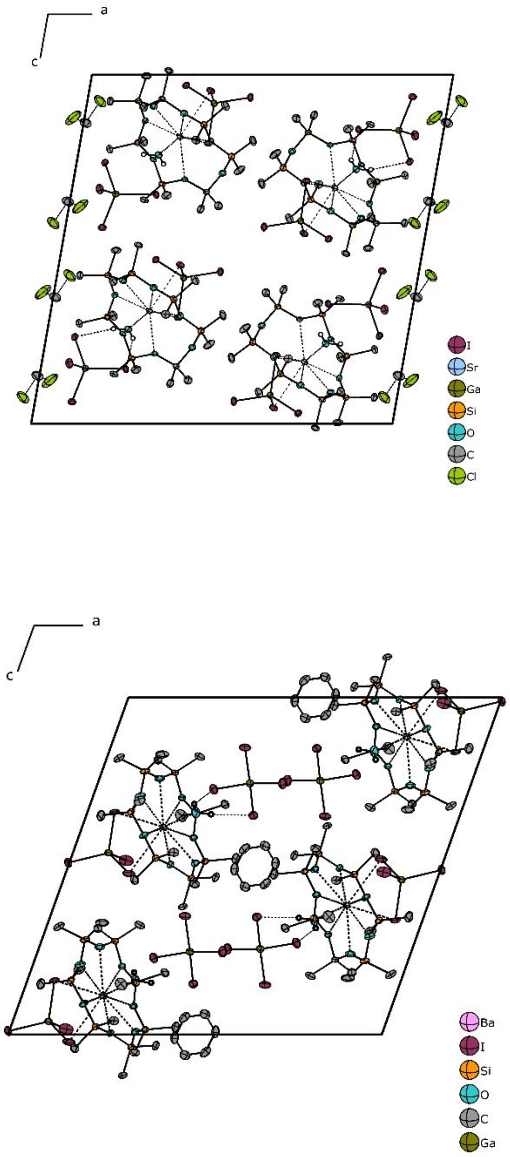

Figure S7. Cell plot of compound **4b**·DCM (top, along [010]) and compound **5a**·C_6H_6 (bottom, along [010]).

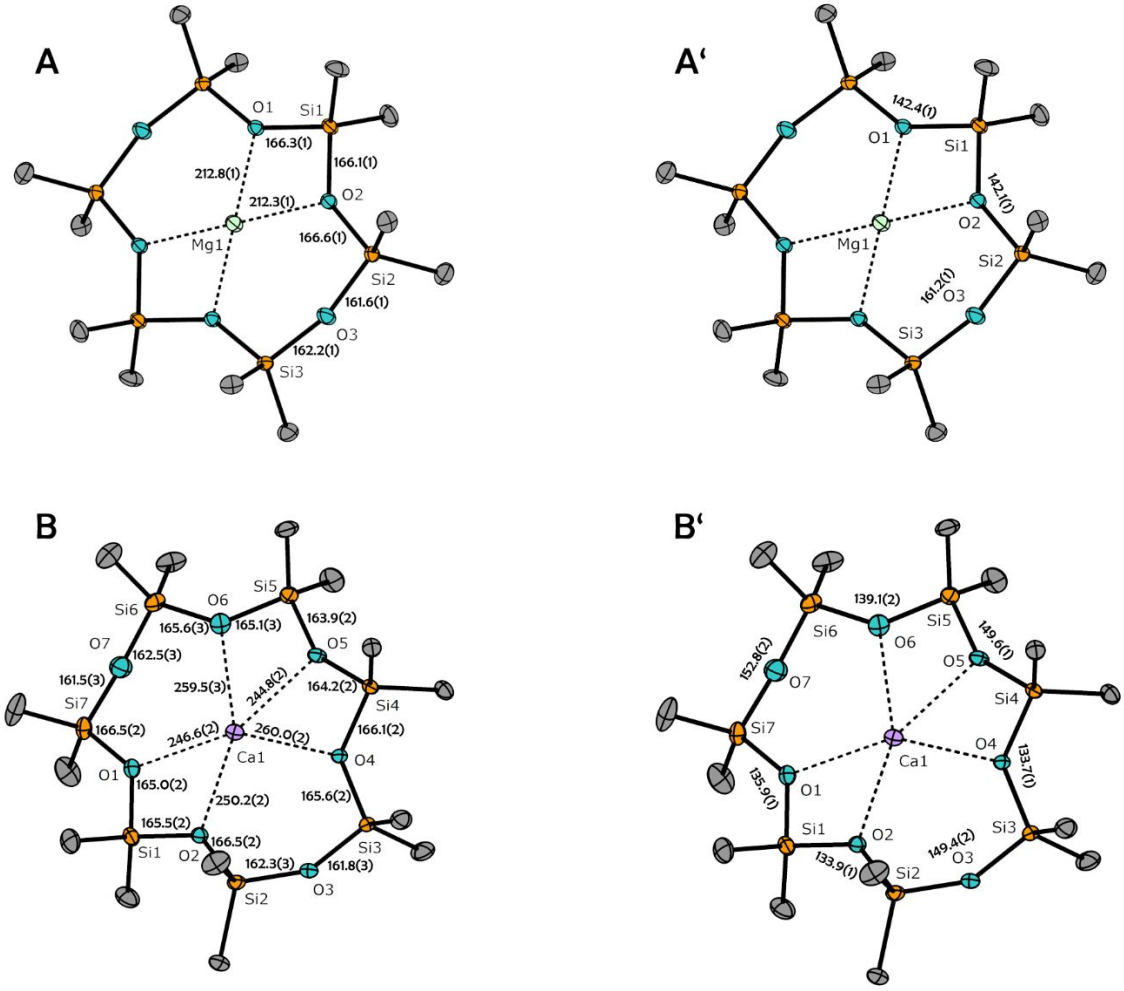

Figure S8. Top-view of the alkaline earth metal complexes **1** and **2**. (A) and (B): Bond-lengths and (A') and (B'): Si-O-Si angles of the respective coordination compounds. Not-depicted bond-lengths and angles are symmetry generated over 1-x, 1-y, 1-z.

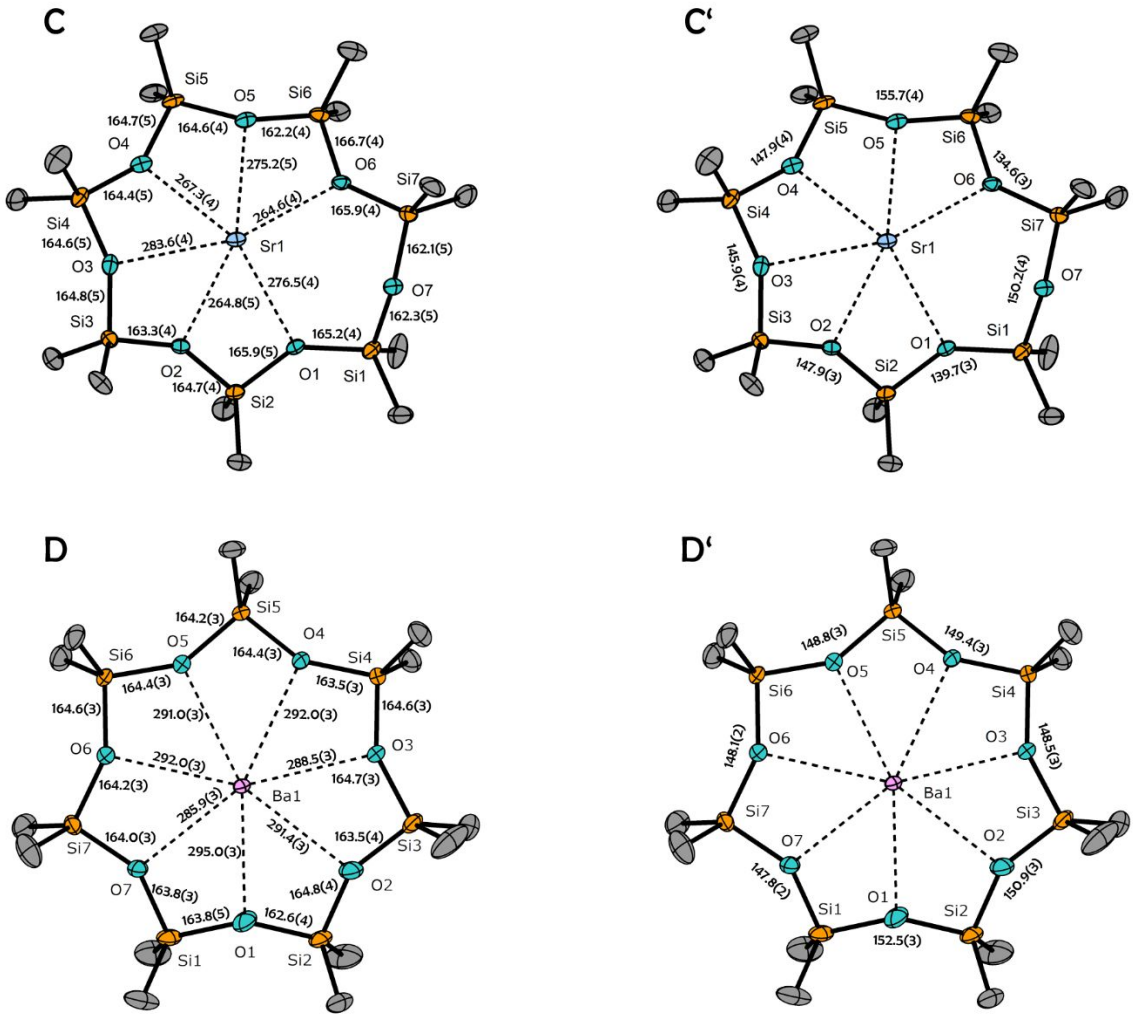

Figure S9. Top-view of the alkaline earth metal complexes **4b** and **5a**. (C) and (D): Bond-lengths and (C′) and (D′): Si-O-Si angles of the respective coordination compounds.

3. Quantum chemical calculations

3.1 General Information

The following Born-Haber cycle is calculated:

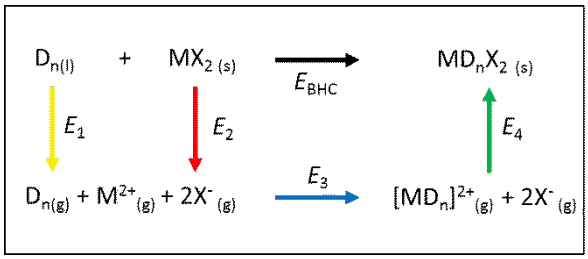

The desired energy E is obtained as follows:

$$E = E_1 + E_2 + E_3 + E_4$$

$$E_1 = 22.8 + 5.6 \cdot n \text{ kJ/mol}$$

$$E_2 = \left(2 \cdot 1^2 + 1 \cdot 2^2\right)\left(\frac{\alpha}{\sqrt[3]{V\left(\mathrm{MX_2}\right)}} + \beta\right) \text{ kJ/mol}$$

$$E_3 = E\left(\mathrm{MD}_n^{2+}\right) - \left\{E\left(\mathrm{M}^{2+}\right) + E\left(\mathrm{D}_n\right)\right\}$$

$$E_4 = -\left(2 \cdot 1^2 + 1 \cdot 2^2\right)\left(\frac{\alpha}{\sqrt[3]{V\left(\mathrm{MD}_n\mathrm{X}_2\right)}} + \beta\right) \text{ kJ/mol}$$

All structures were optimized at the level B3LYP[4]/dhf-TZVP[5] (Table S3) as well as BP86[6]/dhf-TZVP (Table S4) yielding the energies for M^{2+}, D_n and MD_n^{2+}. The molecular volumes of MX_2 and MD_nX_2 are identified with the cavity volumes from the conductor-like screening model (COSMO)[7] used with default radii amounting to 1.300/2.000/1.720/2.200/2.223/2.223/2.320 for H/C/O/Si/Sr/Ba/I, as proposed by Preiss et al.[8] For Ga the radius was slightly increased from 2.223 to 2.28 to ensure the definition of a closed cavity by the COSMO algorithm. We note in passing that for

the experimentally obtained compounds 1, 3, 4b, 5a one could obtain molecular volumes also from the crystal structures, which are larger by about 20%. We desisted from using them, as they are not available for all compounds and thus do not allow for a consistent calculation of energies for all reactions. The equation for obtaining E_1 was taken from Wilcock[9], that for E_2 and E_4 from Jenkins et al.[10]. The numbers in Table S5 are obtained for parameter values α = 133.5 kJmol^{-1}nm and β = 60.9kJmol^{-1}, which were recommended for MX_2 compounds in Ref. 10, the numbers in Table S5 for α = 138.7kJmol^{-1}nm and β = 27.6kJmol^{-1}, which were obtained from a more general fit in Ref. 10.

We note that the quality of the chosen basis is sufficient also for the M^{2+} and the I^- ion. This was checked by comparing the ionization energy Ba→Ba^{2+} obtained with the dhf-TZVP basis to that obtained with its decontracted variant moreover extended with steep functions. The improvement is less than 1kJ/mol. Analogous calculations were done for I/I^- with a basis extended by diffuse functions leading to a change of ca. 5 kJ/mol. Both changes are small compared to the reaction energies discussed and probably also much smaller than the errors of the empirical formulae for obtaining the other energies.

3.2 Calculated energy values and Cartesian coordinates of optimized structures

Table S3. Total energies of M^{2+}, D_n and $(MD_n)^{2+}$ for M=Mg,Ca,Sr,Ba, n=5,6 and resulting gas phase reaction energies at levels B3-LYP/dhf-TZVP and BP86/dhf-TZVP.

		B3-LYP				BP86			
M	n	$E(M^{2+})$	$E(D_n)$	$E(MD_n^{2+})$	$-E_3$	$E(M^{2+})$	$E(D_n)$	$E(MD_n^{2+})$	$-E_3$
Mg	6	-199.20009	-2667.77468	-2867.40248	1123	-199.24624	-2668.72640	-2868.39950	1120
Ca	6	-676.83559	-2667.77468	-3344.93038	840	-676.96303	-2668.72640	-3346.01860	864
Sr	6	-30.04033	-2667.77468	-2698.08733	715	-30.09728	-2668.72640	-2699.10637	742
Ba	6	-24.84866	-2667.77468	-2692.85250	602	-24.91472	-2668.72640	-2693.88341	636
Mg	7	-199.20009	-3112.40260	-3312.04341	1157	-199.24624	-3113.50937	-3313.20122	1170
Ca	7	-676.83559	-3112.40260	-3789.56967	870	-676.96303	-3113.50937	-3790.81730	906
Sr	7	-30.04033	-3112.40260	-3142.73365	763	-30.09728	-3113.50937	-3143.91100	799
Ba	7	-24.84866	-3112.40260	-3137.50647	670	-24.91472	-3113.50937	-3138.69414	709

Table S4. Molecular volumes, in nm^3, calculated at levels B3-LYP/dhf-TZVP and BP86/dhf-TZVP for the systems MD_nX_2 with M=Mg,Ca,Sr,Ba, n=5,6 X=I as well as X=GaI_4 and resulting energies E2 and E4. In the third line, '1' denotes the parameter set optimized specifically for MX_2 compounds, '2' the set optimized at a broader set of molecules.

			Volumes				E_2				$-E_4$			
			B3-LYP		BP86		B3-LYP		BP86		B3-LYP		BP86	
M	n	X	MX_2	MD_nX_2	MX_2	MD_nX_2	1	2	1	2	1	2	1	2
Mg	6	I	0.110	0.633	0.110	0.641	1733	1765	1732	1764	994	997	990	993
Ca	6	I	0.130	0.655	0.130	0.659	1642	1671	1643	1671	983	986	981	984
Sr	6	I	0.133	0.662	0.133	0.668	1629	1657	1631	1658	980	982	977	980
Ba	6	I	0.137	0.657	0.137	0.677	1615	1642	1616	1644	982	985	973	975
Mg	7	I	0.110	0.730	0.110	0.732	1733	1765	1732	1764	951	952	950	951
Ca	7	I	0.130	0.748	0.130	0.746	1642	1671	1643	1671	943	944	955	945
Sr	7	I	0.133	0.779	0.133	0.769	1629	1657	1631	1658	931	932	935	936
Ba	7	I	0.137	0.789	0.137	0.772	1615	1642	1616	1644	928	928	934	935
Sr	6	GaI_4	0.456	0.970	0.455	0.960	1102	1109	1103	1110	870	868	873	871
Ba	6	GaI_4	0.460	0.990	0.458	0.979	1099	1106	1100	1107	864	862	868	866
Sr	7	GaI_4	0.456	1.096	0.455	1.099	1102	1109	1103	1110	838	835	837	834
Ba	7	GaI_4	0.460	1.108	0.458	1.104	1099	1106	1100	1107	835	832	836	833
Ba	6	$+H_2O$		1.002		1.029					861	859	854	852
Ba	7	$+H_2O$		1.123		1.131					832	828	830	836

Table S5. Energies E_{BHC} (see equations), in kJ/mol, for the reactions $MD_{n(l)} + MX_{2(s)} \rightarrow MD_nX_{2(s)}$ with energies E_2 and E_4 from Table S4 and E_3 from Table S3. E_1 amounts to 56 kJ/mol for n=6 and to 62 kJ/mol for n=7. In the third line, '1' denotes the parameter set optimized specifically for MX_2 compounds, '2' the set optimized at a broader set of molecules.

M	*n*	*X*	*E*			
			B3LYP		BP86	
			1	2	1	2
Mg	6	I	-328	-299	-322	-293
Ca	6	I	-125	-99	-146	-121
Sr	6	I	-10	16	-32	-8
Ba	6	I	87	111	63	89
Mg	7	I	-313	-282	-326	-295
Ca	7	I	-109	-81	-156	-118
Sr	7	I	-3	24	-41	-15
Ba	7	I	79	106	35	62
Sr	6	GaI_4	-427	-418	-456	-447
Ba	6	GaI_4	-311	-302	-348	-339
Sr	7	GaI_4	-437	-427	-471	-461
Ba	7	GaI_4	-344	-334	-383	-373

Table S6. Changes in E_2 and E_4 when replacing I with GaI_4. See also Table S4.

	E_2					E_4			
	B3-LYP		BP86			B3-LYP		BP86	
M	1	2	1	2	n	1	2	1	2
Sr	527	548	528	548	6	110	114	104	109
Ba	516	536	516	537	6	118	123	105	109
Sr					7	93	97	98	102
Ba					7	93	96	98	102

Table S7. Cartesian coordinates of D_6 and D_7 obtained at level B3LYP/dhf-TZVP.

D_6				D_7			
Si	-2.3448	-1.1543	1.0276	O	2.4425	0.4990	-0.6148
Si	2.5839	1.4426	-0.0167	O	-2.6503	-0.5500	2.0189
O	-2.4352	-0.0525	-0.1799	O	-0.1276	-1.0059	2.7467
O	2.2038	-0.1468	0.0031	O	1.2873	-1.0159	-2.4666
O	-1.3866	-2.3959	0.5589	O	-1.3411	-0.5597	-2.5501
O	1.2418	2.2917	0.3572	O	1.9636	0.4430	2.0058
C	-4.0576	-1.8266	1.3430	Si	2.7727	1.2194	0.8143
C	-1.6041	-0.3778	2.5549	Si	2.4135	0.1394	-2.2094
C	3.8826	1.7926	1.2803	Si	-1.6916	-1.3540	3.0722
C	3.1693	1.9135	-1.7279	Si	-3.0612	0.7381	1.0950
Si	-2.3127	1.3832	-0.9512	Si	1.4976	-0.8768	2.8544
Si	2.4154	-1.7693	0.0186	Si	-0.1707	-1.6796	-2.7901

Si	-0.3975	-3.2237	-0.4482	Si	-2.7730	0.0403	-2.0382
Si	-0.0756	3.2580	0.3919	C	4.6109	1.1066	1.1439
H	-4.4735	-2.2688	0.4345	C	2.1920	2.9924	0.7780
H	-4.7389	-1.0384	1.6728	C	4.0716	-0.5601	-2.7070
H	-4.0406	-2.6003	2.1145	C	1.9799	1.6737	-3.1838
H	-1.5190	-1.1093	3.3623	C	-1.9829	-3.1823	2.8373
H	-2.2175	0.4513	2.9160	C	-2.1030	-0.8020	4.8105
H	-0.6051	0.0102	2.3440	O	-2.6479	0.4359	-0.4575
H	3.5217	1.5185	2.2745	C	-2.1372	2.2562	1.6649
H	4.8004	1.2305	1.0892	C	-4.9131	0.9546	1.2206
H	4.1420	2.8540	1.3014	C	1.9844	-0.6230	4.6404
H	3.3998	2.9800	-1.7897	C	2.2784	-2.4134	2.1333
H	4.0719	1.3614	-2.0019	C	-0.4184	-3.1319	-1.6435
H	2.4048	1.6920	-2.4765	C	-0.2098	-2.1932	-4.5864
O	-1.3981	2.4103	-0.0624	C	-3.1336	1.5845	-3.0231
C	-4.0174	2.1257	-1.1139	C	-4.1097	-1.2497	-2.2590
C	-1.5163	1.0906	-2.6154	H	4.9430	0.0656	1.1637
O	1.0550	-2.4723	-0.5519	H	4.8664	1.5572	2.1064
C	3.8208	-2.2276	-1.1234	H	5.1864	1.6234	0.3711
C	2.7368	-2.3216	1.7750	H	2.7162	3.5659	0.0089
C	-1.1280	-3.2843	-2.1642	H	2.3686	3.4819	1.7390
C	-0.1631	-4.9305	0.2730	H	1.1218	3.0483	0.5673
C	-0.3354	3.8433	2.1434	H	4.2990	-1.4609	-2.1319
C	0.1727	4.6853	-0.7901	H	4.8771	0.1584	-2.5362
H	-4.4585	2.3025	-0.1298	H	4.0828	-0.8295	-3.7659
H	-3.9836	3.0829	-1.6402	H	1.0024	2.0592	-2.8856
H	-4.6865	1.4618	-1.6665	H	1.9425	1.4602	-4.2549
H	-2.1174	0.4090	-3.2223	H	2.7162	2.4665	-3.0291
H	-1.4074	2.0237	-3.1740	H	-3.0317	-3.4377	3.0071
H	-0.5243	0.6476	-2.5000	H	-1.3785	-3.7746	3.5291
H	3.6153	-1.8943	-2.1434	H	-1.7254	-3.4886	1.8208
H	3.9666	-3.3104	-1.1506	H	-1.4849	-1.3161	5.5508
H	4.7623	-1.7737	-0.8037	H	-3.1495	-1.0075	5.0495
H	3.6323	-1.8448	2.1815	H	-1.9388	0.2720	4.9283
H	2.8816	-3.4034	1.8309	H	-2.4071	2.5259	2.6892
H	1.8974	-2.0618	2.4245	H	-2.3575	3.1144	1.0252
H	-2.1013	-3.7812	-2.1629	H	-1.0594	2.0822	1.6369
H	-0.4738	-3.8291	-2.8493	H	-5.4339	0.0544	0.8855
H	-1.2650	-2.2765	-2.5620	H	-5.2604	1.7921	0.6102
H	0.2610	-4.8748	1.2784	H	-5.2155	1.1471	2.2530
H	0.5089	-5.5331	-0.3431	H	1.5105	0.2719	5.0505
H	-1.1167	-5.4593	0.3446	H	3.0661	-0.5022	4.7391
H	0.5214	4.4210	2.4989	H	1.6878	-1.4731	5.2602
H	-1.2231	4.4758	2.2203	H	2.0021	-2.5326	1.0833
H	-0.4698	2.9940	2.8171	H	1.9543	-3.3090	2.6693
H	0.3300	4.3303	-1.8116	H	3.3691	-2.3697	2.1902
H	-0.6993	5.3440	-0.7966	H	0.3862	-3.8621	-1.7598
H	1.0415	5.2860	-0.5091	H	-1.3639	-3.6433	-1.8409
				H	-0.4240	-2.8023	-0.6021
				H	-0.0664	-1.3287	-5.2395
				H	-1.1671	-2.6518	-4.8475
				H	0.5787	-2.9160	-4.8098
				H	-2.3462	2.3280	-2.8791
				H	-4.0810	2.0364	-2.7188
				H	-3.1949	1.3661	-4.0920
				H	-4.1837	-1.5680	-3.3020
				H	-5.0867	-0.8599	-1.9620
				H	-3.9075	-2.1347	-1.6509

Table S8. Cartesian Coordinates of MI_2 (M=Mg, Ca, Sr, Ba) obtained at level B3LYP/dhf-TZVP.

MgI_2				CaI_2				SrI_2				BaI_2			
Mg	0.0000	0.0000	0.0000	Ca	0.0000	0.0000	0.0000	Sr	0.0000	0.0000	-0.0000	Ba	0.0000	0.0000	-0.0000
I	0.0000	0.0000	2.5449	I	0.0000	0.0000	2.8542	I	0.0000	0.0000	3.0172	I	0.0000	0.0000	3.1812
I	0.0000	0.0000	-2.5449	I	0.0000	0.0000	-2.8542	I	0.0000	0.0000	-3.0172	I	0.0000	0.0000	-3.1812

Table S9. Cartesian Coordinates of GaI_4^- obtained at level B3LYP/dhf-TZVP.

Ga	-0.0000	0.0000	0.0000
I	1.2499	-2.1649	0.0000
I	1.2499	2.1649	-0.0000
I	-2.4998	0.0000	-0.0000

Table S10. Cartesian coordinates of $(MD_6)^{2+}$ (M=Mg, Ca, Sr, Ba) obtained at level B3LYP/dhf-TZVP.

$(MgD_6)^{2+}$				$(CaD_6)^{2+}$				$(SrD_6)^{2+}$				$(BaD_6)^{2+}$			
Mg	-0.0001	0.0003	0.0001	Ca	0.0001	0.0007	-0.0001	Sr	-0.0000	0.0000	0.7503	Ba	0.0001	1.1491	-0.0001
Si	0.0012	-0.0029	2.8136	Si	0.3988	0.1074	3.2484	Si	0.0000	-3.2688	-0.1157	Si	2.0617	-0.3104	-2.5064
Si	-0.0011	0.0072	-2.8136	Si	-0.3988	0.1075	-3.2482	Si	0.0000	3.2688	-0.1157	Si	-2.0618	-0.3102	2.5065
O	1.2226	0.0023	1.6241	O	1.4862	0.0229	1.9707	O	1.2564	-2.1761	0.1210	O	0.4169	0.0311	-2.5038
O	-1.2226	-0.0028	-1.6241	O	-1.4866	0.0222	-1.9714	O	-1.2564	2.1761	0.1210	O	-0.4167	0.0302	2.5024
O	-1.2211	-0.0026	1.6251	O	-0.9674	0.1116	2.2702	O	-1.2564	-2.1761	0.1210	O	2.3716	0.0243	-0.8897
O	1.2211	0.0044	-1.6250	O	0.9671	0.1125	-2.2696	O	1.2564	2.1761	0.1210	O	-2.3731	0.0259	0.8903
C	-0.0091	1.5542	3.8024	C	0.5655	1.7033	4.1621	C	0.0000	-4.5482	1.2161	C	2.9521	0.9021	-3.5801
C	0.0122	-1.5654	3.7940	C	0.4762	-1.4114	4.2972	C	0.0000	-3.9366	-1.8401	C	2.3931	-2.0850	-2.9125
C	0.0105	-1.5460	-3.8084	C	-0.4739	-1.4116	-4.2969	C	0.0000	3.9366	-1.8401	C	-2.3940	-2.0848	2.9121
C	-0.0134	1.5735	-3.7878	C	-0.5663	1.7031	-4.1625	C	0.0000	4.5482	1.2161	C	-2.9504	0.9020	3.5819
Si	2.9622	0.0172	1.6027	Si	3.0132	-0.0922	1.2798	Si	2.8309	-1.6344	-0.1157	Si	-1.1395	-0.3038	-3.0405
Si	-2.9621	-0.0220	-1.6028	Si	-3.0133	-0.0923	-1.2797	Si	-2.8309	1.6344	-0.1157	Si	1.1395	-0.3038	3.0404
Si	-2.9608	-0.0107	1.6048	Si	-2.6157	-0.0152	1.9699	Si	-2.8309	-1.6344	-0.1157	Si	3.1997	-0.3128	0.5326
Si	2.9608	0.0109	-1.6048	Si	2.6156	-0.0151	-1.9700	Si	2.8309	1.6344	-0.1157	Si	-3.1995	-0.3127	-0.5325
H	-0.0145	2.4508	3.1801	H	0.5167	2.5706	3.5005	H	0.0000	-4.1094	2.2162	H	2.7335	1.9378	-3.3104
H	0.8652	1.6022	4.4559	H	1.5157	1.7457	4.7007	H	0.8787	-5.1930	1.1355	H	2.6775	0.7684	-4.6294
H	-0.8872	1.5894	4.4521	H	-0.2265	1.8071	4.9082	H	-0.8787	-5.1930	1.1355	H	4.0338	0.7632	-3.5104
H	-0.8628	-1.6180	4.4463	H	-0.3173	-1.4053	5.0489	H	-0.8769	-4.5665	-2.0097	H	3.4602	-2.3053	-2.8287
H	0.8897	-1.6032	4.4444	H	1.4240	-1.4582	4.8396	H	0.8769	-4.5665	-2.0097	H	2.1090	-2.3031	-3.9449
H	0.0191	-2.4585	3.1668	H	0.3788	-2.3298	3.7147	H	0.0000	-3.1510	-2.5981	H	1.8558	-2.7785	-2.2633
H	0.0177	-2.4450	-3.1897	H	-0.3759	-2.3299	-3.7143	H	0.0000	3.1510	-2.5981	H	-1.8578	-2.7785	2.2623
H	-0.8643	-1.5926	-4.4614	H	-1.4213	-1.4596	-4.8401	H	-0.8769	4.5665	-2.0097	H	-2.1088	-2.3031	3.9442
H	0.8882	-1.5772	-4.4590	H	0.3201	-1.4045	-5.0480	H	0.8769	4.5665	-2.0097	H	-3.4613	-2.3045	2.8295
H	0.8618	1.6298	-4.4395	H	0.2258	1.8071	-4.9085	H	0.8787	5.1930	1.1355	H	-4.0323	0.7636	3.5133
H	-0.8907	1.6130	-4.4384	H	-1.5165	1.7447	-4.7011	H	-0.8787	5.1930	1.1355	H	-2.6748	0.7675	4.6308
H	-0.0217	2.4641	-3.1571	H	-0.5181	2.5705	-3.5010	H	0.0000	4.1094	2.2162	H	-2.7318	1.9380	3.3127
O	3.2323	0.1394	-0.0014	O	2.4485	-0.1333	-0.3022	O	2.5127	0.0000	0.1210	O	-1.9568	0.0280	-1.6105
C	3.5710	-1.5921	2.2772	C	3.8346	-1.6832	1.7318	C	3.4092	-1.9683	-1.8401	C	-1.3265	-2.0750	-3.5418
C	3.5626	1.5210	2.4901	C	4.0116	1.4281	1.6029	C	3.9388	-2.2741	1.2161	C	-1.6299	0.9164	-4.3392
O	-3.2321	-0.1407	0.0016	O	-2.4478	-0.1328	0.3021	O	-2.5127	0.0000	0.1210	O	1.9582	0.0292	1.6115
C	-3.5753	1.5839	-2.2815	C	-4.0115	1.4281	-1.6030	C	-3.9388	2.2741	1.2161	C	1.6276	0.9161	4.3402
C	-3.5583	-1.5298	-2.4863	C	-3.8353	-1.6834	-1.7303	C	-3.4092	1.9683	-1.8401	C	1.3265	-2.0751	3.5413
C	-3.5622	1.6052	2.2704	C	-3.4987	1.5331	2.4542	C	-3.9388	-2.2741	1.2161	C	4.5784	0.8976	0.7567
C	-3.5670	-1.5066	2.5015	C	-3.3145	-1.5721	2.6763	C	-3.4092	-1.9683	-1.8401	C	3.7134	-2.0882	0.6205
C	3.5606	-1.6050	-2.2717	C	3.3134	-1.5722	-2.6774	C	3.4092	1.9683	-1.8401	C	-3.7132	-2.0882	-0.6194
C	3.5684	1.5069	-2.5002	C	3.4988	1.5330	-2.4543	C	3.9388	2.2741	1.2161	C	-4.5781	0.8972	-0.7596
H	3.1342	-2.4526	1.7659	H	3.2052	-2.5516	1.5268	H	2.7289	-1.5755	-2.5981	H	-1.0319	-2.7748	-2.7578

H	4.6556	-1.6519	2.1527	H	4.7672	-1.8079	1.1755	H	4.3931	-1.5238	-2.0097	H	-2.3635	-2.2900	-3.8112
H	3.3692	-1.6928	3.3459	H	4.0945	-1.6996	2.7932	H	3.5162	-3.0426	-2.0097	H	-0.7229	-2.2891	-4.4272
H	3.3825	1.4662	3.5660	H	4.2734	1.4997	2.6617	H	4.0579	-3.3575	1.1355	H	-1.0315	0.7847	-5.2440
H	4.6439	1.6103	2.3549	H	4.9521	1.4012	1.0467	H	4.9366	-1.8355	1.1355	H	-2.6767	0.7833	-4.6234
H	3.1086	2.4386	2.1109	H	3.4842	2.3433	1.3266	H	3.5588	-2.0547	2.2162	H	-1.5061	1.9502	-4.0085
H	-3.1408	2.4470	-1.7727	H	-3.4841	2.3434	-1.3268	H	-3.5588	2.0547	2.2162	H	1.5048	1.9502	4.0102
H	-4.6600	1.6410	-2.1570	H	-4.9519	1.4013	-1.0466	H	-4.9366	1.8355	1.1355	H	2.6738	0.7824	4.6265
H	-3.3741	1.6821	-3.3506	H	-4.2736	1.4996	-2.6617	H	-4.0579	3.3575	1.1355	H	1.0274	0.7839	5.2439
H	-3.3783	-1.4774	-3.5623	H	-4.0951	-1.7009	-2.7918	H	-3.5162	3.0426	-2.0097	H	0.7223	-2.2897	4.4262
H	-4.6394	-1.6218	-2.3509	H	-4.7681	-1.8076	-1.1742	H	-4.3931	1.5238	-2.0097	H	2.3633	-2.2907	3.8109
H	-3.1018	-2.4451	-2.1046	H	-3.2060	-2.5517	-1.5245	H	-2.7289	1.5755	-2.5981	H	1.0321	-2.7742	2.7566
H	-3.3590	1.7108	3.3384	H	-3.4955	1.6531	3.5407	H	-4.0579	-3.3575	1.1355	H	5.3467	0.7581	-0.0079
H	-4.6466	1.6691	2.1465	H	-4.5457	1.4993	2.1428	H	-4.9366	-1.8355	1.1355	H	5.0621	0.7622	1.7272
H	-3.1221	2.4609	1.7541	H	-3.0475	2.4272	2.0192	H	-3.5588	-2.0547	2.2162	H	4.2381	1.9339	0.6982
H	-3.1173	-2.4284	2.1274	H	-2.7641	-2.4602	2.3592	H	-2.7289	-1.5755	-2.5981	H	2.8803	-2.7800	0.4850
H	-4.6488	-1.5919	2.3674	H	-4.3566	-1.6987	2.3717	H	-4.3931	-1.5238	-2.0097	H	4.1780	-2.3072	1.5851
H	-3.3861	-1.4461	3.5769	H	-3.3062	-1.5435	3.7688	H	-3.5162	-3.0426	-2.0097	H	4.4616	-2.3100	-0.1445
H	3.3572	-1.7095	-3.3397	H	3.3044	-1.5435	-3.7699	H	3.5162	3.0426	-2.0097	H	-4.4626	-2.3092	0.1445
H	4.6449	-1.6701	-2.1480	H	4.3556	-1.6995	-2.3733	H	4.3931	1.5238	-2.0097	H	-4.1761	-2.3080	-1.5846
H	3.1197	-2.4608	-1.7561	H	2.7626	-2.4600	-2.3602	H	2.7289	1.5755	-2.5981	H	-2.8803	-2.7800	-0.4818
H	3.1199	2.4289	-2.1250	H	3.0478	2.4271	-2.0191	H	3.5588	2.0547	2.2162	H	-4.2383	1.9338	-0.7025
H	4.6504	1.5908	-2.3664	H	4.5458	1.4987	-2.1428	H	4.9366	1.8355	1.1355	H	-5.0605	0.7601	-1.7306
H	3.3871	1.4478	-3.5756	H	3.4959	1.6534	-3.5408	H	4.0579	3.3575	1.1355	H	-5.3475	0.7586	0.0040

Table S11. Cartesian coordinates of MD_6I_2 (M=Mg, Ca, Sr, Ba) obtained at level B3LYP/dhf-TZVP.

MgD_6I_2				CaD_6I_2				SrD_6I_2				BaD_6I_2			
I	4.2032	8.7517	3.5110	I	4.1705	8.9280	3.3870	I	4.1633	9.0180	3.2675	I	4.2569	8.4995	3.6974
Mg	4.6927	6.6271	5.3639	Ca	4.6927	6.6270	5.3639	Sr	4.6927	6.6271	5.3639	Ba	4.9319	5.5615	6.2785
I	5.1822	4.5024	7.2168	I	5.2150	4.3261	7.3408	I	5.2222	4.2361	7.4603	I	5.4553	3.1832	8.4435
Si	5.1792	8.5975	7.4848	Si	5.2360	8.8163	7.7310	Si	5.2393	8.8319	7.7472	Si	5.2569	8.7368	7.7697
Si	4.2063	4.6566	3.2430	Si	4.1494	4.4378	2.9968	Si	4.1461	4.4222	2.9806	Si	4.1688	4.3694	3.0643
O	6.2135	7.8756	6.3927	O	6.3047	8.1258	6.6709	O	6.3300	8.1523	6.6896	O	6.4106	7.8706	6.9392
O	3.1720	5.3785	4.3351	O	3.0808	5.1283	4.0569	O	3.0554	5.1018	4.0382	O	3.1137	4.8292	4.2687
O	3.7805	7.8361	6.9865	O	3.8239	8.0828	7.2692	O	3.8047	8.1169	7.2978	O	3.8755	7.8346	7.5397
O	5.6049	5.4180	3.7413	O	5.5615	5.1713	3.4586	O	5.5807	5.1372	3.4300	O	5.6528	4.8522	3.6482
C	5.0859	10.4322	7.2207	C	5.1359	10.6476	7.4435	C	5.1443	10.6624	7.4593	C	5.0577	10.4744	7.1580
C	5.6113	8.1436	9.2317	C	5.6654	8.3458	9.4748	C	5.6667	8.3458	9.4861	C	5.6928	8.6467	9.5734
C	4.2996	2.8219	3.5071	C	4.2496	2.6065	3.2843	C	4.2411	2.5917	3.2685	C	4.1739	2.5079	2.9876
C	3.7741	5.1105	1.4961	C	3.7200	4.9083	1.2530	C	3.7188	4.9083	1.2417	C	3.7587	5.1681	1.4461
Si	7.7956	7.7512	5.8499	Si	7.7137	7.7578	5.8822	Si	7.7352	7.7658	5.8857	Si	7.7338	7.6624	5.9515
Si	1.5899	5.5029	4.8779	Si	1.6717	5.4963	4.8456	Si	1.6502	5.4883	4.8421	Si	1.7006	5.4537	4.8947
Si	2.1288	7.6702	7.2257	Si	2.2185	7.6786	7.2119	Si	2.1981	7.6880	7.2261	Si	2.2488	7.6040	7.2721
Si	7.2566	5.5839	3.5021	Si	7.1670	5.5755	3.5159	Si	7.1873	5.5661	3.5017	Si	7.1815	5.5103	3.5681
H	4.8288	10.6582	6.1849	H	4.8789	10.8536	6.4025	H	4.8895	10.8703	6.4179	H	4.7822	10.4870	6.1030
H	6.0421	10.9079	7.4542	Si	6.0898	11.1331	7.6650	Si	6.0993	11.1451	7.6821	Si	5.9708	11.0597	7.2919
H	4.3323	10.8819	7.8727	H	4.3772	11.1064	8.0826	H	4.3852	11.1220	8.0971	H	4.2684	10.9688	7.7309
H	4.8678	8.5358	9.9305	H	4.9216	8.7255	10.179	H	4.9243	8.7233	10.1938	H	4.9274	9.1184	10.1954
H	6.5786	8.5657	9.5166	H	6.6349	8.7578	9.7664	H	6.6384	8.7508	9.7798	H	6.6400	9.1555	9.7651
H	5.6573	7.0597	9.3454	H	5.7094	7.2594	9.5737	H	5.7057	7.2583	9.5768	H	5.7958	7.6089	9.8978
H	4.5567	2.5959	4.5429	H	4.5066	2.4005	4.3253	H	4.4960	2.3838	4.3099	H	4.4212	2.0671	3.9562
H	3.3433	2.3462	3.2736	H	3.2956	2.1210	3.0628	H	3.2862	2.1090	3.0457	H	3.1984	2.1161	2.6880
H	5.0531	2.3722	2.8551	H	5.0082	2.1477	2.6452	H	5.0002	2.1321	2.6307	H	4.9093	2.1534	2.2611
H	4.5176	4.7183	0.7973	H	4.4639	4.5286	0.5480	H	4.4611	4.5308	0.5339	H	4.4783	4.8885	0.6729
H	2.8068	4.6884	1.2112	H	2.7505	4.4963	0.9614	H	2.7470	4.5033	0.9480	H	2.7720	4.8414	1.1083
H	3.7282	6.1944	1.3824	H	3.6760	5.9947	1.1541	H	3.6798	5.9958	1.1510	H	3.7539	6.2544	1.5473
O	7.7229	6.6704	4.6282	O	7.1670	6.6614	4.7670	O	7.2153	6.6591	4.7566	O	7.3005	6.3716	4.9916
C	8.8664	7.0883	7.2163	C	8.9103	6.9484	7.0478	C	8.9233	6.9543	7.0569	C	9.1688	7.1398	7.0212
C	8.3553	9.3998	5.2001	C	8.3858	9.2630	5.0284	C	8.4003	9.2710	5.0285	C	8.0718	9.1864	4.9563
O	1.6625	6.5837	6.0996	O	2.2184	6.5927	5.9608	O	2.1701	6.5950	5.9712	O	2.2251	6.3169	6.2173
C	0.5190	6.1658	3.5115	C	0.4752	6.3057	3.6800	C	0.4622	6.2998	3.6709	C	0.7558	6.4997	3.6865
C	1.0302	3.8543	5.5277	C	0.9997	3.9911	5.6994	C	0.9851	3.9831	5.6993	C	0.7089	4.0165	5.5337
C	1.2923	9.3004	6.9155	C	1.1946	9.1638	6.7752	C	1.1734	9.1708	6.7872	C	1.4217	9.1002	6.5650

C	1.8179	6.9895	8.9266	C	1.7101	6.8443	8.7904	C	1.7028	6.8465	8.8038	C	1.4827	7.0343	8.8681
C	8.0931	3.9537	3.8123	C	8.1908	4.0903	3.9526	C	8.2120	4.0833	3.9406	C	8.4011	4.1121	3.6952
C	7.5676	6.2646	1.8012	C	7.6753	6.4098	1.9374	C	7.6826	6.4076	1.9240	C	7.4195	6.5691	2.0601
H	8.4628	6.1452	7.5897	H	8.4499	6.0761	7.5159	H	8.4594	6.0819	7.5219	H	8.9467	6.2444	7.6054
H	9.8825	6.9097	6.8556	H	9.8127	6.6217	6.5245	H	9.8279	6.6267	6.5379	H	10.0527	6.9225	6.4159
H	8.9326	7.7873	8.0538	H	9.2203	7.6392	7.8362	H	9.2289	7.6440	7.8478	H	9.4363	7.9360	7.7217
H	8.4125	10.1487	5.9941	H	8.6756	10.0291	5.7520	H	8.6863	10.0398	5.7506	H	8.3156	10.0285	5.6100
H	9.3488	9.3190	4.7520	H	9.2712	9.0182	4.4360	H	9.2862	9.0278	4.4361	H	8.9221	9.0353	4.2878
H	7.6627	9.7623	4.4378	H	7.6328	9.6874	4.3613	H	7.6456	9.6911	4.3602	H	7.1963	9.4516	4.3593
H	0.9227	7.1089	3.1381	H	0.9356	7.1780	3.2119	H	0.9260	7.1722	3.2059	H	1.3490	7.3413	3.3246
H	-0.4971	6.3444	3.8722	H	-0.4273	6.6324	4.2033	H	-0.4424	6.6274	4.1899	H	-0.1483	6.8931	4.1603
H	0.4529	5.4668	2.6740	H	0.1651	5.6149	2.8916	H	0.1566	5.6101	2.8800	H	0.4356	5.9028	2.8278
H	0.9730	3.1054	4.7337	H	0.7099	3.2250	4.9758	H	0.6991	3.2143	4.9772	H	0.4003	3.3618	4.7165
H	0.0366	3.9351	5.9758	H	0.1142	4.2359	6.2918	H	0.0993	4.2263	6.2917	H	-0.1955	4.3557	6.0455
H	1.7228	3.4918	6.2900	H	1.7527	3.5667	6.3665	H	1.7398	3.5630	6.3676	H	1.2923	3.4197	6.2379
H	1.5891	10.0529	7.6506	H	1.2498	9.9257	7.5573	H	1.2292	9.9338	7.5679	H	1.4706	9.9327	7.2731
H	0.2065	9.1921	6.9749	H	0.1421	8.8952	6.6529	H	0.1214	8.9004	6.6656	H	0.3657	8.8826	6.3832
H	1.5463	9.6755	5.9220	H	1.5476	9.6045	5.8406	H	1.5250	9.6110	5.8516	H	1.8879	9.4036	5.6256
H	2.3699	6.0583	9.0700	H	2.3480	5.9795	8.9841	H	2.3448	5.9830	8.9908	H	1.9880	6.1401	9.2352
H	0.7539	6.7843	9.0703	H	0.6731	6.5029	8.7402	H	0.6669	6.5013	8.7575	H	0.4240	6.7949	8.7342
H	2.1255	7.6922	9.7050	H	1.7905	7.5276	9.6398	H	1.7865	7.5271	9.6549	H	1.5586	7.8036	9.6406
H	7.7963	3.2012	3.0772	H	8.1357	3.3284	3.1705	H	8.1562	3.3203	3.1599	H	8.3272	3.4344	2.8409
H	9.1790	4.0620	3.7529	H	9.2433	4.3589	4.0749	H	9.2640	4.3537	4.0622	H	9.4245	4.4960	3.7338
H	7.8392	3.5786	4.8058	H	7.8378	3.6496	4.8872	H	7.8605	3.6431	4.8762	H	8.2356	3.5275	4.6027
H	7.0156	7.1958	1.6578	H	7.0374	7.2746	1.7437	H	7.0407	7.2711	1.7370	H	6.6939	7.3857	2.0499
H	8.6315	6.4698	1.6575	H	8.7124	6.7512	1.9876	H	8.7185	6.7528	1.9703	H	8.4259	6.9969	2.0359
H	7.2599	5.5619	1.0228	H	7.5949	5.7265	1.0880	H	7.5990	5.7270	1.0729	H	7.2926	5.9832	1.1441

Table S12. Cartesian coordinates of $(MD_7)^{2+}$ (M=Mg, Ca, Sr, Ba) obtained at level B3LYP/dhf-TZVP.

$(MgD_7)^{2+}$				$(CaD_7)^{2+}$				$(SrD_7)^{2+}$				$(BaD_7)^{2+}$			
Mg	-0.0453	0.1337	0.0018	Ca	-0.1596	-0.0222	-0.2026	Sr	0.0012	0.0046	-0.0068	Ba	0.0036	0.0005	0.0001
O	-1.0825	1.9150	0.3088	O	-1.1191	2.2234	0.0707	O	2.6468	0.8442	0.1827	O	0.0213	2.2456	-1.8165
O	-0.1261	0.6033	2.1265	O	-0.3543	0.9150	2.0540	O	-2.4598	0.2223	0.9626	Si	-0.0576	1.5873	-3.3505
O	1.9830	-0.3375	0.0369	O	2.1736	-0.5959	0.3423	O	-0.8556	-0.9488	2.5066	Si	0.0892	3.6063	-0.8490
O	-1.2357	0.6709	-1.7862	O	-1.5668	0.9800	-2.0374	O	1.9291	-0.5239	-1.8059	O	-0.0739	-0.0192	-2.8935
O	0.1384	-1.8312	-0.6097	O	0.6668	-2.2397	-0.7690	O	-0.4453	-0.5768	-2.6096	C	-1.6417	2.0508	-4.1898
Si	-1.1359	1.9579	1.9973	Si	-1.1543	2.3728	1.7415	O	1.3811	0.1705	2.2427	C	1.4636	1.9910	-4.3257
Si	-1.8030	2.1552	-1.1987	Si	-1.8084	2.5270	-1.4329	Si	2.8137	0.9489	1.8419	O	0.0711	2.8208	0.6256
Si	0.9647	0.0282	3.3355	Si	0.5759	0.2966	3.3531	Si	3.2957	0.2756	-1.2501	C	1.6848	4.5132	-1.0934
Si	1.8396	-1.9051	-0.6082	Si	2.2882	-2.1352	-0.3477	Si	-2.4978	-0.6720	2.3841	C	-1.4210	4.6555	-1.0663
Si	3.1168	0.3850	1.1267	Si	3.0892	0.2973	1.4830	Si	-3.3355	0.9889	-0.2458	Si	-0.0584	-1.6316	-3.3299
Si	-1.5444	-0.2165	-3.2393	Si	-2.2128	-0.3729	-2.7973	Si	0.5288	-0.6938	3.4044	H	-1.7395	1.5374	-5.1497
Si	-1.0978	-2.7059	-1.4423	Si	-0.5698	-2.9164	-1.6887	Si	1.0671	-1.0669	-3.1364	H	-1.6745	3.1226	-4.4004
C	-0.4095	3.5384	2.6138	C	-0.2006	3.8673	2.2653	Si	-1.8741	0.2157	-2.9876	H	-2.5187	1.8020	-3.5885
C	-2.8251	1.5797	2.6417	C	-2.8858	2.3050	2.3897	C	4.2878	0.0373	2.4908	H	2.3801	1.7048	-3.8054
C	-1.0168	3.5767	-2.0745	C	-0.7756	3.7389	-2.3679	C	2.7383	2.7245	2.3564	H	1.5194	3.0624	-4.5343
C	-3.6404	2.2558	-1.0357	C	-3.5981	2.9736	-1.3043	C	4.6717	-0.9338	-0.9885	H	1.4553	1.4819	-5.2926
O	2.4207	0.1355	2.5876	O	2.1151	0.3645	2.7984	C	3.7432	1.7081	-2.3330	Si	0.0121	2.9133	2.2929
C	0.4846	-1.7268	3.6827	C	0.0188	-1.4634	3.5677	C	-3.3685	-2.2834	2.1199	H	2.5546	3.8664	-0.9600
C	0.9312	1.1071	4.8365	C	0.3956	1.3227	4.8800	C	-3.1818	0.3393	3.7744	H	1.7749	5.3426	-0.3873
C	2.5653	-1.9563	-2.3056	C	3.3653	-2.0885	-1.8515	O	-2.1986	0.8186	-1.4604	H	1.7404	4.9444	-2.0960
C	2.4475	-3.2474	0.5055	C	2.7246	-3.4661	0.8594	C	-3.5389	2.7823	0.1602	H	-1.4520	5.0922	-2.0676
C	4.7597	-0.4529	1.0309	C	4.6754	-0.5536	1.9053	C	-4.9253	0.1121	-0.6044	H	-1.4227	5.4891	-0.3595
C	3.1661	2.1802	0.6654	C	3.3311	1.9810	0.7369	C	0.2503	0.3396	4.9145	H	-2.3445	4.0916	-0.9197
O	-1.3736	-1.7714	-2.7537	O	-1.4709	-1.5084	-1.8093	C	1.3474	-2.3185	3.7435	O	0.0194	-2.2704	-1.7878
C	-0.2589	0.2530	-4.4852	C	-1.6149	-0.4604	-4.5443	C	1.1304	-2.9144	-3.2061	C	1.4633	-2.0477	-4.2991
C	-3.2737	0.0844	-3.8250	C	-4.0486	-0.4761	-2.6070	C	1.5817	-0.2320	-4.7056	C	-1.6422	-2.1027	-4.1656
C	-2.5512	-2.7204	-0.2893	C	-1.4920	-4.1673	-0.6910	C	-1.5995	1.6219	-4.1590	O	-0.0492	1.2717	2.5966
C	-0.5012	-4.3814	-1.9373	C	0.0484	-3.5321	-3.3187	C	-3.1372	-1.0088	-3.5621	C	1.5660	3.6595	2.9688
H	0.6267	3.6852	2.3061	H	0.8467	3.8301	1.9615	H	4.2997	-1.0158	2.2062	C	-1.5395	3.7503	2.8592
H	-0.4568	3.6040	3.7020	H	-0.2372	4.0108	3.3465	H	4.3117	0.0900	3.5827	Si	0.0769	-3.6181	-0.8018
H	-0.9937	4.3759	2.2212	H	-0.6449	4.7585	1.8128	H	5.2154	0.4938	2.1369	H	1.4566	-1.5497	-5.2719
H	-3.2335	0.6518	2.2364	H	-3.4294	1.4236	2.0426	H	3.6229	3.2643	2.0095	H	1.5183	-3.1215	-4.4955
H	-3.5248	2.3880	2.4161	H	-3.4532	3.1906	2.0935	H	2.7099	2.8182	3.4447	H	2.3794	-1.7565	-3.7810

H	-2.7988	1.4801	3.7301	H	-2.8844	2.2818	3.4825	H	1.8618	3.2386	1.9550	H	-2.5197	-1.8441	-3.5692
H	-1.2546	4.5178	-1.5720	H	-0.8172	4.7272	-1.9032	H	4.3711	-1.7864	-0.3768	H	-1.6772	-3.1769	-4.3629
H	-1.3914	3.6615	-3.0979	H	-1.1409	3.8488	-3.3921	H	5.5372	-0.4640	-0.5164	H	-1.7367	-1.6008	-5.1319
H	0.0701	3.4859	-2.1230	H	0.2732	3.4386	-2.4198	H	5.0105	-1.3239	-1.9522	Si	-0.0916	0.0237	3.7068
H	-4.0766	1.3751	-0.5616	H	-4.1821	2.2506	-0.7330	H	2.9108	2.4000	-2.4778	H	1.5703	3.6327	4.0614
H	-4.1183	2.3868	-2.0081	H	-4.0439	3.0569	-2.2988	H	4.0861	1.3791	-3.3164	H	1.6521	4.7097	2.6788
H	-3.9085	3.1300	-0.4354	H	-3.7131	3.9511	-0.8286	H	4.5635	2.2730	-1.8822	H	2.4622	3.1428	2.6188
H	-0.4518	-1.7629	4.2451	H	-1.0121	-1.5106	3.9261	H	-4.4318	-2.1342	1.9184	H	-2.4372	3.2884	2.4428
H	1.2467	-2.2179	4.2925	H	0.6423	-1.9716	4.3071	H	-3.2965	-2.9069	3.0147	H	-1.5423	4.8046	2.5718
H	0.3472	-2.3201	2.7769	H	0.0789	-2.0463	2.6442	H	-2.9453	-2.8531	1.2893	H	-1.6240	3.7203	3.9485
H	1.3080	2.1127	4.6474	H	0.8086	2.3255	4.7647	H	-3.0995	-0.1871	4.7280	O	0.0663	-2.8130	0.6621
H	1.5816	0.6583	5.5928	H	0.9466	0.8416	5.6928	H	-4.2468	0.5247	3.6094	C	-1.4424	-4.6571	-1.0037
H	-0.0638	1.1801	5.2818	H	-0.6437	1.4059	5.2062	H	-2.6893	1.3075	3.8774	C	1.6644	-4.5424	-1.0345
H	2.3930	-2.9199	-2.7890	H	3.3426	-3.0436	-2.3819	H	-4.1766	2.9158	1.0375	O	-0.0317	-1.2378	2.6133
H	3.6490	-1.8252	-2.2417	H	4.4065	-1.9056	-1.5741	H	-4.0141	3.3146	-0.6675	C	-1.6949	0.0193	4.6333
H	2.1757	-1.1750	-2.9584	H	3.0690	-1.3058	-2.5533	H	-2.5859	3.2758	0.3645	C	1.4099	0.0429	4.7900
H	3.5341	-3.3368	0.4508	H	3.7839	-3.4388	1.1211	H	-4.7908	-0.9494	-0.8172	Si	0.0279	-2.8833	2.3309
H	2.0383	-4.2054	0.1733	H	2.5369	-4.4436	0.4056	H	-5.4360	0.5655	-1.4574	H	-1.4499	-5.4819	-0.2867
H	2.1676	-3.1103	1.5497	H	2.1445	-3.4136	1.7822	H	-5.6049	0.2000	0.2476	H	-1.4792	-5.1057	-1.9996
H	4.7384	-1.4776	1.4025	H	4.5186	-1.4953	2.4326	H	-0.1815	1.3158	4.6883	H	-2.3609	-4.0837	-0.8621
H	5.4673	0.0979	1.6570	H	5.2524	0.0945	2.5707	H	1.1999	0.5080	5.4299	H	2.5401	-3.9018	-0.9108
H	5.1662	-0.4520	0.0169	H	5.2973	-0.7404	1.0269	H	-0.4067	-0.1654	5.6263	H	1.7155	-4.9884	-2.0310
H	3.6376	2.3182	-0.3106	H	3.9763	1.9288	-0.1435	H	1.5046	-2.9038	2.8346	H	1.7473	-5.3626	-0.3170
H	3.7596	2.7390	1.3932	H	3.8163	2.6469	1.4547	H	0.7333	-2.9201	4.4184	H	-1.7782	0.9005	5.2743
H	2.1777	2.6442	0.6275	H	2.3948	2.4587	0.4359	H	2.3170	-2.1826	4.2282	H	-1.7673	-0.8543	5.2860
H	0.7590	0.1769	-4.1001	H	-0.5301	-0.3675	-4.6230	H	2.1423	-3.2621	-3.4283	H	-2.5597	0.0095	3.9665
H	-0.4059	1.2779	-4.8345	H	-2.0573	0.3496	-5.1301	H	0.4773	-3.2975	-3.9940	H	2.3384	0.0461	4.2152
H	-0.3314	-0.3983	-5.3598	H	-1.9122	-1.3966	-5.0220	H	0.8211	-3.3785	-2.2665	H	1.4277	-0.8289	5.4488
H	-3.4582	-0.5638	-4.6866	H	-4.4129	-1.4155	-3.0314	H	1.5408	0.8565	-4.6467	H	1.4136	0.9250	5.4353
H	-3.4333	1.1098	-4.1653	H	-4.5534	0.3306	-3.1433	H	0.9437	-0.5493	-5.5345	C	-1.5151	-3.7136	2.9297
H	-4.0268	-0.1556	-3.0730	H	-4.3666	-0.4425	-1.5633	H	2.6026	-0.5169	-4.9730	C	1.5916	-3.6174	2.9973
H	-2.8792	-1.7159	-0.0068	H	-1.8371	-3.7649	0.2639	H	-0.8458	2.3261	-3.8005	H	-2.4187	-3.2572	2.5200
H	-2.3335	-3.2763	0.6255	H	-0.8672	-5.0388	-0.4808	H	-2.5300	2.1794	-4.2947	H	-1.5834	-3.6679	4.0195
H	-3.4036	-3.2075	-0.7696	H	-2.3694	-4.5240	-1.2363	H	-1.2929	1.2702	-5.1465	H	-1.5227	-4.7720	2.6575
H	-1.3007	-4.8894	-2.4835	H	-0.7815	-3.8642	-3.9475	H	-2.8318	-1.4297	-4.5240	H	1.6741	-4.6724	2.7244
H	-0.2593	-5.0043	-1.0735	H	0.6943	-4.4020	-3.1710	H	-4.1122	-0.5418	-3.7169	H	1.6119	-3.5713	4.0890
H	0.3639	-4.3498	-2.6013	H	0.6154	-2.7844	-3.8752	H	-3.2642	-1.8404	-2.8665	H	2.4823	-3.1067	2.6250

Table S13. Cartesian coordinates of MD_7I_2 (M=Mg, Ca, Sr, Ba) obtained at level B3LYP/dhf-TZVP.

MgD_7I_2				CaD_7I_2				SrD_7I_2				BaD_7I_2			
I	-1.7024	-1.5540	1.4617	I	-1.9259	-1.7622	1.5696	I	-0.0222	3.1908	0.0159	Ba	0.2270	-0.0005	-0.0010
I	1.6364	1.6895	-1.3679	I	1.7712	1.9276	-1.5771	I	0.0273	-3.1650	-0.0568	O	0.1495	2.9540	0.2946
Mg	0.1506	0.1652	0.3754	Ca	-0.0596	0.0684	0.0028	Sr	0.0024	0.0150	0.0018	Si	0.0297	3.4810	-1.2668
O	-1.6170	1.8423	0.1722	O	-1.6987	2.0076	0.2144	O	2.8004	-0.0196	-0.8233	Si	0.0943	3.1663	1.9323
O	0.0542	1.6447	2.0585	O	-0.0282	1.7539	2.1059	O	-2.1659	-0.0394	1.9663	O	0.1015	2.0696	-2.1232
O	1.9455	-1.1437	0.9044	O	2.0331	-1.2272	0.8586	O	0.1820	0.0688	2.9481	C	-1.6052	4.3216	-1.5422
O	-2.2763	0.5464	-1.9992	O	-2.0695	0.4554	-1.7566	O	1.1028	0.0385	-2.7216	C	1.4961	4.5461	-1.6854
O	0.8691	-1.9906	-1.2938	O	0.8907	-1.9633	-1.3040	O	-1.4433	0.0488	-2.5822	O	0.1455	1.6135	2.4937
Si	-1.2001	2.6397	1.5514	Si	-1.2336	2.7758	1.6029	O	2.3985	0.0395	1.6911	C	1.6052	4.0909	2.4988
Si	-2.6694	1.8578	-1.1264	Si	-2.6805	1.8529	-1.1075	Si	3.6298	-0.0549	0.5997	C	-1.5035	3.9794	2.4266
Si	0.9967	1.4755	3.4396	Si	0.9478	1.4713	3.4289	Si	2.7291	-0.0192	-2.4699	Si	0.0050	1.1787	-3.5116
Si	1.9991	-2.4259	-0.1920	Si	2.0608	-2.4753	-0.2395	Si	-1.3954	0.0631	3.4190	H	-1.7264	4.6188	-2.5871
Si	2.9991	-0.6595	2.1244	Si	2.9909	-0.6656	2.1121	Si	-3.5200	-0.1616	1.0354	H	-1.6927	5.2251	-0.9335
Si	-2.4694	-0.6843	-3.0683	Si	-2.4002	-0.6698	-2.9418	Si	1.8035	0.1265	3.2251	H	-2.4273	3.6518	-1.2804
Si	0.3030	-2.3459	-2.8161	Si	0.3540	-2.3700	-2.8366	Si	-0.2282	0.0670	-3.6918	H	2.4278	4.0062	-1.5032
C	-0.5716	4.3509	1.1909	C	-0.5621	4.4622	1.2099	Si	-3.0213	0.0088	-2.1185	H	1.5082	5.4572	-1.0819
C	-2.5846	2.6311	2.7937	C	-2.6379	2.8073	2.8229	C	4.5366	-1.6684	0.7843	H	1.4797	4.8489	-2.7355
C	-2.3879	3.4069	-2.1209	C	-2.4372	3.2884	-2.2611	C	4.7392	1.4330	0.7416	Si	0.0361	0.4645	3.6760
C	-4.4162	1.7280	-0.4867	C	-4.4478	1.6295	-0.5713	C	3.4384	-1.5981	-3.1506	H	2.5135	3.5691	2.1894
O	2.1530	0.4107	3.0181	O	2.0647	0.4013	2.9185	C	3.5442	1.5087	-3.1517	H	1.6244	4.1889	3.5872
C	-0.0204	0.7772	4.8285	C	-0.0520	0.7201	4.8036	C	-1.7576	-1.4434	4.4502	H	1.6332	5.0992	2.0781
C	1.7852	3.1078	3.8666	C	1.8016	3.0511	3.9295	C	-1.8251	1.6582	4.2737	H	-1.5798	4.9876	2.0113

C	3.6921	-2.5167	-0.9713	C	3.7194	-2.5787	-1.0823	O	-2.8773	-0.0676	-0.4781	H	-1.5821	4.0675	3.5132
C	1.5412	-4.0158	0.6558	C	1.5656	-4.0731	0.5665	C	-4.6573	1.2778	1.3550	H	-2.3565	3.3984	2.0688
C	3.4429	-2.1109	3.2054	C	3.4225	-2.0783	3.2496	C	-4.3326	-1.8146	1.2903	O	0.1121	-0.3696	-2.9456
C	4.4936	0.1808	1.4082	C	4.4895	0.1910	1.4238	C	2.2715	1.7459	4.0106	C	1.4624	1.5540	-4.6048
O	-1.1471	-1.6350	-2.9832	O	-1.0853	-1.6295	-2.9993	C	2.3429	-1.3543	4.2166	C	-1.6371	1.4492	-4.3400
C	-2.5912	0.0266	-4.7904	C	-2.6036	0.1898	-4.5834	C	-0.2932	-1.4646	-4.7463	O	0.0675	-0.9397	2.8070
C	-3.9660	-1.6912	-2.6031	C	-3.8852	-1.6790	-2.4623	C	-0.2745	1.6433	-4.6789	C	1.5258	0.5559	4.7856
C	0.0771	-4.1940	-2.9627	C	0.1029	-4.2137	-2.9441	C	-3.8825	1.5796	-2.6204	C	-1.5796	0.6223	4.5831
C	1.4887	-1.6787	-4.0878	C	1.5465	-1.7251	-4.1076	C	-3.8505	-1.5252	-2.7672	Si	0.0754	-2.0124	-3.1165
H	0.2420	4.3106	0.4642	H	0.2471	4.3833	0.4808	H	3.8440	-2.5077	0.6911	H	1.4550	2.5972	-4.9304
H	-0.2049	4.8423	2.0948	H	-0.1741	4.9569	2.1034	H	5.0274	-1.7367	1.7583	H	1.4549	0.9305	-5.5024
H	-1.3679	4.9766	0.7793	H	-1.3401	5.1058	0.7905	H	5.3099	-1.7791	0.0196	H	2.3986	1.3715	-4.0728
H	-2.9138	1.6107	2.9980	H	-2.9994	1.7961	3.0206	H	5.5179	1.4223	-0.0254	H	-2.4541	1.2167	-3.6534
H	-3.4407	3.1971	2.4179	H	-3.4729	3.4008	2.4417	H	5.2393	1.4621	1.7129	H	-1.7423	0.8150	-5.2239
H	-2.2809	3.0937	3.7360	H	-2.3306	3.2532	3.7722	H	4.1621	2.3530	0.6282	H	-1.7504	2.4861	-4.6665
H	-2.6302	4.3072	-1.5504	H	-2.7498	4.2250	-1.7917	H	2.9262	-2.4621	-2.7216	Si	-0.0121	-2.5822	2.6497
H	-3.0128	3.4080	-3.0177	H	-3.0219	3.1704	-3.1764	H	4.5036	-1.6857	-2.9212	H	1.5097	-0.2372	5.5377
H	-1.3436	3.4710	-2.4321	H	-1.3837	3.3773	-2.5337	H	3.3338	-1.6441	-4.2376	H	1.5645	1.5100	5.3174
H	-4.5342	0.8348	0.1295	H	-4.5407	0.7725	0.0987	H	3.0894	2.4063	-2.7272	H	2.4446	0.4539	4.2042
H	-5.1273	1.6666	-1.3148	H	-5.1079	1.4693	-1.4275	H	3.4460	1.5585	-4.2391	H	-2.4172	0.5664	3.8843
H	-4.6931	2.5969	0.1156	H	-4.8107	2.5164	-0.0453	H	4.6122	1.5263	-2.9190	H	-1.6431	1.5737	5.1169
H	-0.7812	1.4805	5.1743	H	-0.7911	1.4209	5.1996	H	-2.8178	-1.4992	4.7100	H	-1.6989	-0.1751	5.3212
H	0.6206	0.5372	5.6808	H	0.5979	0.4219	5.6304	H	-1.1927	-1.4291	5.3857	O	0.0961	-2.5319	-1.5487
H	-0.5257	-0.1365	4.5086	H	-0.5841	-0.1647	4.4467	H	-1.4933	-2.3526	3.9063	C	-1.5043	-2.5400	-3.9449
H	2.3325	3.5169	3.0151	H	2.3562	3.4795	3.0921	H	-1.2646	1.7699	5.2056	C	1.6073	-2.5915	-3.9966
H	2.4925	2.9736	4.6890	H	2.5100	2.8578	4.7391	H	-2.8880	1.7018	4.5246	O	0.0536	-2.7824	1.0115
H	1.0491	3.8487	4.1870	H	1.0931	3.8019	4.2879	H	-1.5910	2.5104	3.6321	C	-1.6327	-3.2130	3.3082
H	3.7128	-3.2992	-1.7351	H	3.7182	-3.3487	-1.8585	H	-5.0257	1.2672	2.3841	C	1.4726	-3.3688	3.4468
H	4.4665	-2.7642	-0.2415	H	4.5057	-2.8447	-0.3713	H	-5.5294	1.2499	0.6972	Si	0.0385	-3.6877	-0.3697
H	3.9569	-1.5713	-1.4482	H	3.9853	-1.6267	-1.5458	H	-4.1372	2.2236	1.1902	H	-1.5732	-3.6292	-4.0052
H	2.2745	-4.2961	1.4148	H	2.2874	-4.3679	1.3318	H	-3.6231	-2.6202	1.0885	H	-1.5657	-2.1524	-4.9650
H	1.4905	-4.8315	-0.0702	H	1.5113	-4.8836	-0.1643	H	-5.1904	-1.9413	0.6249	H	-2.3709	-2.1744	-3.3896
H	0.5647	-3.9233	1.1339	H	0.5864	-3.9695	1.0388	H	-4.6936	-1.9268	2.3159	H	2.5021	-2.2625	-3.4635
H	2.5502	-2.6012	3.5985	H	2.5230	-2.5786	3.6143	H	1.9297	2.5806	3.3947	H	1.6531	-2.1955	-5.0142
H	4.0383	-1.7637	4.0540	H	3.9756	-1.7066	4.1159	H	3.3545	1.8310	4.1300	H	1.6353	-3.6818	-4.0671
H	4.0380	-2.8583	2.6755	H	4.0521	-2.8243	2.7578	H	1.8236	1.8484	5.0026	H	-1.7222	-3.0305	4.3822
H	5.1341	-0.5155	0.8638	H	5.1622	-0.5088	0.9228	H	2.0546	-2.2800	3.7141	H	-1.7318	-4.2901	3.1505
H	5.0900	0.6254	2.2093	H	5.0524	0.6771	2.2248	H	1.8868	-1.3508	5.2099	H	-2.4679	-2.7175	2.8082
H	4.1943	0.9727	0.7187	H	4.1941	0.9524	0.6984	H	3.4270	-1.3663	4.3558	H	2.3949	-2.9672	3.0212
H	-1.7052	0.6205	-5.0267	H	-1.7248	0.7926	-4.8223	H	0.5519	-1.5090	-5.4384	H	1.4738	-4.4520	3.2997
H	-3.4661	0.6733	-4.8944	H	-3.4779	0.8454	-4.5945	H	-1.2065	-1.4917	-5.3464	H	1.4873	-3.1851	4.5242
H	-2.6748	-0.7660	-5.5383	H	-2.7367	-0.5443	-5.3821	H	-0.2692	-2.3607	-4.1226	C	-1.5501	-4.6480	-0.4885
H	-4.0866	-2.5447	-3.2748	H	-4.0422	-2.4922	-3.1755	H	-0.2370	2.5094	-4.0148	C	1.5606	-4.7523	-0.4472
H	-4.8821	-1.0969	-2.6523	H	-4.7970	-1.0772	-2.4407	H	-1.1886	1.7105	-5.2745	H	-2.4095	-3.9758	-0.4390
H	-3.8632	-2.0721	-1.5845	H	-3.7426	-2.1133	-1.4702	H	0.5706	1.7071	-5.3693	H	-1.6379	-5.3721	0.3257
H	-0.6111	-4.5635	-2.1994	H	-0.5834	-4.5615	-2.1694	H	-3.3521	2.4486	-2.2243	H	-1.6067	-5.2046	-1.4274
H	1.0226	-4.7325	-2.8579	H	1.0416	-4.7637	-2.8413	H	-4.9093	1.6084	-2.2473	H	1.6060	-5.3110	-1.3855
H	-0.3378	-4.4509	-3.9407	H	-0.3237	-4.4780	-3.9151	H	-3.9277	1.6761	-3.7083	H	1.5780	-5.4804	0.3681
H	1.0996	-1.8345	-5.0973	H	1.1487	-1.8723	-5.1150	H	-3.8816	-1.5260	-3.8598	H	2.4606	-4.1379	-0.3734
H	2.4633	-2.1694	-4.0281	H	2.5110	-2.2354	-4.0547	H	-4.8810	-1.6013	-2.4113	I	-3.1486	0.1170	-0.0102
H	1.6428	-0.6079	-3.9392	H	1.7219	-0.6574	-3.9580	H	-3.3122	-2.4180	-2.4417	I	3.5633	-0.1520	0.0202

Table S14. Cartesian coordinates of $MD_n(GaI_4)_2$ (M= Sr, Ba; n=6,7) obtained at level B3LYP/dhf-TZVP.

$SrD_6(GaI_4)_2$				$BaD_6(GaI_4)_2$				$SrD_7(GaI_4)_2$				$BaD_7(GaI_4)_2$			
Sr	0.3513	0.0083	-1.1535	Si	-0.0269	-3.1717	0.3590	Sr	-0.0066	0.0141	-0.0556	Ba	0.0742	0.0161	-0.1911
Si	-0.6569	-3.0444	0.1654	Si	0.1230	3.2895	0.3843	O	0.3717	2.8144	-0.0930	O	0.3856	2.9356	-0.1332
Si	1.4779	3.0750	0.0590	O	1.2730	-2.1986	-0.0266	Si	-1.1575	3.4376	0.0688	Si	-1.1740	3.4961	-0.0297
O	-1.5139	-1.6509	-0.1731	O	-1.1855	2.3121	0.0691	Si	2.0024	3.1148	-0.1759	Si	2.0247	3.1879	-0.0927
O	2.3156	1.6837	-0.3359	O	-1.2828	-2.1273	0.0248	O	-2.0099	2.0187	0.0393	O	-2.0071	2.0613	-0.0595
O	0.8811	-2.4987	-0.1766	O	1.3741	2.2519	0.0246	C	-1.3639	4.2937	1.7026	C	-1.4484	4.3751	1.5823
O	-0.0738	2.5170	-0.1493	C	-0.0057	-3.7061	2.1283	C	-1.5956	4.5099	-1.3820	C	-1.5912	4.5196	-1.5204
C	-1.1460	-4.3870	-1.0198	C	-0.0826	-4.5932	-0.8356	O	2.5785	1.5730	-0.0936	O	2.5802	1.6278	-0.0956

C	-0.8346	-3.5910	1.9229	C	0.1417	4.7018	-0.8219	C	2.4342	3.9043	-1.8006	C	2.5750	4.0754	-1.6286
C	1.8096	3.6370	1.7918	C	0.1664	3.8587	2.1470	C	2.5630	4.1130	1.2892	C	2.5142	4.0493	1.4783
C	1.8668	4.4132	-1.1680	Si	2.8004	-1.6252	0.3091	Si	-3.4447	1.1865	0.0522	Si	-3.4247	1.1970	0.0263
Si	-2.7821	-0.5957	0.0701	Si	-2.7073	1.7293	0.4148	H	-2.3912	4.6457	1.8275	H	-2.4916	4.6842	1.6860
Si	3.5925	0.6242	-0.2132	Si	-2.7808	-1.4924	0.3817	H	-0.7124	5.1681	1.7745	H	-0.8358	5.2779	1.6478
Si	2.5361	-2.4385	-0.0578	Si	2.8755	1.6015	0.3344	H	-1.1365	3.6291	2.5381	H	-1.2042	3.7371	2.4342
Si	-1.7197	2.4659	0.0994	H	0.0383	-2.8616	2.8177	H	-1.5120	3.9697	-2.3272	H	-1.4383	3.9587	-2.4450
H	-1.0662	-4.0738	-2.0609	H	0.8560	-4.3474	2.3291	H	-0.9442	5.3863	-1.4310	H	-0.9735	5.4204	-1.5622
H	-2.1796	-4.6922	-0.8371	H	-0.8995	-4.2877	2.3675	H	-2.6217	4.8776	-1.2966	H	-2.6350	4.8427	-1.4940
H	-0.5179	-5.2712	-0.8802	H	-0.9800	-5.1971	-0.6799	Si	3.8215	0.4871	0.0072	Si	3.7816	0.4898	-0.0053
H	-0.1965	-4.4591	2.1109	H	0.7808	-5.2482	-0.6944	H	2.0850	3.2990	-2.6394	H	2.2696	3.5342	-2.5264
H	-1.8629	-3.9032	2.1251	H	-0.0810	-4.2530	-1.8730	H	3.5155	4.0287	-1.9015	H	3.6622	4.1843	-1.6530
H	-0.5728	-2.8150	2.6410	H	0.1227	4.3536	-1.8564	H	1.9837	4.8963	-1.8890	H	2.1463	5.0797	-1.6773
H	1.6036	2.8645	2.5321	H	-0.7235	5.3522	-0.6706	H	2.1223	5.1131	1.2794	H	2.0896	5.0552	1.5249
H	2.8532	3.9467	1.8965	H	1.0381	5.3126	-0.6885	H	3.6487	4.2402	1.2802	H	3.6000	4.1530	1.5462
H	1.1915	4.5073	2.0285	H	1.0635	4.4548	2.3332	H	2.2873	3.6299	2.2284	H	2.1724	3.4966	2.3557
H	1.2409	5.2909	-0.9869	H	-0.6936	4.4986	2.3614	O	-2.8239	-0.3477	-0.0452	O	-2.8168	-0.3455	-0.0821
H	2.9080	4.7307	-1.0650	H	0.1562	3.0311	2.8586	C	-4.4682	1.5909	-1.4404	C	-4.5172	1.5758	-1.4228
H	1.7118	4.0952	-2.1988	O	2.5862	-0.0011	-0.0095	C	-4.3611	1.4421	1.6434	C	-4.2613	1.4643	1.6582
O	-1.9947	0.8483	-0.2263	C	3.9897	-2.3330	-0.9297	O	2.9903	-0.9314	0.0472	O	2.8884	-0.9055	-0.0247
C	-3.4567	-0.6930	1.7897	C	3.3079	-1.9310	2.0615	C	4.8951	0.5799	-1.5087	C	4.8804	0.5824	-1.5003
C	-4.0609	-0.8606	-1.2481	O	-2.5051	0.1191	0.0400	C	4.7744	0.7332	1.5846	C	4.7174	0.6462	1.5920
O	2.7822	-0.8212	-0.4084	C	-3.1706	1.9933	2.1880	Si	-3.0260	-1.9927	-0.0797	Si	-3.0335	-1.9937	-0.0794
C	4.7345	0.8751	-1.6552	C	-3.9325	2.4743	-0.7654	H	-4.8042	2.6309	-1.4106	H	-4.8524	2.6159	-1.3944
C	4.4389	0.7374	1.4306	C	-3.2642	-1.7669	2.1440	H	-5.3636	0.9648	-1.4752	H	-5.4119	0.9481	-1.4076
C	3.3137	-3.4737	-1.3876	C	-4.0257	-2.1542	-0.8278	H	-3.9154	1.4445	-2.3703	H	-4.0042	1.4140	-2.3727
C	3.1344	-2.8890	1.6362	C	4.0919	2.2874	-0.8901	H	-3.7487	1.2245	2.5203	H	-3.6030	1.2616	2.5050
C	-2.1766	2.9293	1.8305	C	3.4051	1.8589	2.0905	H	-5.2486	0.8052	1.6841	H	-5.1386	0.8196	1.7532
C	-2.5845	3.4978	-1.1781	H	3.6677	-2.1433	-1.9554	H	-4.7045	2.4765	1.7287	H	-4.6100	2.4963	1.7503
H	-2.6820	-0.5772	2.5481	H	4.9860	-1.9013	-0.8049	Si	2.7482	-2.5546	0.0926	Si	2.7396	-2.5550	0.0300
H	-4.2103	0.0814	1.9536	H	4.0831	-3.4143	-0.8007	H	5.6710	-0.1899	-1.4892	H	5.6271	-0.2160	-1.4869
H	-3.9453	-1.6566	1.9550	H	3.3841	-3.0031	2.2589	H	5.4000	1.5471	-1.5740	H	5.4219	1.5315	-1.5282
H	-4.5242	-1.8453	-1.1483	H	4.2944	-1.5008	2.2543	H	4.3062	0.4442	-2.4176	H	4.3069	0.4930	-2.4247
H	-4.8570	-0.1156	-1.1723	H	2.6072	-1.5083	2.7829	H	4.1155	0.6997	2.4544	H	4.0471	0.5942	2.4519
H	-3.6341	-0.7919	-2.2513	H	-2.4529	1.5483	2.8790	H	5.2899	1.6969	1.5869	H	5.2571	1.5955	1.6388
H	4.2009	0.8131	-2.6062	H	-4.1532	1.5622	2.3966	H	5.5348	-0.0425	1.7069	H	5.4575	-0.1522	1.6917
H	5.5249	0.1205	-1.6634	H	-3.2368	3.0621	2.4076	O	-1.4235	-2.4259	-0.0742	O	-1.4456	-2.4833	-0.1158
H	5.2164	1.8546	-1.6057	H	-4.0151	3.5531	-0.6110	C	-3.9000	-2.5959	1.4401	C	-3.8677	-2.5516	1.4792
H	4.9178	1.7131	1.5466	H	-4.9256	2.0447	-0.6109	C	-3.8578	-2.5309	-1.6467	C	-3.9238	-2.5396	-1.6106
H	5.2235	-0.0188	1.5157	H	-3.6506	2.3041	-1.8060	O	1.0883	-2.6176	0.0366	O	1.0904	-2.7189	-0.0396
H	3.7409	0.6002	2.2577	H	-3.3782	-2.8341	2.3499	C	3.3769	-3.2705	1.6882	C	3.3934	-3.2133	1.6383
H	3.0817	-4.5318	-1.2409	H	-4.2279	-1.2978	2.3586	C	3.4834	-3.3751	-1.4047	C	3.5320	-3.3309	-1.4602
H	4.4020	-3.3727	-1.3671	H	-2.5329	-1.3713	2.8499	Si	-0.2501	-3.5950	-0.0172	Si	-0.2778	-3.6600	-0.0364
H	2.9657	-3.1870	-2.3812	H	-3.7277	-1.9707	-1.8617	H	-3.9771	-3.6864	1.4334	H	-3.9557	-3.6411	1.5008
H	2.6661	-2.2843	2.4137	H	-5.0024	-1.6895	-0.6707	H	-4.9196	-2.2034	1.4794	H	-4.8812	-2.1464	1.5414
H	4.2184	-2.7679	1.7100	H	-4.1527	-3.2323	-0.7006	H	-3.3902	-2.3034	2.3599	H	-3.3266	-2.2442	2.3761
H	2.9136	-3.9394	1.8443	H	4.2385	3.3587	-0.7297	H	-3.3227	-2.1950	-2.5370	H	-3.4069	-2.2351	-2.5227
H	-1.9323	3.9787	2.0154	H	5.0665	1.8042	-0.7843	H	-4.8774	-2.1399	-1.6982	H	-4.9344	-2.1239	-1.6400
H	-3.2519	2.8180	1.9910	H	3.7565	2.1445	-1.9188	H	-3.9285	-3.6208	-1.6918	H	-4.0216	-3.6282	-1.6312
H	-1.6576	2.3290	2.5785	H	2.6957	1.4432	2.8078	H	4.4621	-3.1609	1.7611	H	4.4687	-3.0377	1.7254
H	-2.3133	3.2019	-2.1924	H	4.3778	1.3923	2.2675	H	3.1534	-4.3378	1.7617	H	3.2345	-4.2918	1.7158
H	-3.6692	3.4058	-1.0763	H	3.5185	2.9252	2.3028	H	2.9287	-2.7720	2.5495	H	2.9035	-2.7367	2.4898
H	-2.3344	4.5549	-1.0562	I	-2.4354	-2.3692	6.2957	H	3.0923	-2.9422	-2.3274	H	3.1234	-2.9193	-2.3853
I	0.6119	0.0338	3.0866	Ga	-0.1357	-1.1830	6.3331	H	3.2703	-4.4469	-1.4161	H	3.3726	-4.4122	-1.4710
Ga	-0.1962	-0.0061	5.6912	I	0.0960	0.1352	3.9878	H	4.5706	-3.2615	-1.4129	H	4.6122	-3.1632	-1.4626
I	-1.8515	-1.9770	5.8957	I	1.8051	-2.8942	6.3642	C	-0.3950	-4.6067	1.5332	C	-0.4103	-4.6113	1.5515
I	-1.3350	2.2677	6.1237	I	0.0203	0.5751	8.1996	C	-0.2730	-4.6173	-1.5665	C	-0.3340	-4.7293	-1.5519
I	1.9479	-0.3450	7.0605	Ba	0.0220	0.0552	-1.3477	H	-0.4032	-3.9785	2.4262	H	-0.4132	-3.9497	2.4204
I	1.3536	-0.0164	-7.5685	I	2.3660	0.0947	-4.2457	H	0.4369	-5.3105	1.6220	H	0.4233	-5.3098	1.6614
Ga	-0.2570	-0.0092	-5.6006	Ga	-0.0384	0.1198	-5.3227	H	-1.3155	-5.1960	1.5300	H	-1.3307	-5.2001	1.5777
I	0.2999	-2.0255	-3.9476	I	-1.2155	-1.9627	-4.2186	H	-1.1944	-5.2018	-1.6316	H	-1.2548	-5.3176	-1.5780
I	0.2944	2.0198	-3.9584	I	-1.1948	2.1848	-4.1616	H	0.5597	-5.3252	-1.5866	H	0.5009	-5.4349	-1.5678
I	-2.7562	-0.0069	-6.1257	I	-0.0805	0.1532	-7.8456	H	-0.2089	-3.9932	-2.4601	H	-0.2923	-4.1344	-2.4667
								I	0.6843	0.1780	3.1832	I	0.7375	0.1906	3.2593
								Ga	-0.8252	-0.1311	5.4791	Ga	-0.7669	-0.1675	5.5316
								I	-2.0076	-2.4096	5.2760	I	-1.9379	-2.4517	5.2911
								I	-2.4570	1.8570	5.4941	I	-2.4299	1.7979	5.5693
								I	0.9288	-0.0663	7.3351	I	0.9625	-0.1150	7.4148
								I	0.9186	-0.1123	-3.2464	I	1.1408	-0.1029	-3.5448

								Ga	-0.6755	-0.0605	-5.4824	Ga	-0.6745	-0.1731	-5.5809
								I	-1.9038	-2.3211	-5.5047	I	-1.8458	-2.4644	-5.4172
								I	-2.2579	1.9503	-5.1632	I	-2.2914	1.7921	-5.1310
								I	0.9596	0.2414	-7.4232	I	0.7098	0.1208	-7.7075

Table S15. Cartesian coordinates of $MD_n(GaI_4)_2H_2O$ (M= Sr, Ba; n=6,7) obtained at level B3LYP/dhf-TZVP.

$SrD_6(GaI_4)_2H_2O$				$BaD_6(GaI_4)_2H_2O$				$SrD_7(GaI_4)_2H_2O$				$BaD_7(GaI_4)_2H_2O$			
I	-0.4454	1.0027	4.4155	I	-2.4118	-1.7882	4.3079	I	13.6194	10.3435	6.7518	I	-2.2287	3.9085	0.1652
Ga	0.3119	-1.2742	5.5629	Ga	-0.1486	-1.4241	5.5936	Ga	12.8806	10.4661	9.3071	Ga	-2.8535	3.9948	2.7484
I	2.7720	-1.0805	6.2408	I	0.4698	1.0810	5.0568	I	14.3562	12.1631	10.5454	I	-1.1413	5.4539	3.9742
I	0.0850	-2.9081	3.4747	I	1.5668	-2.8178	4.1707	I	13.5138	7.9909	10.0605	I	-2.4968	1.4546	3.4604
I	-1.3196	-1.9393	7.3970	I	-0.2218	-1.9721	8.0607	I	10.3521	10.8247	9.4832	I	-5.2942	4.6589	3.0473
I	2.1656	1.2602	-4.2827	I	2.1258	1.7256	-4.4499	I	19.9562	4.3258	5.5393	I	4.2630	-2.4446	-1.1118
Ga	0.0987	0.9044	-5.9091	Ga	0.1617	1.0569	-6.0878	Ga	19.0429	2.7699	3.5650	Ga	3.3556	-3.9762	-3.0919
H	0.7777	0.5998	-2.0241	H	0.7681	0.6916	-2.1506	H	17.6223	5.3286	5.9519	H	1.9332	-1.3553	-0.7481
I	0.1380	-1.5007	-6.8187	I	0.4441	-1.4216	-6.7469	I	19.9002	0.3825	3.9421	I	4.2186	-6.3629	-2.7671
I	-2.0461	1.2100	-4.3772	I	-2.0469	1.3126	-4.6600	I	16.3733	2.7251	3.7222	I	0.6964	-4.0188	-2.9141
I	0.1133	2.7186	-7.7083	I	0.0993	2.6770	-8.0687	I	19.6971	3.8681	1.3296	I	3.9928	-2.8729	-5.3217
O	0.0060	0.4111	-1.4576	O	0.0134	0.4171	-1.6017	O	16.6467	5.4827	5.9137	O	0.9679	-1.2057	-0.8017
H	-0.7379	0.5501	-2.0736	H	-0.7275	0.5284	-2.2217	H	16.3467	4.7848	5.2819	H	0.6769	-1.9256	-1.3972
Sr	-0.0569	-0.2591	1.1243	Ba	-0.0289	-0.4357	1.6647	Sr	15.2791	7.2124	7.0426	Ba	-0.5547	0.6210	0.4424
Si	2.3974	2.0579	0.9260	Si	2.4628	1.9922	0.8136	O	17.7314	8.5629	8.0535	O	2.0493	1.7764	1.3191
Si	-2.4659	-2.1474	-0.3121	Si	-2.4561	-2.0804	-0.3948	O	13.3884	5.1543	6.9300	O	-2.4639	-1.6714	0.3482
O	2.4611	0.3961	0.7474	O	2.5270	0.3390	0.6233	O	15.0466	4.8187	8.8435	O	-0.7186	-1.8408	2.2132
O	-2.5491	-0.6088	0.3415	O	-2.5557	-0.5776	0.3208	O	17.0503	8.8568	5.6191	O	1.3472	2.3343	-1.0741
O	0.7523	2.2967	0.9913	O	0.8404	2.2270	1.1069	O	15.1334	7.9621	4.2076	O	-0.6327	1.4716	-2.4485
O	-0.8262	-2.4172	-0.2449	O	-0.8548	-2.4642	-0.1303	O	17.0415	6.3724	9.1508	O	1.2578	-0.2676	2.6283
C	3.1533	2.9315	-0.5230	C	3.0376	2.9037	-0.6920	Si	18.1381	7.6106	9.3529	Si	2.4225	0.9097	2.6839
C	3.1735	2.5282	2.5421	C	3.4358	2.4570	2.3250	Si	18.1631	9.4441	6.7136	Si	2.5035	2.7346	0.0415
C	-3.3441	-3.3339	0.8119	C	-3.5213	-3.2841	0.5353	Si	13.7367	4.0757	8.1656	Si	-2.0103	-2.6676	1.5968
C	-3.1035	-2.1913	-2.0497	C	-2.8850	-2.0324	-2.1957	Si	12.3024	5.4060	5.6770	Si	-3.3655	-1.3536	-1.0045
Si	3.0910	-1.0697	0.2423	Si	3.0755	-1.1021	-0.0086	Si	16.4571	4.9117	9.7046	Si	0.6473	-1.7231	3.1390
Si	-3.1696	0.9202	0.6029	Si	-3.0990	0.9856	0.5124	Si	16.5470	8.8134	4.0276	Si	0.7717	2.3301	-2.6298
Si	-0.7031	3.0662	0.7393	Si	-0.6055	3.0203	0.8638	Si	13.7212	7.3856	3.5408	Si	-1.9701	0.7031	-3.0434
Si	0.6487	-2.9968	-0.7682	Si	0.6022	-3.0848	-0.6577	C	19.8866	6.9776	9.2259	C	4.1218	0.1650	2.5668
H	2.6790	2.6722	-1.4709	H	2.4601	2.6692	-1.5866	C	17.8340	8.5307	10.9382	C	2.2018	1.9736	4.1881
H	4.2172	2.6945	-0.6040	H	4.0850	2.6718	-0.9016	C	19.8998	9.0649	6.1546	C	4.1974	2.2788	-0.5729
H	3.0740	4.0141	-0.3927	H	2.9755	3.9825	-0.5260	C	17.8995	11.2559	7.0285	C	2.3581	4.5224	0.5182
H	3.0622	3.5994	2.7287	H	3.3353	3.5241	2.5388	C	14.1918	2.4022	7.4949	C	-1.4933	-4.3343	0.9631
H	4.2435	2.3051	2.5365	H	4.4987	2.2512	2.1744	C	12.3204	3.9896	9.3716	C	-3.3739	-2.7721	2.8558
H	2.7213	1.9937	3.3794	H	3.1075	1.9074	3.2086	O	13.0568	6.6098	4.8429	O	-2.4618	-0.1555	-1.7079
H	-2.9518	-3.2925	1.8294	H	-3.2451	-3.3459	1.5887	C	10.6818	6.0222	6.3495	C	-5.0236	-0.6797	-0.5076
H	-4.4138	-3.1126	0.8497	H	-4.5744	-2.9977	0.4774	C	12.1160	3.8661	4.6467	C	-3.4861	-2.8473	-2.1023
H	-3.2345	-4.3599	0.4519	H	-3.4304	-4.2844	0.1038	C	16.1120	4.9818	11.5334	C	0.2025	-1.6393	4.9422
H	-2.9737	-3.1902	-2.4752	H	-2.7671	-3.0258	-2.6370	C	17.6118	3.5215	9.2663	C	1.8330	-3.0999	2.7570
H	-4.1738	-1.9704	-2.0712	H	-3.9328	-1.7493	-2.3262	C	17.7608	7.8881	2.9687	C	1.9454	1.4464	-3.7631
H	-2.6036	-1.4798	-2.7088	H	-2.2826	-1.3365	-2.7795	C	16.2243	10.5351	3.3917	C	0.4057	4.0667	-3.1849
O	1.6835	-1.9137	-0.0329	O	1.6862	-2.0192	0.0282	C	12.6181	8.7859	3.0026	C	-3.2793	1.9349	-3.5143
C	4.0296	-1.8450	1.6394	C	4.3304	-1.8265	1.1528	C	14.0867	6.2048	2.1515	C	-1.5197	-0.4328	-4.4411
C	4.1019	-0.8975	-1.2998	C	3.7505	-0.9219	-1.7232	H	20.0598	6.4028	8.3057	H	4.2324	-0.4705	1.6864
O	-1.7636	1.7803	0.8309	O	-1.7010	1.7669	0.9738	H	20.1255	6.3205	10.0755	H	4.3358	-0.4450	3.4483
C	-4.1308	1.5409	-0.8536	C	-3.8121	1.6809	-1.0483	H	20.6120	7.8048	9.2485	H	4.8885	0.9426	2.5212
C	-4.1663	0.9093	2.1667	C	-4.3146	1.0563	1.9132	H	18.5064	9.3978	11.0192	H	2.9258	2.7925	4.1960
C	-0.7651	3.8863	-0.9217	C	-0.6702	3.8624	-0.7862	H	18.0202	7.8911	11.8132	H	2.3529	1.3941	5.1023
C	-1.0418	4.2664	2.1147	C	-0.8967	4.1915	2.2758	H	16.8001	8.8963	11.0036	H	1.2028	2.4118	4.2287
C	0.9327	-4.7043	-0.0981	C	0.8438	-4.7541	0.1206	H	20.0415	8.0008	5.9159	H	4.2639	1.2259	-0.8550
C	0.7961	-2.9354	-2.6120	C	0.7269	-3.1161	-2.5044	H	20.6380	9.3432	6.9214	H	4.9577	2.4740	0.1871
H	3.4239	-1.9353	2.5429	H	3.9543	-1.8901	2.1750	H	20.1462	9.6436	5.2509	H	4.4606	2.8759	-1.4500
H	4.3705	-2.8462	1.3642	H	4.6170	-2.8325	0.8363	H	16.8811	11.4608	7.3876	H	1.3588	4.7570	0.8907
H	4.9146	-1.2532	1.8871	H	5.2368	-1.2157	1.1642	H	18.0598	11.8473	6.1146	H	2.5604	5.1750	-0.3350
H	4.9720	-0.2603	-1.1214	H	4.6332	-0.2770	-1.7174	H	18.6065	11.6262	7.7858	H	3.0763	4.7764	1.3019
H	4.4780	-1.8755	-1.6120	H	4.0706	-1.8966	-2.1012	H	13.3334	1.9059	7.0193	H	-2.3371	-4.8606	0.5099

H	3.5395	-0.4748	-2.1339	H	3.0429	-0.5030	-2.4391	H	14.5337	1.7443	8.3086	H	-1.1245	-4.9610	1.7794
H	-3.5397	1.5693	-1.7699	H	-3.1080	1.6951	-1.8803	H	14.9948	2.4591	6.7461	H	-0.7036	-4.2621	0.2127
H	-4.4994	2.5516	-0.6589	H	-4.1532	2.7059	-0.8804	H	12.5906	3.3809	10.2475	H	-3.0559	-3.3522	3.7259
H	-5.0037	0.9086	-1.0355	H	-4.6840	1.1000	-1.3599	H	11.4351	3.5220	8.9149	H	-4.2543	-3.2678	2.4389
H	-5.0452	0.2683	2.0596	H	-5.2127	0.4810	1.6737	H	12.0298	4.9865	9.7308	H	-3.6757	-1.7822	3.2032
H	-4.5202	1.9148	2.4075	H	-4.6251	2.0883	2.0952	H	10.1952	5.2649	6.9816	H	-5.6075	-1.4323	0.0282
H	-3.5850	0.5488	3.0171	H	-3.9024	0.6593	2.8421	H	9.9850	6.2637	5.5331	H	-5.6037	-0.3759	-1.3825
H	-0.0146	4.6792	-0.9818	H	0.0882	4.6474	-0.8451	H	10.8159	6.9312	6.9543	H	-4.9224	0.1905	0.1445
H	-1.7399	4.3544	-1.0807	H	-1.6404	4.3429	-0.9340	H	13.0839	3.4863	4.2898	H	-2.5023	-3.2274	-2.3841
H	-0.5884	3.1935	-1.7440	H	-0.5054	3.1729	-1.6139	H	11.4871	4.0591	3.7644	H	-4.0319	-2.6141	-3.0202
H	-1.0070	3.7902	3.0951	H	-0.8759	3.6746	3.2368	H	11.6296	3.0621	5.2196	H	-4.0286	-3.6538	-1.6023
H	-2.0287	4.7206	1.9927	H	-1.8681	4.6827	2.1773	H	15.4566	5.8231	11.7978	H	-0.4785	-0.8115	5.1479
H	-0.3082	5.0768	2.1069	H	-0.1346	4.9747	2.2966	H	17.0456	5.0834	12.1068	H	1.0950	-1.5047	5.5587
H	0.2040	-5.4059	-0.5127	H	0.0945	-5.4649	-0.2371	H	15.6277	4.0542	11.8737	H	-0.2793	-2.5644	5.2692
H	1.9257	-5.0640	-0.3805	H	1.8271	-5.1615	-0.1285	H	17.8547	3.5040	8.1949	H	2.0999	-3.1287	1.6992
H	0.8575	-4.7398	0.9892	H	0.7679	-4.7039	1.2088	H	17.1712	2.5478	9.5291	H	1.4034	-4.0693	3.0221
H	0.6443	-1.9355	-3.0168	H	0.5697	-2.1356	-2.9533	H	18.5604	3.6047	9.8171	H	2.7571	-2.9896	3.3301
H	1.7849	-3.2753	-2.9300	H	1.7106	-3.4740	-2.8182	H	18.7233	8.4175	2.9092	H	2.8977	1.9783	-3.8312
H	0.0647	-3.5981	-3.0813	H	-0.0107	-3.8013	-2.9296	H	17.3900	7.7778	1.9387	H	1.5394	1.3822	-4.7758
								H	17.9616	6.8799	3.3558	H	2.1551	0.4305	-3.4245
								H	15.5232	11.0871	4.0331	H	-0.2660	4.5765	-2.4921
								H	15.8062	10.5046	2.3741	H	-0.0591	4.0721	-4.1742
								H	17.1586	11.1139	3.3364	H	1.3254	4.6534	-3.2566
								H	12.3694	9.4536	3.8394	H	-3.5432	2.5772	-2.6724
								H	11.6768	8.4020	2.5806	H	-4.1872	1.4278	-3.8516
								H	13.0965	9.3926	2.2187	H	-2.9411	2.5742	-4.3337
								H	14.5590	6.7263	1.3059	H	-1.1321	0.1372	-5.2897
								H	13.1637	5.7471	1.7667	H	-2.3959	-0.9810	-4.7969
								H	14.7636	5.3958	2.4593	H	-0.7608	-1.1634	-4.1553

Table S16. Cartesian coordinates of BaD_7H_2O obtained at level B3LYP/dhf-TZVP.

H	0.7808	-3.6170	0.0461
O	0.0105	-3.0338	0.0300
H	-0.7543	-3.6246	0.0216
Ba	0.0007	-0.2594	-0.0010
O	2.8995	-0.0168	-0.2933
O	-2.4738	0.0220	1.5124
O	-0.3588	0.1255	2.8794
O	1.5712	0.0829	-2.4348
O	-0.9299	0.1303	-2.7466
O	2.0268	0.0907	2.0686
Si	3.4867	0.1155	1.2627
Si	3.1626	0.1156	-1.9362
Si	-2.0088	0.1813	3.1081
Si	-3.6897	0.0855	0.3722
Si	1.1843	0.2308	3.5024
Si	0.4569	0.2295	-3.6681
Si	-2.5934	0.1725	-2.6458
C	4.5050	-1.3686	1.7033
C	4.3618	1.7282	1.5186
C	4.0784	-1.3650	-2.5697
C	3.9612	1.7317	-2.3627

C	-2.5829	-1.2708	4.1052
C	-2.5335	1.8196	3.7953
O	-2.7345	-0.0049	-0.9922
C	-4.6059	1.6945	0.4519
C	-4.7854	-1.4036	0.4991
C	1.4712	1.8844	4.2866
C	1.5461	-1.2040	4.6165
C	0.5769	-1.2055	-4.8337
C	0.5870	1.8846	-4.4928
C	-3.2522	1.8119	-3.2077
C	-3.3439	-1.2764	-3.5213
H	3.9607	-2.3042	1.5586
H	4.8244	-1.3288	2.7476
H	5.4123	-1.4140	1.0956
H	5.2778	1.7785	0.9248
H	4.6576	1.8475	2.5639
H	3.7411	2.5850	1.2484
H	3.5805	-2.3020	-2.3112
H	5.0919	-1.4022	-2.1624
H	4.1747	-1.3297	-3.6577
H	3.4036	2.5866	-1.9742
H	4.0443	1.8516	-3.4457
H	4.9764	1.7864	-1.9620
H	-3.6735	-1.2953	4.1720
H	-2.2040	-1.2171	5.1289
H	-2.2529	-2.2202	3.6783
H	-2.1409	1.9616	4.8053
H	-3.6220	1.8827	3.8688
H	-2.1910	2.6574	3.1844
H	-5.1594	1.7814	1.3901
H	-5.3404	1.7652	-0.3542
H	-3.9418	2.5578	0.3755
H	-4.2225	-2.3384	0.4558
H	-5.5186	-1.4195	-0.3114
H	-5.3481	-1.3982	1.4360
H	1.2527	2.7102	3.6061
H	2.5083	1.9878	4.6151
H	0.8456	2.0099	5.1738
H	1.3633	-2.1629	4.1270
H	0.9278	-1.1660	5.5169
H	2.5877	-1.1905	4.9470
H	1.5293	-1.1969	-5.3698
H	-0.2117	-1.1642	-5.5892
H	0.4942	-2.1637	-4.3164
H	0.5145	2.7094	-3.7808
H	-0.2062	2.0121	-5.2337
H	1.5355	1.9850	-5.0257
H	-2.8016	2.6491	-2.6707
H	-4.3346	1.8703	-3.0699
H	-3.0622	1.9584	-4.2739
H	-3.1725	-1.2160	-4.5989
H	-4.4264	-1.3046	-3.3735
H	-2.9344	-2.2267	-3.1724

4. References

[1] Sheldrick, G. M. Crystal structure refinement with SHELXL. *Acta Crystallogr., Sect. C: Cryst. Struct. Commun.*, 2015, **71**, 3–8.

[2] Sheldrick, G. M. SHELXT - Integrated space-group and crystal-structure determination. *Acta Crystallogr., Sect. A: Fundam. Crystallogr.*, 2015, **A71**, 3–8.

[3] Dolomanov, O. V.; Bourhis, L. J.; Gildea, R. J.; Howard, J. A. K.; Puschmann H., *OLEX2*: a complete structure solution, refinement and analysis program. *J. Appl. Crystallogr.*, 2009, **42**, 339–341.

[4] Lee, C.; Yang, W.; Parr, R. G. Development of the Colle-Salvetti correlation-energy formula into a functional of the electron density. *Phys. Rev. B* 1988, **37**, 785–789.

[5] Weigend, F.; Baldes, A. Segmented contracted basis sets for one- and two-component Dirac–Fock effective core potentials. *J. Chem. Phys*. 2010, **133**, 174102.

[6] a) Becke, A. D. Density-functional exchange-energy approximation with correct asymptotic behavior. *Phys. Rev. A* **1988**, 38, 3098–3109. b) Perdew, J. P. Density-functional approximation for the correlation energy of the inhomogeneous electron gas. *Phys. Rev. B* **1986**, *33*, 8822–8837.

[7] Klamt, A.; Schüürmann, G. COSMO: a new approach to dielectric screening in solvents with explicit expressions for the screening energy and its gradient. *J. Chem. Soc. Perkin Trans*. **1993**, 799–805.

[8] Preiss, U.; Slattery, J.M.; Krossing, I., In Silico Prediction of Molecular Volumes, Heat Capacities, and Temperature-Dependent Densities of Ionic Liquids. *Ind. Eng. Chem. Res*., 2009, **48**, 2290-2296.

[9] Wilcock, D.F. Vapor Pressure-Viscosity Relations in Methylpolysiloxanes, *J. Am. Chem. Soc.* 1946, **68**, 691-696.

[10] Jenkins, H. D. B.; Roobottom, H. K.; Passmore, J; Glasser, L., Relationships among Ionic Lattice Energies, Molecular (Formula Unit) Volumes, and Thermochemical Radii *Inorg. Chem.* 1999, **38**, 3609-3620.

Journal of Inorganic and General Chemistry
ZAAC
Zeitschrift für anorganische und allgemeine Chemie
DOI: 10.1002/zaac.201900297
ARTICLE

C–F Bond Cleavage Reactions with Beryllium, Magnesium, Gallium, Hafnium, and Thorium Halides

Fabian Dankert,[a] H. Lars Deubner,[b] Matthias Müller,[c] Magnus R. Buchner,[c] Florian Kraus,[b] and Carsten von Hänisch*[a]

Dedicated to Professor Bernd Harbrecht on the Occasion of his 70th Birthday

Abstract. The work describes unexpected stoichiometric C–F bond cleavage reactions of beryllium, magnesium, gallium, hafnium and thorium halides with *α,α,α*-trifluorotoluene. The reaction of $BeBr_2$ / $GaBr_3$ or $MgBr_2$ / $GaBr_3$ mixtures as well as neat GaI_3 with *α,α,α*-trifluorotoluene in the presence of $(OSi_2Me_4)_2$ (**I**) yields the carbenium ion containing compounds $[Ph\text{-}C(O_2Si_2Me_4)][GaX_4]$ (X = Br: **1**, X = I/F: **2**). Both compounds were successfully characterized and a defluorination type reaction under incorporation of a siloxy unit was observed. Compound **1** was also characterized by single-crystal X-ray diffraction analysis. The conversion of *α,α,α*-trifluorotoluene with BeI_2, HfI_4 or ThI_4 turned out to be a halodefluorination-type reaction with formation of *α,α,α*-triiodotoluene (**3**). An adequate NMR spectroscopic and the X-ray crystallographic characterization of **3** were performed for the first time.

Introduction

Fluorinated compounds are of high importance especially as pharmaceuticals, agrochemicals and functional materials.[1–5] Because of this, C–F bond formation and activation has evolved into an essential research area.[6–9]

From the chemists' point of view, however, this chemistry is synthetically challenging due to the fact that a C–F bond is the strongest one in organic chemistry. Both C–F bond formation as well as C–F bond cleavage needs innovative, best possible, simple (catalytic) systems to be achieved efficiently. With that being said, many review articles were recently published, giving an overview about latest findings in C–F bond activation.[6,7,10] So for example, *Ichikawa* and co-workers were very recently reviewing this topic and presented a wide ranged selection of transition metal C–F bond cleavage reactions.[10] All of these reactions combine the use of metal centers which are employed for catalytic and/or stoichiometric C–F bond activation. So far, a lot of different metal centers were used in several reaction protocols.

Therein, especially transition metals and lanthanides play a major role, but also main group elements found application.[8] Plenty of metal centers are used and to mention a few (non-exhaustive listing), there are examples of Pd^{2+},[15–18] Zr/Hf^{4+},[19–23] Ni^{2+},[24–28] Ag^{+},[29,30] Rh^{3+},[31–35] $Al^{1+/3+}$,[36–38] Ce^{3+},[39] Yb^{3+},[40] and $Ti^{3+/4+}$.[41,42] The mechanisms around the C-F activations are quite different in these examples. Whereas the hard ions Ti^{4+}, Zr^{4+}, Hf^{4+}, Al^{3+}, and Yb^{3+} mainly act as a *Lewis* acids which promote C–F activation, the other metal centers, especially Pd^{2+} and Ni^{2+} undergo more sophisticated mechanisms before such a bond is about to be broken. In general, C–F bond cleavage reactions can be divided into two-electron reduction by transition metals, single electron reductions (e.g. by low-valent metals) or fluoride abstraction (e.g. by strong Lewis-acids, no change in oxidation number).[8]

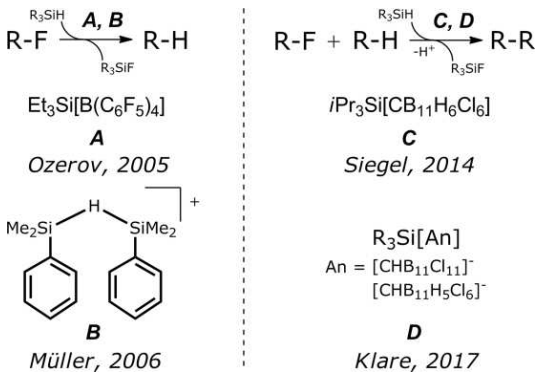

Scheme 1. C–F bond cleavage reactions employing silylium cations: Some eminent examples from past works, also in catalytic fashion.[11–14] The proton of the reactions depicted on the right is neutralized by different reagents. See cited works.

* Prof. Dr. C. von Hänisch
E-Mail: haenisch@chemie.uni-marburg.de
[a] Fachbereich Chemie and Wissenschaftliches Zentrum für Materialwissenschaften (WZMW)
Philipps-Universität Marburg
Hans-Meerwein Str. 4
35032 Marburg, Germany
[b] Fachbereich Chemie: Anorganische Chemie – Fluorchemie
Philipps-Universität Marburg
Hans-Meerwein Str. 4
35032 Marburg, Germany
[c] Fachbereich Chemie: Anorganische Chemie – Nachwuchsgruppe Berylliumchemie
Philipps-Universität Marburg
Hans-Meerwein Str. 4
35032 Marburg, Germany
© 2019 The Authors. Published by Wiley-VCH Verlag GmbH & Co. KGaA. · This is an open access article under the terms of the Creative Commons Attribution-NonCommercial License, which permits use, distribution and reproduction in any medium, provided the original work is properly cited and is not used for commercial purposes.

 © 2020 The Authors. Published by Wiley-VCH Verlag GmbH & Co. KGaA, Weinheim

However, all of them lead to deconstruction of chemically inert C–F bonds (see cited works above for details).

For a few years now, one of our main research topics is the synthesis and coordination ability of silicon-based ligands. Silyl ethers and related metal···silyl ether bonding are examined for quite some time now.[43–50] The research topic is of current interest giving insights into the Si–O bond as well as the *Lewis*-basicity of siloxanes.[51,52] Siloxanes coordinate especially to cations which are chemically hard such as the early s-block metal cations.[47,53–55] Applying the wrong reaction conditions or using tetravalent cations such as Th^{4+} or Hf^{4+}, however, no coordination of siloxanes but C–F bond cleavage reactions of the solvent occurs. These serendipitous C-F-cleavage reactions are presented herein. Putting the C–F bond cleavage into the context of siloxanes, the results presented herein might be of importance regarding the recent discussion around C–F bond activation with silylium cations. Silylium cations mainly found applications as effective catalysts in hydrodefluorination[11,12,56] reactions but recently also in C–H arylation under simultaneous C–F bond activation[13,14] (see Scheme 1 for eminent examples).

Results and Discussion

Our original goal was to obtain exclusively-silicon based crown ether analogues. As it is known from previous works, hybrid silicon-based crown ethers are sensitive towards *Lewis* acids and ring-opening polymerization reactions due to template effects.[57] Thus, we applied the reaction protocol which is represented in Scheme 2 (top). A suitable solvent here is *α,α,α*-trifluorotoluene which is polar, non-coordinating, and allows the heating of reaction mixtures up to 102 °C if necessary. Therefore, this solvent was already used successfully in the synthesis of complexes with silicon based crown ethers.[47,48,57] Applying the reaction conditions in Scheme 2 (bottom), however, we did not observe the formation of sila-crown complexes. To our surprise, the sila precursor as well as the solvent are cleaved to form the carbenium ion containing compound [Ph-C($O_2Si_2Me_4$)][$GaBr_4$] (**1**). The corresponding iodide/fluoride compound [Ph-C($O_2Si_2Me_4$)][GaX_4] (**2**, X = I/F) could be obtained by reaction of **I** with GaI_3. In these compounds the carbenium ion is embedded in a five-membered Si_2O_2C ring, which derives from $(OSi_2Me_4)_2$ (**I**). As presented, the observed reaction can be understood as a defluorination type reaction with substitution of the F atoms by a $Si_2Me_4O_2$ fragment. These unusual compounds are rare examples[58] of siloxane-stabilized carbenium ions. In the case of compound **1**, colorless platelets were obtained from DCM/*n*-pentane solution so that a crystallographic characterization of such a siloxane stabilized carbenium ion could be performed for the first time. In the case of compound **2**, a black oil is obtained. The NMR spectroscopic investigations of all NMR active nuclei give characteristic resonances. The carbenium ionic character of these compounds is supported by a ^{13}C NMR resonance of 180.3 ppm in the case of compound **1** and 182.8 ppm in the case of compound **2**. Furthermore, a ^{29}Si NMR chemical shift is observed for both compounds. With 37.1 ppm (**1**) and

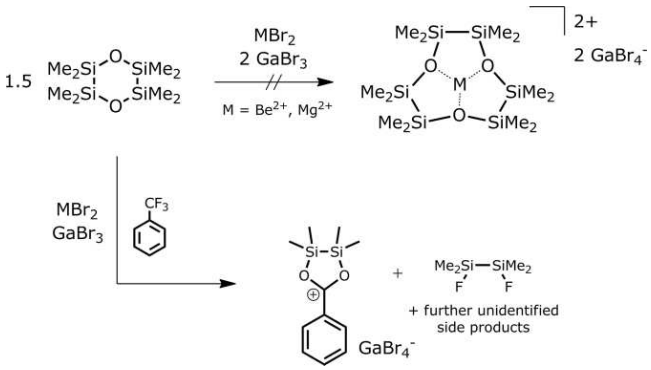

Scheme 2. Attempted pathway to obtain Si-based crown-ethers (top) and observed C–F bond cleavage (bottom).

38.5 ppm (**2**) a strong low-field shift is observed for the silicon-based part of the cationic structure as can be seen by comparing these species with **I** [$\delta(^{29}Si)$ = 3.6 ppm]. ^{19}F NMR spectroscopy of the solution of **2** shows high field signals at –169.72, –174.13, –175.85, –177.56, and –177.76 ppm. While the signals at –177.56 and –174.13 ppm are assigned to compound **II**[59] and an additional methylfluorosilane[60] respectively, the other three resonances exhibit line broadening, which is indicative for fluorine nuclei bound to quadrupolar nuclei like ^{69}Ga or ^{71}Ga. These chemical shifts also compare well with different gallium fluorides with a coordination number of four.[61,62] Furthermore no signal for $[GaF_4]^-$ (–149.7 ppm) could be observed via ^{19}F NMR spectroscopy.[62] Accordingly the signals at –169.72, –175.85, and –177.76 ppm are tentatively assigned to $[GaIF_3]^-$, $[GaI_2F_2]^-$, and $[GaI_3F]^-$, respectively, and the anionic species of **2** is best described as $[GaI_{4-x}F_x]^-$.

Figure 1 displays the ^{13}C NMR spectrum of compound **1** as an example. As determined by means of single-crystal X-ray diffraction analysis, compound **1** crystallizes in the monoclinic space group $P2_1/n$ (no. 14). The ionic structure in the solid reveals that the $[GaBr_4]^-$ ions are discrete and no direct contact with the C5 atom is observed. The closest Br–C5 contacts measure 348.4(3) pm. As a cause of CH–π interactions in the solid state, no fully planar molecular structure is observed for the cation. These interactions measure closest C···C atom distances of 346.0(5) pm and do also form a polymeric structure motif along [100]. The two planes constituted by the aryl ring as well as the disilane backbone are twisted against each other by 24.0(1)° (Figure 2).

For the silicon-based part of the structure, quite strained O–Si–Si angles are present forming this unprecedented five-membered ring. These angles measure 88.5(1)° and 88.7(1)° which are considerably smaller than those, for example, in hybrid silicon based crown ether analogues.[44,45,48] The O1–C5 and O2–C5 atom distances measure 128.1(5) and 128.8(5) pm and are only slightly longer than those in carboxylic acids such as benzoic acid, in which the C–O atom distances measure 124.9(1) and 125.0(1) pm.[63] Thus, a partial C–O double bond character and backbonding of the lone-pairs of the O1 and O2 atoms into the empty *p*-Orbital of the C5 atom is indicated. This also causes long silicon oxygen atom distances of

© 2020 The Authors. Published by Wiley-VCH Verlag GmbH & Co. KGaA, Weinheim

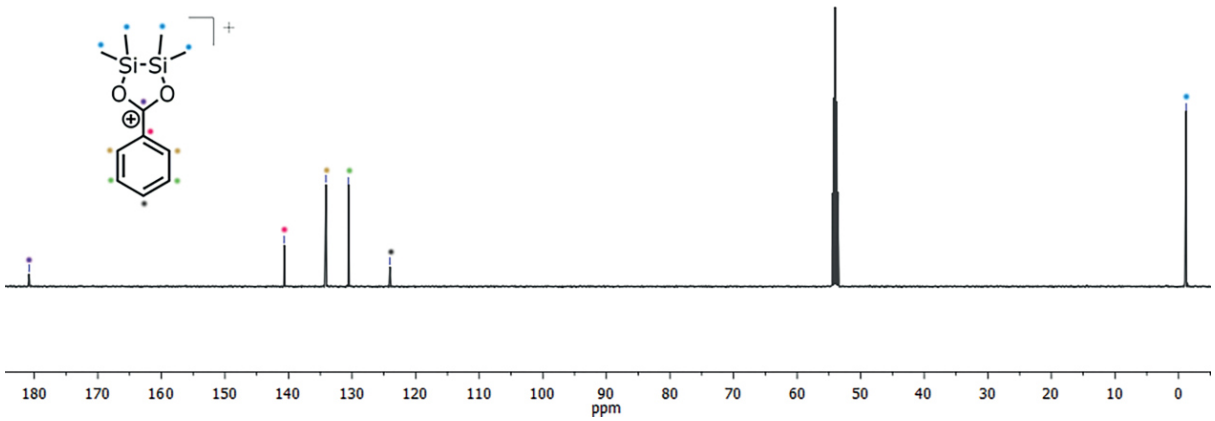

Figure 1. $^{13}C\{^{1}H\}$ NMR spectrum of compound **1** in CD_2Cl_2 (125 MHz, 300 K).

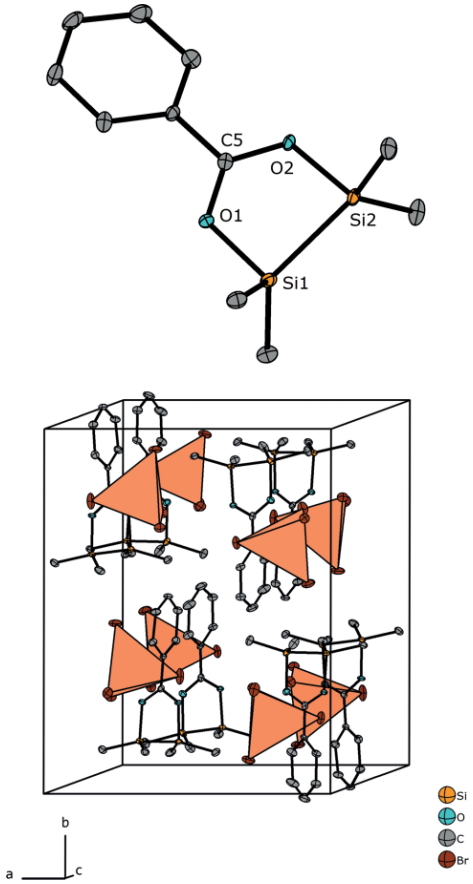

Figure 2. Molecular structure of the cationic part of compound **1** in the solid state (top) and a section of the crystal structure (bottom). Selected bond lengths /pm: Si1–O1 177.9(3), Si2–O2 177.5(3), O1–C5 128.0(5), O2–C5 128.7(5), Si1–Si2 233.0(1). Selected bond angles /°: O1–C5–O2 122.2(4), Si1–O1–C5 120.3(3), Si2–O2–C5 120.1(3), O1–Si1–Si2 88.5(1), O2–Si2–Si1 88.7(1).

177.6(3) and 177.9(3) pm. In comparison to related disilanyl-bearing systems[44,45,47,64,65] the Si–O bond is clearly elongated which is accompanied by the lack of negative hyperconjugation interactions p(O) → σ*(Si–C).[66,67] This further explains the observed low-field shift in the ^{29}Si NMR spectrum. It is somehow unclear what the driving force of the reaction is. For this reason we performed NMR spectroscopic investigations of the reaction mixture with a TMS (TMS = tetramethylsilane) capillary. By means of ^{29}Si NMR spectroscopy we observed a doublet of doublets at δ = 27.7 ppm and according to our interpretation it is most likely that $(Me_2SiF)_2$ (**II**) had formed, which is accompanied by the fluorophilic character of organosilicon compounds.[68] This respective resonance was also observed in a past work and is characteristic.[69] Also the coupling constants of $^{1}J_{SiF}$ = 303.3 Hz and $^{2}J_{SiF}$ = 34.1 Hz prove the finding, as these compare well with those published before. Further resonances were also observed but could not be assigned.

However, after workup and crystallization, compound **1** can be obtained without impurities. In the case of using GaI_3, we were able to synthesize compound **2** without a halide salt. To evaluate the role of the different reaction components, control experiments were performed which included only two components of the above mentioned reaction mixture. If $MgBr_2$ is reacted with siloxane **I** no reaction can be observed. In contrast to this, beryllium halides react with compound **I** with formation of complex, multinuclear beryllium silanolato compounds, which are related to previously described multinuclear beryllium polyolates.[46] These reactions are currently investigated in more detail and will be published in due course. The reaction of $MgBr_2$ or $BeBr_2$ with $GaBr_3$ leads to the formation of insoluble colorless precipitates. Even though $GaBr_3$ or GaI_3 are only little soluble in *α,α,α*-trifluorotoluene, strongly colored suspensions are obtained.

In case of $GaBr_3$, ^{13}C NMR spectroscopy shows aromatic signals, which are shifted downfield compared to neat *α,α,α*-trifluorotoluene. This indicates coordination of the CF_3 group towards the *Lewis*-acidic $GaBr_3$. An analogous coordination has been observed for $PhCCl_3$ / $AlCl_3$ mixtures.[70] However no additional signals could be observed for GaI_3, which is a weaker *Lewis* acid than $GaBr_3$. Furthermore, no halide exchange was observed between the gallium halides and the CF_3-group. While $MgBr_2$ does not react with *α,α,α*-trifluorotoluene on its own, $BeBr_2$ and BeI_2 react rapidly under the formation of *α,α,α*-tribromotoluene and *α,α,α*-triiodotoluene (**3**) as apparent from the ^{13}C NMR signals for the CBr_3 group at δ = 35.5 ppm[71] and CI_3 group at –38.8 ppm.

 © 2020 The Authors. Published by Wiley-VCH Verlag GmbH & Co. KGaA, Weinheim

Even though the NMR spectrum of **3** was unknown, the three iodine atoms bound to the carbon nucleus result in relativistic shielding effects, which lead to the observed high-field shift.[72] Such stoichiometric halodefluorination reactions were reported before.[73] Thus, we suspected a similar stepwise mechanism. However, in the experiments with the beryllium halides no intermediates with CF_2I/CF_2Br- or $CFI_2/CFBr_2$-groups could be observed via NMR spectroscopy. We assumed this was caused by the extremely fast reaction rates. Therefore, we evaluated the reactivity of other hard metal iodides towards *α,α,α*-trifluorotoluene. For this purpose we selected HfI_4 and ThI_4, due to their easy synthesis in pure form by the reaction of the metal powder or metal oxide with elemental iodide (see experimental section).[74,75] Reaction monitoring via ^{13}C NMR spectroscopy of ThI_4 in *α,α,α*-trifluorotoluene revealed the formation of *α,α,α*-triiodotoluene, however, again no intermediates were observed. Simple stirring of these salts in the solvent leads to slow conversion of the suspended MI_4 crystals under precipitation of a black powder. After workup, light yellow platelets were obtained and investigated via SC-XRD. It turned out that halodefluorination reactions took place for both metal ions in seemingly similar manner as both, Hf^{4+} and Th^{4+} ions initiate this reaction. These reactions perturb silyl ether bonding when a siloxane is added but give first examples of facile C–F bond activation. As can be seen, the fluorine atoms are replaced with three iodine atoms from the salts.

The halodefluorination itself was also described for other group 13 salts such as AlX_3 (X = Cl^-, Br^-, I^-) but exclusively *α,α,α*-triiodotoluene (**3**) has not yet been characterized properly.[73] Similar to the group of *Young* we observed quantitative iodide transfer but in our case we were able to characterize the quite air, temperature and light sensitive compound **3** by means of NMR and IR spectroscopy. The $^{13}C\{^1H\}$ NMR spectrum shows characteristic resonances for aromatic compounds and a single, distinctive high field resonance for the carbon atom substituted with the three iodine atoms at –38.8 ppm. As determined via single-crystal X-ray diffraction analysis (see Figure 3) the compound crystallizes in the orthorhombic space group $Pna2_1$ (no. 33). A section of the crystal structure shows that the iodine atoms as well as the aryl groups are separated. The aryl groups are held together by weak π···π interactions. To account π-stacking in this case is somehow controversial[76] but as observed, the aryl planes are twisted against each other by 43.3(1)° and the plane centroid···aryl edge distances measure 339.0(1) to 346.0(1) pm. For this reason, there might be evidence for a weak interaction.

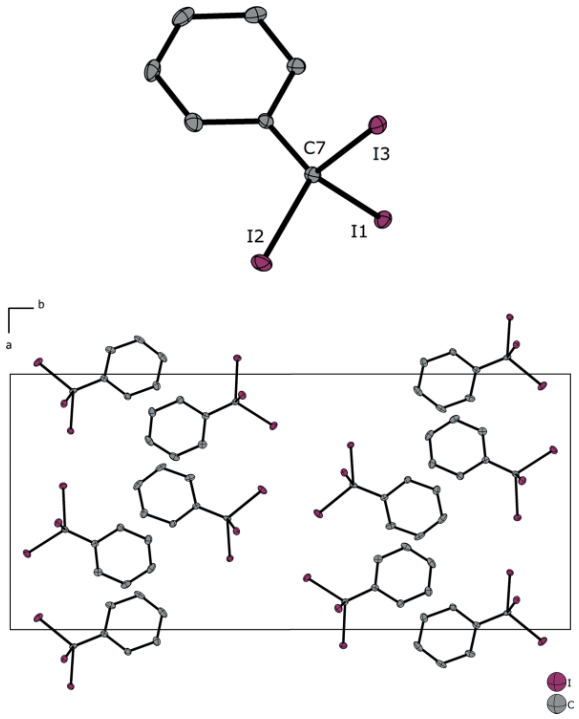

Figure 3. Molecular structure of the cationic part of compound **3** in the solid (top) and excerpt of the crystal structure (bottom). Selected bond lengths /pm: I1–C7 219.8(3), I2–C7 215.8(3), I3–C7 218.9(3). Selected bond angles /°: I1–C7–I2 105.6(1), I1–C7–I3 107.6(1), I2–C7–I3 107.3(1).

Conclusions

In this contribution we have presented facile stoichiometric C–F bond cleavage reactions by simple stirring of *Lewis* acidic beryllium bromide or iodide or tetravalent transition/actinoid metal iodides (Hf, Th) in *α,α,α*-trifluorotoluene. Even though we assume this is a stepwise process at the solid liquid interface, no intermediates could be observed. This might be caused by the significantly weaker C–F, C–Br, and C–I bonds in the mixed intermediates,[77] which leads to fast conversion to *α,α,α*-triiodotoluene (**3**) or *α,α,α*-tribromotoluene, the most stable iodo and bromo compounds. The halodefluorination product **3** was isolated and characterized also by means of single-crystal X-ray diffraction analysis. Employing *α,α,α*-trifluorotoluene, the fluorophilic silicon source **I** and the *Lewis* acid GaI_3 or the *Lewis* acid systems $MgBr_2/GaBr_3$ or $BeBr_2/GaBr_3$ results in the formation of the carbenium ionic compounds $[Ph\text{-}C(O_2Si_2Me_4)][GaX_4]$ (X = Br: **1**, X = F/I: **2**). The formation of these compounds can be formally understood as a siloxy-defluorination type reaction.

We assume the *Lewis* acid abstracts one fluoride from the CF_3 group. The transient $[PhCF_2]^+$ ion then reacts with siloxane **I** which acts as a fluorine atom abstractor and additionally stabilizes the positive charge at the carbon atom. In the absence of compound **I** the above mentioned halo-defluorination occurs. In case of $MgBr_2$, $GaBr_3$ is presumably necessary to increase the *Lewis* acidity of the magnesium ion to an extent that C–F bond cleavage occurs, while in case of $BeBr_2$, $GaBr_3$ most likely only acts as a bromide acceptor. The X-ray structure of compound **1** was determined and discrete ion pairs are present in the solid state showing the carbenium ionic character of this organosilicon compound. NMR spectroscopic investigations are conclusive and support the assumption. The driving force of this reaction is presumably the formation of **II**. All results are summarized in Scheme 3 and a proposed mechanism for the formation of the cation of **1** is depicted in Scheme 4. In the future we hope that there will be broader applications of

© 2020 The Authors. Published by Wiley-VCH Verlag GmbH & Co. KGaA, Weinheim

our presented reactions across different protocols such as catalysis or organofluorine chemistry in general.

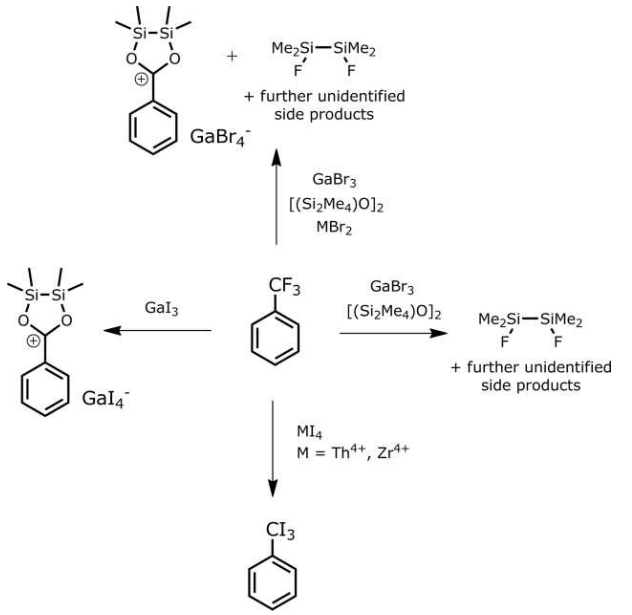

Scheme 3. The C–F-bond cleavage reactions presented herein.

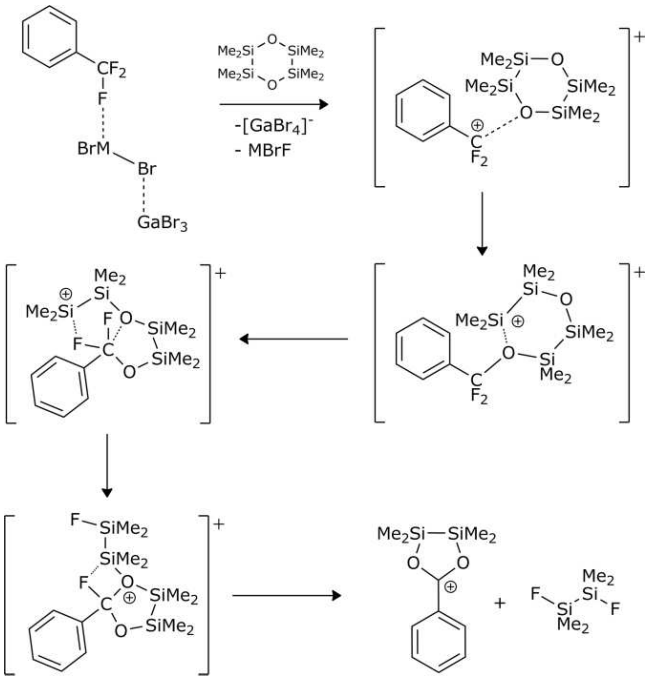

Scheme 4. Proposed mechanism for the formation of the cation of **1**.

Experimental Section

Caution! Beryllium and its compounds are regarded as toxic and carcinogenic. As the biochemical mechanisms that cause beryllium associated diseases are still unknown, special (safety) precautions are strongly advised.[78]

General: All work was carried out excluding moisture and air in an atmosphere of dried and purified argon (5.0, Praxair) using vacuum glass lines and a glovebox (MBraun). Solvents were dried and freshly distilled before use and subsequently stored over molecular sieves (3 Å). Elemental iodine was sublimed in vacuo several times, the last time from phosphorus pentoxide. Aluminum powder (Fluka, purum >99 %) was dried in vacuo at 250 °C. Th(IV) oxide (Merck, p. a.) was dried in vacuo at 350 °C. Hafnium powder (Alfa Aesar, 99.6 %) was used without further purification. $MgBr_2$ (Aldrich, > 99 %), $GaBr_3$ (Alfa Aesar >99 %) and GaI_3 (ABCR >99 %) were used as received. $BeBr_2$ and BeI_2 was synthesized according to literature procedures.[79] Compound **I** has been reported before[80] but we have optimized the reaction protocol (see below).

For the synthesis of ThI_4 and HfI_4 borosilicate glass vessels were flame-dried several times under dynamic vacuum (1×10^{-3} mbar) before use. The glass ampoules had a length of 16 cm, an outer diameter of 18 mm, and a wall thickness of 1.5 mm as described previously.[74,75] The top of the ampoule carries an NS14.5 inner ground joint for filling of the starting materials and a constriction for easier flame sealing. The second constriction at one-third of the length of the ampoule was used to allow for easier opening of the ampoule after the reaction.

Synthesis and Crystallization

Preparation of ThI_4:[74] An ampoule was charged with 1000 mg ThO_2 (3.79 mmol), 204 + 1 mg Al powder (7.58 mmol + transport agent) and 2883 + 256 mg I_2 (7.58 mmol + transport agent) and flame sealed under vacuum (1×10^{-3} mbar). Heating the mixture for 5 d up to 450 °C (source) and 350 °C (sink) yields 2297 mg canary yellow crystals of ThI_4 (3.11 mmol, 82 %), which could be extracted after transport.

Preparation of HfI_4:[74,75] An ampoule (12 mm, 1.5 mm wall thickness) was charged with 125 mg Hf powder (0.700 mmol) and 355.32+10 mg I_2 (2.800 mmol and 10 mg excess) and flame sealed under vacuum (1×10^{-3} mbar). The reactants were heated up to 300 °C for 48 h. HfI_4 (427.7 mg, 0.689 mmol, 98.4 %) in the form of orange crystals was obtained.

$[(Si_2Me_4)O]_2$ (I): 2 mL of 1,1,2,2-tetramethyldichlorodisilane (10.58 mmol) were dissolved in 50 mL of *n*-pentane. Subsequently, 10 mL (excess) of H_2O were added. After stirring overnight, the aqueous phase was extracted with three 50 mL portions of *n*-pentane and the organic phase was then dried with $MgSO_4$ followed by filtration. The solvent was removed under reduced pressure and the greasy residue was sublimed in static fine-vacuum (4×10^{-2} mbar) for several hours. **I** was then obtained as large colorless blocks (1.12 g, 80 %). **^{1}H NMR** (300 MHz, CD_2Cl_2): δ = 0.20 [s, 24 H, Si(CH_3)$_2$] ppm. **^{13}C{^{1}H} NMR** (75 MHz, CD_2Cl_2): δ = 2.6 (s, SiCH_3) ppm. **^{29}Si NMR** (99 MHz, CD_2Cl_2): δ = 3.6 [s, *Si*(CH_3)$_2$] ppm.

[Ph-C($O_2Si_2Me_4$)]$GaBr_4$ (1): 75 mg of **I** (0.38 mmol, 1.0 equiv.) were dissolved in 5 mL *α,α,α*-trifluorotoluene. Subsequently, 117 mg of $GaBr_3$ (0.38 mmol, 1.0 equiv.) and MBr_2 (0.38 mmol, 1.0 eq, M = Be^{2+}, Mg^{2+}) were added. The suspension was heated to reflux twice using a heatgun and then stirred overnight at ambient temperature. The solvent was removed under reduced pressure and DCM (5 mL) was added. The resulting suspension was filtered to obtain a greenish, dark solution which was layered with 20 mL of *n*-pentane. Large colorless platelets were obtained after a few days (191 mg, 80 %). **^{1}H NMR** (300 MHz, CD_2Cl_2): δ = 0.94 [s, 12 H, Si(CH_3)$_2$], 7.69–7.72 (m, 2 H, CH_{ar}), 8–01–8.04 (m, 1 H, CH_{ar}), 8.34–8.37 (m, 2 H, CH_{ar}) ppm.

© 2020 The Authors. Published by Wiley-VCH Verlag GmbH & Co. KGaA, Weinheim

$^{13}C\{^1H\}$ NMR (75 MHz, CD_2Cl_2): δ = –1.2 (s, SiCH_3), 124.0 (s, CH_{ar}), 130.6 (s, CH_{ar}), 134.1 (s, CH_{ar}), 140.7 (s, CH_{ar-q}), 180.8 [s, $CH(SiMe_2O)_2$] ppm. **$^{29}Si\{^1H\}$ NMR** (99 MHz, CD_2Cl_2): δ = 37.1 [s, $Si(CH_3)_2$] ppm. **IR**: $\tilde{\nu}$ = 3065 (vw), 1599 (w), 1498 (m), 1476 (s), 1424 (vs), 1313 (w), 1251 (m), 1181 (w), 1154 (w), 1097 (w), 1070 (w), 1024 (w), 908 (m), 841 (s), 806 (vs), 788 (s), 711 (s), 677 (s), 653 (m), 589 (s), 421 (w) cm^{-1}. $C_{11}H_{17}Br_4Ga_1O_2Si_2$: calcd. C, 21.08; H, 2.73 %; found C, 21.04; H, 2.89 %.

[Ph-C($O_2Si_2Me_4$)]$GaI_{4-x}F_x$ (2): 100 mg of **I** (0.38 mmol, 1.0 equiv.) were dissolved in 5 mL *α,α,α*-trifluorotoluene. Subsequently, 100 mg of GaI_3 (0.38 mmol, 1.0 equiv.) were added. The suspension was stirred overnight and freed of the solvent. Subsequently DCM (5 mL) was added. The resulting suspension was filtered to obtain a greenish, dark solution. After removal of the solvent, washing with several *n*-pentane portions and drying the residue in vacuo for several hours yielded compound **2** as a black oil (0.291 g, >94 %). **^1H NMR** (300 MHz, CD_2Cl_2): δ = 0.98 [s, 12 H, Si(CH_3)$_2$], 7.71–7.77 (m, 2 H, CH_{ar}), 8–01–8.04 (m, 1 H, CH_{ar}), 8.34–8.37 (m, 2 H, CH_{ar}) ppm. **$^{13}C\{^1H\}$ NMR** (75 MHz, CD_2Cl_2): δ = –0.85 (s, SiCH_3), 123.8 (s, CH_{ar}), 130.8 (s, CH_{ar}), 134.4 (s, CH_{ar}), 141.2 (s, CH_{ar-q}), 181.0 [s, $C(SiMe_2O)_2$] ppm. **$^{29}Si\{^1H\}$ NMR** (99 MHz, CD_2Cl_2): δ = 38.5 [s, $Si(CH_3)_2$] ppm. **IR**: $\tilde{\nu}$ = 2958 (vw), 2896 (vw), 1598 (w), 1498 (m), 1474 (m), 1420 (vs), 1315 (w), 1256 (m), 1182 (vw), 1152 (w), 1024 (w), 1001 (w), 836 (m), 793 (m), 752 (m), 712 (m), 673 (m), 590 (w) cm^{-1}.

***α,α,α*-Triiodotoluene (3):** 75 mg of MI_4 (M = Hf^{4+}, Th^{4+}) were dissolved in 2 mL of *α,α,α*-trifluorolouene (excess). The suspension was stirred for 5 h followed by filtration. The clear, yellow-red solution was concentrated in vacuo and stored at –24 °C. Large pale-yellow platelets were obtained overnight. The conversion was quantitative. **^1H NMR** (300 MHz, CD_2Cl_2): δ = 7.11–7.14 (m, 2 H, CH_{ar}), 7.30–7.33 (m, 1 H, CH_{ar}), 7.94–7.96 (m, 2 H, CH_{ar}) ppm. **$^{13}C\{^1H\}$ NMR** (75 MHz, CD_2Cl_2): δ = –38.8 (s, CI_3), 127.0 (s, CH_{ar}), 128.0 (s, CH_{ar}), 128.0 (s, CH_{ar}), 151.4 (s, C_{ar-q}) ppm. **IR**: $\tilde{\nu}$ = 1586 (w), 1572 (w), 1519 (m), 1479 (m), 1435 (w), 1387 (w), 1329 (w), 1306 (w), 1294 (w), 1234 (w), 1185 (w), 1154 (w), 1104 (w), 1076 (w), 1027 (w), 984 (w), 916 (w), 840 (w), 818 (m), 802 (s), 760 (vs), 680 (m), 652 (s), 585 (m) 571 (vs), 458 (w) cm^{-1}.

Control Experiments: For a ^{13}C NMR monitoring of the respective C–F bond cleavage reactions we were placing 30 mg of the respective salt in a J. Young NMR tube. An excess of 0.58 mL of *α,α,α*-trifluorotoluene was subsequently added. We allowed reacting the salt with the solvent for 2 d. After this period we employed a measurement at a Bruker AV III 500 MHz spectrometer using the *α,α,α*-trifluorotoluene as an internal standard.

Crystallography: Single crystal X-ray diffraction experiments were carried out with a Bruker D8 Quest diffractometer at 100(2) K with Mo-K_α radiation (λ = 0.71073). All structures were solved by Direct Methods (SHELXT) and refined with full-matrix-least-squares cycles against F^2 using SHELXL-2015 on OLEX2 platform.[81–83] Visualization of all structures was performed with the Diamond software package Version 4.6.0. All Ellipsoid plots represent the 50 % probability level.

Crystallographic data (excluding structure factors) for the structures in this paper have been deposited with the Cambridge Crystallographic Data Centre, CCDC, 12 Union Road, Cambridge CB21EZ, UK. Copies of the data can be obtained free of charge on quoting the depository numbers CCDC-1961377 (**1**) and CCDC-1961376 (**3**) (Fax: +44-1223-336-033; E-Mail: deposit@ccdc.cam.ac.uk, http://www.ccdc.cam.ac.uk).

Crystal Data of 1: $C_{11}H_{17}Br_4GaO_2Si_2$, monoclinic, $P2_1/n$, Z = 8, 100(2) K, a = 12.9816(6) Å, b = 16.5903(8) Å, c = 18.8676(9) Å, β = 101.723(2)°, V = 3978.7(3) Å^3, ρ = 2.093 g·cm^{-3}, multiscan absorption correction using SADABS2016,[84] μ = 9.535 mm^{-1}, T_{min}, T_{max} = 0.2273, 0.7461, 2Θ range 4.276–52.998°, reflections measured 152075, independent reflections 8229 [R(int) = 0.0645], 370 parameters, R-index [$I \geq 2\sigma(I)$] 0.0371, wR_2 (all data) 0.0953, GoF 1.049, $\Delta\rho_{max}$, $\Delta\rho_{min}$ 3.16/–2.80 e·Å^3.

Crystal Data of 3: $C_7H_5I_3$, orthorhombic, $Pna2_1$, Z = 8, 100(2) K, a = 11.5191(5) Å, b = 25.2908(10) Å, c = 6.7947(3) Å, V = 1979.48(15) Å^3, ρ = 3.153 g·cm^{-3}, multiscan absorption correction using SADABS2016,[84] μ = 9.406 mm^{-1}, T_{min}, T_{max} = 0.5708, 0.7462, 2Θ range 4.784–63.174°, reflections measured 92174, independent reflections 6607 [R(int) = 0.0383], 182 parameters, R-index [$I \geq 2\sigma(I)$] 0.0158, wR_2 (all data) 0.0286, GoF 1.138, $\Delta\rho_{max}$, $\Delta\rho_{min}$ 0.69/–0.65 e·Å^3.

Acknowledgements

This work was financially supported by the Deutsche Forschungsgemeinschaft (DFG). F.D. thanks the X-ray Department (*M. Marsch*, *R. Riedel*, and *Dr. S. Ivlev*), Philipps-Universität, Marburg, for measurement time and their kind advice. Open access funding enabled and organized by Projekt DEAL.

Keywords: Lewis acids; C–F bond cleavage; Carbenium ions; Actinides; Silicon; Fluorine; Defluorination

References

[1] T. Fujiwara, D. O'Hagan, *J. Fluorine Chem.* **2014**, *167*, 16–29.
[2] Y. Zhou, J. Wang, Z. Gu, S. Wang, W. Zhu, J. L. Acenã, V. A. Soloshonok, K. Izawa, H. Liu, *Chem. Rev.* **2016**, *116*, 422–518.
[3] J. Wang, M. Sánchez-Roselló, J. L. Aceña, C. Del Pozo, A. E. Sorochinsky, S. Fustero, V. A. Soloshonok, H. Liu, *Chem. Rev.* **2014**, *114*, 2432–2506.
[4] P. Shah, A. D. Westwell, *J. Enzyme Inhib. Med. Chem.* **2007**, *22*, 527–540.
[5] G. Theodoridis, *Chapter 4 Fluorine-Containing Agrochemicals: An Overview of Recent Developments*, in *Advances in Fluorine Science 2C*, Elsevier **2006**.
[6] Q. Shen, Y. G. Huang, C. Liu, J. C. Xiao, Q. Y. Chen, Y. Guo, *J. Fluorine Chem.* **2015**, *179*, 14–22.
[7] T. A. Unzner, T. Magauer, *Tetrahedron Lett.* **2015**, *56*, 877–883.
[8] T. Stahl, H. F. T. Klare, M. Oestreich, *ACS Catal.* **2013**, *3*, 1578–1587.
[9] D. O'Hagan, *Chem. Soc. Rev.* **2008**, *37*, 308–319.
[10] T. Fujita, K. Fuchibe, J. Ichikawa, *Angew. Chem. Int. Ed.* **2019**, *58*, 390–402.
[11] R. Panisch, M. Bolte, T. Müller, *J. Am. Chem. Soc.* **2006**, *128*, 9676–9682.
[12] V. J. Scott, R. Çelenligil-Çetin, O. V. Ozerov, *J. Am. Chem. Soc.* **2005**, *127*, 2852–2853.
[13] O. Allemann, S. Duttwyler, P. Romanato, K. K. Baldridge, J. S. Siegel, *Science* **2014**, *346*, aaa4609–aaa4609.
[14] H. F. T. Klare, *ACS Catal.* **2017**, *7*, 6999–7002.
[15] M. R. Cargill, G. Sandford, A. J. Tadeusiak, D. S. Yufit, J. A. K. Howard, P. Kilickiran, G. Nelles, *J. Org. Chem.* **2010**, *75*, 5860–5866.
[16] S. Sabater, J. A. Mata, E. Peris, *Nat. Commun.* **2013**, *4*, 1–7.

 © 2020 The Authors. Published by Wiley-VCH Verlag GmbH & Co. KGaA, Weinheim

[17] N. A. Jasim, R. N. Perutz, A. C. Whitwood, T. Braun, J. Izundu, B. Neumann, S. Rothfeld, H. G. Stammler, *Organometallics* **2004**, *23*, 6140–6149.
[18] R. T. Thornbury, F. D. Toste, *Angew. Chem. Int. Ed.* **2016**, *55*, 11629–11632.
[19] R. R. Schrock, J. Adamchuk, K. Ruhland, L. P. H. Lopez, *Organometallics* **2003**, *22*, 5079–5091.
[20] B. M. Kraft, R. J. Lachicotte, W. D. Jones, *J. Am. Chem. Soc.* **2000**, *122*, 8559–8560.
[21] M. Fujiwara, J. Ichikawa, T. Okauchi, T. Minami, *Tetrahedron Lett.* **1999**, *40*, 7261–7265.
[22] W. D. Jones, *Dalton Trans.* **2003**, *3*, 3991–3995.
[23] B. L. Edelbach, A. K. F. Rahman, R. J. Lachicotte, W. D. Jones, *Organometallics* **1999**, *18*, 3170–3177.
[24] J. Zhou, J. H. J. Berthel, M. W. Kuntze-Fechner, A. Friedrich, T. B. Marder, U. Radius, *J. Org. Chem.* **2016**, *81*, 5789–5794.
[25] A. D. Sun, J. A. Love, *Org. Lett.* **2011**, *13*, 2750–2753.
[26] T. Schaub, M. Backes, U. Radius, *J. Am. Chem. Soc.* **2006**, *128*, 15964–15965.
[27] A. Steffen, M. I. Sladek, T. Braun, B. Neumann, H. G. Stammler, *Organometallics* **2005**, *24*, 4057–4064.
[28] P. Fischer, K. Götz, A. Eichhorn, U. Radius, *Organometallics* **2012**, *31*, 1374–1383.
[29] W. W. Ji, E. Lin, Q. Li, H. Wang, *Chem. Commun.* **2017**, *53*, 5665–5668.
[30] T. Fujita, Y. Watabe, S. Yamashita, H. Tanabe, T. Nojima, J. Ichikawa, *Chem. Lett.* **2016**, *45*, 964–966.
[31] M. Aizenberg, D. Milstein, *Science* **1994**, *265*, 359–361.
[32] V. V. Grushin, *Acc. Chem. Res.* **2010**, *43*, 160–171.
[33] T. Braun, F. Wehmeier, *Eur. J. Inorg. Chem.* **2011**, 613–625.
[34] M. Aizenberg, D. Milstein, *J. Am. Chem. Soc.* **1995**, *117*, 8674–8675.
[35] R. P. Hughes, D. C. Lindner, *J. Am. Chem. Soc.* **1997**, *119*, 11544–11545.
[36] J. Terao, M. Nakamura, N. Kambe, *Chem. Commun.* **2009**, 6011–6013.
[37] C. Bakewell, A. J. P. White, M. R. Crimmin, *Angew. Chem. Int. Ed.* **2018**, *57*, 6638–6642.
[38] N. Suzuki, T. Fujita, K. Y. Amsharov, J. Ichikawa, *Chem. Commun.* **2016**, *52*, 12948–12951.
[39] T. Fujita, M. Takazawa, K. Sugiyama, N. Suzuki, J. Ichikawa, *Org. Lett.* **2017**, *19*, 588–591.
[40] A. M. Träff, M. Janjetovic, L. Ta, G. Hilmersson, *Angew. Chem. Int. Ed.* **2013**, *52*, 12073–12076.
[41] T. Akiyama, K. Atobe, M. Shibata, K. Mori, *J. Fluorine Chem.* **2013**, *152*, 81–83.
[42] M. F. Kuehnel, P. Holstein, M. Kliche, J. Krüger, S. Matthies, D. Nitsch, J. Schutt, M. Sparenberg, D. Lentz, *Chem. Eur. J.* **2012**, *18*, 10701–10714.
[43] K. Reuter, G. Thiele, T. Hafner, F. Uhlig, C. von Hänisch, *Chem. Commun.* **2016**, *52*, 13265–13268.
[44] K. Reuter, M. R. Buchner, G. Thiele, C. von Hänisch, *Inorg. Chem.* **2016**, *55*, 4441–4447.
[45] K. Reuter, F. Dankert, C. Donsbach, C. von Hänisch, *Inorganics* **2017**, *5*, 11.
[46] M. R. Buchner, M. Müller, F. Dankert, K. Reuter, C. von Hänisch, *Dalton Trans.* **2018**, *47*, 16393–16397.
[47] F. Dankert, C. Donsbach, C.-N. Mais, K. Reuter, C. von Hänisch, *Inorg. Chem.* **2018**, *57*, 351–359.
[48] F. Dankert, K. Reuter, C. Donsbach, C. von Hänisch, *Dalton Trans.* **2017**, *46*, 8727–8735.
[49] S. Harder, B. Freitag, P. Stegner, J. Pahl, D. Naglav, *Z. Anorg. Allg. Chem.* **2015**, *641*, 2129–2134.
[50] B. Freitag, P. Stegner, K. Thum, C. A. Fischer, S. Harder, *Eur. J. Inorg. Chem.* **2018**, *2018*, 1938–1944.
[51] J. S. Ritch, T. Chivers, *Angew. Chem. Int. Ed.* **2007**, *46*, 4610–4613.
[52] M. Fugel, M. F. Hesse, R. Pal, J. Beckmann, D. Jayatilaka, M. J. Turner, A. Karton, P. Bultinck, G. S. Chandler, S. Grabowsky, *Chem. Eur. J.* **2018**, *24*, 15275–15286.
[53] F. Dankert, C. von Hänisch, *Inorg. Chem.* **2019**, *58*, 3518–3526.
[54] F. Dankert, J. Heine, J. Rienmüller, C. von Hänisch, *CrystEngComm* **2018**, *20*, 5370–5376.
[55] J. Pahl, H. Elsen, A. Friedrich, S. Harder, *Chem. Commun.* **2018**, *54*, 7846–7849.
[56] C. Douvris, C. M. Nagaraja, C. H. Chen, B. M. Foxman, O. V. Ozerov, *J. Am. Chem. Soc.* **2010**, *132*, 4946–4953.
[57] F. Dankert, C. Donsbach, J. Rienmüller, R. Richter, C. von Hänisch, *Chem. Eur. J.* **2019**, *25*, 15934–15943..
[58] W. Kirmse, M. Guth, S. Steenken, *J. Am. Chem. Soc.* **1996**, *118*, 10838–10849.
[59] K. G. Sharp, P. A. Sutor, *J. Am. Chem. Soc.* **1977**, *99*, 8046–8048.
[60] S. G. Frankiss, *J. Phys. Chem.* **1967**, *71*, 3418–3421.
[61] B. Neumüller, *Coord. Chem. Rev.* **1997**, *158*, 69–101.
[62] C. Bour, J. Monot, S. Tang, R. Guillot, J. Farjon, V. Gandon, *Organometallics* **2014**, *33*, 594–599.
[63] R. Feld, M. S. Lehmann, K. W. Muir, J. C. Speakman, *Z. Kristallogr., Cryst. Mater.* **1981**, *157*, 215–231.
[64] F. Dankert, K. Reuter, C. Donsbach, C. von Hänisch, *Inorganics* **2018**, *6*, 15.
[65] K. Reuter, S. S. Rudel, M. R. Buchner, F. Kraus, C. von Hänisch, *Chem. Eur. J.* **2017**, *23*, 9607–9617.
[66] F. Weinhold, R. West, *J. Am. Chem. Soc.* **2013**, *135*, 5762–5767.
[67] F. Weinhold, R. West, *Organometallics* **2011**, *30*, 5815–5824.
[68] J. Horstmann, M. Niemann, K. Berthold, A. Mix, B. Neumann, H.-G. Stammler, N. W. Mitzel, *Dalton Trans.* **2017**, *46*, 1898–1913.
[69] D. A. Stanislawski, R. West, *J. Organomet. Chem.* **1981**, *204*, 307–314.
[70] U. S. Racherla, T. Daniel, P. R. Rajamohanan, N. R. Ayyangar, *J. Am. Chem. Soc.* **1989**, *111*, 7659–7661.
[71] Q. Sun, X. Yu, M. Bao, M. Liu, J. Pan, Z. Zha, L. Cai, H. Ma, C. Yuan, X. Qiu et al., *Angew. Chem. Int. Ed.* **2018**, *57*, 4035–4038.
[72] R. V. Viesser, L. C. Ducati, C. F. Tormena, J. Autschbach, *Phys. Chem. Chem. Phys.* **2018**, *20*, 11247–11259.
[73] K. K. K. Goh, A. Sinha, C. Fraser, R. D. Young, *RSC Adv.* **2016**, *6*, 42708–42712.
[74] H. L. Deubner, S. S. Rudel, F. Kraus, *Z. Anorg. Allg. Chem.* **2017**, *643*, 2005–2010.
[75] B. Krebs, D. Sinram, *J. Less-Common Met.* **1980**, *76*, 7–16.
[76] C. R. Martinez, B. L. Iverson, *Chem. Sci.* **2012**, *3*, 2191.
[77] G. Glockler, *J. Phys. Chem.* **1959**, *63*, 828–832.
[78] D. Naglav, M. R. Buchner, G. Bendt, F. Kraus, S. Schulz, *Angew. Chem. Int. Ed.* **2016**, *55*, 10562–10576.
[79] M. Müller, F. Pielnhofer, M. R. Buchner, *Dalton Trans.* **2018**, *47*, 12506–12510.
[80] T. Takano, N. Kasai, M. Kakudo, *Bull. Chem. Soc. Jpn.* **1963**, *36*, 585–590.
[81] G. M. Sheldrick, *Acta Crystallogr., Sect. C: Struct. Chem.* **2015**, *71*, 3–8.
[82] G. M. Sheldrick, *Acta Crystallogr., Sect. A: Found. Adv.* **2015**, *71*, 3–8.
[83] O. V. Dolomanov, L. J. Bourhis, R. J. Gildea, J. A. K. Howard, H. Puschmann, *J. Appl. Crystallogr.* **2009**, *42*, 339–341.
[84] Bruker, SADABS, Bruker AXS Inc., Madison, Wisconsin, USA, **2016**.

Received: November 15, 2019
Published Online: February 11, 2020

 © 2020 The Authors. Published by Wiley-VCH Verlag GmbH & Co. KGaA, Weinheim

Volume 7 | Number 11 | 7 June 2020

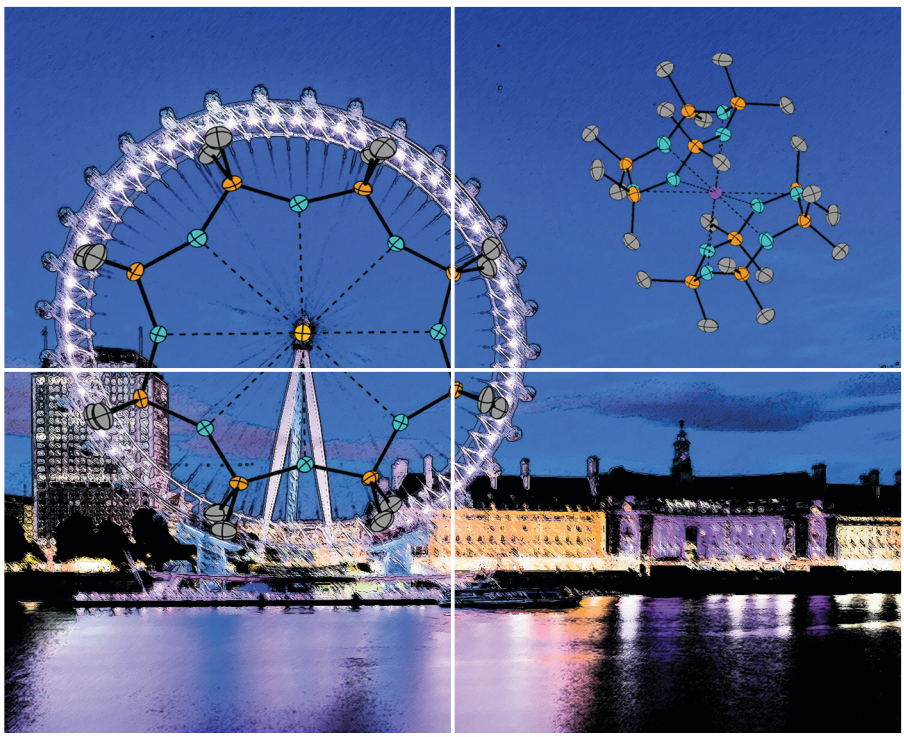

INORGANIC CHEMISTRY

FRONTIERS

CCS 中国化学会 CHINESE CHEMICAL SOCIETY

PEKING UNIVERSITY 1898

ROYAL SOCIETY OF CHEMISTRY

rsc.li/frontiers-inorganic

INORGANIC CHEMISTRY
FRONTIERS

RESEARCH ARTICLE

View Article Online
View Journal | View Issue

Check for updates

Cite this: *Inorg. Chem. Front.*, 2020, **7**, 2138

Published on 12 March 2020. Downloaded on 7/6/2020 9:12:51 PM.

On the molecular architectures of siloxane coordination compounds: (re-)investigating the coordination of the cyclodimethylsiloxanes D_n (n = 5–8) towards alkali metal ions†

Fabian Dankert, Lukas Erlemeier, Christian Ritter and Carsten von Hänisch *

In this study we present a (re-)investigation into cyclodimethylsiloxanes in relation to silyl-ether bonding towards alkali metal ions. We demonstrate that all (non-radioactive) alkali metal ions can be incorporated into D_n cyclosiloxane frameworks (D = $(SiMe_2O)$, n = 5–8), employing appropriate cation–anion combinations. Starting with the Li^+ cation we were able to observe the coordination of D_5 with Li^+ based on a suitable X-ray structure after reacting D_5 with LiI and GaI_3. Due to template effects, the dinuclear coordination compound $[Li_2(D_5)(D_6)(GaI_4)_2]$ (**1**) was obtained. The direct reaction of D_6 with LiI and GaI_3 yields $[Li(D_6)GaI_4]$ (**2**) in quantitative yield. Na^+ ions could be trapped in D_6 and D_7 ligand moieties after the conversion of NaI, GaI_3, and the respective siloxane. The molecular structure of $[Na(D_6)GaI_4]$ (**3**) reveals a six-fold coordinated Na^+ ion, which is located on top of the siloxane D_6. In the case of $[Na(D_7)(DCM)GaI_4]$ (**4**), the larger ligand D_7 provides 15-crown-5-like geometry in which the sodium ion is coordinated by the ligand in a coplanar fashion and further saturated by the solvent DCM (DCM = dichloromethane). The K^+ ion was bound within the D_7 ligand in a similar manner and $[K(D_7)(DCM)GaI_4]$ (**5**) could be characterized. Due to the resemblance of NH_4^+ to K^+, this cation was also employed for complex formation. Counterintuitively, we were able to synthesize and characterize the first ever non-metal-cyclosiloxane coordination compound. After the conversion of D_6 with NH_4I and GaI_3, the compound $[NH_4(D_7)][Ga_2I_7]$ (**6**) was obtained. The ammonium cation favors D_7 coordination over D_6, and the willing formation of hydrogen bonding in such a siloxane moiety was realized. As these compounds could be obtained, we also tested the limits of silyl-ether bonding. Therefore, we reacted D_8 with *in situ* generated $Rb[GaI_4]$ and $Cs[GaI_4]$. In the case of Rb^+, we could cumbersomely characterize $[Rb(D_8)(DCM)GaI_4]$ (**7**) *via* an X-ray structure, as well as by means of mass spectrometry, but the compound starts decomposing readily in solution. The reaction with the Cs^+ salt failed. To obtain meaningful spectroscopic data from a Rb^+ compound and to somehow obtain a Cs^+ complex, we employed the weakly coordinating anion $[Al_F]^-$ (Al_F^- = $[Al\{OC(CF_3)_3\}_4]^-$). The conversion of $M[Al_F]$ then yielded $^1_\infty[M(D_8)AL_F]$ (M = Rb: **8**; M = Cs^+: **9**) in the solid state. Both compounds **8** and **9** were fully characterized. Finally, we aimed at synthesizing 2 : 1 complexes of such siloxanes. The reactions of excess D_5 with $K[Al_F]$ and D_6 with $Cs[Al_F]$ turned out to be expedient and, in the forms of $[K(D_5)_2][Al_F]$ (**10**) and $[Cs(D_6)_2][Al_F]$ (**12**), the first ever sandwich-type complexes observed bearing a cyclosiloxane ligand were characterized.

Received 27th January 2020,
Accepted 24th February 2020

DOI: 10.1039/d0qi00109k

rsc.li/frontiers-inorganic

Introduction

For a few years now, silicon analogues of crown ethers have been widely presented as ligands for metal bonding.[1] Since the accidental discovery of a potassium compound[2] and early extraction experiments in the 1990s,[3] fundamental research into these siloxanes has crucially moved on. However, it took a long time to obtain coordination compounds, even though cyclosiloxanes were discovered long before Pedersen reported on crown ethers.[4,5] Until 2018, metal ions embedded in silacrowns with different ring sizes were limited to four ions: Li^+ (D_5/D_6);[6] K^+ (D_7);[2,7] Zr^{4+} (D_6);[8] and Ag^+ (D_6, D_7) (D_n = $(Me_2SiO)_n$).[9,10] Over time, different explanations were then presented that explained the reduced capability of (cyclo-)siloxanes for binding Lewis acids. First, considering the Si–O-bond

Fachbereich Chemie and Wissenschaftliches Zentrum für Materialwissenschaften (WZMW), Philipps-Universität Marburg, 35032 Marburg, Germany.
E-mail: haenisch@chemie.uni-marburg.de

†Electronic supplementary information (ESI) available. CCDC 1979351–1979364. For ESI and crystallographic data in CIF or other electronic format see DOI: 10.1039/d0qi00109k

This journal is © the Partner Organisations 2020

Published on 12 March 2020. Downloaded on 7/6/2020 9:12:51 PM.

to be covalent, $n_O \rightarrow d_{Si}$ backbonding interactions were described as a reason for the reduced metal bonding capabilities.[11] As the d-orbitals on Si were found to be too high in energy, this theoretical concept was later predominantly replaced with negative hyperconjugation interactions of the $n_O \rightarrow \sigma^*_{Si-C}$ type.[12,13] In these respective interactions, the Si–O-bond is strengthened; however, subsequent metal bonding requires weakening of the Si–O-bond first before shifting electron density towards the metal centre. Thus, metal bonding is hindered and, according to Weinhold and West, the respective hyperconjugation interactions significantly alter the Lewis basicity of permethylated siloxanes.[13] Second, considering the Si–O-bond to be ionic, the electron pairs around the oxygen atoms are spatially diffuse and thus do not readily support donation towards Lewis acids.[14] Furthermore, $Si^{\delta+}\cdots M^{n+}$ repulsive interactions perturb silyl ether bonding.[10,15] As the Si–O-bond is substantially more ionic than the C–O bond, the effect is more distinct in siloxanes than in ethers. Covalency and ionicity were long considered opposed to each other but, according to complementary bonding analysis, Grabowsky and co-workers showed that both aspects have to be taken into account and should not oppose each other, as both increase simultaneously and significantly when approaching larger Si–O–Si angles.[16] In other words, the basicity of siloxanes increases with smaller Si–O–Si angles.[17,18] Recent research emphasizes that siloxanes prefer early group 2 cations for complexation, as stable complexes were obtained when employing iodides. Simple salts, like MgI_2 and CaI_2, could be dissolved in dichloromethane, and silyl ether bonding was observed by means of SC-XRD and ^{29}Si NMR spectroscopy analysis in solution.[19] Furthermore, the Harder group enabled HMDSE (HMDSE = hexamethyldisiloxane) to undergo complexation and introduced the complex $[Mg(BDI)(HMDSE)]^+$ (BDI = CH[C(CH$_3$)N-Dipp]$_2$ and Dipp = 2,6-diisopropylphenyl), the first ever simple silyl ether adduct to be characterized.[20] Thus, metal–silyl ether bonding was found to be stronger than previously thought. Silyl ether bonding highly depends on the choice of metal. It is evident from carefully performed quantum chemical calculations using suitable Born–Haber cycles and from ^{29}Si NMR experiments in solution that the lattice energy of the chosen salt for complexation is of less importance than the nature of the cation.[19] According to gas-phase reactions, decreasing energy gains are observed for the formation of $[M(D_n)]^{2+}$ from $M = Mg^{2+}$ to $M = Ba^{2+}$. Reactions have been calculated to be slightly enthalpically positive for the reaction of MI_2 ($M = Sr^{2+}$, Ba^{2+}) with $D_{6,7}$ to form solid $[M(D_n)I_2]$, giving rise to the question of whether it is possible to also obtain stable complexes of these cations. It turned out that the $[GaI_4]^-$ anion is the most promising candidate, as GaI_3 can abstract I^- in combination with minimizing metal–anion interactions. Hence Sr^{2+} and Ba^{2+} complexes were successfully characterized. Overall it was shown that simple anions, such as I^-, are suitable for the correct choice of M.[19] Furthermore, it was illustrated that an iodide abstractor can support silyl ether coordination to such an extent that no perfluorinated alkoxymetallate is necessary for establishing silyl-ether coordination.[19]

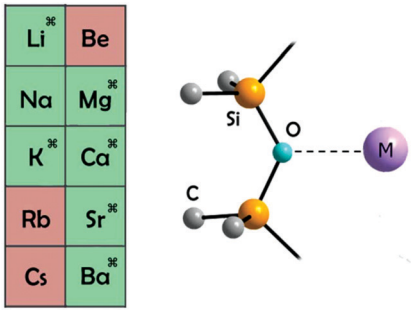

Fig. 1 The $(Me_xSi_y)_2O\cdots M^{n+}$ coordination modes of the s-block metals observed to-date: coordination compounds that have been characterized are marked in green, while for those marked in red, no neutral-ligand complexes have been characterized to-date. Elements depicted with a ribbon have also been bound within cyclic D_n-ligands. M = Li^+,[6,21] Na^+,[22] K^+,[2,7,23] Mg^{2+},[19,20,22] Ca^{2+},[19,22] Sr^{2+},[19,22,24–26] and Ba^{2+}.[19,22]

For this reason, an experimental *in-depth* investigation into the coordination of D_n with alkali metal salts is overdue. As can be seen in Fig. 1, (cyclic) silyl ether coordination has been observed for early alkalis over time, especially the alkaline earth metals. However, it is still unclear to what extent Rb^+ and Cs^+ are able to polarize the Si–O bond to yield stable complexes of these cations. So far, sila-ethers have strictly avoided silyl-ether bonding with soft Lewis-acids.[27] In addition it should be noted that Li^+ and K^+ are the only alkali metals that have been incorporated into such macrocycles and that, exclusively, D_6 and D_7 ligands have been observed in suitable X-ray analyses.[2,6–10,19,23] A question remains about smaller and larger ring sizes being used in combination with different alkali metals, which is common in conventional crown-ether chemistry[28] In this work, we report a handful of alkali metal complexes with D_n ligands, which exhibit coordination modes, molecular architectures and behaviours in solution that are unprecedented to-date.

Results and discussion

Li^+, as the smallest alkali metal ion, has been incorporated into D_6 and D_5 in previous work.[6] However, it should be noted that no suitable crystal structure of a lithium-D_5 complex could be obtained due to the presence of severe disorder. Passmore and co-workers performed quantum chemical calculations and, combining both theoretical and X-ray approaches, the ligand moiety demonstrated fourfold coordination towards Li^+.[6] The respective coordination mode is displayed in the left panel of Scheme 1. As we were able to identify $[GaI_4]^-$ as a suitable anion for siloxane coordination chemistry,[19] we tried to isolate $[Li(D_5)GaI_4]$ from the direct reaction of LiI, GaI_3 and D_5 in α,α,α-trifluorotoluene (Scheme 2). To our surprise, NMR spectroscopy analysis of our reaction product revealed two resonances from all NMR active nuclei. Resonances in the ^{29}Si{^{1}H} NMR spectrum were observed at −7.4 and −9.0 ppm, both of which indicate that there are strong interactions

Published on 12 March 2020. Downloaded on 7/6/2020 9:12:51 PM.

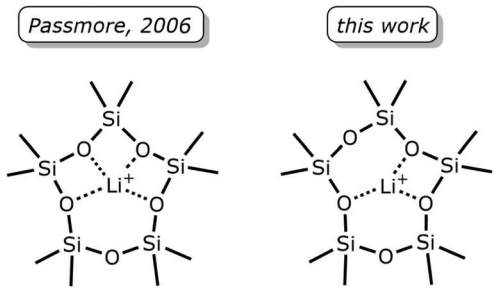

Scheme 1 The binding modes of D_5 towards Li^+: (left) as described by Passmore and co-workers;[6] and (right) as observed in this work.

between the two different siloxanes and Li^+ in solution. Passmore and co-workers mostly performed NMR spectroscopy in liquid SO_2 and, as can be seen in their work from 2006, no chemical shifts were observed when comparing the free ligand D_5 and a 1 : 1 mixture with $Li[Al_F]$ ($Al_F^- = [Al\{OC(CF_3)_3\}_4]^-$).[6] In our case, employing deuterated DCM (DCM = dichloromethane) as a solvent, we were able to observe a chemical shift.

After recrystallizing from DCM/benzene-d_6 solution, the X-ray structure revealed that ring opening had occurred. Li^+ acts as a template in solution and supports the formation of D_6 from D_5 (see Scheme S1† for a mechanistic proposal). Two species crystallize side by side in a triclinic crystal system with the space group $P\bar{1}$ (Fig. 2). What can be seen here is the dinuclear complex $[Li_2(D_5)(D_6)(GaI_4)_2]$ (**1**). The exact assignment of the respective NMR resonances in solution was then possible after D_6 was reacted with LiI and GaI_3. The reaction in α,α,α-trifluorotoluene quantitatively yielded $[Li(D_6)GaI_4]$ (**2**), which could be characterized by state of the art methods, including SC-XRD (Fig. 3). NMR spectroscopy analysis of the compound showed that the observed resonances compare well with one of the signal sets of **1**. From this, all resonances can be assigned properly. In contrast to the earlier work of

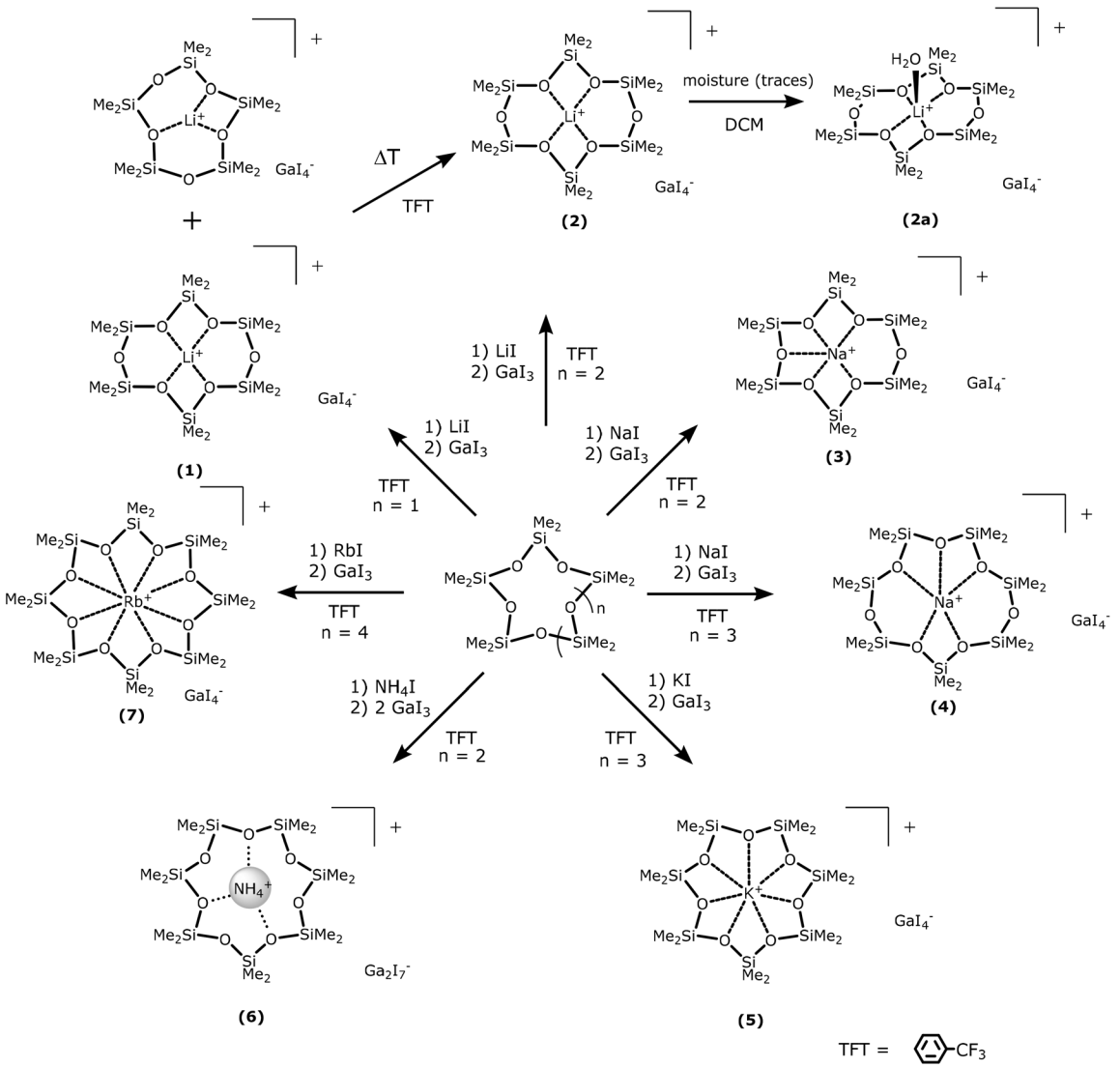

Scheme 2 A schematic representation of the synthesis and binding modes of compounds **1**–**7**.

 This journal is © the Partner Organisations 2020

Published on 12 March 2020. Downloaded on 7/6/2020 9:12:51 PM.

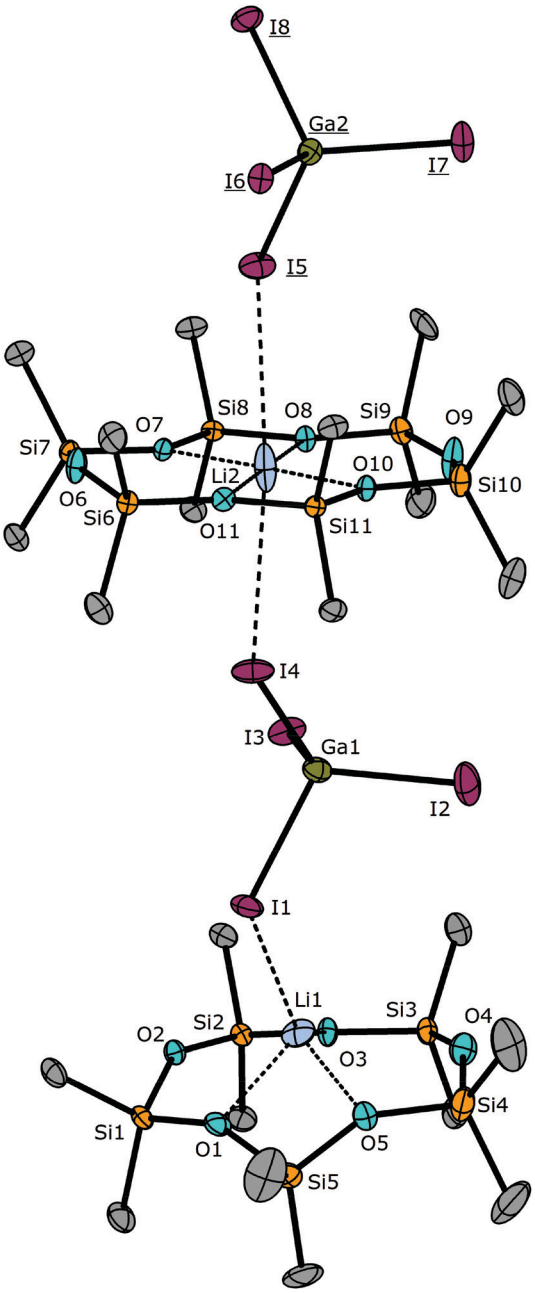

Fig. 2 The connectivity of $[Li(D_5)GaI_4]$ and $[Li(D_6)GaI_4]$ in the crystal structure of $[Li_2(D_5)(D_6)(GaI_4)_2]$ (**1**). The thermal ellipsoids represent the 50% probability level. Atoms with underlined labels are symmetry generated using $1 + x, y, -1 + z$. Selected bond lengths [pm]: O1–Li1: 208.2(1); O2···Li1: 260.3(1); O3–Li1: 194.7(1); O4···Li1: 280.6(1); O5–Li1: 204.4(1); I1–Li1: 275.2(1); O6···Li2: 330.0(1); O7–Li2: 202.7(1); O8–Li2: 204.7(1); O9···Li2: 326.3(1); O10–Li2: 202.9(1); I4–Li2: 343.6(1); I5–Li2: 337.9(1). Selected bond angles [°]: O1–Li1–O3: 115.3(6); O1–Li1–O5: 74.2(5); O3–Li1–O5: 111.5(6); Si1–O2–Si2: 145.4(3); Si1–O1–Si5: 152.4(3); Si2–O3–Si3: 140.5(3); Si3–O4–Si4: 149.3(4); Si4–O5–Si5: 150.0(4); O7–Li2–O8: 75.2(4); O10–Li2–O11: 75.1(4); Si6–O6–Si7: 148.0(3); Si6–O11–Si11: 139.3(3); Si7–O7–Si8: 139.3(3); Si8–O8–Si9: 141.5(3); Si9–O9–Si10: 152.1(3); Si10–O10–Si11: 140.6(3); I4–Li2–I5: 173.9(4).

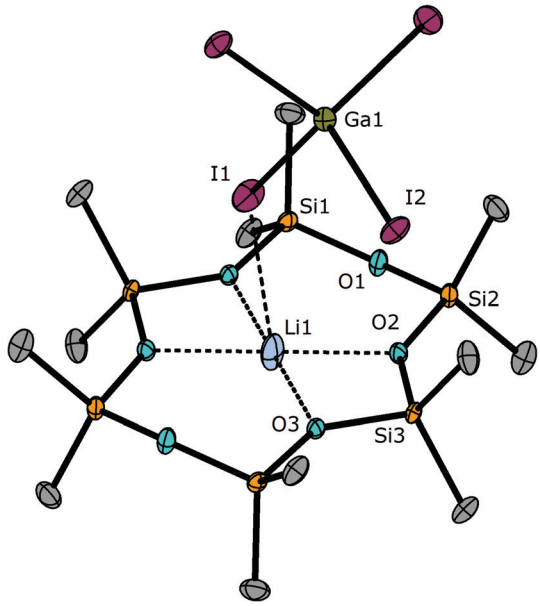

Fig. 3 The molecular structure of $[Li(D_6)GaI_4]$ (**2**) in crystal form. The thermal ellipsoids represent the 50% probability level. Non-labelled atoms are symmetry generated using $1 - x, 1 - y, -1 - z$ or $1 - x, y, 1/2 - z$, respectively. Selected bond lengths [pm]: O1···Li1: 326.2(1); O2–Li1: 206.1(2); O3–Li1: 203.1(1); I1–Li1: 351.0(2). Selected bond angles [°]: O2–Li1–O3: 74.51(6); Si1–O1–Si2: 145.1(1); Si1#–O3–Si3: 141.1(1); Si2–O2–Si3: 141.7(1).

Passmore and co-workers, the coordination mode of D_5 towards Li^+ is different. In this work, D_5 provides three oxygen atoms for metal bonding (Scheme 1: right). Lithium is therefore coordinated in a tetrahedral rather than tetragonal-pyramidal manner, and the coordination number decreases from five to four. As we have employed the $[GaI_4^-]$ anion, the stronger interaction with Li^+ lifts the central ion away from the siloxane. Li^+ is located about 89 pm above the spanned mean plane of the oxygen atoms. The $Li–O_{coord.}$ atom distances range from 194.7(1) pm to 208.2(1) pm. The $Li–O_{noncoord.}$ atom distances range from 260.3(1) to 280.6(1) pm. No coordination of $O_{6,9}$ towards Li^+ is indicated. As an X-ray structure of D_5 was obtained by Parsons and co-workers,[29] a side by side comparison of coordinated and non-coordinated species is possible for the first time and this gives further insights into the influence of a Lewis acid on siloxane binding. As can be seen from the D_5 moiety of the molecular structure of **1**, the $Si_{D_5}–O_{coord.}$ bonds range from 163.7(1) to 167.3(1) pm and the $Si_{D_5}–O_{coord.}–Si_{D_5}$ angles have values of 140.5(3)°, 150.0(4)° and 152.4(3)°. In the free ligand species, the Si–O bonds have values ranging from 161.8(2) to 163.6(2) pm. The Si–O–Si angles are quite strained, measuring from 138.6(1) to 156.8(1)°. Comparing these values, it is notable that the Si–O bond is clearly elongated due to coordination, which is in-line with a decrease in negative hyperconjugation interactions. The $Si_{D_5}–O_{coord.}–Si_{D_5}$ angles in **1** are quite large, even though the Li^+ ion is coordinated by D_5. As it is evident from a number of works,[16,17] the Si–O–Si angle should preferably be small for the strong binding of Lewis acids. This is most likely one of the main

Published on 12 March 2020. Downloaded on 7/6/2020 9:12:51 PM.

reasons why D_5 is cleaved by $Li[GaI_4]$ to form D_6. The D_6 moieties in **1** and **2** involve Si_{D_6}–$O_{coord.}$–Si_{D_6} angles that range from 139.3(3) to 141.5(3)°, as in **1**, and from 141.1(1) to 141.7(1)°, as in **2**. Furthermore, the coordination geometry of D_6 towards Li^+ in **1** and **2** is the same as in $[Li(D_6)Al_F]$ and $[Li(D_6)Al_{PhF}]$ (Al_{PhF}^- = $[Al\{OCPh(CF_3)_2\}_4]^-$), presenting an almost coplanar arrangement of the four oxygen atoms of the D_6 moiety when coordinating towards Li^+. Taking all observations into account, the formation of D_6 involves smaller Si–O–Si angles and, thus, more basic oxygen atoms coordinating with Li^+.

In solution, these observations and, hence, stronger bonding are well represented, as an also stronger $^{29}Si\{^1H\}$ NMR chemical low-field shift is observed upon D_6 formation (−7.4 ppm for Li@D_6 *vs.* −9.0 ppm for Li@D_5). The strong coordination of D_6 with Li^+ is also underlined by the fact that compound **2** can be recrystallized following exposure to moisture, forming the aqua complex $[Li(D_6)(H_2O)][GaI_4]$ (**2a**) (see Fig. S1†).

$[Na(D_6)GaI_4]$ (**3**) was obtained as a colourless powder in a straightforward reaction of D6 with $Na[GaI_4]$ in α,α,α-trifluorotoluene. Recrystallization from DCM solution yields colourless platelets. **3** crystallizes in the monoclinic crystal system with the space group $P2_1/n$. As can be seen from the molecular structure, five out of six oxygen atoms coordinate with the Na^+ ion (Fig. 4). The compound crystallizes as monomeric contact ion pairs. Less pronounced than in the case of Li^+ in **1**, the sodium ion shifts 60 pm out of the spanned mean plane of the oxygen atoms. The O···Na atom distances have quite different values, as four of these atom distances are small and one is comparatively large. The strong contacts between O1, O2, O4, O5 and Na1 measure between 242.5(4) and 249.2(5) pm. The weaker contact between O3 and Na1 measures 261.2(4) pm. O6 and Na1 do not undergo an interaction in the solid state. The atom distance of 324.2(6) pm is too large. Apparent from NMR experiments in solution, the sodium ion switches sites and, thus, a single resonance is observed. The single resonance in the $^{29}Si\{^1H\}$ NMR spectrum is found at −14.9 ppm, different to the free ligand D_6 (δD_6 = −22.2 ppm).[18] This respective shift is far less pronounced than in the lithium compounds, which demonstrates that silyl ether coordination is already far less supported as the sodium ion polarizes the Si–O bonds less strongly, resulting in a decreased low-field shift. The ionic radius of Na^+ with CN = 7 is 112 pm and compares for this reason quite well with that of Ca^{2+} ($r_i[Ca^{2+}]_{CN7}$ = 106 pm).[30] As can be seen from the molecular structure of $[Ca(D_7)I_2]$ in crystal form, the calcium ion matches perfectly with D_7 as "pseudo-[15]-crown-5"-like geometry is obtained for metal bonding.[19] For this reason, we also reacted $Na[GaI_4]$ with D_7 in α,α,α-trifluorotoluene. This yields a colourless microcrystalline powder that can be recrystallized from DCM solution at −24 °C. Once again colourless platelets were obtained and, as can be seen in the molecular structure determined *via* SC-XRD, the sodium ion is bound in the same way as Ca^{2+} and Ag^+ were bound by D_7 in past work (Fig. 5).[9,19]

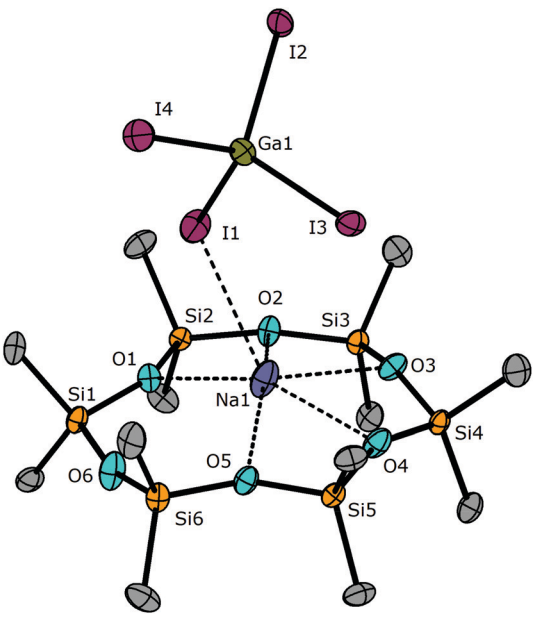

Fig. 4 The molecular structure of $[Na(D_6)GaI_4]$ (**3**) in crystal form. The thermal ellipsoids represent the 50% probability level. Only one of two independent molecules within the asymmetric unit is shown. Selected bond lengths [pm]: O1–Na1: 242.5(4); O2–Na1: 246.6(3); O3–Na1: 261.2(4); O4–Na1: 249.2(5); O5–Na1: 242.9(4); O6···Na1: 324.2(6); I1–Na1: 323.8(3). Selected bond angles [°]: O1–Na1–O2: 62.2(1); O2–Na1–O3: 60.1(1); O3–Na1–O4: 59.6(1); O4–Na1–O5: 62.0(1); Si1–O1–Si2: 144.9(3); Si1–O6–Si6: 162.6(4); Si2–O2–Si3: 152.7(3); Si3–O3–Si4: 153.3(3); Si4–O4–Si5: 156.9(3); Si5–O5–Si6: 146.3(3).

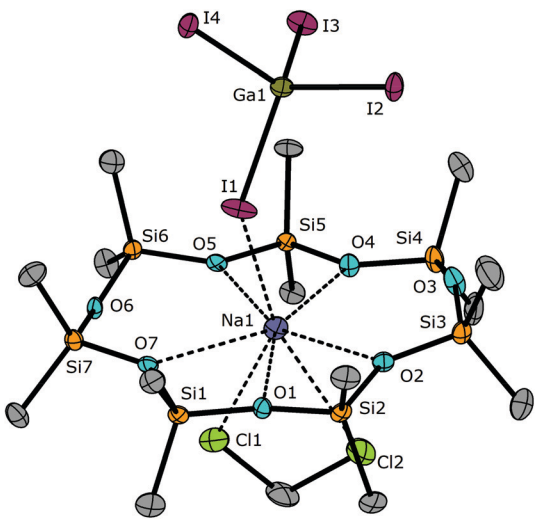

Fig. 5 The molecular structure of $[Na(D_7)(DCM)GaI_4]$ (**4**) in crystal form. The thermal ellipsoids represent the 50% probability level. Only one of two independent molecules within the asymmetric unit is shown. Selected bond lengths [pm]: O1–Na1: 253.1(6); O2–Na1: 265.1(4); O3···Na1: 356.1(19); O4–Na1: 251.0(7); O5–Na1: 253.0(5); O6···Na1: 367.6(5); O7–Na1: 276.2(7); I1–Na1: 322.6(3). Selected bond angles [°]: O1–Na1–O2: 58.6(1); O1–Na1–O7: 52.2(1); O3–Na1–O4: 93.6(2); O4–Na1–O5: 61.1(1); O5–Na1–O7: 90.0(1); Si1–O1–Si2: 150.7(4); Si1–O7–Si7: 141.1(4); Si2–O2–Si3: 141.5(4); Si3–O3–Si4: 156.7(9); Si4–O4–Si5: 138.1(4); Si5–O5–Si6: 136.7(3); Si6–O6–Si7: 151.5(4).

This journal is © the Partner Organisations 2020

Published on 12 March 2020. Downloaded on 7/6/2020 9:12:51 PM.

The good match with the ligand environment is also indicated by the placement of Na^+ in the ring. It is now positioned in the centre of the spanned mean plane of the oxygen atoms. Furthermore, a more distinct low-field shift is observed of −12.7 ppm in the $^{29}Si\{^1H\}$ NMR spectrum. Unlike the D_5-ligand-Li^+ compounds, these sodium compounds are not as sensitive towards ring opening polymerization when employing the reaction conditions reported herein. Both D_6 and D_7 are suitable ligands for complexation. Comparing the Si–O···Na^+ atom distances of **4** with those of **3**, it is notable that these are only slightly larger on average (251.0(7) to 276.2(7) pm in **4** *vs.* 242.5(4) to 261.2(4) pm in **3**). This can be related to the higher coordination number of Na^+, which, as the central ion in **4**, is further saturated by rare C–Cl···Na^+ contacts with DCM and a less strained ligand environment. Taking these observations into account, D_7 is a more suitable ligand than D_6 for binding Na^+. This assumption is strengthened also by observations made using ESI MS (ESI MS = electrospray ionization mass spectrometry). ESI^+ MS indicates the willing formation of D_7 from D_6 when investigating a sample of **3** under gas-phase conditions. Both species, $[D_6 + Na]^+$ and $[D_7 + Na]^+$, were found at *m*/*z* values of 467.1018 and 541.1208, respectively.

Potassium compounds of the cyclodimethylsiloxane D_7 have been known for quite some time. The potassium ion matches very well with the cavity of this ligand. Previous studies revealed a coplanar D_7 ring that coordinates K^+.[2,7,23] Also, in our study, it was possible to incorporate the potassium ion into this ligand. The reaction of $K[GaI_4]$ with D_7 yields a colourless powder that was recrystallized from DCM solution. Suitable crystals for SC-XRD studies were obtained in the form of colourless platelets. $[K(D_7)(DCM)GaI_4]$ (**5**) crystallizes in the triclinic space group $P\bar{1}$ (Fig. 6). The X-ray structure reveals that the ring is rather twisted around the central ion. This twisting causes quite variable potassium–oxygen atom distances. These distances range from 277.6(2) to 307.2(3) pm. Compared with previously characterized complexes, these atom distances fit well if the average atom distances are considered. Whereas the closest O···K^+ contact of 277.6(2) pm is shorter than those reported, 307.2(3) pm is the longest atom distance for this type of compound reported so far. The average atom distance is 288.8(2) pm. The atom distances reported by Churchill *et al.* have an average value of 293 pm,[2] those reported by Lerner of 287 pm.[23] Thus, the average K–O atom distance lies in between these values. As evident from the ligand sphere of compound **5**, the ligand does not have to strain into a planar ring. Most probably, the ligand behaviour of such macrocycles is also dependent on the counter anion and on the solvent used. So, as can be seen from compounds **4** and **5**, these are rare examples of DCM coordinating with M^+ in the solid state. This, however, does also indicate that the silyl ether coordination of such ligands gets worse the softer the cation is. The central ion now also supports being saturated further, even by the weakly coordinating solvent DCM. However, the power of many such silyl-ether···M^+ bonds allows for quantitative conversion. To sum up, this ligand is suitable for coordinating K^+

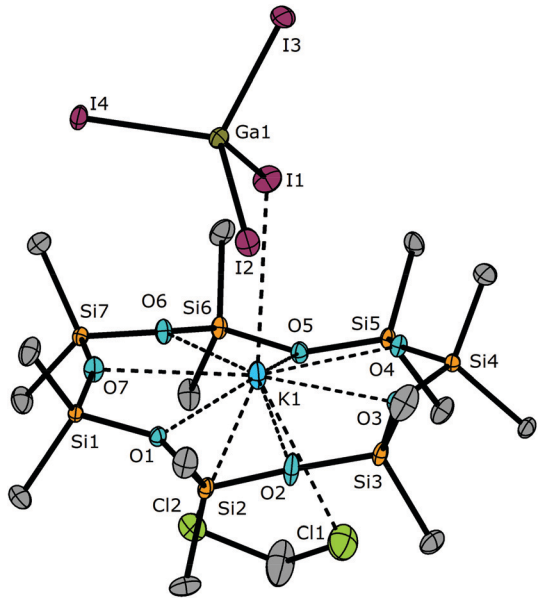

Fig. 6 The molecular structure of $[K(D_7)(DCM)GaI_4]$ (**5**) in crystal form. Thermal ellipsoids represent the 50% probability level. Selected bond lengths [pm]: O1–K1: 277.6(2); O2–K1: 307.2(3); O3–K1: 286.2(2); O4–K1: 281.8(2); O5–K1: 306.7(2); O6–K1: 293.1(2); O7–K1: 295.1(2); I1–K1: 355.1(1); Cl1–K1: 349.0(1); Cl2–K2: 361.9(1). Selected bond angles [°]: O1–K1–O2: 51.8(1); O1–K1–O7: 53.1(1); O2–K1–O3: 50.7(7); O3–K1–O4: 53.8(7); O4–K1–O5: 51.8(7); O5–K1–O6: 50.7(6); O6–K1–O7: 51.6(7); Si1–O1–Si2: 147.0(1); Si1–O7–Si7: 158.2(1); Si2–O2–Si3: 163.3(2); Si3–O3–Si4: 152.3(1); Si4–O4–Si5: 149.6(1); Si5–O5–Si6: 151.3(1); Si6–O6–Si7: 150.7(1).

and enables all oxygen atoms to be involved in coordination. As we recognized that the potassium ion can be coordinated well in such siloxanes, we thought that the ammonium cation, which is often also described as a "pseudo-alkali" metal due to its ion size and close relation to the potassium ion, might also be incorporated into these systems. First, however, the ammonium cation has no metal centre and has to be stabilized *via* hydrogen bonding. Second, most ammonium complexes strive for a C_3-symmetric hydrogen-bonding pattern, which is evident from the high number of characterized [18]-crown-6 complexes.[31–33]

As we were able to incorporate ammonium cations into hybrid disila-[18]-crown-6 ethers,[34] it was clear that, from a practical point of view, a D_6 ring should be used for complexation. With that in mind, we applied 1 : 1 : 1 stoichiometry of NH_4I, GaI_3, and D_6. After conversion in α,α,α-trifluorotoluene, workup and crystallization, we indeed observed siloxane bonding towards NH_4^+. Colourless platelets were investigated *via* SC-XRD. As can be seen from the molecular structure of the crystal (Fig. 7), D_7 from D_6 and a $[Ga_2I_7]^-$ anion was formed. The respective complex $[NH_4(D_7)Ga_2I_7]$ (**6**) crystallizes in the monoclinic space group $P2_1/n$ and, as can be seen in Fig. 7, the ammonium cation forms three hydrogen bonds with the D_7 ring. These were located crystallographically. One additional hydrogen bond is formed with an iodide atom from the anion. The reaction for obtaining this complex is reprodu-

Published on 12 March 2020. Downloaded on 7/6/2020 9:12:51 PM.

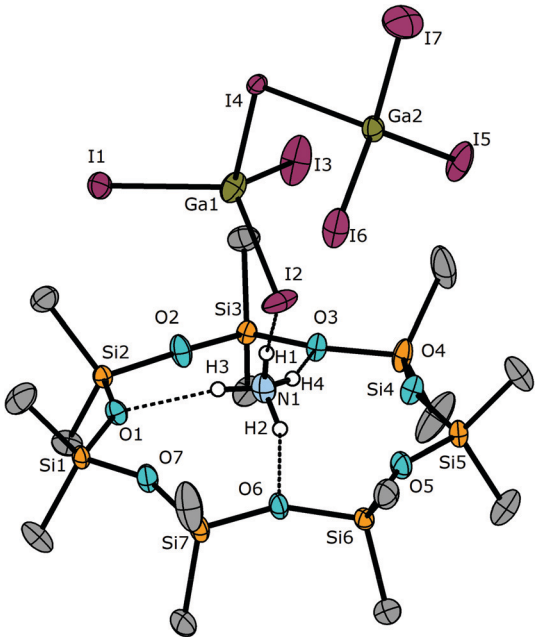

Fig. 7 The molecular structure of $[NH_4(D_7)][Ga_2I_7]$ (**6**) in crystal form. The thermal ellipsoids represent the 50% probability level. Solvent DCM molecules and the disordered part of the structure are omitted for clarity. Hydrogen atoms located at N1 were treated with DFIX [0.91] commands. Selected bond lengths [pm]: H1–I2: 276(5); H2–O6: 212(4); H3–O1: 200(5); H4–O3: 211(3). Selected bond angles [°]: Si1–O1–Si2: 145.7(2); Si1–O7–Si7: 157.9(2); Si2–O2–Si3: 159.0(2); Si3–O3–Si4: 150.1(2); Si4–O4–Si5: 150.6(2); Si5–O5–Si6: 148.7(1); Si6–O6–Si7: 144.5(2).

cible also when employing the correct stoichiometry. However, complex **6** is the first example of a non-metal complex of this type of pseudo-crown ether. Hydrogen bonding involving the siloxane linkage has always been briskly discussed in the literature. In a lot of works, HMDSE and related silyl ethers were investigated and the hydrogen bonding affinity was determined to decrease in the order: R_3COCR_3 > R_3COSiR_3 ≫ $R_3SiOSiR_3$. This order can be found in a lot of different studies, from IR and NMR spectroscopy investigations and from quantum chemical calculations.[11,35–37] There have been attempts to force the siloxane linkage to form hydrogen bonds through straining the Si–O–Si angle[17] but experimental data regarding hydrogen bonding involving the siloxane linkage is ultimately very rare. Most Si–O···H bonds occur only occasionally in the solid state and are not purposefully realized. In a recent work, we showed that establishing hydrogen bonds on purpose is possible through utilizing cooperative effects when ethylene-oxy as well as siloxy groups are present.[34] In **6**, however, there are exclusively Si–O–Si units present.

Considering all these observations and publications, it is very counter-intuitive that the ammonium cation can be trapped in such a ligand without further cooperative effects. Furthermore, it is astonishing that the ring size was willingly adapted, forming D_7 from D_6. The molecular structure reveals hydrogen···oxygen atom distances ranging from 200(5) to 212(4) pm. With these atom distances the hydrogen bonding situation is roughly the same as in the cases of $[NH_4$(1,2-disila-[18]-crown-6)$][PF_6]$ and also $[NH_4$(1,2-disila-benzo-[18]-crown-6)$][PF_6]$.[34] The ammonium ion is lifted 73.2 pm out of the spanned mean plane of the oxygen atoms. The Si–O–Si angles in complex **6** vary from 144.5(2) to 159.0(2)°. The Si–O_{donor}–Si angles measure 144.5(2), 145.7(2) and 150.1(2)°. Also, by means of IR-spectroscopy, a single broad NH– stretching vibration is observed at 3165 cm^{-1}, which is characteristic for a H-bonded NH group and further proves the interactions of the hydrogen atoms with the siloxane moieties. The $^{29}Si\{^1H\}$ NMR chemical shift is −15.51 ppm at 253 K. This chemical shift is in the range of that of compound **5**. It should be noted that spectroscopic analysis of this compound is challenging as the complex starts decomposing readily in solution. To provide meaningful NMR spectroscopic data we dissolved single crystals of **6** in freshly distilled dichloromethane-d_2 in a J. Young NMR tube. An immediate measurement at 253 K was then successful. Otherwise or upon storing for a few minutes in solution, decomposition into various unknown species occurs, which was apparent from monitoring with $^{29}Si\{^1H\}$ NMR spectroscopy.

This unique example of a trapped ammonium cation inside a siloxane moiety motivated us to test the limits of siloxane coordination chemistry. Several of our latest works convincingly show that siloxanes coordinate better[19,21,22] than was assumed in earlier studies.[1,6] Even though the Lewis basicity is impaired compared to organic ethers, we can at this point demonstrate that siloxanes can be activated for coordination towards a wide range of metal centres. Coordination is most likely to those that are chemically hard but it is possible in many more cases than most inorganic chemists would have previously assumed. So far, however, silyl ether coordination towards Rb^+ and Cs^+ has been strictly avoided, as we have mentioned in past works.[27,38] Employing the $[GaI_4]^-$ anion rather than a triflate or simple iodide anion, we could cumbersomely observe the chemical reaction. The reaction of D_8 with *in situ* generated $Rb[GaI_4]$ yielded a greasy residue that could be recrystallized at −24 °C from DCM solution. The resulting very air- and moisture-sensitive colourless platelets were investigated *via* SC-XRD and, indeed, with $[Rb(D_8)(DCM)GaI_4]$ (**7**), a respective complex was obtained (Fig. 8).

The molecular structure of the crystal reveals a twelve-fold coordinated Rb atom, which is saturated by a sila-crown but also by a chelating anion and the solvent DCM. The complex crystallizes in the orthorhombic crystal system with the space group *Pbcn*. As can be seen from this molecular structure, the cyclosiloxane is highly distorted, giving the ligand a boat-like shape encapsulating the central ion. This conformation enables four close contacts with the central ion and four remote contacts. The close contacts measure 311.3(1) and 314.2(1) pm, and the remote contacts measure 320.6(1) and 344.5(2) pm. However, after workup and crystallization, compound **7** shows major instabilities. Upon handling under a glovebox atmosphere and allowing the compound to warm to ambient temperature, the isolated single crystals began to decompose and melt. The freshly prepared, fine-shaped, colourless platelets turned opaque and greasy. For this reason,

 This journal is © the Partner Organisations 2020

Published on 12 March 2020. Downloaded on 7/6/2020 9:12:51 PM.

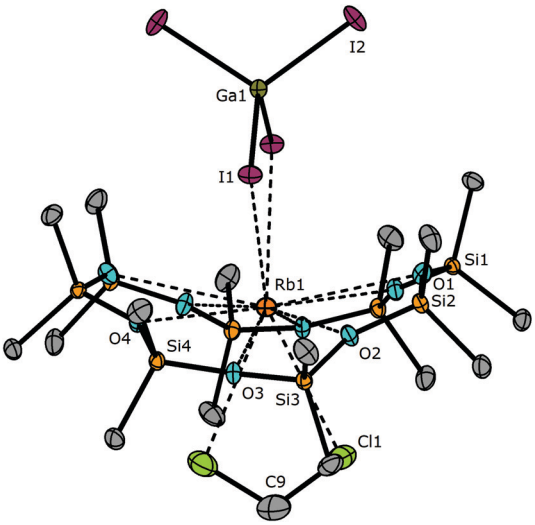

Fig. 8 The molecular structure of $[Rb(D_8)(DCM)GaI_4]$ (**7**) in crystal form. The thermal ellipsoids represent the 50% probability level. Non-labelled atoms are symmetry generated using # = 1 − *x*, *y*, 1/2 − *z*. Selected bond lengths [pm]: O1–Rb1: 344.5(2); O2–Rb1: 311.3(1); O3–Rb1: 320.6(1); O4–Rb1: 314.2(1); I1–Rb1: 373.7(1); Cl1–Rb1: 355.4(1). Selected bond angles [°]: O1–Rb1–O2: 45.9(1); O2–Rb1–O3: 47.8(1); O3–Rb1–O4: 47.5(1); Si1–O1–Si2: 153.2(1); Si1–O4#–Si4#: 144.4(1); Si2–O2–Si3: 143.8(1); Si3–O3–Si4: 150.3(1).

characterization is somewhat restricted. Elemental analysis failed after several attempts. Furthermore, NMR spectroscopy (also at lower temperatures) should reveal a single resonance for all NMR active nuclei. This, however, is not the case, as several resonances are found within all spectra, revealing that the siloxane moiety does not remain completely intact when the single crystals begin to dissolve. Only a freshly prepared assay of compound 7 could be analysed by means of SC-XRD, IR and MS. Besides SC-XRD, the ESI^+ MS spectrum reveals an *m*/*z* value of 677.0614 $[Rb + D_8]^+$ and proves convincingly the existence of ligand···metal interactions and an intact cationic part of 7. This silyl-ether coordination, however, is highly unsupported and for this reason represents one of the limits of silyl ether coordination in combination with the small WCA $[GaI_4]^-$. Overall, the ligand strives to remain uncoordinated, as we also reported for hybrid sila-ethers.[27] Further, the possibility of I^- acting as a nucleophile is the most likely reason explaining why a complex comprised of unsupported silyl ether coordination bonds is even more unstable due to Si–O bond cleavage. Attempts at coordinating D_8 towards Cs^+ employing the $[GaI_4]^-$ anion failed. We applied the same reaction conditions, but we could not observe an NMR chemical shift or a suitable *m*/*z* value from MS. To provide meaningful spectroscopic data related to an Rb^+ complex and to somehow obtain a Cs^+ complex, we applied large, bulky WCAs. Conventional alkoxyaluminates[39] are suitable candidates, and the effectiveness of WCAs at minimizing lattice energy in combination with their robust, non-nucleophilic characteristics is very useful regarding the creation of such unsupported silyl ether coordination with heavy alkali metal compounds. Salts

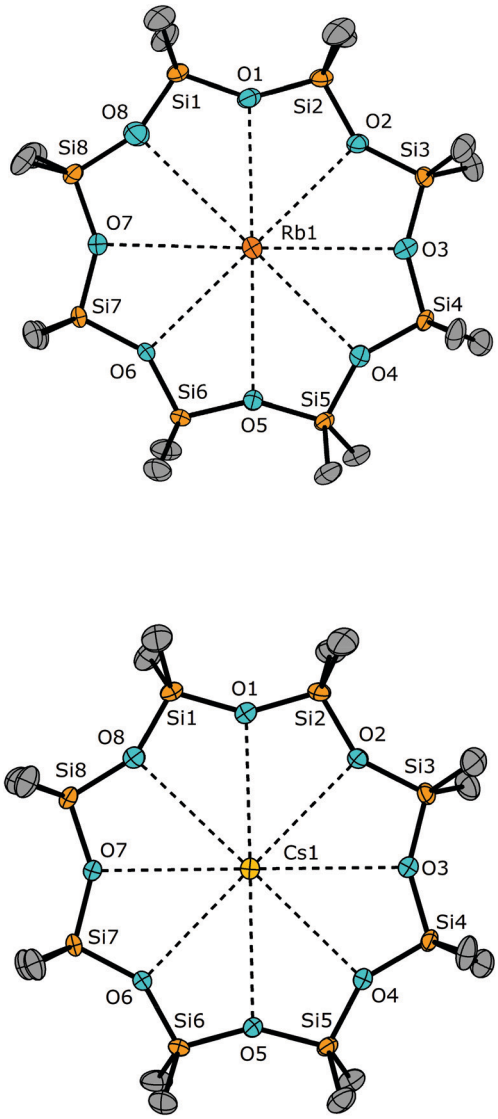

Fig. 9 The top-view of the coordination sphere of $^1_\infty[Rb(D_8)AL_F]$ (**8**) in crystal form (top) and the top-view of the isostructural coordination sphere of $^1_\infty[Cs(D_8)AL_F]$ (**9**) (bottom). The thermal ellipsoids represent the 50% probability level. Only one out of two independent ligand spheres is drawn. Co-crystalline DCM molecules and $[Al_F]^-$ anions are omitted for clarity. (**8**): selected bond lengths [pm]: O1–Rb1: 325.5(3); O2–Rb1: 321.5(1); O3–Rb1: 333.5(3); O4–Rb1: 331.7(3); O5–Rb1: 331.5(3); O6–Rb1: 322.6(3); O7–Rb1: 335.1(3); O8–Rb1: 351.9(4). Selected bond angles [°]: O1–Rb1–O2: 46.3(1); O2–Rb1–O3: 45.4(1); O3–Rb1–O4: 44.7(1); O4–Rb1–O5: 45.5(1); O5–Rb1–O6: 45.5(1); O6–Rb1–O7: 45.7(1); O7–Rb1–O8: 43.4(1); Si1–O1–Si2: 144.9(3); Si1–O8–Si8: 154.5(3); Si2–O2–Si3: 145.4(3); Si3–O3–Si4: 150.4(3); Si4–O4–Si5: 147.7(3); Si5–O5–Si6: 150.1(3); Si6–O6–Si7: 144.2(2); Si7–O7–Si8: 146.4(3). (**9**): selected bond lengths [pm]: O1–Cs1: 330.7(2); O2–Cs1: 328.4(2); O3–Cs1: 334.4(2); O4–Cs1: 334.4(2); O5–Cs1: 337.3(2); O6–Cs1: 329.1(2); O7–Cs1: 332.7(2); O8–Cs1: 340.0(2). Selected bond angles [°]: O1–Cs1–O2: 45.7(1); O2–Cs1–O3: 45.4(1); O3–Cs1–O4: 45.0(1); O4–Cs1–O5: 44.8(1); O5–Cs1–O6: 45.0(1); O6–Cs1–O7: 45.5(1); O7–Cs1–O8: 44.5(1); Si1–O1–Si2: 147.8(1); Si1–O8–Si8: 150.9(1); Si2–O2–Si3: 147.3(1); Si3–O3–Si4: 150.1(1); Si4–O4–Si5: 147.7(1); Si5–O5–Si6: 150.3(1); Si6–O6–Si7: 146.1(1); Si7–O7–Si8: 147.7(1).

Published on 12 March 2020. Downloaded on 7/6/2020 9:12:51 PM.

of the heavy alkali metal WCAs are synthesized *via* either procedures reported in the literature[40] or those reported in the Experimental section. In the case of the potassium salt, we have also provided the crystal structure (see Fig. S2†). The Cs^+ salt is known in the literature[40] and for the Rb salt, no suitable crystals for SC-XRD analysis were obtained.

The reaction of D_8 with $Rb[Al_F]$ (Al_F^- = $[Al\{OC(CF_3)_3\}_4]^-$) in DCM yields $^1_\infty[Rb(D_8)AL_F]$ (**8**) (Fig. 9). The conversion and yield are quantitative. Large colourless platelets were obtained overnight from a saturated DCM solution at 6 °C. The resulting colourless platelets were investigated *via* SC-XRD and **8**, a one-dimensional coordination polymer along the [100] direction, was determined to exist in the triclinic crystal system with the space group $P\bar{1}$ (see also Fig. S3†). The ligand architecture is less distorted compared to **7**, as the Rb^+ centre is coordinated in an almost coplanar fashion by all of the oxygen atoms. This is probably due to the bulkier anion, which enforces coplanar coordination. Associated with this ligand conformation, it is notable that the average O–Rb atom distances have larger values, even though the anion is more weakly coordinating (322.6(3)–351.9(4) pm in **8** *vs.* 311.3(1)–344.5(2) pm in **7**).

With this respective Rb^+ complex, the first ever silyl-ether coordination of a neutral ligand with Rb^+ was established and characterized satisfactorily. The $^{29}Si\{^1H\}$ NMR chemical shift appears at −16.07 ppm. Even though a chemically softer cation was complexed, the respective resonance was shifted to a slightly more low-field value than the potassium species **5**; however, it should be noted that the metal–anion interactions involving the bulky non-nucleophilic $[Al_F]^-$ anion are far less pronounced. This makes the coordination of the Si–O–Si moiety much more favourable in solution. Nevertheless, this chemical shift in combination with $[Al_F]^-$ does once again demonstrate that silyl ether coordination significantly weakens as soon as Rb^+ is employed as a cation. Even more unsupported is the coordination of D_8 towards Cs^+. As mentioned, $[GaI_4]^-$ is an unsuitable anion for complexation in this case. $[Al_F]^-$, however, also allows for attraction between the siloxane moiety and Cs^+. Therefore, finally, it was possible to obtain $^1_\infty[Cs(D_8)AL_F]$ (**9**), isotypic to **8** (Fig. 9 and Fig. S3†). The molecular structure of the crystal was determined from colourless platelets that were grown from DCM solution. As we were able to determine the molecular structure of the crystal, it should be noted at this point that this is the first communicated structure bearing Si–O···Cs^+ contacts in combination with a neutral ligand. In this context also, deprotonated silsesquioxane ligand complexes have been published in the literature,[41] but forcing Si–O···M^+ (M = Rb^+, Cs^+) contacts remains a challenge if a neutral silicon-based ligand is used for complexation. So

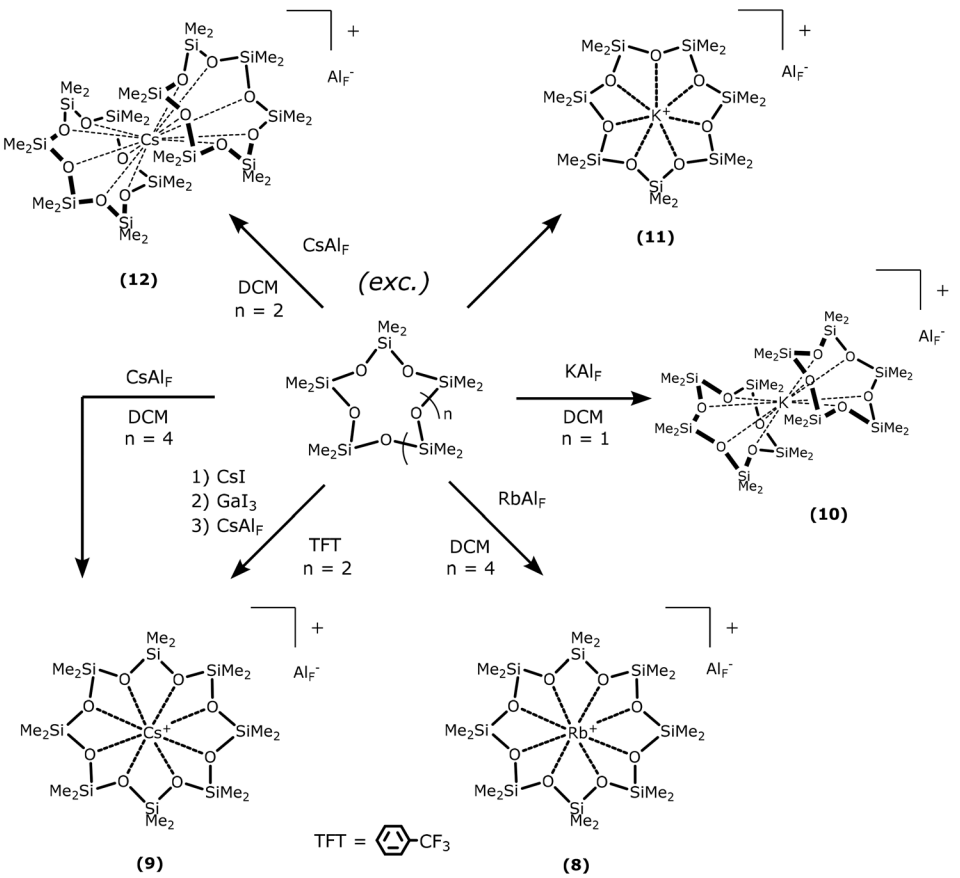

Scheme 3 A schematic representation of the synthesis and binding modes of compounds **8–12** employing the weakly coordinating anion $[Al_F]^-$ as well as different siloxanes.

 This journal is © the Partner Organisations 2020

Published on 12 March 2020. Downloaded on 7/6/2020 9:12:51 PM.

far, commercially available siloxanes are only able to coordinate with Cs^+ employing this weakly coordinating anion. The $^{29}Si\{^1H\}$ NMR chemical shift is −17.39 ppm, which is even less pronounced than that of **8**, which is why Si–O···Cs^+ attraction is even less supported than Si–O···Rb^+. This $^{29}Si\{^1H\}$ NMR chemical shift is the most high-field shifted value observed so far out of all characterized siloxane coordination compounds bearing a neutral pseudo-crown ligand. The metal–anion interactions involving the $[GaI_4]^-$ anion are too strong to yield a stable Cs^+ complex. Employing the bulky $[Al_F]^-$ anion extends the limits of siloxane coordination chemistry (Scheme 3).

As we were able to obtain stable 1 : 1 complexes in various pseudo-crown ether environments, we also tried to vary the stoichiometry in combination with ligand moieties that are too small for 1 : 1 complexation. Doing so, we tried to isolate sandwich-type complexes, but a number of reactions failed, which is closely related to the template chemistry involved. The presence of a nucleophilic I^- source, such as $[GaI_4]^-$, perturbs sandwich formation and supports ring opening polymerization. The reactions presented in Scheme 3 give an overview of the different reaction protocols that were performed. The reaction of excess D_5 with *in situ* generated $K[GaI_4]$ yields $[K(D_7)GaI_4]$ (**5**) due to the oligomerisation of the cyclosiloxane. However, the reaction of $K[Al_F]$ with D_5 allowed the sandwich complex $[K(D_5)_2][Al_F]$ (**10**) to be isolated. The caesium complex $[Cs(D_6)_2][Al_F]$ (**12**) was obtained *via* a similar reaction of D_6 with $Cs[Al_F]$. These compounds are, to the best of our knowledge, the first sandwich complexes involving these pseudo-crowns to be reported. The reaction of D_6 with $Cs[Al_F]$ together with *in situ* generated $Cs[GaI_4]$ again yields compound **9**, which contains the D_8 ligand that was formed upon oligomerisation from D_6. The synthesis of **10** was made possible by cooling an excess of D_5 together with $K[Al_F]$ in DCM to −12 °C. It is notable that placing a sample at a higher temperature, such as 6 °C, exclusively leads to the recrystallization of the potassium salt in the form of colourless blocks (see Fig. S2† for the crystal structure). Only lower temperatures lead to sandwich formation; the D_5 ligands do not support coordination with potassium ions at higher temperatures and only act as auxiliaries,[27] increasing the solubility of the potassium salt. This behaviour was understood based on the performance of variable temperature ^{29}Si NMR experiments. Dissolving isolated crystals of **10** in deuterated DCM and cooling from ambient temperature to 220 K significantly increases the interactions of the siloxane with potassium ions, which are obviously in equilibrium between siloxane and solvent coordination. At ambient temperature, a chemical shift of −21.1 ppm is observed, which indicates no significant coordination between D_5 and K^+. Upon cooling the sample, the single resonance undergoes a downfield shift, which is characteristic[22] of siloxane coordination (see Fig. S7† for a representation of this). Thus, the amount of complex **10** is higher at low temperatures, with the crystallization of **10** at −12 °C. The chemical shift of **10** at 220 K is −16.6 ppm, and this fits well with the D_7 complex of **5** where a chemical shift of −16.4 ppm is observed. To make an even more suitable comparison, we also converted D_7 with $K[Al_F]$,

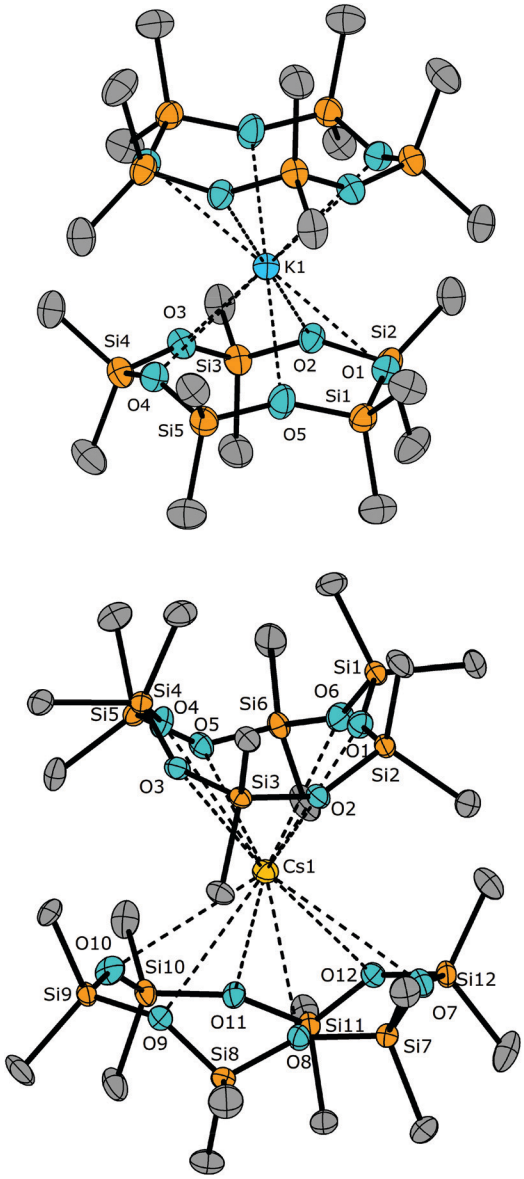

Fig. 10 The molecular structures of the coordination spheres of **10** (top) and **12** (bottom) in crystal form. The thermal ellipsoids represent the 30% probability level (top) and the 50% probability level (bottom). Non-labelled atoms are symmetry generated using # = 1–*x*, –*y*, 1 – *z*. Only one out of two independent molecules of **12** is drawn. The $[Al_F]$ anions are omitted for clarity. (**10**): selected bond lengths [pm]: O1–K1: 310.7(3); O2–K1: 296.0(3); O3–K1: 293.8(4); O4–K1: 312.0(3); O5–K1: 286.9(3). Selected bond angles [°]: O1–K1–O2: 50.7(1); O2–K1–O3: 52.2(1); O3–K1–O4: 50.8(1); O4–K1–O5: 50.8(1); Si1–O1–Si2: 145.3(2); Si1–O5–Si5: 153.0(2); Si2–O2–Si3: 146.8(2); Si3–O3–Si4: 148.0(2); Si4–O4–Si5: 145.3(2). (**12**): selected bond lengths [pm]: O1–Cs1: 329.9(7); O2–Cs1: 332.3(6); O3–Cs1: 367.2(7); O4–Cs1: 334.5(7); O5–Cs1: 339.8(7); O6–Cs1: 361.0(8); O7–Cs1: 352.2(7); O8–Cs1: 332.1(7); O9–Cs1: 356.2(7); O10–Cs1: 352.2(8); O11–Cs1: 319.1(6); O12–Cs1: 353.1(7). Selected bond angles [°]: O1–Cs1–O2: 45.8(1); O1–Cs1–O6: 43.6(1); O2–Cs1–O3: 43.9(1); O3–Cs1–O4: 43.0(1); O4–Cs1–O5: 45.4(1); O5–Cs1–O6: 43.8(1); O7–Cs1–O8: 44.5(1); O7–Cs1–O12: 44.5(1); O8–Cs1–O9: 43.6(1); O9–Cs1–O10: 43.7(1); O10–Cs1–O11: 45.1(1); O11–Cs1–O12: 44.7(1); Si1–O1–Si2: 146.2(5); Si1–O6–Si6: 151.4(5); Si2–O2–Si3: 146.2(4); Si3–O3–Si4: 150.1(4); Si4–O4–Si5: 144.2(4); Si5–O5–Si6: 145.3(5); Si7–O7–Si12: 147.3(5); Si7–O8–Si8: 143.3(5); Si8–O9–Si8: 149.2(5); Si9–O10–Si10: 148.8(5); Si10–O11–Si11: 139.9(4); Si11–O12–Si12: 145.3(5).

Published on 12 March 2020. Downloaded on 7/6/2020 9:12:51 PM.

which leads to the formation of $[K(D_7)Al_F]$ (**11**) (see Fig. S5† for the crystal structure). The $^{29}Si\{^1H\}$ NMR chemical shift of **11** appears at −16.2 ppm, which also compares very well with the above. If a sample of **10** is kept at ambient temperature, solvent coordination prevails again. Overall this reaction is reversible. The same behaviour in solution was observed for the Cs^+ species **12** (see Fig. S8†).

According to the solid-state structure, the D_5 rings of **10** coordinate fivefold towards the potassium centre, which results in CN = 10 (Fig. 10). The K–O contacts have an average distance of 299.9(3) pm. In comparison with the aforementioned K^+ complexes, this value is higher, most likely because of steric effects. The Si–O–Si angles are overall quite small. They measure from 145.3(2) to 153.0(2)° and are on average smaller than those of compound **4**. For this reason, the siloxane moiety is indicated to have notable basicity and backbonding in the case of $n_O \rightarrow \sigma^*_{Si-C}$ negative hyperconjugation interactions is decreased. This is also an explanation for the high tendency of silicon-based systems to be ring-opened if a suitable nucleophile is present. Pre-coordination withdraws electron density from the Si–O–Si linkages, which are then vulnerable to nucleophilic attack. Depending on the ion size, a novel silicon-based ligand environment is then formed. These observations compare well with those reported before and, thus, the mechanism related to the reaction is related to those proposed in recent works.[24,26] Comparing **10** with **5** and **11**, it is notable that the Si–O–Si angles might be larger in **5** and **11**, but coplanar coordination together with smaller O···K^+ atom distances is favoured over a higher coordination number, together with smaller siloxane angles. From the observations made herein, cyclosiloxanes prefer coplanar coordination with the metal centre placed inside the ligand moiety. That is also the exact case for the D_6/Cs[GaI_4]/Cs[Al_F] systems. As long as the $[GaI_4]^-$ anion is present, the D_8 moiety is formed. If there is the exclusive presence of Cs[Al_F], the D_6 entities sandwich Cs^+. The solid-state structure of **12** reveals a twelvefold coordinated Cs^+ cation. The D_6 ligands are highly distorted and present a highly unusual conformation. The ligands are squeezed and adopt a boat-like shape. This enables the two ligands to coordinate in a six-fold manner with the Cs^+ cation. The Si–O–Si angles range from 139.9(4) to 151.4(5)° and the O···Cs^+ atom distances range from 319.1(6) to 367.2(7) pm.

Conclusions

In this work we have convincingly shown that it is very possible to obtain alkali metal complexes of cyclodimethylsiloxanes employing suitable cation–anion combinations. All non-radioactive alkali metal cations could be incorporated with matching ligand moieties. Compounds with unprecedented coordination modes, as well as novel molecular architectures, were isolated and characterized.

Starting with the Li^+ cation, we were able to observe the coordination of D_5 with Li^+ from a suitable X-ray structure after reacting D_5 with LiI and GaI_3. Due to template effects, the dinuclear coordination compound $[Li_2(D_5)(D_6)(GaI_4)_2]$ (**1**) was characterized. The direct reaction of D_6 with LiI and GaI_3 yielded $[Li(D_6)GaI_4]$ (**2**) in quantitative yield. D_6 is a more suitable ligand for complexation, as D_5 readily undergoes ring opening polymerization forming D_6 in the presence of $Li[GaI_4]$, and **2** is also stable towards traces of moisture as $[Li(D_6)H_2O][GaI_4]$ (**2a**) could be characterized *via* SC-XRD. The first sodium cyclodimethylsiloxane complexes were isolated upon reacting NaI, GaI_3 and D_n (n = 6, 7). Both ligands, D_6 and D_7, provide suitable coordination geometry. The complexes $[Na(D_6)GaI_4]$ (**3**) and $[Na(D_7)(DCM)GaI_4]$ (**4**) were isolated and characterized. Rare DCM coordination was additionally observed when using D_7 as a ligand. Similar to **4**, the potassium ion was also trapped inside D_7, and DCM saturated the metal centre, allowing $[K(D_7)(DCM)GaI_4]$ (**5**) to be characterized. At this point, the D_n-MI-GaI_3 system was working well for silyl-ether coordination chemistry so we also tried to bind the NH_4^+ cation due to its great resemblance to K^+. Upon forming the $[Ga_2I_7]^-$ anion and ring opening, the very unusual complex $[NH_4(D_7)][Ga_2I_7]$ (**6**) was isolated and hydrogen bonding towards Si–O-donors could be experimentally verified by means of $^{29}Si\{^1H\}$ NMR, IR spectroscopy and SC-XRD studies. This compound is the first ever characterized non-metal cyclosiloxane complex; rare hydrogen···siloxane-donor bonding was purposefully realized, and experimental data is provided. As this compound was counterintuitively obtained, we stepwise explored the limits of silyl-ether coordination chemistry. Therefore, we first reacted D_8 with *in situ* generated Rb[GaI_4] and then Cs[GaI_4]. In the case of Rb^+, we could cumbersomely characterize $[Rb(D_8)(DCM)GaI_4]$ (**7**) based on an X-ray structure and mass spectrometry data, but the compound started to decompose readily in solution as soon as solvent was added. The reaction with Cs^+ salt failed. To obtain meaningful spectroscopic data from an Rb^+ compound and to somehow obtain a Cs^+ complex, we employed the weakly coordinating anion $[Al_F]^-$. The conversion of M[Al_F] then yielded $^1_\infty[M(D_8)AL_F]$ (M = Rb^+: **8**; M = Cs^+: **9**) in the solid state. Both compounds, **8** and **9**, were fully characterized. These weakly coordinating, large, non-nucleophilic anions are the only way to overcome the issues related to Rb^+ and Cs^+ silyl-ether coordination.

Finally, we aimed at synthesizing 2 : 1 complexes of such siloxanes. It could be shown that ligand moieties that are too small for 1 : 1 complexation can be cleaved in the presence of $[GaI_4]^-$ salt and are ring opened in the case of ion-specific ligands. Thus, 2 : 1 complexes can only be obtained with a chemically inert, weakly coordinating anion, such as the aforementioned $[Al_F]^-$ ion. The reaction of excess $D_{5/6}$ with M[Al_F] (M = K^+, Cs^+) turned out to be expedient, and $[K(D_5)_2][Al_F]$ (**10**) and $[Cs(D_6)_2][Al_F]$ (**12**), the first ever observed sandwich-type complexes consisting of two cyclosiloxane ligands, were characterized. The behaviour of these complexes in solution was investigated by means of VT NMR experiments, which indicated that such sandwich-type complexes are only stable at low temperatures.

To sum up, the coordination of the alkali metal ions Li^+–K^+ is very much possible when $[GaI_4]^-$ is employed as an anion.

 This journal is © the Partner Organisations 2020

Published on 12 March 2020. Downloaded on 7/6/2020 9:12:51 PM.

For the large Rb^+ and Cs^+ cations, the chemically inert $[Al_F]^-$ ion is strongly recommended for obtaining stable complexes in suitable yields. For the formation of sandwich-type complexes, the use of $[Al_F]^-$ is mandatory. The compounds presented herein convincingly show that metal centres can be attracted to silicon-bonded oxygen atoms. This is also of considerable significance in the context of Si–O bond activation reactions. Such silyl-ether coordination reactions could be the starting point for templated (cyclo-)siloxane synthesis from polydimethylsiloxanes. In conclusion, we want to emphasize that recent advances in silyl-ether bonding should be transferred to three-dimensional silyl ethers, such as silsesquioxanes, in order to obtain cage-like (polymeric) coordination compounds, which could be of potential interest for various applications in materials science and/or electrochemistry.

Experimental section

All manipulations were carried out with the rigorous exclusion of oxygen and moisture using basic Schlenk techniques under argon gas, if not stated otherwise. Solvents were dried and freshly distilled before use and subsequently stored over molecular sieves (3 Å). The alkali metal salts LiI (Alfa Aesar, 99.996%), NaI (Acros Organics, ≥99%), KI (Sigma-Aldrich, ≥99.99%), RbI (99.8%, Alfa Aesar), and CsI (99.9% Alfa Aesar), and the salts NH_4I (Acros Organics, ≥99%) and GaI_3 (abcr, 99%) were used as received. The cyclosiloxanes D_5, D_6, D_7 and D_8 (≥95%) were purchased from TCI and used as received as well.

$Li[Al_F]$[42] and $Cs[Al_F]$[40] were synthesized using methods described in the literature. We emphasize that the synthesis of $K[Al_F]$ and $Rb[Al_F]$ was also performed according to known literature procedures[40] but with small manipulations (see below). All salts were handled under an argon atmosphere using an MBraun-type glovebox.

For all reactions, we strictly avoided the use of silicon-grease. For all glass valves and joints we used PTFE paste (Carl Roth). NMR spectra were recorded using different Bruker spectrometers, *e.g.*, AV III HD 300 MHz or AV III HD 500 MHz at 300 K if not stated otherwise (*e.g.*, compound **6**). Infrared (IR) spectra of the respective samples were obtained using attenuated total reflectance (ATR) mode on a Bruker-type Alpha FT-IR spectrometer. The OPUS-Software package was applied throughout. ESI mass spectra were acquired with an LTQ-FT Ultra mass spectrometer (Thermo Fischer Scientific). The resolution was set to 100.000. Elemental analysis was performed using Vario MicroCube (CHN analysis) or Bruker M4 Tornado (micro X-ray fluorescence spectroscopy) apparatus, equipped with an Rh-target X-ray tube and Si drift detector. The values obtained from elemental analyses (CHN) are outside the range viewed as establishing analytical purity for compounds **5**, **6** and **10**. We provide these values regardless to illustrate the best values obtained to date. In the case of compound **12**, the obtained colorless blocks readily start to decompose at ambient temperature forming a sticky grease that could not be analyzed by means of elemental analysis. Possible reasons for the low C values are the formation of SiC or the presence of $[Ga_nI_{3n+1}]^-$ anions in the bulk compounds where GaI_3 was used. Increased Ga and I values are indicated by means of μ-XFS (μ-XFS = micro X-ray fluorescence spectroscopy) for example in the case of compound **5**.

Synthesis and crystallization

$K[Al_F]$. 250 mg of KF (4.30 mmol, 1.40 eq.) together with 3 g of $Li[Al_F]$ are placed in a Schlenk tube. Subsequently, 15 mL of a DCM/Et_2O mixture (2 : 1) is added. The resulting suspension is warmed to 35 °C and placed in a supersonic bath overnight. After filtration, the solvent is removed under reduced pressure and dried *in vacuo* for several days using an oil diffusion pump. $K[Al_F]$ is obtained as a colourless powder with a total yield of 89% (2.75 g, 2.74 mmol). Single crystals of $K[Al_F]$ are obtained from DCM/D_5 solution at 6 °C.

$^{13}C\{^1H\}$ NMR (75 MHz, D_2O, ppm): δ = 78.6 (br, s, $C\{CF_3\}_3$), 121.0 (q, $^1J_{CF}$ = 291.7 Hz, $C\{CF3\}_3$). ^{19}F NMR (283 MHz, D_2O, ppm): δ = −76.01 (br, s, $C\{CF_3\}_3$). ^{27}Al NMR (130 MHz, D_2O, ppm): δ = 34.6 (s, $Al[OC(CF_3)_3]_4^-$). IR (cm^{-1}): 2964 (w), 1351 (w), 1298 (m), 1270 (m), 1238 (m), 1212 (s), 1167 (w), 1028 (s, br), 971 (s), 858 (m), 813 (s), 795 (s), 726 (s), 714 (m), 560 (w), 534 (m), 444 (m). CHN calcd for $C_{16}AlF_{36}KO_4$ C: 19.10; found C: 19.64.

$Rb[Al_F]$. 250 mg of RbF (2.41 mmol, 1.40 eq.) together with 1.67 g of $Li[Al_F]$ (1.72 mmol, 1.00 eq.) are placed in a Schlenk tube. Subsequently, 15 mL of DCM is added. The resulting suspension is warmed to 35 °C and placed in a supersonic bath overnight. After filtration, the solvent is removed under reduced pressure and dried *in vacuo*. $Rb[Al_F]$ is obtained as a colourless powder with a total yield of 30% (0.54 g, 2.74 mmol). No suitable single crystals for SC-XRD analysis could be obtained.

$^{13}C\{^1H\}$ NMR (75 MHz, D_2O, ppm): δ = 121.0 (q, $^1J_{CF}$ = 291.4 Hz, $C\{CF3\}_3$). The quaternary C atom is not observed. ^{19}F NMR (283 MHz, D_2O, ppm): δ = −76.04 (br, s, $C\{CF_3\}_3$). ^{27}Al NMR (130 MHz, D_2O, ppm): δ = 34.6 (s, $Al[OC(CF_3)_3]_4^-$). IR (cm^{-1}): ν = 1353 (w), 1242 (br, s), 1214 (br, s), 958 (s), 833 (w), 798 (w), 755 (w), 724 (s), 560 (w), 536 (m), 442 (m). CHN calcd for $C_{16}AlF_{36}RbO_4$ C: 18.26; found C: 19.01.

$[Li_2(D_5)(D_6)(GaI_4)_2]$ (1). 38 mg of LiI (0.28 mmol, 1.00 eq.) together with 126 mg of GaI_3 (0.28 mmol, 1.00 eq.) are suspended in 5 mL of α,α,α-trifluorotoluene. The mixture is stirred for 10 min and, subsequently, a slight excess of D_5 (0.31 mmol, 114 mg, 1.10 eq.) is added *via* a syringe. As soon as the salt is dissolved, the reaction is immediately stopped, and the solvent is removed under reduced pressure. The residue is dissolved in 5 mL of DCM followed by filtration. The solvent is again removed, and the microcrystalline residue is gently washed with 2 mL of *n*-pentane. **1** is obtained as a colourless to slightly brown powder (178 mg, 0.09 mmol, 64% based on D_5). For single crystal growth, 50 mg of **1** is dissolved in 2 mL of DCM together with 1 mL of benzene-d_6. After concentrating and adjusting the solution to −24 °C, colourless needles of **1**·C_6D_6 were obtained overnight.

Published on 12 March 2020. Downloaded on 7/6/2020 9:12:51 PM.

^{1}H NMR (300 MHz, CD_2Cl_2, ppm): δ = 0.34 (s, 36H, D_6: Si(CH_3)$_2$), 0.35 (s, 30H, D_5: Si(CH_3)$_2$). ^{13}C{^{1}H} NMR (75 MHz, CD_2Cl_2, ppm): 1.38 (s, D_5: Si*C*H$_3$), 1.42 (s, D_6: Si*C*H$_3$). ^{29}Si{^{1}H} NMR (99 MHz, CD_2Cl_2, ppm): δ = −7.4 (s, D_6: Si(CH$_3$)$_2$), −9.0 (s, D_5: Si(CH$_3$)$_2$). ^{7}Li NMR (117 MHz, CD_2Cl_2, ppm): δ = 0.1 (br-s, *Li*GaI$_4$). IR (cm^{-1}): 2961 (w), 1621 (w), 1412 (w), 1263 (m), 990 (m), 856 (m), 799 (s), 708 (m), 574 (w), 525 (w). CHN calcd for $C_{22}H_{66}Ga_2I_8Li_2O_{11}Si_{11}$ C: 13.32; H: 3.35; found C: 13.16; H: 3.27.

[Li(D$_6$)GaI$_4$] (2). 31 mg of LiI (0.23 mmol, 1.00 eq.) together with 104 mg of GaI$_3$ (0.23 mmol, 1.00 eq.) are suspended in 5 mL of α,α,α-trifluorotoluene. The mixture is stirred for 10 min and, subsequently, 102 mg of D_6 (0.23 mmol, 1.00 eq.) are added *via* a syringe. The mixture is stirred for one hour and, subsequently, the solvent is removed under reduced pressure. The residue is dissolved in 5 mL of DCM followed by filtration. The solvent is again removed and **2** is obtained as a colourless to slightly brown (micro-)crystalline powder. The yield is quantitative. A few single crystals in the shape of colourless platelets were obtained directly upon removing the solvent. Dissolving 50 mg of **2** in DCM, exposing to moisture and placing at −24 °C yields colourless platelets of [Li(D_6)(H_2O)][GaI$_4$] (**2a**) within a few hours.

^{1}H NMR (300 MHz, CD_2Cl_2, ppm): δ = 0.34 (s, 36H, Si(CH_3)$_2$). ^{13}C{^{1}H} NMR (75 MHz, CD_2Cl_2, ppm): 1.42 (s, Si*C*H$_3$). ^{29}Si{^{1}H} NMR (99 MHz, CD_2Cl_2, ppm): δ = −7.4 (s, *Si*(CH$_3$)$_2$). ^{7}Li NMR (117 MHz, CD_2Cl_2, ppm): δ = −0.5 (s, *Li*GaI$_4$). IR (cm^{-1}): 2958 (w), 1412 (w), 1263 (m), 1090 (m), 980 (s), 852 (m), 814 (s), 796 (s), 713 (m), 620 (w), 554 (m), 459 (w). HR-MS ESI(+) *m*/*z*: 451.1283 [M − GaI$_4$]$^+$ (100). CHN calcd for $C_{12}H_{36}Ga_1I_4Li_1O_6Si_6$ C: 14.00; H: 3.53; found C: 13.32; H: 3.54.

[Na(D$_6$)GaI$_4$] (3). 40 mg of NaI (0.27 mmol, 1.00 eq.) together with 122 mg of GaI$_3$ (0.27 mmol, 1.00 eq.) are suspended in 5 mL of α,α,α-trifluorotoluene. The mixture is stirred for 10 min and, subsequently, 120 mg of D_6 (0.27 mmol, 1.00 eq.) is added *via* a syringe. The mixture is stirred for another 10 min and, subsequently, the solvent is removed under reduced pressure. The residue is dissolved in 5 mL of DCM, followed by filtration. The solvent is again removed and **3** is obtained as a colourless to slightly brown powder (271 mg, 96%). Single crystals in the shape of colourless platelets were obtained overnight after placing a saturated DCM solution of **3** at −24 °C.

^{1}H NMR (300 MHz, CD_2Cl_2, ppm): δ = 0.27 (s, 36H, Si(CH_3)$_2$). ^{13}C{^{1}H} NMR (75 MHz, CD_2Cl_2, ppm): 1.44 (s, Si*C*H$_3$). ^{29}Si{^{1}H} NMR: (99 MHz, CD_2Cl_2, ppm): δ = −14.9 (s, *Si*(CH$_3$)$_2$). IR (cm^{-1}): 2960 (w), 1263 (m), 1021 (s), 857 (m), 797 (s), 709 (m), 518 (w). HR-MS ESI(+) *m*/*z*: 467.1018 [M − GaI$_4$]$^+$ (100), 541.1208 [D_7 + Na–GaI$_4$] (100). CHN calcd for $C_{12}H_{36}Ga_1I_4Na_1O_6Si_6$ C: 13.79; H: 3.47; found C: 13.65; H: 3.40.

[Na(D$_7$)(DCM)GaI$_4$] (4). 32 mg of NaI (0.21 mmol, 1.00 eq.) together with 95 mg of GaI$_3$ (0.21 mmol, 1.00 eq.) are suspended in 5 mL of α,α,α-trifluorotoluene. The mixture is stirred for 10 min and, subsequently, 110 mg of D_7 (0.21 mmol, 1.00 eq.) is added *via* a syringe. The mixture is stirred and as soon as everything has dissolved, the solvent is removed under reduced pressure. The residue is dissolved in 7 mL of DCM followed by filtration. The solvent is again removed and **4** is obtained as a colourless to slightly brown powder in quantitative yield. Single crystals in the shape of colourless platelets are obtained overnight after placing a saturated DCM solution of **4** at −24 °C.

^{1}H NMR (300 MHz, CD_2Cl_2, ppm): δ = 0.27 (s, 42H, Si(CH_3)$_2$). ^{13}C{^{1}H} NMR (75 MHz, CD_2Cl_2, ppm): 1.6 (s, Si*C*H$_3$). ^{29}Si{^{1}H} NMR (99 MHz, CD_2Cl_2, ppm): δ = −12.7 (s, *Si*(CH$_3$)$_2$). IR (cm^{-1}): 2960 (w), 1413 (vw), 1263 (s), 995 (vs), 857 (s), 793 (vs), 714 (s), 619 (w), 549 (m), 523 (w). HR-MS ESI(+) *m*/*z*: 541.1208 [M − GaI$_4$]$^+$ (100). CHN calcd for $C_{14}H_{42}Ga_1I_4Na_1O_7Si_7$ C: 15.02; H: 3.78; found C: 15.42; H: 3.84.

[K(D$_7$)(DCM)GaI$_4$] (5). 35 mg of KI (0.21 mmol, 1.00 eq.) together with 95 mg of GaI$_3$ (0.21 mmol, 1.00 eq.) are suspended in 5 mL of α,α,α-trifluorotoluene. The mixture is stirred for 10 min and, subsequently, 110 mg of D_7 (0.21 mmol, 1.00 eq.) is added *via* a syringe. The mixture is stirred for 15 min and a greyish powder precipitates from the solution. After the removal of the solvent *in vacuo*, the residue is dissolved in 7 mL of DCM, followed by filtration. The solvent is again removed and **5** is obtained as a colourless to slightly brown powder in quantitative yield. Single crystals in the shape of colourless platelets are obtained from a saturated DCM solution of **5** at ambient temperature. The respective complex can also be obtained in quantitative yields *via* converting excess D_5 (200 mg, 0.54 mmol, 2.6 eq.) instead of D_7.

^{1}H NMR (300 MHz, CD_2Cl_2, ppm): δ = 0.22 (s, 42H, Si(CH_3)$_2$). ^{13}C{^{1}H} NMR (75 MHz, CD_2Cl_2, ppm): 1.38 (s, Si*C*H$_3$). ^{29}Si{^{1}H} NMR: (99 MHz, CD_2Cl_2, ppm): δ = −16.4 (s, *Si*(CH$_3$)$_2$). IR (cm^{-1}): 2959 (w), 1413 (vw), 1263 (s), 1026 (vs), 858 (m), 795 (vs), 712 (s), 528 (m). HR-MS ESI(+) *m*/*z*: 557.0942 [M − GaI$_4$]$^+$ (100). CHN calcd for $C_{14}H_{42}Ga_1I_4K_1O_7Si_7$ C: 14.81; H: 3.73; found C: 13.02; H: 3.20.

[NH$_4$(D$_7$)][Ga$_2$I$_7$] (6). 46 mg of NH_4I (0.31 mmol, 1.00 eq.) together with 282 mg of GaI$_3$ (0.62 mmol, 2.00 eq.) are suspended in 5 mL of α,α,α-trifluorotoluene. The mixture is stirred for 10 min and, subsequently, excess D_6 (192 mg, 1.40 eq.) is added *via* a syringe. The mixture is stirred for 60 min and after the removal of the solvent *in vacuo*, the residue is dissolved in 7 mL of DCM followed by filtration. Concentrating the filtrate and storing at −24 °C for several days yields **6·DCM** as large colourless platelets. After drying *in vacuo*, a yield of 272 mg (56% based on NH_4I) is obtained.

^{1}H NMR (300 MHz, CD_2Cl_2, 253 K, ppm): δ = 0.19 (s, 42H, Si(CH_3)$_2$), 6.54 (*t*, $^1J_{NH}$ = 49.3 Hz, 4H, NH_4). ^{13}C{^{1}H} NMR (75 MHz, CD_2Cl_2, 253 K, ppm): 1.2 (s, Si*C*H$_3$). ^{29}Si{^{1}H} NMR (99 MHz, CD_2Cl_2, 253 K, ppm): δ = −15.6 (s, *Si*(CH$_3$)$_2$). IR (cm^{-1}): 3165 (*br*-m, $\tilde{\nu}_s$ N–H), 2958 (m), 1395 (m), 1262 (s), 1015 (vs), 853 (m), 791 (vs), 706 (s), 522 (m). HR-MS ESI(+) *m*/*z*: 541.1222 [M–Ga_2I_7–NH_4 + Na]$^+$ (100). CHN calcd for $C_{14}H_{46}Ga_2I_7N_1O_7Si_7$ C: 10.75; H: 2.96; N: 0.90; found C: 9.49; H: 2.60; N: 1.09.

 This journal is © the Partner Organisations 2020

Published on 12 March 2020. Downloaded on 7/6/2020 9:12:51 PM.

[Rb(D$_8$)(DCM)GaI$_4$] (7). 50 mg of RbI (0.24 mmol, 1.00 eq.) together with 108 mg of GaI$_3$ (0.24 mmol, 1.00 eq.) are suspended in 5 mL of α,α,α-trifluorotoluene. The mixture is stirred for 15 min and, subsequently, 140 mg of D$_8$ (0.24 mmol, 1.00 eq.) is added *via* a syringe. The mixture is stirred for 3 h and then the solvent is removed. The greasy residue is dissolved in 7 mL of DCM followed by filtration. Concentrating the filtrate and storing at −24 °C for several days yields **7** as colourless platelets (58 mg, 18%).

HR-MS ESI(+) *m*/*z*: 677.0614 $[M - I]^+$ (100). IR (cm^{-1}): 2959 (m), 2903 (vw), 1412 (vw), 1260 (s), 1015 (vs), 857 (m), 790 (vs), 713 (s), 529 (m).

[Rb(D$_8$)Al$_F$] (8). 139 mg of Rb[AL$_F$] (0.13 mmol, 1.00 eq.) together with 78 mg of D$_8$ (0.13 mmol, 1.00 eq.) are dissolved in 3 mL of DCM. The mixture is stirred overnight, and the solvent is removed until saturation is reached. Placing the solution at 6 °C yields **8·DCM** as large colourless platelets. Removing the solvent under reduced pressure yields **8** in quantitative yield.

^{1}H NMR (300 MHz, CD_2Cl_2, ppm): δ = 0.20 (s, 48H, Si(CH_3)$_2$). ^{13}C{^{1}H} NMR (75 MHz, CD_2Cl_2, ppm): δ = 1.26 (s, SiCH_3), 121.8 (q, $^1J_{CF}$ = 293.2 Hz, C{$CF3$}$_3$). The quaternary C atom is not observed. ^{19}F NMR (283 MHz, CD_2Cl_2, ppm): δ = −75.89. ^{27}Al NMR (130 MHz, CD_2Cl_2, ppm): δ = 34.3 (s, *Al*[OC(CF$_3$)$_3$]$_4^-$). ^{29}Si{^{1}H} NMR (99 MHz, CD_2Cl_2, ppm): δ = −16.1 (s, *Si*(CH$_3$)$_2$). IR (cm^{-1}): 2964 (w), 1351 (w), 1299 (m), 1268 (m), 1238 (m), 1212 (s), 1168 (w), 1018 (br, m), 971 (s), 858 (m), 810 (s), 791 (s), 726 (s), 717 (s), 559 (w), 536 (m), 444 (m). MS HR-LIFDI(+) MS *m*/*z* (%): 593.16042 $[M–Al_F + H]^+$ (100), 677.06178 $[M - Al_F]^+$ (100). CHN calcd for $C_{32}H_{48}Al_1F_{36}O_{12}Rb_1Si_8$ C: 23.35; H: 2.94; found C: 23.55; H: 3.03.

[Cs(D$_8$)Al$_F$] (9). 111 mg of Cs[Al$_F$] (0.10 mmol, 1.00 eq.) together with 60 mg of D$_8$ (0.10 mmol, 1.00 eq.) are dissolved in 3 mL of DCM. The mixture is stirred overnight, and the solvent is removed until saturation is reached. Placing the solution at 6 °C yields **9·DCM** as large colourless platelets. Removing the solvent under reduced pressure instantaneously yields **9** in quantitative yield. The respective complex can also be obtained by converting excess D$_6$ with equimolar amounts of CsI, Cs[Al$_F$], and GaI$_3$. After recrystallizing, **9** is obtained as large colorless platelets.

^{1}H NMR (300 MHz, CD_2Cl_2, ppm): δ = 0.17 (s, 48H, Si(CH_3)$_2$). ^{13}C{^{1}H} NMR (75 MHz, CD_2Cl_2, ppm): δ = 1.3 (s, SiCH_3), 121.8 (q, $^1J_{CF}$ = 291.2 Hz, C{CF_3}$_3$). The quaternary C atom is not observed. ^{19}F NMR (283 MHz, CD_2Cl_2, ppm): δ = −75.83. ^{27}Al NMR (130 MHz, CD_2Cl_2, ppm): δ = 34.3 (s, *Al*[OC(CF$_3$)$_3$]$_4^-$). ^{29}Si{^{1}H} NMR (99 MHz, CD_2Cl_2, ppm): δ = −17.4 (s, *Si*(CH$_3$)$_2$). MS HR-LIFDI(+) MS *m*/*z* (%): 593.16042 $[M–CsAl_F + H]^+$ (100), 677.06178 $[M - Al_F]^+$ (100). IR (cm^{-1}): 2964 (w), 1351 (w), 1298 (m), 1266 (m), 1237 (m), 1212 (s), 1167 (w), 1021 (s), 970 (s), 859 (m), 808 (s), 792 (s), 725 (s), 717 (m), 560 (w), 536 (m), 444 (m). CHN calcd for $C_{32}H_{48}Al_1F_{36}O_{12}Cs_1Si_8$ C: 22.70; H: 2.86; found C: 22.69; H: 2.92.

[K(D$_5$)$_2$][Al$_F$] (10). 75 mg of K[Al$_F$] (0.07 mmol, 1.00 eq.) together with a large excess of D$_5$ (0.3 mL, 0.78 mmol, 11.00 eq.) are dissolved in 5 mL of DCM. The solution is stirred for 30 min and is then reduced to a volume of approximately 2 mL. Placing this solution at −12 °C overnight yields large colourless blocks of **10**. After decanting off the solvent and excess D$_5$, large colourless blocks are obtained (99 mg, 81%).

^{1}H NMR (300 MHz, CD_2Cl_2, ppm): δ = 0.09 (s, 60H, Si(CH_3)$_2$). ^{13}C{^{1}H} NMR (75 MHz, CD_2Cl_2, ppm): δ = 1.1 (s, SiCH_3), 121.8 (q, $^1J_{CF}$ = 293.0 Hz, C{CF_3}$_3$). The quaternary C atom is not observed. ^{19}F NMR (283 MHz, CD_2Cl_2, ppm): δ = −75.83. ^{27}Al NMR (130 MHz, CD_2Cl_2, ppm): δ = 34.9 (s, *Al*[OC(CF$_3$)$_3$]$_4^-$). ^{29}Si{^{1}H} NMR (99 MHz, CD_2Cl_2, ppm): δ = −20.9 (s, *Si*(CH$_3$)$_2$). IR (cm^{-1}): 2968 (w), 1352.27 (w), 1299 (m), 1271 (s), 123 (s), 1215 (vs), 1167 (m), 1037 (s), 970 (vs), 857 (w), 806 (s), 725 (s), 706 (m), 560 (w), 535 (m), 514 (w), 442 (m), 410 (w). CHN calcd for $C_{36}H_{60}AlF_{36}KO_{14}Si_{10}$ C: 24.74; H: 3.46; found C: 23.95; H: 2.85.

[K(D$_7$)Al$_F$] (11). 75 mg of K[Al$_F$] (0.07 mmol, 1.00 eq.) together with 37 mg of D$_7$ are dissolved in 3 mL of DCM. The mixture is stirred overnight, and the solvent is removed until saturation is reached. Placing the solution at 6 °C yields **11** as large colourless platelets. Removing the solvent under reduced pressure yields **11** in quantitative yield as a colourless powder.

^{1}H NMR (300 MHz, CD_2Cl_2, ppm): δ = 0.19 (s, 48H, Si(CH_3)$_2$). ^{13}C{^{1}H} NMR (75 MHz, CD_2Cl_2, ppm): δ = 1.0 (s, SiCH_3), 121.8 (q, $^1J_{CF}$ = 293.1 Hz, C{CF_3}$_3$). The quaternary C atom is not observed. ^{19}F NMR (283 MHz, CD_2Cl_2, ppm): δ = −75.83. ^{27}Al NMR (130 MHz, CD_2Cl_2, ppm): δ = 34.3 (s, *Al*[OC(CF$_3$)$_3$]$_4^-$). ^{29}Si{^{1}H} NMR (99 MHz, CD_2Cl_2, ppm): δ = −16.2 (s, *Si*(CH$_3$)$_2$). IR (cm^{-1}): 2964 (w), 1351 (w), 1298 (m), 1270 (m), 1238 (m), 1212 (s), 1167 (w), 1028 (br, s), 971 (s), 858 (m), 813 (s), 795 (s), 726 (s), 714 (m), 560 (w), 534 (m), 444 (m). CHN calcd for $C_{36}H_{60}AlF_{36}KO_{14}Si_{10}$ C: 23.62; H: 2.78; found C: 24.08; H: 3.03.

[Cs(D$_6$)$_2$][Al$_F$] (12). 75 mg of Cs[Al$_F$] (0.07 mmol, 1.00 eq.) together with a large excess of D$_6$ (0.3 mL, 0.65 mmol, 9.20 eq.) are dissolved in 5 mL of DCM. The mixture is stirred for 2 h and the solvent is removed to a volume of approximately 2 mL. Placing the solution at −32 °C yields **12** as large colourless blocks after a few days (104 mg, 75%).

^{1}H NMR (300 MHz, CD_2Cl_2, ppm): δ = 0.10 (s, 72H, Si(CH_3)$_2$). ^{13}C{^{1}H} NMR (75 MHz, CD_2Cl_2, ppm): δ = 1.2 (s, SiCH_3), 121.8 (q, $^1J_{CF}$ = 292.6 Hz, C{CF_3}$_3$). The quaternary C atom is not observed. ^{19}F NMR (283 MHz, CD_2Cl_2, ppm): δ = −75.77. ^{27}Al NMR (130 MHz, CD_2Cl_2, ppm): δ = 34.9 (s, *Al*[OC(CF$_3$)$_3$]$_4^-$). ^{29}Si{^{1}H} NMR (99 MHz, CD_2Cl_2, ppm): δ = −20.8 (s, *Si*(CH$_3$)$_2$). IR (cm^{-1}): 2962 (w), 1413 (vw), 1352 (w), 1299 (s), 1259 (m), 1240 (s), 1217 (vs), 1167 (w), 1055 (vs), 969 (s), 857 (m), 796 (m), 726 (s), 703 (m), 658 (w), 559 (w), 536 (w), 443 (m).

Conflicts of interest

There are no conflicts to declare.

Published on 12 March 2020. Downloaded on 7/6/2020 9:12:51 PM.

Acknowledgements

This work was financially supported by the Deutsche Forschungsgemeinschaft (DFG). F. D. thanks the NMR- (Dr X. Xie and especially C. Mischke), MS- (especially J. Bamberger), and X-ray (M. Marsch, R. Riedel and Dr. S. Ivlev) departments at Philipps-Universität Marburg for measurement time and their kind advice. In particular, Dr S. Ivlev is gratefully acknowledged for his valuable help with X-ray crystallographic data.

Notes and references

1 J. S. Ritch and T. Chivers, Siliciumanaloga von Kronenethern und Cryptanden: ein neues Kapitel in der Wirt-Gast-Chemie?, *Angew. Chem.*, 2007, **119**, 4694–4697, (Silicon analogues of crown ethers and cryptands: A new chapter in host-guest chemistry?, *Angew. Chem., Int. Ed.*, 2007, **46**, 4610–4613).

2 M. R. Churchill, C. H. Lake, S.-H. L. Chao and O. T. Beachley, Silicon Grease as a Precursor to a Pseudo Crown Ether Ligand: Crystal Structure of $[K^+]_3[K(Me_2SiO)_7^+][InH(CH_2CMe_3)_3^-]_4$, *J. Chem. Soc., Chem. Commun.*, 1993, **1**, 1577–1578.

3 C. Marsmann and M. Seifert, Kieselsäureester als Komplexliganden, *Z. Naturforsch.*, 1991, **46b**, 693–694.

4 W. Patnode and D. F. Wilcock, Methylpolysiloxanes, *J. Am. Chem. Soc.*, 1946, **68**, 358–363.

5 C. J. Pedersen, Cyclic polyethers and their complexes with metal salts, *J. Am. Chem. Soc.*, 1967, **89**, 7017–7036.

6 A. Decken, J. Passmore and X. Wang, Cyclic Dimethylsiloxanes as Pseudo Crown Ethers: Syntheses and Characterization of $Li(Me_2SiO)_5[Al\{OC(CF_3)_3\}_4]$, $Li(Me_2SiO)_6[Al\{OC(CF_3)_3\}_4]$, and $Li(Me_2SiO)_6[Al\{OC(CF_3)_2Ph\}_4]$, *Angew. Chem.*, 2006, **118**, 2839–2843, (Cyclic Dimethylsiloxanes as Pseudo Crown Ethers: Syntheses and Characterization of $Li(Me_2SiO)_5[Al\{OC(CF_3)_3\}_4]$, $Li(Me_2SiO)_6[Al\{OC(CF_3)_3\}_4]$, and $Li(Me_2SiO)_6[Al\{OC(CF_3)_2Ph\}_4]$, *Angew. Chem., Int. Ed.*, 2006, **45**, 2773–2777).

7 C. Eaborn, P. B. Hitchcock, K. Izod and J. D. Smith, Zwei Diorganopotassate und die Struktur von $[K(C_6H_6)][K\{C(SiMe_3)_2(SiMe_2Ph)\}_2]$ im Kristall, *Angew. Chem.*, 1995, **107**, 2936–2937, (Two Diorganopotassates: Crystal Structure of $[K(C_6H_6)][K\{C(SiMe_3)_2(SiMe_2Ph)\}_2]$, *Angew. Chem., Int. Ed. Engl.*, 1996, **34**, 2679–2680).

8 R. D. Ernst, A. Glöckner and A. M. Arif, Crystal structure of hexakis(dimethyl-μ-oxosilane)dibromozirconium(IV) bis(nonabromodizirconate(IV)), $[Zr\{(CH_3)_2SiO\}_6Br_2][Zr_2Br_9]_2$, *Z. Kristallogr. - New Cryst. Struct.*, 2007, **222**, 333–334.

9 A. Decken, F. A. LeBlanc, J. Passmore and X. Wang, Cyclodimethylsiloxane $(Me_2SiO)_m$ (m = 3–6) Ring Transformations on Reactions with $AgSbF_6$; Crystal Structure of $Ag(Me_2SiO)_7SbF_6$, *Eur. J. Inorg. Chem.*, 2006, **2006**, 4033–4036.

10 T. S. Cameron, A. Decken, I. Krossing, J. Passmore, J. M. Rautiainen, X. Wang and X. Zeng, Reactions of a Cyclodimethylsiloxane $(Me_2SiO)_6$ with Silver Salts of Weakly Coordinating Anions; Crystal Structures of $[Ag(Me_2SiO)_6][Al]$ ([Al] = $[FAl\{OC(CF_3)_3\}_3]$, $[Al\{OC(CF_3)_3\}_4]$) and Their Comparison with $[Ag(18\text{-Crown-6})]_2[SbF_6]_2$, *Inorg. Chem.*, 2013, **52**, 3113–3126.

11 R. West, L. S. Whatley and K. J. Lake, Hydrogen Bonding Studies. V. The Relative Basicities of Ethers, Alkoxysilanes and Siloxanes and the Nature of the Silicon-Oxygen Bond, *J. Am. Chem. Soc.*, 1961, **83**, 761–764.

12 F. Weinhold and R. West, The nature of the silicon-oxygen bond, *Organometallics*, 2011, **30**, 5815–5824.

13 F. Weinhold and R. West, Hyperconjugative Interactions in Permethylated Siloxanes and Ethers: The Nature of the SiO Bond, *J. Am. Chem. Soc.*, 2013, **135**, 5762–5767.

14 R. J. Gillespie and E. a. Robinson, Models of molecular geometry, *Chem. Soc. Rev.*, 2005, **34**, 396.

15 J. Passmore and J. M. Rautiainen, On The Lower Lewis Basicity of Siloxanes Compared to Ethers, *Eur. J. Inorg. Chem.*, 2012, **2012**, 6002–6010.

16 M. Fugel, M. F. Hesse, R. Pal, J. Beckmann, D. Jayatilaka, M. J. Turner, A. Karton, P. Bultinck, G. S. Chandler and S. Grabowsky, Covalency and Ionicity Do Not Oppose Each Other-Relationship Between Si–O Bond Character and Basicity of Siloxanes, *Chem. – Eur. J.*, 2018, **24**, 15275–15286.

17 S. Grabowsky, M. F. Hesse, C. Paulmann, P. Luger and J. Beckmann, How to Make the Ionic Si-O Bond More Covalent and the Si-O-Si Linkage a Better Acceptor for Hydrogen Bonding, *Inorg. Chem.*, 2009, **48**, 4384–4393.

18 S. Grabowsky, J. Beckmann and P. Luger, The Nature of Hydrogen Bonding Involving the Siloxane Group, *Aust. J. Chem.*, 2012, **65**, 785.

19 F. Dankert, F. Weigend and C. von Hänisch, Not Non-coordinating at all: Coordination Compounds of the Cyclodimethylsiloxanes D_n (D = Me_2SiO; n = 6, 7) and Group-2-Metal Cations, *Inorg. Chem.*, 2019, **58**, 15417–15422.

20 J. Pahl, H. Elsen, A. Friedrich and S. Harder, Unsupported metal silyl ether coordination, *Chem. Commun.*, 2018, **54**, 7846–7849.

21 K. Reuter, G. Thiele, T. Hafner, F. Uhlig and C. von Hänisch, Synthesis and coordination ability of a partially silicon based crown ether, *Chem. Commun.*, 2016, **52**, 13265–13268.

22 F. Dankert and C. von Hänisch, Insights into the Coordination Ability of Siloxanes Employing Partially Silicon Based Crown Ethers: A Comparative Analysis of s-Block Metal Complexes, *Inorg. Chem.*, 2019, **58**, 3518–3526.

23 I. Sänger, M. Gärtner, M. Bolte, M. Wagner and H.-W. Lerner, New Aspects with Regard to Silanide Chemistry in Particular Formation and Structure of the First Disilyl Sodate $[K(Me_2SiO)_7][(^tBu_3Si)_2MeSi\text{-}Na\text{-}SiMe(^tBu_3Si)_2]$, *Z. Anorg. Allg. Chem.*, 2018, **644**, 925–929.

24 S. Harder, B. Freitag, P. Stegner, J. Pahl and D. Naglav, Strontium Chemistry with Silicone Grease, *Z. Anorg. Allg. Chem.*, 2015, **641**, 2129–2134.

 This journal is © the Partner Organisations 2020

Published on 12 March 2020. Downloaded on 7/6/2020 9:12:51 PM.

25 B. Freitag, P. Stegner, K. Thum, C. A. Fischer and S. Harder, Tetranuclear Strontium and Barium Siloxide/Amide Clusters in Metal-Ligand Cooperative Catalysis, *Eur. J. Inorg. Chem.*, 2018, **2018**, 1938–1944.

26 C. von Hänisch, F. Dankert, C. Donsbach, J. Rienmüller and R. Richter, Alkaline earth metal template (cross-)coupling reactions with hybrid disila-crown ether analogues, *Chem. – Eur. J.*, 2019, **25**, 15934–15943.

27 F. Dankert, J. Heine, J. Rienmüller and C. von Hänisch, Sila-polyethers as innocent crystallization reagents for heavy alkali metal compounds, *CrystEngComm*, 2018, **20**, 5370–5376.

28 S. Chadwick and K. Ruhlandt-Senge, The Remarkable Structural Diversity of Alkali Metal Pyridine-2-thiolates with Mismatched Crown Ethers, *Chem. – Eur. J.*, 1998, **4**, 1768–1780.

29 S. Parsons, D. Rankin and P. A. Wood, DOI: 10.5517/cc89wzd, Decamethylcyclopentasiloxane, *CSD Commun.*, (private communication to the Cambridge Structural Database, CCDC 247844), The Cambridge Crystallographic Data Centre, 2004.

30 R. D. Shannon, Revised Effective Ionic Radii and Systematic Studies of Interatomic distances in Halides and Chalcogenides, *Acta Crystallogr., Sect. A: Cryst. Phys., Diffr., Theor. Gen. Crystallogr.*, 1976, **32**, 751–767.

31 P. Dapporto, P. Paoli, I. Matijašić and L. Tušek-Božić, Crystal structures of complexes of ammonium and potassium hexafluorophosphate with dibenzo-18-crown-6. Molecular mechanics studies on the uncomplexed macrocycle, *Inorg. Chim. Acta*, 1996, **252**, 383–389.

32 V. V. Ponomarova, J. A. Rusanova, E. B. Rusanov and K. V. Domasevitch, Unusual centrosymmetric structure of $[M\ (18\text{-crown-}6)]^+$ (M = Rb, Cs and NH_4) complexes stabilized in an environment of hexachloridoantimonate(V) anions, *Acta Crystallogr., Sect. C: Struct. Chem.*, 2015, **71**, 867–872.

33 M. Cheng, X. Liu, Q. Luo, X. Duan and C. Pei, Cocrystals of ammonium perchlorate with a series of crown ethers: preparation, structures, and properties, *CrystEngComm*, 2016, **18**, 8487–8496.

34 F. Dankert, K. Reuter, C. Donsbach and C. von Hänisch, Hybrid Disila-Crown Ethers as Hosts for Ammonium Cations: The O–Si–Si–O Linkage as an Acceptor for Hydrogen Bonding, *Inorganics*, 2018, **6**, 15.

35 R. West, L. S. Wilson and D. L. Powell, Basicity of siloxanes, alkoxysilanes and ethers toward hydrogen bonding, *J. Organomet. Chem.*, 1979, **178**, 5–9.

36 E. Popowski, J. Schulz, K. Feist, H. Kelling and H. Jancke, Basizität und ^{29}Si-NMR-spektroskopische Untersuchungen von Ethoxysiloxanen, *Z. Anorg. Allg. Chem.*, 1988, **558**, 206–216.

37 E. Yilgör, E. Burgaz, E. Yurtsever and I. Yilgör, Comparison of hydrogen bonding in polydimethylsiloxane and polyether based urethane and urea copolymers, *Polymer*, 2000, **41**, 849–857.

38 F. Dankert, C. Donsbach, C.-N. Mais, K. Reuter and C. von Hänisch, Alkali and Alkaline Earth Metal Derivatives of Disila-Bridged Podands: Coordination Chemistry and Structural Diversity, *Inorg. Chem.*, 2018, **57**, 351–359.

39 I. Krossing and I. Raabe, Nichtkoordinierende Anionen – Traum oder Wirklichkeit? Eine Übersicht zu möglichen Kandidaten, *Angew. Chem.*, 2004, **116**, 2116–2142, (Noncoordinating Anions—Fact or Fiction? A Survey of Likely Candidates, *Angew. Chem., Int. Ed.*, 2004, **43**, 2066–2090).

40 I. Krossing, H. Brands, R. Feuerhake and S. Koenig, New reagents to introduce weakly coordinating anions of type $Al(OR_F)_4^-$: synthesis, structure and characterization of Cs and trityl salts, *J. Fluorine Chem.*, 2001, **112**, 83–90.

41 A. A. Korlyukov, A. V. Vologzhanina, M. I. Buzin, N. V. Sergienko, B. G. Zavin and A. M. Muzafarov, Cu(II)-Silsesquioxanes as Secondary Building Units for Construction of Coordination Polymers: A Case Study of Cesium-Containing Compounds, *Cryst. Growth Des.*, 2016, **16**, 1968–1977.

42 I. Krossing, The Facile Preparation of Weakly Coordinating Anions: Structure and Characterisation of Silverpolyfluoroalkoxyaluminates $AgAl(OR_F)_4$, Calculation of the Alkoxide Ion Affinity, *Chem. – Eur. J.*, 2001, **7**, 490–502.

Electronic Supplementary Material (ESI) for Inorganic Chemistry Frontiers.
This journal is © the Partner Organisations 2020

Electronic Supplementary Information

On molecular architectures of siloxane coordination compounds: (Re-)investigating the coordination of the cyclodimethylsiloxanes D_n (n=5-8) towards alkali metal ions

F. Dankert,[a] L. Erlemeier[a], C. Ritter[a] and C. von Hänisch[a]*

*Email: haenisch@staff.uni-marburg.de

[a] Department of Chemistry and Material Sciences Center, Philipps-Universität Marburg, Hans-Meerwein-Straße, 35032 Marburg, Germany.

Content

1. Notes on template-driven ring-opening polymerization S3

2. Single crystal X-Ray diffraction analysis S4

2.1 General Information S4

2.2 Crystallographic Data S6

2.3 Representation of additional X-ray structures S11

2.3.1 $[Li(D_6)(H_2O)]GaI_4$ (**2a**) S11

2.3.2 $K[Al_F]$ S12

2.3.3 $^1_\infty[M(D_8)Al_F]$ (M = Rb^+: **8**, M = Cs^+: **9**) S13

2.3.4 $[K(D_5)_2Al_F]$ (**10**) S14

2.3.5 $[K(D_7)Al_F]$ (**11**) S15

2.3.6 $[Cs(D_6)_2Al_F]$ (**12**) S16

3. NMR spectroscopy S17

3.1 General Information S17

3.2 Behavior in solution of compound 10 ..... S18

3.3 Behavior in solution of compound 12 ..... S19

4. References S20

1. Notes on template-driven ring-opening polymerizations

The depicted mechanism in Scheme S1 gives a proposal for the ring expansion from D_5 to D_6 in the presence of $[GaI_4]^-$ and a Li^+ template. Due to coordination it is most likely that the Li^+ ion will polarize the Si atoms. This makes the Lewis-acidic Si-centres vulnerable for nucleophilic attack of I^-. The ring is eventually cleaved to form an iodosilanolate which is itself nucleophilic. Another equivalent of $[Li(D_5)]^+$ is attacked and the ring is expanded under Li^+ templation. As depicted here, the $ISiMe_2(OSiMe_2)_nOSiMe_2O^-$ anions are the $SiMe_2O$-source for ring expansion. The ring expansion for the formation of larger ring (e.g. using K^+ or Cs^+ as a template) proceeds in seemingly similar manner.

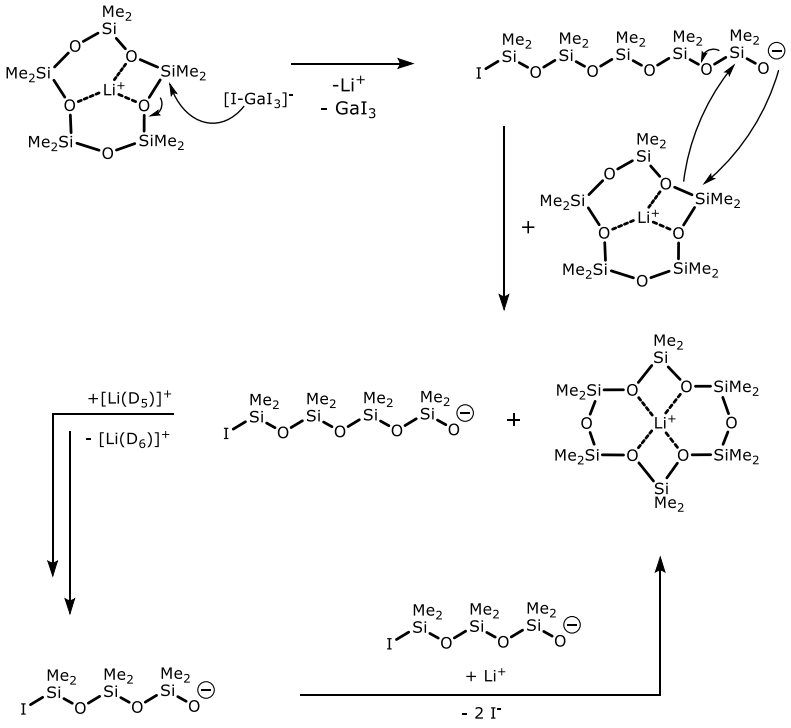

Scheme S1: Tentative Li^+ directed ring transformation process referring to *Passmore* and co-workers.[1]

2. Single crystal X-Ray diffraction analysis

2.1 General Information

Single crystal X-ray diffraction experiments were carried out on a Bruker D8 Quest diffractometer at 100(2)K with MoKα radiation and respective X-ray optics (λ = 0.71073). For compound **10** the experiment was carried out on a STOE STADIVARI diffractometer with CuKα radiation (λ = 1.54186) at 130K. All structures were solved by direct methods and refinement with full-matrix-least-squares against F^2 using SHELXT- and SHELXL-2015 on OLEX2 platform.[2-4] To fix the disordered anions in compound **10, 11** as well as **12** we also used DSR[5] (=disordered model refinement) and placed an OLEX2 implemented initial, rigid $[Al_F]^-$ restraint. In case of **12**, we also refined the residual electron density more precisely using implemented $OCCF_3$ restraints. As a cause, the atom labelling is sometimes quite unconventional around the anions. The intrinsically disorder of these anions, legitimates these high numbers of restraints and it should be noted that the siloxane moieties aren't disordered and thus restraints had only been used for the anion. It should be further noted that due to twisting and tilting of the respective anions, more atom positions of the refined atom positions are possible. However, without the restraints we could not refine the anions properly. It should at this point also be noted that we improved the disorder behaviour of these anions as we placed the crystal at a higher temperature of -20°C to the diffractometer and then cooled down slowly to 100K/130K at a rate of 250K/h. The diffraction experiment for compound **10** had to be performed at a higher temperature due to phase transition at temperatures below this value and/or cracking of the crystal.

The crystallographic data for the compounds **1-12** and K[AlF] are denoted as follows: CCDC Nos. 1979351 (**1**), 1979352 (**2**), 1979354 (**2a**), 1979358 (**3**), 1979356 (**4**), 1979353 (**5**), 1979357 (**6**), 1979355 (**7**), 1979359 (**8**), 1979361 (**9**), 1979360 (**10**), 1979363 (1**1**), 1979364 (1**2**), 1979362 ($KAlF$). Crystallographic information files (CIF) can be obtained free of charge from the Cambridge Crystallographic Data Centre (CCDC) (link: www.ccdc.cam.ac.uk/data_request/cif). The respective crystal data and selected experimental parameters of the structure determinations are summarized in table S1-S4. Visualization of all structures was performed with the Diamond software package Version 4.6.0.

2.2 Crystallographic Data

Table S1. Selected crystal structure data of the structure determinations of the compounds **1·C$_6$D$_6$**, **2**, and **2a**

Compound	**1·C$_6$D$_6$**	**2**	**2a**
Empirical formula	$C_{28}H_{72}Ga_2I_8Li_2O_{11}Si_{11}$	$C_{12}H_{36}GaI_4LiO_6Si_6$	$C_{12}H_{38}GaI_4LiO_7Si_6$
Formula weight	2068.40	1029.21	1047.22
Crystal colour, habit	Colourless, needle	Colourless, platelet	Colourless, platelet
Temperature/K	100(2)	100(2)	100(2)
Crystal system	triclinic	monoclinic	triclinic
Space group	*P*-1	*C*2/*c*	*P*-1
a/Å	11.1168(4)	18.8841(7)	10.5200(4)
b/Å	16.9018(6)	10.4111(4)	11.1154(4)
c/Å	19.8102(8)	19.2669(8)	16.6027(7)
α/°	98.9980(10)	90	88.3260(10)
β/°	95.0500(10)	112.8520(10)	78.6540(10)
γ/°	102.9710(10)	90	69.4900(10)
Volume/Å^3	3553.2(2)	3490.6(2)	1781.15(12)
Z	2	4	2
ϱ_{calc}g/cm^3	1.933	1.958	1.953
μ/mm^{-1}	4.457	4.554	4.466
F(000)	1948.0	1944.0	992.0
Crystal size/mm^3	0.262 × 0.193 × 0.121	0.133 × 0.129 × 0.071	0.177 × 0.125 × 0.089
Radiation	Mo$K\alpha$ (λ = 0.71073)	Mo$K\alpha$ (λ = 0.71073)	Mo$K\alpha$ (λ = 0.71073)
2Θ range for data collection/°	4.486 to 52.84	4.56 to 53.594	4.456 to 56.7
Reflections collected	14525	29905	33652
Independent reflections	14525 [*]	3736 [R_{int} = 0.0423, R_{sigma} = 0.0237]	8849 [R_{int} = 0.0325, R_{sigma} = 0.0334]
Data/restraints/parameters	14525/0/582	3736/0/153	8849/2/301
Goodness-of-fit on F^2	1.099	1.069	1.020
Final R indexes [I>=2σ (I)]	R_1 = 0.0436, wR_2 = 0.0800	R_1 = 0.0221, wR_2 = 0.0417	R_1 = 0.0250, wR_2 = 0.0374
Final R indexes [all data]	R_1 = 0.0651, wR_2 = 0.0873	R_1 = 0.0313, wR_2 = 0.0438	R_1 = 0.0381, wR_2 = 0.0400
Largest diff. peak/hole / e Å^{-3}	1.62/-1.11	0.54/-0.57	1.72/-1.38
Absolute structure parameter	-	-	-

* refined as a two-component twin

Table S2. Selected crystal structure data of the structure determinations of the compounds **3-5**

Compound	**3**	**4**	**5**
Empirical formula	$C_{12}H_{36}GaI_4NaO_6Si_6$	$C_{15}H_{44}Cl_2GaI_4NaO_7Si_7$	$C_{15}H_{44}Cl_2GaI_4KO_7Si_7$
Formula weight	1045.26	1204.34	1220.45
Crystal colour, habit	Colourless, platelet	Colourless, platelet	Colourless, platelet
Temperature/K	100(2)	100(2)	100(2)
Crystal system	monoclinic	triclinic	triclinic
Space group	$P2_1/n$	P-1	P-1
a/Å	19.4191(10)	11.6548(5)	10.8831(4)
b/Å	19.9922(10)	20.5389(9)	11.2425(5)
c/Å	19.9247(11)	21.1652(10)	18.6043(7)
α/°	90	114.0800(10)	89.9390(10)
β/°	113.151(2)	99.536(2)	81.6520(10)
γ/°	90	103.956(2)	74.7930(10)
Volume/Å^3	7112.5(7)	4285.0(3)	2171.68(15)
Z	8	4	2
ϱ_{calc}g/cm^3	1.952	1.867	1.866
μ/mm^{-1}	4.482	3.882	3.916
F(000)	3952.0	2304.0	1168.0
Crystal size/mm^3	0.281 × 0.256 × 0.184	0.257 × 0.161 × 0.089	0.301 × 0.172 × 0.132
Radiation	MoKα (λ = 0.71073)	MoKα (λ = 0.71073)	MoKα (λ = 0.71073)
2Θ range for data collection/°	4.276 to 53.63	4.276 to 50.998	4.206 to 56.702
Reflections collected	264211	103252	40306
Independent reflections	15192 [R_{int} = 0.0453, R_{sigma} = 0.0172]	15885 [R_{int} = 0.0398, R_{sigma} = 0.0264]	10795 [R_{int} = 0.0359, R_{sigma} = 0.0363]
Data/restraints/parameters	15192/0/565	15885/0/687	10795/0/348
Goodness-of-fit on F^2	1.144	1.147	1.029
Final R indexes [I>=2σ (I)]	R_1 = 0.0475, wR_2 = 0.0843	R_1 = 0.0575, wR_2 = 0.1553	R_1 = 0.0338, wR_2 = 0.0629
Final R indexes [all data]	R_1 = 0.0650, wR_2 = 0.0975	R_1 = 0.0665, wR_2 = 0.1582	R_1 = 0.0495, wR_2 = 0.0676
Largest diff. peak/hole / e Å^{-3}	2.63/-1.98	2.62/-1.27	3.33/-1.67
Absolute structure parameter	-	-	-

Table S3. Selected crystal structure data of the structure determinations of compounds **6-8**

Compound	**6·DCM**	**7**	**8·DCM**
Empirical formula	$C_{15}H_{48}Cl_2Ga_2I_7NO_7Si_7$	$C_{17}H_{50}Cl_2GaI_4O_8RbSi_8$	$C_{33}H_{50}AlCl_2F_{36}O_{12}RbSi_8$
Formula weight	1649.81	1340.98	1730.80
Crystal colour, habit	Colourless, platelet	Colourless, platelet	Colourless, platelet
Temperature/K	100(2)	100(2)	100(2)
Crystal system	monoclinic	orthorhombic	triclinic
Space group	$P2_1/n$	$Pbcn$	P-1
a/Å	11.2628(5)	18.0474(7)	14.1058(8)
b/Å	20.6445(18)	13.5623(6)	19.3758(11)
c/Å	22.3771(11)	19.3971(8)	26.4291(15)
α/°	90	90	89.960(2)
β/°	98.338(2)	90	75.318(2)
γ/°	90	90	89.615(2)
Volume/Å^3	5148.0(6)	4747.7(3)	6987.3(7)
Z	4	4	4
ϱ_{calc}g/cm^3	2.129	1.876	1.645
μ/mm^{-1}	5.539	4.545	1.077
F(000)	3064.0	2568.0	3456.0
Crystal size/mm^3	0.400 × 0.132 × 0.106	0.251 × 0.176 × 0.13	0.315 × 0.218 × 0.194
Radiation	MoKα (λ = 0.71073)	MoKα (λ = 0.71073)	MoKα (λ = 0.71073)
2Θ range for data collection/°	4.174 to 52.844	4.304 to 56.702	4.264 to 52.998
Reflections collected	198653	78935	210484
Independent reflections	10511 [R_{int} = 0.0475, R_{sigma} = 0.0166]	5924 [R_{int} = 0.0465, R_{sigma} = 0.0209]	28938 [R_{int} = 0.0421, R_{sigma} = 0.0286]
Data/restraints/parameters	10511/6/483	5924/0/196	28938/6/1691
Goodness-of-fit on F^2	1.155	1.074	1.047
Final R indexes [I>=2σ (I)]	R_1 = 0.0338, wR_2 = 0.0834	R_1 = 0.0244, wR_2 = 0.0498	R_1 = 0.0469, wR_2 = 0.1237
Final R indexes [all data]	R_1 = 0.0390, wR_2 = 0.0860	R_1 = 0.0341, wR_2 = 0.0528	R_1 = 0.0537, wR_2 = 0.1263
Largest diff. peak/hole / e Å^{-3}	1.58/-1.20	1.31/-0.86	1.05/-0.69
Absolute structure parameter	-	-	-

Table S4. Selected crystal structure data of the structure determinations of compounds **9**, **10 and 11**

Compound	**9·DCM**	**10**	**11·DCM**
Empirical formula	$C_{33}H_{50}AlCl_2CsF_{36}O_{12}Si_8$	$C_{36}H_{60}AlF_{36}KO_{14}Si_{10}$	$C_{31}H_{44}AlCl_2F_{36}KO_{11}Si_7$
Formula weight	1778.24	1747.82	1610.27
Crystal colour, habit	Colourless, platelet	Colourless, block	Colourless, platelet
Temperature/K	100(2)	130(2)	100(2)
Crystal system	Triclinic	Orthorhombic	Monoclinic
Space group	*P*-1	*Pbcm*	$P2_1/c$
a/Å	14.1058(8)	11.097(2)	26.8104(18)
b/Å	19.3758(11)	23.519(5)	23.8671(16)
c/Å	26.4291(15)	28.345(6)	30.129(2)
α/°	89.960(2)	90	90
β/°	75.318(2)	90	95.933(2)
γ/°	89.615(2)	90	90
Volume/Å^3	6987.3(7)	7398(3)	19176(2)
Z	4	4	12
ϱ_{calc}g/cm^3	1.690	1.569	1.673
μ/mm^{-1}	0.899	3.611	0.463
F(000)	3528.0	3536.0	9672.0
Crystal size/mm^3	0.315 × 0.218 × 0.194	0.241 × 0.23 × 0.222	0.540 × 0.462 × 0.192
Radiation	Mo$K\alpha$ (λ = 0.71073)	Cu$K\alpha$ (λ = 1.54186)	Mo$K\alpha$ (λ = 0.71073)
2Θ range for data collection/°	4.312 to 56.792	7.518 to 129.994	4.42 to 50.62
Reflections collected	277295	141479	202464
Independent reflections	34913 [R_{int} = 0.0367, R_{sigma} = 0.0239]	6429 [R_{int} = 0.0225, R_{sigma} = 0.0075]	34849 [R_{int} = 0.0271, R_{sigma} = 0.0190]
Data/restraints/parameters	34913/0/1812	6429/1522/683	34849/1638/2446
Goodness-of-fit on F^2	1.096	1.113	1.033
Final R indexes [I>=2σ (I)]	R_1 = 0.0345, wR_2 = 0.0844	R_1 = 0.0706, wR_2 = 0.1954	R_1 = 0.0760, wR_2 = 0.1922
Final R indexes [all data]	R_1 = 0.0416, wR_2 = 0.0879	R_1 = 0.0752, wR_2 = 0.1996	R_1 = 0.0901, wR_2 = 0.2060
Largest diff. peak/hole / e Å^{-3}	0.65/-0.82	1.12/-0.80	2.34/-1.53
Absolute structure parameter	-	-	-

Table S5. Selected crystal structure data of the structure determinations of compounds **12** and **KAl$_F$**

Compound	**12**	**KAl$_F$**
Empirical formula	$C_{40}H_{72}AlCsF_{36}O_{16}Si_{12}$	$C_{32}Al_2F_{72}K_2O_8$
Formula weight	1989.94	2012.48
Crystal colour, habit	Colourless, block	Colourless, block
Temperature/K	100(2)	100(2)
Crystal system	Monoclinic	Monoclinic
Space group	$P2_1$	$P2_1/c$
a/Å	11.1101(9)	23.8518(16)
b/Å	27.2474(18)	12.9216(8)
c/Å	27.564(2)	20.6513(11)
α/°	90	90
β/°	94.171(3)	115.296(2)
γ/°	90	90
Volume/Å^3	8322.1(11)	5754.5(6)
Z	4	4
ρ_{calc}g/cm^3	1.588	2.323
μ/mm^{-1}	0.760	0.479
F(000)	4000.0	3872.0
Crystal size/mm^3	0.249 × 0.228 × 0.188	0.381 × 0.203 × 0.107
Radiation	MoKα (λ = 0.71073)	MoKα (λ = 0.71073)
2Θ range for data collection/°	4.328 to 50.612	4.364 to 50.154
Reflections collected	337172	88440
Independent reflections	30281 [R_{int} = 0.0419, R_{sigma} = 0.0193]	10202 [R_{int} = 0.0869, R_{sigma} = 0.0386]
Data/restraints/parameters	30281/1557/1911	10202/0/1034
Goodness-of-fit on F^2	1.028	1.165
Final R indexes [I>=2σ (I)]	R_1 = 0.0603, wR_2 = 0.1566	R_1 = 0.0986, wR_2 = 0.2133
Final R indexes [all data]	R_1 = 0.0628, wR_2 = 0.1590	R_1 = 0.1173, wR_2 = 0.2207
Largest diff. peak/hole / e Å^{-3}	1.55/-1.44	1.22/-0.64
Absolute structure parameter	0.179(16)	-

2.3 Representation of additional X-ray structures

2.3.1 [Li(D$_6$)(H$_2$O)]GaI$_4$ (2a)

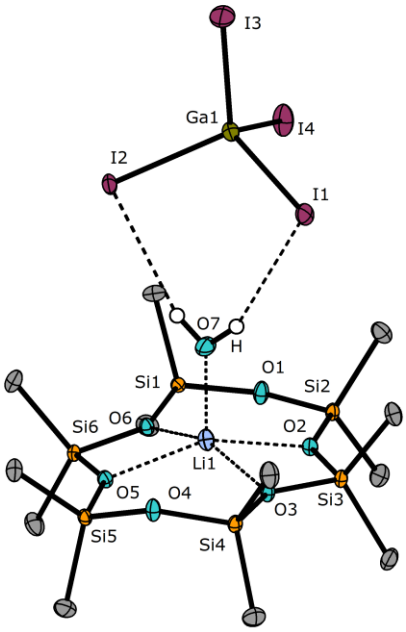

Figure S1. Molecular structure of **2a** in the crystal. Thermal displacement ellipsoids are drawn at 50% probability. Hydrogen atoms were crystallographically localized and fixed with DFIX [0.84] commands. Selected bond lengths [pm]: O1···Li1 326.4(4), O2-Li1 215.4(5), O3-Li1 213.1(5), O4···Li1 321.8(5), O5-Li1 213.7(4), O6-Li1 210.1(4), O7-Li1 192.3(5). Selected bond angles [°]: O2-Li1-O3 71.1(1), O2-Li1-O6 103.6(1), O3-Li1-O5 103.0(1), O5-Li1-O6 71.7(1), Si1-O1-Si2 154.1(1), Si1-O6-Si6 142.1(1), Si2-O2-Si3 143.4(1), Si3-O3-Si4 142.7(1), Si4-O4-Si5 145.7(1), Si5-O5-Si6 143.7(1).

2.3.2 K[AlF]

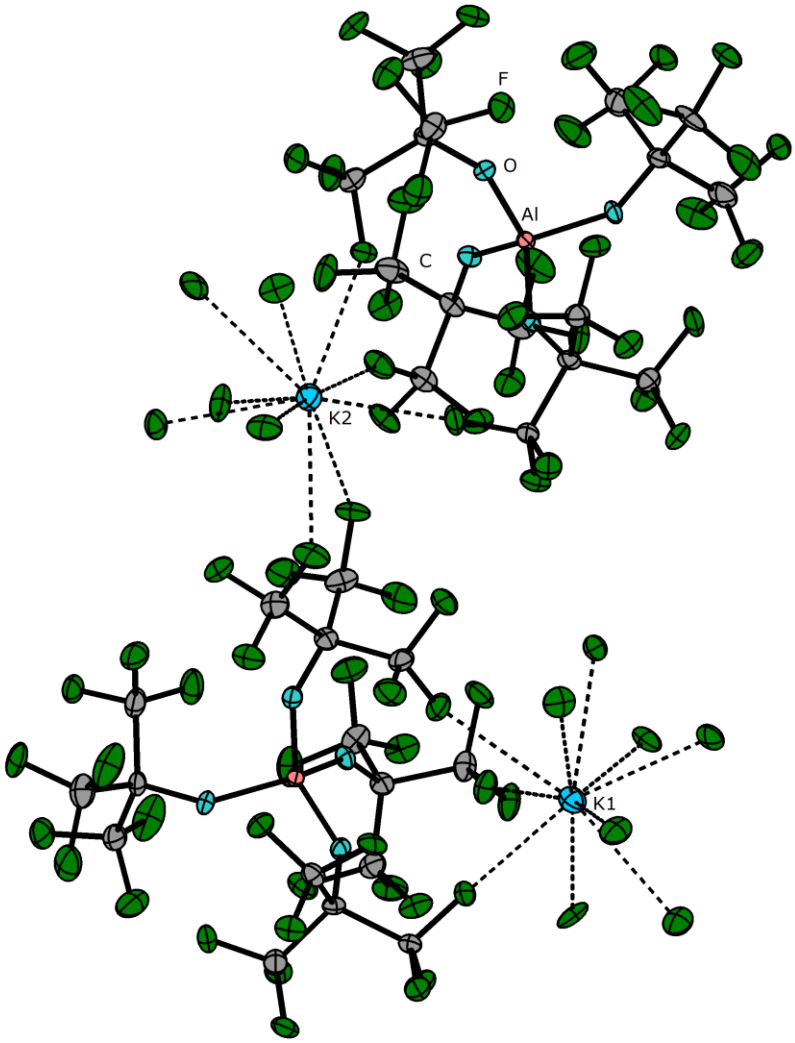

Figure S2. Molecular structure of **K[ALF]** in the crystal and additional fluorine atoms representing the coordination sphere of K1 and K2. Additional fluorine atoms are symmetry generated over x, 1/2-y, 1/2+z; x, 3/2-y, 1/2+z or 1-x, 1-y, 1-z (attached to K1) and x, -1+y, z or 2-x, -1/2+y, 3/2-z (attached to K2). Thermal displacement ellipsoids are drawn at 50% probability. The potassium ions are tenfold coordinated by the anions (CN = 10). The coordination of the CF_3 groups towards K1 have atom distance values of 267.5(4)-302.0(7). The coordination of the CF_3 groups towards K2 have atom distance values of 270.9(6)-294.0(6).

2.3.3 $^{1}_{\infty}[M(D_8)Al_F]$ (M = Rb^+: 8, M = Cs^+: 9)

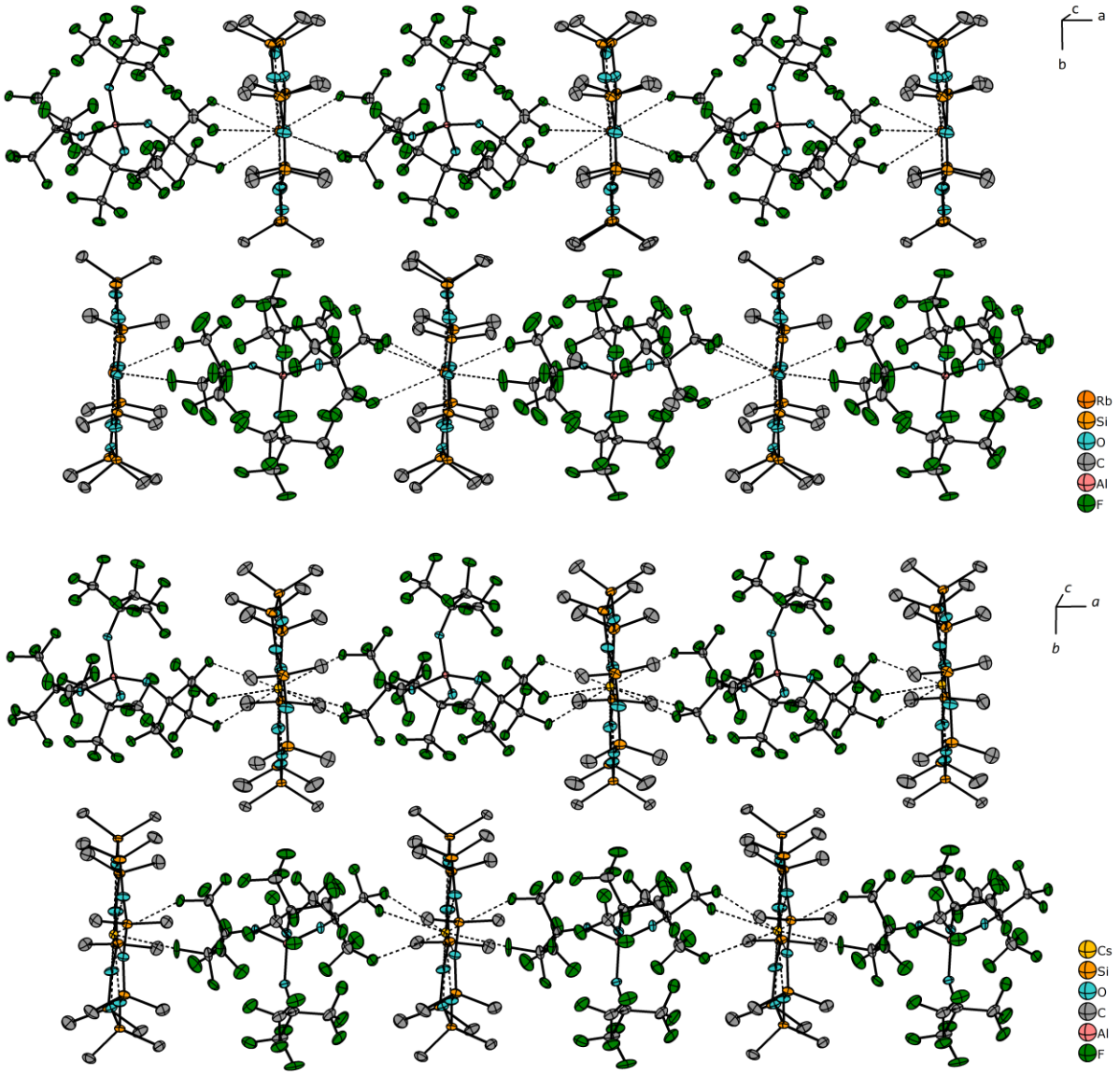

Figure S3. Infinite chains of **8** (top) and **9** (bottom) along [100] in the crystal. Thermal displacement ellipsoids are drawn at 50% probability. DCM molecules are omitted for clarity.

2.3.4 [K(D5)2AlF] (10)

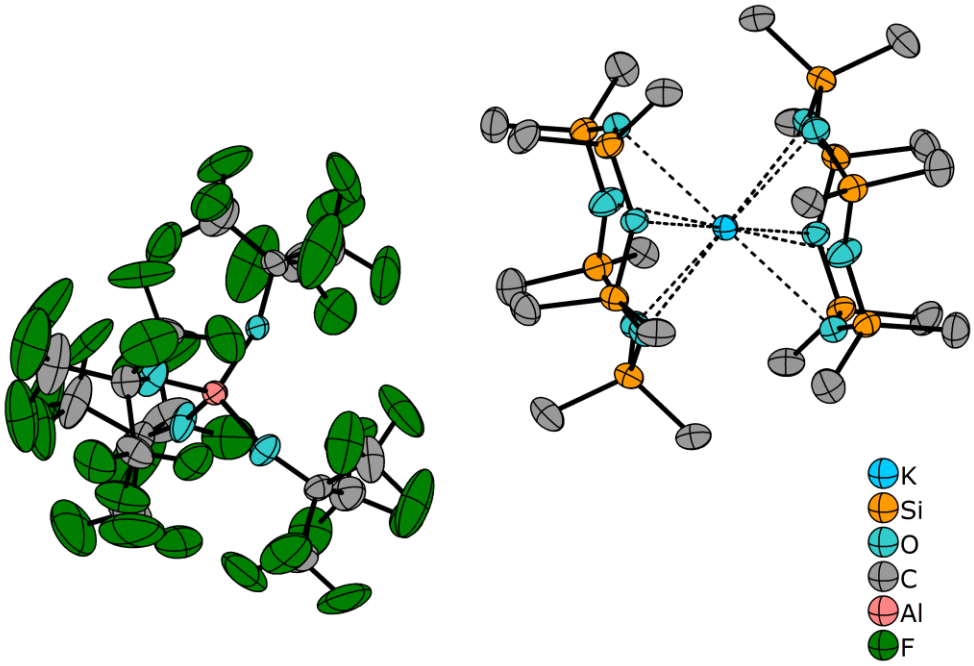

Figure S4. Molecular structure of **10** in the crystal showing the siloxane complex as well as the restraint of the WCA. The disordered part of the anion (x, y, 3/2-z) has not been displayed for clarity. Thermal displacement ellipsoids are drawn at the 30% probability level.

2.3.5 [K(D7)AlF] (11)

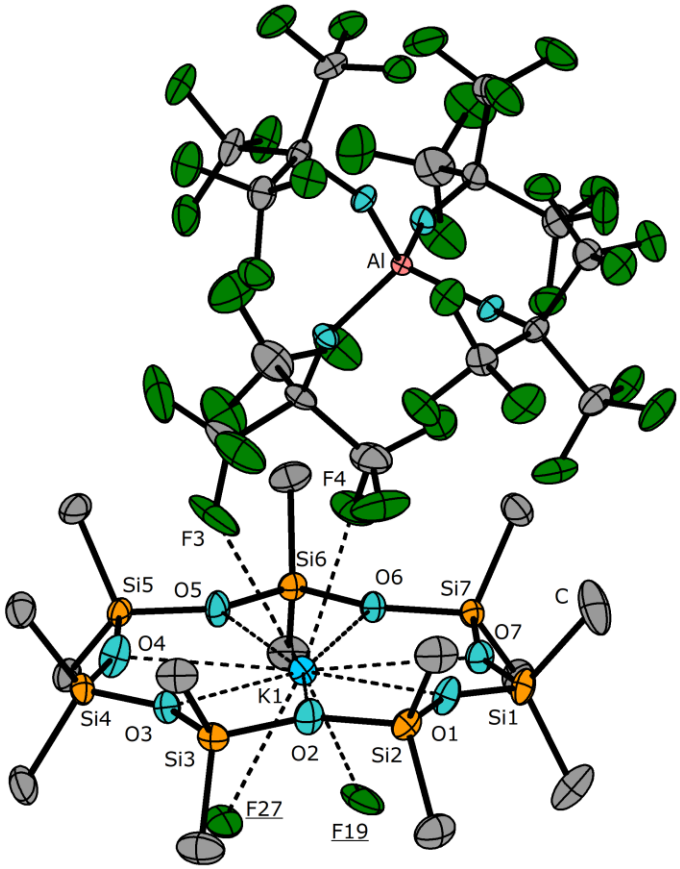

Figure S5. Molecular structure of **11** in the crystal. Only one out of three independent molecules is shown and solvent molecules are omitted for clarity. Thermal displacement ellipsoids are drawn at 50% probability. Underlined atom labels indicate symmetry generation over 1-x, -1/2+y, -1/2z. O1-K1 291.0(3), O2-K1 288.0(3), O3-K1 286.7(3), O4-K1 311.6(3), O5-K1 285.9(3), O6-K1 287.1(3), O7-K1 299.7(3), F3-K1 336.4(4), F4-K1 278.5(3), F27-K1 283.8(3), F19-K1 307.8(3). Selected bond angles [°]: O1-K1-O2 51.9(1), O1-K1-O7 51.2(1), O2-K1-O3 52.5(9), O3-K1-O4 50.0(1), O4-K1-O5 50.4(1), O5-K1-O6 52.7(1), O6-K1-O7 51.2(1), Si1-O1-Si2 152.3(2), Si1-O7-Si7 157.7(2), Si2-O2-Si3 157.7(2), Si3-O3-Si4 149.6(2), Si4-O4-Si5 162.9(3), Si5-O5-Si6 149.6(2), Si6-O6-Si7 152.4(2).

2.3.6 [Cs(D6)2AlF] (12)

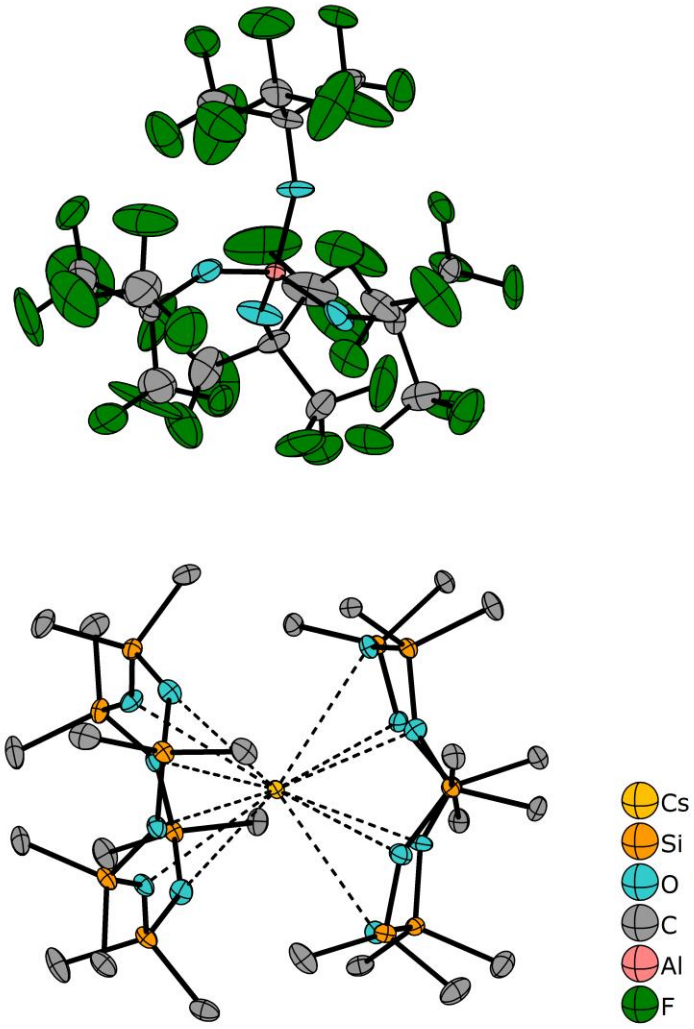

Figure S6. Molecular structure of **12** in the crystal showing the siloxane complex as well as the restraint of the WCA. Only one out of two independent molecules is shown for clarity. Thermal displacement ellipsoids are drawn at the 30% probability level.

3. NMR spectroscopy

3.1 General Information

NMR spectra were recorded on different Bruker Spectrometer types e.g. AV III HD 300 MHz or AV III HD 500 MHz. For the VT NMR we have performed a measurement on the 500 MHz spectrometer. For this purpose, a freshly prepared sample of D5 and KAl_F in the stoichiometric ratio 2:1 was filled into a *J. Young* NMR tube. We started the ^{29}Si NMR (dept) measurement at ambient temperature (300K) and cooled down slowly in 10K steps. All spectra have been visualized with the MestReNove software package 9.0.1.

3.2 Behavior in solution of compound 10

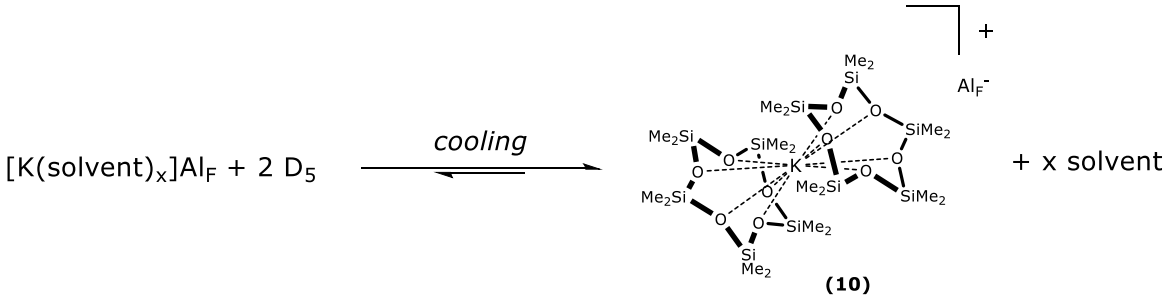

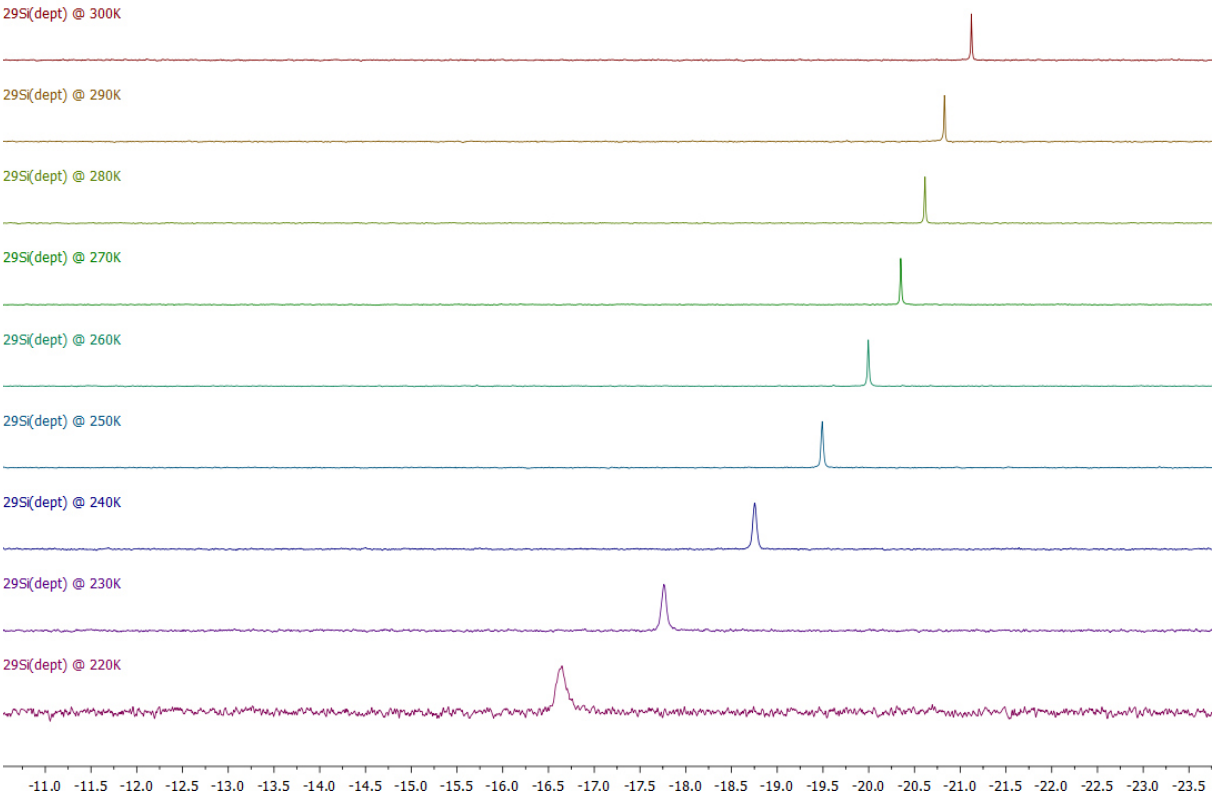

Figure S7. VT ^{29}Si NMR (dept) of compound **10**: A characteristic low-field shift is observed at lower temperatures and thus silyl-ether coordination is present. The sample precipitates from the solvent at temperatures below 230K which results in broad resonances.

3.3 Behavior in solution of compound 12

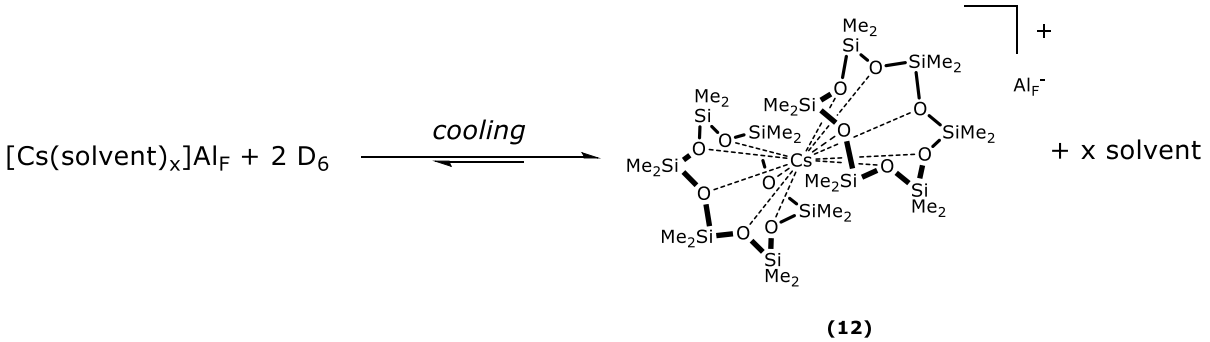

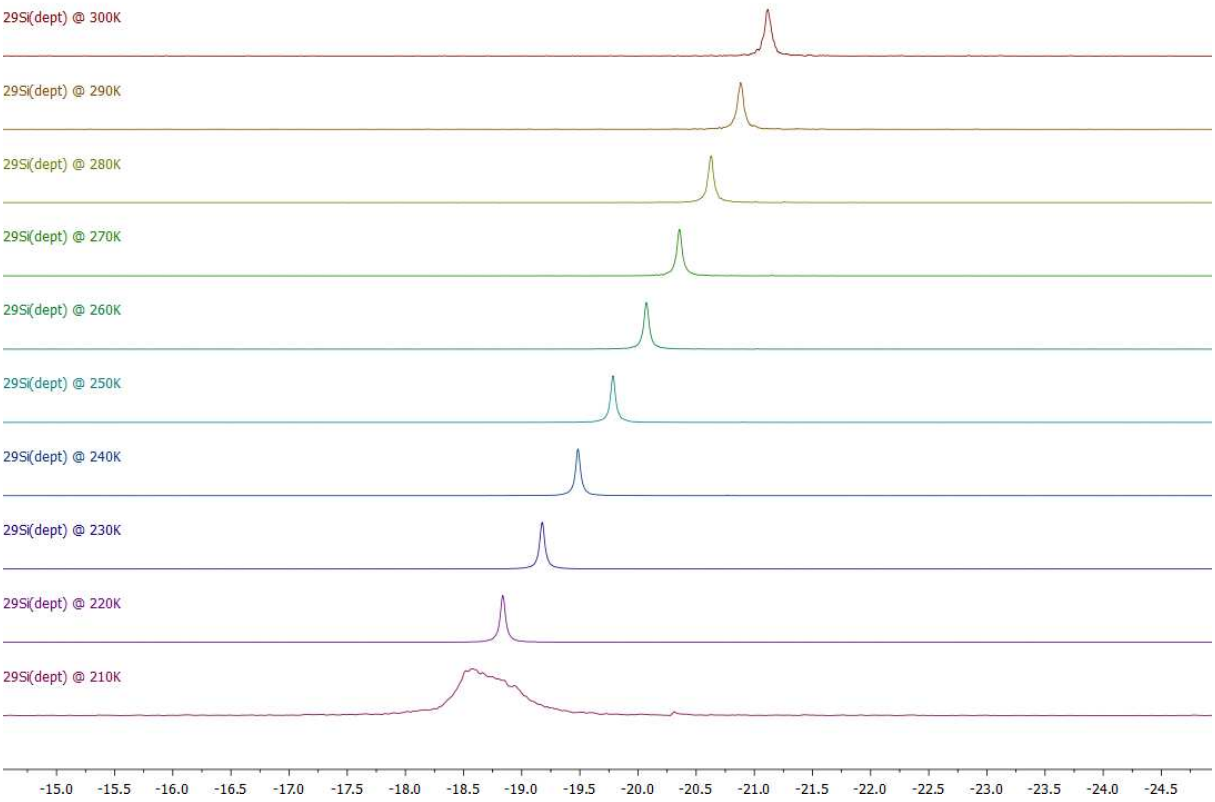

Figure S8. VT ^{29}Si NMR (dept) of compound **12**: A characteristic low-field shift is observed at lower temperatures and thus silyl-ether coordination is present. The sample precipitates from the solvent at temperatures below 220K which results in broad resonances.

4. References

[1] Decken, A.; LeBlanc, F. A.; Passmore, J.; Wang, X. Cyclodimethylsiloxane $(Me_2SiO)_m$ (m = 3–6) Ring Transformations on Reactions with $AgSbF_6$; Crystal Structure of $Ag(Me_2SiO)_7SbF_6$, *Eur. J. Inorg. Chem.* 2006, **2006**, 4033–4036

[2] Sheldrick, G. M. Crystal structure refinement with SHELXL. *Acta Crystallogr., Sect. C: Cryst. Struct. Commun.*, 2015, **71**, 3–8.

[3] Sheldrick, G. M. SHELXT - Integrated space-group and crystal-structure determination. *Acta Crystallogr., Sect. A: Fundam. Crystallogr.*, 2015, **A71**, 3–8.

[4] Dolomanov, O. V.; Bourhis, L. J.; Gildea, R. J.; Howard, J. A. K.; Puschmann H., *OLEX2*: a complete structure solution, refinement and analysis program. *J. Appl. Crystallogr.*, 2009, **42**, 339–341.

[5] Kratzert, D.; Holstein, J. J.; Krossing, I., DSR: enhanced modelling and refinement of disordered structures with SHELXL. *J. Appl. Crystallogr.*, 2015, **48**, 933–938.

EurJIC
European Journal of Inorganic Chemistry

Full Paper
doi.org/10.1002/ejic.202000299

Chalcogen Bonds

Chalcogen Bonding of SO_2 and s-Block Metal Iodides Near Room Temperature: A Remarkable Structural Diversity

Fabian Dankert,[a][‡] Anne Feyh,[a][‡] and Carsten von Hänisch*[a]

Abstract: In this contribution we have systematically explored the coordination chemistry of the iodide anion towards SO_2. While employing large organocations like s-block metal complexes of crown-ethers, we discovered a remarkable structural diversity within the herein characterized compounds together with novel architectures of SO_2 solvates. The observed $O_2S\cdots I^-$ interactions are observed to be strong enough to determine the crystal packing and dimensionality. In the light of chalcogen bonding, the small molecule SO_2 is introduced as a supramolecular synthon. In the light of a chemistry in non-aqueous solutions, the ISO_2^- anion is revisited. Chalcogen bonding was established to form one-dimensional networks in the compounds [Li([12]crown-4)H_2O]I•SO_2 (**1**), [Na([15]crown-5)(SO_2)I] (**2**), [K([18]crown-6)(SO_2)I] (**4**), [NH_4([18]crown-6)]I•SO_2 (**5**), [Rb([18]crown-6)I(SO_2)]•$2SO_2$ (**6**) and [Cs([18]crown-6)(SO_2)$_2$I] (**7**) all of which were obtained by 1:1 complexation of the respective iodide salt and respective crown-ether in SO_2 solution. Two-dimensional networks were obtained within the alkaline earth metal compounds [Mg([12]crown-4)$_2$]I_2•$4SO_2$ (**9**) and [Ba_2([18]crown-6)$_2$(SO_2I)(SO_2)$_2I_3$]•SO_2 (**11**). The iodosulfite ion ISO_2^- was obtained either by shielding Na^+ ions with [12]crown-4, conversion of MgI_2 with [15]crown-5, conversion of CaI_2 with [18]crown-6 or conversion of BaI_2 with [18]crown-6 (**11**, as aforementioned). [Na([12]crown-4)$_2$]ISO_2 (**3**), [Mg([15]crown-5)(ISO_2)$_2$] (**8**) and [Ca_2([18]crown-6)(SO_2I)$_3$]I_3 (**10**) were characterized. In these respective compounds the S···I atom distances are considerably shorter than those previously reported. Experimental data around the chemistry of halosulfites is provided. Besides network structures and the iodosulfite formation, an SO_2-rich aggregate could be observed. An SO_2 adduct of the composition $[I_2(SO_2)_5]^{2-}$ was found to be present in [Na([12]crown-4)$_2$]I•$2.75SO_2$ (**3a**).

Introduction

As a non-aqueous polar aprotic solvent,[1] sulfur dioxide has attracted much attention in chemical synthesis over the past years. As also reviewed by *Mews*, especially the synthesis of salts with WCAs (WCA = weakly coordinating anion) such as $[AlCl_4]^-$, $[AsF_6]^-$, and $[SbF_6]^-$ is widely spread in literature.[2] Later on also the formation of salts with even more weakly coordinating anions such as $[Al_F]^-$ (Al_F^- = $[Al\{OC(CF_3)_3\}_4]^-$) were described.[3–5] The combination of poorly interacting anions, a weakly coordinating solvent such as SO_2 and its volatility makes the synthesis of solvent-free salts bearing various weakly coordinating anions quite practicable.[2] As these salts are predominant in general inorganic chemistry,[6] also applications within organic chemistry were established. Sulfur dioxide can be used in a large variety of reactions which allow functionalization due to SO_2 insertion into multiple bonds.[7,8] Consequently, SO_2 was also described as a useful molecule to establish C–C bonds,[9] which is generally one of the key targets in organic chemistry.

Sulfur dioxide as a solvent is established for more than 70 years now which was, not least, ascribed to a comprehensively summary by *Jander* in the late 40s.[10] Yet, there are still open questions in how sulfur dioxide is solvating cations and anions even in simple salts like the s-block halides. Even though this solvent has established as one of the most important inorganic solvents, it has not been dealt with it exhaustively. By early examinations, the number of SO_2 molecules which coordinate to different metal centres were determined to vary from 0.5 to 4 which is accompanied by a comparatively large molecular volume together with the low dielectric constant of 13.8 at 15 °C.[1,10] The solvates of the alkali metal iodides NaI•$4SO_2$, KI•$4SO_2$, RbI•$3SO_2$ and CsI•$3SO_2$ were postulated but no crystal structure revealing the coordination mode toward these simple salts have been published ever since.[10] The respective chlorides MCl•$3SO_2$ (M = Rb^+, Cs^+) were described lately.[11] Yet, most of the hitherto characterized compounds were crystal structures of s-block SO_2 adducts with different WCAs: $[Li_2\{AlF(OR_F)_3\}\{(Al(OR_F)_4\}]$•$2SO_2$ (R_F = $C(CF_3)_3$),[5] $[Li(AlCl_4)]$•$3SO_2$,[12] $[Li_2(SO_2)_8][B_{12}Cl_{12}]$,[13] $[Na(AlCl_4)]$•$1.5SO_2$[12,14] $Na_2[B_{12}Cl_{12}]$•$4SO_2$,[13] $K_2[B_{12}F_{12}]$•$6SO_2$[15] $Na[Me_3NB_{12}Cl_{11}]$•SO_2,[16] $M_2[B_{12}Cl_{12}]$•$8SO_2$[13] (M = K^+, Rb^+), $Cs_2[B_{12}Cl_{12}]$•SO_2[13] or $[Mg(SO_2)_2\{AsF_6\}_2]$.[17] In these characterized compounds, however, exclusively coordination of SO_2 towards the metal centre

[a] *F. Dankert, A. Feyh, Prof. Dr. C. von Hänisch*
Fachbereich Chemie and Wissenschaftliches Zentrum für Materialwissenschaften (WZMW), Philipps-Universität Marburg, Hans-Meerwein Str. 4, 35032 Marburg, Germany
E-mail: haenisch@chemie.uni-marburg.de
https://www.uni-marburg.de/de/fb15/arbeitsgruppen/ag-haenisch
[‡] These authors contributed equally.
Supporting information and ORCID(s) from the author(s) for this article are available on the WWW under https://doi.org/10.1002/ejic.202000299.
© 2020 The Authors. Published by Wiley-VCH Verlag GmbH & Co. KGaA. • This is an open access article under the terms of the Creative Commons Attribution License, which permits use, distribution and reproduction in any medium, provided the original work is properly cited.

© 2020 The Authors. Published by Wiley-VCH Verlag GmbH & Co. KGaA, Weinheim

Full Paper
doi.org/10.1002/ejic.202000299

was observed. In how far anions can be solvated remains unclear. *Jander* summarized the solubilities of a handful of salts in combination with different anions. Especially for those of the s-block metals. As can be seen in Table 1, the highest solubility according simple halide salts is achieved employing iodide (and thiocyanate) salts but it is known from a number of studies that all halides can be somehow dissolved forming so called halosulfite ions or sharing at least electrostatic interactions with the positively polarized S atom of SO_2.

Table 1. Solubilities of different alkali and alkaline earth metal salts as well as ammonium salts in 1000 g of liquid sulfur dioxide at 0 °C given in [mmol].[a][10]

Cation	F^-	Cl^-	Br^-	I^-	SCN^-
Li^+	23	2.82	6	1490	n.d.[b]
Na^+	6.9	insol.	1.36	1000	80.5
K^+	3.1	5.5	ca. 40	2490	502
Rb^+	n.d.	27.2	n.d.	n.d.	n.d.
NH_4^+	n.d.	1.67	6	580	6160
Be^{2+}	n.d.	5.8	n.d.	n.d.	n.d.
Mg^{2+}	n.d.	1.47	1.3	0.5	n.d.
Ba^{2+}	n.d.	insol.	insol.	18.15	insol.

[a] Values of missing s-block salts are not determined. [b] n.d. = not determined.

Different types of such adducts were characterized and discussed in literature: whereas the fluorosulfite anion could also be characterized as a simple salt of MSO_2F-type (M = K^+, Rb^+, Cs^+),[18–20] the higher homologous halosulfites were only obtained using (large) organocations which make the obtained compounds stable enough for single crystal structure determinations.[11,20–27]

As sulfur dioxide is a gas above temperatures of −10 °C,[1] sulfur dioxide solvates are quite unstable at ambient temperature and SO_2 loss makes a satisfactorily characterization of its coordination compounds challenging. Employing cold temperatures are mandatory and especially preparation of single crystals which combine both, moisture and temperature sensitivity is not trivial.[11] The introduction of large organocations such as tetraalkylammoniumcations, metal-organic ligand complexes, carbene complexes or employing crown-ethers increases stability as well as solubility and enhances the possibility of structure determinations. So has the chlorosulfite anion SO_2Cl^- been crystallographically characterized upon reduction of SO_2Cl_2 with a carbene[21] or as a complex ligand in the sila-crown-ether complex [Li(1,2-disila[12]crown-4)SO_2Cl].[11] A discrete bromosulfite ion has not yet been crystallographically characterized but it should be mentioned that $O_2S\cdots Br^-$ contacts were observed in tetraalkylammonium bromide salts crystallized from SO_2.[22,23]

Iodosulfites have been characterized in the compounds $[PPh_3Bz]SO_2I$,[24] $[Pt(CH_3)(PPh_3)_2SO_2I]$[25] or in $[Pt(depe)_2]SO_2I_2$[26] (depe = 1,2-bis(dimethylphosphino)ethane). The latter compound represents a dianionic iodide-sulfur dioxide adduct which is considered as a diiodosulfite anion and was characterized by *Nagasawa* and co-workers.[26] Most recently also methylsulfonyl iodide was characterized by *Stanbury*.[27] Scheme 1 gives an overview of the different described $O_2S\cdots$halide compounds. These compounds were, however, characterized as a single example of the respective compounds and thus no structural study has been performed where the use of different organocations in combination with different stoichiometries was employed. In this contribution we want to present a more sophisticated work which contributes to the recent discussion around chalcogen-bonds. These are known as an attractive interactions formed by group 16 elements with nucleophiles.[28–32] An outlook has been given in a past work where we characterized alkali metal chloride complexes from SO_2 which finally allowed the crystal structure determination of aforementioned $MCl{\cdot}3SO_2$ (M = Rb^+, Cs^+) together with the observation of rare $O_2S\cdots Cl^-$ contacts.[11] All of these compounds, however, were extremely sensitive towards moisture and temperature.

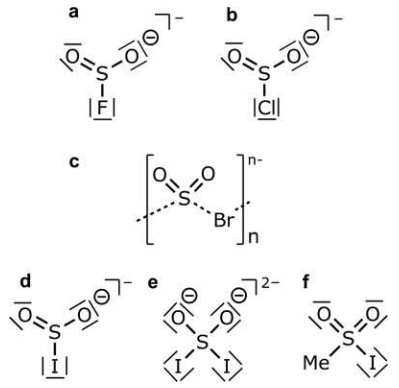

Scheme 1. Different SO_2 adducts of halides and related compounds. (a) Fluorosulfite as characterized in (a)[18,19] MSO_2F (M = K^+, Rb^+, Cs^+, $(Me_2N)_3S^+$, $(Me_2N)_3SO^+$, $N(CH_3)_4^+$), (b)[20,21] Chlorsulfite ion as characterized as the anion of a chloro-carbene adduct or in [Li(1,2-disila[12]crown-4)SO_2Cl], (c)[11,22,23] $O_2S\cdots Br^-$ infinite chains in $NR_4Br{\cdot}SO_2$ (R = CH_3, CH_2CH_3), (d)[24,25] iodosulfite as characterized in $[PPh_3Bz]SO_2I$ and $[Pt(CH_3)(PPh_3)_2SO_2I]$, (e)[26] diiodosulfite as characterized in $[Pt(depe)_2]SO_2I_2$, (f)[27] recently characterized methanesulfonyl iodide in the compounds $(CH_3SO_2I)_2{\cdot}RbI_3$ and $(CH_3SO_2I)_4{\cdot}KI_3{\cdot}2I_2$.

Herein we employ different crown-ethers and the s-block metal iodides for a structural study of iodosulfites and $O_2S\cdots I^-$ contacts. Single crystals can be prepared at ambient temperature from such reaction mixtures and show that SO_2 can not only be embedded in the architecture of discrete SO_2I^- or $SO_2I_2^{2-}$ anions, but furthermore in a variety of different coordination networks. Therein, one- and two-dimensional structures with and without an embedded crown ether complex are observed. In the light of the great potential of chalcogen bonds which find applications as for example in catalysis,[33,34] ion sensing and transport,[35–37] substrate recognition[38] and drug design,[39,40] it is overdue that chalcogen-bonding towards small molecules such as SO_2 should be examined to an extent.

Results and Discussion

SO_2 Adducts with Alkali Metal Crown-Ether Complexes

In starting to investigate the SO_2 coordination we straight forwardly converted different crown ethers with the alkali metal iodides in anhydrous SO_2 employing various stoichiometries. At first, we reacted [12]crown-4 with LiI in liquid SO_2 in a 1:1 stoichiometry of salt and ether. Indeed the salt readily dissolves in the solvent and a clear, pale yellow solution is obtained. An

© 2020 The Authors. Published by Wiley-VCH Verlag GmbH & Co. KGaA, Weinheim

Full Paper
doi.org/10.1002/ejic.202000299

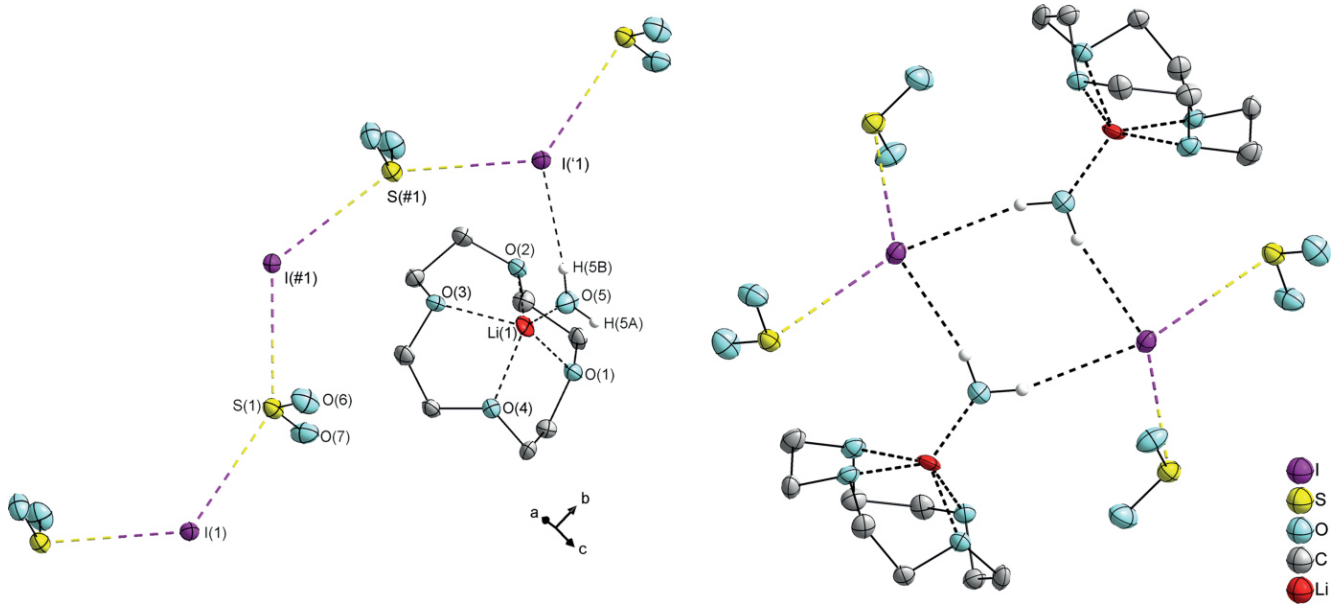

Figure 1. The structure of **1** showing the $O_2S\cdots I^-$ infinite chain along [b] in the crystal (left) and linkage of the one-dimensional infinite chains by hydrogen bonding of H_2O ligands (right). Atoms depicted with # or ′ are symmetry generated over 1/2 – *x*, 1/2+y, 1/2 – *z* or x, 1+y, z. Thermal displacement ellipsoids represent the 50 % probability level. Selected bond lengths [pm]: S(1)–I(1) 343.5(1), S(1)–I(1a) 349.3(1), O(1)–Li(1) 210.9(11), O(2)–Li(1) 210.7(10), O(3)–Li(1) 210.5(11), O(4)–Li(1) 204.7(10), O(5)–Li(1) 188.7(10). Selected bond angles [°]: O(6)–S(1)–O(7) 116.7(3), I(1)–S(1)–I(#1) 145.4(1), S(1)–I(#1)–S(#1) 123.8(1).

orange oil is obtained as the solvent is carefully removed. If the oil is kept at ambient temperature for several days, we observed redox-chemistry as the oil turns dark brown. Colourless needles were obtained after several days which turned out to be γ-S_8. Thus, redox chemistry is crucial which compares well with the observations made by *Jander* earlier on.[10] By allowing the obtained orange oil to react with traces of moisture for about one minute opening the reaction vessel, yields yellow platelets within the oil in minutes.

As determined via SC-XRD (SC-XRD = single-crystal X-ray diffraction) analysis we observed the formation of the SO_2 containing adduct [Li([12]crown-4)H_2O]I•SO_2 which crystallizes in the monoclinic space group $P2_1/n$. As can be seen by the structure in the crystal, the Li^+ ion is coordinated fivefold by the crown ether as well as an additional H_2O molecule. The latter forms hydrogen bonds with the iodide ion (Figure 1: right). The coordination pattern of I^- and SO_2 is a one-dimensional infinite network along the crystallographic [b] axis (Figure 1: left). The S–I atom distances measure 343.5(1) and 349.3(1) pm and the S–I–S angles within the infinite chain measure 123.8(1) and 145.4(1)°. This $I^-\cdots SO_2$ infinite chain is highly related to the $Br^-\cdots SO_2$ infinite chain in [NEt_4]Br•SO_2.[22] Under consideration of the hydrogen bonding between these strands, a two-dimensional coordination polymer is obtained.

Sodium iodide has also been employed for establishing $O_2S\cdots I^-$ contacts. Starting with [15]crown-5 as a ligand, we observed the formation of a clear, pale yellow solution. After removal of the solvent, a sticky orange oil is obtained from which orange platelets can be obtained at ambient temperature. The crystal structure could be determined and turned out to be [Na([15]crown-5)(SO_2)I]. As can be seen in Figure 2, SO_2 as well as I^- are now coordinating towards the metal centre. The compound crystallizes in the monoclinic crystal system, space group $P2_1/c$ with four molecules per unit cell. A closer look reveals a short S(1)···I(1) contact of 311.8(1) pm within this complex. This contact represents actually a shorter chalcogen bond in comparison with those considered close enough to form an "iodosulfite" or also "iodosulfinate".[24,25] However, to consider such a $O_2S\cdots I^-$ fragment to be an "iodosulfite" is in our eyes debatable. Even though literature[24,25] considers such fragments as SO_2I^-, we cannot quite follow this argumentation due to the fact, that significantly shorter $O_2S\cdots I^-$ contacts (<300pm) are observed within this study (e.g compounds **3**, **8** and **10** which are presented later on). In our eyes one could argue, that a $O_2S\cdots I^-$ fragment should be considered as "iodosulfite" when the $O_2S\cdots I^-$ contact is closer to the S–I single bond radii sum of 236 pm[25,41] than to the van der Waals radii sum of 378 pm[42] or 400 pm if the ionic radius of I^- (220 pm at CN = 6)[43] is considered. This would mean an iodosulfite is present with a value below 307 pm or 318 pm, respectively. We want to emphasize that this range is a rough approximation as the vdW radii are anisotropic. Selected structures from literature bearing a covalent S–I bond are in agreement with our interpretation, though. The S–I atom distance in cationic [I-SEt_2]$^+$ has a value of 249.9 pm.[44] In the neutral compounds ($Ph_2PN)_2$NSI and $(PhCN)_2$NSI values of 266.5 and 271.4 pm are found.[45,46] As for an anionic species the S–I atom distance should then only be slightly larger which fits the postulated range and indeed such atom distances are found in our study (see compounds **3**, **8** and **10**).

Assuming that an iodosulfite is established in this case, we observe very close $O_2S\cdots I^-$ contacts within the asymmetric unit of **2** (Figure 2: top). Furthermore, weak $O_2S\cdots I^-$ contacts are observed to the next formula unit which eventually leads to a one-dimensional coordination polymer including the crown-ether complex with twofold coordinated S atoms of SO_2 (Figure 2:

© 2020 The Authors. Published by Wiley-VCH Verlag GmbH & Co. KGaA, Weinheim

Full Paper
doi.org/10.1002/ejic.202000299

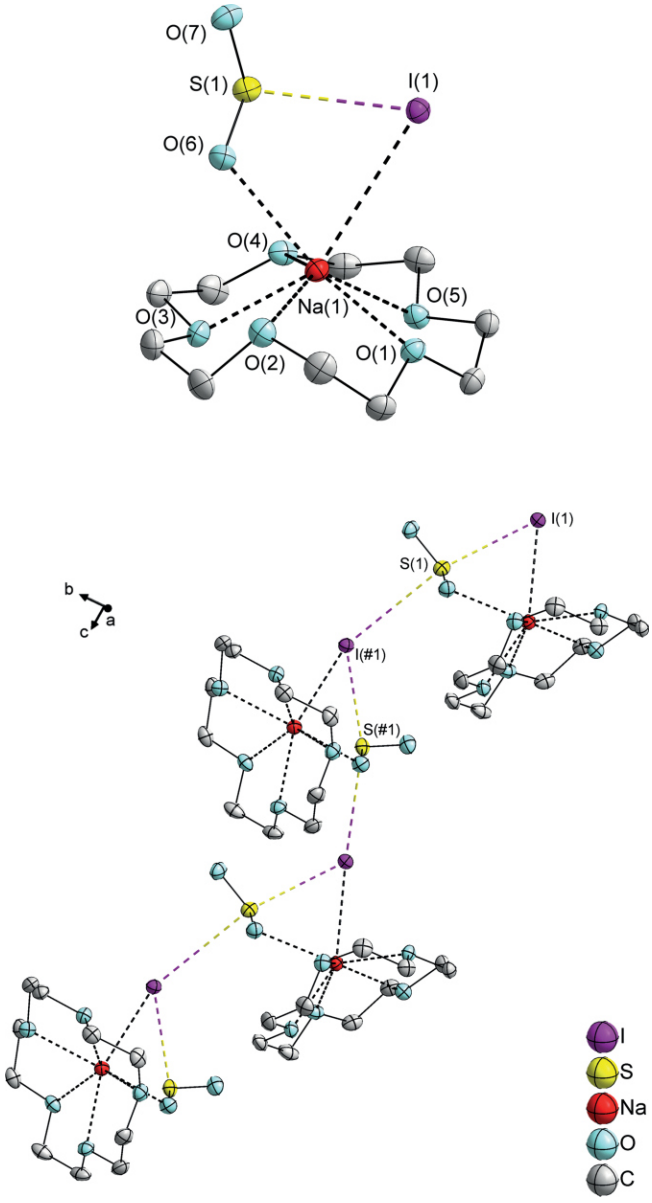

Figure 2. The molecular structure of **2** in the crystal (top) as well as the $[Na([15]crown-5)]^+$ attached $O_2S\cdots I^-$ infinite chain approximately along [c] (bottom). Atoms depicted with # are symmetry generated over x, 3/2 – *y*, –1/2+z. Thermal displacement ellipsoids represent the 50 % probability level. Selected bond lengths [pm]: S(1)–I(1) 311.8(1), S(1)–I(#1) 370.9(2), O(1)–Na(1) 244.0(2), O(2)–Na(1) 245.0(2), O(3)–Na1 240.1(2), O(4)–Na(1) 248.2(2), O(5)–Na(1) 245.7(2), O(6)–Na(1) 257.8(2), I(1)–Na(1) 332.1(2). Selected bond angles [°]: O(6)–S(1)–O(7) 115.8(1), O(6)–Na(1)–I(1) 71.4(1), I(1)–S(1)–I(#1) 161.8(1), S(1)–I(#1)–S(#1) 122.6(1).

bottom). What can be learned from this compound is, that a coordination of SO_2 at a metal centre is observed as long as the metal centre has room for such SO_2 ligand and is capable of being saturated further.

To examine a structural difference, we converted NaI with two equivalents of [12]crown-4 to form sandwich-type complexes in which the iodide ion is isolated from the central ion. This should make the iodide ion somehow "naked" and more reactive towards SO_2. Indeed we could observe a substantially difference in comparison to **2**. A pale yellow solution is observed from which yellow platelets crystallize as the solvent is carefully removed in an argon flush. The obtained platelets could be investigated by means of SC-XRD and during the cell measurements of different crystals we could observe, that two compounds have crystallized as yellow platelets from the solution, both of which are SO_2 solvates of $[Na([12]crown-4)_2]I$. With $[Na([12]crown-4)_2]SO_2I$ (**3**) a first compound could be obtained, where an isolated iodosulfite can be observed (see Figure 3). The compound crystallizes in the triclinic crystal system, space group $P\bar{1}$. In this respective compound, the S–I atom distance is with 293(1) pm distinctly closer to the S–I single bond radii sum than to the van der Waals radii sum. Due to disorder around SO_2I^- this value should be somehow interpreted carefully but this value still proves existence of SO_2I^- within the standard deviation. Due to sandwich formation this anion is isolated from the metal centre and represents a rare example of a halosulfite ion which is not formed and/or stabilized by metal coordination. The iodosulfite ion formulated as $SO_2I_2^{2-}$ has been obtained following a similar strategy as a Pt^{2+} cation was shielded with depe ligands.[26] The molecular structure of **3** clearly indicates a high affinity of I^- to bind SO_2, the second molecular structure follows this observation. The shielding of the central ion has also another effect as there are now higher coordination numbers present at I^-.

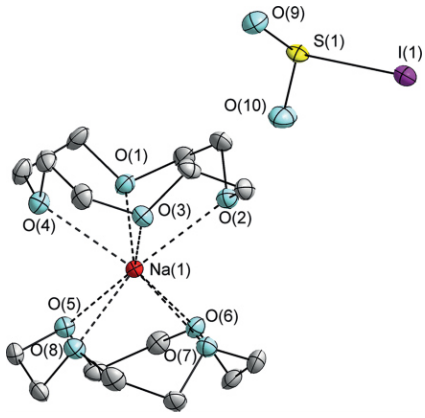

Figure 3. The molecular structure of **3** in the crystal. Thermal displacement ellipsoids represent the 50 % probability level. Hydrogen atoms of the crown-ether as well as the respective disordered part of the iodosulfite are omitted for clarity. The iodosulfite is reduced to the highest occupied atom positions. Selected bond lengths [pm]: I(1)–S(1) 293.5(12), O(1)–Na(1) 246.6(1), O(2)–Na(1) 248.2(1), O(3)–Na(1) 244.4(1), O(4)–Na(1) 250.8(1), O(5)–Na(1) 247.5(1), O(6)–Na(1) 245.3(1), O(7)–Na(1) 252.0(1), O(8)–Na(1) 245.3(1), O(9)–S(1) 143(1), O(10)–S(1) 143.4(8). Selected bond angles [°]: O(9)–S(1)–O(10) 116.6(9), O(9)–S(1)–I(1) 101.0(5), O(10)–S(1)–I(1) 99.9(4).

As was determined by SC-XRD, $2[Na([12]crown-4)_2]I{\cdot}5.5SO_2$ (**3a**, depicted as the reduced formula $[Na([12]crown-4)_2]I{\cdot}2.75SO_2$) has been obtained. The compound does also crystallize in the triclinic space group $P\bar{1}$. Under consideration of the sum of vdW radii, cation-separated $[I_2(SO_2)_5]^{2-}$ strands are observed in this crystal structure (Figure 4). The strands described by this formula sum are explained by disorder of terminal SO_2 molecules. The cationic part of the structure is distinguished by $[Na([12]crown-4)_2]^+$ sandwich complexes. The "naked" I^- ions are thus also able to coordinate towards multiple SO_2 molecules. Solvation numbers observed herein are 3 and 4

© 2020 The Authors. Published by Wiley-VCH Verlag GmbH & Co. KGaA, Weinheim

Full Paper
doi.org/10.1002/ejic.202000299

which compares well with the early examinations of *Jander*.[10] The $[I_2(SO_2)_5]^{2-}$ strands consist out of two crystallographic different iodide ions. Inside the cavity spanned by four of such strands, a further SO_2 molecule is incorporated co-crystalline.

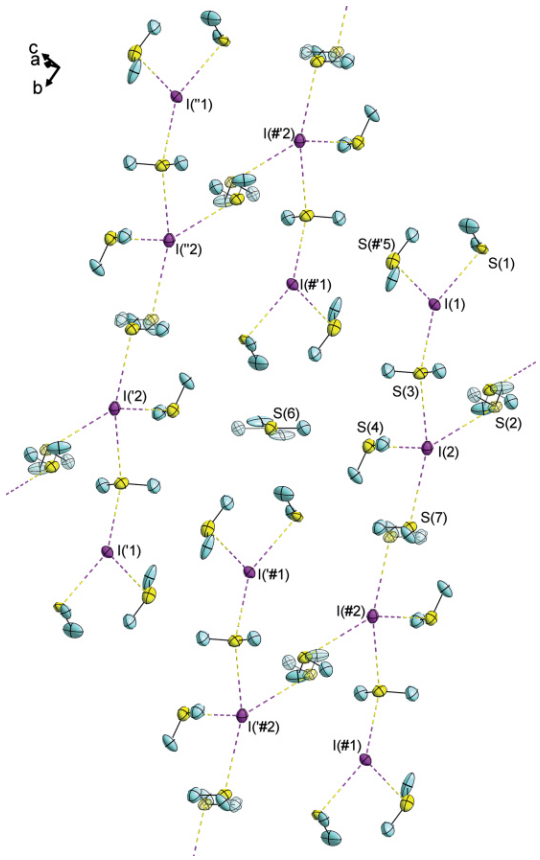

Figure 4. Section of the $O_2S\cdots I^-$ coordination pattern of **3a** in the crystal. Thermal displacement ellipsoids represent the 50 % probability level. The disordered SO_2 molecules are drawn transparent and the $[Na([12]crown\text{-}4)_2]^+$ cations are omitted for clarity. Atoms depicted with ', '', #, '# or #' are symmetry generated over 1 – *x*, 2 – *y*, 1 – *z*; x, y, 1+z; 1 – *x*, 2 – *y*, –z; x, 1+y, z or 1 – *x*, 1 – *y*, 1 – *z*. Selected bond lengths [pm]: I(1)–S(1) 324.9(3), I(1)–S(3) 353.1(4), I(1)–S(#'5) 330.9(3), I(2)–S(2) 374.3(7), I(2)–S(3) 336.1(3), I(2)–S(4) 306.5(3), I(2)–S(7) 354.9(7). Selected bond angles [°]: I(1)–S(3)–I(2) 133.5(1), S(1)–I(1)–S(3) 147.6(1), S(1)–I(1)–S(#'5) 93.1(1), S(3)–I(1)–S(#'5) 94.5(1), S(2)–I(2)–S(3) 73.3(1), S(3)–I(2)–S(4) 76.8(1), S(3)–I(2)–S(7) 158.5(1), S(4)–I(2)–S(7) 81.6(1).

Unfortunately, these crystals were twinned and a suitable refinement was problematic in general. Restraints were used to fix the refinement around the SO_2 solvates. For this reason, the depicted atom distances as well as angles in the caption of Figure 4 should also be considered carefully. However, the shielding of metal centres can obviously enforce the formation of halosulfites and can also lead to SO_2 rich compounds. The obtained coordination pattern gives an idea on what kind of SO_2 aggregates can be present. To obtain such solvent-rich coordination compounds, we also tried to shield the sodium ion with [18]crown-6 or [2.2.2]crypt. In case of [18]crown-6 a yellow solution can be obtained, but crystallization of the initially formed species failed due to redox processes as explained above and the SI (SI = supporting information). Further, exposing to moisture was not successful. [2.2.2]crypt leads to an insoluble precipitate from which no suitable crystals for SC-XRD could be obtained. Shielding a cation by [2.2.2]crypt as a strategy to obtain solvates was abandoned as the formation of insoluble compounds was observed for all herein chosen s-block metal iodides.

[18]crown-6 as a ligand has then been chosen as ligand for the remaining alkali metal and ammonium iodides MI (M = K^+, NH_4^+, Rb^+, Cs^+). These salts readily dissolve in SO_2 in combination with [18]crown-6 and different network structures could be obtained after investigating yellow platelets via SC-XRD. In case of KI, a one-dimensional network including the crown-ether complex $[K([18]crown\text{-}6)I(SO_2)]$ was observed. The potassium ion is trapped inside the middle of the crown-ether as evident from O-K-O transannular angles of 174.2(4) to 177.6(4)°. In this respective network, the potassium ions are coordinated by the crown-ether, a single SO_2 molecule as well as the iodide anion. The coordination geometry around potassium is a slightly distorted hexagonal bipyramid. The vertices are occupied by I^- and SO_2. Close contacts between the iodide anions and the SO_2 molecules of the next formula unit are observed. Different to the half-sandwich-like structure motif of **1** and **2**, the coordination network proceeds alongside the crown-ether plane (Figure 5). The one-dimensional network arises along [b] with $O_2S\cdots I^-$ chalcogen bonding interactions of 303.0(1) pm and S(1)–I(#1)–K(#1) angles of 113.7(1)°. As the potassium ion was successfully embedded into a SO_2 coordination network, we also converted NH_4I with [18]crown-6. The purpose was to obtain a SO_2-rich network and/or multiple SO_2 contacts at I^- without the [18]crown-6 complex embedded into the structure. Indeed we could observe network formation, but the network is very similar to that of compound **1** and a representation of the crystal structure has thus moved to the SI. The architecture around the one-dimensional network in $[NH_4([18]crown\text{-}6)]I{\cdot}SO_2$ (**5**) is also stair-like but almost rectangular as the S–I–S angle has a value of 88.0(1)°. In comparison to **1**, however, the one-dimensional strands are not connected by hydrogen bonds. Finally, we could also obtain compounds of RbI and CsI. As both salts were converted with [18]crown-6, yellow platelets were grown from clear yellow solutions. Two related structures were found. The rubidium compound crystallizes in the monoclinic space group $P2_1/n$ with four molecules per unit cell. $[Rb([18]crown\text{-}6)I(SO_2)]{\cdot}2SO_2$ (**6**) consists, similar to **2**, out of a one-dimensional coordination network which is build up by $O_2S\cdots I^-$ contacts and a Rb^+ half-sandwich complex of [18]crown-6 (Figure 6). The iodide anions are in this case bound to the metal centre and furthermore embedded into a fourfold coordination with SO_2. One of the SO_2 molecules coordinates to the metal centre which is at the same time twofold coordinated by I^- anions which eventually enables the network formation. Two more SO_2 molecules are embedded in the structure which are saturated by the I^- anion within the respective asymmetric unit. The coordination pattern around I^- can be understood as a $[I(SO_2)_4]^-$ unit which is related to $[Cl(SO_2)_4]^-$ as observed in $[Li([12]crown\text{-}4)Cl]{\cdot}4SO_2$ as well as $[M([12]crown\text{-}4)_2(SO_2)]Cl{\cdot}4SO_2$ (M = K^+, Rb^+).[11] In comparison to these mentioned structures, the distorted square-like $[I(SO_2)_4]^-$ units are corner-sharing forming a polymeric structure rather than an iso-

© 2020 The Authors. Published by Wiley-VCH Verlag GmbH & Co. KGaA, Weinheim

Full Paper
doi.org/10.1002/ejic.202000299

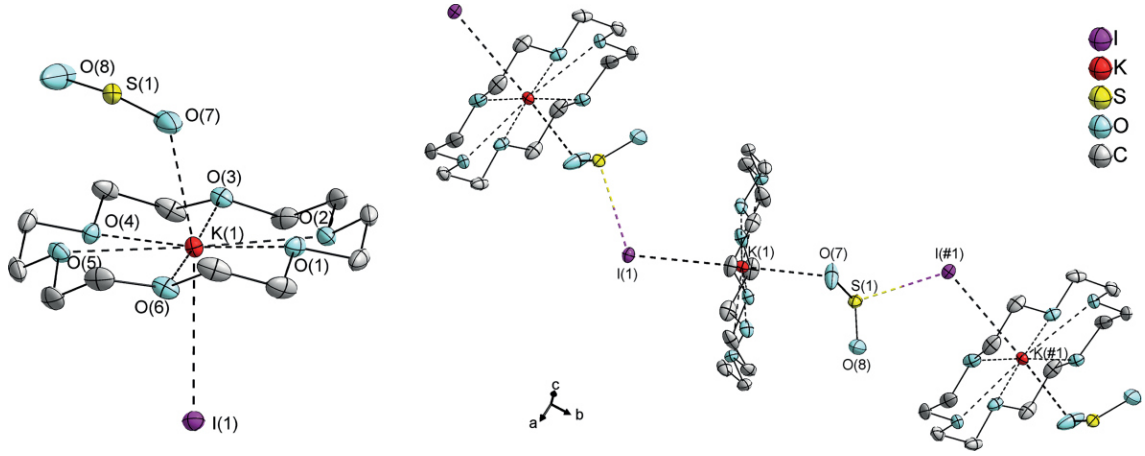

Figure 5. The molecular structure of **4** (left) as well as the 1D $I^-\cdots SO_2\cdots[K([18]crown-6)]^+$ infinite chain along [b] in the crystal (right). Atoms depicted with # are symmetry generated over 1/2 – *x*, 1/2+y, 1/2 – *z*. Selected bond lengths [pm]: I(1)–K(1) 352.1(1), O(1)–K(1) 277.8(1), O2–K(1) 281.5(1), O(3)–K(1) 283.2(1), O(4)–K(1) 279.7(1), O(5)–K(1) 286.8(1), O(6)–K(1) 278.7(1), O(7)–K(1) 280.6(2), S(1)···I(#1) 303.0(1). Selected bond angles [°]: I(1)–K(1)–O(7) 159.0(1), I(#1)–S(1)–O(7) 102.1(1), K(1)–O(7)–S(1) 133.7(1), O(7)–S(1)–O(8) 116.4(1), S(1)–I(#1)–K(#1) 113.7(1).

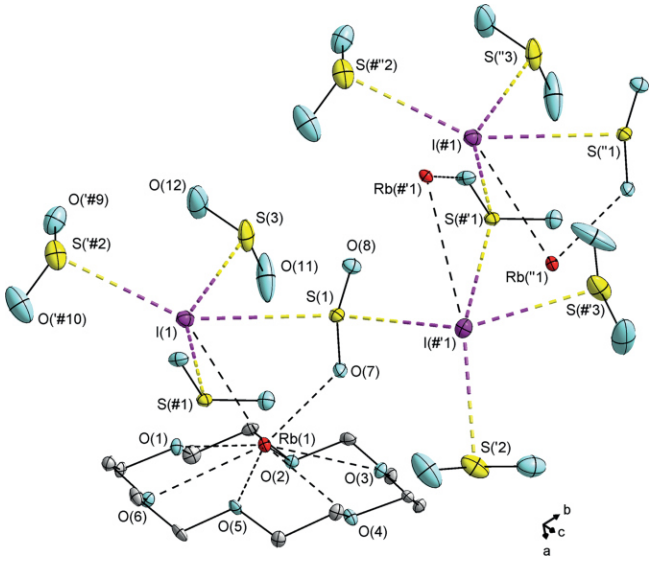

Figure 6. The structure of **6** in the crystal as well as adjacent $[I(SO_2)_4]^-$ units. Adjacent crown-ethers are omitted for clarity. Thermal displacement ellipsoids represent the 50 % probability level. Atoms depicted with #, '#, #', #'' or '' are symmetry generated over 1/2 – *x*, –1/2+y, 3/2 – *z*; 1 – *x*, –y, 1 – *z*; 1/2 – *x*, 1/2+y, 3/2 – *z*; 1 – *x*, 1 – *y*, 1 – *z* or x, 1+y, z. Selected bond lengths [pm]: I(1)–Rb(1) 384.5(1), O(1)–Rb(1) 290.1(3), O(2)–Rb(1) 304.3(3), O(3)–Rb(1) 292.8(3), O(4)–Rb(1) 300.2(3), O(5)–Rb(1) 288.8(3), O(6)–Rb(1) 301.2(3), O(7)–Rb(1) 290.2(4), I(1)–S(1) 354.5(1), I(1)–S('#2) 335.2(1), I(1)–S(3) 326.8(1). Selected bond angles [°]: I(1)–S(1)–I(#'1) 157.6(1), S(1)–I(1)–S(#1) 76.5(1), S(1)–I(1)–S(3) 69.6(1), S(#1)–I(1)–S('#2) 106.9(1), S('#2)–I(1)–S(3) 100.6(1).

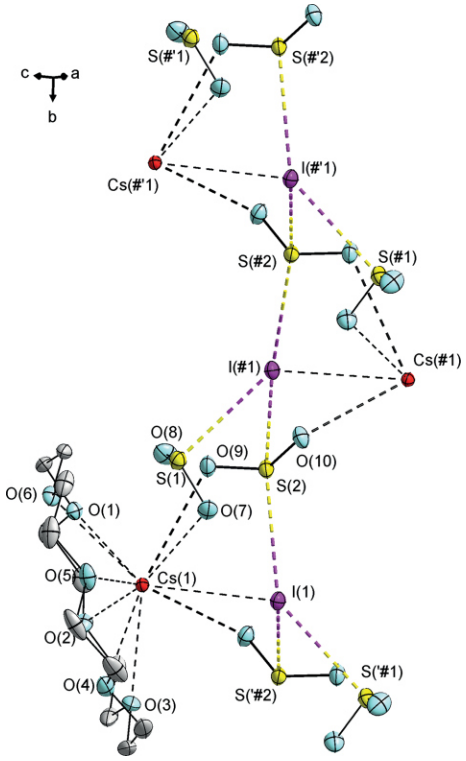

Figure 7. The structure of **7** in the crystal as well as adjacent $[I(SO_2)_3]^-$ units. Adjacent crown-ethers are omitted for clarity. Thermal displacement ellipsoids represent the 50 % probability level. Atoms depicted with #, '# or #' are symmetry generated over 1 – *x*, –1/2+y, 1/2 – *z*; 1 – *x*, 1/2+y, 1/2 – *z* or x, –1+y, z. Selected bond lengths [pm]: I(1)–Cs(1) 389.0(1), I(1)–S('#1) 317.8(1), I(1)–S('#2) 356.6(1), I(1)–S(2) 352.7(1), O(1)–Cs(1) 309.7(1), O(2)–Cs(1) 317.5(1), O(3)–Cs(1) 301.3(1), O(4)–Cs(1) 316.7(1), O(5)–Cs(1) 304.7(1), O(6)–Cs(1) 318.3(1), O(7)–Cs(1) 322.7(1), O(9)–Cs1 337.9(1). Selected bond angles [°]: I(1)–S(2)–I(#1) 156.1(1), S(1)–I(#1)–S(#2) 135.9(1), S(1)–I(#1)–S(2) 67.2(1), S(2)–I(1)–S('#2) 95.6(1).

lated aggregate. Again, the solvation number around M^+ or I^- is not higher than 4 but the comparably large ionic radius of Rb^+ (r_i[CN8] = 161 pm)[43] and probably also the position of the metal centre slightly outside the crown-ether plane (d(plane···Rb^+) = 95 pm) allows for the attraction with a higher number of SO_2 molecules, so half-sandwich complex formation of a cation with a large ionic radius is actually another strategy to fixate multiple SO_2 molecules per formula unit.

The cesium compound $[Cs([18]crown-6)(SO_2)_2I]$ (**7**, Figure 7) represents also a one-dimensional coordination network along [b]. The I^- ions are in this case coordinating three SO_2 molecules. The $[I(SO_2)_3]^-$

© 2020 The Authors. Published by Wiley-VCH Verlag GmbH & Co. KGaA, Weinheim

solvates formed in this structure show a trigonal pyramidal coordination motif as the iodide anion is placed 125.2(1) pm on top of the spanned plane by the S atoms. Similar to the SO_2···I^- building blocks in **6**, the $[I(SO_2)_3]^-$ units are corner-sharing which results in the described one-dimensional coordination motif. The larger ionic radius of Cs^+ allows for the attraction of I^- as well as now three SO_2 ligands from one of which is part of the adjacent formula unit. This leads to a coordination number of ten at Cs^+. The SO_2 molecules coordinate the Cs^+ ion and are themselves coordinated by I^-. Within this coordination network one SO_2 molecule is in a bridging position between two cesium ions. This is probably the reason, why the iodide anions are not saturated by more SO_2 molecules. The crown ether units are closely packed side by side, so no more voids can be occupied by SO_2. To shortly sum up the alkali metal iodide chemistry in SO_2, we can distinguish different strategies to obtain possible O_2S···I^- chalcogen bonding interactions with solvation numbers between 1 and 4. By employing the 1:1 crown-ether complexes we obtained mainly one-dimensional coordination polymers. These are structures, where the crown-ether is embedded into the coordination polymer. However, by shielding the metal centres, we avoided a respective interaction of SO_2 with the cation. This results in two major differences. On the one hand, the attractive chalcogen bonding is stronger than in 1:1 coordination compounds as an isolated iodosulfite was observed with considerably shorter S···I atom distances than those reported before. On the other hand, the I^- ion has more space in the crystal lattice which allows for the attraction with a higher number of SO_2 molecules. Thus, for example the $[I_2(SO_2)_5]^{2-}$ aggregate was formed. As the latter mentioned aggregate is formed by two crystallographic independent iodide anions it was at this point plausible, that the alkaline earth metal iodides should allow for the formation of related compounds and/or multidimensional networks with $(O_2S$···$I)^-_n$ building blocks.

SO_2 Adducts with Alkaline Earth Metal Crown-Ether Complexes

The alkaline earth metal iodides turned out to be even more redox-sensitive than the alkali metal iodides. We have obtained compounds exclusively for Mg^{2+} and Ba^{2+} which did not suffer redox-chemistry. In case of Sr^{2+} we were unable to obtain any SO_2 solvates of SrI_2 even after employing various crown ethers like [15]crown-5 and [18]crown-6. In case of CaI_2, we did only obtain one respective example with [18]crown-6 employed as ligand. This, however, shows I_3^- formation. The chemistry around the alkaline earth metal iodides is thus somehow reduced to Mg^{2+} and Ba^{2+}. The representation of the obtained Ca^{2+} compound $[Ca_2([18]crown\text{-}6)_2(SO_2I)_3]I_3$ (**10**) has been moved to the ESI. In the ESI, we have also provided a comment on the redox chemistry around these SO_2 adducts which contains a proposal for the redox-cascade in combination with literature-known[10,47] redox-chemistry in SO_2. The redox-cascade is basically characterized by sulfur- and iodide formation both of which were proved to be existent by means of SC-XRD.

However, the alkaline earth metal compounds presented herein are very rare examples of alkaline earth metal coordination compounds with SO_2 ligands in general. To the best of our knowledge, the only reported crystal structure bearing both, alkaline earth metal and SO_2 ligand is the aforementioned complex $[Mg(SO_2)_2\{AsF_6\}_2]$.[17] The related structure $[Ca(SO_2)_{1.5}(AsF_6)_{6/3}]_n$ was briefly mentioned as a preliminary result but no crystal structure has been deposited ever since.[2]

The conversion of MgI_2 with [15]crown-5 gives a red-orange solution from which small red-orange blocks were grown after slow reduction of the volume. The molecular structure in the crystal shows the willingly formation of two iodosulfites which are coordinating towards Mg^{2+} (Figure 8). The compound $[Mg([15]crown\text{-}5)(SO_2I)_2]$ (**8**) crystallises in the monoclinic space group *C*2/*c* with four molecules per unit cell. The S···I atom distances are with 275.8(2) pm even smaller than those in compound **3**. A considerably lower value by almost 20 pm is observed here. This is the closest value by far. Thus, an iodosulfite with reasonable S···I atom distances bears significantly shorter values than those reported before and we want to emphasize that this atom distance is now 40 pm close to the single bond radii sum of 236 pm.[25] The formation of this iodosulfite ion might be due to a high polarization of the SO_2 molecules by the hard metal cation Mg^{2+}. Due to coordination, the shift of electron density from the sulfur atom to the oxygen atoms is increased, which allows I^- to interact even stronger with the sulfur atom. This argument is strengthened by the fact, that the O(4)–S(1)–O(5) angle has a value of 112.3(1)° and approximates to a tetrahedral angle. These observations are in line with basic VSEPR (= valence shell electron pair repulsion) considerations which predict a Ψ-tetrahedral-like geometry for the iodosulfite SO_2I^-.

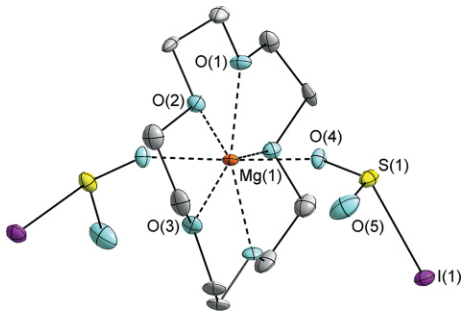

Figure 8. The molecular structure of **8** in the crystal. Thermal displacement ellipsoids represent the 50 % probability level. Hydrogen atoms of the crown-ether are omitted for clarity. Non-labelled atoms are symmetry generated over 1 – *x*, y, 3/2 – *z*. Selected bond lengths [pm]: I(1)–S(1) 275.8(1), O(1)–Mg(1) 213.0(1), O(2)–Mg(1) 221.6(1), O(3)–Mg(1) 214.9(1), O(4)–Mg(1) 203.9(1), O(4)–S(1) 146.0(1), O(5)–S(1) 144.8(1). Selected bond angles [°]: O(4)–S(1)–O(5) 112.3(1), O(4)–S(1)–I(1) 103.5(1), O(5)–S(1)–I(1) 103.3(1).

Further, the S–O atom distances are elongated which measure 144.8(1) and 146.0(1) pm in comparison to uncoordinated SO_2 in which the S–O atom distance measures 143(1) pm.[48] S–O bond elongation, however, is also caused by coordination of SO_2I^- towards Mg^{2+}. Similar as applied for compound **3**, MgI_2 was also reacted with [12]crown-4. A reaction mixture of 1 eq of MgI_2 and two equivalents of [12]crown-4 in liquid sulfur dioxide yields a red-orange, opaque suspension which was stirred overnight. We were able to grow some small orange platelets from the suspension. The structure determined from these respective platelets is $[Mg([12]crown\text{-}4)_2]I_2{\cdot}4SO_2$ (**9**, Figure 9). Apparent from two crystallographic independent iodide ions, we observed the formation of a two-dimensional network which is build up by the coordination sphere around these anions (Figure 10). One building block resembles a highly distorted tetrahedral coordination sphere of SO_2 molecules around I^-. The tet-

© 2020 The Authors. Published by Wiley-VCH Verlag GmbH & Co. KGaA, Weinheim

Full Paper
doi.org/10.1002/ejic.202000299

rahedron exhibits S–I–S angles of 86.3(1) and 122.1(1)°. Another building block is a nearly perfect shaped $[I(SO_2)_4]^-$ square of which every corner is attached to such tetrahedron (Figure 10). The S–I–S angles have a value of 89.9(1)° and the transannular S–I–S angles measure 176.6(1)°. The solvation number around I^- is in both cases 4. Indeed the isolation of two rather than one iodide anion leads to the formation of a two dimensional network constituted by $O_2S\cdots I^-$ contacts. The network is a rare example of such structure determined by chalcogen bonding. This result represents crown-ethers to be activating anions to bind SO_2 in such way that the chalcogen bonds are strong enough to control the conformation and packing of cations in the solid. Maybe this result can give an outlook on SO_2 based layered materials and interfaces or even SO_2 based host-lattices as the multidimensionality of such networks can build a porous design. As the SO_2 chemistry around Ca^{2+} and Sr^{2+} is skipped at this point due to severe redox-chemistry (see ESI) we present the conversion of [18]crown-6 with BaI_2 in SO_2. The conversion yields a yellow solution which turns slightly orange upon reduction of the volume. Slow reduction of the volume eventually leads to the formation of orange platelets which were investigated via SC-XRD.

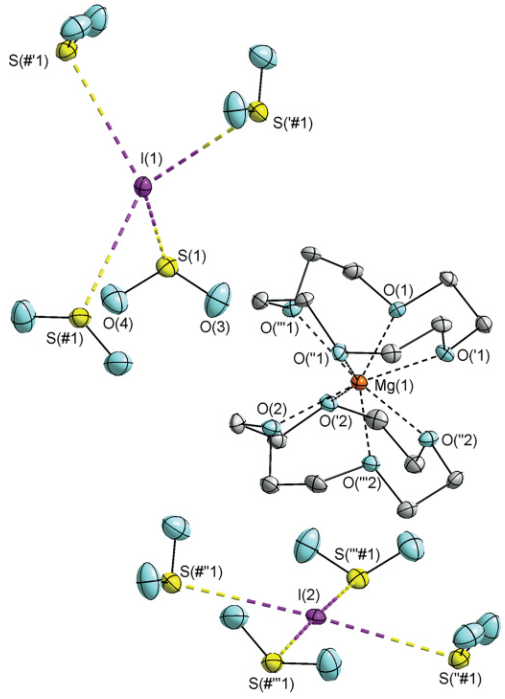

Figure 9. The molecular structure of **9** in the crystal including the coordination sphere around Mg^{2+} and I^-. Thermal displacement ellipsoids represent the 50 % probability level. Hydrogen atoms of the crown-ether are omitted for clarity. Atoms depicted with #, #', #'', #''', '#,''#, '''#, ', '' or ''' are symmetry generated over 3/2 – *x*, 1/2 – *y*, *z*; 1 – *y*, –1/2+*x*, 2 – *z*; 1/2+*y*, 1 – *x*, 1 – *z*; 1/2+*x*, 1/2+*y*, 1 – *z*; 1/2+*y*, 1 – *x*, 2 – *z*; 1 – *y*, 1/2+*x*, 1 – *z*; 1 – *x*, 1 – *y*, 1 – *z*; *y*, 3/2 – *x*, *z*; 3/2 – *x*, 3/2 – *y*, *z* or 3/2 – *y*, *x*, *z*. Selected bond lengths [pm]: I(1)–S(1) 353.2(1), I(2)–S(2) 344.8(1), O(1)–Mg(1) 225.0(2), O(2)–Mg(1) 224.0(2). Selected bond angles [°]: S(#'1)–I(1)–S('#1) 86.3(1), S(#'1)–I(1)–S(#1) 122.1(1), S(#''1)–I(2)–S('''#1) 89.9(1), S(''#1)–I(2)–S(#''1) 176.6(1).

The molecular structure in the crystal reveals a dinuclear Ba^{2+} complex. In this respective complex, one SO_2 molecules is connecting the metal ions and is further polarized in such way, that the attraction with I^- is strong enough to form the iodosulfite ion (S2–I(#1) 298.4(1) pm). Close contacts of I^- and coordinating SO_2 molecules as well as one further attached SO_2 molecule are present. The compound is best described as $[Ba_2([18]crown\text{-}6)_2(SO_2I)(SO_2)_2I_3]\cdot SO_2$ (**11**) and crystallizes in the monoclinic space group $P2_1/c$. As can be seen in the structure depicted in Figure 11, the barium ions have next to the crown ether ligand four coordination sites, which allows for the formation of an extensive network. These are occupied by the iodide anions and by oxygen atoms of linking SO_2 ligands. Figure 11 (bottom) shows the 2D-network which is build. In comparison to the alkali-metals, the alkaline earth metal barium strives a different binding mode and the coordination of SO_2 enables the formation of a dinuclear species. Polarized SO_2 molecules attached to the side positions of the complex as well as nucleophilic iodide-head positions enables chalcogen bonding. A 2D network with the crown-ether embedded is the outcome and

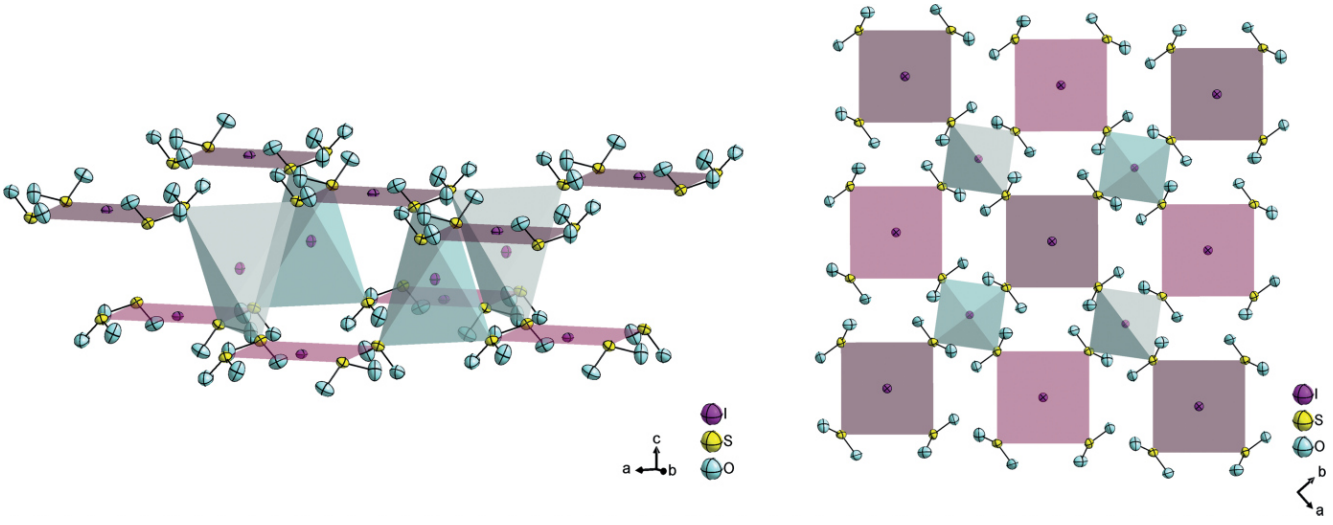

Figure 10. The building blocks of the $[I(SO_2)_2]_n^{n-}$ network of compound **9**. The distorted $[I(SO_2)_4]^-$ tetrahedra and corner-sharing $[I(SO_2)_4]^-$ squares approximately along [b] (left) and along [c] (right) forming a two-dimensional network along [a] and [b].

© 2020 The Authors. Published by Wiley-VCH Verlag GmbH & Co. KGaA, Weinheim

Full Paper
doi.org/10.1002/ejic.202000299

proceeds along [b] and [c]. This is another nice example of chalcogen bonds strong enough to determine the crystal packing and most likely also morphology as the two-dimensionality is in line with the formation of platelets. Crystal engineering around multiple chalcogen bonds has been established and the possibility of crystal engineering with small molecules such as SO_2 is indicated. Furthermore, **11** does also contain the SO_2I^- anion. In how far small molecules like SO_2 can be a supramolecular synthon should be debate for future research.

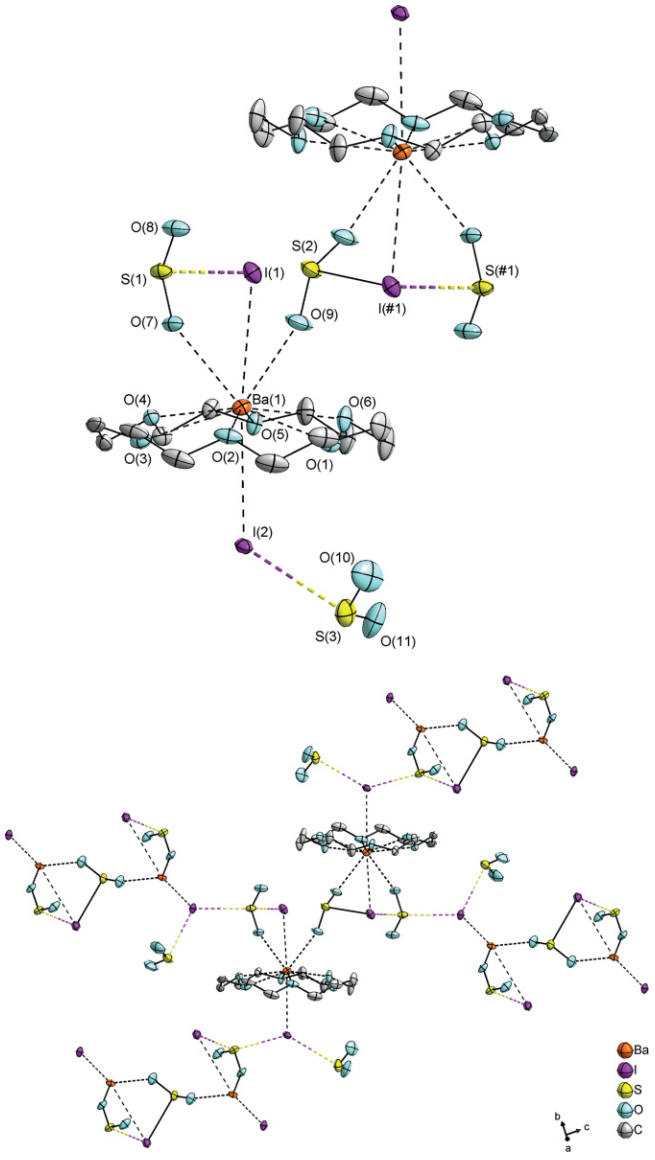

Figure 11. The structure of **11** in the crystal (top) as well as including the adjacent SO_2 adducts approximately along [a]. Adjacent crown-ethers (bottom) are omitted for clarity. Further, the disordered part of the structure is omitted in both representations. Thermal displacement ellipsoids represent the 50 % probability level. Non-labelled atoms and atoms depicted with # (top) are symmetry generated over 2 – *x*, 1 – *y*, 1 – *z*. Selected bond lengths [pm]: I(1)–S(1) 310.9(1), I(#1)–S(2) 298.4(1), I(2)–S(3) 328.4(1), I(1)–Ba(1) 389.8(1), I(2)–Ba(1) 349.5(1), O(1)–Ba(1) 281.9(1), O(2)–Ba(1) 283.9(1), O(3)–Ba(1) 283.1(1), O(4)–Ba(1) 283.1(1), O(5)–Ba(1) 276.5(1), O(6)–Ba(1) 283.1(1). Selected bond angles [°]: I(1)–Ba(1)–I(2) 144.7(1), I(2)–Ba(1)–O(7) 140.9(1), I(2)–Ba(1)–O(9) 141.0(1), O(7)–S(1)–O(8) 114.1(1).

Brief Comparison with Related Compounds

The architectures of the herein characterized compounds are zig-zag typed in one-dimensional networks, tetragonal planar and distorted tetrahedral in two-dimensional networks or simple adduct of SO_2 and I^- as shown in the revisited iodosulfite ion ISO_2^- and non-planar $[I_2(SO_2)_5]^{2-}$. As the presented SO_2-chemistry is mainly characterized as an interaction of a nucleophile with an electrophile, this chemistry is highly related to the recent research of polyhalides or polypseudohalides in general.[49,50] So do the one-dimensional chains compare well with zig-zag shaped $[X_8]^{2-}$ (X = Cl, Br, I)[51–53] or $[I(Br_4)]^-$[54] anions, tetragonal shaped architectures compare well with the $[Cl(I_2)_4]^-$[55] or $[I_5Br_2]^-$[56] anion and iodosulfite $[ISO_2]^-$ is most likely analogous to the simple trihalides $[X_3]^-$ (X = Cl, Br, I)[52,57,58] and also mixed (pseudo-)halides such as $[Br(BrCN)]^-$ (arbitrarily chosen).[59] The non-planar aggregate $[I_2(SO_2)_5]^{2-}$ is highly related to for example $[Cl_{12}]^{2-}$ which represents a non-planar building-block of a three-dimensional network in $[NMe_3Ph]_2[Cl_{12}]$.[60]

These are just a few parallels but they demonstrate that the structural motifs which are obtained in a lewis acid-base chemistry including halides and SO_2 has the potential to form various species in the form of $[X_m(SO_2)_n]^{m-}$ as it is well-known for polyhalides or poly-pseudohalides such as $[X_m(X_2)_n]^{m-}$, $[X_m(Y_2)_n]^{m-}$, $[X_m(XY)_n]^{m-}$ and $[X_m(YZ)_n]^{m-}$ (X, Y, Z = halogen).[50]

Conclusion

The presented paper discussed the chalcogen bonding of I^- towards SO_2 on a structural level. We have shown that employing large organo-cations such as s-block metal complexes of crown-ethers form sufficient stable compounds, which could be crystallized and prepared at room temperature. Thereby, even alkaline earth metal complexes could be obtained, in which we could observe very rare SO_2 coordination to an alkaline earth metal cation. The iodide anions in the respective compounds (see Scheme 2 for alkali metal (top) and alkaline earth metal (bottom) compounds) adapt solvation numbers of one to four.

The chalcogen bonding around the iodide anions, however, is substantially different and a structural diversity far beyond a simple adduct formation was discovered. SO_2 takes place in the formation of one- (**1**, **2**, **4–7**) and two-dimensional networks (**9** and **11**) as well as in the SO_2-rich aggregate $[I_2(SO_2)_5]^{2-}$ (as in **3a**). This lets us conclude that the observed $O_2S\cdots I^-$ interactions are strong enough to determine the crystal packing and dimensionality and might be a useful tool for the formation of molecular frameworks with SO_2 spacers. The relationship to the chemistry of polyhalides and polypseudohalides was pointed out. Redox-chemistry plays a major role and it was demonstrated that these compounds are redox-sensitive in concentrated solutions. Especially alkaline earth metal derivatives have been observed to be sensitive. Further, the iodosulfite anion has been revisited. The compounds **3, 8** and **11** contain this anion and it was shown that the atom distances can be considerably shorter than those observed in past works.

© 2020 The Authors. Published by Wiley-VCH Verlag GmbH & Co. KGaA, Weinheim

Full Paper
doi.org/10.1002/ejic.202000299

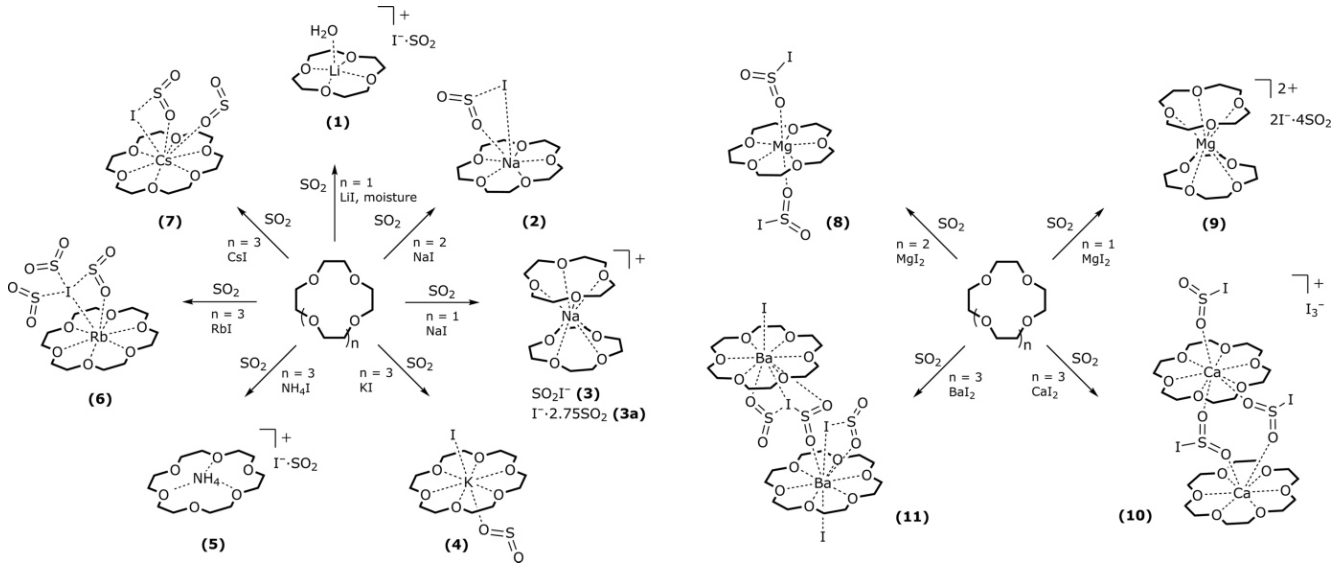

Scheme 2. The SO_2 containing compounds presented herein. Alkali-metal complexes (left) and alkaline earth metal complexes (right). To see the polymeric aspects of these compounds, please see Figure 1–Figure 10, S1 and S2.

Experimental Section

General: All manipulations were carried out with rigorous exclusion of oxygen and moisture using basic Schlenk techniques under SO_2 (Air Liquide, 99.999 %) or argon gas if not stated otherwise. For chemical reaction, glass vessels equipped with fine thread glass spindles were used. $SO_{2(l)}$ has been dried with P_2O_5 before it was condensed in the respective reaction vessel. The salts LiI (Alfa Aesar, 99.996 %), NaI (acros organics, ≥99 %), KI (sigma aldrich, ≥99.99 %), RbI (99.8 %, Alfa Aesar), CsI (99.9 % Alfa Aesar), MgI_2 (Alfa Aesar, 99.996 %), CaI_2, SrI_2 (both Alfa Aesar, 99 %), BaI_2 (abcr, 99.995 %) and NH_4I (acros organics, ≥99 %) were used as received. All salts were handled under argon atmosphere using a glovebox of MBraun-type. NMR spectra were recorded on the Bruker Spectrometer device AV III HD 300 MHz or AV III HD 500 MHz at 300K using TMS as an external standard. For the respective measurement, *J. Young* NMR tubes with PTFE valve were used. The tube was charged with 20 mg of the respective sample and a TMS capillary. 1 mL of SO_2 were subsequently condensed into the tube. Infrared (IR) spectra of the respective samples were measured using attenuated total reflectance (ATR) mode on the Bruker-type spectrometer Alpha FT-IR. The OPUS-Software package was applied throughout.[61] All compounds are sensitive towards moisture and solvolysis. The compounds release SO_2 as soon as the glass-vessel is opened and the SO_2 atmosphere is released. Thus, compounds being stored in the aforementioned glovebox are not long-time stable. For crystallographic details, see SI.

Reactions to Obtain Single Crystals and Spectroscopic Data

[Li([12]crown-4)(H_2O)]I·SO_2 (1): 0.020 g of LiI (0.149 mmol, 1.00 equiv.) together with 0.026 g of [12]crown-4 (0.149 mmol, 1.00 equiv.) are placed in a high-pressure *J. Young* Schlenk flask with a fine thread glass spindle and stir bar. Under stirring, 5 mL of SO_2 were condensed into the flask. As soon as a pale yellow solution is obtained, the reaction is stopped and the SO_2 is evaporated from the flask under Ar flush at ambient temperature. As soon as an orange, sticky oil is obtained, the crop compound is exposed to moisture for one minute. **1** is obtained as yellow-orange platelets within minutes at room temperature.

Note: It is important that the sample does only interact with traces of moisture and is kept under Ar again, otherwise redox-chemistry prevails and **1** decomposes readily to [Li([12]crown-4)]I_n^-, γ-S_8 and further unidentified side products. We cannot afford quantitative H_2O incorporation but we have in principle detected H_2O also by means of NMR and IR spectroscopy. After preparing a fresh sample and letting the solvent evaporate under moisture, we immediately prepared and characterized the sample. NMR chemical shift of H_2O is found at 3.37 ppm as a broad singlet. No quantitative H_2O incorporation could be observed. Estimating the integrals in the ^{1}H NMR spectrum, every tenth crown ether complex bears one H_2O molecule. IR spectroscopy of the obtained, greasy colourless platelets revealed small broad vibrations at 3441 as well as 3342 cm^{-1} which can tentatively assigned to two different symmetric stretching vibrations $\tilde{\nu}_s$ (O-H) which is in accordance with the solid-state structure. Further, characteristic vibrations are found in the IR spectrum: $\tilde{\nu}$ = 1358 (w, $\tilde{\nu}_{as}$: S–O), 1132 (s, $\tilde{\nu}_s$: S–O) and 527 (w, δ: SO_2). Thus, the greasy and sticky crop of the compound should be interpreted as $[LiI_{0.9}(H_2O)_{0.1}([12]crown-4)]I_{0.1}{\cdot}nSO_2$.

^{1}H NMR: (500 MHz, SO_2): δ [ppm] = 3.37 (br, s, 0.2H, H_2O)*, 4.43 (s, 16H, CH_2). $^{13}C\{^1H\}$ NMR: (126 MHz, SO_2): δ [ppm] = 68.3 (s, CH_2). ^{7}Li NMR: (117 MHz, SO_2): δ [ppm] = 0.74 (s). *The incorporation of H_2O is not quantitative. IR: $\tilde{\nu}$[cm^{-1}] = 3441 (w), 3342 (w), 2962 (w), 2918 (w), 2871 (w), 1476 (w), 1443 (w), 1358 (w, $\tilde{\nu}_{as}$: S–O), 1277 (w), 1244 (m), 1132 (s, $\tilde{\nu}_s$: S–O), 1079 (s), 1015 (s), 923 (s), 855 (s), 557 (m), 527 (w, δ: SO_2).

[Na([15]crown-5)(SO_2)I] (2): 0.080 g of NaI (0.53 mmol, 1.00 equiv.) together with 0.117 g [15]crown-5 (0.53 mmol, 1.00 equiv.) are placed in a high-pressure *J-Young* Schlenk flask with a fine thread glass spindle and stir bar. Under stirring, 5 mL of SO_2 were condensed into the flask. As soon as a pale yellow solution is obtained, the reaction is stopped and the SO_2 is evaporated from the flask under Ar flush at ambient temperature. As soon as a red-orange oil is obtained, red-orange platelets are obtained within a few hours at ambient temperature. ^{1}H NMR: (300 MHz, SO_2): δ [ppm] = 3.96

© 2020 The Authors. Published by Wiley-VCH Verlag GmbH & Co. KGaA, Weinheim

(s, 20H, CH_2). $^{13}C\{^1H\}$ NMR: (126 MHz, SO_2): δ [ppm] = 69.5 (s, *C*H_2). IR: $\tilde{\nu}$[cm^{-1}] = 2917 (w), 2873 (w), 1117 (vw), 1476 (w), 1456 (w), 1351 (m, $\tilde{\nu}_{as}$: S–O), 1281 (m), 1253 (m), 1085 (vs, $\tilde{\nu}_s$: S–O), 1048 (s), 1035 (s), 944 (s), 861 (w), 827 (m), 527 (m, δ: SO_2).

[Na([12]crown-4)$_2$]SO$_2$I (3) & [Na([12]crown-4)$_2$]I·2.75SO$_2$ (3a): 0.017 g of NaI (0.114 mmol, 1.00 equiv.) together with 0.040 g [12]crown-4 (0.228 mmol, 2.00 equiv.) are placed in a high-pressure *J. Young* Schlenk flask with a fine thread glass spindle and stir bar. Under stirring, 5 mL of SO_2 were condensed into the flask. As soon as a pale yellow solution is obtained, the reaction is stopped and the SO_2 is evaporated from the flask under Ar flush at ambient temperature to a total volume of approximately 0.2 mL. Yellow platelets of **3** and **3a** are obtained within minutes at ambient temperature. ^1H NMR: (500 MHz, SO_2): δ [ppm] = 4.31 (s, 32H, *C*H_2). $^{13}C\{^1H\}$ NMR: (126 MHz, SO_2): δ [ppm] = 66.5 (s, *C*H_2). IR: $\tilde{\nu}$ = [cm^{-1}] = 2957 (w), 2906 (w), 2867 (w), 1486 (w), 1471 (w), 1443 (w), 1401 (w), 1364 (w, $\tilde{\nu}_{as}$: S–O), 1290 (w), 1242 (m), 1133 (s, $\tilde{\nu}_s$: S–O), 1087 (s), 1019 (s), 913 (s), 847 (s), 554 (m), 520 (w, δ: SO_2).

[K([18]crown-6)(SO$_2$)I] (4): 0.015 g of KI (0.09 mmol, 1.00 equiv.) together with 0.024 g [18]crown-6 (0.09 mmol, 1.00 equiv.) are placed in a high-pressure *J. Young* Schlenk flask with a fine thread glass spindle and stir bar. Under stirring, 5 mL of SO_2 were condensed into the flask. As soon as a pale yellow solution is obtained, the reaction is stopped and the SO_2 is evaporated from the flask under Ar flush at ambient temperature to a total volume of approximately 0.5 mL. Yellow platelets of **4** are obtained within minutes at ambient temperature. ^1H NMR: (500 MHz, SO_2): δ [ppm] = 4.28 (s, 24H, *C*H_2). $^{13}C\{^1H\}$ NMR: (126 MHz, SO_2): δ [ppm] = 71.0 (s, *C*H_2). IR: $\tilde{\nu}$ [cm^{-1}] = 2898 (w), 2860 (w), 2824 (vw), 1471 (w), 1453 (w), 1348 (m, $\tilde{\nu}_{as}$: S–O), 1278 (m), 1245 (w), 1132 (w), 1096 (s, $\tilde{\nu}_s$: S–O), 960 (s), 836 (m), 524 (m, δ: SO_2).

[NH$_4$([18]crown-6)]I·SO$_2$ (5): 0.015 g of NH_4I (0.103 mmol, 1.00 equiv.) together with 0.027 g [18]crown-6 (0.103 mmol, 1.00 equiv.) are placed in a high-pressure *J. Young* Schlenk flask with a fine thread glass spindle and stir bar. Under stirring, 5 mL of SO_2 were condensed into the flask. As soon as a pale yellow solution is obtained, the reaction is stopped and the SO_2 is evaporated from the flask under Ar flush at ambient temperature to a total volume of approximately 0.5 mL. Yellow platelets of **5** are obtained within minutes at ambient temperature. ^1H NMR: (500 MHz, SO_2): δ [ppm] = 4.32 (s, 24H, *C*H_2), 7.19 (t, $^1J_{NH}$ = 53 Hz, NH_4). $^{13}C\{^1H\}$ NMR: (126 MHz, SO_2): δ [ppm] = 71.0 (s, *C*H_2). IR: $\tilde{\nu}$ [cm^{-1}] = 3131 (w), 3070 (w), 3034 (w), 2899 (w), 2825 (w), 1455 (m), 1427 (m), 1349 (m, $\tilde{\nu}_{as}$: S–O), 1294 (m), 1249 (m), 1128 (m), 1093 (s, $\tilde{\nu}_s$: S–O), 955 (s), 867 (w), 831 (m), 598 (w), 573 (w), 527 (m, δ: SO_2).

[Rb([18]crown-6)(SO$_2$)I]·2SO$_2$ (6): 0.030 g of RbI (0.141 mmol, 1.00 equiv.) together with 0.037 g [18]crown-6 (0.141 mmol, 1.00 equiv.) are placed in a high-pressure *J. Young* Schlenk flask with a fine thread glass spindle and stir bar. Under stirring, 5 mL of SO_2 were condensed into the flask. As soon as a pale yellow solution is obtained, the reaction is stopped and the SO_2 is evaporated from the flask under Ar flush at ambient temperature to a total volume of approximately 0.5 mL. Yellow platelets of **6** are obtained after three days at ambient temperature. ^1H NMR: (500 MHz, SO_2): δ [ppm] = 4.28 (s, 24H, *C*H_2). $^{13}C\{^1H\}$ NMR: (126 MHz, SO_2): δ [ppm] = 70.9 (s, *C*H_2). IR: $\tilde{\nu}$ = [cm^{-1}] = 2897 (w), 2863 (w), 2823 (w), 1471 (w), 1454 (w), 1349 (w, $\tilde{\nu}_{as}$: S–O), 1284 (w), 1248 (w), 1100 (s, $\tilde{\nu}_s$: S–O), 961 (m), 837 (m), 530 (m, δ: SO_2).

[Cs([18]crown-6)(SO$_2$)$_2$I] (7): 0.030 g of CsI (0.115 mmol, 1.00 equiv.) together with 0.031 g [18]crown-6 (0.115 mmol, 1.00 equiv.) are placed in a high-pressure *J. Young* Schlenk flask with a fine thread glass spindle and stir bar. Under stirring, 5 mL of SO_2 were condensed into the flask. As soon as a pale yellow solution is obtained, the reaction is stopped and the SO_2 is evaporated from the flask under Ar flush at ambient temperature to a total volume of approximately 0.5 mL. Yellow platelets of **7** are obtained after a few hours at ambient temperature. ^1H NMR: (500 MHz, SO_2): δ [ppm] = 4.28 (s, 24H, *C*H_2). $^{13}C\{^1H\}$ NMR: (126 MHz, SO_2): δ [ppm] = 70.7 (s, *C*H_2). IR: $\tilde{\nu}$ = [cm^{-1}] = 2882 (m), 2824 (w), 2744 (w), 1478 (w), 1464 (w), 1451 (w), 1350 (m, $\tilde{\nu}_{as}$: S–O), 1277 (m), 1250 (m), 1135 (w), 1099 (s, $\tilde{\nu}_s$: S–O), 956 (s), 859 (w), 836 (s), 775 (w), 597 (w), 574 (w), 528 (m, δ: SO_2), 447 (w), 429 (w), 412 (w).

[Mg([15]crown-5)(SO$_2$I)$_2$] (8): 0.105 g of MgI_2 (0.378 mmol, 1.00 equiv.) together with 0.085 g [15]crown-5 (0.378 mmol, 1.00 equiv.) are placed in a high-pressure *J. Young* Schlenk flask with a fine thread glass spindle and stir bar. Under stirring, 5 mL of SO_2 were condensed into the flask. The suspension is stirred overnight to give a red-orange solution. The SO_2 is then evaporated from the flask under Ar flush at ambient temperature to a total volume of approximately 0.5 mL. red-orange blocks of **8** are obtained after a few hours at ambient temperature. ^1H NMR: (300 MHz, SO_2): δ [ppm] = 4.68 (s, 20H, CH_2). $^{13}C\{^1H\}$ NMR: (126 MHz, SO_2): δ [ppm] = 69.1 (s, *C*H_2). IR: $\tilde{\nu}$ = [cm^{-1}] = 2940 (w), 2882 (w), 1615 (w), 1465 (w), 1350 (w, $\tilde{\nu}_{as}$: S–O), 1247 (w), 1165 (m, $\tilde{\nu}_s$: S–O), 1084 (s), 1060 (s), 1040 (s), 966 (s), 839 (w), 651 (w), 640 (w), 569 (w), 545 (w), 524 (w, δ: SO_2), 461 (w), 424 (w).

[Mg([12]crown-4)$_2$]I$_2$·4SO$_2$ (9): 0.030 g of MgI_2 (0.108 mmol, 1.00 equiv.) together with 0.038 g [12]crown-4 (0.216 mmol, 2.00 equiv.) are placed in a high-pressure *J. Young* Schlenk flask with a fine thread glass spindle and stir bar. Under stirring, 5 mL of SO_2 were condensed into the flask. The suspension is stirred overnight to give a red-orange solution. The SO_2 is then evaporated from the flask under Ar flush at ambient temperature to a total volume of approximately 0.5 mL. Yellow platelets of **9** are obtained after a few hours at ambient temperature. ^1H NMR: (300 MHz, SO_2): δ [ppm] = 4.61–4.68 (m, 16H, CH_2), 4.72–4.80 (m, 16H, CH_2). $^{13}C\{^1H\}$ NMR: (126 MHz, SO_2): δ [ppm] = 67.3 (s, *C*H_2). IR: $\tilde{\nu}$ = [cm^{-1}] = 2977 (w), 2944 (w), 2883 (w), 1620 (w), 1448 (w), 1410 (w), 1362 (w), 1349 (w), 1280 (m, $\tilde{\nu}_{as}$: S–O), 1241 (m), 1128 (m), 1070 (s, $\tilde{\nu}_s$: S–O), 1016 (s), 935 (s), 863 (s), 656 (w), 611 (w), 565 (m), 527 (m, δ: SO_2), 505 (w).

[Ca$_2$([18]crown-6)$_2$(SO$_2$I)$_3$]I$_3$ (10): 0.020 g of CaI_2 (0.068 mmol, 1.00 equiv.) together with 0.018 g [18]crown-6 (0.068 mmol, 1.00 equiv.) are placed in a high-pressure *J. Young* Schlenk flask with a fine thread glass spindle and stir bar. Under stirring, 5 mL of SO_2 were condensed into the flask. The suspension is stirred for 30 min. to give a yellow solution. The SO_2 is then evaporated from the flask under Ar flush at ambient temperature to a total volume of approximately 0.5 mL. A few red-brown needles of **10** are obtained after three days at ambient temperature.

[Ba$_2$([18]crown-6)$_2$(SO$_2$I)(SO$_2$)$_2$I$_4$]·SO$_2$ (11): 0.040 g of BaI_2 (0.102 mmol, 1.00 equiv.) together with 0.027 g [18]crown-6 (0.102 mmol, 1.00 equiv.) are placed in a high-pressure *J. Young* Schlenk flask with a fine thread glass spindle and stir bar. Under stirring, 5 mL of SO_2 were condensed into the flask. The obtained solution is stirred overnight and the SO_2 is evaporated from the flask under Ar flush at ambient temperature to a total volume of approximately 0.5 mL. Yellow-orange platelets of **11** are obtained after one day at ambient temperature.

^1H NMR: (500 MHz, SO_2): δ [ppm] = 4.54 (s, 24H, *C*H_2). $^{13}C\{^1H\}$ NMR: (126 MHz, SO_2): δ [ppm] = 71.5 (s, *C*H_2). IR: $\tilde{\nu}$ = [cm^{-1}] = 2923 (m), 2875 (w), 2819 (vw), 1469 (m), 1348 (m), 1282 (m), 1244 (m, $\tilde{\nu}_{as}$: S–O), 1075 (vs, $\tilde{\nu}_s$: S–O), 958 (s), 826 (s), 530 (m, δ: SO_2).

© 2020 The Authors. Published by Wiley-VCH Verlag GmbH & Co. KGaA, Weinheim

Crystallography: Single crystal X-ray diffraction experiments were carried out on a Bruker D8 Quest diffractometer at 100(2) K with MoK_α radiation and respective X-ray optics (λ = 0.71073). All structures were solved by direct methods and refinement with full-matrix-least-squares against F^2 using SHELXT- and SHELXL-2015 on *OLEX2* platform.[62–64] The respective crystal data and selected experimental parameters of the structure determinations are summarized in the Tables S1-S4 (see ESI). Visualization of all structures was performed with the Diamond software package Version 4.4.0. All Ellipsoid plots represent the 50 % probability level. "*Checkcif*" of the international union of crystallography (IUCR) of the respective .cif files show plenty of A, B and C alerts regarding short S···I atom distances ("PLAT431_ALERT_2_A", "PLAT431_ALERT_2_B" or also "PLAT431_ALERT_2_C"). We want to emphasize that this was the purpose of our study and should be considered negligible.

Deposition Numbers 1992742 (**1**), 1992744 (**2**), 1992745 (**3**), 1992743 (**3a**), 1992749 (**4**), 1992753 (**5**), 1992746 (**6**), 1992748 (**7**), 1992752 (**8**), 1992747 (**9**), 1992750 (**10**), 1992751 (**11**). Crystallographic information files (CIF) can be obtained free of charge from the Cambridge Crystallographic Data Centre (CCDC) (link: www.ccdc.cam.ac.uk/data_request/cif). The respective crystal data and selected experimental parameters of the structure determinations are summarized in the Tables S1-S4 (see ESI). Visualization of all structures was performed with the Diamond software package Version 4.4.0. All Ellipsoid plots represent the 50 % probability level. "*Checkcif*" of the international union of crystallography (IUCR) of the respective .cif files show plenty of A, B and C alerts regarding short S···I atom distances ("PLAT431_ALERT_2_A", "PLAT431_ALERT_2_B" or also "PLAT431_ALERT_2_C") contain the supplementary crystallographic data for this paper. These data are provided free of charge by the joint Cambridge Crystallographic Data Centre and Fachinformationszentrum Karlsruhe Access Structures service www.ccdc.cam.ac.uk/structures.

Acknowledgments

R.-M. Richter is gratefully acknowledged for assistance in the laboratory and characterization of **2**. F. D. thanks the NMR (C. Mischke and Dr. X. Xie) and X-ray departments (Dr. S. Ivlev, M. Marsch and R. Riedel). C. Ritter is acknowledged for his help with X-ray crystallographic data refinement. This work was financially supported by the DFG. Open access funding enabled and organized by Projekt DEAL.

Keywords: Sulfur dioxide · Chalcogen bonds · Solvent effects · Crown ethers · Structure chemistry · Alkali metals · Alkaline earth metals

[1] H. Spandau, V. Gutmann, *Angew. Chem.* **1952**, *64*, 93–102.
[2] R. Mews, E. Lork, P. G. Watson, B. Görtler, *Coord. Chem. Rev.* **2000**, *197*, 277–320.
[3] A. Martens, P. Weis, M. C. Krummer, M. Kreuzer, A. Meierhöfer, S. C. Meier, J. Bohnenberger, H. Scherer, I. Riddlestone, I. Krossing, *Chem. Sci.* **2018**, *9*, 7058–7068.
[4] A. Decken, C. Knapp, G. B. Nikiforov, J. Passmore, J. M. Rautiainen, X. Wang, X. Zeng, *Chem. Eur. J.* **2009**, *15*, 6504–6517.
[5] T. S. Cameron, G. B. Nikiforov, J. Passmore, J. M. Rautiainen, *Dalton Trans.* **2010**, *39*, 2587.
[6] I. M. Riddlestone, A. Kraft, J. Schaefer, I. Krossing, *Angew. Chem. Int. Ed.* **2018**, *57*, 13982; *Angew. Chem.* **2018**, *130*, 14178–14221.
[7] D. Zheng, J. Wu, *Sulfur Dioxide Insertion Reactions*. In: *Sulfur Dioxide Insertion Reactions for Organic Synthesis*, SpringerBriefs in Molecular Science, Springer, Singapore. **2007**. See DOI: https://doi.org/10.1007/978-981-10-4202-7_3.
[8] J. Ross, J. H. Percy, R. L. Brandt, A. I. Gebhart, J. E. Mitchell, S. Yolles, *Ind. Eng. Chem.* **1942**, *34*, 924–926.
[9] P. Vogel, M. Turks, L. Bouchez, D. Marković, A. Varela-Álvarez, J. Á. Sordo, *Acc. Chem. Res.* **2007**, *40*, 931–942.
[10] G. Jander, *Die Chemie in verflüssigtem Schwefeldioxyd* In: *Die Chemie in Wasserähnlichen Lösungsmitteln. Anorganische und Allgemeine Chemie in Einzeldarstellungen*, vol 1. Springer, Berlin, Heidelberg. **1949**. See DOI: https://doi.org/10.1007/978-3-662-21788-7_8.
[11] K. Reuter, S. S. Rudel, M. R. Buchner, F. Kraus, C. von Hänisch, *Chem. Eur. J.* **2017**, *23*, 9607–9617.
[12] A. Simon, K. Peters, E.-M. Peters, H. Kühnl, B. Koslowski, *Z. Anorg. Allg. Chem.* **1980**, *469*, 94–100.
[13] J. Derendorf, M. Keßler, C. Knapp, M. Rühle, C. Schulz, *Dalton Trans.* **2010**, *39*, 8671.
[14] K. Peters, A. Simon, E.-M. Peters, H. Kühnl, B. Koslowski, *Z. Anorg. Allg. Chem.* **1982**, *492*, 7–14.
[15] M. Malischewski, D. V. Peryshkov, E. V. Bukovsky, K. Seppelt, S. H. Strauss, *Inorg. Chem.* **2016**, *55*, 12254–12262.
[16] C. Jenne, V. Van Lessen, *Acta Crystallogr., Sect. E* **2019**, *75*, 607–610.
[17] R. Hoppenheit, W. Isenberg, R. Mews, *Z. Naturforsch. B* **1982**, *37*, 1116–1121.
[18] U. Kessler, L. Van Wüllen, M. Jansen, *Inorg. Chem.* **2001**, *40*, 7040–7046.
[19] U. Keßler, M. Jansen, *Z. Anorg. Allg. Chem.* **1999**, *625*, 385–388.
[20] E. Lork, R. Mews, D. Viets, P. G. Watson, T. Borrmann, A. Vij, J. A. Boatz, K. O. Christe, *Inorg. Chem.* **2001**, *40*, 1303–1311.
[21] N. Kuhn, H. Bohnen, D. Bläser, R. Boese, A. H. Maulitz, *J. Chem. Soc. Chem. Commun.* **1994**, *53*, 2283–2284.
[22] A. Kumar, G. S. McGrady, J. Passmore, F. Grein, A. Decken, *Z. Anorg. Allg. Chem.* **2012**, *638*, 744–753.
[23] A. Kornath, O. Blecher, *Z. Anorg. Allg. Chem.* **2002**, *628*, 570–574.
[24] P. G. Eller, G. J. Kubas, *Inorg. Chem.* **1978**, *17*, 894–897.
[25] M. R. Snow, J. A. Ibers, *Inorg. Chem.* **1973**, *12*, 224–229.
[26] I. Nagasawa, H. Amita, H. Kitagawa, *Chem. Commun.* **2009**, 204–205.
[27] P. Rajakaruna, J. D. Gorden, D. M. Stanbury, *Inorg. Chem.* **2019**, *58*, 14752–14759.
[28] P. Scilabra, G. Terraneo, G. Resnati, *Acc. Chem. Res.* **2019**, *52*, 1313–1324.
[29] A. Bauzá, D. Quiñonero, P. M. Deyà, A. Frontera, *CrystEngComm* **2013**, *15*, 3137–3144.
[30] K. T. Mahmudov, M. N. Kopylovich, M. F. C. Guedes da Silva, A. J. L. Pombeiro, *Dalton Trans.* **2017**, *46*, 10121–10138.
[31] G. Cavallo, P. Metrangolo, T. Pilati, G. Resnati, G. Terraneo, *Cryst. Growth Des.* **2014**, *14*, 2697–2702.
[32] V. Oliveira, D. Cremer, E. Kraka, *J. Phys. Chem. A* **2017**, *121*, 6845–6862.
[33] S. Benz, J. López-Andarias, J. Mareda, N. Sakai, S. Matile, *Angew. Chem. Int. Ed.* **2017**, *56*, 812–815.
[34] P. Wonner, A. Dreger, L. Vogel, E. Engelage, S. M. Huber, *Angew. Chem. Int. Ed.* **2019**, *58*, 16923–16927.
[35] G. E. Garrett, E. I. Carrera, D. S. Seferos, M. S. Taylor, *Chem. Commun.* **2016**, *52*, 9881–9884.
[36] S. Scheiner, *Chem. Eur. J.* **2016**, *22*, 18850–18858.
[37] S. Benz, M. Macchione, Q. Verolet, J. Mareda, N. Sakai, S. Matile, *J. Am. Chem. Soc.* **2016**, *138*, 9093–9096.
[38] R. J. Fick, G. M. Kroner, B. Nepal, R. Magnani, S. Horowitz, R. L. Houtz, S. Scheiner, R. C. Trievel, *ACS Chem. Biol.* **2016**, *11*, 748–754.
[39] S. P. Thomas, D. Jayatilaka, T. N. Guru Row, *Phys. Chem. Chem. Phys.* **2015**, *17*, 25411–25420.
[40] B. R. Beno, K. S. Yeung, M. D. Bartberger, L. D. Pennington, N. A. Meanwell, *J. Med. Chem.* **2015**, *58*, 4383–4438.
[41] P. G. Eller, G. J. Kubas, R. R. Ryan, *Inorg. Chem.* **1977**, *16*, 2454–2462.
[42] M. Mantina, A. C. Chamberlin, R. Valero, C. J. Cramer, D. G. Truhlar, *J. Phys. Chem. A* **2009**, *113*, 5806–5812.
[43] R. D. Shannon, *Acta Crystallogr., Sect. A* **1976**, *32*, 751–767.
[44] S. A. Snyder, D. S. Treitler, A. P. Brucks, *J. Am. Chem. Soc.* **2010**, *132*, 14303–14314.
[45] T. Chivers, M. N. S. Rao, J. F. Richardson, *J. Chem. Soc. Chem. Commun.* **1983**, *23*, 700–702.
[46] A. W. Cordes, S. L. Craig, M. S. Condren, R. T. Oakley, R. W. Reed, *Acta Crystallogr., Sect. C* **1986**, *42*, 922–923.

© 2020 The Authors. Published by Wiley-VCH Verlag GmbH & Co. KGaA, Weinheim

[47] G. S. Calabrese, M. S. Wrighton, *J. Am. Chem. Soc.* **1981**, *103*, 6273–6280.
[48] B. Post, R. S. Schwartz, I. Fankuchen, *Acta Crystallogr.* **1952**, *5*, 372–374.
[49] H. Haller, S. Riedel, *Z. Anorg. Allg. Chem.* **2014**, *640*, 1281–1291.
[50] K. Sonnenberg, L. Mann, F. A. Redeker, B. Schmidt, S. Riedel, *Angew. Chem. Int. Ed.* **2020**, *59*, 5464–5493; *Angew. Chem.* **2020**, *132*, 5506–5535.
[51] R. Brückner, P. Pröhm, A. Wiesner, S. Steinhauer, C. Müller, S. Riedel, *Angew. Chem. Int. Ed.* **2016**, *55*, 10904–10908.
[52] K. Sonnenberg, P. Pröhm, S. Steinhauer, A. Wiesner, C. Müller, S. Riedel, *Z. Anorg. Allg. Chem.* **2017**, *643*, 101–105.
[53] A. Gräfe-Kavoosian, S. Nafepour, K. Nagel, K. Tebbe, *Z. Naturforsch. B* **1998**, *53*, 641–652.
[54] R. Babu, G. Bhargavi, M. V. Rajasekharan, *Eur. J. Inorg. Chem.* **2015**, *2015*, 4689–4698.
[55] C. Walbaum, M. Richter, U. Sachs, I. Pantenburg, S. Riedel, A.-V. Mudring, G. Meyer, *Angew. Chem. Int. Ed.* **2013**, *52*, 12732–12735.
[56] A. Parlow, H. Hartl, *Z. Naturforsch. B* **1985**, *40*, 45–52.
[57] M. P. Bogaard, J. Peterson, A. D. Rae, *Acta Crystallogr., Sect. B* **1981**, *37*, 1357–1359.
[58] R. C. L. M. Slater, *Acta Crystallogr.* **1959**, *12*, 187–196.
[59] B. Schmidt, B. Schröder, K. Sonnenberg, S. Steinhauer, S. Riedel, *Angew. Chem. Int. Ed.* **2019**, *58*, 10340–10344; *Angew. Chem.* **2019**, *131*, 10448–10452.
[60] K. Sonnenberg, P. Pröhm, N. Schwarze, C. Müller, H. Beckers, S. Riedel, *Angew. Chem. Int. Ed.* **2018**, *57*, 9136–9140.
[61] *OPUS*; Version 7.2; Bruker Opt. GmbH: Ettlingen, Germany, **2012**.
[62] G. M. Sheldrick, *Acta Crystallogr., Sect. C* **2015**, *71*, 3–8.
[63] G. M. Sheldrick, *Acta Crystallogr., Sect. A* **2015**, *71*, 3–8.
[64] O. V. Dolomanov, L. J. Bourhis, R. J. Gildea, J. A. K. Howard, H. Puschmann, *J. Appl. Crystallogr.* **2009**, *42*, 339–341.

Received: March 30, 2020

© 2020 The Authors. Published by Wiley-VCH Verlag GmbH & Co. KGaA, Weinheim

EurJIC
European Journal of Inorganic Chemistry

Supporting Information

Chalcogen Bonding of SO_2 and s-Block Metal Iodides Near Room Temperature: A Remarkable Structural Diversity

Fabian Dankert, Anne Feyh, and Carsten von Hänisch*

Content

1. Single crystal X-Ray diffraction analysis S2

1.2 Crystallographic Data S2

1.3 Representation of additional X-ray structures S6

1.3.1 $[NH_4([18]crown\text{-}6)]I{\cdot}SO_2$ (**5**) S6

1.3.2 $[Ca_2([18]crown\text{-}6)_2(SO_2I)_3]I_3$ (**10**) S7

2. Comment on redox-chemistry S8

3. References S11

1. Single crystal X-Ray diffraction analysis

1.1 Crystallographic Data

Table S1. Selected crystal structure data of the structure determinations of compounds **1-3**

Compound	**1**	**2**	**3**
Empirical formula	$C_8H_{18}ILiO_7S$	$C_{10}H_{20}INaO_7S$	$C_{16}H_{32}INaO_{10}S$
Formula weight	392.12	434.21	566.36
Crystal colour, habit	orange, platelet	orange, platelet	yellow, platelets
Temperature/K	100(2)	100(2)	100(2)
Crystal system	monoclinic	monoclinic	triclinic
Space group	$P2_1/n$	$P2_1/c$	P-1
a/Å	11.1114(18)	8.523(8)	10.0800(8)
b/Å	11.6558(19)	16.694(9)	10.9215(8)
c/Å	11.5933(19)	11.942(9)	10.9989(9)
α/°	90	90	89.782(4)
β/°	97.535(5)	107.14(3)	77.059(4)
γ/°	90	90	84.185(4)
Volume/Å^3	1488.5(4)	1624(2)	1173.81(16)
Z	4	4	2
ϱ_{calc}g/cm^3	1.750	1.776	1.602
μ/mm^{-1}	2.310	2.151	1.518
F(000)	776.0	864.0	576.0
Crystal size/mm^3	0.386 × 0.367 × 0.112	0.174 × 0.131 × 0.092	0.214 × 0.133 × 0.106
Radiation	MoKα (λ = 0.71073)	MoKα (λ = 0.71073)	MoKα (λ = 0.71073)
2Θ range for data collection/°	4.774 to 52.762	4.324 to 63.882	4.97 to 52.836
Reflections collected	13187	36275	47689
Independent reflections	3009 [R_{int} = 0.0669, R_{sigma} = 0.0615]	5573 [R_{int} = 0.0470, R_{sigma} = 0.0244]	4815 [R_{int} = 0.0333, R_{sigma} = 0.0160]
Data/restraints/parameters	3009/0/164	5573/0/181	4815/3/316
Goodness-of-fit on F^2	1.105	1.082	1.057
Final R indexes [I>=2σ (I)]	R_1 = 0.0441, wR_2 = 0.0834	R_1 = 0.0308, wR_2 = 0.0735	R_1 = 0.0273, wR_2 = 0.0664
Final R indexes [all data]	R_1 = 0.0702, wR_2 = 0.0899	R_1 = 0.0425, wR_2 = 0.0778	R_1 = 0.0334, wR_2 = 0.0689
Largest diff. peak/hole / e Å^{-3}	0.72/-1.20	1.00/-1.17	0.69/-0.48
Absolute structure parameter	-	-	-

Table S2. Selected crystal structure data of the structure determinations of compounds **3a-5**

Compound	**3a**	**4**	**5**
Empirical formula	$C_{32}H_{64}I_2Na_2O_{27}S_{5.5}$	$C_{12}H_{24}IKO_8S$	$C_{12}H_{28}INO_8S$
Formula weight	1356.94	494.37	473.31
Crystal colour, habit	yellow, platelet	yellow, platelet	yellow, platelet
Temperature/K	100(2)	100(2)	100(2)
Crystal system	triclinic	monoclinic	orthorhombic
Space group	*P*-1	$P2_1/n$	$P2_12_12_1$
a/Å	12.5295(11)	8.3143(6)	8.7123(4)
b/Å	14.4749(13)	17.2979(13)	13.9145(6)
c/Å	15.4608(14)	13.9724(11)	16.1858(7)
α/°	89.498(3)	90	90
β/°	72.953(3)	101.344(3)	90
γ/°	87.058(3)	90	90
Volume/Å^3	2677.2(4)	1970.3(3)	1962.16(15)
Z	2	4	4
ϱ_{calc}g/cm^3	1.683	1.667	1.602
μ/mm^{-1}	1.487	1.974	1.773
F(000)	1376.0	992.0	960.0
Crystal size/mm^3	0.328 × 0.179 × 0.032	0.269 × 0.167 × 0.05	0.38 × 0.127 × 0.085
Radiation	MoKα (λ = 0.71073)	MoKα (λ = 0.71073)	MoKα (λ = 0.71073)
2Θ range for data collection/°	4.968 to 50.798	4.71 to 56.7	5.034 to 56.68
Reflections collected	9726	84847	32083
Independent reflections	9726 [*]	4915 [R_{int} = 0.0373, R_{sigma} = 0.0146]	4902 [R_{int} = 0.0463, R_{sigma} = 0.0363]
Data/restraints/parameters	9726/49/593	4915/0/208	4902/5/225
Goodness-of-fit on F^2	1.119	1.067	1.027
Final R indexes [I>=2σ (I)]	R_1 = 0.0778, wR_2 = 0.1867	R_1 = 0.0226, wR_2 = 0.0499	R_1 = 0.0269, wR_2 = 0.0416
Final R indexes [all data]	R_1 = 0.0886, wR_2 = 0.1913	R_1 = 0.0286, wR_2 = 0.0518	R_1 = 0.0389, wR_2 = 0.0437
Largest diff. peak/hole / e Å^{-3}	3.06/-3.01	0.65/-0.77	0.64/-0.53
Absolute structure parameter	-	-	-0.004(8)

* refined as a two-component twin

Table S3. Selected crystal structure data of the structure determinations of compounds **6-8**

Compound	**6**	**7**	**8**
Empirical formula	$C_{12}H_{24}IO_{12}RbS_3$	$C_{12}H_{24}CsIO_{10}S_2$	$C_{10}H_{20}I_2MgO_9S_2$
Formula weight	668.86	652.24	626.49
Crystal colour, habit	yellow, platelet	yellow, platelet	orange, block
Temperature/K	100(2)	100(2)	100(2)
Crystal system	monoclinic	orthorhombic	monoclinic
Space group	$P2_1/n$	$P2_12_12_1$	$C2/c$
a/Å	13.0494(8)	9.7988(4)	9.923(6)
b/Å	8.4209(5)	10.2557(4)	16.798(10)
c/Å	21.7886(13)	22.0522(9)	11.938(7)
α/°	90	90	90
β/°	98.415(2)	90	95.00(2)
γ/°	90	90	90
Volume/Å^3	2368.5(2)	2216.10(15)	1982(2)
Z	4	4	4
ϱ_{calc}g/cm^3	1.876	1.955	2.099
μ/mm^{-1}	3.710	3.294	3.452
F(000)	1320.0	1264.0	1208.0
Crystal size/mm^3	0.336 × 0.22 × 0.196	0.24 × 0.161 × 0.103	0.053 × 0.043 × 0.027
Radiation	MoKα (λ = 0.71073)	MoKα (λ = 0.71073)	MoKα (λ = 0.71073)
2Θ range for data collection/°	5.194 to 55.084	4.38 to 56.714	4.782 to 50.528
Reflections collected	5477	49561	7443
Independent reflections	5477 [*]	5521 [R_{int} = 0.0341, R_{sigma} = 0.0183]	1735 [R_{int} = 0.0632, R_{sigma} = 0.0590]
Data/restraints/parameters	5477/0/264	5521/0/236	1735/0/111
Goodness-of-fit on F^2	1.194	1.073	1.115
Final R indexes [I>=2σ (I)]	R_1 = 0.0307, wR_2 = 0.0921	R_1 = 0.0129, wR_2 = 0.0260	R_1 = 0.0425, wR_2 = 0.0929
Final R indexes [all data]	R_1 = 0.0335, wR_2 = 0.0936	R_1 = 0.0142, wR_2 = 0.0263	R_1 = 0.0649, wR_2 = 0.0988
Largest diff. peak/hole / e Å^{-3}	0.81/-0.58	0.43/-0.38	0.93/-0.85
Absolute structure parameter	-	-0.014(4)	-

* refined as a two-component twin

Table S4. Selected crystal structure data of the structure determinations of compounds **9-11**

Compound	**9**	**10**	**11**
Empirical formula	$C_{16}H_{32}I_2MgO_{16}S_4$	$C_{24}H_{48}Ca_2I_6O_{18}S_3$	$C_{24}H_{48}Ba_2I_4O_{22}S_5$
Formula weight	886.76	1562.36	1631.20
Crystal colour, habit	orange, platelet	brown, needle	yellow-orange, platelet
Temperature/K	100(2)	100(2)	100(2)
Crystal system	tetragonal	orthorhombic	Monoclinic
Space group	*P*4/*n*	$P2_12_12_1$	$P2_1/c$
a/Å	11.6974(19)	12.8246(7)	8.4679(4)
b/Å	11.6974(19)	17.5810(9)	13.4183(7)
c/Å	11.4976(18)	20.8518(10)	22.0213(13)
α/°	90	90	90
β/°	90	90	94.800(2)
γ/°	90	90	90
Volume/Å^3	1573.2(6)	4701.4(4)	2493.4(2)
Z	2	4	2
ϱ_{calc}g/cm^3	1.872	2.207	2.173
μ/mm^{-1}	2.349	4.377	4.324
F(000)	876.0	2968.0	1544.0
Crystal size/mm^3	0.181 × 0.069 × 0.064	0.256 × 0.077 × 0.076	0.307 × 0.148 × 0.14
Radiation	MoKα (λ = 0.71073)	MoKα (λ = 0.71073)	MoKα (λ = 0.71073)
2Θ range for data collection/°	4.924 to 50.512	4.39 to 50.644	4.796 to 50.782
Reflections collected	21677	70398	38352
Independent reflections	1430 [R_{int} = 0.0781, R_{sigma} = 0.0294]	8561 [R_{int} = 0.0692, R_{sigma} = 0.0385]	4571 [R_{int} = 0.0439, R_{sigma} = 0.0232]
Data/restraints/parameters	1430/0/91	8561/0/479	4571/43/291
Goodness-of-fit on F^2	1.032	1.097	1.042
Final R indexes [I>=2σ (I)]	R_1 = 0.0232, wR_2 = 0.0482	R_1 = 0.0480, wR_2 = 0.1109	R_1 = 0.0211, wR_2 = 0.0324
Final R indexes [all data]	R_1 = 0.0295, wR_2 = 0.0499	R_1 = 0.0603, wR_2 = 0.1159	R_1 = 0.0297, wR_2 = 0.0339
Largest diff. peak/hole / e Å^{-3}	0.47/-0.42	2.14/-2.16	0.81/-1.01
Absolute structure parameter	-	0.42(5)	-

1.2 Representation of additional X-ray structures

1.2.1 [NH4([18]crown-6)]I·SO2 (5)

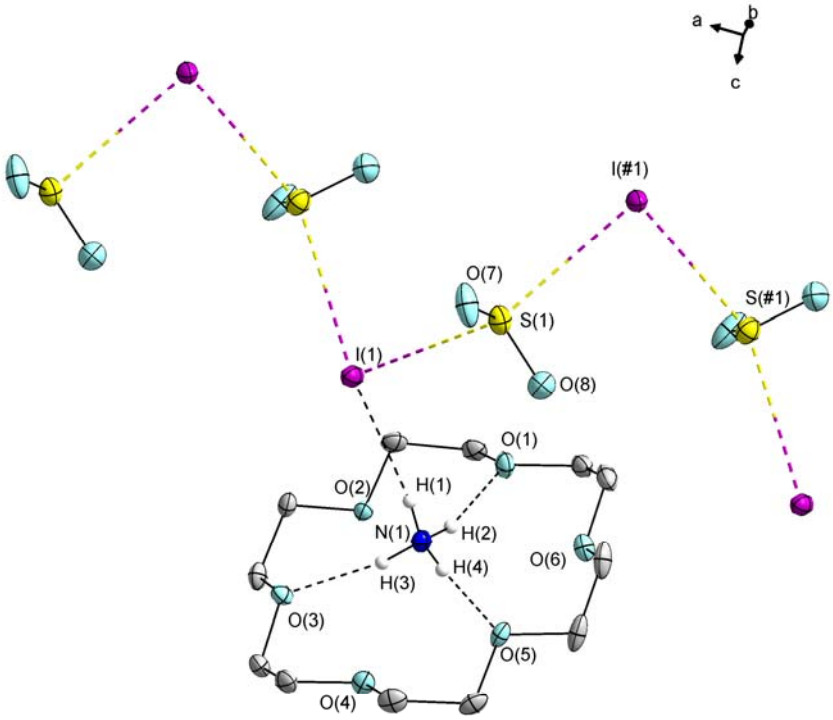

Figure S1. Structure of **5** in the crystal. Thermal displacement ellipsoids are drawn at 50% probability. Hydrogen atoms were crystallographically localized and fixed with DFIX [0.91] commands. Selected bond lengths [pm]: H(1)-I(1) 265(2), H(2)-O(1) 196(2), H(3)-O(3) 199(3), H(4)-O(5) 196(3), I(1)-S(1) 330.3(1), I(#1)-S(1) 337.1(1). Selected bond angles [°]: I(1)-S(1)-I(#1) 150.0(1), S(1)-I(#1)-S(#1) 88.0(1).

1.2.2 $[Ca_2([18]crown\text{-}6)_2(SO_2I)_3]I_3$ (10)

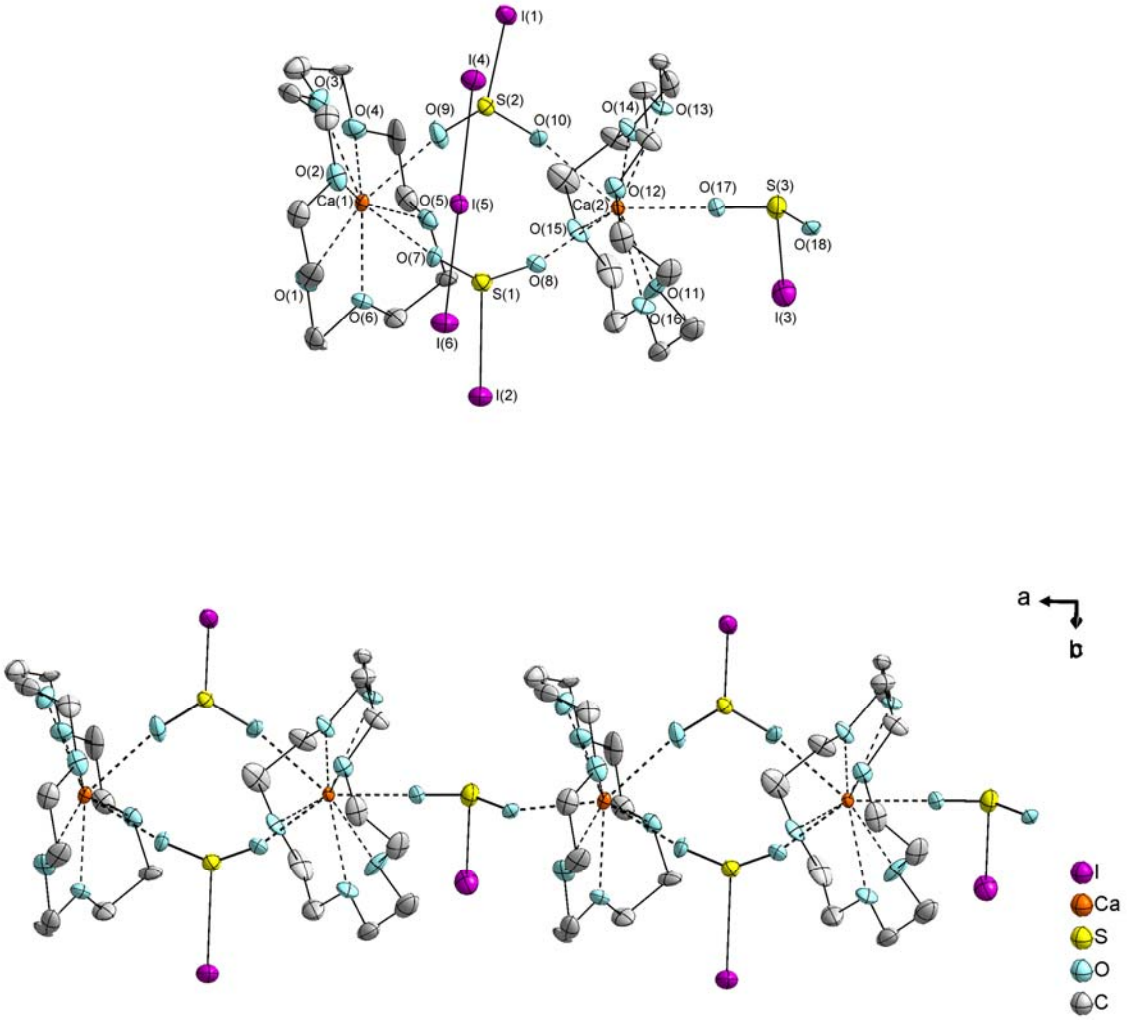

Figure S2. Structure of **10** in the crystal. Asymmetric unit (top) and a section of the coordination polymer along [c] (bottom). I_3^- anions are omitted for clarity (bottom). Thermal displacement ellipsoids are drawn at 50% probability. Selected bond lengths [pm]: I(1)-S(2) 287.6(1), I(2)-S(1) 277.9(1), I(3)-S(3) 267.3(1), O(1)-Ca(1) 261.2(1), O(2)-Ca(1) 253.4(1), O(3)-Ca(1) 260.9(1), O(4)-Ca(1) 263.8(1), O(5)-Ca(1) 254.3(1), O(6)-Ca(1) 250.0(1), O(7)-Ca(1) 241.9(1), O(8)-Ca(2) 239.4(1), O(9)-Ca(1) 242.5(1), O(10)-Ca(2) 247.1(1), O(11)-Ca(2) 256.0(1), O(12)-Ca(2) 256.8(1), O(13)-Ca(2) 265.5(1), O(14)-Ca(2) 250.8(1), O(15)-Ca(2) 252.3(1), O(16)-Ca(2) 257.7(1), O(17)-Ca(2) 233.8(1).

2. Comment on redox-chemistry

Despite the fact that the s-block metal iodides turned out to be the most suitable salts for the exploration of chalcogen bonding towards SO_2, it is unmistakable that this chemistry suffers redox chemistry. The redox chemistry has been investigated by *Jander* back in the 1940s and is nothing new. However, by observations made herein the use of crown ethers increases the sensitivity of these compounds even more. *Jander* reported on different time periods in which the respective salts are undergoing solvolysis which range from days to years.[1] Employing crown-ethers, we have also experienced redox-chemistry within hours. Especially using strontium iodide. The crown-ethers most likely additionally act as an auxiliary to dissolve the salts and activates the iodide anions through shielding of the metal centers. In our studies we could convincingly show the formation of various $SO_2\cdots I^-$ adducts and we were able to substantiate the formation of elemental sulfur in combination with I_3^- formation. We want at this point expand upon the early considerations and assume the following reaction-cascade for Sr^{2+} as an example (see Scheme S1). In the depicted Scheme, the initial step is the dissolution of SrI_2 in SO_2 using [18]crown-6. Subsequently, the solvation of SO_2 around I^- occurs. As it is evident from the results presented herein, the iodosulfite formation occurs. At this point, the redox-chemical part begins. Upon formation of SO_3^{2-} as well as instable SOI_2, elemental sulfur as well as unbound iodine are formed. SO_3^{2-} is eventually oxidized to SO_4^{2-}.

Elemental sulfur and I_2 (also as part of I_3^-) have been several times detected by means of SC-XRD. The reaction of LiI and [12]crown-4 lead several times to a brownish solution upon reducing the volume for single-crystal growth. Also applying various stochiometries.

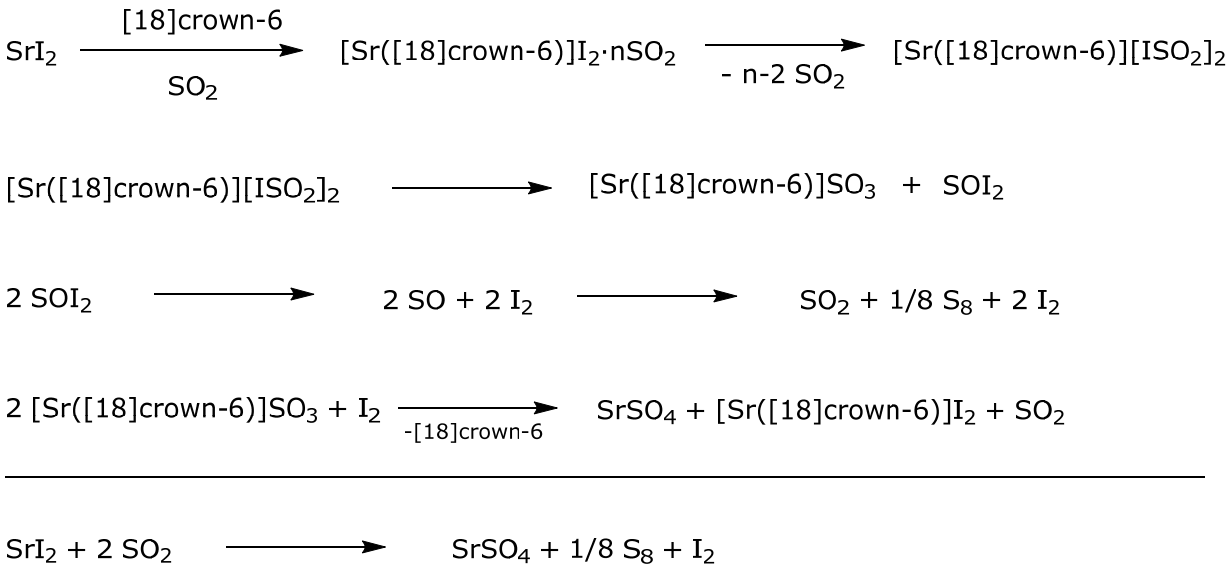

Scheme S1. Proposed redox-cascade for solvolysis reactions employing SO_2, s-block metal iodides and crown-ethers based on the results presented herein as well as suggestions by *Jander*.[1] SrI_2 has been arbitrarily chosen as an example here.

For instance, two equivalents of [12]crown-4 were reacted with one equivalent of LiI. Upon reducing the volume for single crystal growth, the solution turned brown after several hours and at some point, single crystals grew in the residue. These turned out to be γ-S_8 on the one hand (yellow needle, mP (no. 13, *P*2/*c*), a = 8.50, b = 13.05, c = 9.27, β = 124.88 and V = 838Å^3).[2] On the other hand, brown needles, oF (initially refined: no. 43, *Fdd*2), a = 36.05, b = 12.33, c = 33.06, $\alpha = \beta = \gamma$ = 90° and V = 14678Å^3 turned out to be $[Li([12]crown\text{-}4)_2]I_3$. Similar observations were made for SrI_2 in SO_2. Reacting SrI_2 with [18]crown-6 in SO_2 or with [15]crown-5 (2.0 eq) yields a brownish dark solution within a few hours in both cases. Whereas the conversion with [18]crown-6 yielded exclusively γ-S_8, the conversion with [15]crown-5 also yielded $[Sr([15]crown\text{-}5)(I_3)_2]\cdot 2I_2$ (brown platelet, oC, initially

refined: no. 20; $C222_1$ with a = 12.48, b = 17.73, c = 19.73, $\alpha = \beta = \gamma = 90°$ and V = 4368Å^3). We want to emphasize, that SO_2I^- was tentatively assigned as the electroactive species in a I_3^-/I^- mediation system for SO_2 oxidation in a past work by *Wrighton*.[3] Experimental data around the SO_2I^- anion is provided within this work and gives insights into this reaction.

3. References

[1] Jander, G. *Die Chemie in verflüssigtem Schwefeldioxyd*. In: Die Chemie in Wasserähnlichen Lösungsmitteln. Anorganische und Allgemeine Chemie in Einzeldarstellungen, **1949**, vol 1. Springer, Berlin, Heidelberg, Germany. DOI: 10.1007/978-3-662-21788-7_8.

[2] Yasunari, W. The Crystal Structure of Monoclinic γ-Sulphur. *Acta Crystallogr., Sect. B: Struct. Sci., Cryst. Eng. Mater.*, 2015, **B30**, 1396–1401.

[3] Wrighton, M. S.; Calabrese, G. S. Photoelectrochemical oxidation of sulfur dioxide in strong acid solution: iodide-mediated oxidation at illuminated metal dichalcogenide electrodes. *J. Am. Chem. Soc.*, 1981, **103**, 6273-6280.

This document is confidential and is proprietary to the American Chemical Society and its authors. Do not copy or disclose without written permission. If you have received this item in error, notify the sender and delete all copies.

A Second Modification of Beryllium Bromide: β-BeBr2

Journal:	*Inorganic Chemistry*
Manuscript ID	ic-2020-02832n.R1
Manuscript Type:	Featured Article
Date Submitted by the Author:	14-Oct-2020
Complete List of Authors:	Buchner, Magnus; Philipps-Universitat Marburg Fachbereich Chemie, Dankert, Fabian; Philipps-Universitat Marburg Fachbereich Chemie, Faculty of Chemistry Spang, Nils; Philipps-Universitat Marburg Fachbereich Chemie Pielnhofer, Florian; Universitat Regensburg, Anorganische Chemie von Hänisch, Carsten; Philipps-Universitat Marburg Fachbereich Chemie, Fachbereich Chemie and Wissenschaftliches Zentrum für Materialwisenschaften (WZMW)

SCHOLARONE™
Manuscripts

A Second Modification of Beryllium Bromide: β-$BeBr_2$

Magnus R. Buchner,*,† Fabian Dankert,‡ Nils Spang,† Florian Pielnhofer,¶ and Carsten von Hänisch*,‡

†*Fachbereich Chemie, Philipps-Universität Marburg*

‡*Fachbereich Chemie and Wissenschaftliches Zentrum für Materialwissenschaften (WZMW), Philipps-Universität Marburg*

¶*Institut für Anorganische Chemie, Universität Regensburg*

E-mail: magnus.buchner@chemie.uni-marburg.de; haenisch@chemie.uni-marburg.de

Abstract

The synthesis of a second beryllium bromide modification, β-$BeBr_2$, was accomplished through recrystallization of α-$BeBr_2$ from benzene in the presence of *cyclo*-decamethylpentasiloxane. This phase was analyzed *via* single crystal X-ray diffraction and IR and Raman spectroscopy as well as density functional theory calculations. This enabled a comparison to α-$BeBr_2$ and the α- and β-phases of beryllium chloride and iodide.

Introduction

Beryllium is the lightest metal, which is stable against air and humidity, due to a passivating layer of beryllium oxide. Therefore it is widely applied in high technology applications and indispensable for many of these.[1] Owing to the highest electronegativity among the s-block metals the chemistry of beryllium is more diverse than of the other alkaline earth or alkali metals. Furthermore, beryllium coordination chemistry is unique since Be^{2+} is by far the smallest metal ion.[2,3] However, there are serious health hazards associated with beryllium and its compounds.[4] This is the reason why there is little systematic knowledge on this element's chemistry.

The main starting material for organometallic and coordination chemistry of beryllium are $BeCl_2$, $BeBr_2$ and BeI_2.[3] Synthetic procedures yielding these in a pure form have been known for roughly a century.[5] Despite this fact, there is still surprisingly little known about these compounds and we presented the first complete set of IR and Raman spectra of these only recently.[6] Also the structure elucidation of these compounds was protracted in relation to other, simple metal halides. While already 30 years ago the modifications of BeF_2 were determined from powder X-ray data to be analogous to α- and β-quartz,[7] the single crystal structure of α-BeF_2 was only presented in 2011.[8] The constitution of α-$BeCl_2$ on the other hand has been known since 1952. It crystallizes in the orthorhombic space group *Ibam* (No. 72) and exhibits the SiS_2 structure type. In this solid state modification the beryllium atoms are tetrahedrally coordinated by four chlorine atoms and two beryllium atoms are μ_2-linked by two chlorine atoms. This generates infinite chains of edge connected $[BeCl_{4/2}]$ tetrahedra as shown in figure 1 (left).[9] In 1995 a second phase of $BeCl_2$ was described. This low temperature phase, β-$BeCl_2$, crystallizes in the tetragonal space group $I4_1/acd$ (No. 142) and adopts the $Mg(NH_2)_2$ structure type. In this polymorph the beryllium atoms are also tetrahedrally coordinated by four chlorine atoms. However, these $[BeCl_{4/2}]$ tetrahedra are corner connected to form super tetrahedra ($[Be_4Cl_6Cl_{4/2}]$) as illustrated in figure 1 (right).[10] In general mixtures of both $BeCl_2$ phases are obtained during synthesis.[6] However, pure

α-$BeCl_2$ can be obtained by fast sublimation while pure β-$BeCl_2$ can be made by gas phase deposition at 300 °C.[10]

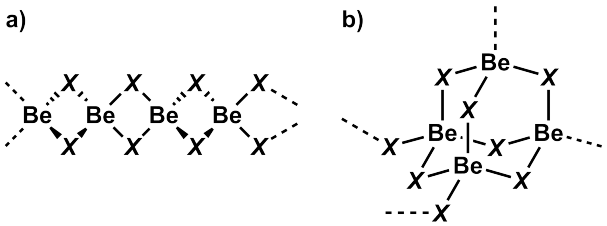

Figure 1: Structure of **a)** α- and **b)** β-beryllium chloride and iodide (X = Cl, I).[9–11]

Based on powder X-ray data, *Lazarini* suggested in 1975 that $BeBr_2$ is isostructural to α-$BeCl_2$.[12] This was verified in 2000 by *Trojanov* through the single crystal structure of α-$BeBr_2$, which is depicted in figure 2. This is also the only phase that is obtained directly from the synthesis of $BeBr_2$ from the elements.[6] *Trojanov* was also able to show that BeI_2 adopts two different structures. The α-phase of BeI_2 is isostructural to α-$BeCl_2$, while β-BeI_2 is isostructural to β-$BeCl_2$ (Fig. 1).[11] β-BeI_2 is obtained phase pure from the synthesis out of the elements at 400 °C.[6]

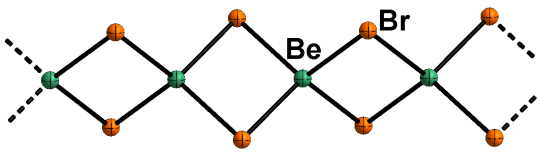

Figure 2: Structure of α-$BeBr_2$ in the solid state.[11]

$BeCl_2$ and $BeBr_2$ show very similar reactivity and in general form complexes with the same constitution and geometry, while BeI_2 behaves differently.[13,14] Therefore, we thought it was astonishing that there was no evidence in the literature, that a beryllium bromide phase does exist, which is isostructural to β-$BeCl_2$ and β-BeI_2. This was emphasized by the fact that calculations came to the conclusion that the β-phases of $BeCl_2$ and BeI_2 are more stable than their α counterparts.[6,15] Given that $BeBr_2$ is emerging as one of the best starting materials for beryllium chemistry in solution,[13,16] we decided to investigate whether a second phase of $BeBr_2$ does exist.

Experimental Section

Caution! *Beryllium and its compounds are regarded as toxic and carcinogenic. As the biochemical mechanisms that cause beryllium associated diseases are still unknown,[4] special (safety) precautions are strongly advised.*[17]

General Experimental Techniques

All manipulations were performed either under solvent vapor pressure or dry argon using glovebox and *Schlenk* techniques. Benzene was dried over sodium and subsequently distilled under argon. C_6D_6 was dried over NaK alloy and subsequently vacuum distilled. *Cyclo*-decamethylpentasiloxane ($\geq 95\,\%$) was purchased from TCI and used as received. $BeBr_2$ and BeI_2 were prepared from the elements according to the literature.[6] Due to the expected extreme toxicity of the obtained compounds no elemental analysis could be performed.

Powder X-Ray diffraction

Inside a glovebox the samples were filled into borosilicate capillaries with a diameter of 0.5 mm, which were subsequently sealed with a hot tungsten filament. The powder X-ray patterns were recorded with a *Stoe & Cie* StadiMP diffractometer in Debye-Scherrer geometry. The diffractometer was operated with Cu-K_α radiation (1.5406 Å, germanium monochromator) and was equipped with a MYTHEN 1K detector. The diffraction patterns were examined using the WinXPOW software suite.[18]

Single Crystal X-Ray Diffraction

Single crystals were selected under exclusion of air in perfluorinated polyether (Fomblin YR 1800, Solvay Solexis) and mounted using the MiTeGen MicroLoop system. X-ray diffraction data were collected using the monochromated Mo-K_α radiation of a Bruker D8 Quest diffractometer equipped with a microfocus source and a CMOS Photon 100 detector. The structures

were solved using Direct Methods (SHELXT)[19] and refined against F2 (SHELXL)[20] using the OLEX2 software package.[21]

IR Spectroscopy

IR spectra were recorded on a *Bruker* alpha FTIR spectrometer equipped with a diamond ATR unit in an argon filled glovebox. Processing of the spectra was performed with the OPUS software package[22] and OriginPro 2017.[23] Single crystals of the compounds were used for the IR spectroscopic measurements.

Raman spectroscopy

The Raman spectra were recorded on a *S&I* Confocal Raman Microscope MonoVista CRS+ at ambient temperature. The Raman spectrometer was equipped with four laser diodes with excitation lines of 488, 532, 633 and 785 nm. The best spectra were obtained with an excitation wavelength of 488 nm.

Tempering of $BeBr_2$

A fused silica ampule was charged with 30 mg α-$BeBr_2$ and flame sealed under vacuum. The ampule was heated to 573 K for 42 days and subsequently cooled to ambient temperature with a cooling rate of 0.02 K min^{-1}. The ampule was opened inside a glovebox and a sample was filled into a 0.5 mm borosilicate capillary for powder X-Ray diffraction.

Formation of β-BeI_2

A 15 mg portion of β-BeI_2 (0.057 mmol, 1.0 eq.) was placed in a *J-Young* NMR tube. Subsequently, 32 mg of *cyclo*-decamethylpentasiloxane (0.086 mmol, 1.5 eq.) together with 1 ml of C_6D_6 were added. The suspension was sonicated for about 30 min and subsequently stored

at ambient temperature for two weeks. During this time block-shaped, colorless crystals of β-BeI_2 formed at the bottom of the reaction vessel.

Preparation of β-$BeBr_2$

A 10 mg portion of α-$BeBr_2$ (0.059 mmol, 1.0 eq.) was placed in a *J-Young* NMR tube. Subsequently, 33 mg of *cyclo*-decamethylpentasiloxane (0.089 mmol, 1.5 eq.) together with 1 ml of C_6H_6 were added. The suspension was sonicated for about 30 min and subsequently stored at ambient temperature for two weeks. During this time block-shaped, colorless crystals of β-$BeBr_2$ formed at the bottom of the reaction vessel. FT-IR (cm^{-1}): 510 (s), 412 (s); Raman (cm^{-1}): 552 (m), 426 (w), 188 (s).

Computational Details

Quantum chemical calculations were performed in the framework of density functional theory (DFT) using a linear combination of Gaussian-type functions (LCGTF) scheme as implemented in CRYSTAL17.[24] Full structural optimizations were performed using the PBE[25] xc-functional with D3 dispersion correction.[26] Basis sets were selected according to literature.[27] The convergence criterion considering the energy was set to 10^{-8} a.u. with a k-mesh sampling of $8 \times 8 \times 8$. Energy-volume plots were fitted to a Birch-Murnaghan equation of state. The vibrational frequencies including Raman intensities were computed on the basis of the relaxed structures using the coupled-perturbed Kohn-Sham (CPKS) mode.[28] The modes were visualized with J-ICE.[29]

Results and discussion

Synthesis

β-$BeCl_2$ and β-BeI_2 can be synthesized through slow gas phase deposition at 300 °C and 400 °C respectively.[6,10] Accordingly we heated α-$BeBr_2$ in a fused silica ampule under vacuum to 300 °C for six weeks and subsequently cooled the sample to ambient temperature with a cooling rate of 0.02 K min^{-1}. However, this only gave phase pure α-$BeBr_2$ according to the powder X-ray diffraction pattern (Supporting Information Fig. S1). Also slow heating of a sample of low crystallinity, with consecutive measurement of powder X-ray diffractograms, did not give any evidence for the existence of a second $BeBr_2$ phase (Supporting Information Fig. S3). Therefore, it was evident that recrystallization in solution at ambient temperature had to be employed. But the choice of solvent was significantly reduced by the fact that $BeBr_2$ forms stable adduct complexes with *O*- and *N*-donor solvents and ligands.[14,30] Chlorinated solvents are also capable to dissolve low amounts of beryllium halides. However, in case of $BeBr_2$ and BeI_2 exchange of the bromide and iodide against chloride can occur through activation of the C−Cl bonds.[31] Therefore, chlorinated solvents had to be excluded as well. Other non-coordinating aromatic and aliphatic solvents do not dissolve beryllium halides in an extent necessary to perform recrystallization.

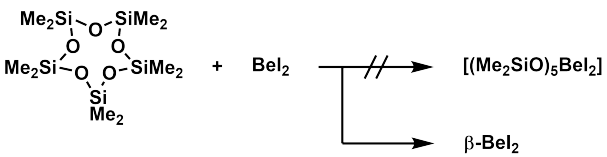

Scheme 1: Attempt to coordinate *cyclo*-decamethylpentasiloxane to BeI_2 in C_6D_6.

However, serendipitously we discovered a way to recrystallize BeI_2 from benzene. Since crown ether complexes of $BeCl_2$ were known, we wanted to expand this field with other polydentate *O*-donor ligands.[32] In accordance to the synthesis of alkali and alkaline earth complexes of *cyclo*-methylsiloxanes,[33] we reacted BeI_2 with *cyclo*-decamethylpentasiloxane in C_6D_6. However, instead of the anticipated formation of methylsiloxane beryllium complexes,

we obtained single crystals of β-BeI_2 according to scheme 1. We assume that the *cyclo*-decamethylpentasiloxane acts as a solubilizer. An analogous reactivity was described for open chain sila-polyethers, which help to recrystallize rubidium and caesium salts.[34] Motivated by these observations we reacted α-$BeBr_2$ with *cyclo*-decamethylpentasiloxane in benzene. This led to the formation of block shaped single crystals of β-$BeBr_2$ according to equation (1).

$$\alpha\text{-}BeBr_2 \xrightarrow[(C_6H_6)]{(Me_2SiO)_5} \beta\text{-}BeBr_2 \quad (1)$$

However, this reaction only works on a small scale and if the reaction suspensions are kept for more than two weeks all of the solid dissolves. This is presumably caused by reaction of $BeBr_2$ with the siloxane under formation of beryllium siloxanato compounds, which is in analogy to the reaction of $BeCl_2$ with siloxanes or partially silicon-based crown ethers.[35] This is currently under investigation and will be published in due course.

Structure

β-$BeBr_2$ crystallizes in the tetragonal space group $I4_1/acd$ (No. 142) with 32 formula units per unit cell. The beryllium atoms are surrounded by four bromine atoms, which form a tetrahedral coordination sphere. Four of these $[BeBr_{4/2}]$ tetrahedra are corner connected to each other to from a structure analogous to P_4O_{10} as shown in figure 3. These $[Be_4Br_6Br_{4/2}]$ supertetrahedra are again connected to each other *via* their corners to form a three dimensional coordination network. The eight super tetrahedra per unit cell form two independent coordination frameworks, which are interpenetrating each other (Fig. 3, bottom). This structure type corresponds to the structure of $Mg(NH_2)_2$[36] and is also found for β-$BeCl_2$,[10] β-BeI_2,[11] $ZnBr_2$,[37] ZnI_2[38] and $Be(NH_2)_2$.[39]

The Be–Br distances in β-$BeBr_2$ are between 2.174(5) and 2.191(6) Å and are, for this reason, identical to α-$BeBr_2$ (2.1852(11) Å).[11] This is in accordance with identical Be–Cl

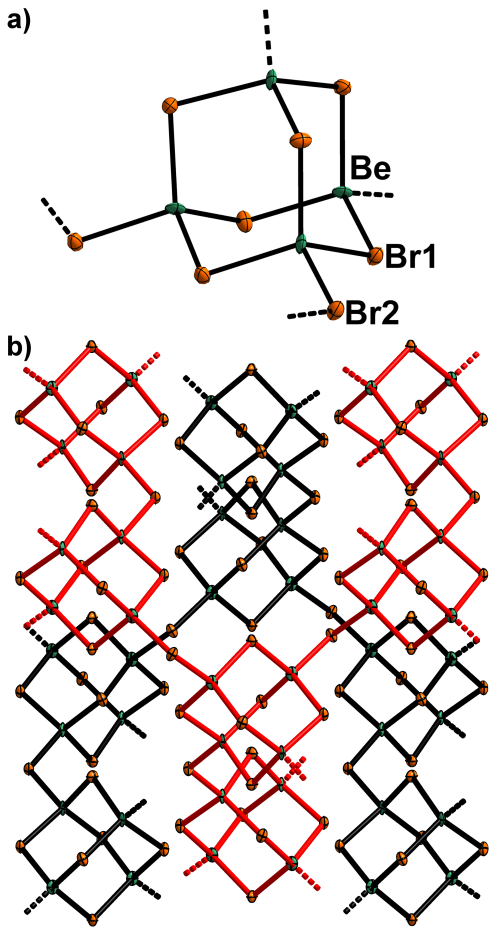

Figure 3: Structure of **a)** $[Be_4Br_6Br_{4/2}]$ supertetrahedra and **b)** the two independent coordination networks in the solid state structure of β-$BeBr_2$. Ellipsoids are depicted at 70 % probability at 100 K.

or Be–I distances in α-$BeCl_2$ (2.0260(8) Å) and β-$BeCl_2$ (2.0224(12)–2.0323(12) Å) or α-BeI_2 (2.4167(7) Å) and β-BeI_2 (2.395(13)–2.447(12) Å), respectively.[11] The Br–Be–Br angles range from 103.8(2) to 112.0(2)°, which is identical to the respective Cl–Be–Cl and I–Be–I angles in β-$BeCl_2$ and β-BeI_2.[11] The Be–Br1–Be angles within the supertetrahedra range from 105.4(3) to 105.7(3)°, which is slightly smaller than the corresponding Be–Cl1–Be angles in β-$BeCl_2$ (106.93(4)–107.08(5)°) and slightly larger than the Be–I1–Be angles in β-BeI_2 (103.8(4)–104.0(4)°).[11] This trend is also observed for the Be–X2–Be angles between the supertetrahedra (Cl: 116.27(4)°, Br: 114.0(3)°, I: 112.4(4)°), which are all significantly larger than the ones within the supertetrahedra.[11] The unit cell dimensions lie in between the ones

of β-$BeCl_2$ and β-BeI_2 as would be expected from the atomic radii.[11] Details on the crystal data and the structure determination of β-$BeBr_2$ are compiled in table 1.

Table 1: Crystal data and details of the structure determination of β-$BeBr_2$.

Empirical formula	$BeBr_2$
Relative molecular mass	168.81
Radiation / Å	(Mo-K_α), 0.71073
Crystal System	tetragonal
Space group (No.)	$I4_1/acd$ (142)
a / Å	11.2117(7)
c / Å	19.2922(13)
V / Å^3	2425.1(3)
T / K	100(2)
Z	32
F(000)	2368
d_{calc} / g cm^{-1}	3.7
µ / mm^{-1}	26.4
Θ / °	3.326–27.138
Range of Miller indices	$-14 \leq h \leq 14$
	$-14 \leq k \leq 14$
	$-24 \leq l \leq 24$
reflections collected / unique	18109 / 657
restraints / parameters	0 / 30
R_{Int}	0.0610
R_1 $I \geq 2\sigma(I)$	0.0327
R_1 (all data)	0.0332
wR_2 $I \geq 2\sigma(I)$	0.0883
S	1.273
$\Delta\rho_{min,\ max}$ /e Å^{-3}	−1.0, 1.4

Vibrational Spectra

The infra red spectrum of β-$BeBr_2$ consists of two bands with almost equal intensity at 412 and 510 cm^{-1} as shown in figure 4. According to quantum chemical calculations (*vide infra*) the band at 412 cm^{-1} is composed of three IR frequencies with E_u symmetry (408, 411 and 414 cm^{-1}) and one with A_{2u} symmetry (409 cm^{-1}). The second band is also caused by three E_u vibrations (505, 521 and 523 cm^{-1}) and one with A_{2u} symmetry (521 cm^{-1}). In α-$BeBr_2$ also two bands are observed at comparable wavenumbers (404 and 477 cm^{-1}), however here the intensity of the band at 404 cm^{-1} is significantly larger than the one at 477 cm^{-1}.[6]

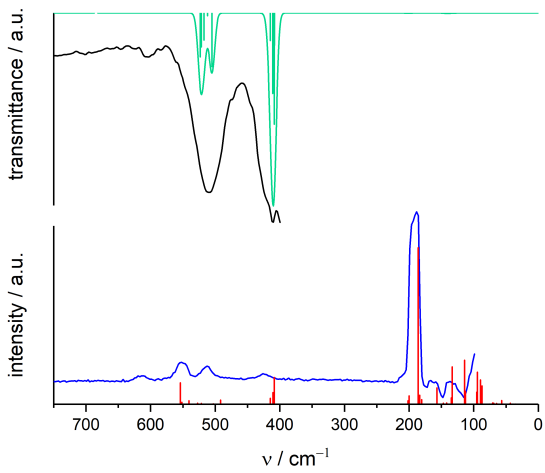

Figure 4: Measured (black) and simulated IR spectrum as well as calculated IR frequencies (green) and measured Raman spectrum (blue) as well as calculated Raman frequencies (red) of β-$BeBr_2$. The intensity is given in arbitrary units.

The Raman spectrum of β-$BeBr_2$ is dominated by one intense band at 188 cm^{-1}, which is of A_{1g} symmetry according to calculations (calculated value: 188 cm^{-1}). The corresponding A_{1g} mode of α-$BeBr_2$ is observed at 203 cm^{-1}.[6] β-$BeBr_2$ has two additional but very weak Raman bands at 426 and 552 cm^{-1}. The prior comprises of one B_{2g} (409 cm^{-1}) and one E_g (411 cm^{-1}) band according to quantum chemistry. The second band is caused by an A_{1g} mode which is calculated to be at 554 cm^{-1}.

The IR and Raman spectra of β-$BeCl_2$ and β-BeI_2 show similar patterns, though the Be−Cl bands are observed at higher and the Be−I bands at lower wavenumbers compared to the Be−Br bands.[6] This is in accordance with the decreasing Be−X bond strength from chloride *via* bromide to iodide.

Theoretical Investigation

Density functional theory (DFT) calculations were carried out in order to investigate the relative stability of both $BeBr_2$ polymorphs. Optimized lattice parameters as obtained with the D3 corrected PBE functional for both modifications are in good agreement with experimental values (table 2). The cell volume is only slightly underestimated by 0.63 % (α-$BeBr_2$)

and 0.03 % (β-$BeBr_2$). The vibrational properties (*vide supra*) were computed on the basis of the optimized structures.

Table 2: Optimized lattice parameters in Å and cell volumes per formula unit in Å^3 of α-$BeBr_2$ and β-$BeBr_2$ as obtained with PBE-D3.

modification	a	b	c	V
α-$BeBr_2$	5.478	10.477	5.561	79.8
β-$BeBr_2$	11.121		19.601	75.8

As already mentioned above and previously reported, the β-modification is energetically preferred over the α-modification for all other beryllium halides.[6] Therefore, it is not surprising, that β-$BeBr_2$ is found to be 6.6 kJ mol^{-1} more stable than α-$BeBr_2$, which is displayed by the E-V curves in figure 5. The calculated bulk moduli B_0 are extremely small and account for high compressibilty of both polymorphs. B_0 of β-$BeBr_2$ (12.7 GPa) is marginally larger than the value for α-$BeBr_2$ (10.1 GPa) and is in line with the fact that β-$BeBr_2$ exhibits a lower cell volume per formula unit. Further, the calculated bandgaps are very similar for both modifications (α: 5.5 eV, β: 5.3 eV).

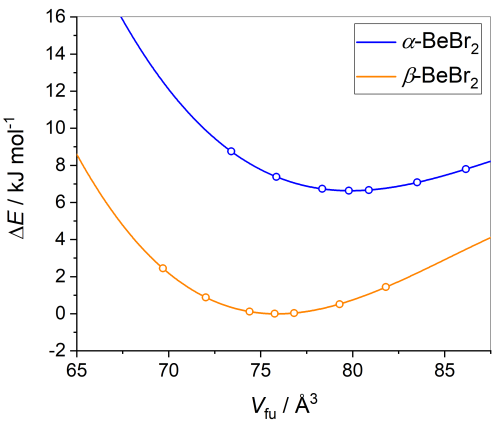

Figure 5: Birch-Murnaghan equation of state (EOS) curves for α-$BeBr_2$ (blue) and β-$BeBr_2$ (orange).

Conclusions

We could show that β-$BeBr_2$ can be synthesized by recrystallizing α-$BeBr_2$ from benzene in the presence of *cyclo*-decamethylpentasiloxane, which acts as a solubilizer. The solid state structure of β-$BeBr_2$ consists of two interpenetrating three dimensional coordination networks of $[Be_4Br_6Br_{4/2}]$ super tetrahedra and is isostructural to β-$BeCl_2$ and β-BeI_2. Quantum chemical calculations show that β-$BeBr_2$ is more stable than α-$BeBr_2$. This is in line with $BeCl_2$ and BeI_2 where also the β-modifications are more stable than the corresponding α-phases. The shape of the vibrational spectra of β-$BeBr_2$ correspond well to the ones of β-$BeCl_2$ and β-BeI_2, while the bands of α-$BeBr_2$ and β-$BeBr_2$ are observed at similar energies. The experimental and computational results are in good agreement and through a combination of these findings, a complete assignment of all IR and Raman bands was possible.

Acknowledgement

The authors express their gratitude to H. Lars Deubner, Jascha Bandemehr and Matthias Müller for their help with the temperature dependent powder X-ray diffraction experiments. M.R.B. thanks Prof. Florian Kraus for the provision of laboratory space. F.D., N.S., C.v.H. and M.R.B. gratefully acknowledge the DFG for financial support (BU 2725/8–1, HA 3466/8–3). F.P. thanks Prof. Bettina Lotsch, Dr. Ulrich Wedig and the Computer Service group from the Max-Planck-Institute for Solid State Research (Stuttgart, Germany) for access to CRYSTAL17 and computational facilities.

Supporting Information Available

The following files are available free of charge.

- CSD 2031947 contains the supplementary crystallographic data for this paper, which can be obtained free of charge *via* www.ccdc.cam.ac.uk/data_request/cif, or by emailing data_request@ccdc.cam.ac.uk, or by contacting The Cambridge Crystallographic Data Centre, 12 Union Road, Cambridge CB2 1EZ, UK; fax: +44 1223 336033.
- Powder X-ray diffraction data.
- Optimized lattice parameters.

This material is available free of charge via the Internet at `http://pubs.acs.org/`.

Conflict of Interest

There are no conflicts to declare.

References

(1) (a) Puchta, R. A brighter beryllium. *Nat. Chem.* **2011**, *3*, 416–416; (b) Fröhlich, P.; Lorenz, T.; Martin, G.; Brett, B.; Bertau, M. Valuable Metals–Recovery Processes, Current Trends, and Recycling Strategies. *Angew. Chem. Int. Ed.* **2017**, *56*, 2544–2580.

(2) (a) Perera, L. C.; Raymond, O.; Henderson, W.; Brothers, P. J.; Plieger, P. G. Advances in beryllium coordination chemistry. *Coord. Chem. Rev.* **2017**, *352*, 264–290; (b) Buchner, M. R. Recent Contributions to the Coordination Chemistry of Beryllium. *Chem. Eur. J.* **2019**, *25*, 12018–12036.

(3) Buchner, M. R. Beryllium coordination chemistry and its implications on the understanding of metal induced immune responses. *Chem. Commun.* **2020**, *56*, 8895–8907.

(4) Buchner, M. R. Beryllium-associated diseases from a chemist's point of view. *Z. Naturforsch., B: J. Chem. Sci.* **2020**, *75*, 405–412.

(5) (a) Messerknecht, C.; Blitz, W. Über die Dichten der Berylliumhalogenide. *Z. Anorg. Allg. Chem.* **1925**, *148*, 152–156; (b) Hönigschmidt, O.; Johannsen, T. Das Atomgewicht des Berylliums. *Z. Naturforsch.* **1946**, *1*, 650–655; (c) Bell, N. A. Beryllium Halides and Pseudohalides. *Adv. Inorg. Chem. Radiochem.* **1972**, *14*, 255–332.

(6) Müller, M.; Pielnhofer, F.; Buchner, M. R. A facile synthesis for $BeCl_2$, $BeBr_2$ and BeI_2. *Dalton Trans.* **2018**, *47*, 12506–12510.

(7) (a) Narten, A. H. Diffraction Pattern and Structure of Noncrystalline BeF_2 and SiO_2 at 25℃. *J. Chem. Phys.* **1972**, *56*, 1905–1909; (b) Wright, A. F.; Fitch, A. N.; Wright, A. C. Preparation and structure of the alpha quartz and beta quartz polymophism of BeF_2. *J. Solid State Chem.* **1988**, *73*, 298–304.

(8) Ghalsasi, P.; Ghalsasi, P. S. Single Crystal X-Ray Structure of BeF_2: α-Quartz. *Inorg. Chem.* **2011**, *50*, 86–89, PMID: 21141831.

(9) Rundle, R. E.; Lewis, P. H. Electron Deficient Compounds. VI. The Structure of Beryllium Chloride. *J. Chem. Phys.* **1952**, *20*, 132–134.

(10) Spundflasche, E.; Fink, H.; Seifert, H. J. Zur Thermochemie und Struktur von Berylliumchlorid. *Z. Anorg. Allg. Chem.* **1995**, *621*, 1723–1726.

(11) Trojanov, S. I. Crystal modifications of beryllium dihalides $BeCl_2$, $BeBr_2$, and BeI_2. *Russ. J. Inorg. Chem.* **2000**, *45*, 1481–1486.

(12) Lazarini, F. New crystal data for beryllium(II) bromide. *J. App. Cryst.* **1975**, *8*, 568.

(13) Müller, M.; Buchner, M. R. Beryllium-Induced Conversion of Aldehydes. *Chem. Eur. J.* **2019**, *25*, 11147–11156.

(14) Müller, M.; Buchner, M. R. Solution Behavior of Beryllium Halides in Dimethylformamide. *Inorg. Chem.* **2019**, *58*, 13276–13284.

(15) Zwijnenburg, M. A.; Corà, F.; Bell, R. G. Isomorphism of Anhydrous Tetrahedral Halides and Silicon Chalcogenides: Energy Landscape of Crystalline BeF_2, $BeCl_2$, SiO_2, and SiS_2. *J. Am. Chem. Soc.* **2008**, *130*, 11082–11087.

(16) (a) Himmel, D.; Krossing, I. $[BeBr_2(SMe_2)_2]$, a Versatile Starting Material for Beryllium Chemistry – One Pot Synthesis from Beryllium Powder. *Z. Anorg. Allg. Chem.* **2006**, *632*, 2021–2023; (b) Himmel, D.; Scherer, H.; Kratzert, D.; Krossing, I. Synthesis and Characterization of Cp*Be-F-Al$(OR^F)_3$. *Z. Anorg. Allg. Chem.* **2015**, *641*, 655–659; (c) Naglav, D.; Bläser, D.; Wölper, C.; Schulz, S. Synthesis and Characterization of Heteroleptic 1-Tris(pyrazolyl)borate Beryllium Complexes. *Inorg. Chem.* **2014**, *53*, 1241–1249; (d) Naglav, D.; Tobey, B.; Neumann, A.; Bläser, D.; Wölper, C.; Schulz, S. Synthesis, Solid-State Structures, and Computational Studies of Half-Sandwich Cp*BeX (X = Cl, Br, I) Compounds. *Organometallics* **2015**, *34*, 3072–3078; (e) Paparo, A.; Smith, C. D.; Jones, C. Diagonally Related s- and p-Block Metals Join Forces: Synthesis and Characterization of Complexes with Covalent Beryllium-Aluminum Bonds. *Angew. Chem. Int. Ed.* **2019**, *58*, 11459–11463; (f) Müller, M.; Buchner, M. R. Understanding the Localization of Berylliosis: Interaction of Be^{2+} with Carbohydrates and Related Biomimetic Ligands. *Chem. Eur. J.* **2019**, *25*, 16257–16269.

(17) Naglav, D.; Buchner, M. R.; Bendt, G.; Kraus, F.; Schulz, S. Off the beaten track – a hitchhiker's guide to beryllium chemistry. *Angew. Chem. Int. Ed.* **2016**, *55*, 10562–10576.

(18) WinXPOW, STOE & Cie GmbH, Darmstadt, Germany, WinXPOW, STOE & Cie GmbH, Darmstadt, Germany. 2015.

(19) Sheldrick G. M., SHELXT-2018/2, Göttingen, Germany, SHELXT-2018/2, G. M Sheldrick., Göttingen, Germany. 2018.

(20) Sheldrick G. M., SHELXL-2018/3, Göttingen, Germany, SHELXL-2018/3, G. M Sheldrick Göttingen, Germany. 2018.

(21) Dolomanov, O. V.; Bourhis, L. J.; Gildea, R. J.; Howard, J. A. K.; Puschmann, H. *OLEX2*: a complete structure solution, refinement and analysis program. *J. Appl. Crystallogr.* **2009**, *42*, 339–341.

(22) OPUS, Bruker Optik GmbH, Ettlingen, Germany, OPUS, Bruker Optik GmbH, Ettlingen, Germany. 2009.

(23) OriginPro 2017, OriginLab, Northampton, MA, USA, OriginPro 2017, OriginLab, Northampton, MA, USA. 2017.

(24) (a) Dovesi, R.; Erba, A.; Orlando, R.; Zicovich-Wilson, C. M.; Civalleri, B.; Maschio, L.; Rérat, M.; Casassa, S.; Baima, J.; Salustro, S.; Kirtman, B. Quantum-mechanical condensed matter simulations with CRYSTAL. *Wiley Interdiscip. Rev.: Comput. Mol. Sci.* **2018**, *8*, e1360; (b) Dovesi, R. et al. CRYSTAL17 User's Manual. University of Torino, Torino, 2017.

(25) Perdew, J. P.; Burke, K.; Ernzerhof, M. Generalized gradient approximation made simple. *Phys. Rev. Lett.* **1996**, *77*, 3865.

(26) (a) Grimme, S.; Antony, J.; Ehrlich, S.; Krieg, H. A consistent and accurate ab initio parametrization of density functional dispersion correction (DFT-D) for the 94 elements H-Pu. *J. Chem. Phys.* **2010**, *132*, 154104; (b) Grimme, S.; Ehrlich, S.; Goerigk, L. Effect of the damping function in dispersion corrected density functional theory. *J. Comput. Chem.* **2011**, *32*, 1456–1465; (c) Grimme, S.; Hansen, A.; Brandenburg, J. G.; Bannwarth, C. Dispersion-corrected mean-field electronic structure methods. *Chem. Rev.* **2016**, *116*, 5105–5154.

(27) (a) Baima, J.; Erba, A.; Rérat, M.; Orlando, R.; Dovesi, R. Beryllium oxide nanotubes and their connection to the flat monolayer. *J. Phys. Chem. C* **2013**, *117*, 12864–12872;

(b) Doll, K.; Stoll, H. Ground-state properties of heavy alkali halides. *Phys. Rev. B* **1998**, *57*, 4327.

(28) (a) Ferrero, M.; Rérat, M.; Orlando, R.; Dovesi, R. The calculation of static polarizabilities of 1-3D periodic compounds. the implementation in the crystal code. *J. Comput. Chem.* **2008**, *29*, 1450–1459; (b) Ferrero, M.; Rérat, M.; Kirtman, B.; Dovesi, R. Calculation of first and second static hyperpolarizabilities of one-to three-dimensional periodic compounds. Implementation in the CRYSTAL code. *J. Chem. Phys.* **2008**, *129*, 244110.

(29) Canepa, P.; Hanson, R. M.; Ugliengo, P.; Alfredsson, M. J-ICE: a new Jmol interface for handling and visualizing crystallographic and electronic properties. *J. Appl. Crystallogr.* **2011**, *44*, 225–229.

(30) (a) Paparo, A.; Jones, C. Beryllium Halide Complexes Incorporating Neutral or Anionic Ligands: Potential Precursors for Beryllium Chemistry. *Chem. Asian J.* **2019**, *14*, 486–490; (b) Neumüller, B.; Dehnicke, K. Direktsynthese und Kristallstruktur von $[BeBr_2(CH_3CN)_2]$. *Z. Anorg. Allg. Chem.* **2010**, *636*, 1438–1440; (c) Müller, M.; Buchner, M. R. Preparation and crystal structures of the beryllium ammines $[Be(NH_3)_4]X_2$ (X = Br, I, CN, SCN, N_3) and $Be(NH_3)_2X'_2$ (X' = Cl, Br, I). *Chem. Commun.* **2019**, *55*, 13649–13652; (d) Paparo, A.; Best, S. P.; Yuvaraj, K.; Jones, C. Neutral, Anionic, and Paramagnetic 1,3,2-Diazaberyllacyles Derived from Reduced 1,4-Diazabutadienes. *Organometallics* **2020**, doi: 10.1021/acs.organomet.0c00017; (e) Müller, M.; Karttunen, A. J.; Buchner, M. R. Speciation of Be^{2+} in acidic liquid ammonia and formation of tetra- and octanuclear beryllium amido clusters. *Chem. Sci.* **2020**, *11*, 5414–5422.

(31) (a) Buchner, M. R.; Müller, M.; Spang, N. Probing the electronic boundaries between trigonal and tetrahedral coordination at beryllium. *Dalton Trans.* **2020**, *49*, 7708–7712; (b) Buchner, M. R.; Spang, N.; Müller, M.; Rudel, S. S. Formation and Properties of the Trichloroberyllate Ion. *Inorg. Chem.* **2018**, *57*, 11314–11317.

(32) (a) Neumüller, B.; Dehnicke, K. [BeCl(12-Krone-4)][$SbCl_4$]: Ein neuer kationischer Berylliumkomplex. *Z. Anorg. Allg. Chem.* **2006**, *632*, 1681–1686; (b) Neumüller, B.; Dehnicke, K.; Puchta, R. Die Kristallstruktur von [$BeCl_2$(15-Krone-5)]. *Z. Anorg. Allg. Chem.* **2008**, *634*, 1473–1476; (c) Puchta, R.; Kolbig, R.; Weller, F.; Neumüller, B.; Massa, W.; Dehnicke, K. [$(BeCl_2)_2$(18-Krone-6)] und sein Hydrolyseprodukt [$Be_3(\mu\text{-}OH)_3(H_2O)_6$-(18-Krone-6)]$Cl_3 \cdot 3\,H_2O$: Kristallstrukturen und DFT-Rechnungen. *Z. Anorg. Allg. Chem.* **2010**, *636*, 2364–2371; (d) Buchner, M. R.; Müller, M. Beryllium Crown Ether Complexes Reinvestigated. *Z. Anorg. Allg. Chem.* **2018**, *644*, 1186–1189; (e) Raymond, O.; Henderson, W.; Lane, J. R.; Brothers, P. J.; Plieger, P. G. An electrospray ionization mass spectrometric study of beryllium chloride solutions and complexes with crown ether and cryptand macrocyclic ligands. *J. Coord. Chem.* **2020**, *73*, 1–16.

(33) (a) Dankert, F.; Weigend, F.; von Hänisch, C. Not Non-Coordinating at All: Coordination Compounds of the Cyclodimethylsiloxanes D_n (D = Me_2SiO; n = 6, 7) and Group 2 Metal Cations. *Inorg. Chem.* **2019**, *58*, 15417–15422; (b) Dankert, F.; Erlemeier, L.; Ritter, C.; von Hänisch, C. On the molecular architectures of siloxane coordination compounds: (re-)investigating the coordination of the cyclodimethylsiloxanes D_n (n = 5–8) towards alkali metal ions. *Inorg. Chem. Front.* **2020**, *7*, 2138–2153.

(34) Dankert, F.; Heine, J.; Rienmüller, J.; von Hänisch, C. Sila-polyethers as innocent crystallization reagents for heavy alkali metal compounds. *CrystEngComm* **2018**, *20*, 5370–5376.

(35) (a) Neumüller, B.; Dehnicke, K. Synthese, Schwingungsspektrum und Kristallstruktur des Disiloxanato-Chloroberyllats $(Ph_4P)_2[Be_4Cl_6(OSiMe_2OSiMe_2O)_2]$. *Z. Anorg. Allg. Chem.* **2004**, *630*, 1846–1850; (b) Buchner, M. R.; Müller, M.; Dankert, F.; Reuter, K.; von Hänisch, C. The coordination behaviour and reactivity of partially silicon based crown ethers towards beryllium chloride. *Dalton Trans.* **2018**, *47*, 16393–16397.

(36) Jacobs, H. Die Kristallstruktur des Magnesiumamids. *Z. Anorg. Allg. Chem.* **1971**, *382*, 97–109.

(37) Chieh, C.; White, M. A. Crystal structure of anhydrous zinc bromide. *Z. Kristallogr.* **1984**, *166*, 189–197.

(38) Fourcroy, P. H.; Carré, D.; Rivet, J. Structure cristalline de l'iodure de zinc ZnI_2. *Acta Crystallogr., Sect. B: Struct. Crystallogr. Cryst. Chem.* **1978**, *34*, 3160–3162.

(39) Jacobs, V. H. Die Kristallstruktur von Berylliumamid, $Be(NH_2)_2$. *Z. Anorg. Allg. Chem.* **1976**, *427*, 1–7.

Graphical TOC Entry

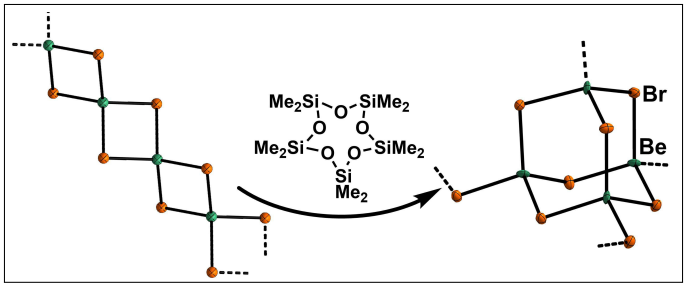

Cyclo-decamethylsiloxane was used as a solubilizer to facilitate the recrystallization of α-$BeBr_2$ into the previously unknown β-modification of beryllium bromide. This polymorph was analyzed *via* X-ray diffraction, IR and Raman spectroscopy as well as quantum chemistry.

Supporting Information for

A Second Modification of Beryllium Bromide: β-$BeBr_2$

Magnus R. Buchner,*[,1] Fabian Dankert,[1] Nils Spang,[1]
Florian Pielnhofer,[2] and Carsten von Hänisch*[,1]

[1] *Philipps-Universität Marburg*
[2] *Universität Regensburg*

Table of Contents

Powder X-ray diffraction data.....S2–S3

References.....S3

1 Powder X-ray diffraction data

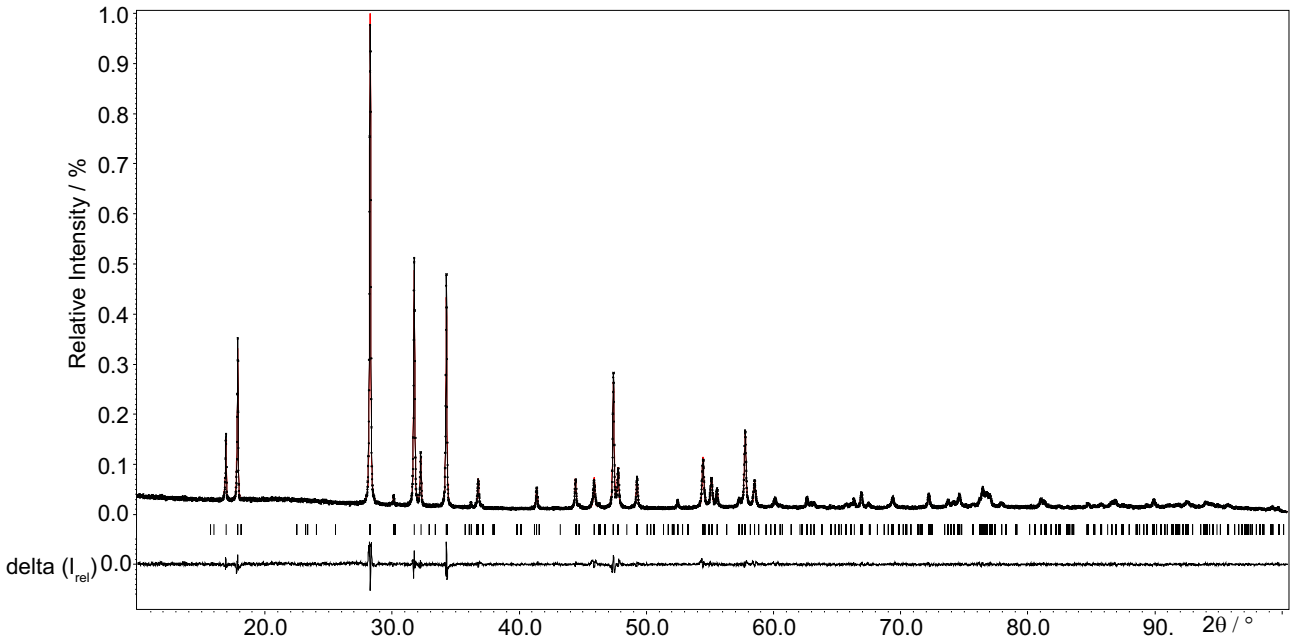

Figure S1 X-ray powder diffractogram of $BeBr_2$ tempered at 300 °C with LeBail profile fit, difference plot and related reference for α-$BeBr_2$.[1]

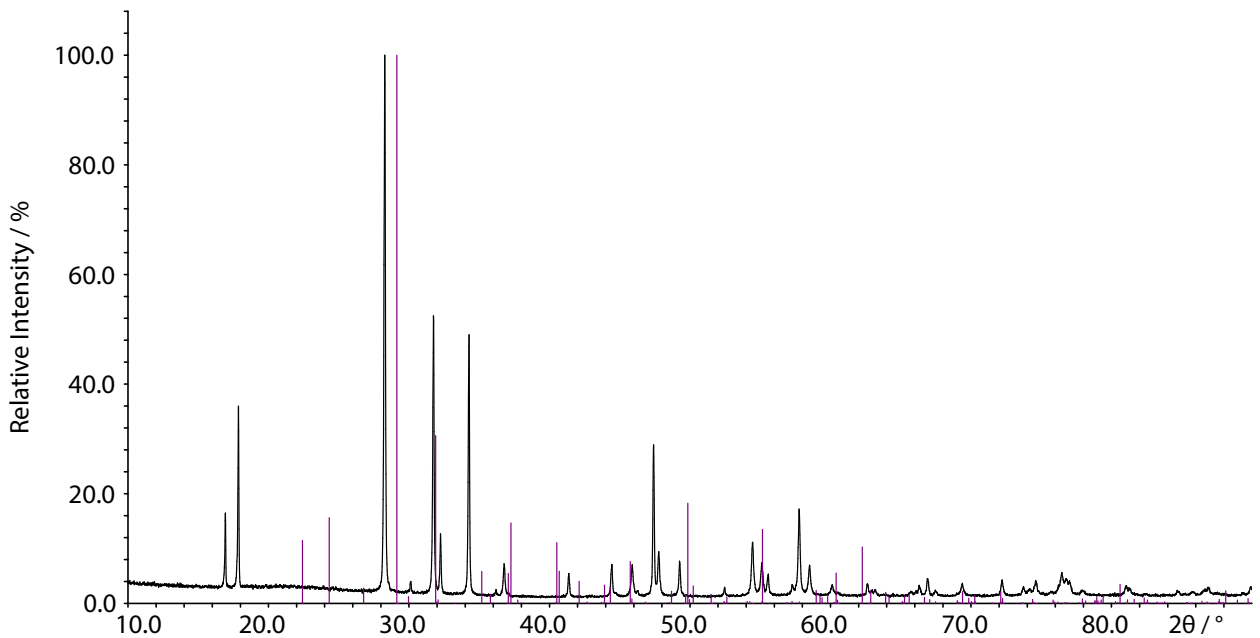

Figure S2 X-ray powder diffractogram of $BeBr_2$ tempered at 300 °C and reference reflex positions of β-$BeBr_2$.

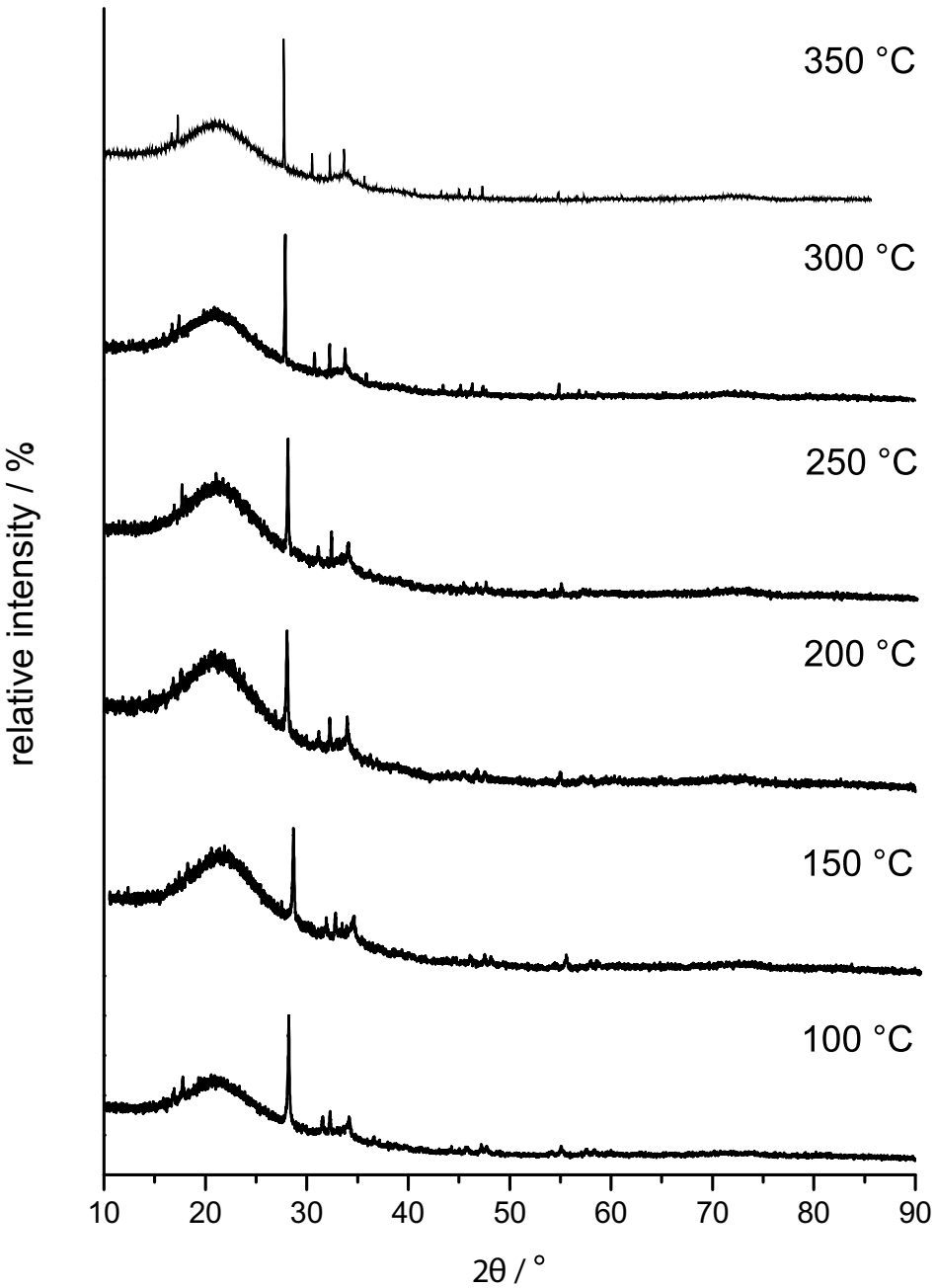

Figure S3 X-ray powder diffractograms of $BeBr_2$ at various temperatures.

References

[1] Trojanov, S. I. *Russ. J. Inorg. Chem.* **2000**, *45*, 1481–1486.

Architecting inorganic crown-ethers by s-block-metal templated Si-O bond activation

Fabian Dankert,[a] Roman-Malte Richter,[a] Florian Weigend,*[b] Xiulan Xie,[b] Markus Balmer,[a]

Carsten von Hänisch*[a]

[a] F. Dankert, R.-M. Richter, Dr. M. Balmer, Prof. Dr. C. von Hänisch
Fachbereich Chemie and Wissenschaftliches Zentrum für Materialwissenschaften (WZMW)
Philipps-Universität Marburg
Hans-Meerwein-Straße 4, 35032 Marburg, Germany
E-mail: carsten.vonhaenisch@staff.uni-marburg.de

[b] Dr. F. Weigend, Dr. X. Xie
Fachbereich Chemie
Philipps-Universität Marburg
Hans-Meerwein-Straße 4, 35032 Marburg, Germany
E-mail: florian.weigend@staff.uni-marburg.de

Supporting information for this article is given via a link at the end of the document.

Abstract: We herein report the synthesis, structures, coordination ability and formation mechanism of crown-ether analogues which are constructed by an inorganic skeleton of ^2D_n-type (^2D_n = $(Me_4Si_2O)_n$). A $^2D_2/GaI_3/MI_x$ system has been established for oligomerization of $^2D_2$ (**I**) *via* metal templation. In case of MI_x = LiI, $[Li(^2D_3)GaI_4]$ (**1**) is formed. In case of MI_x = NaI, MgI_2, CaI_2 and SrI_2, $[M(^2D_4)(GaI_4)_x]$ (M = Mg^{2+} (**3**), Ca^{2+} (**4**), Sr^{2+} (**5**) is formed. Furthermore the proton complex $[H(^2D_3)]Ga_2I_7$ (**6**) was isolated and structurally characterized. All complexes were characterized by means of multinuclear NMR spectroscopy, DOSY NMR (DOSY = diffusion ordered spectroscopy) experiments and except for compound **3**, also by means of SC-XRD (SC-XRD = single-crystal X-ray diffraction analysis). Solid-state structures compare well with observations made in solution proving that these inorganic crown-ethers are stable as long as a suitable metal template is present. A crucial step for the formation of such poly-silylethers is an exocyclic pre-coordination of **I** with M^{n+} which is evident from an obtained intermediate product in the reaction of **I** with $LiGaI_4$. $[Li_2(^2D_2)(GaI_4)_2]$ (**II**) was isolated and characterized. Coordination indicates Si-O bond activation as elongated Si-O bonds and smaller Si-O-Si angles are found. The metal centres can be readily removed from the obtained macrocycles upon MeCN addition. Bulk extraction shows that an unoccupied ligand can in principle be obtained, but combined NMR-spectroscopic and mass spectrometric studies reveal that even higher oligomers are formed as soon as the metal template is removed. $^2D_4$ (**7**) is obtained as the main product followed by $^2D_5$ (**8**) and $^2D_6$ (**9**). Quantum chemical calculations were carried out to compare the M^+ affinity of the crown-ether analogs among themselves and with respect to crown ethers and to shed light on the formation of larger rings from smaller ones, in particular concerning the role of M^+ and I^-.

Introduction

Since their discovery in the mid-sixties, crown ethers and related compounds such as cryptands, spherands and podands came a long way. Due to their fantastic coordination ability, they were several times reviewed, gained many fields of applications and it was in 1987 when C.J. *Pedersen*, J.M. *Lehn* and D. J. *Cram* were awarded with the noble prize in chemistry for their research in supramolecular chemistry.[1–5] However, much less attention was paid to silicon analogues of crown-ethers even though there has been a major interest in 'inorganic' macrocycles over the years.[6–15] Furthermore, many works of the last few decades dealt with the Si-imitation of organic chemistry: compounds were characterized which represent silicon-silicon multiple bonds,[16–20] silanones[21–23] silanoic esters,[24,25] silacarboxylates,[26] silanoic/silaform amides[27,28] or also radicaloids[29] (see Scheme 1 for a selection of examples). Such species are highly sensitive towards air, moisture and most of the compounds also to oligomerization. A skilled handling of such compounds is required as the reactivity is substantially different to that of organic counterparts.

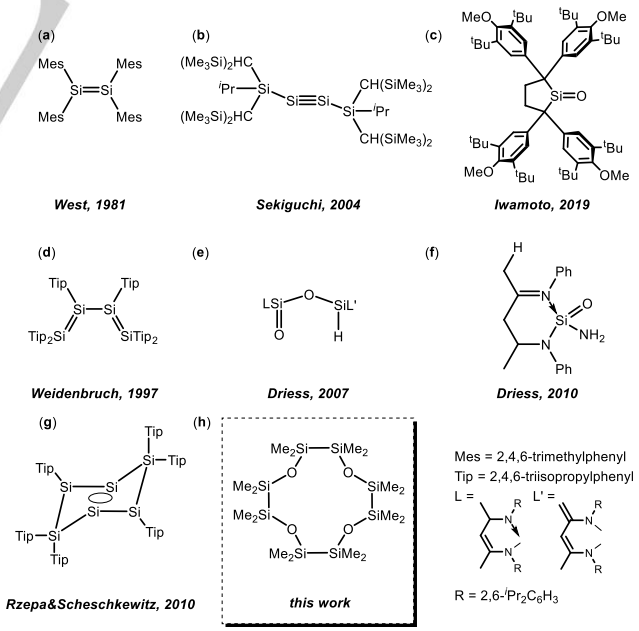

Scheme 1: A selection of advances in a silicon chemistry imitating important organic compounds: (a)[16] alkene → silylene, (b)[17] alkyne → silylyne, (c)[23] ketone → silanone, (d)[19] diene → siladiene, (e)[24] ester → silanoic ester, (f)[27] amide → silanoic amide, (g)[18] benzene → hexasilabenzene, (h) [12]crown-4 (cyclic polyether) → octasila[12]crown-4 (cyclic sila-polyether).

The problem with obtaining inorganic crown ethers imitating the organic counterpart, however, is probably ascribed to the specific Si-O-bond character. This is to date controversially discussed and regards siloxane donors as poorly coordinating. Various explanations in literature conclude a lower basicity of the Si-O-linkage in comparison to the C-O-linkage which made silicon based ligands somehow unattractive for their use in coordination chemistry: Negative hyperconjugation interactions of $n_O \rightarrow \sigma^*_{Si\text{-}C}$ type are nowadays discussed.[30–32] When siloxanes coordinate Lewis acids, this $n_O \rightarrow \sigma^*_{Si\text{-}C}$ interaction competes with the $n_O \rightarrow M^{n+}$ interaction. A recent work considers $n_O \rightarrow \sigma^*_{Si\text{-}C}$ but also less pronounced $n_O \rightarrow d_{Si}$ interactions to be important.[33] Due to the described orbital overlaps, covalency is responsible for the low basicity of siloxanes according to the aforementioned explanations. On the other hand, the Si-O-bond is, according to the basic electronegativity concept, much more polarized and thus ionic compared to ethers. However, the oxygen atoms don't readily provide electron density for metal bonding. The electron density around the O-atom is spatially diffuse,[34] and $metal^{+}\cdots Si^{\delta+}$ repulsive interactions disrupt metal binding.[35,36] Covalency and ionicity were long time opposed to each other but, according to meticulously performed quantum chemical calculations, have about the same importance as both increase simultaneously and significantly when approaching larger Si-O-Si angles.[37] As mentioned, Si-O donors are described as weakly coordinating and thus coordination compounds of neutral siloxane ligands were mostly obtained using highly reactive compounds or WCA's such as perfluorinated alkoxy aluminates (WCA = weakly coordinating anion).[35,38–43] However, the understanding of siloxane ligands has crucially moved in the past few years. As several works show, early group one and especially group two ions can be effectively bound within siloxane moieties and the nature of the cation has to be considered when siloxanes are used for silyl-ether coordination.[44–48] Another key factor to compare organic (crown-) ethers with siloxane ligands is the architecture of the ligand moiety. Since the most silicon based ligands are constructed out of $–SiMe_2–$ units rather than $–C_2H_4–$ units, there is structural repugnance.[49,50] For a few years now we therefore investigated the coordination ability sila-(crown-) ethers with one, two or three $–Si_2Me_4–$ units between the oxygen atoms.[51–58] According to NMR experiments, DFT calculations as well as single crystal X-ray diffraction we could demonstrate that these hybrid ligands coordinate well and the cooperative effects of siloxane-oxygen donors as well as etheric oxygen donors yields stable complexes.[51–58] To date, however, exclusively silicon based crown-ether analogues of ^2D_n type (^2D_n = $(Si_2Me_4O)_n$) were unavailable and for this reason their coordination compounds could not be characterized. A comparison of silicon-based crown-ethers with organic crown-ethers or the cyclosiloxanes D_n was for this reason not possible.

In this contribution we report on exclusively disilanyl-bearing cyclosiloxanes and their metal complexes which are available by s-block-metal templated Si-O bond activation. Behavior in solution, single crystal X-Ray diffraction experiments as well as quantum chemical calculations were carried out to impart an understanding of these, to the best of our knowledge, first ever characterized (metal) complexes of silicon based crown-ether analogues of ^2D_n type.

Results and Discussion

Synthesis and Structure

As it is evident from a number of publications, ligands containing siloxane moieties can be ring-opened and also deconstructed by either strong acids, various metal-organic bases or suitable metal-anion combinations.[58–61] ROP (ROP = ring opening polymerization) of cyclic silaethers, however, is a challenge as metal organic bases can initiate Si-Si bond cleavage and cationic ROP requires very strong acids such as triflic acid.[59] As we demonstrate in this contribution, a milder approach turned out to be expedient for the synthesis of inorganic crown-ethers. Combining the small WCA $[GaI_4]^-$, a chemically rather hard metal cation and a suitable sila-precursor has been established as the method of choice. A suitable sila-precursor for ROP, is $^2D_2$ (**I**). The proton affinity and the basicity of **I** are described to be significantly higher than those of siloxanes of the D_n type, including very reactive D_3.[62,63] For this reason, we started investigating $^2D_2$/s-block metaliodide/gallium(III)iodide systems and used LiI at first. Indeed, the ring is opened by Li^+ metal templated ring opening polymerization. However, the outcome of the reaction highly depends on the reaction time and stoichiometry of the metal salt. By stirring 1.0 eq of *in situ* generated $LiGaI_4$ and 1.5 eq **I** for 2h at 70°C in Ph-F, we observed formation of $[Li_2(^2D_2)(GaI_4)_2]$ (**II**), which shows two Li^+ ions coordinated by one $^2D_2$ ligand and $[GaI_4]^-$ counterions (Figure 1 and S2). According to single crystal X-ray diffraction analysis, a one-dimensional coordination polymer is obtained (see Figure S2). The stoichiometry of the reaction protocol does not fit for this compound, but the reaction is finely reproducible under these conditions. In CD_2Cl_2 solution, a single resonance of 8.7 ppm can be observed in the ^{29}Si NMR spectrum.

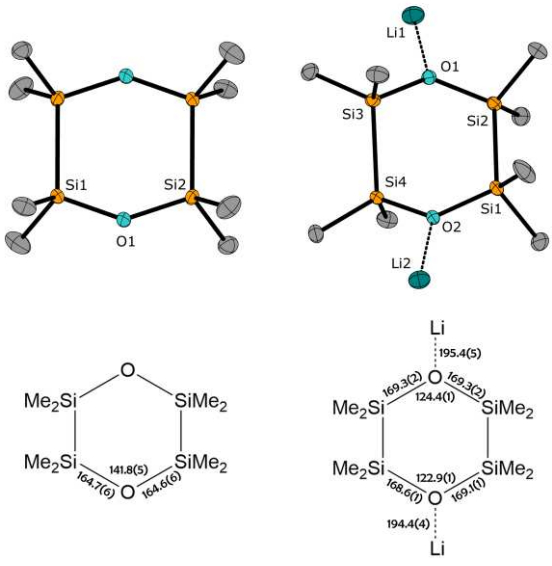

Figure 1: Structural comparison of the molecular structures of **I** and **II** in the crystal. Thermal displacement ellipsoids represent the 50% probability level. Half a molecule of **I** is symmetry-generated over 1-x, 1-y, 1-z. Hydrogen atoms as well as attached $[GaI_4]^-$ anion of **II** are omitted for clarity. Bond lengths are depicted in [pm] and angles in [°].

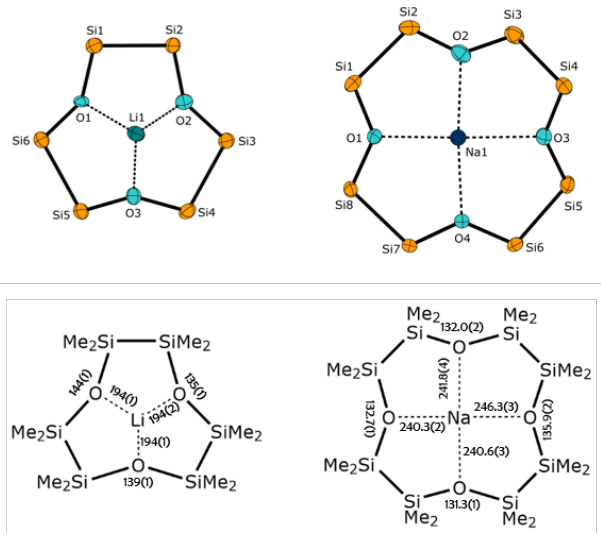

Figure 2: Comparison of the geometric features of alkali metal complexes of inorganic crown-ethers. The molecular structures of **1** (left) and **2** (right) in the crystal are reduced to the inorganic skeleton. Anions as well as disordered parts are omitted for clarity. Thermal displacement ellipsoids represent the 50% probability level. Atom distances are depicted in [pm] and angles in [°].

Comparing the observed resonance with that found for **I** [$\delta(^{29}Si)$ = 3.6 ppm] proves the interaction of **I** with Li^+ in solution. From this respective intermediate product, we concluded that ring opening requires effective Si-O bond activation and we repeated the reaction procedure with 2.0 eq of $LiGaI_4$ and longer reaction times. Stirring **I** and $LiGaI_4$ or isolated **II** in Ph-F overnight at 70°C selectively yields the compound $[Li(^2D_3)GaI_4]$ (**1**) ($^2D_3$ = $(Me_4Si_2O)_3$ *e.g.* 1,2,4,5,7,8-hexasila[9]crown-3) under precipitation of the excess $LiGaI_4$ as a white powder. The reason is most likely the effective Si-O bond activation of **I** which causes a significant change in the bonding situation of the Si-O linkage. For **II**, the Si-O-Si angles are smaller and the Si-O distances are longer than for **I** due to coordination. As can be seen from a redetermined crystal structure of **I**, the Si-O bond lengths measure 164.6(6) and 164.7(6) pm (Figure 1: left). The respective Si-O-Si angle measures 142.1(5)°. In the presence of $LiGaI_4$, the Si-O atom distances are elongated to values of 168.6(1) and 169.3(1) pm. The Si-O-Si angle is reduced to values of 122.9(1) and 124.4(1)° indicating a high basicity towards the Li^+ center and a diminishing of $n_O \rightarrow \sigma^*_{Si\text{-}C}$ backbonding (Figure 1: right). The Si-O bond is thus activated and *Lewis*-acidic Si-centers can be more easily attacked by nucleophiles such as I^-. Compound **II** clearly shows the pre-coordination of an s-block metal center as a crucial step before the precursor is ring-opened to form a silicon-based crown-ether. Li^+ templated ROP yields **1**, in which the silicon based crown ether $^2D_3$ is threefold coordinating the lithium ion (Figure 2, left). With an Li-I atomic distance of 287(1) pm, a monomeric contact ion pair is observed. As the Si-Si bonds in **1** measures 235.6(6) to 241.3(6) pm it is clear that the cavity of silicon based crown ethers is much larger than the cavity of purely organic ones.

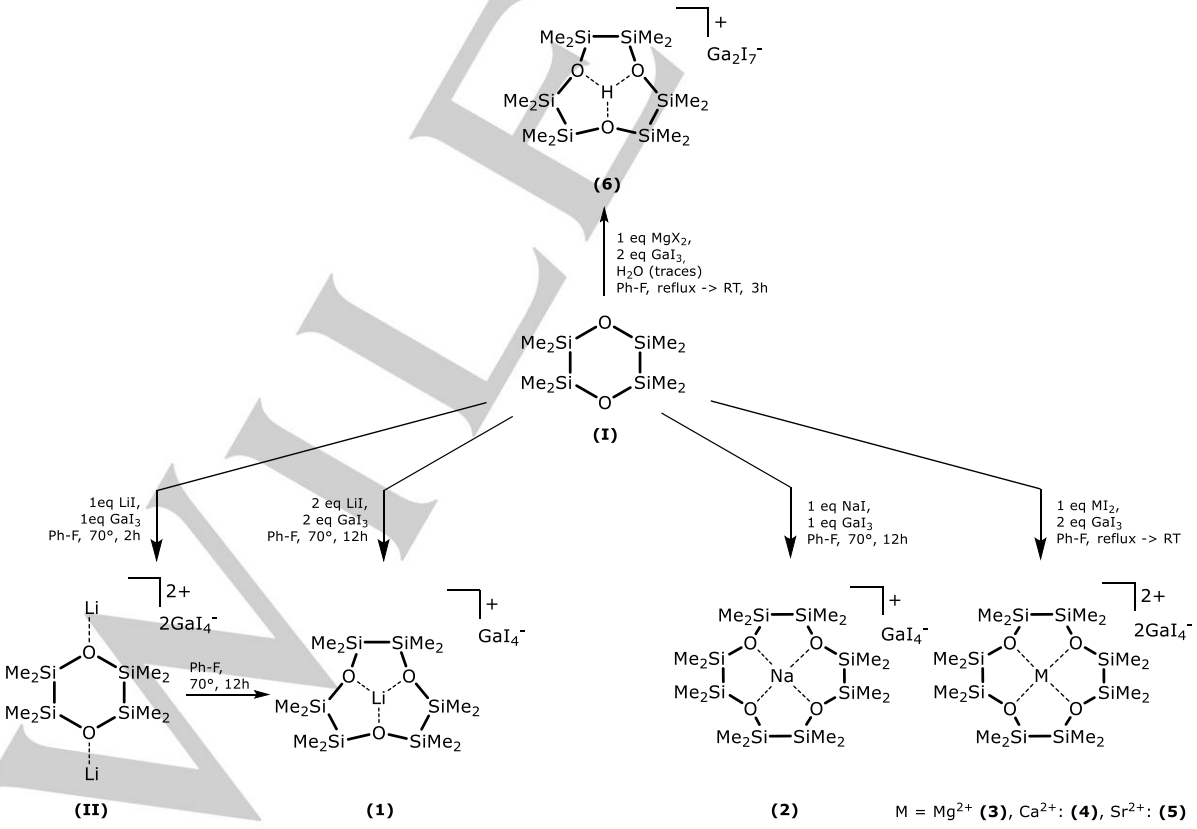

Scheme 2: Synthesis of inorganic crown-ether complexes of the s-block elements.

[9]crown-3, the smallest member of the crown-ether family is barely used for coordination chemistry and for this reason complexes of this ether are rare. The Li^+ ion in $[Li(naphtho[9]crown\text{-}3)_2]ClO_4$, for instance, is located 139.5 pm above the spanned mean plane.[64] In **1**, the Li^+ ion is much more sunken into the cavity of the ligand as it is now 69.2 pm above the spanned plane of the oxygen atoms. Due to a lower coordination number at Li^+, the O-Li atom distances are slightly smaller as for example in $[Li(D_6)Al_F]$ (Al_F = $[Al(OCCF_3)_4]^-$) (194(1) – 194(2) pm in **1** and 201(1) – 208(1) pm in the D_6 complex). The Si-O-Si angles of **1** vary from 135(1) to 144(1)°. Thus, the ligands' architecture in the complex bears Si-O-Si angles comparable with those in the mentioned D_6 complex where Si-$O_{coord.}$-Si angles of 139.5(4)-141.6(4)° are present. In CD_2Cl_2 solution, the ^{29}Si NMR resonance is shifting towards even lower field as a single resonance of 15.5 ppm is observed for **1** which compares very well with the hybrid crown-compound [Li(1,2,4,5-tetrasila[12]crown-4)OTf] where a single resonance is observed at 15.9 ppm for the inner Si-atoms. As can be seen from both structures **II** and **1,** the siloxane coordination highly depends on the reaction conditions with exocyclic metal-coordination as a crucial step due to Si-O bond activation. Metal templation then enables the formation of a macrocycle which in turn enables a higher number of silyl-ether contacts. To obtain a larger inorganic crown-ether, the Na^+ ion was chosen for macrocycle-formation and $^2D_2$ was converted with one equivalent of sodium iodide as well as one equivalent of GaI_3 employing similar reaction conditions as for **1**. Indeed the larger silicon based crown ether $^2D_4$ ($^2D_4$ = $(Me_4Si_2O)_4$ *e.g.* 1,2,4,5,7,8,10,11-octasila[12]crown-4) is formed (Figure 2, right). The solid state structure of $[Na(^2D_4)GaI_4]$ (**2**) shows a sodium ion bound by all of the crown ethers oxygen atoms in coplanar fashion. The cavity is now enlarged to such extent, that the twelve-membered cycle is capable of binding a larger sodium ion in-plane ($r_i[Na^+]_{CN5}$ = 100 pm)[65].

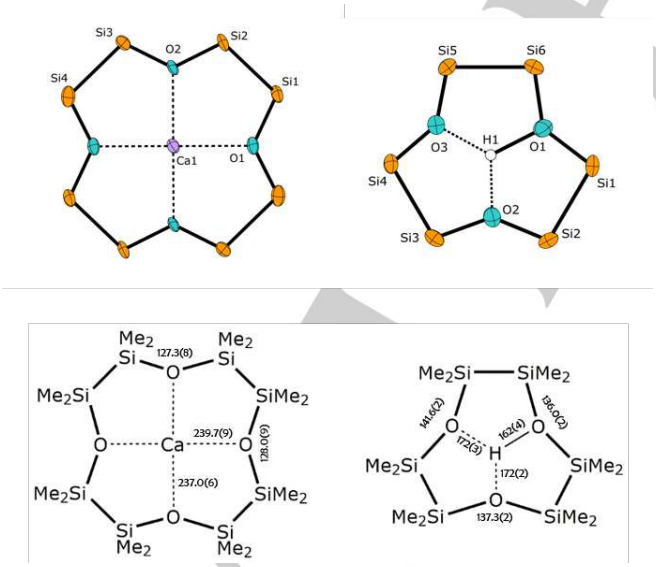

Figure 3: Comparison of the geometric features of an alkaline earth metal and proton complex of an inorganic crown-ether. The molecular structures of **4** (left) and **6** (right) in the crystal are reduced to the inorganic skeleton. Anions as well as disordered parts are omitted for clarity. Thermal displacement ellipsoids represent the 50% probability level. Non-labelled atoms are symmetry generated over 1-x, 1-y, 1-z. Atom distances are depicted in [pm] and angles in [°].

The Si-O-Si angles measure 131.3(1) to 135.9(2)° which compare well with the Si-O-Si angle in [Na(1,2,4,5-tetrasila-benzo[15]crown-5)I].[44] In solution, the ^{29}Si-NMR resonance is observed at 13.1 ppm in deuterated dichloromethane and reveals ligand-metal interaction also present in solution. At this point we also employed the in-situ generated, higher homologous alkali-metal salts $MGaI_4$ (M = K^+-Cs^+) but all our attempts to isolate respective crown-ether complexes failed so far as we could only observe **I** by means of multinuclear NMR spectroscopy. This is probably due to the nature of the respective cations which are too soft and are not activating the Si-O bond properly for ROP. For this reason, we also employed the harder alkaline earth metals for the synthesis of such inorganic crown-ethers. The alkali-metal ions Mg^{2+}-Sr^{2+} turned out to be suitable templates yielding $[M(^2D_4)(GaI_4)_2]$ (M = Mg^{2+} (**3**), Ca^{2+} (**4**), Sr^{2+} (**5**)) but crystal structures could only be obtained for **4** and **5**. Salts of Be^{2+} and Ba^{2+} had also been reacted with **I**. Whereas beryllium halides form literature-related[57] polyolate complexes which will be published in due course, $Ba(GaI_4)_2$ shows no reactivity towards $^2D_2$. **4**·DCM crystallizes as colorless planks in the triclinic crystal system, space group *P*-1 (Figure 4, top). As also observed in **2**, the metal ion is situated in plane but the Si-O-Si angles are smaller in comparison to **2** (131.3(1) to 135.9(2)° in **2** and 126.9 to 127.9° in **4**) and the O_{Si}-M atom distances are shorter (240.4-246.3 as in **2** and 236-240 pm as in **4**). Thus, silyl ether bonding of this silicon based macrocycle is stronger towards the group 2 metal cation and the ligand shows an enhanced basicity even though there are now two metal-anion interactions which are known to perturb silyl ether coordination.[40] These values compare well with the atom distances as well as Si-O-Si angles found in the hybrid crown-ether complex [Ca(1,2,4,5-tetrasila-benzo[15]crown-5)I_2].[44] In solution, a distinct low-field shifted resonance of 19.2 ppm is observed which proves the strong coordination of the ligand in solution. Interestingly and in contrast to all other herein characterized compounds, **4** is stable towards moisture as $[Ca(^2D_4)(GaCII_3)_2]$ (**4a**) crystallizes in an NMR tube from CD_2Cl_2 solution exposed to moisture (see Figure S11). The ligand moiety is maintained at air and the metal center remains inside the cavity. Stabilization may come from the halogen exchange with the solvent. The crystal structure determination of the Sr^{2+} species **5** had been a challenge. The compound reveals an intrinsically disorder-problem and the only suitable crystals for SC-XRD could be grown from a Ph-F solution so no other solvents could be applied. We were still able to determine the molecular structure but have in this case used a completely restrained model to fix the refinement with $P2_12_12_1$ as the most suitable space group (Figures S6 and S9). In solution, the respective singlet of **5** in ^{29}Si NMR spectroscopy is observed at 16.6 ppm proving strong interactions of the Si-O moiety with Sr^{2+}.

As above-mentioned, for compound **3** no crystal structure could be obtained. This is most likely due to the very high sensitivity of the compound. The compound can only be obtained using MgI_2 which purity is 99.996% (denoted as 'ultra dry'). We could detect several decomposition products (compounds S1-2) while attempting to determine the crystal structure of the compound (see ESI for a comment and brief discussion). However, one respective compound was obtained which aroused our special interest. We were able to obtain and characterize a compound of a caged proton in $^2D_3$. $[H(^2D_3)]Ga_2I_7$

(**6**) was obtained after contaminating a Ph-F solution of **3** with immersion oil which is basically used for preparing single crystals for SC-XRD. The compound could be reproduced employing various reaction conditions, the most suitable routes are converting $^2D_2$ with MgI_2 (>98% purity) and GaI_3 in *α*,*α*,*α*-trifluorotoluene or with $MgCl_2$ (>99% purity) and GaI_3 in Ph-F whose date of destillation is past more than one week. We assume that the formation of a GaI_3/MgX_2 *Lewis*-acidic system can activate smallest traces of H_2O to such extent that protons are readily served to the silyl-ether. The Mg^{2+} is released in the favor of complexing the "naked" proton. The small proton can act as a template as well, forming $^2D_3$ from $^2D_4$ or directly from $^2D_2$. The field of proton complexes has been reviewed by *Chambron* and *Meyer*[66] but as outlined, proton complexes are limited to organic-type ligands. Most of them resemble crown ether- or cryptand-like macrocycles. A handful of open-chained complexes are also characterized[67–69] but compound **6** is the very first example of proton coordination within a cyclic siloxane. Crystals of **6** generally exhibit a high quality so that it was possible to determine the molecular structure precisely. The encircled proton was located and refined as an independent isotropic atom in the middle of the crown-ether moiety. Due to oscillation of the refined hydrogen atom, very soft SADI (SADI = same atomic distance) restraints were employed, though. Within the standard deviation, however, the O···H atom distances are much larger than those in the above mentioned crown-ether and cryptand compounds[66] or diverse silanols[70] and silanolates[71] proving the existence of a threefold coordination of the hydrogen atom. The observation of NMR signals of **6** in solution turned out to be a challenge due to rapid formation of various decomposition products (see ESI, p. S36-S37). Fortunately, with enough amount of crystals of good quality, we were able to carry out multinuclear NMR spectroscopy. In the ^1H spectrum, a major signal at 0.52 ppm was observed, which was readily assigned to the Me_2Si-O-$SiMe_2$ moiety. In addition, two broad signals at 7.89 and 9.38 ppm were observed. An integral of these signals revealed relative intensities of 36 : 0.8 : 0.5. We proposed these two broad signals to be due to the trapped proton. The observation of twin resonance signals was also reported for protons trapped in crown ethers.[72] Our efforts tried to obtained long-range correlation and exchange spectroscopy failed. Nevertheless, we observed the disappearance of these two signals together with the major signal at about 3 hours after sample preparation, which may serve as an indirect evidence to our proposed assignment. Protonated siloxane-linkages are very rare in general. To the best of our knowledge, there are only two structurally characterized disiloxoniumions, one from *Sekiguchi*[73] and the other one from *Müller*[74]. Even though the Brønstedt acid/base chemistry is not exactly part of our study we want to emphasize that this compound might be interesting in a context of proton chelators. Siloxanes prove to be an interesting new possibility to establish such a chemistry, even though siloxanes were long-time assumed to be not very basic at all. Investigations on siloxane acids and various *Lewis*-acidic systems, however, should be part of future research so further studies are underway.

To shortly sum up, the herein characterized compounds are obtained by Si-O bond activation and complexes of inorganic crown-ethers are stable as evident from SC-XRD and ^{29}Si NMR. As the cavities of the Si-based ligands are much larger than those of the organic counterpart, the cation selectivity, however, is substantially different to that known from organic crown-ethers: H^+ and Li^+ are coordinated by Si_6[9]crown-3 instead of [12]crown-4 and Na^+, Ca^{2+}, Sr^{2+} are coordinated by Si_8[12]crown-4 instead of [3n]crown-n (n = 5, 6) according to the solid state structures.

NMR spectroscopic investigations

Due to the fact that solid-state structures are not inevitably represented in solution, especially when molecules have a high tendency to form oligomers[75] like the compounds herein, further investigations are necessary to proof existence of the respective ligand moiety in solution. By taking advantage of the pulsed field gradient (PFG), diffusion ordered spectroscopy (DOSY) experiments provide us diffusion coefficients of molecules in solution. Thus, in related works, PFG diffusion experiments proved to be powerful in study of various aggregates in solution.[75,76] According to *Stoke-Einstein* equation the size of the molecules under study can be determined. Stejskal-Tanner plots are used to display the diffusion behavior of molecules in solution, whereby the attenuation of signal intensities in response to the applied gradient strength is plotted in logarithmic scale.[77,78]

Table 1. NMR Chemical Shifts and diffusion coefficients in CD_2Cl_2 at 298 K.

compound	^1H (ppm)	^{13}C (ppm)	^{29}Si (ppm)	D^{exp} (10^{-9} m^2s^{-1})	r_{exp} (Å)[a]	r_{cal} (Å)
$^2D_2$ (**I**)	0.20	2.6	3.6	1.53	3.5	3.5[b]
$[Li_2(^2D_2)]^{2+}$ (cation of **II**)	0.36	2.7	8.7	1.21	4.4	4.3[b]
$[Li(^2D_3)]^+$ (cation of **1**)	0.47	3.1	15.5	1.03	5.1	4.7[b]
$[Na(^2D_4)]^+$ (cation of **2**)	0.45	2.9	13.1	0.99	6.0	5.2[b]
$[Mg(^2D_4)]^{2+}$ (cation of **3**)	0.71	3.5	25.7	0.87	6.1	n.d.[c]
$[Ca(^2D_4)]^{2+}$ (cation of **4**)	0.47	4.0	19.2	0.87	6.1	5.6[d]
$[Sr(^2D_4)]^{2+}$ (cation of **5**)	0.64	4.4	16.6	0.86	6.1	5.2[d]
$[H(^2D_3)]^+$ (cation of **6**)	0.52	1.7	21.2	1.09	4.9	4.4[d]

[a]Hydrodynamic radius based on the experimental diffusion coefficients measured in CD_2Cl_2 at 298 K and Stoke-Einstein equation $D = k_BT/6\pi\eta r$. [b]Radius calculated from molecular hard-sphere volume increments.[79] [c]Not determined. [d]Radius estimated from X-Ray.

Therefore, the slope of the *Stejskal-Tanner* plot corresponds directly to the diffusion coefficient of the molecule. For example, an overlay of the Stejskal-Tanner plots of the solvent CD_2Cl_2, $^2D_2$ (**I**), the Li^+ complex of a nine-membered macrocycle $[Li(^3D_2)]^+$ and the sodium complex of a twelve-membered macrocycle $[Na(^4D_2)]^+$ is shown in Figure S51 which demonstrates clearly the correlation of ligand size with the respective cation incorporated. The obtained diffusion coefficients for all herein characterized compounds and the molecular radii are summarized in Table 1. In this study, the so obtained molecular radii agree well with those of the molecules in solid-state.

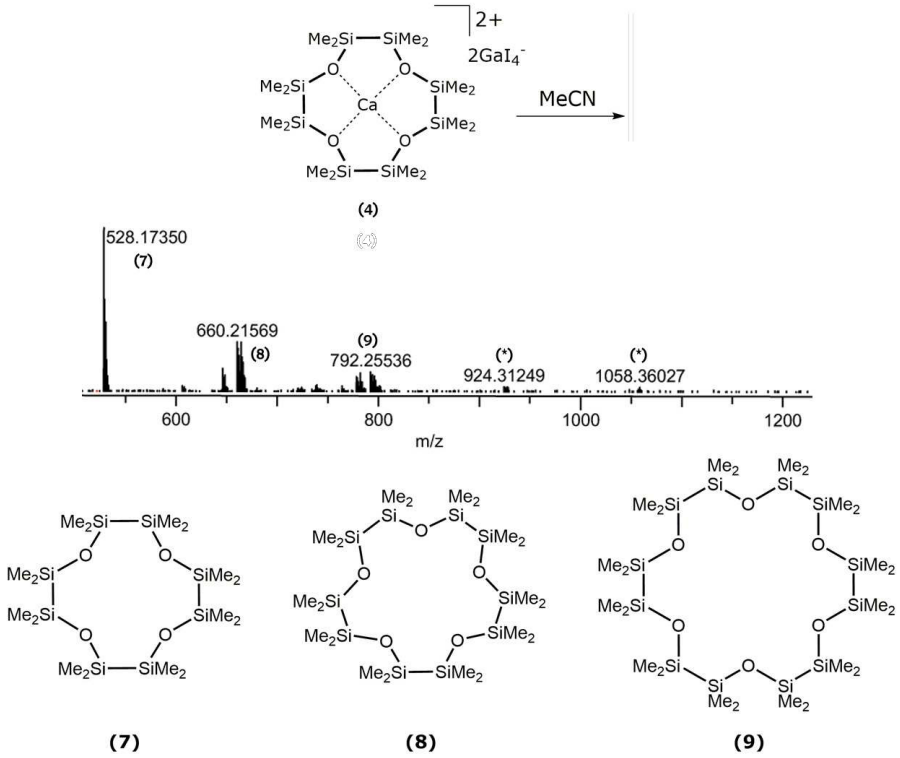

Scheme 3: LIFDI(+) MS spectrum of a ^2D_n mixture after conversion of compound (4) with MeCN. Compounds (**7**)-(**9**) were detected as $^+$-species. For the respective HR-MS spectra, please see the SI. The m/z relations marked with asterisk (*) can tentatively be assigned to even higher oligomers of $^2D_2$ such as $^2D_7$ and $^2D_8$, but no suitable HR-MS was obtained due to poor signal to noise ratio.

We verified that the compounds $[Li_2(^2D_2)]^{2+}$ and $[Li(^2D_3)]^+$ bear a six- and nine-membered (macro-)cyclic ligand in solution, while $[Na(^2D_4)]^+$, $[Mg(^2D_4)]^{2+}$, $[Ca(^2D_4)]^{2+}$ and $[Sr(^2D_4)]^{2+}$ all bear a twelve-membered macrocyclic ligand in solution.

Extraction of unoccupied ^2D_n ligands

As we have convincingly shown inorganic, macrocyclic complexes are obtained and are, except for compound **6**, somewhat stable in solution. A remaining question at this point is, if the cation which is used for the template synthesis can be removed from the respective ligands to obtain a free ligand species. For this purpose, we have chosen compound **4** as it shows the highest stability in general and the yields, when synthesizing **4**, are fine. After isolating the crystalline product **4**, the crystals were dissolved in MeCN which is a strong donor solvent. It could be observed by means of ^{1}H NMR spectroscopy, that the metal ion is indeed readily displaced in the favor of MeCN coordination. Adding *n*-pentane to a MeCN/$[Ca(^2D_4)GaI_4]$ solution results in the formation of two separate phases. The sila ligands can therefore be extracted from the mixture by carefully separating the n-pentane solution from the MeCN solution. After workup procedures, an oily residue is obtained from the *n*-pentane phase. NMR spectroscopy revealed, that the oil contained several species indicating that free ligand $^2D_4$ is not stable without a suitable template as partial ring cleavage occurred during the extraction process. The ^{1}H NMR spectrum (CD_2Cl_2, 300MHz, 300 K) shows overlapping resonances at 0.16, 0.17 and 0.20 ppm. These respective peaks can be tentatively assigned to $^2D_4$ (**7**, 0.16 ppm), $^2D_5$ (**8**, 0.17 ppm) and $^2D_2$ (0.20 ppm). This assignment is supported by ^{1}H-^{29}Si HMBC, ^{1}H-^{13}C HMQC and especially due to combined LIFDI$^+$ MS (LIFDI = liquid injection field desorption ionization; MS = mass spectrometry) studies. The main product of a freshly prepared ^2D_n mixture according to the LIFDI$^+$ MS is $^2D_4$ (relative abundance of 100%, calc. 528.17067 m/z; found 528.17196 m/z), and thus the ^{1}H NMR main peak at 0.16 ppm and the respective correlating peaks from ^{13}C and ^{29}Si NMR are assigned to $^2D_4$ (^{13}C NMR: 2.38 ppm, ^{29}Si NMR: 0.4 ppm). $^2D_5$ (relative abundance of 30%, calc. 660.21334 m/z; found 660.21494 m/z) is therefore assigned to the ^{1}H NMR peak of 0.17 ppm and its respective correlations (^{13}C NMR: 2.35 ppm, ^{29}Si NMR: 0.9 ppm). The peak at 0.20 ppm and the respective correlations (^{13}C NMR: 2.36 ppm, ^{29}Si NMR: 3.4 ppm) could be assigned to **I** as we were using this as our starting material and the resonances compared well with it.[80] LIFDI$^+$ MS further proofs the existence of $^2D_6$ (**9**) in traces (relative abundance of 8%, calc. 792.25601 m/z; found 792.25693 m/z). As evident from the small relative abundance it is most likely that these traces were to small to detect the compound by means of NMR spectroscopy. As the HR-MS spectrum compares well with the calculated one, it is clear that this compound is also part of the extracted oil and/or is formed under gas-phase conditions. Is the oil considered as a mixture of $(Me_4Si_2O)_n$ (n = 2-6), the turnover to free ligand species is quantitative which is evident from NMR spectroscopy as coordinated species are found no longer upon MeCN addition. In solution, free ligand species are in equilibrium: another measurement of the same sample revealed, that the amounts of the respective species change. As there is $^2D_4$ the main product right after the extraction, there is $^2D_5$ the main product after four days. Also, the integral of $^2D_2$ has higher

values, indicating that also the starting material **I** is formed by time. That the equilibrium is on the side of **I** is proved by another ^{1}H NMR experiment after nine weeks, where exclusively **I** is found to be present. Hence, we observe a reversible reaction behavior here. We assume this back-reaction to be entropically driven as quantum chemical calculation of the reaction of $^2D_2$ + $^2D_2 \rightarrow {}^2D_4$ is enthalpically insignificant (see next section).

This ligand behavior might serve as an interesting possibility in terms of separation techniques. The precursors are recognizing hard metal ions, forming specific ligands which are efficiently binding the metal cation. When separated from a bulk and treated with MeCN, ligands can be replaced and the starting material is recycled by time. Another cycle for ion extraction can in principle be established. The evaluation of such a system is about to be examined in more detail and will be part of upcoming work. From the respective observations herein, we were able to detect even higher oligomers of **I** such as Si_{10}[15]crown-5 ($^2D_5$) and Si_{12}[18]crown-6 ($^2D_6$) could in general show that it is possible to obtain the oligomerized ligand from the complex. Back-reaction of the starting material slowly occurs when the template is removed.

Quantum chemical calculations

Quantum chemical calculations were carried out estimate the ability of the different ^2D_n-type species to coordinate M^+ ions, also relative to D_n-type species as well as to crown ethers. Further, they were done to shed light on the formation of larger rings from $^2D_2$, in particular on the role of Na^+ and GaI_4^- for this process. The first issue was tackled by the calculation of energies for exchange reactions of the type

$$[ML_2]^+ + L_1 \rightarrow [ML_1]^+ + L_2$$

which directly allow for a comparison of the attractivity of L_1 and L_2 for a metal ion M^+. These reactions were calculated for L = $^2D_2$, $^2D_3$, $^2D_4$, D_5, D_6, as well as for the crown ethers [3*n*]-crown-*n*, *n* = 4, 5, 6 and for M = Li, Na. The calculations were done for reactions in the gas phase as well as in solvents with dielectric constants ε = 6 and ε = 9 (oriented at Ph-F and DCM) within the conductor-like screening model (COSMO[81]). For instance, for L_1 = $^2D_4$, L_2 = $^2D_3$, the reaction energy for the gas phase (ε = 1)

$$E_{M,\varepsilon}(L_1,L_2) = E_\varepsilon(L_1M^+) + E_\varepsilon(L_2) - E_\varepsilon(L_2M^+) - E_\varepsilon(L_1) \quad (1)$$

amounts to −65(−35) kJ/mol for M = Na(Li). Thus, for both metal types $^2D_4$ is significantly more attractive than $^2D_3$. When including solvent effects (ε = 6), this preference is less pronounced, −35(−17) kJ/mol. All reaction energies are listed in Tables S5−S8 in the Supporting Information in compact manner, for the gas phase also for other functionals, yielding similar results. For a more comprehensive picture – and finally for ranking the M^+ affinity for each ligand L_i with respect to the other seven ligands L_j, it is helpful to calculate the corresponding average reaction energies according to equation (2).

$$\bar{E}_{M,\varepsilon}(L_i) = \frac{1}{7}\sum_{\substack{j=1 \\ j\neq i}}^{8} E_{M,\varepsilon}(L_i,L_j) \quad (2)$$

The energies $\bar{E}$ are listed in Table 2 for M = Li, Na for ε = 1 (gas phase) and ε = 6 (the latter yields results very similar to ε = 9 see Tables S5−S8).

Table 2. Average reaction energies according to equations 1 and 2 in kJ/mol. Negative values indicate overall preference for the corresponding ligand to bind Na/Li in the gas phase (ε = 1) or in a solvent with ε = 6. C_n is a short-hand notation for [3*n*]-crown-*n*.

	$^2D_2$	$^2D_3$	D_5	$^2D_4$	D_6	C_4	C_5	C_6
Li, ε=1	155	1	16	-39	-22	-24	-55	-31
Na, ε=1	121	30	11	-45	-24	25	-20	-99
Li, ε=6	91	8	24	-11	-7	-35	-55	-16
Na, ε=6	60	30	16	-11	-8	1	-26	-63

As expected, lowest values for $\bar{E}$, and thus highest tendencies to incorporate M^+, are observed for [15]crown-5 or [18]crown-6, depending on M and ε. $^2D_4$ and D_6 both show similar trends for $\bar{E}$ which are in the range of C_5 for the gas phase. They are preferred over $^2D_3$ or D_5. The binding of M^+ to $^2D_2$ is clearly de-preferred. This de-preference is less pronounced for ε = 6, as for $^2D_2$ the M^+ is outside the ring and thus the stabilization by the solvent is larger for $^2D_2$ than for the other ligands.

The formation of larger rings from smaller ones was investigated exemplarily for $^2D_4$ formed from two $^2D_2$ rings. The energy gain for the (hypothetic) reaction $^2D_2$ + $^2D_2 \rightarrow {}^2D_4$ is insignificant, –4 kJ/mol. Matters are different as soon Na is present. The energy of the corresponding reaction, $[Na^2D_2]^+ + {}^2D_2 \rightarrow Na^+ + [Na(^2D_4)]^+$, amounts to –149 kJ/mol for ε=1, and still –50 kJ/mol for ε = 6. So, the presence of M^+ obviously is the driving force for the reaction. Instead of starting from $[Na(^2D_2)]^+$ + $^2D_2$, it is more realistic to start from a complex where Na is bound to two $^2D_2$ rings, $[Na(^2D_2)_2]^+$, see Figure 5 (top left). This which is favored towards $[Na(^2D_2)]^+$ + $^2D_2$ by 102(11) kJ/mol for ε = 1(6). Consequently, the formation of $[Na(^2D_4)]^+$ from this complex is exothermic by 47(39) kJ/mol.

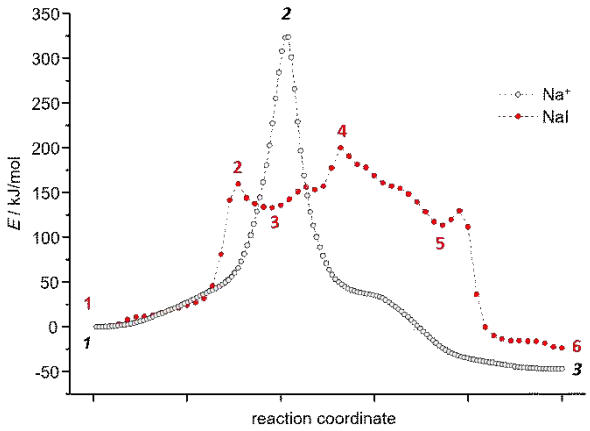

Figure 4: Energy profiles for the pathways from $[Na(^2D_2)_2]^+$ to $[Na(^2D_4)]^+$, black with italic numbers, and from $[NaI(^2D_2)_2]$ to $[NaI(^2D_4)]$, red. The numbers label the structures shown in Figure 5.

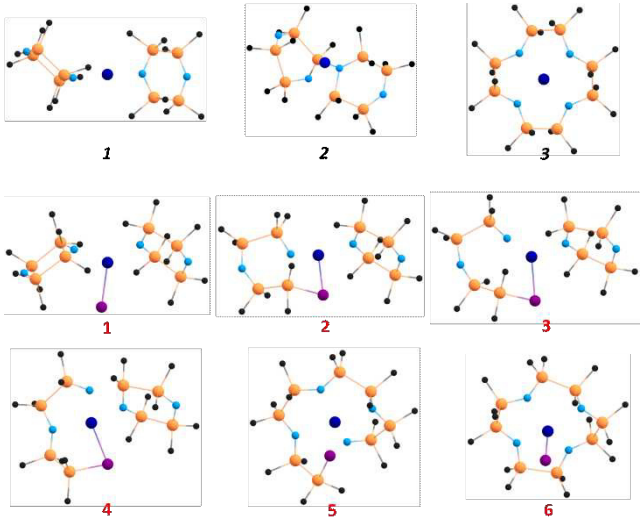

Figure 5: Extremum structures for the pathways from $[Na(^2D_2)_2]^+$ to $[Na(^2D_4)]^+$, first row, with black italic numbers, and from $[NaI(^2D_2)_2]$ to $[Na(^2D_4)I]$, second and third row, with red numbers. The numbers refer to the labelling in Figure 4. Hydrogen atoms are omitted for clarity.

Nevertheless, of course a significant energy barrier is expected, which is investigated in detail now. The pathway (=P) P(Na^+) for the transformation from $[Na(^2D_2)_2]^+$ to $[Na(^2D_4)]^+$ was optimized with the method proposed by *Plessow*.[82] Moreover, the pathway P(NaI) from $[NaI(^2D_2)_2]$ to $[NaI(^2D_4)]$, P(NaI), was treated in order to clarify the influence of the presence of I^-, as model for GaI_4^-. The energy profiles for P(Na^+) and P(NaI) are shown in Figure 4, selected intermediate structures for P(Na^+) and P(NaI) are displayed in Figure 5. Movies of these transformation pathways and corresponding data for a model where Me was replaced with H are available in the Supporting Information, Figures S57 – S58, together with details of the optimization. P(Na^+) exhibits a single barrier, see Figure 4. As shown in Figure 5 (first row, middle), at the maximum energy point one Si atom of the right $^2D_2$ unit gets in contact with an O atom of the left $^2D_2$ unit which leads to the opening of one Si-O bond in the former, accompanied by the formation of a second bond between the two units. In this way the electronic closed-shell character is maintained along the rearrangement, yet the barrier is quite high, 324 kJ/mol. For P(NaI) matters are different. The I^- ion approaches an Si atom of the left $^2D_2$ unit (point 2), which simultaneously opens the Si-O bond in this ring. This requires ca. 160 kJ/mol, that is half of the energy for opening the corresponding bond in P(Na^+).Next, the dangling O atom approaches an Si atom of the right $^2D_2$ unit, which, after slight rearrangement of the Me groups (point 4), enables the formation of a bond between the two units and simultaneously opens one Si-O bond in the second ring (point 5). The re-connection of I to Na is accompanied with the formation of the second bond between the units without a significant barrier. With COSMO (ε = 6) the energy profile is qualitatively the same, but for P(Na^+) the barrier is somewhat lower, 294 kJ/mol; P(NaI) is almost unchanged, see Figure S61 in the Supporting Information. Overall, the calculations show that the presence of I^- facilitates a mechanism with a barrier that is less than half as high as that for the mechanism without I^-.

Experimental Part

General Information

All manipulations were carried out with rigorous exclusion of oxygen and moisture using basic Schlenk techniques under argon gas if not stated otherwise. Solvents were dried and freshly distilled before use and subsequently stored over molecular sieve (3Å). The siloxane $^2D_2$ (**I**) was synthesized by a reported method in literature,[80] but was sublimated from P_2O_5. The alkali metal salts NaI (acros organics, ≥99%) and LiI (Alfa Aesar, 99.996%), the alkaline earth metal salt MgI_2 (Sigma Aldrich, 98% and alfa aesar, ≥99.99%, ultradry), $MgCl_2$ (Alfa Aesar, ≥99.99%, ultradry), CaI_2 (Alfa Aesar, 99.5%), SrI_2 (Sigma Aldrich ≥99.99%), and GaI_3 (abcr, 99%) were used as received. All parceled salts were received as packed under argon and handled under argon atmosphere using a MBraun glovebox.

In all respective reactions we strictly avoided the use of silicon-grease. Silicon grease is a potential monosilane source and is cleaved and/or complexed by the salts used herein.[38,39,43,45,46,60,61,83–85] For all glass valves and joints we therefore used PTFE paste (Carl Roth). NMR measurements were performed on Bruker AVIII HD 300 with a BBO probe and Bruker AVIII 500 with a cryo probe Prodigy BB-H&F with z-gradient at 298 K. DOSY experiments were done using the double stimulated echo method with long eddy current delay.[86] The gradient shape used was smoothed square SMSQ10.100 and gradient length (δ) was between 1 and 2 ms. The optimized diffusion delays (Δ) were between 30 and 50 ms. Diffusion attenuation was realized with 9 to 10 steps in gradient ramp. The DOSY 2D spectra were recorded with 9 to 10 experiments and each with 16 to 32 transients. Relaxation delays were 3 s. Spectra were processed with Bruker software package Topspin 4.0. Infrared (IR) spectra of the respective samples were measured using attenuated total reflectance (ATR) mode on the Bruker-type spectrometer Alpha FT-IR. The OPUS software package was applied throughout. ESI mass spectra were acquired with a LTQ-FT Ultra mass spectrometer (Thermo Fischer Scientific). The resolution was set to 100.000. Elemental analysis was performed on a Vario MicroCube. No suitable CHN analysis was obtained for **3** which we attribute to the very high sensitivity of the compound.

Synthesis and Crystallization

$[Li_2(^2D_2)(GaI_4)_2]$ (**II**). 0.034 g of LiI (0.25 mmol, 1.00 eq) are suspended in 8 mL of Ph-F. Subsequently, 0.114 g of GaI_3 (0.25 mmol, 1.00 eq) are added. The suspension is vigorously stirred for 30 min. and several times gently warmed to reflux. Then, at ambient temperature, 0.100 g of **I** (0.38 mmol, 1.5 eq) are added and the obtained solution is stirred at 70°C for 2h. The solvent is removed under reduced pressure and 10 mL of DCM are added. The suspension is then filtered and reduced until saturation is reached. Placing the solution at -32°C for three days yields colorless planks of **1**·DCM. After decantation and drying in fine vacuum, **1** is obtained as a colourless powder (0.147 g, 82%).
^{1}H NMR: (300 MHz, CD_2Cl_2) δ = 0.36 (s, 24H, Si(CH_3)$_2$) ppm. ^{7}Li NMR δ = -1.66 (177 MHz, CD_2Cl_2) ppm. ^{13}C{^{1}H} NMR: (75 MHz, CD_2Cl_2) δ = 2.7 (s, SiCH_3) ppm. ^{29}Si NMR: (99 MHz, CD_2Cl_2) δ = 8.7 (s, *Si*(CH$_3$)$_2$) ppm. IR (cm^{-1}): 2950 (w), 2890 (vw), 1431 (vw), 1397 (w), 1255 (s), 925 (w), 877 (s), 852 (s), 803 (s), 780 (vs), 739 (s), 683 (m), 665 (m), 645 (m), 579 (s). CHN calcd. for $C_8H_{24}Ga_2I_8Li_2O_2Si_4$·DCM C, 7.12; H, 1.73; found C, 7.70; H, 1.86.

[Li(²D₃)(GaI₄)] (**1**). 0.051 g of LiI (0.38 mmol, 2.00 eq) are suspended in 8 mL of Ph-F. Subsequently, 0.171 g of GaI_3 (2.00 eq, 0.38 mmol) are added. The suspension is stirred for 30 min. several times gently warmed to reflux. Then, at ambient temperature, 0.050 g of **I** (0.19 mmol, 1.0 eq) are added. The obtained solution is warmed to 70°C and stirred overnight. The solvent is then removed under reduced pressure and 10 mL of DCM are added. After filtration and removing the solvent under reduced pressure, a colorless to light beige powder is obtained (0.101 g, 54%) as a colorless powder. For single crystal growth, **1** was dissolved in DCM and a saturated solution was placed at -32°C. Colorless blocks of **2** are obtained after a few days.
^{1}H NMR: (300 MHz, CD_2Cl_2) δ = 0.47 (s, 36H, Si(C*H*$_3$)$_2$) ppm. ^{7}Li NMR δ = 0.38 (177 MHz, CD_2Cl_2) ppm. ^{13}C{^{1}H} NMR: (75 MHz, CD_2Cl_2) δ = 3.1 (s, Si*C*H$_3$) ppm. ^{29}Si NMR: (99 MHz, CD_2Cl_2) δ = 15.5 (s, *Si*(CH$_3$)$_2$) ppm. IR (cm^{-1}): 2948 (w), 2888 (vw), 1404 (w), 1254 (m), 1086 (vw), 1021 (vw), 944 (vs), 853 (m), 810 (m), 781 (s), 719 (w), 686 (m), 536 (w), 484 (m), 456 (w). CHN calcd. for $C_{12}H_{36}GaI_4LiO_3Si_6$ C, 14.69; H, 3.70; found C, 14.63; H, 3.77.

[Na(²D₄)(GaI₄)] (**2**). 0.042 mg of NaI (0.28 mmol, 1.00 eq) are suspended in 8 mL Ph-F. Subsequently, 0.128 g of GaI_3 (1.00 eq, 0.28 mmol) are added. The yellow suspension is then stirred for 30 min. and several times gently warmed to reflux. Then, at ambient temperature, 0.075 g of **I** (0.28 mmol, 1.0 eq) are added. The obtained solution is warmed to 70°C and stirred overnight. The solvent is then removed under reduced pressure and 10 mL of DCM are added. After filtration and removing the solvent under reduced pressure, **2** is obtained as a colorless grease (0.120 g, 76%) For single crystal growth, **2** was dissolved in a DCM/toluene mixture (2:1) and concentrated until saturation was reached. A few colorless platelets are obtained after a few hours at ambient temperature.
^{1}H NMR: (300 MHz, CD_2Cl_2) δ = 0.45 (s, 48H, Si(C*H*$_3$)$_2$) ppm. ^{13}C{^{1}H} NMR: (75 MHz, CD_2Cl_2) δ = 2.9 (s, Si*C*H$_3$) ppm. ^{29}Si NMR: (99 MHz, CD_2Cl_2) δ = 12.9 (s, *Si*(CH$_3$)$_2$) ppm. IR (cm^{-1}): 2991 (vw), 2946 (m), 2893 (w), 2828 (vw), 1460 (vw), 1402 (vw), 1253 (s), 1202 (vw), 1131 (m), 987 (m), 927 (s), 850 (vs), 811 (s), 772 (vs), 692 (s), 448 (m). CHN calcd. for $C_{16}H_{48}GaI_4NaO_4Si_8$ C, 17.01; H, 4.28; found C, 16.76; H, 4.20.

[Mg(²D₄)(GaI₄)₂] (**3**). 0.079 g of MgI_2 (0.28 mmol, 1.00 eq) are suspended in 10 mL of Ph-F. Subsequently, 0.252 g of GaI_3 (2.00 eq, 0.56 mmol) are added. The yellow suspension is then stirred for 60 min. and several times gently warmed to reflux. Then, at ambient temperature, 0.075 g of **I** (0.28 mmol, 1.0 eq) are added and the obtained solution is further three times very gently refluxed using a heatgun. The so obtained suspension is filtered and immediately placed at 6°C. Compound **3** is obtained as a colorless pale-white powder overnight (0.050 g, 21%).
^{1}H NMR: (300 MHz, CD_2Cl_2) δ = 0.71 (s, 48H, Si(C*H*$_3$)$_2$) ppm. ^{13}C{^{1}H} NMR: (75 MHz, CD_2Cl_2) δ = 3.5 (s, Si*C*H$_3$) ppm. ^{29}Si NMR: (99 MHz, CD_2Cl_2) δ = 25.7 (s, *Si*(CH$_3$)$_2$) ppm. IR (cm^{-1}): 2949 (w), 2892 (w), 1391 (w), 1256 (s), 1017 (m), 884 (m), 837 (vs), 804 (vs), 782 (vs), 686 (s), 549 (m), 445 (m).
[Ca(²D₄)(GaI₄)₂] (**4**). 0.056 g of CaI_2 (0.19 mmol, 1.00 eq) are suspended in 8 mL of Ph-F. Subsequently, 0.171 g of GaI_3 (2.00 eq, 0.38 mmol) are added. The yellow suspension is then stirred for 30 min. and several times gently warmed to reflux. Then, at ambient temperature, 0.050 g of **I** (0.19 mmol, 1.0 eq) are added The obtained solution is again several times refluxed using a heatgun. After filtration and concentration, the solution is placed at -12°C. Large colorless blocks are obtained overnight (0.107 g, 65%). For single crystal growth of suitable crystals for SC-XRD, **4** was dissolved in DCM and concentrated until saturation was reached. Colorless planks of **4**·DCM are obtained within hours at -12°C. Colorless blocks of **4a** are obtained from CD_2Cl_2 solution after slowly evaporating the solvent for three days in an NMR tube.
^{1}H NMR: (300 MHz, CD_2Cl_2) δ = 0.47 (s, 48H, Si(C*H*$_3$)$_2$) ppm. ^{13}C{^{1}H} NMR: (75 MHz, CD_2Cl_2) δ = 4.0 (s, Si*C*H$_3$) ppm. ^{29}Si NMR: (99 MHz, CD_2Cl_2) δ = 19.2 (s, *Si*(CH$_3$)$_2$) ppm. IR (cm^{-1}): 2947 (w), 2895 (vw), 1626 (w), 1394 (w), 1352 (w), 1258 (s), 1071 (w), 1035 (w), 885 (m), 835 (vs), 805 (vs), 775 (vs), 688 (s), 660 (s), 560 (w), 487 (w), 455 (m). CHN calcd. for $C_{16}H_{48}CaGa_2I_8O_4Si_8$·DCM C, 11.29; H, 2.79; found C, 11.76; H, 2.91.

[Sr(²D₄)(GaI₄)₂] (**5**). 0.065 g of SrI_2 (0.19 mmol, 1.00 eq) are suspended in 8 mL of Ph-F. Subsequently, 0.171 g of GaI_3 (2.00 eq, 0.38 mmol) are added. The yellow suspension is then stirred for 30 min. and several times gently heated to reflux. Then, at ambient temperature, 0.050 g of **I** (0.19 mmol, 1.0 eq) are added. The obtained solution is again several times refluxed using a heatgun. After filtration and concentration, the solution is placed at 6 °C. Large colorless prisms are obtained after a few days (0.114 g, 68%).
^{1}H NMR: (300 MHz, CD_2Cl_2) δ = 0.64 (s, 48H, Si(C*H*$_3$)$_2$) ppm. ^{13}C{^{1}H} NMR: (75 MHz, CD_2Cl_2) δ = 4.4 (s, Si*C*H$_3$) ppm. ^{29}Si NMR: (99 MHz, CD_2Cl_2) δ = 16.6 (s, *Si*(CH$_3$)$_2$) ppm. IR (cm^{-1}): 2945 (w), 2893 (w), 1394 (w), 1257 (s), 889 (s), 841 (vs), 807 (s), 776 (vs), 687 (s), 554 (m), 446 (m). CHN calcd. for $C_{16}H_{48}SrGa_2I_8O_4Si_8$ C, 10.85; H, 2.73; found C, 10.95 ; H, 2.70.

[H(²D₃)](Ga₂I₇) (**6**). *Protocol 1:* 0.100 g of **I** (0.38 mmol, 2.00 eq) together with 0.053 g of MgI_2 (98% (Aldrich), 0.19 mmol, 1.00 eq,) are dissolved in 5 mL of freshly distillated *α*,*α*,*α*-trifluorotoluene. Subsequently, GaI_3 (0.170 g, 0.38 mmol, 2.00 eq) is added. The obtained suspension is refluxed once, slowly brought to ambient temperature and stirred for 10 further minutes. Then, the solvent is removed under reduced pressure and 10 mL of DCM are added. After filtration, concentration and stirring the solution at -24°C yields **6** up to 64% yield (0.16 mmol, 0.230 g) as colorless needles/blocks. Needles and blocks were both investigated by SC-XRD and turned out to be the same molecular structure in the crystal.
Protocol 2: 0.30 mmol $MgCl_2$ (99.99% (Alfa aesar), 0.30 mmol, 2.5 eq) together with GaI_3 (0.110 g, 0.24 mmol, 2.00 eq) are dissolved in 5 mL of Ph-F which has been distillated more than a week ago. The obtained suspension is stirred for 30 min. and 0.032 g of **I** (0.12 mmol, 1.00 eq) is added. The solution is stirred further 3h and several times refluxed using a heatgun followed by filtration at ambient temperature. Reducing the volume to approximately 3 mL and placing the solution at -24°C yields **6** as colorless needles/blocks (54%, 0.061 g).
^{1}H NMR: (300 MHz, CD_2Cl_2) δ = 0.52 (s, 36H, Si(C*H*$_3$)$_2$), 7.89+9.38 (br, s, Si(CH$_3$)$_2$O*H*) ppm. ^{13}C{^{1}H} NMR: (75 MHz, CD_2Cl_2) δ = 2.2 (s, Si*C*H$_3$) ppm. ^{29}Si NMR: (99 MHz, CD_2Cl_2) δ = 21.2 (s, *Si*(CH$_3$)$_2$) ppm. IR (cm^{-1}): 3384+3081 (m, w, ν_s(Si-*OH*)), 2949 (w), 2892 (vw), 1621 (vw), 1593 (vw), 1493 (w), 1394 (s), 1255 (m), 1186 (s), 1034 (s), 994 (s), 964 (m), 900 (w), 812 (s),

778 (vs), 684 (s), 653 (m), 635 (m), 560 (vw), 520 (vw), 443 (vw), 426 (vw). CHN calcd. for $C_{12}H_{37}Ga_2I_7O_3Si_6$, 10.25; H, 2.62; found C, 10.11 ; H, 2.64.

^2D_n (**7**-**9**) 0.159 g of **4** are dissolved in 5 mL of MeCN and subsequently 15 mL of n-pentane are added. The solution is stirred for 18h followed by separation of the phases. The n-pentane is removed under reduced pressure to obtain 44 mg of a ^2D_n mixture as a colourless oil.
1H NMR (300 MHz, CD_2Cl_2): δ = 0.16 (s, $^2D_4$), 0.17 (s, $^2D_5$), 0.20 (s, $^2D_2$) ppm. $^{13}C\{^1H\}$ NMR (75 MHz, CD_2Cl_2): δ = 2.35 (s, $^2D_5$), 2.36 (s, C-1), 2.38 (s, $^2D_4$) ppm. ^{29}Si NMR (99 MHz, CD_2Cl_2): δ = 0.4 (s, $^2D_4$), 0.9 (s, $^2D_5$), 3.4 (s, $^2D_2$) ppm. HR LIFDI$^{(+)}$ MS: *m*/*z* calculated (found) for $[^2D_4]^{\bullet+}$ = 528.17067 (528.17196), $[^2D_5]^{\bullet+}$ = 660.21334 (660.21494), $[^2D_6]^{\bullet+}$ = 792.25601 (792.25693).

Crystal structure determination

A respective single crystal X-ray diffraction analysis was carried out on a Bruker D8 Quest or IPDS2 diffractometer at 100(2) K with MoKα radiation and respective X-ray optics or graphite monochromatization, respectively (λ = 0.71073). All structures were solved by direct methods and refinement with full-matrix-least-squares against F^2 using SHELXT- and SHELXL-2015 on the OLEX2 application.[87–89] The molecular structure of **2** is disordered around the center of inversion, centrosymmetric space group *C*2/*c*, which is why the disordered part is constrained to an occupancy of 0.5. Disordered oxygen atoms within the crown ether moiety were also disordered. The split positions were constrained to occupancies of 0.32 and 0.18 respectively. This enables for successful anisotropic refinement of these split positions. The $[GaI_4]^-$ anion of compound **3** is rotationally disordered. The split positions were constrained to a reasonable occupancy of 0.5. In compound **4**·DCM, the siloxane ligand as well as the anion are rotationally disordered. A disorder model was established using free variables (FVAR) for the siloxane and the $[GaI_4]^-$ anion is constrained to occupancies of 0.5. The crystallographic determination of **5** had been a challenge. Both, $[GaI_4]^-$ and siloxane ligand are intrinsically disordered. Furthermore, the $[GaI_4]^-$ switch coordination modes causing even more disorder. For one independent molecule of **5**, we therefore had to refine an additional Sr^{2+} split-position. As a cause, several restraints had to be employed to stabilize the refinement. Recrystallization from other solvents than Ph-F or DCM failed. Recrystallized from both solvents, the intrinsic disorder problem could not be avoided. Crystallographic data for the compounds are assigned as follows: CCDC Nos. 2035390 (**I**), 2035394 (**II**·DCM), 2035392 (**1**), 2035388 (**2**), 2035391 (**4**·DCM), 2035387 (**4a**), 2035396 (**5**), 2035389 (**6**) 2035393 (**S1**), 2035395 (**S2**) Crystallographic information files (CIF) can be obtained free of charge from the Cambridge Crystallographic Data Centre (CCDC) (link: www.ccdc.cam.ac.uk/data_request/cif). The respective crystal data and selected experimental parameters of the structure determinations are summarized in Table S1-S4. Visualization of all structures was performed with the Diamond software package Version 4.6.0 All Ellipsoid plots represent the 50% probability level.

DFT calculations

The calculations were done with TURBOMOLE[90] employing the PBE[91] functional and def2-TZVP basis sets.[92] Solvent effects were treated within the conductor-like screening model, COSMO.[81] The transformation pathways were optimized with the method proposed by *Plessow*.[82] Further details are given in the Supporting Information.

Acknowledgements

This work was financially supported by the Deutsche Forschungsgemeinschaft (DFG, HA 3466/8-3). F. Dankert gratefully acknowledges Dr. S. Ivlev and R. Riedel (X-ray department, Phillipps-Universität Marburg) for their kind advice and measurement time. C. Mischke (NMR department, Philipps-Universität Marburg) and J. Bamberger (MS department, Philipps-Universität Marburg) are gratefully acknowledged for the collection of several NMR- and MS spectra of these extremely sensitive compounds and their kind advice.

Keywords: Si–O bond activation · Host-guest systems · Ion Recognition · Templates · Inorganic Macrocycles · Inorganic Crown Ethers · Reaction Mechanism

References

[1] Gokel, G. W. Leevy, W. M. Weber, M. E. *Chem. Rev.* **2004**, *104*, 2723–2750.
[2] Swidan, A.; Macdonald, C. L. B. *Chem. Soc. Rev.* **2016**, *45*, 3883–3915.
[3] Steed, J. W. *Coord. Chem. Rev.* **2001**, *215*, 171–221.
[4] Pedersen, C. J. *J. Am. Chem. Soc.* **1967**, *89*, 7017–7036.
[5] Pedersen, C. J. *Angew. Chem., Int. Ed.* **1988**, *27*, 1021–1027.
[6] Chivers, T.; Manners, I. *Inorganic Rings and Polymers of the p-Block Elements: From Fundamentals to Applications*, Royal Society Of Chemistry, Cambridge, **2009**.
[7] Xuan, W.; Surman, A. J.; Zheng, Q.; Long, D.-L.; Cronin, L. *Angew. Chem.* **2016**, *128*, 12895–12899.
[8] Plajer, A. J.; García-Rodríguez, R.; Benson, C. G. M.; Matthews, P. D.; Bond, A. D.; Singh, S.; Gade, L. H.; Wright, D. S. *Angew. Chem., Int. Ed.*. **2017**, *56*, 9087–9090.
[9] Donsbach, C.; Reiter, K.; Sundholm, D.; Weigend, F.; Dehnen, S. *Angew. Chem., Int. Ed.* **2018**, *57*, 8770–8774.
[10] Calera, S. G.; Wright, D. S. *Dalton Trans.* **2010**, *39*, 5055–5065.
[11] Nordheider, A.; Chivers, T.; Thirumoorthi, R.; Vargas-Baca, I.; Woollins, J. D. *Chem. Commun.* **2012**, *48*, 6346–6348.
[12] Nishio, M.; Inami, S. Hayashi, Y. *Eur. J. Inorg. Chem.* **2013**, 1876–1881.
[13] Block, E.; Dikarev, E. V.; Glass, R. S. Jin, Li, B. Li, X. Zhang, S.-Z. *J. Am. Chem. Soc.* **2006**, *128*, 14949–14961.
[14] Martínez-Martínez, A. J.; Armstrong, D. R.; Conway, B.; Fleming, B. J.; Klett, J.; Kennedy, A. R.; Mulvey, R. E.; Robertson, S. D.; O'Hara, C. T. *Chem. Sci.* **2014**, *5*, 771–781.
[15] Krebs, B.; Hürter, H.-U. *Angew. Chem., Int. Ed.* **1980**, *19*, 481–482.
[16] West, R.; Fink, M. J.; Michl, J. *Science.* **1981**, *214*, 1343–1344.
[17] Sekiguchi, A.; Kinjo, R.; Ichinohe, M. *Science.* **2004**, *305*, 1755–1757.
[18] Abersfelder, K.; White, A. J. P.; Rzepa, H. S.; Scheschkewitz, *Science.* **2010**, *327*, 564–566.
[19] Weidenbruch, M.; Willms, S.; Saak, W.; Henkel, G. *Angew. Chem.* **1997**, *109*, 2612–2613.
[20] Inoue, S.; Epping, J. D.; Irran, E.; Driess, M. *J. Am. Chem. Soc.* **2011**, *133*, 8514–8517.
[21] Xiong, Y.; Yao, S.; Driess, M. *Angew. Chem.* **2013**, *125*, 4398–4407.
[22] Filippou, A. C.; Baars, B.; Chernov, O.; Lebedev, Y. N.; Schnakenburg, G. *Angew. Chem., Int. Ed.* **2014**, *53*, 565–570.
[23] Kobayashi, R.; Ishida, S.; Iwamoto, T. *Angew. Chem., Int. Ed.* **2019**, *58*, 9425–9428.
[24] Yao, S.; Xiong, Y.; Brym, M.; Driess, M. *J. Am. Chem. Soc.* **2007**, *129*, 7268–7269.
[25] Epping, J. D.; Yao, S.; Karni, M.; Apeloig, Y.; Driess, M. *J. Am. Chem. Soc.* **2010**, *132*, 5443–5455.
[26] Xiong, Y.; Yao, S.; Driess, M. *Angew. Chem.* **2010**, *122*, 6792–6795.
[27] Xiong, Y.; Yao, S.; Müller, R.; Kaupp, M.; Driess, M. *J. Am. Chem.*

Soc. **2010**, *132*, 6912–6913.
[28] Yao, S.; Brym, M.; van Wüllen, C.; Driess, M. *Angew. Chem.* **2007**, *119*, 4237–4240.
[29] Yildiz, C. B.; Leszczyńska, K. I.; González-Gallardo, S.; Zimmer, M.; Azizoglu, A.; Biskup, T.; Kay, C. W. M.; Huch, V.; Rzepa, H. S.; Scheschkewitz, D. *Angew. Chem.* **2020**, *132*, 15199–15204.
[30] Weinhold, F.; West, R. *Organometallics* **2011**, *30*, 5815–5824.
[31] Weinhold, F.; West, R. *J. Am. Chem. Soc.* **2013**, *135*, 5762–5767.
[32] Ritch, J. S.; Chivers, T. *Angew. Chem., Int. Ed.* **2007**, *46*, 4610–4613.
[33] Moraru, I. T.; Petrar, P. M.; Nemeş, G. *J. Phys. Chem. A* **2017**, *121*, 2515–2522.
[34] Gillespie, R. J.; Robinson, E. A. *Chem. Soc. Rev.* **2005**, *34*, 396.
[35] Cameron, T. S.; Decken, A.; Krossing, I.; Passmore, J.; Rautiainen, J. M.; Wang, X.; Zeng, X. *Inorg. Chem.* **2013**, *52*, 3113–3126.
[36] Passmore, J.; Rautiainen, J. M. *Eur. J. Inorg. Chem.* **2012**, 2012, 6002–6010.
[37] Fugel, M.; Hesse, M. F.; Pal, R.; Beckmann, J.; Jayatilaka, D.; Turner, M. J.; Karton, A.; Bultinck, P.; Chandler, G. S.; Grabowsky, S. *Chem. Eur. J.* **2018**, *24*, 15275–15286.
[38] Churchill, M. R.; Lake, C. H.; Chao, S.-H. L.; Beachley, O. T. *J. Chem. Soc. Chem. Commun.* **1993**, *1*, 1577–1578.
[39] Eaborn, C.; Hitchcock, P. B.; Izod, K.; Smith, J. D. *Angew. Chem., Int. Ed.* **1996**, *34*, 2679–2680.
[40] Decken, A.; Passmore, J.; Wang, X. *Angew. Chemie* **2006**, *118*, 2839–2843.
[41] Decken, A.; LeBlanc, F. A.; Passmore, J.; Wang, X. *Eur. J. Inorg. Chem.* **2006**, *2006*, 4033–4036.
[42] Ernst, R. D.; Glöckner, A.; Arif, A. M. *Z. Kristallogr. - New Cryst. Struct.* **2007**, *222*, 333–334.
[43] Sänger, I.; Gärtner, M.; Bolte, M.; Wagner, M.; Lerner, H.-W. *Z. Anorg. Allg. Chem.* **2018**, *644*, 925–929.
[44] Dankert, F.; von Hänisch, C. *Inorg. Chem.* **2019**, *58*, 3518–3526.
[45] Dankert, F.; Weigend, F.; von Hänisch, C. *Inorg. Chem.* **2019**, *58*, 15417–15422.
[46] Dankert, F.; Erlemeier, L.; Ritter, C.; von Hänisch, C. *Inorg. Chem. Front.* **2020**, *7*, 2138-2153.
[47] Dankert, F.; Heine, J.; Rienmüller, J.; von Hänisch, C. *CrystEngComm* **2018**, *20*, 5370–5376.
[48] Pahl, J.; Elsen, H.; Friedrich, A.; Harder S. *Chem. Commun.* **2018**, *54*, 7846–7849.
[49] Ouchi, M.; Inoue, Y.; Kanzaki, T.; Hakushi, T. *Bull. Chem. Soc. Jpn.* **1984**, *57*, 887–888.
[50] Inoue, Y.; Ouchi, M.; Hakushi, T. *Bull. Chem. Soc. Jpn.* **1985**, *58*, 525–530.
[51] Reuter, K.; Buchner, M. R.; Thiele, G.; von Hänisch, C. *Inorg. Chem.* **2016**, *55*, 4441–4447.
[52] Reuter, K.; Thiele, G.; Hafner, T.; Uhlig, F.; von Hänisch, C. *Chem. Commun.* **2016**, *52*, 13265–13268.
[53] Reuter, K.; Dankert, F.; Donsbach, C.; von Hänisch, C.. *Inorganics* **2017**, *5*, 11.
[54] Dankert, F.; Reuter, K.; Donsbach, C.; von Hänisch, C. *Dalton Trans.* **2017**, *46*, 8727–8735.
[55] Dankert, F.; Donsbach, C.; Mais, C.-N.; Reuter, K.; von Hänisch, C. *Inorg. Chem.* **2018**, *57*, 351–359.
[56] Dankert, F.; Reuter, K.; Donsbach, C.; von Hänisch, C. *Inorganics* **2018**, *6*, 15.
[57] Buchner, M. R.; Müller, M.; Dankert, F.; Reuter, K.; von Hänisch C. *Dalton Trans.* **2018**, *47*, 16393–16397.
[58] Dankert, F.; Donsbach, C.; Rienmüller, J.; Richter, R. M.; von Hänisch, C. *Chem. Eur. J.* **2019**, *25*, 15934–15943.
[59] Cypryk, M. Polymerization of Cyclic Siloxanes, Silanes, and Related Monomers. In: *Ref. Modul. Mater. Sci. Mater. Eng.*, Elsevier, **2016**, pp. 1–35. DOI: 10.1016/B978-0-444-53349-4.00112-6.
[60] Pop, L.-C.; Saito, M. *Coord. Chem. Rev.* **2016**, *314*, 64–70.
[61] Haiduc, I. *Organometallics* **2004**, *23*, 3–8.
[62] Cypryk, M.; Kurjata, J.; Chojnowski, J. *J. Organomet. Chem.* **2003**, *686*, 373–378.
[63] Cypryk, M. *Macromol. Theory Simul.* **2001**, *10*, 158–164.
[64] Buchanan, G. W.; Rastegar, M. F.; Yap, G. P. A. *J. Mol. Struct.* **2002**, *605*, 1–8.
[65] Shannon, R. D. *Acta Crystallogr. Sect. A* **1976**, *32*, 751–767.
[66] Chambron, J. C.; Meyer, M. *Chem. Soc. Rev.* **2009**, *38*, 1663–1673.
[67] Krossing, I.; Reisinger, A. *Eur. J. Inorg. Chem.* **2005**, 1979–1989.
[68] Stasko, D.; Hoffmann, S. P.; Kim, K. C.; Fackler, N. L. P.; Larsen, A. S.; Drovetskaya, T.; Tham, F. S.; Reed, C. A.; Rickard, C. E. F.; Boyd, P. D. W.; Stoyanov, E. S., *J. Am. Chem. Soc.* **2002**, *124*, 13869–13876.
[69] Jutzi, P.; Müller, C.; Stammler, A.; Stammler, H. G. *Organometallics* **2000**, *19*, 1442–1444.
[70] Morisue, M.; Kusukawa, T.; Watase, S. *Eur. J. Inorg. Chem.* **2020**, *2020*, 1885–1893.
[71] Weitkamp, R. F.; Neumann, B.; Stammler, H.; Hoge, B. *Angew. Chemie* **2020**, *132*, 5536–5541.
[72] Tun, Z. M.; Panzner, M. J.; Scionti, V.; Medvetz, D. Wesdemiotis, C.; Youngs, W. J.; Tessier, C. *J. Am. Chem. Soc.* **2010**, *132*, 17059–17061.
[73] Ichinohe, M.; Takahashi, N.; Sekiguchi, A. *Chem. Lett.* **1999**, *28*, 553–554.
[74] Schäfer, A.; Reißmann, M.; Schäfer, A.; Schmidtmann, M. Müller, T. *Chem. Eur. J.* **2014**, *20*, 9381–9386.
[75] Xie, X.; Auel, C.; Henze, W.; Gschwind, R. M. *J. Am. Chem. Soc.* **2003**, *125*, 1595–1601.
[76] Neufeld, R.; John, M.; Stalke, D. *Angew. Chemie Int. Ed.* **2015**, *54*, 6994–6998.
[77] Tanner, J. E. *J. Chem. Phys.* **1970**, *52*, 2523–2526.
[78] Johnson, C. S. *Prog. Nucl. Magn. Reson. Spectrosc.* **1999**, *34*, 203–256.
[79] Ben-Amotz, D.; Willis, K. G. *J. Phys. Chem.* **1993**, *97*, 7736–7742.
[80] Dankert, F.; Deubner, H. L.; Müller, M.; Buchner, M. R.. Kraus, F.; von Hänisch, C. *Z. Anorg. Allg. Chem.* **2020**, 1–8.
[81] Klamt, A.; Schüürmann, G. *J. Chem. Soc. Perkin Trans. 2* **1993**, 799–805.
[82] Plessow, P. *J. Chem. Theory Comput.* **2013**, *9*, 1305–1310.
[83] Pop, L. C.; Kurokawa, N.; Ebata, H.; Tomizawa, K.; Tajima, T.; Ikeda, M.; Yoshioka, M.; Biesemans, M.; Willem, R.; Minoura, M.; Saito, M. *Can. J. Chem.* **2014**, *92*, 542–548.
[84] Harder, S.; Freitag, B.; Stegner, P.; Pahl, J.; Naglav, D. *Z. Anorg. Allg. Chem.* **2015**, *641*, 2129–2134.
[85] Freitag, B.; Stegner, P.; Thum, K.; Fischer, C. A.; Harder, S. *Eur. J. Inorg. Chem.* **2018**, *2018*, 1938–1944.
[86] Jerschow, A.; Müller, N. *J. Magn. Reson.* **1997**, *125*, 372–375.
[87] Sheldrick, G. M. *Acta Crystallogr. Sect. A Found. Adv.* **2015**, *71*, 3–8.
[88] Sheldrick, G. M. *Acta Crystallogr. Sect. C Struct. Chem.* **2015**, *71*, 3–8.
[89] Dolomanov, O. V.; Bourhis, L. J.; Gildea, R. J.; Howard, J. A. K.; Puschmann, H. *J. Appl. Crystallogr.* **2009**, *42*, 339–341.
[90] TURBOMOLE V7.5 **2020**, a development of University of Karlsruhe and Forschungszentrum Karlsruhe GmbH, 1989-2007, TURBOMOLE GmbH, since 2007; available from http://www.turbomole.com.
[91] Perdew, J. P.; Burke, K.; Ernzerhof, M. *Phys. Rev. Lett.* **1996**, *77*, 3865–3868.
[92] Weigend, F.; Ahlrichs, R. *Phys. Chem. Chem. Phys.* **2005**, *7*, 3297.

Entry for the Table of Contents

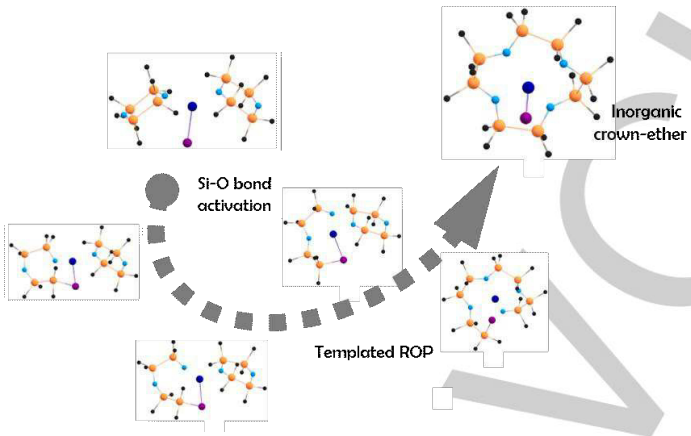

Inorganic crown-ethers: All-silicon versions of crown-ethers were isolated and characterized. These silicon-based macrocycles are obtained from $^{2}D_2$/s-block metaliodide/gallium(III)iodide ($^{2}D_2$ = $(Me_4Si_2O)_2$) Lewis-acidic systems which enable s-block metal templated Si-O bond activation and subsequent ring-opening polymerization. The coordination ability of these macrocycles is evaluated and the formation-mechanism is suggested by means of DFT calculations.

Institute and/or researcher Twitter usernames: @Uni_MR, @haenisch_group

WILEY-VCH

Architecting inorganic crown ethers by s-block-metal templated Si-O bond activation

F. Dankert,[a] R.-M. Richter,[a] F. Weigend,[a]* X. Xie,[b] M. Balmer[a] and C. von Hänisch[a]*

*Email:

haenisch@staff.uni-marburg.de

florian.weigend@chemie.uni-marburg.de

[a] Fachbereich Chemie and Wissenschaftliches Zentrum für Materialwissenschaften (WZMW), Philipps-Universität, Hans-Meerwein-Straße 4, 35032 Marburg, Germany.

[b] Fachbereich Chemie, Philipps-Universität Marburg, Hans-Meerwein-Straße 4, 35032 Marburg, Germany

Content

1. Crystal structure representations 3
1.1 Compound I 3
1.2 Compound II 4
1.3 Compound 1 5
1.4 Compound 2 6
1.5 Compound 4 7
1.6 Compound 5 8
1.7 Compound 6 9
1.8 Comparison of compounds 1 and 2 10
1.9 Comparison of compounds 4 and 5 11
1.10 Top-view of compounds 6 12
2. Additional X-ray structures 13
2.1 Compound 4a 13
3. Attempts crystallizing [Mg(^{2}D$_4$)(GaI$_4$)$_2$] (3) 14
3.1 Crystal structure of S1 16
3.2 Crystal structure of S2 17
4. Crystallographic Data 18
5. NMR spectra and plots obtained by DOSY 22
5.1 Compound I 22
5.2 Compound II 22
5.3 Compound 1 25
5.4 Compound 2 27
5.5 Compound 3 30
5.6 Compound 4 32
5.7 Compound 5 34
5.8 Compound 6 36
5.9 Compounds 7 and 8 38
5.10 Stejskal-Tanner Plots 44
6. HR-MS spectra 46
6.1 Compound 7 46
6.2 Compound 8 46
6.3 Compound 9 47
7. Quantum chemical calculations 48
8. References 61

1. Crystal structure representations

1.1 Compound I

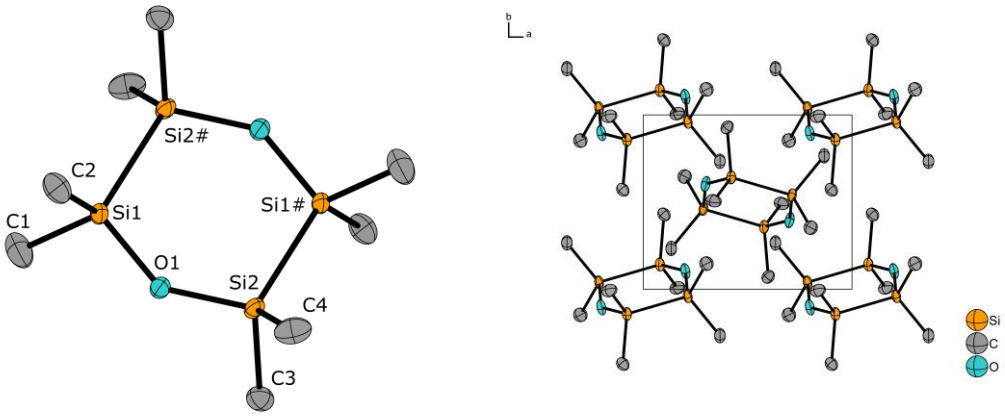

Figure S1: The molecular structure of **I** in the crystal (left) and cell package along [001] (right). The disordered oxygen atoms as well as hydrogen atoms are omitted for clarity. Atoms marked with # are symmetry generated over 1-x, 1-y, 1-z. Thermal ellipsoids are drawn at 50% probability level. Please note that two polymorphs of the same molecular structure were already published.[1,2] Selected bond lengths [pm]: Si1-O1 164.7(6), Si1-C1 186.5(1), Si1-C2 186.2(1), Si1-Si2# 236.2(1), Si2-O1 166.0(6), Si2-C3 186.5(1), Si2-C4 186.0(1). Selected bond angles [°]: Si1-O1-Si2 141.8(5), Si2#-Si1-O1 106.9(3).

1.2 Compound II

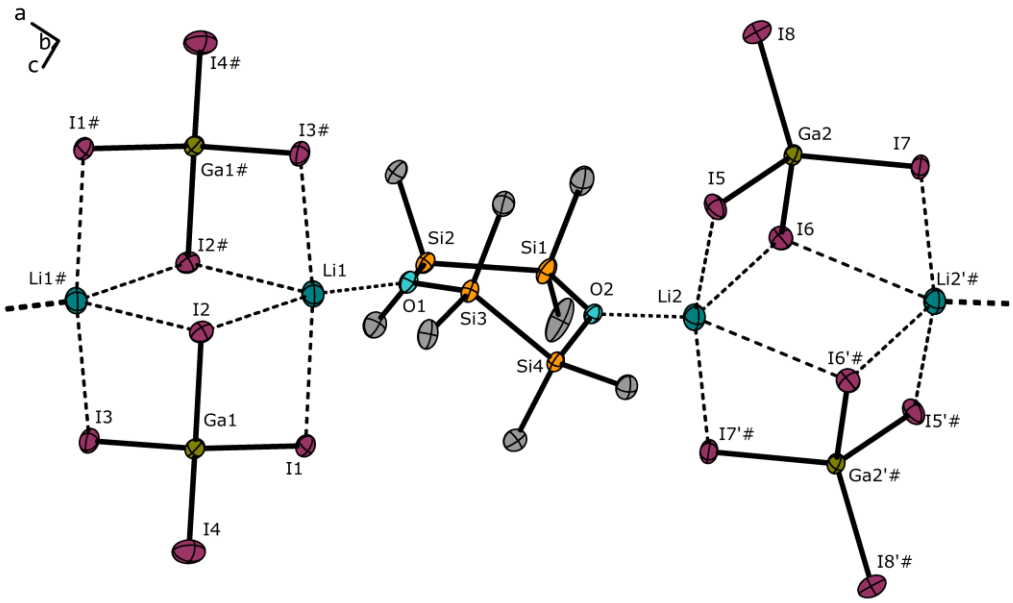

Figure S2: A section of the polymeric structure motif of **II** in the crystal. Atoms depicted with # or '# are symmetry generated over 2-x, 1-y, 1-z and 1-x, 1-y, -z. Hydrogen atoms and co-crystalline DCM molecules are omitted for clarity. Thermal ellipsoids are drawn at 50% probability level. Selected bond lengths [pm]: I1-Li1 294.3(5), I2-Li1 327.5(5), I3#-Li1 295.2(5), Li1···Li1# 460.9(6), Li2···Li2'# 464.7(6), O1-Li1 195.4(5), O1-Si2 169.3(2), O1-Si3 169.3(2), O2-Li2 194.4(4), I5-Li2 297.4(5), I6-Li2 289.1(5), I6'#-Li2 346.5(4), I7'#-Li2 294.1(5). Selected bond angles [°]: Li1-I2-Li1# 95.2(1), I1-Li1-I3# 161.4(2), I2-Li1-I2# 84.7(1), I2-Li1-O1 151.2(2), Si1-O2-Si4 122.9(1), Si2-O1-Si3 124.4(1), Li2-I6-Li2'# 93.5(1), O2-Li2-I6 124.0(2), I5-Li2-I7'# 159.5(2).

1.3 Compound 1

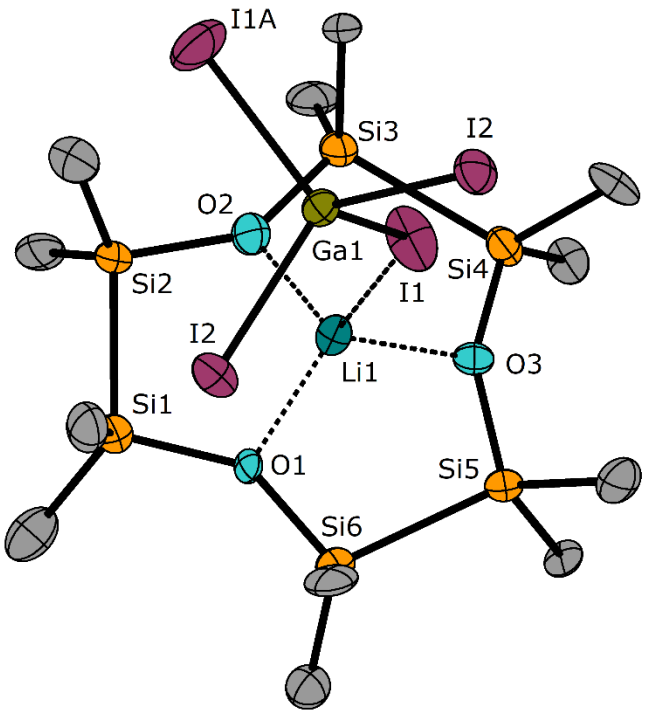

Figure S3: The molecular structure of **1** in the crystal. I1A is symmetry generated over 1-x, y, 3/2-z. The disordered parts as well as hydrogen atoms are omitted for clarity. Thermal ellipsoids are drawn at 50% probability level. Selected bond lengths [pm]: I1-Li1 287(1), O1-Li1 194(2), O2-Li1 194(1), O3-Li1 194(1), Si1-Si2 235.6(6), Si3-Si4 238.5(6), Si5-Si6 241.3(6). Selected bond angles [°]: Si1-O1-Si6 144(1), Si2-O2-Si3 135(1), Si4-O3-Si5 139(1), O1-Li1-O2 103.9(9), O1-Li1-O3 110.7(9), O2-Li1-O3 109.4(9).

1.4 Compound 2

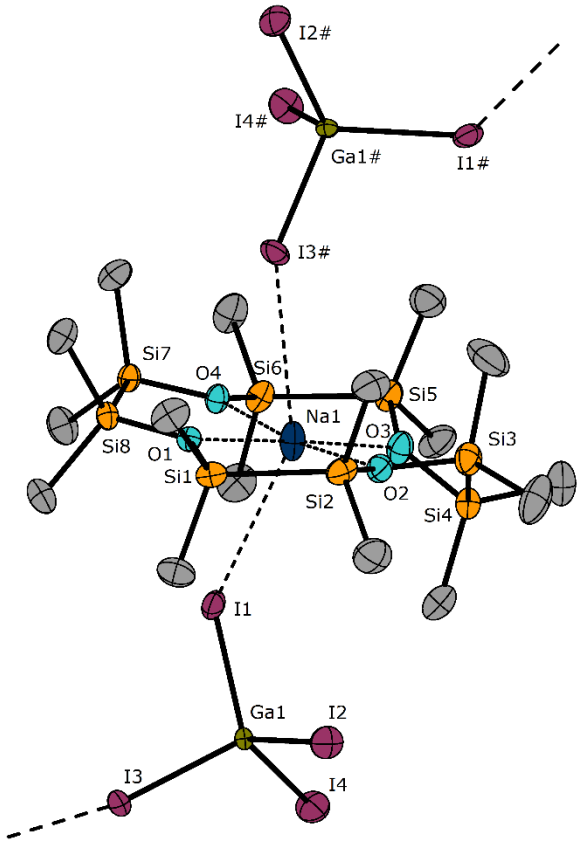

Figure S4: The molecular structure of **2** in the crystal including a $[GaI_4]^-$ anion from the next formula unit indicating a coordination polymer. Atoms depicted with # are symmetry generated over x, 3/2-y, 1/2+z. The disordered parts as well as hydrogen atoms are omitted for clarity. Thermal ellipsoids are drawn at 50% probability level. Selected bond lengths [pm]: I1-Na1 341.9(4), I3#-Na 367.6(3), O1-Na1 240.3(2), O2-Na1 241.8(4), O3-Na1 246.3(3), O4-Na1 240.6(3). Selected bond angles [°]: I1-Na1-I3# 150.5(1), Si1-O1-Si8 132.7(1), Si2-O2-Si3 132.0(2), Si4-O3-Si5 135.9(2), Si6-O4-Si7 131.3(1).

1.5 Compound 4

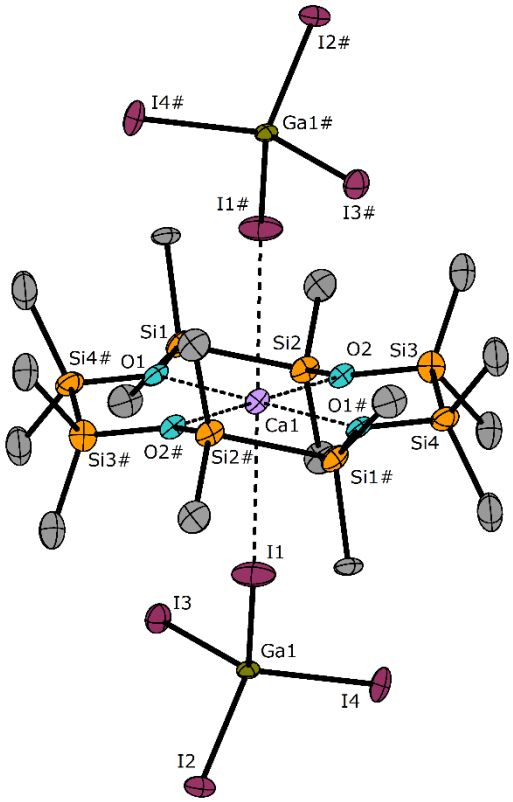

Figure S5: The molecular structure of **4** in the crystal. Atoms depicted with # are symmetry generated over 1-x, 1-y, 1-z. The disordered parts, co-crystalline DCM as well as hydrogen atoms are omitted for clarity. Thermal ellipsoids are drawn at 50% probability level. Selected bond lengths [pm]: I1-Ca1 317.3(4), O1-Ca1 239.7(9), O2-Ca1 237.0(6). Selected bond angles [°]: Si1-O1-Si4# 128.0(9), Si2-O2-Si3 127.3(8), I1-Ca1-I1# 179.9(1).

1.6 Compound 5

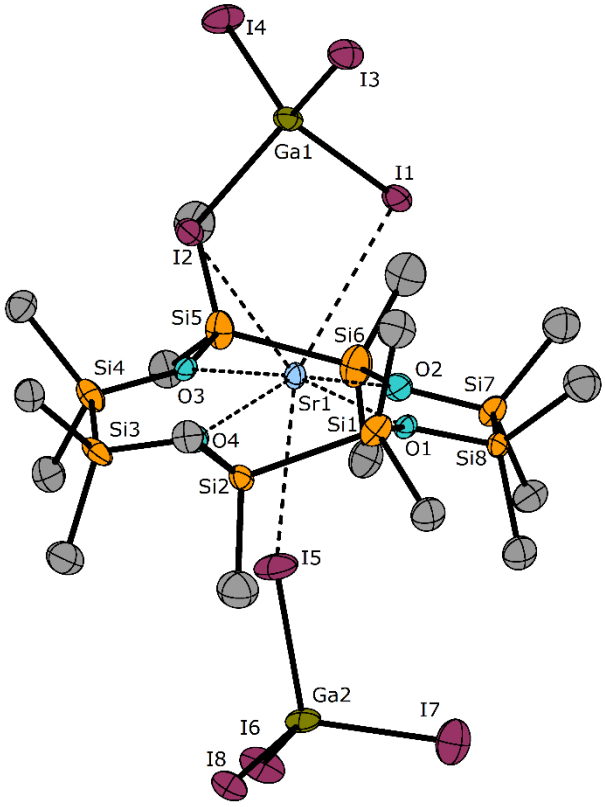

Figure S6: The molecular structure of **5** in the crystal. Restraints were used to fix the refinement. The disordered parts and hydrogen atoms are omitted for clarity. Only one out of two independent molecules is shown. Thermal ellipsoids are drawn at 30% probability level. Selected bond lengths [pm]: I1-Sr1 339.6(3), I2-Sr1 345.5(3), I5-Sr1 342.9(4), O1-Sr1 250(3), O2-Sr1 259(3), O3-Sr1 251(3), O4-Sr1 252(3). Selected bond angles [°]:I1-Sr1-I5 146(1), I2-Sr1-I5 141(1), Si1-O1-Si8 129(2), Si2-O4-Si3 132(2), Si4-O3-Si5 131(2), Si6-O2-Si7 133(2).

1.7 Compound 6

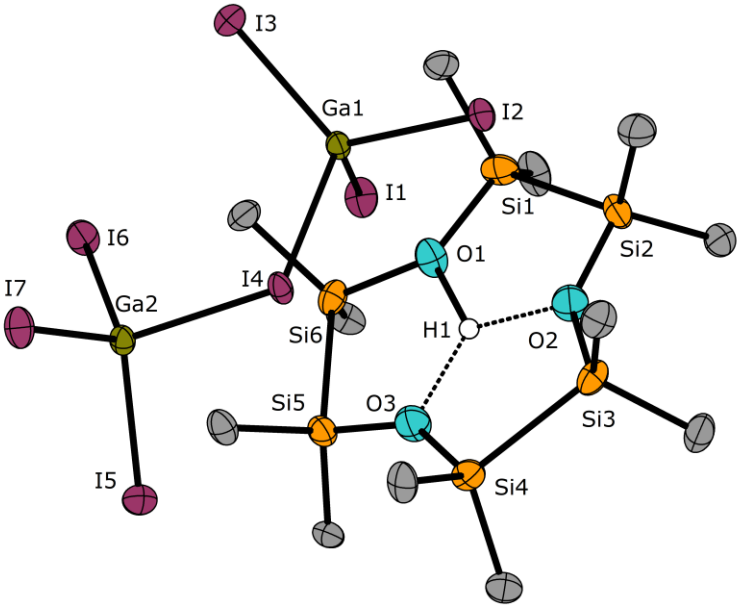

Figure S7: The molecular structure of **6** in the crystal. Thermal ellipsoids are drawn at 50% probability level. Selected bond lengths [pm]: O1-H1 162(4), O2-H1 172(2), O3-H1 172(3). Selected bond angles [°]: Si1-O1-Si6 136.0(2), Si2-O2-Si3 137.3(2), Si4-O3-Si5 141.6(2).

1.8 Comparison of compounds 1 and 2

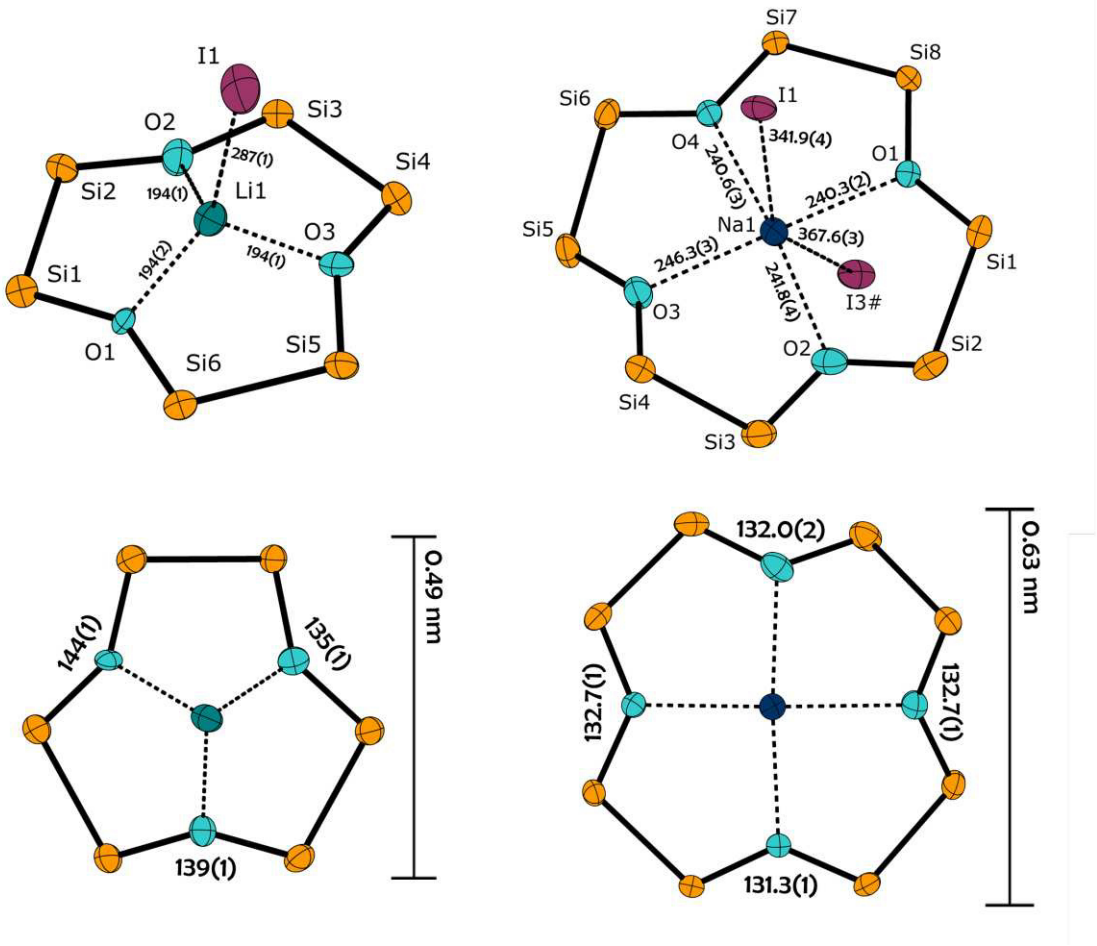

Figure S8: Comparison of the geometric features of alkali metal complexes of inorganic crown-ethers. The molecular structures of **1** (left) and **2** (right) in the crystal are reduced to the inorganic skeleton and the closest $M^{+}\cdots I–GaI_3$ contact. The disordered part of 1 and 2 are omitted for clarity. Thermal displacement ellipsoids represent the 50% probability level. Atoms depicted with # are symmetry generated over x, 3/2-y, 1/2+z. Atom distances are depicted in [pm] and angles in [°].

1.9 Comparison of compounds 4 and 5

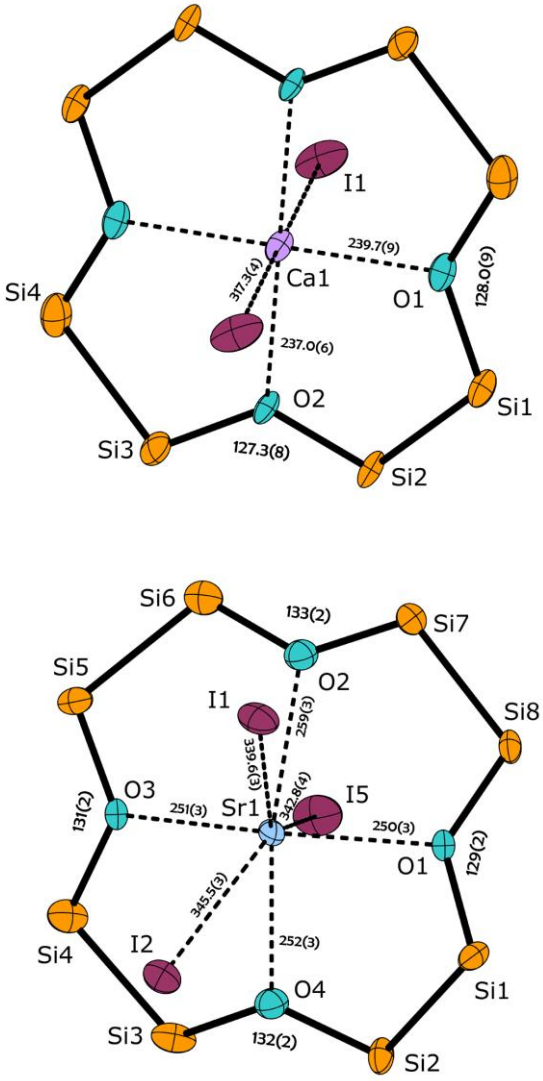

Figure S9: Geometric features of alkaline-earth metal complexes of inorganic crown-ethers. The molecular structures of **4** (top) and **5** (bottom) in the crystal are reduced to the inorganic skeleton and the closest $M^{+}\cdots I–GaI_3$ contacts. For the crystal structure of **5**, a restrained model was used which is the reason for large standard deviations. The disordered parts of **4** and **5** are omitted for clarity. Thermal displacement ellipsoids represent the 50% probability level (top) and the 30% probability level (bottom). Non-labelled atoms are symmetry generated over 1-x, 1-y, 1-z. Atom distances are depicted in [pm] and angles in [°].

1.10 Top-view of compounds 6

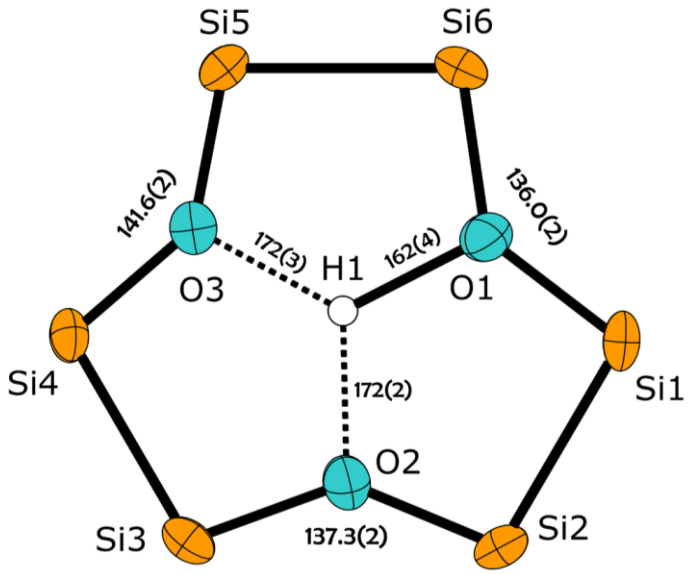

Figure S10: Geometric features of a proton complex of an inorganic crown-ether. The molecular structure of **6** in the crystal is reduced to the inorganic skeleton. The proton has been refined as an isotropic atom and is crystallographically located in the middle of the crown-ether moiety. Soft SADI restraints were employed to stabilize the refinement. Thermal displacement ellipsoids represent the 50% probability level.

2. Additional X-ray structures

2.1 Compound 4a

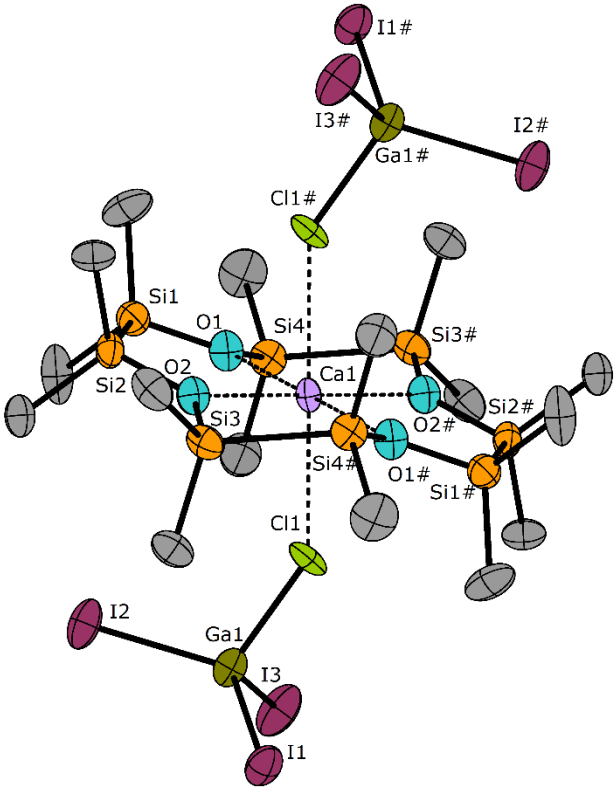

Figure S11: The molecular structure of **4a** in the crystal. Atoms depicted with # are symmetry generated over 1-x, 1-y, 1-z. Hydrogen atoms are omitted for clarity. Thermal ellipsoids are drawn at 50% probability level. Selected bond lengths [pm]: Cl1-Ca1 278.9(3), Cl1-Ga1 225.9(4), I1-Ga1 251.2(1), I2-Ga1 251.0(1), I3-Ga1 250.4(1), O1-Ca1 238.6(7), O2-Ca1 238.8(8). Selected bond angles [°]:Cl1-Ca1-Cl1# 180.0, Si1-O1-Si4 127.4(5), Si2-O2-Si3 127.1(5).

3. Attempts crystallizing [Mg(^{2}D$_4$)(GaI$_4$)$_2$] (3)

After conversion of ^{2}D$_2$ (**I**) with MgI$_2$ (1.0 eq, 99.996% ultra dry) and GaI$_3$ (1.0 eq) a colourless, microcrystalline powder of **3** is obtained after placing a freshly filtered Ph-F solution of **3** at 6 °C. Thus, we systematically tried to vary the solvent, crystallization procedure and even reaction conditions in order to obtain a crystal structure which further proves ^{2}D$_4$ coordination towards Mg^{2+} which is indicated by DOSY NMR. All our attempts, however, failed. This is especially due to the extremely high sensitivity of the compound. Even though solvents were distilled three or four days before a crystallization attempt was started, we observed a readily decomposition to various unidentified products. Most of them could be characterized by means of SC-XRD and partially also NMR spectroscopy. As we have already mentioned in the main-text article, compound **6** is one of them. Another decomposition product is the pincer complex [Mg(L)(GaI$_4$)$_2$] (L = O(Si$_2$Me$_4$OH)$_2$, compound **S1**) which is shown in Figure S8. The related decomposition product [Mg(L')](GaI$_4$)$_2$ (compound **S2**, Figure S8: right) (L' = (SiMe$_2$OH)$_2$) was also obtained, which itself is probably a decomposition product of **S1**. We propose that the Mg^{2+} ion (r_i[CN6]= 72 pm[3]) is too small for the large cavity of ^{2}D$_4$ what makes the compound very instable. Even the smallest traces of H$_2$O readily deconstruct the ligand moiety and form ligands coordinating Mg^{2+} in a common octahedral coordination sphere. Probably caused by even higher amounts of H$_2$O, the pincer ligand is hydrolysed forming (SiMe$_2$OH)$_2$ which is eventually coordinating Mg^{2+}. The molecular structure of **S1** reveals a six-coordinate heteroleptic coordinated Mg^{2+} centre. Stabilized by coordination, a neutral silanol ligand is coordinating threefold. A chelating as well as single coordinating counter ion complete the coordination sphere. The molecular structure of **S2** reveals a six-coordinate

homoleptic coordinated Mg^{2+} center. Three silanols are shielding the metal center in such way that no contact to the anions is observed any more. Eventually, the octahedral coordination of the magnesium salt of the small WCA $[GaI_4]^-$ is favoured in such way, that powdery compound **3** and even the single crystals of **S1** and **S2** stored under immersion oil readily decompose to afford single crystals of $[Mg(H_2O)_6](GaI_4)_2$ (**S3**, not deposited) and $[Mg(H_2O)_6](GaI_4)_2 \cdot H_2O$. Scheme S1 summarizes a possible pathway for the decomposition of **3** to **S3**. The formation of **6** is more complicated but from basic text-book chemistry it is most likely that the established *Lewis*-acidic system causes olation and oxolation. Even though these results were not intended, it can clearly be concluded that metal centers can form silanols from siloxanes. In further studies, we will therefore evaluate s-block metals as catalysts for the formation of silanols from siloxanes.

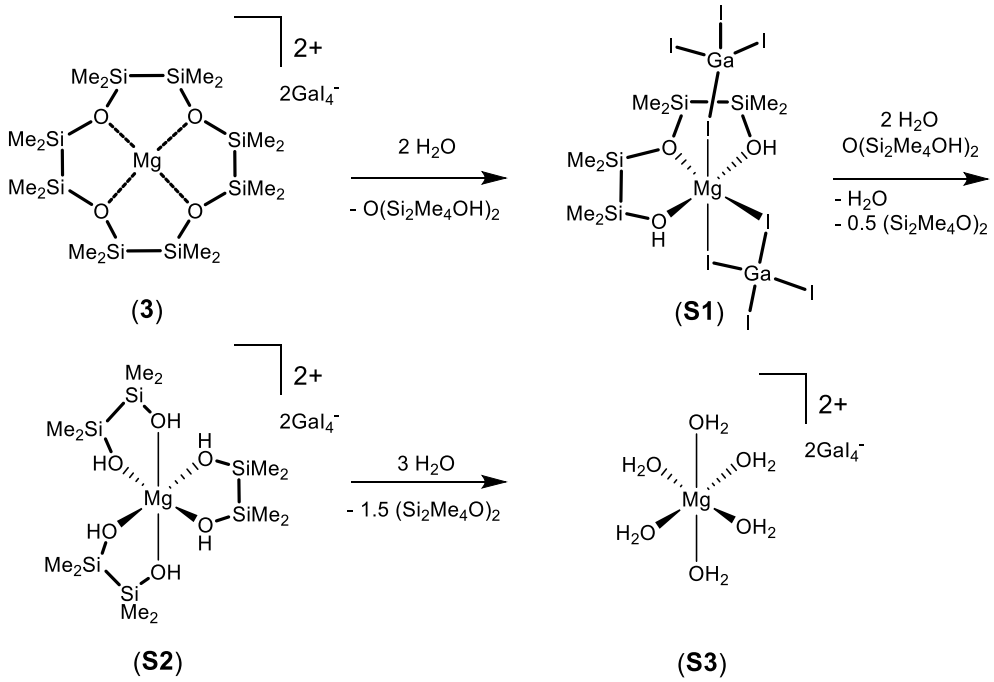

Scheme S1: Proposed pathway for the decomposition of **3**.

3.1 Crystal structure of S1

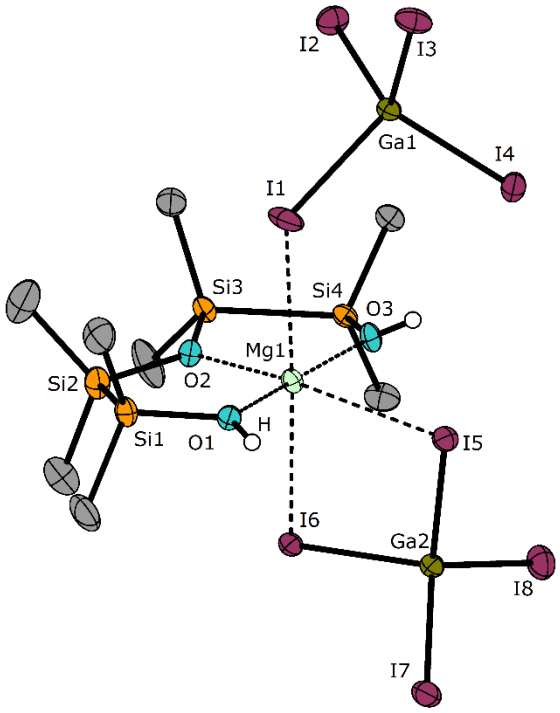

Figure S12: The molecular structure of **S1** in the crystal. Carbon-bond hydrogen atoms are omitted for clarity. Thermal ellipsoids are drawn at 50% probability level. Selected bond lengths [pm]: I1-Mg1 306.4(1), I5-Mg1 305.2(2), I6-Mg1 296.4(1), O1-Mg1 200.2(4), O2-Mg1 209.6(4), O3-Mg1 200.6(4). Selected bond angles [°]: I1-Mg1-I6 174.5(1), O2-Mg1-I5 172.5(1), O1-Mg1-O3 169.1(1), O1-Mg1-O2 94.9(1), O2-Mg1-O3 94.3(1), Si2-O2-Si3 124.8(2).

3.2 Crystal structure of S2

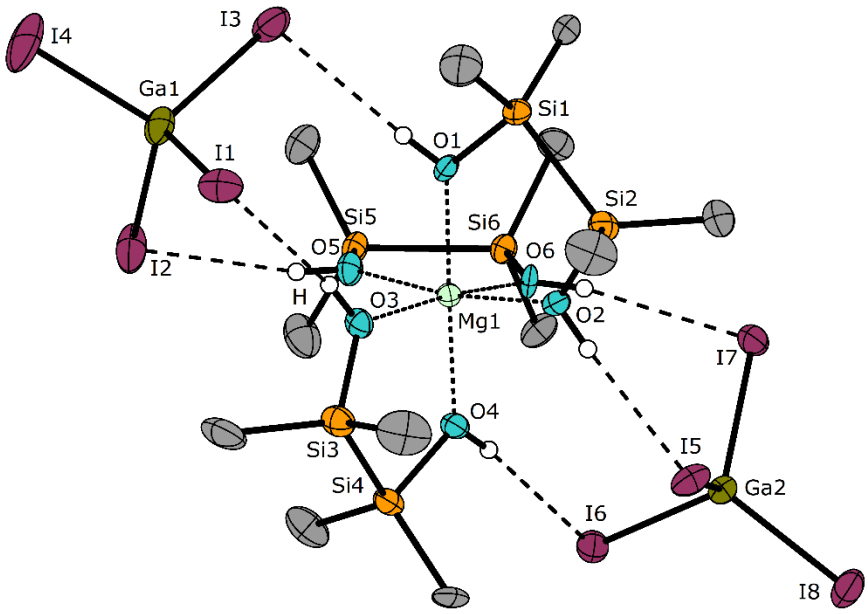

Figure S13: The molecular structure of **S2** in the crystal. Carbon-bond hydrogen atoms are omitted for clarity. Thermal ellipsoids are drawn at 50% probability level. Selected bond lengths [pm]: O1-Mg1 205.7(4), O2-Mg1 207.7(4), O3-Mg1 209.1(4), O4-Mg1 207.0(4), O5-Mg1 207.8(4), O6-Mg1 208.2(4). Selected bond angles [°]: O1-Mg1-O2 85.5(1), O3-Mg1-O4 85.3(1), O5-Mg1-O6 85.8(1), O1-Mg1-O4 172.7(2), O2-Mg1-O5 171.0(1).

4. Crystallographic Data

Table S1. Selected crystal structure data of the structure determinations of the compounds **I**, **II·DCM** and **1**

Compound	**I**	**II·DCM**	**1**
Empirical formula	$C_8H_{24}O_2Si_4$	$C_9H_{25}Cl_2Ga_2I_8Li_2O_2Si_4$	$C_{12}H_{36}GaI_4LiO_3Si_6$
Formula weight	264.63	1475.61	981.21
Crystal colour, habit	colourless, platelet	colourless, plank	colourless,block
Temperature/K	100(2)	100(2)	100(2)
Crystal system	monoclinic	monoclinic	monoclinic
Space group	$P2_1/n$	$P2_1/c$	$C2/c$
a/Å	7.5980(3)	20.7530(8)	18.3592(7)
b/Å	6.4048(3)	13.2339(6)	10.4671(4)
c/Å	16.1625(8)	13.1794(6)	19.2576(7)
α/°	90	90	90
β/°	94.5040(10)	91.8150(10)	113.0990(10)
γ/°	90	90	90
Volume/Å^3	784.10(6)	3617.8(3)	3404.0(2)
Z	2	4	4
ϱ_{calc}g/cm^3	1.121	2.709	1.915
μ/mm^{-1}	0.360	8.529	4.658
F(000)	288.0	2628.0	1848.0
Crystal size/mm^3	0.346 × 0.153 × 0.151	0.287 × 0.125 × 0.1	0.164 × 0.106 × 0.05
Radiation	MoKα (λ = 0.71073)	MoKα (λ = 0.71073)	MoKα (λ = 0.71073)
2Θ range for data collection/°	8.13 to 56.674	4.362 to 50.656	4.578 to 51.992
Reflections collected	22870	98606	57405
Independent reflections	1948 [R_{int} = 0.0241, R_{sigma} = 0.0109]	6584 [R_{int} = 0.0408, R_{sigma} = 0.0145]	3342 [R_{int} = 0.0452, R_{sigma} = 0.0153]
Data/restraints/parameters	1948/6/79	6584/3/271	3342/12/272
Goodness-of-fit on F^2	1.048	1.052	1.122
Final R indexes [I>=2σ(I)]	R_1 = 0.0192, wR_2 = 0.0551	R_1 = 0.0149, wR_2 = 0.0282	R_1 = 0.0215, wR_2 = 0.0363
Final R indexes [all data]	R_1 = 0.0211, wR_2 = 0.0562	R_1 = 0.0188, wR_2 = 0.0293	R_1 = 0.0280, wR_2 = 0.0375
Largest diff. peak/hole / e Å^{-3}	0.33/-0.20	0.66/-0.47	0.53/-0.36
Absolute structure parameter	-	-	-

Table S2. Selected crystal structure data of the structure determinations of the compounds **2**, **4·DCM** and **4a**

Compound	**2**	**4·DCM**	**4a**
Empirical formula	$C_{16}H_{48}GaI_4NaO_4Si_8$	$C_{18}H_{52}CaCl_4Ga_2I_8O_4Si_8$	$C_{16}H_{48}CaCl_2Ga_2I_6O_4Si_8$
Formula weight	1129.57	1893.83	1541.08
Crystal colour, habit	colourless, platelet	colourless, needle	colourless, block
Temperature/K	100(2)	100(2)	100(2)
Crystal system	monoclinic	triclinic	triclinic
Space group	$P2_1/c$	P-1	P-1
a/Å	20.6215(11)	10.6509(7)	10.8414(5)
b/Å	11.3075(6)	11.3868(8)	11.5561(5)
c/Å	19.2534(10)	12.4312(8)	11.8996(5)
α/°	90	105.155(2)	107.514(3)
β/°	112.792(2)	93.396(2)	91.819(4)
γ/°	90	97.281(2)	91.968(4)
Volume/Å^3	4138.9(4)	1436.75(17)	1419.50(11)
Z	4	1	1
ϱ_{calc}g/cm^3	1.813	2.189	1.803
μ/mm^{-1}	3.910	5.700	4.583
F(000)	2168.0	878.0	722.0
Crystal size/mm^3	0.253 × 0.199 × 0.112	0.561 × 0.473 × 0.176	0.363 × 0.184 × 0.183
Radiation	Mo$K\alpha$ (λ = 0.71073)	Mo$K\alpha$ (λ = 0.71073)	Mo$K\alpha$ (λ = 0.71073)
2Θ range for data collection/°	4.27 to 50.566	4.328 to 56.758	3.592 to 50.998
Reflections collected	56417	56782	18425
Independent reflections	7522 [R_{int} = 0.0469, R_{sigma} = 0.0276]	7145 [R_{int} = 0.0312, R_{sigma} = 0.0193]	5279 [R_{int} = 0.0279, R_{sigma} = 0.0316]
Data/restraints/parameters	7522/0/368	7145/0/347	5279/0/186
Goodness-of-fit on F^2	1.043	1.125	1.043
Final R indexes [I>=2σ(I)]	R_1 = 0.0318, wR_2 = 0.0685	R_1 = 0.0342, wR_2 = 0.0928	R_1 = 0.0698, wR_2 = 0.1900
Final R indexes [all data]	R_1 = 0.0468, wR_2 = 0.0744	R_1 = 0.0415, wR_2 = 0.0962	R_1 = 0.0861, wR_2 = 0.1976
Largest diff. peak/hole / e Å^{-3}	1.61/-0.67	2.01/-1.34	5.60/-1.53
Absolute structure parameter	-	-	-

Table S3. Selected crystal structure data of the structure determinations of the compounds **5, S1, S2**

Compound	**5**	**6**	**S1**
Empirical formula	$C_{16}H_{48}Ga_2I_8O_4Si_8Sr$	$C_{12}H_{37}Ga_2I_7O_3Si_6$	$C_8H_{26}Ga_2I_8MgO_3Si_4$
Formula weight	1771.52	1425.69	1461.60
Crystal colour, habit	colourless, prism	colourless, block	colourless, block
Temperature/K	100(2)	100(2)	100(2)
Crystal system	orthorhombic	triclinic	triclinic
Space group	$P2_12_12_1$	P-1	P-1
a/Å	20.021(3)	10.2301(4)	11.1269(14)
b/Å	20.094(2)	11.9594(4)	11.8662(13)
c/Å	24.955(3)	17.8622(7)	13.8845(13)
α/°	90	106.0610(10)	80.508(3)
β/°	90	94.710(2)	76.009(4)
γ/°	90	108.9140(10)	89.295(4)
Volume/Å^3	10040(2)	1950.88(13)	1753.8(3)
Z	8	2	2
ϱ_{calc}g/cm^3	2.344	2.427	2.768
μ/mm^{-1}	7.256	7.118	8.741
F(000)	6496	1300.0	1304.0
Crystal size/mm^3	0.409 × 0.186 × 0.123	0.218 × 0.091 × 0.08	0.159 × 0.121 × 0.102
Radiation	Mo$K\alpha$ (λ = 0.71073)	Mo$K\alpha$ (λ = 0.71073)	Mo$K\alpha$ (λ = 0.71073)
2Θ range for data collection/°	4.37 to 50	4.286 to 53.632	4.244 to 51.592
Reflections collected	186404	51449	53610
Independent reflections	17629 [R_{int} = 0.0707, R_{sigma} = 0.0380]	8322 [R_{int} = 0.0356, R_{sigma} = 0.0238]	6715 [R_{int} = 0.0441, R_{sigma} = 0.0227]
Data/restraints/parameters	17629/1127/890	8322/3/287	6715/2/251
Goodness-of-fit on F^2	1.064	1.013	1.036
Final R indexes [I>=2σ(I)]	R_1 = 0.0890, wR_2 = 0.2204	R_1 = 0.0283, wR_2 = 0.0611	R_1 = 0.0307, wR_2 = 0.0778
Final R indexes [all data]	R_1 = 0.0926, wR_2 = 0.2227	R_1 = 0.0381, wR_2 = 0.0648	R_1 = 0.0358, wR_2 = 0.0799
Largest diff. peak/hole / e Å^{-3}	6.04/-3.15	1.96/-1.15	3.77/-1.97
Absolute structure parameter	0.40(3)	-	-

Table S4. Selected crystal structure data of the structure determinations of the compound **S2**

Compound	**S2**
Empirical formula	$C_{12}H_{42}Ga_2I_8MgO_6Si_6$
Formula weight	1629.94
Crystal colour, habit	colourless, block
Temperature/K	100(2)
Crystal system	monoclinic
Space group	$P2_1/c$
a/Å	17.149(5)
b/Å	13.926(3)
c/Å	20.954(7)
α/°	90
β/°	95.600(9)
γ/°	90
Volume/Å^3	4980(2)
Z	4
ϱ_{calc}g/cm^3	2.174
μ/mm^{-1}	6.219
F(000)	2976.0
Crystal size/mm^3	0.109 × 0.072 × 0.062
Radiation	MoKα (λ = 0.71073)
2Θ range for data collection/°	4.774 to 50.756
Reflections collected	83241
Independent reflections	9108 [R_{int} = 0.0957, R_{sigma} = 0.0459]
Data/restraints/parameters	9108/18/347
Goodness-of-fit on F^2	1.006
Final R indexes [I>=2σ(I)]	R_1 = 0.0372, wR_2 = 0.0675
Final R indexes [all data]	R_1 = 0.0614, wR_2 = 0.0733
Largest diff. peak/hole / e Å^{-3}	1.86/-1.67
Absolute structure parameter	-

5. NMR spectra and plots obtained by DOSY

5.1 Compound I

I has been synthesized according to literature-known procedures.[4] The observed resonances by multinuclear NMR spectroscopy compare well with the values published before.

5.2 Compound II

After dissolving single crystals of **II** in freshly distillated CD_2Cl_2 we could instantaneously detect **II** as the main species but also traces of other species which immediately form after dissolution of **II**. Further species are $[Li(^2D_3)]GaI_4$ (**1**), species of $[Li(^2D_n)_x]GaI_4$-type (**a**) and polymeric $[Li_n(^2D_2)_n]nGaI_4$ (**b**) which is evident from reasonable ^{29}Si NMR chemical shifts. Assignments were backed up by a ^1H-^{29}Si HMBC NMR spectrum (Figure S13) and DOSY.

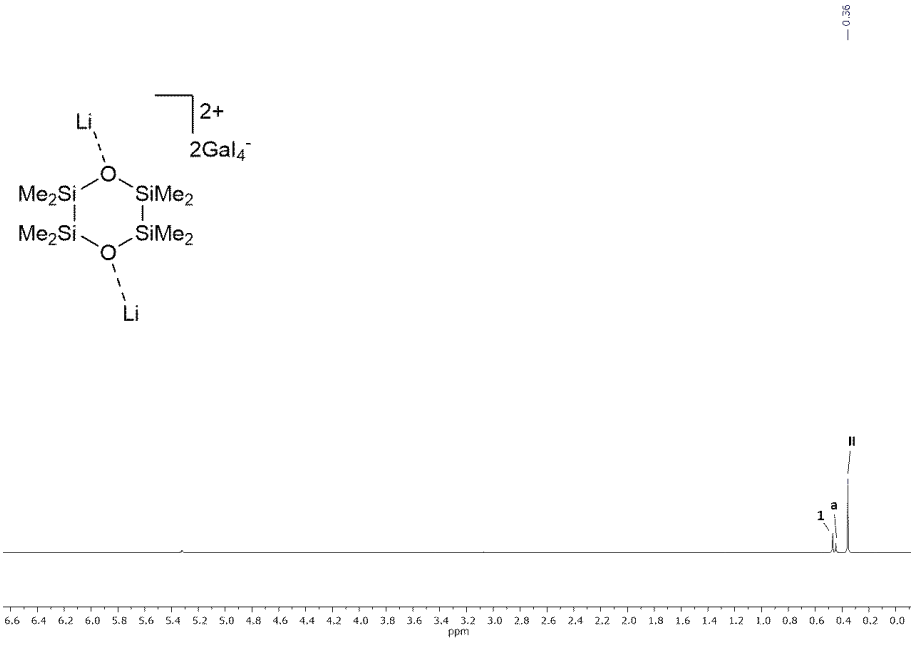

Figure S14: ^1H NMR spectrum of compound **II** in CD_2Cl_2.

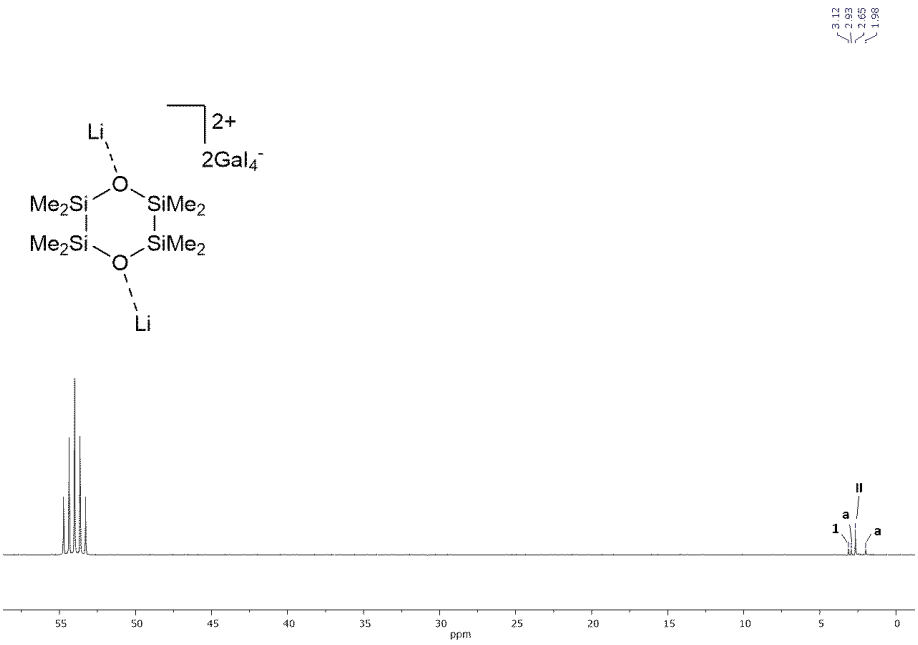

Figure S15: $^{13}C\{^{1}H\}$ NMR spectrum of compound **II** in CD_2Cl_2.

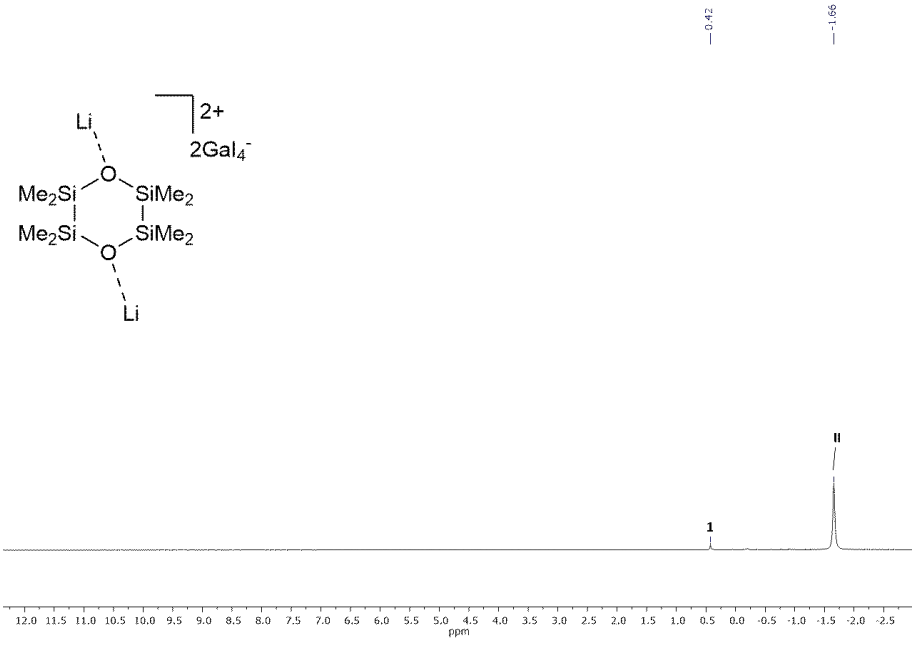

Figure S16: ^{7}Li NMR spectrum of compound **II** in CD_2Cl_2.

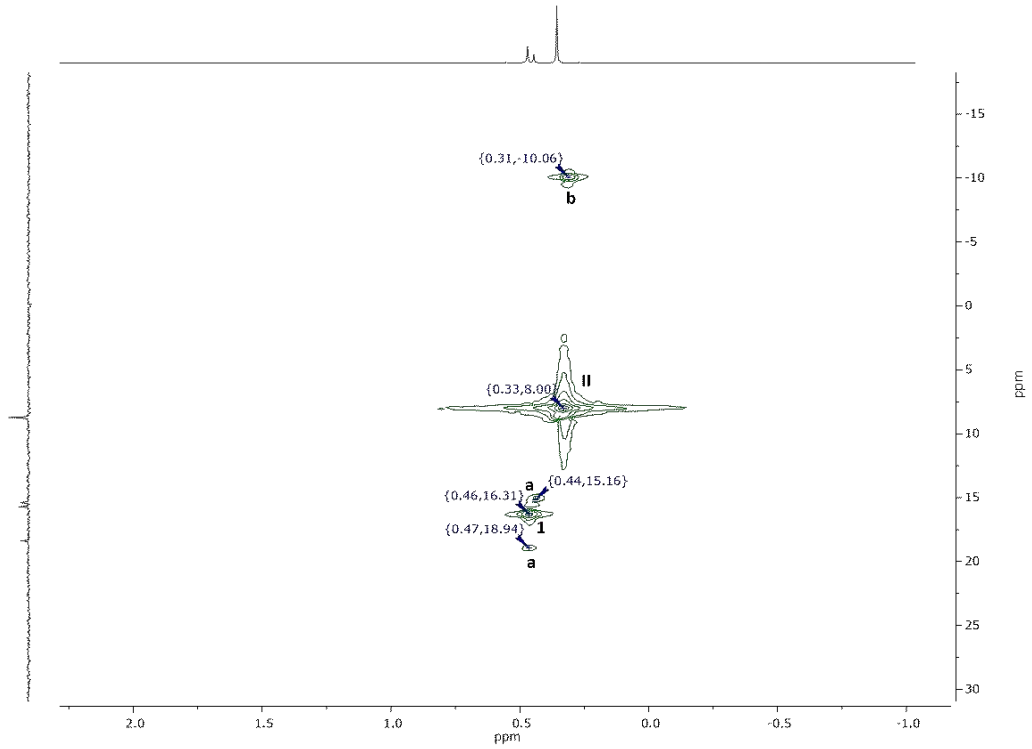

Figure S17: ^{1}H-^{29}Si HMBC NMR spectrum of compound **II** in CD_2Cl_2.

5.3 Compound 1

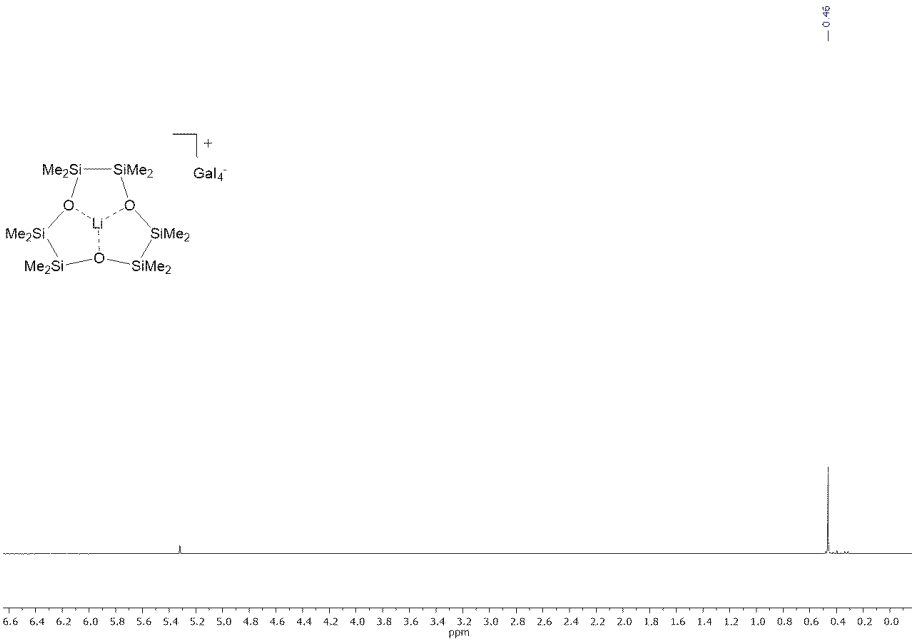

Figure S18: ^{1}H NMR spectrum of compound **1** in CD_2Cl_2.

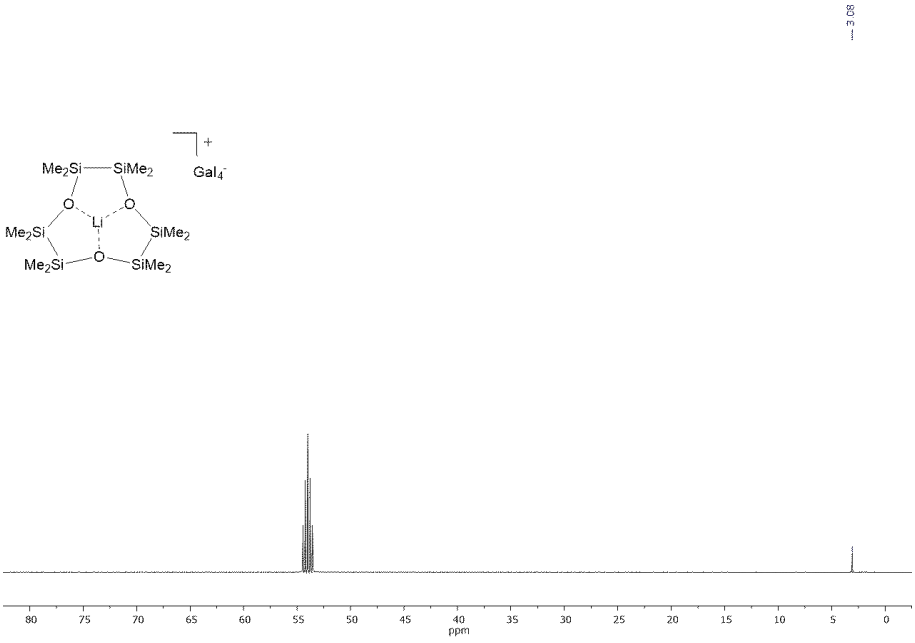

Figure S19: $^{13}C\{^{1}H\}$ NMR spectrum of compound **II** in CD_2Cl_2.

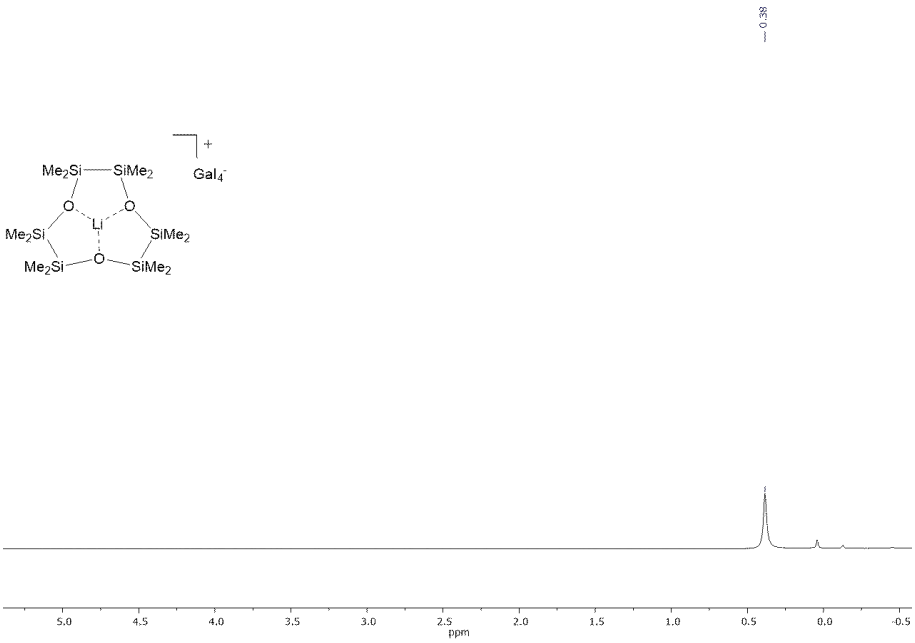

Figure S20: ^{7}Li NMR spectrum of compound **1** in CD_2Cl_2.

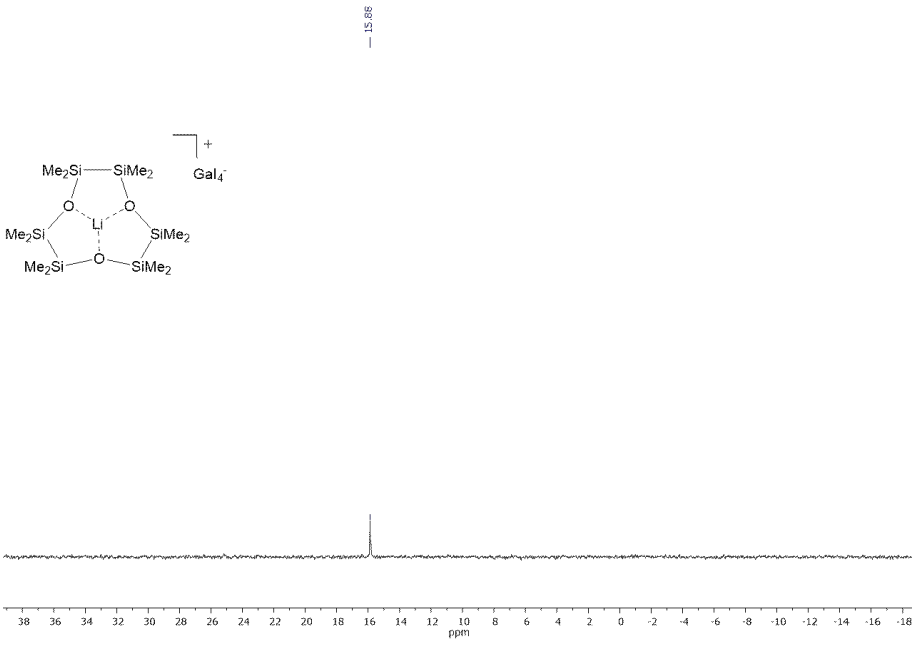

Figure S21: ^{29}Si NMR spectrum of compound **1** in CD_2Cl_2.

5.4 Compound 2

Compound **2** decomposes upon dissolving in CD_2Cl_2. We observe the formation of significant amounts of **I** in solution. Assignments were for this reason backed up by 2D NMR experiments. ^{1}H-^{13}C HSQC as well as ^{1}H-^{29}Si HMBC are provided.

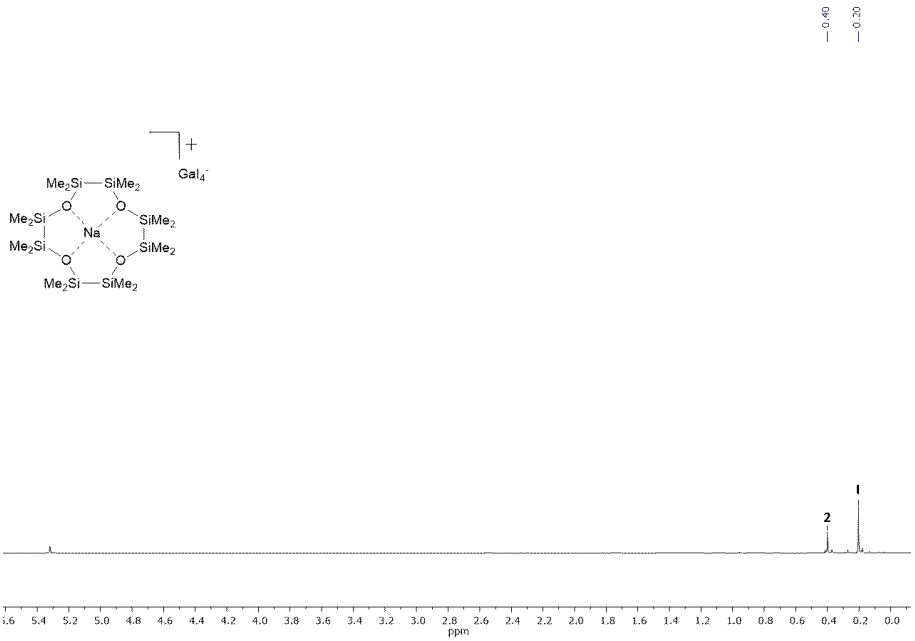

Figure S22: ^{1}H NMR spectrum of compound **1** in CD_2Cl_2.

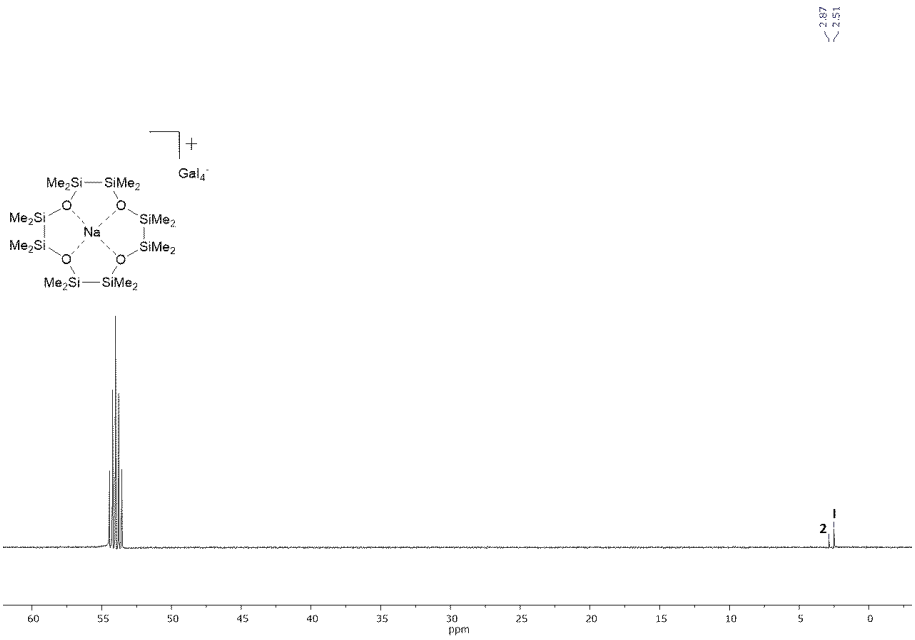

Figure S23: $^{13}C\{^{1}H\}$ NMR spectrum of compound **2** in CD_2Cl_2.

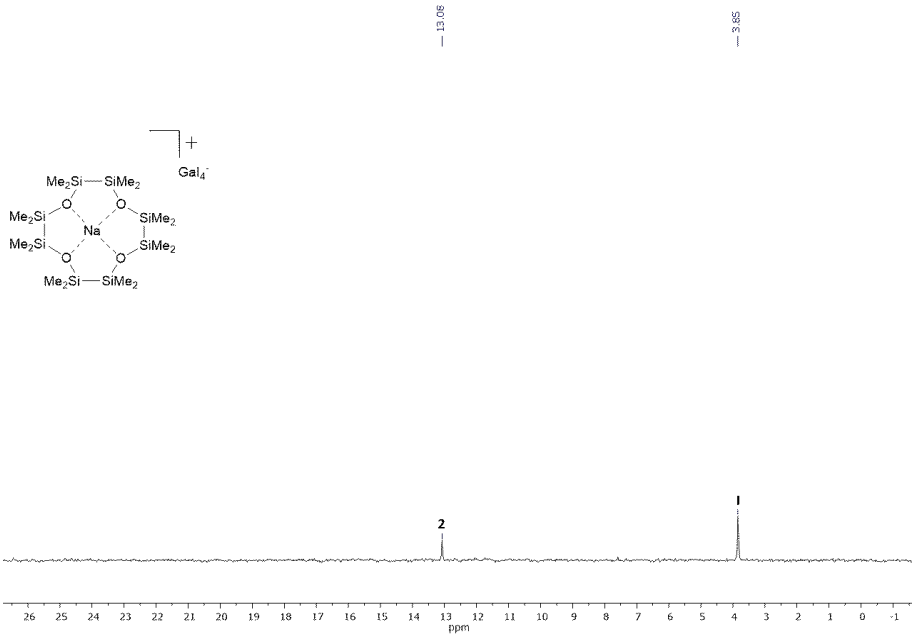

Figure S24: ^{29}Si NMR spectrum of compound **2** in CD_2Cl_2.

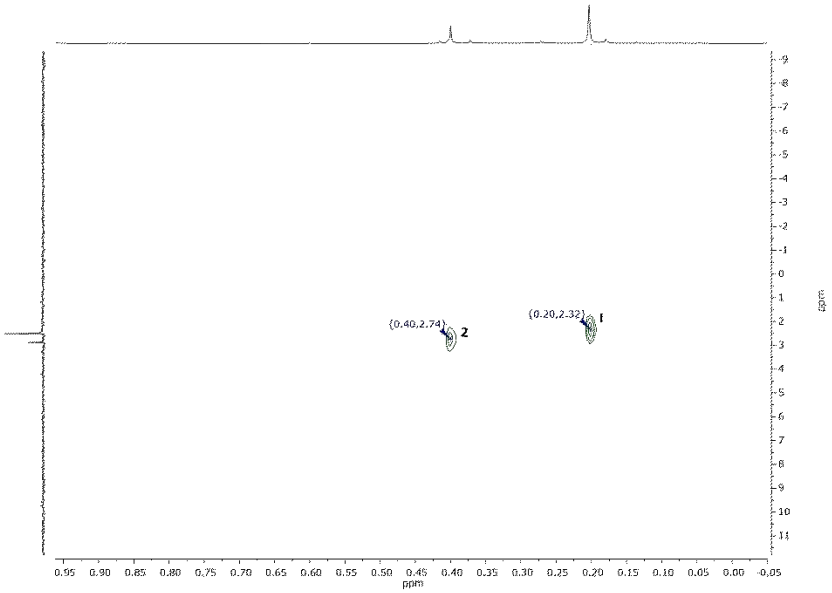

Figure S25: ^{1}H-^{13}C HSQC NMR spectrum of compound **2** in CD_2Cl_2.

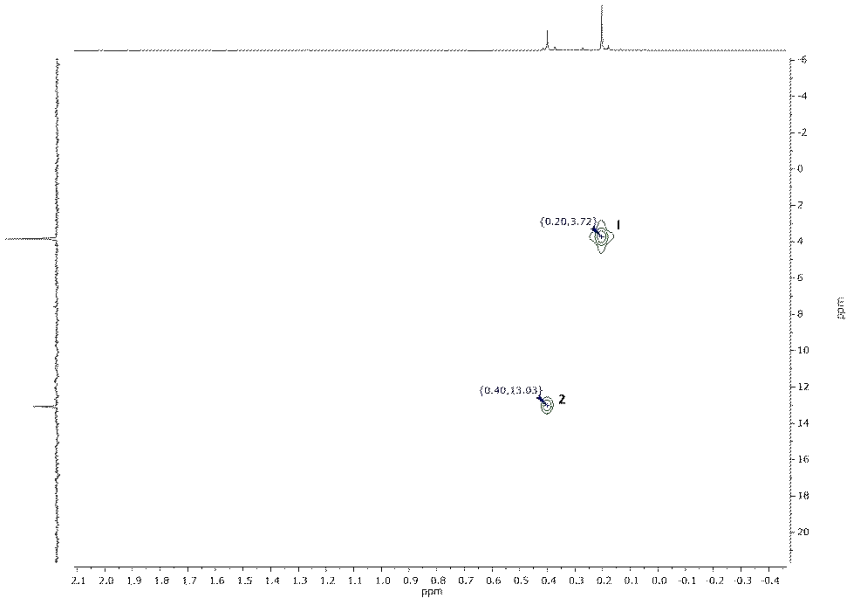

Figure S26: ^{1}H-^{29}Si HMBC NMR spectrum of compound **2** in CD_2Cl_2.

5.5 Compound 3

Compound **3** could only be obtained in low yields and is decomposing fast due to its high sensitivity. We were unable to detect a ^{29}Si NMR resonance in a 1D ^{29}Si(dept) spectrum. Making use of a higher sensitivity of the measurement method, we were still able to detect the signal in a 2D ^{1}H-^{29}Si HMBC spectrum (Figure S25).

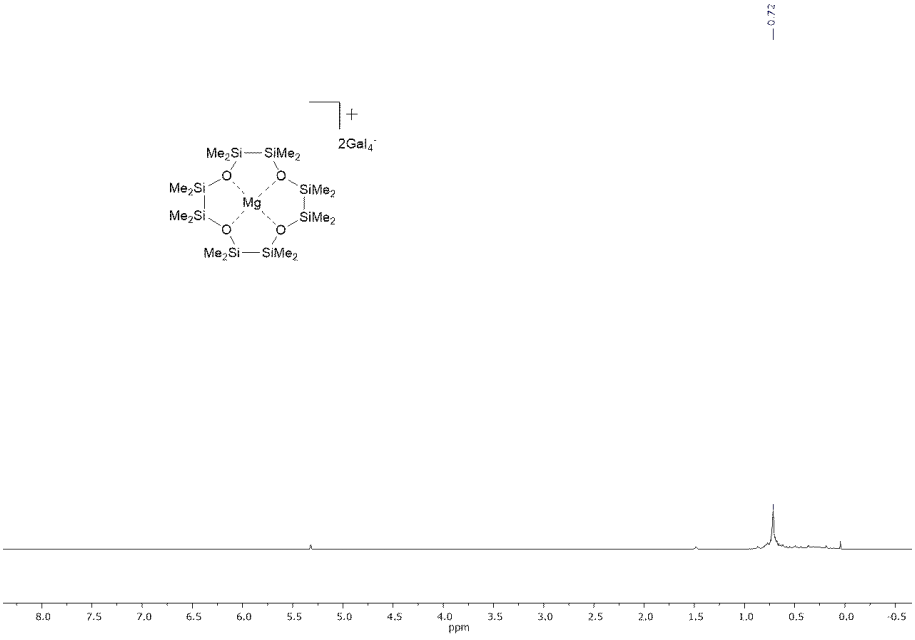

Figure S27: ^{1}H NMR spectrum of compound **3** in CD_2Cl_2.

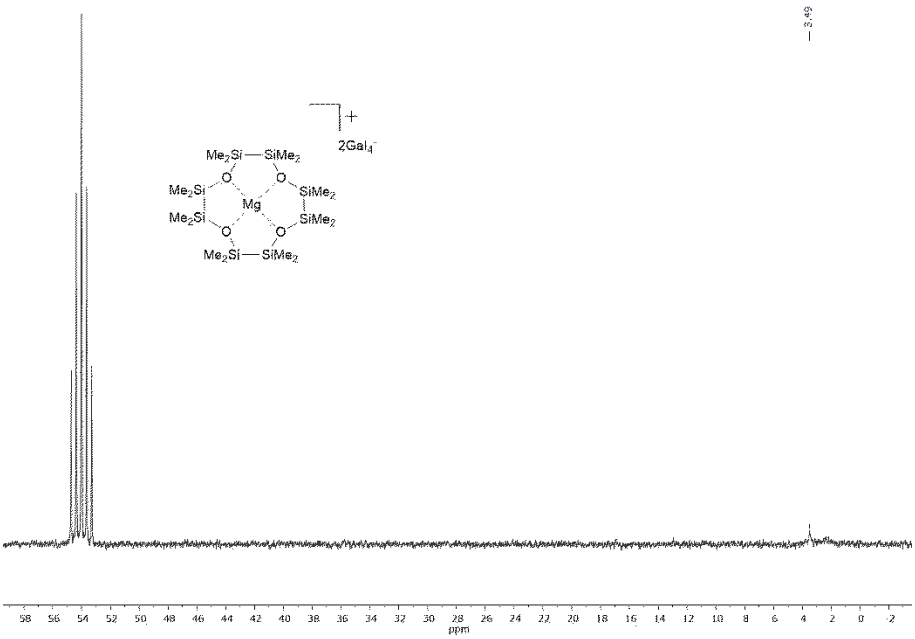

Figure S28: $^{13}C\{^{1}H\}$ NMR spectrum of compound **3** in CD_2Cl_2.

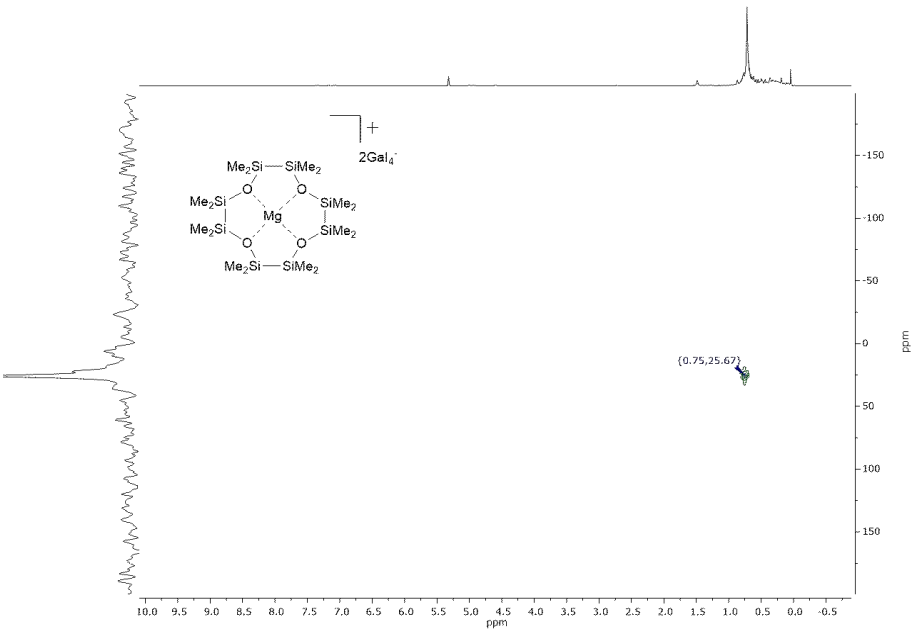

Figure S29: ^{1}H-^{29}Si HMBC NMR spectrum of compound **3** in CD_2Cl_2.

5.6 Compound 4

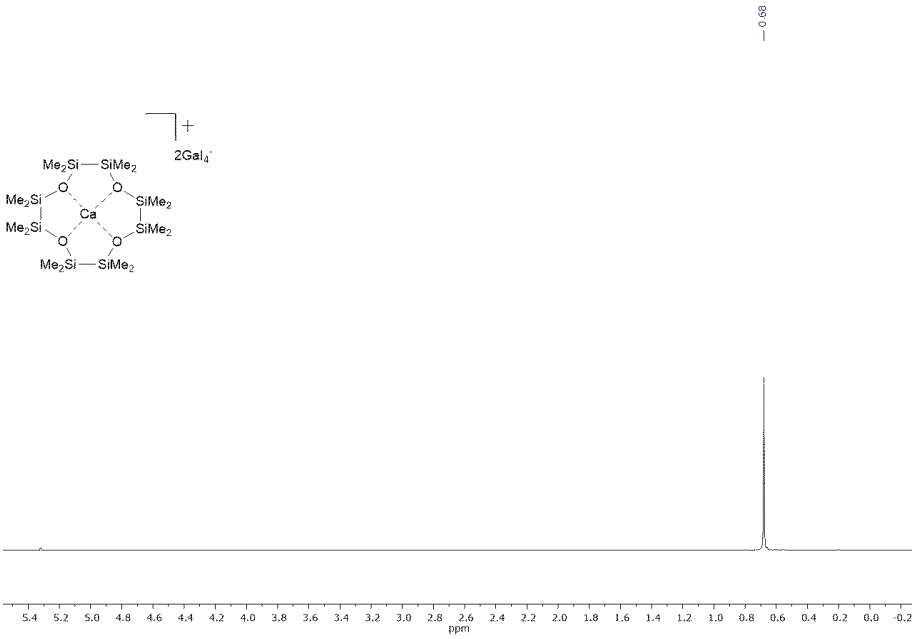

Figure S30: ^{1}H NMR spectrum of compound **4** in CD_2Cl_2.

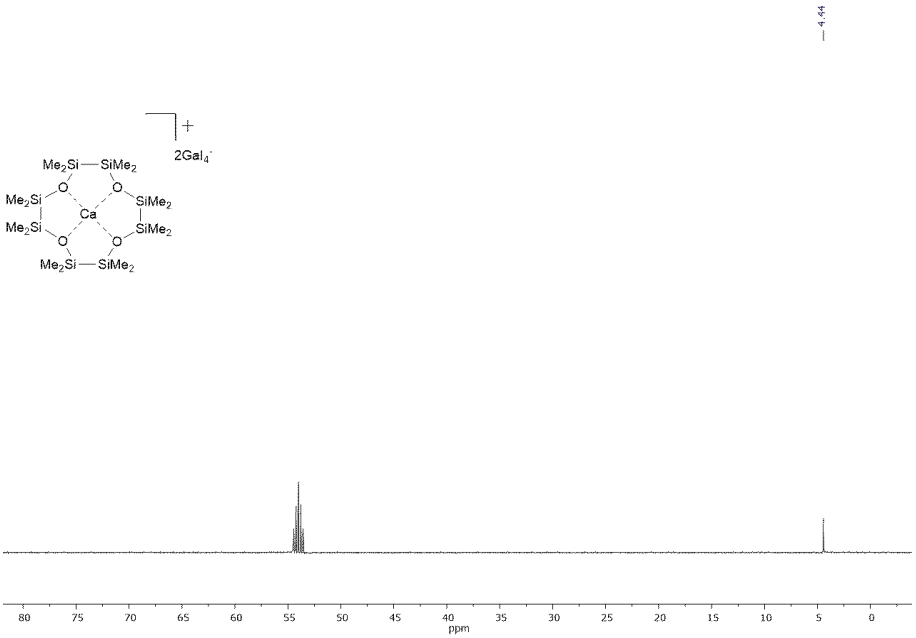

Figure S31: $^{13}C\{^{1}H\}$ NMR spectrum of compound **4** in CD_2Cl_2.

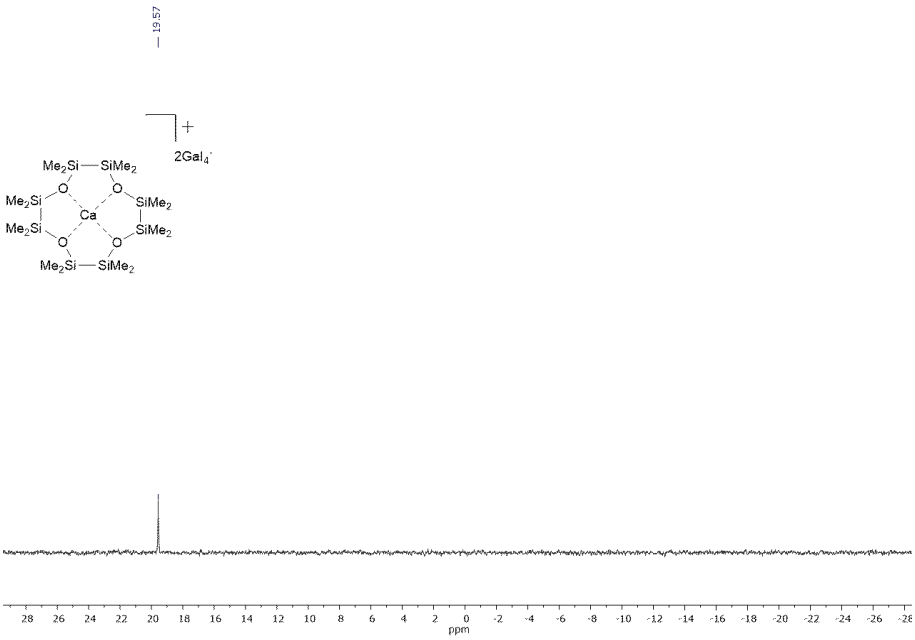

Figure S32: ^{29}Si NMR spectrum of compound **4** in CD_2Cl_2.

5.7 Compound 5

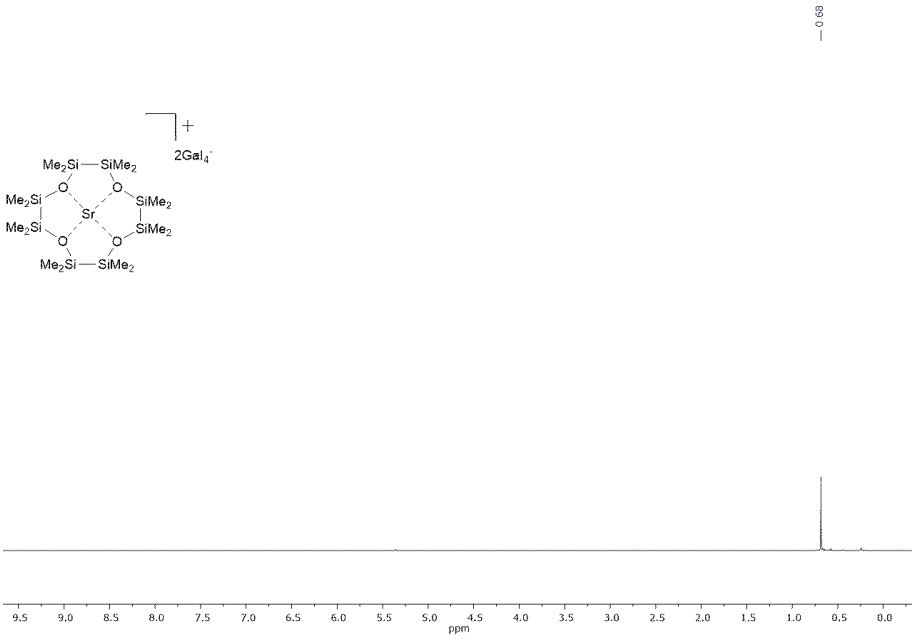

Figure S33: ^{1}H NMR spectrum of compound **4** in CD_2Cl_2.

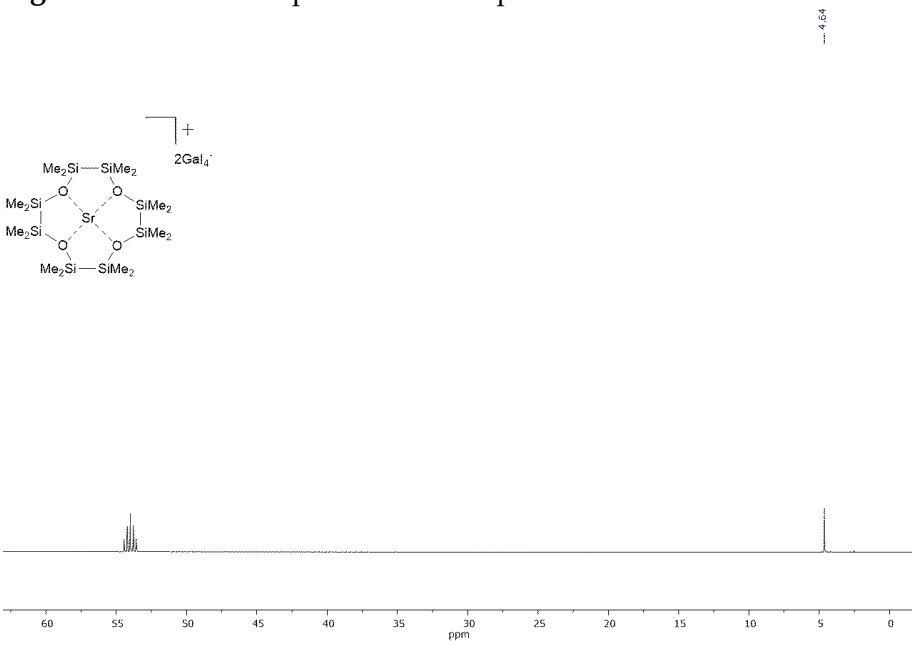

Figure S34: $^{13}C\{^{1}H\}$ NMR spectrum of compound **4** in CD_2Cl_2.

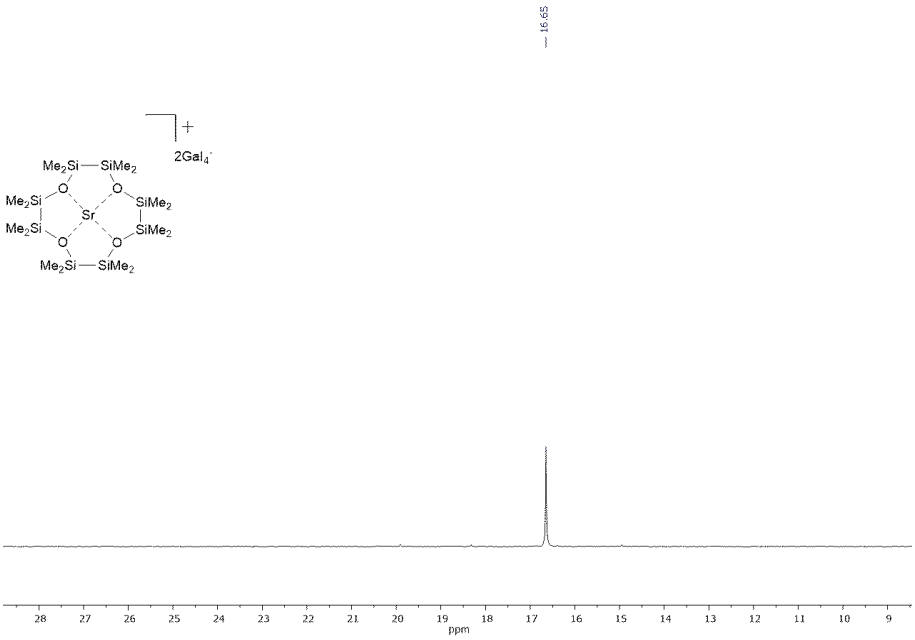

Figure S35: ^{29}Si NMR spectrum of compound **5** in CD_2Cl_2.

5.8 Compound 6

As also mentioned in the main-text, the NMR spectroscopic investigation of compound **6** turned out to be a challenge. Upon dissolving single crystals of **6**, decomposition occurred quickly during the measurement period. As we have observed **6** as the main species during the measurement of ^{1}H and DOSY NMR, the compound has decomposed during ^{13}C measurement which takes generally longer than ^{1}H NMR. Thus, we obtained a more or less clean proton spectrum but ^{13}C and ^{29}Si NMR spectra already contain various decomposition products which we tentatively assign to $[H_x(^2D_n)]^{x+}$ which is evident from reasonable ^{29}Si NMR chemical shifts. To properly assign the ^{13}C and ^{29}Si NMR chemical shift of **6** we decided to roughly record 2D spectra of the respective nucleus in order to save time which causes decomposition. Thus, ^{13}C and ^{29}Si NMR spectra are provided as 2D spectra. All decomposition products of $[H_x(^2D_n)]^{x+}$ are depicted with an asterisk (*). So far, our attempts isolating and crystallizing $[H_x(^2D_n)]^{x+}$ species failed. The described difficulty does also explain why our efforts to obtain long-range correlation and an exchange spectroscopy failed.

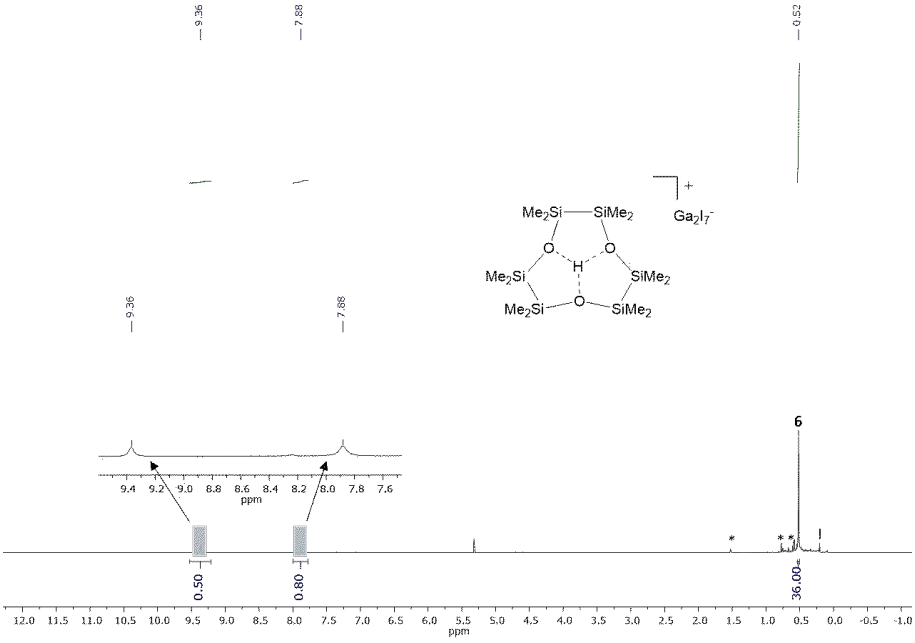

Figure S36: ^{1}H NMR spectrum of compound **6** in CD_2Cl_2.

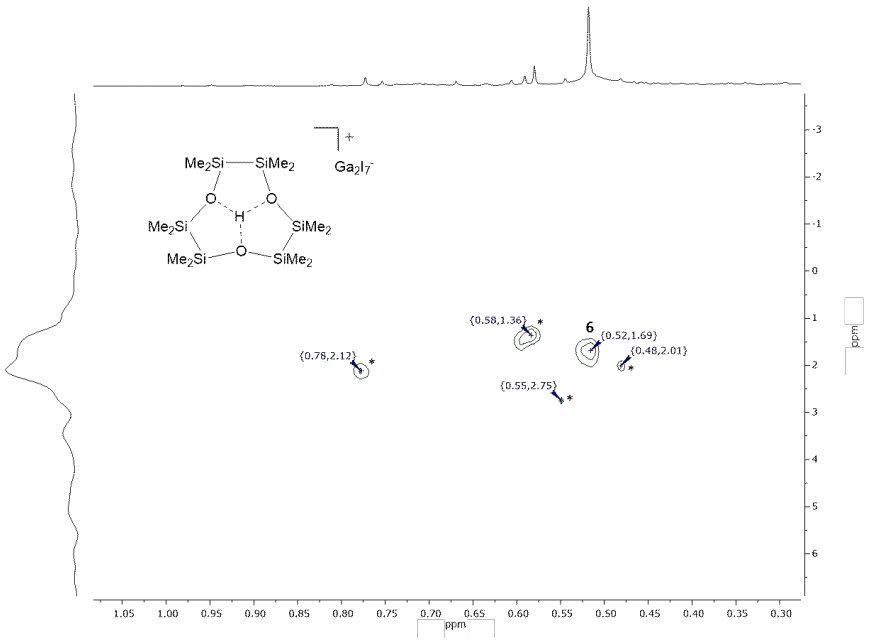

Figure S37: ^{1}H-^{13}C HSQC NMR spectrum of compound **6** in CD_2Cl_2.

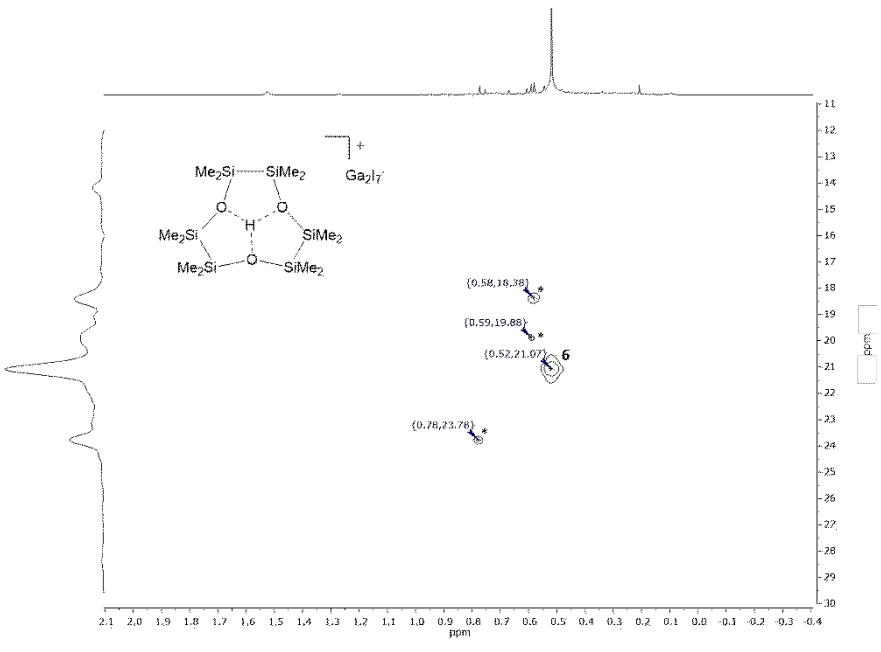

Figure S38: 1H-^{29}Si HMBC NMR spectrum of compound **5** in CD_2Cl_2.

5.9 Compounds 7 and 8

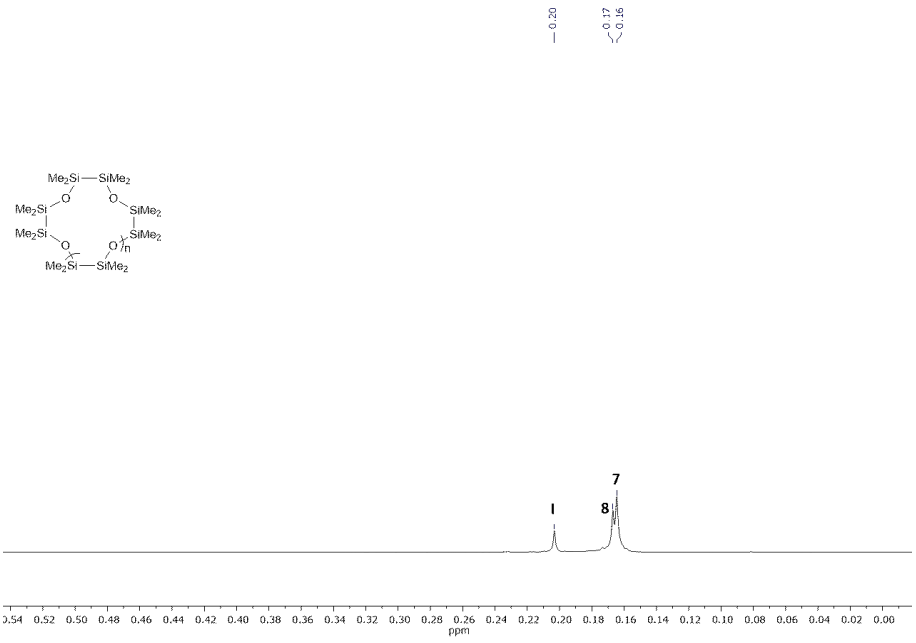

Figure S39: ^{1}H NMR spectrum of compound **7** and **8** in CD_2Cl_2 (freshly prepared).

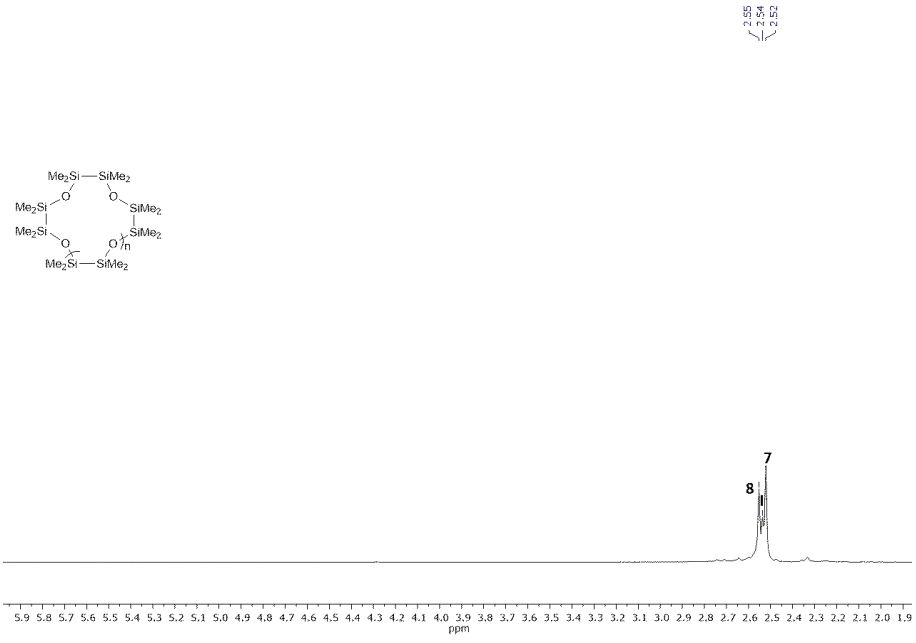

Figure S40: ^{13}C NMR spectrum of compound **7** and **8** in CD_2Cl_2 (freshly prepared).

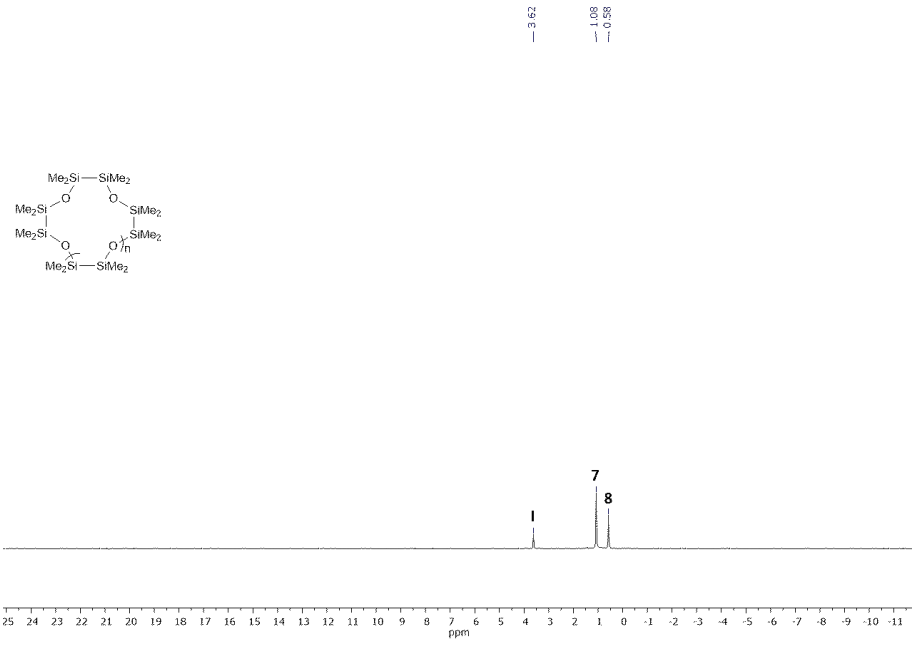

Figure S41: ^{29}Si NMR spectrum of compound **7** and **8** in CD_2Cl_2 (freshly prepared).

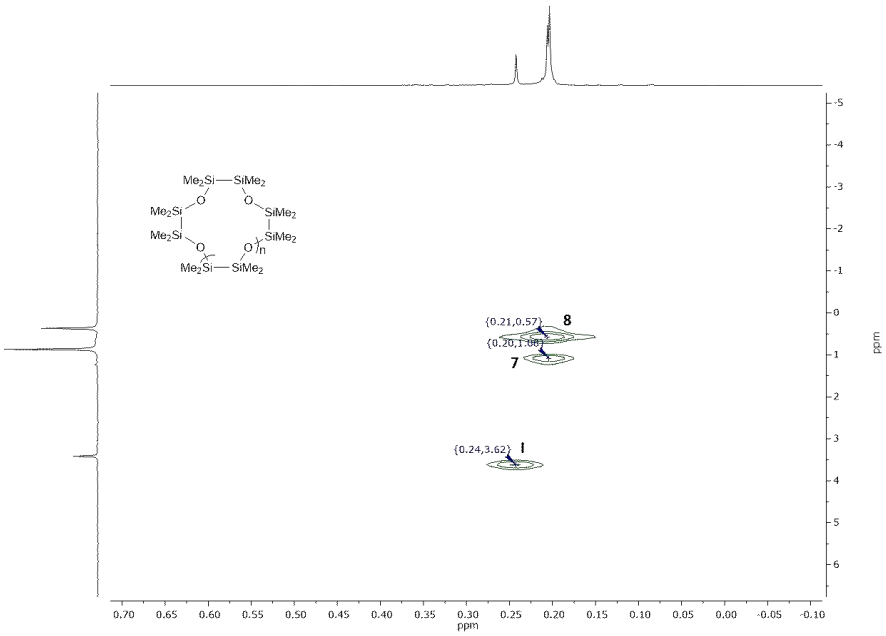

Figure S42: ^{1}H-^{29}Si HMBC NMR spectrum of compound **7** and **8** in CD_2Cl_2 (freshly prepared).

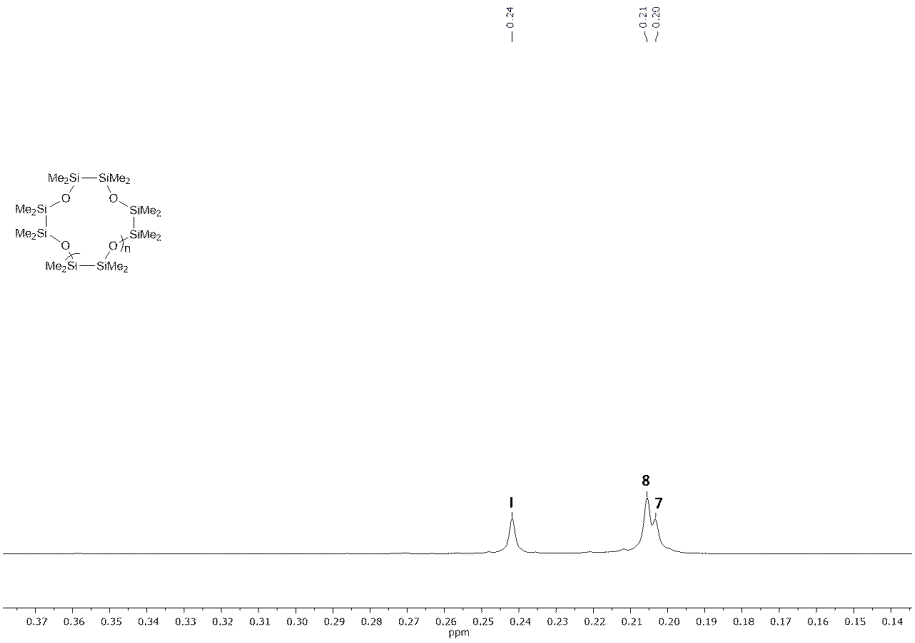

Figure S43: ^{1}H NMR spectrum of compound **7** and **8** in CD_2Cl_2 (after 4 days).

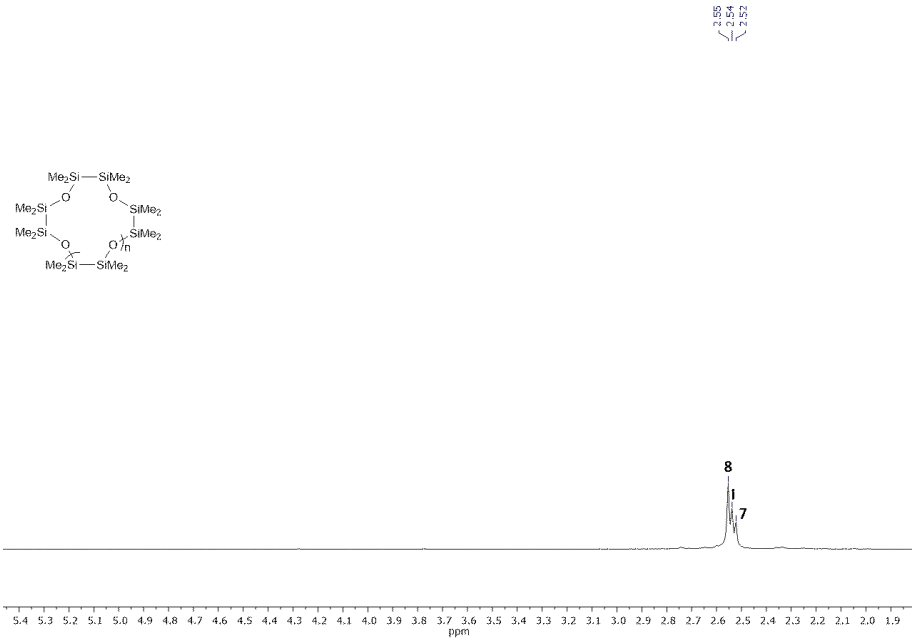

Figure S44: ^{13}C NMR spectrum of compound **7** and **8** in CD_2Cl_2 (4 days).

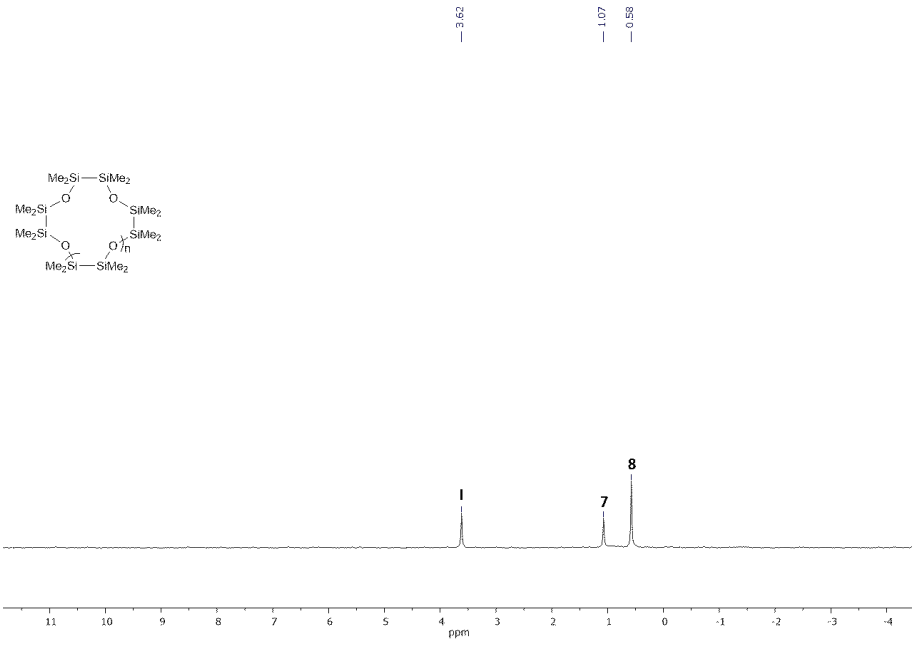

Figure S45: ^{29}Si NMR spectrum of compound **7** and **8** in CD_2Cl_2 (after 4 days).

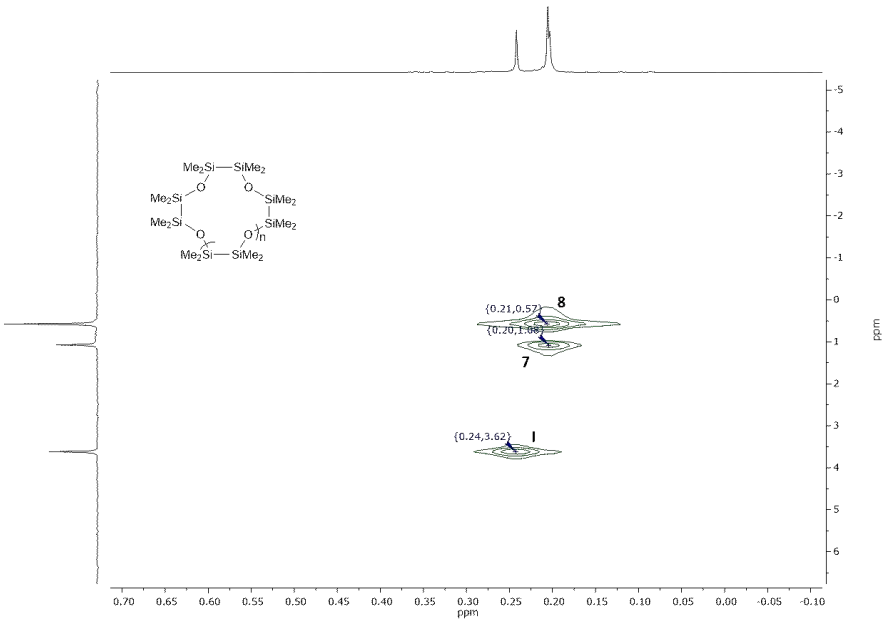

Figure S46: ^{1}H-^{29}Si HMBC NMR spectrum of compound **7** and **8** in CD_2Cl_2 (after 4 days).

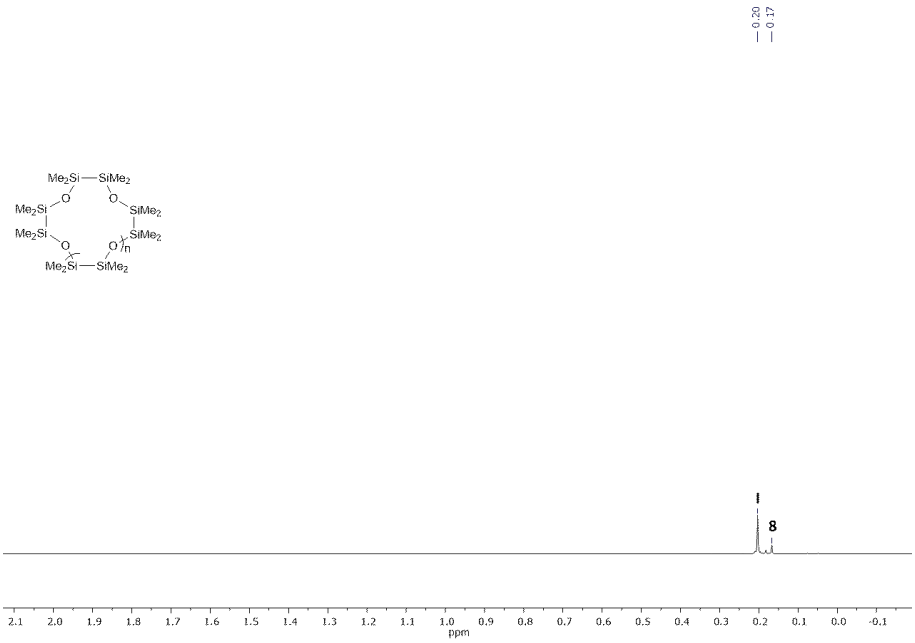

Figure S47: ^{1}H NMR spectrum of compound **7** and **8** in CD_2Cl_2 (after 9 weeks).

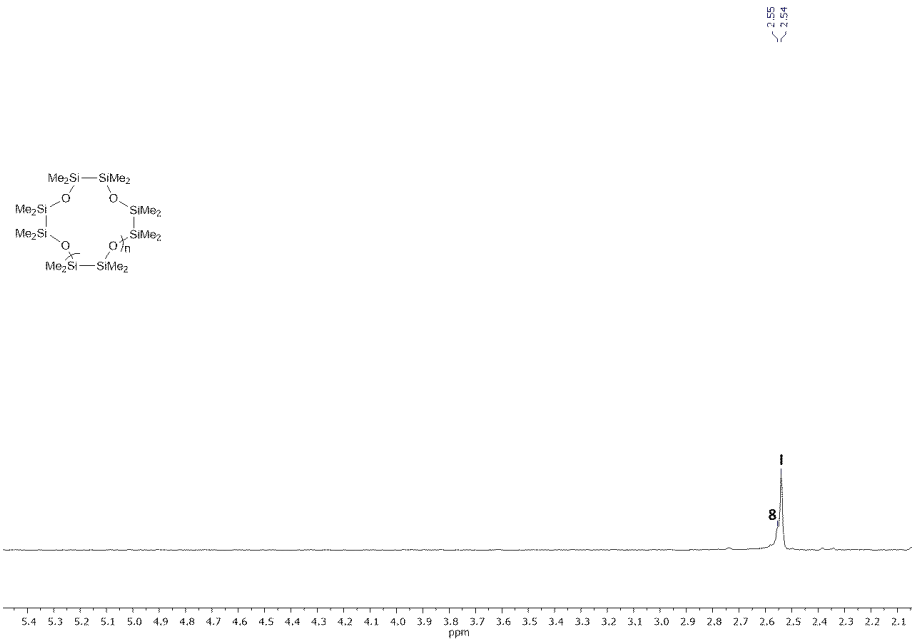

Figure S48: ^{13}C NMR spectrum of compound **7** and **8** in CD_2Cl_2 (after 9 weeks).

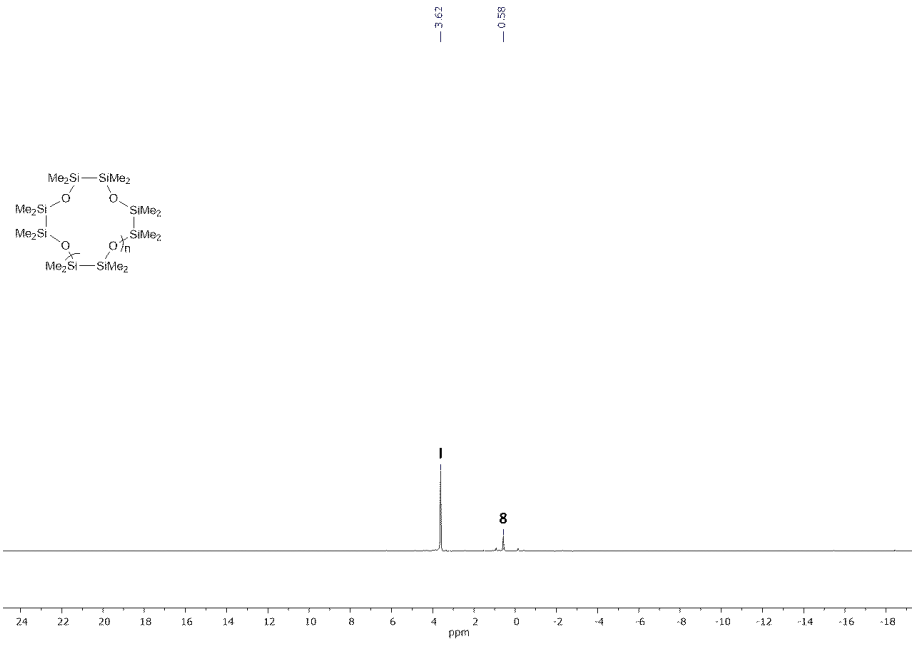

Figure S49: ^{29}Si NMR spectrum of compound **7** and **8** in CD_2Cl_2 (after 9 weeks).

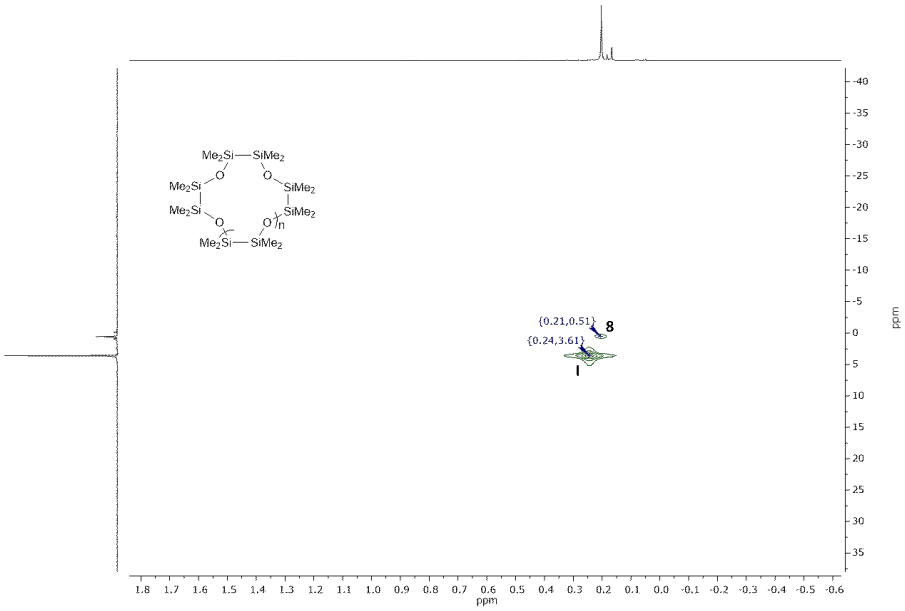

Figure S50: ^{1}H-^{29}Si HMBC NMR spectrum of compound **7** and **8** in CD_2Cl_2 (after 9 weeks).

5.10 Stejskal-Tanner Plots

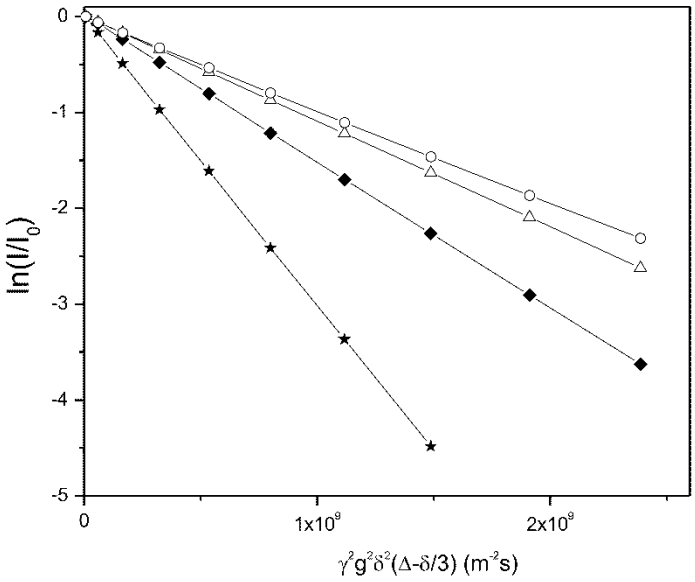

Figure S51: Stejskal-Tanner plot of the solvent CD_2Cl_2 (star), **I** (diamond), dissolved **1** (triangle) and dissolved **2** (circle) for comparison.

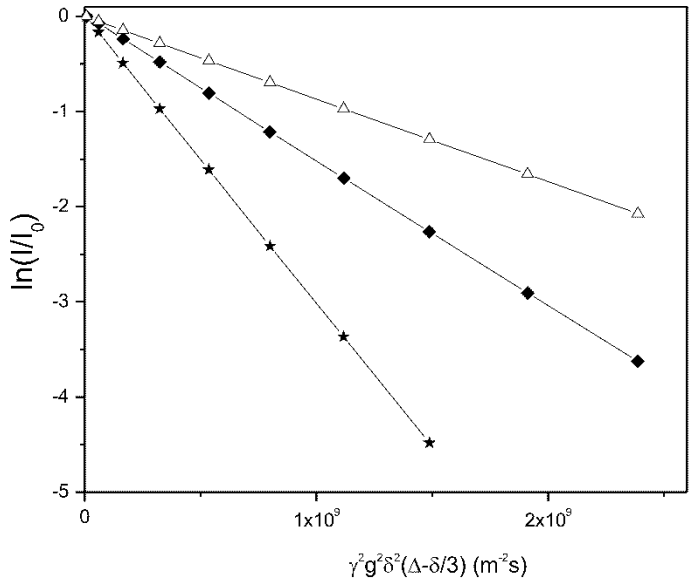

Figure S52: Stejskal-Tanner plot of the solvent CD_2Cl_2 (star), **I** (diamond), and dissolved **4** (triangle) for comparison.

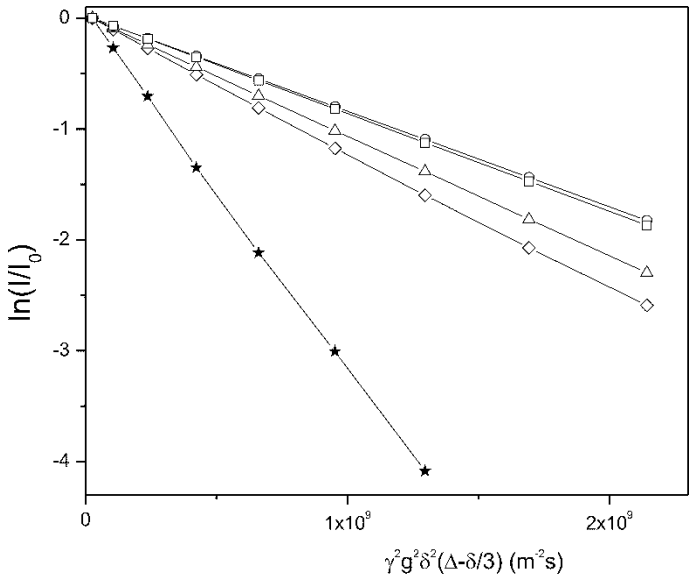

Figure S53: Stejskal-Tanner plot of the solvent CD_2Cl_2 (star), **II** (diamond), dissolved **6** (triangle), dissolved **3** (square) and dissolved **5** (circle) for comparison.

6. HR-MS spectra

6.1 Compound 7

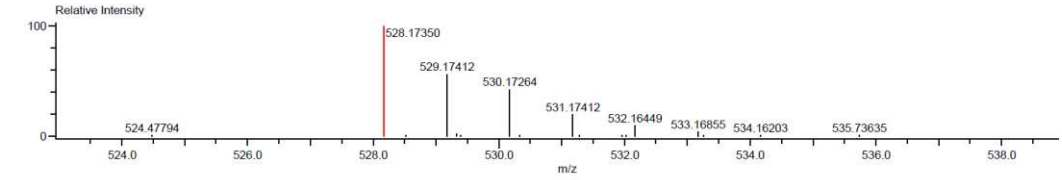

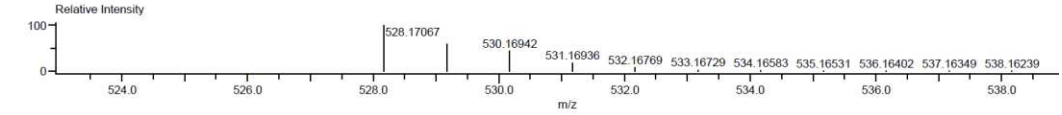

Mass	Intensity	Relative Intensity	Calc. Mass	Mass Difference [mDa]	Mass Difference [ppm]	Possible Formula	Unsaturation Number
528.17350	15195.02	100.00	528.17067	2.83	5.37	$^{12}C_{16}{}^{1}H_{48}{}^{16}O_{4}{}^{28}Si_{8}$	1.0

Figure S54: HR-LIFDI(+) MS spectrum of **7**.

6.2 Compound 8

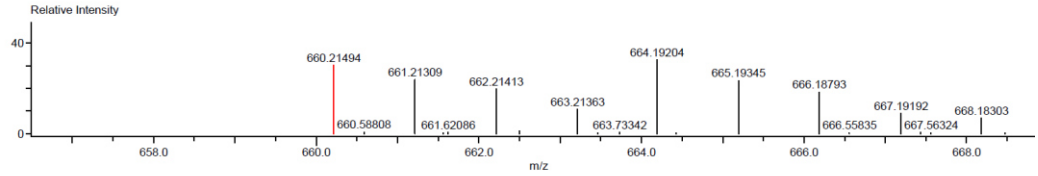

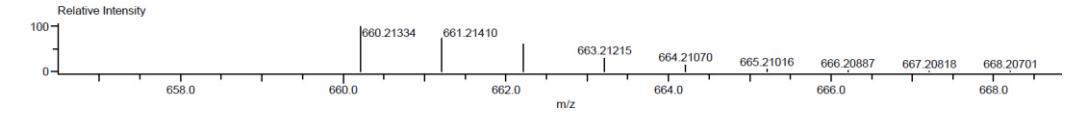

Mass	Intensity	Relative Intensity	Calc. Mass	Mass Difference [mDa]	Mass Difference [ppm]	Possible Formula	Unsaturation Number
660.21494	23069.63	30.02	660.21334	1.60	2.42	$^{12}C_{20}{}^{1}H_{60}{}^{16}O_{5}{}^{28}Si_{10}$	1.0

Figure S55: HR-LIFDI(+) MS spectrum of **8**.

6.3 Compound 9

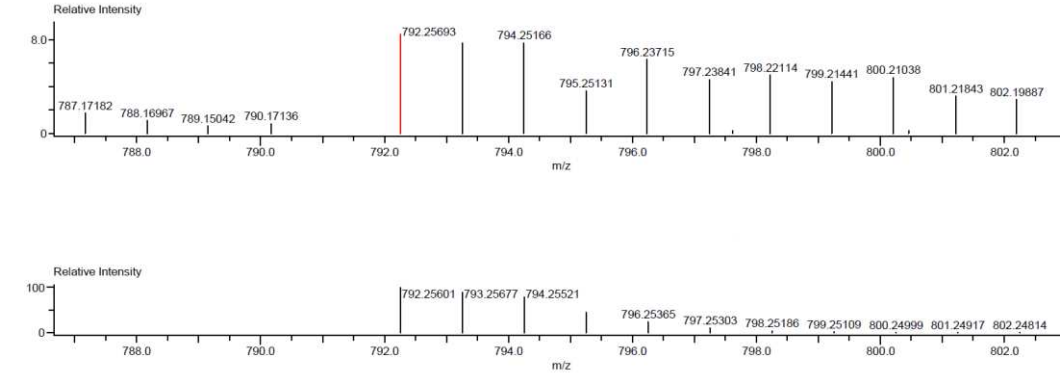

Mass	Intensity	Relative Intensity	Calc. Mass	Mass Difference [mDa]	Mass Difference [ppm]	Possible Formula	Unsaturation Number
792.25693	6455.76	8.40	792.25601	0.92	1.16	$^{12}C_{24}{}^{1}H_{72}{}^{16}O_{6}{}^{28}Si_{12}$	1.0

Figure S56: HR-LIFDI(+) MS spectrum of **9**.

7. Quantum chemical calculations

Quantum chemical calculations[4] were carried out at the level of density functional theory. For the calculation of minimum structures of L and ML^+, (L = $^2D_2$, $^2D_3$, $^2D_4$, D_5, D_6, as well as 3*n*-crown-*n*, *n*=4-7) and ML^+ (M=Li, Na) the functionals PBE[5], PBE0[6] and TPSS[7] evaluated at medium-sized grids (grid 3)[8], together with def2-TZVP basis sets[9] were employed. For the RI approximation[10] corresponding auxiliary bases[11] were used. Solvent effects were modelled with the conductor-like screening model[12] with the dielectric constant, ε, as input parameter. From the total energies of L and ML^+ energies for reactions $[ML_1]^+ + L_2 \rightarrow [ML_2]^+ + L_1$ were calculated and sampled in Tables S5 (M=Li, ε=1,6,9, functional PBE), S6 (M=Li, ε=1, functionals PBE0 and TPSS), S7 (M=Na, ε=1,6,9, functional PBE) and S8 (M=Na, ε=1, functionals PBE0 and TPSS).

Reaction pathways P(Na^+) and P(NaI) for the transformations from $[Na^+(^2D_2)_2]^+$ to $[Na^2D_4]^+$ and from $[NaI(^2D_2)_2]$ to $[NaI^2D_4]$ were explored with the reaction path optimization tool proposed by *Plessow*[13] using the PBE functional and def2-TZVP basis sets. For both cases we started with simplified models where Me was replaced with H, $P^H(Na^+)$ and P^H(NaI). For $P^H(Na^+)$ the optimized structures of $[Na^+(^2D^H_2)_2]^+$ and $[Na^2D^H_4]^+$ were used as input for the initial path, which consisted of 75 interpolated structures for discretization; for P^H(NaI), additionally to the corresponding optimized structures a roughly pre-optimized intermediate structure with a broken Si-O bond and I connecting to this Si atom was used for the initial path. Cartesian coordinates for the two input structures for $P^H(Na^+)$ are listed in Table S9, and for the three input structures for P^H(NaI) in Table S10. The energy profiles of the two optimized pathways are shown in Figure S57, structures of selected extrema along these pathways in Fig. S58. The converged pathways $P^H(Na^+)$ and P^H(NaI) served as starting points for the

optimization of pathways, P(Na^+) and P(NaI). H was replaced with Me and the coordinates of the Me groups were optimized while keeping the positions of O, Si and Na fixed, except for the first and the last structure, which were fully optimized. In case of $P^H(Na^+)$ the first, the last and another 7 structures equally distributed along the path, were used as input for the initial path, after the H atoms of each CH_3 group were permuted so that that rotations of these groups along the path were avoided. For the more complicated P(NaI) it turned out that replacement of H with Me significantly influences the energy profile of the pathway, as evident from Figure S59, which shows this pathway after H being replaced with Me and optimization of the coordinates of the Me groups while keeping the positions of O, Si and Na fixed. Thus, for the optimization of P(NaI) the initial path was set up by first fully optimizing the structures labelled 1 and 10 in figures S59 and S60 and taking structures 2–8 as intermediates. The energy profile of the converged pathways P(Na^+) and P(NaI) resulting from optimizations starting from these initial pathways are shown in the main document (Figure 4) together with images of extremum structures (Figure 5) and are also available as movies in files path_without_i.mp4 and path_with_i.mp4. Finally, the entire pathways were reoptimized within COSMO (ε=6); energy profiles are shown in Figure S61. For clarity we note that this procedure does not exactly yield transition states (stationary points with exactly one imaginary frequency), but due to the large number of intermediate points on the pathway we are confident that the qualitative picture of the pathway is realistic.

Table S5. Reaction energies (PBE functional) for reactions $L_2Li^+ + L_1 \rightarrow L_1Li^+ + L_2$ in kJ/mol. The rows refer to L_1 and the columns to L_2. (L_1, L_2 = $^2D_2$, $^2D_3$, $^2D_4$, D_5, D_6, C_4, C_5, C_6; C_n is an abbreviation for [3*n*]crown-*n*). For instance, the energy for the reaction $[Li(^2D_2)]^+ + {}^2D_3 \rightarrow [Li(^2D_3)]^+ + {}^2D_2$, which amounts to −135 kJ/mol is found in the row labelled $^2D_3$ and the column labelled $^2D_2$. The numbers in the last column, *avg*, are the averages of the seven nonzero numbers in the columns before.

ε=1	$^2D_2$	$^2D_3$	$^2D_4$	D_5	D_6	C_4	C_5	C_6	*avg*
$^2D_2$	0	135	170	122	155	157	184	163	155
$^2D_3$	-135	0	35	-13	20	22	49	28	1
$^2D_4$	-170	-35	0	-48	-15	-13	14	-7	-39
D_5	-122	13	48	0	32	35	62	41	16
D_6	-155	-20	15	-32	0	2	29	8	-22
C_4	-157	-22	13	-35	-2	0	27	6	-24
C_5	-184	-49	-14	-62	-29	-27	0	-21	-55
C_6	-163	-28	7	-41	-8	-6	21	0	-31
ε=6	$^2D_2$	$^2D_3$	$^2D_4$	D_5	D_6	C_4	C_5	C_6	*avg*
$^2D_2$	0	72	89	58	85	111	127	93	91
$^2D_3$	-72	0	17	-14	13	38	55	21	8
$^2D_4$	-89	-17	0	-31	-4	21	38	4	-11
D_5	-58	14	31	0	27	52	69	35	24
D_6	-85	-13	4	-27	0	25	42	8	-7
C_4	-111	-38	-21	-52	-25	0	17	-17	-35
C_5	-127	-55	-38	-69	-42	-17	0	-34	-55
C_6	-93	-21	-4	-35	-8	17	34	0	-16
ε=9	$^2D_2$	$^2D_3$	$^2D_4$	D_5	D_6	C_4	C_5	C_6	*avg*
$^2D_2$	0	64	80	50	77	105	120	84	83
$^2D_3$	-64	0	15	-14	13	40	56	20	9
$^2D_4$	-80	-15	0	-29	-3	25	41	4	-8
D_5	-50	14	29	0	27	54	70	34	25
D_6	-77	-13	3	-27	0	27	43	7	-5
C_4	-105	-40	-25	-54	-27	0	16	-20	-36
C_5	-120	-56	-41	-70	-43	-16	0	-36	-55
C_6	-84	-20	-4	-34	-7	20	36	0	-13

Table S6. Gas phase reaction energies obtained with functionals PBE0 and TPSS for reactions $[LiL_2]^+ + L_1 \rightarrow [LiL_1]^+ + L_2$ in kJ/mol. See also Table S5.

PBE0	$^2D_2$	$^2D_3$	$^2D_4$	D_5	D_6	C_4	C_5	C_6	*avg*
$^2D_2$	0	136	169	121	156	167	193	173	159
$^2D_3$	-136	0	33	-15	20	32	57	37	4
$^2D_4$	-169	-33	0	-48	-13	-1	24	4	-34
D_5	-121	15	48	0	35	47	72	52	21
D_6	-156	-20	13	-35	0	11	37	17	-19
C_4	-167	-32	1	-47	-11	0	25	5	-32
C_5	-193	-57	-24	-72	-37	-25	0	-20	-61
C_6	-173	-37	-4	-52	-17	-5	20	0	-38
TPSS	$^2D_2$	$^2D_3$	$^2D_4$	D_5	D_6	C_4	C_5	C_6	*avg*
$^2D_2$	0	130	158	118	152	174	198	178	158
$^2D_3$	-130	0	28	-13	21	44	67	47	9
$^2D_4$	-158	-28	0	-41	-7	16	39	19	-23
D_5	-118	13	41	0	34	56	80	60	24
D_6	-152	-21	7	-34	0	22	46	26	-15
C_4	-174	-44	-16	-56	-22	0	23	4	-41
C_5	-198	-67	-39	-80	-46	-23	0	-20	-68
C_6	-178	-47	-19	-60	-26	-4	20	0	-45

Table S7. Reaction energies (PBE functional) for reactions $[NaL_2]^+ + L_1 \rightarrow [NaL_1]^+ + L_2$ in kJ/mol. See also Table S5.

ε=1	$^2D_2$	$^2D_3$	$^2D_4$	D_5	D_6	C_4	C_5	C_6	*avg*
$^2D_2$	0	80	145	96	127	84	123	192	121
$^2D_3$	-80	0	65	16	47	4	43	112	30
$^2D_4$	-145	-65	0	-49	-18	-61	-22	47	-45
D_5	-96	-16	49	0	31	-11	27	96	11
D_6	-127	-47	18	-31	0	-42	-4	66	-24
C_4	-84	-4	61	11	42	0	39	108	25
C_5	-123	-43	22	-27	4	-39	0	69	-20
C_6	-192	-112	-47	-96	-66	-108	-69	0	-99
ε=6	$^2D_2$	$^2D_3$	$^2D_4$	D_5	D_6	C_4	C_5	C_6	*avg*
$^2D_2$	0	26	61	38	60	51	75	107	60
$^2D_3$	-26	0	35	12	33	25	49	81	30
$^2D_4$	-61	-35	0	-23	-2	-10	14	46	-11
D_5	-38	-12	23	0	21	13	37	69	16
D_6	-60	-33	2	-21	0	-8	15	47	-8
C_4	-51	-25	10	-13	8	0	24	56	1
C_5	-75	-49	-14	-37	-15	-24	0	32	-26
C_6	-107	-81	-46	-69	-47	-56	-32	0	-63
ε=9	$^2D_2$	$^2D_3$	$^2D_4$	D_5	D_6	C_4	C_5	C_6	*avg*
$^2D_2$	0	20	52	31	51	46	69	96	52
$^2D_3$	-20	0	32	11	31	26	49	76	29
$^2D_4$	-52	-32	0	-21	0	-5	18	45	-7
D_5	-31	-11	21	0	20	16	39	66	17
D_6	-51	-31	0	-20	0	-5	18	45	-6
C_4	-46	-26	5	-16	5	0	23	50	-1
C_5	-69	-49	-18	-39	-18	-23	0	27	-27
C_6	-96	-76	-45	-66	-45	-50	-27	0	-58

Table S8. Gas phase reaction energies obtained with functionals PBE0 and TPSS for reactions $[NaL_2]^+ + L_1 \rightarrow [NaL_1]^+ + L_2$ in kJ/mol. See also Table S5.

PBE0	$^2D_2$	$^2D_3$	$^2D_4$	D_5	D_6	C_4	C_5	C_6	*avg*
$^2D_2$	0	77	143	93	127	91	128	201	123
$^2D_3$	-77	0	65	15	49	14	51	124	34
$^2D_4$	-143	-65	0	-50	-16	-52	-15	58	-40
D_5	-93	-15	50	0	34	-1	36	109	17
D_6	-127	-49	16	-34	0	-35	2	75	-22
C_4	-91	-14	52	1	35	0	37	110	19
C_5	-128	-51	15	-36	-2	-37	0	73	-24
C_6	-201	-124	-58	-109	-75	-110	-73	0	-107
TPSS	$^2D_2$	$^2D_3$	$^2D_4$	D_5	D_6	C_4	C_5	C_6	*avg*
$^2D_2$	0	71	132	87	125	92	129	201	120
$^2D_3$	-71	0	61	16	54	21	58	130	38
$^2D_4$	-132	-61	0	-45	-7	-41	-3	69	-31
D_5	-87	-16	45	0	38	5	42	115	20
D_6	-125	-54	7	-38	0	-33	4	76	-23
C_4	-92	-21	41	-5	33	0	37	110	15
C_5	-129	-58	3	-42	-4	-37	0	72	-28
C_6	-201	-130	-69	-115	-76	-110	-72	0	-110

Table S9. Cartesian coordinates in Å of the minimum structure of $[Na^+(^2D^H_2)_2]^+$ and $[Na(^2D^H_4)]^+$ used as input for the generation of the initial pathway of $P^H(Na^+)$.

	$[Na^+(^2D^H_2)_2]^+$				$[Na^2D^H_4]^+$		
Na	0.0971130	-0.4073673	-0.0976626		0.0023483	-0.0056353	-0.0102128
Si	3.0485984	-0.4151484	-1.7357993		3.4601611	-0.0085105	0.0065816
Si	4.3105188	1.4550235	-2.4831654		2.6480040	2.2203878	-0.0086581
Si	4.4026986	2.5179334	0.4358918		-0.0570916	3.3318044	-0.9148711
Si	3.1223955	0.6416571	1.1377233		-1.9525430	2.2120923	-1.7977906
Si	-3.1913806	0.3385905	-0.6211185		-3.3299946	-0.3601286	-0.8691672
Si	-4.9398865	0.5083861	0.9805987		-2.7861017	-1.8319679	0.9099240
Si	-4.2672701	-2.3459350	1.9865866		-0.0766431	-2.9585303	1.7838469
Si	-2.5383905	-2.4913873	0.3624375		2.0927300	-2.6031810	0.8929920
O	2.3183555	0.0169464	-0.2440167		2.1188901	-0.9672934	0.4264727
O	4.9191607	2.1541002	-1.1028165		1.0064815	2.0924511	-0.4383428
O	-2.1186330	-0.8894717	-0.0876107		-2.0375964	0.7442103	-0.9410458
O	-5.1936481	-1.0440153	1.5232945		-1.0856692	-1.8768918	0.9428786
H	1.8628423	-0.7719009	-2.5887641		3.9388410	-0.4407671	-1.3425074
H	3.8518422	-1.6562600	-1.5034241		4.5444372	-0.2097699	1.0147181
H	3.4094928	2.4108885	-3.1995379		3.3540880	3.0721145	-1.0130254
H	5.4393871	1.0409144	-3.3627062		2.7283175	2.8596012	1.3407492
H	3.5348475	3.7365697	0.4198716		0.6172952	4.1929957	-1.9328587
H	5.5881923	2.7324213	1.3123261		-0.3958309	4.1476912	0.2916341
H	1.9878522	0.9571270	2.0708605		-1.7912266	1.8945686	-3.2501774
H	3.9266343	-0.4719792	1.7315057		-3.2167155	2.9803024	-1.5869360
H	-3.6451782	-0.0256935	-1.9999610		-3.4108760	-1.0707688	-2.1824782
H	-2.2955474	1.5413137	-0.7212892		-4.6008238	0.3854371	-0.6201669
H	-6.1964414	1.0249762	0.3693334		-3.3097621	-3.2131799	0.6842133
H	-4.5014644	1.3906970	2.1067192		-3.2661462	-1.3203548	2.2305338
H	-5.1151799	-3.5706764	1.9996653		-0.5584477	-4.3552796	1.5607812
H	-3.6670096	-2.1059361	3.3359547		-0.1474535	-2.6274995	3.2404490
H	-2.9173934	-3.2263488	-0.8848936		2.3449154	-3.4392659	-0.3209283
H	-1.2325083	-3.0454251	0.8599969		3.1663537	-2.8448018	1.9037001

Table S10. Cartesian coordinates in Å of the minimum structure of [NaI(^{2}D$_2$)$_2$], [NaI(^{2}D$_4$)] and one intermediate structure used as input for the generation of the initial pathway of P^H(NaI).

	[NaI(^{2}D$_2$)$_2$]				intermediate				[NaI^{2}D$_4$]		
Na	1.7318900	0.0111825	-0.1775403		2.0882793	0.1779650	-1.6294605		-0.2677894	-0.2090484	0.0536879
Si	1.1047886	2.7992302	-1.8051356		1.5772622	2.3365355	0.5867782		0.3017405	2.9400251	1.0858987
Si	-1.1493366	3.5463611	-1.6988209		1.1658848	4.5451028	-0.1107081		-0.1138882	3.0097726	-1.2421463
Si	-0.9584435	3.6384628	1.4063873		-1.7463560	3.7982661	-0.8041309		-1.2280814	0.9079457	-3.0934995
Si	1.2958082	2.8955718	1.2768547		-2.7327564	1.8364976	-0.0187806		-1.9449109	-1.3027570	-2.6491628
Si	1.2007849	-2.7871674	-1.7855086		-0.2375999	-2.2605804	-2.3057033		-0.4703611	-3.5262642	-1.1293881
Si	-1.0506650	-3.5514284	-1.7669909		-1.5828469	-3.9642632	-1.3536010		0.1022339	-3.5565756	1.1680078
Si	-0.9663682	-3.6705505	1.3401940		-0.3403346	-3.4835273	1.4197436		1.2550827	-1.4426346	3.0208093
Si	1.2783883	-2.8868542	1.2980138		0.8682937	-1.6313824	0.5915675		1.8496331	0.8238156	2.6810963
O	1.7196146	2.3797717	-0.2812271		0.5294697	1.4827343	-0.4433361		0.8299602	1.3657552	1.4697280
O	-1.5156682	3.9458645	-0.1278566		-0.4937358	4.6394192	-0.0867662		-0.1614640	1.4622357	-1.9111320
O	1.7528307	-2.3567463	-0.2417109		0.5024722	-1.3767317	-1.0505703		-0.9186158	-1.9462948	-1.4501173
O	-1.4734674	-3.9649134	-0.2147057		-0.8728707	-4.3471189	0.1050407		0.6538561	-2.0006882	1.5406677
H	1.2987863	1.5722129	-2.6499433		2.9156272	1.7469813	0.1822483		1.4715775	3.8320072	1.4141346
H	2.0142596	3.8599403	-2.3550742		1.3549161	1.9649363	2.0188601		-0.8306356	3.3370047	1.9699858
H	-2.1087477	2.5504210	-2.2573133		1.6749859	4.5944196	-1.5226591		1.0607686	3.6867218	-1.8916750
H	-1.2569794	4.8097673	-2.5012387		1.7547385	5.6342298	0.7100731		-1.3409977	3.7960800	-1.5689527
H	-1.8345901	2.6760086	2.1345268		-1.8212911	4.1330139	-2.2600105		-0.4299379	0.8781754	-4.3669109
H	-0.9744352	4.9459808	2.1421134		-3.0211820	4.1496433	-0.1176056		-2.3780553	1.8414030	-3.2885535
H	1.5965976	1.7180192	2.1618963		-4.1471755	2.1933670	-0.4421489		-1.7101496	-2.1618457	-3.8648994
H	2.2637446	3.9813820	1.6489080		-2.6736468	2.0171557	1.4745305		-3.3718988	-1.4646518	-2.2500967
H	2.1412382	-3.8370798	-2.3025252		0.9077284	-2.7457098	-3.1455134		0.6987021	-3.9041164	-1.9868366
H	1.4129192	-1.5569080	-2.6226636		-0.9860622	-1.2598719	-3.1334853		-1.5933448	-4.4752846	-1.4165876
H	-1.1191068	-4.8076888	-2.5845176		-1.5987738	-5.1751499	-2.2190602		1.1884135	-4.5455419	1.4693503
H	-1.9931583	-2.5552380	-2.3530587		-2.9671578	-3.4374401	-1.1441506		-1.0696805	-3.8724843	2.0454867
H	-0.9810636	-4.9894787	2.0555405		0.5037234	-4.3390640	2.2964065		2.4292194	-2.2854171	3.4200691
H	-1.8830405	-2.7362634	2.0548325		-1.4917423	-2.9059052	2.1816070		0.1913089	-1.6056298	4.0626068
H	2.2471432	-3.9631782	1.6955176		2.3766061	-1.6546241	0.5899092		3.2751197	0.9519841	2.2379453
H	1.5290872	-1.7141191	2.2027523		0.4955549	-0.4053463	1.3631297		1.6712139	1.6219242	3.9360010
I	-1.1485768	-0.0094002	-0.0398755		-2.8620764	-0.6632209	-0.3232537		-2.8815047	1.0398691	0.2168136

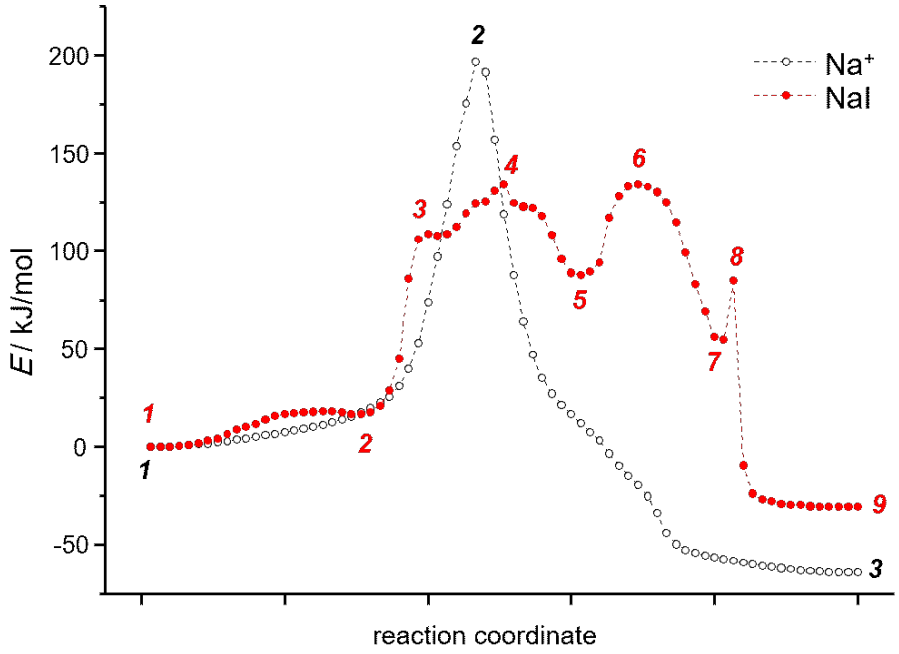

Figure S57. Energy profiles for the pathways $P^{H}(Na^{+})$ (black, open circles) and $P^{H}(NaI)$ (red, filled circles). The numbers refer to the structures shown in Fig. S58.

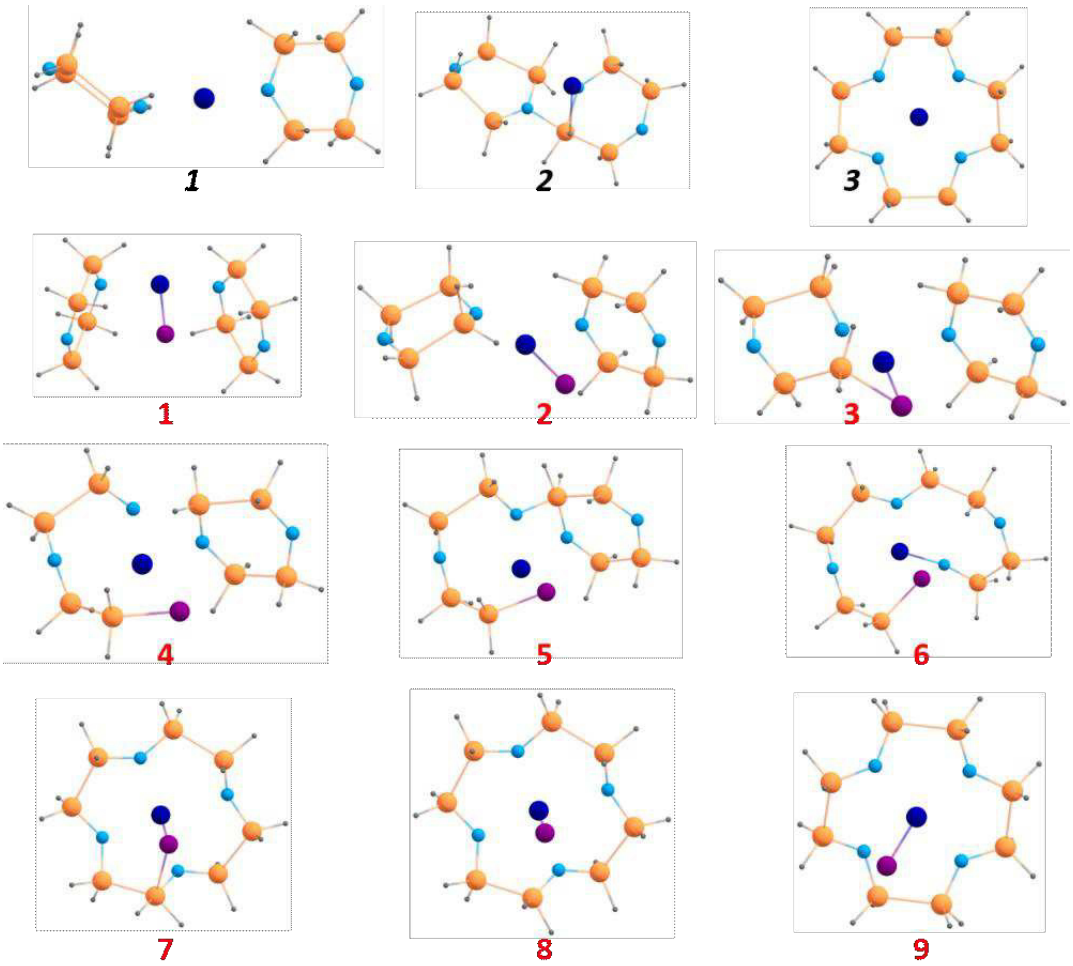

Figure S58. Images of labelled structures for the pathways $P^{H}(Na^{+})$, first row, italic black numbers, and $P^{H}(NaI)$, rows 2−4, red numbers; see also Figure S57.

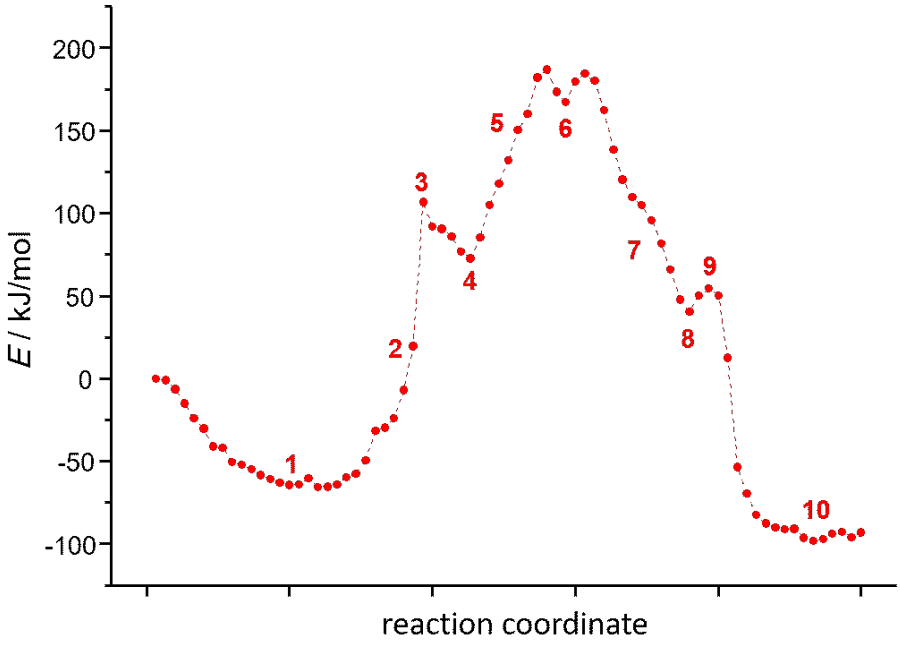

Figure S59. Energy profile for the pathway derived from P^{H}(NaI) after H being replaced with Me and optimization of the coordinates of the Me groups while keeping the positions of O, Si and Na fixed. The numbers indicate the structures chosen for the initial path in the optimization of P(NaI), corresponding images are shown in Figure S60.

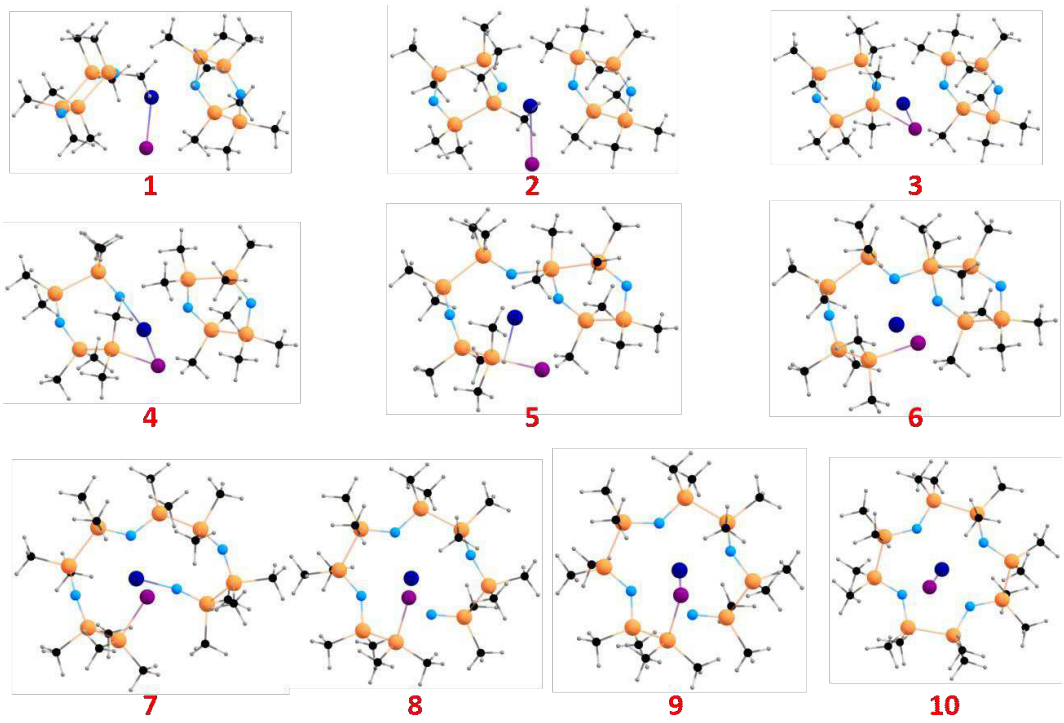

Figure S60. Images of labelled structures for the pathway P^{H}(NaI) after H being replaced with Me and optimization of the coordinates of the Me groups while keeping the positions of O, Si and Na fixed; see also Figure S59.

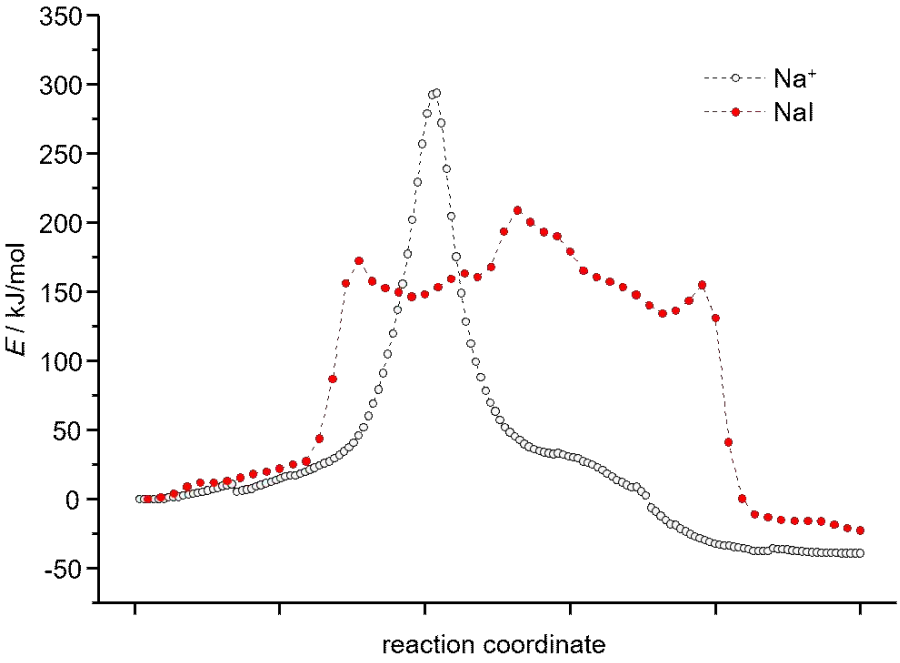

Figure S61. Energy profiles for the pathways P(Na^+) (black, open circles) and P(NaI) (red, filled circles) employing the conductor-like screening model (ε=6) for solvent effects.

8. References

[1] Takano, T.; Kasai, N.; Kakudo, M. The Crystal Structure of Bistetramethyldisilanilenedioxide ($(CH_3)_4Si_2O)_2$, *Bull. Chem. Soc. Jpn.*, **1963**, 36, 585-590.

[2] Korlyukov, A. A.; Chernyavskaya, N. A.; Antipin, M. Yu.; Lysenko, K. A. Molecular and Crystal Structure of Octamethyl-1,4-dioxacyclohexasilane, *Chem. Heterocycl. Compd. (N. Y., NY, U. S.)*, **2005**, 41, 536-541.

[3] Shannon, R. D.; Revised Effective Ionic Radii and Systematic Studies of Interatomic distances in Halides and Chalcogenides, *Acta Crystallogr., Sect. A: Cryst. Phys., Diffr., Theor. Gen. Crystallogr.*, **1976**, 32, 751–767.

[4] TURBOMOLE V7.5 **2020**, a development of University of Karlsruhe and Forschungszentrum Karlsruhe GmbH, 1989-2007, TURBOMOLE GmbH, since 2007; available from http://www.turbomole.com.

[5] Perdew, J.P.; Burke, K.; Ernzerhof, M. K. Generalized gradient approximation made simple, *Phys. Rev. Lett.* **1996**, *77*, 3865-3868.

[6] Perdew, J.P.; Ernzerhof, M.; Burke, K. Rationale for mixing exact exchange with density functional approximations. *J. Chem. Phys.* **1996,** *105*, 9982–9985.

[7] Tao, J.; Perdew, J.P.; Staroverov, V.N.; Scuseria, G.E. Climbing the density functional ladder: Nonempirical meta-generalized gradient approximation designed for molecules and solids. *Phys. Rev. Lett.* **2003**, *91*, 146401.

[8] Treutler, O.; Ahlrichs, R. Efficient molecular numerical-integration schemes. *J. Chem. Phys.* **1995**, *102*, 346-354.

[9] Weigend, F.; Ahlrichs, R. Balanced basis sets of split valence, triple zeta valence and quadruple zeta valence quality for H to Rn: Design and assessment of accuracy. *Phys. Chem. Chem. Phys.* **2005**, *7*, 3297-3305.

[10] Eichkorn, K.; Weigend, F.; Treutler, O.; Ahlrichs, R. Auxiliary basis sets for main row atoms and transition metals and their use to approximate Coulomb potentials. *Theor. Chem. Acc.* **1997**, *97*, 119-124.

[11] Weigend, F. Accurate Coulomb-fitting basis sets for H to Rn. *Phys. Chem. Chem. Phys.* **2006**, *8*, 1057-1065.

[12] Klamt, A.; Schüürmann, G. COSMO: A New Approach to Dielectric Screening in Solvents with Explicit Expressions for the Screening Energy and its Gradient. *J. Chem. Soc., Perkin Trans.* **1993**, *2*, 799–805.

[13] Plessow, P. Reaction Path Optimization without NEB Springs or Interpolation Algorithms *J. Chem. Theory Comput.* **2013,** *9,* 1305–1310.